UNIVERSITEIT GENT

FACULTEIT WETENSCHAPPEN
Vakgroep Geologie en Bodemkunde
Laboratorium voor Toegepaste Geologie en Hydrogeologie

Hydrogeological and Hydrogeochemical Investigation of a Precambrian Basement Aquifer in Bugesera Region (Burundi)

Charles BAKUNDUKIZE

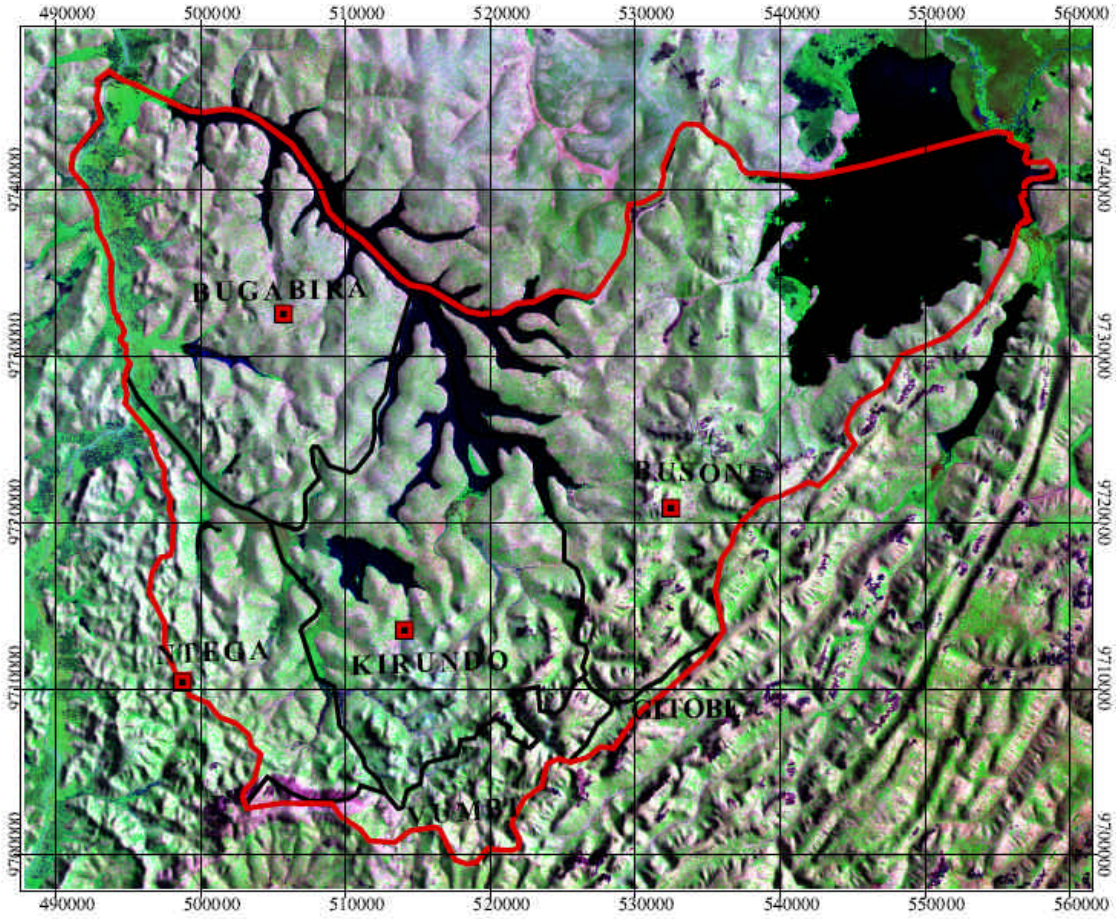

Dissertation submitted in fulfilment of the requirements for the award of the degree of Doctor in Sciences: Geology

Academic year: 2011-2012

Promotor: Prof. Dr. Kristine Walraevens

Hydrogeological and Hydrogeochemical Investigation of a Precambrian Basement Aquifer in Bugesera Region (Burundi)

Charles BAKUNDUKIZE

Dissertation submitted in fulfilment of the requirements for the award of the degree of Doctor in Sciences: Geology

Academic year: 2011-2012

Promotor: Prof. Dr. Kristine Walraevens

Dedication.

To my wife Anne-Marie NDIKUMANA, my sons Aldo-Miguel, Aurel and Melvin-Liesol BAKUNDUKIZE,
To my parents, Bernadette BERAHINO and Joseph BAKUNDUKIZE,
To my elder sister and "second mother", late Marie-Thérèse BAKUNDUKIZE,
To the rest of my family, my sisters and brothers,

This PhD thesis is yours

Acknowledgements

The completion of this research would not have been possible without the substantial contribution of several persons and organisations who, through their advises and various supports, have helped me to bring this work to a successful conclusion. I am deeply thankful to all those who, in a way or another, have assisted me in the course of this challenging and long journey, but I would like to specifically mention some persons and organisations for their special inputs.

First of all, I would like to extend my sincere and heartfelt gratitude to Professor Dr. Kristine Walraevens, my Promoter and Head of the Laboratory for Applied Geology and Hydrogeology for her wise guidance and patience in the course of this work. You have sacrificed a lot of your precious time both in Burundi and Belgium to help me to shape the work as it is today. You deserve a special respect from my family and I, not only for your scientific achievements, but also for your human qualities. You have kept on encouraging me to go ahead even when the chips were down.

I would like also to express my deep thanks to the Applied Training Project of the Nile Basin Initiative and more specifically to Dr. Canisius Kanangire, Dr. William Kudoja and Ernest Kagoro, respectively former Head of the Applied Training Project, Lead Training Specialist and Procurement Specialist for having provided me with substantial means to carry out the important part of this work.

The government of Burundi through the Minister of High Education and Scientific Research, Professor Dr. Julien Nimubona, is equally thanked for having accepted to provide me with an extension of the scholarship after the closing of the Applied Training Project. Without this extension, it would have been complicated to bring this work to a successful end.

Special thanks are also conveyed to the VLIR for awarding me a scholarship which enabled me to serenely finalise the manuscript of this PhD thesis.

I would like to express my deep and sincere appreciation to the members of the jury: Prof. Dr. Jacques Verniers (UGent), Prof. Dr. Dirk Raes (KUL), Prof. Dr. Jean Pierre Cnudde (UGent), Prof. Dr. Morgan De Dapper (UGent), Dr. Max Fernandez-Alonso and Dr. Kristine Martens for accepting to be members of the jury and for their critical review of the manuscript and invaluable inputs which helped to improve this work.

I have highly appreciated the support and collaboration of my colleagues at the Laboratory for Applied Geology and Hydrogeology: Dr. Kristine Martens, Marc Van Camp, Dr. Ibrahim Chikira Mjemah, Yohana Mtoni, Dr. Nawal Al Farrah, Dr. Marleen Coetsiers, Antonia Balazova, Dr. Ammar Da'as, Dr. Mahdi Radfar, Dr. Tesfamichael G.Yohannes Tewolde and Josué Bahati Chishugi. The discussions we had were scientifically enriching and have significantly contributed to the completion of this work. Specifically, I feel morally indebted towards Marc Van Camp for his tireless willingness to advise and help me while I was carrying out this work. I have always been dropping into his office whenever I was stuck, sometimes without considering the deadlines of his own work. Dr. Kristine Martens is equally heartedly thanked for her invaluable help in the arrangement of the final layout of this work.

I owe a special gratitude to the Royal Museum for Central Africa and particularly to Dr. Johan Lavreau, Dr. Max Fernandez-Alonso, Dr. Luc Tack, Dr. Pierre-Denis Plisnier and Daniel Baudet for their constant willingness to assist me and to provide me with an up-to-date documentation, especially maps and information on the geology of Central Africa, in the course of the entire period of this work.

The personnel of the Institut Géographique du Burundi (IGEBU) and specifically the Head of the Department of Meteorology, Aloys Rurantije, and Jean Crystostome Nzeyimana, are deeply thanked for having accepted to provide me with weather data each time I have contacted them.

I deeply thank Mrs. Gilberte Verschueren, former secretary at the Laboratory for Applied Geology and Hydrogeology for her kindness and willingness to help whenever she was contacted. Jill Van Reybrouck also should find in the completion of this PhD thesis the result for her significant contribution in laboratory analysis.

I wish also to express my deep acknowledgements to my colleagues of the University of Burundi: Prof. Dr. Ir. Gaston Hakiza, the Rector of the University of Burundi, prof. Dr. Deo-Douglas Niyonzima, Dean of the Faculty of Sciences, Prof. Dr. Pascal Nkurunziza, Head of the Department of Earth Sciences, Prof, Dr. Louis Nahimana, Dr. Gilbert Midende, Dr. David Nahimana, Dr. Aloys Katihabwa, Prof. Dr. Leonard Hari, Anicet Sindayihebura, Théodose Simuzeye, Menus Nkurunziza, Rénovat Nyandwi and Laurent Habonimana for their support and encouragements in the course of this work.

Last but not the least I would like to thank all those who helped me during the 3 field campaigns conducted in Bugesera region. The former Minister of Energy and Mines, Dr. Samuel Ndayiragije, is specially thanked for having allowed me to use the generator of the Department of Geology during the pumping tests. Special gratitude is also extended to MSc. Ir. Didace Didi, the Director of GEOSCI, for his assistance to print all the maps I used in the field. I am deeply grateful to those courageous guys who, in a way or another, have gently helped me to gather invaluable field data in the field. My special thoughts go to late Gérard Nkundabahizi, Lazare Sindakira, Bernard Gasongo, Bernard Nzirubusa, Libère Mudende, Mukurarinda Pascal, Sungura Jean Bosco, Eddy Niyongabo, Evariste Sinzumusi, Nzeyimana Martin, Madori Normand, Barthélemy Harusha, Munongo, Bernard, Vincent Nzisabira, Jean Claude Harerimana, Jean Claude Nduwayo and Dismas. Without their contribution, this work would not have been as it is now.

SUMMARY

Water, the blue gold, is a vital commodity for human life, the survival of water-related biodiversity and natural ecosystems. Burundi, as many Sub-Saharan countries, is still far from achieving the Millennium Development Goal related to access to safe drinking water and adequate sanitation. Recent figures indicate a global drinking water coverage of 83% and 55% in urban and rural areas respectively. Despite several attempts to resolve the issue of drinking water in water-scarce areas by tapping groundwater resources, the problem is still unsolved, mainly due to the poor knowledge of hydrogeological conditions and limited financial investments. The present study is therefore a comprehensive contribution to the scientific understanding of the hydrogeological framework and the hydrogeochemical environment of a basement aquifer in Bugesera region, one of the most water-scarced areas in Burundi.

Bugesera region, which covers an important part of northeastern Burundi and southeastern Rwanda, is one of the numerous depressions known in the inter-lacustrine zone of East Africa. Despite a large complex of interconnected swamps and small lakes, this region is impressively marked by a lack of natural springs. For domestic needs, local population, who believe that the lack of drinking water is "damnation", heavily relies on groundwater which is tapped through hand-dug wells. Where these hand-dug wells are not operating, the population resorts to often polluted surface water from the lakes and marshlands. The study area mainly consists of a depression surrounded by a more rugged landscape to the South and East. It covers an area of 1050 km^2 and stretches over 5 main watersheds: Kanyaru 9, Nyavyamo, Cohoha South, Cohoha North and Rweru.

The main source of groundwater recharge in the study area is precipitation. The long-term average groundwater recharge estimated using the soil moisture budget technique for a period of 35 hydrologic years (1974/75-2008/2009) is 218 mm/year calculated by the Thornthwaite Monthly Water-Balance Model (TMWB model). The latter, which is on a monthly basis, using Hamon's PET (185 mm/year), was found to perform very well, as it fairly approximates average recharge values obtained on a daily basis with Penman-Monteith PET (243 mm/year) for the period 1999-2009 where a complete set of climatic parameters is available. This study clearly demonstrates that the use of small time steps in recharge calculations, which better corresponds to the reality in nature, leads to increased recharge. Four evapotranspiration calculation methods namely Hamon, Hargreaves, Thornthwaite, and a modification of the original Thornthwaite method were evaluated in comparison to the reference Penman-Monteith equation for the period 1999-2009. The results of evapotranspiration calculations show that the Hargreaves method aberrantly overestimates evapotranspiration by 51 % with a RMSE of 48 mm/month and should be avoided in the study area. This study draws the attention on the risk of generating erroneous estimates of recharge by using inappropriate PET methods. The calculation of groundwater balance in the study area shows that groundwater exploitation, which represents only 0.16 % of the recharge, is still underdeveloped despite the scarcity of drinking water. The important baseflow explains the existence of the perennial complex of marshlands and lakes. A comparison of the volume of water available (3806000 m^3/year) to the water demand (3334000 m^3/year) shows an apparent surplus of 14 % which is mainly due to the springs concentrated in the southern and eastern highlands and which flow round-the-clock.

The study area, which entirely belongs to the Western Domain of the Karagwe-Ankole Belt, is predominantly underlain by Precambrian crystalline rocks consisting of metasedimentary rocks and magmatic intrusions. They form five geological formations: (1) the Undifferentiated Complex, which occurs in the centre of the depression, is mainly composed of granitic and pegmatitic intrusions; (2) the Formation of Murehe (or Mugendo) girdles the Undifferentiated Complex; it is made up of pelitic and quartzitic metasediments intruded by granites, pegmatites and quartzitic veins; (3) the Formation of Ngozi occupies the South-West of the study area where it forms a L-shaped set of metasediments and metavolcanites with sporadic dykes of pegmatites; (4) the Formation of Ruganza, which is mainly composed of quartzites, underlies the Formation of Ngozi in the South-West; (5) the Formation of Nyagisozi (or Nyabihanga) forms a NE-SW elongated feature made up of psammites to psammoschists (micaceous sandstones) with intercalation of conglomerates. Cenozoic formations comprise various types of soils and alluvium in valley bottoms and lower terraces. The hydrogeological structure was inferred from the re-interpretation of two existing batches of vertical electrical soundings (VES) which were constrained by available geological and lithological information. The interpretation of the VES shows sequences of 3 to 6 geoelectrical layers organised in different sequences which, overall, show an upwards fining of weathering material reflecting the upwards increasing intensity of the weathering process. The hydrogeological model of the study area shows that the aquifer tapped by the hand-dug wells is hosted by the weathered overburden and consists of a mixture of clay, sand, gravel and rock fragments in variable proportions (with a resistivity between 28-150 Ωm), which is topped by a clay-rich layer (with a resistivity between 3-28 Ωm) acting as the (semi-) confining layer. The top soil is formed by a wide variety of materials which are characterised by a wide range of resistivities (7-600 Ωm). The weathered overburden is underlain by the fractured weathered basement (150-500 Ωm) which may form the prolongation of the aquifer. The weathered/fractured basement overlies the fresh basement which is characterised by high values of resistivity (>500 Ωm). The Undifferentiated Complex Formation, which is characterised by the highest thicknesses of the two components of the aquifer, i.e. weathered overburden and the weathered/fractured basement, has the highest groundwater potential compared to the two metasedimentary formations: Murehe and Nyagisozi in which VES were performed.

The hydraulic parameters are evaluated based on the analysis of 41 constant-rate pumping tests conducted during two field campaigns, organised from September to December in 2007 and from July to October in 2008. Pumping and recovery test data were analysed using different analytical methods namely: Theis (1945), Hantush (1960), Cooper & Jacob (1946), Papadopoulos & Cooper (1967), double porosity method and the specific capacity method. The results of pumping test data analysis show a widespread conformity of the aquifer response to the analytical Hantush method (27 pumping and recovery tests), thus confirming the proposed hydrological model which reveals leaky conditions. In the western part of the study area, most of the pumping tests conform to the double porosity model and this reflects the tectonic fracturing associated with the North-South trending fault along which flows the River Kanyaru. Overall, the transmissivity varies between 1 m^2/d and 377 m^2/d with an average of 33 m^2/d, whereas the hydraulic conductivity ranges between 0.1 m/d and 166 m/d with an average of 14.8 m/d. Specific capacity values calculated for the 41 pumping tests are in the range of 6.6 -1134 m^2/d with an average of 113.6 m^2/d. The wide variability is typical of basement aquifers as this was reported by several authors. The

hydraulic parameters obtained using the Hantush, and Cooper & Jacob methods, both for the pumping and recovery phases are generally closely comparable. The spatial distribution of hydraulic parameters confirms the high groundwater potential of the Undifferentiated Complex Formation (T = 2.1-377 m^2/d, K = 0.3-166 m/d, S_c = 6.6-1134 m^2/d) in comparison to the metasedimentary formations of Nyagisozi (T = 5.7-60 m^2/d, K = 1.6-41 m/d, S_c = 24-222 m^2/d) and Murehe (T = 1-30 m/d, K= 0.2-34 m/d, S_c = 7-104 m^2/d).

The groundwater flow system was reconstructed based on 157 piezometric measurements and 126 topographic elevations of springs located in the southern highlands. An analysis of the groundwater flow pattern shows a local component towards the perennial and ephemeral streams and a regional component flow from the southern and eastern highlands towards the complex of marshlands and lakes which forms the main discharge area. Analysis of the inter-annual variation of groundwater levels shows a decreasing trend between 1991 and 2006, whereas between 2006 and 2008, a maximum is observed in 2007. This pattern of groundwater level fluctuation is in agreement with the amount of recharge calculated for each hydrologic year, the highest groundwater level corresponding to high recharge. Analysis of the seasonal variations of groundwater levels for 2008 shows a trend which closely follows that of the monthly rainfall. However, it was observed that the peak of groundwater level occurs at different times in northeastern (May), central (April) and southwestern pasts (June). This important observation is related to duration of the travel of the recharge across the unsaturated zone and confirms the high hydraulic conductivity which characterises the Undifferentiated Complex Formation situated in the central part of the study area.

A simple steady state groundwater flow model of Bugesera region was successfully developed and calibrated using the finite difference code Visual Modflow 3.0. Considering the low level of groundwater exploitation in the study area, steady state conditions were assumed. Taking into account the defined hydrogeological model, 3 layers, comprising the top clay-rich layer, the weathered overburden and the weathered/fractured basement were considered. The model domain was discretised into a grid consisting of 225 rows and 278 columns with a spatial resolution of 180 m * 180 m for each grid cell. The calibration of the model through a trial and error process has enabled to reach a satisfactory match between the observed and calculated piezometric levels with a RMSE of 5.24 %. The groundwater flow model shows that the average hydraulic conductivity for the weathered overburden is 0.30 m/d instead of 0.66 m/d deduced from pumping tests which appears to be overestimated. The simulated groundwater flow confirms both the local flow towards the myriad of V-shaped valleys where flow ephemeral and perennial streams, and the regional flow towards the marshlands and the lakes. The potentiometric map generated by the model is closely similar to the piezometric map constructed manually based on groundwater level measurements. The groundwater balance shows a small discrepancy (0.01 %) between the inputs and outputs of the model, which confirms a good convergence of the model.

The hydrogeochemical study is based on the analytical results of 143 water samples collected from wells (66), springs (61) and lakes (16). The spatial distribution of different hydrochemical parameters shows a general increasing trend from the highlands where water samples, mainly from springs, show low mineralisation (TDS = 26-152 mg/l) and low pH (field pH = 4.6-6.6). The classification of water types based on the

dominant ion and representation of water samples on a Piper diagram highlights the existence of clusters which clearly show an evolutionary sequence from the lowly mineralised springs, mainly of NaCl types (19 %), towards a suite of water types along the flowpath which are dominated by $NaHCO_3$ (49 %) and $CaHCO_3$ (13%). The anthropogenic pollution is underlined by the occurrence of $NaNO_3$, $CaNO_3$, KNO_3 and $NaSO_4$ types even in spring water. The main hydrogeochemical factor controlling groundwater evolution in Bugesera region is the weathering of aluminosilicates. The evaporative concentration, the leaching of evaporitic salts and the anthropogenic pollution play a secondary role. This important finding is but tressed by the predominance of $NaHCO_3$ and $CaHCO_3$ water types (62 %), the stability diagrams which show that all water samples are in thermodynamic equilibrium with the weathering products of aluminosilicates (gibbsite and kaolinite) and the cross-plots which confirm an increasing trend of the alkaline and alkaline earth cations ($Na^+ + K^+ + Ca^{2+} + Mg^{2+}$) released from the weathering of aluminosilicates along the flowpath. The poor correlation between the concentrations of SiO_2 and Na^+, Ca^{2+}, Mg^{2+}, K^+, HCO_3^- and TDS confirms the incongruent character of the weathering of aluminosilicates which causes part of the silica released from the weathering of silicates to be retained into the formation of clay minerals.

This study clearly shows that Bugesera region has a real groundwater potential which could be circumscribed and tapped in order to provide enough drinking water to the inhabitants of these areas. Thus, this study recommends further investigations among which are geophysical investigations coupled to reconnaissance drillings, the installation of a network of piezometers to monitor the groundwater level variation, measurements of the discharge rate and water level fluctuation in the complex of marshlands and lakes, monitoring of groundwater quality and further pumping tests in order to refine the distribution of hydraulic parameters in the study area.

SAMENVATTING

Water, het blauwe goud, is vitaal voor het menselijk leven, de biodiversiteit en natuurlijke ecosystemen. Burundi, als zovele Sub-Sahara landen, staat ver van het bereiken van de Millenium Ontwikkelings Doelstellingen wat betreft de toegang tot veilig drinkwater en een adequaat afvalwaterbeheer. Recente cijfers geven aan dat globaal 83 % van de stedelijke bevolking en 55 % op het platteland, toegang hebben tot drinkwater. Ondanks verscheidene pogingen om het probleem van drinkwater in waterschaarse gebieden op te lossen door de grondwatervoorraden aan te spreken, is het probleem nog steeds onopgelost, hoofdzakelijk als gevolg van de beperkte kennis van hydrogeologische condities en ontoereikende financiële middelen. De voorliggende studie vormt daarom een bijdrage tot het wetenschappelijk begrip van het hydrogeologisch kader en de hydrogeochemische toestand van een sokkelaquifer in het Bugesera gebied, een van de meest waterschaarse gebieden van Burundi.

Het Bugesera gebied, dat een belangrijk gedeelte van noordoost Burundi en zuidoost Rwanda omvat, is een van de talrijke depressies in de interlacustriene zone van Oost-Afrika. Ondanks een groot complex van verbonden moerassen en kleine meren, wordt dit gebied gekenmerkt door het ontbreken van natuurlijke bronnen. De locale bevolking gelooft dat het gebrek aan drinkwater een vloek is. Voor huishoudelijke doeleinden zijn zij sterk aangewezen op grondwater, dat gewonnen wordt d.m.v. handgegraven putten. Waar deze putten niet functioneren, nemt de bevolking dikwijls haar toevlucht tot verontreinigd oppervlaktewater van de meren en moerassen. Het studiegebied bestaat grotendeels uit een depressie omringd door een reliëfrijker landschap in het zuiden en oosten. Het beslaat een oppervlakte van 1050 km² en strekt zich uit over 5 waterbekkens: Kanyaru 9, Nyavyamo, Cohoha Zuid, Cohoha Noord en Rweru.

De belangrijkste bron van grondwateraanvulling in het studiegebied is neerslag. De lange-termijn gemiddelde grondwateraanvulling werd geschat met de bodemvochtbalansmethode voor een periode van 35 hydrologische jaren (1974/1975-2008/2009) en bedraagt 218 mm/jaar berekend met het Thornthwaite Maandelijkse WaterBalans Model (TMWB model). Dit model, op maandelijkse basis, en gebruik makend van de PET volgens Hamon (185 mm/jaar), bleek goed te voldoen, aangezien het een goede benadering vormt voor gemiddelde grondwateraanvullingswaarden verkregen op dagelijkse basis met de PET volgens Penman-Monteith (243 mm/jaar), voor de periode 1999-2009 waarvoor een volledige set van klimaatsparameters beschikbaar is. Deze studie toont duidelijk aan dat het gebruik van kleine tijdsstappen in grondwatervoedingsberekeningen, wat beter overeenkomt met de realiteit, leidt tot een hogere aanvulling. Vier evapotranspiratie berekeningsmethoden, met name Hamon, Hargreaves, Thornthwaite, en een aanpassing van de Thornthwaite methode, werden geëvalueerd in vergelijking met de referentie Penman-Monteith methode voor de periode 1999-2009. De resultaten van de evapotranspiratie berekeningen tonen dat de Hargreaves methode de evapotranspiratie sterk overschat met 51 % met een RMSE van 48 mm/maand; deze methode dient dus vermeden te worden in het studiegebied. Dit onderzoek brengt het risico van verkeerde PET schattingen door het gebruik van onaangepaste methoden onder de aandacht. De berekening van de grondwaterbalans in het studiegebied toont dat grondwaterwinning, die slechts 0.16 % van de aanvulling bedraagt, nog onderontwikkeld is in het studiegebied, de schaarsheid van water ten spijt. De belangrijke baseflow verklaart het bestaan van het complex van moerassen en meren. Een vergelijking van het beschikbaar watervolume (3.806.000 m³/jaar) met de

vraag naar water (3.334.000 m³/jaar) toont een schijnbare surplus van 14 %, die hoofdzakelijk te wijten is aan de bronnen die geconcentreerd zijn in de zuidelijke en oostelijke hooglanden, en die permanent stromen.

Het studiegebied, dat vol ledig behoort tot het Westelijk Domein van de Karagwe-Ankole Belt, rust voornamelijk op Precambrische kristallijne gesteenten, bestaande uit metasedimentaire gesteenten en magmatische intrusies. Ze vormen vijf geologische formaties: (1) het Ongedifferentieerd Complex, dat in het centrum van de depressie voorkomt, en vooral bestaat uit granitische en pegmatitische intrusies; (2) de Formatie van Murehe (of Mugendo) omgordelt het Ongedifferentieerd Complex; ze bestaat uit pelitische en kwartsietische metasedimenten die geïntrudeerd worden door granieten, pegmatieten en kwartsietaders; (3) de Formatie van Ngozi beslaat het zuidwesten van het studiegebied, waar ze een L-vormig stel metasedimenten en metavolcanieten vormt met sporadische pegmatietdykes; (4) de Formatie van Ruganza, die hoofdzakelijk bestaat uit kwartsieten, en onder de Formatie van Ngozi voorkomt in het zuidwesten; (5) de Formatie van Nyagisozi (of Nyabihanga) vormt een NE-SW strook bestaande uit psammieten tot psammo-schists (micahoudende zandstenen) met intercalatie van conglomeraten. Cenozoïsche formaties omvatten diverse typen van bodems en alluvium in valleibodems en lagere terrassen. De hydrogeologische structuur werd afgeleid uit de herinterpretatie van twee bestaande stellen van verticale elektrische sonderingen (VES), die gijkt werden op beschikbare geologische en lithologische informatie. De interpretatie van de VES toont sekwenties van 3 tot 6 geo-elektrische lagen vervat in verschillende sequenties die, in het algemeen, een opwaarts verfijnende trend vertonen van het verweringsmateriaal, hetgeen een opwaarts toenemende verwering weerspiegelt. Het hydrogeologisch model van het studiegebied toont dat de aquifer die aangetapt wordt door de handgegraven putten zich situeert in de verweringsmantel en uit een mengsel van klei, zand, grint en gesteentefragmenten bestaat, in wisselende proporties (met een resistiviteit begrepen tussen 28 en 150 Ωm). Daarboven bevindt zich een sterk kleihoudende laag (met een resistiviteit tussen 3 en 28 Ωm) die dienst doet als (half-)afsluitende laag. De bodem wordt gevormd door een ruime waaier aan materialen die gekenmerkt worden door een variatie in de resistiviteit (7 tot 600 Ωm). Onder de verweringsmantel komt de gefractureerde en verweerde sokkel voor (150-500 Ωm) die de voortzetting van de aquifer kan vormen. De verweerde/gefractureerde sokkel ligt bovenop de onverweerde sokkel die gekarakteriseerd wordt door hoge resistiviteitswaarden (> 500 Ωm). Het Ongedifferentieerd Complex, dat gekenmerkt wordt door de grootste dikten van beide componenten van de aquifer, met name de verweringsmantel en de verweerde/gefractureerde sokkel, heeft het grootste grondwaterpotentieel in vergelijking met beide metasedimentaire formaties: Murehe en Nyagisozi, waarin VES werden uitgevoerd.

De hydraulische parameters werden afgeleid op basis van 41 pompproeven, uitgevoerd tijdens twee terreincampagnes in september-december 2007 en juli-oktober 2008. Pomp- en recovery-testgegevens werden geanalyseerd met verschillende analytische methoden, met name: Theis (1945), Hantush (1960), Cooper & Jacob (1946), Papadopoulos & Cooper (1967), dubbelporositeitsmethode en de specifieke putcapaciteit-methode. De resultaten van de pompproefinterpretatie tonen een algemeen beantwoorden van de aquifer-respons aan de analytische Hantush methode (27 pomp- en recovery testen), hetgeen het voorgestelde hydrologische model van half-afgesloten condities bevestigt. In het westelijk deel van het studiegebied beantwoorden de meeste pompproeven aan het dubbele porositeitsmodel, en dit reflecteert de tektonische

fracturatie geassocieerd met de N-S breuk waarlangs de Kanyaru Rivier stroomt. De transmissiviteit varieert tussen 1 m²/dag en 377 m²/dag, met een gemiddelde van 33 m²/d, terwijl de hydraulische doorlatendheid schommelt tussen 0.1 m/d en 166 m/d met een gemiddelde van 14.8 m/d. De specifieke put capaciteit berekend voor 41 pompproeven varieert van 6.6 m²/d tot 1134 m²/d met een gemiddelde van 113.6 m²/d. De grote variabiliteit is typisch voor schokelaquifers, zoals gerapporteerd door verscheidene auteurs. De hydraulische parameters afgeleid met de Hantush en Cooper & Jacob methoden, zowel voor de pomp- als de recovery testen, zijn in het algemeen goed vergelijkbaar. De spatiale verdeling van de hydraulische parameters bevestigt het hoge grondwaterpotentieel van het Ongedifferentieerd Complex (T = 2.1-377 m²/d, K = 0.3-166 m/d, S_c = 6.6-1134 m²/d) in vergelijking met de metasedimentaire formaties van Nyagisozi (T = 5.7-60 m²/d, K = 1.6-41 m/d, S_c = 24-222 m²/d) en Murehe (T = 1-30 m²/d, K = 0.2-34 m/d, S_c = 7-104 m²/d).

Het grondwaterstromingssysteem werd gereconstrueerd op basis van 157 piëzometrische metingen en 126 topografische hoogten van bronnen in de zuidelijke hooglanden. Een analyse van het grondwaterstromingspatroon toont een lokale component naar de permanente en tijdelijke waterlopen en een regionale component van de zuidelijke en oostelijke hooglanden naar het complex van moerassen en meren, die het belangrijkste uitvloeigebied vormen. De analyse van de interjaarlijkse variatie van grondwaterstanden toont een afnemende trend tussen 1991 en 2006, terwijl tussen 2006 en 2008 een maximum wordt vastgesteld in 2007. Dit patroon van grondwaterstanden komt overeen met de hoeveelheid grondwateraanvulling die berekend werd voor elk hydrologisch jaar, waarbij de hoogste grondwaterstand correspondeert met een grote aanvulling. De analyse van de seizoenale variatie van de grondwaterstanden voor 2008 toont een trend die goed overeenkomt met deze van de maandelijkse neerslag. Nochtans werd vastgesteld dat de grondwaterstandspiek op verschillende momenten optreedt in het noordoosten (mei), centraal (april) en in het zuidwesten (juni). Deze belangrijke vaststelling houdt verband met de reistijd van de grondwateraanvulling doorheen de onverzadigde zone, en bevestigt de hoge hydraulische conductiviteit die het Ongedifferentieerd Complex kenmerkt, in het centraal deel van het studiegebied.

Een eenvoudig steady state grondwaterstromingsmodel van het Bugesera gebied werd met succes ontwikkeld en gecalibreerd aan de hand van het eindig-verschil model Visual Modflow 3.0. Gezien de beperkte grondwaterwinning in het gebied konden steady state condities worden aangenomen. Uitgaande van het ontwikkelde hydrogeologisch model werden 3 lagen beschouwd, met name de bovenste kleirijke laag, de verweringsmantel en de verweerde/gefractureerde schokkel. Het modeldomein werd gediscretiseerd tot een netwerk, bestaande uit 225 rijen en 278 kolommen met een spatiale resolutie van 180 m x 180 m voor elke cel. De calibratie van het model met een trial-and-error proces leidde tot een aanvaardbare overeenkomst tussen waargenomen en berekende stijghoogten met een RMSE van 5.24 %. Het grondwaterstromingsmodel toont dat de gemiddelde hydraulische doorlatendheid voor de verweringsmantel 0.30 m/d is i.p.v. 0.66 m/d zoals afgeleid uit de pompproeven, wat een overschatting blijkt te zijn. De gesimuleerde grondwaterstroming bevestigt zowel de lokale stroming naar de talrijke V-vormige valleien waarin permanente en tijdelijke waterlopen stromen, als de regionale stroming naar de moerassen en meren. De stijghoogtekaart berekend met het model is goed vergelijkbaar met de kaart die manueel werd geconstrueerd op basis van de stijghoogtemetingen. De grondwaterbalans toont een kleine discrepantie (0.01 %) tussen inputs en outputs van het model, en bevestigt een goede modelconvergentie.

De hydrogeochemische studie is gebaseerd op de analyseresultaten van 143 waterstalen verzameld uit putten (66), bronnen (61) en meren (16). De spatiale verdeling van de hydrochemische parameters toont een algemeen toenemende trend vanaf de hooglanden, waar de waterstalen, vnl. van de bronnen, een lage mineralisatie tonen (TDS = 26-152 mg/l) en een lage pH (veld pH = 4.6-6.6). De klassificatie van watertypes op basis van het dominant ion en de voorstelling van de waterstalen op een Piper diagram brengt het bestaan van clusters aan het licht, die duidelijke evolutietonen van de minst gemineraliseerde bronnen (meestal van NaCl-type (19 %)), tot een reeks van watertypes langs een stroomlijn die gedomineerd worden door $NaHCO_3$ (49 %) en $CaHCO_3$ (13 %). De anthropogene verontreiniging wordt aangetoond door het voorkomen van $NaNO_3$, $CaNO_3$, KNO_3 en $NaSO_4$ types, zelfs in bronwater. De belangrijkste hydrogeochemische factor die de grondwaterevolutie in het Bugesera gebied bepaalt, is de verwering van aluminosilikaten. Evaporatieve concentratie, de uitloging van evaporitische zouten en de anthropogene verontreiniging spelen een ondergeschikte rol. Deze belangrijke vaststelling wordt onderstreept door het overheersen van $NaHCO_3$ en $CaHCO_3$ watertypes (62 %), de stabiliteitsdiagrammen die aantonen dat alle waterstalen in thermodynamisch evenwicht zijn met de verweringsprodukten van aluminosilikaten (gibbsiet en kaoliniet) en de cross-plots die de toenemende trend bevestigen van de alkali- en aardalkali-elementen ($Na^+ + K^+ + Ca^{2+} + Mg^{2+}$) die langs een stroomlijn vrijkomen bij de verwering van aluminosilikaten. De zwakke correlatie tussen de concentraties van SiO_2 en Na^+, Ca^{2+}, Mg^{2+}, K^+, HCO_3^- en TDS bevestigt het incongruent karakter van de verwering van aluminosilikaten, waardoor een deel van de silica die vrijgesteld wordt bij de silikaatverwering, opgenomen wordt in de vorming van kleimineralen.

Deze studie toont duidelijk aan dat het Bugesera gebied een werkelijk grondwaterpotentieel heeft, dat nader kan omschreven worden en aangesproken om in voldoende drinkwater voor de inwoners van dit gebied te voorzien. De studie beveelt dan ook verder onderzoek aan, waaronder geofysische metingen gekoppeld aan verkenningsboringen, de installatie van een peilbuizennetwerk om de variatie van de stijghoogten op te volgen, metingen van de afvoerdebieten en waterpeilfluctuaties in het complex van moerassen en meren, monitoring van de grondwaterkwaliteit en bijkomende pompproeven om de verdeling van de hydraulische parameters te verfijnen.

aCKNOWLEDGEMENTS
Summary
SAMENVATTING

TABLE OF CONTENT

LIST OF SYMBOLS
LIST OF ABBRIVIATION AND ACRONYMS
LIST OF FIGURES
LIST OF TABLES

List of Figures

LIST OF TABLES

LIST OF APPENDICES

List of symbols

Δh: Rise of groundwater level (L)
ΔS: Change in groundwater storage (L^3/T)
ΔS_B: Change in soil moisture storage (L)
AET: Actual evapotranspiration (L)
APWL: Accumulated potential water loss (L)
CAP: Water content at field capacity (L)
D: Well diameter (L)
DEF: Deficit (L)
EC: Electrical conductivity (µS/cm-25°C)
ET_g: Evapotranspiration from the groundwater (L)
G_r: Gibbs free energy (kJ/mol)
K: Hydraulic conductivity (m/d)
K_h: Horizontal hydraulic conductivity (L/T)
K_v: Vertical hydraulic conductivity (L/T)
n: porosity (%)
n_e: Effective porosity (%)
P: Precipitation (L)
PAW: Plant available water (L)
PET: Potential evapotranspiration (L)
Q_i: Return flow (L^3/T)
Q_O: Baseflow (L^3/T)
Q_p: Groundwater abstraction from wells (L^3/T)
R_a: Extraterrestrial radiation (MJ m^{-2} day^{-1})
RH: Relative humidity (%)
R_N: Natural groundwater recharge (L)
Ro: Runoff (L or L^3/T)
S: storage coefficient (%)
s: drawdown (L)
S_B: Soil moisture storage (L)
S_{Bn+1}: soil moisture storage at the end of a new time step (L)
Sc: Specific capacity (L^2/T)
S_{g+s}: Ground and surface water storage (L^3/T)
SMW: Soil moisture withdrawal (L)
Ss: specific storage (unitless)
SUR: Surplus (mm)
SWL: Static water level (L)
S_y: specific yield (unitless)
T: temperature (°C)
T: Transmissivity (L^2/T)
TDS: Total dissolved solids (mg/l)
T_{eff}: Effective temperature (°C)
T_{max}: Max temperature (°C)
T_{mean}: mean temperature (°C)
T_{min}: Minimum temperature (°C)
WPWP: Water content at permanent wilting point (L)
ρ: restivity (Ωm)

List of abbreviation and acronyms

AIDR: Association internationale pour le développement rural
AMC: Antecedent soil moisture condition
BGR: Bundesanstalt für Geowissenschaften und Rohstoffe (German federal institute for geosciences and natural resources)
BTC: Belgian Technical Cooperation
CN: Curve number
CSLP: Cadre stratégique de lutte contre la pauvreté
DEM: Digital Elevation Model
DRC: Democratic Republic of Congo
ED: Eastern domain
FAO: Food and Agriculture Organisation
FMAM: February, March, April and May
GEOSCI: Geosciences & Civil Engineering
GPS: Global positioning system
HS: Hargreaves-Samani
IGEBU: Institut géographique du Burundi
INEAC: Institut National pour l'Etude Agronomique du Congo Belge
ISABU: Institut des Sciences Agronomiques du Burundi
JFMAM: January, February, March, April and May.
JMP: Joint monitoring programme
KAB: Karagwe-Ankole Belt
KIB: Kibaran Belt
l/c/d: litre per capita per day
Ma: Mega-annum
Max: Maximum
Min: Minimum
MDG: Millenium development goal
NASA: National Aeronotics and Space Administration
NE: North-East
NGO: Non governmental organisation
NRCS: Natural resources conservation service
NW: North-West
PM: Penman-Monteith
REGIDESO: Régie de distribution de l'eau et de l'electricité
RMSE: Root mean square error
SHER: Société pour l'hydraulique, l'environnement et la réhabilitation
SON: September, October and November
SONDJFMAM: September, October, November, December,
SRTM: Shuttle Radar Topography Mission
SW: South-West
TH: Original Thornthwaite's PET equation
TH (k = 0.69): Modification of the orginal Thornthwaite's PET equation with k = 0.69
TMWB: Thornthwaite monthly water balance
UNEP: United Nations Environment Programme
UNESCO: United Nations Educational, Scientific and Cultural Organisation
UNICEF: United Nations Children's Fund
US: United States
USDA: United States department of agriculture
UTM: Universal transverse mercator
VES: Vertical electrical sounding
W/N: Well number
WD: Western domain
WHO: World Health Organisation

CHAPTER I. INTRODUCTION

I.1. General background

Water, the blue gold, is a vital commodity for human life, the survival of water-related biodiversity and natural ecosystems on the earth. Availability of water resources in sufficient quantity and quality is a key factor for economical growth for any country. However, with the ever growing world population, the expending urbanisation and the consequent increase of water demand for industry, agricultural and households, the climatic change and the attendant capricious trends of rainfall, the increasing threat of pollution associated with the agricultural, urbanisation and industrial expansion, fresh water resources availability is decreasing year after year, especially in the developing world where infrastructures to tap, treat and convey water are not adapted to cope with the aftermaths of our ever changing world.

The last report of the UNICEF/WHO Joint Monitoring Programme for water supply and sanitation indicates that from 1990 to 2010, the proportion of global population with access to safe drinking water has risen from 76 % to 89 %, which shows that the Millenium Development Goal (MDG) objective with respect to safe drinking water has been achieved 5 years ahead of the deadline. For the MDG sanitation target, only 63 % of the global population has nowadays access to improved sanitation and this is still very far from the objective of 75 % set for 2015 (UNICEF/WHO JMP, 2012). However, this global coverage of safe drinking water seems to mask considerable disparities between regions, countries and even at the country level, where rural and urban, poor and rich populations do not enjoy the same access to safe drinking water and sanitation facilities. More specifically, Sub-Saharan Africa, where the drinking water coverage is estimated at 65 %, is still lagging far behind, with respect to the MDG drinking water target.

In Burundi, according to the second generation of the Strategic Framework for Economical Growth and Poverty Alleviation (CSLP II), the drinking water coverage was estimated at 55 % and 83 % in 2009, respectively in rural and urban areas (République du Burundi, 2011). To address this vital issue of drinking water in water-scarce areas, efforts have been engaged, since several decades, to tap groundwater resources through deep wells and hand-dug wells, but so far, the problem is still unsolved, mainly due to the poor knowledge on the potential, quality and spatial distribution of groundwater resources in Burundi, but also due to limited financial investments. Indeed, to date and for the whole country, only 73 water boreholes and 250 hand-dug wells are reported, mainly in Bugesera region, the central province of Gitega, Bujumbura, Rumonge (southwestern Burundi) and Moso (Barrat *et al.*, 2011). However, as other Sub-Saharan countries, Burundi still has a long walk to go before meeting the

MDG objective related to access to drinking water, especially in rural areas where safe drinking water coverage is still very low. Moreover, even in urban areas, the rural-urban migration, which is a typical facet of developing countries, increases the urban population to the level that the gravity-driven water supply systems can no longer cope with the increasing water demand, especially with the whimsical variation of spring discharge resulting from climate change. In some urban agglomerations like in Gitega, Rumonge and Kirundo, the water supply company Regideso, private companies and organisations are timidly starting to resort to groundwater resources.

The above facts show that there is an important need in Burundi to undertake countrywide hydrogeological investigations aimed at evaluating groundwater potentialities and quality, their spatial distribution, circumscribing potential sources of pollution and proposing adequate measures for protecting groundwater resources, which constitute a precious alternative to the currently and widely used spring water. This study, "**Hydrogeological and hydrogeochemical investigation of a Precambrian Basement aquifer in Bugesera region (Burundi)**", is therefore a comprehensive contribution to the scientific understanding of the hydrogeological framework and the hydrochemical environment of water resources in Bugesera region, one of the most drinking water-deprived regions in Burundi, in order to help decision-makers and actors in water resources domain to take well-informed decisions while addressing the critical issue of drinking water resource in this area. This study is based on field data, meteorological data and laboratory analyses which have been synthesised and presented in easily interpretable sketches, maps, graphs and tables.

I.2. Statement of the problem

Besides the disparities of access to safe drinking water, mainly based on economical conditions, the availability of this commodity is also a function of natural conditions (climate, geomorphology and geology), such that uneven spatial distribution of water resources still poses real challenges, even in small countries like Burundi. Indeed, while overall Burundi enjoys abundant rainfall, a dense network of rivers and streams, abundant natural springs from which approximately 90 % of domestic water demand is covered, the low-lying regions of Bugesera in NE, Imbo in W, Moso in SE Burundi are the most underprivileged and local populations are still facing a severe scarcity of safe drinking water and its consequent water-related diseases. Hydrogeological information is still lacking in Burundi and only a few detailed hydrogeological studies have been, so-far conducted, even in regions where access to potable water is still a real challenge. As a matter of fact, the present PhD thesis is the second comprehensive and recent research work conducted on groundwater in Burundi after the one performed by Hakiza

(2002) on the groundwater potential of the Rusizi Plain, to the North of the Lake Tanganyika.

Bugesera region is one of the most potable water-scarce areas in Burundi. Several attempts have been made since the colonial period to address the issue of potable water but the problem remains unsolved as, to date, an important part of the depression of Bugesera still does not have access to sufficient and safe drinking water. Indeed, except the complex of swamps where stagnate polluted waters, the depression of Bugesera impressively lacks natural springs. Hence, for domestic needs, local population heavily relies on hand-dug wells. Where these wells are not operating, local villagers resort to surface water from lakes and swamps, whose chemical and bacteriological quality is not guaranteed. In such conditions, evaluation of the potentialities, the quality and the spatial distribution of groundwater in a drinking water-deprived area, appears to be of prime importance with a view to solving the problem of current water demand and to draw up plans for the future, taking into account the rapid population growth, economical growth and unpredictable challenges like climate change.

I.3. Significance of the study

In the past, Burundians were not measuring enough the importance of water. Burundi was said to be a country where flow milk and honey. This assertion is more related to peace, which was fully prevailing at that time, but seems to show also that there was no worry about water, which could be found every where, at reasonable distances, owing to the abundance of spring waters across the country. Water was not the main concern of Burundians for whom a rich family was considered as the one whose members would rarely need water for quenching their thirst. However, as time goes on and with the ever increasing population, with cyclic civil wars which compel populations to leave their homesteads and live in refugee camps where access to water may not be guaranteed, the recurring drought which causes many springs to dry, the increasing need for irrigation due to erratic rainfall, the still high death toll from water-related diseases, the importance of water is progressively gaining the minds of the majority of Burundians.

In the light of the preceding considerations, this study finds its place as a pioneering and comprehensive study within the efforts which are timidly starting in Burundi, with a view to achieving a comprehensive understanding of the groundwater resources potential, their quality, their spatial distribution, the mechanisms of replenishment, potential sources of pollution and the behaviour of aquifers in response to exploitation and climate change. Indeed, within the bilateral cooperation with Germany, the BGR (Bundesanstalt für Geowissenschaften und Rohstoffe) is implementing a countrywide project whose main objective is a qualitative and quantitative evaluation of groundwater

resources as well as their spatial distribution. To this effect, a preliminary study completed by a team of the French BRGM (Bureau de Recherches Géologiques et Minières) has already pointed out the lack of sufficient hydrogeological information in Burundi and the still lower level of groundwater exploitation, despite the acute scarcity of drinking water in some areas and the global increasing water demand.

I.4. Objective of the study

This study is aimed at a comprehensive understanding of the hydrogeological framework and the hydrochemical environment of groundwater resources in Bugesera, a region whose inhabitants believe that it is "a cursed area" due to the scarcity of potable water despite the existence of a complex of wide marshlands connected to more than 10 small lakes. Specifically, this study addresses the following aspects:

- Estimation of groundwater recharge using the soil moisture balance technique and meteorological data
- Understanding the hydrogeological structure based on interpretation of geophysical soundings and lithological descriptions of shallow wells, auger soundings and field observations
- Characterisation of groundwater hydrodynamics for Bugesera region based on hydraulic parameters determined from the analysis of pumping tests
- Mapping the groundwater flow system using piezometric measurements and evaluate inter-seasonal and inter-annual groundwater level fluctuations
- Hydrochemical characterisation of groundwater, surface water and spring water and determination of the main hydrochemical processes controlling groundwater evolution.
- Conceptualisation and simulation of a groundwater flow model under steady state conditions.

I.5. Scope and outline of thesis

This study is built on a substantial set of detailed information including 41 pumping tests conducted across the study area, meteorological data covering 36 calendar years (1974 to 2009), available soil data, landuse map, two available sets of vertical electrical soundings (VES) executed by AIDR (1984) and GEOSCI (2001), lithological descriptions done by AIDR (1984), GEOSCI (2001), Tandamba (2008, personal communication), field observations during 3 field campaigns, piezometric measurements performed in 1991 (SHER, 1991), 2006 to 2008 within the framework of this research and chemical analyses of 143 water samples. It proposes a comprehensive hydrogeological and hydrochemical evaluation of the basement aquifer in Bugesera which allows to conclude that local populations should not worry about the availability

of potable water resources, but a well-informed approach is indispensable in siting wells. The findings of this pioneering study are presented in a way accessible to decision-makers and other water resources stakeholders, who may take advantage of it in defining water-related policies.

This study deals with a transboundary aquifer stretching over the Burundian and Rwandan portions of the Bugesera region. In the beginning of the work, our ambition was to collect data both in Burundi and Rwanda. However, several attempts to obtain existing data from the Rwandan side remained unsuccessful. But on the other hand, it is important to note that both on the Rwandan and Burundian sides, this aquifer drains into the Lake Cohoha, Lake Rweru and River Kanyaru which actually form hydrologic boundaries. Recharge occurs in the highlands surrounding the depression of Bugesera on both sides, whereas discharge mainly occurs in the lakes and rivers which separate the two portions of the aquifer. Therefore, given that the two portions of the transboundary aquifer are separated by hydrologic boundaries, it is possible to study and model each portion separately.

The dissertation is structured in eight chapters:

- Chapter I gives the general framework of the study, including general introduction, statement of the problem, significance, objective and scope of the study, research methodology and presentation of the study area including a brief presentation of Burundi.
- Chapter II concerns the geological and hydrogeological context of the study area wherein the regional geology and the geological framework of Burundi are briefly presented. In a more detailed way are subsequently presented the geology of the study area and the hydrogeological structure of the aquifer system, as inferred from the interpretation of vertical electrical soundings which were constrained with lithological information from auger soundings and wells.
- Chapter III discusses the hydrology and groundwater balance where the hydrological context of Burundi and more specifically that of the study area is presented. Also, in this chapter, groundwater recharge is estimated using the soil moisture balance technique and several methods of estimating potential evapotranspiration.
- Chapter IV deals with the hydraulic parameters of the basement aquifer which are evaluated based on information from 41 pumping tests conducted in the study area between September and December 2007 and between July and October 2008.
- Chapter V builds on piezometric measurements carried out in August 1991 (SHER, 1991) and within the framework of this research in September 2006,

October 2007 and October 2008, to determine the groundwater system ands its relationships with the complex of marshlands and lakes. Also, inter-annual and inter-seasonal variations of groundwater levels are evaluated.

- Chapter VI is devoted to a comprehensive characterisation of hydrochemical quality of groundwater, surface water from lakes and spring water. This chapter analyses the main hydrochemical processes which control groundwater from the recharge area to the discharge area. Chemical and RX analyses of evaporitic salts occurring in Mago (Busoni) and Rubirizi (Bugabira) are discussed and compared to the chemistry of water samples.
- Chapter VII describes the process of conceptualisation and simulation of a groundwater flow model of the study area under steady state conditions.
- Chapter VIII presents general conclusions and recommendations of this study.

I.6. Research approach and methodology

Figure I.1 depicts the detailed methodology applied in this research. The study is the result of a coordinated approach including the following steps:

I.6.1. Desk study and literature review

This step was important as it allows to gather and treat all information available on the subject including previous works and methods applied in the study area or elsewhere. More specifically, this step consisted of analysing and compiling reports of non governmental organisations working in water resources, consulting firms, government institutions and a few BSc theses. Moreover, available literature on groundwater investigations and particularly pumping tests, water sampling and storage, and piezometric measurements were analysed so as to have a wide and substantial background with respect to the subject.

I.6.2. Field work

Field work research was oriented towards gathering as much as possible data. Three field campaigns were organised from July to October 2006, September to December 2007 and July to October 2008. The first campaign was devoted to a reconnaissance survey wherein all wells were mapped using a GPS, alongside groundwater level measurements. During the following campaigns, more detailed work including pumping tests, piezometric measurements and water sampling was conducted. Besides, these field campaigns also offered an opportunity to interview, on each site, local villagers about the characteristics of the wells and the quality of water pumped from the well. These three stays in Burundi were also an occasion of going to the IGEBU (Institut Geographique du Burundi) to collect monthly and daily data of weather parameters.

I.6.3. Analysis of data

Field data such as location of wells, sampling sites and pumping test sites were compiled using ArcView 3.2. The same software was used to process and produce maps of all parameters (hydraulic, hydrochemical, geophysical parameters,…) discussed in this work. Other softwares such as Surfer 8 Golden software and Phreeqc version 2.17.01 (Parkhurst & Appelo, 1999) were respectively used for drawing and for calculation of saturation indices. Pumping and recovery test data were analysed using Aquifer Test Professional 4.2, a software developed by Schlumberger Water Services. The two batches of vertical electrical soundings conducted by AIDR (Association Internationale de Développement Rural) (1984) and a consulting firm, GEOSCI (2001) were all re-interpreted using RES1D version 1.0, an inversion software. Chemical analyses of water samples were done at the Laboratory for Applied Geology and Hydrogeology of Ghent University.

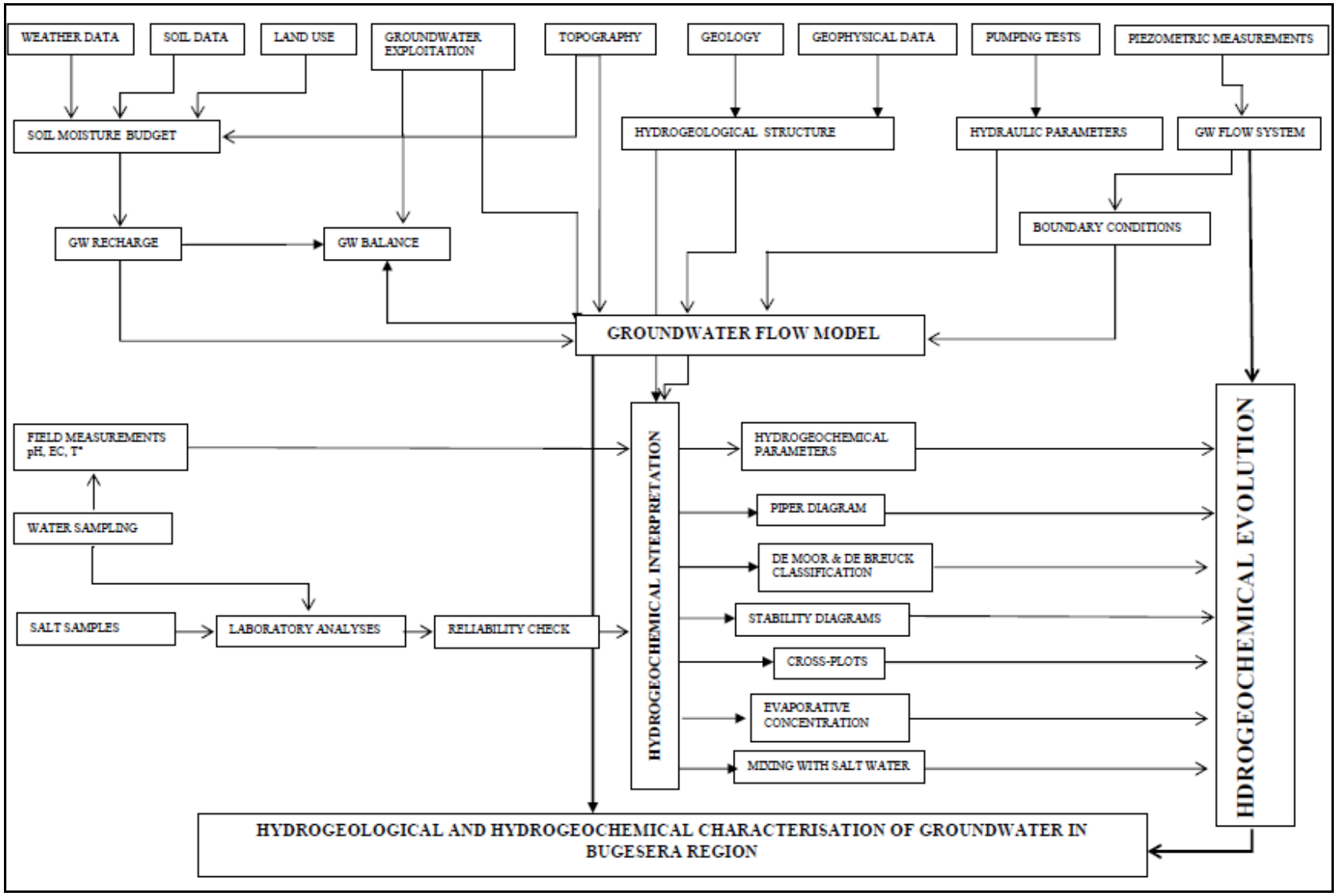

Figure I.1. Methodology flow chart

I.7. Description of the study area

I.7.1. Presentation of Burundi

I.7.1.1. Location

Often called "the heart of Africa", Burundi forms a sort of hinge between East and Central Africa. With an area of 27 834 km^2, Burundi stretches between 2°45' and 4°28' of latitude South and between 28°50' and 30°50' of longitude East. It shares its borders with Rwanda to the North, Democratic Republic of Congo (DRC) to the West, and Tanzania to the East and South (Ministère de l'Aménagement du Territoire et de l'Environnement, 2001). Burundi is a landlocked country. The nearest maritime port, Dar-es-Salaam, is situated at 1200 km, on the Indian Ocean (Figure I.2). Burundi is part of the Great Lakes Region of Eastern Africa. What is called Great Lakes of Africa is actually a chain of small and large lakes located with or in between the two branches of the East African rift system. Lake Tanganyika which occupies an important part of Burundi's western border (177 km) is located within the western branch of the East African Rift Valley system in the same alignment with lakes Albert, Edward and Kivu.

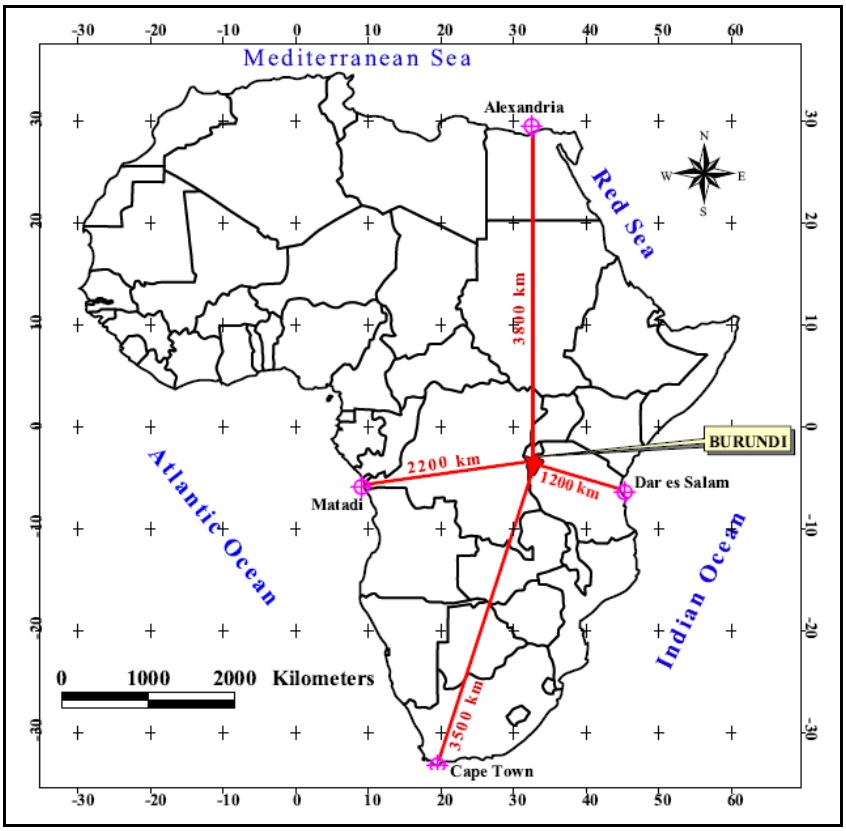

Figure I.2. Geographical position of Burundi in Africa

I.7.1.2. Climate

Overall, Burundi enjoys a tropical highland climate with a considerable daily temperature range in many areas. Temperature varies considerably from one region to another, chiefly as a result of differences in altitude. The average annual temperature varies with altitude from 23 to 17°C. The Imbo plain which is located around Lake Tanganyika and along the Rusizi river is the hottest area with an annual average temperature around 25°C. The rest of the country is rather mild. The country has two important seasons: the long dry season from June to September and the long rainy season from February to May. The remaining time encompasses a short rainy season between September and November and a short dry season between December and January. The average annual rainfall is about 1274 mm (Bidou *et al.*, 1991; Ministère de l'Aménagement du Territoire et de l'Environnement, 2001; Aquastat FAO Info, 2005).

I.7.1.3. Main morpho-climatic units

Burundi is characterized by hilly and mountainous landscapes dissected by numerous valleys and is often described as "the country of thousand hills". Five morpho-climatic zones can be distinguished (Bidou *et al.*, 1991; http://www.fao.org) (Figure I.3):

- **The Imbo or Rusizi plain** in which lies Lake Tanganyika in western Burundi and where flows one of the important rivers in Burundi, namely Rusizi river. This plain has an altitude varying between 774 and 1000 m. It is characterized by a hot tropical climate (25°C), relatively low rainfall (800-1000 mm/ year) and a 5 to 6-month dry season. This zone occupies 7 % of the Burundian territory.
- **The western escarpments** also known as **the Mirwa escarpments** correspond to the western slopes of the Congo-Nile crest and form the eastern flank of the western portion of the East African Rift System. Their elevation varies from 1000 to 2000 m. Annual precipitations oscillate between 1100 and 1800 mm while temperatures are in the range 17-23°C depending on the altitude. This zone accounts for 10 % of the national territory.
- **The Congo–Nile ridge** constitutes an important water divide between Congo (Zaire) and Nile basins and has an altitude which varies between 2000 and 2 670 m. With an annual rainfall of 1500 to 2000 mm, it the most watered area in Burundi. This zone is characterized by a mountain climate with an equatorial tendency. The average annual temperature ranges between 12 and 16°C. This zone occupies 15 % of the Burundian territory.
- **The central plateaus** are characterized by rolling hills and a landscape dissected by several valleys. Its altitude varies between 1500 and 2000 m while the mean annual

rainfall fluctuates between 1 150 and 1 500 mm. The temperatures are rather fresh, the average ranging between 16 and 18°C. This zone covers 44 % of the total surface area of Burundi.

- **The northeastern and eastern depressions** form 24 % of the whole Burundian territory. These lowlands are marked by low precipitation which rarely exceeds 1100 mm per year and which can even fall below 600 mm. The dry season can last for 5 to 8 consecutive months while the mean annual temperature exceeds 20°C. Two entities can be distinguished:
  - The depression of Bugesera in northeastern Burundi, whose altitude varies between 1.200 and 1.500 m.
  - The depression of Mosso situated in southeastern Burundi with altitudes comprised between 1.200 and 1.400 m.

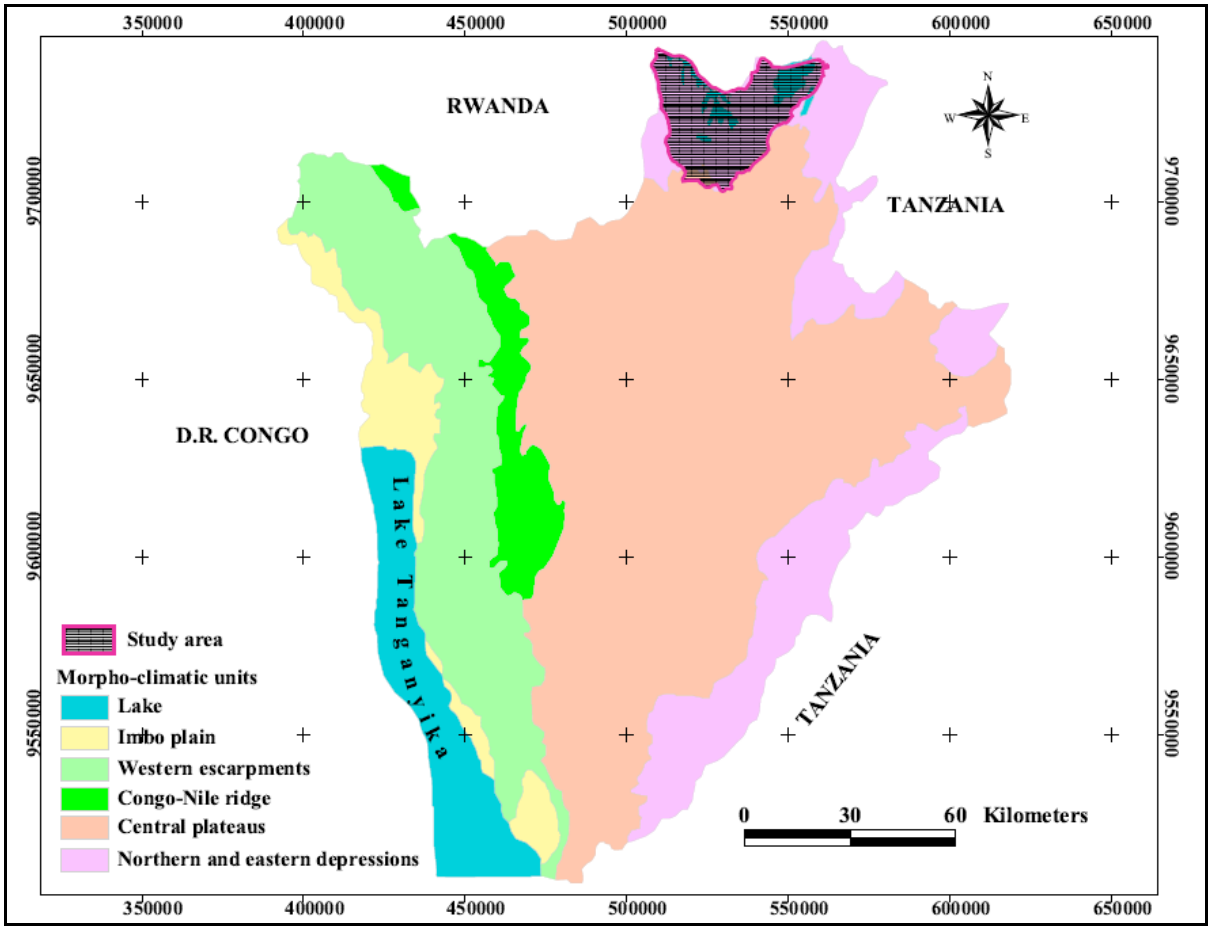

Figure I.3. Main morpho-climatic units in Burundi

I.7.2. Study area

1.7.2.1. Location

Bugesera is one of the numerous depressions known in the inter-lacustrine zone of East Africa. It covers an important part of northeastern Burundi and southeastern Rwanda. It is surrounded, to the North, East and South, by dissected plateaus whose quartzitic crests overhang the depression. To the West, the depression of Bugesera is bounded by the North-South trending valley of the Kanyaru River both in Burundi and Rwanda (Moeyersons, 1977). In Burundi, Bugesera region is one of the 11 natural regions and covers the northern extremity of the provinces of Muyinga and Kirundo (Figure I.4). According to local saying, this region is called "*mu Bugesera*" which literally means, "*a damned*", "*a cursed*" area, most probably due to the generalized scarcity of potable water in this area. Yet, one of the most striking features in this region is the presence of a complex of interconnected swamps in which lie several small shallow lakes, which form the head waters for the Kagera River. The area is impressively marked by a lack of natural water springs. Hence, for domestic needs, the population heavily relies on groundwater resources which are tapped through several large diameter hand-dug wells scattered throughout the area. Moreover, the area is also remarkably marked by dry conditions with a typical recurring drought which negatively impacts on the agricultural yield, thereby bringing about food shortage, which periodically compels the population to flee the region.

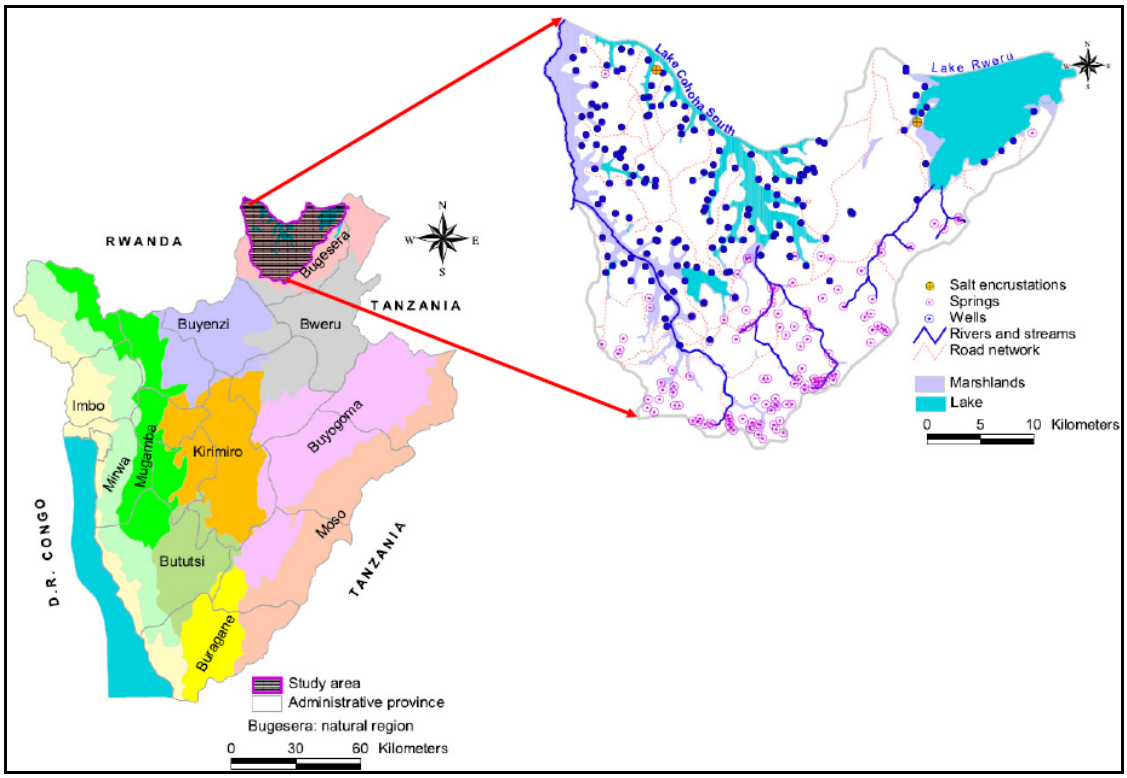

Figure I.4. Location of the study area

The study area stretches between longitudes 29° 56' 36.2''E and 30 23' 38.9"E; latitudes 2° 19'45.2" S and 2°41'37.4" S, with an area of approximately 1050.41 km^2 of which 152.80 km^2 are occupied by lakes.

I.7.2.2. Development of Bugesera depression

The present-day depression of Bugesera is thought to have been formed in the wake of the Miocene tectonic movements which led to the creation of the western branch of the African Rift Valley. Indeed, many authors agree, to date, that prior to this major tectonic disturbance, an important river system flowed from East to West into the River Congo in a peneplain covering Burundi and Rwanda, accross what is now Lake Victoria and Bugesera depression (Peeters, 1957; Moeyersons, 1977 & 1979a & b; Pouclet, 1978; Giddelo *et al.*, 2002). The main rivers comprising this network were Kagera (also known as Akagera), Katonga, Kafu and their tributaries (Figure I.5). This hydrographical pattern was broken up by faulting and central collapse of the western branch of the East African Rift Valley which was accompanied by the uplift of its shoulders, Mitumba Mountain on the Congolese side and the Congo-Nile ridge on the eastern side. The uplift of the eastern border of the rift valley, the so-called Congo-Nile water divide, entailed a tilting of the topographic surface towards the East, thereby reversing the flow direction of the rivers to the East towards the Lake Victoria basin. It is this back tilting of the river system which resulted into the drowning of the valleys of Bugesera region evolving into small lakes (Figure I.5). Further downwarping of the Bugesera area might have been favoured by a system of North-South trending faults like the one along which flows the river Kanyaru. Indeed, E-W topographic cross-sections show that, due to this fault, the Butare plateau was slightly uplifted relative to Bugesera area which went down (Figure I.6). Hence, the formation of the western branch of the Great Rift Valley, through the associated North-South faults, parcelled out a former peneplain-like surface (also known as Buganda surface, which was defined in Uganda) (Moeyersons, 1979b). The relicts of this landscape are still preserved on some prominent quartzitic crests around and inside the depression of Bugesera in the form of a lateritic carapace both in Burundi and Rwanda (Moeyersons, 1977 & 1979b). It is also established that the depression of Bugesera was impounded by rivers diverted from their westerly flow and might have formed an endoreic basin whose waters eventually overflowed to the East through the Kagera river. This is evidenced by the presence of fluvial material on interfluves in Bugesera region (Moeyersons, 1977).

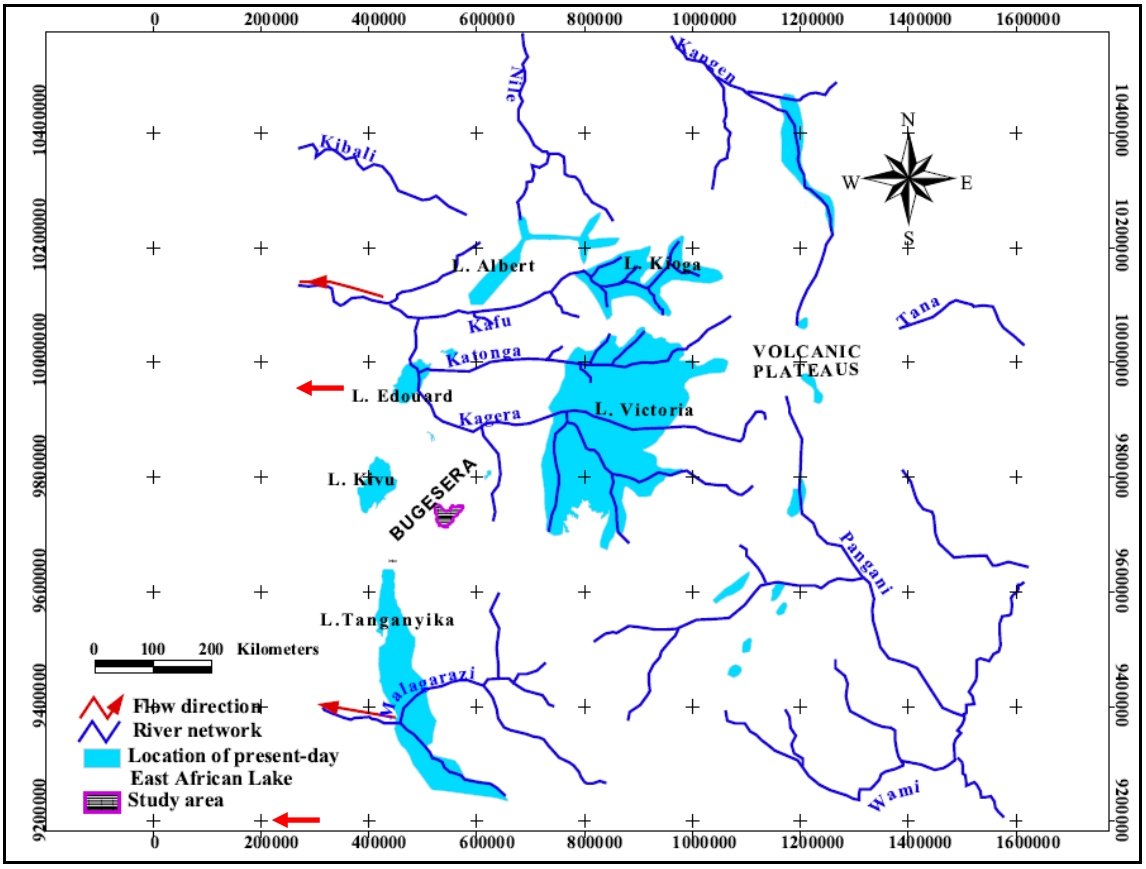

Figure I.5. Assumed drainage pattern in East Africa during the Miocene (modified after Beadle, 1974 as quoted by Ntakimazi, 1985)

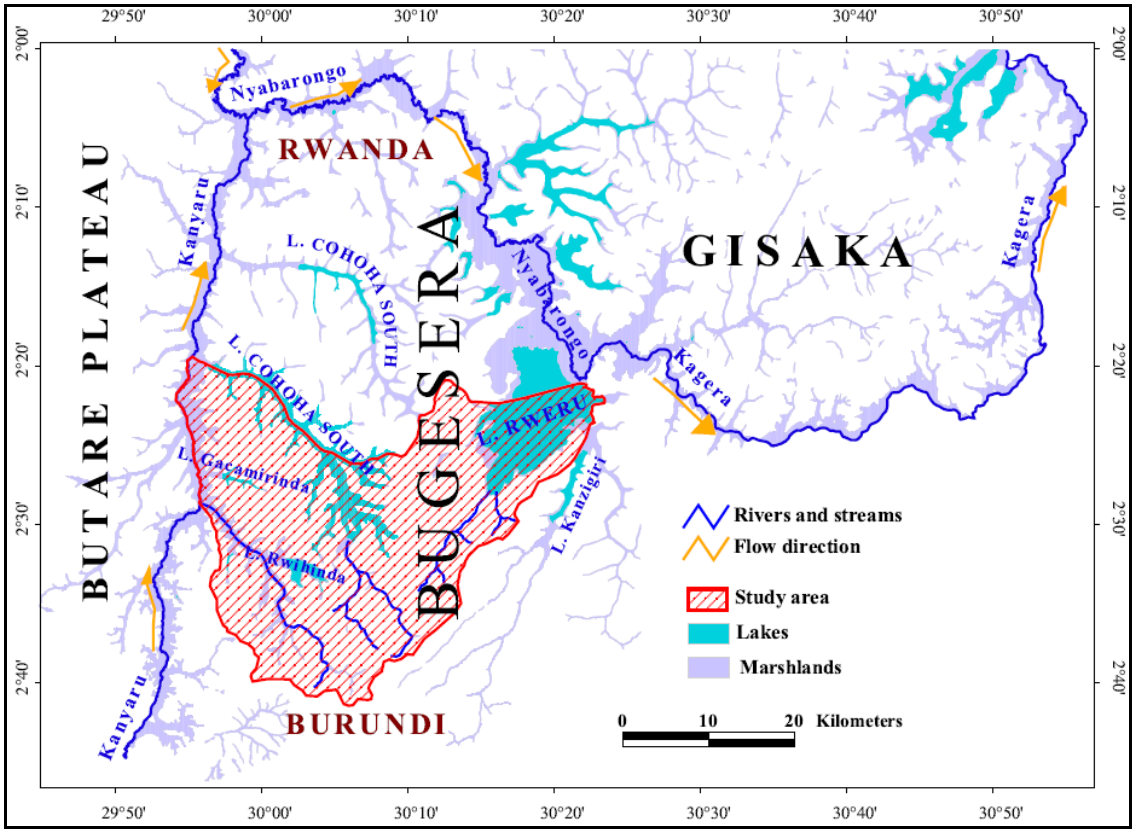

Figure I.6. Drainage pattern within and around the Bugesera depression after the formation of the western branch of the East African Rift System

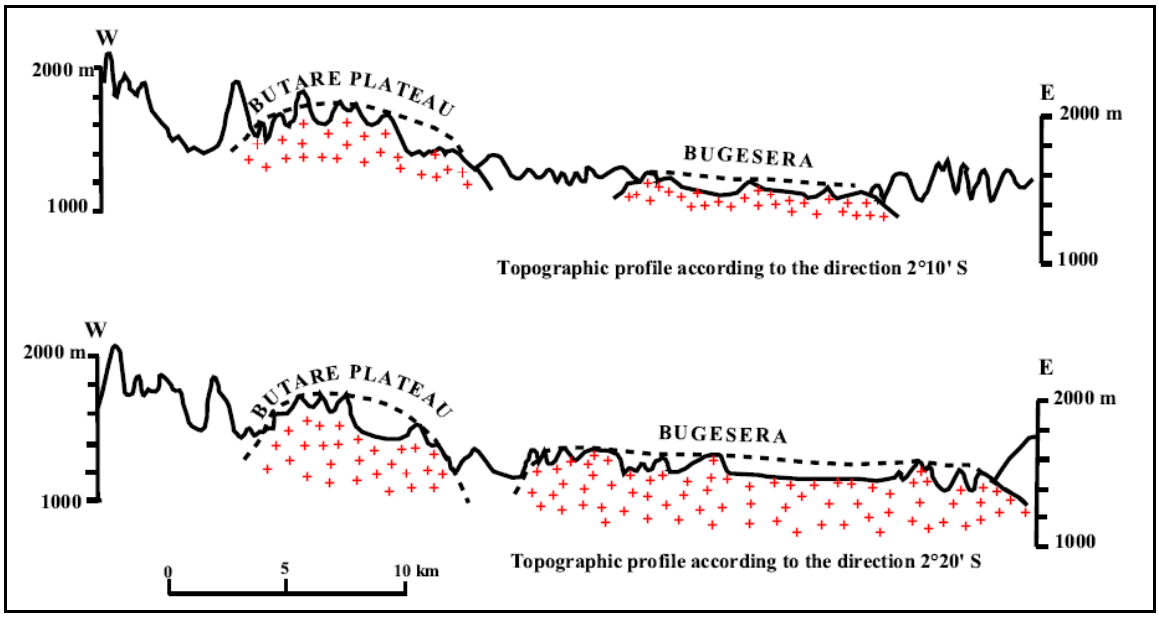

Figure I.7. E-W topographic profiles showing the dome-shaped Butare plateau and the depression of Bugesera (after Moeyersons, 1979b)

I.7.1.3. Topography and landform

Topographic information is derived from the Shuttle Radar Topography Mission (SRTM) data which provides elevation data on a near-global scale. SRTM refers to a specially modified radar system that was flown onboard the Space Shuttle Endeavour during an 11-day mission in February 2000**.** This mission was co-sponsored by the National Aeronautics and Space Administration (NASA) and US National Geospatial-Intelligence Agency (NGA)**.** Thanks to this mission, a global coverage of digital elevation models with a resolution of 90 m is freely available, which allows to generate the most complete high-resolution digital topographic database of Earth. The topographic information used in this study is extracted from the third version of SRTM data, which is a result of the processing of the original DEMs by Jarvis *et al.* (2006), in order to fill in the no-data voids in the original data.

Figures I.8, I.9 and I.10 show the main topographic features of the study area namely the elevation (m), slope (%) and the topographic contours generated at 50 m interval. Overall, the elevation ranges between 1321 m and 1873 m above the mean sea level with a mean elevation of 1427 m. The highest elevations are observed to the South and East of the study area where a more rugged topography marks the transition from the Bugesera depression towards the highlands of Bweru. The slope grid (Figure I.8-A) was generated from the digital elevation model using the surface tools of Arcview 3.2. It can be noted that, for the whole study area, the slope varies from 0 % for flats areas including swampy valleys and narrow plains surrounding the lakes, to 64.1 % mostly for the steeply sloping topography to the South and East of the study area. The mean slope for the study area is 10.8 %.

According to the Africover project (FAO, 2003), four landform classes can be distinguished within the study area (Figure I.8): depression, hills and mountain foot ridges, alluvial plain, plateau.

- The depression: located around the so-called “Lacs du Nord” (northern lakes); the centre of the depression is geologically underlain by the Undifferentiated Complex, a deeply weathered complex of granite and pegmatite with sporadic relicts of the country rocks consisting of quartzitic and pelitic metasediments. The Undifferentiated Complex is girdled by a metasedimentary belt also known as the Formation of Mugendo (or Murehe). The depression is characterized by a slightly undulating topography with elevations ranging between 1350 and 1500 m while percentage slope varies between 0 % and 58.4 %, with a mean value of 9.4 %. This landform was initially classified as a plain by the FAO Africover project (2003), but based on our knowledge of the study area, this landform class denomination is

not appropriate at all, because some isolated peaks within what is referred to as a "plain" can reach an elevation exceeding 1600 m (Moeyersons, 1979). Therefore, we have modified the landform class name as a depression. This depression is the most dominant landform. It covers 53 % of the whole study area.

- Hills and mountain foot ridges: the depression is surrounded, to the South and East, by a more rugged landscape with steep slopes made up of metasediments which comprise a wide range of lithologies: quartzites, phyllites, schists, quartzophyllades, psammites, psammoschists and conglomerates. These lithologies are grouped into four geological formations namely: Nyagisozi (or Nyabihanga), Mugendo (or Murehe), Ngozi and Ruganza. The landscape is characterized by several ridges, hills and mountains whose crests peak up to more than 1800 m, while valley bottoms lie at 1322 m. The mean elevation for this landform class is 1500.9 m. Percentage slope ranges between 0 % and 64.3 % with a mean value of 18.3 %. These mountains, hills and escarpments which are classified as hills and mountain foot ridges represent 27 % of the study area and form a transition towards the highlands of Bweru region. This landform is dissected by numerous V-shaped valleys in which flow small perennial streams. Most of the water springs are located within the hills and mountain foot ridges.
- Alluvial plains: the depression is dissected by an important network of large valleys where lie Holocene sediments, swamps and a number of shallow lakes. In some areas, this complex of swampy valleys and lakes is surrounded by alluvial plains where sediments from highlands are deposited. Indeed, alluvial plains are formed at the foot of the hills and mountain foot ridges. This landform is not so important in terms of areal extension as it represents only 3 %, while water bodies occupy 15 % of the study area. Alluvial plains are underlain by a geological substratum made up of the Undifferentiated Complex or the Mugendo (Murehe) Formation. Topographically, the alluvial plain shows an elevation which varies from 1354 m to 1651 m with a slope ranging from 0.4 % to 62.2 %.
- Plateau: developed over the quartzitic Formation of Ruganza, this landform is perched over the Mutumba mountain range in the Southwest of the study area. With an areal coverage of 1 % of the whole study area, this landform is of minor importance in terms of spatial extension. The plateau is characterized by percentage slope comprised between 1.2 % and 59 % whereas the elevation varies from 1425 m to 1803 m. This landform contains the highest elevations for the whole study area.

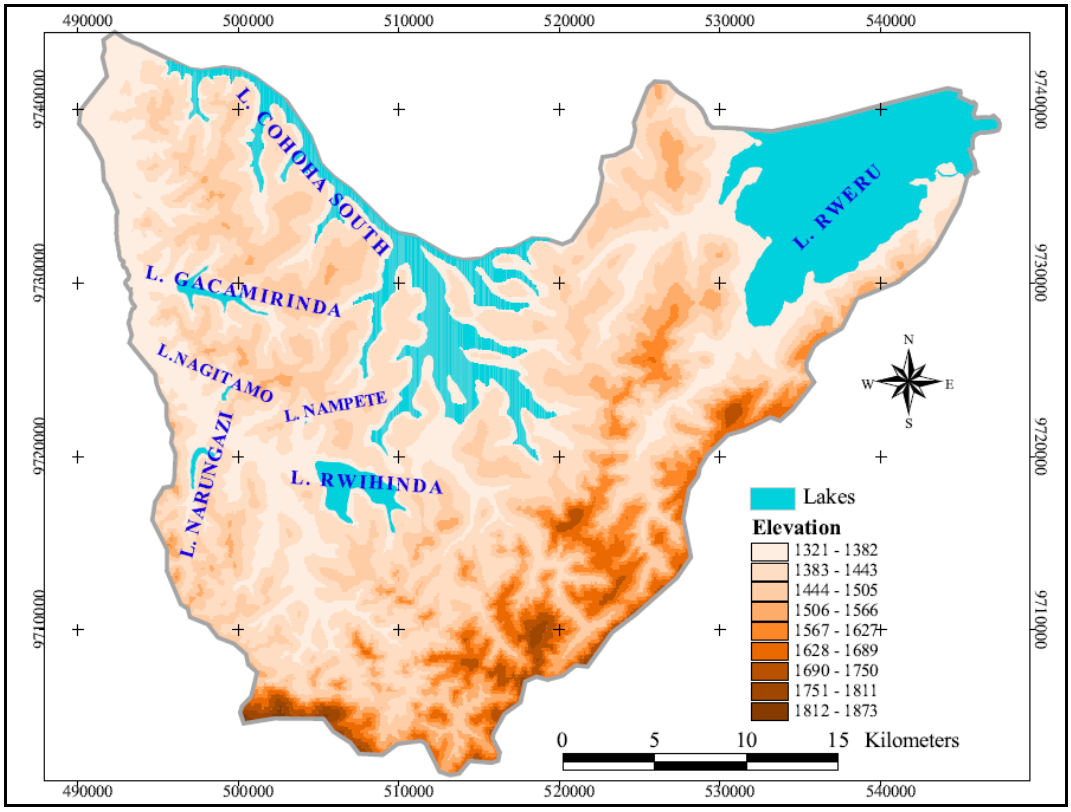

Figure I.8. Digital Elevation Model of the study area (based on Jarvis *et al.*, 2006)

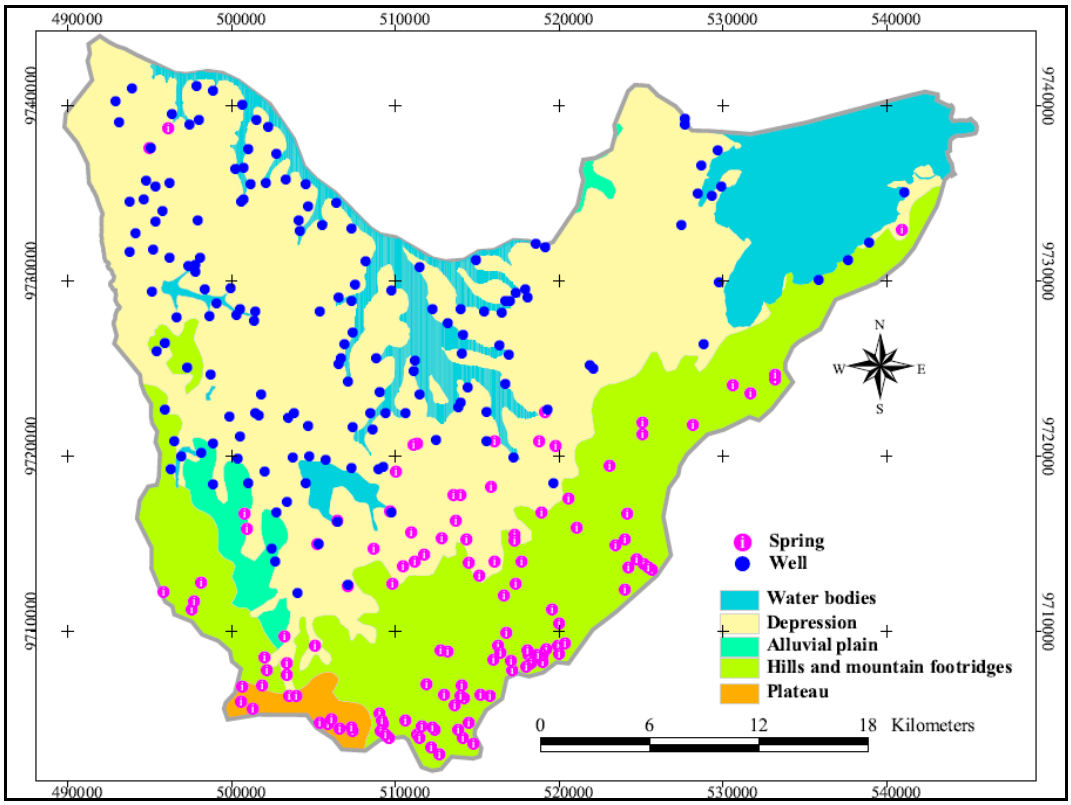

Figure I.9. Landforms in the study area (FAO, 2003, modified)

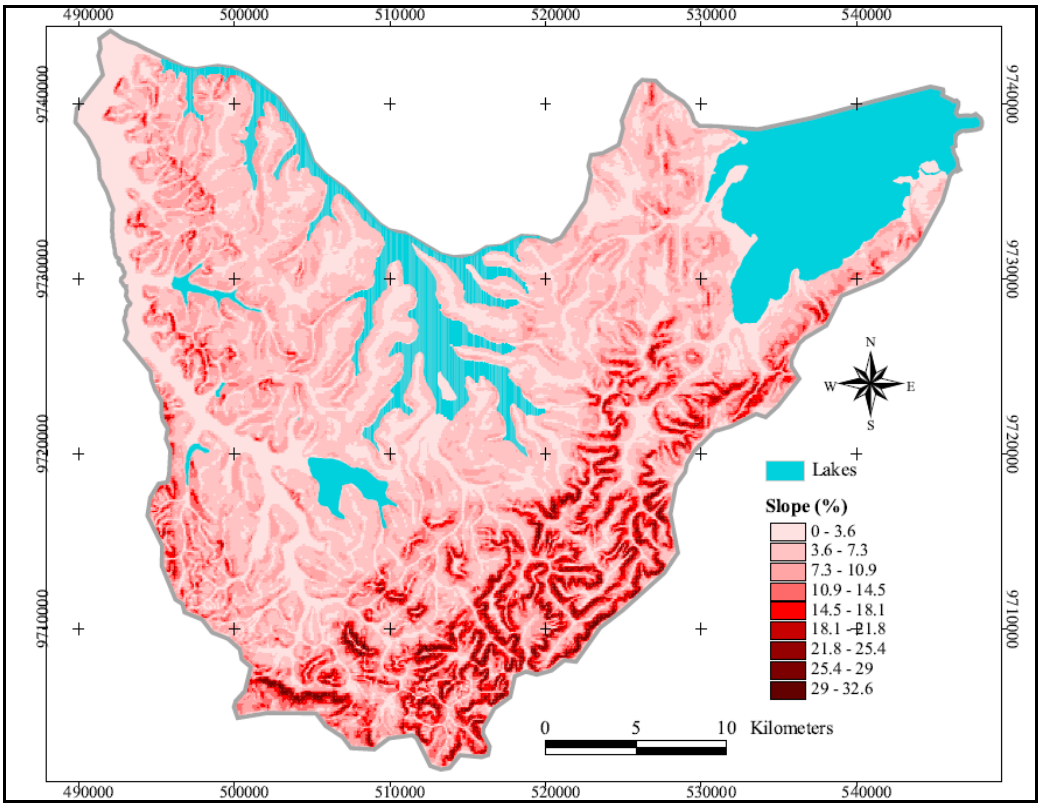

Figure I.10. Surface slope (%) derived from the digital elevation model

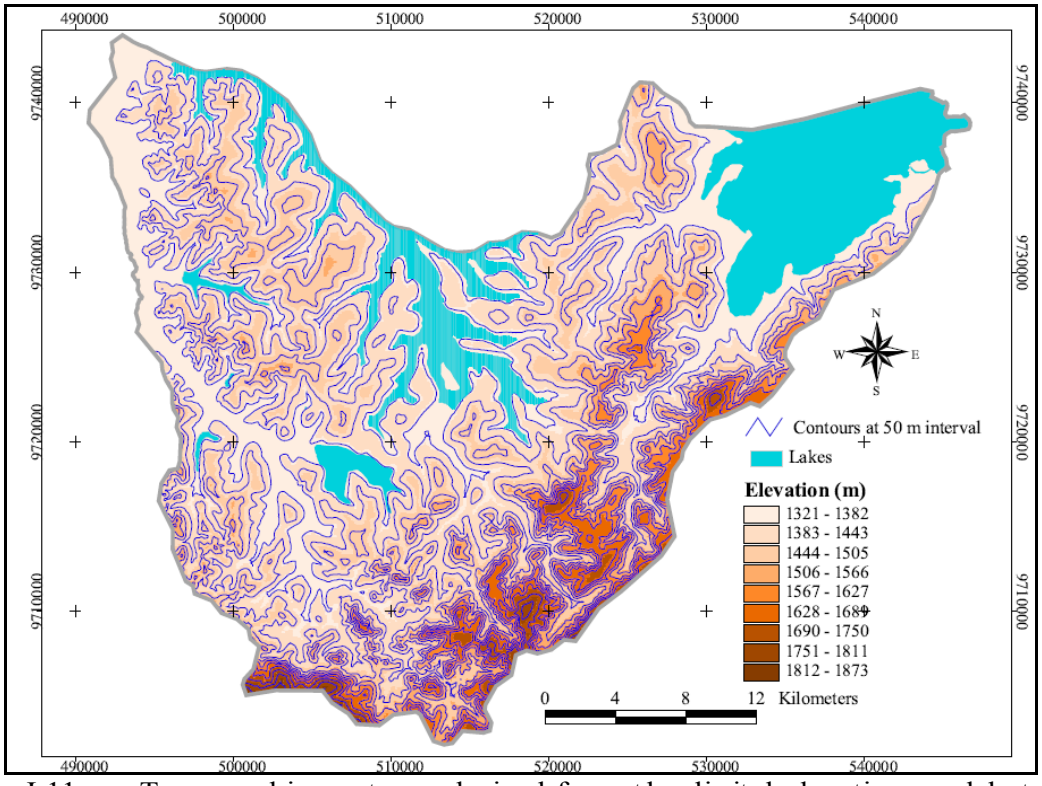

Figure I.11. Topographic contours derived from the digital elevation model at 50 m interval

I.7.1.4. Land use

Land use in Bugesera region has tremendously changed over the last decades. What used to be natural vegetation and forests, formerly populated by several species of wildlife, has been progressively transformed into croplands and settled areas (Nzigidahera *et al.*, 2005). This phenomenon has been accelerated by the arrival of populations from the densely populated provinces of Kayanza and Ngozi who, since the 1970's, came massively to seek agricultural land. Furthermore, the out break of the civil war in Burundi and Rwanda respectively in 1993 and 1994 has significantly contributed to the de forestation of the region. Indeed, large numbers of refugees and internally displaced persons fleeing war in the two countries have been compelled to settle into camps spread over the whole region and this new phenomenon has contributed to the destruction of the natural vegetation cover.

Nowadays, the land use in our study area is dominated by agricultural land with sparse forest plantations and some relicts of natural vegetation. Human settlement is characterized by a dispersed pattern which is typical of most of the developing countries. The only urban settlement is the small city of Kirundo.

Land cover classification in the study area is adopted and adapted from the recently published Kagera Monograph (BRL Ingénierie, 2008) and can be summarized as follows (Figure I.12):

- **Marshlands:** permanent or temporary flooded areas with natural vegetation typical of wetlands and marshlands (papyrus) and post flooding herbaceous crops.
- **Closed forest –** natural forest (mountain and dry forests) or forest plantation with a canopy density between 60-80 %.
- **Very high vegetation cover/ Natural** – combination of trees and shrubs, closed herbaceous vegetation, natural vegetation dominant, vegetation cover density between 40-60 %.
- **High vegetation cover / Agricultural –** combination of crops and natural vegetation (trees and shrubs), agricultural dominant, vegetation cover density between 40-60 %.
- **Medium vegetation cover / Agricultural –** combination of crops and vegetation (trees and shrubs), agricultural dominant, vegetation cover density between 20 - 40 %.
- **Low vegetation cover / Rangeland –** combination of herbaceous vegetation (savannah), open shrubs, natural vegetation density between 10-20 %.

- **Very low vegetation cover / Bare soil / Urban –** very open deciduous herbaceous natural vegetation, close to bare soil or bare soil, artificial surface and urban areas, vegetation cover less than 10 %.

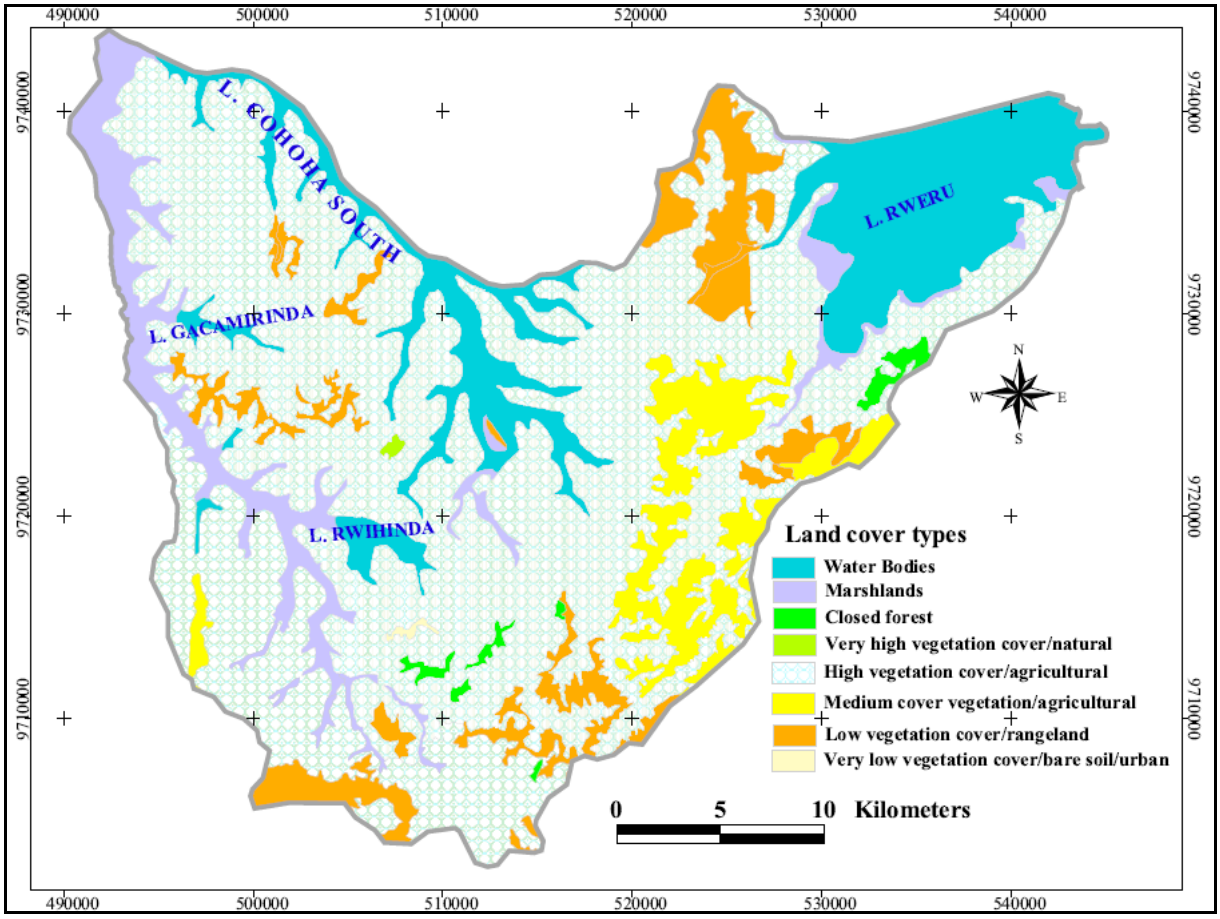

Figure I.12. Land cover classification (BLR Ingénierie, 2008)

Agricultural land (high vegetation cover and medium vegetation cover) is by far the most dominant land use type in the study area. It covers 68.6 % of the study area, thereby confirming the agricultural vocation of this region which, under favourable weather conditions, becomes the agricultural granary for the country. There are three growing seasons in Burundi. The first one also known as agricultural season A coincides with the short rainy season. Crops are planted in September and are harvested in January. The second also called season B corresponds to the long rainy season and covers the period February to May. The last growing season is termed C or "dead season", and corresponds to the long dry season. During this season, crops are planted in June/July in marshlands and are harvested in September/October.

Of second importance in terms of spatial extension are water bodies which cover 15.3 % of the study area, thereby highlighting the importance of this complex of interconnected lakes and marshlands. The latter form 6.7 % of the study area. Low vegetation cover, which includes shrubs and savannah, represents 8.2 % of the study area. Closed forest and natural dense vegetation represent respectively 0.8 and 0.1 %, underlying the continuing expansion of agricultural land to the detrimental of natural vegetation and forests. With only 0.1 % of the study area, urban area, along with natural dense vegetation, are the least important land use types in the study area.

I.7.1.5. Soils

Soils deriving from the weathering of Precambrian metasediments and magmatic intrusions are predominantly clayey (Figure I.13), as illustrated by the soil map of the study area extracted from the pedological map of Burundi (Carte des sols du Burundi au 1/250000) (Sottiaux *et al.*, 1988). Other soil types such as loamy sand, sandy loam and organic soils are less important in terms of spatial extension. The soil classification utilised for the original map is based on the principles of the INEAC (Institut National pour l'Etude Agronomique du Congo Belge) soil classification system as defined by Sys *et al.* (1961) and Tavernier and Sys (1965) (in Sottiaux *et al.*, 1988 ; Tessens *et al.*, 1991). In this soil classification system, the different soil units are designated using a formula consisting of a numerator and a denominator (e.g. $\frac{Yt0i}{cFb}$). The numerator includes symbols relating to the profile development (e.g. Yt), the type of unit (simple or composite) (e.g. 0) and texture (e.g. i). The denominator comprises symbols corresponding to the colour/drainage (e.g. c), the presence of a humic horizon (e.g. F) and the slope (e.g. b). The texture is represented by a symbol which relates to the parent materials and the proportion of the soil fraction smaller than 20 microns in size (Sottiaux *et al.*, 1988; Tessens *et al.*, 1991). In this study, only the information on texture was extracted. The textural classification used in the pedological map of Burundi was translated into the USDA textural classes using information on grain size analysis from soil profiles described and sampled in the study area by ISABU (Tessens *et al.*, 1991). The result is represented on the map in Figure I.13.

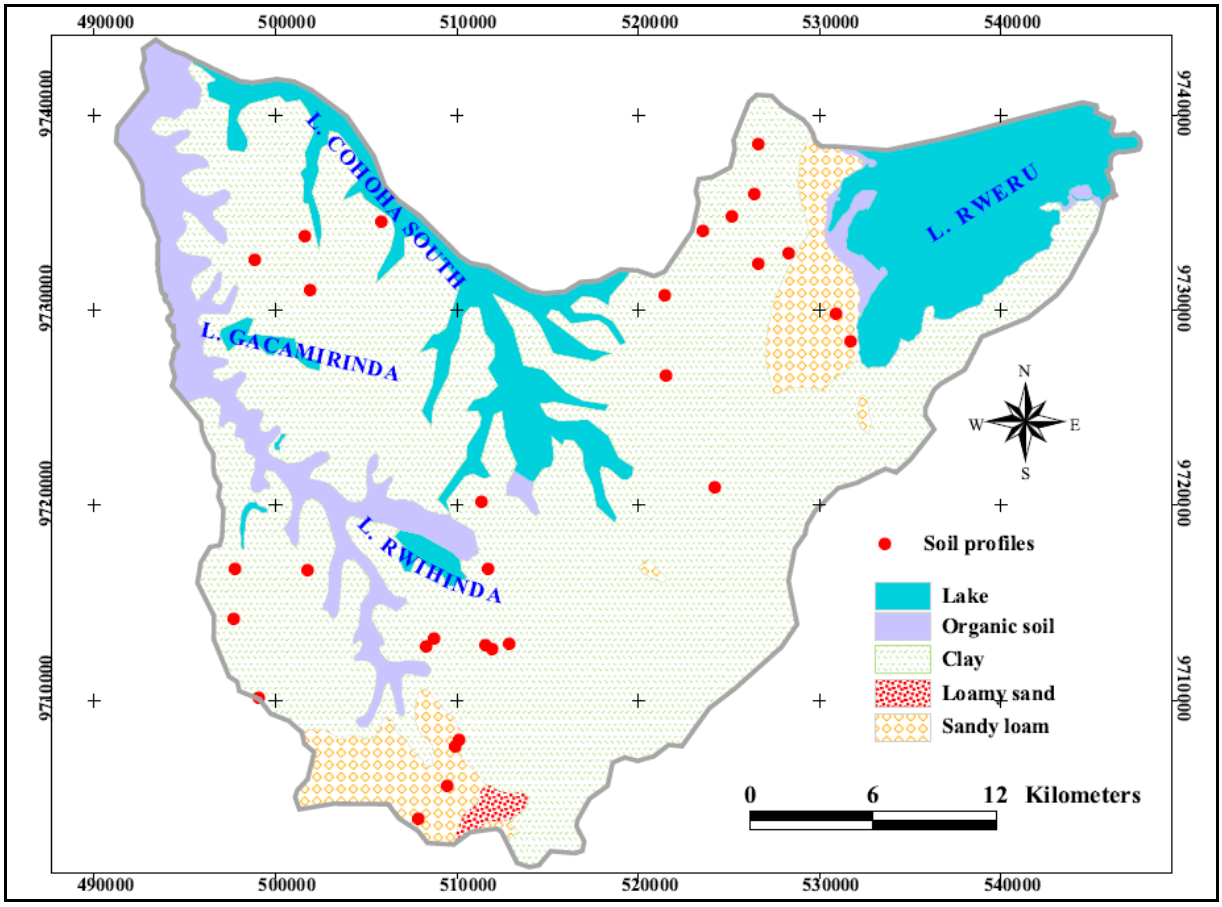

Figure I.13. Soil texture distribution in the study area

CHAPTER II. GEOLOGY AND HYDROGEOLOGICAL STRUCTURE

II.1. Geology

II.1.1. Regional geology

The most important part of Burundi is underlain by Mesoproterozoic metasediments and minor metavolcanites which are intruded by abundant s-types granitoids, tin-granites and subordinate mafic rocks (Buchwaldt *et al.*, 2007; Deblond & Tack, 1999). In previous literature, this part of Burundi was considered as belonging to the so-called Kibaran Belt, a 1300 km-long Mesoproterozoic belt stretching from the Katanga region (Kibara mountains), in Democratic Republic of Congo, to the Ankole region, in SW Uganda through Burundi, NW Tanzania and Rwanda (Buchwaldt *et al.*, 2007; Fernandez-Alonso *et al.*, 2006; Tack *et al.*, 2006).

However, recent developments in the knowledge of the "Kibaran Belt", which are supported by satellite imagery and derived products (e.g. Landsat, SRTM DEM) show that, what was hitherto considered as a continuous belt, is actually split into two structurally distinct portions by the Palaeoproterozoic Ubende Belt which extends NW across Lake Tanganyika into the Kivu-Maniema region, where it is locally mapped as the Palaeoproterozoic Rusizian basement. Hence, to avoid any further confusion of terminologies, Tack *et al.* (2010) propose to use the name Kibaran Belt (KIB) only for the portion of the belt occurring in the Katanga region, including the Kibara Mountains type area, while the northeastern part is termed Karagwe-Ankole Belt (KAB), after local terminologies used in Tanzania (Karagwe) and Uganda (Ankole) (Figure II.1).

In Burundi, the portion of Karagwe-Ankole Belt is termed Burundian (Tack *et al.*, 2010). The latter is flanked in the eastern part of the country by the Neoproterozoic deposits of the Malagarazi Supergroup, whereas Tertiary and Quaternary sediments are mainly found in the plain surrounding the Lake Tanganyika and River Rusizi, which are both located within the Albertine Rift valley (western branch of the East African Rift Valley System).

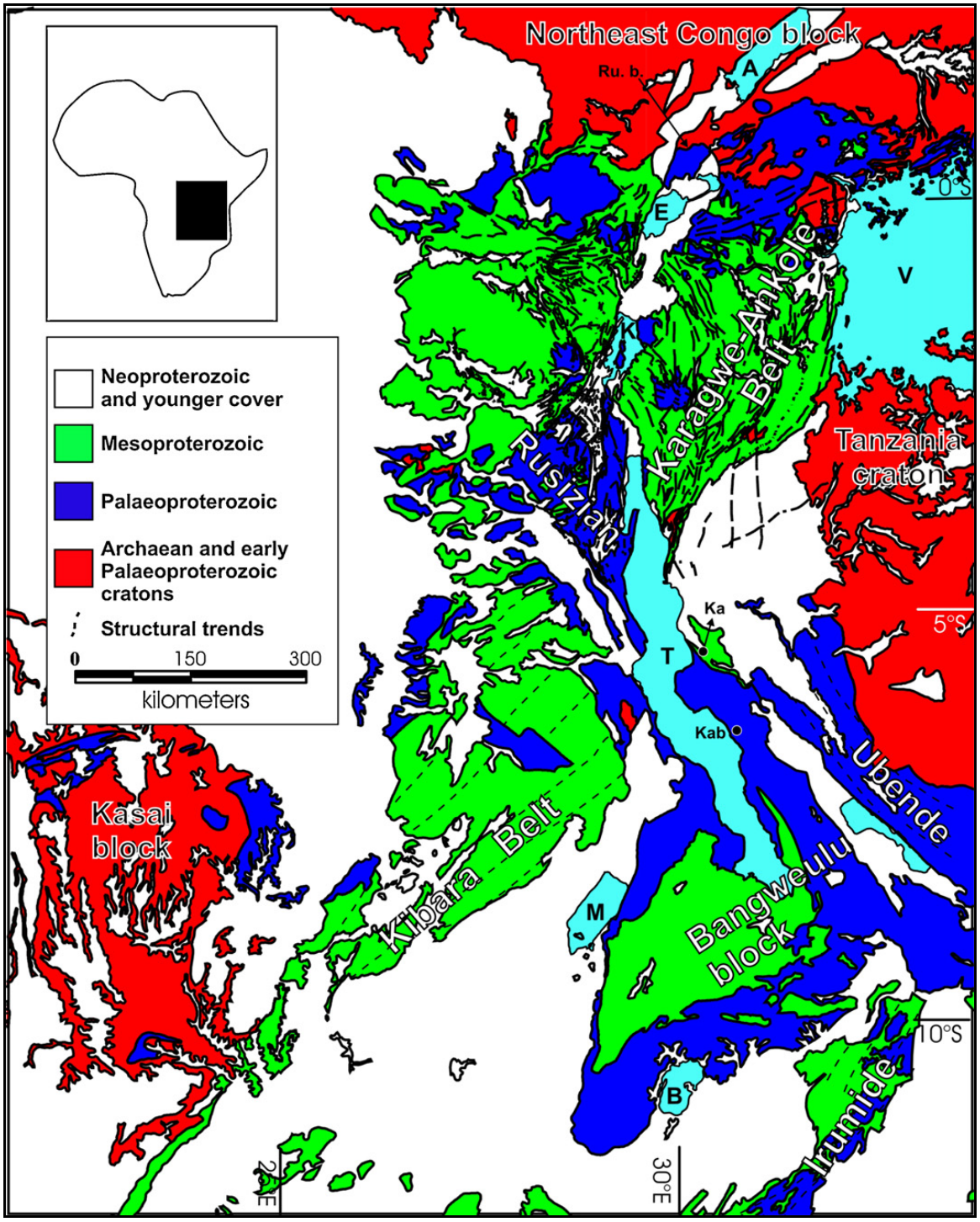

Figure II.1. Regional geological setting showing the Karagwe-Ankole and the Kibaran belts in their Proterozoic and Archaean framework (Fernandez-Alonso, 2007 in Tack *et al.*, 2010)

Tack *et al*. (1994) define, within the Karagwe-Ankole Belt, two structurally contrasting domains: a Western Domain (WD) and an Eastern Domain (ED), which are separated by a boundary zone consisting of a 350 km -long narrow alignment of mafic and ultramafic intrusions (Deblond & Tack, 1999), also termed the Kabanga-Musongati ultramafic and mafic belt, after the Kabanga intrusion, a Ni-sulphides deposit in northeastern Tanzania and the Musongati ultramafic intrusion in southeastern Burundi, which host an important Ni-V-Ti-Fe-PGE (Platinium Group Elements) mineralisation (Figure II.2). These intrusive complexes of mafic to ultramafic rocks are accompanied by small bodies A-type granitoids which are alkaline.

The WD consists of deformed metasediments and interlayered metavolcanites which are extensively intruded by peraluminous granitoids and accessorily by mafic rocks. Underlain by the Palaeoproterozoic basement, the WD is also characterised by a relatively high-grade metamorphism. The ED is dominated by relatively undisturbed to subhorizontal sedimentary or low-grade metamorphism sequences overlying the Archaean Tanzania Craton (Fernandez-Alonso *et al*., 2006 ; Tack *et al*., 2010) . This domain is also characterised by the lack of granitic intrusions.

Recently, Fernandez-Alonso *et al*. (2006) designed new uniform lithostratigraphies which take into account the existence of the two structural domains of the Karagwe-Ankole belt using up-to-date litho stratigraphical information (Figure II.3; Table II.1). For the WD (Rwanda, western Burundi, and southwestern Uganda), the detailed lithostratigraphy of the Rwanda Supergroup is used as a guideline for correlation and the Rwanda Supergroup is referred to as **"**Akanyaru Supergroup**"** (the "Akanyaru or Kanyaru" being the river which forms part of the boundary between Rwanda and Burundi). This supergroup comprises 4 groups which are, from bottom to top: Gikoro, Pindura, Cohoha and Rugezi. The lithostratigraphy of the ED (eastern Burundi, northwestern Tanzania and southwestern Uganda) is redefined using the detailed stratigraphic units of eastern Burundi, which were extended, along-strike, into NW Tanzania and SW Uganda. The new lithostratigraphy for the ED is referred to as "*Kagera Supergroup" (*Kagera being the name for a river forming part of the border between Burundi and Rwanda, and between Rwanda and Tanzania. Kagera is also the name for the administrative district in NW Tanzania*)*. The newly defined Kagera Supergroup includes, amongst others, the "Bukoba Sandstone", "Kavumwe" and "Nkoma" Groups, erstwhile considered as Neoproterozoic.

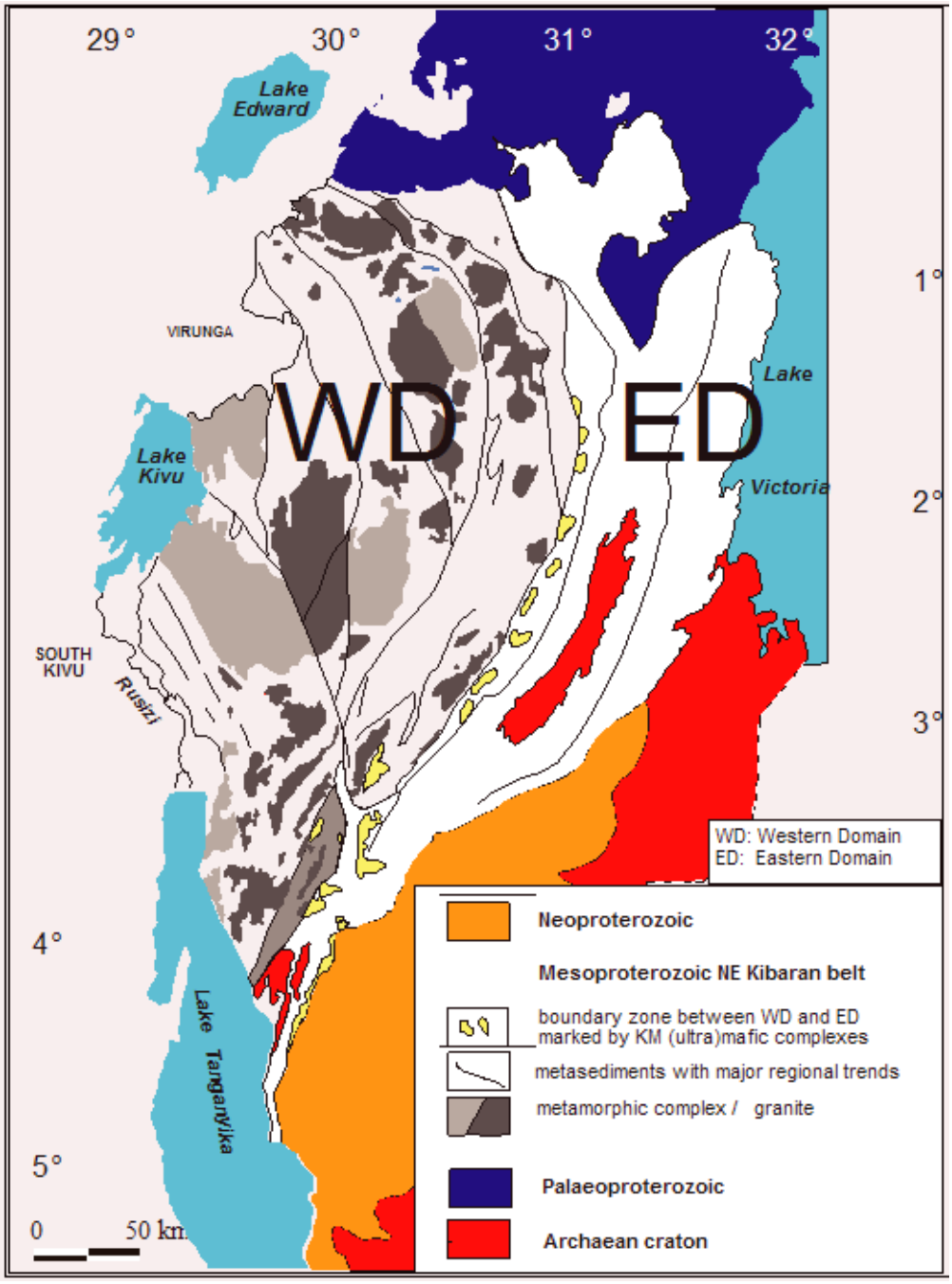

Figure II.2. Map of the Karagwe-Ankole Belt featuring the two structural domains, i.e. the Eastern Domain and the Western Domain (Fernandez-Alonso *et al.*, 2006)

The new "*Kagera Supergroup"* of the ED, comprises two distinct but adjacent (sub) basins, separated by a structural discontinuity, with two different lithostratigraphic columns: 1) to the West, the former "Lower Burundian" and Nkoma groups are redefined as the *"Muyaga Group* overlain by *Ruvubu Group"*, and 2) to the East, the "Bukoba sandstone" and "Kavumwe" groups, redefined together as the *"Bukoba Group"* **(**Figure II.3**).**

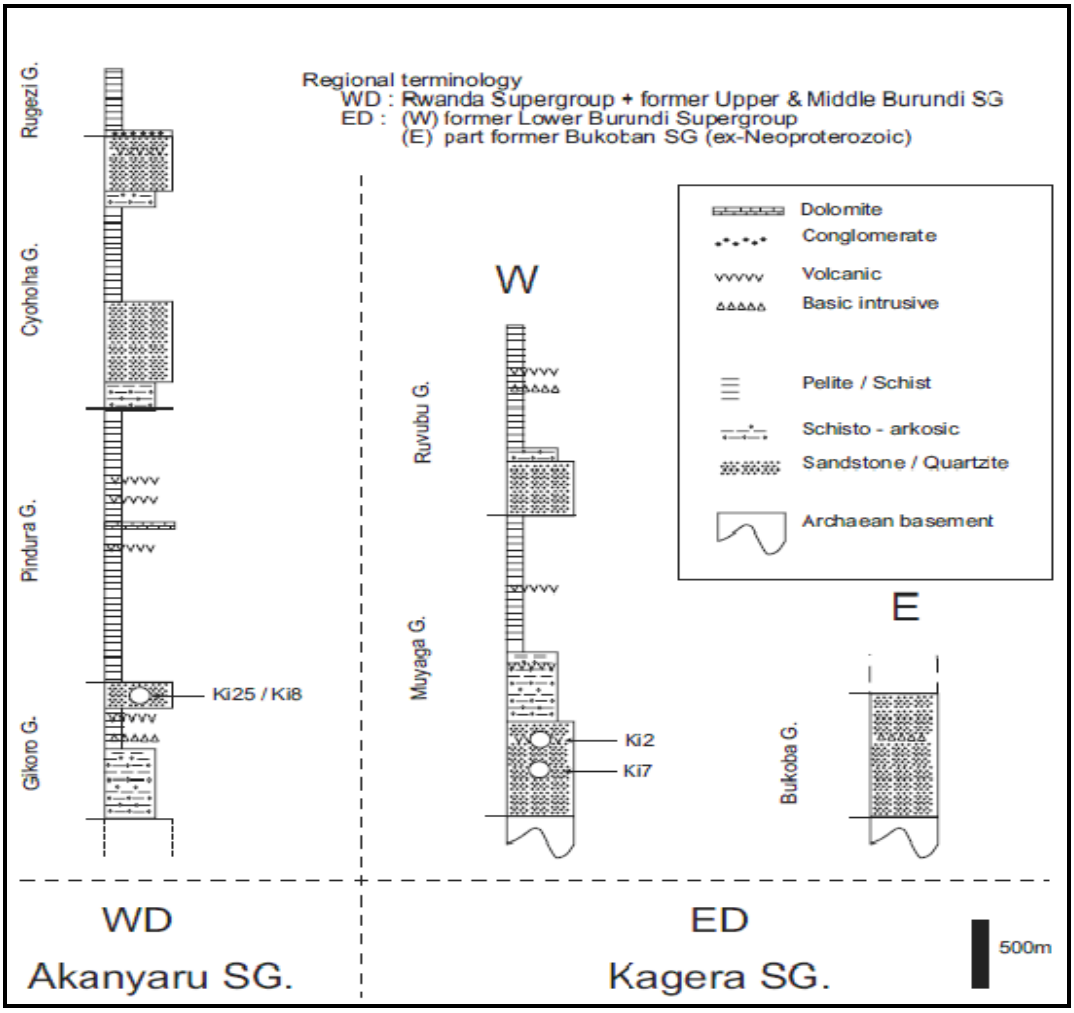

Figure II.3. Synthetic lithostratigraphy of the Karagwe-Ankole Belt (Fernandez-Alonso *et al.*, 2006)

The three newly defined lithostratigraphies, i.e. the whole WD, the western ED and the eastern ED subdomains, can not be intercorrelated because they correspond to different structural domains with different sedimentary environments, each of them being accompanied by volcanic events (Figure II. 3).

II.1.2. Geology of Burundi

II.1.2.1. General

The geological setting of Burundi comprises four geological formations, which are, from the more recent to the oldest (Figure II.4):

- **Cenozoic formations** comprise loose sediments which fill the plain of Imbo in the West of Burundi, some basaltic flows in northwestern Burundi as well as different soil types, Neogene sediments and peat bogs which lie in valley bottoms throughout the country.
- **Neoproterozoic formations** (ca. 800-1000 Ma) comprise the magmatic intrusions forming the Alcaline Complex of the Upper Ruvubu and the Malagarazi Supergroup. The latter comprises shallow water sediments associated with mafic volcanic and shallow depth intrusive rocks, which outcrops in southeastern Burundi. They were deposited in local isolated sedimentary basins, which developed during episodic reactivation of the Palaeoproterozoic Ubendian Belt (Theunissen *et al*., 1996; Klerkx *et al*., 1998). The lithostratigraphy of the Malagarazi Supergroup comprises three groups, which are from the top to the bottom: the Kibago, Mosso and Mutsindozi groups (Deblond *et al.*, 2001; Fernandez-Alonso *et al*., 2006).
- **Mesoproterozoic formations** occupy the largest part of the country. They are part of the Karagwe-Ankole Belt. These formations are bordered to the East by the Malagarazi Supergroup and to the West by Cenozoic deposits filling the Albertine Rift Valley. Mesoproterozoic formations are represented in Burundi by what was hitherto known as the Supergroup of Burundi which is nowadays split into two structural domains with two different lithostratigraphic sequences. In the light of the newly designed lithostratigraphy, which shows that the two structural domains, i.e. ED and WD, can not be intercorrelated, the former subdivision of the Burundi Supergroup referring to the Lower Burundian (or lower group of the Burundi Supergroup) in ED, and the Middle and Upper Burundian in the WD, is nowadays obsolete and should no longer be used. Indeed, the ED is formed by the former Lower Burundian and Nkoma Groups to the West, which are now replaced by the Muyaga and Ruvubu Groups, and the former Bukoba and Kavumwe groups to the East, which are now taken together in the Bukoba Group (Figure II.3) (Tack *et al.*, 1994; Fernandez-Alonso *et al.*, 2006, Fernandez-Alonso *et al*., 2009)
- **Archaean rocks** in Burundi outcrop in SW Burundi (Nyanza-Lac), in W Burundi (the region of Bujumbura) and in eastern Burundi (the region of Mugera). They consist of migmatites, granitic gneisses and gneisses with local intercalations of amphibolites and metaquartzites.

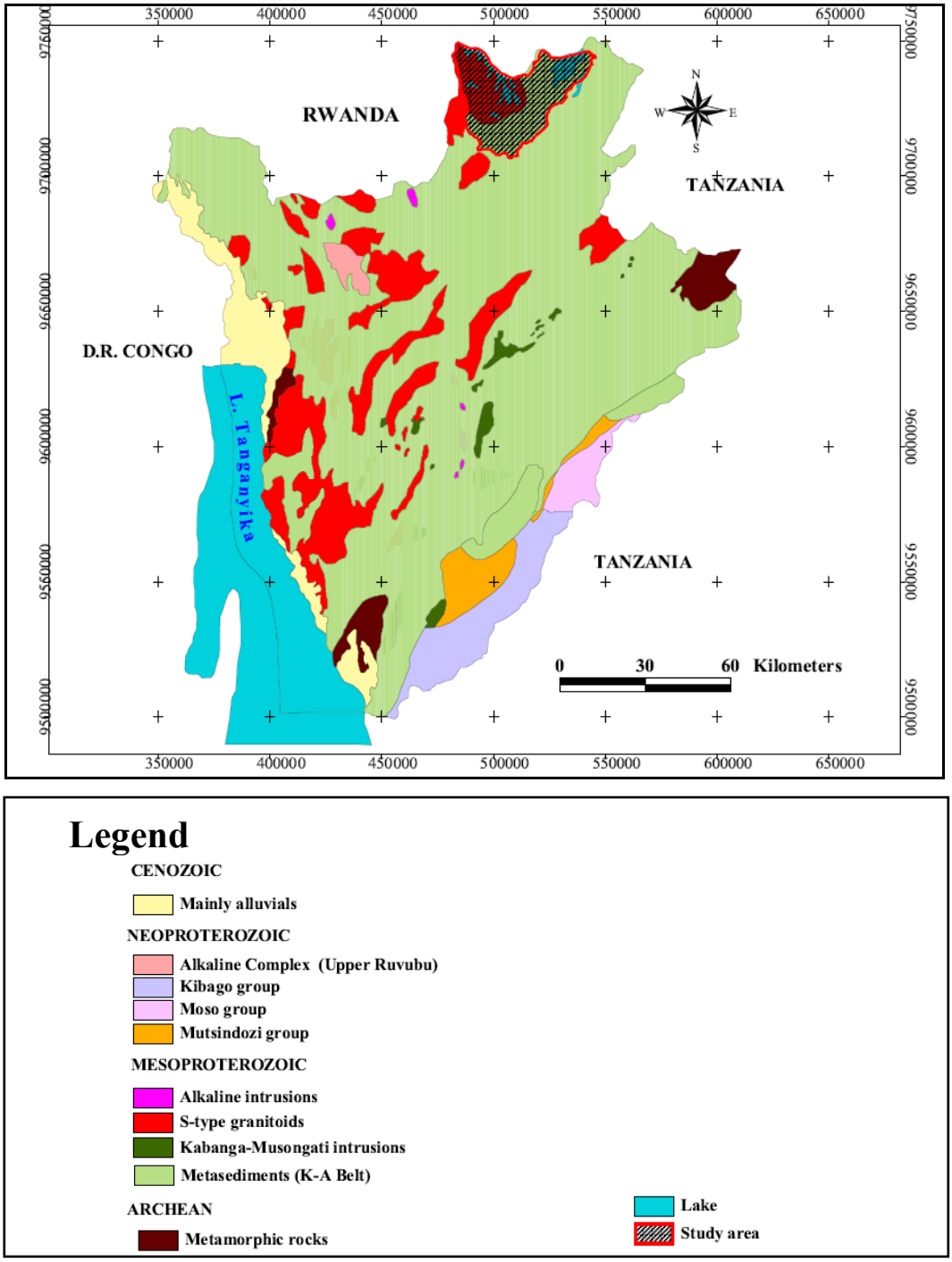

Figure II.4. Geological overview of Burundi (after Deblond, 1990, modified)

Figure II.5 shows an extended view of the geological setting of the whole Bugesera region including the Rwandan and Burundian parts. Table II.1 shows the new lithostratigraphic sequence of the Karagwe-Ankole Belt wherein the former lithostratigraphic terminologies are related to the newly defined ones.

Table II.1. The new lithostratigraphy ofthe Karagwe-Ankole Belt (Fernandez-Alonso *et al.*, 2006)

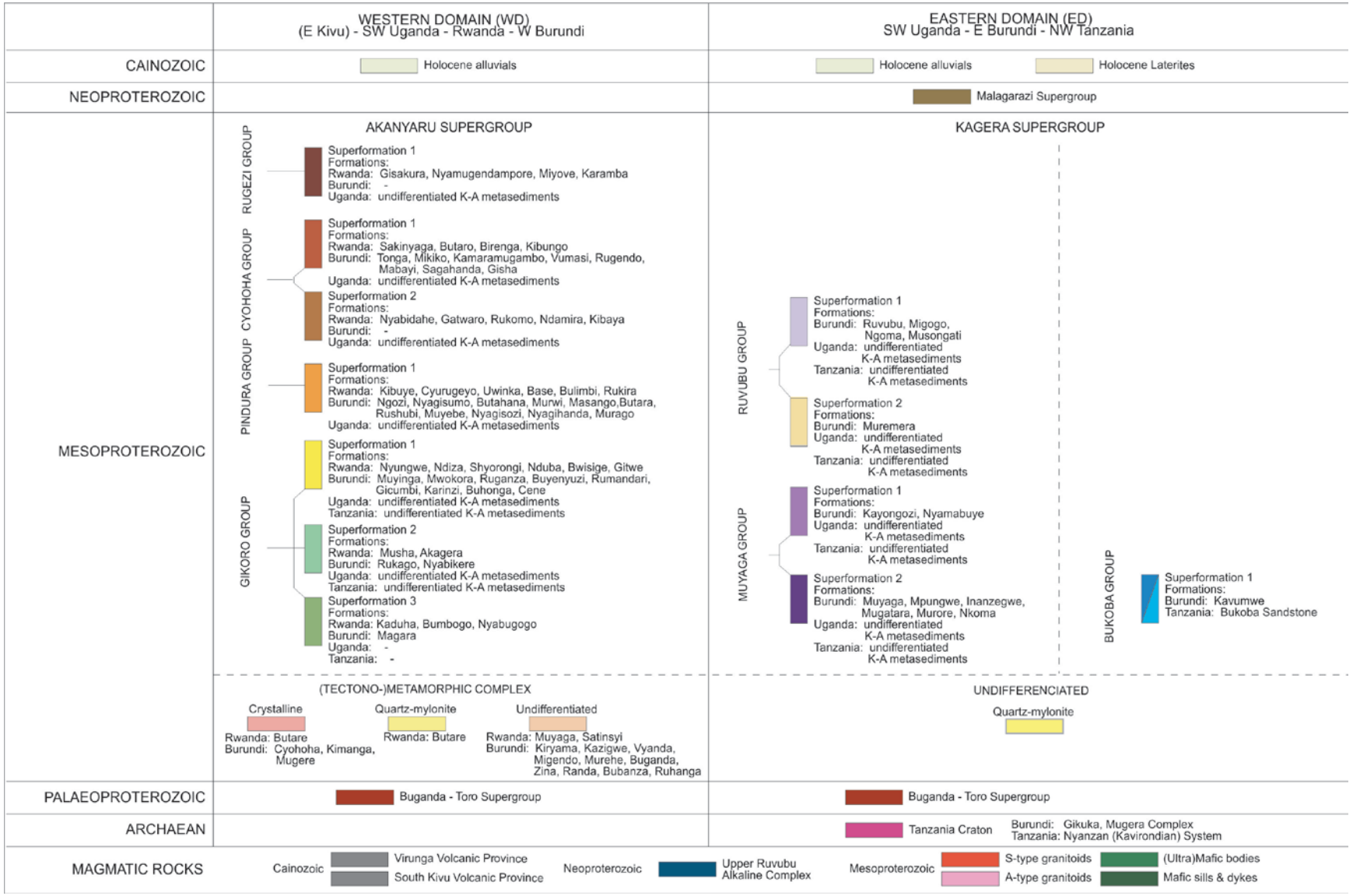

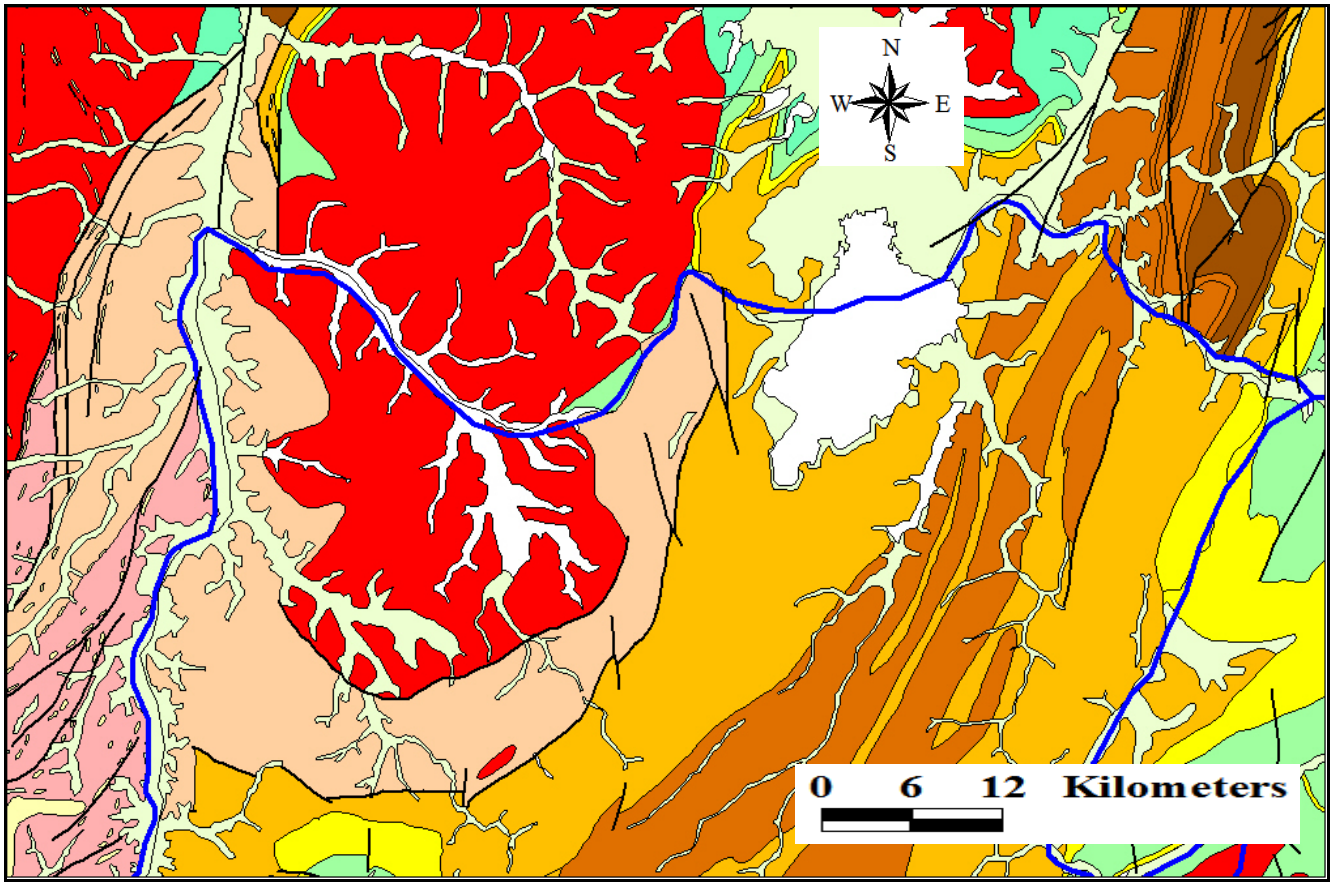

Figure II.5. Geological setting of the Bugesera region (Rwandan and Burundian parts). The legend of the map is given in Table II.1. The blue line on the map represents the country border between Rwanda and Burundi

II.1.2.2. Magmatism

One of the prominent features of the Karagwe-Ankole Belt in Burundi is the widespread occurrence of granitoids, mainly of peraluminous S-type, which are accompanied by subordinate mafic intrusions. Several studies in the recent past have classified these granitoids into 5 generations (Gr1 to Gr5) based on structural and petrographical observations along with geochronological data (mainly Rb-Sr and to a lesser extent bulk zircon U-Pb ages) (Pohl, 1987; Pohl & Günther, 1991; Kokonyangi *et al.*, 2001; Kokonyangi *et al.*, 2004; Dewaele *et al.*, 2010; Tack *et al.*, 2008; De Clercq *et al.*, 2008; Baudet *et al.*, 1989). Gr1 to Gr3 granitoids are mainly calco-alkaline, with limited modal and geochemical compositional variations (Tack *et al.*, 2010). These S-type granitoids are always associated with small bodies of mafic rocks, mainly dolerite and gabbros. Gr4 granitoids (A-type) are alkaline with a typical pinkish colour and a marked absence of muscovite. According to Dewaele *et al.*, 2010, the crystallisation of the first four generations of granitoids did not result in economically important mineralisations. Gr5

granitoids, also called "tin granites", are small bodies of granites, pegmatitic granites and pegmatites which are the source of tin and tungsten mineralisations. They are sub-alkaline, strongly peraluminous and equigranular (Pohl & Gunther, 1991).

Recently, high precision ages based on U-Pb Sensitive High Resolution Ion MicroProbe (U-Pb SHRIMP), 40Ar/39Ar and laser-ablation zircon Hf dating techniques in different parts of the Karagwe-Ankole Belt converge to the existence of an important magmatic event at around 1375 Ma, which corresponds to a prominent coeval bimodal magmatism marked by: (1) the emplacement of the Kabanga-Musongati (KM) alignment of mafic and ultramafic complexes, (2) abundant S-type granitoid magmatism and accompanying subordinate mafic intrusive bodies. This important magmatic event was followed, at 1205 Ma, by the emplacement of the A-type granites and later on, at 986 Ma, by the tin-granites and the associated Sn-metallogenic province (Tack *et al.*, 2010). The 1375 Ma coeval bimodal magmatic event took place in an intra-cratonic extensional environment.

II.1.2.3. Tectonics

Several works conducted on the Kibara and Karagwe-Ankole belts converge to the fact that the present-day morpho-structural features of the two belts have been fashioned by three major deformations referred to as D1, D2 and D3 (Klerkx *et al.*, 1984, Klerkx *et al.*, 1987; Kokonyangi *et al.*, 2006) The deformation D1 is ascribed to a regional extensional environment whereby the crustal thinning led to the emplacement of a bimodal magmatism. The tangential deformation D1 is responsible for the widespread occurrence of a schistosity S_1 parallel to the sedimentary bedding S_0, mainly in the WD (Fernandez-Alonso & Theunissen, 1998, Tack *et al.*, 2006). The absence of this prominent schistosity in the ED confirms the fact the two structural domains correspond to two different sedimentary basins. The deformation D2 is expressed by upright cylindrical folds trending NE-SW. These cylindrical folds form a prominent characteristic in the morpho-structural setting of the Karagwe-Ankole Belt, typically in the ED. This regional folding is associated with the development of a crenulation cleavage S_2 (Baudet *et al.,* 1989; Dewaele *et al.,* 2010). The deformation D3 is a conjugate shear deformation, trending N-S, which affects the cylindrical folds associated with the deformation D2 (Fernandez- Alonso & Theunissen, 1998; Tack *et al.*, 2006).

II.1.3. Geology of the study area

Considering the two structural domains as defined by Tack *et al.* (1994), the study area entirely belongs to WD. Thus, apart from various types of soil including the widespread lateritic cover and the alluvial deposits in valley bottoms and low terraces, the study area is

underlain by Precambrian formations which belong to the Upper and Middle Burundian Supergroup (now incorporated into the Akanyaru Supergroup), and thus to the Karagwe-Ankole Belt. So far, there have not yet been detailed geological investigations in this part of Burundi and many unsolved questions remain. The only available sources of geological information include the three geological maps at the scale of 1/100 000: Busoni, Muyinga and Ngozi (anonymous, 1988) which cover the study area, next to localised research studies (Kabundege, 1999), and some consultancy works (TBW Ingénieurs Conseils, 1994 & 1998; GEOSCI, 2001).

Physiographically, the study area features two distinct entities: the northern part located around the so-called "*Lacs du Nord*" (Northern Lakes) which is a depression with altitudes ranging between 1320 m and 1600 m; and the southern part which is characterised by a more rugged landscape where crests peak up to more than 1800 m. The two entities are in tectonic contact although the exact nature of the contact has not yet been clearly defined due to the lack of rock exposures in the critical zone.

Although the whole study area belongs to the WD, the geological setting shows a clear difference between the eastern part characterised by the absence of magmatic intrusions and a low-grade metamorphism, and the western part where metasediments are intruded by abundant granites and pegmatites and feature a relatively high-grade metamorphism.

This eastern part of the study area comprises one geological formation, **the Formation of Nyagisozi (Busoni geological map) or Nyabihanga (Muyinga geological map)** (Figure II.5). This formation occurs in anticlines and forms NE-SW steep crests. The base of this formation consists of bedded psammites whose layering is expressed by an alternation of light sandy beds and dark fine-grained ones. The bedding planes of the psammites are coated by flat spangles of detrital muscovite. In the middle of this formation occurs a 100 m-thick layer of quartzite with small conglomeratic lenses. The top of this formation is made up of grey to mauve bedded psammites and psammoschists (micaceous sandstones) interbedded with thin layers of greys iltstone. It contains also small lenses of intraformational conglomerates which are mainly composed of quartzite pebbles. Sedimentary structures such as cross-bedding, mudcracks and tidal channels are observed, reflecting a depositional environment of shallow water. In the new lithostratigraphy of the Akanyaru Supergroup, Fernandez-Alonso *et al.* (2007) define the Nyagisozi/Nyabihanga Formation as belonging to the Pindura Group. The layers of this formation are steeply dipping and are, from place to place, cut by important faults which can serve as conduits for groundwater (SHER, 1992). In low lying areas, psammites are covered by important

lateritic soils or crusts. An important contrasting feature with the adjacent depression of Bugesera is the occurrence of several springs which originate on the flanks or at the foot of the NE-SW elongated crests. These springs feed some perennial streams which flow NE or N.

The western part of the study area comprises four geological formations which are:

- **The Formation of Ngozi** is only found in the SW of the study area. It consists of an important and homogeneous set of grey-blackish phyllites with intercalation of metavolcanites at the base of the formation. These metavolcanites comprise grey-green metabasalts associated with chloritous phyllites. Fresh outcrops show NE-SW trending bedding planes which subvertically dip towards the NW (Kabundege, 1999). Dykes of pegmatite intruding the phyllites are observed from place to place. Several natural springs have been identified in this formation (Kabundege, 1999; TBWIngenieurs Conseil, 1994 & 1998). They are found to originate at the foot of the hills, at altitudes lower than 1450 m. According to the recently redefined lithostratigraphy of the Karagwa-Ankole Belt, the Formation of Ngozi is part of the Pindura Group (Figure II.3) and is correlated to the Formation of Nyagisozi/Nyabihanga (Fernandez-Alonso *et al.*, 2007)
- **The Formation of Ruganza** outcrops in the SW extremity of the study area and covers the mountain of Mutumba whose culminating point peaks at 1856 m above the national datum (Arc 1950 for Burundi). It consists of white and well bedded metaquartzites with local gravelly to conglomeratic levels. The quartzite often splits into decimetric to centrimetric plates but alignments of metric beds of compact quartzite are equally observed. Pegmatite veins are intruded along the stratification planes which trends NE-SW with high dip angles (40-80°) towards the NW. This formation comprises also some isolated outcrops of mafic rocks. This quartzite shows local evidence of recrystallization which may be related to the proximity of magmatic intrusions (granitic and mafic). In the newly designed lithostratigraphic sequence (Fernandez-Alonso *et al.*, 2006), the Formation of Ruganza is included into the Gikoro Group. While thick layers of compact and recrystallized quartzite may form poor aquifers, the important weathered overburden which covers the top of this unit, the presence of conglomeratic and gravelly layers and the intense fracturing that characterises the quartzite are likely to enhance the aquifer properties and may explain the numerous springs which originate from this formation (Kabundege, 1999; SHER, 1992).
- **The Formation of Murehe** (geological map of Busoni) or **Mugendo** (geological map Muyinga) forms an amphitheatre-like feature, surrounding the centre of the

depression. It is made up of micaschists which are interbedded with quartzite layers. This formation is also dotted by sporadic granitic and pegmatitic intrusions as well as quartz veins in which are emplaced cassiterite and columbo-tantalite mineralisations in Murehe (NE of the study area) and some sporadic occurrences of wolframite, which are reported mainly to the SW of Lake Rweru (Anonymous, 1988). Overall, this formation is characterised by a widespread lack of rock exposures and the presence of micas pangles within a clayey regolith which mantles the bedrock. Thus, the few sparse rock outcrops are drowned into what seems to be a granitic or pegmatitic arena, which most probably derives from the weathering of the granitic and pegmatitic intrusions. The latter consists of silty to clayey alterites with a variable proportion of sand and/or gravel. Where some rare rock exposures are observed, like at the entrance of the police station of Ntega, this formation also features a NE-SW trending with a subvertical dip towards the NW. Depending on the relative proportion of fine (clay, silt) and coarse fractions (sand and gravel) in the surficial overburden, this formation may host locally productive aquifers. Moreover, contact zones of this formation with the Undifferentiated Complex, particularly where fractured and faulted zones are filled with coarse materials, are likely to form potentially interesting aquifers (SHER, 1991). Indeed, it is well recognized that fracturing can transform an otherwise unproductive formation into a viable aquifer, or conversely enhance the transmissivity of rocks with low matrix permeability (Finn *et al.*, 2003**).** The quartzite is often recrystallized and this may limit its groundwater potential a priori; however the intercalation of micaschists with a laminated structure and the folding which affects this formation may give rise to an increased permeability (TBW Ingénieurs Conseils, 1994). According to Fernandez-Alonso *et al.* (2007), this formation forms a separate tectono-metamorphic complex.

- **The Undifferentiated Complex** occupies the centre of the Bugesera depression where it is girdled by the Formation of Murehe (or Mugendo). The morphology of this area is characterized by a slightly undulating topography dissected by large valleys where lie recent sediments, a number of small lakes and peaty papyrus marshlands. Lithologically, the Undifferentiated Complex is profoundly weathered and its granitic and pegmatitic nature is only recognisable by a widespread typical granitic arena. The original fresh rock does not outcrop in any place and the occurrence of this arena may indicate that a substratum formed by granite and pegmatite is hidden by a thick weathered overburden, whose thickness may vary between 30 m and 40 m (AIDR, 1984). This granitic intrusion is the prolongation of the granite of Kigali and is part of the numerous massifs of S-type granites

emplaced with the metasediments of the Karagwe-Ankole Belt. At certain places within this Undifferentiated Complex, quartzitic metasediments are observed and may represent the relicts of the country rocks. The new lithostratigraphy of the Karagwe-Ankole Belt considers the Undifferentiated Complex as an intrusion of S-types granitoids. This central zone is also strongly marked by a widespread occurrence of yellowish-brown to reddish laterite. At various altitudes, ferruginous cement often has agglomerated large quartz grains resulting from the disaggregation of the substratum (SHER, 19921). According to GEOSCI (2001), several phases of lateritization could have taken place and contributed to the current shape of the Bugesera depression as well as its hydrogeological properties. Low altitude laterite, generally indurated and cemented by clay, is impermeable, whereas on plateaus, where its thickness can reach 3 to 5 m (Moeyersons, 1978), the laterite is permeable owing to the leaching of clay minerals. Moeyersons (1978) demonstrated that these lateritised crests, which are flat, might be the remnants of an ancient landscape surface, reworked and dissected, originally much less incised, but however significantly undulating.

Figure II.6 shows the geological setting of the study area and the location of the 3 geological cross-sections which present a more detailed geological view. Figures II.7 to II.9 present the three cross-sections which show that the depression of Bugesera is mainly underlain by the Undifferentiated Complex which is surrounded by the metasedimentary formations of Murehe (Mugendo), Ngozi and Nyagisozi. The 3 cross-sections also show that the magmatic intrusions comprising the Undifferentiated Complex are in a faulted contact with the metasediments of the Murehe/Mugendo Formation. Moreover, physiographically, it can be observed from the 3 cross-sections that, despite its overall low-lying topography, the depression of Bugesera is actually formed by alternation of crests and swampy valleys in which lie the small lakes.

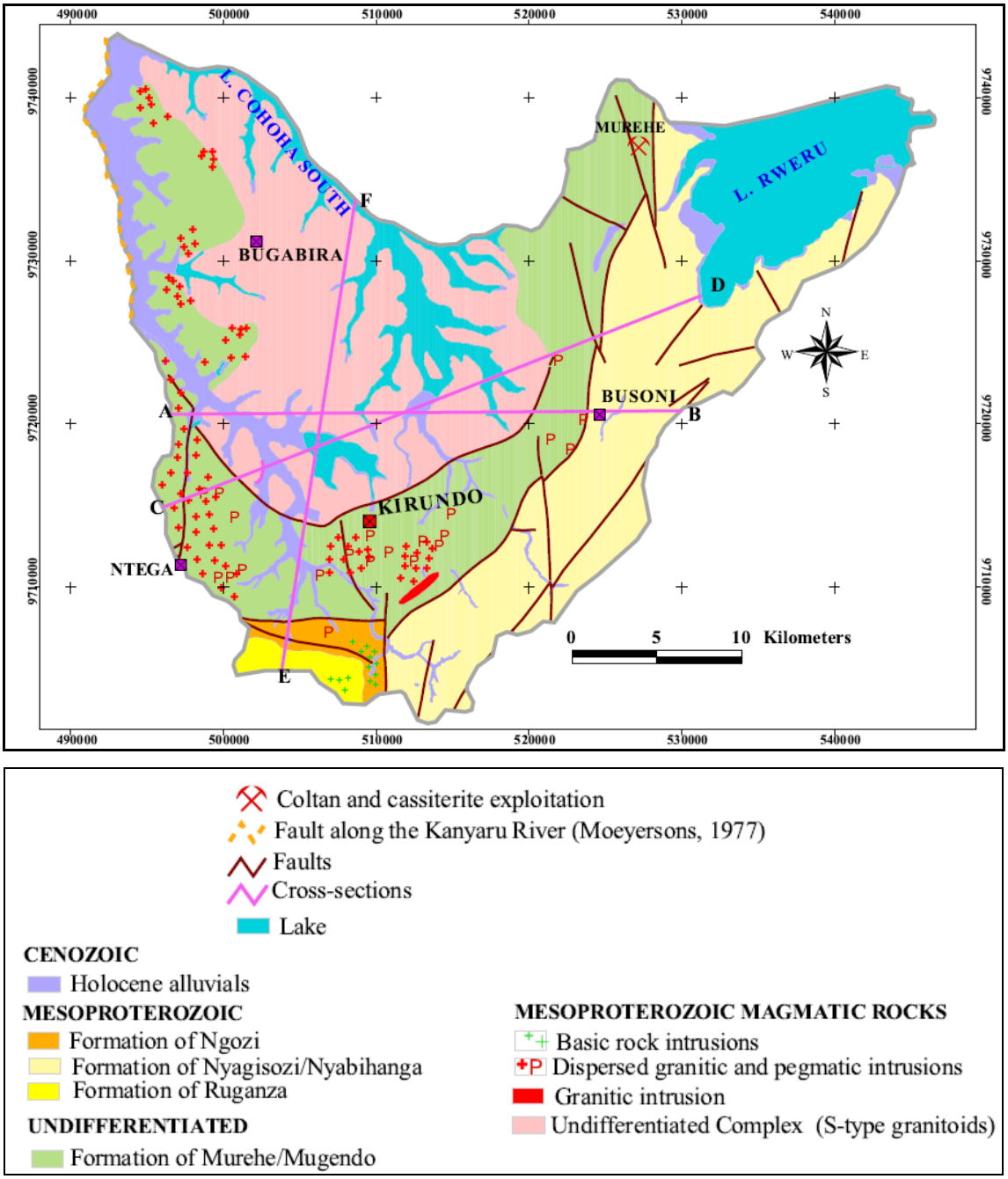

Figure II.6. Geological setting (source: Cartes géologiques au 1/100000: sheets Ngozi (1983), Muyinga (1986) and Busoni (1989)

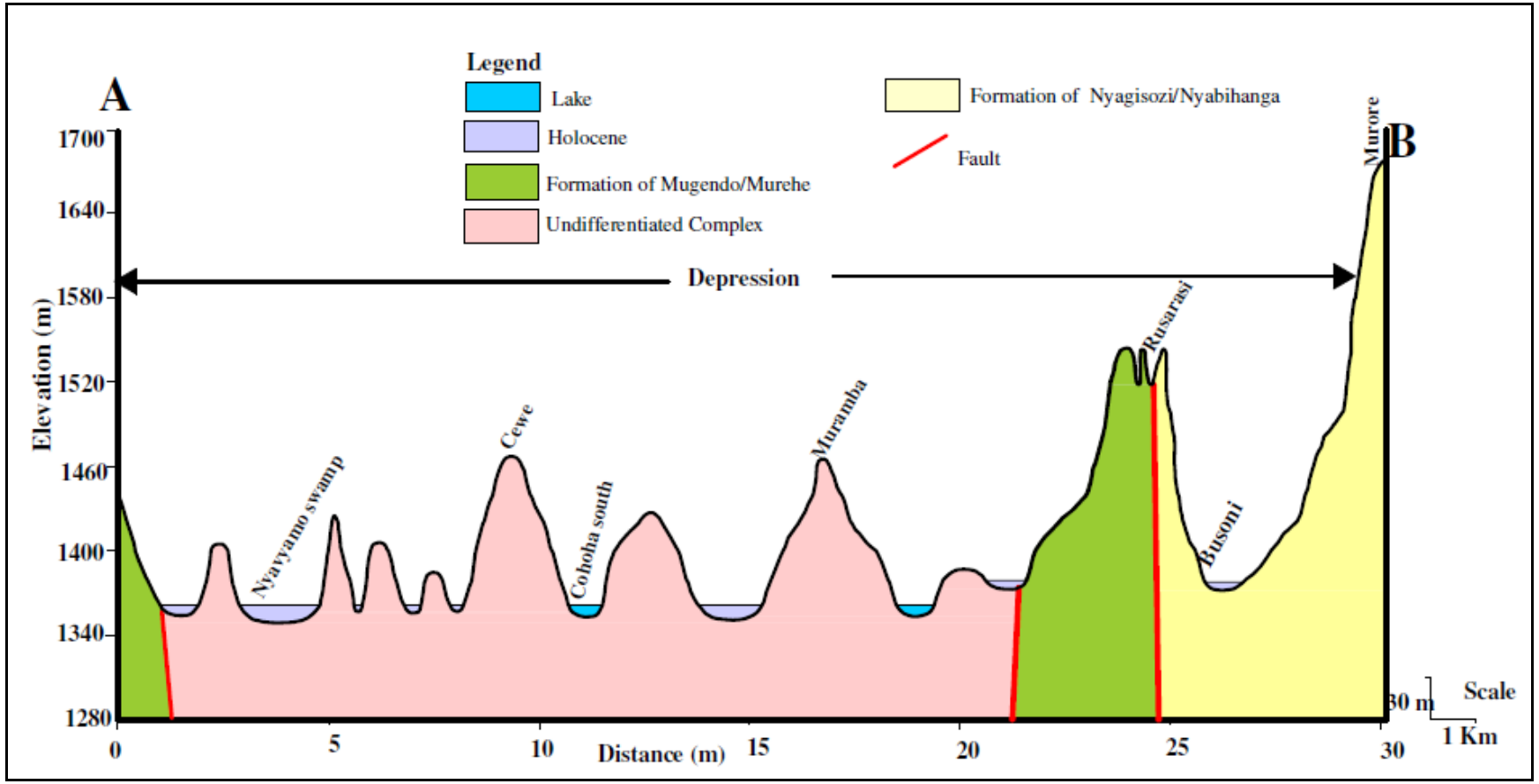

Figure II.7. Geological cross-section A-B (Figure II.5) showing the geological setting of the study area

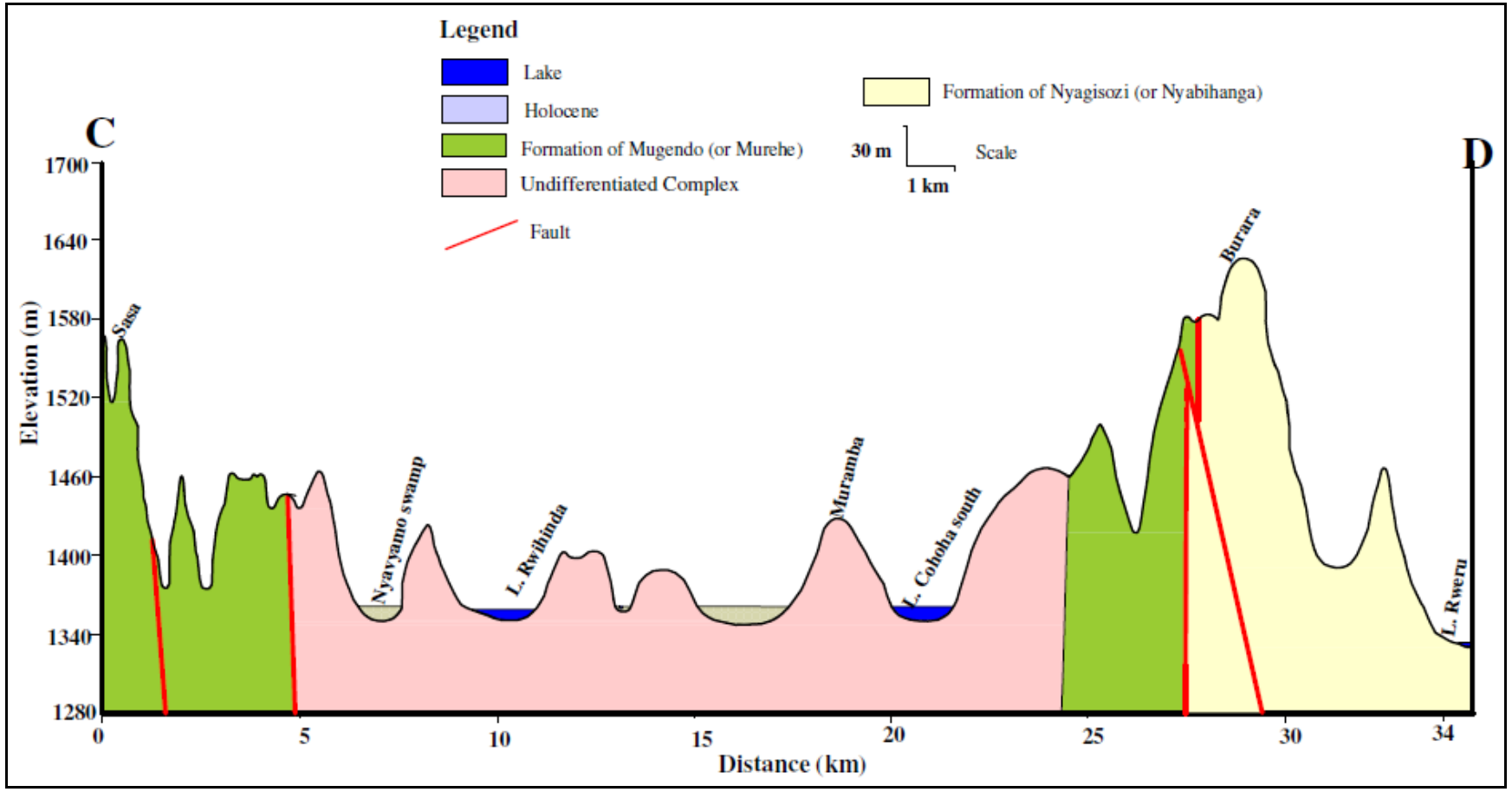

Figure II.8. Geological cross-section C-D (Figure II.5) showing the geological setting of the study area

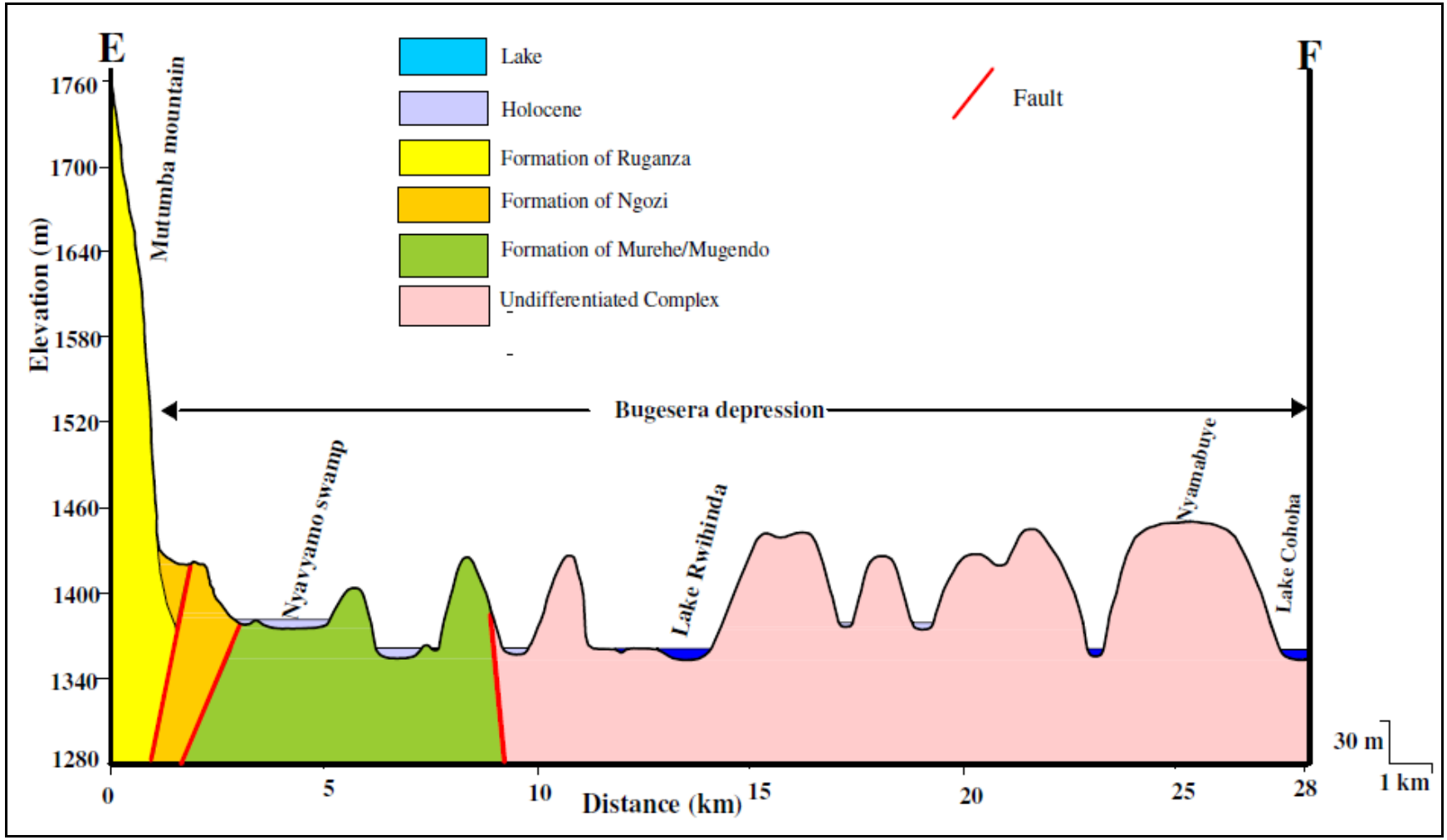

Figure II.9. Geological cross-section E-F (Figure II.5) showing the geological setting of the study area.

II.2. Hydrogeological structures

II.2.1. Overview of knowledge on basement aquifers

A good knowledge of the geological structure of groundwater reservoirs is the main open sesame to a good understanding of groundwater dynamics and hydrogeochemistry. Mainly underlain by Precambrian metasediments, granitic and pegmatitic intrusions as well as some subordinate mafic rocks, the study area falls well within the African crystalline basement complexes also known as shields. African crystalline basements are mainly Precambrian but also, accessorily, Archaean in age. Crystalline basements are widespread in Africa where, for only sub-Saharan Africa, they occupy 40 % of the land area (Figure II.10). They comprise granites and metamorphic rocks of various metamorphic grades (Chilton & Foster, 1995). In Burundi, basement complexes form nearly 90 % of the land surface (Figure II.11). In such geological environments, groundwater aquifers are likely to develop within the weathering cover which is mainly composed of two stratiform and superimposed layers namely the regolith and the underlying fissured/fractured layer of the bedrock (Wright, 1992; Chilton & Foster, 1995; Dewandel *et al*., 2006; Chandra *et al*., 2008). Despite the low productivity of basement aquifers (2-20 m^3/h), their widespread occurrence is well suited for the scattered pattern of human settlement and small to medium cities, which are typical of developing countries. Moreover, crystalline basement aquifers are characterised by shallow groundwater tables which can be exploited at low cost using hand- or foot-operated pumps, bucket and windlass systems (Wright, 1992).

In the past, basement aquifers have not received enough attention in groundwater investigations probably due to their presumed poor groundwater potential. However, with the increasing water demand due to the global population growth in the 20th century and particularly the green revolution in developing nations, a lot of advances have been achieved towards the understanding of the hydrogeology of basement aquifer around the world (Nyagwambo, 2006). Indeed, several studies conducted in many parts of the world (Chilton & Smith-Carington, 1984; Wright, 1992; Chilton & Foster, 1995; Taylor & Howard, 2000; Dewandel *et al*., 2006; Chandra *et al*., 2008) nowadays converge towards a common understanding of groundwater flow in basement environments: "*groundwater flow in crystalline rocks predominantly occurs in a shallow higher-permeability zone ("active" zone) that overlies a deeper lower permeability zone hosting little flow ("inactive" zone ")* (Maréchal, 2010).

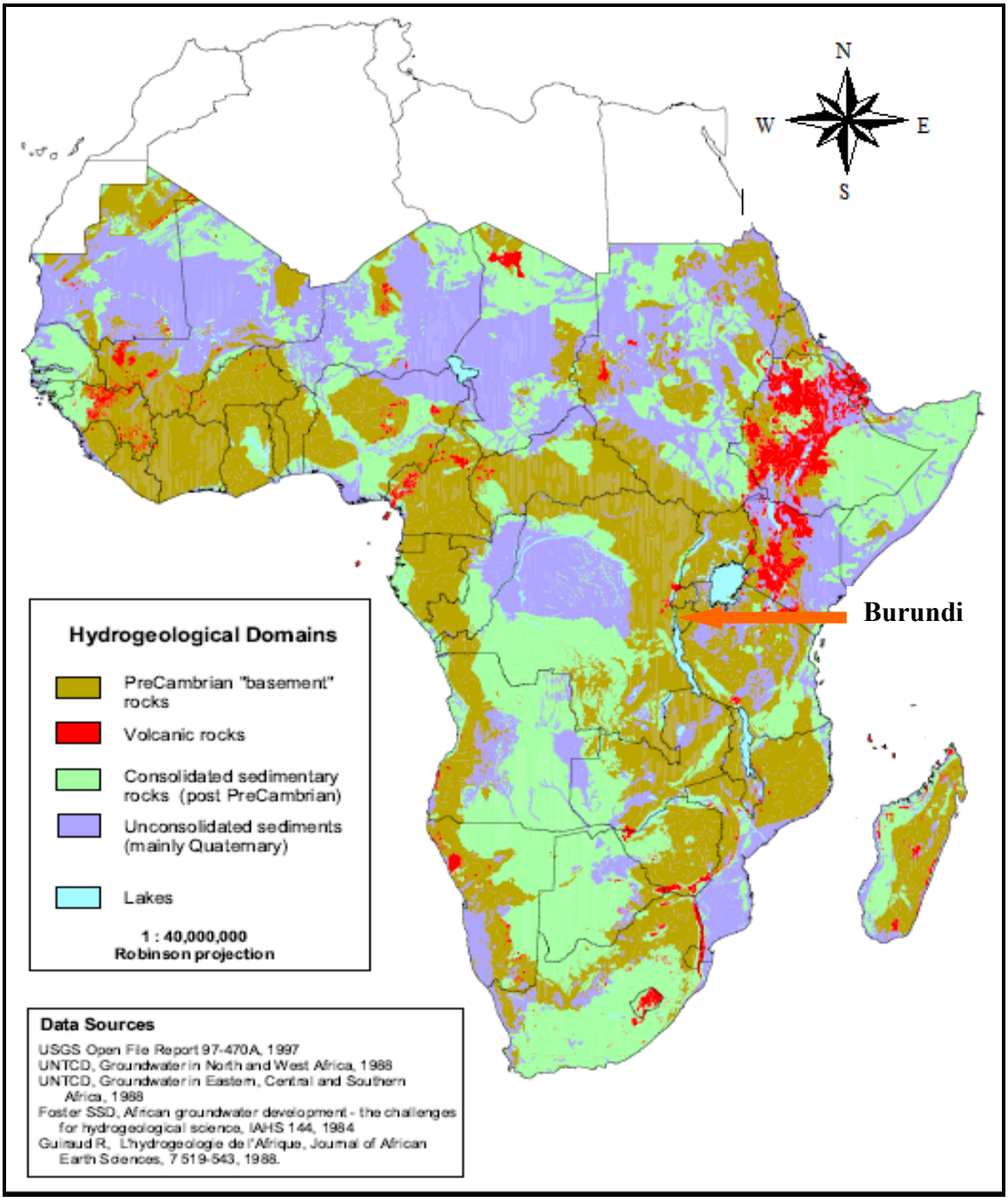

Figure II.10. The hydrogeological environments of sub-Saharan Africa (MacDonald & Davies, 2000; MacDonald *et al.,* 2005)

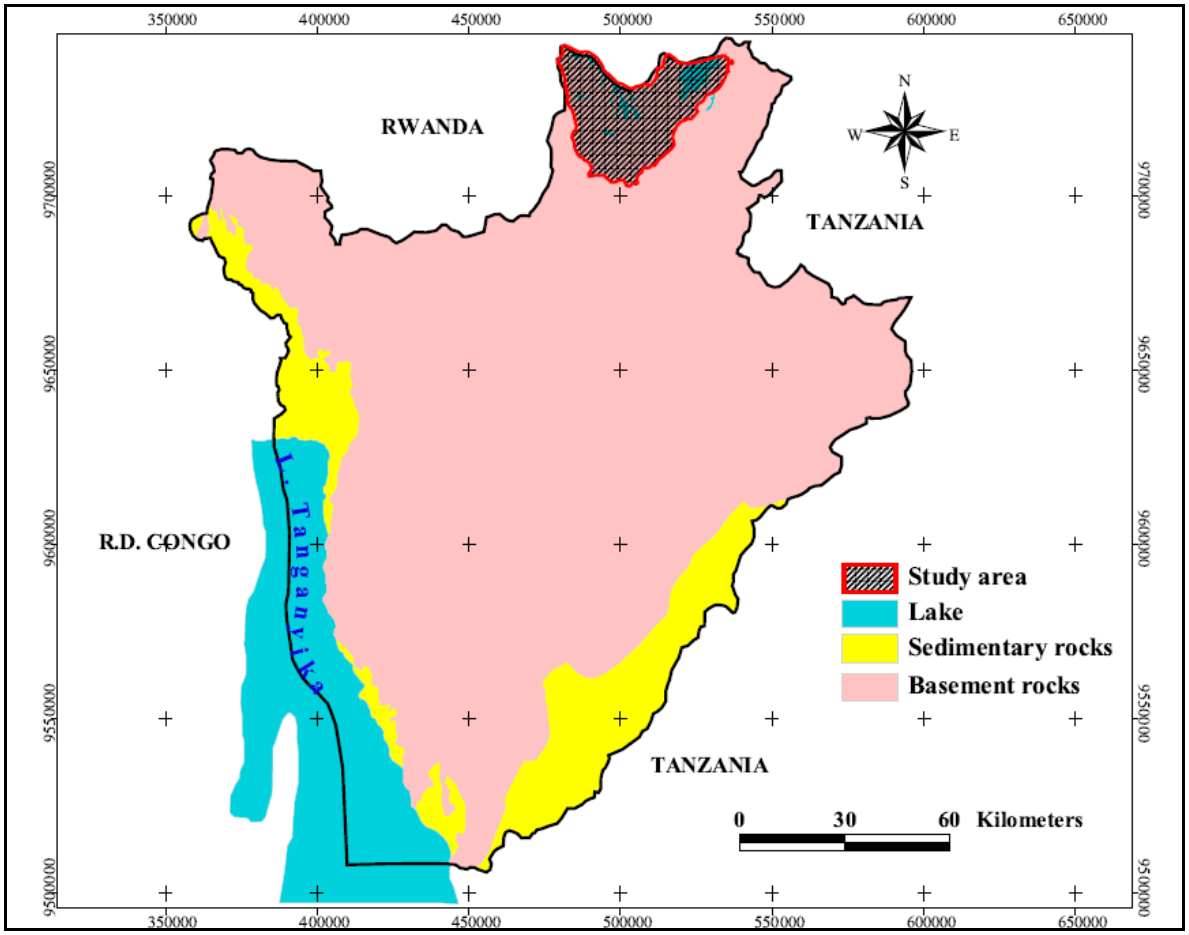

Figure II.11. Hydrogeological environments in Burundi (based on the geological map of Burundi; after Deblond, 1990)

Taylor & Howard (2000) observed that the hydrogeological characteristics of the weathered overburden and the underlying bedrock result from a combination of processes of deep weathering and stripping through colluvial and fluvial erosion. Deep weathering, involving biogeochemical hydrolysis of rock-forming minerals, is favoured by percolating rainfall during periods of tectonic quiescence, while stripping occurs during periods of tectonic uplift. Several research works conducted on crystalline basement rocks in tropical and subtropical environments across the world (Chilton & Smith-Carington, 1984; Acworth, 1987; Wright, 1992; Chilton & Foster, 1995; Taylor & Howard, 2000; Dewandel *et al.*, 2006; Wyns *et al.*, 2004; Chandra *et al.*, 2008) have come up with a typical weathering profile which, if not truncated by erosion, consists of the following layers (from the top to the bottom) (Figures II.12 & II.13):

- **The residual soil or collapsed layer** develops from the underlying saprolite by further dissolution and leaching combined with other chemical, physical and biological processes. It comprises the surface soils including other features such as laterites, calcretes, illuviated clayey layers and stone lines. The surface material is

typically sandy on quartz-rich rocks but changes to sandy clays and clays in valley bottoms (Wright, 1992). The laterite (iron or bauxitic crust) can be absent due to erosion or rehydratation of hematite into a latosol (for iron crusts), or resilicification of gibbsite/boehmite (Dewandel *et al*., 2006).

- **The saprolite** is a clay-rich layer, a few tens of metres thick, which results from prolonged in situ decomposition of bedrock. This layer can be further divided into two sub-units namely the alloterite and the isalterite (Dewandel *et al*., 2006).
- **The alloterite** is mostly a clayey horizon wherein the structure of the bedrock is lost due to mineralogical transformations resulting from weathering processes (Dewandel *et al.,* 2006). This upper saprolite may be distinguished by a higher proportion of more advanced secondary clay mineral (kaolinite). Since weathering is most effective in the vadose zone and in the zone of water table fluctuations, the upper saprolite will tend to be more clayey and when saturated will have relatively low permeability and specific yields (Wright, 1992).
- **The isalterite** is the part of the regolith where the weathering processes have not induced profound changes and where the original structure of the bedrock is thus preserved. The lower saprolite is composed of highly weathered parent rock with coarse sand-size clasts texture and a dense horizontal lamination crosscutting the phenocrysts. In igneous rocks like granites, the base of this layer is laminated. Because of its clay-sand composition, the saprolite may have a relatively high porosity depending on the mineralogy of the parent rocks (Figure II.12). Permeability of this layer is generally low, especially when the regolith is derived from rocks rich in minerals, such as ferromagnesians, which produce secondary clay minerals (Wright, 1992).
- **The fissured layer or saprock** reflects the first stage of weathering of the bedrock. The rock is slightly weathered and therefore maintains all the fabric and structural features of the fresh rock (Wright, 1992; Chilton & Foster, 1995; Panabokke *et al.*, 2007; Taylor & Eggleton, 2001). This layer is generally characterized by a dense network of diversely oriented fissures whose density decreases with depth. According to several authors (e.g. Lachassagne *et al.*, 2001; Dewandel *et al*., 2006), the saprock forms a layer of coarse materials at the base of the saprolite that has a higher hydraulic conductivity than the entire weathered overburden (Figure II.12). The boundary between the saprolite and the saprock may be sharp in coarse-grained and massive rocks or transitional in banded and finer-grained rocks (Wright, 1992). According to Panabokke *et al.* (2007), most of dug wells penetrate only the top of the saprock layer as it becomes difficult to dig further with hands when the saprock is reached. In the study area most of the more

productive wells are those which reach the upper part of the saprock (Figure II.14 & II.15). Several processes such as cooling stresses in the magma, tectonic activity, weathering processes and lithostatic decompression are often invoked to explain the origin of the fissures. Decompression fissures tend to be horizontal while tectonic ones tend to be subvertical and show zonal concentrations (Wright, 1992) (Figure II.12).

- **The fresh basement** may be locally permeable depending on the presence and density of tectonic fractures. However, their density decreases with depth and this leads to consider the fresh basement, at the catchment scale, as impervious and of very low storativity. Therefore, further deepening a borehole into the basement in the desperate hope of increasing the yield of the well will, most of the time, entail unjustified expenses, that Maréchal (2010) considers as "*the sink cost fallacy*". The only exceptions are situations where there are deep water-bearing faults or fractured zones associated with the tectonic activity (Maréchal, 2010).
- **The regolith** or **weathered mantle** is a superficial blanket of loose particulate rock materials sitting atop of the fresh bedrock. According to Eggleton (2001), the regolith includes the saprock (weathered and fractured basement), saprolite, soil, organic accumulations, volcanic material, glacial deposits, colluvium, alluvium, evaporitic sediments, aeolian deposits and groundwater. In simple words, regolith is all what is between the fresh rock and fresh air.

The development of such a typical weathering profile is governed by combination of factors among which the characteristics of the parent rock (mineralogy, petrography, structure and chemistry), climatic conditions (rainfall and temperature), tectonic activity, topography and time (Wright, 1992). A relatively flat topography is required for the development of a complete profile as described above. On steep landscapes, part of or the whole saprolite may be washed away by erosion. In absence of erosion, the saprolite along with the fissured layer form a composite aquifer wherein the saprolite layer plays a storage function (thick saturated layer) while the fissured zone and the fractures of the basement, where well developed, assume a transmissive role (Dewandel *et al.*, 2006) (Figure II.13).

Although basement aquifers may have a regional extent, they respond to abstraction in a discontinuous way due to variability of local features such as discontinuities, barrier boundaries or variations in lithologies and structures of the regolith (Wright, 1992).

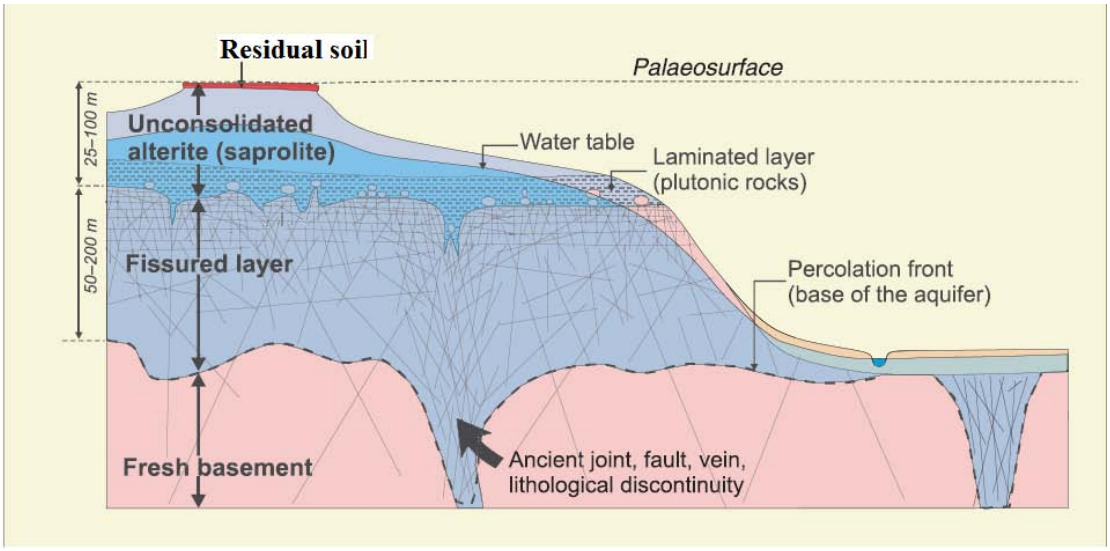

Figure II.12. Stratiform conceptual model of the structure and the hydrogeological properties of hard rock aquifers (after Wyns *et al.*, 2004, modified)

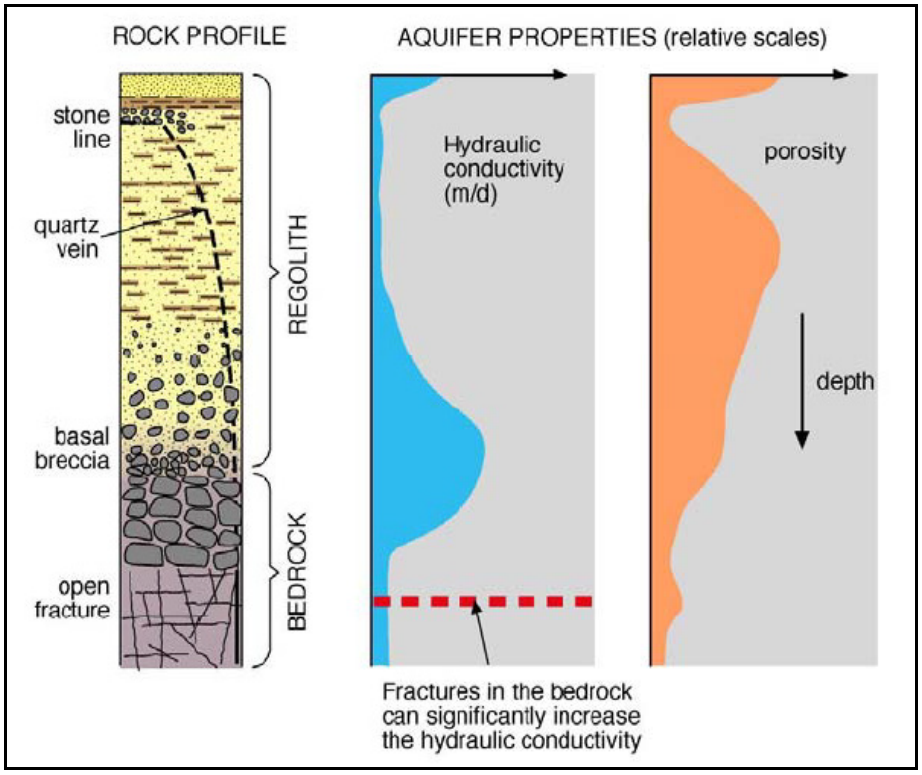

Figure II.13. The variation of permeability and porosity with depth in basement aquifers (after Chilton & Foster, 1995)

This discontinuous behaviour of basement aquifers is reflected in the large number of borehole failures and a wide range of yields, even over short distances, despite the apparent

regional homogeneity of the controlling factors such as climate, morphology and geology (Wright, 1992; Dewandel *et al*., 2006). Basement aquifers, even when continuous, are characterized by a low hydraulic conductivity. Table II.2 shows the values of transmissivity (T) of weathered mantle (regolith) in different parts of Africa, based on pumping test results. Wright (1992) observed that basement aquifers are essentially phreatic in character but may respond to localized abstraction in a semi-confined fashion, if the static water level occurs within the clayey saprolite. This semi-confined behaviour of basement aquifers was recently confirmed in Uganda by Taylor & Howard (2000).

Table II.2. Transmissivity (T) of weathered mantle (regolith) in parts of Africa based on pumping test results (Taylor & Howard, 2000)

T range (m^2/d)	**T mean[a] (m^2/d)**	**Number of sites**	**Area**	**Reference**
1-20	5.5	134	Livulezi, Malawi	Chilton & Smith-Carington (1984)
0.2-5	2.1	81	Dowa West, Malawi	Chilton & Smith-Carington (1984)
1-60	5.2	64	Masvingo, Zimbabwe	Houston & Lewis (1988)
2-10	3.4	27	Masvingo, Zimbabwe	Houston & Lewis (1988)
0.2-40	4.6	6	Various sites	Wright (1992)
0.4-170	4.8	40	Mukono, Uganda	Taylor & Howard (2000)

II.2.2. Hydrogeological structure of the study area

II.2.2.1. Materials and methods

The hydrogeological structure of an area is generally inferred from field information such as lithological logs of wells and geophysical data which are complemented by available information on geology and geomorphology of the area under study. Linking geological and geomorphological data to lithogical logs of boreholes and geophysical data can help give a clear picture of the subsurface stratigraphy and therefore a good hydrogeological framework for the study. However, hitherto, there have been little detailed geological investigations in the study area. Except lithological descriptions of recently constructed hand-dug wells, there is only one deep borehole which was drilled at Rukuramigabo (Kirundo), within the Undifferentiated Complex. This borehole did not reach the fresh basement down to the depth of 32 m.

[a] Geometric mean

The large diameter wells investigated in this study were constructed since the 1960's, but no records of the hydrogeological structure of the wells were kept. This may testify to the fact that these wells were not constructed by groundwater professionals and explain the high rate of well failure as, manifestly, the well siting and construction were not founded on conclusive geological considerations. For this study, we have tried, as much as possible, to infer the hydrogeological structure from available geological and lithological information, which was complemented by information derived from geoelectrical soundings.

Two batches of vertical electrical soundings conducted by AIDR (Association Internationale de Développement Rural) (1984) and a local consulting firm, GEOSCI (2001) were all re-interpreted using RES1D version 1.0, an inversion software. These vertical electrical soundings were performed within the framework of development projects with a view to identifying sites with good groundwater prospects where hand-dug wells for rural water supply should be constructed. In total 136 vertical electrical soundings distributed over 27 transects were processed and re-interpreted.

The first batch of geophysical investigations were conducted by AIDR in 1984 and were first interpreted by the "Laboratoire de Géologie de l'Ingénieur" of the University of Liège in Belgium. A total of 60 vertical electrical soundings distributed along 16 transects were executed (Figure II.16). For each transect, A1 to A16, VES were executed at an equidistance of mostly 50 m (14 transects), or 100 m (A1) or 25 m (A16) from each other depending on the configuration of the terrain. Therefore, in Figure II.16, only the locations of transects have been indicated. The interpretation of the 60 VES were calibrated using lithological information from 21 shallow auger soundings performed by the same organisation (AIDR) and which reached a maximum depth of approximately 15 m.

The second batch of geophysical measurements was carried out in 2001 by a local consulting firm Geosciences & Civil Engineering (GEOSCI). They were interpreted by GEOSCI (2001) using information from 5 shallow auger soundings and 2 shallow wells, which reached a maximum depth of approximately 10 m. In total, this batch of geophysical soundings comprises 150 vertical electrical soundings (VES) located along 26 transects (Figure II.16). However, most of the VES of the second batch (GEOSCI, 2001) were executed near or in the same sites as those performed by AIDR in 1983 and were not re-interpreted in this study. Therefore, all the 60 VES of the first batch (AIDR, 1984) and only 76 VES of the second batch (GEOSCI, 2001), which make a total of 136 VES aligned on 27 transects were re-interpreted in the framework of this study, using the software RES1D (Loke, 2001) so as to have a common benchmark.

Moreover, geophysical information was complemented with lithological information from 30 hand-dug wells recently constructed in the study area within the framework of a project funded by the Belgian Technical Cooperation. Lithological descriptions were done by the civil engineer who was supervising the project in the field (Tandamba, 2008, personal communication) and were enriched by the observations made by the author, while carrying out the last field campaign of this research, between July and October 2008. Figures II.14 and II.15 present the stratigraphy of 4 hand-dug wells recently constructed through this BTC-funded projet. They illustrate the variability of the composition and sequence of lithological layers in the basement rocks of the study area.

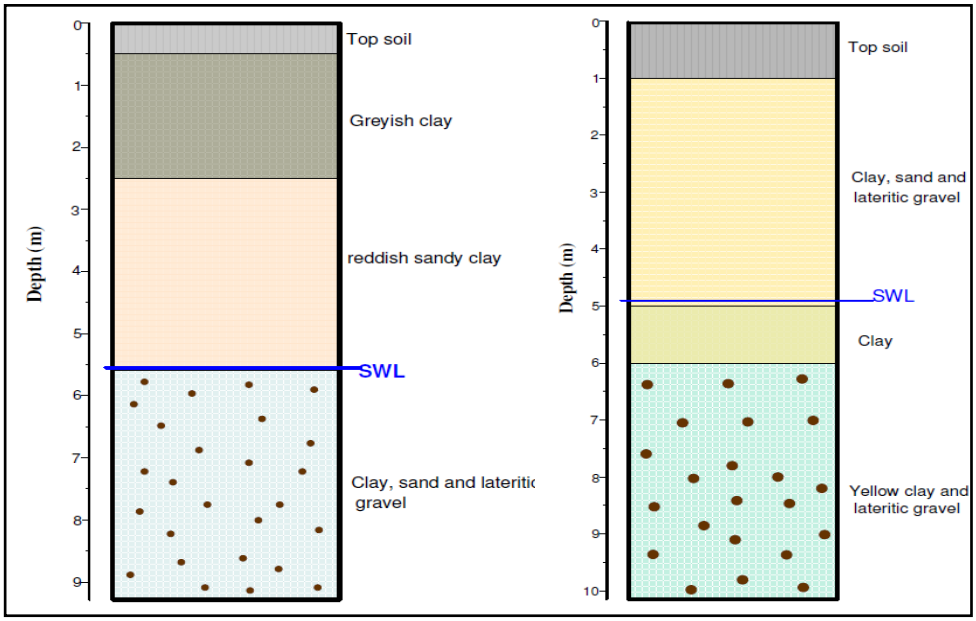

Figure II.14. Lithological sequence of hand-dug wells in Kiruhura II - Kiyanza (A: Well BTC - Kirundo 11) and Rutonde - Kigoma (B: Well BTC – Busoni 1) showing the lithological heterogeneity of the weathering profile and the occurrence of clay layers at different levels within the weathering profile.

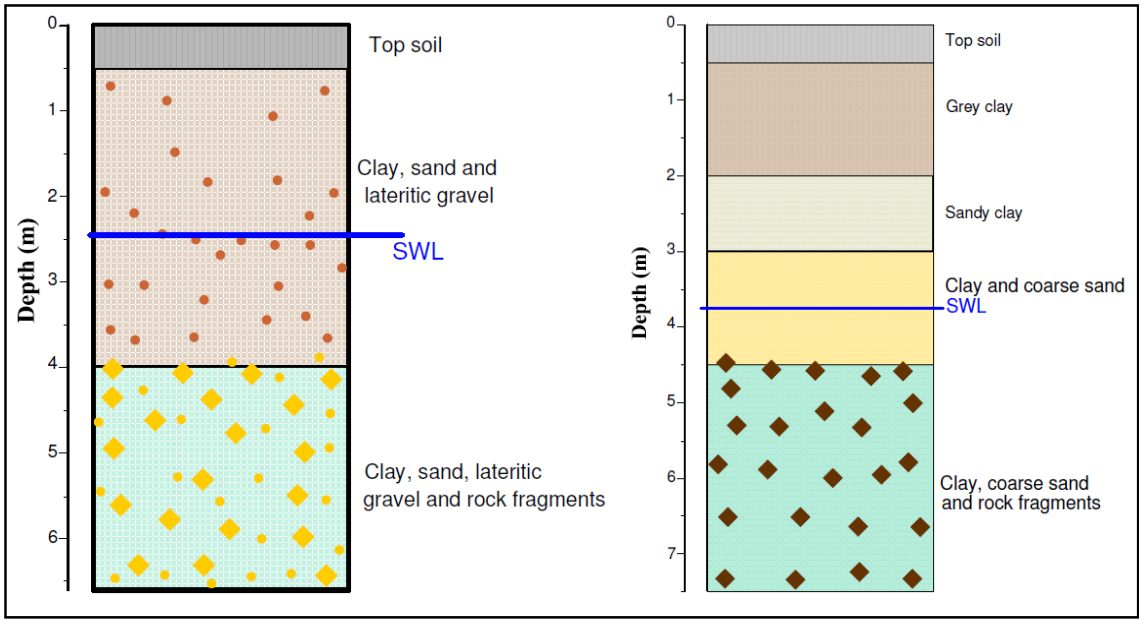

Figure II.15. Lithological sequence of hand-dug wells in Rukori - Nyagisozi (A: Well BTC - Busoni 8) and Ninda - Rubuga (B: Well BTC - Bugabira 5) showing the heterogeneity of the weathering profile and the increase of the coarse fraction with depth.

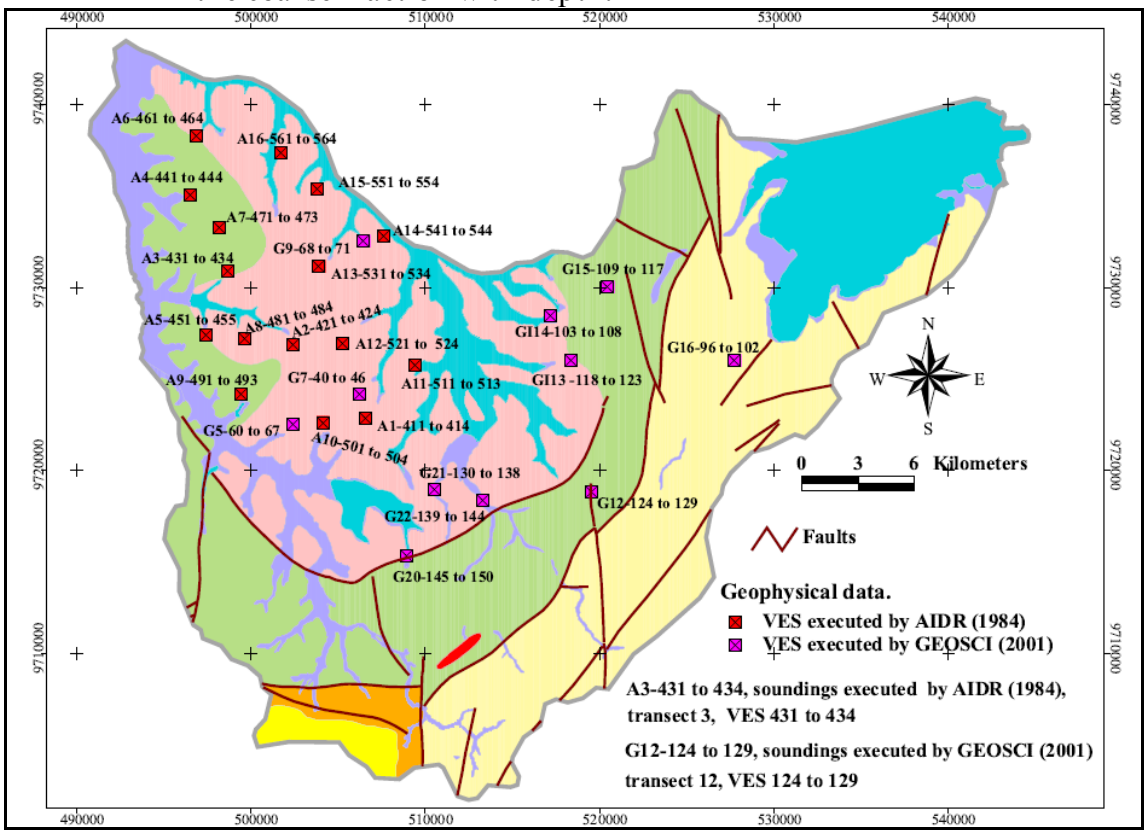

Figure II.16. Location of geophysical prospection sites

II.2.2.2. Geophysical investigation

II.2.2.2.1. Introduction

A wide range of geophysical methods are extensively used in hydrogeological investigations. Electrical methods (Vertical Electrical Sounding), electromagnetic (Time Domain Electromagnetic, Frequency Domain Electromagnetic), ground penetrating radar and seismic methods (seismic refraction) are some of the geophysical methods applied in groundwater investigations (Weight, 2008). The electrical resistivity technique is the most commonly applied geophysical method for groundwater research. Geophysical methods allow to map the subsurface stratigraphy, the lithological composition and geological structures, and thereby to locate and characterise potentially interesting aquifer targets. Over the last decades, geophysical methods have gained an increasing popularity owing to the development of efficient field equipment and computer interpretation techniques, but also because they offer a relatively low-cost tool in hydrogeological investigations **(**Sandberg *et al*., 2002).

Resistivity is defined as the resistance opposed by a material to the flow of electrical current through it, resulting in a potential drop between two considered points of that material. In case of inhomogeneous materials, the measured resistivity is termed apparent resistivity. The latter should be understood as the true resistivity of a hypothetical homogeneous and isotropic medium (Krishnamurthy *et al*., 2009**)**. Apparent resistivity is not a physical property characteristic of geological materials as the true resistivity is. Thus, all field measurements give apparent resistivities, which have to be converted into true resistivities by interpretation techniques **(**Reynolds, 1997**).** From true resistivities and thicknesses obtained from field measurements, it is possible to infer the lithology of different subsurface layers if the different resistivity values can be correlated to known lithologies in the study area.

Measurement is typically performed using 4 electrodes: 2 current electrodes A and B, by means of which an electrical current is passed through the ground, and two potential electrodes m and N, in between which the potential difference is measured. Different types of electrode configurations can be applied depending upon the purpose of the resistivity investigations. Each of these configurations has its own advantages, disadvantages and sensitivities. Resistivity surveys are conducted as either soundings or profiles. Profiling is applied to determining lateral variation of resistivity up to a certain depth, whereas vertical electrical sounding is used to determine vertical changes in resistivity.

The geophysical measurements executed both by AIDR (1984) and GEOSCI (2001) were all vertical soundings and were performed using the Schlumberger array. The latter uses collinear point electrodes, whereby the potential gradient is measured at the mid-point. In this configuration, the spacing between the current electrodes (A and B) is much bigger than the spacing between the potential electrodes (M and N). The apparent resistivity is given by the following relation:

$$\rho_a = K(\Delta V / I)$$

where the geometric factor $K = \pi (L^2 - l^2) / 2l$. L and l are the spacing of the current electrodes and the potential electrodes respectively.

The VES were performed in Bugesera with a maximum current electrodes spacing (L = AB) of 400 m and 300 m for VES executed by GEOSCI and AIDR respectively. The maximum potential electrode separation (l = MN) is 40 m for the VES conducted by AIDR and 20 m for the VES executed by GEOSCI.

Resistivity values of geological materials exhibit the widest range of variation among all other physical properties. Reynolds (1997) observed that the resistivity of a rock is controlled by its nature, composition and age. Table II.3 presents typical resistivity values for different geological materials. Igneous rocks tend to have the highest resistivities whereas sedimentary rocks are the least resistive, owing probably to the high fluid content in pore space. Metamorphic rocks have intermediate but overlapping resistivities. Old rocks tend to be more resistive than younger ones because, with age, their pore spaces become strongly reduced by compaction or recrystallisation. As for rocks with a variable composition, their resistivity will mirror the proportions of the different geologic materials comprising the rock. For sedimentary rocks, their resistivity can strongly decrease as clay becomes the dominant constituent (Reynolds, 1997).

Table II.3. Resistivities of common geologic materials (Reynolds, 1997)

Lithology	**Nominal resistivity (Ωm)**
Granite	$3x10^2 – 3x10^6$
Granite weathered	$3x10^{-5} – 3x10^2$
Schist (calcareous and mica)	$20 - 10^4$
Schist (Graphite)	$10 -10^2$
Slates	$6x10^2 - 4x10^7$
Consolidated shales	$20 – 2x10^3$
Conglomerates	$2x10^3 - 2x10^4$
Sandstones	$1 – 7.4x10^8$
Limestones	$5x10-10^7$
Dolomite	$3.5x10^2 - 5x10^3$
Clays	$1-10^2$
Alluvium and sand	$10 – 8x10^2$
Soil (40 % clay)	8
Soil (20 % Clay)	33
Top soil	250 - 1700
Clay (very dry)	50-150
Gravel (dry)	1400
Gravel (saturated)	100
Quaternary/recent sands	50-100
Laterite	800 - 1500
Lateritic soil	120 - 750
Dry sandy soil	80 - 1050
Sandy clay/Clayey sand	30 - 215
Sand and gravel	30 - 225
Fresh basement	> 1000
Weathered/Fractured basement	100-500

The interpretation of a sounding curve can be done qualitatively using curve shapes, and quantitatively with graphical model curves or computer modeling. For three geoelectrical layers, the shape of the sounding curve can be classified into one of the four basic curve shapes (Figure II.17). The H-type curve is a basin-shaped curve which is typical of crystalline basement aquifers. It indicates a low resistivity material underlain and overlain by more resistive materials (Olayinka & Mbachi, 1992**).** The upper high resistivity layer corresponds to the residual soil, whereas the lower high resistivity values indicate the fresh basement**.** The intermediate values of resistivity in between the two layers reflect the clay-rich layer, i.e. the saprolite**.** The A-type curve represents a progressively increasing resistivity wherein the middle layer has an intermediate resistivity between upper and lower layers. This curve shape can be typical for outcrops of crystalline rocks wherein the water content of the materials decreases with depth due to the decrease of weathering with depth**.** The K-type is a bell-shaped curve and indicates a high resistivity formation underlain by lower resistivity material. The Q-type shows a decrease of the resistivity with depth and may characterize formations intruded by salt water **(**Lloyd, 1999**).** A combination of these elementary curve shapes can be used to describe more complex field curves which may represent several more layers (e.g. types HK and KH in Figure II.17).

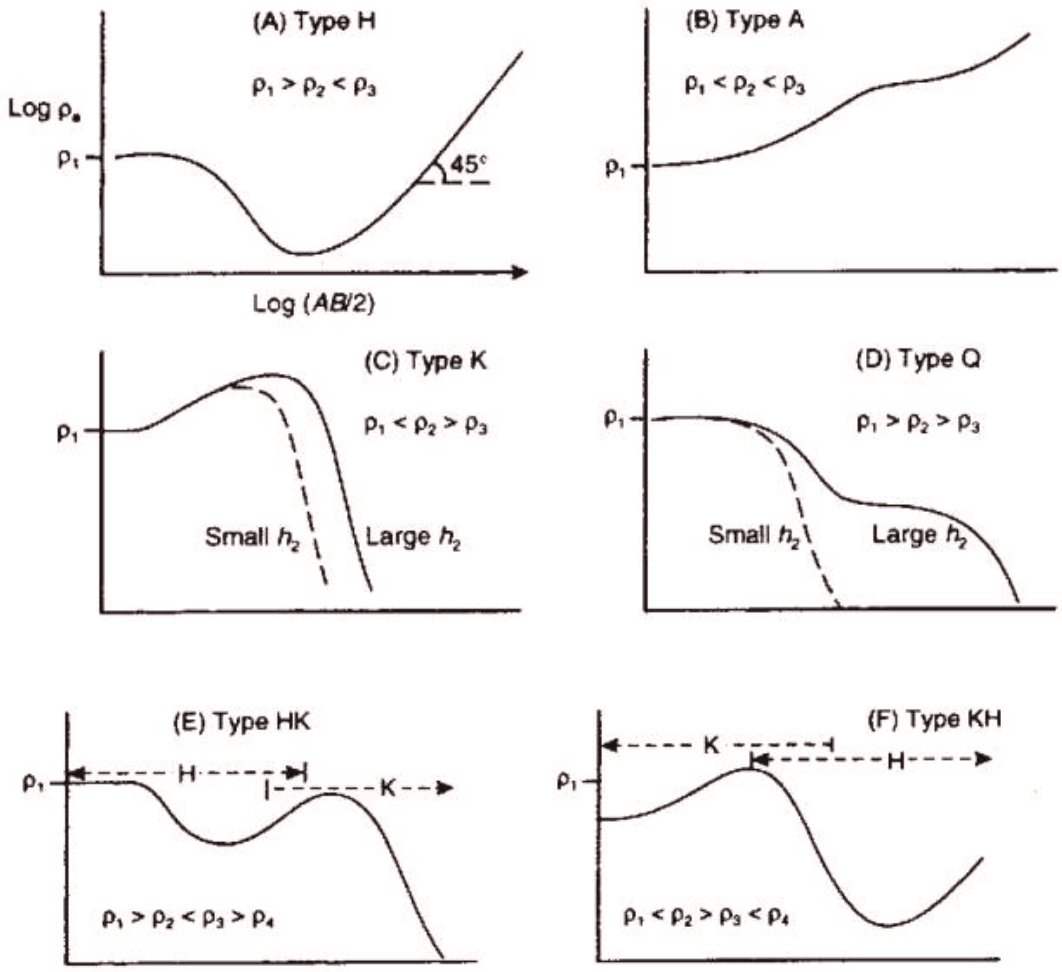

Figure II.17. Apparent resistivity curve shapes for different resistivity structures: (A) to (D) are three-layer models, (E) and (F) are four-layer models (Reynolds, 1997).

In crystalline rock environments, the fresh basement and the regolith have a marked resistivity contrast. The presence of a geoelelectric substratum is marked, on the log-log graph, by a 45° rising arm after the curve trough **(**Lloyd, 1999). On the contrary, a low value for the resistivity of the basement may reflect the presence of some saturating component such as groundwater, and this could suggest a high aquifer potential related to the expected high fracture permeability (K'Orowe *et al*., 2008; Jatau & Bajeh, 2007**).**

Interpretation of VES conducted in different basement environments around the world proved that there are no standard values of resistivity for the different parts of crystalline basements **(**K'Orowe *et al*., 2008; Nyagwambo, 2006**).** Olayinka & Sogbetum (2002) argue that the values of resistivity are rather site specific as they are determined by the rock

mineralogy and the degree of weathering. Martinelli and Hubert (1985, in Nyagwambo, 2006) attempt to simplify and generalize resistivity values for granites, gneisses and paragneisses in the African and Post-African erosional surfaces as shown in Table II.4.

Table II.4. Resistivity ranges for granites, gneisses and paragneisses in the African and Post-African surfaces (after Martinelli & Hubert, 1985 in Nyagwambo, 2006)

Lithological succession	**Resistivity range (Ωm)**	**Aquifer characteristics**
Various top soil	80 – 1000^{+}	Superficial layer, dry. Resistivity depends on clay/sand ratio.
Highly weathered granite, gneiss and paragneiss	20 - 50	Main water bearing horizon when thickness of overburden exceeds 25 m.
Weathered granite, gneiss and paragneiss	50 - 100	Important water bearing horizon when thickness of overburden exceeds 25 m.
Partly weathered granite, gneisses and paragneiss	100 - 150	Moderate to important aquifer.
Poorly weathered granites, gneisses and paragneiss	150 - 250	Marginal aquifer.
Unweathered and unfractured granite, gneiss and paragneiss	500 - 2000^{+}	Hydrogeological bedrock.

Note: Interpretations are based on electrical resistivity data only.

The limits set by Martinelli & Hubert (1984) should not be considered as strict guidelines for interpreting resistivity values, as local variations are common. Furthermore, there is no agreement among different authors on typical values of resistivity for various lithologies. As an example, Curruthers and Smith (1992) (in Nyagwambo, 2006**)** found that the upper limit of 250 Ωm for potentially water-bearing layers as suggested by Martinelli and Hubert (1984) is rather low and proposed that an upper limit of 400 Ωm should be considered. Table II.5 shows a farther clustering and simplification of resistivity values as regards to groundwater potential.

Table II.5. Aquifer and resistivity (Ωm) of layered regolith (Wright, 1992)

Resistivity (Ωm)	**Groundwater potential**
<20	Clays with limited potential (or saline)
20-100	Optimum weathering and groundwater potential
100-150	Medium conditions and potential
150-200	Little weathering and poor potential
>250	Negligible

II.2.2.2.2. Interpretation of geophysical data

The hydrogeological structure of the study area was inferred from the re-interpretation of all the 60 VES of the first batch (AIDR, 1984) and 76 VES out of 150 VES of the second batch (GEOSCI, 2001). From the very start, a quick visual inspection of inversion results shows a clear contrasting boundary between the regolith, which is characterized by low to moderate resistivity values, and the basement which, in most of the cases, is typically marked by high resistivity values (Appendix, II.1). However, the weathered cover displays further geoelectrical subdivisions which may reflect the heterogeneities in relation to the rock type variations as well as weathering and pedological processes. The inversion and interpretation of the 136 VES show 3 to 6 geoelectrical layers but the number and the sequence of the different layers varies from one site to another and even within the same transect. Indeed, there is an important variability of the geoelectrical structure, such that even two adjacent VES may feature a different sequence of geoelectrical layers. In the following discussion, an attempt is made to cluster the different VES interpreted into 2 different groups based on the sequence of geoelectrical layers and to infer hydrogeological conditions. Detailed results of the inversion of the 136 VES are presented in appendix II.1.

1. Vertical electrical soundings showing the typical weathering profile of the basement rock in the study area.

This is the most typical subsurface sequence of geoelectrical layers inferred from the inversion and interpretation of the different VES conducted in the study area. This sequence of geoelectrical layers depicts a subsurface composed of 3 to 6 geoelectrical layers, whose resistivity values show a clear upwards decreasing trend, suggesting an upwards fining of the weathering materials, in agreement with the fact that the weathering process is generally more intense in the upper parts of the weathering profile, and more specifically in the vadose zone and the zone of water table fluctuations (e.g. A1-411 to 414; A2-421 to 424; A4-441 to 444; A8-481 to 484; A13-531 to 534; G14-103 to 108).

The lowest layer of the sequence, which corresponds to the basement, is characterised by remarkably high but variable values of resistivity, which reflect the nature and the state of weathering of the basement. Figure II.18 shows the average values (per transect) of resistivity for the basement, found in geoelectrical transects where the resistivity signature of the lowest geoelectrical layer hints to the fresh basement. The low value of resistivity for the basement that was found in transect G12 (520 Ωm), corresponds to metapelitic metasediments such as micaschists or schists, whereas extremely high values of resistivity

may be suggestive of fresh granitic (G14: 133000 Ωm), psammitic (G16: 222000 Ωm) or quartzitic (A7: 24000 Ωm) basement. The remarkable contrast of average resistivity of the fresh basement in the geoelectrical transect G12 (520 Ωm) on one hand, and G20 (9600 Ωm) and G21 (10000 Ωm) on the other hand, seems to confirm the granitic nature of the fresh basement at the sites where the geoelectrical transects G20 and G21 were performed, as opposed to the metapelitic metasediments in G12.

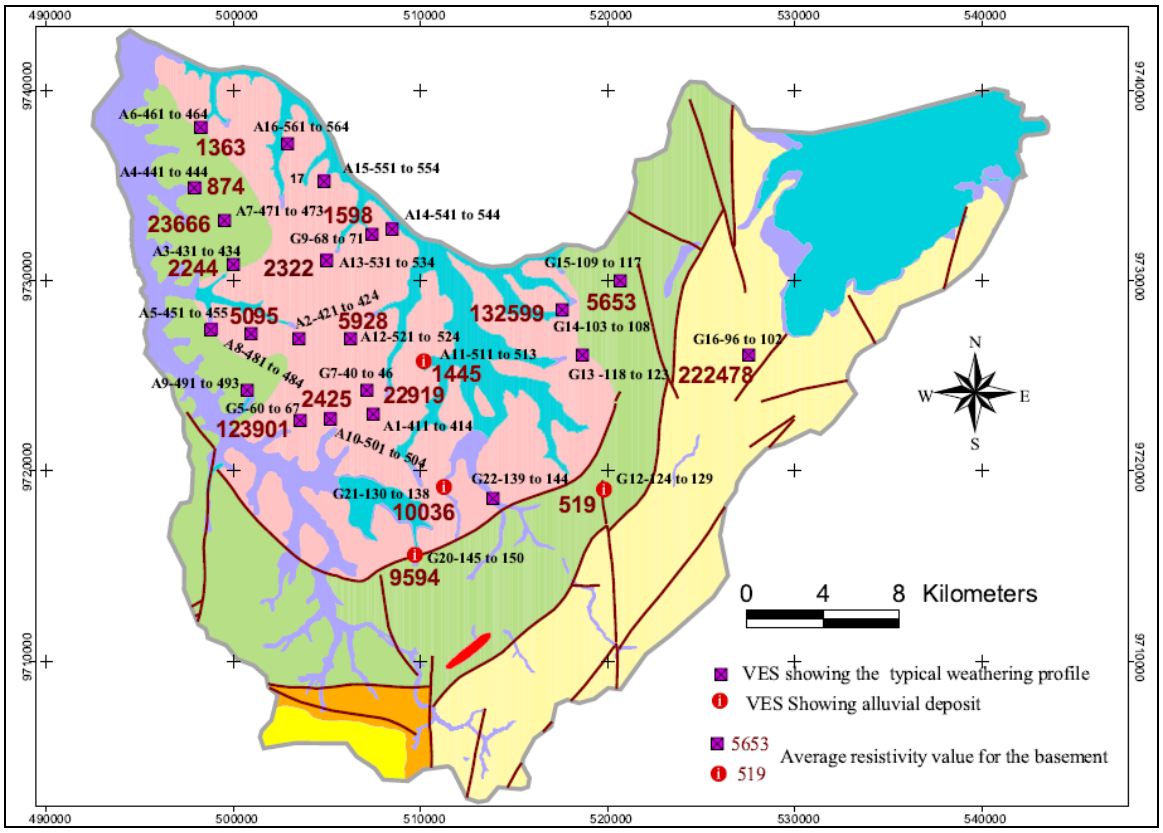

Figure II.18. Average resistivity values (average per transect) for the fresh basement in different geoelelectric (in Ωm)

The fresh basement is overlain by a geoelectrical layer which shows moderately high but variable values of resistivity (150-500 Ωm) which correspond to the weathered/fractured part of the basement. This geoelectrical layer is the lowest layer of the sequence in most of the VES executed by AIDR (1984), because the maximum current electrode spacing AB (L = 300 m) did not allow to reach the fresh basement. The geoelectrical transect A3 (Figure II.19) shows a typical illustration of a complete weathering profile where both the fractured/weathered and fresh basement are present with a clear contrast of resistivity between the two geoelectrical layers, i.e. an average resistivity of 356 Ωm for the weathered/fractured basement and 2244 Ωm for the fresh basement. In some geoelectrical

soundings (e.g. A6, A7 & A8), the resistivity signature of the fractured/weathered basement does not appear due to the principle of suppression according to which a thin layer of intermediate resistivity may not appear when sandwiched between two thick layers with a high contrast of resistivity values.

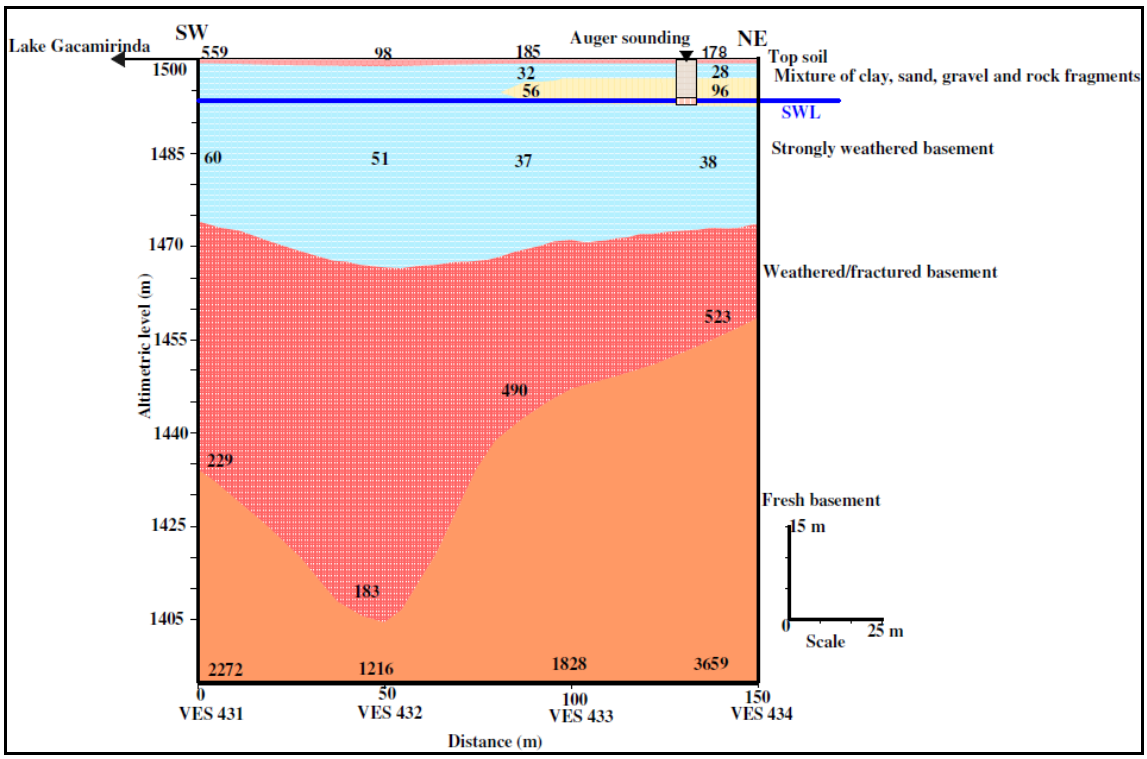

Figure II.19. Geoelectrical cross-section A3 howing 4 to 6 geoelectrical layers (resistivity values in Ωm)

The top of the fractured/weathered basement shows an irregular topography but within sounding transects perpendicular to the shore of the lakes or to the axes of the swampy valleys, it appears clearly that the basement tends to slope towards the swampy valleys (e.g. A4) or the lakes (e. g. A1; A9; A15, A16) (Figures II.20 & II.21). This observation suggests that the thickness of the weathered overburden increases downslope towards the valleys or lakes, which may explain why most of the wells are constructed close to the lakes or valleys, where the combination of alluviation and weathering processes increases the thickness of the weathered overburden and thus the groundwater potential.

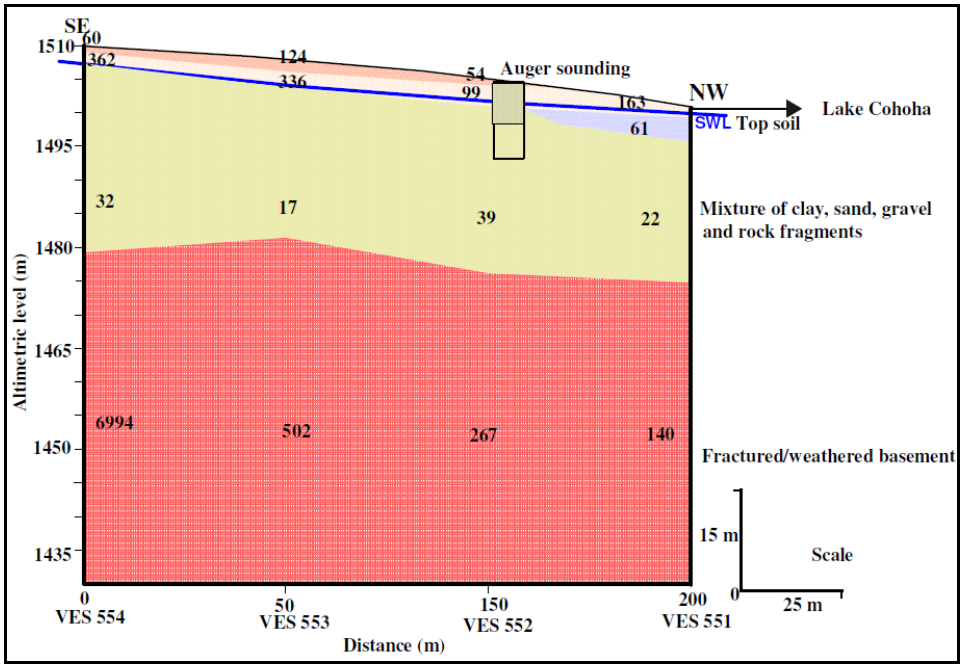

Figure II.20. Geoelectrical cross-section A15 showing 4 geoelectrical layers (resistivity values in Ωm)

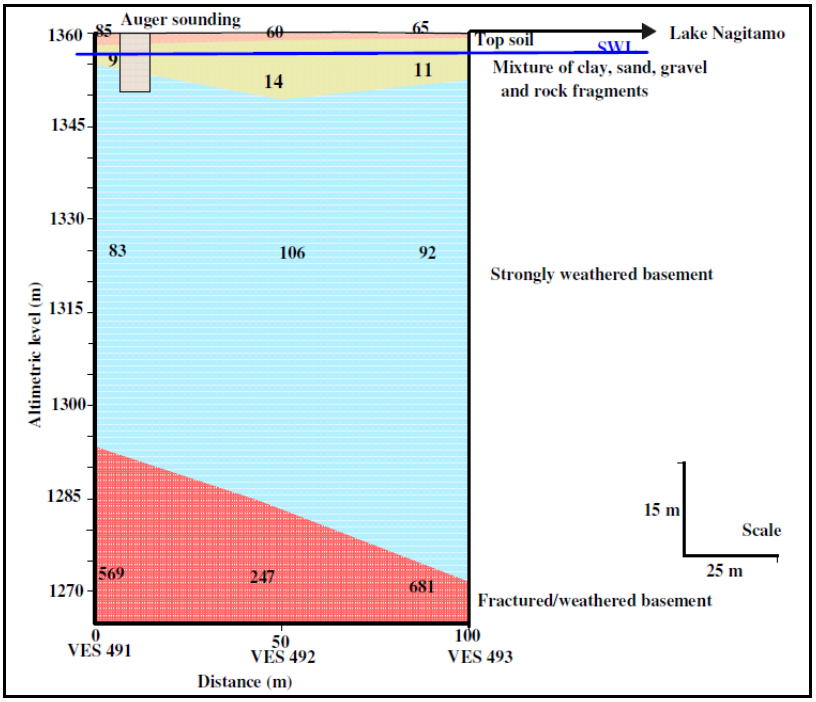

Figure II.21. Geoelectrical cross-section A9 showing 4 geoelectrical layers (resistivity values in Ωm)

Above the weathered/fractured basement occurs the weathered overburden with a variable resistivity (3-150 Ωm) and thickness (3-140 m). The wide variation of resistivity values for the weathered overburden reflects the heterogeneity of its lithological composition which

varies from clay/sandy clay to a mixture of clay, sand, gravel and rock fragments but with a clear upwards fining of the weathering products which, in some transects, results in a distinct clay-rich layer on the top of the sequence (3-28 Ωm) in which lies the groundwater table. This layer acts as a semi-confining layer. The relative importance of coarse and fine materials is reflected by the wide variability of resistivity values, higher values of resistivity indicating the predominance of coarse materials. Figure II.22 presents two photos showing the aquifer materials excavated at the bottom of recently constructed wells in the study area which confirm the downwards increase of the proportion of unweathered materials, which explains the increasing trend of resistivity values with depth. Figure II.23 represents the resistivity values of the two geoelectrical layers overlying the fresh basement which confirm the quite generalised trend of upwards decrease of resistivity which is in line with the upwards fining of the weathering materials. This is a typical characteristic of the weathering profile in the study area which may explain the quite generalised semi-confined response of the aquifer in the study area as corroborated by the interpretation of pumping test data (Chapter III).

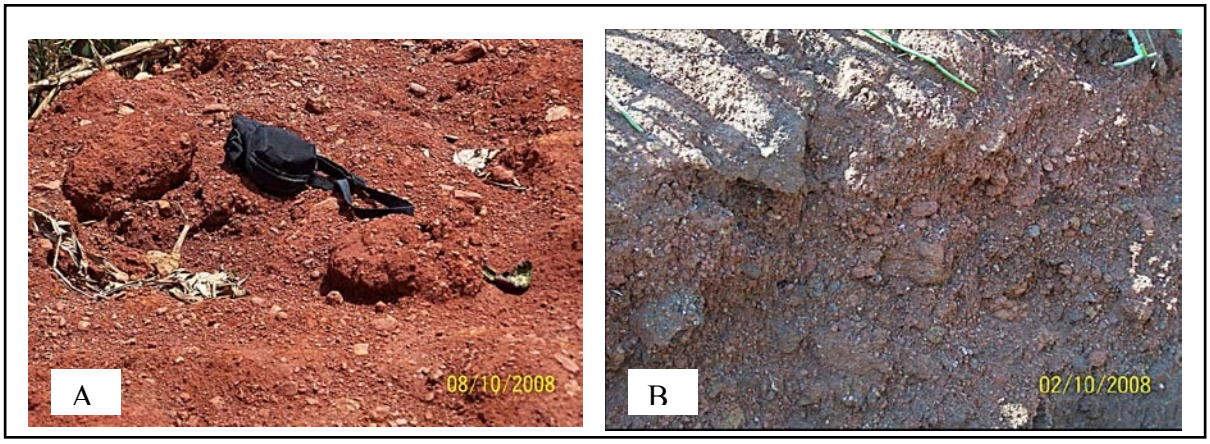

Figure II.22. Photos showing the materials excavated at the bottom of recently constructed wells at Senga-Nyagisozi (A) and Kiyanza-Kiruhura (B) confirming the downwards decrease of the weathering intensity.

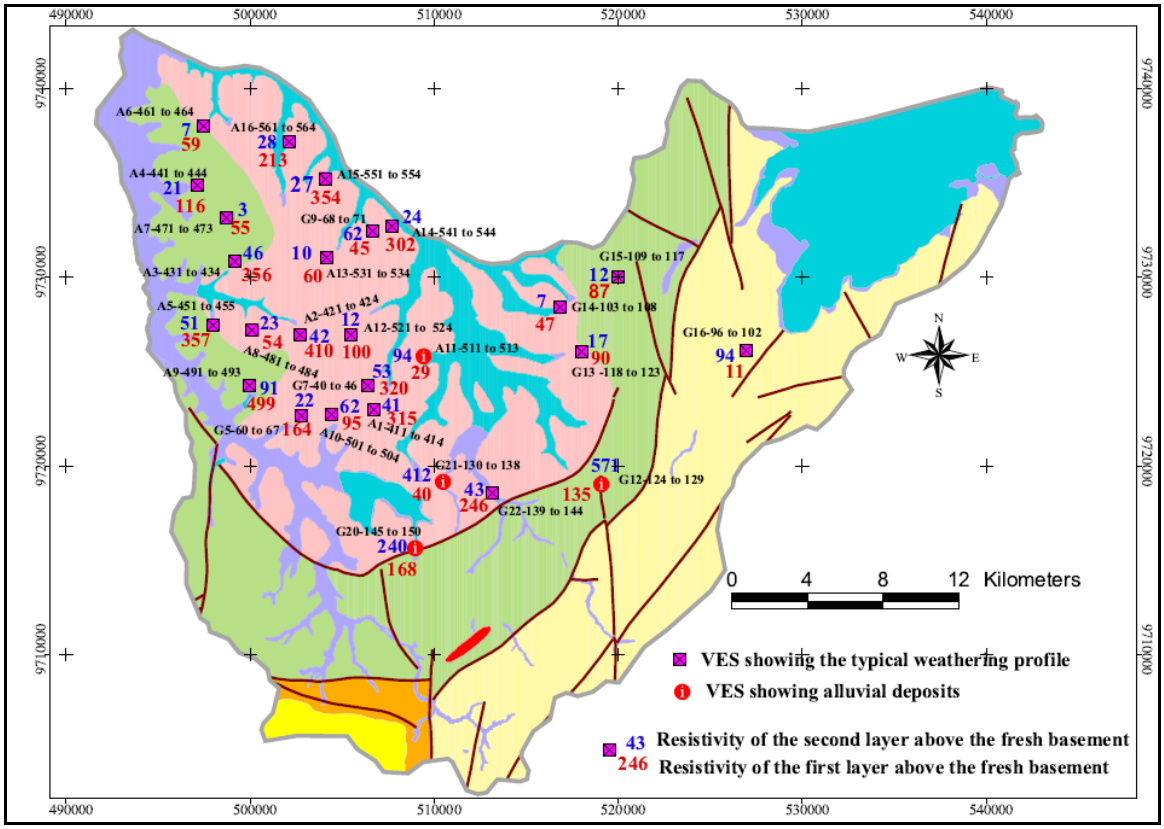

Figure II.23. esistivity values (average of layer par transect) of the two geoelectric layers overlying the fresh basement

The second layer above the fresh basement, which is actually a profoundly weathered part of the weathered/fractured basement generally features relatively high and variable values of resistivity (e.g. Figure II.24: A4: 102-144 Ωm; Figure II.25: A13: 44-76 Ωm), which denote a still high proportion of coarse materials. With the upwards increasing intensity of the weathering, this layer evolves into a mixture of clay, sand, gravel and rock fragments in variable proportions but with a clear predominance of clay in most of the cases, as this is evidenced by the low values of resistivity (e.g. A4: 19-25 Ωm; A13: 7-15 Ωm; A14:21-29 Ωm). In some situations, this layer is topped by a distinct clayey layer (e.g. transects A4, A9, A13 & A14) (Figures II.21, II.24, II.25 & II.26). It is in this layer that the auger soundings have struck the groundwater table in most of the geoelectrical transects, at a depth varying between 1.4 to 9 m. When the proportion of coarse materials increases, the resistivity of this geoelectrical layer increases accordingly, although the clay is still ubiquitously present as revealed by the auger soundings (A1 & A3;) (Figures II.27 & II.19)

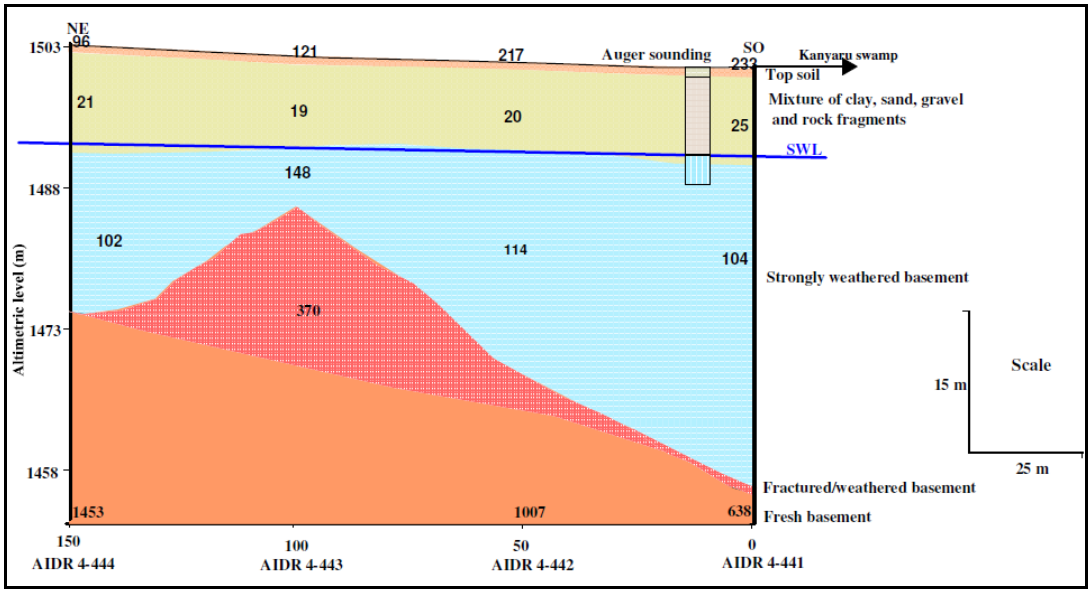

Figure II.24. Geoelectrical cross-section A4 showing 4 geoelectrical layers (resistivity values in Ωm).

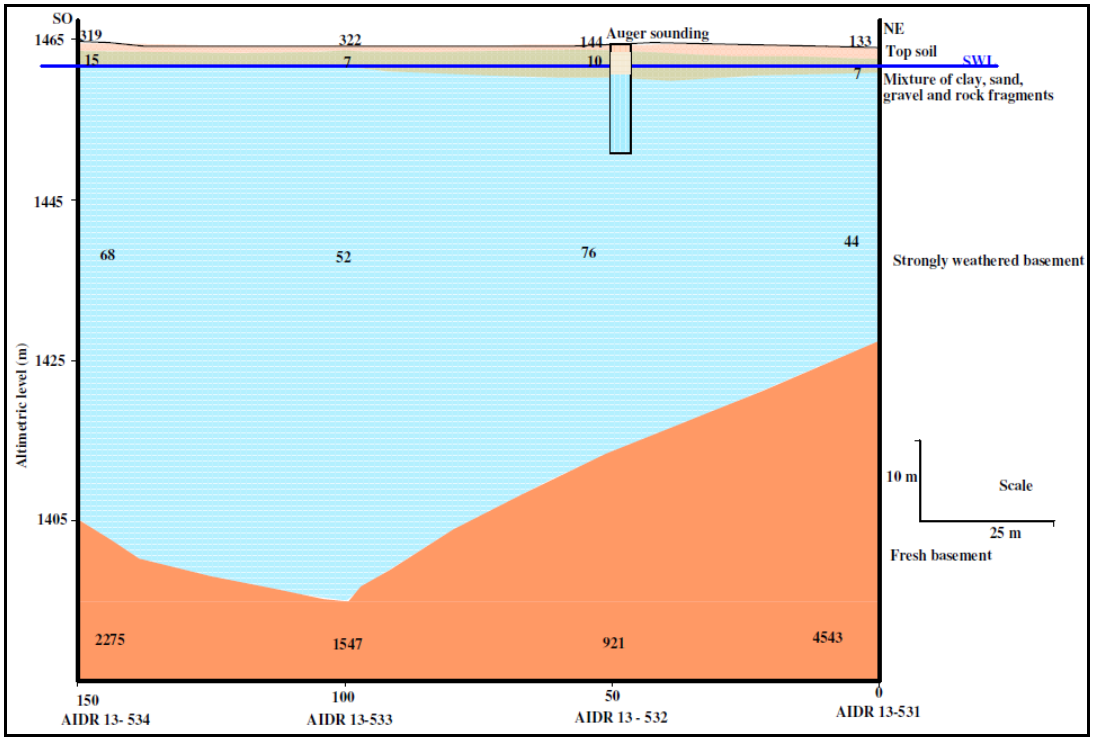

Figure II.25. Geoelectrical cross-section A13 showing 4 geoelectrical layers (resistivity values in Ωm).

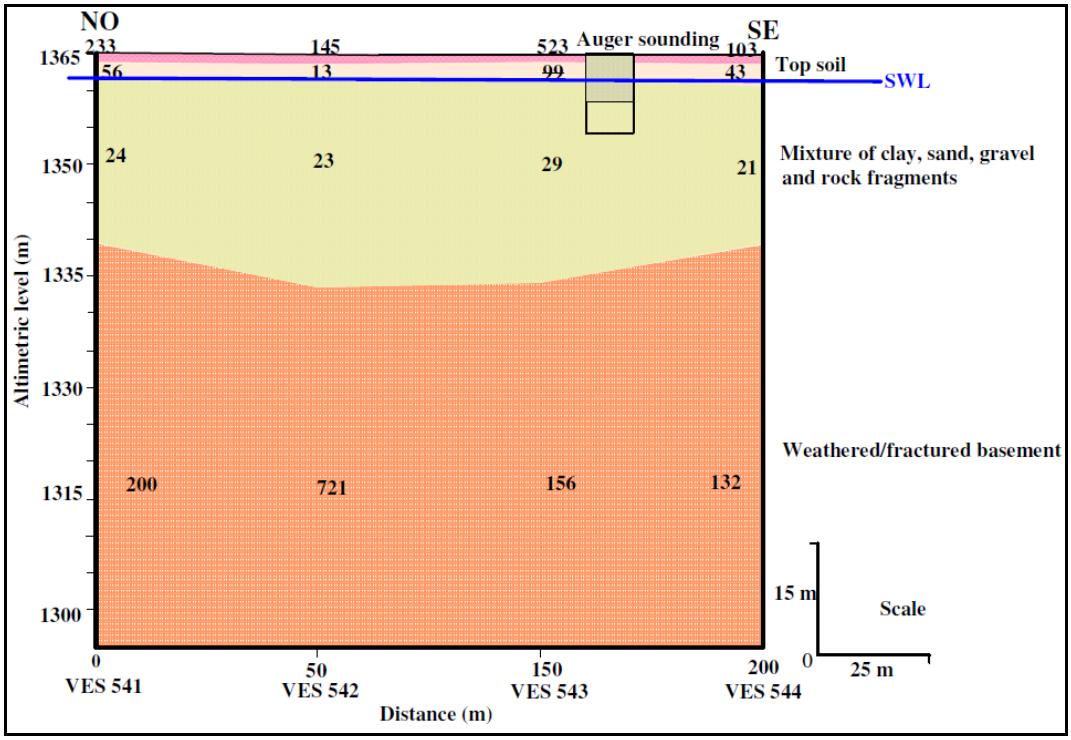

Figure II.26. Geoelectrical cross-section A14 showing 4 geoelectrical layers (resistivity values in **Ω**m).

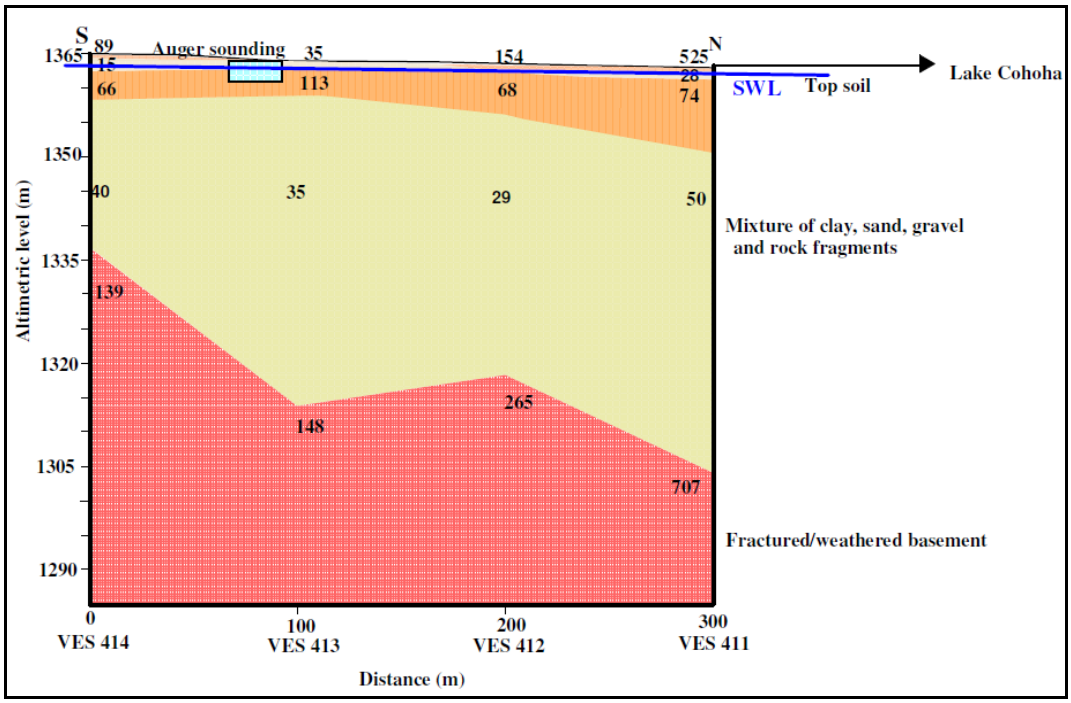

Figure II.27. Geoelectrical cross-section A1 showing 4 to 5 geoelectrical layers (resistivity values in **Ω**m).

However, it should be noted that the sequence of the different geoelectrical layers comprised in this typical weathering profile is not always complete. Despite the obvious and general upwards decrease of resistivity within the weathering profile, one or another geoelectrical layer may be missing in the interpretative cross-sections due to the principle of suppression. The boundaries between the various geoelectrical layers are not as sharp as they appear on the cross-section but are rather smooth and gradual. Moreover, this upwards decrease of resistivity which reflects the upwards increasing intensity of the weathering may be hidden by alluviation or colluviation processes which superimpose materials characterised by various resistivity values (e.g. Figures II.27 & II.28). This wide variability of resistivity values for the top soil denotes the heterogeneities of the materials comprising this layer which can include laterite or other coarse materials (e.g. A3 & A14) or more clayey alterites (e.g. G5).

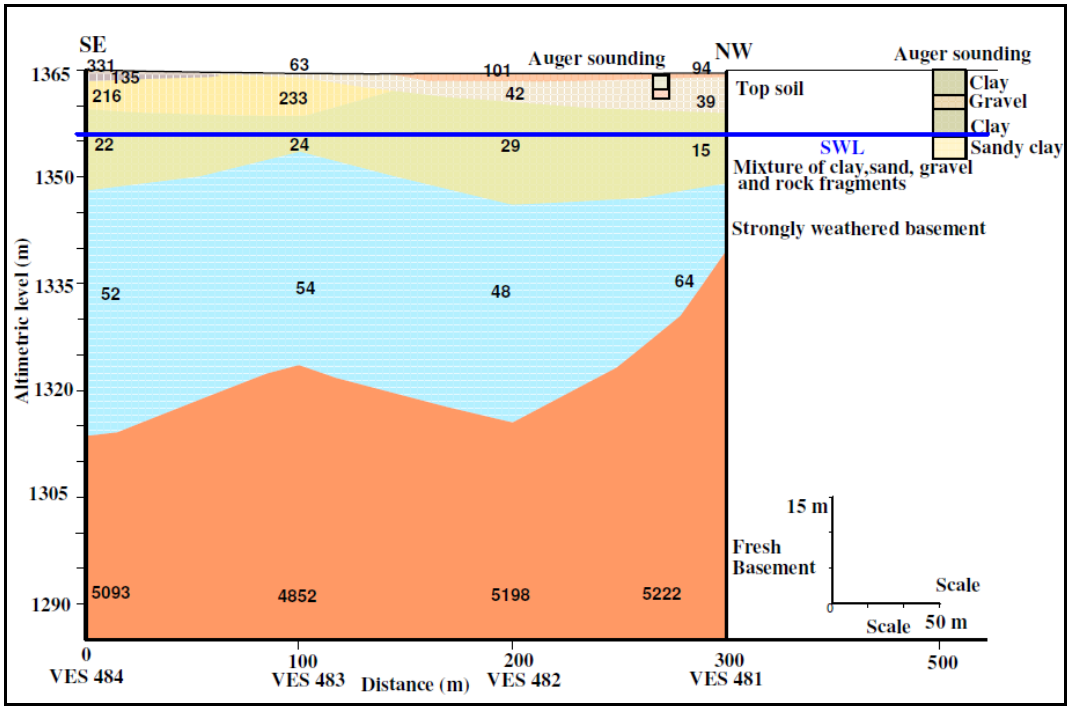

Figure II.28. Geoelectrical cross-section A8 showing 5 to 6 geoelectrical layers (resistivity values in Ωm).

2. Vertical soundings showing a sequence of geoelectrical layers corresponding to alluvial deposits

This type of subsurface is illustrated by the geoelectrical transects A11, G12, G20 and G21. Unlike the above geoelectrical transects where the different geoelectrical layers derive from the weathering of the underlying basement, these 4 transects show a complex sequence of 5 to 6 geoelectrical layers which is characterized by an alternation of lower and higher resistivity values in a pattern which may pertain to an alluvial origin. The geoelectrical transects G12, G20 and G21 (Figure II.29) were performed in dry valleys originating from the southern highlands, while the transect A11 (Figure II.30) was executed on a narrow alluvial valley adjoining the Lake Cohoha at Rukuramigabo (Kirundo). The saw-toothed pattern of the alluvial deposits depicted by the geoelectrical transect G21 (Figure II.29) reflects the incision of the fresh basement, which may pertain to the important slope gradient between the southern highlands and the depression.

The resistivity values of the geoelectrical layers within the alluvial overburden vary over a wide range, between 12 Ωm (G21) and 3077 Ωm (G12) reflecting heterogeneous materials due to different hydrodynamic conditions prevailing during the deposition. While a demarcation between the alluvial deposit and the underlying basement can be established in most of the VES based on the contrast of resistivity values, the presence of layers within the alluvial deposit which feature extremely highly values of resistivity (G12, G21 & G21) suggests an important deposition of coarse materials such as rock fragments and rock blocks brought from the highlands by strong torrents during the rainy season.

The thickness of the alluvial deposit shows a wide variation ranging from 12 m (G12-VES 125) to 127 m (G20- VES 148). Such a thick alluvial deposit where layers of fine materials alternate with layers of coarse materials may constitute a good prospect for groundwater resource.

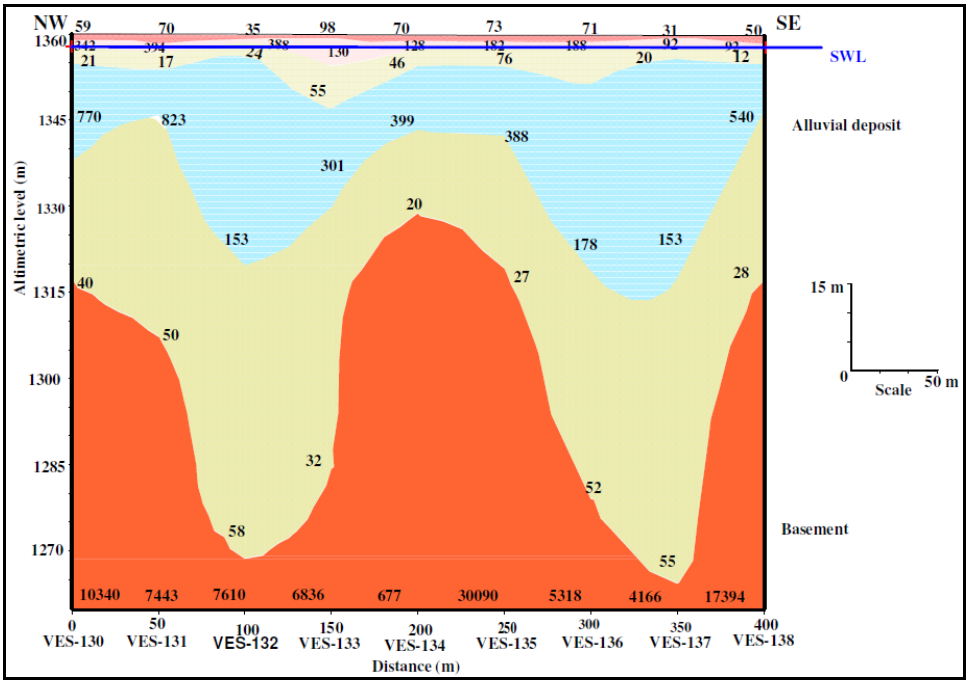

Figure II.29. Geoelectrical cross-section G21 showing 5 to 6 geoelectrical layers, comprising an alluvial deposit on top of the fresh basement (resistivity values in Ωm).

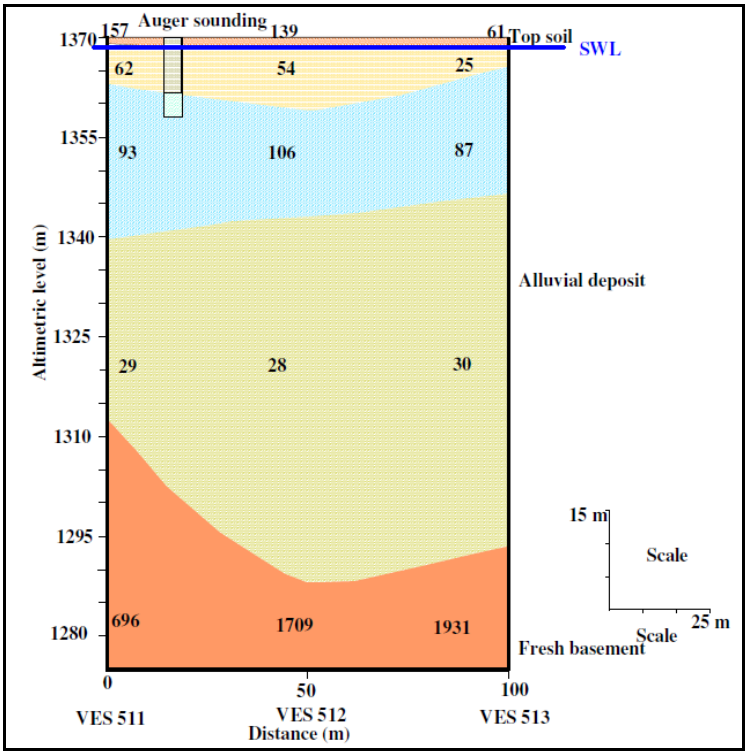

Figure II.30. Geoelectrical cross-section A11 showing 5 geoelectrical layers (resistivity values in Ωm).

II.2.2.2.3. Hydrogeological conditions and aquifer potential

The Precambrian metasediments and the associated magmatic intrusions underlying the study area have been exposed to prolonged weathering processes which have created thin to relatively thick layers of alteration products, composed of clay, sand, gravel, laterite and rock fragments in variable proportions. In addition to the weathering processes, the weathered overburden undergoes further phenomena like dissolution, leaching and other chemical, physical and biological processes which result in a sequence of several layers with different physical, chemical, mineralogical, geoelectrical and hydraulic features. Hence, the occurrence of the more clayey layer in the upper parts of the weathering profile and the attendant hydrogeological conditions, are the result of these complex processes combining weathering and pedogenetic phenomena. Indeed, for normal conditions, a number of authors (Chilton & Smith-Carington, 1984; Acworth, 1987; Foster, 1984; Chilton & Foster, 1995; Wright, 1992) have proposed a more generalized conceptual hydrogeological model in which relatively impermeable layers of clay are found in the upper parts of the profile, while with increasing depth, the weathering materials become progressively coarser (Figures II.31 & II.32). With this regard, Wright (1992) confirms that the upper saprolite tends to be more clayey and thus to have low hydraulic conductivity but high storativity when saturated owing to the fact that weathering is most effective in the vadose zone and the zone of water table fluctuations. This model shows that semi-confined to confined conditions may arise when the static water level occurs within the clayey layer whereas unconfined conditions may occur when the static water levels rests deeper, in the more coarse part of the weathering profile (Figure II.31). The weathering profile depicted in Figure II.31 shows that the regolith which is characterised by a high clay content has a low hydraulic conductivity but a high porosity which decreases with depth, towards the bed rock. On the contrary, the fractured/weathered basement has a high hydraulic conductivity owing to the presence of fractures, but its storativity strongly decreases because the fractures do not represent a significant volume of the rock.

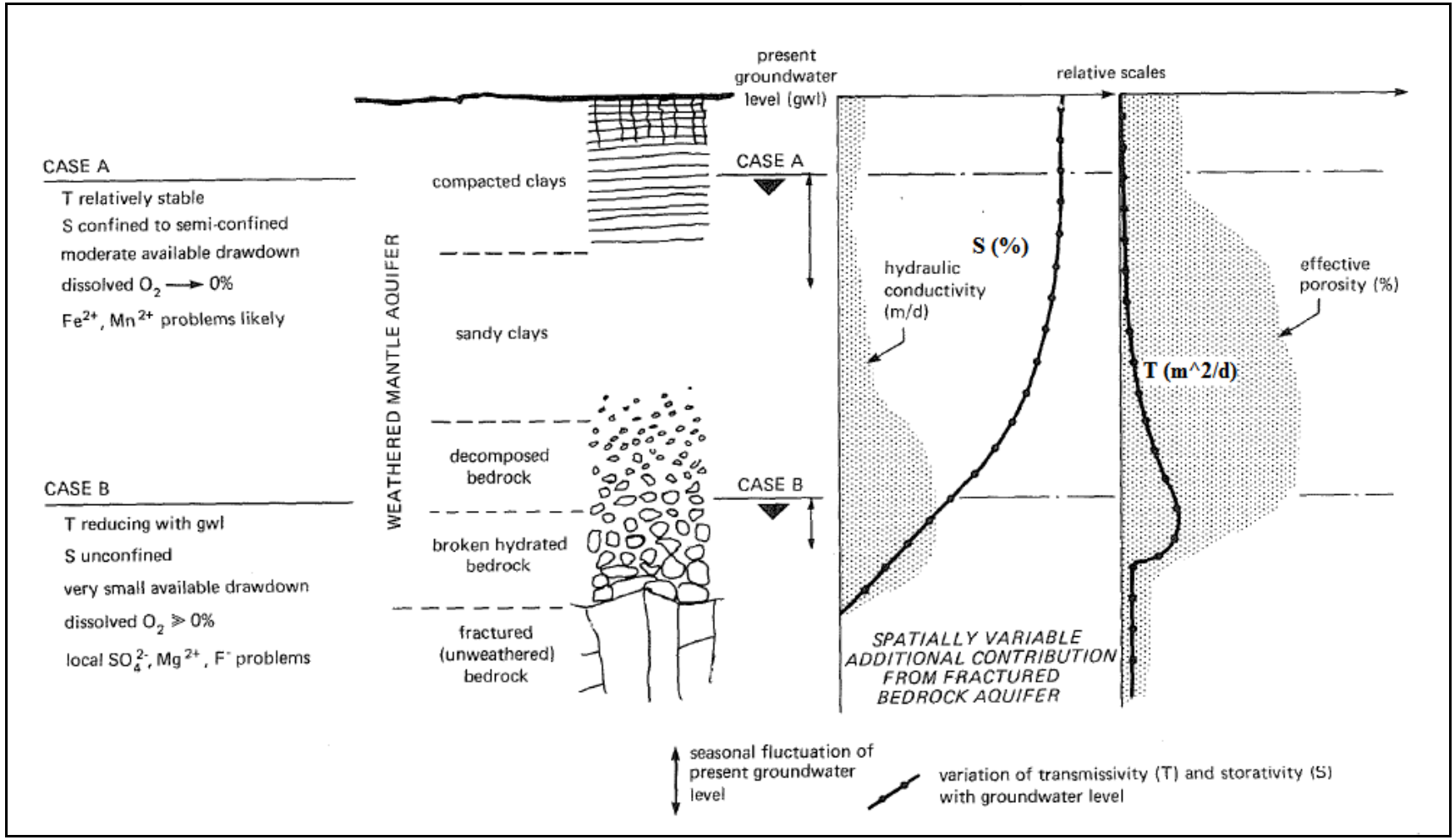

Figure II.31. Tentative conceptual model of weathered mantle aquifer of basement shield (modified after Foster, 1984)

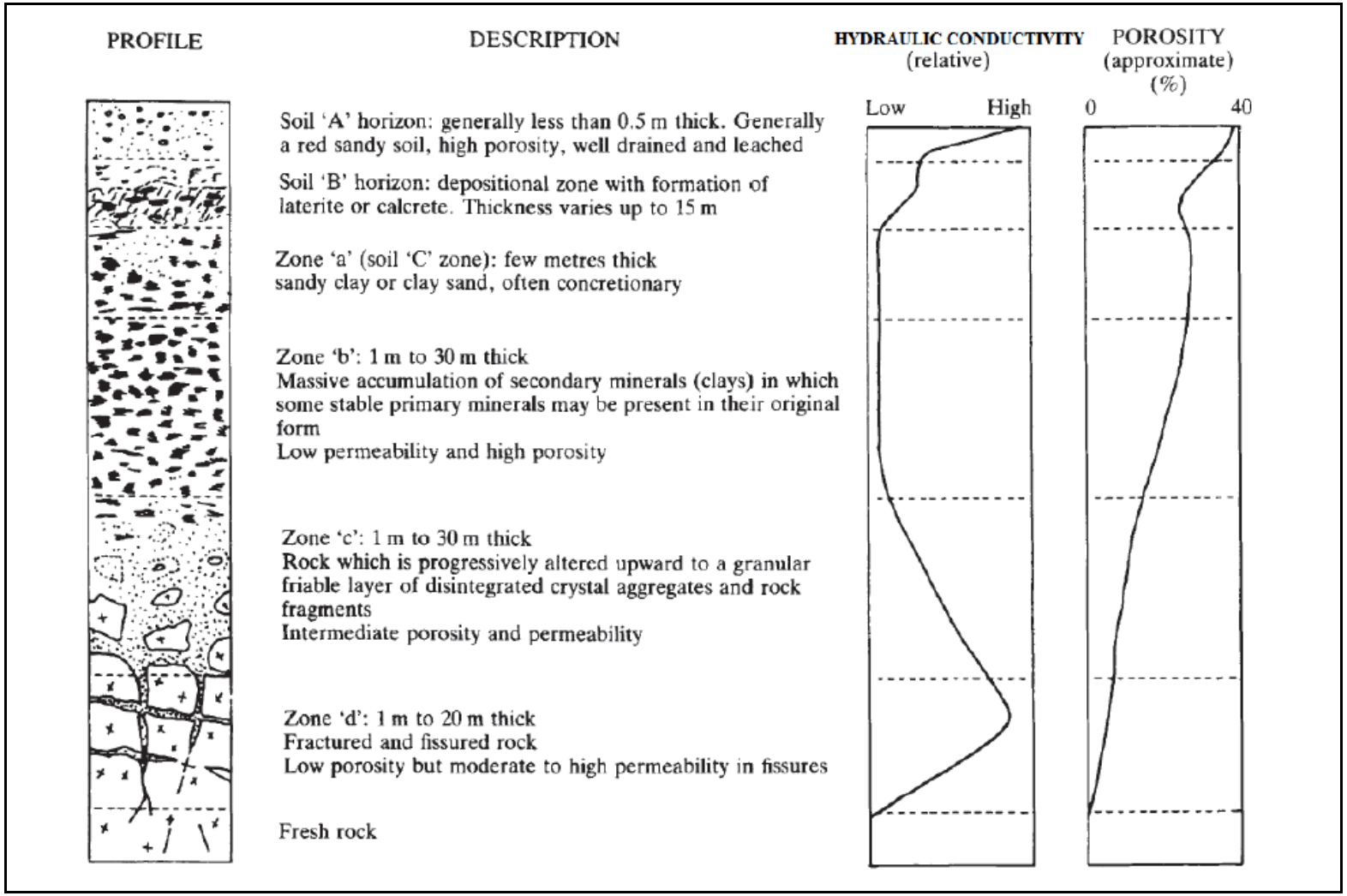

Figure II.32. Typical weathering profile on crystalline basement rock and resulting hydraulic parameters (modified after Acworth, 1987)

It stems from the inversion and interpretation of the VES that, overall, the structure of the subsurface in the study area comprises a clay-rich regolith with highly variable thickness and resistivity values which is contrastingly underlain by a more resistive basement. The geoelectrical signatures of the regolith and the basement reveal a complex and variable sequence of 3 to 6 geoelectrical layers.

Shallow auger soundings performed along with the different VES, coupled with field observations, provide some lithological constraints which enable to infer the lithological and the attendant hydrogeological structure of the subsurface. The complexity and the variability of the layer sequence, even on the same investigation site, reflect the complexity of the pedological, geomorphological and tectonic processes which are typical of basement complexes, especially when catalysed by a humid tropical environment (Chilton & Foster, 1995).

The study area is underlain by Precambrian metasediments mainly composed of quartzites, phyllites, micaschists, schists, psammites, psammoschists (micaceous sandstones), quartzophyllades which are intruded by a series of magmatic intrusions, chiefly of granitic and pegmatitic nature with sparse minor basic intrusions. These rocks are forming the basement.

The weathered overburden or regolith is composed of a series of 2 to 5 geoelectrical layers which, alongside the fresh basement, form a sequence which conforms to the typical weathering profile of basement rock environments: an evident succession of the fresh basement, the weathered/fractured basement, the strongly weathered basement (e.g. Figure II.24), a mixture of clay, sand, gravel and rock fragments, and various top soils. This typical weathering profile is characterised by an overall tendency of upwards decreasing resistivity, which mirrors the upwards increasing intensity of weathering. Hence, the top layer of the weathering profile, in which the groundwater table lies, is generally characterised by fine-grained weathering products, wherein the clay fraction is dominant, and which acts as the semi-confining layer. This upwards decrease of the grain-size in the

weathered overburden, which results in semi-confined to confined conditions, has been already pointed out by previous studies (e.g. Taylor & Howard, 1999; Acworth, 1987).

This typical weathering profile is topped by a soil layer with a variable thickness (0.2-3 m) and resistivity (7-600 Ωm) which may sometimes blur this characteristic upwards decrease of the grain-size. The wide range of resistivity values within the top soil reflects the lithological heterogeneity of this layer which comprises variable proportions of clay, sand, gravel, laterite, and rock fragments, resulting from a combination of pedogenetic, alluviation and colluviation processes.

The weathered overburden overlies the basement which is formed by two distinct parts: the weathered/fractured and the fresh basement. The interpretation of the different VES seems to indicate that resistivity values ranging between 150 Ωm and around 500 Ωm correspond to a basement weathered or fractured at different degrees. Higher values of resistivity (>500 Ωm) suggest the fresh basement. The different interpretative cross-sections corroborate this subdivision and reveal that, depending on the maximum electrode spacing, only the weathered/fractured part of the basement may be reached and thus appears to have an infinite thickness. On the other hand, the absence of the weathered/fractured part of the basement in the interpretation of many VES data may pertain to the principle of suppression, according to which, the large contrast in resistivity between the bedrock and the regolith may mask the presence of layers of intermediate resistivity corresponding to the weathered/fractured basement (Ghosh, 1971 in Batte *et al*., 2008).

From the hydrogeological point of view, the above discussion suggests that the aquifer system may comprise two superimposed parts, namely the weathered overburden and the partially weathered/fractured part of the basement. The thickness of the whole weathered cover varies from 3 m (G15–VES 110) to 95 m (A10- VES 502). The groundwater table as revealed by shallow auger soundings is found at a depth varying between 1.4 m (A11) and 9 m (A8). As for the typology of the aquifers, a thorough analysis of the geoelectrical structure of the subsurface coupled with the lithological information from auger soundings shows that confined to semi-confined conditions prevail. Indeed, a number of interpretative

geoelectrical cross-sections show that the static water level lies within the uppermost part of the weathering profile where fine-grained materials predominate, as evidenced by the low values of resistivity (3- 28 Ωm). Despite the apparent clayey nature of this layer, which may be inferred from the low resistivity values, the auger soundings show that this water table layer contains a small proportion of sand and/or gravel.

By combining all geological information, the lithological information from shallow auger soundings (AIDR, 1984 & GEOSCI, 2001), the interpretation of the VES and the stratigraphy of hand-dug wells (Tandamba, 2008, personal communication), the hydrogeological structure of the basement aquifer in the study area can be summarized into the following conceptual hydrogeological model which confirms confined to semi-confined conditions (Figure II.33).

The aquifer structure is composed of two stratiform and superimposed units, i.e. the weathered overburden and the fractured/weathered part of the basement. The weathered overburden aquifer which derives from a profound weathering of the underlying fractured/weathered basement is formed by a mixture of clay, sand, gravel and rock fragments with a clear upwards increase of the fine-grained fraction as revealed by the values of resistivity and corroborated by lithological information from auger soundings. At the top of the weathering profile, with the increasing intensity of the weathering, a distinct clay-rich layer occurs wherein the groundwater table lies and which acts as the (semi-)confining layer. The productivity of the weathered cover aquifer depends on the depth of the well. Shallow wells completed in the more clayey part of the weathered overburden will be less productive and may run dry from time to time, whereas those which penetrate into the coarser part of the weathering profile will be more productive.

The weathered overburden aquifer is prolonged within the fractured/weathered basement which is characterised by relatively low values of resistivity as compared to the fresh bedrock. This unit, which is revealed by the interpretation of the VES, has been struck neither by the auger soundings nor by the hand-dugs wells in the study area. The presence of fractures within the weathered/fractured basement implies higher transmissivity and may

increase the yield of wells which would tap this part of the basement. This fractured/weathered basement overlies the fresh basement whose higher values of resistivity seem to preclude any prospect of viable aquifer.

However, it should be understood that this model represents the general configuration of the hydrogeological structure of the study area, which is a simplification of more complex situations which may arise from the complexity and variability of the factors presiding to the weathering and subsequent formation of aquifer systems. For instance, the geoelectrical transects A11, G12, G20 and G21 show thick and complex sequences of 5 to 6 geoelectrical layers, characterised by an alternation of higher and lower resistivity values which point to an alluvial origin.

From the proposed hydrogeological model, it becomes easy to understand the seasonal failure or the intermittence of some wells as observed in the study area. First of all, it is important to note here that in the whole study area, the shallow hand-dug wells have a depth varying between 5 m and 17.5 m. Three hydrogeological conditions can be therefore distinguished.

The first hydrogeological situation corresponds to areas where the weathered cover is relatively thin and consequently part of the well is dug within the coarse part of the weathering profile (saprock) so as to ensure there is a water column of 5 m in the well (e.g. wells at Senga-Nyagisozi, Kiruhura I-Kiyanza, Muhero II-Yaranda). Indeed, due to poor knowledge in hydrogeology, people involved in the construction of wells in the study area have always considered that a water column of 5 m is sufficient whether the well is completed in low permeability materials or not (Tandamba, 2008, personal communication). Due to the high hydraulic conductivity which characterises the saprock (Figure II.32), wells which tap this part of the weathering profile are highly productive and do not run dry even during peak time of the day, when many people are fetching water. Thus, such areas offer most favourable natural conditions in the sense that the thin weathered overburden allows the hand-digging, which is a common practice in the

construction of the wells in the study area, to reach the coarser part of the weathering profile, at the base of the regolith.

The second hydrogeological condition concerns areas which are underlain by a very thick weathered overburden and shallow water table. From the fact that the shallow wells are dug by hand, it is obvious that the lack of appropriate equipments (powerful evacuation pumps) will progressively hamper the work of excavating below the water table and eventually prevent the deepening of the well down to the bottom of the weathered cover, which shows more coarse materials with good hydraulic conductivity (Figure II.31). In such circumstances, the aquifer being tapped in its most clayey part (Figure II.31) with its attendant low hydraulic conductivity, is likely to run dry, at some peak time of the day when many people are fetching water (e.g. wells at Marembo-Marembo; Kigoma-Busoni, Kinyamateke-Nyabikenke). This is quite frequent in the study area and people are therefore obliged to wait until the well is replenished again.

The third instance is illustrated by areas where the wells tap the maximum thickness of the weathered mantle including the lower part with abundant coarse weathering materials. This hydrogeological situation may arise when the groundwater table is deep and thus the wells are dug deeper such that they tap the whole regolith and part of the fractured basement, which, thanks to its high hydraulic conductivity, increases the yield. Similarly to the first situation, such wells are highly productive and do not run dry even during peak time of the day (e.g. wells at Cimbogo-Gatete II, Gaturanda-Bugabira).

Of the three hydrogeological conditions discussed above, the second and third situations depict a thick weathered overburden and consequently a thick aquifer, which implies a high natural groundwater potential. The problem of some wells constructed in such hydrogeologic conditions, which, despite the high groundwater potential, function intermittently, simply resides in the fact that those wells are not deepened enough such that they can tap the coarser part of the weathering profile with a high hydraulic conductivity, at the base of the regolith.

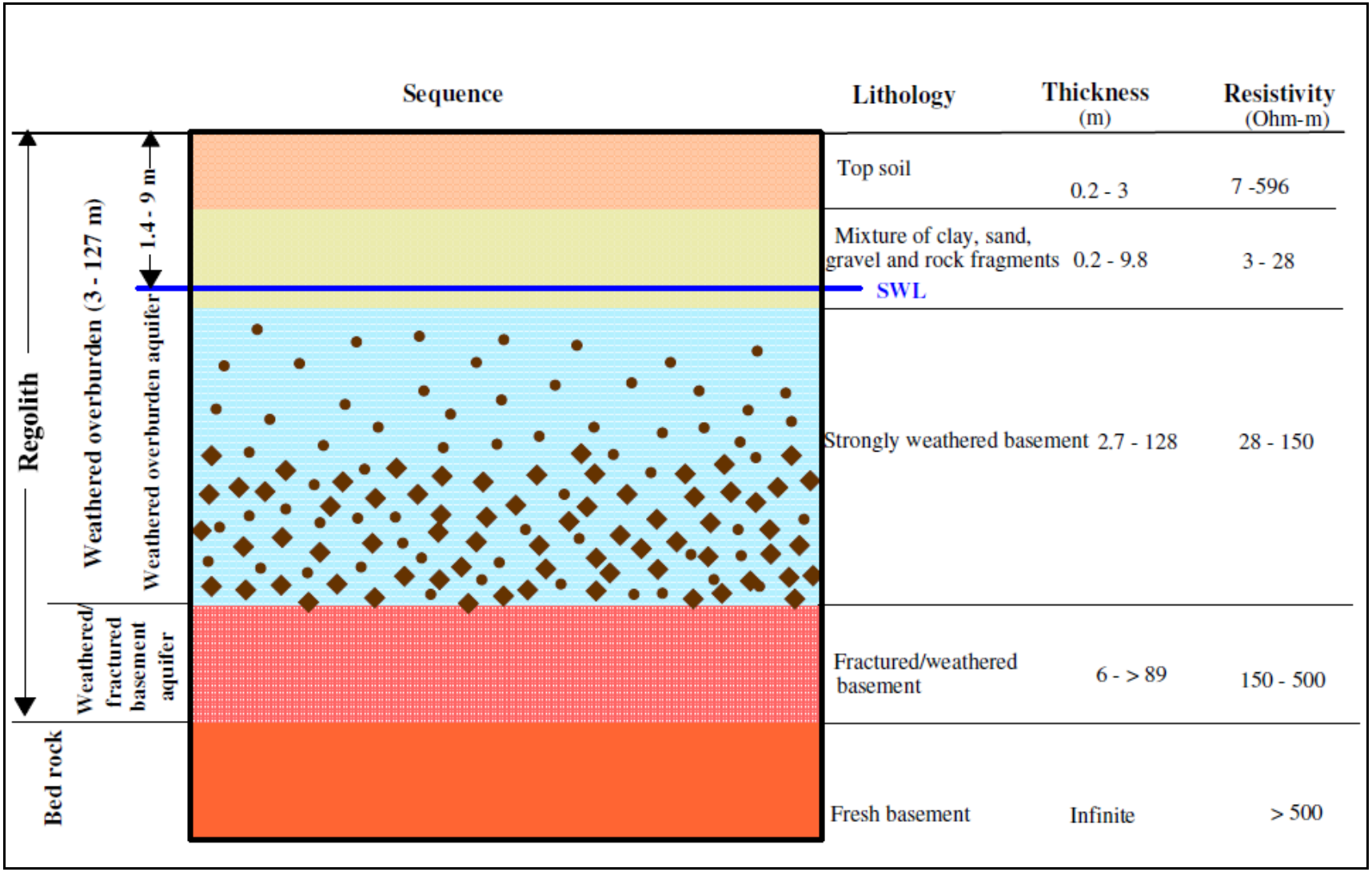

Figure II.33. Conceptual hydrogeological model showing confined to semi-confined conditions

Figure II.34 shows the estimated average depth to the fresh basement, which gives an indication of the aquifer potential across the study area. Indeed, the depth to the fresh basement indicates the total thickness of the weathered overburden and the fractured/weathered basement, which determines the groundwater potential in basement rock environments. In such environments, the existence of a thick zone of weathered overburden and weathered/fractured basement above the fresh basement indicates that important quantities of recharge water can be stored and eventually exploited through wells. Overall, it can be noted that, except the alluvial deposits which are characterised by extremely large thicknesses, the Undifferentiated Complex which is made up of granitic and pegmatitic intrusions shows the highest average thicknesses for the potential aquifer (25- >85 m), i.e. the weathered overburden and the fractured/weathered basement, and therefore offers the highest aquifer potential in the study area. The fractured/weathered basement, whose thickness varies between 6 m and more that 89 m, appears to be thicker in areas where the weathered overburden is thin (e.g. transect G15 & transect G22), which means that, in such conditions, the bedrock is not well hidden from weathering processes.

Figure II.35 which depicts the spatial distribution of the average thicknesses of the weathered overburden (without the fractured/weathered basement) confirms that, despite a wide variability (12-85 m), the Undifferentiated Complex shows the highest thickness of the weathered overburden, which increases the groundwater potential of this geological formation. Indeed, a thick weathered overburden forms an important reservoir in which infiltrating rain water can accumulate and which, when superimposed over a fractured/weathered basement, plays a capacitive role, delivering water to wells through the more transmissive fractured/weathered basement. A thin weathered overburden may result from the erosion which strips away part of the weathered overburden.

The metasediments surrounding the Undifferentiated Complex and particularly the Formation of Nyagisozi which is topped by psammites (transect G16) show the lowest value for the average thickness of the weathered cover and the fractured/weathered basement and therefore offer limited prospects for aquifer potential.

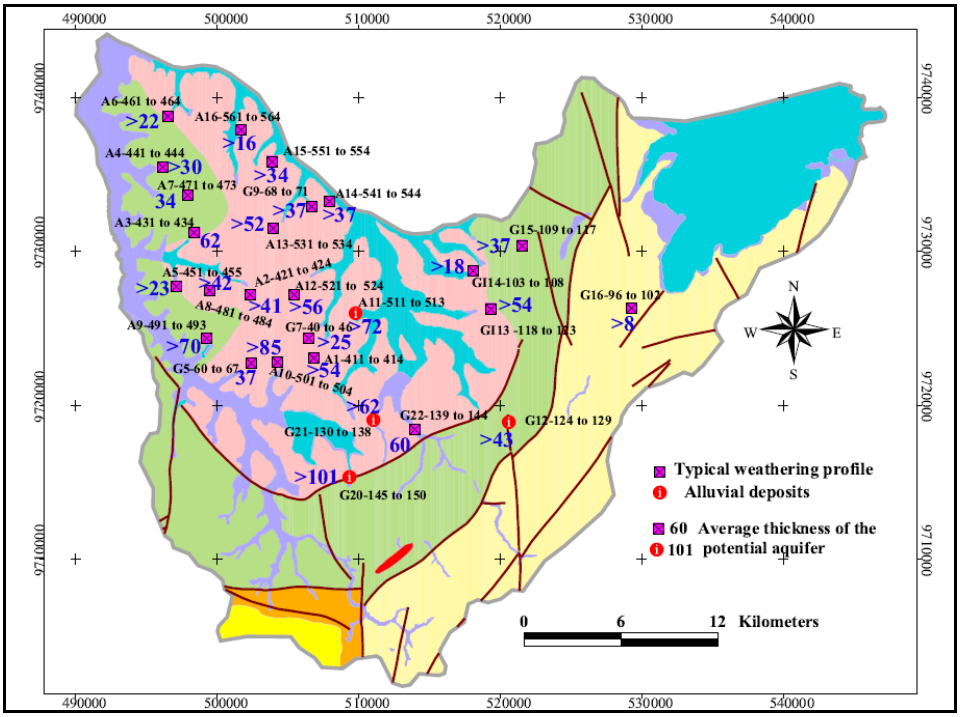

Figure II.34. Average thickness of the potential aquifer (weathered overburden + fractured/weathered basement)

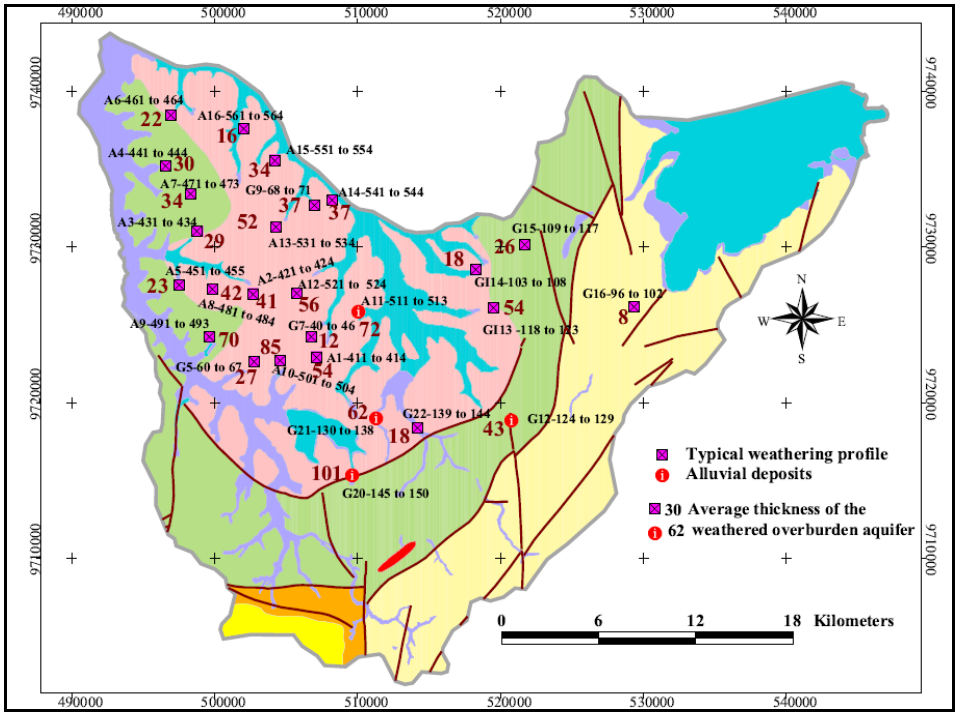

Figure II.35. Average thickness of the weathered overburden aquifer

II.3. Conclusions and recommendations

Geologically, Burundi is part of the Karagwe-Ankole belt, a Mesoproterozic belt which comprises two structurally contrasting domains: the Western Domain (WD) and Eastern Domain (ED) which are separated by a boundary zone consisting of a 350 km-long alignment of mafic and ultramafic intrusions also known as the Kabanga-Musongati ultramafic and mafic belt. Burundi is predominantly underlain by folded Precambrian metasedimentary and metavolcanic rocks, which are abundantly intruded by S-type granitoids, mainly in the WD, and subordinate mafic rocks. In southeastern Burundi, shallow water sediments associated with mafic rocks form the Neoproterozoic Malagarazi Supergroup. Cenozoic formations are mostly represented by the sediments filling the graben of the Lake Tanganyika, the basaltic flows outcropping in northwestern Burundi and to a lesser extent by the different surficial soils, Neogene sediments and peat bogs.

The study area, which entirely belongs to the WD, is predominantly underlain by Precambrian crystalline rocks which mainly consist of metasedimentary rocks (micaschists, schists, psammites, psammoschists (micaceous sandstones), quartzites, quartzophyllades and conglomerates) and magmatic intrusions (granitoids, pegmatites and sparse mafic intrusions). Cenozoic formations comprise various types of soils and alluvium in valley bottoms and lower terraces.

From the hydrogeological point of view, the geological setting of the study area falls well within the African crystalline basement complexes, also known as shields, which form nearly 90 % of the land surface in Burundi. Nowadays, several researchers agree that the hydrogeological structure in basement rock environments comprises two stratiform and superimposed aquifers: the regolith playing a capacitive role and the underlying weathered/fractured part of the bedrock which may assume a transmissive function. The development of such a structure is governed by several factors whose variation in time and space may account for the heterogeneous hydrogeological characteristics of this type of aquifers and the variability of yield, even over short distances.

The interpretation of the different VES and the inferred interpretative cross-sections reveals that the subsurface structure of the study area comprises a complex sequence of 3 to 6 geoelectrical layers, which can be broadly grouped into two clearly contrasting units, namely the weathered overburden and the basement. The variability of the number of geoelectrical layers may be ascribed to the lithological complexity and heterogeneity which are typical of basement rock environments.

These geoelectrical layers are organised in complex sequences which however show a general upwards trend of decreasing grain-size in the weathering materials, which is corroborated by a similar upwards decrease of resistivity. This typical weathering profile which is characteristic of the study area, reflects an upwards increasing intensity of the weathering which has already been described in similar geological environments. Hence, except 4 geoelectrical transects which show sequences of geoelectrical layers comprising alluvial deposits, all other geoelectrical transects show sequences of layers which conform to this typical weathering profile. This typical weathering profile is capped by a highly variable top soil, which derives from pedogenetic processes and other geomorphologic processes. The wide range of resistivity values for the different geoelectrical layers comprising the weathered mantle mirrors the variability of the lithological composition which can change from highly clay-rich materials with low resistivity (3-28 Ωm) to mixtures of clay, sand, gravel and rock fragments in variable proportions with resistivity values ranging between 28 Ωm and 150 Ωm. The weathered overburden is important as it forms the aquifer which is tapped by the shallow hand-dug wells investigated in this study.

The basement is characterised by remarkably high values of resistivity which vary over a wide range. Low resistivity values (<500 Ωm) for the bedrock correspond to the weathered/fractured part of the basement whereas higher values of resistivity (> 500 Ωm) indicate relatively fresh basement.

By combining all the geological information available for this study, the hydrogeological structure of the basement aquifer in the study area can be summarised into a conceptual hydrogeological model from which semi-confined to confined conditions can be inferred. The aquifer is composed of a mixture of clay, sand, gravel and rock fragments in variable proportions which represent the advanced stage of weathering of the fractured/ weathered basement. This upwards increasing intensity of weathering results in the occurrence of a distinct clay-rich layer at the top of the weathering profile in which the groundwater table lies and which acts as the (semi-)confining layer. The regolith aquifer is underlain by the fractured/weathered basement, which is characterised by relatively low values of resistivity compared to the fresh bedrock (Figure II.32). This weathered/fractured basement, which may form the second aquifer, is in continuity with the weathered overburden aquifer. The presence of a fractured/weathered basement, even of small thickness, when coupled with a thick saturated regolith may tremendously increase the groundwater potential of an area. These findings are supported by the hydrogeological structure of some wells recently constructed under a BTC-funded project which show that some wells are completed in the

coarser part of the weathering profile, at the base of the weathered overburden (Figures II.14 & II.15).

The depth to the fresh basement, which corresponds to the total thickness of the weathered overburden and the fractured/weathered basement, gives an interesting clue as regards to the groundwater potential across the study area. The existence of a thick zone formed by the weathered overburden and the fractured/weathered basement is suggestive of an increased storage capacity, mainly in the weathered overburden, for the aquifer and thus the availability of groundwater resource. The spatial distribution of the average depth to the fresh basement across the study area indicates that, with the largest thicknesses of the two components of the aquifer system, the Undifferentiated Complex is endowed with the highest groundwater potential in the study area, while in the metasedimentary formations, prospects of groundwater resources appear to be limited.

This study recommends to perform a VES at prospective sites for well construction, which would focus on exploring the groundwater potential of both the weathered overburden and the fractured/weathered basement. Deepening wells up to the fractured/weathered part of the basement can indeed help increase the yield of the wells as this part of the weathering profile is endowed with a high hydraulic conductivity.

CHAPTER III. HYDROLOGY AND GROUNDWATER BALANCE

III.1. Introduction

Water is continuously flowing between its different reservoirs through an endless process called hydrological cycle which is powered by solar energy. The latter triggers the vaporisation of water from surface water bodies on the earth (oceans, lakes and rivers), and from soils and plants (Sophocleous, 2004). Water vapour rises into the atmosphere where it cools, condenses and eventually returns anew to the earth in the form of rainfall, hail or snow. Precipitation constitutes the largest flow of water and the source of virtually all freshwater in the hydrologic cycle. Precipitation falls nearly everywhere, but with a highly variable distribution (Winter *et al.*, 1998). Part of the precipitation will reach streams and rivers as overland flow but also through subsurface routes such as interflow and baseflow. Another fraction of the precipitation infiltrates deeply into the ground where it replenishes underground water bodies called aquifers. This process which is also termed natural groundwater recharge marks the entrance door to the groundwater component of the hydrological cycle. Natural discharge from aquifer systems will eventually feed streams, rivers, wetlands, lakes and oceans (Chilton & Seiler, 2006). Hence, computing the water balance for a hydrological entity consists of quantifying the different components of the hydrological cycle within that entity.

Surface water catchments and underground aquifers form an interlinked hydrological system which is connected to the water-dependent ecosystems. Therefore, while studying the water balance of a hydrological basin, it is important to consider and quantify surface water-groundwater interactions in three possible ways (Winter *et al.*, 1998):

- In arid and semi-arid areas, groundwater may be recharged by surface water bodies such as streams, rivers and lakes, which lose water to the groundwater seepage through their beds.
- In humid zones, surface water bodies may gain water from inflow of groundwater through the streambed. River flow measurements are often the best data available for resource analysis, and integrate the catchment's behaviour.
- In some other environments, flow direction can vary along a river course: some reaches receive groundwater outflow while others lose water to the groundwater system. Furthermore, flow direction can change in very short timeframes as a result of individual storms causing focused recharge near the streambank, temporary flood peaks moving down the channel, or transpiration of groundwater by streamside vegetation.

III.2. Background: hydrological features of Burundi

Overall, Burundi is endowed with abundant water resources compared to most African countries. Owing to its geographical situation, Burundi receives abundant rainfalls which feed its surficial as well as its underground water resources. However, water resources are unevenly distributed throughout the country. While highland regions like Mugamba, Mumirwa and Bututsi are well gifted with abundant spring water (specific flows exceeding 0.3 l/s/km^2), low-lying regions such as Imbo, Kumoso and Bugesera are, by far, the most underprivileged. In these regions, the lack of natural springs compels the inhabitants to resort to surface water which is not always potable or groundwater which they access through hand-dug wells or boreholes.

The hydrological and hydrogeological knowledge in Burundi is still at the lowest level. Hydrogeological data are sparse. To date, there have never been countrywide hydrogeological investigations to appraise the quality, quantity and spatial distribution of groundwater resources. However, according to the National Water Master Plan (TBW Ingénieurs Conseils, 1994 & 1998), the total discharge from natural springs across the country amounts approximately to 6600 l/s which correspond to 208.14 Mm^3/year. As for surface waters, the mean discharge rate of water courses is estimated at 319 m^3/s, which represents 10060 Mm^3/year. Table III.1 shows the hydrological balance of the whole Burundi for an average year. It can be noticed that, for an average annual precipitation amounting to 1274 mm, the main components of the hydrological balance, namely evapotranspiration, groundwater recharge and surface runoff, represent respectively 68 %, 23 % and 9 % (Table III.1).

Table III.1. Hydrological balance for an average year (AQUASTAST, FAO INFO 2005, modified)

Precipitation	**Evapotranspiration**	**Groundwater recharge**	**Runoff**
1274 mm/year	872 mm/year	299 mm/year	103 mm/year
1011 m^3/s	692 m^3/s	237 m^3/s	82 m^3/s
100 %	68 %	23 %	9 %

The dense network of rivers and streams in Burundi belongs to two major continental catchments which share almost equitably the country's surface area with 13800 km^2 for the Nile Basin and 14034 km ^{2} for the Congo Basin (Figure III.1). Watersheds in Burundi are classified into five hierarchical levels (TBW Ingénieurs Conseils, 1994 &1998). The two major watersheds in Burundi, i.e. Congo and Nile basin form the first level. In the North, they are separated by the Congo-Nile Ridge, a North-South trending mountain range which serves as a major water divide.

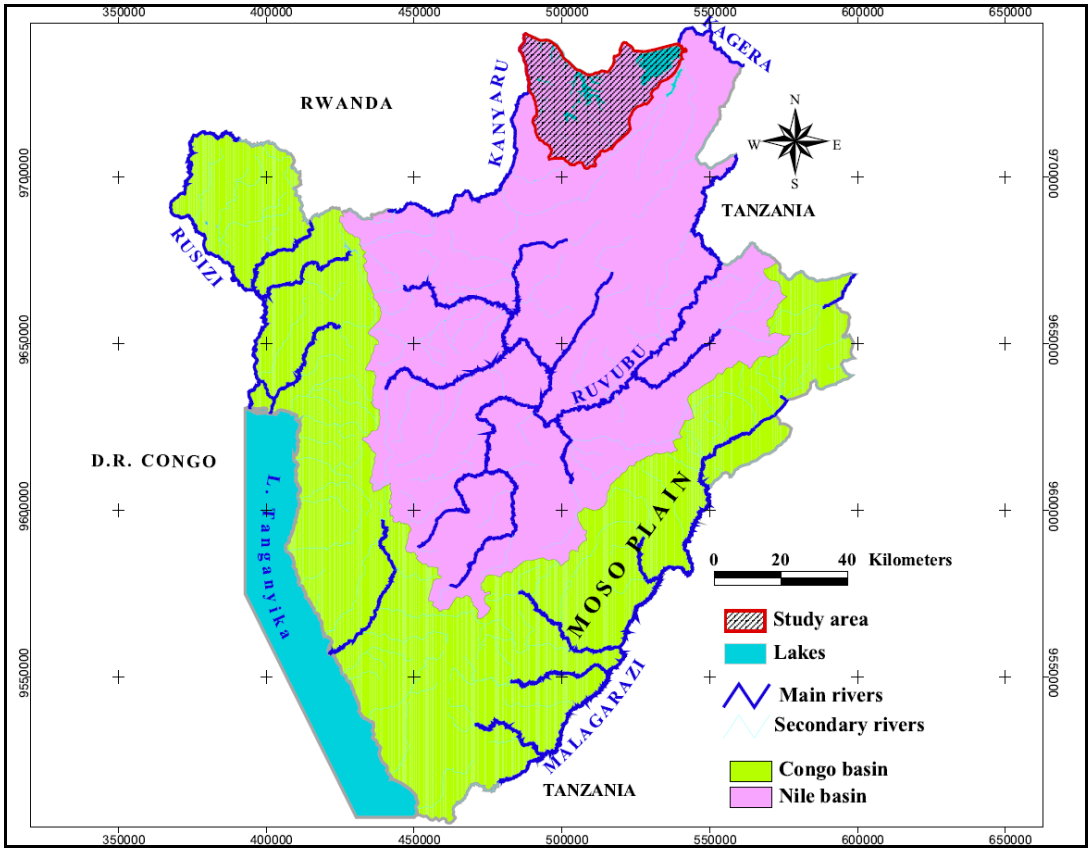

Figure III.1. Main hydrological basins in Burundi

The Congo Basin comprises water courses situated to the West of the Congo-Nile water divide and the Plain of Moso in eastern Burundi. All these water courses flow to the Lake Tanganyika which in turn drains into the River Congo through the River Lukuga in Democratic Republic of Congo. Lake Tanganyika is known to be the second deepest lake (1477 m) in the world after Lake Baikal in Russian Federation. With a total volume of 20000 km^3 of which 1820 km^3 belong to Burundi, Lake Tanganyika constitutes an important reserve of freshwater.

Three subbasins can be distinguished within the Congo Basin: 1) the one in which water courses flow directly to the Lake Tanganyika, (2) the sub-basin of the River Rusizi, and (3) the subbasin of Kumoso located in the East of the country wherein Malagarasi River and its tributaries flow (Figure III.2). These three basins form the second level in the hierarchical classification of watersheds. The total discharge in this basin amounts to 182 m^3/s which represents 57 % of the total surface water for the country.

The Nile Basin includes water courses flowing to the East of the Congo-Nile Ridge except the Plain of Moso. This basin is mainly drained by the rivers Ruvubu and Kanyaru which

are both tributaries of the River Kagera. The Nile Basin comprises 3 subwatersheds of the second level namely Ruvubu, Kagera and Kanyaru (Figure III.2). It is worth to mention here that the southernmost source of the Nile River is located in southern Burundi where it coincides with the source of the Ruvyironza River, a tributary of Ruvubu River. Kagera River is the main tributary of Lake Victoria which is the source of the White Nile. The total discharge of the Burundian part of the Nile basin is 137 m^3/s, which represents 43 % of the total surface water resources of Burundi (TBW Ingénieurs Conseils, 1998) (Table III.2).

Table III.2. Surface water in Burundi (TBW Ingenieurs Conseils, 1998)

Basin	**Burundi**	**Average discharge**	
	Area (km^2)	**m^3/sec**	**l/sec/km^2**
Congo	14034	182	15.4
Nile	13800	137	10.4
Total	27834	319	12.9

With an estimated length of 6800 km, the Nile River is the longest river in the world, flowing from South to North over 35 degrees of latitude to its mouth on the Mediterranean Sea. With an area of 3254555 km^2, the basin drains about 10 percent of the African continent (Figure III.3).

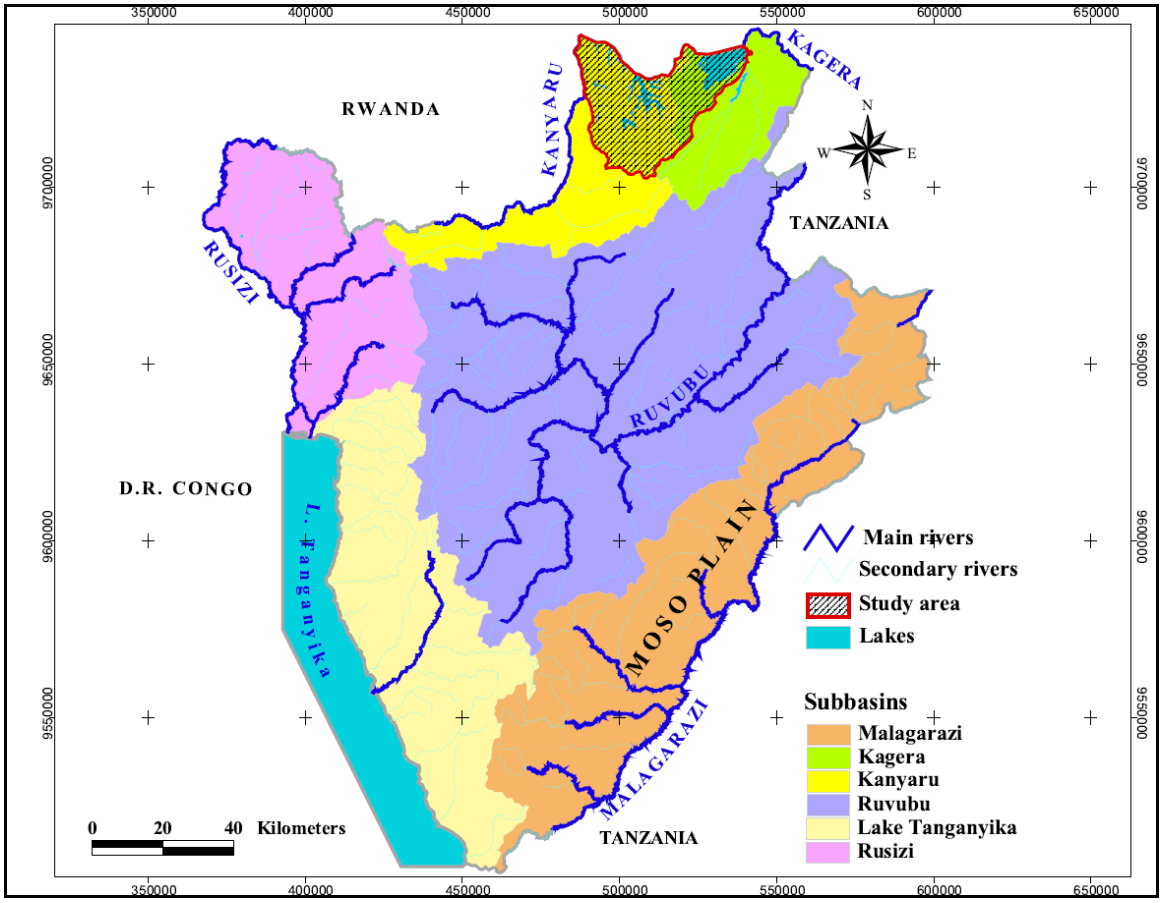

Figure III.2. Subbasins in the two main basins

Figure III.3. Nile River Basin (Abrams, 2001)

III.3. Hydrology of the study area

One of the most striking features of the Bugesera depression on either side of the border between Rwanda and Burundi is the existence of a complex of interconnected swamps, rivers and lakes within an environment yet characterized by an overall weak drainage density. The latter ranges from 0 to 0.42 km per km^2 within the depression of Bugesera, while in surrounding highlands it varies between 0.67 to 1.28 km per km^2 (Cambezy, 1981 as quoted by Ntakimazi, 1985). According to Ntakimazi (1985), the depression of Bugesera may receive water masses from well watered highlands in Burundi and Rwanda through Kanyaru and Nyabarongo rivers.

III.3.1. Main subwatersheds

The study area extends over two subbasins of the second level namely Kanyaru and Kagera (Figure III.2). The two subbasins comprise five subwatersheds of the third level which are Nyavyamo, Kanyaru 9, Cohoha South, Cohoha North, and Rweru (Figure III.4). The subbasins Kanyaru 9, Cohoha South, Cohoha North, and Nyavyamo belong to the Kanyaru subbasin while only Rweru subwatershed is included into the Kagera subbasin. Table III.3 presents the characteristics of the five watersheds of the third level among which the perimeter, area, elevation and slope. With an area of 314.8 km^2 and a perimeter of 258.7 km, Cohoha South is the largest subbasin in the study area. The smallest one is the portion of Cohoha North which has an area of 16.1 km^2 and a perimeter of 21.48 km. This lake is located in Rwanda and only a small portion of its watershed extends in Burundi. The maximum elevation (1873 m) is observed in Nyavyamo subwatershed whereas the minimum elevation (1321 m) is found in Lake Rweru subwatershed. This maximum elevation corresponds the Mutumba mountain which is located in the southwest of the study area. The elevation data were derived from an SRTM DEM (Jarvis *et al.*, 2006), which was first reprojected into the projection system of Burundi which makes use of a special datum Arc 1950 (for Burundi). The maximum slope (64.2 %) as well as the highest mean slope (13.5 %) is observed in Nyavyamo subbasin. The minimum slope of 0 % corresponds to the narrow plains surrounding the lakes or the marshy valleys.

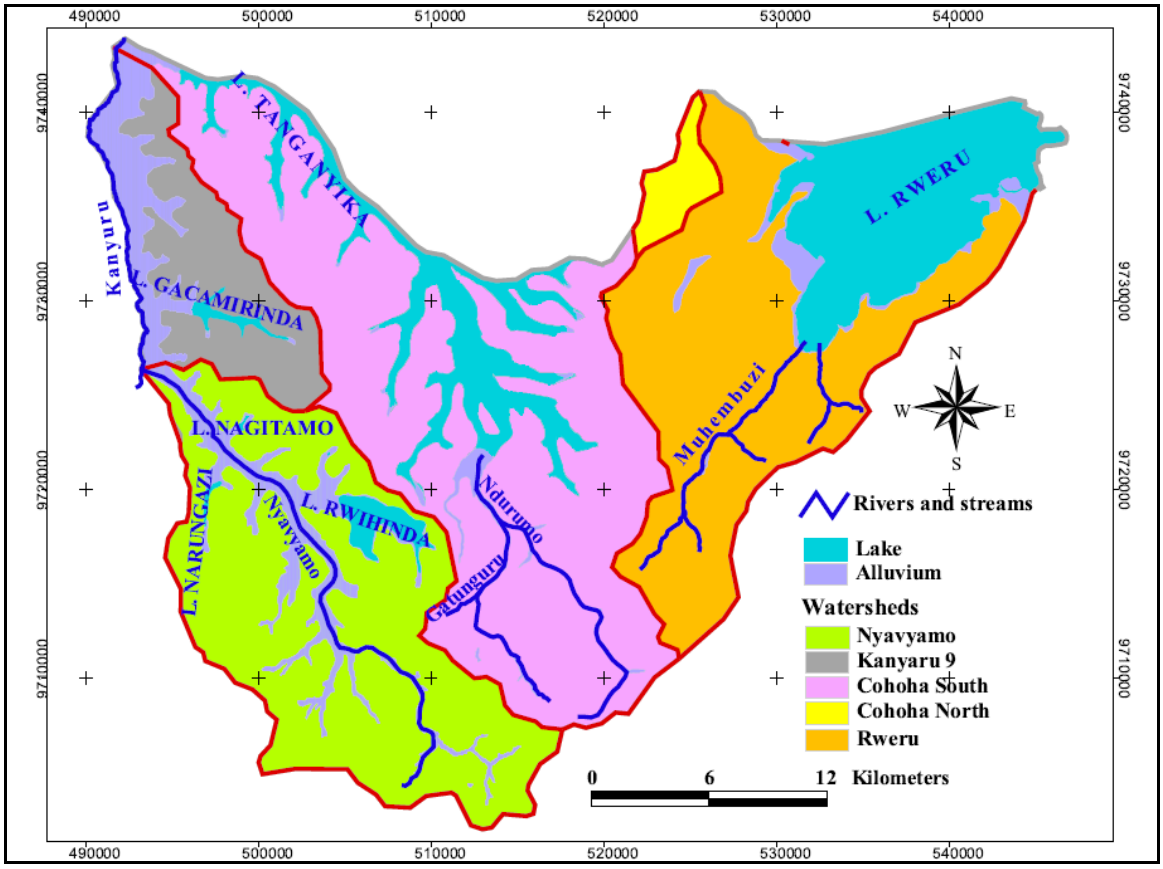

Figure III.4. The main subwatersheds in the study area

Table III.3. Main subwatersheds and their characteristics in the study area

Subwatershed	Perimeter (km)	Area (km^2)	Elevation (m)			Slope (%)		
			Max	Mean	Min	Max	Mean	Min
Kanyaru 9	53.2	98.4	1535	1397.6	1346	35.7	9.5	0
Cohoha South	258.7	314.8	1800	1446.1	1344	61	12.3	0
Cohoha North	21.5	16.1	1566	1440.4	1358	21.8	7.7	0.2
Rweru	119	218	1752	1452.4	1321	56.6	13.1	0
Nyavyamo	82.9	253.1	1873	1446.9	1352	64.1	13.5	0

III.3.2. Rivers

The whole Bugesera region (Burundian and Rwandan portions) is girdled by three major rivers namely Kanyaru, Nyabarongo and Kagera, which are connected to lateral shallow lakes and marshy valleys (Figure III.5).

- **Kanyaru River**: with an overall South-North but meandering course, this river constitutes the western boundary of Bugesera depression where it maintains lateral ties with a number of small lakes through strips of swampy valleys. After crossing the Rwandan border, the River Kanyaru continues to flow northwards in a swampy valley until its confluence with the Nyabarongo River. There is no hydrometeorological station on Kanyaru River but according to estimates made by TBW Ingénieurs Conseils (1994), the annual average discharge of this river at the exit of Burundi territory would amount to 39 m^3/s.
- **Nyabarongo River** originates in southwestern Rwanda and flows over 300 km until the close vicinity of Lake Rweru, in southeastern Rwanda, from where it changes its name to Kagera. The River Nyabarongo does not discharge into Lake Rweru but is connected to the latter through a narrow channel. Nyabarongo River forms the northern border of the Bugesera depression on the Rwandan side. Long term records of discharge (1971-1988) of the discharge of this river at Kanzeze hydrometeorological station (Bugesera, Rwanda) give an average discharge of 4 km^3/year which corresponds to 127 m^3/s (BLR Ingénierie, 2008). This value is not significantly different from the average discharge of 108 m^3/s indicated by Ntakimazi (1985) for the same river and for the period 1956-1973.
- **Kagera River** drains a basin area of 59800 km^2 distributed among the countries of Burundi (22 %), Rwanda (33 %), Tanzania (35 %) and Uganda (10 %) (Nzeyimana, 2003)**.** It acts as an outlet of the fluvio-lacustrine complexes of Bugesera. Indeed, from the outlet of Lake Rweru (Figures III. 5 & III.6), Nyabarongo River takes the name of Kagera and makes a turn to the East where it meanders through a large swampy valley untill it meets the River Ruvubu at about 2 km ahead of Rusumo Falls. Downstream Rusumo Falls, Kagera River flows northwards in a large papyrus swamp of the Kagera National Park where it forms the border between Rwanda and Tanzania over about 230 km. At the northeastern tip of Rwanda, Kagera meets the Kagitumba River and then flows eastwards for 260 km before emptying into Lake Victoria.

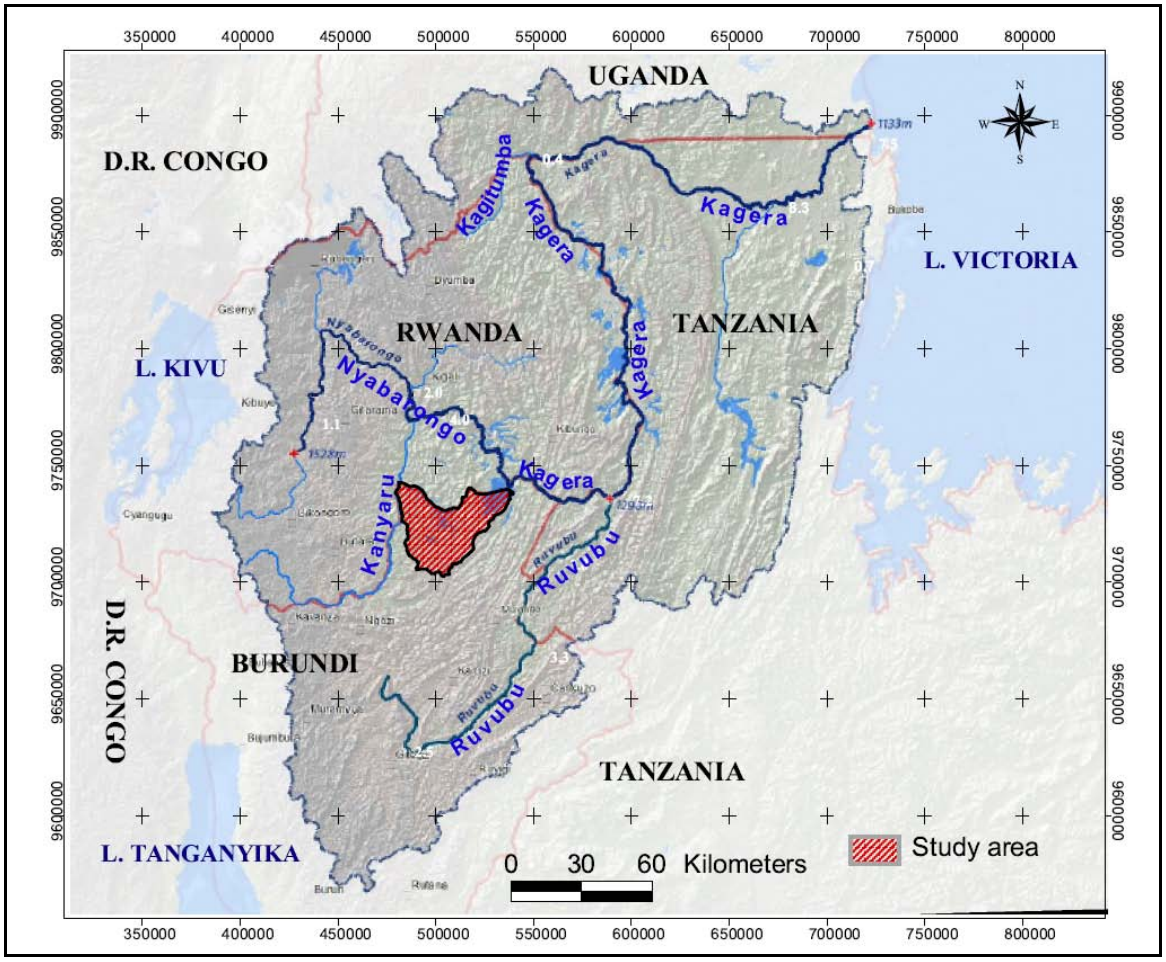

Figure III.5. Kagera Basin (BLR Ingénierie, 2008, modified by the author)

Inside the study area, several ephemeral streams originating from the southern and eastern highlands flow towards the complex of marshlands and lakes through a myriad of V-shaped valleys, mainly during the rainy season. Besides, there are 4 small perennial streams which drain the study area: Nyavyamo, Ndurumo, Gatunguru and Muhembuzi. (Figure III.4). Nyavyamo originates from the southern highlands and flows NW towards the River Kanyaru through the large swamp hosting the lakes Rwihinda, Narungazi, Nagitamo, and Nampete. Discharge measurements performed on Rurata, the main tributary of Nyavyamo by TBW Ingénieurs Conseils in September 1994 indicated a discharge rate of 0.12 m^3/sec. Ndurumo and Gatunguru also originate in the southern highlands and join to form the only tributary of Lake Cohoha south on Burundian side. Discharge measurements performed in September 1994 by TBW Ingénieurs Conseils, downstream the confluence of the two streams gave a discharge of 0.10 m^3/sec. The small stream Muhembuzi originates in the southern highlands, in the mountains of Kagege, and flows in a NE direction towards the Lake Rweru.

III.3.3. Lakes

The rivers which bound the Bugesera depression, both in Burundi and in Rwanda, are laterally connected to several shallow lakes which, as seen before, were formed when the rivers, erstwhile flowing westwards to the Atlantic Ocean, were reversed upon the opening of the western branch of the East Africa Rift System. In the western part of the Bugesera depression (Burundian side), the lakes Mwungere, Narungazi, Gacamirinda, Rwihinda, Nampete, Nagitamo and Cohoha South are connected to the Kanyaru River through swampy valleys. The lakes Narungazi, Rwihinda, Nampete and Gitamo are located in the same swampy valley, namely Nyavyamo. Lake Mwugere is located outside the study area, in the southwest. In the eastern part of the Bugesera depression, on the Burundian side, there are two lakes namely Rweru and Kanzigiri. The latter is a sort of prolongation of Lake Rweru through a marshy valley. Lake Kanzigiri is also situated outside the study area (Figure III.6). Lake Cohoha North, which is situated outside the study area, in the Rwandan part of the Bugesera depression, has almost disappeared since 1981 due to the draining of the marshlands for agricultural purposes. Like Cohoha South, Cohoha North had also a dendritic shape and is connected to the River Kanyaru through a swampy valley which was drained in 1981. Lakes Cohoha South, Rweru and Rwihinda are the most important lakes within the depression of Bugesera, in terms of spatial extension.

Lake Cohoha South: with an area of 78.5 km^2 of which 61.3 km^2 belongs to Burundi, Lake Cohoha South straddles the border between Burundi and Rwanda. It lies between 2°20 and 2°35’ South latitude, 29°58’ and 30°11’ East longitude. The lake features a rather elongated but dendritic shape with 27 km in length and 0.4 to 2.3 km in width. Its shoreline extends over about 230 km. The depth of the lake varies between 5 and 7 m in its northwestern part while it increases between 8 to 11 m in its eastern extremity. Lake Cohoha South is typically characterized by several lateral branches which can be bifid or even several times ramified. This highly dendritic shape explains why this lake is called “*Cohoha*” in Kirundi which literally means a “*wandering*” lake. The lake is connected to the River Kanyaru through a swampy strip of about 2 km in length. It is believed that the present day Lake Cohoha South occupies the medium and low valleys of an ancient river which was flowing westwards before the formation of the western branch of the East Africa Rift System (Albertine Rift). The slope of the ancient river was reversed by the back tilting of the Bugesera area after the uplift of the eastern border of the Albertine rift. This may explain why the highest depths are found in the eastern parts of the lake (Ntakimazi, 1985).

Lake Rweru: unlike Lake Cohoha, Lake Rweru is characterised by a rather spread out but more or less round shape. Located between latitude 2°21' and 2°27' South and between longitude 30°17' and 30°24' East, the lake covers an area of 102 km^2 of which about 70 km^2 belong to Burundi. The major axis (length) of the lake, which approximately coincides with

the NE-SW direction, is about 18 km whereas its minor axis (width) measures about 14.5 km. The depth of the lake varies from 3 to about 5 m, the deepest part being situated to the North-East, close to the river Nyabarongo. The lake is surrounded by a marshy plain covered by papyrus vegetation whose spatial extension has tremendously decreased due to agricultural pressure. Lake Rweru receives water from two main perennial influents which are Muhembuzi and the outlet of Lake Kanzigiri (Ntakimazi, 1985).

Lake Rwihinda: also known as the "*lac aux oiseaux*" (birds lake) because of the wide variety of migratory aquatic birds which seasonally populate its surrounding swampy vegetation of papyrus, Lake Rwihinda is located on the northern periphery of the city of Kirundo, at an altitude of 1420 m. With an area of 4.3 km^2, Lake Rwihinda and its bordering swamps are nowadays part of the nature reserve of Lake Rwihinda (Nzigidahera *et al.*, 2005). It lies between latitude 2°32' and 2°34' South; 30°03' and 30°06'East. Oriented SE-NW, this shallow water body is 6 km in length and 2.5 km in width at its southeastern extremity. The lake drains to the River Kanyaru from its northwestern end through a tract of swampland 11 km long and 2 km wide (Hughes *et al.*, 1992).

Lake Gacamirinda covers an area of 2.4 km^2 and is surrounded by high and steep sloping hills. The lake is about 4 km long and 1 km wide. Located at latitude 2°27'S and longitude 30°01'E, this lake shows a SE-NW elongated but dendritic shape. Its southeastern end adjoins a forested hill while its northwestern edge merges into a papyrus swamp through which it drains for 4 km to the Kanyaru River (Hughes *et al.*, 1992). The lake is flanked by a narrow belt of swampy vegetation dominated by *Typha domingensis (*Nzigidahera & Fofo, 2005). Nowadays, this swampy swathe connecting Lake Gacamirinda to the River Kanyaru has been extensively drained for agricultural purposes and this is likely to compromise the future existence of this lake, as water inflows to the lake from the flooding of River Kanyaru are limited.

Lake Nagitamo is a little, but deep lake, sandwiched between the high and steep sloping hills of Kabirizi and Ntwago. Situated at an altitude of 1460 m, Lake Nagitamo covers an area of 0.18 km^2 and lies within a northern branch of the swampy valley Nyavyamo.

Lake Narungazi is another small lake situated South of Lake Nagitamo, at an altitude of 1380 m. With an N-S elongated shape, this lake is bordered by the hills of Nyange-Kiringanire and Kanyarwe-Mwunguko. With an area of 0.75 km^2, Lake Narungazi lies within a southern branch of the marshy valley of Nyavyamo. Its elongation coincides with a N-S trending fault.

Lake Nampete is just a small but deep pool of water, located within a branch of the marshy valley of Nyavyamo at an altitude of 1380 m. This branch of Nyavyamo valley is sandwiched between the crests of Cewe and Ntwago I. With an area 0.01 km^2, this lake is

the smallest of all the lakes forming the marshy and lake complex of Bugesera, on the Burundian side.

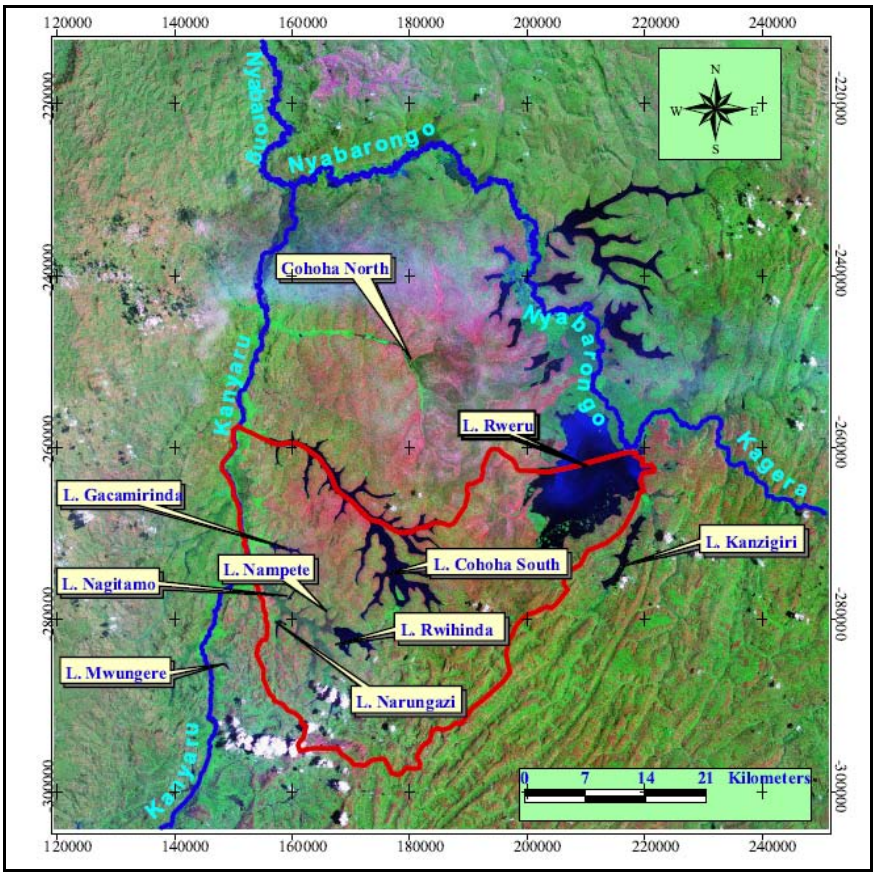

Figure III.6. Satellite image (2000) showing the marshy and lake complex of Bugesera (in UTM coordinates, zone 36)

III.3.4. Interactions between the lakes and the rivers

The marshy complexes of the Bugesera region play an important role in regulation of water level in rivers as well as in the small lakes. Indeed, during the rainy season, mainly between February and May, this marshy complex stores an important quantity of water, which is eventually released slowly to sustain river discharge during the dry season. The drainage of the storage starts in June and reaches a minimum level in October.

The small lakes communicate with the main river channels in two different ways: (1) through a distinct channel or (2) through a strip of swampy valley.

The channel connecting Lake Rweru and the River Nyabarongo illustrates the first type of communication between the small lakes and the main river channel. During low water level, i.e. in August-September, there is no surface connection between the main channel

and Lake Rweru, although the water level in the river is lower than in the lake (difference in elevation). With the short rainy season, from October to December, the water level in the Lake Rweru rises until it starts to drain into the River Nyabarongo through the narrow channel. This flow continues until the water level in the River Nyabarongo exceeds that of Lake Rweru. The flow direction in the channel is therefore reversed; the river starts to empty into the Lake Rweru. This phenomenon is observed in March and April. As the water level in the two systems keeps on increasing, the channel linking Lake Rweru and the River Nyabarongo gets overflowed and the water inundates the surrounding marshland. Eventually, as the water level declines, between June and August, the Lake Rweru starts again to drain into the River Nyabarongo, first through surface overflow and thereafter through the channel.

The second type of connection between the small lakes and the rivers occurs through a strip of marshland. Lakes Cohoha, Rwihinda, Gacamirinda, Narungazi and Nagitamo offer a good example of this type of relationship between the main river and the lateral lakes. These lakes are in communication with the River Kanyaru through a slow diffusion of water at the base of the marshy vegetation. This flow, which becomes significant only during high water stages of the river, contributes, to raise the water level in the lakes. The marshy zone serves as a sort of dike which maintains the water level in the lake when the river discharge falls into the minor bed. Hence, the current tendency to drain the marshy valleys for agricultural purposes may be fatal to these free water bodies, as this has been the case for Lake Cohoha North in 1981 (Ntakimazi, 1985).

Thus, the water level in the rivers Kanyaru and Nyabarongo strongly controls the water level in the different lakes. During the period of high river stage, which occurs generally in April-May following intense rainfall, the conveyance capacity of the river channels becomes rapidly exceeded, resulting in flooding of the marshy valleys and the small lakes. Moreover, at the confluence of the rivers Nyabarongo and Kanyaru, the high water level in the River Nyabarongo blocks the inflow of the Kanyaru River, thereby resulting in the reversal of the flow. This leads to an increased flooding of the flat reaches of the River Kanyaru, including the lateral marshy valleys and lakes.

III.4. Groundwater recharge

III.4.1. Introduction

Groundwater recharge is generally defined as the downward flow of water reaching the water table, forming an addition to the groundwater reservoir. Rushton (1988) made a clear distinction between the potential recharge and the actual recharge. Potential recharge is the

amount of water available for recharge from the soil zone but which may be transformed into runoff due to specific situations such as high water table. Actual recharge is the quantity of water that really reaches the water table. The two quantities may differ due to either the influence of the unsaturated zone or non-acceptance by the aquifer of the potential value.

According to De Vries & Simmers (2002) and Maréchal *et al.* (2008), the total groundwater recharge encompasses three main components namely: (1) direct recharge (or diffuse) recharge, (2) indirect (non-diffuse) recharge and (3) localized recharge (Figure III.7).

- Direct or diffuse recharge represents the portion of precipitation which is added to the groundwater reservoir by direct percolation through the unsaturated zone. Direct or diffuse recharge is spatially distributed and results from widespread percolation through the entire vadose zone (Sophocleous, 2004). This mode of recharge is typical of the humid climate, where regular precipitations maintain the water content to values close to the field capacity.
- Indirect or non-diffuse recharge results from the percolation of a runoff fraction through the bed of surfaces water bodies. This mechanism of groundwater recharge is characteristic of arid climates where percolation to the groundwater may occur in wadi channels.
- Localized or focused is defined as concentrated recharge from depressions, joints, cracks, sloughs, potholes, and playas (Sophocleous, 2004).

The relative proportions of these components fluctuate according to climatic conditions, geomorphology and geology (Marechal *et al.*, 2008; Xu & Beekman, 2003; de Vries & Simmers, 2002).

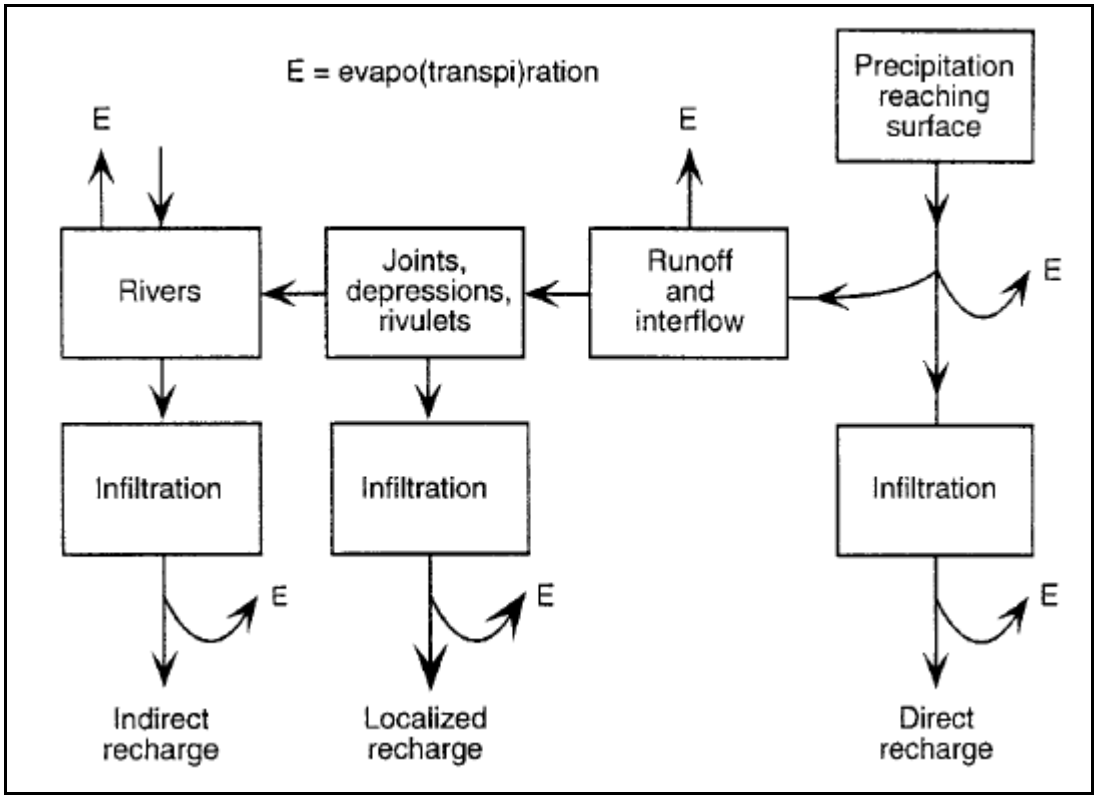

Figure III.7. Various mechanisms of recharge in (semi-) arid area (Lerner 1997 as quoted in De Vries & Simmers, 2002)

The estimation of groundwater recharge is of prime importance for safe, efficient and sustainable management of groundwater resources. In this regard, Sharma (1986) notes that management of groundwater is often carried out with little or no knowledge of recharge rates, resulting in misuse of the resource. This continuously growing interest in recharge estimation studies may find its justification in two important but often ambiguous concepts introduced in the field of water resources studies during the last century namely the safe and sustainable yields (Lee, 1915; Freeze & Cherry, 1979; Bedraft *et al.*, 1982; 1997, 2002; Sophocleous, 1997, 1998, 2000; Alley & Leake, 2004; Kalf & Woolley, 2005; Zhou, 2009).

Lee (1915) who is the pioneer in this domain defines the safe yield as the limit to the quantity of water which can be withdrawn regularly and permanently without dangerous depletion of the storage reserve. In refining the definition, Todd (1959) states that the safe yield should be the amount of water which can be withdrawn from a basin without causing undesirable results. But this definition brought in more confusion and ambiguity, as "undesirable results" can be differently interpreted. Indeed, according to Domenico (1972) for instance, the undesirable results may include the depletion of the groundwater reserves,

the intrusion of water of undesirable quality, the contravention of existing water rights, and the deterioration of the economic advantages of pumping. For Freeze and Cherry (1979), this concept should include the excessive depletion of stream flow by induced infiltration and land subsidence. Furthermore, none of the different authors suggests a clear methodology to quantify these undesirable results. Another misleading confusion and misinterpretation embodied into the concept of safe yield is to consider the development of groundwater as 'safe' as long as the rate of groundwater withdrawal does not exceed the rate of natural recharge. Indeed, under natural conditions, i. e., in absence of groundwater abstraction, aquifers are in a dynamic equilibrium wherein long-term natural discharge balances the long-term natural recharge.

$$R_0 = D_0$$

where R_0 and D_0 are the natural recharge and discharge respectively.

When groundwater development starts, the new discharge by wells must be balanced by loss of storage in the aquifer, an increase in recharge of the aquifer, a decrease in the old natural discharge, or a combination of these (Zhou, 2009):

$$(R_0 + \Delta R_0) - (D_0 - \Delta D_0) - P = dV / dt$$

where ΔR_0 and ΔD_0 are respectively the induced recharge and decrease in discharge caused by pumping, P is the pumping rate and dV/dt is the change in storage due to pumping.

Therefore, even with a pumping rate smaller than the natural recharge, the induced recharge from surface water bodies and the decrease of groundwater discharge to surface water bodies may lead to the depletion of stream flow, thereby endangering dependent ecosystems such as wetlands and riparian ecosystems. Furthermore, during pumping, the storage loss manifests itself as a cone of depression, which may cause intrusion of poor quality water and land subsidence (Zhou, 2009; Kalf & Woolley, 2004; Alley & Leake, 2004). From what precedes, it is clear that the concept of safe yield embodies ambiguities and considering development of groundwater to be safe if only the rate of groundwater withdrawal does not exceed the rate of natural recharge, is questionable, as the dynamic development of groundwater may cause adverse impacts on society, economy and natural environment. The following question may well summarize the whole issue: if one pumps all the natural recharge, where is the water for the discharge to the streams, springs and riparian ecosystems?

The concept of sustainability emerged early in 1980's, centred on the idea of using available resources at a rhythm that can be sustained over the long term. The concept was

adopted in the field of water resources to overcome the shortcomings related to the safe yield. Groundwater sustainability is defined as the development and use of groundwater in a manner that can be maintained for infinite time without causing unacceptable environmental, economic, or social consequences. The basin sustainable yield should be understood as a compromised pumping rate, which can be sustained by groundwater recharge and will not cause unacceptable environmental, economic, or social consequences.

In the light of what precedes, it is clear that without a good estimate of groundwater recharge, it is not possible to properly evaluate the impacts of groundwater abstraction as well as the long-term behaviour of an aquifer under various management schemes. In the following section, an overview of the commonly used methods for estimating groundwater recharge is presented.

III.4.2. Overview of recharge estimation methods

Groundwater recharge is a critical hydrologic parameter which, depending on the objective followed, may be estimated at various temporal and spatial scales. As a matter of fact, evaluation of water resources may require information on recharge at large spatial and temporal scales, while assessment of aquifer vulnerability to pollution needs more detailed information at local and shorter time scales (Xu & Beekman, 2003**)**. Several methods for estimating groundwater recharge are nowadays in use. The use of one method or another depends on the temporal and spatial resolutions of the required estimates (Scanlon *et al.*, 2002). These methods can be broadly grouped into physical and chemical methods. Physical methods comprise: (1) direct method: lysimeters and seepage meters (Xiao *et al.*, 2009; Rushton *et al.*, 2006; Scanlon *et al.*, 2002; Misstear, 2000; Sophocleous, 2004; Kitching & Shearer, 1982; Kitching *et al.*, 1977), (2) the water table fluctuation method (Scanlon *et al.*, 2002; Misstear, 2000), (3) the zero flux plane method (Khalil *et al*, 2003; Scanlon *et al.*, 2002), (4) the Darcy method (Scanlon *et al.*, 2002); (5) inverse modelling (Kendy *et al.*, 2003; Prasad & Rastogi, 2001; Kommadath, 2000), (6) hybrid water fluctuation method (Sophocleous, 1991 & 2004; Kommadath, 2000; (7) empirical methods (Kommadath, 2000; Sophocleous, 2004), and (9) soil water balance models. Chemical methods (10) comprise tracer techniques (Sharma, 1986; Flint *et al*, 2002; Sophocleous, 2004 ; Rushton *et al.* 2006 ; Misstear, 2000; Kommadath, 2000). However, although several methods have been proposed for evaluation of groundwater recharge, this factor is still the most difficult to measure. Groundwater recharge is indeed a complex function of several factors and mechanisms including meteorological conditions, soil types, land use, physiographic characteristics, depth to the water table, antecedent soil moisture, properties

of the geological materials, interaction between surface and groundwater and available groundwater storage… which may not be accurately appraised. Hence, estimates of groundwater recharge are normally and almost inevitably sullied by considerable errors and uncertainties. The best way to minimize these uncertainties is to use a combination of several methods (Scanlon *et al.*, 2002). In the following paragraphs, a detailed description of the methods which will be applied in this research will be presented.

III.4.2.1. The water table fluctuation method

The water table fluctuation method is based on the assumption that rises in groundwater levels in unconfined aquifers are due to recharge water reaching the water table (Scanlon *et al.*, 2002). Groundwater recharge can be then quantitatively estimated by multiplying the rise of the water table due to recharge by the specific yield. Kruseman (1997) (in Misstear, 2000**)** suggests the following relationship for estimation of the recharge from the fluctuation of the water table:

$$R = \Delta h.S_y + Q_p + Q_l$$

Where R = the recharge, Δh = the change in water table elevation, S_y = the specific yield, Q_p = the groundwater abstraction during the period under consideration, Q_l = the difference between lateral subsurface outflow and lateral subsurface inflow during the same period.

In suitable conditions where Q_p and Q_l can be neglected, this method offers a useful rough estimate of groundwater recharge. The main drawbacks in its application are related to the difficulty of obtaining reliable values of specific yield and ensuring that fluctuations in water levels are due to recharge and are not the result of changes in atmospheric pressure, the presence of entrapped air, or other phenomena, such as pumping (Scanlon *et al.*, 2002)

III.4.2.2. Soil moisture budgeting

The soil moisture balance technique can be used for routine recharge estimation in many situations if the important physical processes are represented adequately. It helps analyze the allocation of water among the various components of the hydrologic system at various time scales. This model was developed by Thornthwaite in the 1940s but was later revised. The basic principle of the method is that the soil becomes free draining when the moisture content of the soil reaches a maximum value called the field capacity; excess water drains through the soil towards the water table and becomes recharge (Rushton *et al.*, 2006). Soil moisture budgeting consists of computing soil moisture surpluses and deficits and thus actual evapotranspiration from precipitation and potential evapotranspiration data. The quantity of water stored under variable soil-moisture conditions is determined.

Soil-water budget calculations are commonly made on a daily, monthly or annual basis depending on availability of relevant climatic data sets (Scanlon *et al.,* 2002). However, Healy *et al.* (1989) observe that computing water-budget at small-scale allows an accurate estimation of individual parameters of the water balance equation. The calculations are generally carried out at the catchment or subcatchment scale.

III.4.2.3. Hybrid methods

Hybrid water fluctuation method is a methodology which combines the techniques of soil-moisture budget and water table fluctuation (Sophocleous, 2002**)**. The method is generally reliable for estimating natural groundwater recharge in flat areas having shallow water table. The effective storativity is obtained by dividing the recharge resulting from the soil-water balance analysis by the corresponding water table rise. The site-calibrated effective storativity is computed by averaging several estimates of the effective storativity (Sophocleous, 2004) obtained by associating water table rises to specific rainfall events. The site-calibrated value of effective storativity is then used to translate each major water table rise associated with a specific precipitation event into a corresponding amount of groundwater recharge. This combined methodology is designed to minimize water balance uncertainties. It was successfully applied in the US central Kansas plains region and was found to give more reliable results of recharge estimation than any other approach (Sophocleous, 1991).

III.4.3. Estimation of groundwater recharge using the soil moisture budget method

III.4.3.1. Introduction

Computing the soil moisture balance consists of estimating the various components of the hydrological cycle including: (1) precipitation, (2) potential evapotranspiration, (3) actual evapotranspiration, (4) soil moisture storage, (5) change in soil moisture storage, (6) deficit, and (7) surplus, (8) runoff and (9) recharge (Ritter, 2006). Figure III.8 illustrates some of the components of the soil moisture budget.

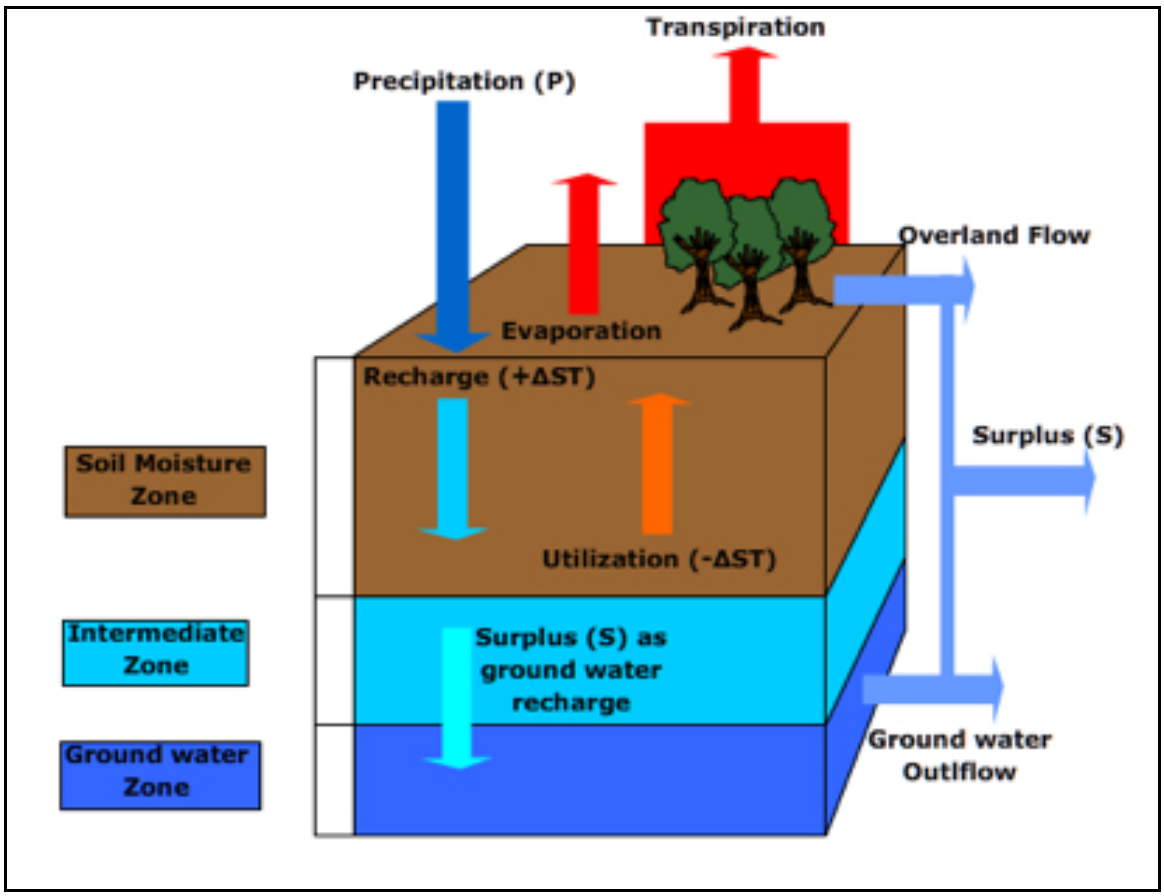

Figure III.8. The soil water balance (Stahler, 2006 as quoted by Ritter, 2006)

III.4.3.2. Methodology

III.4.3.2.1. Data collection and processing

The climatic data used for this study come from the weather station of Kirundo, the only comprehensive meteorological station which is found within the study area, although it is slightly located at its southern periphery. They were collected at the National Geographic Institute of Burundi, located in the city of Gitega, central Burundi. The meteorological parameters recorded at this station include precipitation, maximum and minimum temperature, maximum and minimum relative humidity, radiation and wind speed at 2m above the ground surface. Time series of meteorological data covering 36 calendar years, i.e. 1974-2009 were collected for the parameters air temperature and precipitation. Time series of relative humidity, wind speed and solar radiation are only available for a period of 11 years (1999-2009). Missing data in time series were filled using the arithmetic mean of adjacent days if only one record was missing. Larger gaps were filled using a linear correlation with data from the neighbouring meteorological station of Muyinga or by the long term daily means where satisfactory linear correlation could not be achieved. For the

period 1999-2009, time series data including solar radiation, wind speed, maximum and minimum relative humidity are available and this enabled us to compute the potential evapotranspiration using the standard Penman-Monteith equation. Table III.4 presents averages of monthly weather parameters computed for different time periods depending on the length of the available time series. Averages of monthly precipitation and air temperature are calculated for a period of 36 years (1974-2009) whereas for wind speed, relative humidity and radiation, they were calculated for a time period of 11 years (1999-2009). Averages of monthly air temperature ($T_{average}$) and relative humidity ($RH_{average}$) are calculated as average of maximum and minimum air temperature and relative humidity respectively.

Table III.4. Mean monthly climatic data (Period 1974-2009 for precipitation and temperature; period 1999-2009 for relative humidity, wind speed and solar radiation)

Month	Rain (mm)	T_{max} (°C)	T_{min} (°C)	$T_{average}$ (°C)	Max RH (%)	Min RH (%)	Average RH (%)	Wind speed (m/s)	Radiation (MJm^2)
January	88.37	26.94	15.04	20.99	95.11	51.59	73.35	0.5	13.46
February	95.35	27.52	15.12	21.32	94.41	47.66	71.03	0.52	14.61
March	133.76	26.98	15.19	21.09	96.64	55.68	76.16	0.51	13.77
April	187.65	26.32	15.72	20.73	96.28	58.56	77.42	0.48	13.27
May	109.18	26.35	15.42	20.89	94.86	54.74	74.80	0.47	12.86
June	13.93	27.16	14.84	21.00	89.82	43.89	66.86	0.68	14.28
July	7.61	27.76	14.58	21.17	82.67	36.43	59.55	0.91	15.28
August	24.84	28.59	15.24	21.92	81.23	37.40	59.32	0.74	14.9
September	72.44	28.69	15.45	22.07	88.15	40.79	64.47	0.64	14.98
October	104.91	27.62	15.30	21.46	93.18	46.75	69.96	0.56	14.15
November	123.20	26.32	15.25	20.79	96.44	56.12	76.28	0.42	12.64
December	93.11	26.49	15.10	20.80	95.42	53.91	74.66	0.43	13.9

a) Precipitation

Precipitation is the main supply of water to the land surface and therefore the principal source of groundwater recharge. The annual rainfall regime for the study area is characterised by two distinct wet and dry seasons which are controlled by the south-easterly and the north-easterly monsoon. The longer south-easterly monsoon brings rain between about February and May while the shorter north-easterly monsoon is responsible for the rainfall occurring between September and November (BLR Ingénierie, 2008). The months of June to August are generally dry and constitute the long dry season whereas the months of December and January are characterised by a diminution of precipitation and are thus

called the short dry season (Figure III.9). For the period 1974 through 2009, the average annual precipitation amounts to 1059.24 mm. A hydrologic year in Burundi starts in September with the beginning of the short rainy season and ends in August, at the end of the long dry season.

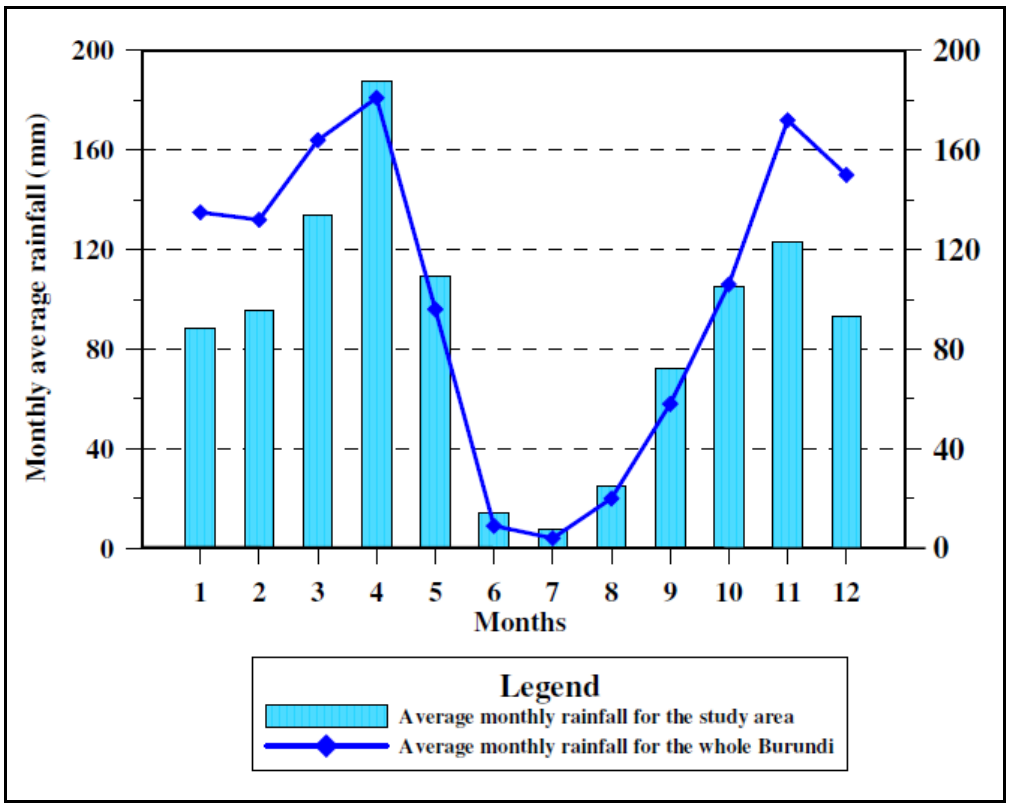

Figure III.9. Long term average of monthly precipitation for the study area and the whole Burundi

Figure III.9 shows the average monthly rainfall for the period 1974 through 2009. The long rainy season, *i.e.* February through May, accounts for 49.4 % of the total rainfall with an important peak in April. The short rainy season, which covers the months of September to November, accounts for 28.1 % of the total annual precipitation with the highest precipitation occurring in November. The long and short dry seasons contribute for respectively 5.5 % and 17 % of the total annual rainfall. Actually, what is called long dry season is really dry, whereas the so-called short dry season is in fact, just a diminution of the amount of rainfall. The whole rainy period, *i. e.* from September to May (SONDJFMAM) accounts for 95.6 % of the annual rainfall. Overall, the precipitation pattern throughout the year follows that of the whole country. It can be also observed from Figure III.9 that average monthly rainfall in Bugesera is slightly above the country mean for the months of April through October, while for the rest of the year, mean monthly precipitations are substantially below the country average.

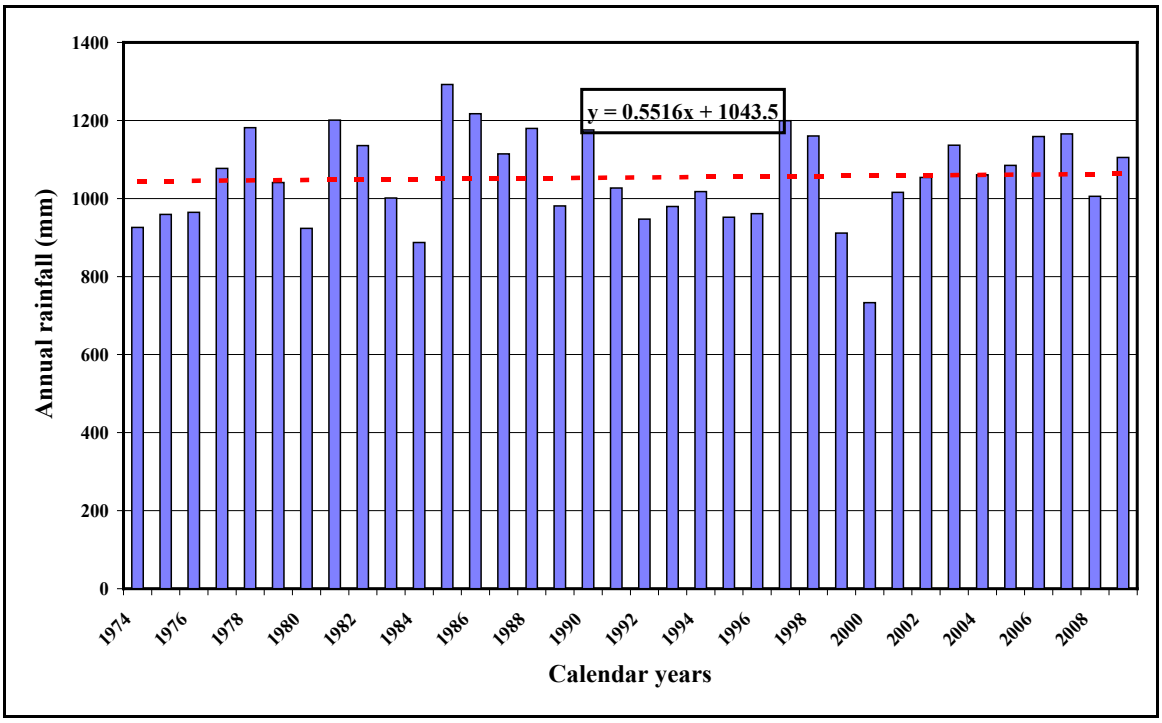

Figure III.10. Annual precipitation for the period 1974 through 2009

Figure III.10 presents the annual precipitation for the calendar years 1974 to 2009 for the climatological station of Kirundo. The yearly rainfall oscillates between a minimum of 733.2 mm and a maximum of 1292.3 mm, respectively recorded in 2000 and 1985. For the whole time period, the mean annual precipitation amounts to 1059.2 mm. The annual precipitation in this region is systematically lower than the long term annual average for Burundi which amounts to 1274 mm, except for the year 1985 where the precipitation (1292 mm) was slightly higher than the long term country average. Overall, there is a slightly increasing trend in annual precipitations from 1974 to 2009, which is however interrupted by periods of relatively low precipitation like 1974-1976, 1979-1980, 1983-1984 and 1999-2001.

In the following discussion, hydrologic years are considered and the different periods of the hydrologic year analysed are designed by the initials of the names of the months. Figure III.11 presents the annual rainfall for the hydrologic years 1974/75 through 2008/2009. The highest rainfall (1460.3 mm) was recorded during the hydrologic 1997/98 while the minimum rainfall occurred in the course of the hydrologic year 1998/99. It can be noted that the maximum and minimum rainfall for the different hydrologic years are significantly higher than the maximum and minimum values calculated for the calendar years. This

observation may be consistent with the fact that a hydrologic year comprises the short and the long rainy seasons of two different calendar years. Table III.5 shows some statistical parameters of the annual as well as the seasonal rainfall for the short rainy season (SON), the long rainy season (FMAM) and the whole rainy period (SONDJFMAM) for the period 1974/75 through 2008/2009. The maximum rainfall (491.1 mm) for the short rainy season (SON) occurred during the hydrologic year 1982/83 while the minimum (164.3 mm) was recorded during the hydrologic year 1979/80. For the long rainy season (FMAM), a maximum rainfall of 680.5 mm was recorded during the hydrologic year 1984/85 whereas the minimum (302.8 mm) occurred in the course of the hydrologic year 2000/2001. It can be therefore noted that the maximum and minimum rainfall for the two rainy seasons, i.e. SON and FMAM, are not necessarily recorded in the same hydrologic years and this may denote an interseasonal variability. This interseasonal variation of rainfall is typical of the rainfall regime in Burundi: for some hydrologic years, precipitations can be abundant during the first rainy season (SON) while they can strongly decrease in the long rainy season (FMAM) or vice versa. Over the entire length of record, statistics regarding the interannual variation of annual and seasonal rainfall indicate that the short rainy season (SON) has a higher variability (26 %) than the long rainy season (FMAM), the two rainy seasons combined (SONDJFMAM) and annual rainfall. For the three latter time periods, the coefficients of variation are not significantly different: 17 % (FMAM), 16 % (SONDJFMAM) and 16 % (annual).

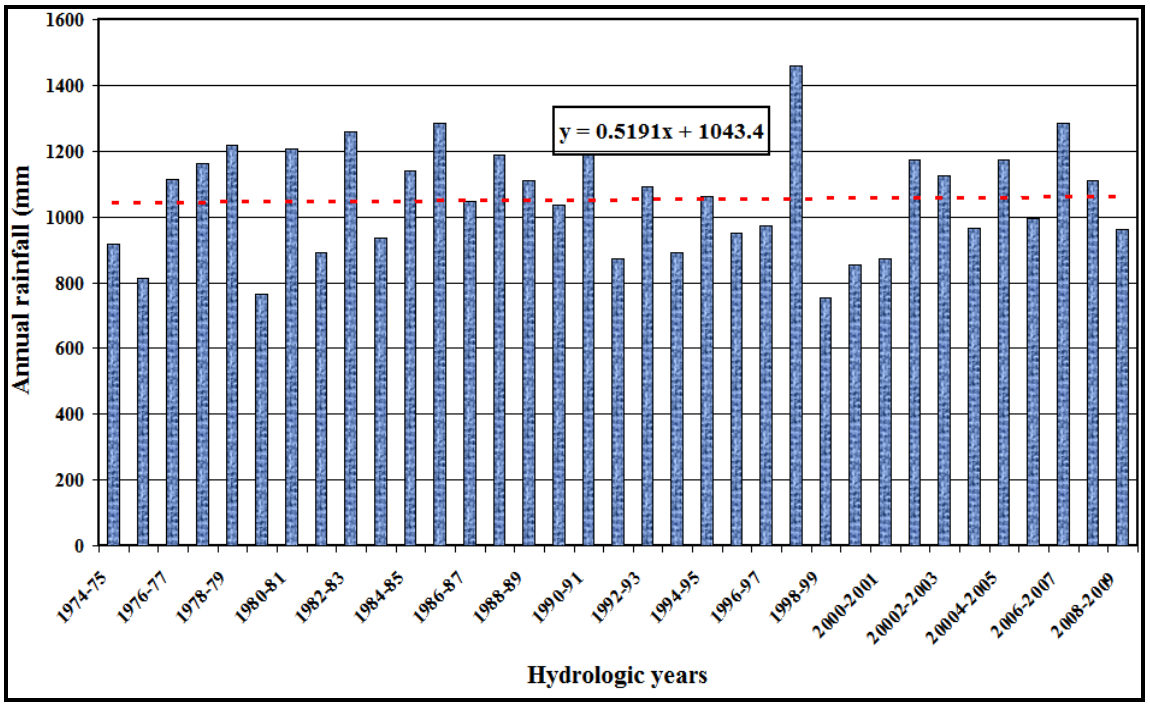

Figure III.11. Annual precipitation for the hydrologic years 1974/75 through 2008/2009

Table III.5. Seasonal and annual rainfall statistics for the hydrologic years 1974/75 through 2008/2009

	SON	FMAM	SONDJFMAM	Hydrologic Year
Maximum (mm)	491.10	680.50	1422.40	1460.30
Minimum (mm)	164.30	302.80	709.60	752.40
Mean	299.64	526.08	1007.07	1053.43
Standard deviation	78.33	90.12	161.31	165.19
Coefficient of variation (%)	26	17	16	16

SON: September, October and November; FMAM: February, March, April and May; SONDJFMAM: September, October, November, December, January, February, March, April and May.

b) Air temperature

Air temperature in Bugesera region does not vary significantly throughout the year. Indeed, the long term average of mean monthly temperature varies between 20.7°C and 22.1°C which are respectively recorded in April and September. On the other hand, long term averages of both maximum and minimum monthly temperatures show a bimodal pattern which is closely related to yearly distribution of precipitation.

The long term average of monthly maximum temperature shows two unequal peaks which correspond to the beginning of the short and long rainy seasons, *i.e.* 28.7°C in September and 27.5°C in February (Figure III.12). The most important peak occurs at the beginning of the short rainy seasons, in September. The two troughs of the average of maximum temperature, which occur during the rainy season, i.e. in April-May and November-December, reflect the cooling effect of rainfall on air.

The long-term average of minimum temperature equally shows two peaks which, unlike the maximum temperature, occur during the long and short rainy seasons, respectively in April (15.7°C) and September (15.5°C). The occurrence of two peaks of minimum temperature during the two rainy seasons may be explained by the abundance of clouds which blocks and refracts the outgoing terrestrial radiation back to the earth, resulting in an increased temperature during the night.

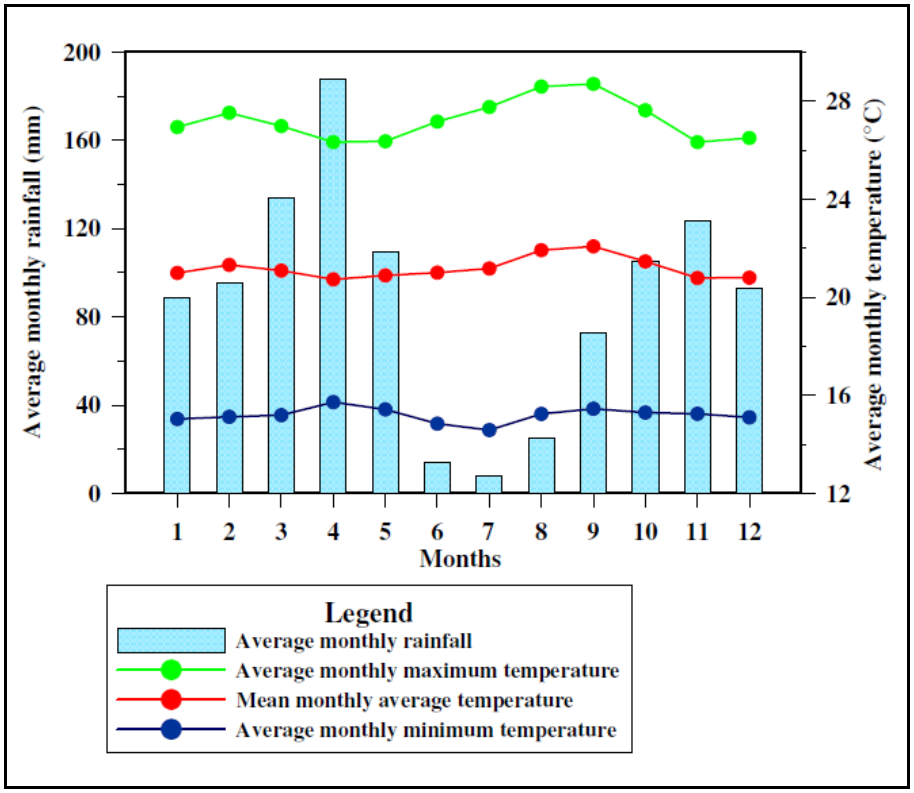

Figure III.12. Long term monthly average of precipitation (mm) and temperature (°C)

c) Relative humidity

Relative humidity indicates the state of moisture in the air. This parameter controls evapotranspiration rates because, as the air becomes progressively saturated, less water is able to evaporate into that air. Therefore, as the relative humidity increases, transpiration decreases. In humid tropical regions, despite the high solar energy input, the high humidity of the air will reduce the evapotranspiration demand (Allen *et al.*, 1998). Thus, Allen *et al.* (1998) draw the attention to the risk of overpredicting evapotranspiration under conditions of high relative humidity if the latter parameter is not incorporated into the estimation equation.

The study area is characterized by relatively high values of relative humidity. The long term average of maximum relative humidity fluctuates between 81.2 % and 96.6 %. On the other hand, the long term average of minimum relative humidity oscillates between 36.4 % and 58.6 %. The distribution of relative humidity throughout the year shows a bimodal pattern which closely resembles to that of the rainfall. Indeed, Figure III.13 shows two peaks of relative humidity which correspond to the two rainy seasons, namely the short (September to November) and the long (February to May) rainy season. The important

trough which occurs between June and September corresponds to the long dry season (Figure III.13). This pattern of long term average of monthly relative humidity reflects the fact that, during the rainy seasons, the relative humidity of air increases while it significantly drops during the dry period (Figure III.9).

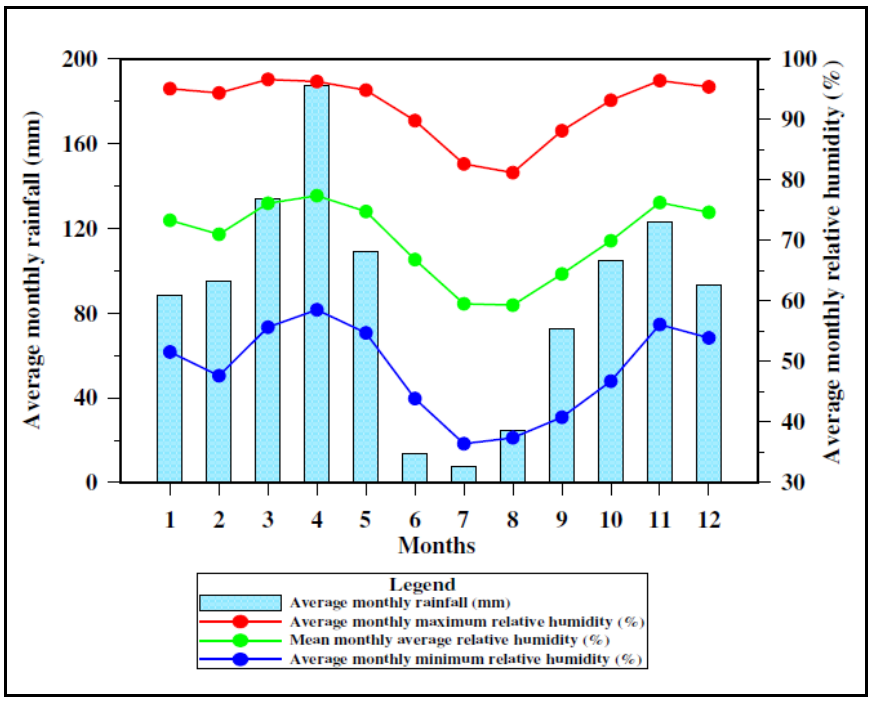

Figure III.13. Long term monthly average of maximum, minimum and mean monthly relative humidity (%)

d) Radiation

Solar radiation provides the necessary energy that transforms water masses into water vapor. The potential radiation at a specific location is determined by its geographical position and the time of the year (Allen *et al.*, 1998). The average solar radiation fluctuates between 12.6 MJm^2 and 15.3 MJm^2 with a mean value of 14 MJm^2. Figure III.14 shows two peaks (February and July) and two troughs (May and November) of solar radiation. The maximum radiation is recorded in July, during the long dry season (June-August), whereas the minimum value occurs in November. It is interesting to note that periods of maximum radiation closely coincide with periods of high potential evapotranspiration (Figure III.14).

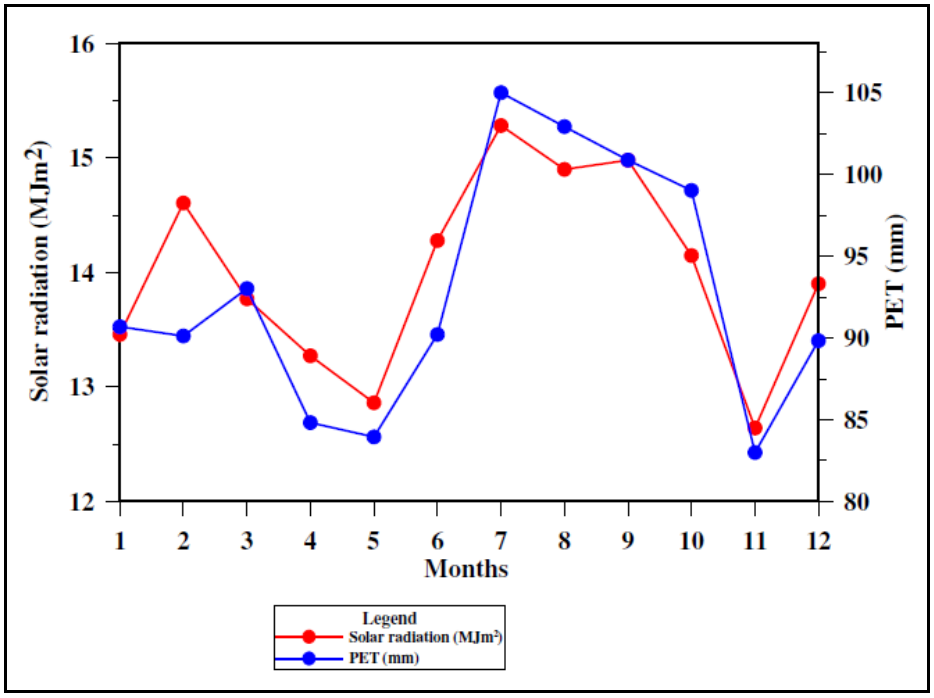

Figure III.14. Long term monthly average of solar radiation (MJm^2)

e) Wind speed

Wind speed is the driving force of water vapor transport. It helps remove the air above the evaporating body which is already saturated with water vapor, thereby allowing much more water vapor to be stored into the air. If dry and hot weather conditions are coupled with high wind speed, then more water vapor is likely to be taken up and this increases the evapotranspiration rate. On the contrary, in humid climates, even under high wind speed conditions, the humidity of the air and the presence of clouds cause the evapotranspiration to be lower. According to Allen *et al.* (1998), the evapotranspiration is likely to be underpredicted under high wind conditions (3 m/s) if this weather parameter is not taken into account in the estimation method.

Wind speed in our study area is rather low. The average monthly wind speed for a period of 11 years (1999-2009) varies between 0.4 m/s and 0.9 m/s; with an average value of 0.7 m/s. Higher wind speed occurs in the dry season (June-August), whereas lower values of wind speed are recorded in the rainy season (November-May) (Figure III.15).

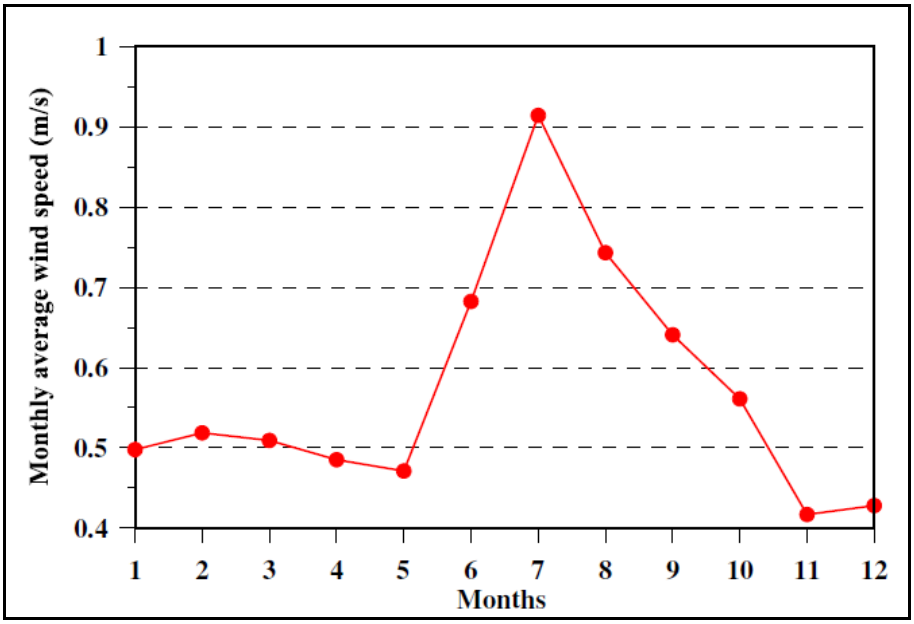

Figure III.15. Long term monthly average of wind speed (m/s)

f) Aridity index

The climatic regime of an area is classified based on the aridity index, a numerical indicator of the degree of dryness of the climate at a given location. The UNESCO (1979) and UNEP (1992) define the aridity index as the ratio of the mean annual rainfall (P) to the average annual potential evapotranspiration (PET). However, while the UNESCO aridity index is calculated using the Penman-Monteith potential evapotranspiration, the UNEP suggests to use the Thornthwaite potential evapotranspiration because the Penman-Montheith equation requires data which are not always available (Table III.6).

Table III.6. Aridity index according to UNESCO (1979) and UNEP (1992) (Tsakiris and Vangelis, 2005)

Zone	UNESCO (1979) P/PET (Penman-Monteith method)	UNEP (1992) P/PET (Thornthwaite method)
Hyper-arid	< 0.03	< 0.05
Arid	0.03-0.20	0.05-0.20
Semi-arid	0.20-0.50	0.20-0.50
Sub-humid	0.50-0.75	0.50-0.65
Humid	> 0.75	> 0.65

Unlike what has been always reported in literature in last decades (e.g. UNEP/UNDP, 2007), Bugesera region should not be classified as a semi-arid area because with an aridity index (A.I.) of 1.10 (UNEP, 1992), this region falls within the humid zone (A.I. > 0.65). On an annual basis, Figure III.16 shows that the aridity index for the whole period (1974/75-2007/2009) is systematically greater than 0.65, even for years of low precipitations like 1979/80 (A.I. = 0.75) and 1998/99 (A.I. = 0.77).

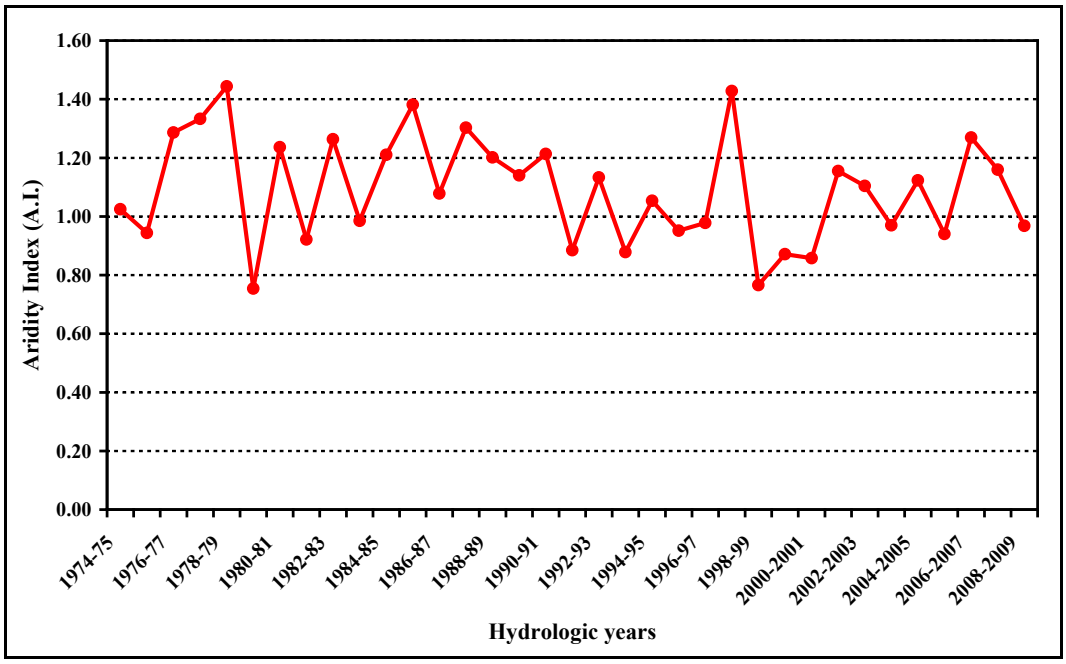

Figure III.16. Annual aridity index (UNEP, 1992) for the period 1974/75-2008/2009

III.4.3.2.2. Potential evapotranspiration

III.4.3.2.2.1 Introduction

Potential evapotranspiration is the water needed for evaporation and transpiration, at a location, given the local environmental conditions. It is the amount of water that would be evapotranspirated under an optimal set of conditions, among which is an unlimited supply of water. If the demand for water largely exceeds that which is actually present, soil moisture is depleted and plants eventually die (Ritter, 2006). Evapotranspiration is one of the discharge mechanisms which control the soil moisture and is therefore a key environmental parameter that deserves a lot of attention for efficient irrigation management and groundwater management schemes.

There are several methods of estimating potential evapotranspiration. They are classified in five groups as: water budget (e.g. Guitjens, 1982), mass-transfer (e.g. Harbeck, 1962), temperature-based (e.g. Thornthwaite, 1948; Hargreaves & Sammani, 1982 and 1985; Blaney & Criddle, 1950; Hamon, 1963), radiation-based (e.g. Priestley & Taylor, 1972; Makkink, 1957) and combination types. Penman-Monteith equation (Allen *et al.*, 1998) is an example of methods where a combination of several weather parameters is used to estimate potential evapotranspiration. The method requires several weather parameters, among which are air temperature, solar radiation, wind speed and relative humidity. Since 1990, the FAO, the International Commision for Irrigation and Drainage and the World Meteorological Organization have recommended to use Penman-Monteith method as the standard procedure for estimating the reference evapotranspiration and for evaluating other methods (Allen *et al.*, 1998; Trakkovic & Kolakovic, 2009; Xu & Singh, 2002; Castaneda & Rao, 2005)

In this study, potential evapotranspiration is estimated using Hamon`s equation (1963) incorporated into Thornthwaite Monthly Water Balance Model (MacCabe & Markstrom, 2007), Hargreaves equation (Hargreaves & Sammani, 1982 & 1985), Thornthwaite equation (1948, 1955 and 1957) for the whole period of data record (1974/75-2008/2009) and the FAO Penman-Monteith equation (Allen *et al.*, 1998) for the period 1999/2000 to 2008/2009 where all the required parameters are available.

III.4.3.2.2.2. Penman-Monteith equation

The standard Penman-Monteith method for estimating evapotranspiration can be mathematically expressed as follows (Allen *et al.,* 1998):

$$PET = \frac{0.408\Delta(R_n - G) + \gamma \frac{900}{T+273} u_2 (e_s - e_a)}{\Delta + \gamma(1 + 0.34u_2)}$$

where PET = reference potential evapotranspiration (mm day^{-1}), R_n = net radiation at the crop surface ($MJm^{-2}day^{-1}$), G = solar heat density (MJm^{-2} day^{-1}), γ = psychrometric constant ($kPa°C^{-1}$), T= mean air temperature (°C), u_2 = wind speed at 2 m height (m s^{-1}), e_s= saturation vapour pressure (kPa), e_a = actual vapour pressure (kPa), e_s - e_a = saturation vapour pressure deficit (kPa), Δ= slope of the saturation vapour pressure curve ($kPa°C^{-1}$).

One of the advantages of the Penman-Monteith method is the possibility of calculating automatically the PET on a daily or monthly basis, depending on the availability of data series, by using excel sheets designed by Snyder & Eching (2003).

Although Penman-Monteith equation has proven to be the best method to estimate potential evapotranspiration worldwide, its major drawback is that it requires a lot of weather parameters which are not always available in many parts of the world, especially in developing countries.

III.4.3.2.2.3. Hamon's equation

Hamon's formula for estimation of potential evapotranspiration requires only latitude, which is converted into daylength, and mean temperature which is converted into saturation vapor density. It can be mathematically expressed as follows:

$$PET = 13.97 * d * D^2 * W_t$$

Where PET = potential evapotranspiration in mm per month, d = the number of days in a month, D = the mean monthly hours of daylight in units of 12 hours and W_t = saturated water vapor (g m^{-3}).

$$W_t = \frac{4.95e^{0.62T}}{100}$$

Where T = the mean monthly temperature (°C).

In addition to its simplicity, Hamon potential evapotranspiration can be generated automatically through the computer-based Thornthwaite Monthly Water Balance (TMWB) model developed by McCabe & Markstrom (2007).

III.4.3.2.2.4. Thornthwaite equation

Thornthwaite's method is a simple and empirical scheme for calculating potential evapotranspiration which requires only temperature as input data. The method is based on an exponential relationship between mean monthly temperature and mean monthly consumptive use. The Thornthwaite equation can be expressed as:

$$PET = 16 * \left(10\frac{T}{I}\right)^a, 0° \leq \mathrm{T} \leq 26°\mathrm{C}$$

where I = the temperature-efficiency index, which is the sum of 12 monthly values of the heat index i, and a = function of I.

$i = \left(\frac{T}{5}\right)^{1.514}$ where T = mean monthly temperature (°C)

$$I = \sum_{i=1}^{12} i$$

$$a = 0.000000675I^3 - 0.0000771I^2 + 0.01792I + 0.49239$$

However, the estimates of potential evapotranspiration given by Thornthwaite equation have to be adjusted with a factor which takes into account the actual number of days in the month (28-31) and the number of daylight hours, the latter being a function of the altitude and the season.

The major shortcoming of this method is that it overestimates potential evapotranspiration in humid climates while it underestimates the parameter in arid climates (Castaneda & Rao, 2005, Alkaeed *et al.*, 2006; Pereira & Pruit, 2004; Trajkovic & Kolakovic, 2009). Hence, several attempts have been undertaken to adjust the constants of the empirical equations with a view to adapting the formulation to different geographical areas of interest (Castaneda & Rao, 2005; Pereira & Pruitt, 2004; Trajkovic & Kolakovic, 2009). One of these modifications was introduced by Camargo *et al.* (1999) (in Pereira & Pruitt, 2004) who suggested to replace the monthly average temperature in Thornthwaite equation by an effective temperature empirically computed as a function of the average temperature and the daily amplitude (A= T_{max}-T_{min}). The effective temperature (T_{eff}) can be therefore mathematically expressed as:

$$T_{eff} = k(Tm + A) = 1/2k(3T_{\max} - T_{\min})$$

where T_m = mean air temperature

A value k = 0.72 was proposed by Camargo *et al.* (1999) (in Pereira & Pruitt, 2004) as statistically the best value. However, in this study k = 0.69 has been adopted. The value k = 0.69 was found by Perreira & Pruit (2004) to give better estimate of PET. In case there are two days with the same effective temperature but very different photoperiods, Camargo *et al.* (1999) (in Pereira & Pruitt, 2004) suggested to correct the T_{eff} parameter with the day-night length ratio as follows:

$$T_{eff}^{*} = T_{eff}\,\frac{N}{24 - N} \text{ with the following condition: } T_m \le T_{eff}^{*} \le T_{\max}$$

with N = the photoperiod (daylight length) for a given day.

III.4.3.2.2.5. Hargreaves equation

Hargreaves equation is one of the simplest equations used to estimate potential evapotranspiration. It is expressed as (Hargreaves & Samani, 1985; Allen *et al.*, 1998):

$$PET = 0.023(T_{mean} + 17.8)(T_{\max} - T_{\min})^{0.5} R_a$$

where PET = reference evapotranspiration (mm day^{-1}), T_{mean} = daily mean air temperature (ºC), T_{max} = daily maximum air temperature, T_{min}= daily minimum air temperature (ºC), R_a = extraterrestrial radiation (MJ $m^{-2}day^{-1}$).

Many studies have pointed out the poor performances of the Hargreaves method in estimating potential evapootranspiration (Trajkovic & Kolakovic, 2009; Xu & Singh, 2002; Castaneda & Rao, 2005). This method was found to substantially overestimate the potential evapotranspiration. However, some few studies still present the method as the reliable alternative to the standard Penman-Monteith equation when there are not enough climatic data (Lopez-Urrea *et al.*, 2006; Alkaeed *et al.*, 2006; Allen *et al.*, 1998). Like Penman-Monteith method, Hargreaves' PET can be automatically computed on a daily or monthly basis by using the same excel sheets (Snyder & Eching, 2003), depending on the availability of the weather parameters.

III.4.3.2.3. Soil moisture balance

III.4.3.2.3.1. Introduction

The different terms of the soil moisture budget are computed in two different manners: (1) automatically using the Thornthwaite Monthly Water Balance (TMWB) model program (McCabe & Markstrom, 2007); and (2) each term separately in an excel sheet using PET values estimated by different methods (Penman-Monteith, Hargreaves, Thornthwaite and modified Thornthwaite methods). In both methods, the concept of water balance of the unsaturated zone (Thornthwaite & Mather, 1957) is applied. It consists of keeping track of the accumulated potential water loss (APWL) and the amount of water stored in the soil (S_B). Calculations to determine S_B and APWL are performed for each month or day using monthly or daily precipitation (P) and potential evapotranspiration (PET) (Table III.7).

Table III.7. Annual soil-water budget calculations used in excel sheet calculations

TERMS	**WET SEASON** **SUR = (P-Ro)-PET > 0**			**DRY SEASON** SUR = (P-Ro)-PET < 0
	S_B = CAP	S_B < CAP		
		(P-Ro)-PET ≤ CAP - S_B	(P-Ro)-PET > CAP - S_B	
S_{Bn+1}	CAP	S_B + (P-Ro)-PET	CAP	PAW*$e^{-APWL/PAW}$+WPWP
R_N	(P-Ro)-PET	0	P-Ro-PET-(CAP-S_B)	0
AET	PET	PET	PET	(P-Ro) + ΔS_B
DEF	0	0	0	PET-AET

P = precipitation (mm); Ro = runoff (mm); PET = potential evapotranspiration (mm); APWL= accumulated potential water loss (mm) (PET – (P – R_O)) accumulated for subsequent dry months; AET = actual evapotranspiration (mm); S_B = water stored in soil: S_B = PAW*$e^{-APWL/PAW}$ +WPWP; S_{Bn+1} = soil moisture storage at the a end of a new time step (mm); PAW = Plant available water = the difference between water content at field capacity (CAP) and water content at permanent wilting point (WPWP); WPWP = average rooting depth (mm) * PWP (in volume %) (e.g. 250 mm*15 % = 37.5 mm), CAP (mm) = maximum water content of soil, without gravitational water (= average rooting depth (mm) * water content at field capacity (in volume %) (e.g. 250 mm * 45 % = 112.5 mm) ; ΔS_B = change in soil moisture storage; $\Delta S_B = S_{Bn+1}-S_B$; DEF = deficit (PET-AET) (mm); SUR = surplus ((P- Ro)-AET) (mm); R_N = natural groundwater recharge (SUR-ΔS_B) (mm).

This way of calculating the water balance, which takes into account the exponential decrease of soil moisture during the dry period, was refined at the Laboratory for Applied Geology and Hydrogeology, building on the concept developed by Thornthwaite & Mather (1957). Indeed, as the soil moisture diminishes, water in the soil becomes more and more tightly bound to the soil particles and is therefore difficult to be removed and this explain the exponential shape of the soil moisture depletion curve. However, unlike the concept of exponential decrease of soil moisture used in excel sheet calculations, TMWB model considers that the soil moisture storage withdrawal linearly decreases with decreasing soil moisture storage. When total precipitation for a month is less than the PET, then the AET is equal to the sum of precipitation and the soil moisture that can be withdrawn from the soil. The soil moisture storage withdrawal (STW) is calculated as follows (McCabe & Markstrom, 2007):

$$STW = ST_{i-1} - \left[absolute\left(P_{total} - PET\right) x \left(\frac{ST_{i-1}}{STC} \right) \right]$$

where ST_{i-1} is the soil moisture storage for the previous month and STC is the soil moisture storage at field capacity.

Moreover, the TMWB model uses the Hamon method for estimating PET and the runoff is calculated using a runoff factor representing the fraction (%) of the monthly rainfall which becomes direct runoff. This is not totally correct because every rainfall event does not generate runoff. One of the important shortcomings of the TMWB model is the fact that entering data into the model is accomplished through a graphical interface which does not allow to consider the decimal values for some parameters like the altitude and the soil moisture storage capacity. In addition, the model does not enable to consider the water content at permanent wilting point when balancing the soil moisture such that, for dry months, the soil moisture content drops down to zero, while according to Raes *et al.* (2010), the lowest level of soil moisture in dry periods is the water content at permanent wilting point.

The monthly and daily climatic data, whenever available, were first rearranged into hydrologic years. As already mentioned above, a hydrologic year in Burundi starts with September, which is the beginning of the rainy season, and terminates at the end of August, i.e. the end of the dry season. This way of organizing data has the advantage of facilitating the computation of the change in soil moisture storage at the beginning of the calculations, because the soil moisture storage at the end of the dry season can be considered as being at its lowest level, i.e. the water content at permanent wilting point. Moreover, the concept of

hydrologic year reflects the natural climatic reality in the sense that it commences with the start of the season of soil moisture recharge, includes the season of maximum groundwater recharge, if any, and terminates with the season of maximum soil moisture utilisation (Ritter, 2006).

III.4.3.2.3.2. Actual evapotranspiration

It is the quantity of water which is actually removed from the soil due to the combined processes of evaporation and transpiration. Actual evapotranspiration (AET) is an output of water that is dependent on moisture availability, temperature and humidity. It increases with temperature as long as there is water to evaporate and for plants to transpire. The amount of actual evapotranspiration also depends on the plant available water (PAW). Practically, the concept of AET can be understood in the following way:

- In wet months, when there is enough rain, i.e. when P-Ro > PET, the AET is at its maximum value, which is equal to the PET.
- In dry months, when there is not enough rain, i.e. when P-Ro < PET, the precipitation is no longer able to meet the evapotranspiration demand. Therefore, the unmet amount of water required by the evapotranspiration demand is progressively taken from the soil moisture storage until the latter reaches the permanent wilting point (PWP). Hence, even if there is not enough precipitation, the AET can still approach the PET when there is still enough water within the soil moisture storage.

III.4.3.2.3.3. Soil moisture storage

Soil moisture storage represents the total amount of water which is held within the plants root zone. The soil texture and crop rooting depth are the main determinant factors for this parameter. A deeper rooting zone means that there is a larger volume of water stored in the soil zone and therefore a reduced amount of water going to the groundwater reservoir as recharge. The maximum amount of water that can be held within the soil zone is referred to as the field capacity (CAP). The soil moisture comprises two components, namely the water content at permanent wilting point (WPWP) and the plant available water (PAW).

- **Plant available water (PAW)** is the difference between the water content at field capacity (CAP) and the water content at permanent wilting point (WPWP).
- **Water content at permanent wilting point (WPWP)** is the minimal soil water moisture, at which the plant starts to wilt.

The values of PAW and WPWP depend on the soil properties as well as the rooting depth. The total soil water-holding capacity of the root zone (CAP) is typically expressed in mm and can be obtained by multiplying the water content at field capacity by the effective depth of the root-zone (Figure III.17 and Table III.8). For instance, in our study area, soils are predominantly clayey and the land cover is dominated by agricultural land with shallow rooted crops. Hence, assuming a uniform PAW of 30 % over the entire root-zone (Table III.8) and a rooting depth of 0.25 m for shallow rooted crops, the PAW at field capacity becomes 75 mm (Table III.8) while the CAP is 75 mm plus 37.5 mm (water content at field capacity (CAP) = 112.5 mm). Previous studies have proposed a water holding capacity of 100 mm (TWB, Ingénieurs Conseils, 1994) but no scientific explanation was given as regards to the way this figure was estimated.

Table III.8. Suggested plant available water (PAW) for combinations of soil textures and vegetation types (Thornthwaite & Mather, 1957)

Vegetation	Soil texture	Available Water capacity (% volume)	Rooting depth (m)	Plant available water in the root-zone (mm) at field capacity (PAW)
Shallow rooted crops (spinach, peas, beans, beets, carrots etc.)	Fine sand	10	0.50	50
	Fine sandy loam	15	0.50	75
	Silt loam	20	0.62	125
	Clay loam	25	0.40	100
	Clay	30	0.25	75
Moderately rooted crops (corn, cereals, cotton, tobacco)	Fine sand	10	0.75	75
	Fine sandy loam	15	1.00	150
	Silt loam	20	1.00	200
	Clay loam	25	0.80	200
	Clay	30	0.50	150
Deep rooted crops (alfalfa, pasture, grass, shrubs)	Fine sand	10	1.00	100
	Fine sandy loam	15	1.00	150
	Silt loam	20	1.25	250
	Clay loam	25	1.00	250
	Clay	30	0.67	200
Orchards	Fine sand	10	1.50	150
	Fine sandy loam	15	1.67	250
	Silt loam	20	1.50	300
	Clay loam	25	1.00	250
	Clay	30	0.67	200
Mature forest	Fine sand	10	2.50	250
	Fine sandy loam	15	2.00	300
	Silt loam	20	2.00	400
	Clay loam	25	1.60	400
	Clay	30	1.17	350

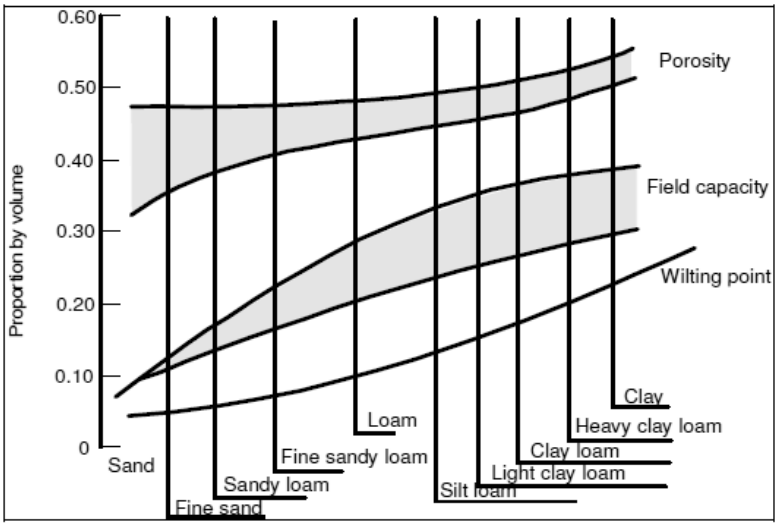

Figure III.17. Water-holding properties of different soil types based on texture (Dunne and Leopold, 1978 as quoted by Asmamaw, 2003)

III.4.3.2.3.4. Change in soil moisture storage

The change in moisture storage is the amount of water which is added or removed to water in storage. The change in soil moisture storage fluctuates between the WPWP and the CAP. This parameter is computed, depending on the time scale used, as the difference between the current soil moisture and the previous one. Withdrawals of water from the moisture storage take place during the dry months ($PET>P-R_o$) wherein a certain amount is taken to meet the evapotranspiration demand. Water is added to the soil moisture storage during the wet months ($PET<P-R_o$) until the water content at field capacity (CAP) of the root-zone, i.e. 112.5 mm in our study area, is reached. The excess moisture is drained to the groundwater reservoir in the form of groundwater recharge.

III.4.3.2.3.5. Deficit (D)

A soil moisture deficit occurs when the demand for water exceeds the amount which is actually available. Deficits occur when potential evapotranspiration exceeds actual evapotranspitration (PET>AET). The amount of deficit is therefore calculated as the difference between potential and actual evapotranspiration (Ritter, 2006).

III.4.3.2.3.6. Surplus (S)

Surplus water occurs when P-Ro exceeds potential evapotranspiration and the soil moisture is at its field capacity, i.e**.** when there is more water than what is actually needed given the local environmental conditions. Surplus (SUR) is computed as the difference between P-Ro and the actual evapotranspiration (AET). The existence of surplus water indicates the

possibility of groundwater recharge although the soil moisture storage must be brought to its field capacity at first.

III.4.3.2.3.7. Runoff estimation

Introduction

Surface runoff is the fraction of precipitation, in mm, that flows on impervious surfaces or over the land surface. Surface runoff is subtracted from the precipitation to compute the residual amount of precipitation which participates into the further steps of the soil water balance process.

Several approaches have been proposed in an attempt to decipher the complexity of direct runoff estimation from precipitation data. Among these methods, we can mention the artificial neural networks (Govindaraju, 2000; Govindaraju & Rao, 2000; Rajurkar *et al.*, 2004; Daliakopoulos *et al.*, 2005; Yazdani *et al.*, 2009), Justin method (Justin, 1915), Fergusson method (Fergusson & Debo, 1990), geomorphological instantaneous unit hydrograph (Bhadra *et al.*, 2008; Kumar *et al.*, 2007) and the NRCS-Curve Number method (USDA-SCS, 1972). The latter method was used for estimation of direct runoff for this study.

NRCS-Curve number (CN) method

The NRCS-CN method is widely accepted and used by scientists in different domains for estimation of runoff. This method was originally developed by the Soil Conservation Service of the United States Department of Agriculture (USDA) using total storm rainfall and an index of initial abstractions to compute total storm runoff volume (USDA-SCS, 1972; Patil *et al.*, 2008; Terzoudi *et al.*, 2007). Curve number values have been determined experimentally from rainfall and runoff data over different geographic, soil and land use conditions (Huang *et al.*, 2006). The generation of runoff is indeed governed by the interaction of precipitation with the topography, land use and soil properties of the land surface (Patil *et al.*, 2008). However, this method was strongly criticised for the fact that the amount of generated runoff does not take into account the rainfall intensity (Terzoudi *et al.*, 2007) nor the slope factor (Huang *et al.*, 2006)

The NRCS-CN method is underlain by an empirical equation predicting runoff from rainfall, using a shape factor S which combines the effects of soil, vegetation, land use and soil moisture prior to a rainfall event. The factor S is also called the potential maximum retention. At the start of the rain, the first water will be intercepted by the crop, stored in

small depressions and infiltrated in the soil as initial abstraction, I_a. After runoff has started, some of the additional precipitation will infiltrate forming the actual retention (F). With increasing precipitation, the actual retention eventually reaches a maximum value which is the potential maximum retention (S) (Figure III.18).

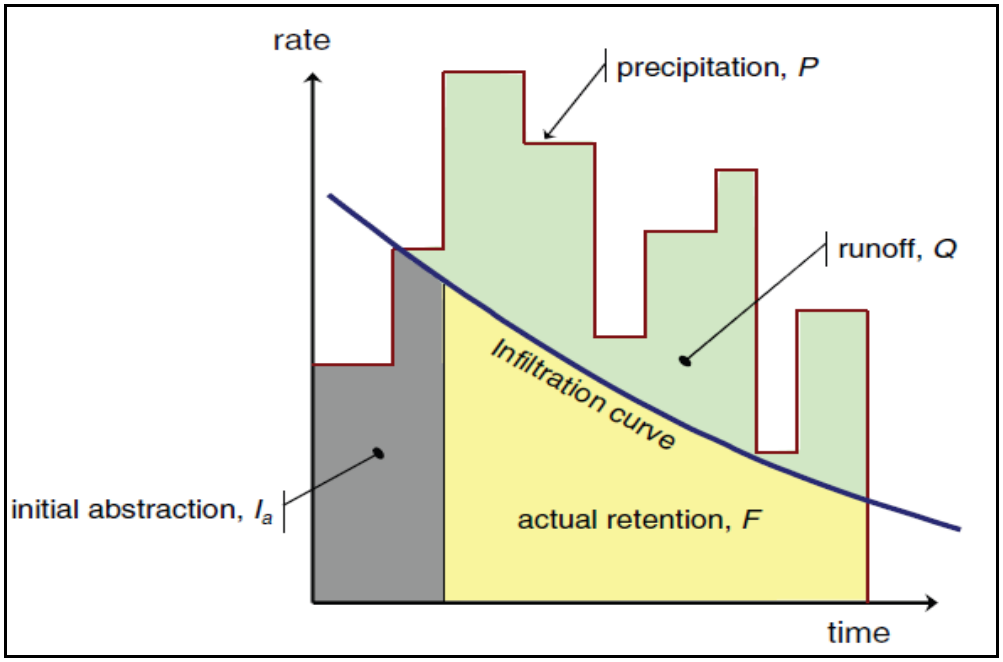

Figure III.18. The division of precipitation between initial abstraction, actual retention, and runoff (Bos *et al.*, 2009)

Mathematically, this empirical equation can be expressed as follows:

$$R_O = \frac{(P - I_a)^2}{P - I_a + S}$$

where R_O is the runoff (mm), P is the precipitation (mm), I_a is the initial abstraction (mm) and S is the potential maximum retention (m).

$I_a = \lambda S$ where $\lambda = 0.2$ (SCS, 1972)

Therefore the above equation becomes:

$$R_O = \frac{(P - 0.2S)^2}{P + 0.8S} \text{ for } P \geq 0.2\ S$$

$$R_O = 0 \text{ for } P < 0.2S$$

The retention parameter S (mm) can be calculated using the following equation:

$$S = \frac{25400}{CN} - 254$$

where CN is the curve number, a dimensionless parameter whose value ranges from 0 to 100. The CN indicates the runoff response characteristics of an area which depend on the

land use, land treatment, hydrological condition, hydrological soil group and antecedent soil moisture of the area.

Factors influencing the curve number value

- ***Land use or land cover***

Land use or land cover represents the surface conditions of the area and corresponds to the degree and type of the cover of the soil surface. In the CN method, the following categories of land cover or land use are distinguished (Bos *et al.*, 2009):

Fallow is the agricultural land use with the highest potential for runoff because the land is kept bare.

Row crops are field crops planted in rows far enough apart that most of the soil surface is directly exposed to precipitation

Small grain is planted in rows close enough that the soil is not directly exposed to precipitation.

Close-seeded legumes or rotational meadow are either planted in close rows or broadcasted. This kind of crop usually protects the soil throughout the year.

Pasture range is native grassland used for grazing.

Woodlands are usually small isolated groves of trees being raised for farm use (Orchards)**.**

As already mentioned in chapter I, the study area is dominated by agricultural land (68 %) where subsistence crops, mainly beans are cultivated. Hence, overall, the land cover was classified as "close-seeded legumes or rotational meadow".

- ***Land treatment or practice***

Land treatment represents the way the agricultural land is managed and the agricultural practices which are applied. This includes mechanical practices such as contouring or terracing and management practices among which rotation of crops, grazing control or burning. The ease with which water can infiltrate into the soil is qualitatively qualified as good, fair or poor (Bos *et al.*, 2009).

There is no special land treatment applied in the study area, local villagers are practicing subsistence agriculture in a rather traditional fashion. Hence, for this study the "contoured" practice was adopted as the land treatment or practice.

- ***Hydrologic conditions***

Hydrologic condition refers to the effect of cover type and treatment on infiltration and runoff. It is generally determined by the density of plant and residue cover of an area. Hydrologic condition is one of the factors used to select a curve number. Good hydrologic condition reduces the runoff potential, whereas poor hydrologic condition indicates that

surface factors increase runoff to the detrimental of infiltration. The following factors are considered in estimating the effect of cover on infiltration and runoff: canopy or density of lawns, crops, or other vegetative areas, amount of year-around cover, amount of grass or close-seeded legumes in rotations, percent of residue cover and degree of surface roughness (USDA-NRCS, 1986; Bos *et al.*, 2009).

In our study area, there are two rainy seasons, viz. September to November and February to May which are separated by two dry seasons, i.e. December to January and June to August. However, in reality, December to January is not a dry season as such, but just a decrease of the amount of precipitations. Therefore, for the period September to May, during which runoff may occur, the ground surface is well covered by either broadcasted crops or a dense meadow after the harvest. In the light of what precedes, the hydrological condition of our study area was characterised as good.

- ***Hydrological soil group***

Soil properties strongly influence the amount of infiltration and runoff. In the NRCS-CN method, the soil properties are represented by a hydrological parameter which indicates the runoff potential of the soil. All soils are qualitatively classified into four hydrological soil groups as shown in Table III.9 (USDA-NRCS, 1972).

Table III.9. Hydrological soil groups (USDA-NRCS, 1972)

Group	Description	Infiltration rate
Group A	Soils having high infiltration rates even when thoroughly wetted and a high rate of water transmission. Examples are deep, well to excessively drained sands or gravels.	Final infiltration rate: 8-12 mm/h
Group B	Soils having moderate infiltration rates when thoroughly wetted and a moderate rate of water transmission. Examples are moderately deep to deep, moderately well to well drained soils with moderately fine to coarse texture.	Final infiltration rate: 4-8 mm/h
Group C	Soils having low infiltration rates when thoroughly wetted and a low rate of water transmission. Examples are soils with a layer that impedes the downward movement of water or soils of moderately fine to fine texture	Final infiltration rate : 1-4 mm/h
Group D	Soils having a very low infiltration rate when thoroughly wetted and a very low rate of water transmission. Examples are: clays, soils with high swelling potential, soils with a permanent high watertable, soils with a clay pan or clay layer at or near the surface or shallow soils over nearly impervious material.	Final infiltration rate: less than 1 mm/h

In our study area, soils are predominantly clayey and were therefore classified into group D.

- ***Antecedent soil moisture conditions***

The soil moisture condition before runoff occurs is another important factor which determines the final CN value. The soil moisture condition is classified into three antecedent soil moisture condition (AMC) classes (Table III.10):

AMC I: the soils in the area are practically dry, viz. the soil moisture content is at wilting point

AMC II: average conditions

AMC III: the soils in the area are practically saturated from antecedent precipitation or irrigation water application, viz. the soil moisture content is at field capacity.

These classes are based on the accumulated soil moisture during the 5 days preceding the runoff under consideration. The original NRCS-CN method distinguishes the dormant and the growing season in order to highlight the differences in actual evapotranspiration. The values of CN given in the table of SCS (Table III.11) (USDA-NRCS, 1972) are valid for an average relationship $I_a = 0.2S$ and for average antecedent soil moisture condition (AMC II). Thus, if the 5-day antecedent precipitation plus irrigation water is classified as class I or class III, then the CN value given in the USDA-NRCS table must be corrected with an appropriate factor (Table III.12).

Table III.10. Seasonal precipitation (plus irrigation) limits for AMC classes (USDA-NRCS, 1972)

Antecedent moisture content class	**5-day antecedent rainfall plus irrigation application (mm/5 days)**	
	Dormant season	**Growing season**
AMC I	<13	<36
AMC II	13-28	36-53
AMC III	>28	>53

By considering the land use or cover (close-seeded legumes or rotational meadow), the land treatment or practice (contoured), the hydrological condition (good) and the soil group (D), the CN for average antecedent soil moisture conditions in our study area, i.e. AMC II, was determined as 83. Furthermore, this CN value for average conditions was adjusted to the two other antecedent soil moisture conditions AMC III and AMC I using linear interpolation based on Table III.12. CN values for antecedent soil moisture conditions AMC III and AMC I were determined as 92.5 and 66.8 respectively.

Table III.11. Curve number (CN)values for the combined hydrological soil complex for average antecedent soil moisture (Class AMC II), flat or slightly sloping areas, and Ia = 0.2S (USDA-NRCS, 1972 in Bos et al. 2009)

Land use or cover	**Treatment or practice**	**Hydrological conditions**	**Hydrological soil group**			
			A	**B**	**C**	**D**
Fallow	Straight row	Poor	77	86	91	94
Row crops	Straight row	Poor	72	81	88	91
	Straight row	Good	67	78	85	89
	Contoured	Poor	70	79	81	88
	Contoured	Good	65	75	82	86
	Terraced	Poor	66	74	80	82
	Terraced	Good	62	71	78	81
Small grain	Straight row	Poor	65	76	84	88
	Straight row	Good	63	75	83	87
	Contoured	Poor	63	74	82	85
	Contoured	Good	61	73	81	84
	Terraced	Poor	61	72	79	82
	Terraced	Good	59	70	78	81
Closed-seeded	Straight row	Poor	66	77	85	89
	Straight row	Good	58	72	81	85
or rotational meadow	Contoured	Poor	64	75	83	85
	Contoured	**Good**	55	69	78	**83**
	Terraced	Poor	63	73	80	83
	Terraced	Good	51	67	67	80
Pasture range		Poor	68	79	86	89
		Fair	49	69	79	84
		Good	39	61	74	80
	Contoured	Poor	47	67	81	88
	Contoured	Fair	25	69	75	83
	Contoured	Good	6	35	70	79
Meadows (Permanent)		Good	30	58	71	78
Woodlands (farm woodlots)		Poor	45	66	77	83
		Fair	36	60	73	79
		Good	25	55	70	77
Farmsteads			59	74	82	86

Table III.12. Conversion table for curve number (CN) values from antecedent moisture class II to classes I and III (USDA-NRCS, 1972)

	Corrected for AMC I and III			Corrected for AMC I and III	
AMC II	**AMC I**	**AMC III**	**AMC II**	**AMC I**	**AMC III**
100	100	100	56	36	75
96	89	99	54	34	73
92	81	97	50	31	70
90	78	96	48	29	68
86	72	94	44	25	64
84	68	93	42	24	62
80	63	91	38	21	58
78	60	90	36	19	56
74	55	88	32	16	52
72	53	86	30	15	50
68	48	84	20	9	37
66	46	82	15	6	30
62	42	79	5	2	13
60	40	78	0	0	0

Incorporating the slope factor into the curve number method

The CN values proposed in Table III.11 and Table III.12 are only valid for flat or slightly sloping areas (slopes ≤ 5 %) (Bos *et al.*, 2009). Therefore, by using the standard CN method, the surface runoff may not be correctly estimated. Indeed, Huang *et al.* (2006) observed that the standard CN method underpredicts large runoff events while small ones are overpredicted; the discrepancy between observed and predicted runoff increases with slope. Notwithstanding this important fact, there are few models in literature which incorporate a slope factor to improve prediction of surface runoff volume.

Huang *et al.* (2006) developed a CN slope-adjusted equation based on the relationship between observed and theoretical CN values and slope. This equation was found to yield the best predicted runoff depth in the steep areas of the Chinese Loess Plateau, where the percent slope varies between 14 and 140 %. The CN slope-adjusted equation is mathematically expressed as follows:

$$CN_{2,\alpha} = CN_2 \frac{322.79 + 15.63(\alpha)}{\alpha + 323.52}$$

where $CN_{2,\alpha}$ is the slope-adjusted CN for the antecedent soil moisture condition AMC II, CN_2 is the original CN value for average antecedent soil moisture condition (AMC II) and α is the slope.

Application to the study area

For our study area, the CN slope-adjusted equation by Huang *et al.* (2006) was applied as, to date, it is the best method which has successfully imbedded the slope factor into the original CN method. The slope α was derived from the slope map of the study area. The latter was first classified into 10 slope gradient classes pursuant to the guidelines for soil description (Table III.13) (FAO, 2006).

Table III.13. Slope gradient classes (FAO, 2006)

Class	Description	Slope α (%)
1	Flat	0-0.2
2	Level	0.2-0.5
3	Nearly level	0.5-1.0
4	Very gently sloping	1-2
5	Gently sloping	2-5
6	Sloping	5-10
7	Strongly sloping	10-15
8	Moderately steep	15-30
9	Steep	30-60
10	Very steep	>60

The number of slope gradient classes was further reduced to 7 by combining the slope classes 2 through 5 into one class because original CN values are valid for those slightly sloping areas which encompass all slope angles less than 5 % (USDA-NRCS, 1972; Bos *et al.*, 2009). The class 1, *i.e.* slope angle comprised between 0 % and 0.2 %, was excluded from the calculations as there should not be runoff on flat areas (table III.14). For each slope gradient class, an average slope was determined and it is this value which was used to adjust the CN values 66.8, 83 and 92.5 respectively for antecedent soil moisture conditions AMC I, AMC II and AMC III for slopes angles greater than 5 %.

The runoff was calculated for each slope class using daily rainfall data for a period of 35 hydrologic years (1974/75-2008/2009). An average daily runoff depth was subsequently calculated over the entire study area based on the runoff values of the different slope classes. Figure III.19 shows the annual precipitation for each hydrologic year and runoff computed using the slope-adjusted CN method. The long-term average runoff factor, 4.6 %, used in the Thornthwaite Monthly Water Balance Model, was estimated by averaging the annual runoff factors for each hydrologic year. This value is comparable to the typical runoff factor of 5 % suggested by McCabe & Markstrom (2007). According to the classification proposed by Ramakrishnan *et al.*, (2009), the surface runoff in our study area

is rather low (< 20 %). The annual runoff factor (%) for each hydrologic year was calculated as the ratio between the annual runoff and rainfall.

Table III.14. Redefinition of slope gradient classes and corresponding slope-adjusted curve numbers

Class	Slope range (%)	Average slope (%)	Area (m^2)	CN for AMC II	CN for AMC I	CN for AMC III
1	0-0.2	0.01	123152400			
2	0.2-5	2	253173600	83	66.8	92.5
3	5-10	8	153146700	83.11	66.89	92.63
4	10-15	12	253475100	83.26	67.01	92.79
5	15-30	20	190212300	83.56	67.25	93.13
6	30-60	37	47166300	84.20	67.77	93.84
7	> 60	62	32400	85.14	68.52	94.88

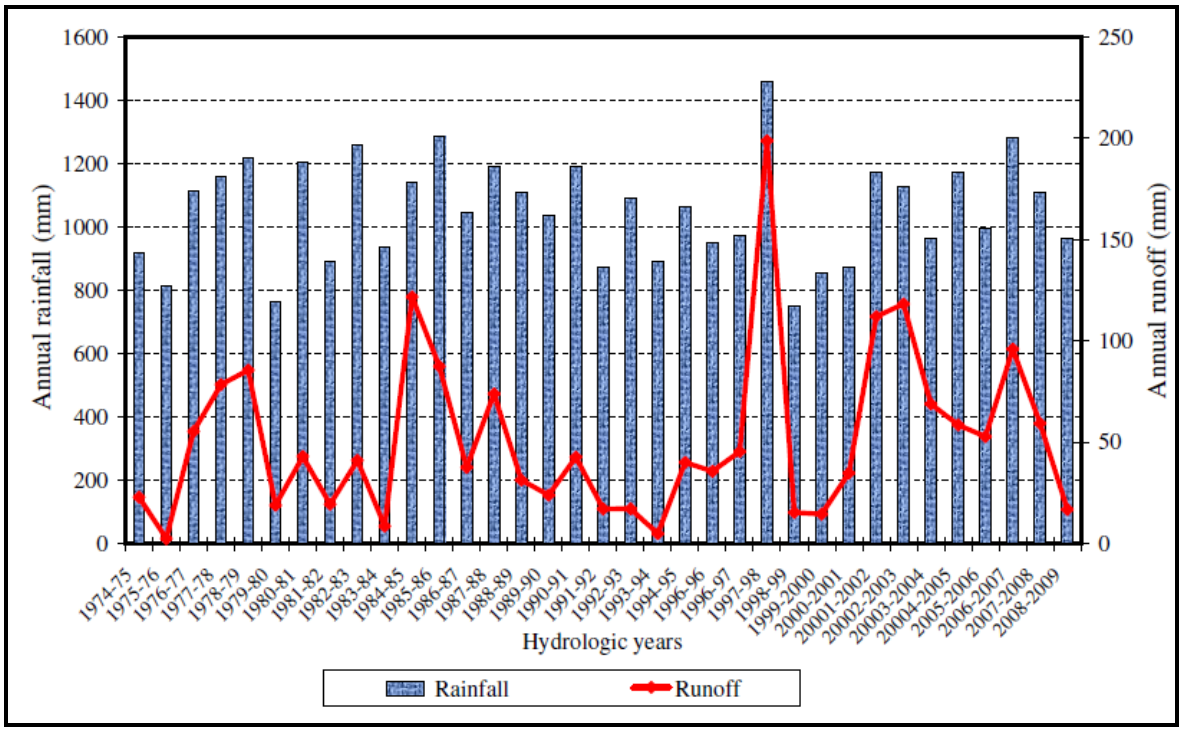

Figure III.19. Annual precipitation and runoff for the period 1974/75 through 2008/2009

Figure III.20 shows monthly rainfall and the monthly runoff estimated using the curve number method for the period 1974 through 2009. In general, Figures III.19 and III.20 show that important rainfall depths may lead to increased runoff but this is not always the

case. Indeed, the amount of runoff depends on several factors including the rainfall intensity and the antecedent soil moisture status. Hence, even an important rainfall amount in a month or a year may not generate a significant runoff depending on the intensity of the different daily rainfall events or the soil moisture status. For example the monthly rainfall for November 1987 was 252.1 mm and the estimated runoff was 51.8 mm, while for April 1988, with a monthly rainfall 263.7 mm the calculated runoff is only 12 mm.

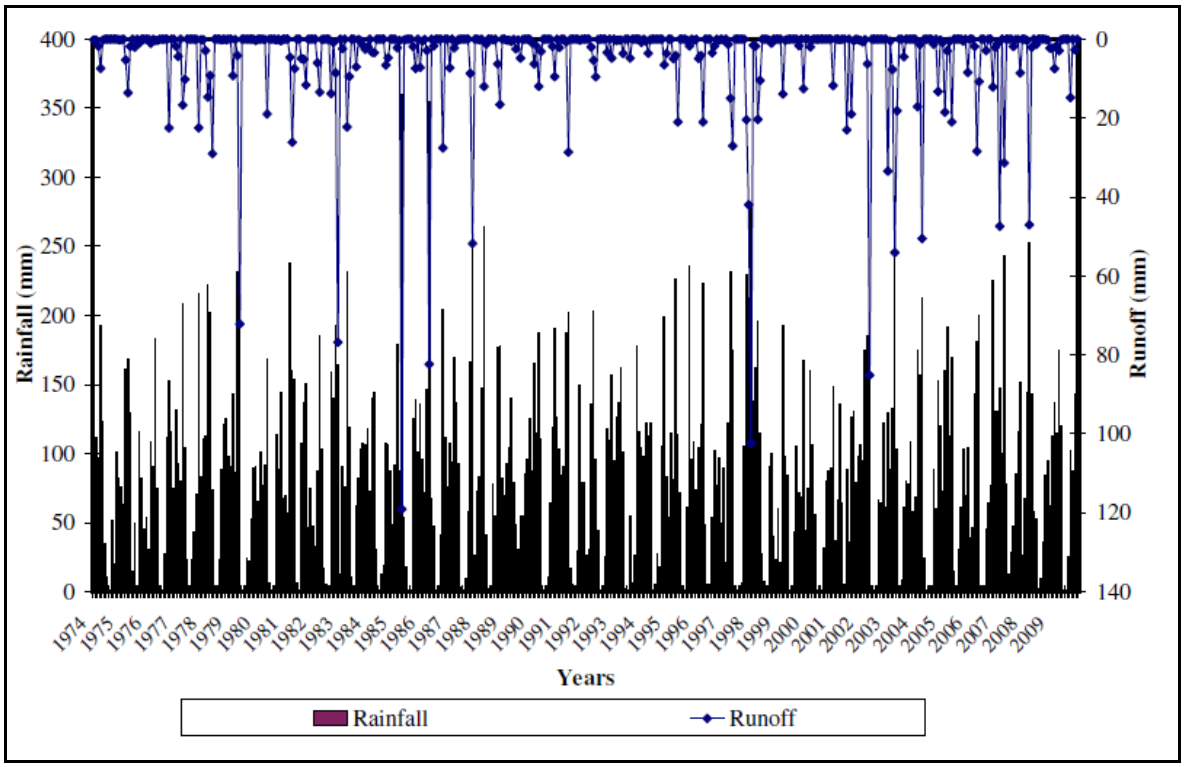

Figure III.20. Monthly rainfall and runoff for the period 1974 through 2009

III.4.3.2.3.8. Natural groundwater recharge (R_N)

After determining all the factors controlling the natural groundwater recharge (R_N), this important parameter was eventually calculated as the fraction of the precipitation which reaches the groundwater water table using the soil moisture balance method according to the procedure presented in Table III.7.

III.4.3.3. Results and discussion

III.4.3.3.1. Potential evapotranspiration

The potential evapotranspiration was calculated on monthly and daily basis using available data: monthly data for the period 1974 to 2009 and daily data for the period 1999 to 2009. Figure III.21 represents the comparison between the monthly average values of potential evapotranspiration calculated using five methods: Hamon, Thornthwaite and the modification of the original Thornthwaite method (k = 0.69), Hargreaves and Penman-Monteith for the period between 1999 and 2009. In the absence of direct measurement of evapotranspiration, the Penman-Montheith equation was used as a criterion to evaluate the performances of the four other methods of estimating evapotranspiration as recommended by FAO (Allen *et al.*, 1998; Xu & Sing, 2002; Castaneda & Rao, 2005; Jabloun & Sahli, 2008; Gonzalez-Dugo *et al.*, 2009; Sentelhas *et al.*, 2010). A visual inspection of Figure III.21 clearly shows that the Hargreaves method aberrantly overestimates the potential evapotranspiration, whereas the Hamon and Thornthwaite methods slightly underestimate it with respect to the standard Penman-Monteith equation. The modification of the original Thornthwaite method using k = 0.69 slightly overestimates the potential evapotranspiration as compared to the standard Penman-Monteith method.

An evaluation of the performances of the different PET methods in comparison to the standard Penman-Monteith method was made through the computation of the Root Mean Square Error (RMSE) between the average monthly PET estimated by Penman-Monteith equation and other methods (Table III.15). With a RMSE error of 48 mm/month, Hargreaves method appears to be the worst performing method for PET estimation in our study area, while the modification of the Thornthwaite method with k = 0.69 gave the lowest RMSE (RMSE = 5 mm/month), thereby indicating a good performance of the method. It can be also noted that the Thornthwaite method performs slightly better (RMSE = 10 mm/month) as compared to the Hamon's method (RMSE = 13 mm/month). Figure III.21 also indicates that, when PET is calculated with Hargreaves method, surplus and eventually recharge occur only during the long rainy season (rainfall > PET only in March-April), while with the other PET methods, surplus can occur both in short and long rainy seasons, thereby leading to an enhanced recharge.

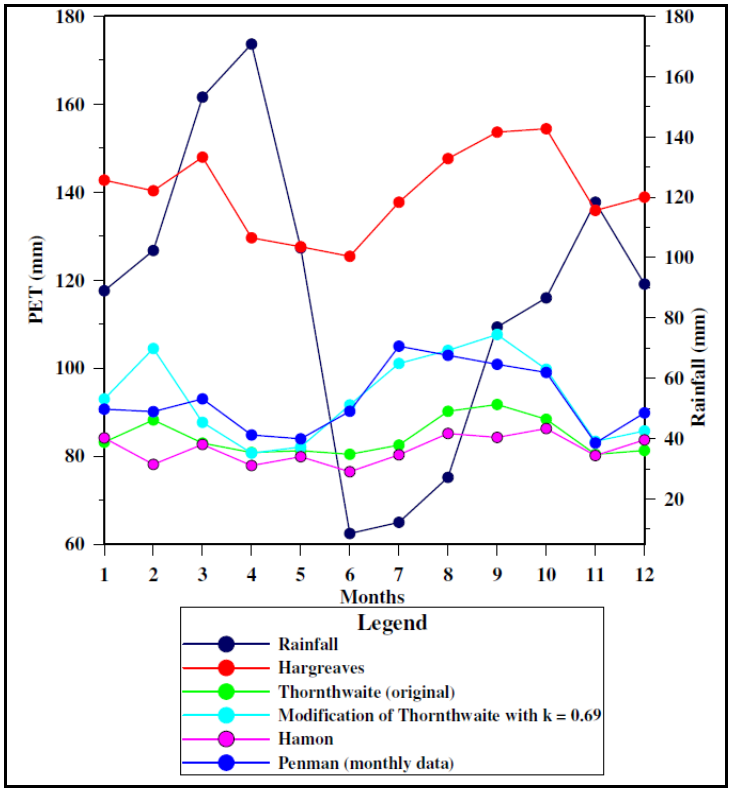

Figure III.21. Comparison of monthly average PET computed using different methods for the period 1999 through 2009

Table III.15. Comparison of average monthly PET computed by different methods for the period 1999-2009

Month	Hamon (mm)	Original TH (mm)	Modified TH (k = 0.69) (mm)	Hargreaves (mm)	PM (mm)
January	84.15	83.16	92.97	142.73	90.68
February	78.12	88.23	104.45	140.32	90.11
March	82.65	82.97	87.69	147.96	93.02
April	77.87	80.83	80.69	129.63	84.81
May	79.88	81.25	82.09	127.59	83.94
June	76.46	80.42	91.63	125.41	90.20
July	80.30	82.51	101.07	137.71	105.00
August	85.16	90.19	104.04	147.63	102.92
September	84.25	91.74	107.63	153.65	100.87
October	86.28	88.40	99.75	154.42	99.02
November	80.14	80.41	83.37	135.83	82.99
December	83.69	81.30	85.73	138.87	89.83
RMSE	13	10	5	48	0

TH: Thornthwaite, PM: Penman-Monteith

Table III.16 shows the annual average of the potential evapotranspiration calculated using the different methods over the period 1999-2009. It can be observed that the Hargreaves method overestimates the potential evapotranspiration by more than 50 %, whereas Hamon and Thornthwaite methods underestimate it respectively by 12 % and 9 %, with respect to reference PET computed by the standard Penman-Monteith equation. On the other hand, the modification of the original Thornthwaite method using the effective temperature instead of the mean air temperature seems to give good results. Indeed, by using this modification with k= 0.69, the PET is overestimated by only 1 % with respect to the reference PET estimated by the Penman-Monteith method. These results confirm the poor performance of Hargreaves method in estimating PET, as already reported by several previous studies (Trajkovic & Kolakovic, 2006; Xu & Singh, 2002; Castaneda & Rao, 2005; Jabloun & Sahli, 2008). Moreover, such aberrant PET results could be expected for our study area due to rather high relative humidity (annual average 70.3 %). Indeed, Allen *et al.* (1998) highlighted the tendency of Hargreaves equation to overpredict PET under conditions of high relative humidity.

Table III.16. Comparison of average annual PET computed on monthly basis by different methods for the period 1999-2009

Calculation method	Maximum (mm)	Minimum (mm)	Annual average (mm)	Departure from PM (%)
Hamon	1004.90	948.10	978.96	-12
Original Thorthwaite	1045.50	973.40	1011.40	-9
Modified Thornthwaite (k = 0.69)	1179.76	1059.52	1121.12	1
Hargreaves	1743.90	1601.05	1681.75	51
Penman-Monteith (PM) (monthly data)	1157.92	1053.83	1113.40	0
Penman-Monteith (PM) (daily data)	1169.93	1038.58	1100.74	

III.4.3.3.2. Groundwater recharge

Tables III.17 and III.18 illustrate the concept utilised to compute the groundwater balance based on different PET methods, by means of an example hydrologic year 2008-2009. The Hamon equation for estimation of the potential evapotranspiration is embedded into the TMWB model (McCabe & Markstrom, 2007). Thus, while the TMWB model program generates automatically the potential evapotranspiration and recharge (surplus), the computation of the soil moisture balance using other evapotranspiration methods through excel sheets is rather fastidious and time-consuming.

The results of calculation of annual groundwater recharge are given in Table III.19. For the period 1999/2000-2007/2009, the average annual recharge computed on a monthly basis using the Penman-Monteith PET is equal to 149.8 mm. By applying the evapotranspiration calculated using Hargreaves method, for the same period, the average annual groundwater recharge drastically drops to 12.3 mm, which represents a decrease of 92 % of the recharge estimated using the PET calculated by Penman-Monteith method. On the other hand, with the PET estimated by the modification of Thornthwaite method with k = 0.69, the groundwater recharge is overestimated by 0.4 % whereas, by applying the evapotranspiration calculated using the original equation of Thornthwaite and the equation of Hamon, the groundwater recharge is overestimated by 20 % and 24 % respectively.

Moreover, the time discretisation used in calculations has important consequences, the use of smaller time steps leading to enhanced recharge. Indeed, with recharge computation performed on a daily basis, precipitation sometimes greatly exceeds evapotranspiration on a single day, even in arid settings, and this leads to increased recharge. Averaging data over long time periods (monthly or annual) tends to overestimate actual evapotranspiration and thereby to deaden extreme precipitation events which are normally liable to recharge events (Walraevens & Van Camp, 2008; Walraevens *et al.*, 2009; Scalon *et al.*, 2002; Giambelluca, 1987; Xu & Chen, 2005). Hence, computing recharge on daily basis has the advantage of considering each of the individual small rainfall events which are actually the source of groundwater recharge. On the contrary, in summing up all the precipitations of one month, it is wrongly considered that all the small daily rainfall events form one big event which might still be smaller than the total monthly evapotranspiration, thereby resulting in reduced groundwater recharge.

Table III.17. Example of the calculation of recharge in excel sheet with PET calculated by Penman-Monteith method for the hydrologic year 2008-2009

Year	**2008**	**2008**	**2008**	**2008**	**2009**	**2009**	**2009**	**2009**	**2009**	**2009**	**2009**	**2009**
Month	**9**	**10**	**11**	**12**	**1**	**2**	**3**	**4**	**5**	**6**	**7**	**8**
P	35.50	84.60	94.30	62.50	112.90	136.90	115.10	175.00	120.05	0.70	0.00	25.70
R_O	0.00	0.02	0.19	2.27	2.26	7.48	1.65	2.92	0.11	0.00	0.00	0.00
P-R_O	35.50	84.58	94.11	60.23	110.64	129.42	113.45	172.08	119.94	0.70	0.00	25.70
PET(PM)	102.81	96.67	93.24	99.56	93.16	83.63	97.17	77.80	82.33	94.28	113.57	112.65
(P-Ro)-PET	-67.31	-12.10	0.86	-39.32	17.47	45.79	16.29	94.27	37.61	-93.58	-113.57	-86.95
PET-(P-Ro)	67.31	12.10	-0.86	39.32	-17.47	-45.79	-16.29	-94.27	-37.61	93.58	113.57	86.95
APWL	325.50	337.59	0.00	39.32	0.00	0.00	0.00	0.00	0.00	93.58	207.15	294.10
APWL/PAW	4.34	4.50	0.00	23.18	0.00	0.00	0.00	0.00	0.00	1.25	2.76	3.92
S_B	38.48	38.33	39.20	37.50	54.97	100.76	112.50	112.50	112.50	59.04	42.24	38.99
ΔS_B	-1.42	-0.15	0.86	-1.70	17.47	45.79	11.74	0.00	0.00	-53.46	-16.80	-3.25
AET (P-Ro+ΔS_B)	36.92	84.72	93.24	61.93	93.16	83.63	97.17	77.80	82.33	54.16	16.80	28.95
DEF (PET- AET)	65.89	11.95	0.00	37.63	0.00	0.00	0.00	0.00	0.00	40.12	96.77	83.70
SUR ((P-Ro)-AET)	-1.42	-0.15	0.86	-1.70	17.47	45.79	16.29	94.27	37.61	-53.46	-16.80	-3.25
R_N (SUR-ΔS_B)	0.00	0.00	0.00	0.00	0.00	0.00	4.55	94.27	37.61	0.00	0.00	0.00
R_N hydrologic year												136.43

P = precipitation (mm), Ro = runoff (mm), PET = potential evapotranspiration (mm), S_B = soil moisture storage (mm), ΔS_B = change in moisture storage (mm), AET = actual evapotranspiration (mm), DEF = deficit (mm), SUR = surplus (mm), R_N = natural recharge (mm), APWL= accumulated potential water loss (mm), PAW = plant available water (mm)

Table III.18. Example of computation of groundwater recharge in TMWB model program (McCabe & Markstrom, 2007) for the hydrologic year 2008-2009

	PET (mm)	**P (mm)**	**Ro (mm)**	**(P-Ro)-PET (mm)**	**P-PET (mm)**	**Soil moisture storage (mm)**	**AET (mm)**	**PET-AET (mm)**	**Groundwater recharge (mm)**
September 2008	84.4	35.5	1.775	-50.68	-50.7	2.8	36	48.4	0
October 2008	82.1	84.6	4.23	-1.73	-1.7	2.7	80.4	1.7	0
November 2008	78.7	94.3	4.715	10.89	10.9	13.6	78.7	0	0
December 2008	78.5	62.5	3.125	-19.13	-19.1	11.3	61.7	16.8	0
January 2009	73.9	112.9	5.645	33.36	33.4	44.7	73.9	0	0
February 2009	71.7	136.9	6.845	58.36	58.3	103	71.7	0	0
March 2009	83	115.1	5.755	26.35	26.4	112	83	0	17.4
April 2009	76.6	175.0	8.75	89.65	89.6	112	76.6	0	89.6
May 2009	81.7	120.0	6	32.30	32.3	112	81.7	0	32.3
June 2009	82.1	0.7	0.035	-81.44	-81.5	30.5	82.1	0	0
July 2009	84.3	0	0	-84.30	-84.3	7.5	23	61.4	0
August 2009	91.0	25.7	1.285	-66.59	-66.6	3.1	28.9	62.1	0
September 2009	86.8	102.2	5.11	10.29	10.2	13.3	86.8	0	0
R_N hydrologic year									139.3

P = precipitation (mm), Ro = runoff (mm), PET = potential evapotranspiration (mm), S_B = soil moisture storage (mm), ΔS_B = change in moisture storage (mm), AET = actual evapotranspiration (mm), DEF = deficit (mm), SUR = surplus (mm), R_N = natural recharge (mm), APWL= accumulated potential water loss (mm), PAW = plant available water (mm).

For the calendar years 1999 through 2009, daily values of meteorological parameters are available. Calculation of recharge on a daily basis using evapotranspiration computed by FAO Penman-Monteith equation gives 243.2 mm, which is 62 % higher than the recharge value obtained on a monthly time scale by applying monthly averages of meteorological parameters (149.8 mm). Of even more spectacular significance is the increase of the recharge for PET calculated with Hargreaves equation, from 12.3 mm on a monthly time scale to 72.2 mm on a daily time scale.

Calculations of groundwater recharge on daily time scale assume a swift drainage of water in the top soil. However, given the clayey nature of the top soil, the drainage may be slow and soil water content in the root zone may remain at field capacity for several days after rainfall. In such conditions, daily calculations might overestimate groundwater recharge. Hence, it would be interesting to calculate the recharge on a 10-day basis in order to take into account the slow drainage through the clayey top soil.

In our study, groundwater recharge computed by the TMWB model, on a monthly scale, using the Hamon equation for PET calculation was adopted. Compared to the recharge values obtained on a daily basis with Penman-Monteith PET (which represents the best approximation of reality) (average recharge of 243.2 mm for the period 1999/2000-2008/2009), of all attempted methods, the TMWB method which is on a monthly basis, using Hamon's PET, performs best (average recharge of 185.4 mm). The latter method presents the advantage of needing much less data.

For the period 1974/75-2008/2009, the average annual recharge computed using the TMWB model amounts to 218.4 mm, which represents 196.2 Mm^3 per year for the whole study area. Annual recharge for the whole period of records (1974-2009) varies between a minimum value of 0 mm and a maximum of 611.7 mm respectively for the hydrologic years 2000/2001 and 1997/1998 which were exceptionally dry and wet. Figure III.22 shows the distribution of the average monthly recharge calculated using the PET estimated by different methods for the period 1999/2000-2008/2009. It can be observed that the distribution pattern of monthly recharge features a bimodal pattern somewhat similar to that of the monthly rainfall. Indeed, groundwater recharge mainly occurs during the long rainy season (March to May) and to a lesser extent during the short rainy season, in November. By using the TMWB model, recharge during the long rainy season accounts for more than 93 % of the total annual recharge with an important peak in April, whereas recharge occurring during the short rainy season contributes to only 2 % of the total annual recharge with a small peak in November. There is always a time lag between the onset of the rainy

season (February for the long rainy season and September for the short one) and the peak of groundwater recharge, which must be expected from the fact that the soil moisture must be brought to its maximum water holding capacity, i.e. field capacity, before recharge can occur. It is also interesting to note that, although the period December-January is considered as the short dry season due to the decrease of precipitations, groundwater recharge can still occur depending on the amount of precipitations during and after the short rainy season, and therefore the state of soil moisture storage. This is not the case for the long dry season where groundwater recharge is systematically nil.

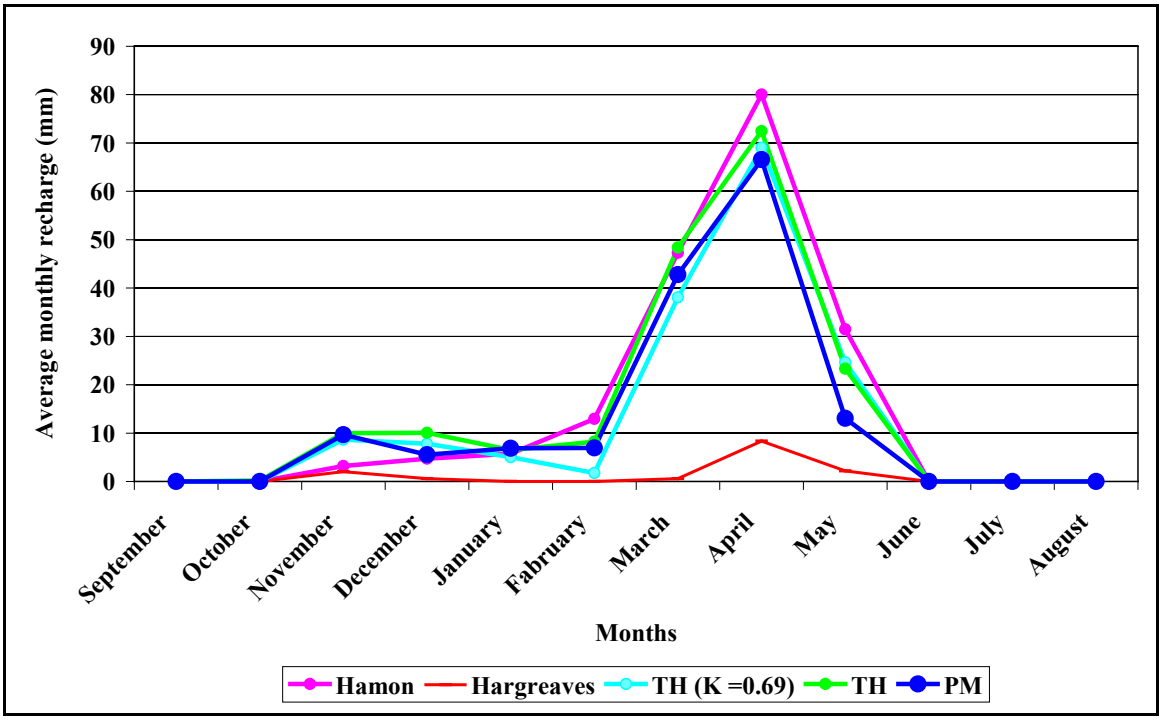

Figure III.22. Monthly average recharge for the period 1999/2000-2008/2009 (TH: Original Thorthwaite's PET equation, TH (k = 0.69): Modification of Thornthwaite's PET equation with k = 0.69, PM: Penman-Monteith equation)

There is no contribution to recharge from return flow because there is nearly no irrigation practice in the study area. Indeed, in our study area, as for the whole country, there are three agricultural seasons. Two agricultural seasons which cover the two rainy seasons (September to May), i.e. the agricultural season A, from September to January, and the agricultural season B from January to June, whereas during the third one, the agricultural season O, which runs from June to September, crop production is concentrated on marshlands where there is no need for irrigation.

Figure III.23 presents the results of annual groundwater recharge computed using values of potential evapotranspiration estimated by different methods. It can be observed that the evapotranspiration plays a significant role in groundwater balance. It is the main mechanism whereby part of the precipitations is lost back to the atmosphere. Thus, the higher the evapotranspiration, the lower the amount of groundwater recharge. Evapotranspiration can have a direct as well as an indirect impact on groundwater resources. The direct impact is related to the groundwater transpiration through deep root systems and/or evaporation from the groundwater table. The indirect impact consists of the moisture uptake by plant root systems in the soil and the evaporation from the unsaturated zone. Phillips (1963) observed that in dry climates groundwater uptake by roots may reach the depth of more that 50 m, whereas according to Walvoord *et al.* (2002), evaporation from the groundwater table and capillary transport may take place at more than 20 m depth. Moreover, Figure III.23 shows that, overall, TMWB model gives a higher annual recharge compared to the recharge, calculated using PET estimated by other methods.

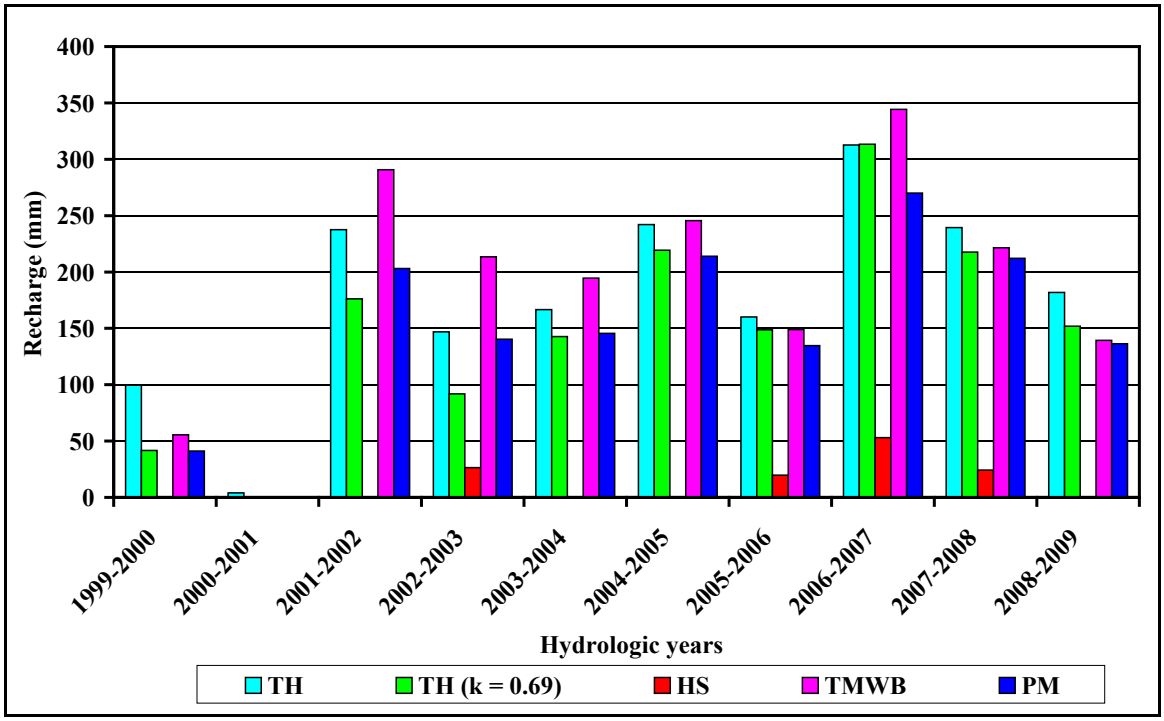

Figure III.23. Average annual recharge computed using different PET methods, on a monthly basis, for the period 1999/2000-2008/2009 (TH: Original Thorthwaite's PET equation, TH (k = 0.69): Modification of Thornthwaite's PET equation with k = 0.69, PM: Penman-Monteith equation, HS: Hargreaves-Samani, TMWB: Thorthwaite monthly water balance, PM: penman-Monteith)

Table III.19. Results of groundwater recharge calculation using potential evapotranspiration estimated by different methods

Hydrologic year	Monthly data					Daily Data	
	TH	TH (k = 0. 69)	HS	TMWB	PM	HS	PM
1974-75	183.74	116.67	15.06	146.6			
1975-76	127.34	54.36	0.00	75.7			
1976-77	305.54	119.82	0.00	290.5			
1977-78	414.74	290.12	39.04	391.1			
1978-79	425.50	229.37	16.97	412.5			
1979-80	76.18	19.72	0.00	12.9			
1980-81	266.61	241.06	52.95	235.7			
1981-82	121.87	85.49	0.00	71.5			
1982-83	269.55	240.10	9.67	316.2			
1983-84	173.21	139.99	0.00	122.7			
1984-85	248.79	197.67	53.95	317.9			
1985-86	371.77	305.56	69.28	401.9			
1986-87	252.52	133.10	0.00	223.8			
1987-88	355.46	304.82	58.16	339.4			
1988-89	264.36	186.45	29.58	180.9			
1989-90	296.39	168.00	0.00	256.1			
1990-91	341.59	310.87	43.91	317.5			
1991-92	109.94	93.41	0.00	73.5			
1992-93	293.55	236.50	0.00	227.8			
1993-94	127.97	96.70	0.00	146.3			
1994-95	224.62	190.94	21.14	187.2			
1995-96	309.39	248.47	73.65	256.4			
1996-97	168.60	160.15	37.69	162.5			
1997-98	472.42	429.82	91.27	611.7			
1998-99	51.06	38.07	0.00	12.7			
1999-2000	99.55	41.65	0.00	55.6	41.22	0.00	100.20
2000-2001	4.05	0.00	0.00	0	0.00	0.00	60.02
2001-2002	237.59	176.17	0.00	290.8	203.05	98.15	361.85
2002-2003	146.87	91.86	26.48	213.4	140.40	81.66	264.72
2003-2004	166.61	142.70	0.00	194.6	145.57	61.48	226.12
2004-2005	242.13	219.36	0.00	245.6	214.03	73.37	342.68
2005-2006	160.04	148.68	19.66	148.9	134.64	98.58	209.38
2006-2007	312.68	313.39	53.06	344.3	270.07	177.29	386.96
2007-2008	239.46	217.69	24.18	221.5	212.13	82.80	284.09
2008-2009	181.91	151.95	0.00	139.3	136.43	48.66	195.76
Average 1999/2000-2008/2009	**179.09**	**150.34**	**12.34**	**185.40**	**149.75**	**72.20**	**243.18**
Average all data	**229.82**	**175.45**	**21.02**	**218.43**	**149.75**	**72.20**	**243.18**

HS = Hargreaves-Samani PET method; TH = Original Thornthwaite PET method; TH (k = 0.69) = modification of Thornthwaite PET equation with k = 0.69; TMWB = Hamon PET method; PM = Penman-Monteith PET method.

The computation of the soil moisture balance was performed using a rooting depth of 0.25 m as suggested by Thornthwaite & Mather (1957) (Table III.8). However, such a small rooting depth may neglect the upwards flow of water from the wet subsoil towards the dry top soil. To evaluate the effect of the rooting depth on groundwater recharge, increased values of effective rooting depth, 0.50 and 0.75 m, were tested on a daily and monthly time scale for a period of 10 hydrologic years (1999/2000-2008/2009), using the Penman-Monteith PET. Increased values of effective rooting depth imply increased values of water content at field capacity (CAP) within the root zone and consequently reduced amount of groundwater recharge. Table III.20 shows a comparison of groundwater recharge calculated using the different values of effective rooting depth on daily and monthly time scales. Table III.21 shows the details of the calculation of groundwater recharge using an effective rooting depth of 0.75 m for the sample hydrologic year 2008-2009.

Table III.20. Comparison of groundwater recharge estimated using different effective rooting depths

	Rooting depth = 0.25 m		**Rooting depth = 0.50 m**		**Rooting depth = 0.75 m**	
	CAP = 112.50 mm		**CAP = 187.50 mm**		**CAP = 262.5 mm**	
Hydrologic year	**Monthly**	**Daily**	**Monthly**	**Daily**	**Monthly**	**Daily**
1999-2000	41.22	100.2	0.00	10.59	0.00	0.00
2000-2001	0.00	60.02	0.00	0.00	0.00	0.00
2001-2002	203.05	361.85	128.35	268.84	53.35	191.69
2002-2003	140.4	264.72	77.03	173.21	32.01	107.38
2003-2004	145.57	226.12	94.08	156.10	63.96	108.77
2004-2005	214.03	342.68	146.06	241.79	94.27	160.70
2005-2006	134.64	209.38	67.89	126.48	17.57	52.90
2006-2007	270.07	386.96	210.63	295.71	170.75	218.20
2007-2008	212.13	284.09	159.04	184.55	131.77	137.30
2008-2009	136.43	195.76	63.00	120.47	10.05	59.29
Average	**149.75**	**243.18**	**94.61**	**157.77**	**57.37**	**103.62**

As this could be expected, Table III.20 and Figure III.24 show that increasing the effective rooting depth results into a substantial reduction of groundwater recharge as a consequence of the increased water content at field capacity (CAP) in the root zone, which is largely evaporated in the dry period requiring replenishment before groundwater recharge can occur. It is interesting to note that the average values of groundwater recharge calculated on a daily time scale using increased effective rooting depths (0.50 m and 0.75 m) and the

attendant increased CAP, are fairly comparable to the rough estimates of recharge calculated using the water level fluctuation (121.6 m) and the hybrid water level fluctuation method (143.1 mm). The monthly estimates of groundwater recharge calculated using increased effective rooting depths are far below the rough estimates calculated using the water level fluctuation (121.6 m) and the hybrid water level fluctuation method (143.1 mm).

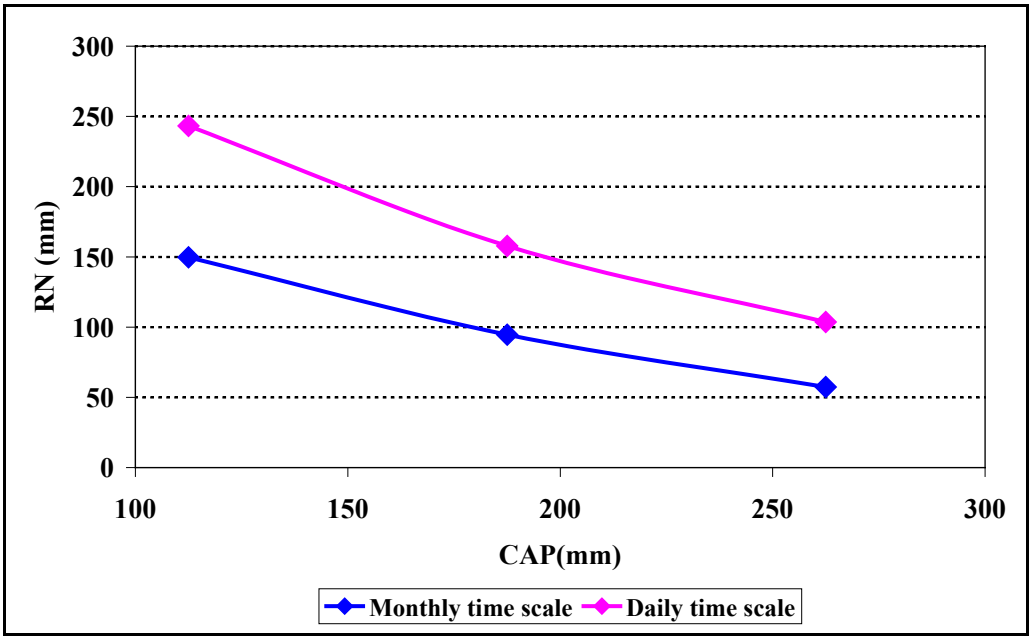

Figure III.24. Variation of groundwater recharge in function of the effective rooting depth, changing CAP.

Table III.21. Example of the calculation of groundwater recharge using an effective rooting depth of 0.75 mm and PET calculated by Penman-Monteith method for the hydrologic year 2008-2009

Year	**2008**	**2008**	**2008**	**2008**	**2009**	**2009**	**2009**	**2009**	**2009**	**2009**	**2009**	**2009**
Month	9	10	11	12	1	2	3	4	5	6	7	8
P	35.50	84.60	94.3	62.5	112.90	136.90	115.10	175.00	120.05	0.70	0.00	25.70
R_o	0.00	0.02	0.19	2.27	2.26	7.48	1.65	2.92	0.11	0.00	0.00	0.00
P-R_o	35.50	84.58	94.11	60.23	110.64	129.42	113.45	172.08	119.94	0.70	0.00	25.70
ET(PM)	102.81	96.67	93.24	99.56	93.16	83.63	97.17	77.80	82.33	94.28	113.57	112.65
(P-R_o)-PET	-67.31	-12.10	0.86	-39.32	17.47	45.79	16.29	94.27	37.61	-93.58	-113.57	-86.95
PET-(P-R_o)	67.31	12.10	-0.86	39.32	-17.47	-45.79	-16.29	-94.27	-37.61	93.58	113.57	86.95
APWL	325.50	337.59	0.00	39.32	0.00	0.00	0.00	0.00	0.00	93.58	207.15	294.10
APWL/PAW	1.45	1.50	0.00	0.77	0.00	0.00	0.00	0.00	0.00	0.42	0.92	1.31
S_B	90.45	87.68	88.55	61.13	78.60	124.39	140.67	234.95	262.50	185.94	127.11	98.39
ΔS_B	-18.47	-2.77	0.86	-27.42	17.47	45.79	16.29	94.27	27.55	-76.56	-58.83	-28.72
AET (P-R_o+ΔS_B)	53.97	87.35	93.24	87.65	93.16	83.63	97.17	77.80	82.33	77.26	58.83	54.42
D (PET- AET)	48.84	9.32	0.00	11.90	0.00	0.00	0.00	0.00	0.00	17.02	54.74	58.23
SUR ((P-R_o)-AET)	-18.47	-2.77	0.86	-27.42	17.47	45.79	16.29	94.27	37.61	-76.56	-58.83	-28.72
R_N (SUR-ΔS_B)	0.00	0.00	0.00	0.00	0.00	0.00	0.00	0.00	10.05	0.00	0.00	0.00
R_N hydrologic year												**10.05**

P = precipitation (mm), Ro = runoff (mm), PET = potential evapotranspiration (mm), S_B = soil moisture storage (mm), ΔS_B = change in moisture storage (mm), AET = actual evapotranspiration (mm), DEF = deficit (mm), SUR = surplus (mm), R_N = natural recharge (mm), APWL= accumulated potential water loss (mm), PAW = plant available water (mm)

III.4.4. Estimation of groundwater recharge using the water table fluctuation method

Estimation of groundwater recharge using the water table fluctuation method was performed thanks to water level measurements taken from January to December 2008. These water level measurements show a continuing rising of the water table from January with a peak in April or May (Figure III.25). Thereafter, the water level in wells starts to decline during the dry season and starts to rise again from October or November. Table III.22 presents the water level rises in selected wells which were calculated, for each well, as the difference of groundwater levels of two consecutive months. Thus, the water level fluctuation for January 2008 could not be calculated because there are no water level measurements for December 2007. For the dry period, the water level progressively declines, resulting in negative water level fluctuations which are not reported in Table III.20. The rising of water table in wells reflects recharge which can be quantified using the relationship devised by Kruseman (1997) (in Misstear, 2000):

$$R_N = \Delta h.S_y + Q_a + Q_l$$

Q_a = the groundwater abstraction during the period under consideration (can be neglected as the measurements were taken in abandoned wells); Q_l = the difference between lateral subsurface outflow and lateral subsurface inflow during the same period. This factor was also neglected by assuming that recharge water is the main cause of water level rise in the well.

Table III.22. Monthly rises of water level compared to previous month, in selected wells across the study area (mm).

Well location	Jan	Feb	Mar	Ap	May	June	July	Aug	Sept	Oct	Nov	Dec
Sigu	n.d.	100	230	315	200	-	-	-	-	-	140	60
Gikombe	n.d.	85	220	255	225	-	-	-	-	-	125	60
Vyanzo II	n.d.	60	200	300	210	-	-	-	-	-	65	25
Renga II	n.d.	5	76	154	12	-	-	-	-	48	33	7
Gikomero	n.d.	94	26	172	108	45	-	-	-	76	98	43
Kariba	n.d.	40	15	60	89	11	-	-	-	28	138	40

n.d.: no data, -: groundwater level decline

The 6 wells used to compute the groundwater recharge were selected in such a way that the variability of the weather conditions in the study area is taken into account. Hence, the first three wells in Table III.22 (Sigu: III.25 C, Gikombe: III.25 D and Vyanzo II: III.25 E) are located in the northern part of the depression where drier conditions prevail, while the last three wells (Kariba: III.25 A, Gikomero: III. 25 B, Renga II:

III.25 F) are situated in southwestern part of the depression, in the transition zone towards the highlands where more humid conditions are expected.

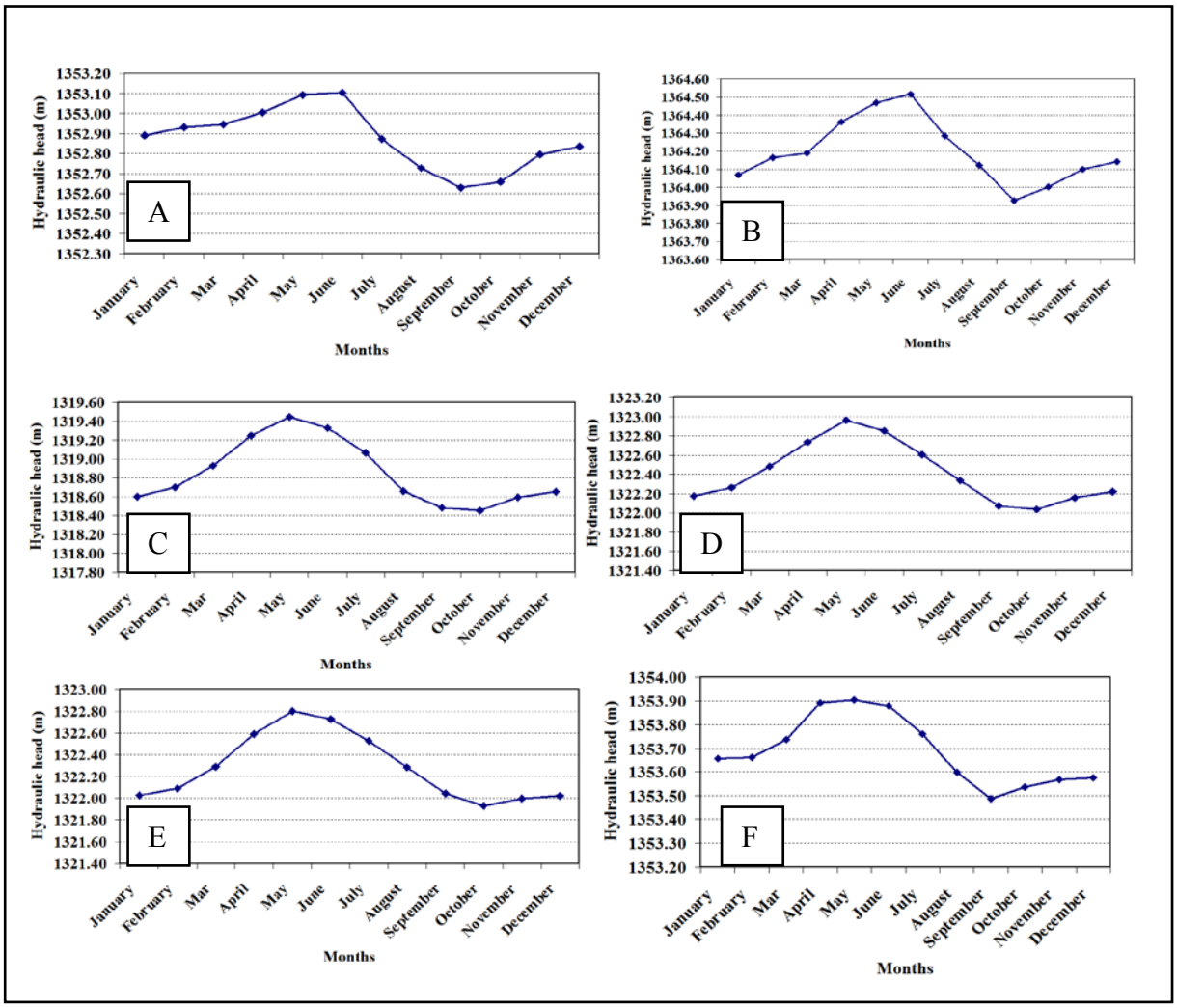

Figure III.25. Groundwater level fluctuations in wells at Kariba-Kanyagu (A), Gikomero-Susa (B), Sigu-Kumana (C), Gikombe-Nyagisozi (D), Vyanzo II-Gatete (E), Renga II-Gitwenzi (F) for the year 2008.

Table III.23 shows groundwater recharge estimated based on the water table fluctuation method using a specific yield (S_y) value of 0.17, which is the optimised value obtained after calibration of the groundwater flow model (Chapter VII). Compared to the recharge estimated using the TMWB model for the calendar year 2008 (Table III.22), it can be observed that the water table fluctuation method seems to significantly underestimate the recharge, although it performs better than the soil moisture balance calculation based on Hargreaves PET. Most probably this underestimation is due to the fact that the average value of specific yield used, may not correctly reflect the heterogeneities characterising the weathered overburden, which is a mixture of clay, sand, gravel and rock fragments in variable proportions. Furthermore, if evapotranspiration from groundwater occurs, this leads to lower groundwater level and

consequently results in underestimation of water level rise due to recharge as shown by the following equations:

$$R_N - ET_g + Q_i - Q_O = \Delta S$$

Where R_N is the natural groundwater recharge (mm), ET_g is the evapotranspiration (mm) from the groundwater, Q_i is return flow (mm) and Q_o is the baseflow (mm), ΔS is the change in storage expressed by change in water level (mm).

$$\Delta S = \Delta h * S_y.$$

Where Δh is the groundwater rise (mm) and S_y is the specific yield.

Results of the water table fluctuation method show that groundwater recharge occurs both during the short rainy season (October to December) and the long rainy season (February to May), which corresponds to the reality, while the soil moisture balance method for 2008 (Table III.24) (on a monthly basis) indicates that the recharge occurs only during the long rainy season as a result of important rainfall events. Groundwater recharge in different wells varies between a minimum of 57 mm and a maximum of 178 mm with an average of 122 mm.

The water table fluctuation method gives recharge estimates which are more spread in time and is therefore more realistic. The large discrepancy between estimates of recharge obtained using the water fluctuation and the TMWB may be ascribed to the fact that the average value of specific yield is underestimated. Moreover, the soil storage capacity may have been overestimated in the soil moisture balance method, and this precludes the occurrence of recharge except in periods of intense rainfall, mainly during the long rainy season, when the soil moisture storage is brought to its full capacity.

Table III.23. Monthly groundwater recharge calculated using the water level fluctuation method.

Well location	**Jan**	**Feb**	**Mar**	**Ap**	**May**	**June**	**July**	**Aug**	**Sept**	**Oct**	**Nov**	**Dec**	**Total**
Sigu	n.d.	17.0	39.1	53.5	34.0	-	-	-	-	-	23.8	10.2	177.7
Gikombe	n.d.	14.5	37.4	43.3	38.3	-	-	-	-	-	21.3	10.2	164.9
Vyanzo II	n.d.	10.2	34.0	51.0	35.7	-	-	-	-	-	11.0	4.3	146.2
Renga II	n.d.	0.9	12.9	26.2	2.0	-	-	-	-	8.2	5.6	1.2	57.0
Gikomero	n.d.	16.0	4.4	29.2	18.4	7.7	-	-	-	12.9	16.7	7.3	112.5
Kariba	n.d.	6.8	2.5	10.2	15.1	1.9	-	-	-	4.8	23.5	6.8	71.6
Average	n.d.	**10.9**	**21.7**	**35.6**	**23.9**	**4.8**	-	-	-	**8.6**	**17.0**	**6.7**	**121.6**

n.d. no data, -: groundwater level decline

Table III.24. Groundwater recharge estimated using the TMWB model on a monthly basis for the calendar year 2008

Month	PET (mm)	P (mm)	P-PET (mm)	Soil moisture (mm)	AET (mm)	PET-AET (mm)	R_N (mm)
Jan	79.1	67	-15.4	49.3	71.5	7.6	0
Feb	72.1	144	64.7	112	72.1	0	2
Mar	77.9	252.1	161.6	112	77.9	0	161.6
April	78.2	143.3	57.9	112	78.2	0	57.9
May	83	58	-27.8	84.2	83	0	0
June	78.1	52.6	-28.1	63.1	71.1	7	0
July	82.9	2.4	-80.7	17.6	47.7	35.2	0
Aug	88.9	9.5	-79.8	5.1	21.6	67.3	0
Sept	84.4	35.5	-50.7	2.8	36	48.4	0
Oct	82.1	84.6	-1.7	2.7	80.4	1.7	0
Nov	78.7	94.3	10.9	13.6	78.7	0	0
Dec	78.5	62.5	-19.1	11.3	61.7	16.8	0
Total							**221.5**

III.4.5. Estimation of groundwater recharge using hybrid water level fluctuation method (Sophocleous, 1991)

For the estimation of groundwater recharge using the hybrid method, an average value of specific yield, S_y, is first calculated by averaging the different values obtained by dividing the groundwater recharge calculated from the soil moisture balance method by the corresponding rise in groundwater table in each well. Tables III.25 to III.27 show the procedure used to compute the monthly recharge using the hybrid water level fluctuation method. Overall, specific yield values estimated from water level rises appear to be very small for February 2008, while they are extremely large and even physically unrealistic (>100 %) for March (Table II.26). Hence the average value of specific yield obtained from the groundwater rise in April for the wells situated in Sigu, Gikombe and Vyanzo, i.e. 0.20, was found to be realistic and was used to estimate the recharge.

For the 6 wells, the annual groundwater recharge varies between 67 mm and 209 mm with an average of 143.1 mm (Table III.27). The discrepancy between the value of recharge computed with the soil moisture balance and the one obtained from the hybrid water fluctuation method may be explained by the fact that one average value of field capacity used in the former and one average specific yield in the latter method do not correctly reflect the variability of lithological composition over the whole study area. Similarly to the water table fluctuation method, the hybrid method shows that recharge occurs both in short and long rainy seasons, while with the soil moisture balance

method for 2008, recharge occurs only during the long rainy season. It is interesting to note that the wells at Sigu, Gikombe and Vyanzo II, which are located in the same zone, around Lake Rweru, show fairly comparable, higher values of recharge, compared to the wells Renga II, Gikomero and Kariba which are located in the southwestern part of the study area.

Table III.25. Monthly water level rises (mm) and monthly recharge (mm) estimated using the TMWB model

Wells	Jan	Feb	Mar	Ap	May	June	July	Aug	Sept	Oct	Nov	Dec
Sigu	n.d.	100	230	315	200	-	-	-	-	-	140	60
Gikombe	n.d.	85	220	255	225	-	-	-	-	-	125	60
Vyanzo II	n.d.	60	200	300	210	-	-	-	-	-	65	25
Renga II	n.d.	5	76	154	12	-	-	-	-	48	33	7
Gikomero	n.d.	94	26	172	108	45	-	-	-	76	98	43
Kariba	n.d.	40	15	60	89	11	-	-	-	28	138	40
Recharge (TWBM) (mm)		**2**	**162**	**58**								

n.d. no data, -: groundwater level decline

Table III.26. Specific yield values estimated using monthly water level rises and recharge computed with the TMWB model

Well location	Jan	Feb	March	April	May	June	July	Aug	Sept	Oct	Nov	Dec
Sigu	n.d.	0.02	0.70	0.18	n.r.e	-	-	-	-	-	n.r.e	n.r.e
Gikombe	n.d.	0.02	0.73	0.23	n.r.e	-	-	-	-	-	n.r.e	n.r.e
Vyanzo II	n.d.	0.03	0.81	0.19	n.r.e	-	-	-	-	-	n.r.e	n.r.e
Renga II	n.d.	0.40	(2.13)	0.38	n.r.e	n.r.e	-	-	-	n.r.e	n.r.e	n.r.e
Gikomero	n.d.	0.02	(6.22)	0.34	n.r.e	n.r.e	-	-	-	n.r.e	n.r.e	n.r.e
Kariba	n.d.	0.05	(10.77)	(0.96)	n.r.e	n.r.e	-	-	-	n.r.e	n.r.e	n.r.e
Average* S_y		**0.02**	**0.75**	**0.20**								

* average only for the first 3 wells, n.d.: no data, n.r.e: no recharge estimate from soil moisture balance

Table III.27. Monthly groundwater recharge calculated using the hybrid water level fluctuation method

Well location	Jan	Feb	Mar	Ap	May	June	July	Aug	Sept	Oct	Nov	Dec	Total
Sigu	n.d.	20.0	46.0	63.0	40.0	-	-	-	-	-	28.0	12.0	209.0
Gikombe	n.d.	17.0	44.0	51.0	45.0	-	-	-	-	-	25.0	12.0	194.0
Vyanzo II	n.d.	12.0	40.0	60.0	42.0	-	-	-	-	-	13.0	5.0	172.0
Renga II	n.d.	1.0	15.2	30.8	2.4	-	-	-	-	9.6	6.6	1.4	67.0
Gikomero	n.d.	18.8	5.2	34.4	21.6	9.0	-	-	-	15.2	19.6	8.6	132.4
Kariba	n.d.	8.0	3.0	12.0	17.8	2.2	-	-	-	5.6	27.6	8.0	84.2
Average	**n.d.**	**12.8**	**25.6**	**41.9**	**28.1**	**5.6**	-	-	-	**10.1**	**20.0**	**7.8**	**143.1**

n.d.: no data, -: groundwater level decline

III.5. Groundwater exploitation

Groundwater exploitation in the study area is only accomplished through shallow hand-dug wells equipped with hand- or foot-operated pumps whose nominal capacity is 1.5 m^3 per hour. These wells were constructed since the colonial period (before 1960) as a way to supply drinking water to local rural populations, mainly in the depression of Bugesera where natural springs are rather scarce. Well construction was intensified in late 1980's and beginning of the 1990's thanks to a project funded by the European Fund for Development through the so-called *"projet Kirundo"* (Kirundo project). In the late 1990's, a number of new wells were also constructed by humanitarian NGO's along with the rehabilitation of some of the wells vandalized during the civil war. With a depth varying between 5 m and 17.5 m, these shallow wells only tap the shallow aquifer, hosted within the weathered overburden covering the substratum. In total, there are 176 wells in the study area, among which only 86 are functioning. Among these 86 wells which are operating nowadays, 30 were constructed by a BTC-funded project in the course of the year 2008. The large number of non-operating wells is to be linked to 3 main factors: (1) pump failure, (2) well abandonment due to poor water quality (bad smell or taste due to anthropogenic pollution or high mineralisation) or (3) theft of the pump.

Most of the wells are equipped with hand- or foot-operated pumps and have therefore been assigned the same yield of 1.5 m^3 per hour which is the nominal discharge capacity of this type of pumps. The well located at Kigina-Gisenyi I is highly productive and has been assigned a yield of 20 m^3/day. Indeed, even population from surrounding villages where wells are not operating or where water quality from wells is deemed not good come to collect water from this well. The well also supplies water to the small commercial centre of Kubaniro (Zone Gisenyi). This well is operating all day long. The pump of this well was stolen during the civil was (1993-2005) and local villagers decided to remove the concrete cover of the well so that they can directly fetch water from the well using buckets suspended to long sticks. By considering the total number of producing wells in the study area (86 wells) with an average pumping time of 6 hours per day, the annual groundwater abstraction from these shallow wells is equal to 286721 m^3/year for the whole study area. The water supply company (REGIDESO) in the city of Kirundo also exploits a well at the pumping station located at the outskirts of the city. With a pumping rate of 0.8 l/sec, the annual production of this well amounts to 25246 m^3 per year. In total, the groundwater exploitation in the whole study area is equal to 311967 m^3 per year or 0.312 Mm^3 per year.

III.6. Groundwater balance

The water balance equation which is commonly used to quantify the components of the hydrologic balance at the basin scale can be written as (Domenico & Schwartz, 1990):

$$P - ET - Ro = \Delta S_{g+s}$$

where P = precipitation, ET = evapotranspiration, Ro = runoff of rivers to the sea and ΔS = the change in storage for all subsurface and terrestrial surface waters. The components of the above equation have the units of discharge or volume per unit time. For the groundwater component of the hydrologic cycle, the water balance equation can be presented as follows:

$$R_N + Q_i - Q_o - ET_g = \Delta S$$

where RN = natural groundwater recharge; Q_i = groundwater input from irrigating surface waters when streams lose water to the groundwater reservoir or return seepage from irrigated fields; Q_o = base flow when streams and other surface water bodies receive water from the groundwater reservoir; and ΔS = the change in groundwater storage. Over long periods and in the absence of groundwater exploitation, long-term average recharge is equal to discharge and no significant change in storage occurs, ΔS = 0. Hence, the groundwater balance equation can be rearranged as:

$$R_N + Q_i = Q_o + ET_g$$

This means that the groundwater component in the basin is hydrologically in equilibrium. However, if there is groundwater exploitation through pumping wells, the groundwater balance equation becomes:

$$RN + Q_i - Q_o - ET_g = \Delta S$$

where $\Delta S = Q_p$ = groundwater abstraction from wells, which is true in the long term (neglecting seasonal fluctuation), and assuming stable climatic conditions. In this case the system is said to be in a transient or unsteady state.

Return flow, Q_i, in the study area can be neglected as there is no irrigation practice and no losing streams. Besides the groundwater recharge, the other components of the groundwater balance equation could be determined except for the groundwater baseflow (Q_o). The baseflow, which includes the groundwater discharge to surface water courses either as groundwater seepage to lakes, marshlands and rivers or as spring discharge appears to be the most difficult parameter to determine in our study area. This is complicated by the presence of the complex of interconnected swamps and shallow lakes which does not allow the measurement of the surface water discharge. The springs are mostly located in the southern and southeastern parts of the study area which form the transition between the depression of Bugesera and Bweru highlands. In total, 136 springs are documented in our study area with a total discharge of 9564.25 m^3/d, which is equivalent to 3.494 Mm^3 per year. However, the information about spring discharge is not reliable as most of the time only one measurement is available. Hence, the baseflow was taken as the only unknown parameter and determined indirectly taking into account the groundwater recharge and groundwater abstraction through pumping

wells. The latter can be considered as fairly equal to the change in storage. Table III.28 presents the groundwater budget estimated for the whole study area.

Table III.28. Groundwater budget

Component		**Quantity (Mm^3/year)**	**Fraction of the recharge (%)**
Recharge R_N		196.152	100
Groundwater abstraction through hand-dug wells	$\mathbf{Q_p = \Delta S}$	-0.287	0.15
Groundwater abstraction at the pumping station in Kirundo by REGIDESO (water supply company)		- 0.025	0.01
Spring discharge		-3.494	1.78
Total baseflow Q_O		+ 192.35	98.06

Such an important baseflow in this depression coupled with the low-lying topography may explain the presence of the complex of interconnected swamps, associated with perennial shallow lakes which do not dry up, even in periods of severe drought. During the prolonged drought which took place from 1998/1999 through 2000/2001, one small lake, Gacamirinda was reported to have dried up but according to Vincent Nzisabira (personal communication), the sanitation technician in Bugabira commune, the main reason was not the drought as such, but because local populations in their desperate conquest of agricultural land, resorted to drain the marshy strip situated between the lake and the River Kanyaru, which before had been playing the role of a natural stopper, thereby entailing the emptying of the lake into the river.

III.7. Potable water demand

Water is an indispensable commodity for human beings worldwide. Access to safe water, supplied both in sufficient quantity and adequate quality, is certainly one of the main requirements to achieve a sustainable development. A country's level of freshwater use has long been taken as one of the key measures of its level of economic development. Unfortunately, in many regions of the world, especially in developing countries, the amount and quality of water available to meet human needs are already limited. In its Millennium Declaration, the United Nations set eight Development Goals (MDGs), among which a commitment was made to halve, by 2015, the global proportion of people without access to safe drinking water (Chenoweth, 2008).

Minimum requirement of water consumption at the household level includes the quantities of water required for ingestion and hygiene uses and does not consider amenity and productive uses. However, hitherto, there is no consensus on the minimum amount of fresh water per capita required to satisfy human health and economic development (Chenoweth, 2008; Hirotsugu, 2003). Table III.29 shows different

estimates of the minimum quantity of water required for consumption, advanced by different authors. The standards of domestic water use in any society seem to vary in line with climatic conditions, life style, culture, tradition, technology and economy. Hence, water consumption is the highest in the western world, while in many developing countries, even the daily per capita minimum requirement for water consumption of 20 litres in rural and 150 litres in urban areas (WHO & UNICEF, 2000) is still far from being met.

Table III.29. Minimum per capita water requirement estimates (Chenoweth, 2008; Hirotsugu, 2003)

Author	**Estimate (l/c/d)**	**Basis of estimate**
WHO/UNICEF (2000)	20	Basic domestic health and hygiene needs
Gleick (1996, in Chenoweth, 2008)	50	Basic domestic health and hygiene needs
Howard and Batram (2003, in Chenoweth, 2008)	100	All domestic health and hygiene needs
Chenoweth (2008)	135	Minimum water requirement for social and economic development
Hirotsugu (2003)	140	Water consumption that ensures less diarrhoeal incidence among children under 5 years
Shuval (1992, in Chenoweth, 2008)	342	Non-agricultural requirements plus water for essential fresh food production
Falkenmark (1986, in Chenoweth, 2008)	1369	Requirement to run a modern society
World Water Assessment Programme (2003, in Chenoweth, 2008)	4654	Drinking water for active and healthy human life

In his analysis of the household water consumption and the incidence of diarrhoea, Hirotsugu (2003) suggested that a per capita water quantity of 140 litres per day should be considered as the minimum requirement of water consumption to ensure less diarrhoeal incidence among under-5-year-old children. This amount is fairly close to the estimate recently proposed by Chenoweth (2008) who considers that a minimum quantity of 135 litres of water per day and per capita should be taken as the minimum water requirement for social and economic development.

Although Burundi is endowed with abundant water resources, access to potable water is still limited. In urban areas, 83 % of the population has access to potable water while the situation worsens in rural areas where only 55 % of the population has access to clean water (République du Burundi, 2011). Since a long time ago, the region of Bugesera, in Rwanda as in Burundi, is well known for its acute scarcity of potable water. This is mainly due to the fact that this depression is characterised by an impressive lack of natural water springs which constitute the main source of potable water in other rural areas of Burundi, especially in highlands. Overall, in Kirundo province, there is one water point, a well or a standpipe, for 234 households while the

recommended norm is 30 households per water point (Ministère de la Planification du Développement et de la Reconstruction Nationale, 2006). In order to appraise the gravity of this water scarcity issue in our study area, the calculation of the drinking water demand (Table III.28) was made taking into account the standards set by the WHO and UNICEF as adapted by the National Water Master Plan (TBW Ingénieurs Conseils, 1994 & 1998) and HYGECEL, Ingénieur Conseils (2005). For the whole study area, an annual volume of 3334334 m^3 of water is necessary to satisfy the potable water demand.

Table III.30. Drinking water demand in the study area in 2010

	Population per municipality								
Categories	**Bugabira**	**Kirundo**	**Busoni**	**Ntega**	**Vumbi**	**Gitobe**	**Total**	**Factor**	**Water demand (m^3/year)**
Urban	0	10000	0	0	0	0	10000	150 l/c/d	547875
Rural population	94695	90780	127262	43659	22435	2614	381446	20/c/d	2786459
Total									**3334334**

- Population in the study area was calculated for the year 2010 by applying the annual increase rate of 3 % on the basis of the population of the different municipalities in 2008 as given by the results of the national census conducted in 2008
- The water demand for the urban perimeter of Kirundo was calculated for 10000 inhabitants instead of the current population of 8560 inhabitants (Hakizimana, 2012, personal communication) in order to take into account students of the boarding school, Lycée Kanyinya, coming from outside the study area, tourists who regularly visit the "Lacs du Nord" and NGO workers in Kirundo.
- The population of the portions of the municipalities of Busoni, Vumbi and Gitobe included in our study area was calculated by multiplying the total population of the municipality by a coefficient calculated as the ratio of the surface area of the municipality included in the study area to the total area of the municipality.

Table III.29 shows the actual amount of water available in the study area. The total available water in the study area encompasses:

- the water pumped from the 86 hand-dug wells: 286745 m^3/year,
- the water pumped from a well constructed at the pumping station of Kirundo: 25246 m^3/year,
- a rough estimate of the spring discharge: 3493606 m^3/year consisting of:
  - discharge from 126 springs scattered throughout the study area, mainly in the highlands: 3028516 m^3/year

- water conveyed to the city of Kirundo from the springs located on the northern flank of the mountain Mutumba: 27288 m^3/year. This water is not conveyed to the pumping station of Kirundo.
- water conveyed to pumping station of Kirundo from the springs situated in Marimano: 232661m^3/year
- the overflow from the water tank at the pumping station: 205141 m^3/year. This overflow supplies domestic water to rural population in the surroundings of the city of Kirundo, who are not connected to the water supply network.

The water collected at the pumping station of Kirundo from the well and the springs of Marimano is subsequently supplied to the urban population of Kirundo through the distribution network.

In total, available potable water in the study area is 3805597 m^3/year, which represents a surplus of approximately 14 % with respect to the total potable water demand (Table III.28). However, this surplus can not be generalised over the entire study area. The surplus can be explained by the fact that there are several springs concentrated in the southern and eastern highlands, where the population density is low. The part of the study area located within the depression of Bugesera faces a severe scarcity of potable water and local villagers are relying on the few wells which are still operating, or squarely resort to the shallow lakes although their water is of questionable quality (Figure III.25). This 14 % of water surplus with respect to the demand, which is actually formed by spring water which flows continuously, should not be considered as wasted as, by supporting water-depending ecosystems, it contributes to the ecological and environmental equilibrium.

Table III.31. Available potable water in the study area

Source	**Quantity (m^3/month)**	**Quantity (m^3/year)**	**Remarks**
Springs	252376	3028516	Rough estimate often based on one measurement
Hand-dug wells	23895	286745	86 hand-dug wells
Well constructed at the pumping station in Kirundo (REGIDESO)	2104	25246	
Pumping station (REGIDESO- Kirundo). Water from the springs of Marimano	19388	232661	
Water delivered to Kirundo from the springs of the mountain Mutumba	2274	27288	This water is not delivered to the pumping station of Kirundo
Overflow at the pumping station	17095	205141	
Total	**317132**	**3805597**	

Source: REGIDESO, antenne Kirundo (Georges Hakizimana, 2012, personal communication)

Figure III.26. Children fetching water from Lake Cohoha south in an area where wells are not operating (Rukuramigabo)

III.8. Conclusions

Bugesera region is a potable water-scarce area located in northeastern Burundi. The study area mainly consists of a depression surrounded by a more rugged landscape which forms the transition towards the highlands of Bweru region. The depression of Bugesera is impressively marked by a lack of natural water springs, despite the presence of a complex of interconnected swamps and several lakes.

Groundwater recharge has been computed using the soil moisture balance method as a first step towards a proper evaluation of the potential of groundwater resources in this region, which could be an alternative to the lack of natural water springs. In this regard, several methods for estimating potential evapotranspiration (Hargreaves, Thornthwaite, a modification of Thornthwaite method, Hamon) have been tested and compared to the standard Penman-Monteith equation as recommended by FAO. This was done with a view to determining an alternative method for estimating potential evapotranspiration which could give acceptable estimates for this parameter when it is not possible to use the reference evapotranspiration method due to the lack of relevant weather data.

The findings of this study show that, while Thornthwaite and Hamon methods slightly underestimate the potential evapotranspiration by 9 % and 12 % respectively, Hargreaves method overestimates it by 51 % with a RMSE of 48 mm/month. Therefore, the latter method is definitely not appropriate for the study area. Furthermore, the

modification of Thornthwaite method with a coefficient k = 0.69 was also tested and seems to generate a reasonable estimate of potential evapotranspiration with a small overestimation of the PET (1 %) and a small RMSE (5 mm/month). It is important to recall that these empirical methods, like Thornthwaite equation, have been devised with coefficients which are most of the time site-specific. Hence, further research should be carried out to adapt these methods to different geographic and climatic conditions.

Groundwater recharge was computed in two different ways: using Thornthwaite Monthly Water-Balance Model (TMWB model) wherein Hamon equation for PET is embedded, and using excel sheets for other PET methods. The plant available water, an important term of the soil moisture budget, is estimated at 75 mm assuming a water-holding capacity of 30 % over the entire root zone and a rooting depth of 25 cm. Indeed, soils in the study area result from the weathering of Precambrian metasediments and magmatic intrusions and are predominantly clayey, while the land use is dominated by agricultural land (68.6 % of the study area) where shallow rooted plants (subsistence crops) are predominantly grown. Depending on the method used to compute the potential evapotranspiration, recharge can occur only in the long rainy season (Hargreaves method) or both in the long and the short rainy season (other methods). The use of a small effective rooting depth of 0.25 m in groundwater recharge calculation as suggested by Thornthwaite & Mather (1957), taking into account the land use and the soil type, may neglect the upwards flow of water from the wet subsurface to the top dry soil. Calculations of groundwater recharge using larger effective rooting depths, 0.50 m and 0.75 m, on a daily basis result in reduced amounts of groundwater recharge, which are fairly comparable to the rough estimates of groundwater recharge calculated using the groundwater level fluctuation and the hybrid groundwater level fluctuation methods.

Moreover, the time discretisation used in calculations has important consequences, the use of smaller time steps leading to enhanced recharge, even when computed using overestimated values of PET (Hargreaves method). This corresponds to a better approximation of reality. For the calendar years 1999 to 2009, daily time series of all meteorological parameters are available and calculations of groundwater recharge on a daily basis, using evapotranspiration computed by Penman-Monteith and Hargreaves equations, give significantly higher values compared to the monthly basis, i.e. 243.2 mm and 72.2 mm respectively compared to 149.8 mm and 12.3 mm. However, it should be stressed that the calculations of groundwater recharge on a daily basis assume a swift drainage of the unsaturated zone, which may not be fully correct in case of clayey top soils like in Bugesera region. In such conditions, the soil water content in the root zone may remain at field capacity for several days. Therefore, a time scale of 10 days might be used for the calculation of recharge in order to take into account the clayey nature of the top soil and the attendant slow drainage**.**

The recharge values obtained on a daily basis with Penman-Monteith PET represent the best approximation of reality. Indeed, it should be understood that recharge occurs as a surplus fraction of each individual rainfall event, rather than in function of a lump monthly rainfall amount. This method results in 243.18 mm average recharge per year, which is best approximated by the calculations, on a monthly basis, with the TMWB method (185.40 mm). Therefore, we can conclude that, of all attempted methods, the TMWB method, which is on a monthly basis, using Hamon's PET, performs best as it fairly approximates recharge values obtained on a daily basis with Penman-Monteith PET. In addition, the TMWB model presents another added value of needing much less data.

Estimation of groundwater recharge using the groundwater level fluctuation and the hybrid water level fluctuation methods helps acquire rough estimates of groundwater recharge. Compared to the annual value of groundwater recharge obtained using the soil moisture balance for the calendar year 2008 (221.5 mm), it can be observed that the water level fluctuation method strongly underestimates the recharge (121.6 mm), whereas the hybrid water level fluctuation method gives a slightly higher value of groundwater recharge (143.1 mm). The discrepancy between these different methods of estimating groundwater recharge may be due to the use of average values of specific yield and field capacity on one hand, and the fact that the evapotranspiration of the groundwater, which is not evaluated, may lead to a reduced rise of the groundwater level.

Groundwater exploitation in the study area is still underdeveloped. It represents only 0.2 % of the recharge while an important part of the study area, mainly the depression of Bugesera is deprived of potable water. It is noteworthy to recall that the drinking water coverage, which shows an apparent surplus of 14 % with respect to the total water demand, can not be generalised over the whole study area, as there is no even spatial distribution of springs, which are mainly concentrated in the southern and eastern highlands. There is still enough room for groundwater exploitation to meet the urgent drinking water demand. An efficient plan for potable water supply in the study area should be urgently established in order to respond to the lack of drinking water, mainly in the depression of Bugesera.

Due to lack of reliable spring discharge and the impossibility to gauge the river flow in this complex of swampy valleys and lakes, groundwater balance was computed by considering the unmapped spring discharge and groundwater discharge to surface water bodies (lakes, streams and swamps) under the same term namely baseflow. Water balance shows an important baseflow (192.346 Mm^3/annum) which sustains the

perennial complex of marshlands and shallow lakes in the Bugesera depression. The groundwater balance confirms that there is a groundwater potential which, with a good hydrogeological background, can be more efficiently tapped in order to meet the groundwater demand, mainly in the depression of Bugesera.

CHAPTER IV. HYDRAULIC PARAMETERS

IV.1. Introduction

Aquifer parameters are of critical importance for sustainable management of groundwater resources. Indeed, a good knowledge of these parameters allows the prediction of the quantitative and qualitative response of aquifers to abstraction and recharge. Hence, these parameters are instrumental in establishing water resource plans and in developing groundwater flow models which are of utmost importance in predicting current and future trends of water resources availability (Jha *et al.*, 2004). Hydraulic parameters which are commonly determined for aquifers comprise the hydraulic conductivity (K), transmissivity (T), specific capacity, specific yield (Sy) and storage coefficient (S) respectively for unconfined and confined aquifers.

Hydraulic properties of aquifers can vary spatially due to geological heterogeneities. In governing groundwater flow, these properties also control the movement of several solutes and pollutants (Rotzoll & El-Kadi, 2008). These properties can be determined on a local scale by analysis of data from pumping tests or on a regional scale by simulation of a numerical groundwater flow model (Mjemah *et al.*, 2009). Pumping test is the most reliable and commonly used method for determining the hydraulic characteristics (Kruseman & de Ridder, 1994). Besides determination of these parameters, pumping tests can assist in identifying disturbing factors such as lateral flow boundary, hydraulic continuity and recharge.

Pumping tests or aquifer tests consist in imposing an artificial stress on an aquifer system by pumping water from a well and measuring the variation of water levels in the pumped well and observation wells for a certain period of time. The variation of the hydraulic head with time, also called drawdown, can be used to estimate the transmissivity and therefore the hydraulic conductivity. In the absence of observation wells, the determination of the storage coefficient is not feasible by using analytical methods. However, numerical methods can be successful to estimate storage properties (Kruseman & de Ridder, 1994; Halford *et al.*, 2006).

The objective of this chapter is to determine the aquifer parameters through the analysis of pumping test data using traditional analytical methods of curve matching. The pumping tests were performed during two field campaigns conducted from September to December in 2007, and from July to October in 2008. These pumping tests were conducted on shallow hand-dug wells which have been constructed in the study area since the colonial period, within the framework of development projects or recently by humanitarian agencies. In total, there are 176 wells in our study area among which only 80 wells are producing nowadays.

IV.2. Large diameter wells

Large diameter wells are still common in many parts of the world especially in developing countries where they are still playing an important role in local irrigation and domestic water supply systems (Singh, 2008). Hence, these wells are sometimes the only possibility which is offered to hydrogeologists to determine the hydraulic parameters of shallow aquifers hosted by alluvial deposits or the weathered overburden of crystalline basement. These wells are suited for low transmissivity aquifers because of their capacity to store large volumes of readily accessible water which can help meet demand during the day and replenish itself during periods when there is no abstraction.

The depths of hand-dug wells generally range between 5 m and 20 m. Exceptionally, hand-dug wells of over 30 m in depth are constructed to exploit known aquifers. These wells are excavated with an internal diameter of minimum 1.5 m to provide enough working space. This excavation diameter is further reduced to a final internal diameter of about 1 m after the well has been lined. Hand-dug wells with an internal diameter of more than 10 m have been reported in the Kingdom of Saoudi Arabia (Zekai, 1991). The shaft of the well can be lined with stone or brick masonry, reinforced concrete, or plain concrete pre-cast well rings that are lowered into the hole. In Bugesera, a column of perforated concrete rings serve as the well screen. However, often, water enters the well via unlined bottom, through spaced bricks or in between plain rings, i.e. at their junction. Figure IV.1 shows a cross-section of a hard rock aquifer lithological cross-section and the different types of wells that can be constructed.

Standard methods for analysis of pumping test data assume that storage in the well is negligible. However, for large diameter wells, this assumption does not hold given the volume of water stored within the well, which depends on its diameter. The contribution of the well storage to the discharge can be substantial and can not be therefore neglected in the analytical solution (Singh, 2008). At the beginning of the pumping test, the discharge comes not only from the aquifer but also from the well bore storage or from the annular space around the well (gravel and filter pack). Thus, the observed drawdown is reduced compared to the standard Theis solution. The discharge from the pump comprises two components which can be written as:

$$Q_p = Q_s + Q_a$$

where Q_p is discharge rate of the pump, Q_s is the rate at which water is taken from the well bore storage and Q_a is the rate at which water flows from the aquifer into the well.

As pumping continues, the effect of well bore storage becomes progressively negligible and eventually, at later time, the time-drawdown curve follows that of Theis solution.

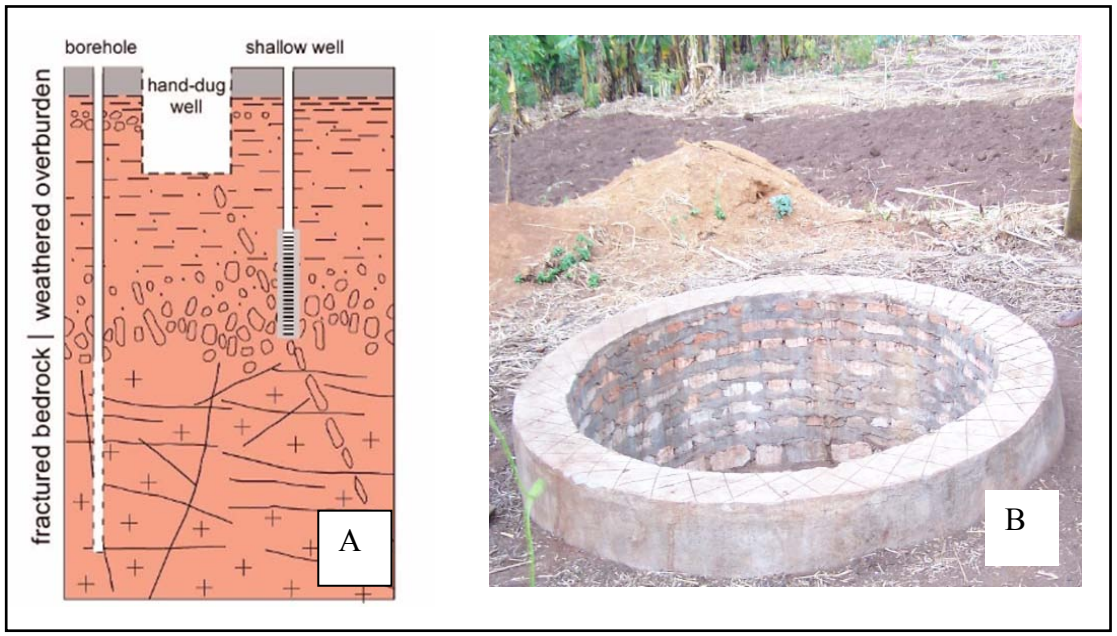

Figure IV.1. Cross-section of hard rock aquifer and well types (A) and a completed large diameter well lined with brick masonry in Bugesera region (B)

IV.3. Classification scheme of transmissivity magnitude occording to Krasny

Krasny (1993) proposed an objective classification scheme of transmissivity magnitude and variation which is very useful for a quantitative evaluation and comparison of the groundwater potential for different hydrogeological environments. This classification has the merits of putting fixed limits between the different classes which are often subjectively used to describe transmissivity in quantitative or semi-quantitative terms such large, small, high, low… . As a matter of fact, people with poor knowledge in hydrogeology tend to erroneously relate the hydrogeological conditions to the water demand rather than to the actual aquifer parameters (Krasny, 1993). Hence, in areas where wells produce sufficient water to meet limited water demand such as in small human settlements, the transmissivity might be described as high, whereas in areas where well yields do not meet large demands, the transmissivity might be designated as low. Such a subjective approach does not allow an objective comparison of transmissivity values at both local and regional scales.

The classification of Krasny (1993) defines a scale of six classes from very high transmissivity (Class I with $T > 1000$ m^2/d) to imperceptible transmissivity (Class VI with $T < 0.001$ m^2/d). Moreover, the classification of Krasny (1993) gives an estimation of groundwater prospects and potential yield for a single well at 5 m drawdown for each class of transmissivity (Table IV.1).

IV.4. Overview of analytical methods used to interpret pumping test data

Several analytical methods are available to analyse drawdown or recovery data depending on the geological conditions of the site: confined, semi-confined, unconfined, and boundary conditions such as partial penetration, well bore storage, recharge and impermeable boundaries (Kruseman & de Ridder, 1994). The choice of theoretical model is an important step in the interpretation of pumping tests. If a wrong model is chosen, the hydraulic parameters calculated will not be correct. Moreover, the non-uniqueness of some theoretical solutions to well-flow problems may further complicate the analysis of pumping test data. Indeed, different theoretical models developed for different aquifer settings may yield similar response to a pumping test, which complicates the system identification and model selection (Kruseman & de Ridder, 1994). In this section, a theoretical overview of analytical methods used to interpret pumping tests data is presented.

Table IV.1. Classification of transmissivity magnitude (Krasny, 1993).

Coefficient of transmissivity ($m^2 d^{-1}$)	**Class of transmissivity magnitude**	**Designation of transmissivity magnitude**	**Specific capacity S_c ($l s^{-1} m^{-1}$)**	**Groundwater supply potential**	**Very approximate expected discharge in $l s^{-1}$ of a single well at 5 m drawdown**
>1000	I	Very high	> 10	Withdrawals of great regional importance	> 50
100 - 1000	II	High	1 - 10	Withdrawals of lesser regional importance	5 – 50
10 -100	III	Intermediate	0.1 - 1	Withdrawals for local water supply (small communities, plants, etc.)	0.5 - 5
1 - 10	IV	Low	0.01 – 0.1	Smaller withdrawals for local water supply with limited consumption	0.05 – 0.50
0.1 - 10	V	Very low	0.001 – 0.01	Withdrawals for local water supply with limited consumption	0.005 – 0.05
< 0.1	VI	Imperceptible	< 0.01	Sources for local water supply are difficult (if possible) to ensure	< 0.005

IV.4.1. Theis method for confined aquifers

The value of this method is that it enables to determine the hydraulic characteristics of an aquifer before development of steady-state conditions. Indeed, under most real aquifer conditions, a new steady-state condition cannot be developed or may be reached after lengthy time periods.

The unsteady-state or Theis equation, which was derived from the analogy between groundwater flow and heat transfer in a homogeneous medium, can be written as follows:

$$s = \frac{Q}{4\pi T} W(u) = \frac{Q}{4\pi T}\left(-5772 - \ln u + u - \frac{u^2}{2.2!} + \frac{u^3}{3.3!} - \frac{u^4}{4.4!} + ... \right)$$

where s is the drawdown in m, Q is the constant discharge rate (m^3/d), T is the transmissivity of the aquifer (m^2/day) and W(u) is the well function.

$$u = \frac{r^2 S}{4Tt}$$

$$S = \frac{4Ttu}{r^2}$$

where r is the radial distance to the point where the drawdown is measured (m), t is the time in days since the pumping started.

Using the equation for drawdown and storativity, Theis developed a curve-fitting method to determine the storativity (S) and the transmissivity (T). In this respect, equations for drawdown and storativity are respectively rearranged as follows:

$$\log s = \log\left(\frac{Q}{4\pi T} \right) + \log(W(u))$$

$$\log\left(\frac{r^2}{t} \right) = \log\left(\frac{4T}{S} \right) + \log(u)$$

Theis's fitting method is based on the fact that if the drawdown (s) is plotted against r^2/t (or t/r^2) and W(u) against u (or 1/u) on the same bi-logarithmic paper, the resulting data and type curves respectively will have the same shape with horizontal and vertical offset corresponding to the two constants $Q/4\pi T$ and 4T/S. The two curves can be therefore matched and at some arbitrary matching point on the overlapping part of the sheets, the coordinates of the latter point allow to read the values of s, r^2/t, u and W(u) which can be substituted into Theis'equations to compute the transmissivity (T) and the storativity (S) of the aquifer.

IV.4.2. Cooper-Jacob's method

It is a simplification of the Theis method which makes use of a semi-logarithmic graph (Kruseman & de Ridder, 1994). Indeed, Cooper and Jacob noted that, for large values of t or small values of r, the sum of the infinite Taylor series used to estimate the well function W(u) is negligible beyond the term ln(u). Thus, for small values of u (u<0.01), the drawdown can be approximated by:

$$s = \frac{Q}{4\pi T}\left(-0.5772 - \ln\frac{r^2 S}{4Tt}\right)$$

By rearranging the above equation and changing into decimal logarithms, it reduces to:

$$s = \frac{2.30Q}{4\pi T}\log\frac{2.25Tt}{r^2 S}$$

Because T, Q and S are constant, a plot of the drawdown s on an arithmetic scale versus time on a logarithmic scale will form a straight line whose slope is proportional to the pumping rate (Q) and the transmissivity (T). When the straight line is extended, the point where it intercepts the horizontal axis has the coordinates s = 0 and t = t_0. Solving the equation of Cooper and Jacob for s = 0 and t = t_0 gives:

$$S = \frac{2.25Tt_0}{r^2}$$

$$T = \frac{2.30Q}{4\pi\Delta s}$$

where Δs (in m) is the drawdown difference per log cycle of time.

IV.4.3. Hantush curve-fitting method for semi-confined aquifers

This is a method for analysis of pumping test data which takes into account the storage changes into the aquitard. For small values of pumping time, the drawdown equation for unsteady flow can be defined as:

$$s = \frac{Q}{4\pi T}W(u,\beta)$$

Where

$$u = \frac{r^2 S}{4Tt}$$

$$\beta = \frac{r}{4}\sqrt{\frac{K'/D'}{T}\cdot\frac{S'}{S}}$$

Where β is the leakage factor in m, K' is the vertical hydraulic conductivity of the leaky aquitard (m/d), D' is the saturated thickness of the leaky aquitard (m), S' and S are the storativities of the aquitard and aquifer respectively (dimensionless).

$$W(u,\beta) = \int_u^\infty \frac{e^{-y}}{y}erfc\frac{b\sqrt{u}}{\sqrt{y(y-u)}}dy$$

IV.4.4. Fractured aquifers

Groundwater flow in a fractured medium can be extremely complex. Hence, conventional flow equations developed mainly for homogeneous porous aquifers can not be applied for fractured aquifers. Several theoretical models have been developed, all assuming a simplified pattern of fractures. Most of these models are based on the concept of double-porosity (Barenblatt *et al.*, 1960 in Kruseman & de Ridder, 1994) which considers a fractured rock formation as consisting of two media namely fractures and the matrix blocks having their own hydraulic properties. The aquifer is modeled as consisting of matrix blocks with primary porosity separated with fractures of low storage capacity and high permeability. However, the radial flow to the pumping well is only controlled by the transmissivity of fractures which drain the matrix.

Using the concept of double porosity, Bourdet & Gringarten (1980) (in Kruseman & de Ridder, 1994) developed an equation which expresses the drawdown response to pumping as follows:

$$s = \frac{Q}{4\pi T_f} F\left(u^*, \lambda, \omega\right)$$

where

$$u^* = \frac{T_f t}{\left(S_f + \beta S_m\right) r^2} \;;\; \lambda = \alpha r^2 \frac{K_m}{K_f} \;;\; \omega = \frac{S_f}{S_f + \beta S_m}$$

where f and m relate to the fractures and matrix blocks respectively, λ is interporosity (flow from matrix into fractures) flow coefficient (dimensionless), α is the shape factor characteristic of the geometry of the fractures and aquifer matrix, β is a factor equal to 0 for early time analysis and for late time, it is equal to 1/3 for orthogonal systems or 1 for strata type systems, r is the radial distance from the pumping well to the observation well (m), T_f is the fracture transmissivity (m^2/d), Q the pumping rate (m^3/d) and t the time (day).

For small pumping times, the drawdown equation reduces to:

$$s = \frac{Q}{4\pi T_f} W(u)$$

where $u = \dfrac{\left(S_f + \beta S_m\right) r^2}{4 T_f t}$

For large values of pumping time the drawdown equation reduces to the Theis equation which then describes the drawdown behaviour of the combined fracture and block system (β equal to 1/3 or 1).

At intermediate pumping times, the drawdown becomes constant, thereby reflecting the transition between fracture flow to combined flow from fractures and matrix blocks. The drawdown at which this transition occurs can be expressed as:

$$s = \frac{Q}{2\pi T_f} K_0\left(\sqrt{\lambda}\right)$$

where $K_0(x)$ is the Bessel function of the second kind and of zero order.

For low values of of λ (< 0.01), the previous equation reduces to:

$$s = \frac{2.30Q}{2\pi T_f} \log \frac{1.26}{\lambda}$$

The drawdown at which the transition occurs is independent of early-and late-time drawdown behaviours and is solely a function of λ.

IV.4.5. Papadopulos and Cooper method for large diameter wells

Papadopulos & Cooper (1967) developed a method that accounts for well bore storage for large diameter wells in confined aquifers, but which can also be applied for unconfined aquifers provided that the Jacob correction is applied (Kruseman & de Ridder, 1994). The drawdown in a large diameter well can be mathematically expressed by the following equation:

$$s = \frac{Q}{4\pi T} F\left(u, \alpha, r/r_{ew}\right)$$

where

$$u = \frac{r^2 S}{4Tt}$$

$$\alpha = \frac{r_{ew}^2}{r_c^2}$$

r_{ew} is the effective radius of the well screen or open hole (m) and r_c is the radius of the unscreened part of the well over which the water level is changing.

For long pumping times, when the drawdown is no longer influenced by well bore storage, the well function can be approximated by the Theis well function W(u).

IV.4.6. Estimation of transmissivity (T) from specific capacity (S_c)

Specific capacity is a measure of the productivity of a well. In mathematical terms, specific capacity is the ratio of the pumping rate to the drawdown in the pumping well at (pseudo-) steady-state conditions. Using different equations for drawdown under different aquifer and hydrodynamic conditions, a number of relationships relating the transmissivity to the specific capacity have been developed (Theis *et al.*, 1963; Mace *et al.*, 1994, Thomasson *et al.,* 1960). The estimate of the transmissivity derived from specific capacity is not as accurate as the one obtained using the standard methods. However, it helps obtain a fairly acceptable estimate of this parameter because the specific capacity itself is controlled by the hydraulic parameters, especially the transmissivity.

The specific capacity is mathematically expressed as:

$$S_c = \frac{Q}{s}$$

Where S_c is the specific capacity (m^2/day), Q is the pumping rate (m^3/day), and s is the drawdown in the pumping well (m).

Thomasson *et al.* (1960) were the first to relate the transmissivity to the specific capacity using the Thiem-Dupuit equation:

$$s_w = \frac{Q}{2\pi T}\ln\left(\frac{R}{r_w}\right)$$

where s_w is the drawdown in the well (m), Q is the pumping rate (m^3/day), T is the transmissivity (m^2/day), R is the radius of influence of the well (m), and r_w is the radius of the pumping well (m).

Solving the above equation for transmissivity at steady-state conditions, they showed that the transmissivity can be linearly related to the specific capacity by a constant C_c:

$$T = \left(\frac{1}{2\pi}\ln\frac{R}{r_w}\right)\frac{Q}{s_w} = C_c\frac{Q}{s_w}$$

According to several authors (Thomasson *et al.*, 1960, Johnson *et al.*, 1966; Adyalkar & Mani, 1972; Adyalkar *et al.*, 1981, Logan, 1964, Bakiewicz *et al.*, 1985), the coefficient C_c can take different values depending on hydrogeological and hydrodynamic conditions (Table IV.2.).

Table IV.2. Values of the constant C_c according to different authors

Author	C_c	Observations
Thomasson *et al.* (1960)	1.01-1.53	For a radius of influence ranging between 100-1000 m
Thomasson *et al.* (1960)	0.9-1.5	For alluvial sediments in California
Theis *et al.* (1963)	0.5-1	In transient conditions
Johnson *et al.* (1966)	1.10	Wells in confined alluvial aquifer with a radius of influence of 1000 m
Adyalkar & Mani (1972)	0.23-0.44	For large diameter wells in a fractured aquifer
Adyalkar *et al.*, (1981)	0.42	For the weathered zone of massive and vesicular basalts of the Deccan Trap
Mace *et al.* (1994)	0.59, 0.63, 0.75	For three sandstone aquifers

IV.5. Methodology

Two batches of pumping test data have been collected during two field campaigns conducted from September to December in 2007 and from July to October in 2008. In total 41 wells out the 176 wells mapped in the study area (Figures IV.2 & IV.3) were submitted to a constant rate pumping test for a duration varying between 9 minutes and a maximum of 9 hours depending on the behaviour of the aquifer. Each well was pumped until (pseudo-) steady-state conditions were reached except in case the well ran dry due to low transmissivity or unsustainable pumping rate.

The recovery phase was monitored until complete recovery or at least until a recovery of 80 % of the initial static water level was obtained, except for very poor aquifers where only a very small recovery of the initial static water level was reached. During the pumping phase, the discharge rate was measured and regular adjustments were made on the control valve so as to keep, as much as possible, a constant discharge rate (Figure IV.4). Prior to the start of the test, the pumping set-up was installed and, in agreement with local administrative authorities, the production was stopped for 12 to 24 hours in order to allow water level to return to its normal static level. The variation of water level in the well during the pumping and recovery phases was monitored manually using an electrical water level meter (Figure IV.5) and automatically using electronic divers. The diver is a datalogger designed to measure water level changes. The diver consists of a pressure sensor meant to measure water pressure, a temperature sensor, memory for storing measurements and a battery. Two divers were used during our pumping tests: the diver and the baro-diver.

The diver was installed within the pumping well (as there was no observation well) using a standard stainless steel cable. To avoid disturbance of the diver due to the turbulence of water in the vicinity of the pump, the diver was installed in a galvanised

pipe. As long as the diver is not submerged in water, it measures the atmospheric pressure, just like a barometer. However, once the diver is submerged in water, the atmospheric pressure is supplemented with the pressure of the water column. Thus, the pressure measured by the diver comprises the atmospheric pressure and the pressure of the water column. The baro-diver is generally installed at the top of the well casing or anywhere in the vicinity of the site where the measurements are being carried out (within a radius of 15 km) and measures the atmospheric pressure. The measurements done by the diver are further compensated for the barometric variations in order to obtain the net pressure of the water column. At the start of the pumping test, it is important to hang the diver at a certain depth and to calibrate diver readings by a manual measurement at the same moment, with reference to a known datum plane. The same manual control is done at the end of the pumping test to make sure that the diver data have not undergone any disturbance. Therefore, the water level in relation to a reference datum can be calculated. The drawdown is thus deduced from the variations of the pressure of the water column during the pumping. For the two divers, a fixed time step of 1 minute for measurement of the barometric and water column pressures was programmed using a computer before the start of the pumping test. During the programming of the divers, the name and other required characteristics of the site to be tested were indicated. Upon completion of the pumping test, data from the divers were downloaded to the computer using a special read-out unit which is connected to the computer.

As a matter of caution and for the sake of translating pressures recorded by divers into water level versus datum, manual measurements of the water level during the pumping test were taken with a water level meter and this helped obtain an additional set of data in case the dataloggers have been disturbed in one way or another during the pumping test. Figures IV.6 and IV.7 show situations in which, without this additional set of manual data, one would be compelled to resume the test, which is time- and money-consuming.

Manual measurements of the dynamic water level were performed at variable time intervals as indicated in Table IV.3. Pumping test data were analysed using the software Aquifer Test Professional 4.2 developed by Schlumberger Water Services. This is flexible and user-friendly software, which allows data from pumping tests and other required information to be entered via the keyboard or imported from any datalogger file. Moreover, pumping test data can also be inserted by cutting and pasting from a windows text editor, spreadsheet or any other database. The aquifer parameters are determined by standard curve matching whereby the data curve can be brought to fit to a type curve using the parameter controls.

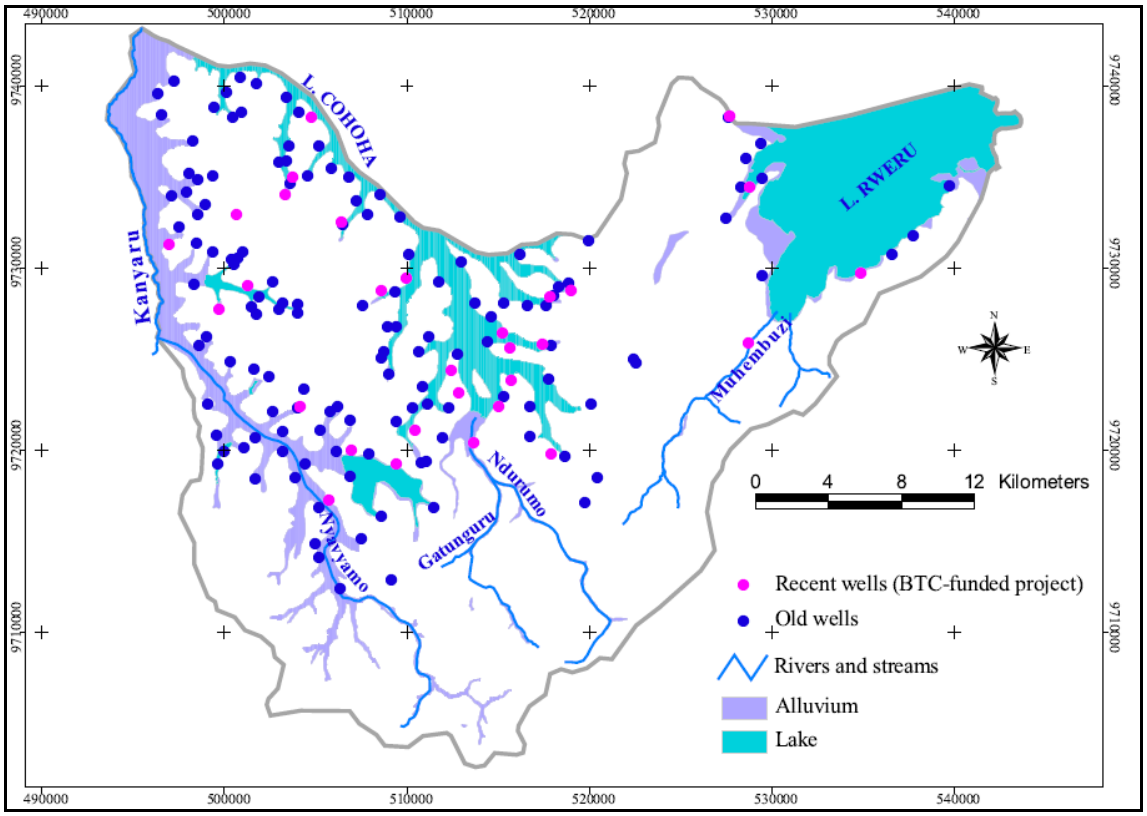

Figure IV.2. Old and recently constructed large diameter wells

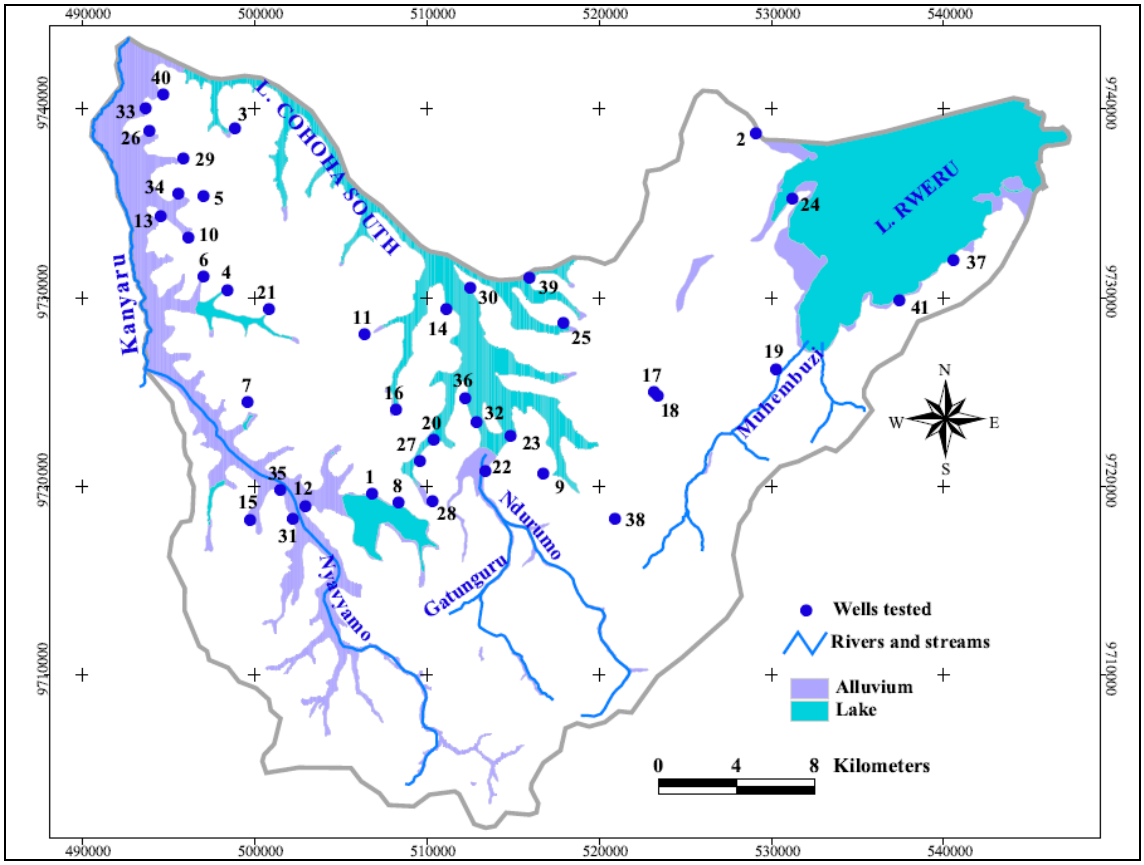

Figure IV.3. Selected wells for pumping tests carried out in 2007 and 2008.

Figure IV.4. Discharge measurement during the pumping test

Figure IV.5. Measurement of the dynamic water level during the pumping test

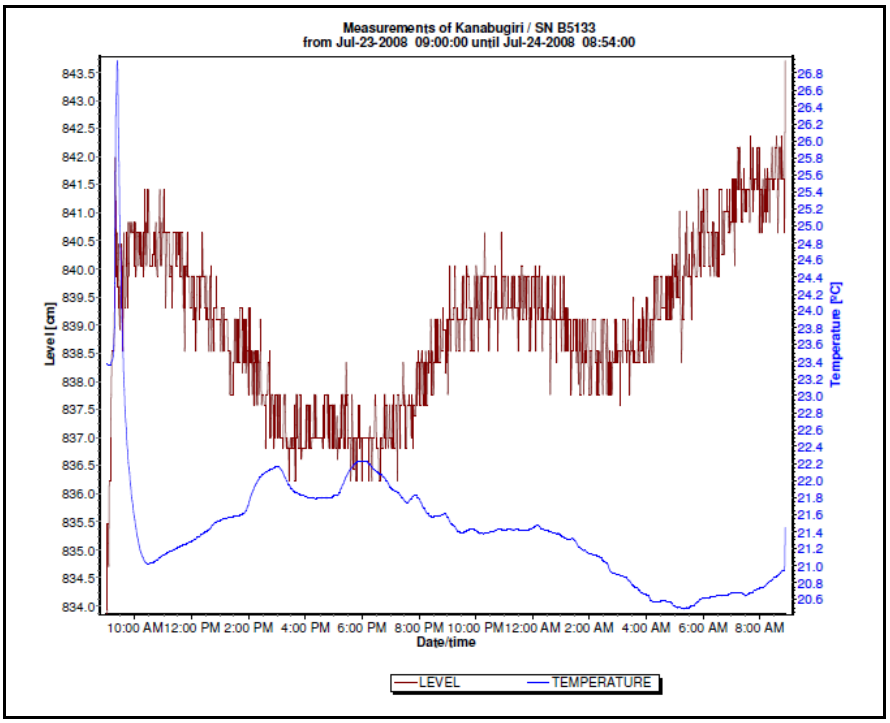

Figure IV.6. Situation where diver data can not be used because the datalogger was disturbed by the turbulence induced by the pump during the test. The datalogger was extending beyond the protection pipe (pumping test Nr.13,Kanabugiri-Bugera).

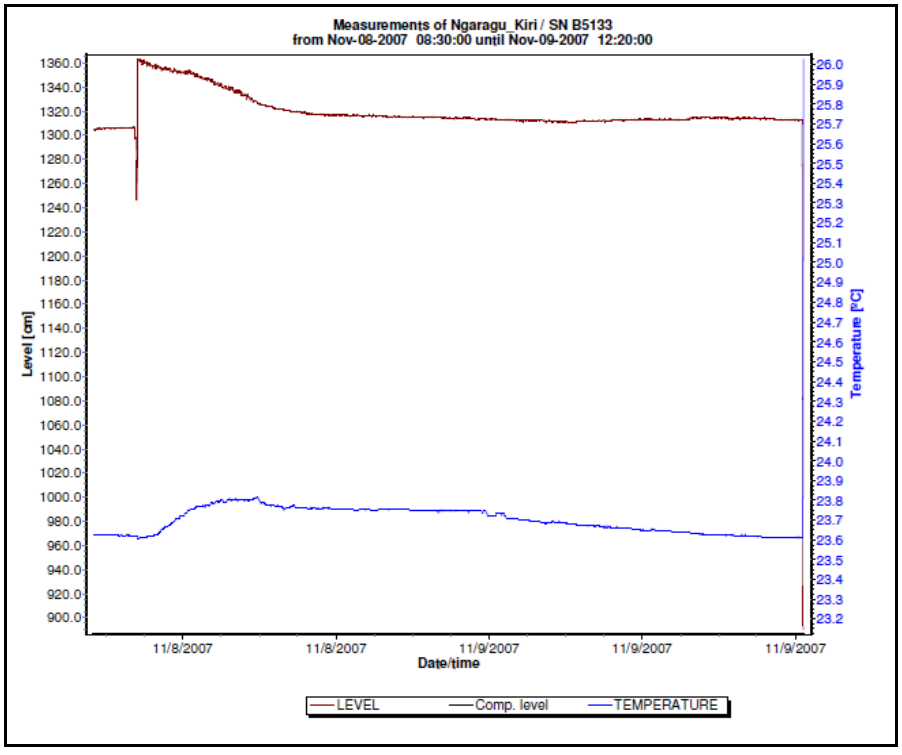

Figure IV.7. Situation where diver data can not be used because the lower end of the protection pipe was lowered too deep and sealed by the muddy bottom of the well and hence, the water level within the pipe did not change during the pumping test (pumping test Nr.33, Ngaragu-Kiri).

Table IV.3. Time intervals for measurement of the dynamic water level during pumping and recovery tests

Pumping phase		Recovery phase	
Time since the start of the pumping (minutes)	**Time interval (minutes)**	**Time since the shutdown of the pump minutes**	**Time interval (minutes)**
0 to 10	1	0 to 10	1
10 to 60	5	10 to 60	5
60 to shutdown of the pump	20	60 to the end of measurement	20

IV.6. Difficulties encountered during the pumping tests

The major challenge during this field campaign was the determination of a sustainable pumping rate. Indeed, there was not any benchmark as regards to the sustainable discharge rate to be applied at different sites tested. Some of these large diameter wells were constructed within the framework of a development project (Kirundo project) in the study area while others were constructed by humanitarian agencies. However, none of these organisations performed pumping tests on the constructed wells and moreover none of them kept a record of the lithological logs of the wells. In such conditions, it was through a repetitive trial and error process that we tried as much as possible to determine a sustainable pumping rate.

For some wells completed in low transmissivity aquifers, it was quite impossible to determine a sustainable pumping rate even after several attempts. As a consequence, some of these wells ran dry before steady-state conditions could be reached. In some other cases it was deemed necessary to stop the pumping phase before steady-state conditions were reached as further lowering of the pumping rate would have endangered the pump. Overall, the applied discharge rate varies between 1.2 m^3/h and 5.6 m^3/h.

A quick analysis of the graphs of water level versus time provided by the electronic divers allows to distinguish 3 main types of aquifer response in the study area: (1) 24 successful pumping tests where steady state conditions and full recovery are reached within a time span depending of the hydraulic properties of the aquifer (Figure IV.8). For these pumping tests, estimates of hydraulic parameters can be obtained from both pumping and recovery phase data; (2) 15 half-successful pumping tests in which, despite a relatively low pumping rate, the drawdown in the well keeps on increasing, eventually leading to the drying up of the well before steady-state conditions were reached, but where a recovery of at least 80 % of the initial static water level was

recorded (Figure IV.9). Sometimes, precaution was taken to shut down the pump before it got emersed so as to prevent it from being damaged. For such pumping tests, an estimate of the hydraulic parameters can still be obtained from the recovery data; and (3) 2 completely unsuccessful pumping tests where the behaviour of the aquifer during the pumping test was similar to the previous one but where a very small recovery of the initial static water level was obtained (Figure IV.10). These are mostly abandoned wells which have been idle for long time and which thus contain a substantial well bore storage with seemingly a significant contribution of rainfall water. For such an aquifer response, hydraulic parameters can not be calculated.

Moreover, the lack of lithological logs information was a very challenging issue as this was rendering complicated the choice of the analytical solution to apply. The lack of this important information for most of the wells tested was eventually overcome through the interpretation of several geoelectrical soundings which, coupled to information from shallow auger soundings and recently acquired lithological information, helped to define a conceptual hydrogeological model of the study area (Chapter III) which could explain the different hydraulic responses of the aquifer. Furthermore, lithological logs from recently constructed wells under a BTC-funded project enabled us to have complementary clues as regard to the hydrogeological structure (Appendix IV.1.1 to IV.1.10).

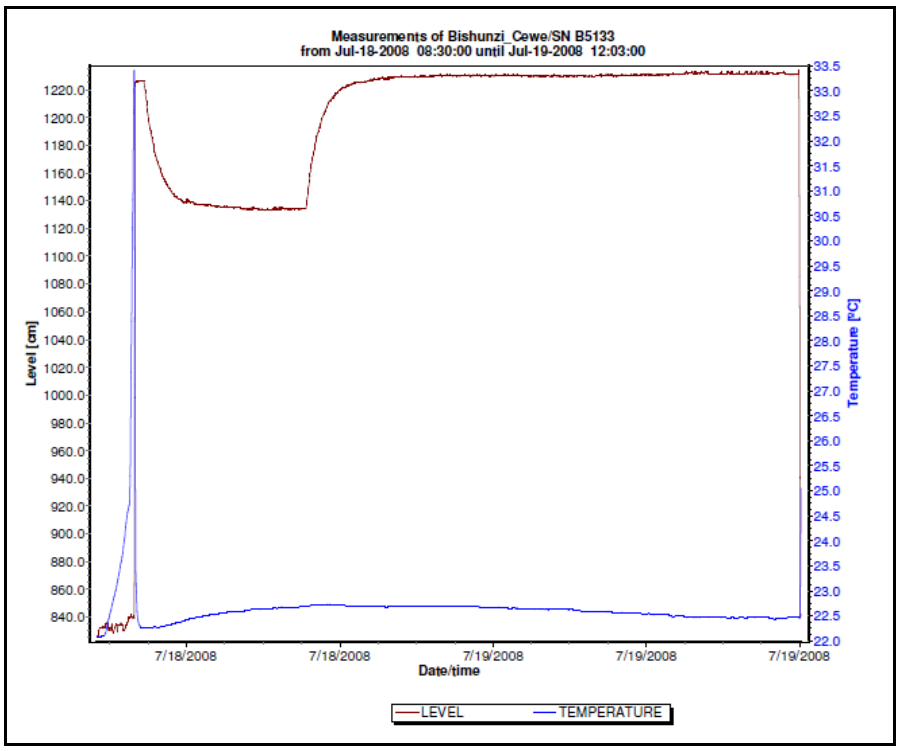

Figure IV.8. Water level versus time from the electronic datalogger showing a representative successful pumping test (pumping test Nr.1, Bishunzi-Cewe).

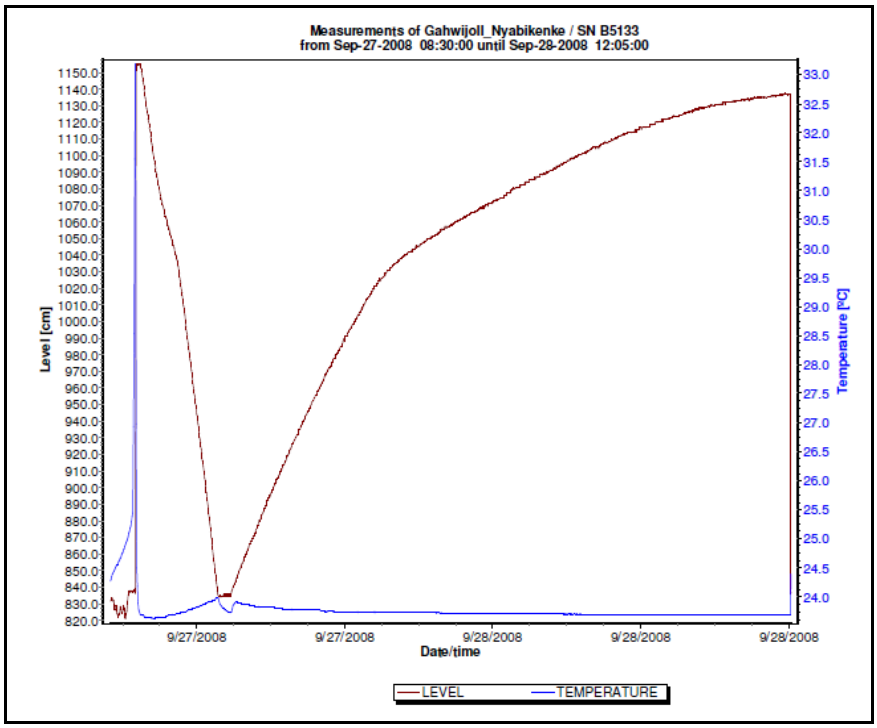

Figure IV.9. Water level versus time from the electronic datalogger showing a representative half-successful pumping test (pumping test Nr. 4, Gahwijo II-Nyabikenke).

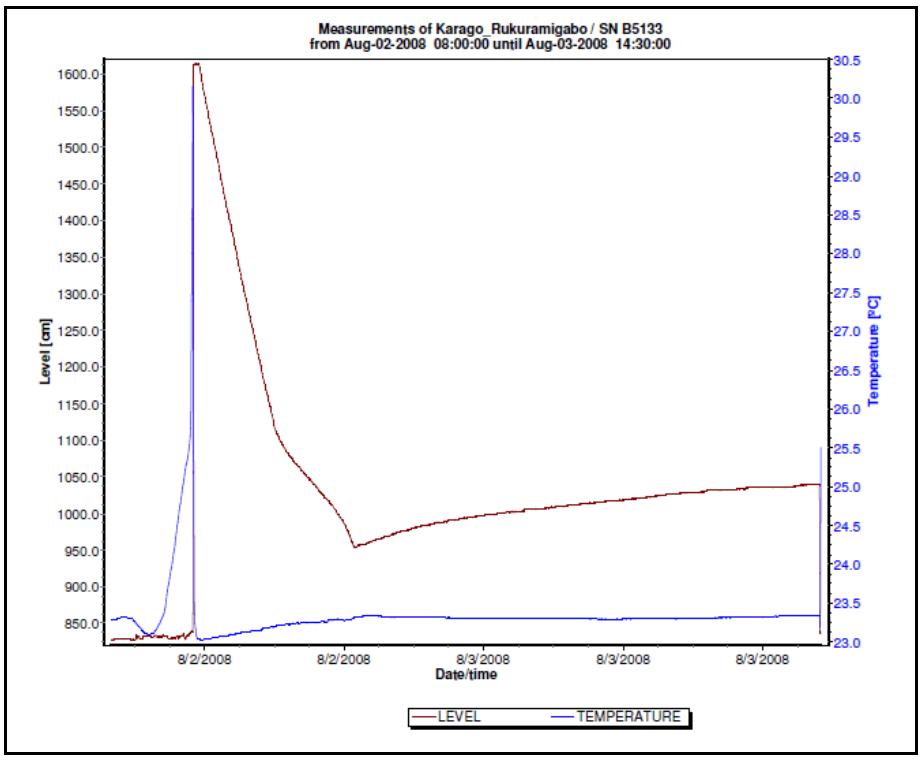

Figure IV.10. Water level versus time from the electronic datalogger showing a representative unsuccessful pumping test (pumping test Nr. 16, Karago-Rukuramigabo)

IV.7. Pumping test analysis and interpretation

Pumping test data were analysed using standard methods for constant rate aquifer tests including: Theis method (1935), Hantush (1960) for wells with a leaky response, double porosity, and Cooper & Jacob (1946) time-drawdown method on one hand, and the specific capacity method for all pumping tests on the other hand. The method of Papadopulos & Cooper (1967) for large diameter wells was also tried and compared to other analytical methods. Analytical curves of all pumping and recovery test data are presented in Appendix IV.2. Recovery tests were interpreted as pumping tests, by considering groundwater rises with respect to final pumping level as drawdowns, assuming that steady state was reached during pumping. Interpreting the data and the diagnostic graphs helped to identify the assumptions that can be made about the data and thus, to choose the appropriate analysis method. The transmissivity of the aquifer was determined by the standard curve matching method, while the hydraulic conductivity was derived from the transmissivity by dividing it by the aquifer thickness. The aquifer thickness was adopted as the total distance from the water table to the bottom of the well (Gingerich, 1999 in Ratzoll & El-Kadi, 2008).

IV.7.1. Analytical methods and interpretation

The software package Aquifer Test Professional 4.2 was used for the interpretation. It offers the possibility of comparing the data curve to a number of type curves and thus to choose the best analytical solution. It is of course obvious that combining this possibility offered by the software with good information about the actual structure of the aquifer can lead to a well-informed and good choice of the analytical solution. The program offers also a number of flexibilities which allows to change and adjust the model assumptions and parameters. It is worth to recall that all wells investigated in the study area are large-diameter wells with a depth varying between 5 m and 17.5 m, while their internal radius is 0.50 m.

Despite the relatively large diameter of all the wells in the study area, weirdly, none of them conforms to the Papadopulos & Cooper (1967) (in Kruseman & de Ridder, 1994) solution for large diameter wells. Even where a relatively good match with the Papadopulos and Cooper (1967) analytical solution was observed, like for the wells Kadobogoro-Muramba (T = 31.6 m^2/d), Kigoma-Gatare (T = 14.4 m^2/d) and Muhero–Yaranda I (T = 36.3 m^2/d), the obtained values of transmissivity were systematically higher than the values obtained by other analytical methods. The reason for this unexpected response of these large diameter wells could be explained by the fact, that for a pumping duration of more than 6 hours, the well bore storage is exhausted within a maximum of 1 hour 30, which means that for the rest of the pumping duration, the aquifer response may conform to the standard analytical solutions.

To illustrate that point, let's take the case of the well Kigoma-Gatare (Appendix IV.2, Figures IV.2.48 to 55). With a radius of 0.5 m and a water column of 3.7 m, the well bore storage is 2.9 m^3. Hence, with a pumping rate of 2.3 m^3/h, the well bore storage will be exhausted after approximately 1h16 min while the entire pumping duration was 8 hours. Hence, at later stages of the pumping test, the contribution from the aquifer significantly dominates the discharge. Moreover, the wells investigated have a moderate diameter if we compare them to the large diameter dug wells reported in India with an average diameter varying between 5 and 10 m (Singhal, 1997).

The analysis and interpretation of the 39 pumping tests (successful and half-successful ones) conducted in the study area reveal that the drawdown response to pumping and recovery tests predominantly conforms to the Hantush leaky conditions model and to a lesser extent to the double porosity model. The quite generalized leaky response of the aquifer system to pumping and recovery tests seems to be consistent with the hydrogeological structure, which shows the static water level lies within the upper part of the saprolite which is more clayey, while the aquifer itself is made up of coarser materials including sand, gravel and rock fragments. Indeed, among the 41 pumping and recovery tests executed in this study, 28 show a leaky response with a good fitting to Hantush type curves, 19 show a somewhat good conformity to the Theis model, 17 show a good match with the Cooper & Jacob model, 13 conform to the Papadopulos & Cooper model, and 10 reveal a response which reflects double porosity conditions. From what precedes, it is evident that several pumping test data reveal a drawdown response which conforms to different analytical models. In this respect, Sammel (1974) noted that data from pumping tests carried out in large diameter wells could be successfully analysed using both the Papadopulos & Cooper method and the Cooper & Jacob modification of the Theis method. Moreover, the same author observed that, if the pumping test is carried out for a sufficient length of time, drawdown in the aquifer can conform to the Theis solution.

Nine (9) out of the 41 pumping tests were conducted on newly constructed wells towards the end of the field campaign, in October 2008. The fact that these new wells were visited and tested just after their completion in dry season provided a good opportunity to observe the nature of fresh geological materials excavated at the bottom of the well and which bear witness to the nature of the aquifer (Figures IV.11 to IV.13).

Figure IV.11. Geological materials excavated at the bottom of the well in Kiruhura II-Muramba (Nr. 22) showing that the aquifer is made up of a mixture of reddish clay, sand and lateritic gravel.

Figure IV.12. Geological materials excavated at the bottom of the well in Kiruhura I-Kiyanza (Nr. 23) showing that the aquifer is mainly made up of a mixture of reddish sand, lateritic gravel and rock fragments.

Figure IV.13. Geological materials excavated at the bottom of the well in Senga-Nyagisozi (Nr. 41) showing that the aquifer is mainly made up of a mixture of reddish clay, sand, lateritic gravel and rock fragments.

IV.7.1.1. Successful pumping tests

In total, 24 pumping tests were successfully conducted in 2007 (September to December) and 2008 (July to October)**.** Successful pumping tests are those in which (pseudo-) steady state conditions were reached during the pumping phase and where a full recovery was monitored. Such pumping tests help acquire estimates of hydraulic parameters both from pumping and recovery data. In the following paragraphs, a discussion of four representative pumping tests selected in the East, centre and West of the study area will be presented.

IV.7.1.1.1. Well in Kiruhura II-Muramba (pumping test Nr. 22)

Figure IV.12 shows the lithological cross-section of the well situated in the locality of Kiruhura within the village of Muramba, which is situated at 10 km NE of the city of Kirundo. It can be observed that the well is entirely completed in the weathered overburden, which, as extensively discussed in Chapter II, is characterised by an upward decreasing of the grain-size of the weathering materials. The well has a depth of 9.3 m and a diameter of 1 m. The static water level, which is situated at a depth of 5.61 m, lies within sandy clay materials overlying a layer of more coarse materials comprising clay, sand and lateritic gravel (Figures IV.11 & IV. 14).

The pumping test was conducted on 04/10/2008 starting from 11h15, at constant discharge rate of 50.8 m^3/d and the recovery test was continued overnight and

terminated on 05/10/2008 at 8h00 in the morning. The pumping and the recovery phases lasted for 4 hours and 16h30 respectively. The dynamic water level was measured in the pumping well both for the pumping and recovery phases as there is no observation well in the study area. The time-drawdown data curve was matched to 4 different analytical solutions including Hantush, Papadopulos & Cooper, Theis, and Cooper & Jacob. A quick visual inspection of the 4 graphs (IV.15 to IV.18) reveals a pretty good match with the Hantush type curve (IV.15) and the Cooper & Jacob solution (IV.16) with somewhat comparable transmissivity values of 12 m^2/d and 18.2 m^2/d respectively. On the other hand, while the data curve shows a seemingly rather good fit to the Papadopulos and Cooper solution (IV.17), the value of transmissivity of 35.7 m^2/d deduced from this analytical method is nearly 3 times higher than the value obtained from the Hantush method. Moreover, the time-drawdown data curve indicates a poor fit to the Theis type curve (IV.18). For all the above analytical solutions examined, it is worth to note that the storage coefficient is exaggeratedly large ($2.8.10^{-2}$ to $4.8.10^{-1}$), which would stem from the fact that, as there is no observation well, these values may represent the well bore storage (Appendix IV.3).

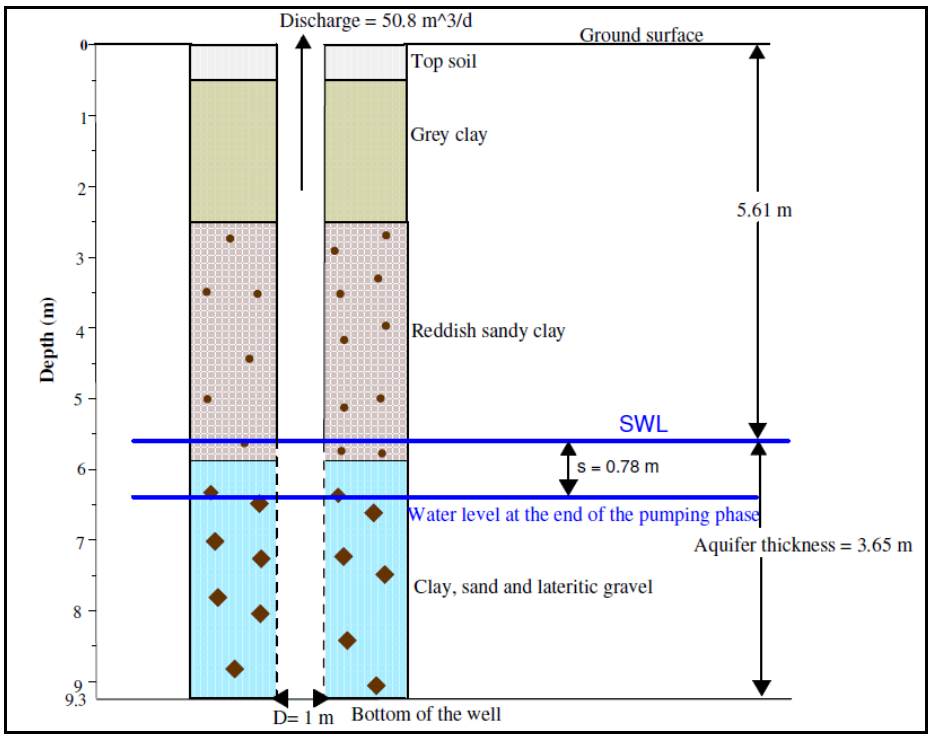

Figure IV.14. Lithological cross-section of the well pumped in Kiruhura II-Muramba in October 2008

Test Conducted by:		Test Date: 04/10/2008
Analysis Performed by: Charles	Hantush	Analysis Date: 06/02/2009
Aquifer Thickness: 3.68 m	Discharge Rate: 2.114959659 [m³/h]	

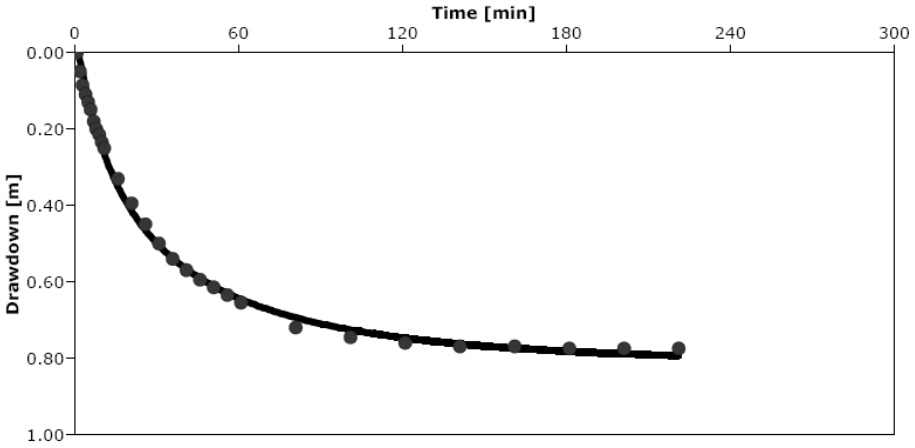

Calculation after Hantush

Observation Well	Transmissivity [m²/d]	Hydraulic Conductivity [m/d]	Storage coefficient	Hydr. resistance [min]	Radial Distance to PW [m]
PW	1.20×10^{1}	3.27×10^{0}	4.84×10^{-1}	2.31×10^{2}	0.5

Figure IV.15. Results of the Hantush analytical method for the pumping test conducted in Kiruhura II –Muramba. Drawdown measurements are done in the pumping well.

Location: Bugesera (Burundi)	Pumping Test: Large diameter Well Muramba_Kiruhura	Pumping Well: PW
Test Conducted by:		Test Date: 04/10/2008
Analysis Performed by: Charles	Cooper & Jacobl	Analysis Date: 06/02/2009
Aquifer Thickness: 3.68 m	Discharge Rate: 2.114959659 [m³/h]	

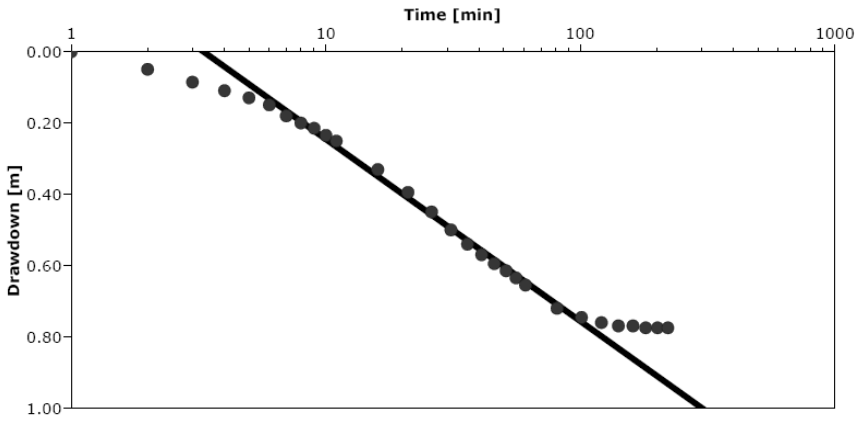

Calculation after Cooper & Jacob

Observation Well	Transmissivity [m²/d]	Hydraulic Conductivity [m/d]	Storage coefficient	Radial Distance to PW [m]	
PW	1.82×10^{1}	4.94×10^{0}	3.76×10^{-1}	0.5	

Figure IV.16. Results of the Cooper & Jacob analytical method for the pumping test conducted in Kiruhura II–Muramba. Drawdown measurements are done in the pumping well.

Location: Bugesera (Burundi)	Pumping Test: Large diameter Well Muramba_Kiruhura	Pumping Well: PW
Test Conducted by:		Test Date: 04/10/2008
Analysis Performed by: Charles	Papadopulos & Cooper	Analysis Date: 06/02/2009
Aquifer Thickness: 3.68 m	Discharge Rate: 2.114959659 [m³/h]	

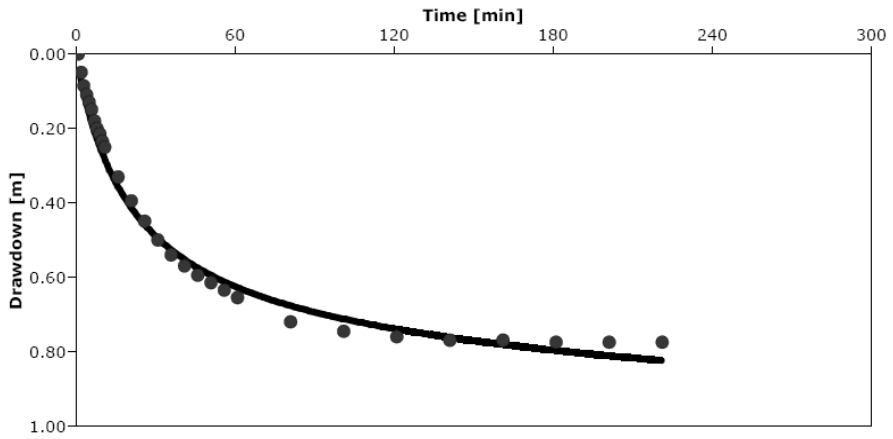

Calculation after Papadopulos & Cooper

Observation Well	Transmissivity [m²/d]	Hydraulic Conductivity [m/d]	Storage coefficient	Radial Distance to PW [m]	
PW	3.57×10^{1}	9.70×10^{0}	2.84×10^{-2}	0.5	

Figure IV.17. Results of the Papadopulos & Cooper analytical method for the pumping test conducted in Kiruhura II–Muramba. Drawdown measurements are done in the pumping well.

Location: Bugesera (Burundi)	Pumping Test: Large diameter Well Muramba_Kiruhura	Pumping Well: PW
Test Conducted by:		Test Date: 04/10/2008
Analysis Performed by: Charles	Theis	Analysis Date: 06/02/2009
Aquifer Thickness: 3.68 m	Discharge Rate: 2.115 [m³/h]	

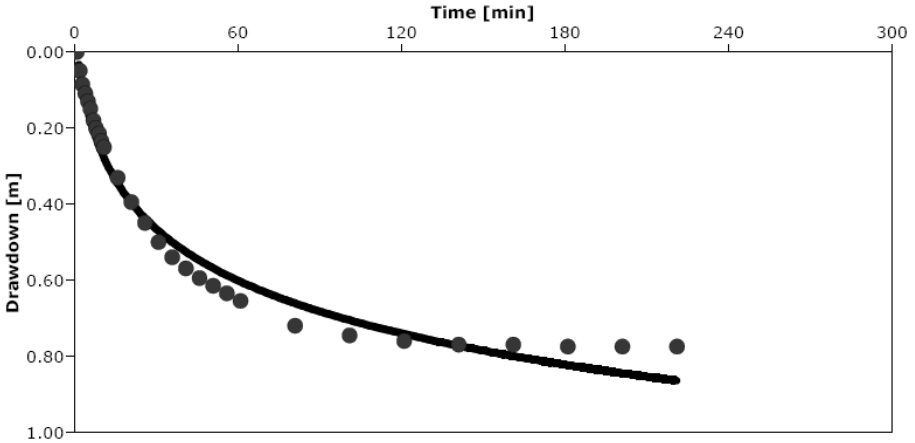

Calculation after Theis

Observation Well	Transmissivity [m²/d]	Hydraulic Conductivity [m/d]	Storage coefficient	Radial Distance to PW [m]	
PW	1.97×10^{1}	5.35×10^{0}	4.07×10^{-1}	0.5	

Figure IV.18. Results of the Theis analytical method for the pumping test conducted in Kiruhura II–Muramba. Drawdown measurements are done in the pumping well.

IV.7.1.1.2. Well in Kiruhura I- Kiyanza (pumping test Nr. 23)

Figure IV.19 presents the lithological cross-section of the well located also in the locality of Kiruhura, but within the village of Kiyanza, which neighbours the village of Muramba to the North. The well is situated at approximately 3 km to the North of the well in Kiruhura II-Muramba. Like in Kiruhura II-Muramba, the well is completed in the weathered overburden with a depth of 6 m and an internal diameter of 1 m. Figures IV.12 and IV.19 show that the bottom of the wells taps a layer of coarser materials comprising clay, sand, lateritic gravel and rock fragments. The static water level lies at a depth of 3.05 m, within a layer made up of a mixture of clay and lateritic gravel.

The pumping test was conducted on 02/10/2008 for 3 hours, from 13h15 to 16h15, whereas the recovery test was continued until the following day (03/10/2008) at 9h00 in the morning, which totalizes a duration of 16h45. A constant pumping rate of 134.8 m^3/day was applied. The time-drawdown data curve shows a good fit to the Hantush type curve (Figure IV.20) and to the Jacob and Cooper analytical solution (Figure IV.21) with values of transmissivity of 19.2 m^2/d and 37.2 m^2/d respectively. On the other hand, despite a good match with the Papadopulos & Cooper type curve (Figure IV.22), the value of transmissivity of 209 m^2/d deduced from this method seems to be extremely high.

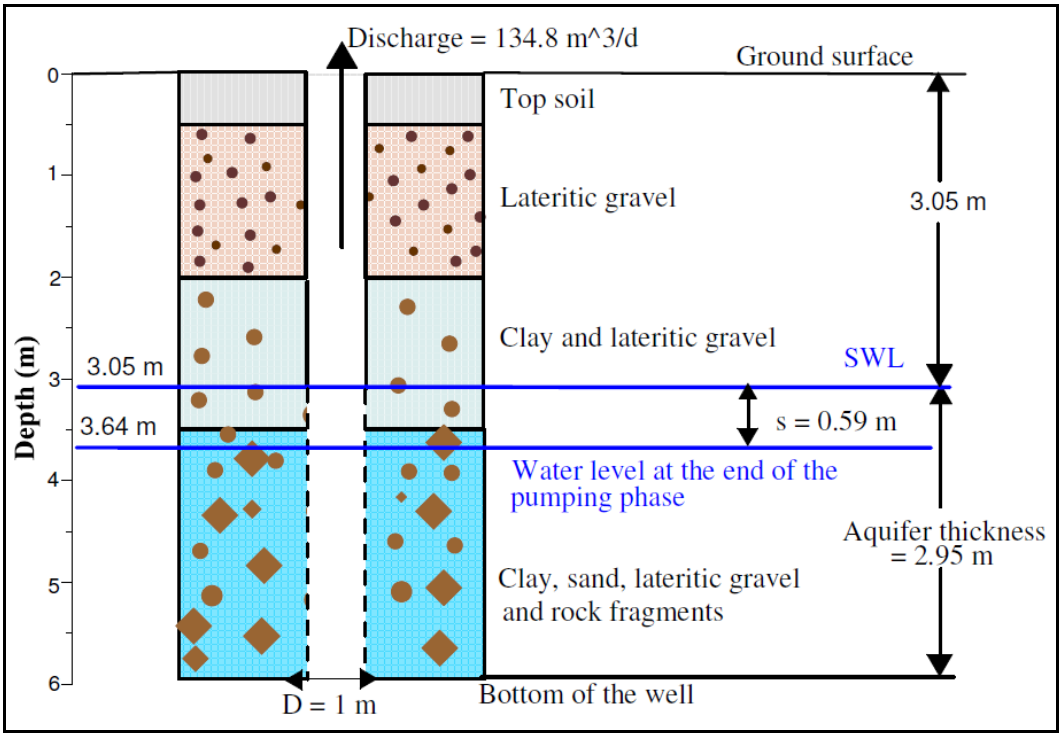

Figure IV.19. Lithological cross-section of the well pumped in Kiruhura I-Kiyanza in October 2008.

Location: Bugesera (Burundi)	Pumping Test: Large diameter well Kiyanza_Kiruhura I	Pumping Well: PW
Test Conducted by: Charles		Test Date: 03/10/2008
Analysis Performed by: Charles	Hantush	Analysis Date: 10/02/2009
Aquifer Thickness: 2.95 m	Discharge Rate: 3.471111111 [m³/h]	

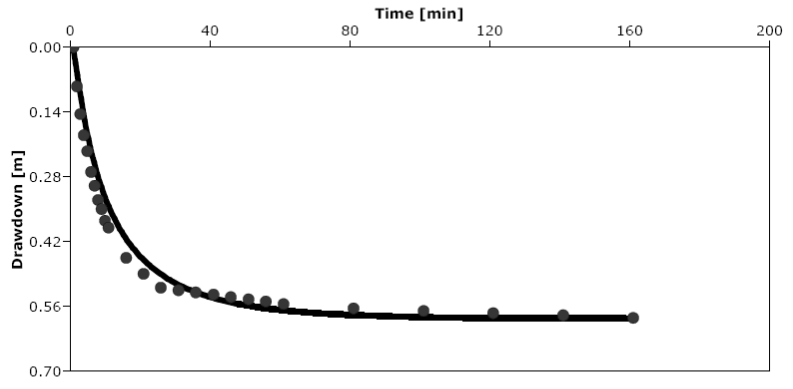

Calculation after Hantush

Observation Well	Transmissivity [m²/d]	Hydraulic Conductivity [m/d]	Storage coefficient	Ratio K(v)/K(h)	Hydr. resistance [min]	Radial Distance to PW [m]
PW	1.92×10^{1}	6.51×10^{0}	5.00×10^{-1}	1.20×10^{-1}	6.25×10^{1}	0.5

Figure IV.20. Results of the Hantush analytical method for the pumping test conducted in Kiruhura I-Kiyanza. Drawdown measurements are done in the pumping well.

Location: Bugesera (Burundi)	Pumping Test: Large diameter well Kiyanza_Kiruhura I	Pumping Well: PW
Test Conducted by: Charles		Test Date: 03/10/2008
Analysis Performed by: Charles	Cooper & Jacob I	Analysis Date: 10/02/2009
Aquifer Thickness: 2.95 m	Discharge Rate: 3.471111111 [m³/h]	

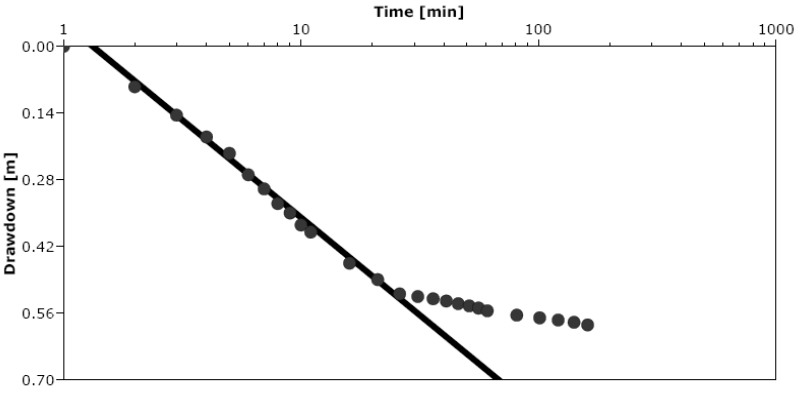

Calculation after Cooper & Jacob

Observation Well	Transmissivity [m²/d]	Hydraulic Conductivity [m/d]	Storage coefficient	Radial Distance to PW [m]	
PW	3.72×10^{1}	1.26×10^{1}	3.08×10^{-1}	0.5	

Figure IV.21. Results of the Cooper & Jacob analytical method for the pumping test conducted in Kiruhura I –Kiyanza. Drawdown measurements are done in the pumping well.

Location: Bugesera (Burundi)	Pumping Test: Large diameter well Kiyanza_Kiruhura I	Pumping Well: PW
Test Conducted by: Charles		Test Date: 03/10/2008
Analysis Performed by: Charles	Papadopulos & Cooper	Analysis Date: 10/02/2009
Aquifer Thickness: 2.95 m	Discharge Rate: 3.471111111 [m³/h]	

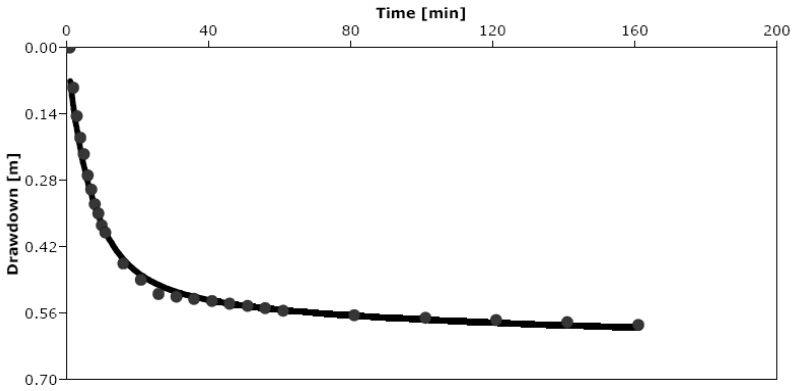

Calculation after Papadopulos & Cooper

Observation Well	Transmissivity [m²/d]	Hydraulic Conductivity [m/d]	Storage coefficient	Radial Distance to PW [m]	
PW	2.09×10^{2}	7.07×10^{1}	1.57×10^{-6}	0.5	

Figure IV.22. Results of the Papadopulos & Cooper analytical method for the pumping test conducted in Kiruhura I–Kiyanza. Drawdown measurements are done in the pumping well.

IV.7.1.1.3. Well in Senga-Nyagisozi (pumping test Nr. 41)

The well is located at approximately 15 km North-East of the chief centre of this municipality of Busoni. Figure IV.23 shows the lithological cross-section of the well located in the locality of Senga, in the village of Nyagisozi. The well presents a lithological sequence similar to the typical weathering profile of the basement rocks in the study area. Indeed, Figure IV.23 shows a clear upwards fining of the weathering materials. The well is completed in the weathered overburden and has a depth of 6.6 m with an internal diameter of 1m. The static water level lies at a depth of 2.62 m below the ground surface (Figure IV.23).

The pumping test was executed on 08/10/2008, between 10h00 and 13h20, and the recovery test was terminated the same day at 15h00 in the afternoon. The well was submitted to a constant pumping rate of 125.8 m^3/d for 3h20, whereas full recovery of the initial static water level was achieved after 1h40. Time-drawdown data curves from the pumping test indicate a good match to the Hantush analytical solution (Figure IV.24) and to the Cooper and Jacob solution (IV.25) with values of transmissivity of 46.5 m^2/d and 56.5 m^2/d respectively. As already observed for other wells in the above discussion, the values of storativity derived from the different analytical methods are exaggeratedly large, thereby reflecting the well bore storage (Appendix IV.3).

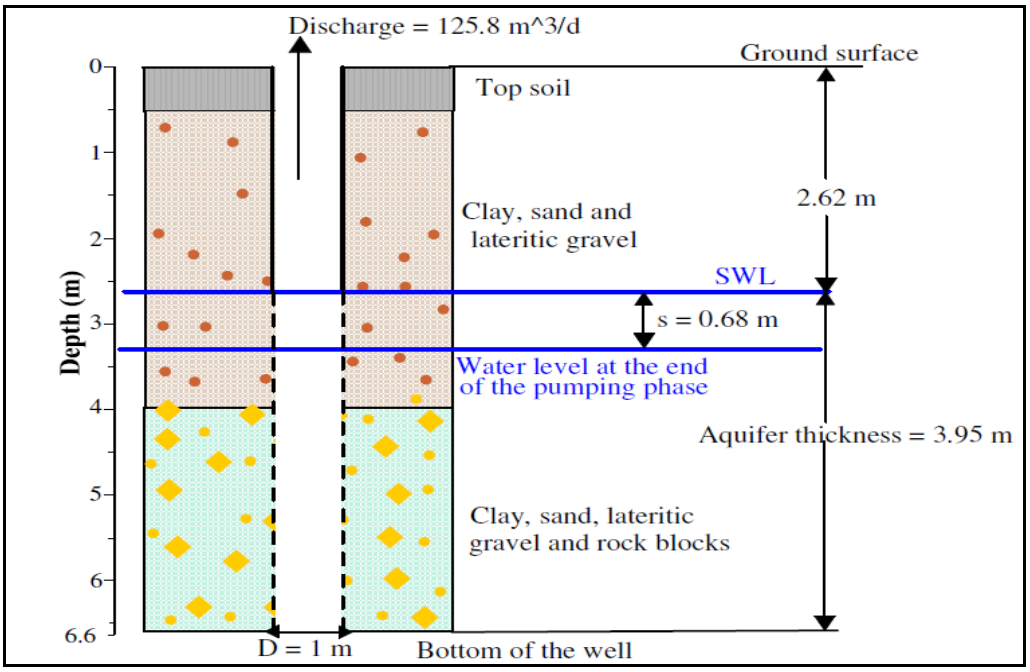

Figure IV.23. Lithological cross-section of the well pumped in Senga-Nyagisozi in October 2008.

Location: Bugesera (Burundi)	Pumping Test: Pumping Large diameter	Pumping Well: PW
Test Conducted by: Charles		Test Date: 07/10/2008
Analysis Performed by: Charles	Hantush	Analysis Date: 13/02/2009
Aquifer Thickness: 3.94 m	Discharge Rate: 5.242997065 [m³/h]	

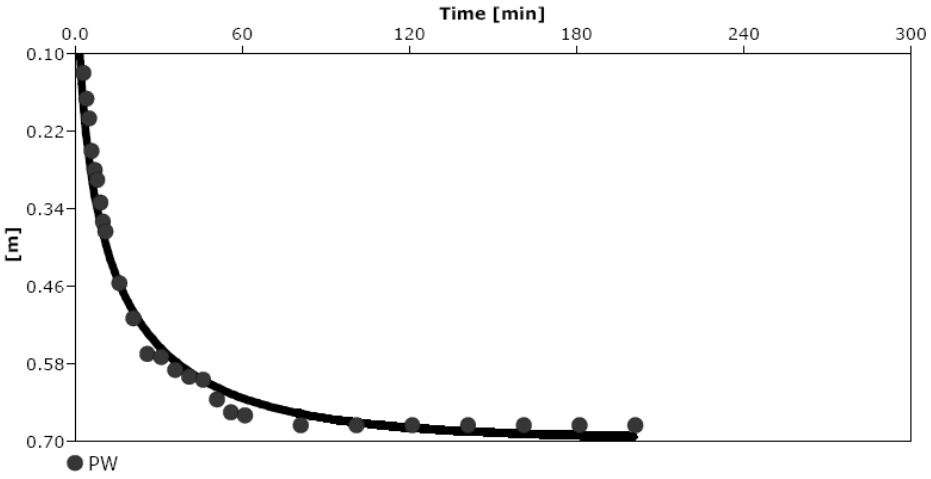

Calculation after Hantush

Observation Well	Transmissivity [m²/d]	Hydraulic Conductivity [m/d]	Storage coefficient	Hydr. resistance [min]	Radial Distance to PW [m]
PW	4.65×10^{1}	1.18×10^{1}	5.00×10^{-1}	1.45×10^{2}	0.5

Figure IV.24. Results of the Hantush analytical method for the pumping test conducted in Senga-Nyagisozi. Drawdown measurements are done in the pumping well.

Location: Bugesera (Burundi)	Pumping Test: Pumping Large diameter	Pumping Well: PW
Test Conducted by: Charles		Test Date: 07/10/2008
Analysis Performed by: Charles	Cooper & Jocob I	Analysis Date: 13/02/2009
Aquifer Thickness: 3.94 m	Discharge Rate: 5.242997065 [m³/h]	

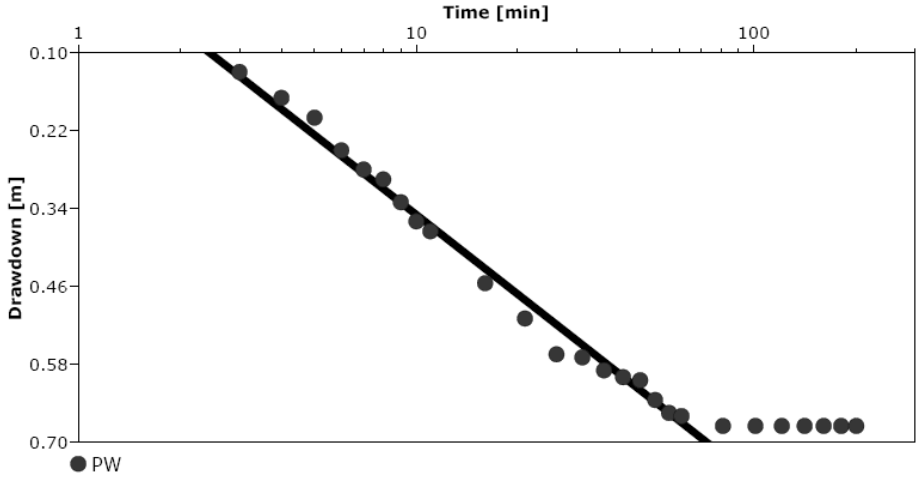

Calculation after Cooper & Jacob

Observation Well	Transmissivity [m²/d]	Hydraulic Conductivity [m/d]	Storage coefficient	Radial Distance to PW [m]	
PW	5.65×10^{1}	1.43×10^{1}	4.91×10^{-1}	0.5	

Figure IV.25. Results of the Cooper & Jacob analytical method for the pumping test conducted in Senga-Nyagisozi. Drawdown measurements are done in the pumping well.

IV.7.1.1.4. Well in Kabirizi II-Kigoma (pumping test Nr. 7)

This well is located in the municipality of Bugabira, North-West of the province of Kirundo. The well is situated at approximately 500 m North of the small lake Nagitamo. The well was constructed in the 1990's by the development project of the province of Kirundo, the so-called "projet Kirundo" (Kirundo project), but, as many other wells in this area, no record regarding its lithological log was found. However, using geoelectrical sounding information, a geoelectrical cross-section of the site, which provides clues as regards to the hydrogeological structure, was inferred (Figure IV.26). This geoelectrical cross-section shows that the static water level lies within a clay-rich layer which overlies a coarse and thick layer made up materials deriving from the deep weathering of the underlying basement, which actually constitutes the aquifer. The well has a total depth of 7.43 m, an internal diameter of 1 m and the static water level lies at a depth of 2.93 m below the ground surface.

The well was submitted to a pumping test on 11/08/2008 for 9 consecutive hours, from 12h00 to 21h00, and a recovery test was conducted until full recovery of the initial static water level for a time span of 12 h, from 21h00 to 9h00 the next morning.

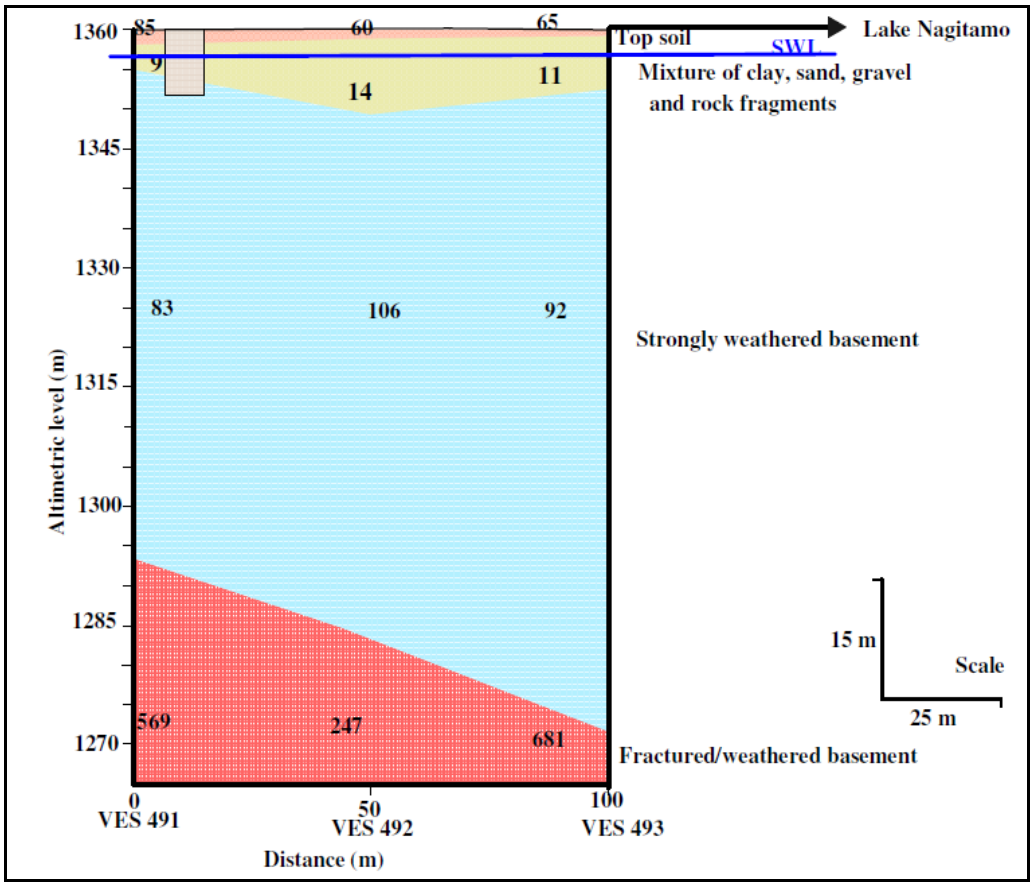

Figure IV.26. Geoelectrical cross-section showing the hydrogeological structure of the site of Kabirizi II-Kigoma based on vertical soundings AIDR-VES 491 to 493.

While the time-drawdown data curve for the pumping phase was expected to match the Hantush analytical solution (IV.27), as per the hydrogeological structure which shows that leaky conditions may prevail, it was noticed that a better fit was rather obtained with the double porosity model with a value of transmissivity of 20.2 m^2/d and a storage coefficient of 2.04 $x10^{-4}$ (Figure IV.28). However, what was even more surprising is the response of the aquifer during the recovery test, which prettily conforms to the Hantush analytical model (Figure IV.29), thereby reflecting leaky conditions with a transmissivity value of 16.2 m^2/d, which is closely comparable to the value obtained from the pumping phase data. The time-drawdown data curve for the recovery phase shows a rather poor match to the double porosity model (Figure IV.30) with an apparently erroneous value for transmissivity of 41.9 m^2/d.

Although such a hybrid response of the aquifer may appear a bit weird, the double porosity response of the aquifer during the pumping phase seems to be at least consistent with our own field observations because, during the pumping test, it was noticed that most of the water flowing to the well was coming from small vertical fractures. This confirms the observations made by El-Fahem (2008) in regolith aquifers in Benin. It was observed that, rather than being a compact homogeneous porous

medium, the regolith may comprise an observable fine network of fissures which result from the original texture and the structural characteristics of the parent rock.

Location: Bugesera (Burundi)	Pumping Test: Large diameter well Kabirizi II	Pumping Well: PW
Test Conducted by: Charles		Test Date: 11/08/2008
Analysis Performed by: Charles	Hantush	Analysis Date: 16/02/2009
Aquifer Thickness: 4.45 m	Discharge Rate: 3.279 [m³/h]	

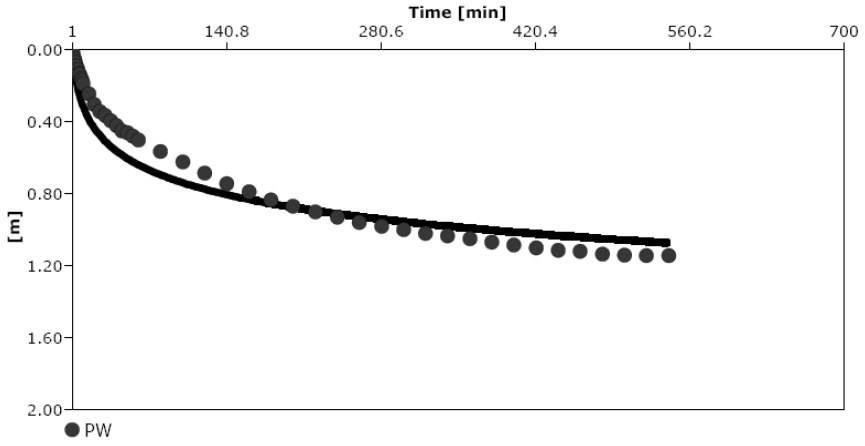

Calculation after Hantush

Observation Well	Transmissivity [m²/d]	Hydraulic Conductivity [m/d]	Storage coefficient	Hydr. resistance [min]	Radial Distance to PW [m]
PW	3.12×10^{1}	7.02×10^{0}	5.00×10^{-1}	1.67×10^{10}	0.5

Figure IV.27. Results of the Hantush analytical method for the pumping test conducted in Kabirizi II-Kigoma. Drawdown measurements are done in the pumping well.

Location: Bugesera (Burundi)	Pumping Test: Large diameter well Kabirizi II	Pumping Well: PW
Test Conducted by: Charles		Test Date: 11/08/2008
Analysis Performed by: Charles	Double porosity	Analysis Date: 16/02/2009
Aquifer Thickness: 4.45 m	Discharge Rate: 3.279 [m³/h]	

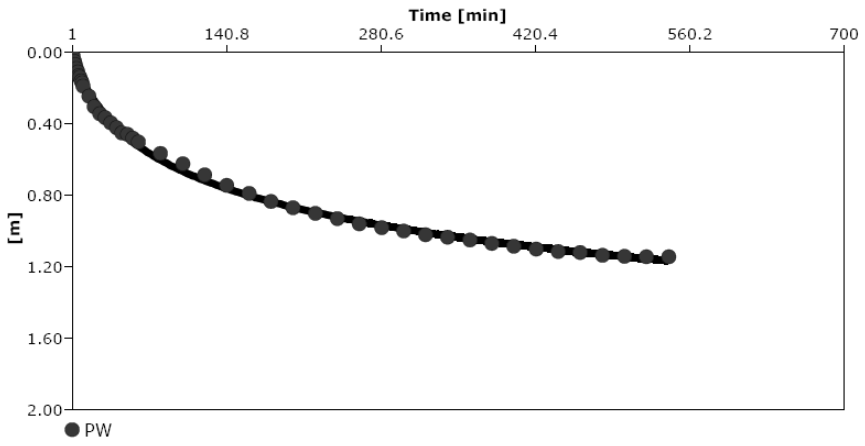

Calculation after Double Porosity

Observation Well	Transmissivity [m²/d]	Hydraulic Conductivity [m/d]	Specific storage	Sigma	Lambda	Radial Distance to PW [m]
PW	2.02×10^{1}	4.55×10^{0}	2.04×10^{-4}	7.80×10^{3}	7.58×10^{0}	0.5

Figure IV.28. Results of the double porosity analytical method for the pumping test conducted in Kabirizi II-Kigoma. Drawdown measurements are done in the pumping well.

Location: Bugesera (Burundi)	Pumping Test: Large diameter well Kabirizi II	Pumping Well: PW
Test Conducted by: Charles		Test Date: 11/08/2008
Analysis Performed by: Charles	Hantush	Analysis Date: 16/02/2009
Aquifer Thickness: 4.45 m	Discharge Rate: 3.278663157 [m³/h]	

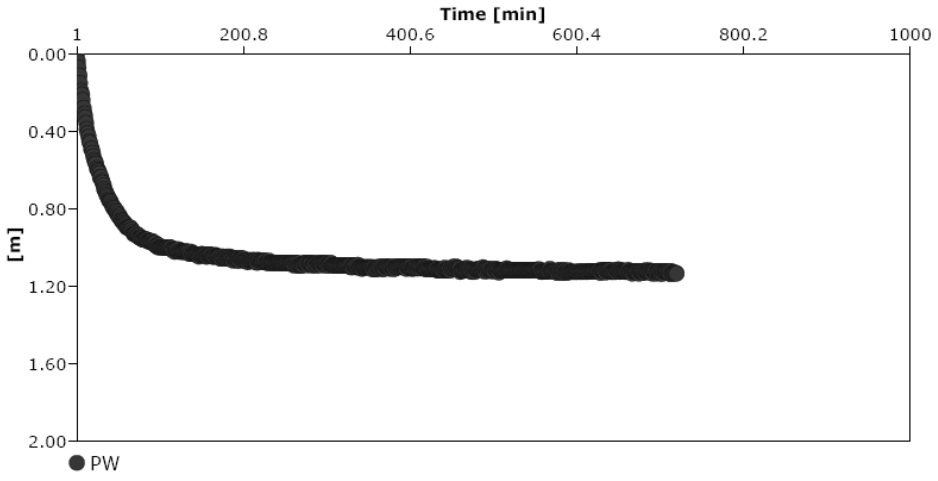

Calculation after Hantush

Observation Well	Transmissivity [m²/d]	Hydraulic Conductivity [m/d]	Storage coefficient	Hydr. resistance [min]	Radial Distance to PW [m]
PW	1.62×10^{1}	3.63×10^{0}	5.00×10^{-1}	2.86×10^{2}	0.5

Figure IV.29. Results of the Hantush analytical method for the recovery test conducted in Kabirizi II-Kigoma. Drawdown measurements are done in the pumping well.

Location: Bugesera (Burundi)	Pumping Test: Large diameter well Kabirizi II	Pumping Well: PW
Test Conducted by: Charles		Test Date: 11/08/2008
Analysis Performed by: Charles	Double Porosity	Analysis Date: 16/02/2009
Aquifer Thickness: 4.45 m	Discharge Rate: 3.278663157 [m³/h]	

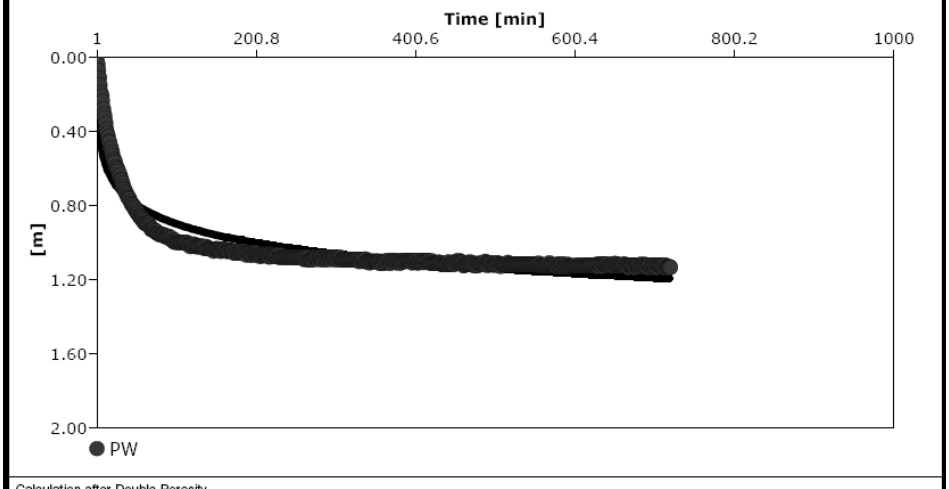

Calculation after Double Porosity

Observation Well	Transmissivity [m²/d]	Hydraulic Conductivity [m/d]	Specific storage	Sigma	Lambda	Radial Distance to PW [m]
PW	4.19×10^{1}	9.42×10^{0}	3.21×10^{-2}	1.00×10^{0}	1.00×10^{1}	0.5

Figure IV.30. Results of the double-porosity analytical method for the Recovery test conducted in Kabirizi II-Kigoma. Drawdown measurements are done in the pumping well.

IV.7.1.1.5. Results and discussion

Table IV.4 & IV.5 represent the values of transmissivity and hydraulic conductivity calculated from the pumping and recovery test data using different analytical methods. Values of transmissivity estimated from the best fit method show a wide variation ranging from as low as 4.4 m^2/d (Marembo-Marembo) to very high values of 377 m^2/d (Muhero II-Yaranda) with an average transmissivity of 50 m^2/d. The hydraulic conductivity ranges between 0.8 m/d (Ngaragu-Kiri) and 166 m/d (Muhero II-Yaranda) with an average of 25 m/d.

This wide range of values of hydraulic parameters reflects the heterogeneity of the regolith aquifer in basement rock environments, whose potential in groundwater is tributary of a number of factors including weathering processes, tectonic activity, mineralogical composition and rock types. Moreover, such a wide range of variation of transmissivity comprising high values exceeding 100 m^2/d reveals that, despite a common belief that the Bugesera region is poor in water resources, there are some localised (sparse) areas within this region with a real groundwater potential. It is interesting to note the way the transmissivity varies sometimes in a rather dramatic way even on short distances.

To illustrate this point, let us consider the village of Yaranda, which is situated at approximately 3 km North of the city of Kirundo. This village is situated within the geological formation called “Undifferentiated Complex”, which mainly comprises granitic and pegmatitic intrusions as well as relicts of the metasedimentary country rocks. Five wells, namely Muhero I-Yaranda, Muhero II-Yaranda, Kigozi-Yaranda, Nunga II-Yaranda and Mutoza-Yaranda have been constructed on the northern and southern flanks of this elongated village, at distances of maximum 2 km from one well to another (Figure IV.3). However, despite the apparent homogeneity as regards to the geology, the five wells show a wide variability of values of hydraulic parameters (Table IV.6). The transmissivity varies between a minimum of 6.1 m^2/d and a maximum of 377 m^2/d with an average of 96 m^2/d and a standard deviation of 159 m^2/d. Similarly, the hydraulic conductivity ranges between 2.2 m/d and 166 m/d with an average of 38.5 m/d and a standard deviation of 71.50 m/d. Both parameters show an extremely large coefficient of variation, reflecting the importance of the heterogeneities within this shallow aquifer system.

Table IV.4. Comparison of transmissivity values (m^2/d) calculated using different analytical methods from fully successful pumping and recovery test data collected during the field work in 2007 and 2008.

W/N	Well name	**Pumping test**					**Recovery test**					Best fit method
		Hantush	Theis	Papadopulos & Cooper	Cooper & Jacob	Double porosity	Hantush	Theis	Papadopulos & Cooper	Cooper & Jacob	Double porosity	
1	Bishunzi-Cewe	7.24	-	-	13.5	-	5.56	-	-	12.4	-	Hantush
2	Cimbogo-Gatete	54.3	-	-	48.4	-	55.5	-	-	50.7	-	Hantush
7	Kabirizi II-Kigoma	31.2	-	-	-	20.2	16.2	-	-	19.8	41.9	Double porosity (pumping)-Hantush (recovery)
8	Kabonde-Runyonza	226	-	-	-	-	188	-	553	-	-	Hantush
9	Kadobogoro-Muramba	15.5	-	31.6	18.7	-	11.1	-	52.4	17.3	-	Hantush
	Kanabugiri-Bugera	61.7	-	-	-	-	64.3	-	-	70.1	-	Hantush
13	Kanigo-Cinuma	6.45	-	-	-	4.78	3.37	-	-	5.74	7.04	Double porosity (pumping)-Hantush (recovery)
17	Kigina I-Gisenyi	27.7	-	-	-	-	12.6		-	29.9	-	Hantush
18	Kigina II-Gisenyi	10.4	-	-	-	-	5.17	-	-	11.0	-	Hantush
19	Kigoma-Gatare	5.67	7.41	14.4	7 .42	-	3.62	8.39	20.8	5.76	-	Hantush
22	Kiruhura II-Muramba	12.0	19.7	35.7	18.2	-	6.97	-	-	14.7	-	Hantush
23	Kiruhura I-Kiyanza	19.2	-	209	37.2	-	12.0	-	-	-	-	Hantush
24	Mago-Gatete	43.9	-	-	-	-	37.3	-	-	-	-	Hantush
25	Marembo-Marembo	4.38	4.38	-	4.55	-	3.67	6.16	-	5.04	-	Hantush
27	Muhero II-Yaranda	377	-	-	-	-	343	-	-	-	-	Hantush
28	Muhero I-Yaranda	21.6	-	36.3	22.2	-	13.1	-	84.9	23.3	-	Hantush
30	Murambo-Murambi	13.1	17.5	47.0	16.5	-	6.30	-	99.1	12.4	-	Hantush
32	Mutoza-Yaranda	8.40	-	23.1	10.3	-	2.72	-	66.5	7.66	-	Hantush
33	Ngaragu-Kiri	5.15	7.46	13.2	5.55	-	4.41	7.46	13.2	6.82	-	Hantush
34	Ntwago-Murungurira	52.1	-	-	-	-	37.0	-	-	54.1	-	Hantush
36	Nunga II-Yaranda	66.9	-	113	70.3	-	58.9	-	172	-	-	Hantush
37	Nyange-Kumana	60.3			61.1	-	12.6			49.1		Hantush
39	Ruranzi-Rwibikara	39.3	39.3	52.7	41.7	-	20.9	-	97.5	-	-	Hantush
41	Senga-Nyagisozi	46.5	-	-	56.5	-	18.4	-	-	45.2	-	Hnatush

Table IV.5. Comparison of hydraulic conductivity values (m/d) calculated using different analytical methods from fully successful pumping and recovery test data collected during the field work in 2007 and 2008.

W/N	Well name	**Pumping test**					**Recovery test**					**Best fit method**
		Hantush	Theis	Papadopulos & Cooper	Cooper & Jacob	Double porosity	Hantush	Theis	Papadopulos & Cooper	Cooper & Jacob	Double porosity	
1	Bishunzi-Cewe	1.56	-	-	2.89	-	1.20	-	-	2.67	-	Hantush
2	Cimbogo-Gatete	30.3	-	-	27.1	-	31.0	-	-	28.3	-	Hantush
7	Kabirizi II-Kigoma	7.02	-	-	-	4.55	3.63	-	-	4.44	9.42	Double porosity (pumping)-Hantush (recovery)
8	Kabonde-Runyonza	104	-	-	-	-	86.4	-	2.54	-	-	Hantush
9	Kadobogoro-Muramba	5.25	-	10.7	6.32	-	3.76	-	17.7	5.86	-	Hantush
12	Kanabugiri-Bugera	41.0	-	-	-	-	42.7	-	-	46.6		Hantush
13	Kanigo-Cinuma	1.14	-	-	-	$8.46x10^{-1}$	$5.96x10^{-1}$	-	-	1.02	1.25	Double porosity (pumping)-Hantush (recovery)
17	Kigina I-Gisenyi	12.0	-	-	-	-	5.41	-	-	12.9	-	Hantush
18	Kigina II-Gisenyi	5.23			5.99	-	2.59	-	-	5.51	-	Hantush
19	Kigoma-Gatare	1.55	2.03	3.94	2.03	-	$9.92x10^{-1}$	2.30	5.70	1.58	-	Hantush
22	Kiruhura II-Muramba	3.27	5.35	9.70	4.95	-	1.89			3.99	-	Hantush
23	Kiruhura I-Kiyanza	6.51	-	70.7	12.6	-	4.07	-	-	-	-	Hantush
24	Mago-Gatete	10. 6	-	-	-	-	9.02	-	-	-	-	Hantush
25	Marembo-Marembo	$8.84x10^{-1}$	$8 .84x10^{-1}$	-	$9.19x10^{-1}$		$7.40x10^{-1}$	1.25	-	1.02	-	Hantush
27	Muhero II-Yaranda	166	-	-	-	-	151	-	-	-	-	Hantush
28	Muhero I-Yaranda	6.06	-	10.2	6.23	-	3.67	-	23.8	6.54	-	Hantush
30	Murambo-Murambi	6.57	8.76	23.5	8.26	-	3.15	-	49.5	6.22	-	Hantush
32	Mutoza-Yaranda	2.15	-	5.94	2.62	-	$6.94x10^{-1}$	-	-	1.96	-	Hantush
33	Ngaragu-Kiri	$8.31x10^{-1}$	1.20	2.13	$8.95x10^{-1}$	-	$7.11x10^{-1}$	1.20	2.14	1.10	-	Hantush
35	Ntwago-Murungurira	26.8	-	-	-		19.0	-	-	27.8	-	Hantush
36	Nunga II-Yaranda	15.7	-	26 .5	16.5	-	13.8	-	40.4	-	-	Hantush
37	Nyange-Kumana	40.7	-	-	41.3	-	8.51	-	-	33.4	-	Hantush
39	Ruranzi-Rwibikara	22.7	22.7	30.5	24.1	-	12.1		56.3			Hantush
41	Senga-Nyagisozi	11.8	-	-	14.3	-	4.67	-	-	11.5		Hnatush

Table IV.6. Variation of hydraulic parameters in 5 wells located within the village of Yaranda, at the outskirts of the city of Kirundo (Q = discharge, D = saturated thickness assumed to be equal to the length of the water column in the well)

W/N	Well-location	Q (m^3/d)	D (m)	T (m^2/d)	K (m/d)	Observation
20	Kigozi-Yaranda	61.3	2.5	6.1	2.5	Half- successful test
27	Muhero II-Yaranda	124.7	2.3	377	166	Fully successful test
28	Muhero I-Yaranda	44.2	3.6	21.6	6.1	Fully successful test
32	Mutoza-Yaranda	48	3.9	8.4	2.2	Fully successful test
36	Nunga II-Yaranda	126.5	4.3	66.9	15.7	Fully successful test
	Maximum			**377**	**166**	
	Minimum			**6.1**	**2.2**	
	Average			**96**	**38.5**	
	Standard deviation			**159**	**71.5**	
	Coefficient of variation (%)			**165.6**	**185.8**	

Tables IV.4 and IV.5 confirm the predominance of leaky response (Hantush method showing bets fit) among the pumping tests in which (pseudo-) steady-state conditions were reached. This observation is consistent with the hydrogeological model inferred by combining geophysical and lithological information, which shows that semi-confined conditions may prevail. On the other hand, most of the wells in which a leaky response was observed conform also to the Cooper & Jacob method, with values of hydraulic parameters which are fairly comparable to those predicted by the Hantush method.

In general, hydraulic parameters derived from pumping test data using the Hantush analytical solution are comparable to those calculated from the recovery test data. However, there are some exceptions like the wells Nyange-Kumana, Senga-Nyagisozi, Mutoza-Yaranda and Ruranzi-Rwibikara which show an important discrepancy between hydraulic parameters derived from pumping test data and those calculated from recovery data. On the other hand, by using the Cooper & Jacob method (1945), which generally gives values of hydraulic parameters comparable to those predicted by the Hantush method, at least for the pumping phase, the difference between hydraulic parameters calculated from pumping and recovery test data is not of great significance. For instance, for the same well Nyange-Kumana, the Cooper & Jacob method gives transmissivity values of 61.1 m^2/d and 49.1 m^2/d respectively for the pumping and recovery phases, while by applying the Hantush method, the values of transmissivity for the pumping and recovery phases are respectively 60.30 m^2/d and 12.6 m^2/d. According to Chilton and Smith-Carington (1984), such a discrepancy between hydraulic parameters derived from pumping and recovery test data may reflect the heterogeneities of aquifers.

The hybrid response of some wells (Kabirizi II-Kigoma and Kanigo-Cinuma) in the western part of the study area, which show double porosity conditions during the pumping phase and leaky conditions during the recovery phase, is somewhat strange and has never been reported in previous studies. A number of studies conducted in basement aquifers across the world reveal unconfined conditions (Wright, 1992, Diop & Tijani, 2008), confined conditions (Taylor & Howard, 2000, Chilton and Smith-Carington, 1984), leaky conditions (Wright, 1992, Chilton & Foster, 1995, Taylor & Howard, 2000, Jalludin & Razack, 2004) and fractured conditions (Taylor & Howard, 2000, Jalludin & Razack, 2004).

This change of aquifer response from double porosity conditions during the pumping test to leaky conditions during the recovery test may be consistent with the observations made by Taylor & Howard (2000) in fractured crystalline aquifers in Uganda. First of all, it appears important to recall that, in the western part of the study area where this unusual drawdown behaviour of aquifers is observed, tectonic fracturing consecutive to the development of the Bugesera depression and particularly the North-South fault separating the depression and the plateau of Butare (Chapter II), may be responsible for this widespread conformity to the double porosity solution. Indeed many wells in this part of the study area, mainly those in which half-successful pumping tests were performed, show a quasi generalised conformity to the double porosity model.

During the pumping phase, the aquifer is submitted to a hydraulic stress and the flow to the well preferentially occurs through the fractures. As the pumping continues, both fractures and the matrix progressively contribute to the flow. In pumping tests conducted in fractured aquifers in Uganda, Howard and Taylor (2000) observed that the drawdown in the weathered mantle occurred several hours after the start of the pumping and continued for 1 to 2 hours after pumping had ceased. This resulted in a rapid recovery thereby confirming a connection between the weathered mantle and the fractures, the former playing a capacitive role and transmitting water to the well through the more transmissive fractures.

Therefore, despite the hydrogeological structure which indicates leaky conditions, it is strongly possible that during the pumping phase, the flow to the well through the fractures predominates over the flow through the matrix pores, thereby leading to a double porosity response of the aquifer. However, during the recovery test, the flow to the well may be mainly dominated by the leakage of the clayey weathered mantle which continues for several hours after the end of the pumping and which may be responsible for the leaky response of the aquifer during the recovery phase.

Furthermore, it is interesting to note how fairly close are values of hydraulic parameters obtained from the pumping and recovery test data despite the use of two different analytical solutions. Indeed, for the well Kabirizi II-Kigoma, the transmissivity obtained for the pumping phase using the double porosity model is 20.2 m^2/d while for the recovery phase, which conforms to Hantush analytical solution, a transmissivity value of 16.2 m^2/d is obtained. Similarly, for the well Kanigo-Cinuma, the transmissivity values calculated from the pumping test data using the double porosity method and from recovery test data using Hantush method are respectively 4.8 m^2/d and 3.4 m^2/d.

Despite the fact that all the wells tested have a large diameter, which implies a substantial well bore storage, the Papadopulos & Cooper method (1967) does not seem to be appropriate for the interpretation of the pumping and recovery test data. Indeed, even when the data curve for the pumping or recovery test perfectly matches the Papadopulos & Cooper type curve, the hydraulic conductivity and the transmissivity are exaggeratedly high and therefore seem unreliable. For instance, for the well Kiruhura I-Kiyanza (Nr. 23), where a good match of the pumping test data is observed with the Papadopulos & Cooper method, the value of transmissivity obtained is 209 m^2/d while the values obtained by using the Hantush, and Cooper & Jacob methods are respectively 19.2 m^2/d and 37.2 m^2/d. The same observation applies to the hydraulic conductivity for which the Papadopulos & Cooper method gives systematically higher values.

The hydraulic parameters (transmissivity and hydraulic conductivity) determined in this study have to be considered with caution. Indeed, the conversion of the transmissivity into hydraulic conductivity or vice-versa requires a good knowledge of the aquifer thickness or the saturated thickness which is, so far, poorly defined in the study area. For most of the wells investigated, there are no lithological descriptions from which the aquifer thickness could be inferred. Moreover, these wells were dug by hands down to a maximum depth of 17.5 m, which implies that they only tap a minimum portion of the saturated thickness. The approach used in this study as suggested by Gingerich (1999) helps obtain maximum estimates of hydraulic conductivity by assuming that the aquifer thickness is equal to the saturated well depth.

According to the classification of transmissivity magnitude and variation proposed by Krasny (1993), most of the values of transmissivity (16 values) derived from fully successful pumping tests fall within the intermediate transmissivity class (T = 10-100 m^2/d). The low transmissivity (T = 1-10 m^2/d) and the high transmissivity (T = 100-1000 m^2/d) classes comprise 6 and 2 values of transmissivity respectively. The two values of transmissivity which fall within the high transmissivity class correspond to the wells Muhero II in the village of Yaranda and Kabonde in the village of Runyonza, which are all located within the Undifferentiated Complex Formation (Table IV.7).

Likewise, 16 values of hydraulic conductivity fall within the intermediate class, while the low transmissivity and high transmissivity classes comprise 6 and 2 values respectively (Table IV.8).

Table IV.7. Classification of values of transmissivity calculated from fully successful pumping test data according to the classification scheme proposed by Krasny (1993)

W/N	Low transmissivity class (1-10 m^2/d)			W/N	Intermediate transmissivity class (10-100 m^2/d)			W/N	High transmissivity class (100-1000 m^2/d)		
	Well name	**Formation**	**T (m^2/d)**		**Well name**	**Formation**	**T (m^2/d)**		**Well name**	**Formation**	**T (m^2/d)**
1	Bishunzi-Cewe	U.C.	7.2	2	Cimbogo-Gatete	Nyagisozi	54.3	8	Kabonde-Runyonza	U.C.	226
13	Kanigo-Cinuma	Murehe	4.8	7	Kabirizi II-Kigoma	Murehe	20.2	27	Muhero II-Yaranda	U.C.	377
19	Kigoma-Gatare	Nyagisozi	5.7	9	Kadobogoro-Muramba	U.C.	15.5				
25	Marembo-Marembo	U.C.	4.4	12	Kanabugiri-Bugera	U.C	61.7				
32	Mutoza-Yaranda	U.C.	8.4	17	Kigina I-Gisenyi	Murehe	27.7				
33	Ngaragu-Kiri	Murehe	5.2	18	Kigina II-Gisenyi	Murehe	10.4				
				22	Kiruhura II-Muramba	U.C	12				
				23	Kiruhura I-Kiyanza	U.C.	19.2				
				24	Mago-Gatete	Nyagisozi	43.9				
				28	Muhero I-Yaranda	U.C.	21.6				
				30	Murambo-Murambi	U.C.	13.1				
				35	Ntwago-Murungurira	U.C.	52.1				
				36	Nunga II-Yaranda	U.C.	66.9				
				37	Nyange-Kumana	Nyagisozi	60.3				
				39	Ruranzi-Rwibikara	U.C.	39.3				
				41	Senga-Nyagisozi	Nyagisozi	46.5				
	Maximum		**8.4**				**66.9**				**-**
	Minimum		**4.4**				**10.4**				**-**
	Average		**5.9**				**35.3**				**301.5**
	Standard deviation		**1.6**				**19.9**				**-**
	Coefficient of variation (%)		**26**				**56.5**				**-**

U.C.: Undifferentiated Complex

Table IV.8. Classification of values of hydraulic conductivity calculated from fully successful pumping test data according to the classification scheme proposed by Krasny (1993)

W/N	Low transmissivity class (1-10 m^2/d)			W/N	Intermediate transmissivity class (10-100 m^2/d)			W/N	High transmissivity class (100-1000 m^2/d)		
	Well name	**Formation**	**K (m/d)**		**Well name**	**Formation**	**K (m/d)**		**Well name**	**Formation**	**K (m/d)**
1	Bishunzi-Cewe	U.C.	1.6	2	Cimbogo-Gatete	Nyagisozi	30.3	8	Kabonde-Runyonza	U.C.	104
13	Kanigo-Cinuma	Murehe	0.8	7	Kabirizi II-Kigoma	Murehe	4.55	27	Muhero II-Yaranda	U.C.	166
19	Kigoma-Gatare	Nyagisozi	1.6	9	Kadobogoro-Muramba	U.C.	5.25				
25	Marembo-Marembo	U.C.	0.9	12	Kanabugiri-Bugera	U.C	41				
32	Mutoza-Yaranda	U.C.	2.2	17	Kigina I-Gisenyi	Murehe	12				
33	Ngaragu-Kiri	Murehe	0.8	18	Kigina II-Gisenyi		5.23				
				22	Kiruhura II-Muramba	U.C	6.51				
				23	Kiruhura I-Kiyanza	U.C.	3.27				
				24	Mago-Gatete	Nyagisozi	10.6				
				28	Muhero I-Yaranda	U.C.	6.06				
				30	Murambo-Murambi	U.C.	6.57				
				35	Ntwago-Murungurira	U.C.	26.8				
				36	Nunga II-Yaranda	U.C.	15.7				
				37	Nyange-Kumana	Nyagisozi	40.7				
				39	Ruranzi-Rwibikara	U.C.	22.7				
				41	Senga-Nyagisozi	Nyagisozi	11.8				
	Maximum		**2.2**				**41**				**-**
	Minimum		**0.8**				**3.3**				**-**
	Average		**1.3**				**15.6**				**135**
	Standard deviation		**0.6**				**12.8**				**-**
	Coefficient of variation (%)		**43.6**				**82.3**				**-**

U.C. : Undifferentiated Complex

Tables IV.9 and IV.10 show some statistical parameters about the values of transmissivity and hydraulic conductivity calculated for the 3 geological formations wherein fully successful pumping tests were conducted, i.e. the Formation of Murehe (Mugendo), the Undifferentiated Complex and the Formation of Nyagisozi (or Nyabihanga). The highest values of hydraulic parameters are found within the Undifferentiated Complex where, for the 14 sites which were fully successfully tested, the transmissivity varies between a minimum of 4.4 m^2/d (Marembo-Marembo) and a maximum of 377 m^2/d (Muhero II-Yaranda) with an average of 66 m^2/d (Table IV.9). The Formation of Murehe (or Mugendo) shows the lowest values of hydraulic transmissivity. For the 5 sites where fully successful pumping tests were performed, the transmissivity ranges between 4.8 m^2/d (Kanigo-Cinuma) and 27.7 m^2/d (Kigina I-Gisenyi) with an average of 13.6 m^2/d. The Formation of Nyagisozi, wherein 5 fully successful pumping tests were performed, is characterised by intermediate values of transmissivity, with a minimum transmissivity of 5.7 m^2/d (Kigoma-Gatare), a maximum of 60.3 m^2/d (Nyange-Kumana) and an average of 42.1 m^2/d.

The highest values of hydraulic parameters found within the Undifferentiated Complex confirm the findings presented in Chapter III which indicate that, with the thickest weathered part of the basement, this formation has the highest groundwater potential compared to the surrounding metasedimentary formations. On the other hand, the high values of the coefficients of variation for the hydraulic properties for the 3 geological formations confirm the heterogeneities, which are typical of basement aquifers. Indeed, several authors have pointed out the fact that aquifers in crystalline rocks are heterogeneous and may have variable hydraulic properties even over short distance (Bannerman & Ayibotele, 1984; Chilton & Smith-Carington, 1984; Jalludin & Razack, 2004; Sighal, 1997).

Table IV.9. Variation of the transmissivity (m^2/d), obtained from fully successful pumping tests, for the different geological formations

Geological formation	Number of tests	Maximum (m^2/d)	Minimum (m^2/d)	Average (m^2/d)	Standard deviation (m^2/d)	Coefficient of variation (%)
Undifferentiated Complex	14	377	4.4	66	106.1	160.6
Murehe (or Mugendo)	5	27.7	4.8	13.6	10	73.4
Nyagisozi (or Nyabihanga)	5	60.3	5.7	42.1	21.4	50.7

Table IV.10. Variation of the hydraulic conductivity (m/d), obtained from fully successful pumping tests, for the different geological formations

Geological formation	Number of wells	Maximum (m^2/d)	Minimum (m^2/d)	Average (m^2/d)	Standard deviation (m^2/d)	Coefficient of variation (%)
Undifferentiated Complex	14	166	0.9	29.2	47.9	164
Murehe (or Mugendo)	5	12	0.8	4.7	4.6	97.8
Nyagisozi (or Nyabihanga)	5	40.7	1.6	21.1	17.7	83.7

IV.7.1.2. Half-successful pumping tests

These are pumping tests in which the pumping phase was ended before (pseudo-) steady-state conditions were attained but where a recovery of at least 80 % of the initial water level was achieved, thus allowing to derive an estimate of the hydraulic parameters from the recovery data. This was achieved by interpreting recovery with standard pumping test interpretation methods, assuming steady-state was reached during pumping, and considering rises with respect to pumping level as drawdowns. In total, 16 pumping tests fall within this group. In the following paragraphs, a description of 4 representative pumping tests of this category will be given.

IV.7.1.2.1. The well in Kinyamateke-Nyabikenke (pumping test Nr. 21)

The well is located at the southern outskirts of the chief centre of the municipality of Bugabira, at approximately 2 km. This well is the only source of domestic water supply for the inhabitants of Ruhehe, the chief centre of the municipality of Bugabira. The well was constructed in 1988. It has a total depth of 9 m and an internal diameter of 1 m.

Figure IV.31 shows a lithological cross-section of the well inferred from the lithological description of a recently constructed well (2008) at 1 km to the west of the old well. The two wells are situated in the same geological formation, i.e. the Undifferentiated Complex. The cross-section shows that the well taps the upper part of the weathered overburden wherein clay is still predomidant, despite a downwards increase of the coarse fractions (sand and rock fragments).

The pumping test was conducted on 14/08/2008, from 12h00 to 16h20, with a pumping rate of 35 m^3/d. The pump was shut down when the groundwater level reached a depth of 7.73 m, before (pseudo-) steady-state conditions, in order to avoid damage to the pump. The recovery was monitored until the following day at 10h00, which totalizes 17h40 for the recovery test. The initial static water level was fully recovered. Thus, an estimate of the hydraulic parameters was derived from recovery data.

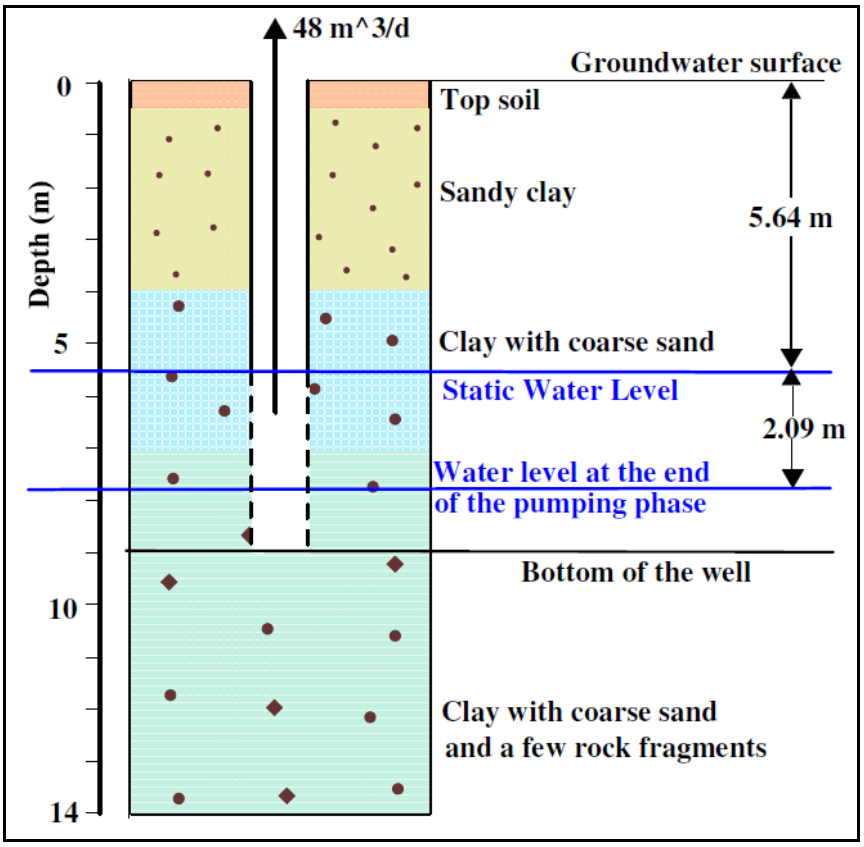

Figure IV.31. Lithological cross-section of the well pumped in Kinyamateke-Nyabikenke

Location: Bugesera (Burundi)	Pumping Test: Large diameter well Kinyamateke	Pumping Well: PW
Test Conducted by:		Test Date: 14/08/2008
Analysis Performed by: Charles	Hantush	Analysis Date: 16/02/2009
Aquifer Thickness: 2.61 m	Discharge Rate: 1.443288174 [m³/h]	

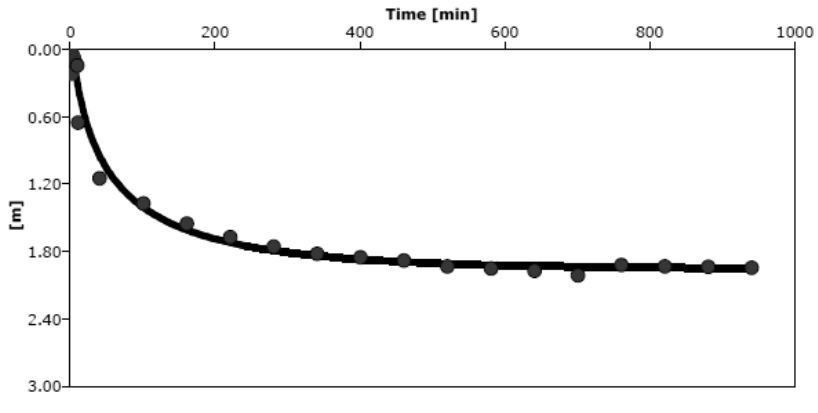

Calculation after Hantush

Observation Well	Transmissivity [m²/d]	Hydraulic Conductivity [m/d]	Storage coefficient	Hydr. resistance [min]	Radial Distance to PW [m]
PW	3.94×10^{0}	1.51×10^{0}	2.76×10^{-1}	1.08×10^{3}	0.5

Figure IV.32. Results of the Hantush analytical method for the recovery test conducted in Kinyamateke-Nyabikenke. Drawdown measurements are done in the pumping well.

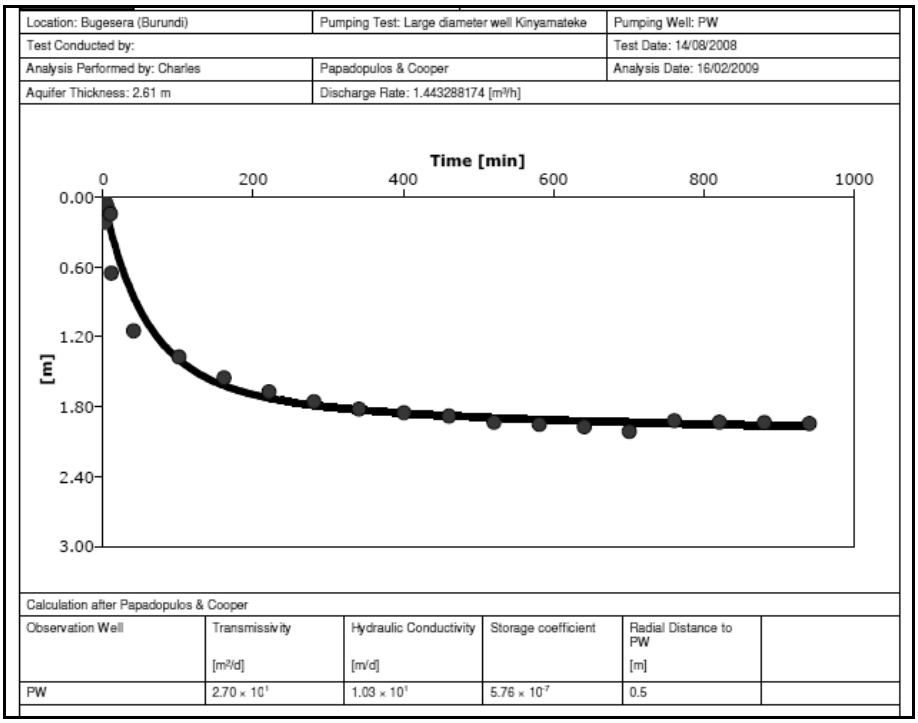

Figure IV.33. Results of the Papadopulos & Cooper analytical method for the recovery test conducted in Kinyamateke-Nyabikenke. Drawdown measurements are done in the pumping well.

Figures IV.32 and IV.33 show values of hydraulic parameters obtained using the analytical methods of Hantush and Papadopulos & Cooper. Despite an apparent good match of the time-drawdown data curve with the Papadopulos & Cooper analytical model (Figure IV.33), this method gives a very high value of transmissivity (27 m^2/d) compared to the value obtained from the analytical method of Hantush (3.9 m^2/d) (Figure IV.32). Considering the low productivity of this well, the value obtained from the method of Hantush seems to be more realistic.

IV.7.1.2.2. The well in Gahwijo II-Nyabikenke (pumping test Nr. 4)

This well is situated in the locality of Gahwijo, at approximately 3.5 km to the West of the chef centre of the municipality of Bugabira. It is located within the Undifferentiated Complex Formation. The well, which was constructed in 2000, is still operating, but can run dry at some peak times of the day, when many people come to fetch water at the same time. The well has a depth of 8.32 m and an internal diameter of 1 m.

Figure IV.34 shows a geoelectrical cross-section of the site of Gahwijo in the village of Nyabikenke where the well is situated. The geoelectrical cross-section is inferred from the vertical sounding performed by AIDR in 1984 and gives a broad view of the subsurface structure of the area. From this figure, it is evident that, with a depth of 8.32 m, the well taps only the upper part of the weathering profile which, as discussed

in Chapter III, comprises fine-grained weathering materials and therefore has a low transmissivity. The static water level lies at a depth of 4.30 m below the ground surface, in the upper layer of the weathering profile.

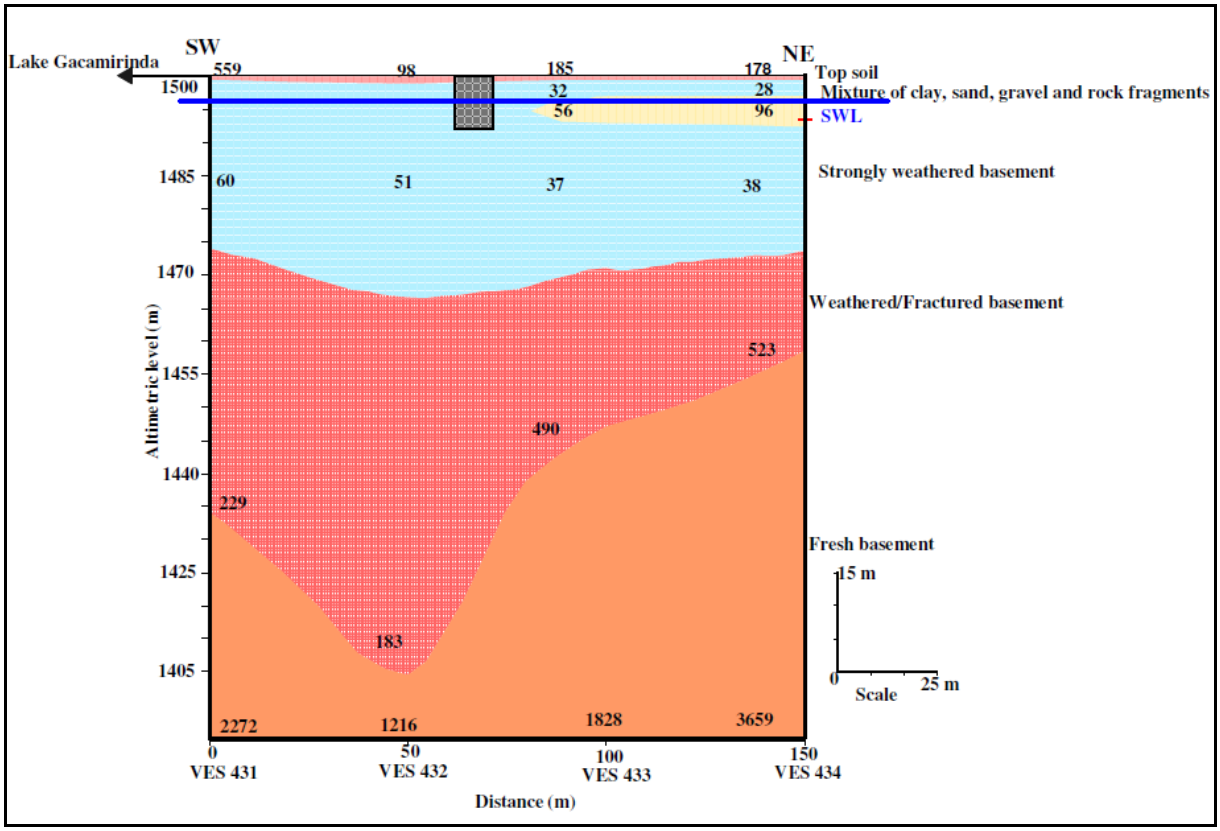

Figure IV.34. Geoelectrical cross-section of the site Gahwijo in the village of Nyabikenke where the well is situated. Numbers in the figure represent the resistivity values (Ωm)

The pumping test at Gahwijo II-Nyabikenke was conducted on 27/09/2008 from 9h40 to 12h55 at a constant discharge rate of 31 m^3/d. The pumping test was stopped when the water level reached the depth of 7.68 m below the ground surface. The recovery test was started immediately after the end of the pumping phase and was terminated the following day (28/09/2008) at 12h00, which corresponds to a total of 23h05 for the whole duration of the recovery test. The recovery test was stopped when the groundwater level had risen up to 4.51 m below the ground surface, which represents a recovery of 94 % of the initial water level. Steady-state conditions having not been reached during the pumping phase, a conservative estimate of the hydraulic parameters is derived from the recovery measurements.

Figure IV.35 shows the time-drawdown data curve of the recovery test which matches well the double porosity model with a transmissivity of 2.2 m^2/d. This value is comparable to the value of transmissivity found for the well in Kinyamateke which is also situated in the Undifferentiated Complex Formation.

Location: Bugesera (Burundi)	Pumping Test: Large diameter well Gahwijol I	Pumping Well: PW
Test Conducted by: Charles		Test Date: 29/09/2008
Analysis Performed by: Charles	Double Porosity	Analysis Date: 17/02/2009
Aquifer Thickness: 4.10 m	Discharge Rate: 1.301014943 [m³/h]	

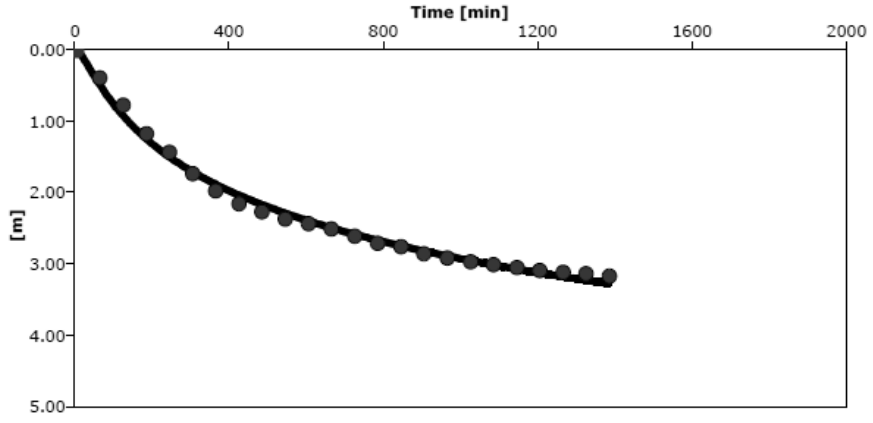

Calculation after Double Porosity

Observation Well	Transmissivity [m²/d]	Hydraulic Conductivity [m/d]	Specific storage	Sigma	Lambda	Radial Distance to PW [m]
PW	2.23×10^{0}	5.44×10^{-1}	5.00×10^{-1}	1.09×10^{0}	1.00×10^{1}	0.5

Figure IV.35. Results of the double porosity analytical method for the recovery test conducted in Gahwijo II-Nyabikenke. Drawdown measurements are done in the pumping well.

IV.7.1.2.3. The well in Gasagara II-Rubuga (pumping test Nr. 5)

This well is situated in the locality of Gasagara, in the village of Rubuga, at approximately 15 km North-West of Ruhehe, the chief centre of the municipality of Bugabira. The well was constructed in 1993 and is still operating. It is located within the metasedimentary Formation of Murehe (Mugendo), but the locality of Gasagara indicates the presence of pegmatitic intrusions which are evidenced by abundant spangles of micas scattered on the ground surface. The well has a depth of 6.5 m and an internal diameter of 1 m.

Figure IV.36 shows a geoelectrical cross-section inferred from a transect of vertical electrical soundings executed at Gasagara by AIDR (1984). The figure clearly shows that the well is completed in the upper layer of the weathering profile, which is composed of a clay-rich mixture of weathering materials. The groundwater table is found at a depth of 2.05 m below the ground surface.

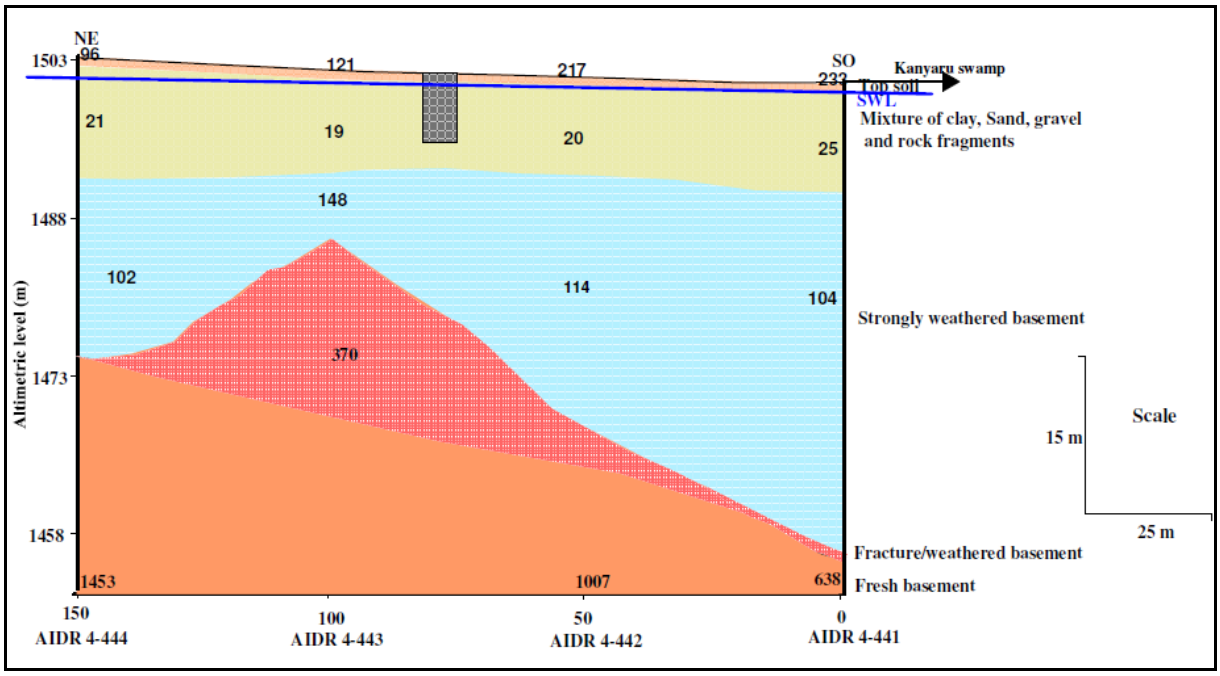

Figure IV.36. Geoelectrical cross-section of the site Gasagara in the village of Rubuga where the well is situated. Numbers in the figure represent the resistivity values (Ωm).

The pumping test was performed on 18/09/2008, from 10h30 to 14h13, at a constant discharge rate of 39 m^3/d. The pumping phase was ended when the groundwater level reached a depth of 5.70 m without attaining steady-state conditions. The recovery test was conducted until the following day (19/09/2008) at 12h00, which totalizes a duration of 21h47 for the recovery test. At the end of the recovery test, the water level had risen again up to a depth of 2.62 m below the ground surface, which represents a recovery of 87 % of the initial static water level. The hydraulic parameters were derived from recovery data.

Figure IV.37 shows the time-drawdown curve from the recovery data, which perfectly fit to the double porosity model, with a value of transmissivity of 2.6 m^2/d and a hydraulic conductivity of 0.6 m/d. The low values of hydraulic parameters, which reflect the clayey nature of the alterites in which the well is completed, are in agreement with the low productivity of this well.

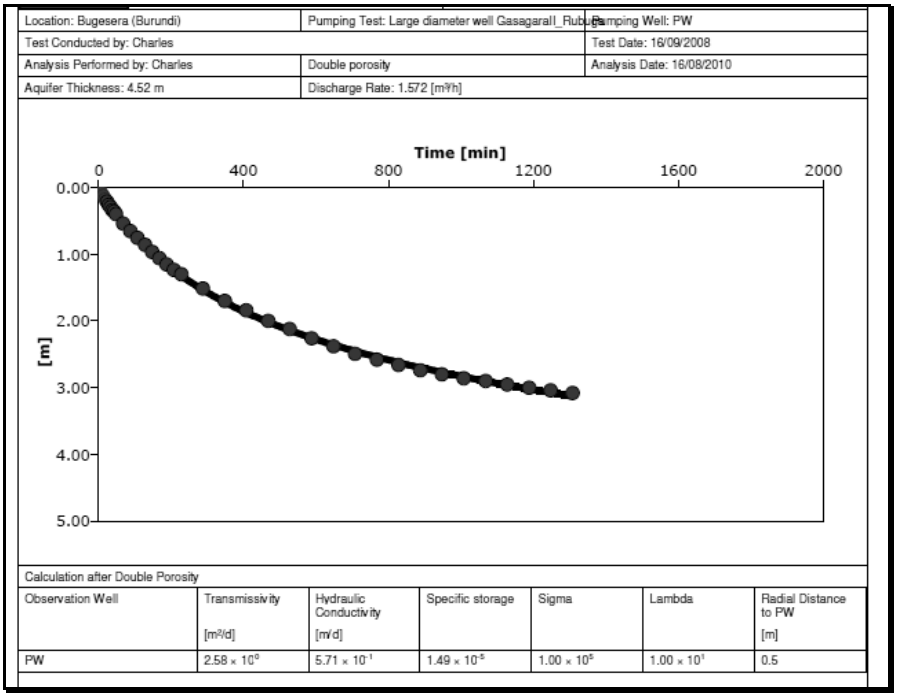

Figure IV.37. Results of the double porosity analytical method for the recovery test conducted in Gasagara II-Rubuga. Drawdown measurements are done in the pumping well

IV.7.1.2.4. The well in Ruseno-Kanyagu (pumping test Nr. 15)

This well is located in the locality of Ruseno, in the village of Kanyagu, at approximately 10 km to the North-East of the chief centre of the municipality of Ntega. The well was constructed in 1989 and was rehabilitated in 2002 within the framework of a project of the Norwegean Refugee Council and UNICEF aimed at coping with the water demand of villagers returning from exile, towards the end of the civil war. It is located within the Undifferentiated Complex Formation. The well has a total depth of 7.61 m and an internal diameter of 1 m. The static water level lies at a depth of 4.01 m below the ground surface.

As for most of old wells in the study area, there are no archives of the lithological stratigraphy for this well. Moreover, there are no recent wells constructed in this area, even no geophysical information from which a tentative structure of the subsurface in the area can be inferred. However, this site being situated in the Undifferentiated Complex Formation, it is very likely that the subsurface structure of this site is similar to the general hydrogeological model, defined by combining available geophysical and lithological information.

The well was tested on 13/10/2008, from 11h30 to 15h30, at a constant discharge rate of 30 m^3/d. During the pumping phase, the groundwater level continued to decline and eventually, the pumping phase was stopped when the groundwater level reached the

depth of 6.76 m without attaining steady-state conditions. The recovery phase was monitored until the following day (14/10/2008) at 8h00, which corresponds to a recovery duration of 16h30. The recovery phase was stopped when the water level reached a depth of 4.06 m below the ground surface, which represents a recovery of 98 %. The hydraulic parameters are derived from the recovery data only.

Figures IV.38 to IV.40 show the analysis of the recovery data using double porosity, Theis, and Papadopulos & Cooper analytical models. It can be seen that the double porosity model (Figure IV.38) offers the best fit with a transmissivity and a hydraulic conductivity value of respectively 2.4 m^2/d and 0.7 m/d. Despite the fact that the recovery data curve does not match perfectly the analytical models of Papadopulos & Cooper (Figure IV.39) and Theis (IV.40), the values of hydraulic parameters obtained from the two models are not significantly different from those obtained with the double porosity analytical solution (Table IV.11 & IV.12).

Location: Bugesera (Burundi)	Pumping Test: Large diameter well Ruseno_Kanyagu	Pumping Well: PW
Test Conducted by: Charles		Test Date: 14/10/2008
Analysis Performed by: Charles	Double Porosity	Analysis Date: 17/02/2009
Aquifer Thickness: 3.60 m	Discharge Rate: 1.238713751 [m³/h]	

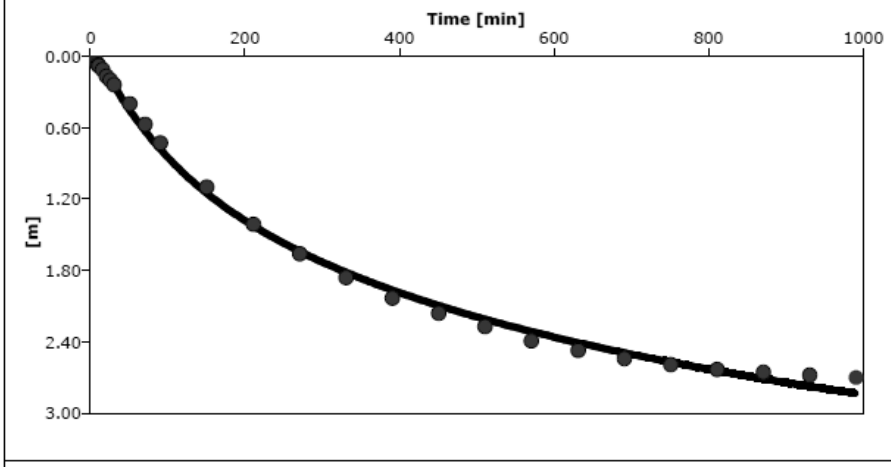

Calculation after Double Porosity

Observation Well	Transmissivity [m²/d]	Hydraulic Conductivity [m/d]	Specific storage	Sigma	Lambda	Radial Distance to PW [m]
PW	2.40×10^{0}	6.66×10^{-1}	4.03×10^{-1}	1.15×10^{0}	8.20×10^{0}	0.5

Figure IV.38. Results of the double porosity analytical method for the recovery test conducted in Ruseno-Kanyagu. Water level measurements are done in the pumping well.

Location: Bugesera (Burundi)	Pumping Test: Large diameter well Ruseno_Kanyagu	Pumping Well: PW
Test Conducted by: Charles		Test Date: 14/10/2008
Analysis Performed by: Charles	Papadopulos & Cooper	Analysis Date: 17/02/2009
Aquifer Thickness: 3.60 m	Discharge Rate: 1.238713751 [m³/h]	

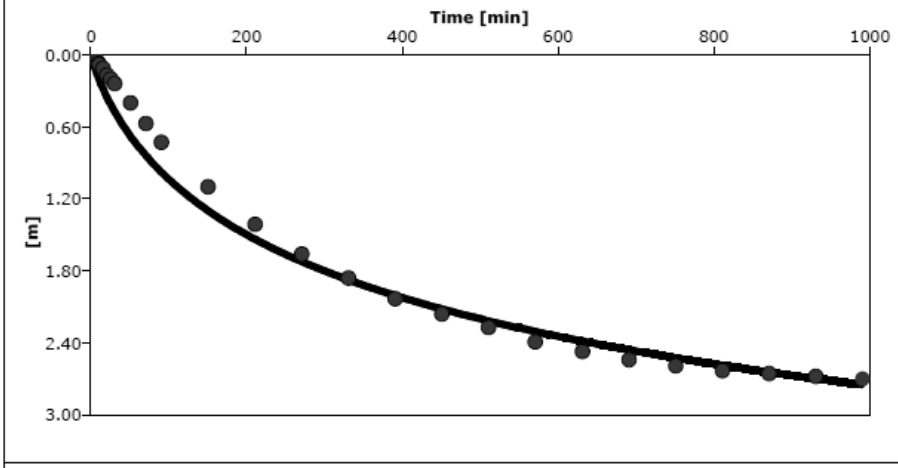

Calculation after Papadopulos & Cooper

Observation Well	Transmissivity [m²/d]	Hydraulic Conductivity [m/d]	Storage coefficient	Radial Distance to PW [m]	
PW	3.06×10^{0}	8.50×10^{-1}	5.00×10^{-1}	0.5	

Figure IV.39. Results of the Papadopulos & Cooper analytical method for the recovery test conducted in Ruseno-Kanyagu. Water level measurements are done in the pumping well.

Location: Bugesera (Burundi)	Pumping Test: Large diameter well Ruseno_Kanyagu	Pumping Well: PW
Test Conducted by: Charles		Test Date: 14/10/2008
Analysis Performed by: Charles	Theis	Analysis Date: 17/02/2009
Aquifer Thickness: 3.60 m	Discharge Rate: 1.238713751 [m³/h]	

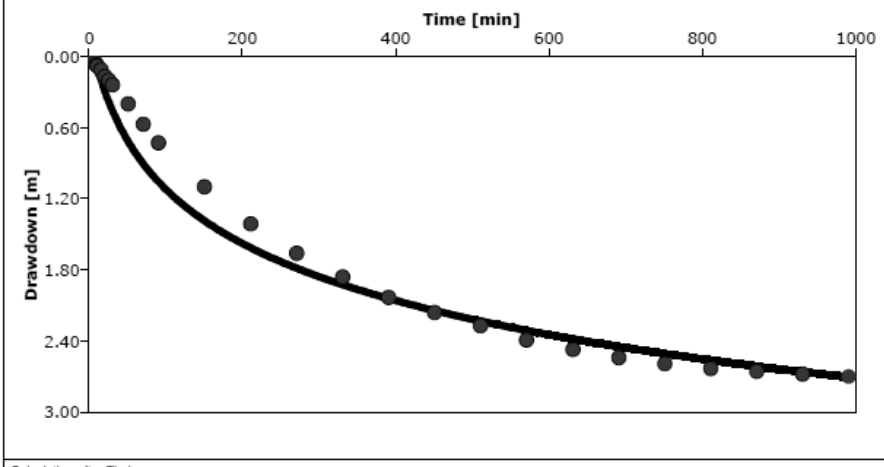

Calculation after Theis

Observation Well	Transmissivity [m²/d]	Hydraulic Conductivity [m/d]	Storage coefficient	Radial Distance to PW [m]	
PW	3.24×10^{0}	8.98×10^{-1}	5.00×10^{-1}	0.5	

Figure IV.40. Results of the Theis analytical method for the recovery test conducted in Ruseno-Kanyagu. Water level measurements are done in the pumping well.

IV.7.1.2.5. Results and discussion

Tables IV.11 and IV.12 show the values of hydraulic parameters estimated from recovery data for wells in which half successful pumping tests were performed. It should be stressed that most of these wells (13) are located in the western part of the study area and mainly in the metasedimentary Formation of Murehe (Mugendo) (6 wells). The metasediments belonging to the Mugendo Formation are reportedly intruded with granites and pegmatites (Carte géologique du Burundi, feuille Busoni). The transmissivity varies between 1 m^2/d (Gifuruguti-Nyakarama) and 29.6 m^2/d (Rugoma-Kagege) with an average of 5.9 m^2/d. The hydraulic conductivity is the range 0.2-34.1 m/d, with an average of 3.5 m/d. Moreover, most of the wells (10) in this group conform to double porosity analytical solution and of the 10 wells, 8 are located in the western study area.

This western part of the study area adjoins the South-North course of the River Kanyaru which separates the Bugesera depression from the elevated Butare plateau in Rwanda. According to Moeyersons (1977), the North-South course of the River Kanyaru coincides with a major North-South trending fault, which separates the uplifted Butare plateau and the depression of Bugesera, which underwent a downwarping. Although this fault is not represented on the geological map, Moeyersons notes that the clear geomorphological contrast between the dome-shaped Butare plateau and the low-lying Bugesera depression points to the existence of this fault (Chapter II). Thus, the quite generalized best fit of the drawdown response to the double porosity model may be speculatively ascribed to the existence of radial faults and consequent fracturing associated with this major fault.

However, it appears paradoxical that, despite the possible tectonic fracturing accompanying the faults, the area is almost systematically characterized by low values of hydraulic parameters. Hence, besides the clayey materials deriving from weathering which may clog the tectonic fractures, hydrothermal processes (weathering and formation of hydrothermal minerals) induced by magmatic intrusions are likely to have tempered the effect of tectonic fracturing. This deduction is consistent with the findings of previous researchers (Jalludin & Razack, 2004; Singhal, 1997), who observed that the same geological unit may undergo locally different hydrothermal effects which increase the heterogeneity of aquifers, resulting in a wide variation of values of transmissivity within the same geological formation.

On the other hand, values of storativity are systematically and aberrantly high and are not therefore reliable. They may certainly reflect the storage in the pumping well as there are not any drawdown data from observation wells which could help compute accurate values of storativity.

Table IV.11. Comparison of transmissivity values (m^2/d) calculated using different analytical methods from recovery test data of half-successful pumping tests collected during the field work in 2007 and 2008.

W/N	Well location	Hantush	Theis	Papadopulos & Cooper	Cooper & Jacob	Double porosity	Best fit method
3	FokoII-Kiyonza	-	-	-	-	2.2	Double porosity
4	Gahwijo II-Nyabikenke	-	-	-	-	2.2	Double porosity
5	Gasagara II-Rubuga	-	-	-	-	2.6	Double porosity
6	Gifuruguti-Nyakarama	-	-	-	-	1	Double porosity
10	Kadobori II-Rubuga	-	-	-	-	1.9	Double porosity
11	Kamwayi II-Nyamabuye	-	-	-	-	6.6	Double porosity
14	Kantuye-Ceru	-	-	-	-	9.6	Double porosity
15	Kanyagu-Ruseno	-	3.24	3.1	-	2.4	Double porosity
20	Kigozi-Yaranda	-	-	-	-	6.1	Double porosity
21	Kinyamateke	3.9	-	27	-	-	Hantush
26	Mugombwa-Kiri	7.2	-	40.1	-	-	Hantush
31	Murehe-Murungurira	6	-	-	-	-	Hantush
34	Ntembe II-Kiri	4.8	-	8.4	5.2	-	Hantush
38	Rugoma-Kagege	29.6	-	-	-	-	Hantush
40	Rwasama-Kiri	-	-	-	-	2.2	Double porosity

Table IV.12. Comparison of hydraulic conductivity values (m/d) calculated using different analytical methods from recovery test data of half-successful pumping tests collected during the field work in 2007 and 2008.

W/N	Well location	Hantush	Theis	Papadopulos & Cooper	Cooper & Jacob	Double porosity	Best fit method
3	FokoII-Kiyonza	-	-	-	-	0.3	Double porosity
4	GahwijoII-Nyabikenke	-	-	-	-	0.5	Double porosity
5	Gasagara II-Rubuga	-	-	-	-	0.6	Double porosity
6	Gifuruguti-Nyakarama	-	-	-	-	1.7	Double porosity
10	Kadobori II-Rubuga					0.2	Double porosity
11	Kamwayi II-Nyamabuye	-	-	-	-	1.4	Double porosity
14	Kantuye-Ceru	-	-	-	-	0.5	Double porosity
15	Kanyagu-Ruseno	-	0.9	0.9	-	0.7	Double porosity
20	Kigozi-Yaranda	-	-	-	-	2.5	Double porosity
21	Kinyamateke	1.5	-	10.3	-	-	Hantush
26	Mugombwa-Kiri	2.4	-	13.2	-	-	Hantush
31	Murehe-Murungurira	2	-	-	-	-	Hantush
34	Ntembe II-Kiri	1.1	-	1.9	1.2	-	Hantush
38	Rugoma-Kagege	34.1	-	-	-	-	Hantush
40	Rwasama-Kiri	-	-	-	-	2.3	Double porosity

Tables IV.13 and IV.14 show the classification of the hydraulic parameters using the classification scheme proposed by Krasny (1993). Except the values of transmissivity and hydraulic conductivity calculated for the well situated in Rugoma-Kagege, which falls in the intermediate transmissivity class, all other values belong to the low transmissivity class. At first glance the transmissivity calculated for this well is comparable to the maximum found for successful pumping tests in this formation (Table IV.9). However, being situated within the Formation of Murehe (Mugendo) which is, overall, characterised by low values of hydraulic parameters (average T = 2.5 m^2/day, average K = 1.2 m/d), it is probable that the values of transmissivity and hydraulic conductivity estimated from recovery data are overestimated.

Table IV.13. Classification of values of transmissivity calculated from half-successful pumping test data according to the classification scheme proposed by Krasny (1993)

W/N	**Low transmissivity class (1-10 m^2/d)**			**W/N**	**Intermediate transmissivity class (10-100 m^2/d)**		
	Well Location	**Formation**	**T (m^2/d)**		**Well location**	**Formation**	**T (m^2/d)**
3	FokoII-Kiyonza	U.C.	2.2	38	Rugoma-Kagege	Murehe	29.6
4	GahwijoII-Nyabikenke	U.C.	2.2				
5	GasagaraII-Rubuga	Murehe	2.6				
6	Gifuruguti-Nyakarama	Murehe	1				
10	Kadobori II-Rubuga	Murehe	1.9				
11	Kamwayi II-Nyamabuye	U.C.	6.6				
14	Kantuye- Ceru	U.C.	9.6				
15	Kanyagu-Ruseno	U.C.	2.4				
20	Kigozi-Yaranda	U.C.	6.1				
21	Kinyamateke	U.C.	3.9				
26	Mugombwa-Kiri	Murehe	7.2				
31	Murehe-Murungurira	U.C.	6				
34	Ntembe II-Kiri	Murehe	4.8				
40	Rwasama-Kiri	Murehe	2.2				
	Maximum		**9.6**				
	Minimum		**1**				
	Average		**4.7**				
	Standard deviation		**2.4**				
	Coefficient of variation (%)		**50.8**				

U.C.: Undifferentiated Complex

Table IV.14. Classification of values of hydraulic conductivity calculated from half-successful pumping test data according to the classification scheme proposed by Krasny (1993)

W/N	Low transmissivity class (1-10 m2/d)			W/N	Intermediate transmissivity class (10-100 m2/d)		
	Well location	Formation	K (m/d)		Well location	Formation	K (m/d)
3	Foko II-Kiyonza	U.C.	0.3	38	Rugoma-Kagege	Murehe	34.1
4	Gahwijo II-Nyabikenke	U.C.	0.5				
5	Gasagara II-Rubuga	Murehe	0.6				
6	Gifuruguti-Nyakarama	Murehe	0.2				
10	Kadobori II-Rubuga	Murehe	0.2				
11	Kamwayi II-Nyamabuye	U.C.	0.1				
14	Kantuye- Ceru	U.C.	5.2				
15	Kanyagu-Ruseno	U.C.	0.7				
20	Kigozi-Yaranda	U.C.	0.3				
21	Kinyamateke-Nyabikenke	U.C.	0.2				
26	Mugombwa-Kiri	Murehe	2.4				
31	Murehe-Murungurira	U.C.	2				
34	Ntembe II-Kiri	Murehe	1.1				
40	Rwasama-Kiri	Murehe	0.2				
	Maximum		**5.2**				
	Minimum		**0.2**				
	Average		**1.3**				
	Standard deviation		**1.2**				
	Coefficient of variation (%)		**87.6**				

U.C.: Undifferentiated Complex

Tables IV.15 and IV.16 show statistics of the distribution of hydraulic parameters in the 2 geological formations where half-successful pumping tests were carried out. The values of transmissivity and hydraulic conductivity calculated for the well in Rugoma-Kagege were excluded because they appear to be exaggerated. These parameters confirm the high groundwater potential of the Undifferentiated Complex Formation. Indeed, similarly to the statistical parameters estimated for the successful pumping tests, the Undifferentiated Complex Formation is characterized by the highest values of hydraulic parameters.

Table IV.15. Variation of the transmissivity (m^2/d), obtained from half-successful pumping tests, for the different geological formations

Geological formation	Number of wells	Maximum (m^2/d)	Minimum (m^2/d)	Average (m^2/d)	Standard deviation (m^2/d)	Coefficient of variation %
Undifferentiated Complex	9	9.6	2.2	4.6	2.6	57.4
Murehe (or Mugendo)	6	4.8	1	2.5	1.4	55.5

Table IV.16. Variation of the hydraulic conductivity (m/d), obtained from half-successful pumping tests, for the different geological formations

Geological formation	Number of wells	Maximum (m/d)	Minimum (m/d)	Average (m/d)	Standard deviation (m/d)	Coefficient of variation (%)
Undifferentiated Complex	9	2.5	0.3	1.1	0.8	71.2
Murehe (or Mugendo)	6	2.3	0.2	1.2	0.8	55.8

IV.7.1.3. Unsuccessful pumping tests

These are pumping tests where the pumping phase was stopped before reaching (pseudo-) steady-state conditions and where, due to low hydraulic parameters, only a small recovery of the initial static water level was obtained despite a long duration of the recovery phase. For these pumping tests, although a rough estimation of the specific capacity can be obtained, the transmissivity and hydraulic conductivity can not be derived.

IV.7.1.3.1. The well at Karago-Rukuramigabo (pumping test Nr. 16)

This is an abandoned well located at nearly 10 km to the North of the city of Kirundo. The well was constructed in 1991 but was vandalized during the civil war. It was rehabilitated in 1998 but subsequently underwent another act of vandalism whereby the foot-operated pump was stolen. Like many hand-dug wells constructed in 1980's and 1990's, there is no lithological description of the well stratigraphy. Figure IV.41 shows a geoelectrical cross-section of the site of Karago, in the village Rukuramigabo where this well is situated. The figure shows that the well was completed in the upper part of the weathering profile, the more clayey part, and this would explain the low productivity of the well. Indeed, local villagers met during the pumping test confirmed that, even before the well was destroyed, it was operating intermittently. The well has a depth of 12 m and the static water level lies at a depth of 3.39 m within the top soil.

The well was tested on 02/08/2008, from 11h45 to 18h25, at discharge rate of 43.7 m^3/day, while the recovery was monitored until the following day (03/08/2008) at 14h00. During the pumping test, which lasted for 6h40, the water level kept on declining up to the depth of 10.01 m. The recovery test was conducted immediately after the pumping phase, and after 17h35 m, the water level was still at a depth of 9.15 m, which represents a recovery of 19.1 %. Figure IV.10 depicts the poor recovery of this well, which reflects its poor productivity.

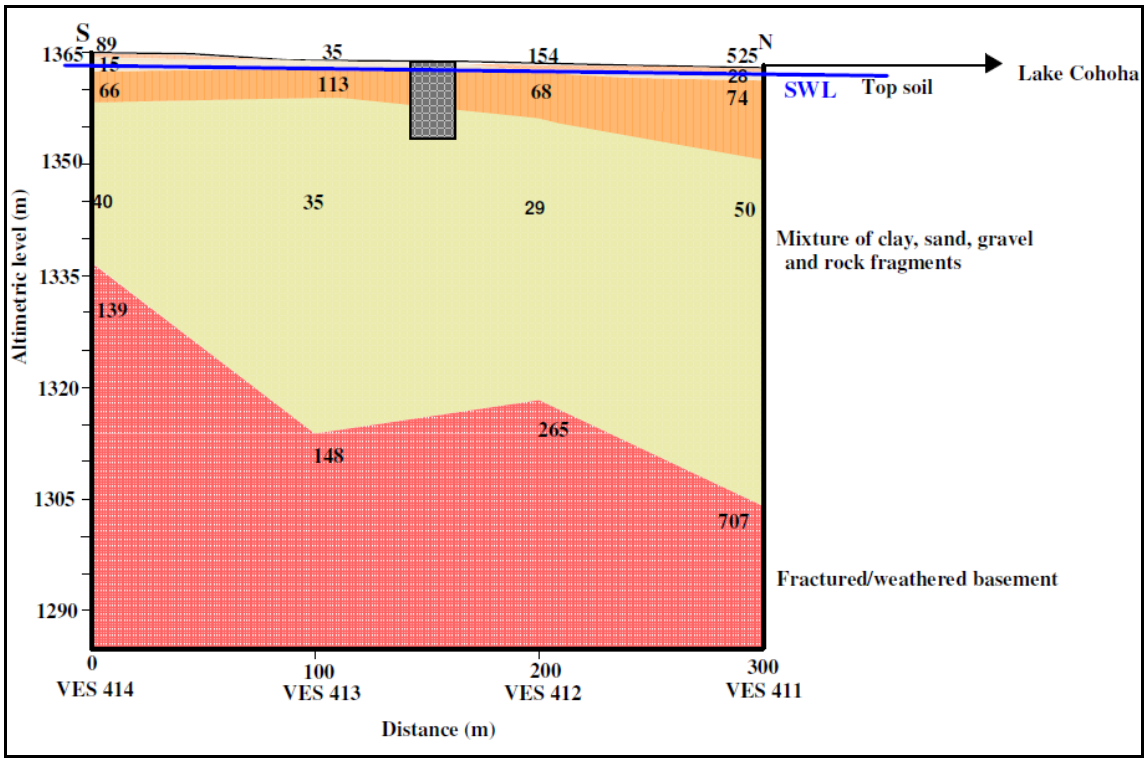

Figure IV.41. Geoelectrical cross-section of the site of Karago in the village of Rukuramigabo, where the well is situated. Numbers in the figure are resistivity values (Ωm).

IV.7.1.3.2. The well at Mukuyo-Kiri (pumping test Nr. 29)

The well is situated in the locality of Mukuyo, in the village of Kiri, at approximately 20 km to the North-West of the chief centre of the municipality of Bugabira. The well was constructed in 1988 but was vandalised during the civil war. It was subsequently abandoned because the pump and its accessories were stolen. Figure IV.42 shows a geoelectrical cross section of the neighbouring site of Mamfu-Kiyonza, where a geoelectrical transect was performed in 1984 by AIDR (AIDR 6-461 to 464). The two sites (Mamfu-Kiyonza and Mukuyo-Kiri) being very close and in the same the geological formation, their subsurface structure is very likely to be the same. The geoelectrical cross-section shows the typical weathering profile in the study area with an upwards decreasing of the grain-size of the weathered overburden (Figure IV.42).

With a total depth of 7.16 m and an internal radius of 1 m, the well taps a small part of the aquifer which is formed by the strongly weathered part of the basement. Indeed, Figure IV.42 shows that the bottom of the well reaches only the upper part of the aquifer, the most important part of the well being completed in the clay-rich upper part of the weathering profile. This would explain the low yield of this well and the intermittent failure. The static water level rests in the upper part of the weathering profile, at 2.17 m below the ground surface.

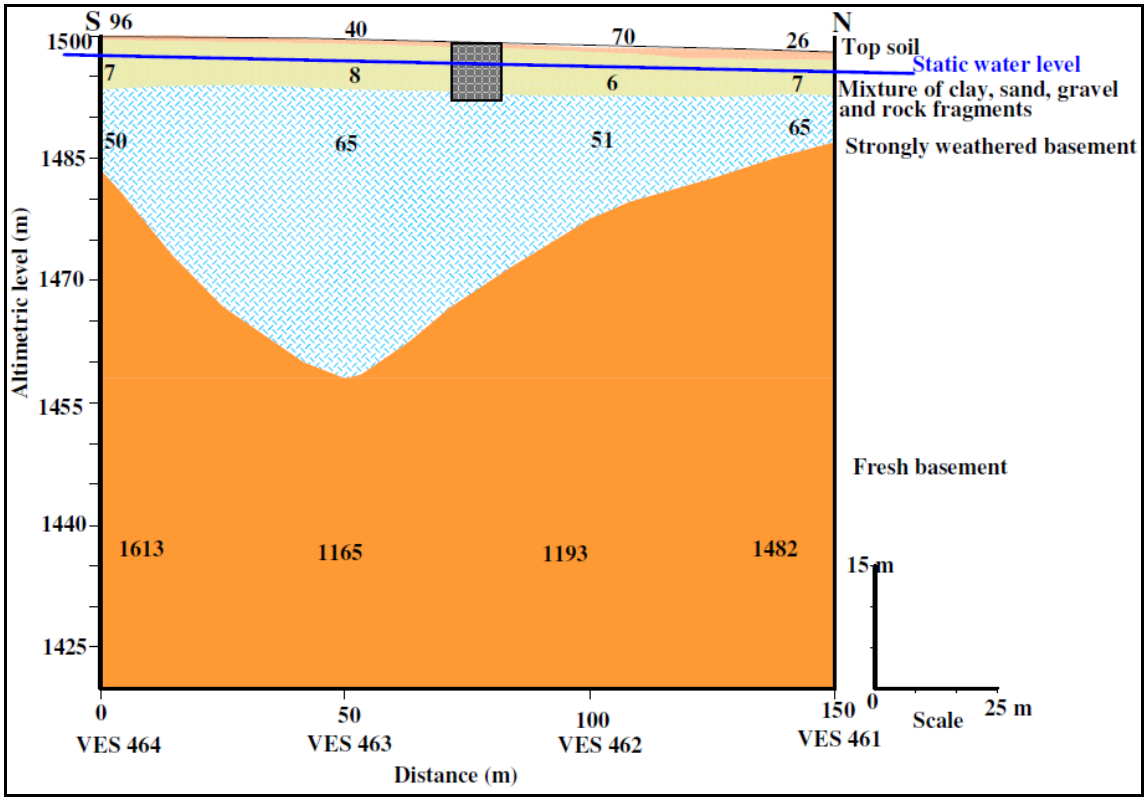

Figure IV.42. Geoelectrical cross-section of the site of Mamfu-Kiyonza which is very close to the site of Mukuyo-Kiri. Numbers on the figure are resistivity (Ωm)

The well was tested on 16/09/2008, from 13h00 to 18h00, at a discharge rate of 34 m^3/d. The recovery was monitored until the following day at 12h00, which represents a duration of 18h for the whole recovery test. During the pumping test, the water level continues to drop, down to a depth of 4.79 m. The recovery was conducted immediately after the shutoff of the pump but, after 18h00, the water level was still at a depth of 4.55 m which represents a recovery of only 9 % of the initial water level. Figure IV.43 depicts the poor recovery of the well which seems to be in agreement with its low productivity.

For such pumping tests, the transmissivity and hydraulic conductivity could not be determined.

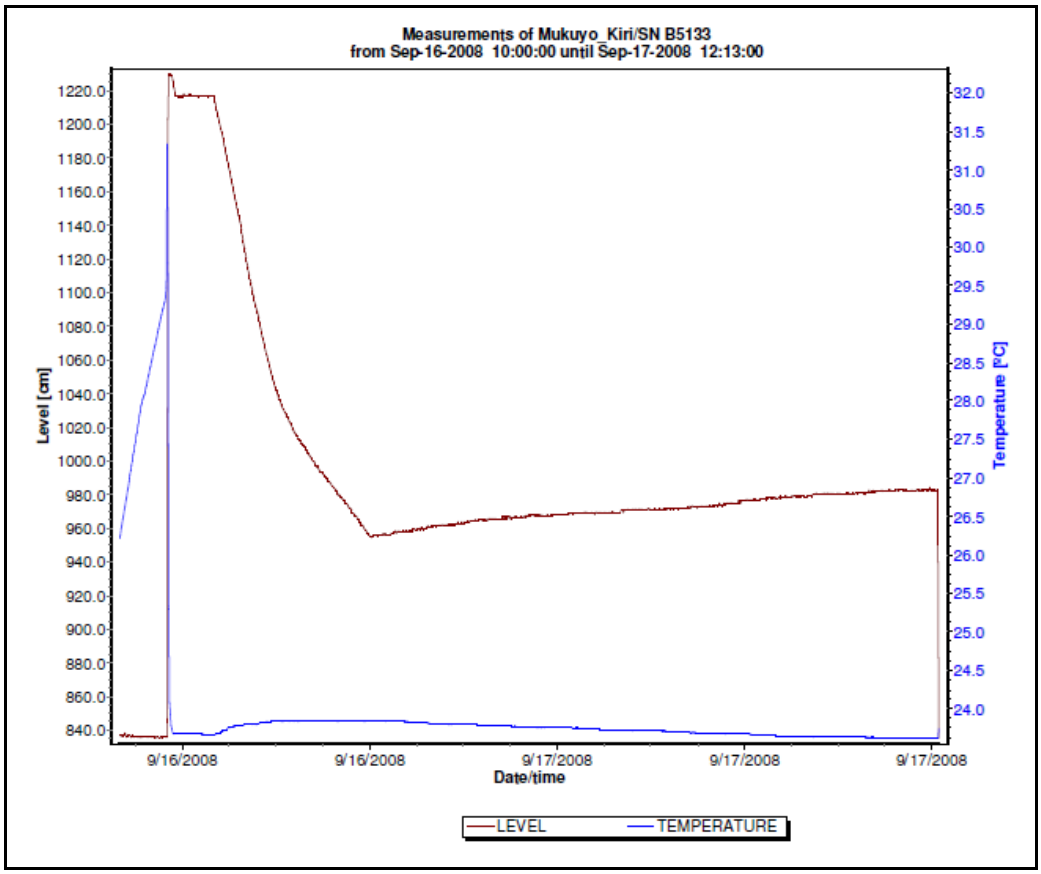

Figure IV.43. Graph of water level versus time from the electronic datalogger showing a representative unsuccessful pumping test, with a poor recovery at Mukuyo-Kiri

IV.7.1.4. Synthesis of results of analytical methods as a function of geology

Table IV.17 portrays a comparison of the different geological formations underlying the study area based on the hydraulic parameters (hydraulic conductivity and transmissivity) derived from fully successful and half successful pumping tests. Figure IV.44 shows the spatial distribution of the values of transmissivity across the different geological formations. A cross-analysis of Table VI.17 and Figure IV.44 shows that the Undifferentiated Complex is characterised by the highest values of hydraulic parameters (hydraulic conductivity and transmissivity), which imply a high groundwater potential for this formation. On the other hand, Table IV.17 and Figure IV.44 also show a wide variation of hydraulic conductivity (166-0.1 m/d) and transmissivity (377-2.2 m^2/d), as this is confirmed by extremely high coefficients of variation: 202.6 % for transmissivity and 211 % for hydraulic conductivity.

The lowest values of hydraulic conductivity (0.2-34.1 m/d) and transmissivity (1-29.6 m^2/d) are found within the Formation of Murehe/Mugendo, with average values of 5.4 m/d and 9.8 m^2/d respectively. The relatively high values of hydraulic conductivity (34.1 m/d) and transmissivity (29.6 m^2/d) found for the well located in Rugoma-Kagege

seem to be overestimated in comparison to the average values for this formation, which are respectively 5.4 m/d and 9.8 m^2/d.

With values of hydraulic conductivity and transmissivity varying repectively between 1.6-40.7 m/d and 5.7-60.3 m^2/d, the Formation of Nyagisozi/Nyabihanga shows intermdiate hydraulic parameters compared to the Formation of Mugendo and the Undifferentiated complex. On average the hydraulic parameters of the Formation of Nyagisozi/Nyabihanga (average T = 42.1 m^2/d and average K = 19 m/d) are closely comparable to those of the Undifferentiated Complex (average T = 43.8 m^2/d and average T = 19 m/d). However, this comparison has to be taken with caution because the average values of hydraulic parameters for the Undifferentiated Complex are based on a ratively large number of pumping tests (22), whereas only 5 pumping tests were performed within the Formation of Nyagisozi/Nyabihanga.

Moreover, similarly to the Undifferentiated Complex, the Formations of Nyagisozi/Nyabihanga and Murehe/Mugendo reveal also a wide variation of hydraulic parameters, as this is reflected by very high coefficients of variation (Table IV.17). Overall, when coupled to Figure IV.44, these high coefficients of variation rather denote a random variation of hydraulic parameters across the study area, which explains this random distribution, even over short distances, of areas with highly productive wells and those with a rather poor yield.

Table IV.17. Comparison of different geological formations based on transmissivity and hydraulic conductivity deduced from fully successful and half-successful pumping tests

Formation	Number of tests	Parameter	Maximum	Minimum	Average	Standard deviation	Coefficient of variation (%)
Undifferentiated Complex	**22**	**T(m^2/d)**	377	2.2	43.8	88.7	202.6
		K(m/d)	166	0.1	19	40	211
Mugendo/Murehe	**12**	**T(m^2/d)**	29.6	1	9.8	10.2	104.3
		K(m/d)	34.1	0.2	5.4	9.7	180.8
Nyagisozi/Nyabihanga	**5**	**T(m^2/d)**	60.3	5.7	42.1	21.4	50.7
		K(m/d)	40.7	1.6	19	16	84.2
All pumping tests	**39**	**T(m^2/d)**	377	1	33.1	68.4	206.5
		K(m/d)	166	0.1	14.8	31.4	211.9

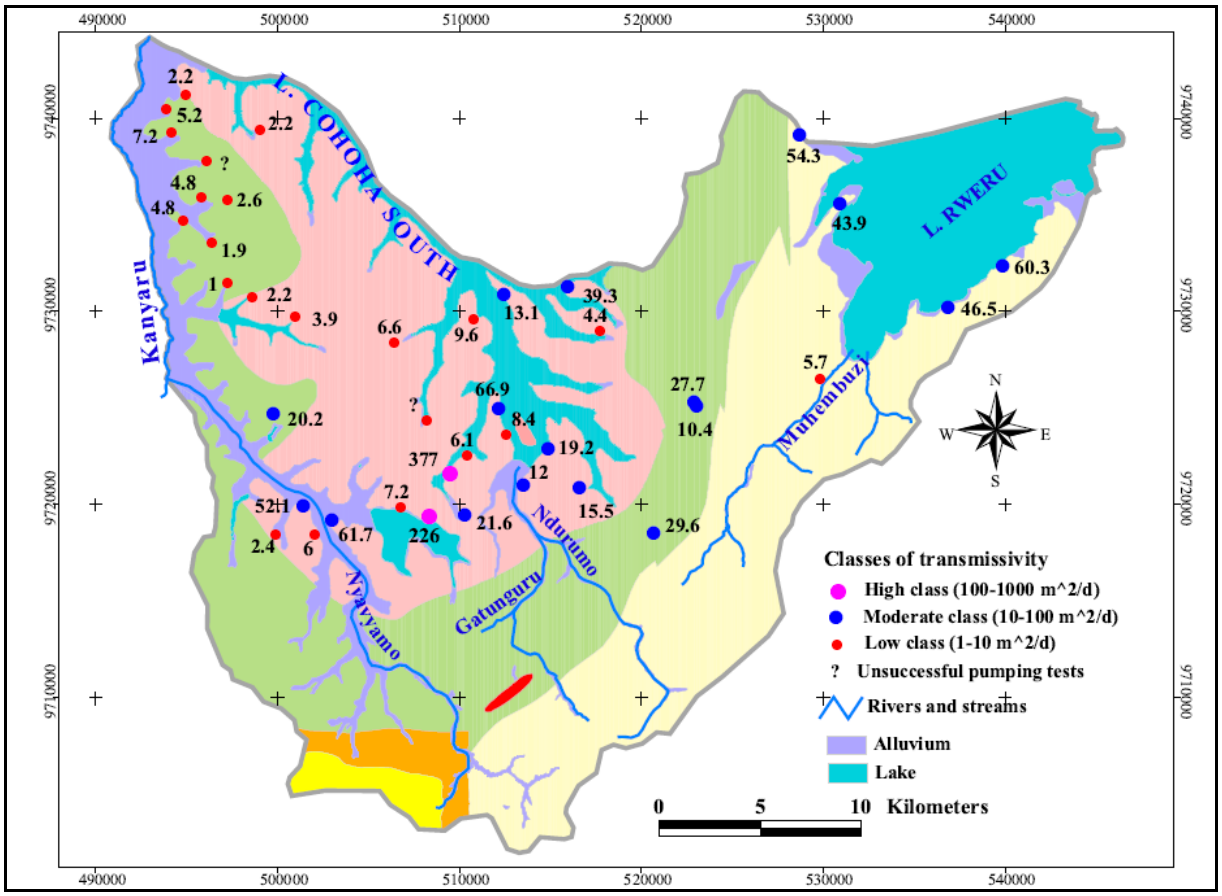

Figure IV.44. Distribution of transmissivity values derived from the best fitting method.

IV.7.2. Specific capacity method

In this study, specific capacity values are calculated for the 41 pumping tests conducted in the study area. In the following discussion, the 41 pumping tests performed are grouped into the categories already presented in the prevous section, i.e. (1) successful pumping tests, (2) half-successful and non-successful pumping tests. Half-successful and non-successful pumping tests are treated together because in both cases, as steady state conditions were not reached, the maximum drawdown reached is used so as to calculate a conservative estimate of the specific capacity.

IV.7.2.1. Successful pumping tests

Table IV.17 shows values of specific capacity calculated for the first category of aquifers in which (pseudo-) steady state conditions were reached during the pumping test. The specific capacity varies between a minimum of 17.4 m^2/d (well in Ngaragu-Kiri) and a maximum of 1133.6 m^2/d (well in Muhero II-Yaranda) with an average value of 179.6 m^2/d and a standard deviation of 254.7 m^2/d.

Considering the classification of transmissivity and specific capacity magnitude as defined by Krasny (1993), the specific capacity values calculated for successful

pumping tests fall within 3 classes, namely intermediate (8.64 to 86.4 m^2/d), high (86.4 to 864 m^2/d) and very high (> 864 m^2/d) (Table IV.17). However, most of the values of the estimated specific capacity fall within the intermediate and high specific capacity classes, while only one value is found within the class of very high specific capacity. The two classes are characterized by very high values of coefficients of variation (Romano *et al.*, 2005), i.e. 47.2 % and 73.2 % respectively, which confirms the heterogeneity of the basement aquifer in Bugesera region. This is even confirmed by the spatial distribution of the specific capacity values, which shows that, even for two neighbouring wells, the values of specific capacity can be dramatically different (Figure IV.42).

Table IV.18. Classification of specific capacity values for wells where (pseudo-) steady-state conditions were reached during the pumping test

W/N	Intermediate (8.64-86.4 m^2/d)			W/N	High (86.4 - 864 m^2/d)			W/N	Very high (> 864 m^2/d)		
	Well	**Fm.**	**S_c (m^2/d)**		**Wells**	**Fm.**	**S_c (m^2/d)**		**Wells**	**Fm.**	**S_c (m^2/d)**
1	Bishunzi-Cewe	U.C.	51.2	2	Cimbogo-Gatete	Nyagisozi	175	27	MuheroII-Yaranda	U.C.	1133.6
7	Kabirizi II-Kigoma	Murehe	68.7	8	Kabonde-Runyonza	U.C.	745				
9	Kadobogoro-Muramba	U.C.	58.9	12	Kanabugiri-Bugera	U.C.	308				
13	Kanigo-Cinuma	Murehe	20	17	Kigina-Gisenyi I	Murehe	104				
18	Kigina-Gisenyi II	Murehe	47.2	23	Kiruhura I - Kiyanza	U.C.	229				
19	Kigoma-Gatare	Nyagisozi	23.7	24	Mago-Gatete	Nyagisozi	189				
22	Kiruhura II - Muramba	U.C.	65.5	35	Ntwago-Murungurira	Murehe	208				
25	Marembo-Marembo	U.C.	17.6	36	Nunga-Yaranda II	U.C.	201				
28	Muhero I-Yaranda	U.C.	70.1	37	Nyange-Kumana	Nyagisozi	222				
30	Murambo-Murambi	U.C.	49.1	39	Ruranzi-Rwibikara	U.C.	91.6				
32	Mutoza Yaranda	U.C.	31.2	41	Senga-Nyagisozi	Nyagisozi	186				
33	Ngaragu-Kiri	Murehe	17.4								
	Maximum		**70.1**				**745**				
	Minimum		**17.4**				**91.6**				
	Average		**43.4**				**242**				
	Standard deviation		**20.5**				**177**				
	Coefficient of variation (%)		**47.2**				**73.2**				

U.C. : Undifferentiated Complex

Table IV.19 shows statistics describing the variation of specific capacity within the three geological formations wherein successful pumping tests were performed. Like for the transmissivity and hydraulic conductivity, the specific capacity confirms the high groundwater potential for the Undifferentiated Complex Formation. Indeed, high values of specific capacity indicate that it is possible to abstract important quantities of

groundwater without too much lowering the groundwater level. This comparison of specific capacity values in different geological formations also confirms that the Formation of Murehe (Mugendo) has the lowest groundwater potential.

Table IV.19. Variation of the specific capacity (m^2/d) deduced from successful pumping tests, for the different geological formations

Geological formation	Number of wells	Maximum (m^2/d)	Minimum (m^2/d)	Average (m^2/d)	Standard deviation (m^2/d)	Coefficient of variation %
Undifferentiated Complex	14	1133.6	17.6	232.7	320.9	137.9
Murehe (or Mugendo)	5	104.1	17.4	51.5	36.2	70.3
Nyagisozi (or Nyabihanga)	5	222.2	23.7	159.1	77.7	48.8

IV.7.2.2. Half-successful and unsuccessful pumping tests

Table IV.20 shows the values of specific capacity for the pumping tests in which the pumping phase was stopped before reaching steady state conditions. The specific capacity varies between a minimum of 6.6 m^2/d and a maximum of 75.5 m^2/d. The maximum value of specific capacity for the site of Rugoma-Kagege, which is located within the Formation of Mugendo, seems to be exaggerated, because, averall, this formation has the lowest hydraulic parameters.

According to the classification of transmissivity and specific capacity magnitude proposed by Krasny (1993), most of the values of specific capacity fall within the intermediate class (8.64-86.4 m^2/d). Only two values of specific capacity fall within the class of low specific capacity (0.864-8.64 m^2/d). Similarly to successful pumping tests, the values of specific capacity derived from half-successful and unsuccessful pumping tests in the intermediate class show also a very high coefficient of variation which can be ascribed to the heterogeneity of the basement aquifer (Figure IV.45).

Table IV.21 presents statistical parameters showing a comparison of the specific capacity calculated within the Undifferentiated Complex and the Formation of Murehe (Mugendo), where half-successful and unsuccessful pumping tests were executed. These statistical parameters confirm the high groundwater potential of the Undifferentiated Complex Formation (Figure IV.45).

Table IV.20. Classification of specific capacity values for wells where (pseudo-) steady-state conditions were not reached during the pumping test.

W/N	Low class (0.864 - 8.64 m^2/d) Well location		S_c (m^2/d)	W/N	Intermediate class (8.64 - 86.4 m^2/d) Wells		S_c (m^2/d)
16	Karago-Rukuramigabo	U.C.	6.6	3	Foko II-Kiri	U.C.	9.2
40	Rwasama-Kiri	Mureh e	7.4	4	Gahwijo II-Nyabikenke	U.C.	9.2
				5	Gasagara II-Rubuga	Mureh e	11
				6	Gifuruguti-Nyakarama	Mureh e	9.2
				10	Kadobori II - Rubuga	Mureh e	12.4
				11	Kamwayi II - Nyamabuye	U.C.	27
				14	Kantuye-Ceru	U.C.	43.8
				15	Kanyagu-Ruseno	U.C.	10.8
				20	Kigozi-Yaranda	U.C.	26.7
				21	Kinyamateke	U.C.	17.9
				26	Mugombwa-Kiri	Mureh e	33.3
				29	Mukuyo-Kiri	Mureh e	13
				31	Murehe-Murungurira	U.C.	18.4
				34	Ntembe II - Kiri	Mureh e	15.2
				38	Rugoma-Kagege	Mureh e	75.5
	Maximum		**-**				**75.5**
	Minimum		**-**				**9.2**
	Average		**7**				**22.2**
	Standard deviation		**-**				**17.9**
	Coefficient of variation (%)		**-**				**80.8**

U.C. : Undifferentiated Complex

Table IV.21. Variation of the specific capacity (m^2/d) deduced from half-successful and unsuccessful pumping tests, for the different geological formations

Geological formation	Number of wells	Maximum (m^2/d)	Minimum (m^2/d)	Average (m^2/d)	Standard deviation (m^2/d)	Coefficient of variation %
Undifferentiated Complex	10	43.8	6.6	18	11.6	64.3
Murehe (or Mugendo)	7	33.3	7.4	16.3	9.1	56

Table IV.22 shows a comparison of the three geological formations covering the study area based on values of specific capacity values calculated from the 41 pumping tests performed withing the framework of this study. Figure IV.45 depicts the spatial

distribution of the specific capacity values across the different geological formations. A cross-inspection of Table IV.22 and Figure IV.45 confirms that the Undifferentiated Complex has the highest specific capacity values, although they vary over a wide range (1133.6-6.6 m^2/d) as this is substantianted by a very high coefficient of variation (180.4 %).

With specific values ranging between 7.4 m^2/d to 104.1 m^2/d and an average value of 33.4 m^2/day, the Formation of Murehe/Mugendo has the lowest values of specific capacity, which confirms that this formation has the lowest hydraulic parameters and consequently the lowest groundwater potential.

The Formation of Nyagisozi, which has intermediate values of specific capacity (23.7-222.2 m^2/d), shows however that the average value of this parameter (159.1 m^2/d) is slightly greater than that of the Undifferentiated Complex. However, it should be recalled that the average value of specific capacity for the Formation of Nyagisozi/nyabihanga is only based on 5 pumping tests, while that of the Undifferentiated Complex is deduced from much more pumping tests (23).

The high coefficients of variation of the specific capacity values (Table IV.22) and the spatial distribution of this parameter across the study area (Figure IV.45), which shows a random distribution of specific capacity values, are in agreement with the random variation of hydraulic parameters as already concluded from the analysis of the spatial distribution and comparison of the hydraulic conductivity across the three geological formations occuring in the studya area.

Table IV.22. Comparison of different geological formations based on specific capacity values deduced from all pumping tests (fully successful, half-successful and unsuccessful pumping tests)

Formation	Number of pumping tests	Maximum (m^2/d)	Minimum (m^2/d)	Average (m^2/d)	Standard deviation (m^2/d)	Coefficient of variation (%)
Undifferentiated Complex	23	1133.6	6.6	149	268.9	180.4
Murehe/Mugendo	13	104.1	7.4	33.4	31.1	93
Nyagisozi/Nyabihanga	5	222.2	23.7	159.1	77.7	48.9
All pumping tests	41	1133.6	6.6	113.6	209.1	184.1

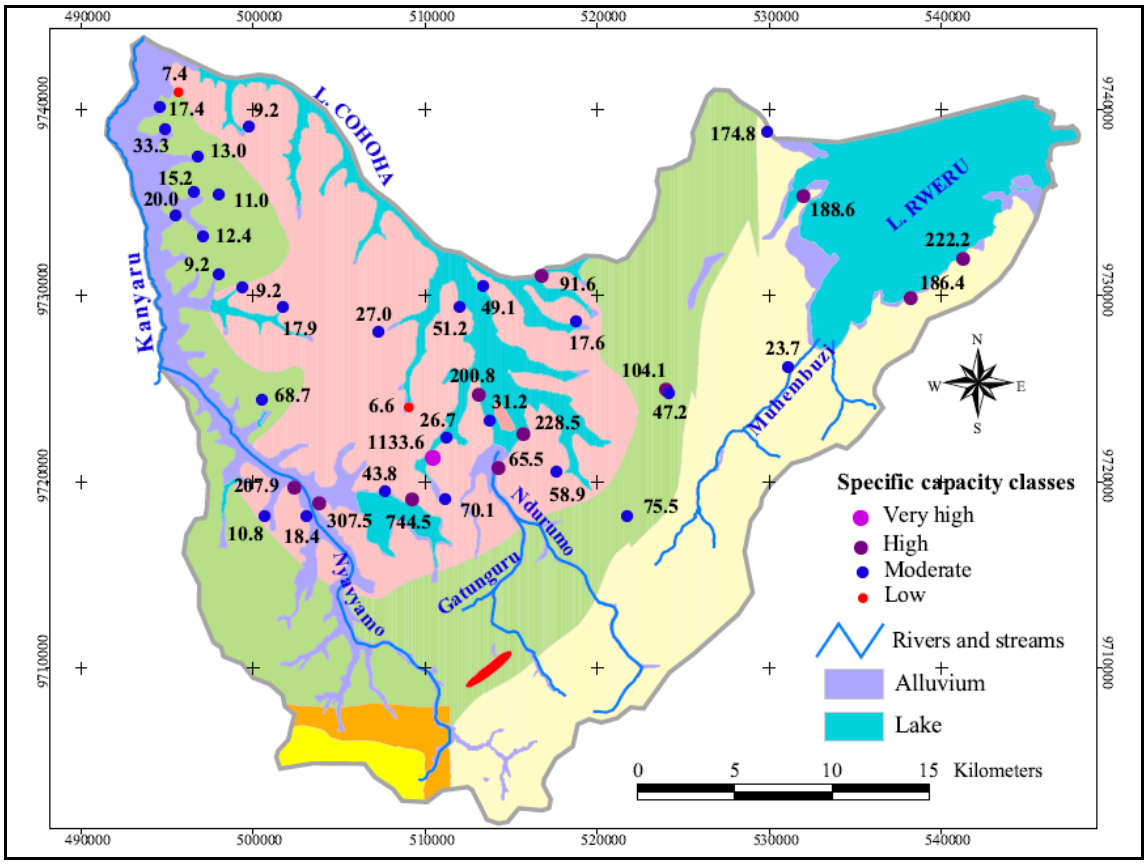

Figure IV.45. Distribution of specific capacity values

IV.7.2.3. Relationship between transmissivity and specific capacity

The relationship between the transmissivity calculated by analytical methods and the specific capacity is evaluated through a regression analysis between the two parameters. In this respect, values of transmissivity are plotted against values of specific capacity on linear and logarithmic scales and a line is fitted through the data points scatter. The use of log transformed values of the transmissivity and specific capacity is justified by the fact that the frequency distributions of the two parameters are log-normally distributed as this was demonstrated by several authors (Razack & Huntley, 1991; Huntley *et al.*, 1992; Krasny, 1993; Mace, 1997; Verbovsek, 2008). Moreover, Limpert *et al.* (2001) suggest the log-transformation as the most accurate way of estimating statistical parameters for log-normally distributed data. From the best-fitting line, an empirical relationship relating the specific capacity to the transmissivity is derived and the correlation between the two parameters is, at first glance, evaluated through the coefficient of determination R^2.

Figures IV.46 and IV.47 show arithmetic and log-log plots of transmissivity (T) against specific capacity (S_c). Both arithmetic and log-log plots show a strong correlation between values of specific capacity and transmissivity as evidenced by very high coefficients of determination. Figure IV.43 shows an arithmetic plot of specific capacity

and transmissivity values estimated from the 41 pumping tests executed. It can be noted that most data points are concentrated in the lower left corner of the graph, thus reflecting low values of transmissivity and specific capacity. The equation representing the best-fit line through the 41 data is:

$T = 0.3181S_c - 4.3663$

where T is transmissivity in m^2/d and S_c is specific capacity in m^2/d with a coefficient of determination R^2 of 0.98.

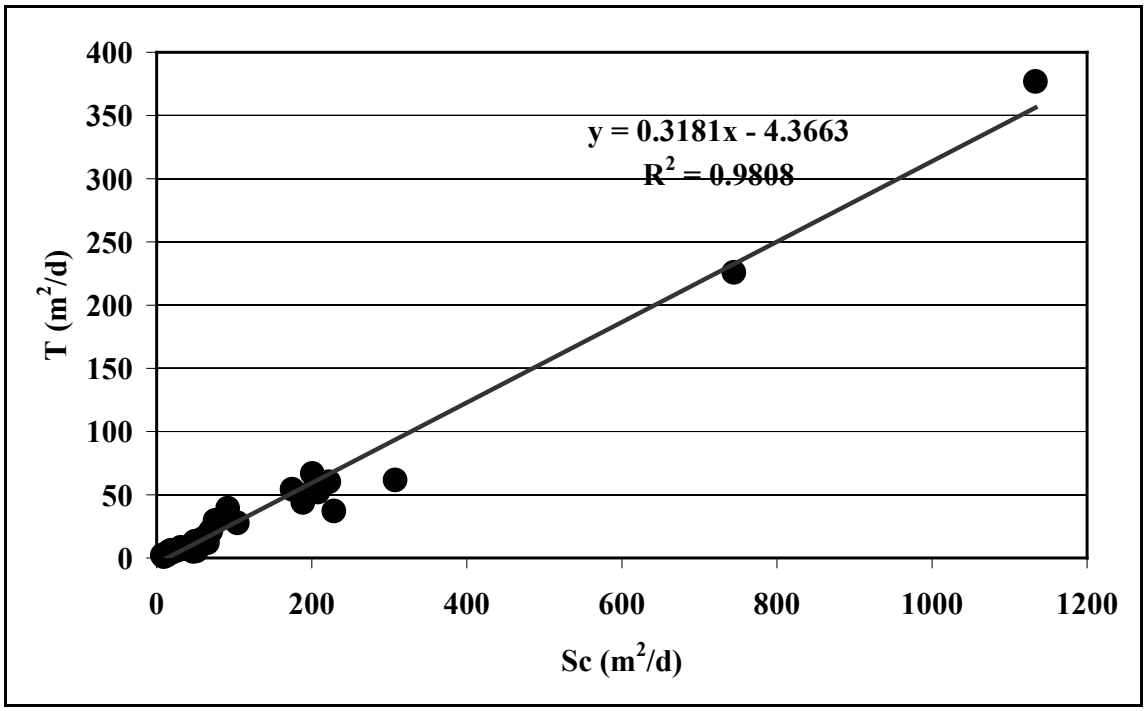

Figure IV.46. Arithmetic plot of transmissivity (m^2/d) versus specific capacity (m^2/d)

Figure IV.44 shows log-log plot of transmissivity versus specific capacity for the entire data set of 41 data pairs including recovery information. The log-log plot shows a better scatter of data points along the best-fit line than for the case of the arithmetic plot. The equation for the bilogarithmic regression line representing the best fit is:

$T = 0.192S_c^{1.0584}$

where T is transmissivity (m^2/d) and S_c is specific capacity (m^2/d) with a coefficient of determination R^2 of 0.95.

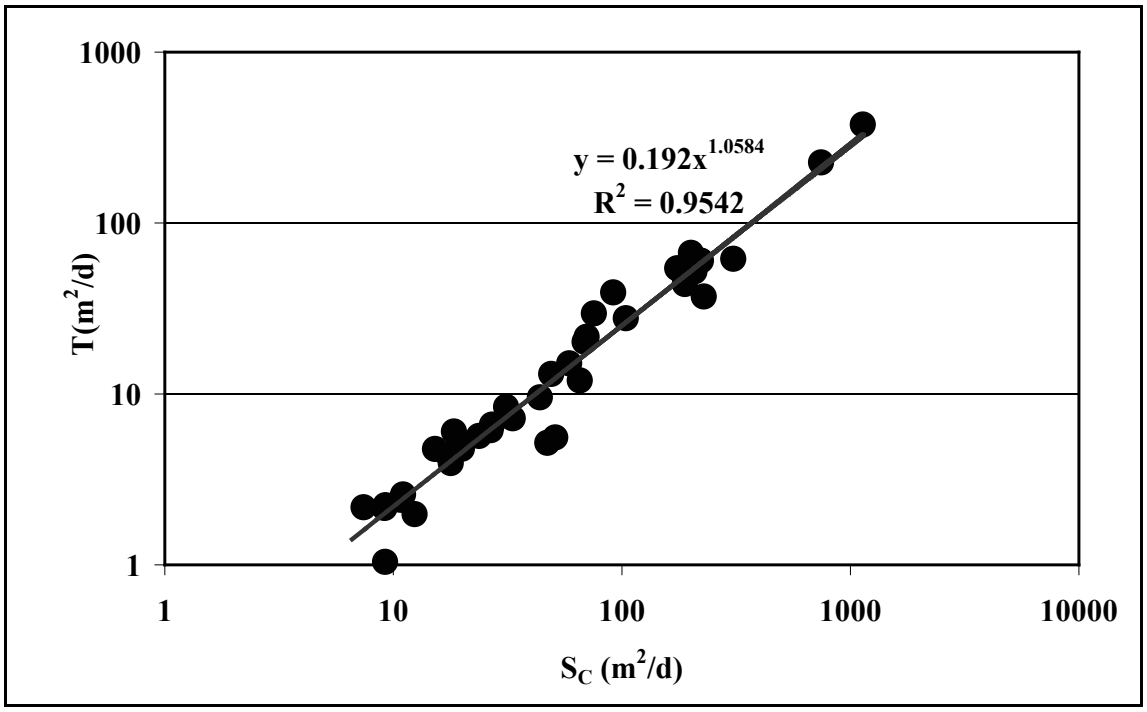

Figure IV.47. Log-log plot of transmissivity (m^2/d) versus specific capacity (m^2/d)

Unlike what many previous authors (Razack & Huntley, 1991; Huntley *et al.*, 1992; Fabbri, 1997; Mace, 1997; Hamm *et al.*, 2005; Rotzoll & El-Kadi, 2008) have suggested, the log-log regression between transmissivity and specific capacity, which conforms to the lognormal character of both parameters, does not necessarily improve the correlation coefficient. This observation is in agreement with recent findings by Verbovsek (2008) and Razack & Lasm (2006) who have concluded that the log-transformation and especially the back-transformation to original values do not necessarily lead to improved results.

The two empirical equations established in this study are similar to other empirical relationships developed by previous authors such as Thomasson *et al.* (1960), Logan (1964), Razack & Huntley (1991), Huntley *et al.* (1992), Mace (1997), El-Naqa (1994), Fabbri (1997), Dixon & Custer (2002), Jalludin & Razack (2004), Ham *et al.* (2005), Razack & Lasm (2006), Verbovsek (2008) (Table IV.23).

Table IV.23. Empirical relationships between specific capacity and transmissivity in different hydrogeological environments.

Empirical relationship	Coefficient of determination	Reference	Number of data pairs	Aquifer
$T = 1.18S_c$	_	Thomasson *et al.* (1960)	-	Valley-fill sediments
$T = 1.22S_c$	-	Logan (1964)	-	Sand and gravel
$T = 15.3S_c^{0.67}$	0.63	Razack & Huntley (1991)	215	Alluvial
$T = 0.12S_c^{1.18}$	0.89	Huntley *et al.* (1992)	129	Fractured granite
$T = 1.81S_c^{0.917}$	0.97	El-Naqa (1994)	237	Karst
$T = 0.76S_c^{1.08}$	0.89	Mace (1997)	71	Karst
$T = 0.85S_c^{1.07}$	0.97	Fabbri (1997)	45	Karst
$T = 0.17S_c^{1.36}$	0.87	Dixon & Custer (2002)	50	Karst
$T = 3.64S_c^{0.938}$	0.91	Jalludin & Razack (2004)	48	Volcanic
$T = 0.99S_c^{0.89}$	0.94	Hamm *et al.* (2005)	117	Volcanic
$T = 0.33S_c^{1.30}$	0.88	Razack & Lasm (2006)	118	Crystalline
$T = 22.9S_c^{0.66}$	0.59	Srivastav *et al.* (2007)	94	Alluvial
$T = 1.537S_c^{1.002}$	0.87	Rotzoll & El-Kadi (2008)	141	Volcanic
$T = 0.192S_c^{1.0584}$	0.95	Bakundukize &Walraevens (2012)	41	Crystalline

Note: Specific capacity (S_c) and transmissivity (T) are expressed in m^2/d

It should be born in mind, however, that each of the empirical relationships is site-specific and depends on the local conditions prevailing at each site, among which are well losses, well penetration, well completion characteristics, heterogeneities, methodology used to determine S_c and T, aquifer type and hydraulic characteristics (Razack & Lasm, 2006; Rotzoll & El-Kadi, 2008; Verbovsek, 2008). Thus, several authors agree that correcting the specific capacity for well losses can significantly reduce the uncertainty by improving the correlation between T and S_c (Ratzoll & El-Kadi, 2008; Jalludin & Razack, 2004).

IV.8. Conclusions and recommendations

The interpretation of 41 pumping and recovery tests performed in the study area using the software Aquifer Test Pro 4.2 confirms the hydrogeological model inferred from the available geophysical and lithological information. Indeed, this model shows that the subsurface structure comprises a weathered overburden which is characterised by an upwards decrease of the grain-size of the weathering materials. Hence, in general, the top of the weathering profile is formed by a clay-rich layer in which rests the groundwater table and which acts as the confining layer. The aquifer is formed by a mixture of weathering materials including clay, sand, and gravel and rock fragments with a clear increase of coarse materials with depth. The weathered mantle is underlain by a fractured basement which in turn overlays the fresh basement. The hydrogeological structure is therefore composed of two superimposed but communicating aquifers namely the weathered overburden and the fractured basement. This structure is confirmed by geoelectrical data.

The shallow wells investigated in this study only tap the weathered overburden aquifer. In the interpretation of the pumping and recovery test data, five methods including Hantush, Theis, Papadopulos & Cooper, Cooper & Jacob, and double porosity were examined and compared. It was observed that the Hantush method offers the best matching analytical solution for most of the wells tested (27 wells) in the study area, while the double porosity method was adopted for several wells in the western part of the study area. In this part of the study area, tectonic fracturing associated with the North-South trending fault, along which flows Kanyaru River, may account for the systematic double porosity response of the aquifer.

The widespread conformity of the drawdown response to the Hantush analytical solution, both for pumping and recovery test data, confirms the hydrogeological model developed for the study area, which shows that leaky conditions should prevail. The hydraulic parameters obtained using the Hantush, and Cooper & Jacob methods, both for the pumping and recovery phases, are generally closely comparable in most of the cases. The discrepancy between the hydraulic parameters obtained during the pumping and recovery phases may be symptomatic of aquifer heterogeneity.

Overall, the transmissivity varies between 1 m^2/d and 377 m^2/d with an average of 33.1 m^2/d, whereas the hydraulic conductivity ranges between 0.1 m/d and 166 m/d with an average of 14.8 m/d. Such a wide variation of hydraulic parameters even on short distance mirrors the importance of heterogeneities which are typical of basement aquifer environments. According to the classification of the transmissivity magnitude developed by Krasny (1993), most of the wells fall in the low transmissivity class (1-10

m^2/d) and the moderate transmissivity class (10-100 m^2/d), while only two wells are found within the high transmissivity class (100-1000 m^2/d).

The distribution of transmissivity across the three geological formations in which pumping tests were conducted confirms that the Undifferentiated Complex Formation, which is mainly formed by pegmatitic and granitic intrusions, has the highest groundwater potential, as this was already concluded from the hydrogeological structure of the study area. Indeed, this formation shows the highest values of transmissivity (2.1-377 m^2/d), hydraulic conductivity (0.3-166 m/d) and specific capacity (6.6-1133.6 m^2/d) in comparison to the two other formations namely Nyagisozi (or Nyabihanga) and Murehe (or Mugendo). The latter is characterised by the lowest values of hydraulic parameters, which confirm its poor groundwater potential.

Specific capacity values calculated for the 41 pumping tests are in the range 6.6-1133.6 m^2/d with an average of 113.60 m^2/d. The wide variation of specific capacity and transmissivity values which is confirmed by the high coefficients of variation is consistent with the typical heterogeneity of basement aquifers. According to the classification of specific capacity magnitudes proposed by Krasny (1993), most of the calculated values lie within the intermediate (8.64-86.4 m^2/d) and high specific capacity (86.4-864 m^2/d) classes while only one value falls within the low (0.864-8.64 m^2/d) and very high (>864 m^2/d) specific capacity classes.

A regression analysis between specific capacity and transmissivity (from the best fit method) was performed in order to establish an empirical relationship between the two parameters. The two empirical relationships derived from both arithmetic and log-log plots show a strong correlation between values of specific capacity and transmissivity, which is reflected by very high coefficients of determination. The best-fit regression line for the arithmetic plot is $T = 0.3181S_c - 4.3663$, with a coefficient of determination R^2 of 0.98. For the log-log plot, the best-fit regression line becomes $T = 0.192S_c^{1.0584}$, with a coefficient of determination R^2 of 0.95.

It stems from this study that the Bugesera region is not as “cursed” as local population seems to believe, especially with respect to the scarcity of water resources. Indeed, this study sheds light to the fact that there is a random distribution of several prospective areas where hydraulic parameters reveal a good groundwater potential, which could be circumscribed and tapped with a view to providing clean water to the population, who are in a serious need of this vital commodity. The only and most limiting factor, as this was shown in this study, is the random nature of variations of hydraulic parameters. Further studies should focus on refining the grid of pumping tests in order to better circumscribe areas of groundwater potential. In this respect, further geophysical

investigations coupled with reconnaissance drilling are strongly necessary and recommended in order to explore the groundwater potential of the fracture/weathered basement. By establishing the connection between the weathered overburden and the underlying fractured aquifer, it would be possible to increase the yield of wells and avoid the upper aquifer which is vulnerable to various sources of pollution.

CHAPTER V. PIEZOMETRIC MEASURMENTS AND GROUNDWATER FLOW SYSTEM

V.1. Introduction

Groundwater flow varies in time and space in response to anthropogenic and climatological constraints which change the boundary conditions, thereby resulting in changes in the drainage network as well as uncertainties in the hydraulic model parameters governing groundwater flow (Vissers & Van der Perk, 2008). Mapping the groundwater flow system is of critical importance for a sound and efficient management of groundwater resources. Groundwater is generally connected to surface water bodies such as lakes, rivers and other potential sources of contamination. Regular measurements of water levels in wells can help to appraise the status of the interactions between groundwater and surface water bodies (rivers, lakes, sea). Indeed, low water levels in the river can induce groundwater flow to the surface water body or conversely high water levels in the surface water body can trigger a reverse situation (Chapman & Kimstach, 1996).

A well-informed analysis and understanding of the spatial pattern of the groundwater flow system, when combined with a good knowledge of potential sources of contamination and possible hydrochemical processes, provide in-depth insights as regards to the spatio-temporal variation of groundwater quality (Vissers & Van der Perk, 2008). However, mapping the groundwater flow system is not an easy task because groundwater is hidden from view and hence, the variations of hydraulic parameters of an aquifer and the topography of the groundwater surface, which are not always perceptible, may result in ambiguities and uncertainties. Like surface water courses, groundwater flows from the topographically elevated areas, also known as recharge areas, towards the low lying areas, also known as discharge areas. This is in line with Darcy's law which states that groundwater flows from high to low hydraulic heads. Flow lines are idealised paths followed by water particles as they move through the aquifers. They are perpendicular to the equipotential lines which are drawn through the aquifer and which connect points of equal hydraulic head.

Seasonal fluctuations of groundwater level can be caused by natural as well as anthropogenic causes including changes in the volume of water stored in the aquifer, variations of atmospheric pressure and the deformation of the aquifer. The change in aquifer storage can result either from the addition of water to the aquifer through recharge or the removal of water through exploitation of pumping wells and evapotranspiration, especially in arid climates.

In their analysis of the effects of multi-annual climate variability on the hydrodynamic evolution (1933 to present) in a shallow aquifer system in northern Belgium, Van Camp *et al.* (2010) observed that amplitudes of seasonal groundwater level fluctuation are generally higher in recharge areas than in discharge areas. The same study demonstrated that the main inter-annual variations of groundwater levels are mainly due to fluctuations in winter peak discharge, whereas summer discharge remains quite constant.

The study area is made up of two distinct geomorphologic units: the depression of Bugesera, which is characterised by a complex of swamps and shallow lakes, and the highlands which surround the depression to the South and East. Hence, groundwater recharge in the study area may mainly occur in the highlands and then, the infiltrated water flows towards the depression where it eventually discharges within the complex of interconnected swamps and lakes. However, localised recharge may also take place within the depression in response to rainfall. During the rainy season, the rise of groundwater level in the highlands results in the appearance of ephemeral streams which flow towards the interconnected complex of marshlands and lakes through numerous small valleys which dissect the flanks of the highlands.

This chapter aims at defining the spatial configuration of the groundwater flow in the study area through the mapping of the depth to the groundwater surface at different locations, with a view to inferring the flow direction and hence the implications with respect to the hydrochemical processes, the interactions between groundwater, the shallow lakes and the potential threats as regards to groundwater quality.

V.2. Water level measurements

There is not any governmental or private groundwater monitoring programme in the study area, and thus there are no historical data available on groundwater level fluctuations. In this study, the groundwater flow system of the study area is defined based on water level measurements performed within the framework of this study in September and October 2006, 2007 and 2008 in the shallow wells scattered throughout the study area. Moreover, for the year 2008, a continuous monitoring of a number of wells in the study area was organised, all year long, in order to observe the seasonal fluctuations of groundwater. The time table of measurement was organised in such a way that, in each well, the water level was, as far as possible, measured at the same period of the month. Each month, piezometric measurements were successively done in the municipality of Ntega (southwestern part), then in the municipality of Busoni (northeastern and of the central part) and they were terminated in the municipality of Kirundo (Central part). They were performed by sanitation technicians of each municipality. It was observed that some wells went completely dry during the dry

season and particularly in the course of the months of August and September. Water level measurements taken in producing wells are characterised by irregular variations which do not follow the general seasonal trend of precipitation fluctuations, probably in response to the daily fetching of water by local villagers which takes place at any time of the day.

Water level measurements were performed using an electrical water level meter which comprises a probe and a measuring tape. The water level meter is lowered into the well and when the level zero of the probe touches the groundwater surface, acoustic and light signals are produced and the depth to the groundwater can be then read on the graduated tape.

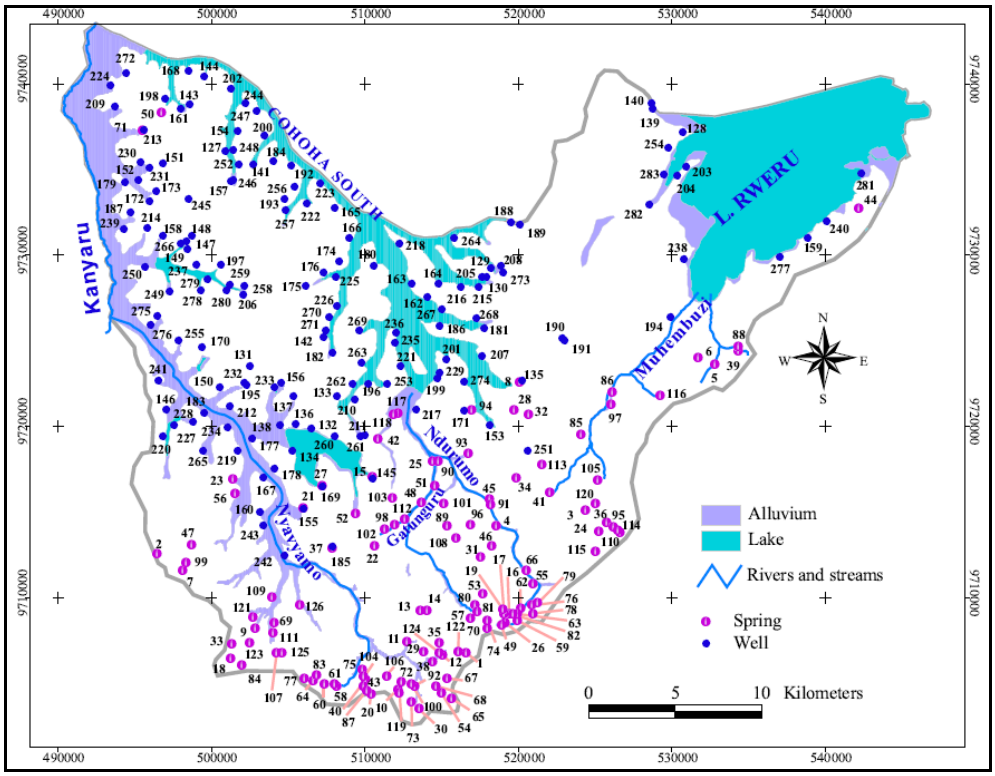

Figure V.1. Map showing the location of piezometric measurements and springs used to define the groundwater flow system in the study area (numbers on the map correspond to the numbers of different wells and springs as presented in Appendix V.1)

In total, groundwater levels were measured in 157 wells which were complemented by the information on the elevation of 126 springs in order to have a good coverage of the study area (Figure V.1). In this regard, a simplifying assumption is adopted which considers that, for a spring, groundwater surface outcrops at the ground surface and therefore the elevation of the spring location can be considered as the local hydraulic head of groundwater. The hydraulic head at each measurement location is computed as the difference between the topographic elevation derived from the digital elevation

model and the depth to groundwater surface which is considered as 0 m for springs. Of the 126 springs, 61 were mapped and sampled for chemical analyses during the field campaigns conducted in 2007 and 2008, while information about the other 65 was taken from an existing database at the General Directorate of Water and Energy in Bujumbura (Ministry of Energy and Mines).

V.3. Results and discussion

V.3.1. Depth to the water table

Figure V.2 and Appendix V.1 present the spatial distribution of the depth to groundwater across the study area based on piezometric measurements from 157 wells and the topographic elevations of 126 springs. The figures on the map represent the depth to the groundwater table for different wells and springs used to define the groundwater flow system. Table V.1 shows some descriptive statistics regarding the variation of the depth to the groundwater table in wells. Overall, it varies between 0.37 m (Well in Gahwijo I-Nyabikenke, Nr. 148) and 15.32 m (well Nr. 206 Appendix V.1) with an average depth of 5.42 m below the ground surface. Of the 157 wells mapped and wherein the groundwater level was measured, 85 wells (55 %) show water levels at a depth lower than or equal to 5 m, 57 wells (36 %) have groundwater levels at depths comprised between 5 and 10 m, whereas only 13 wells (8 %) display water levels at depths exceeding 10 m. These shallow depths to the groundwater table confirm that most of the hand-dug wells investigated tap the shallow aquifer hosted in the weathered mantle.

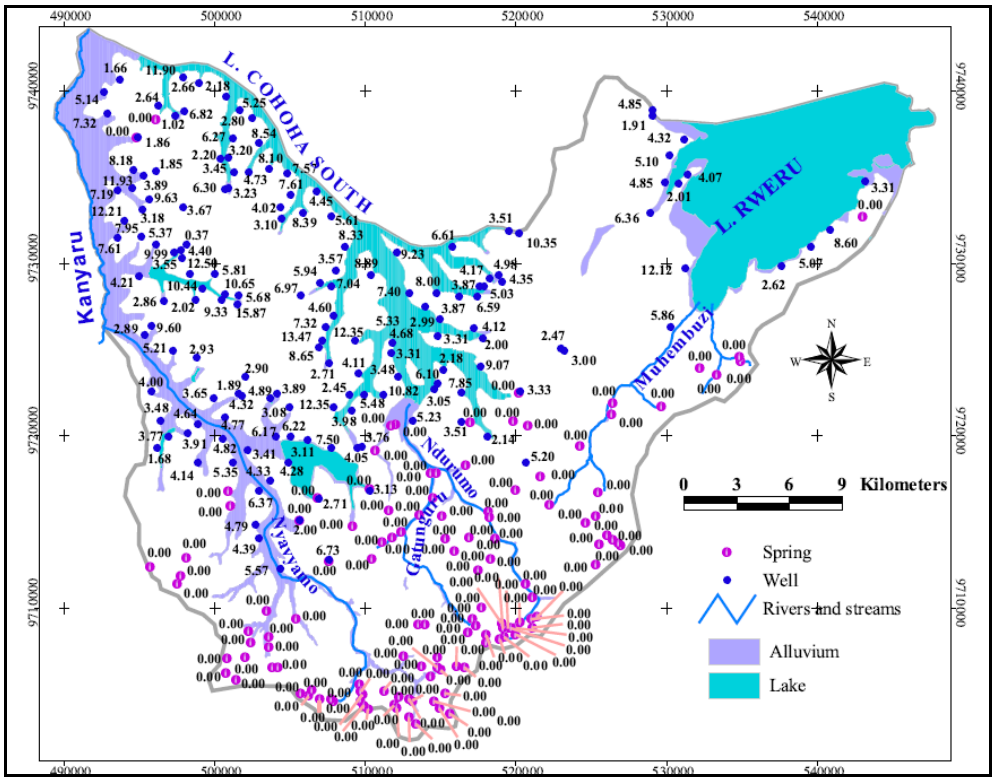

Figure V.2. Depth to the water table (in mbg: meter below ground surface)

Moreover, the abundance of springs in the southern and eastern parts of the study area, which represent the outcrop of groundwater at the land surface, confirms that groundwater has the highest elevations in the highlands which often give rise to ephemeral streams, especially during the rainy season. These streams flow through a myriad of small and tortuous V-shaped valleys which connect the highlands to the complex of interconnected swamps and lakes within the depression.

On the other hand, it can be observed that the depth to the water table is highly variable across the study area even over short distances. For instance, it can be noted that the wells in Bishunzi-Cewe (well Nr. 132), Runyonza–Kabonde (well Nr. 259) and Cewe-Nunga (well Nr. 136), located on the northern shore of Lake Rwihinda, and which are not very distant, show however quite different depth to the water table and therefore completely different hydraulic heads which are respectively 1368.89 m, 1358.50 m and 1372.78 m above the local datum (Arc 1950 for Burundi). The same observation holds for the wells at Karago-Runyonza (well Nr.182), Cinyambo (well Nr. 142), Ruyivyi I (well Nr. 269), Ruyivyi II (well Nr. 270) and Ngugo III (well Nr 226) in the central part of the study area, which show quite contrasting depths to the groundwater over short distances (Figure V.1, Figure V.2 and Appendix V.1). Based on the premise that groundwater surface generally tends to follow the land surface topography, these rapid and sharp variations of the depth to the groundwater surface reflect the abrupt changes of the topography, which is the main physiographic characteristic of the study area.

Indeed, even the part of the study area considered as a depression, features an undulating topography where some peaks can reach up to more than 1600 m, whereas the average elevation for the depression is 1410 m. In this respect, El-Fahem (2008) observed that each morphological unit has its own groundwater level and this is supported by Haitjema & Mitchell-Bruker (2005), who refer to the water table as a subdue replica of topography, although they warn that this observation should not be generalised.

Table V.1. Descriptive statistics of the variation of the depth to the groundwater table (m)

Number of observations	Maximum (m)	Minimum (m)	Average (m)	Standard deviation (m)
157	15.32	0.37	5.42	2.86

V.3.2. Inter-seasonal variations of depth to the water table

Figures V.3 to V.6 and Appendix VI.2 show the inter-seasonal variations of the groundwater elevation during the year 2008 for a number of representative, mainly abandoned wells, which can be considered as observation wells. Figures VI.3 to V.6 represent the fluctuations of the piezometric level in 32 selected wells situated in three different geographical locations of the study area: northeastern part around the Lake Rweru (Figure V.3), the central part around Lakes Cohoha South and Rwihinda (Figure V.4) and the southwestern part around the Nyavyamo marshland (Figure V.5). Figure V.6 shows the fluctuations of groundwater level in operating wells situated in central and southeastern parts of the study area. It can be observed that the fluctuations of the groundwater surface closely follow the seasonal variation of rainfall (Figure V.7), which is the only source of recharge in the study area, with a clear demarcation between the rainy season, where recharge occurs, and the dry season, where the water level declines. Groundwater head progressively increases from January and generally reaches the peak in April (Figure V.4) or May (Figure V.3) or June (Figure V.5). From June, the groundwater surface starts to decline and attains the lowest level in September-October. Thereafter, the groundwater surface starts to rise again and progressively evolves towards another less pronounced peak in December.

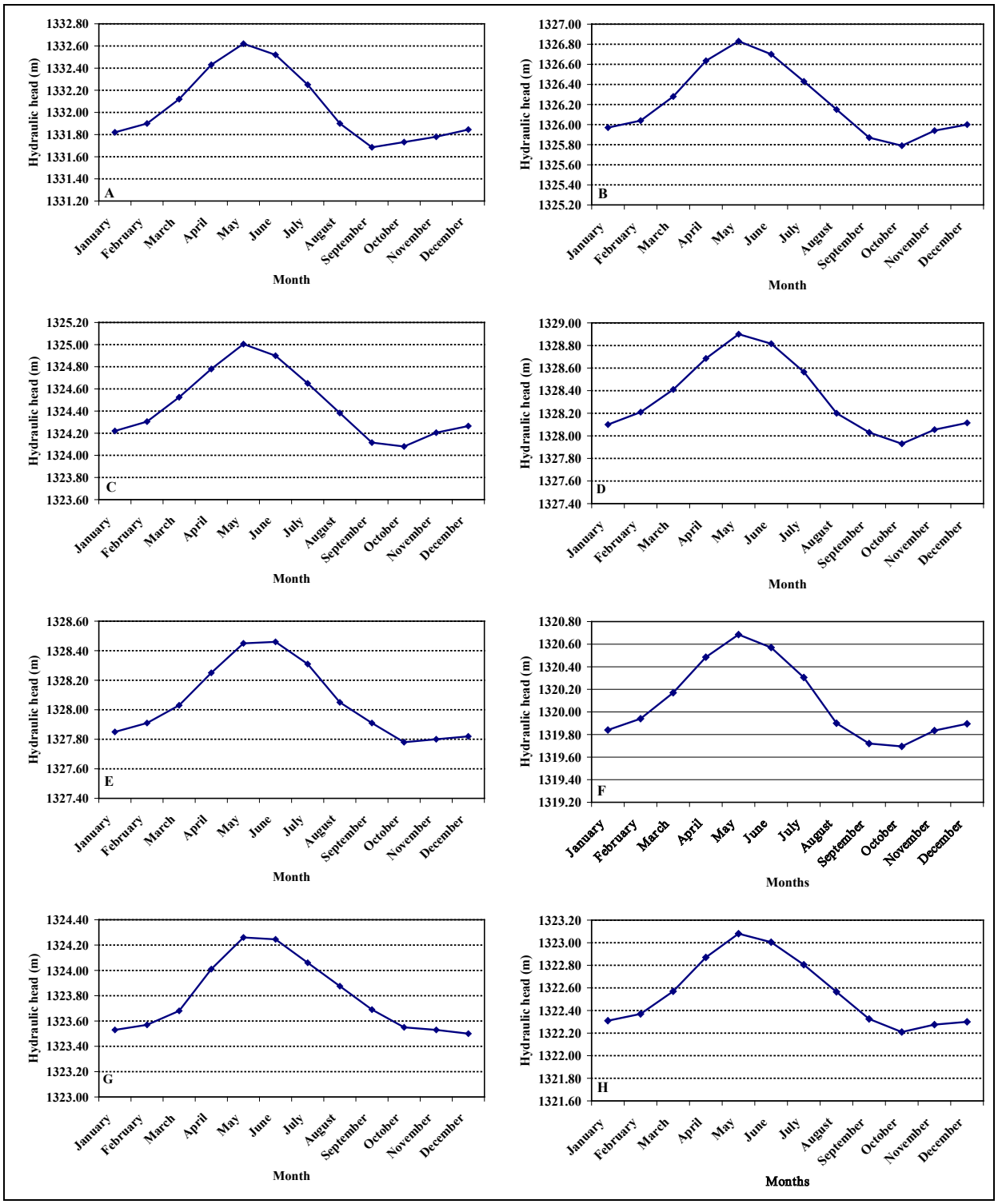

Figure V.3. Groundwater level fluctuations in 2008 in wells in Bidogo-Gatete in the northeastern part: Bidogo-Gatete (A : Nr. 128), Cimbogo-Gatete I (B : Nr. 139), Gikombe-Nyagisozi (C : Nr. 160), Mago-Gatete I (D: Nr. 203), Gatare-Nyakiganga (E : Nr. 154), Sigu-Kumana (F : Nr 280), Vyanzo I-Gatete (G : Nr. 282) and Vyanzo II-Gatete (H: Nr. 283) (hydraulic head in m above the local datum, Arc 1950 for Burundi) (Numbers refer to the Appendix V.2)

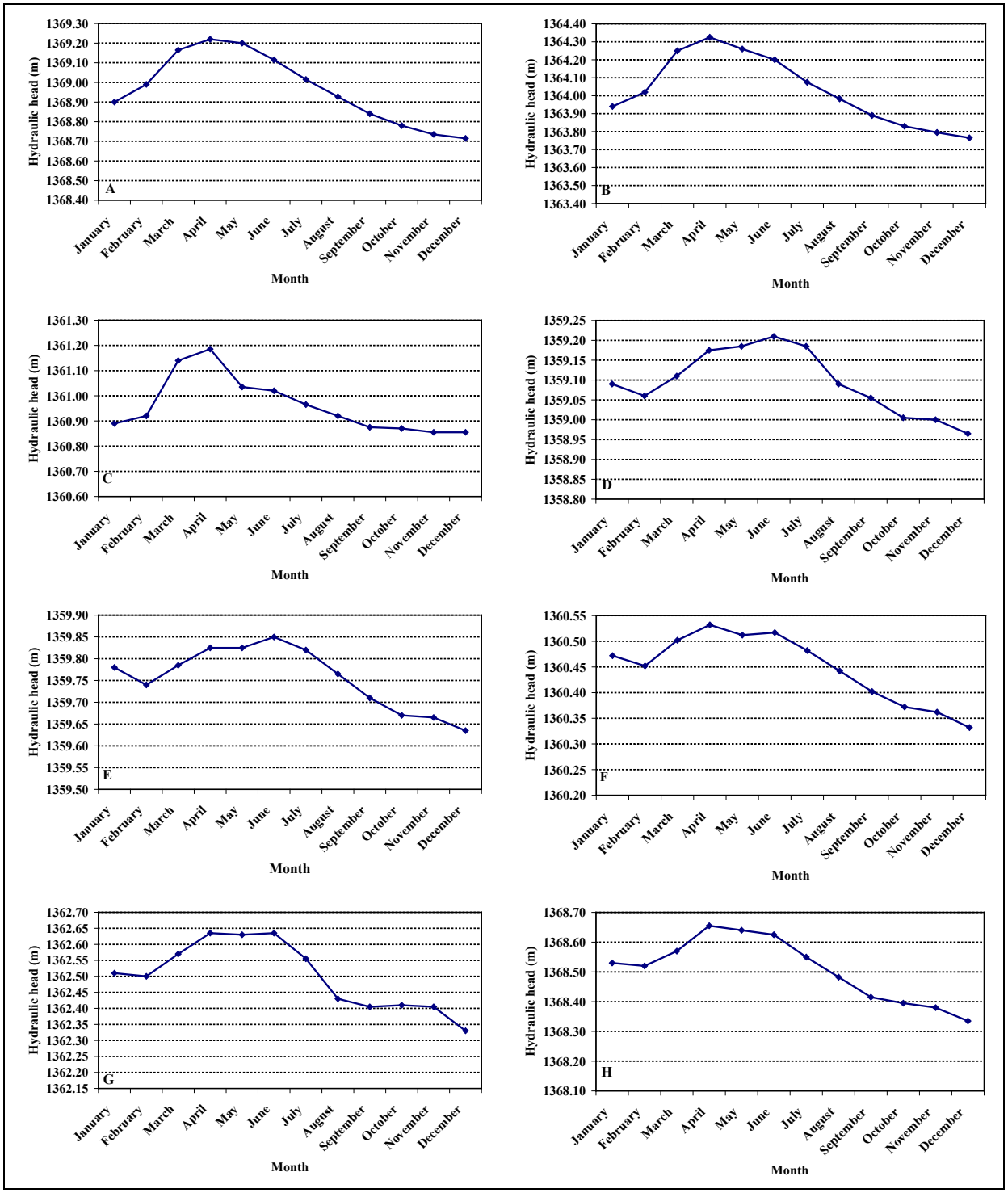

Figure V.4. Groundwater level fluctuations in 2008 in wells in central part: Bishunzi-Cewe (A : Nr. 132), Cewe-Nyakariba (B: Nr. 138), Gaharata-Murama (C: Nr. 145), Gitamo I-Murambi (D: Nr. 164), Gitamo II-Murambi (E : Nr. 163), Kantuye-Ceru (F: Nr. 180), Murama I-Higiro (G: Nr. 215), Ruranzi-Rwibikara (H: Nr. 264) (hydraulic head are in m above the local datum, Arc 1950 for Burundi) (Numbers refer to the Appendix V.2)

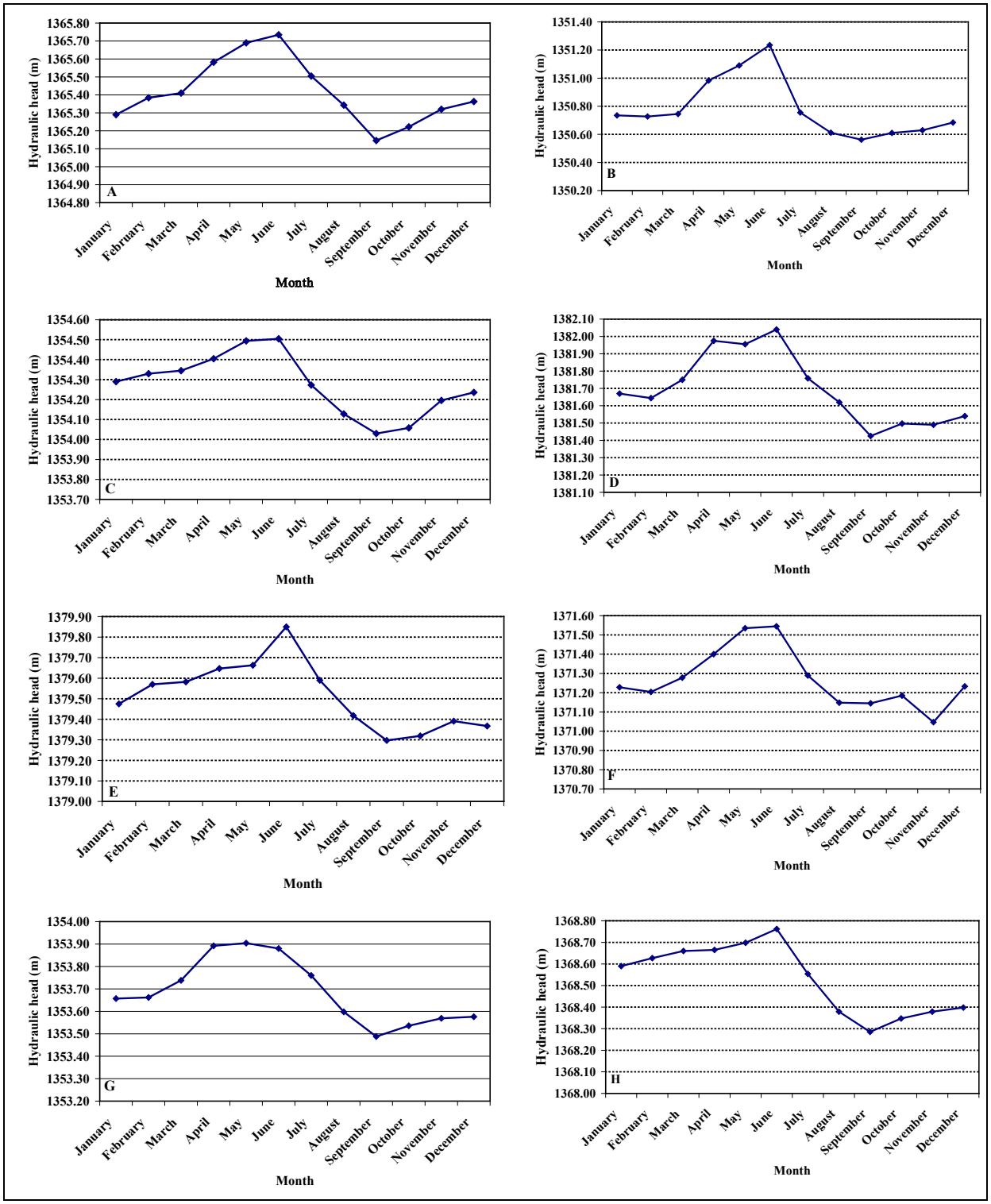

Figure V.5. Groundwater level fluctuations in 2008 in wells in southwestern part: Gikomero-Susa (A: Nr. 160), Haga-Susa (B: Nr. 167), Kariba-Kanyagu (C: Nr. 183), Murehe-Murungurira (D: Nr. 219), Murungazi-Mugendo (E: Nr. 220), Ntwago-Murungurira (F: Nr 234), Renga II-Gitwenzi (G: Nr. 243) and Ngugo II-Kanyagu (H: Nr. 265) (hydraulic head in m above the local datum, Arc 1950 for Burundi) (Numbers refer to the Appendix V.2)

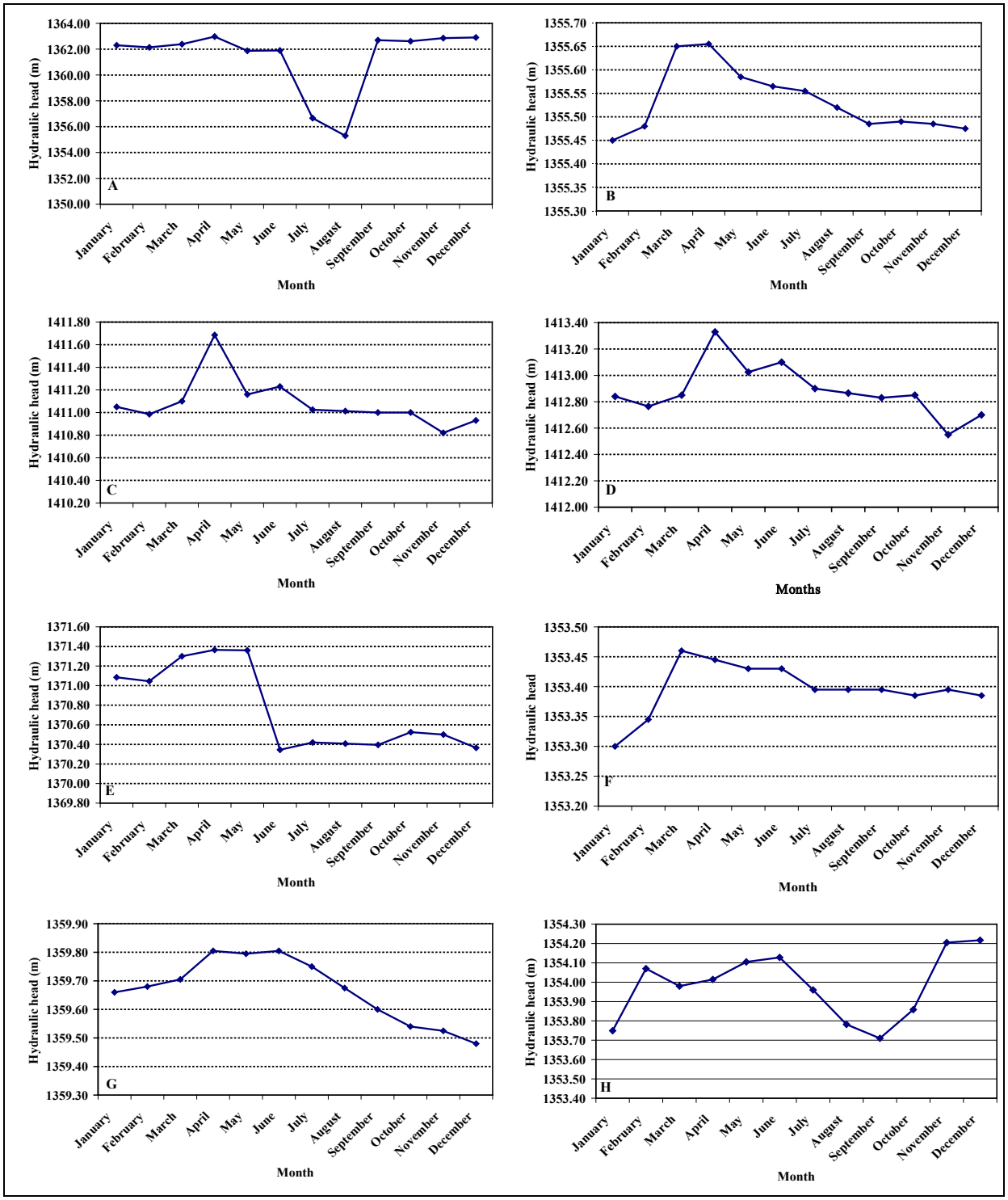

Figure V.6. Groundwater level fluctuations in 2008 in operating wells in Bunyari-Rugarama (A: Nr. 135), Kadobogoro-Muramba (B: Nr. 171), Kigina I-Gisenyi (C: Nr. 190), Kigina II-Gisenyi (D: Nr. 191), Kigozi-Yaranda (E: Nr. 196), Muhero I-Yaranda (F: Nr 211), Murambo-Murambi (G: Nr. 218) and Ruseno-Kanyagu (H: Nr. 265) (hydraulic head in m above the local datum, Arc 1950 for Burundi) (Numbers refer to the Appendix V.2)

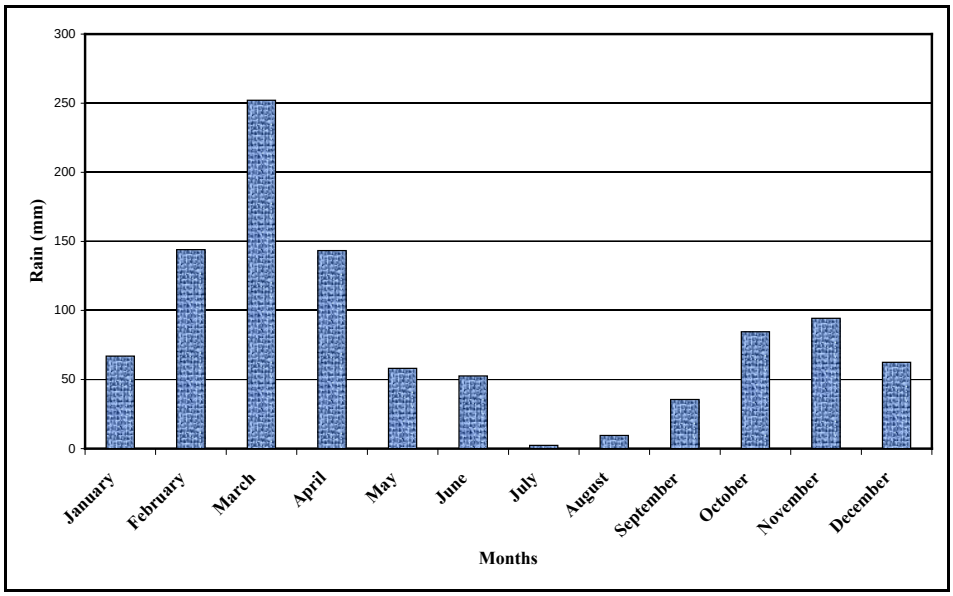

Figure V.7. Monthly rainfall recorded at the meteorological station in Kirundo for the year 2008

Overall, this trend of the fluctuation of groundwater surface reflects the two unequal peaks of the annual recharge. Groundwater table, in each hydrological year, reaches maxima in April-May and December in response to the long (February-May) and short (September-November) rainy seasons (Figure V.7). It can be noted from Figure V.3 A to H, V.4 B, C and V.5 A to F that the peak of the groundwater level does not necessarily correspond to the peak of the precipitation which generally occurs in March or April (Figure V.7) and this can be understood as resulting from the cumulative effect of the groundwater recharge occurring generally in April or May and exceptionally in March depending on the amount of precipitations during the month of February. Figure V.7 shows the monthly rainfall in the course of the year 2008 at the meteorological station of Kirundo.

Figure V.6, which depicts piezometric level fluctuations in producing wells from the central and southwestern parts of the study area, shows saw-teeth-like fluctuations which, in most of the cases, do not correlate to the general trend of monthly precipitations (Figure V.7) and the resulting recharge events. Indeed, these wells being producing, the water level measured depends on whether the measurement was taken before or after local villagers have started to fetch water from the well. However, for highly productive wells where the static water level can recover quickly after pumping, it can be observed that the water level fluctuation is closely similar to that of non producing wells and reflects the seasonal trend of groundwater recharge (Figure V.4 A, B and G). For the well located in Ruseno-Kanyagu (Figure V.6 G), the sharp increase of groundwater level from October may be explained by the failure of the pump in September 2008, as this was confirmed by local villagers in October 2008 when the author was performing a pumping test on this well. The water level fluctuations and

amplitudes of seasonal variations in these wells are not discussed because they are highly tributary of the random fetching of water by local villagers.

Table V.2 also presents the amplitude of seasonal variations of piezometric levels in the three locations namely the northeastern, the central and the southwestern parts of the study area. For each well, the amplitude of groundwater level fluctuation was calculated as the difference between the maximum and minimum piezometric levels in one well. The northeastern part of the study area, Figure V.3, shows the highest amplitudes of seasonal fluctuations, with an average of 0.90 m, whereas the lowest amplitudes are observed in the central part, Figure V.4, where the average amplitude reaches 0.34 m. The southeastern part of the study area, Figure V.5, shows intermediate amplitudes of seasonal variations with an average of 0.54 m.

Table V.2. Descriptive statistics of seasonal fluctuations of the piezometric level

Group of observations	Number of observations	Piezometric level (m above datum)		Amplitude of water level fluctuations (m)		
		Average max (m)	Average min (m)	Max (m)	Min (m)	Average (m)
NE (Figure V.3)	8	1326.23	1325.33	1.04	0.68	0.90
Central (Figure V.4)	8	1363.2	1361.99	0.56	0.2	0.34
SW (Figure V.5)	8	1366.06	1365.51	0.67	0.42	0.54
Producing wells (Figure V.6)	8	1372.81	1371.37	7.67	0.16	1.44
All observations (Appendix V.2)	50	1358.61	1357.63	7.67	0.16	0.69

A comparison of the three areas (NE, central and SW) considered in the analysis of seasonal groundwater level fluctuations seems to indicate a strong control exerted by the hydrologic conductivity and the amount of precipitation (recharge) on the amplitude of seasonal groundwater fluctuations. In the central part, where occurs the Undifferentiated Complex, the amplitude of seasonal fluctuations is strikingly lower that in the southwestern and northeastern parts, where occur the metasedimentary formations of Murehe and Nyagisozi. This lower amplitude can be related to two factors:

- Lower amounts of precipitation and recharge;
- Higher hydraulic conductivity

The amounts of precipitation are decreasing northwards (Figure V.10) and thus could explain the contrast between the southwestern and central parts. For explaining the again higher amplitudes in the northeastern part, we need however to resort to the second explanation: the higher hydraulic conductivities of the Undifferentiated Complex, which were obvious from pumping tests, and were explaining the earliest arrival of the groundwater level maximum (Figure V.4), compared to both other parts of the study area (Figures V.3 & V.5).

In the central part of the study area, the slight rise of groundwater water level resulting from the recharge during the short rainy season, which is observed elsewhere in November (Figures V.3 & V.5), comes later, in January and this seems to be typical of the central part of the study area (Figure V.4). This observation may reflect the spatial variability of rainfall in the course of the year 2008. The occurrence of groundwater level peak in April in the central part of the study area, which is exclusively underlain by the Undifferentiated Complex Formation, seems to confirm that the formation has the highest hydraulic conductivity, which allows a quick travel of the recharge through the unsaturated zone, in comparison to the northeastern and southwestern parts, where wells are all or partly situated in the metasedimentary formations (Chapter IV).

Extremely high amplitudes of groundwater level fluctuations are observed in producing wells (Figure V.6), mainly in Figures V.6 A (well in Bunyari Rugarama, Nr. 135) and V.6 E (well in Kigozi-Yaranda). For the first well, the important drop of groundwater level in June 2008 coincides with the period wherein the road connecting the city of Kirundo to the Rwandan border in Murehe-Gasenyi (NE of the study area) was being constructed. Hence, while building the foundation of the bridge in the marshland of Bunyari-Rugarama, which is not far from this well, the aquifer was partly drained and this explains the significant drop of groundwater level. As for the well in Kigozi-Yaranda, it belongs to a religious community (Sisters) who owns a guest house, and the drop of groundwater level at the beginning of the dry season coincides with the beginning of the seasonal tourism, which implies an increase of water demand at the guest house.

Figure V.8 shows the average groundwater level fluctuations for the 3 parts of the study area considered in the above discussion, pumping wells for all 50 wells where groundwater water level was monthly measured in 2008. As already discussed above, it can be observed that the groundwater table reaches the maximum level in April, May and June respectively for wells situated in the central, northeastern and southwestern parts of the study area. For all 50 wells including producing wells, the seasonal fluctuation of groundwater level shows a peak in April.

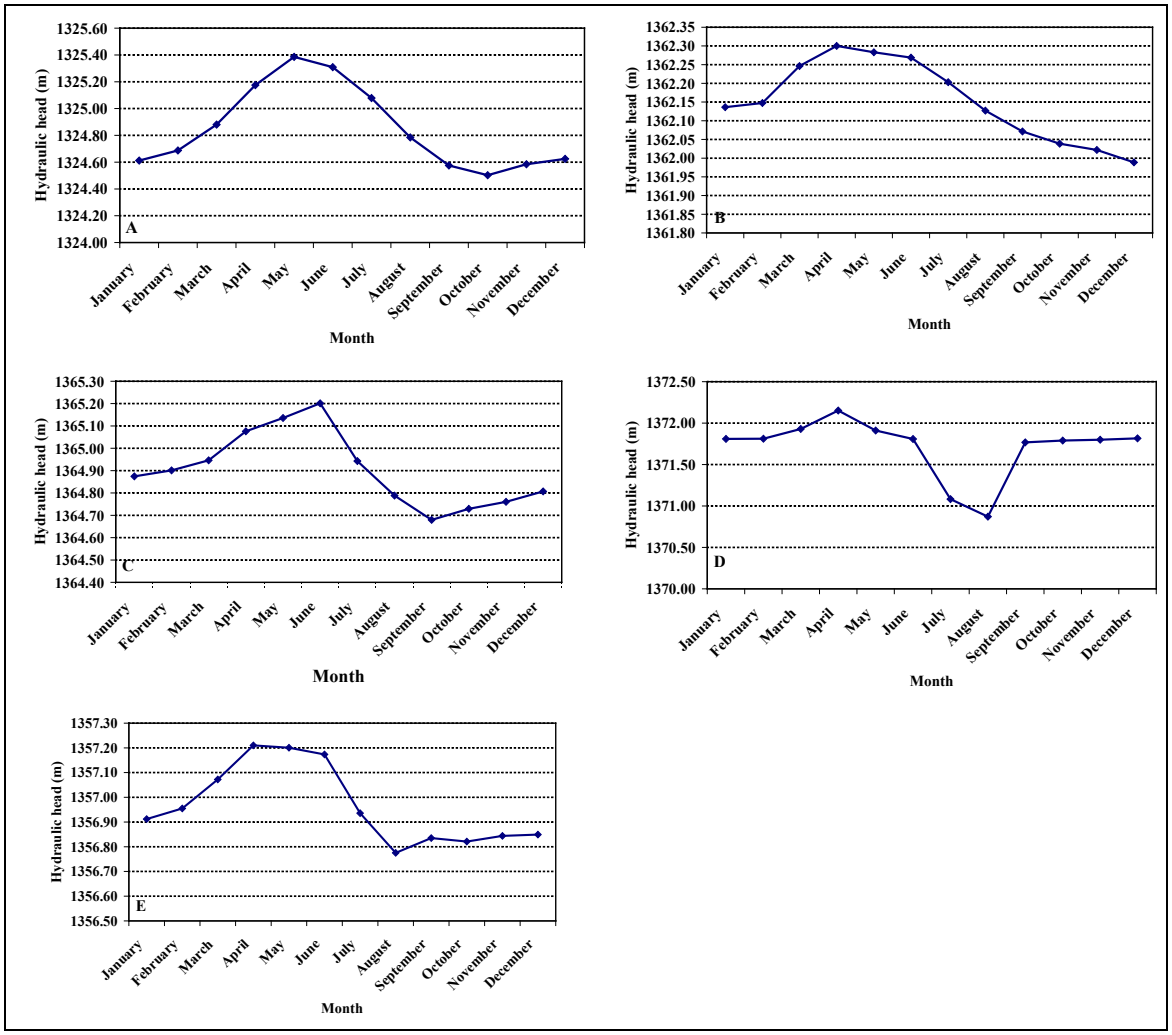

Figure V.8. Average monthly piezometric level fluctuations in northeastern (A), central (B), southwestern (C) parts of the study area, in producing wells (D) and in all monitored wells (E)

The peak of groundwater level observed in June, the beginning of the dry season, for the wells located in the southwestern part of the study area (Figure V.8 C) could be ascribed to three main reasons. First, the recharge has been computed using data from one meteorological station which may not capture all the rainfall variability across the whole study area (Figure V.10). Thus, it is possible that in the southwestern part of the study area, important rainfall may still occur in late May or beginning of June, thereby resulting in additional recharge which would justify the peak of groundwater level in June. On the other hand, measurements of groundwater recharge in that part of the study area (Ntega municipality) were performed at the beginning of each month and thus, it is possible that the peak of groundwater level observed in June could still reflect the recharge which has occurred in May before the water level starts to decline during the dry season. Moreover, a retardation between precipitation peak and highest water table is to be expected, due to delay caused by travel or recharge in unsaturated zone. The

lower the unsaturated hydraulic conductivity and the largest the thickness of the unsaturated zone, the larger will be the delay. Figure V.9 shows the location of wells in which monthly measurements of groundwater level were performed in 2008.

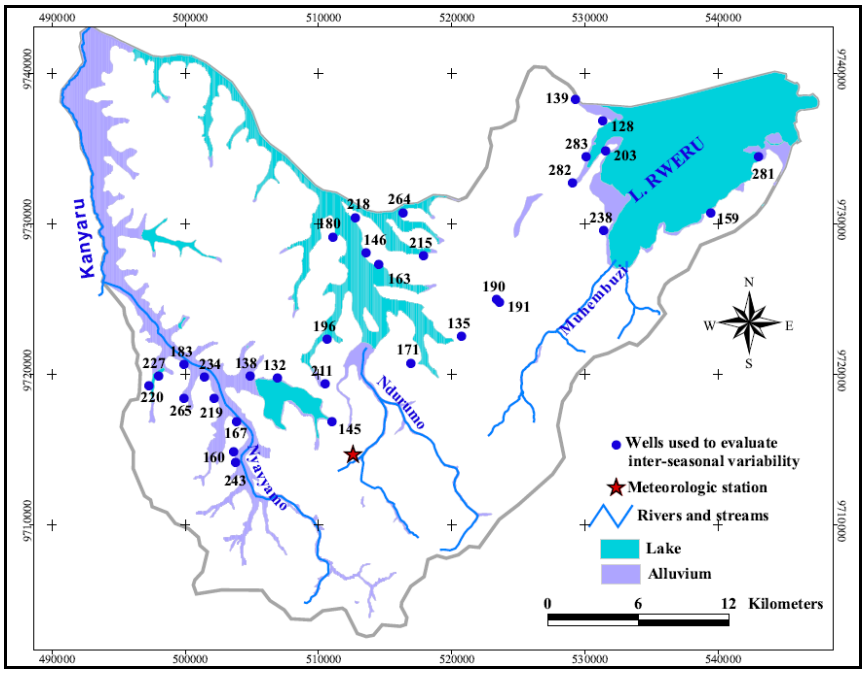

Figure V.9. Location of wells where piezometric measurements performed in 2008 are represented in Figure V.3, V.4 and V.5

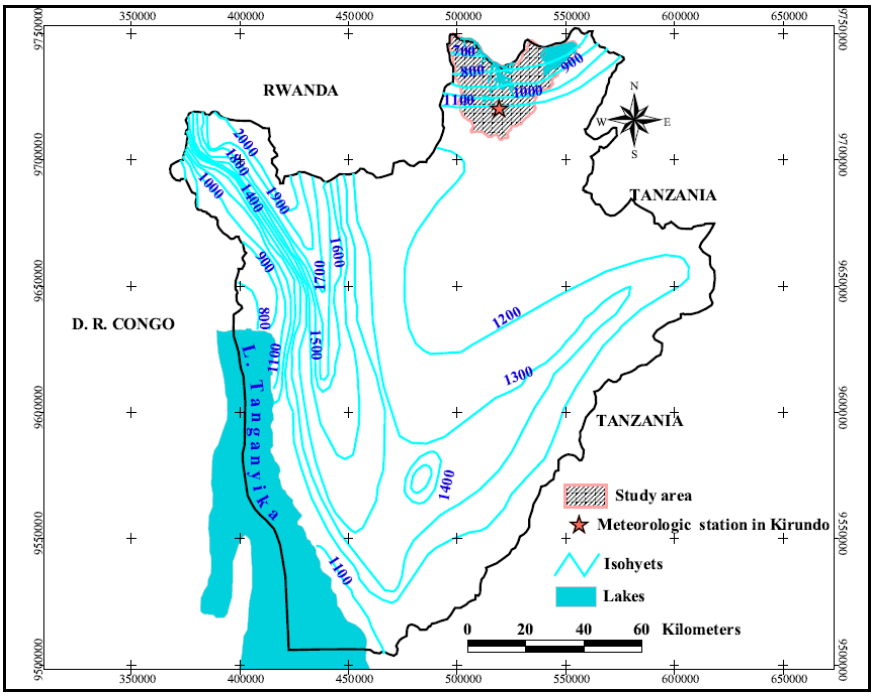

Figure V.10. Map of isohyet contours in Burundi (source: Atlas du Burundi, 1979)

V.3.3. Inter-annual variations of groundwater levels

Inter-annual variations of groundwater levels were assessed by comparing groundwater levels measured in August 1991, September 2006, October 2007 and October 2008 (Appendix V.3). Groundwater level measurements in August 1991 were performed by S.H.E.R Ingénieurs Conseils (1992), a Belgian consulting firm, within the framework of the hydrogeological evaluation of hand-dug wells constructed between 1989 and 1991 by the so-called *projet Kirundo,* a development project of the Kirundo Province, and the siting of new wells which were foreseen to be constructed in 1992 by the same project. Measurements of groundwater levels in 2006, 2007 and 2008 were performed within the framework of the present PhD research. Figure V.11 to V.14 present some representative graphs showing the inter-annual variation of groundwater level in the Northeast (Figure V.11), in the central part (Figure V.12), in the Southwest (Figure V.13) and in the western part of the study area (Figure V.14) for the years 1991, 2006, 2007 and 2008. Wells represented in Figure V.11 to V.14 are shown on a map in Figure V.15.

Overall, although the water level in 1991 was measured in August, i.e. during the dry season, it appears that there is a clear declining trend of the groundwater level between 1991 and 2006. This decline of the groundwater level was systematically observed in most of the hand-dug wells and some of them were further deepened at the end of the 90's and beginning of the 2000's amid a severe drought which prevailed in the region of Bugesera from 1998 to 2001. This might explain the drop of water level between 1991 and 2006 observed in most of the wells (Figures V.11 to V.14, Appendix V.3). Deviations to this general trend of groundwater level fluctuations are due to some external causes including errors taking measurements, random variation of groundwater level in producing wells or waste thrown inside the well. Indeed, during the civil war which prevailed in Burundi from 1993 to 2005, several hand-dug wells were vandalised by people who wanted to steal either the pump or iron bars used to build the wells. Moreover, most of these vandalised wells were left open in agricultural fields where local farmers kept on throwing agricultural waste into the wells. All these materials thrown into the wells may not allow an accurate measurement of the groundwater level. On the other hand, it is also possible that the high amplitude of variation of groundwater level between 1991 and 2006 could be also ascribed to the difference of months of measurements. Indeed, it can be seen from Figures V.3 to V.5 that groundwater level starts to decline from, May or June and reaches the lowest level in October. Hence, when measurements of groundwater level are performed in August (in idle wells) like in 1991, they are likely to give high level because the groundwater level is still declining and has not yet dropped to its lowest level, which is attained in October.

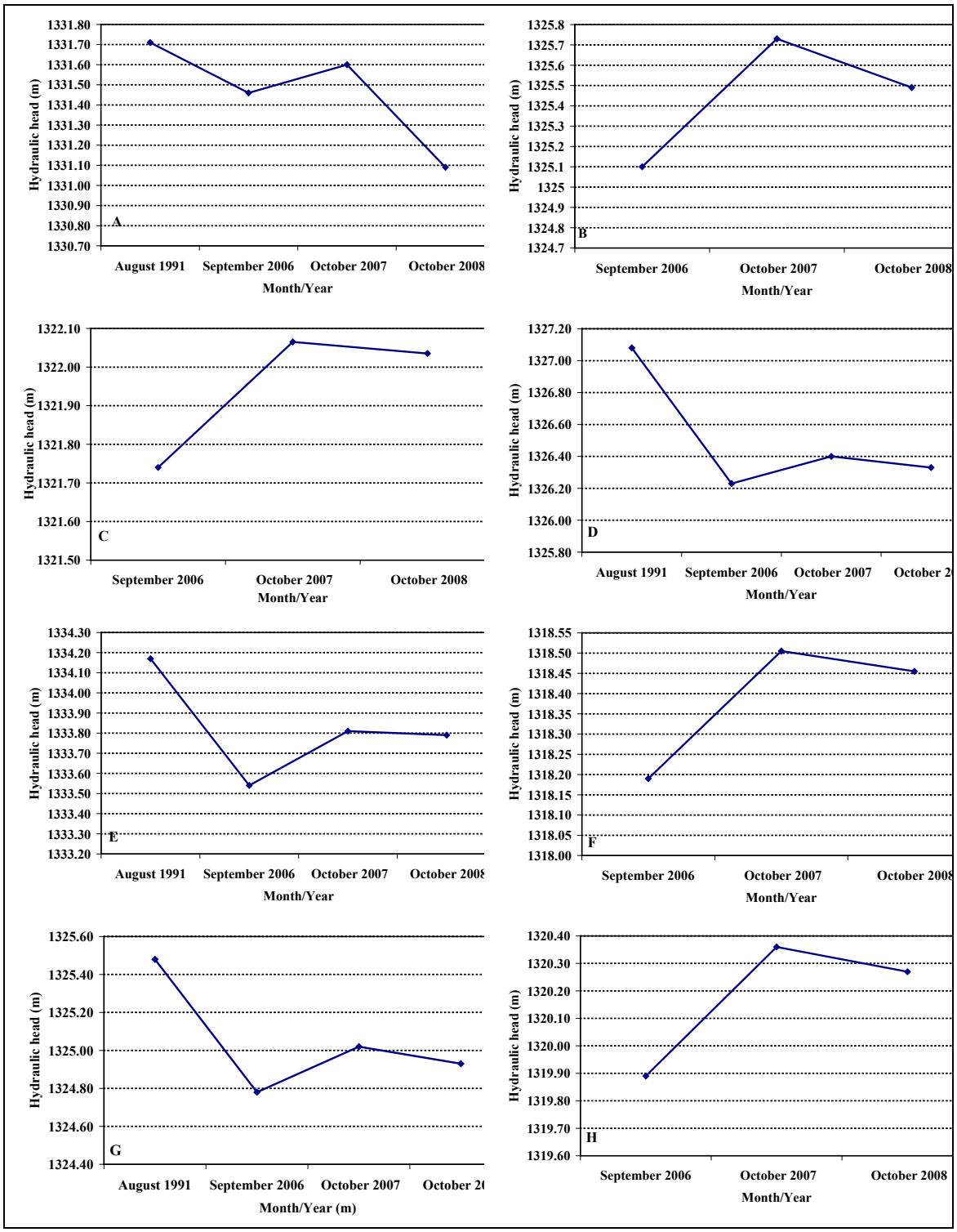

Figure V.11. Inter-annual groundwater level fluctuations in the northeastern part, for the wells at Bidogo-Gatete (A: Nr 128), Cimbogo-Gatete I (B: Nr 139), Gikombe-Nyagisozi (C: Nr 159), Mago I-Gatete (D: Nr 203), Rukera-Gatete (E: Nr 254), Sigu-Kumana (F: Nr 281), Vyanzo I-Gatete (G: Nr 282) and Vyanzo II-Gatete (H: Nr 283) (hydraulic head in m above the local datum Arc 1950 for Burundi). Numbers (Nr) refer to the table in Appendix V.1

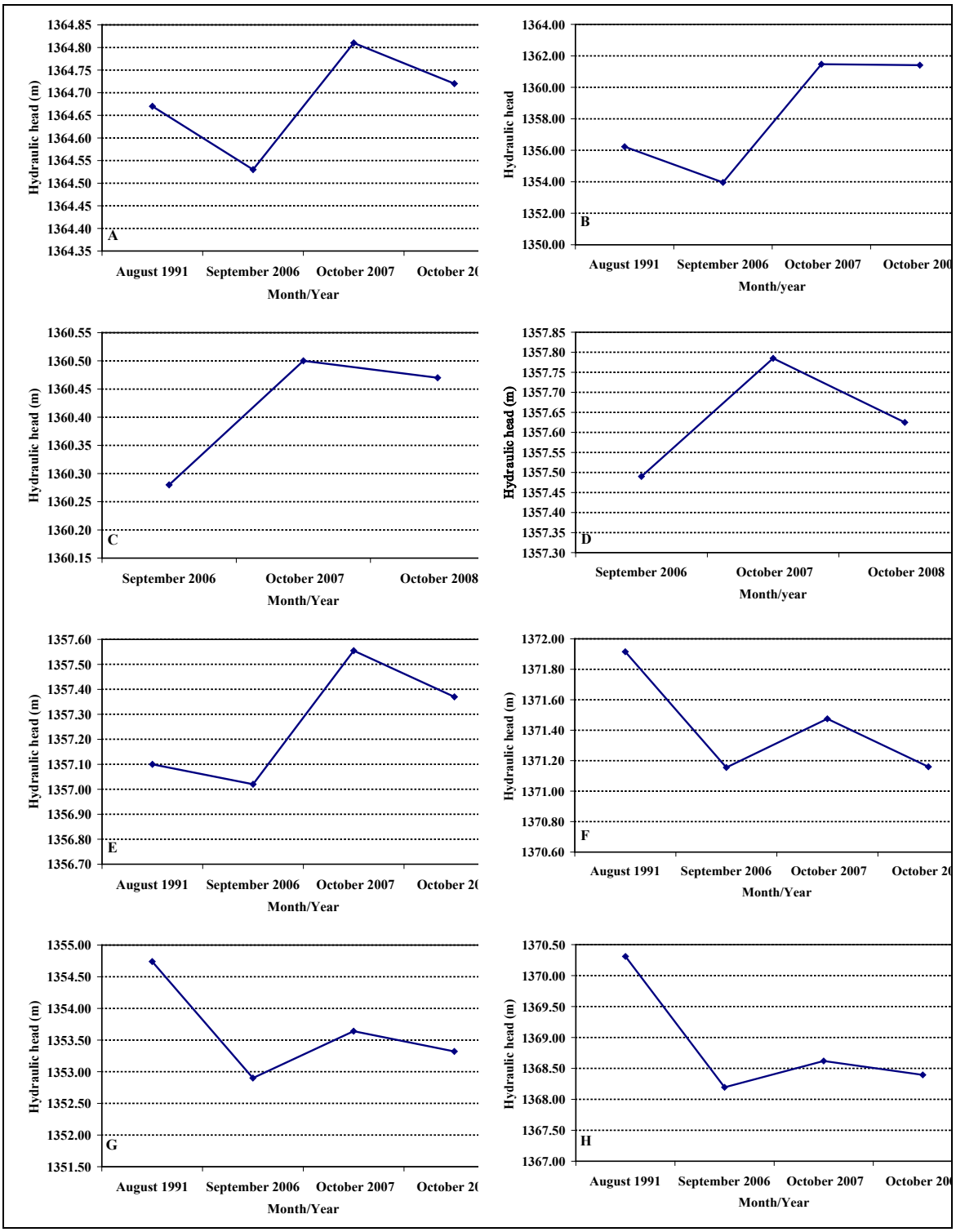

Figure V.12. Inter-annual groundwater level fluctuations in the central part, for the wells at Bugera-Bugera (A: Nr 134), Bunyari-Rugarama (B: Nr 135), Gaharata-Murama (C: Nr 145), Gitamo I-Murambi (D: Nr 163), Gitamo II-Murambi (E: Nr 162), Karago-Runyonza (F: Nr 236), Nunga I-Yaranda (G: Nr 182) and Ruranzi-Rwibikara (H: Nr 265) (hydraulic head in m above the local datum Arc 1950 for Burundi). Numbers (Nr) refer to the table in Appendix V.1

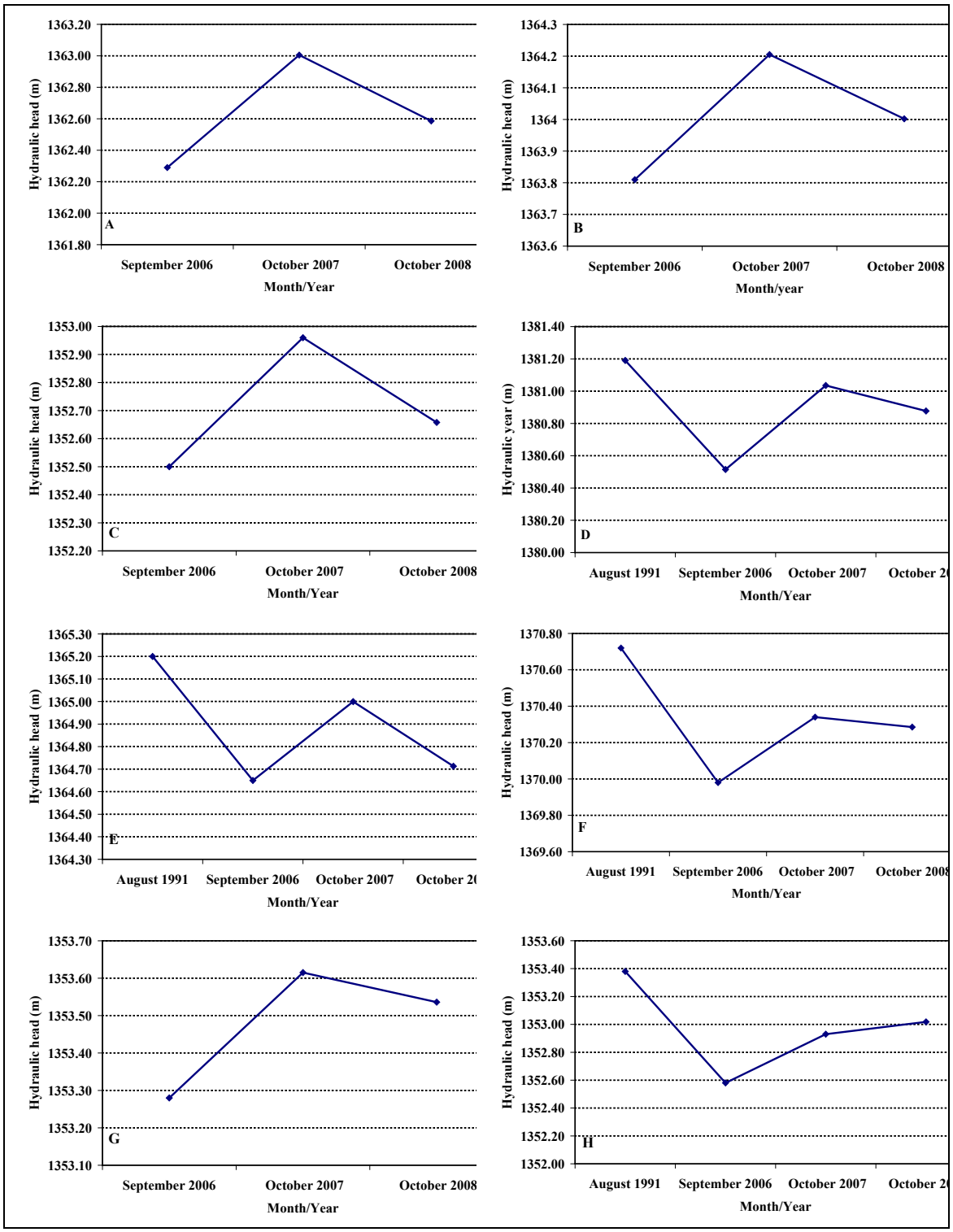

Figure V.13. Inter-annual groundwater level fluctuations in the southwestern part, for the wells at Gahenda-Mugendo (A: Nr 146), Gikomero-Susa (B: Nr 160), Kariba-Kanyagu (C: Nr 183), Murehe-Murungurira (D: Nr 219), Ngugo I-Kanyagu (E: Nr 228), Ntwago-Murungurira (F: Nr 224), Renga II-Gitwenzi (G: Nr 243) and Ruseno-Kanyagu (H: Nr 265) (hydraulic head in m above the local datum Arc 1950 for Burundi). Numbers (Nr) refer to the table in Appendix V.1

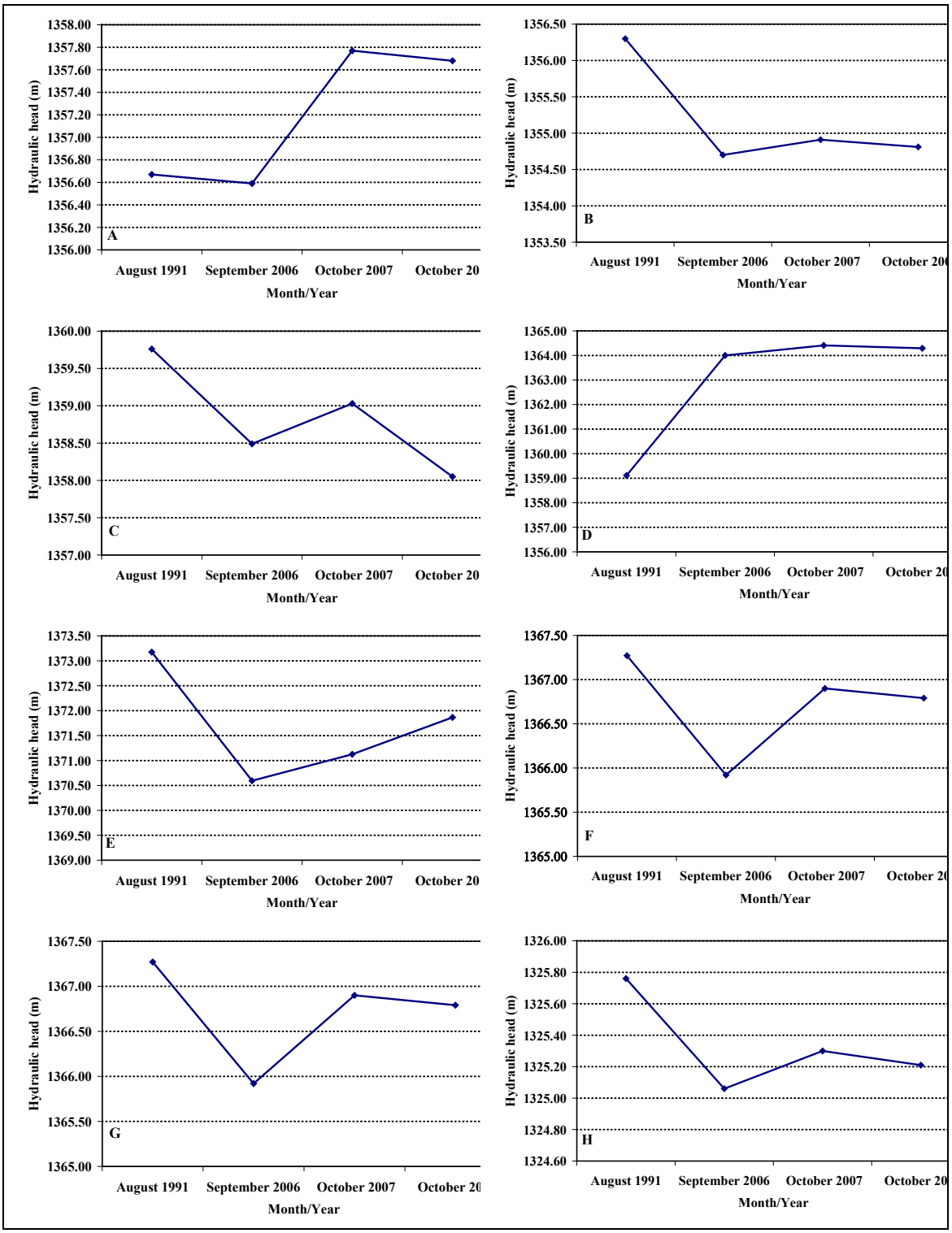

Figure V.14. Inter-annual groundwater level fluctuations in the western part, for the wells at Kabirizi-Kigoma (A: Nr 70), Kanigo-Cinuma (B: Nr 179), Kinyamateke-Nyabikenke (C: Nr 197), Mukuyo-Kiri (D: Nr 213), Ngaragu-Kiri (E: Nr 224), Rubirizi-Gaturanda (F: Nr 244), Rukindo-Rugasa (G: Nr 255) and Saruduha I-Rugasa (H: Nr 276) (hydraulic head in m above the local datum Arc 1950 for Burundi). Numbers (Nr) refer to the table in Appendix V.1

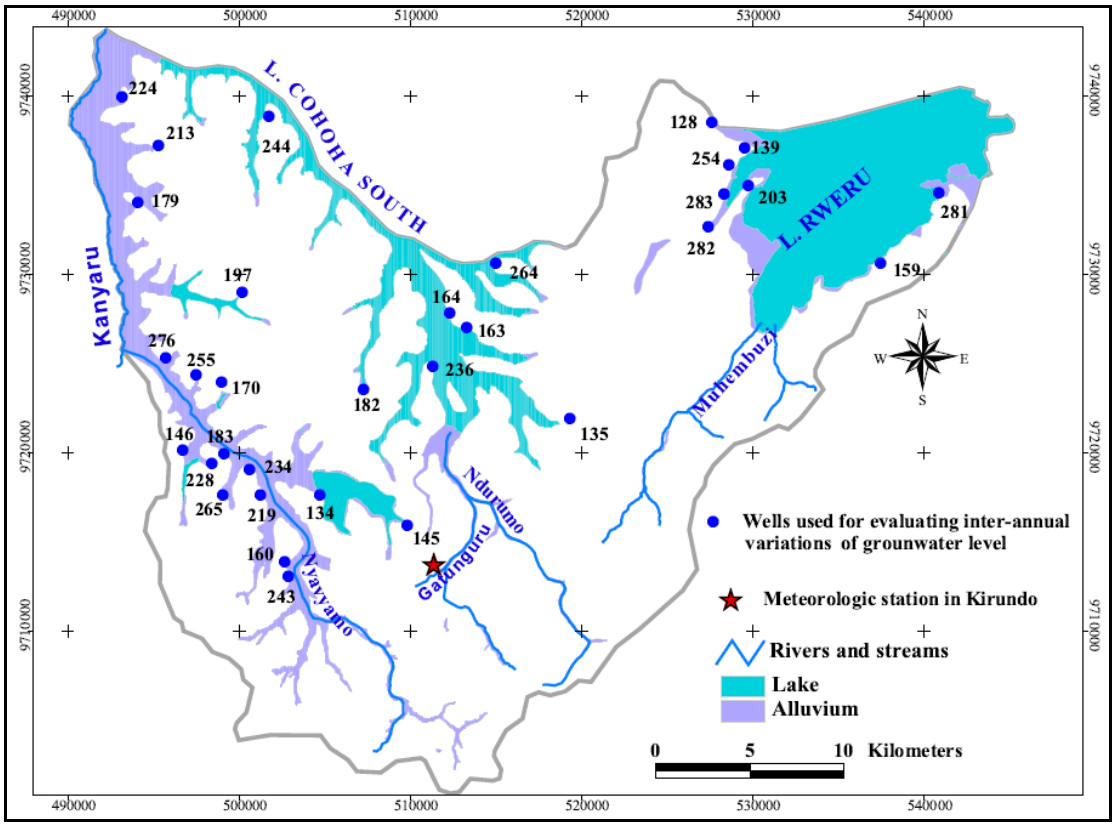

Figure V.15. Wells with piezometric measurements (performed in August 1991, September 2006, October 2007 and October 2008)

Table V.3 shows descriptive statistics of characterising the inter-annual variation of groundwater level between 1991 and 2006 (26 observations), between 2006 and 2007 (46 observations) and between 2007 and 2008 (44 observations). Variation of groundwater level between two years is evaluated by calculating the difference between the available piezometric levels (m above datum) in the same well corresponding to the two years. For instance, variation of groundwater level between August 1991 and September 2006 is calculated as the difference between the piezometric levels in a well observed in september 2006 and August 1991. Positive difference means that there has been a rise of groundwater level between the two considered years, whereas a negative difference indicates that a drop of groundwater level occurred. Only non producing wells are considered. It can be observed from this table that there is an overall decreasing trend of groundwater level between 1991 and 2006 with an average decrease of 0.66 m. However a comparison of the water levels measured in September 2006, October 2007 and October 2008 reveals that, overall, higher levels of groundwater were recorded in 2007, as a result of abundant rainfall and the resulting increased recharge compared to the other two years. On the other hand, a comparison of the years 2006 and 2008 shows that groundwater levels were, in most of the cases, higher in 2008 than in 2006. Between 2006 and 2007, there is an average increase of groundwater level of 0.37 m while between 2007 and 2008, there is an average decrease of 0.17 m. By

considering that nearly no recharge occurs in September-October which is the beginning of the hydrologic year, it can be assumed that the groundwater levels measured in October are mainly attributable to the recharge which occurred during the previous hydrological year. Hence, the differences in groundwater levels observed in August 1991, September 2006, October 2007 and October 2008 are in agreement with the amount of annual recharge calculated for the hydrologic years 1990-1991 (317.5 mm), 2005-2006 (149 mm), 2006-2007 (344 mm) and 2007-2008 (221.5 mm) using the Thornthwaite monthly water balance model (Figure V.16). Compared to an average drop of 0.10 m between September and August calculated from abandoned wells monitored in 2008 (Appendix V.2), the decrease of 0.66 m from August 1991 to September 2006 can not be only explained by seasonal variation of groundwater level. This important decrease of groundwater level is the result of a combination of the general seasonal decrease between August and September on the one hand and, most importantly, the decrease of groundwater level stemming from the significant reduction of groundwater recharge on the other hand. Indeed, groundwater recharge calculated for the hydrologic year 2005-2006 is less than half of that estimated for 1990-1991 (Figure V.16).

However, a deviation from this general trend is observed in some wells such as the wells located in the municipality of Busoni, in Bidogo-Gatete (Figure V.11 A) and Kinyamateke-Nyabikenke, in the municipality of Bugabira (Figure V.14 C) where water levels were higher in 2006 than in 2008, despite a substantially higher groundwater recharge in 2008. This deviation is due to errors in taking measurements or to producing wells, like the well in Kinyamateke-Nyabikenke, where groundwater level randomly varies depending on whether the measurement is taken before or after villagers have already fetched water.

Table V.3. Comparison of amplitude of inter-annual variations

Periods	**1991-2006**	**2006-2007**	**2007-2008**
Number of observations	26	46	44
Maximum (m)	0.77	0.98	0.25
Minimum (m)	-1.96	-0.09	-0.98
Average (m)	-0.66	0.37	-0.17
Standard deviation	0.66	0.23	0.25

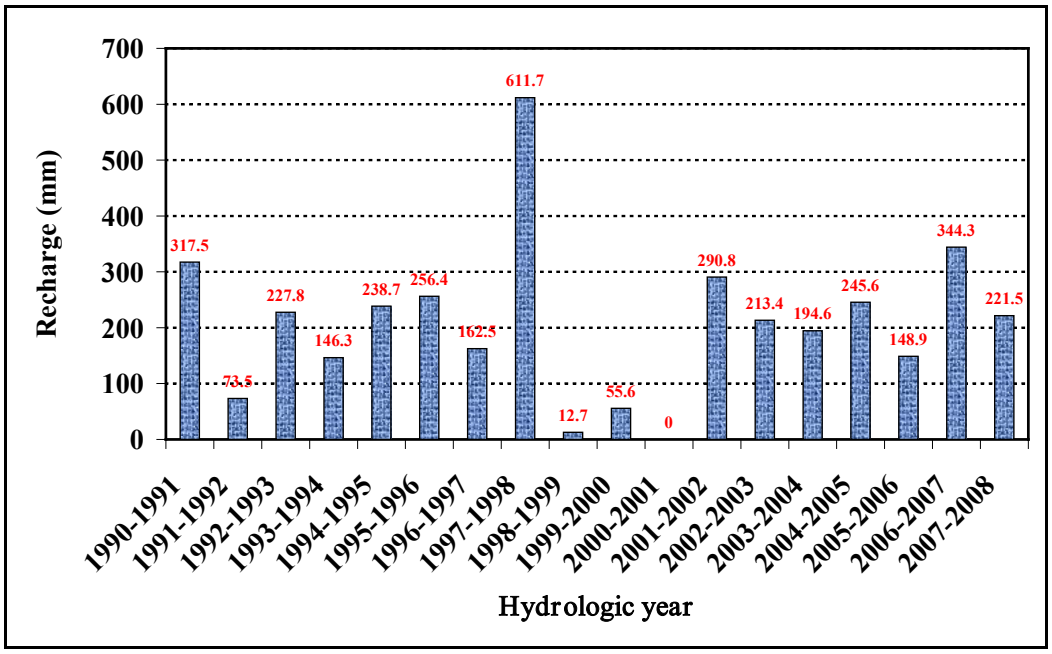

Figure V.16. Annual groundwater recharge (in mm) calculated using the TMWB model from 1991 to 2008

V.3.4. Groundwater flow system

The hydraulic gradient which is defined as the difference of groundwater head over a certain distance between two locations is the driving force of groundwater flow. Groundwater flows in the direction of the maximum hydraulic gradient. The observed hydraulic head, in the study area, varies between 1757 m and 1315 m (above the local datum Arc 1950 for Burundi) respectively for the spring at Muryaruhuma-Muramba situated on the mountain Muramba and the well at Cimbogo-Gatete which is located within the depression. Overall, the highest values of hydraulic heads are found in the southern and eastern highlands, while the lowest values are mostly observed within the depression. This observation indicates that the southern and eastern highlands form the main recharge area, whereas the depression in which lies the complex of marsh lands and lakes, constitutes the discharge area. Figure V.17 presents the piezometric map of the study area as inferred from the information on groundwater level in different wells and the topographic elevation of the numerous springs emerging in the highlands. The lines represent the equipotential lines which connect locations of equal hydraulic head. The arrows represent the flow direction which is perpendicular to the equipotential lines. The complexity of the groundwater flow pattern can be noted, which is a consequence of the complex and rugged topography. The contour lines which represent the elevation of the groundwater table are very close, thus indicating a rapid and abrupt decrease of the hydraulic head over short distances, mainly near the highlands. Hence, on a regional scale, an analysis of the groundwater flow system reveals that, overall, groundwater flows from the recharge area in the highlands towards the depression,

where it discharges into the lakes and marshlands. However, it can be observed that, on a local scale, groundwater flows to the locally draining streams where equipotential lines form V-shapes indicating that the streams are gaining water from the aquifer. Indeed, during the rainy season, most of the small valleys which dissect the highlands are occupied by ephemeral streams whose discharge strongly decreases and eventually disappears during the dry season. The occurrence of these ephemeral streams results from the rising of the groundwater surface in the recharge area during the rainy seasons, which eventually intercepts the banks of the small valleys, thereby causing groundwater to flow into the numerous narrow valleys. The only perennial streams are Nyavyamo, Ndurumo, Gatunguru and Muhembuzi.

Figure V.18 gives a simplified view of the complex flow system presented in Figure V.17 which can be summarised into 5 groundwater flow basins. Numbers in the figure represent the hydraulic heads of some wells and springs which help visualise the direction of groundwater flow. The eastern part of the study area forms the groundwater flow basin of Lake Rweru (IV). It comprises the part of the study area situated at the East of the axis Kiravumba-Rusarasi-Gisenyi-Marembo-Murehe. In this basin, groundwater is mainly drained by the perennial stream Muhembuzi, and occasionally by several other ephemeral streams originating from the highlands, or flows directly to Lake Rweru. The western part of the study area comprises two groundwater flow basins. The northwestern part of the study area forms the Gacamirinda-Kanyaru basin (I) and includes the part of the study area girdled by the axes Kiri-Ruhehe-Kigoma and Kigoma-Rukindo. Groundwater in this part flows directly to the River Kanyaru or to the Lake Gacamirinda. The southwestern part of the study area corresponds to the Rwihinda-Nyavyamo groundwater flow basin (II) and is situated between the axes Rukindo-Kigoma and Kigoma-Yaranda-Rugero-Kiziba. Besides the numerous ephemeral streams flowing from the southern highlands, this groundwater basin is mainly drained by a vast marshy complex comprising the perennial stream Nyavyamo and the lakes Narungazi, Nagitamo, Nampete and Rwihinda. In the central part of the study area, groundwater flows directly to Lake Cohoha south or through the perennial stream Ndurumo and its tributary Gatunguru. Several ephemeral streams also originate from the southern highlands during the rainy season and drain into the two perennial streams. This central part of the study area forms the groundwater flow basin of the lake Cohoha South (III). In the northeastern extremity of the central part of the study area, there is a small portion of the groundwater flow basin of the Lake Cohoha-North whose major part is situated in Rwanda. There are no observations of piezometric levels in this part of the study area.

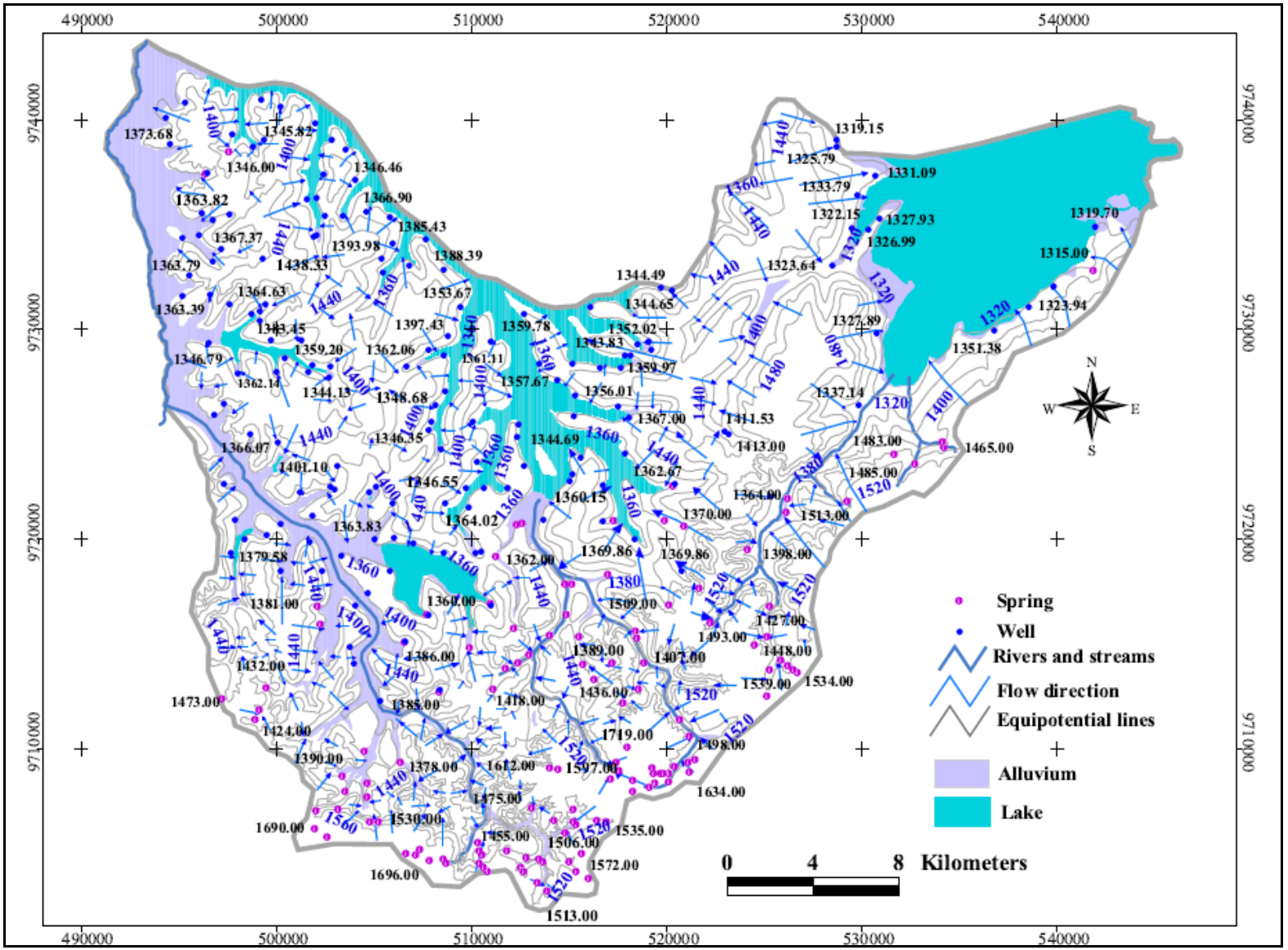

Figure V.17. Piezometric map of the study area (hydraulic head in m above the local datum Arc 1950 for Burundi)

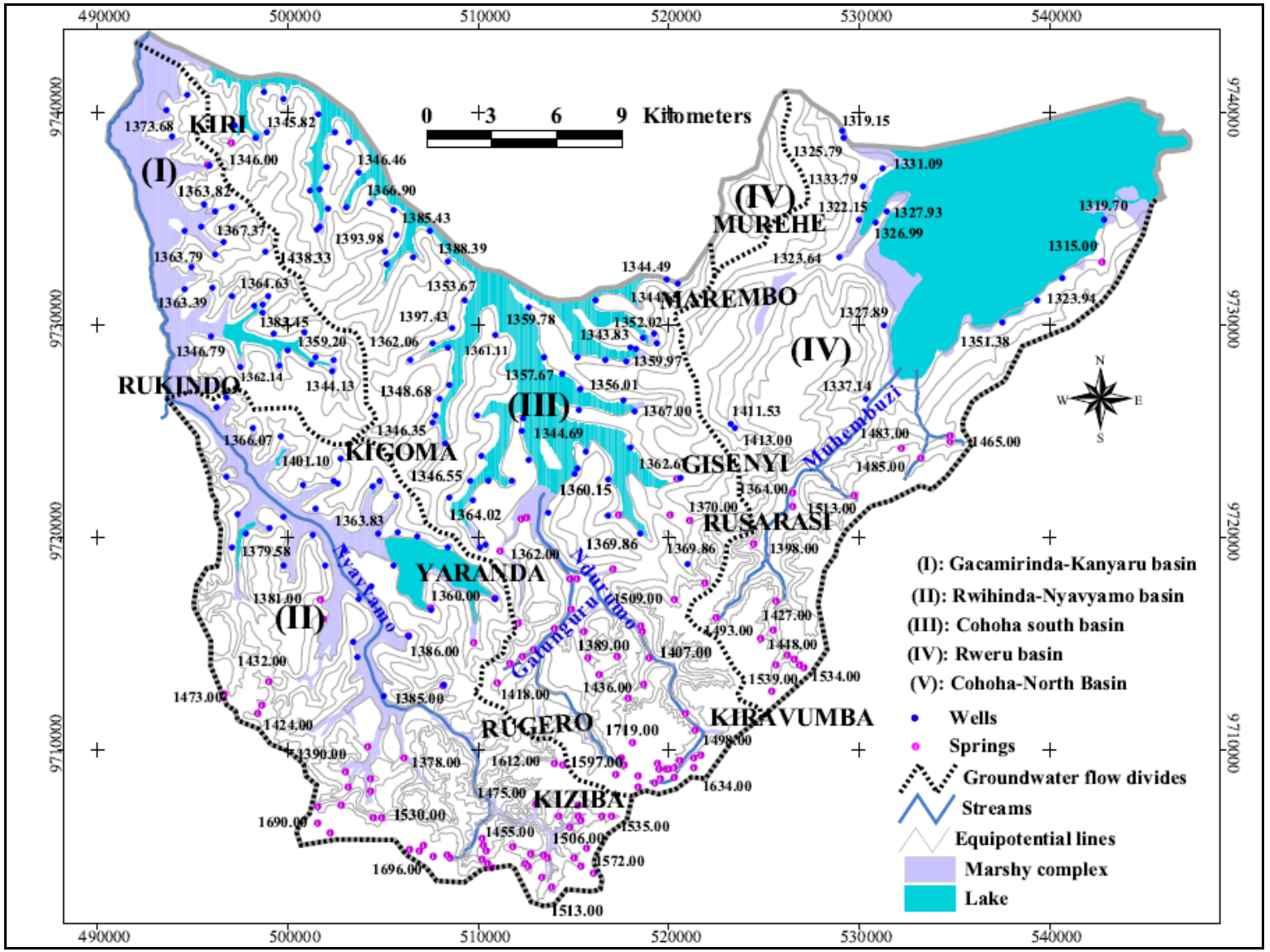

Figure V.18. Groundwater flow basins (numbers are hydraulic heads in m above the local datum Arc 1950 for Burundi)

V.4. Conclusions and recommendations

The groundwater flow system in Bugesera region is defined based on information about the hydraulic head of groundwater in 157 wells, which is complemented by the topographic elevation of 126 springs, mainly in the southern part of the study area which constitutes the main recharge area. The locations where emerge the springs are considered as the "outcrops" of the groundwater and the hydraulic head is assumed to be equal to the topographic elevation. The hydraulic head is computed based on the measurements of groundwater level performed within the framework of this research in September 2006, October 2007 and October 2008, complemented by available groundwater levels measured in August 1991, in order to evaluate the inter-annual variations of groundwater level. In addition, monthly measurements of the fluctuation of groundwater level were performed in 2008 in order to analyse the inter-seasonal fluctuations of groundwater level.

Overall, there is a decreasing trend of groundwater level from 1991 to 2006, while between 2006 and 2008, there is a peak of groundwater level in 2007 compared to 2006 and 2008 and this is in agreement with the amount of annual recharge calculated from 1990/1991 to 2007/2008. Overall the inter-annual fluctuation of groundwater levels are in line with the amount of recharge calculated. Groundwater level in 2008 is generally higher than in 2006 in most of the wells, but there are some cases where a reverse situation is observed and this is due to errors in measurements or measurements taken in producing wells, where random variations of water level occur depending on whether the measurement was taken before of after local villagers have already fetched water from the well. The fluctuation of groundwater level in the course of the year 2008 shows a trend which closely follows that of the recharge, with an important peak mostly in May and a less pronounced peak in December.

Maxima of groundwater levels (average: 1366.06 m) are observed in the southwestern part of the study area, which is close to the southern and eastern highlands forming the recharge area. The lowest water levels (average 1323.33 m) are found in the northeastern part of the study area, around the Lake Rweru. On the contrary, the maximum average amplitude (0.90 m) of seasonal groundwater level fluctuations is found in the northeastern part of the study area, whereas the minimum average amplitude (0.34 m) is found in the central part of the study area. The southwestern part of the study area shows an intermediate average amplitude of water level fluctuations (0.54 m). The amount of recharge and the hydraulic conductivity are the main factors controlling the amplitude of seasonal fluctations of groundwater level. The peaks of seasonal groundwater level in the 3 parts of the study area occur at different times: April in central part, May in northeastern part and June in southwestern part. Beside the

spatial variability of rainfall distribution, the occurrence of the peak of groundwater level at different times of the year implies different duration for the travel of the recharge. This observation seems to confirm that the central part of the study area where the peak of groundwater occurs early (April) has the highest hydraulic conductivity, while the northeastern and southwestern parts of the study area, which are underlain by metasedimentary formations and where the peaks appear respectively in May and in June, have lower hydraulic conductivities. This parameter determines the duration of the travel of the recharge in the unsaturated zone.

An analysis of the groundwater flow pattern reveals both a local flow towards the perennial and ephemeral streams and a more regional flow from the southern and eastern highlands towards the depression, where the complex of marshlands and lakes forms the main discharge area. The groundwater flow system shows a complex pattern which could be expected, given the complexity of the topographic setting. The complex groundwater system can be simplified into 5 groundwater flow basins, which are: the basin of Lake Rweru to the East, the basin of Lake Cohoha South in the centre of the study area, the basin of Lake Cohoha North in the northeastern extremity of the central part, the basin of River Navyamo and Lake Rwihinda in the southwestern part and the basin of River Kanyaru and Lake Gacamirinda in the northwestern part of the study area.

Given the worldwide climatic changes which inevitably affect groundwater resources, this study recommends to the Government of Burundi to start, as soon as possible, a countrywide programme of monitoring groundwater levels, especially in regions where potable water is still scarce like Bugesera, the plain of Imbo (Bujumbura) and the eastern depression of Moso. This would help decision-makers to follow closely the availability of this vital resourse and to envision adequate measurements in case of severe depletion.

CHAPTER VI. GROUNDWATER FLOW MODEL

VI.1. Introduction

Increasing water resources development over the past decades has prompted the application of numerical models in order to predict the effects of management measures of hydrological systems at basin or regional scales. In the recent past, the use of groundwater flow models has been strongly boosted by the wide availability of powerful computers, user friendly modelling and GIS softwares (Yangxiao & Wenpeng, 2011). Nowadays, the use of numerical groundwater models is increasingly becoming a standard and unavoidable tool in groundwater and environmental investigations. Groundwater models allow a better understanding of groundwater flow systems and thus, offer a valuable tool for groundwater resources evaluation and management, groundwater quality assessment, site contamination assessment and remediation, environmental impact review and other environmental related issues. More importantly, groundwater flow models are nowadays serving as a useful and practical tool in modelling the transport of different contaminants for risk evaluation. According to Mace (2001), numerical flow models are efficient tools which can combine a complex array of aquifer variables (hydraulic properties, recharge, groundwater abstractions, surface water bodies, structure and heterogeneities) and simulate their interactions in order to understand the behaviour of an aquifer system under natural and man-induced stresses. In a more general way, a groundwater flow model is a simplified representation of complex aquifer systems by means of mathematical equations and simplifying assumptions with a view to replicating as much as possible the way natural systems operate and may respond to different management scenarios.

Yangxiao & Wenpeng (2011) summarise the main issues which are commonly addressed by groundwater flow models. Groundwater professionals often resort to numerical models as : (1) interpretative tools for understanding groundwater system dynamics and flow patterns; (2) simulation tools for investigating the response of aquifers to different stresses; (3) assessment tools for evaluating the processes of recharge, discharge and storage, as well as quantifying sustainable yield; (4) predictive tools for forecasting future conditions or impacts of human activities on groundwater system; (5) supporting tools for planning field data collection and designing practical solutions; (6) screening tools for evaluating groundwater development scenarios; (7) management tools for assessing alternative policies; and (8) visualization tools for conveying understandable messages to public and decision-makers. On the other hand, according to Mace (2001), regional groundwater flow models can be roughly classified into two groups, namely scientific and management models. While scientific models are aimed at better understanding groundwater flow in aquifer systems and the way they operate, management models are generally meant to make predictions or evaluate

management scenarios. The two groups of models are however somehow complementary in the sense that management models may build on previously developed scientific models, whereas management models can considerably increase the understanding of the aquifer system, i.e. the scientific models.

The use of groundwater flow models dates long back in the history of groundwater investigations (Yangxiao & Wenpeng, 2011; Zhang, 2011). In this long history of groundwater modelling, several software packages such as the USGS 3D finite difference model (Trescott, 1975), the Finite Element subsurface Flow (FEFLOW) model developed since 1979 by the Institute for Water Resources Planning and Systems Research Inc. (WASY GmbH) of Berlin (Germany) (Trefry & Muffels, 2007), the 3D control-volume finite element groundwater model HydroGeoSphere developed jointly by the Groundwater Simulations Group and Hydrogeologic Inc. since 1995 (Therrien *et al.*, 2010) are in use but, as of now, it is undoubtedly the finite difference MODFLOW program (McDonald and Harbaugh, 1988) and its update versions MODFLOW-2000 (Harbaugh *et al.*, 2000) and MODFLOW-2005 (Harbaugh, 2005) conceived by the USGS, and its user-friendly implementation Visual MODFLOW developed by Waterloo Hydrogeologic Inc. since 1994, which are the most popular and widely used by groundwater professionals around the world, owing to their completeness and easy-to-use graphical modelling environment for 3-dimensional groundwater flow and contaminant transport simulations. In this study Visual MODFLOW V.3 (Waterloo Hydrogeologic Inc., 2002) was used to develop and calibrate a groundwater flow model for the aquifer system of Bugesera region in northeastern Burundi.

VI.2. Groundwater flow modelling

VI.2.1. Overview of groundwater flow modelling theory

Mathematical models simulate groundwater flow by means of governing equations that represent the physical processes occurring within the system and equations describing heads and flows along the boundary of the model. Mathematical models can be analytical or numerical. Analytical models are based on the exact solution of a specific flow or transport equation which is the simplification of more complex three-dimensional groundwater flow or solute transport equations. Inevitably analytical models make use of restrictive and simplifying assumptions in order to simulate the otherwise more complex field situations. To deal with more realistic and complicated situations, numerical models are commonly used. Numerical flow models are based on one or more partial differential equations describing the groundwater flow under given conditions and which are solved using numerical and iterative techniques. The differential equations are solved using a number of approximations such as Finite Differences or Finite Elements. Numerical models whether Finite Difference or Finite Element Models, consider the study area as a grid of small cells or elements with given

properties and nodes where the head will be computed. The nodes may be the corners of the cells or their centres. While the shape of cells in the Finite Element Method may be irregularly shaped blocks, the Finite Difference Method involves the division of the modelled area into regular polygonal shapes such as hexagons or rectangles. The finite difference method simulates groundwater flow using a system of polygonal grid cells, commonly with block-centred nodes. The accuracy of a numerical model strongly depends on the quality of model input data, the size of the space and time discretisation and the numerical method used to solve the model equations. Physical parameters such as hydraulic conductivity, transmissivity, storage, porosity and aquifer thickness are defined in each grid cell and are considered to be constant. Hence, each grid cell can be considered as having a unique combination of physical parameters and this can enable to incorporate the space dimension in the variation of these parameters.

VI.2.2. Overview of governing groundwater flow equations

The first step in developing a mathematical model of any system is to translate the conceptual model of the physical system into a mathematical formulation in terms of general equations. In the case of groundwater flow, general equations are differential equations which describe physical principles governing groundwater flow. More precisely, for groundwater flow, the relevant physical principles governing groundwater flow are Darcy's law and mass balance also known as the continuity equation. The partial differential equation governing the general flow equation is derived from the combination of the mathematical relation describing each physical principle.

Darcy's law for one-dimensional groundwater flow is mathematically expressed as:

$$Q = -KA\left(\frac{dh}{dl}\right)$$

where Q is the discharge rate in the l direction in $L^3\ T^{-1}$, K is the hydraulic conductivity in L/T and dh/dl is the hydraulic gradient in the direction l, A is the cross-sectional area perpendicular to the direction l in L^2. The minus sign is consistent with the fact that groundwater flows in the direction of decreasing hydraulic head. Darcy's law can also be expressed in the form of what is known as the Darcy's flux or Darcy's flow or the specific discharge which is the discharge rate per unit cross-sectional area:

$$q = \frac{Q}{A} = -K\left(\frac{dh}{dl}\right)$$

where q is the Darcy's flux in units of velocity (L/T)

However, in the real subsurface, groundwater flow in the three dimensions features a complex pattern which can be mathematically expressed in a similar manner as one-dimensional flow.

$$q = -\left(K_x\frac{dh}{dx} + K_y\frac{dh}{dy} + K_z\frac{dh}{dz}\right)$$

The continuity equation is one of the fundamental principles used in the analysis of uniform flow, also known as the continuity of flow. The principle stems from the fact that mass is always conserved in fluid systems irrespective of the complexity of flow medium or direction of flow. If steady state conditions prevail and the principle of conservation of mass is applied to a system, the continuity of flow can be defined as: "The mean velocity at all cross sections having equal areas are then equal, and if the areas are not equal, the velocities are inversely proportional to the areas of the respective cross sections". This means that if the flow is constant in a reach of the flow medium, the product of the area and velocity will be the same for any two cross sections within that reach. Mathematically, this law can be simply expressed as:

$$Q = A_1V_1 = A_2V_2$$

where Q is the discharge rate (L^3T^{-1}), A is the cross-sectional area (L^2) and V is the mean flow velocity ($L\ T^{-1}$).

The continuity equation for steady state conditions used in finite-difference models is defined by the Laplace equation in which the storage is equated to zero:

$$\frac{\partial q_x}{\partial x} + \frac{\partial q_y}{\partial y} + \frac{\partial q_z}{\partial z} = 0$$

By combining Darcy's law and the continuity equation for steady state conditions, the three-dimensional flow equation can be written:

$$\frac{\partial}{\partial x}\left(K_x \frac{\partial h}{\partial x}\right) + \frac{\partial}{\partial y}\left(K_y \frac{\partial h}{\partial y}\right) + \frac{\partial}{\partial z}\left(K_z \frac{\partial h}{\partial z}\right) = 0$$

For an incompressible fluid, isotropic and homogeneous medium where $K_x = K_y = K_z$, the three dimensional and steady state groundwater flow can be expressed as:

$$\frac{\partial}{\partial x}\left(\frac{\partial h}{\partial x}\right) + \frac{\partial}{\partial y}\left(\frac{\partial h}{\partial y}\right) + \frac{\partial}{\partial z}\left(\frac{\partial h}{\partial z}\right) = 0$$

For transient flow in a saturated porous medium, the law of conservation of mass requires that the net rate of fluid mass flowing into any reference elemental volume is equal to the rate of change of fluid mass storage within the same element. In more simple terms, the mass conservation law can be stated as:

Mass inflow rate – Mass outflow rate = Change in mass storage per unit time

The change in storage can be expressed in terms of the specific storage coefficient (S_s) which is defined as the volume of water released from storage per unit volume of soil per unit decline in hydraulic head over time. Mathematically, the change in storage can be expressed as:

$$\frac{\Delta Q}{V} = S_s . \frac{\Delta h}{\Delta t}$$

By combining the Darcy's equation and the equation expressing the law of mass conservation, the transient three dimensional groundwater flow equation can be expressed as:

$$\frac{\partial}{\partial x}\left(K_x \frac{\partial h}{\partial x}\right)+\frac{\partial}{\partial y}\left(K_y \frac{\partial h}{\partial y}\right)+\frac{\partial}{\partial z}\left(K_z \frac{\partial h}{\partial z}\right)=-S_s \frac{\partial h}{\partial t}$$

where $\frac{\partial h}{\partial (x,y,z)}$ represents the change of hydraulic head per unit length in x, y, and z directions, $\frac{\partial h}{\partial t}$ is the change of hydraulic head over time, K_x, K_y and K_z are the values of hydraulic conductivities along the x, y and z directions ($L\ T^{-1}$) for heterogeneous and anisotropic aquifer systems.

The partial differential equation for three dimensional groundwater flow used in MODFLOW (McDonald & Harbaugh, 1988) can be written as:

$$\frac{\partial}{\partial x}\left(K_{xx} \frac{\partial h}{\partial x}\right)+\frac{\partial}{\partial x}\left(K_{yy} \frac{\partial h}{\partial y}\right)+\frac{\partial}{\partial z}\left(K_{zz} \frac{\partial h}{\partial z}\right)-W=S_s \frac{\partial h}{\partial t}$$

where W is the volumetric flux per unit volume and represents the sources/sinks for water.

For steady state conditions, $\frac{\partial h}{\partial t}=0$ and the equation governing groundwater flow becomes:

$$\frac{\partial}{\partial x}\left(K_{xx} \frac{\partial h}{\partial x}\right)+\frac{\partial}{\partial x}\left(K_{yy} \frac{\partial h}{\partial y}\right)+\frac{\partial}{\partial z}\left(K_{zz} \frac{\partial h}{\partial z}\right)-W=0$$

VI.2.3. Numerical modelling tool used

For this study, the numerical modelling tool used to simulate groundwater flow in the aquifer system of Bugesera region is the 3D groundwater flow model program MODFLOW-2000 developed by the USGS (Harbaugh et al., 2000) which is imbedded into the window-based graphic user interface Visual MODFLOW V.3 (Waterloo Hydrogeologic Inc. (2002). Visual MODFLOW V.3 is a 3D and block-centred groundwater flow model which makes use of the finite difference method to solve the derivatives of the partial differential equation with approximate linear equations for determining the hydraulic head within each cell. The result of the model calculations is a head distribution for the modelled area based on individual head values calculated for each grid cell as well as an accounting of the water flow entering and leaving each cell which is displayed as the hydrologic budget (Waterloo Hydrogeologic Inc., 2002).
Visual MODFLOW offers a user-friendly modelling environment for simulating three dimensional groundwater flow as well as contaminant transport. The program provides the user with the possibility to: (1) graphically design the model grid, properties and

boundary conditions, (2) visualise the model input parameters and results in two or three dimensions, (3) simulate the groundwater flow, path lines and contaminant transport, (4) automatically or manually calibrate the model, and (5) display and interpret the modelling results.
MODFLOW-2000 comprises a main program and a series of independent subroutines called modules. Each module addresses a specific feature of the hydrologic system to be modelled such as river flow, flow into drains or specific methods of solving linear equations which describe the flow system. This fully integrated package combines Modflow, Modpath, and MT3DMS with a user-friendly graphical interface. The latter is subdivided into three modules including: Input Module, Run Module and Output Module. The Input section is used to set up conditions for groundwater flow and contaminant transport. The Run section enables to translate the model conditions created with the Input section into the standard input files for the appropriate models. The 3D-Explorer in the Output section helps visualise the model results (Waterloo, Hydrogeologic Inc., 2002).

VI.3. Methodology for the groundwater flow model of Bugesera region

The groundwater flow model of the study area was constructed, run and calibrated using the Visual MODFLOW V.3 code (Waterloo Hydrogeologic Inc., 2002). The first step in the process of modelling groundwater flow in the study area was to conceptualise the aquifer system into a set of model layers and to define the boundary conditions. Then, input files for the model including the site map, the model layers, *i.e.* the top and the bottom of each model layer, the topography, pumping and observation wells and their characteristics (pumping rate, screen location, start and end time of the pumping, observed head), boundary maps (rivers, lakes and marshlands) were prepared using ArcView 3.2 and a suite of extensions which enable the conversion of the ArcView shape files into dxf files, ASCII or Surfer grid files before being imported into Visual MODFLOW. The a priori input hydraulic parameters of the aquifer applied to the model are average values estimated from the pumping tests conducted across the study area. After compiling all the input parameters and files the model was run. The final step was the calibration of the model so as to minimise as much as possible the discrepancy between the observed and the calculated values of the model parameters. The calibration of the model was conducted through a process of trial and error consisting of manually adjusting the model parameters with a view to reducing as much as possible the Normalized Root Mean Square error (RMS) and the Mean Absolute error (MA) between the measured and the calculated parameters of the aquifers. The two criteria serve as the benchmark for measuring the accuracy of the model. It is generally accepted that a RMS error below 10 % can be accepted to ascertain that a model has converged with a desired degree of correspondence between the model simulations and observations of the groundwater flow system.

VI.4. Conceptual model and aquifer schematisation

The conceptual model of the aquifer system was developed based on the hydrogeological structure as detailed in Chapter III. The interpretation of several electrical soundings coupled to lithological information from recently constructed wells in the study area reveals two main and distinct units: a thick clay-rich regolith which is underlain by the more resistive basement. Based on the vertical sequence of the geoelectrical layers, the hydrogeological structure was found to be composed of a main aquifer composed of a mixture of alterites wherein the coarse fraction is increasing downwards. The main aquifer is overlain by a more clayey layer in which the static water level rests and which acts as a semi-confining layer. On the other hand, this main aquifer is underlain by the weathered/fractured part of the basement below which extremely high values of resistivity may indicate the presence of an unweathered basement.

Taking into account the hydrogeological structure, the aquifer system was schematised as a succession of three layers including: (1) the upper confining layer which is mostly clayey and in which rests the static water level with an average thickness of 8 m. This layer is part of the regolith and is actually made of a mixture of sand, clay and rock fragments but with a clear predominance of the clay fraction which is underlined by low values of resistivity; (2) the main aquifer which consists of a mixture of alterites comprising clay, sand, gravel and rock fragments with an evident dominance of the coarse fraction which increases downwards as this is evidenced by moderate to high values of resistivity. This layer was assigned an average thickness of 30 m, and (3) the fractured/weathered basement which underlies the main aquifer with an average thickness of 10 m. This layer is characterised by high to very high values of resistivity. Figure VI.1 helps visualise the location of the conceptual cross-sections within the model domain. This simplified schematisation of the aquifer structure is shown in Figures VI.2 & VI.3. However, it does not fully portray the complexities and heterogeneities of the aquifer system of the study area as this was extensively discussed in chapters III and VI.

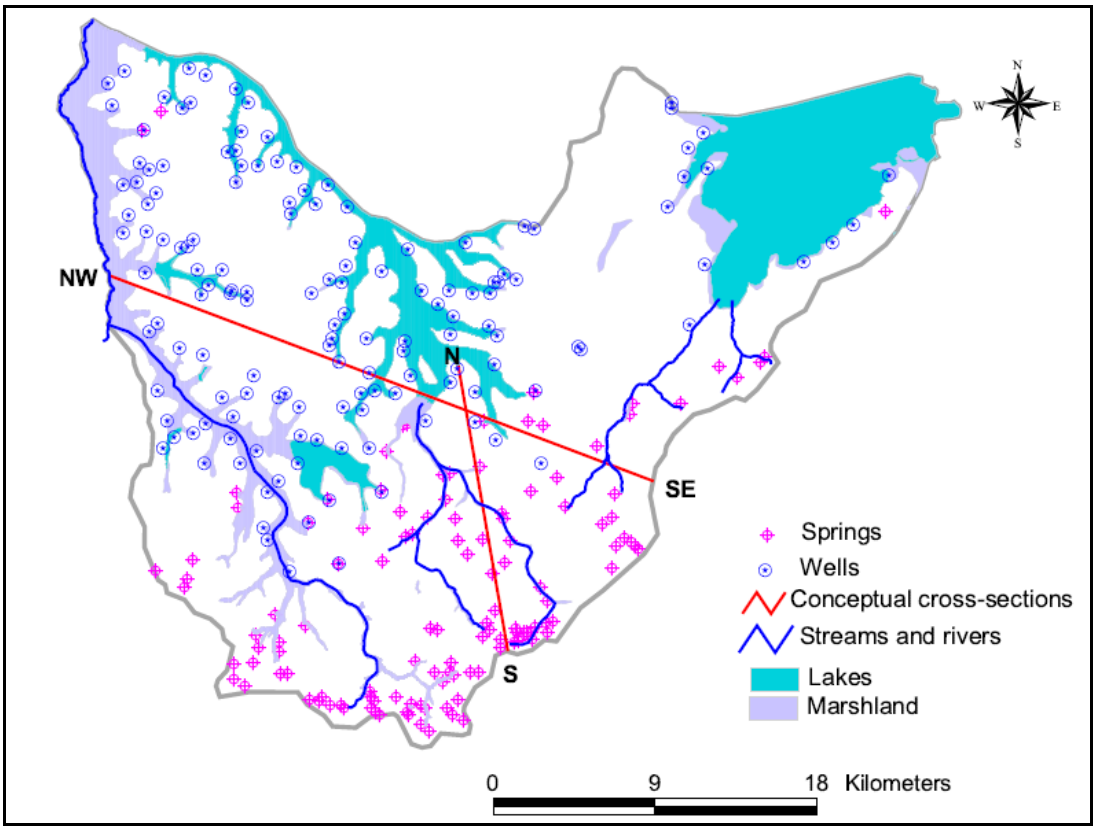

Figure VI.1. Map of the study area showing the model domain and the location of the conceptual cross-sections

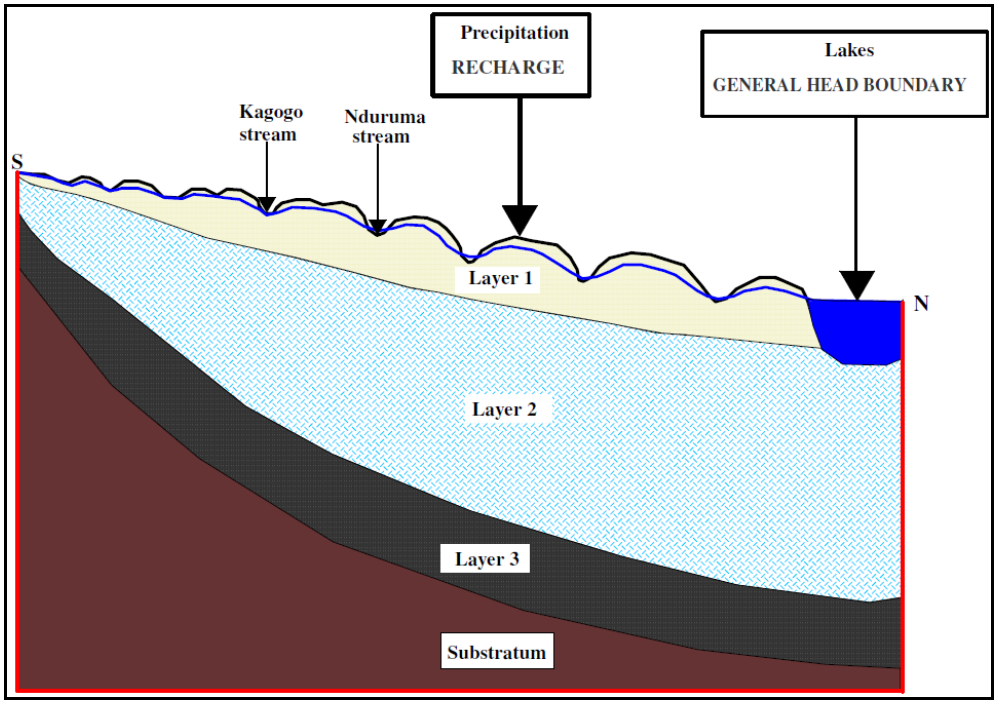

Figure VI.2. Simplified S-N cr oss-section s howing m odel l ayers and bo undary conditions (not to scale)

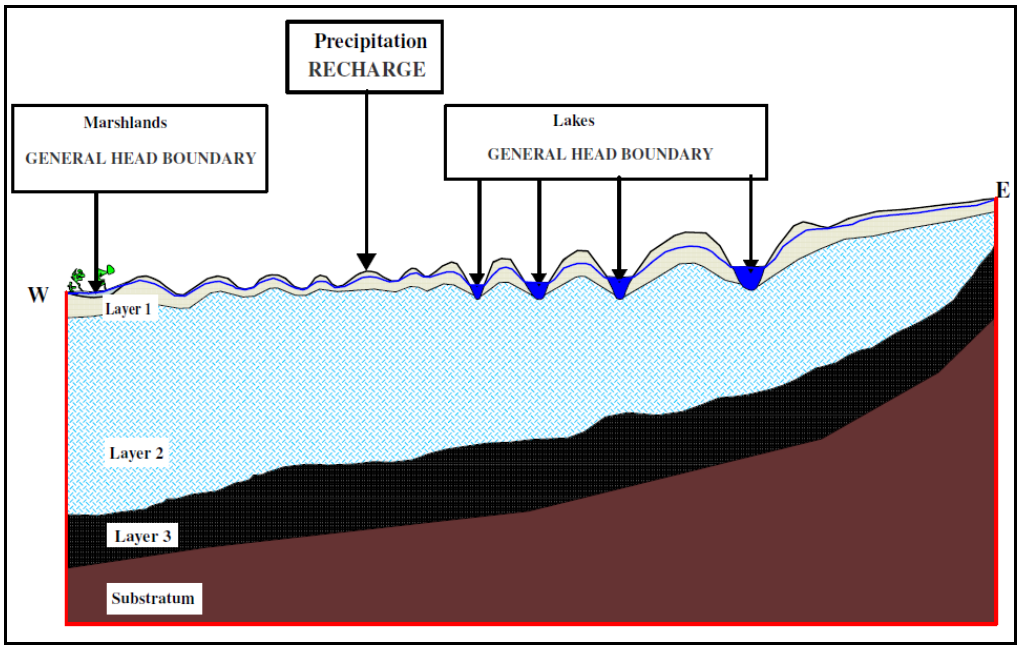

Figure VI.3. Simplified NW-SE cross-sections showing model layers and boundary conditions (not to scale)

VI.5. Model domain and grid definition

The three dimensional groundwater flow model for Bugesera region was developed for an area extending over 1050 km^2. The model domain covers both the southern and eastern highlands as well the depression of Bugesera which is dissected by a complex of marshlands and shallow lakes. It should be recalled here that the highlands are characterised by a rugged topography where the myriad of hills are separated by several V-shaped small valleys in which flow perennial and ephemeral streams. Moreover, even the depression features an undulating topography where alternate large marshy valleys hosting the shallow lakes and rounded hills.

To take into account this rugged topography, the grid was defined as consisting of 225 rows and 278 columns with a spatial resolution of 180 m*180 m for each grid cell. The initial STRM digital elevation model (DEM) with a resolution of 90 m was resampled to a resolution of 180 m. The resampled DEM was used to define the top and the bottom of each layer of the model by subtracting the average thickness of each layer from the elevation of the ground surface given by the DEM. The region outside the model boundary for each of the three layers was set as inactive cells so as to reduce the number of iterations carried out and the memory requirement during the computational process aiming at solving the groundwater flow equation. Figure VI.4 shows the extension of the model domain and the boundary conditions including pumping and observations wells.

VI.6. Hydraulic parameters

The hydraulic parameters used for the model were assigned to the different layers assuming a homogeneous medium in which the hydraulic conductivities in the X (K_x) and Y (K_y) directions are considered to be identical (K_h), while the hydraulic conductivity in the Z direction was assumed to be equal to 1/10 of K_x. Initial estimate of the hydraulic conductivity for the aquifer (second layer), i.e. 0.66 m/d, was adopted considering that the average hydraulic conductivity obtained from the analysis of pumping tests was overestimated due to the fact that the thickness of the aquifer was underestimated. The analysis of 41 pumping tests conducted in the study area during two field campaigns (September to December 2007 and July to October 2008) gave an average transmissivity of 33.10 m^2/d and an average hydraulic conductivity of 14.8 m/d. The value of hydraulic conductivity used in the model for the second layer was obtained by considering an average thickness of 50 m for the weathered overburden and the weathered fractured basement. The average value of transmissivity, i.e. 33.10 m^2/d, (Chapiter IV) was therefore divided by an average thickness of 50 m and the value obtained, i.e. 0.66 m/d, was entered into the model as the initial estimate of the hydraulic conductivity for the second layer. This value of hydraulic conductivity was assigned to the second layer of the model domain because, actually, with a depth varying between 5 m and 17.5 m, most of the hand-dug wells in the study area tap the groundwater resource in the second layer. The hydraulic parameters for the other layers were assigned taking into account their lithology, as revealed by the interpretation of the geoelectrical soundings and the lithological logs of a number of wells recently constructed in the study area. The first layer which is composed of a mixture of sand, clay and rock fragments but where the clay fraction clearly predominates as evidenced by low values of resistivity (Chapter III) was assigned a hydraulic conductivity (K_h) of 0.20 m/day, considering the clayey nature of the layer. The third layer which is formed by the fractured/weathered part of the basement was also assigned a hydraulic conductivity (K_h) of 0.015 m/d, a low value which reflects the low permeability of the basement rocks as well as the fact that most of the shallow wells do not reach this layer.

However, it should be born in mind that these average values are far from reflecting the lithological complexities and heterogeneities which are characteristic of the aquifer system of the study area. In addition, the wells investigated being all hand-dug, they only tap the first and second layers in the model and the relatively high values of hydraulic conductivity can be explained by the fact that, while the transmissivity is deduced from pumping tests, the thickness of the aquifer, which was assumed to be equal to the distance between the static water level and the bottom of the well, may have been substantially underestimated. Table VI.1 shows the initial hydraulic parameters entered into the model and which were further adjusted during the calibration process. The values of specific storage (S_s) and specific yield (S_y), porosity and effective

porosity, which are actually not important for the steady state simulation, where taken from literature considering similar lithologies (Fetter, 2001)

Table VI.1. Initial hydraulic parameters

	K_h	K_v	S_s	S_y	n	n_e	Thickness
Layer 1	0.20	0.020	0.003	0.007	0.4	0.2	8
Layer 2	0.66	0.066	0.002	0.007	0.3	0.15	30
Layer 3	0.015	0.0015	0.00005	0.00007	0.1	0.05	10

VI.7. Boundary conditions for the model

The definition of boundary conditions is an important part of the conceptualisation and modelling process of the groundwater flow system. Boundary conditions act as constraints imposed on the model domain that express the nature of physical boundaries of the aquifer system being modelled. Hence, boundary conditions help determine and quantify the exchange between the aquifer system and the external features which control inflows and outflows along the boundaries of the model. The identification and location of model boundaries must be complemented by a good mathematical representation of the selected features within the model. Indeed, according to Reilly (2001), many features which are hydrologic boundaries can be mathematically represented in several ways and the determination of the best mathematical expression depends on the objectives of the study. Figure VI.4 shows the boundary conditions selected for the model domain of the study area.

VI.7.1. Recharge

The only source of replenishment of groundwater in the study area has been found to be precipitation (Chapter II). The agricultural practices in the study area are mainly dependent on seasonal rhythm with rain-fed agriculture during the rainy seasons (September-December and February-May) and marshy agriculture during the dry seasons. Thus, there is no large scale irrigation practice known in the study area and therefore return flow can not be considered as a significant source of recharge. On the other hand, groundwater in the highlands discharges through the myriad of springs, ephemeral and perennial streams and this may preclude the lateral flow from the mountain aquifer as a potential source of recharge.

The recharge rate was estimated using the soil moisture technique based on meteorological data from the only comprehensive climatological station located within the study area. The long term average recharge rate (218.43 mm/year) computed in

Chapter II was uniformly applied to the whole study area. The recharge boundary was applied only on the model layer 1.

VI.7.2. General Head Boundary

The General Head Boundary (GHB) package is used to simulate head-dependent recharge or discharge across an aquifer boundary. The flow into or out of the groundwater system is always proportional to the difference in head. Conceptually, the General Head Boundary represents the resistance to flow between the cell belonging to the model and a constant head source or sink (Mace *et al.*, 2000). Within the model domain, the marshlands and associated shallow lakes were modelled as General Head Boundary with an estimated conductance value of 5000 m^2/day for the lakes Rweru and Cohoha, 4000 m^2/day for the Lake Rwihinda, 3000 m^2 for the Lake Gacamirinda, 500 m^2/day for the Lake Narungazi and 100 m^2/day for the Lake Nagitamo, and 6500 m^2/day for the vast marshland connecting the lakes Rwihinda, Narungazi, Nagitamo, Gacamirinda and the River Kanyaru. Due to the fact that there are no actual measurements of the conductance in these hydrological features, the values of the conductance used for the model were estimated taking into account the dimensions of each hydrological feature and were adjusted by trial and error during the calibration of the model.

VI.7.3. Rivers

The study area is drained by several ephemeral streams flowing through the myriad of V-shaped valleys. These ephemeral streams generally occur during the rainy season where the groundwater level increases and eventually intercepts the ground surface. They were modelled with DRAIN package. Besides, there are also a number of perennial streams including Ndurumo, Gatunguru, Rurata and Muhembuzi which are however characterised by a very low discharge rate. Discharge measurements performed by TBW Ingénieurs Conseils in September 1994 indicated a discharge rate of 0.12 m^3/sec for Rurata, a tributary of the Nyavyamo marshy system and 0.10 m^3/sec for Ndurumo, which drains into Lake Cohoha. The only important river is Kanyaru whose discharge rate was estimated at 39 m^3/sec. It is the latter only which is modelled as a river with RIVER Package.

VI.7.4. Drains

The drain boundary condition was used to simulate the groundwater discharge through the numerous springs scattered mainly in the southern and eastern highlands as wells as the water flow which occurs through small streams and the multitude of dry valleys

during the rainy season. DRAIN package is designed to simulate the effects on groundwater flow of features such as agricultural drainage which removes water from the aquifer at a rate proportional to the difference between the head in the aquifer and the elevation of the drain. The drain is assumed to run only partially full so that the head within the drain is approximately equal to the median of the drain elevation. The drainage continues as long as the drain elevation is below the head in the aquifer but ceases as soon as the groundwater head in the aquifer drops below the drain elevation (Batelaan & De Smedt, 2004). The DRAIN boundary condition was defined as a polygon covering the whole model domain at a depth of 0.1 m below the ground surface so as to encompass the removal of water through the multitude of springs which are not all mapped and gauged. Moreover, this way of defining the drain helps account for the perennial drainage through the small streams as well as the ephemeral streams which occur in periods of intense rainfall within the multitude of V-shaped valleys. This way of simulating the drainage in Visual MODFLOW was successfully applied by Tesfamichael (2009) while developing a regional groundwater flow model for the Geba basin, in northern Ethiopian and Van Camp *et al.* (2010) in their analysis of the multi-annual climate variability on the hydrodynamic evolution (1833 to present) in a shallow aquifer system in northern Belgium. For the study area investigated in this study, a high value of drain conductance was assigned to the model and was progressively adjusted during the calibration process until a good match between the calculated and measured hydraulic heads was achieved.

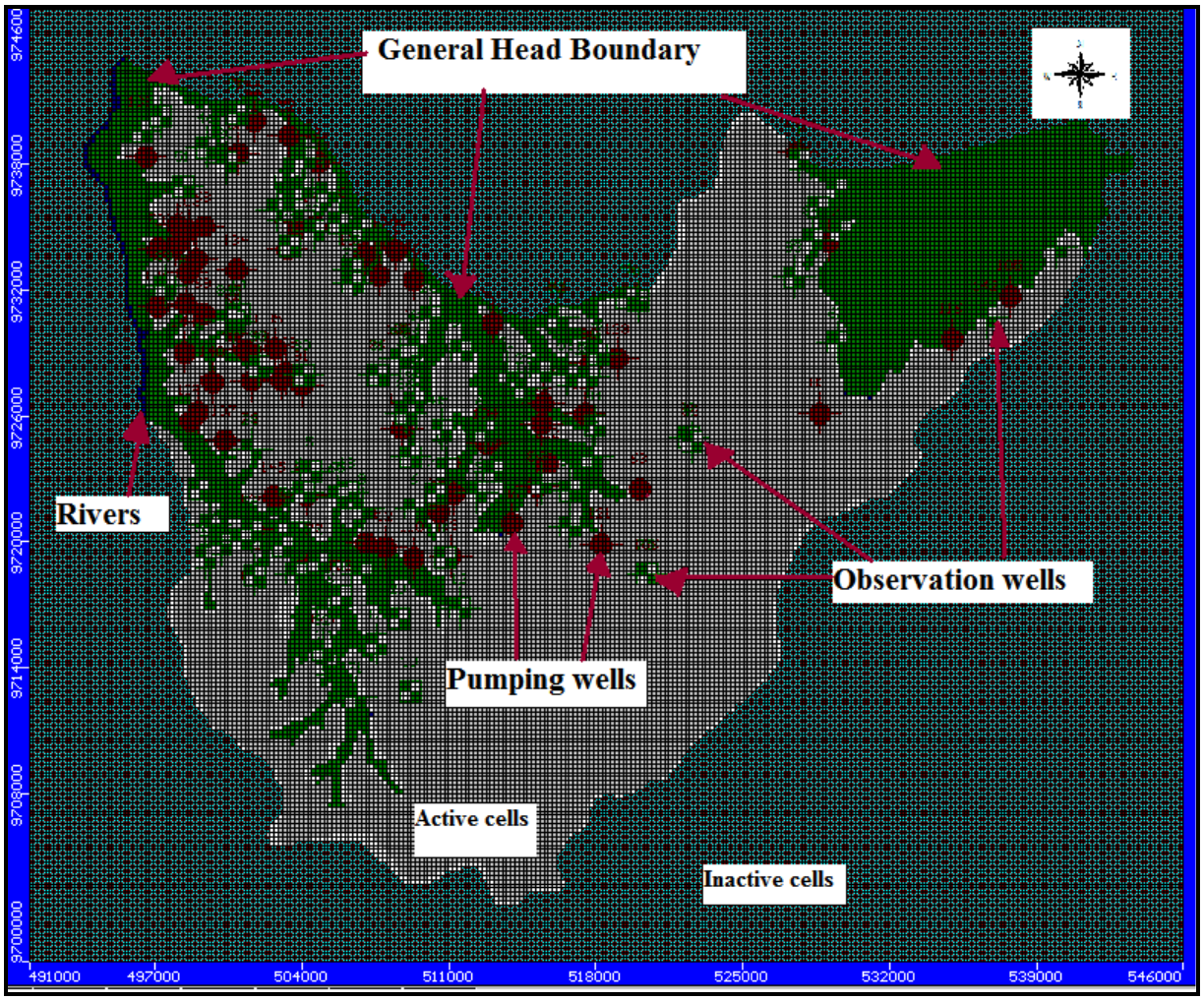

Figure VI.4. Model domain and boundary conditions

VI.8. Model pumping rate

The simulation of groundwater abstraction by wells is an important and widely used feature of groundwater flow models such as Visual MODFLOW. Discharging wells or artificial recharge through injection wells in Visual MODFLOW is simulated using the MODFLOW WELL package. The latter simulates the discharge from a well at a specified rate Q which is independent of the head in the cell and the area of the cell. Recharging wells are simulated in the same way as discharging wells, except that the specified volumetric rate is positive instead of negative (Halford & Hanson, 2002). The WELL package uses the hydraulic conductivity and thickness per model layer to determine the amount of groundwater which is extracted from each layer of the model. Thus, the well discharge is redistributed as the values of hydraulic conductivity are changed during the model calibration.

Pumping rates in the model were assigned based on information collected from 86 pumping wells scattered across the study area (Figure VI.5). All these hand-dug wells

are equipped with hand- or foot-operated pumps with a nominal discharge capacity of 1.5 m^3/hour. These wells are considered to be pumped 6 hours a day and this leads to a total discharge of 9 m^3/day for each well, except for the well situated at Kigina I-Gisenyi which is highly productive and which was assigned a discharge rate of 20 m^3/day. The pump of this well was stolen during the civil war (1993-2005) and local villagers decided to remove the concrete cover of the well so that they can fetch water directly from the well using buckets which are suspended to long sticks. This well is exploited all day long and never runs dry. All villagers from neighbouring villages where wells are broken down, come to fetch water from this well. For the whole study area, groundwater extraction can be estimated by summing up all the estimated daily discharges for the 86 pumping wells and amounts to 785 m^3/day which corresponds to 286 525 m^3/year.

VI.9. Observation wells

Water levels observations used for the calibration of the groundwater flow model were taken from 94 non-operating wells which, for having remained idle for long periods, can be considered as fairly representing average steady state conditions. Moreover, as already mentioned in Chapter III, groundwater exploitation in the study area is still underdeveloped so that the aquifer system in Bugesera can be undoubtedly considered as being in steady state conditions. Indeed, the few operating hand-dug wells are far from tapping the whole groundwater potential in this area where a long term groundwater recharge was estimated at 159.72 mm per year which corresponds to 167.74 Mm^3/year. Compared to an annual water abstraction of 0.29 M m^3/year which represents only 0.17% of the annual recharge, it is evident that the aquifer groundwater system in Bugesera region is not substantially affected by the very low groundwater abstraction through the few hand-dug wells (86 pumping wells) equipped with hand- or foot-operated pumps and can be fairly considered as being in equilibrium conditions. I

n total, 94 measurements performed in October 2008 in non-operating wells were used to calibrate the groundwater flow model. To this effect, the parameters of the model, especially the hydraulic parameters, were adjusted several times until the hydraulic heads calculated by the model match as much as possible those measured in the field. Figure VI.5 shows the spatial distribution of the 86 pumping wells, the 94 head observation wells and the numerous springs mainly located in the southern and eastern highlands surrounding the depression of Bugesera and which were modelled as drains.

Head observation wells and pumping wells have a depth varying between 5 m and 17.5 m and thus tap the first and second layers of the model.

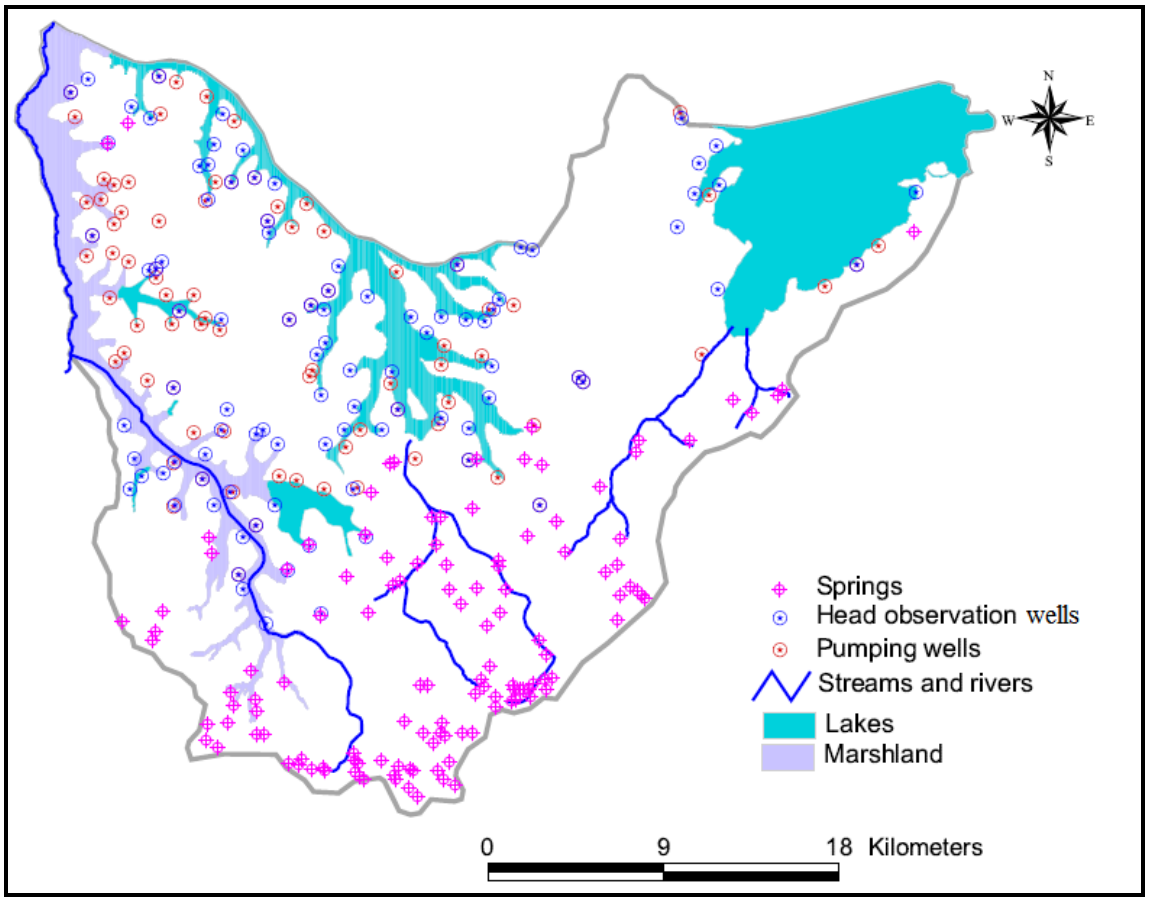

Figure VI.5. Map showing the spatial distribution of pumping wells, head observation wells and the numerous springs which were modelled as drains

VI.10. Calibration of the model

Model calibration is the process consisting of adjusting input model parameters with a view to reaching, as closely as possible, a good match between simulated and field conditions. Calibration is carried out through an iterative process of changing the values of the model parameters in an attempt to minimise as much as possible the discrepancy between the variables measured in the field and those computed by the model. The calibration can be conducted either by manual trial and error or automatically using codes that automatically manipulate parameter values to minimise an objective function such as the sum of squares of the residuals between simulated and observed heads (Petrich, 2004). The calibration of the groundwater flow model developed in this study was achieved under steady state conditions by trial and error, which involves a manual manipulation of model parameter values, mainly the hydraulic conductivity, until simulated head values are close to values measured in the field. Steady state simulation is used to analyse the pre-development (natural) flow conditions or new equilibrium conditions that may develop in response to groundwater development (Franke *et al.*, 1987). Thus steady state calibration is appropriate when the model simulates equilibrium conditions or evaluates long-term aquifer sustainability. Steady state

calibration of model parameters generally consists of manually adjusting the hydraulic conductivity, because in steady state conditions the storage of the aquifer system is not involved. Indeed, steady state conditions assume that the overall mass balance is in equilibrium, which means that total inputs should be equal to total outputs. Moreover, unlike transient state calibration, steady state calibrations provide unambiguous information on hydraulic conductivity and transmissivity (Franke *et al.* 1987). During the calibration process, the drain conductance was also adjusted until a satisfactory agreement between the calculated and measured hydraulic heads was achieved.

The initial values of hydraulic conductivity for the different layers of the model and the conductance for the drain were progressively altered as the calibration process continued until a satisfactory agreement between the hydraulic head measured in the field and the hydraulic head calculated by the model was achieved. Table VI.2 shows the optimised values of horizontal and hydraulic conductivities for the three layers of the model. After calibration, the optimal value of the drain conductance was found to be 45 m^2/day.

Table VI.2. Horizontal and vertical hydraulic conductivities after calibration

Layers	**Lithology**	**K_h**	**K_v**
Layer 1	Mixture of clay, sand and rock fragments with clear predominance of clay	0.12	0.012
Layer 2	Mixture of clay, sand, gravel and rock fragments with a clear increase of the coarse grain size with depth	0.30	0.030
Layer 3	Fractured/weathered basement	0.009	0.0009

The quality of the calibration exercise is depicted by Figure VI.6 which shows a cross-plot of the measured hydraulic heads against those calculated by the model. Data points are well spread along the fit line with, however, most of the points falling slightly below the 1:1 line. A close look to some of the points which plot below the 1:1 line reveals that some of those points correspond to wells which have been vandalised during the civil war in which, due to different materials thrown inside (building materials and grass from agricultural fields), piezometric measurements may not be accurate (e.g. observation wells 14/1 at Gahwijo1-Nyabikenke, 81/1 at Runyonza-Muhero, 70/1 at Rabiro Rutagara). This may partially explain the discrepancy between observed hydraulic heads and those calculated by the model. However, given the physiographic, hydrological and geological complexities as well as the spatial extent of the study area, it can be concluded that there is a satisfactory agreement between the observed and calculated hydraulic heads. Indeed, Figure VI.6 shows a pretty good fit as reflected by low normalised RMSE (5.24 %), a root mean squared error RMSE (5.40 m) and standard error of the estimate (0.56 m). Moreover, Figure VI.6 indicates that residual errors are relatively small and comprised between 0.04 m and 14 m. The discrepancy

between the calculated and measured hydraulic heads may also stem from the fact that the uniform value of hydraulic conductivity used by the model for the whole study area does not fully reflect the complexities and heterogeneities of the geological setting and topography. Furthermore, it is not excluded that errors during the measurement of the water levels in the different wells may contribute also to the discrepancy between the observed and calculated hydraulic heads.

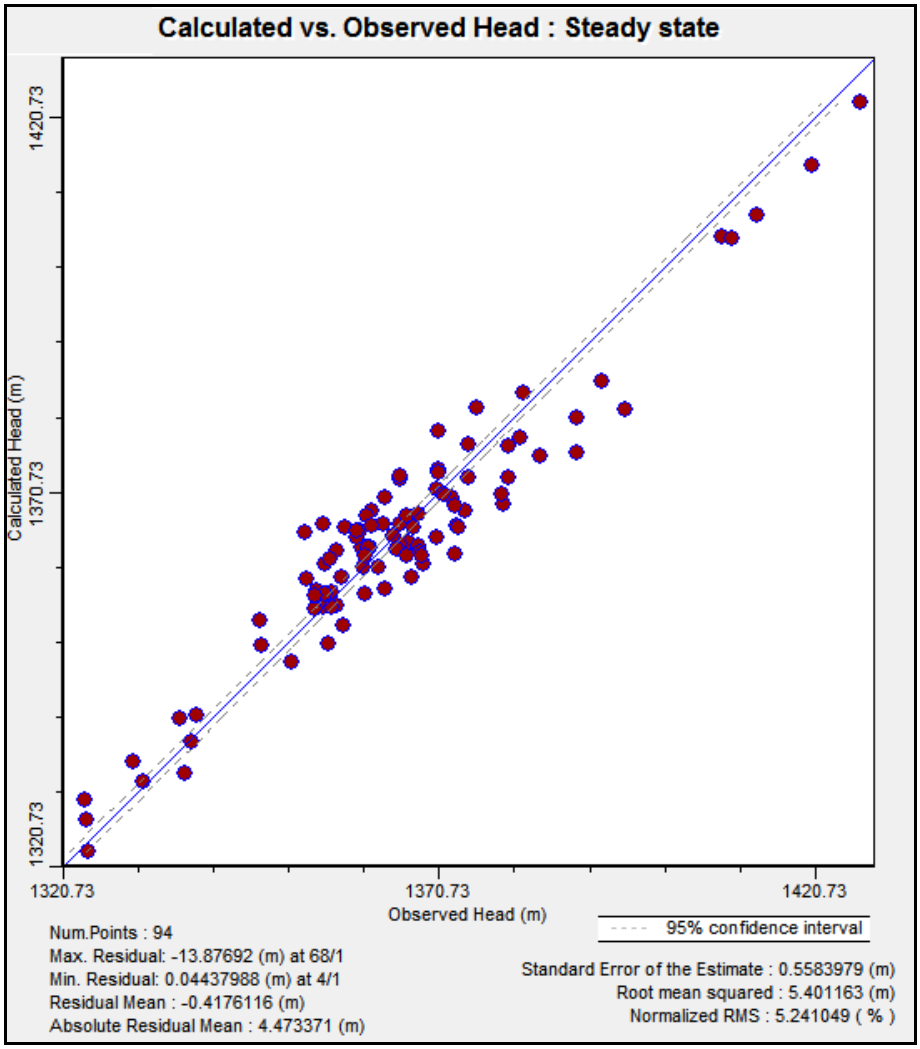

Figure VI.6. Cross-plots showing the comparison between measured and calculated hydraulic heads using the hydraulic parameters shown in table VI. 2

VI.11. Results and discussion of the steady state simulation

VI.11.1. Steady state groundwater balance

Steady state simulation of groundwater flow is based on the law of mass conservation which states that the total volume of water entering the groundwater system from various sources of recharge is equal to the total volume of water leaving the system through the different sinks. Table VI.3 presents the water balance results of the study

area as calculated by the model. The major components of the groundwater balance are the recharge from precipitation (recharge), the recharge from the leakage through the river bed (river leakage), abstraction through pumping wells, the discharge to the lakes and marshlands (head dependent boundary) and discharge to the drains. While the conceptualisation of the model considers precipitation as the only source of recharge (633312.81 m^3/day) of the groundwater system, it can be noticed that there is a small amount of additional recharge (410.87 m^3/day) which is coming from the leakage through river beds. While this leakage may occur naturally whenever the elevation of the river bed is higher than the elevation of the groundwater table, it is also possible that, due to the complex topography of the study area, only a few cells of the river course may have an elevation higher than the groundwater table, as a result of the interpolation of the topography data, during the model development, which sometimes significantly alters the original elevation of the DEM used. As shown in Chapter V, the few small perennial and numerous ephemeral streams as well as the River Kanyaru, at the western border of the study area, seem to be fed by discharge from the groundwater system. The output from the groundwater system includes: discharge by pumping wells (731 m^3/day), baseflow to the river (7751.39 m^3/day), baseflow to the shallow lakes and marshland (244332.50 m^3/day) and discharge to the drains (380785.91 m^3/day). The important discharge through the drains is in agreement with the existence of several springs mainly in the southern and eastern highlands which, besides the perennial and ephemeral streams, drain an important volume of water from the groundwater system. The positive difference between the total inputs and outputs to the groundwater system is very small as evidenced by the small percentage of the discrepancy (0.01%). The small discrepancy indicates that the total volume of inputs (rainfall recharge + leakage through river beds) is in balance with the total volume of outputs (abstraction from pumping wells + discharge to the lakes and marshlands + discharge to the drain + discharge to the river). It can be seen that the abstraction from pumping wells is significantly low compared to the volume of recharge. However, considering all complexities and the small discrepancy, it can be concluded that the groundwater balance components are satisfactorily offsetting, according to the principle of mass conservation which governs the steady state groundwater flow simulation.

Table VI.3. Groundwater balance obtained from the steady state simulation

Source	IN (m^3/day)		OUT (m^3/day)
Pumping wells			731
Drains			380785.91
River leakage	410.87		7751.39
Head dependent boundary			244332.50
Recharge (from precipitation)	633723.68		
TOTAL	633723.68		633600.80
IN-OUT (m^3/day)		**122.88**	
PERCENT DISCREPANCY		**0.01**	

VI.11.2. Piezometric levels

To check whether the results of the steady state groundwater flow simulation are realistic and acceptable, a map of the simulated piezometric levels was generated and compared to the water level contour map prepared based on the piezometric measurements performed in the field (Chapter V). This piezometric map was prepared using mainly measurements taken from abandoned wells which were complemented by the elevation of springs (groundwater surface outcrops), especially in the southern and eastern highlands surrounding the depression of Bugesera. Given the low abstraction of groundwater in the study area through the shallow hand-dug wells, it was assumed that, overall, steady state conditions prevail.

Figure VI.7 portrays steady state equipotential contours with an equidistance of 20 m as generated from the simulated piezometric levels, while Figure VI.8 shows the same map with a satellite image of the study area at the background. The two maps clearly show that the simulated piezometric levels fairly replicate the actual piezometric conditions in the field and confirm the complex groundwater flow pattern, which is strongly controlled by the complex topography characterised by an alternation of hills, hillocks, small V-shaped valleys as well as swampy large valleys in which lie the shallow lakes. Therefore, the groundwater flow model developed in this study satisfactorily reproduces the behaviour of the aquifer system and shows a regional flow trend from the highlands towards the complex of interconnected swamps and shallow lakes within the depression of Bugesera.

However, besides this general flow pattern, another local flow can be noticed towards the myriad of V-shaped valleys in which flow both perennial streams as well as ephemeral streams which mostly occur during the rainy seasons. The development of the groundwater flow model of the study area can be considered as fairly successful in the sense that, on the one hand, it reproduces the piezometric levels with an acceptable

discrepancy (5.97%) between the observed and calculated hydraulic heads and, on the other hand, the simulated piezometric levels clearly conform to the complex topography, thereby reflecting the strong and expected control exerted by the topography over the groundwater flow pattern. The simulated piezometric iso-contour lines (Figure VI.7) fairly replicate the groundwater flow system map (Figure V.6) which was manually constructed using the piezometric levels measured in the field (Chapter V). However, an important discrepancy between simulated and observed piezometric levels appears in the southern and eastern highlands where several springs occur, which were considered as representing outcrops of the groundwater table. Indeed, simulated piezometric levels are far below the actual field conditions, wherein groundwater table was assumed to be close to the ground surface given the multitude of springs. The reason for this discrepancy could be explained by two main reasons: (1) there are no observation wells in the highlands and all the springs were modelled as drains, and (2) the fact of using one uniform hydraulic conductivity to simulate groundwater flow for the whole study area may not fully represent all the complexities and heterogeneities which characterise its geological and topographical settings. Indeed, the hydraulic conductivity being the ratio of the transmissivity to the aquifer thickness, it is possible that, by assuming the model layers to have an average and constant thickness over the whole study area, there was an overestimation of the transmissivity. In reality, the thickness of the weathered overburden, and hence the thickness of the different layers of the model, progressively thins out towards the southern and eastern highlands; the layer may even completely disappear close to the southern and eastern borders of the study area, where basement rocks barely outcrop at the ground surface. Therefore, the use of an overestimated value of transmissivity in the simulation of the steady state groundwater flow model may explain why the water levels in the highlands have been aberrantly lowered.

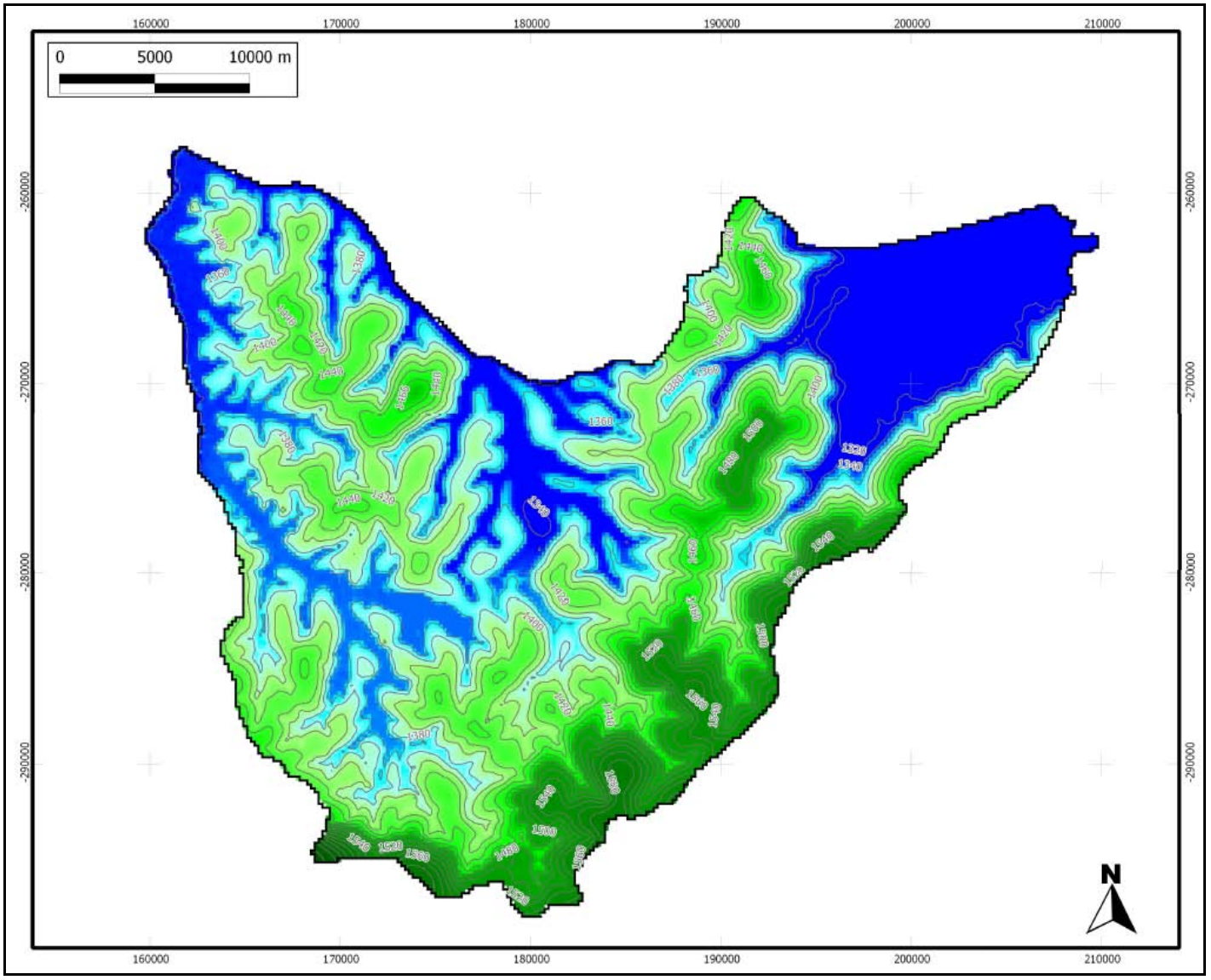

Figure VI.7. Steady state equipotential contours with an equidistance of 20 m (in UTM coordinates)

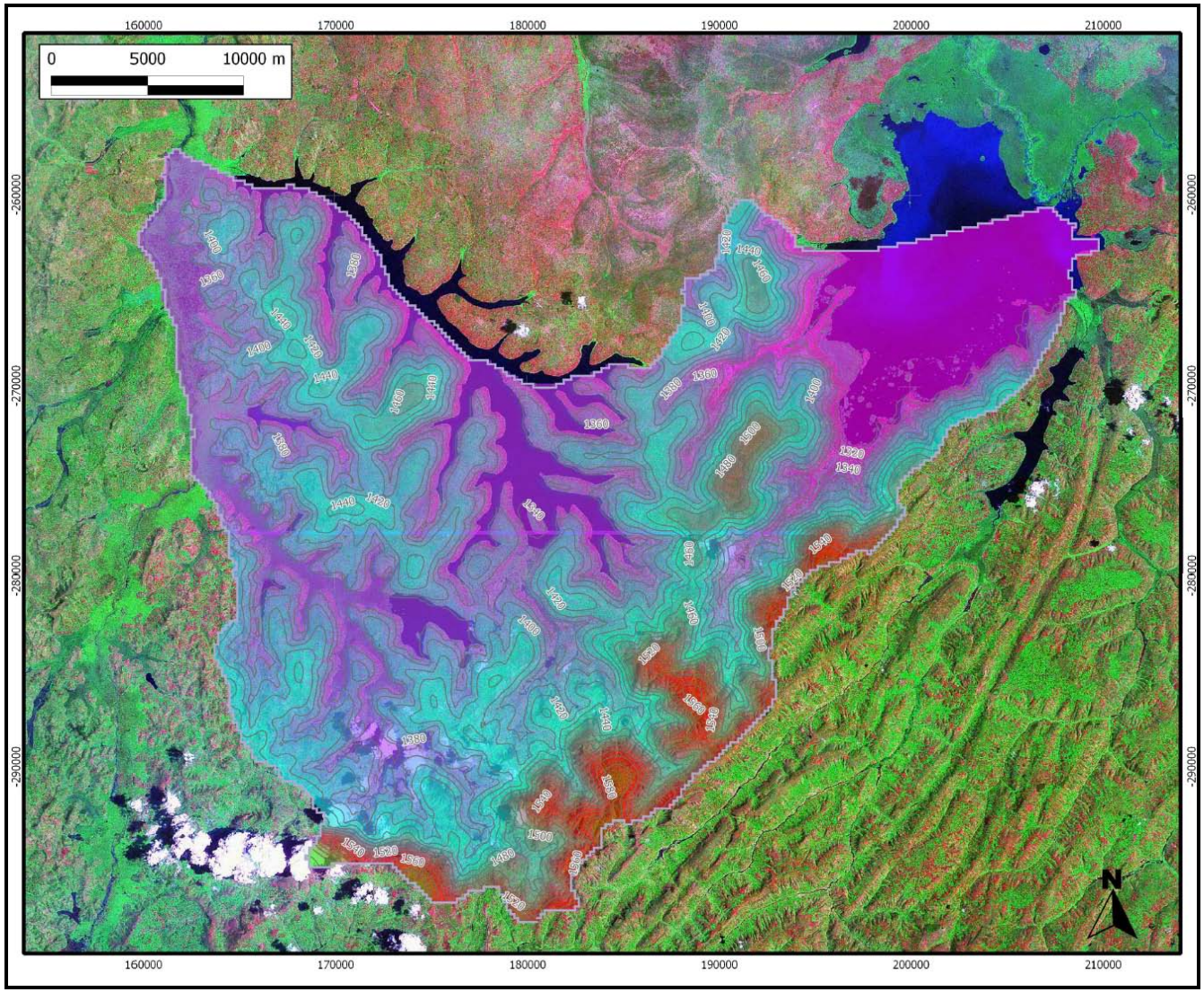

Figure VI.8. Steady state equipotential contours with an equidistance of 20 m with a satellite image at the background (in UTM coordinates

VI.12. Conclusions and recommendations

The steady state groundwater flow model of Bugesera region was successfully conceptualised, constructed, simulated and calibrated using the three dimensional finite difference code, Visual Modflow V.3. Considering the low level of groundwater development in the study area, it was assumed that steady state conditions are prevailing over the whole study area and that the water level measurements performed in abandoned wells were fairly representing long-term steady state conditions. The model domain was discretised into 3 layers, while the grid was defined as consisting of 225 rows and 278 columns with a spatial resolution of 180 m *180 m for each grid cell.

The calibration of the model was carried out through a trial and error process consisting of manually changing the hydraulic parameters and the drain conductance values until a satisfactory agreement between measured and calculated hydraulic heads was obtained. The hydraulic conductivity, i.e. 0.66 m/d, used as the starting point during the calibration process was an average value calculated considering an average transmissivity of 33.10 m^2/d obtained from the analysis of pumping tests and an average thickness of 50 m for the weathered overburden and the fractured weathered basement. This average value was assigned to the second layer which, according to the hydrogeological structure, constitutes the main aquifer tapped by the shallow hand-dug wells. For the first and third layers, estimates of values of hydraulic parameters were assigned taking into account their respective lithological composition as defined in Chapter III. For the first layer which is made up of clayey alterites an average value of hydraulic conductivity of 0.20 m/d was adopted. As for the third layer a hydraulic conductivity K_h of 0.009 m/d was used taking into account the low transmisisvity of the basement

These hydraulic parameters were progressively altered until an acceptable normalized RMSE of 5.24 % was reached, which is far below the maximum accepted normalized RMSE of 10%. Moreover, even the residual mean difference and the standard error of estimate of respectively 0.42 m and 0.56 m prove that the model converged to a solution with a small and acceptable error, considering the topographical and geological complexities and heterogeneities. Despite the fact that rainfall was considered the only source of recharge in the study area, the model calculates that there would be an additional source coming from the leakage through the river bed. The small additional recharge through river bed leakage may just result from the fact that, when elevation data are imported into Visual Modflow V.3, they are re-interpolated and this may result in the elevation of some rivers cells erroneously being higher than the groundwater table, which may explain the small additional recharge from river leakage.

As reflected by the normalised RMSE (5.24 %), the calculated and measured hydraulic heads show, overall, a satisfactory match, while the steady state groundwater flow confirms a regional groundwater flow trend towards the depression and a local flow component towards the myriad of V-shaped valleys in which flow perennial and ephemeral streams. The steady state hydraulic head contours reflect the strong control exerted by the complex topography over the groundwater flow. However, the potentiometric map shows an important discrepancy between the actual conditions in the southern and eastern highlands where, due to the occurrence of a multitude of springs, the groundwater surface was assumed to be close to the ground surface, the springs being an outcrop of the groundwater surface. This discrepancy may be related to the lack of observation wells in this part of the study area, as well as the fact of using one uniform value of hydraulic conductivity for the whole study area, which may not reflect all the topographic complexities and geological heterogeneities. More importantly, the use of a uniform hydraulic conductivity may not be appropriate for the highlands, where the weathered mantle thins out or squarely disappears, thereby resulting in reduced values of transmissivity.

This study recommends more pumping tests with a representative coverage of the study area for the sake of reliable and representative hydraulic parameters for the different hydrogeological units. A regular monitoring of water level fluctuation in the complex of marshlands and lakes, as well as the gauging of discharge in the few streams and rivers should be undertaken in order to allow a better definition of the boundary conditions. It is also highly advisable that a network of observation wells with a good coverage of the study area should be installed, in order to undertake a regular monitoring of the groundwater level fluctuation.

CHAPTER VII. HYDROGEOCHEMISTRY

VII.1. Introduction

The quality of water refers to the physical, chemical, and biological properties which result mainly from natural hydrogeochemical processes as well as anthropogenic activities. Temperature, turbidity, colour, taste, and odour are the main physical water quality parameters. Hydrochemical properties of groundwater are controlled by the composition of different end-members (rainwater, leakage from surface water bodies, sea water intrusion…), the geological environment, the residence time, different hydrogeochemical, biological and microbiological reactions, climate and topography, and the groundwater flow regime of a particular area. The chemical composition of groundwater determines its suitability for different uses including domestic, agricultural or industrial purposes.

The natural chemical composition of groundwater may be strongly altered by anthropogenic pollution resulting from agricultural activities, waste disposal and industrial activities. Thus, elevated levels of nitrate (NO_3^-), and other chemicals used in agriculture may occur in aquifers underlying agricultural or residential areas, whereas high heavy metal concentrations may result from industrial pollution. Moreover, the quality of groundwater can be also compromised by the occurrence of salt water intrusion which, in coastal aquifers, may result from overexploitation. The total mass of dissolved ions is referred to as the total dissolved solids (TDS). The TDS is a very important parameter in the evaluation of the groundwater quality, higher levels of TDS causing water to be inappropriate to some purposes such as domestic, industrial or agricultural uses.

Groundwater in basement aquifers is generally young and has low solute concentration reflected by low levels of TDS, which result from the low solubility and low reactivity of basement rocks. However, high concentrations of some elements such as sulphate can occur as a result of oxidation of sulphides, while elevated concentrations of iron and manganese may be encountered in reducing conditions. Although these elements are not generally harmful to the human or animal health, they can impart an unpleasant taste or colour to water, thereby compromising its quality for some uses.

The study area is underlain by Precambrian rocks (metasediments, granites, pegmatites and accessorily mafic rocks) whose mineralogical composition is dominated by silicate and aluminosilicate minerals. Therefore, the weathering of silicates and aluminosilicates must play a significant role in the hydrochemical evolution of groundwater.

The aim of this chapter is to characterise the hydrochemistry of groundwater and surface water in the study area, and to infer the hydrogeochemical processes and their potential implications for the quality of water resources. This hydrogeochemical study is based on results of laboratory analyses of 143 water samples collected in 2007 and 2008 from shallow hand-dug wells, lakes, and natural springs.

VII.2. Weathering of silicate and aluminosilicaten minerals

It has been established that the chemical composition of groundwater is strongly influenced by the progressive weathering of aquifer-forming lithologies along the flowpath. However, Appelo & Postma (2005) observe that the weathering of silicate minerals is a slow process and its influence on groundwater chemistry is less pronounced than in carbonate terrains. Still, the weathering of silicate and aluminosilicate minerals is an important geochemical process. It contributes about 45 % of the total dissolved content of natural waters and acts as an important sink for CO_2. Weathering of primary aluminosilicate minerals is an incongruent reaction, which results in the formation of secondary minerals such as clays (kaolinite, montmorillonite), gibbsite, and Fe-oxides. These secondary products are mainly due to the insolubility of Al-compounds.

The nature of the weathering product is determined by the hydrological conditions along with the rate of mineral weathering. Thus, montmorillonite will form in relatively dry climate or in low lying areas where the rate of flushing is low, whereas the formation of gibbsite occurs in tropical climates where intense rainfall and well drained conditions prevail. The main effect of aluminosilicate weathering on the water chemistry is the addition of cations and silica as well as the increase of pH resulting from the consumption of acid. The major cations like Na^+, K^+, Ca^{2+}, Mg^{2+} are released from the weathering of feldspars, pyroxenes, amphiboles and micas (biotite). The weathering being promoted by CO_2, the increase in cation concentration is accompanied by an augmentation of bicarbonate, which, in some cases, can lead to the precipitation of carbonate as a result of silicate weathering (reactions 6.1 to 6.3). This is confirmed by the saturation indices of groundwater sampled in this study, which show that, despite the absence of carbonate rocks in the study area, some water samples, mainly those collected from wells, show oversaturation with respect to carbonate minerals (Appendix VII.7).

The following reactions show the weathering of 3 main aluminosilicates, namely albite, K-feldspar and anorthite

$$2NaAlSi_3O_8 + 9H_2O + 4H^+ + 2CO_2 \Leftrightarrow Al_2Si_2O_5(OH)_4 + 2Na^+ + 2HCO_3^- + 4H_4SiO_4 \quad (6.1)$$

albite kaolinite

$$2KAlSi_3O_8 + 9H_2O + 4H^+ + 2CO_2 \Leftrightarrow Al_2Si_2O_5(OH)_4 + 2K^+ + 2HCO_3^- + 4H_4SiO_4 \quad (6.2)$$

K-feldspar kaolinite

$$2CaAl_2Si_2O_8 + 4CO_2 + 6H^+ + 3H_2O \Leftrightarrow 2Al_2Si_2O_5(OH)_4 + 2Ca^{2+} + 4HCO_3^- \quad (6.3)$$

anorthite kaolinite

The above equations show that the dissolution of aluminosilicates is controlled by pH (consumption of protons), lower pH values promoting the dissolution. Natural rainwater which recharges groundwater becomes slightly acid as a result of the dissolution of atmospheric CO_2 in the falling water. The carbonic acid resulting from the CO_2 dissolution breaks down and produces protons (H^+) and bicarbonate (HCO_3^-). Hence, when the rainwater starts to infiltrate through the vadose zone, where the CO_2 pressure is much higher than in atmosphere, the most important CO_2 dissolution occurs and the infiltrating water becomes a slightly to moderately acidic and oxidising solution, which can destroy rock-forming minerals. The dissolution of primary aluminosilicate minerals is a slow and kinetically controlled process (Helgeson *et al.*, 1969 in Appelo & Postma, 2005). The dissolution kinetics of primary aluminosilicate is a main rate limitation in the weathering process.

VII.3. Methodology

VII.3.1. Sampling

Water samples for this study were collected during two field campaigns conducted from September to December 2007 and from July to October 2008 in Bugesera region. The water sampling protocols as proposed by Barcelona *et al.* (1985) were followed as much as possible. These water samples were collected for the determination of hydrochemical parameters including major and minor elements. Physical parameters like electrical conductivity, temperature and pH were measured in the field using a combined pH-electrical conductivity-temperature meter and appropriate electrodes. For each sampling point (well, spring, or lake) two samples were collected in plastic bottles of 250 ml each: one sample was meant for the analysis of cations and was treated with concentrated nitric acid (HNO_3) until a pH value of about 2, whereas the other sample intended for the analysis of anions was left untreated. Acid-treatment of samples intended for the analysis of cations aims at stabilising water samples and preventing the precipitation of metals. Upon returning from the field, samples were stored in a refrigerator until they were shipped to the Laboratory for Applied Geology and Hydrogeology at Ghent University.

In total, 143 samples were collected from the study area of which 66 samples are from wells, 61 samples from springs and 16 samples from the shallow lakes. Sampling locations were chosen so as to have a representative coverage of the whole study area. Water samples from the small lakes were collected at a distance of minimum 20 m from the shores to avoid possible contamination from the land. Water samples from wells were taken during the pumping test and after a pumping duration of at least 1 hour in order to have the water bore storage removed. For operating wells which were not submitted to pumping tests, they were continuously pumped by the villagers fetching water for domestic use and, thus, there was no need for purging them before collecting samples for laboratory analysis. Figure VII.1 shows the location of all sampling sites, i.e. wells, springs, lakes and evaporitic salts. The sample numbers correspond to the S/N numbers in appendix VII.1.

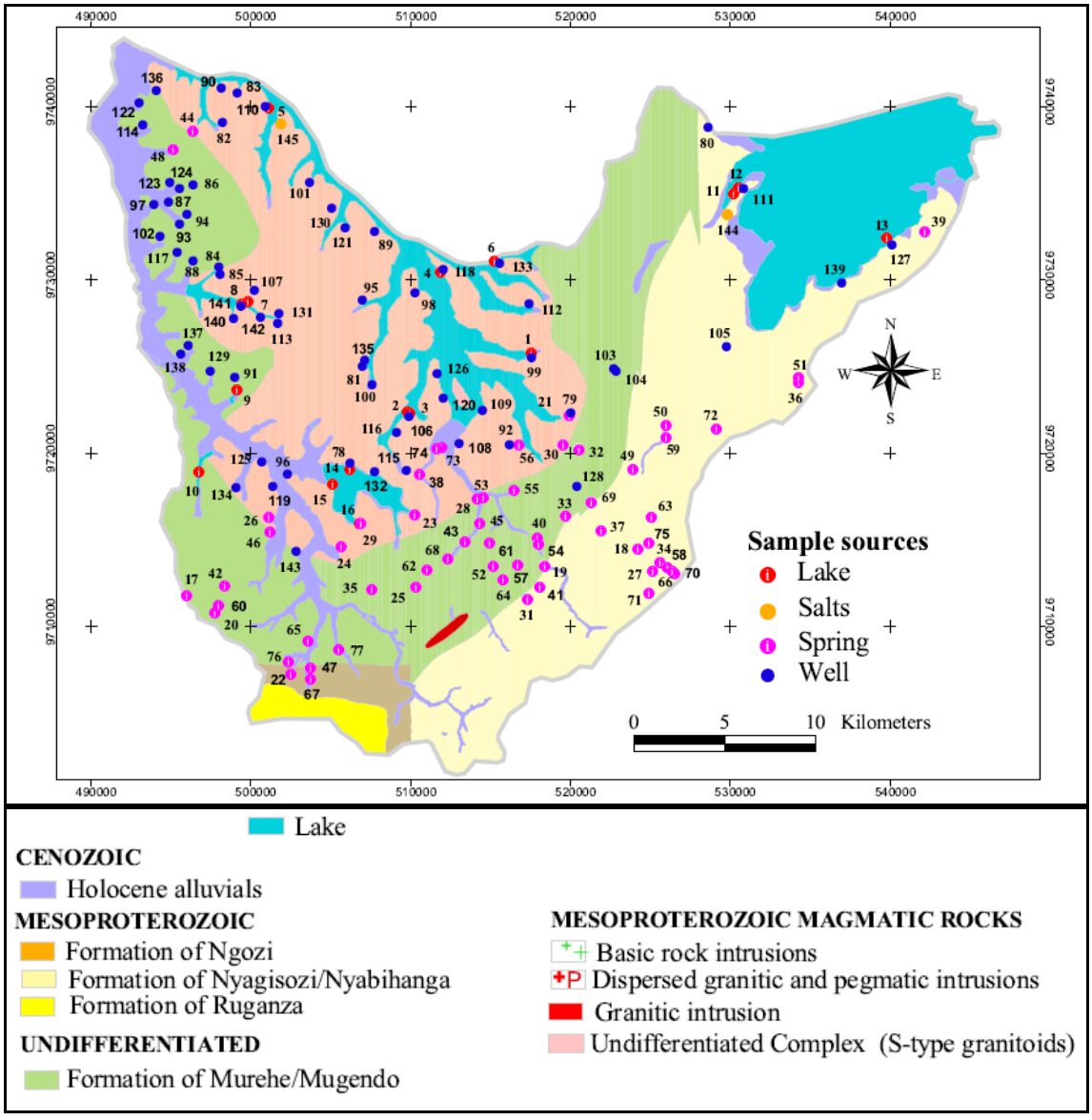

Figure VII.1. Study area with the location of the sampling sites

VII.3.2. Chemical analysis

Chemical analyses were performed in the Laboratory of Applied Geology and Hydrogeology at Ghent University. Different analytical methods were applied for the various hydrochemical parameters studied in this work:

- Flame Atomic Absorption Spectrometry (FAAS) (Varian Zeeman Spectra AA 400) was used to analyse the cations Na^+, K^+, Mn^{2+}, Fe $^{2+/3+}$, Ca^{2+}, Mg^{2+} and SiO_2.
- Al was analysed using Graphite Furnace Atomic Absorption Spectrometry (GF-AAS) with electrothermal atomisation in a graphite furnace (Varian Zeeman Graphite Furnace Spectra AA 400).
- Zn was determined using Varian Spectrometer AA 400 with ACT-80 Atom Concentrator Tube with air and acetylene gas.
- Anions (NO_3^-, NO_2^-, and PO_4^{3-}), and NH_4^+ were analysed by means of Molecular Absorption Spectrophotometer (UV-VIS spectrophotometer Shimadzu UV mini 1240-Heatingplate 105°C).

The ultraviolet-visible light spectroscopy (also known as UV/vis spectrophotometry) measures the intensity of light passing through a sample (I), and compares it to the intensity of original incident light before it passes through the sample (I_o). The ratio I/I_o is termed the transmittance and is usually expressed as a percentage (% T). The absorbance, A, is determined using the Beer-Lambert law which is mathematically expressed as: $A = -\log(I/I_0) = \varepsilon * c * L$ where ε = is a constant known as the molar absorptivity or extinction coefficient, c is the concentration of the absorbing species and L is the path length through the sample.

  - NO_3^- was analysed by spectrophotometry with sodium salicylate
  - NO_2^- was determined using the NED (*N*-(1-naphthyl)-ethylenediamine dihydrochloride) method
  - NH_4^+ was measured using the standard method 4500-NH_3: D-Phenate method
- Chloride and SO_4^{2-} concentrations were determined using the chloridometric and turbidimetric methods respectively.
- The determination of the bicarbonate (HCO_3^-) and carbonate (CO_3^{2-}) concentrations was performed using the titration method with dilute HCl acid (0.01N). This method measures bicarbonate (HCO_3^-), carbonate (CO_3^{2-}) and alkalinity levels in water. The method has a routine detection limit of 0.1 meq/l.
- Fluoride was analysed using an ion selective electrode.

Descriptions of the different analytical methods for major ions and trace elements are extensively explained in the Laboratory Manual and in Standard Methods for Examination of Water and Waste water (APHA, 1992). Detailed results of the laboratory analyses and other physico-chemical parameters determined are presented in Appendix VII.1.

VII.3.3. Reliability of chemical analysis data

Before interpreting chemical analysis data, it is important to check the quality and reliability of laboratory analyses. One method used to assess the accuracy and completeness of groundwater analyses is the computation of the charge balance error (C.B.E). This test is based on the principle that all aqueous solutions must be electrically neutral, meaning that the sum of the positively charged cations must be equal to the sum of the negatively charged anions. Charge balance error is calculated using the following equation:

$$C.B.E(\%) = \frac{\sum Cations - \sum Anions}{\sum Cations + \sum Anions} * 100 \qquad (6.4)$$

where the concentrations of anions and cations are expressed in milli-equivalents per liter (meq/l).

As a general rule, a charge balance error calculated using the above equation should be within the limits ± 5 % although in most of the cases the charge balance will be less than 2 % if correct sampling and laboratory procedures have been followed (Freeze & Cherry, 1979). If groundwater has a very low mineralisation, a charge balance error greater than 5 % can be acceptable.

Apart from the low mineralisation, large charge balance errors can result from a number of causes, among which (Weight, 2008): (1) the list of constituents which have been analysed is incomplete. The absence of a given ion will result in an increase or decrease in charge balance error depending on the concentration of the missing ion and on its associated ionic charge, (2) a serious systematic error has occurred during the analysis (e.g. poor standardization or failure to correct the results for laboratory dilutions), (3) problems with field measurements such as alkalinity or, (4) incorrect assignment of the charge for one or more of the major solutes.

Water samples collected within the framework of this study show a charge balance error ranging between 0.04 and 7.73 %. Values of the charge balance errors greater than 5 % mostly correspond to water samples from springs, with low TDS (Appendix VII.1).

VII.4. Analytical results interpretation and discussion

Detailed results of all physico-chemical and hydrochemical parameters of the 143 water samples analysed in this study are shown in Appendix VII.1. Table VII.1 summarises some descriptive statistics of these physico-chemical and hydrochemical parameters including, for each parameter, minimum and maximum values, average standard deviation and the coefficient of variation.

A quick inspection of Table VII.1 shows a wide range of variation of some parameters which is reflected by very high coefficients of variation and which may be consistent with a geological environment of crystalline basement rocks. Indeed, extreme variations in groundwater quality, even over short distances, have been already revealed in crystalline environments of Malawi, as resulting from the complexity of groundwater flow and weathering processes (Foster *et al.*, 1999). On average, the relative abundance of the ions in the water samples analysed is in the order $Na^{+}>Ca^{2+}>K^{+}>Mg^{2+}>Fe^{2+}>Mn^{2+}>NH_4^{+}$ and $HCO_3^{-}>Cl^{-}>SO_4^{2-}>NO_3^{-}>NO_2^{-}>PO_4^{3-}$ for the cations and anions respectively.

Table VII.1. Descriptive statistics of different physico-chemical and hydrochemical parameters analysed

Parameters	Maximum	Minimum	Average	Standard deviation	Coefficient of variation (%)
T (°C)	29.1	21.6	24.2	1.4	5.8
EC (µS/cm-25°C)	3730.0	22.6	731.9	851.6	116.4
pH	8.5	4.5	6.7	0.8	11.7
TDS (mg/l)	3213.6	24.8	530.1	627.5	118.4
HCO_3^{-} (mg/l	1984.9	3.1	242.7	308.2	127.0
Cl^{-} (mg/l)	499.3	0.04	65.7	90.8	138.3
SO_4^{2-} (mg/l)	504.3	1.04	49.8	93.1	187.1
NO_3^{-} (mg/l)	83.3	0.1	17.6	18.5	104.7
NO_2^{-} (mg/l)	7.2	0.03	0.2	0.9	360.4
NH_4^{+} (mg/l)	5.7	0.0	0.2	0.7	327.2
PO_4^{3-} (mg/l)	0.9	0.04	0.1	0.1	125
Ca^{2+} (mg/l)	169.9	0.4	35.9	39.8	110.9
Mg^{2+} (mg/l)	74.5	0.9	16.6	18.6	111.6
Mn^{2+}(mg/l)	14.5	0.0	0.5	1.6	311.2
$Fe^{2+/3+}$ (mg/l)	54.0	0.01	2	6.3	316.1
K^{+} (mg/l)	252.0	0.11	20.3	31.2	153.9
Na^{+} (mg/l)	630.0	1.9	78.5	112.9	143.8
F^{-} (mg/l)	16.5	0.1	0.9	1.8	189.4
Al^{3+} (mg/l)	1.7	< dl	0.1	0.2	285.4
SiO_2 (mg/l)	30.1	0.1	11.0	6.8	61.9

VII.4.1. Physico-chemical parameters

VII.4.1.1. Temperature

Generally, higher topographic elevations are characterised by lower temperatures, TDS and electrical conductivities which are typical of recharge areas; whereas lower topographic depressions which generally correspond to discharge areas, are marked by higher temperature, TDS and electrical conductivities (Ganyaglo *et al.*, 2010).

Overall, the temperature of water samples from the study area does not vary a lot. It varies between a maximum of 29.1°C and a minimum of 21.6°C with an average of 24.2°C. High temperature values correspond to samples collected from the shallow lakes during the dry season: e.g. Lake Rweru in Mago II (29.1°C) (Appendix VII.1). These high temperatures of water samples from lakes seem to be compatible with the high air temperature which prevails in this area at the period of the year during sampling.

Table VII.2. Descriptive statistics of temperature values for various sources of water samples

	Max (°C)	**Min (°C)**	**Average (°C)**	**Standard deviation (°C)**	**Coefficient of variation (%)**
All samples	29.1	21.6	24.2	1.4	5.8
Lakes	29.1	23	26.11	1.91	7.32
Springs	25.6	21.6	23.44	0.90	3.84
Wells	27.8	22	24.50	1.13	4.63

High temperatures of groundwater, e.g. the well in Kigazi-Nyakarama (27.8°C) are associated with water samples taken from wells which were not submitted to pumping tests during the dry season. Hence, the high temperatures may reflect the influence of prevailing air temperatures which were transmitted to well water through the metallic well equipment. On average, spring waters show the lowest temperature values.

VII.4.1.2. Total dissolved solids (TDS) and electrical conductivity (EC)

Both parameters are treated together because they are intimately related. The TDS reflects the degree of mineralisation of water and refers to the sum of the concentration (in mg/l) of all the elements present in the water sample. Electrical conductivity, which reflects the ease with which electrical current is transmitted through a water sample, is a useful indicator of TDS. The TDS value is a very important parameter which determines the palatability of groundwater. Indeed, high values of TDS may impart a taste, an odour, colour, scaling of domestic utensils and appliances, thereby rendering it unacceptable for domestic consumption. As of now, there is no health-based value for TDS in the various editions of water quality standards proposed by the World Health Organisation (WHO, 2008). The only guideline value nowadays available for TDS is the limit of 1000 mg/l, which was established based on taste considerations (WHO, 1984).

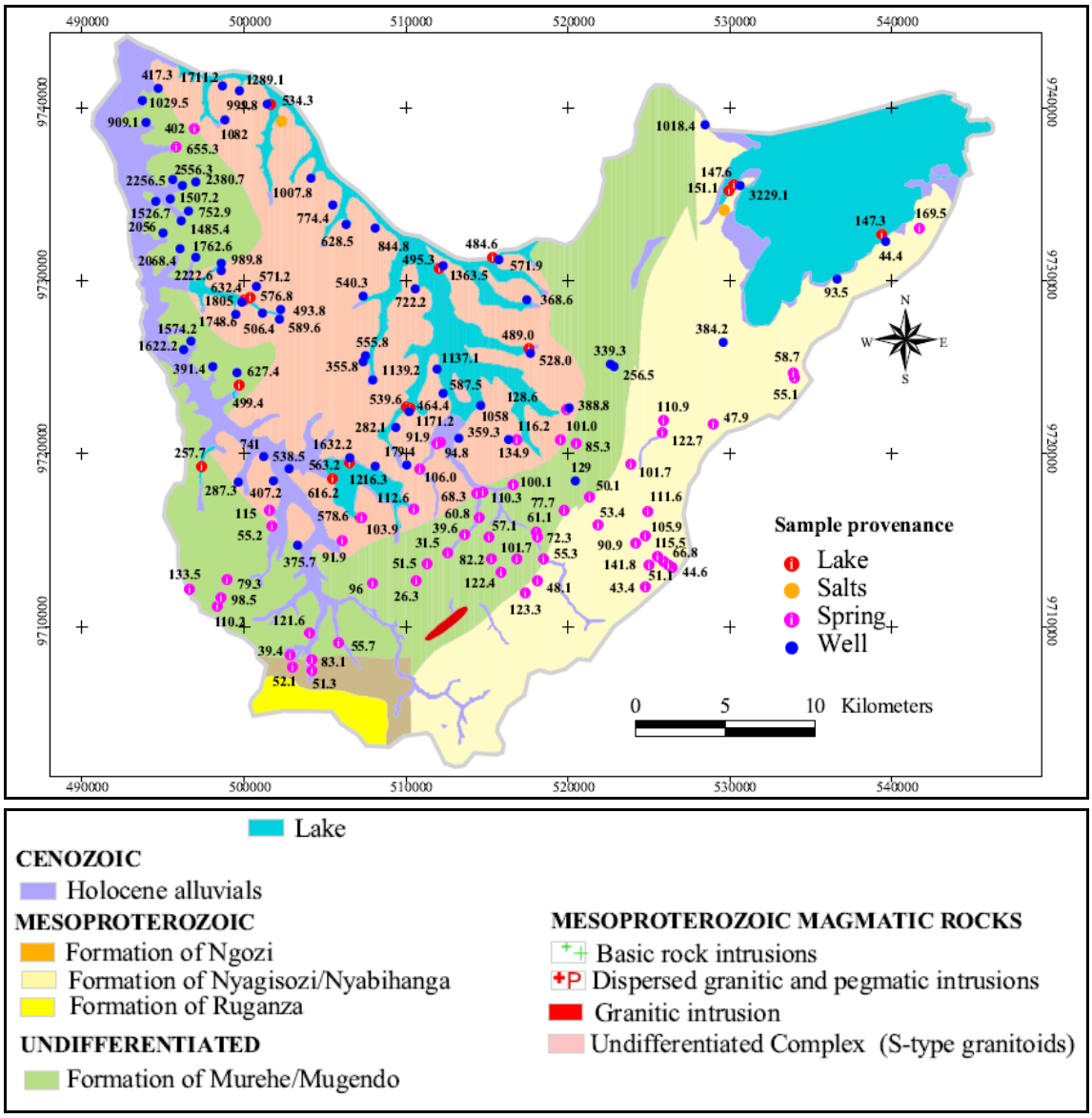

Figure VII.2. Map showing the spatial distribution of TDS (mg/l) across the study area

Overall, TDS values range from 26.3 mg/l to 3229 mg/l, with an average value of 542 mg/l (Table IV.3). Of the 143 water samples, 27 samples, which represent 18.9 % of all water samples analysed, show values of TDS greater than 1000 mg/l. The highest values of TDS are observed in water samples from wells, where this parameter ranges from 44.4 mg/l (Nyange-Kumana: Nr 127 in Appendix IV.1) to 3229 mg/l (Mago-Gatete: Nr 111 in Appendix IV.1) with an average of 974.6 mg/l. All the 27 water samples with TDS values exceeding 1000 mg/l were collected from wells. Figure VII.2 shows the spatial distribution of TDS across the study area. The high TDS values of water samples from wells are consistent with the relatively long flow path and residence time which favour a longstanding contact between the infiltrating water and the rock materials through which the water flows.

A comparison of the average values of TDS for the 16 lakes sampled shows that Lake Rweru is, by far, the least mineralized lake with an average TDS value of 148.8 mg/l, while Lake Gacamirinda appears to be the most mineralized lake with an average TDS of 604.6 mg/l (Appendix VII.1). The low mineralisation of Lake Rweru compared to other lakes of the marshy complex of Bugesera has been already observed by Ntakimazi (1985). This low mineralisation of Lake Rweru, despite the presence of salty encrustations and the well with the highest mineralisation on its western shore, may be related to dilution effect induced by the inflow of water from the River Nyabarongo. Indeed, during the high water stages of the River Nyabarongo, which generally occur in April or in May, an important volume of water overflows towards Lake Rweru through the narrow canal connecting the river and the lake.

While higher values of TDS could be expected in lakes, given the fact that the lakes constitute the ultimate surface reservoirs, to which drain waters after long residence times in underground reservoirs, the direct input of less mineralised water from rain and overland flow may have a dilution effect, which explains the low TDS values in lakes compared to groundwater samples from wells.

Table VII.3. Descriptive statistics of TDS values for various sources of water samples

	Max (mg/l)	**Min (mg/l)**	**Average (mg/l)**	**Standard deviation (mg/l)**	**Coefficient of variation (%)**
All samples	3229	26.3	542	630.7	116.3
Lakes	632.4	147.3	448.6	170.9	38
Springs	655.3	26.3	98.5	88.9	90.2
Wells	3229	44.4	974.6	691.5	71

With an average TDS value of 98.5 mg/l, spring waters show the lowest mineralisation (generally lower than 200 mg/l), which is consistent with the geological setting and, more importantly, with the short flowpaths and residence times. Indeed, most of the springs sampled are located in the southern highlands surrounding the depression of Bugesera. These highlands are underlain by metasedimentary rocks (quartzites, schists, psammoschists and psammites, conglomerates), whose mineral constituents are not easily soluble under normal physico-chemical conditions. Moreover, some of the springs such as Kididiri-Buhasa (Nr.36 in Appendix VII.1) and Rugomero-Nyabugeni (Nr.72 in Appendix VII.1) emerge from rocky beds made up of the above lithology.

However, springs located within the depression of Bugesera such as Mukuyo-Kiri (TDS = 631 mg/l, Nr. 48 in Appendix VII.1) and Mamfu-Kiyonza (TDS = 402 mg/l, Nr. 44 in Appendix VII.1) are characterised by relatively high values of TDS, which may result from long flow paths and residence time.

Electrical conductivity (EC in µS/cm-25°C) variation and distribution show close similarities with TDS. For the bulk of the samples, the EC values vary between a minimum of 22.60 µS/cm and a maximum of 3730 µS/cm with an average of 731.9 µS/cm. Considering that the maximum allowable TDS value in drinking water is 1000 mg/l (WHO, 2008) and that a factor of 1.5 (Goel, 2006) or 2 (Australian Government, 2003) can be used to convert the TDS value (in mg/l) into EC (in µS/cm at 25°C), the maximum allowable EC in drinking water can be roughly estimated at 1500 to 2000 µS/cm. The conversion factor proposed by the Australian Government seems to be highly exaggerated compared to the factor of 1.3 deduced from the correlation between EC (in µS/cm at 25°C) an TDS (mg/l) in this study (Figure VII.3) and the value of 1.5 proposed by Goel (2006). The European Union drinking water standards have established the maximum allowable EC in drinking water at 2500 µS/cm (at 20°C), which is equivalent to 2547.5 µS/m at 25°C. Over the 143 water samples collected in the study area, 15 samples show EC values greater than 2000 µS/cm and all are water samples from wells.

Table VII.4 shows some statistics of electrical conductivity values for various sources of water samples. Not surprisingly, water samples from wells have the highest values of electrical conductivity which confirm their high mineralisation. Overall, the lowest EC values are found in water samples from springs, except the springs in Mukuyo-Kiri (EC = 766 µS/cm-25°C) and Mamfu-Kiyonza (EC = 459 µS/cm-25°C), which show relatively high values of EC. The low values of EC associated with water samples from springs reflect the short residence time of water in rocks whose mineral constituents, i.e. silicates, are not easily soluble.

Table VII.4. Descriptive statistics of electrical conductivity for various sources of water samples (values in µS/cm-25°C)

	Max	**Min**	**Average µS/cm-25°C**	**Standard deviation µS/cm-25°C**	**Coefficient of variation %**
All samples	3730	22.6	731.9	851.6	116.4
Lakes	1027	166	641	280.2	43.7
Springs	766	22.6	136.9	108.3	79
Wells	3730	37.5	1303.9	942.8	72.3

Figure VII.3 represents a scatter diagram of TDS against EC which shows a very good correlation between both parameters, as evidenced by the very high coefficient of correlation (r = 0.99). From this figure, it is clearly shown that spring waters have the lowest TDS and EC, followed by lake water samples, while water samples from wells are spread over a wide range of values reflecting the high variability of factors governing groundwater chemistry, particularly in basement aquifer environments (Foster *et al.*, 1999).

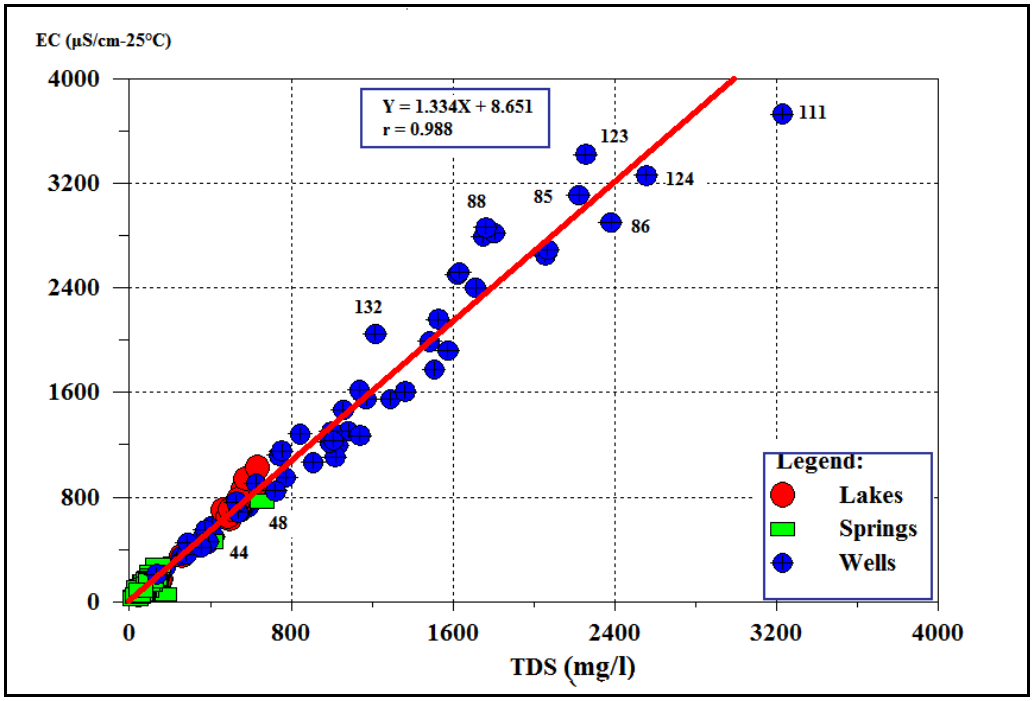

Figure VII.3. Scatter diagram of TDS (mg/l) against EC (µS/cm-25°C) showing a good correlation between both parameters (R = 0.988)

Figure VII.4 shows that, overall, the mineralisation of water is inversely related to the topographic elevation, which is in agreement with the fact that meteoric water recharging the aquifer in highlands further moves vertically and laterally to spring-discharge points downslope. This implies that the lower the topographic elevation of the discharge point, the longer the subsurface residence time and thus the higher the mineralisation of groundwater, contributed both by rock-water interaction and evaporative concentration.

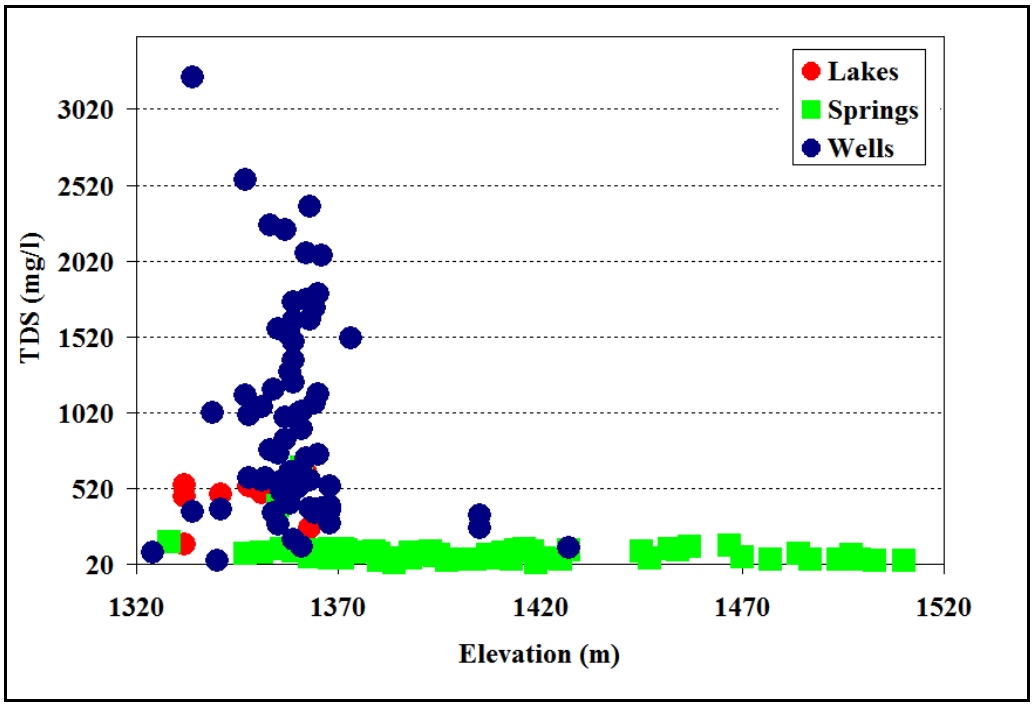

Figure VII.4. Variation of TDS value as a function of elevation (in m above the local datum, Arc 1950 for Burundi).

VII.4.1.3. pH

The pH is an important parameter which controls a number of hydrochemical processes, and thus determines the quality of groundwater. The different editions of WHO standards for drinking water have not yet established a health-based guideline for this parameter. The guideline nowadays in use is a pH range of 6.5-8.5, established based on aesthetic considerations (WHO, 2011). Acidic waters (pH<6.5) could leach metal ions such as iron, manganese, copper, lead, and zinc from the aquifer materials (Ganyaglo *et al.*, 2010).

Tables VII.5 and VII.6 show descriptive statistics of pH values for water samples of various provenances (springs, lakes and wells). Detailed values of pH measured in laboratory and in field are presented in Appendix VII.2. At first glance, there appears an obvious discrepancy between the pH values measured in field and in laboratory. For water samples collected from springs and wells, pH values measured in laboratory are higher than the values obtained in the field. The increase of pH between the field and the laboratory is attributable to the degassing of water (escape of CO_2) which may occur during the transport and storage of samples. On the other hand, for a number of water samples, mainly those collected from the small lakes, there is an opposite phenomenon whereby pH values measured in laboratory become lower than those measured in the field. This discrepancy may be due to measurement errors, but also to the dissolution of CO_2 which may take place between the field and the laboratory and which entails the

decrease of pH. Indeed, lake waters may exhibit very low dissolved CO_2 concentrations during the day, lower than prescribed by equilibrium with atmospheric p_{CO2}, due to photosynthetic CO_2 consumption, raising water pH (Ntakimazi, 1985).

Table VII.5. Descriptive statistics of pH values measured in field for different sources of water samples

	Max	Min	Average	Standard deviation	Coefficient of Variation (%)
All samples	9.4	4.6	6.4	1.2	19.2
Wells	7.7	5.6	6.9	0.5	6.9
Lakes	9.4	8.1	8.7	0.4	4.7
Springs	6.6	4.6	5.2	0.4	8.3

Table VII.6. Descriptive statistics of pH values measured in laboratory for different provenances of water samples

	Max	Min	Average	Standard deviation	Coefficient of variation (%)
All samples	8.5	4.5	6.7	0.8	11.8
Wells	8.5	6.2	7.1	0.4	5.3
Lakes	8.4	6.7	7.3	0.4	5.8
Springs	7.4	4.5	6.1	0.8	13.0

Figure VII.5 shows a crossplot of pH values measured in the laboratory against those measured in the field. This figure helps cluster the 3 provenances of water samples, i.e. lakes, wells and springs, which are clearly distinguished by field pH. Moreover, the figure clearly portrays the change of pH between the field and the laboratory. The figure seems to confirm an overall increase of pH for the majority of water samples from springs and wells between the field and the laboratory, while the pH values of water samples from lakes decrease. This important observation may raise the question of which of the two pH values is the most reliable. On one hand, field values of pH should better represent the actual aquifer conditions, but field conditions may not offer the best environment for measurement of this parameter. Indeed, it has been observed that several measurements of pH performed in the field, on the same sample, using the same meter, may give quite different values of pH. On the other hand, laboratory measurements, although performed with reliable equipment and in appropriate conditions, may not reproduce the actual physico-chemical conditions of the aquifer due to the changes (escape of CO_2, dissolution of CO_2) which occur between the field and the laboratory as a result of transport and storage. In this study the pH measured in the laboratory will be considered, unless otherwise stated.

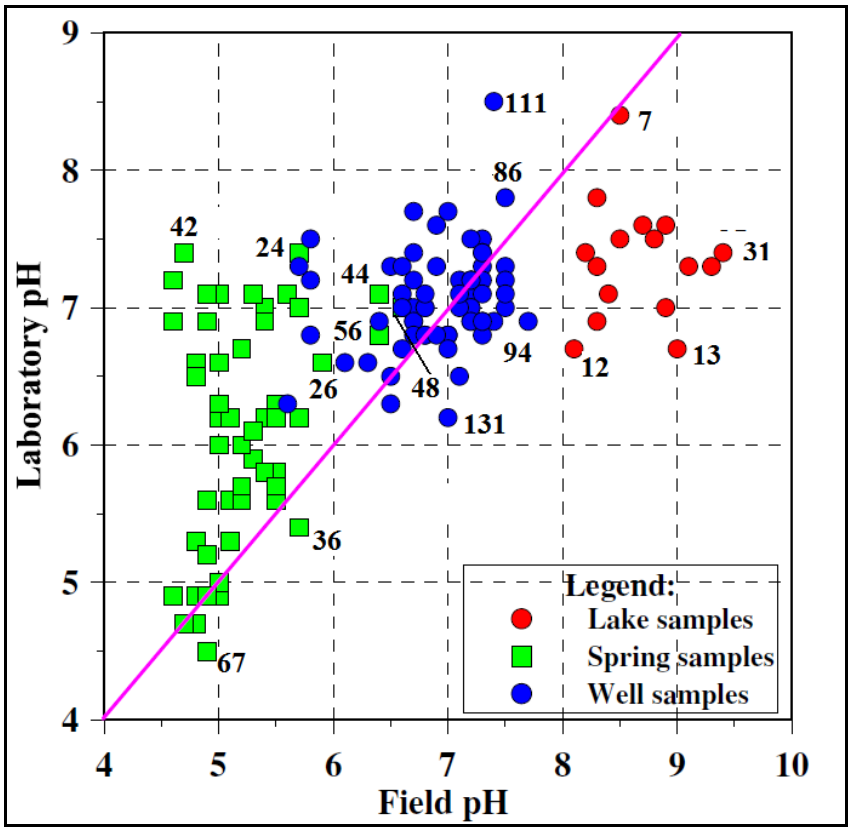

Figure VII.5. Crossplots of pH values measured in laboratory and pH values measured in the field. Numbers in the figure correpond to the sample S/N in appendix VII.2.

Overall, pH values of all water samples vary between a minimum of 4.5 (Rugangazi-Ntogwe) to a maximum of 8.5 (well in Mago-Gatete) with an average of 6.7. Water samples from lakes are clearly characterised by very high values of pH (field pH) which reflect the low levels of dissolved CO_2 in lakes and thus, low concentration of H_2CO_3 (Table VII.5, Appendix VII.2). According to Ntakimazi (1985), the low CO_2 content in lakes especially during the daytime should be ascribed to the aquatic photosynthetic activity which consumes dissolved CO_2 in water. Of the 6 lakes sampled (Cohoha South, Gacamirinda, Nagitamo, Narungazi, Rweru, Rwihinda), Lake Gacamirinda displays the highest average pH value, while Lake Rweru has the lowest average pH value (Table VII.7). It should be recalled that Lakes Gacamirinda and Rweru have also respectively the highest and lowest TDS and EC values.

Table VII.7. Average values of pH for the different lakes sampled

	Cohoha South	**Gacamirinda**	**Nagitamo**	**Narungazi**	**Rweru**	**Rwihinda**
Number of samples	6	2	1	1	3	3
Average pH	7.5	7.7	7	7.3	6.8	7.6

Water samples collected from springs show the lowest values of pH (Table VII.6). Indeed, of the 41 water samples with pH values lower than 6.5, 40 samples are from springs. The low pH values confirm the immaturity of spring waters, which emerge after short flow paths and still reflect the acidic character of the recharge water resulting from the dissolution of CO_2 in rain water both in the atmosphere and mainly in the soil zone, because of its higher p_{CO2}. The prevalence of acidic character of most spring waters is consistent with the low solubility of the rock-forming minerals along which flows the infiltrating water. The short residence time of the spring water in the subsurface allows only small amount of dissolution which does not profoundly modify the chemical character of the recharge water.

Water samples from wells show higher values of pH compared to spring water samples (Table VII.6). The highest value of pH corresponds to the water sample from the well at Mago-Gatete (sample Nr 111 in Appendix VII.2) which is also the water sample with the highest TDS and EC values. This observation indicates that, with increasing residence time, groundwater in the study area evolves mainly by the dissolution of silicate minerals. Indeed, the weathering reaction of silicates consumes carbonic acid, resulting in more alkaline waters due to the release of bicarbonate according to the reaction:

$$2KAlSi_3O_8 + 2H_2CO_3 + 9H_2O \rightleftharpoons Al_2Si_2O_5(OH)_4 + 4H_4SiO_4 + 2K^+ + 2HCO_3^- \quad (6.5)$$
Orthoclase kaolinite

$$2NaAlSi_3O_8 + 2H_2CO_3 + 9H_2O \rightleftharpoons Al_2Si_2O_5(OH)_4 + 4H_4SiO_4 + 2Na^+ + 2HCO_3^- \quad (6.6)$$
Albite kaolinite

The release of bicarbonate in water efficiently buffers the effect of the weak silicic acid resulting from the weathering of aluminosilicates and this would explain the slightly alkaline character of water samples collected from wells. Figure VII.6 shows the spatial distribution of pH values across the study area. As expected, lower pH values are found on the highlands where several springs emerge after short residence time.

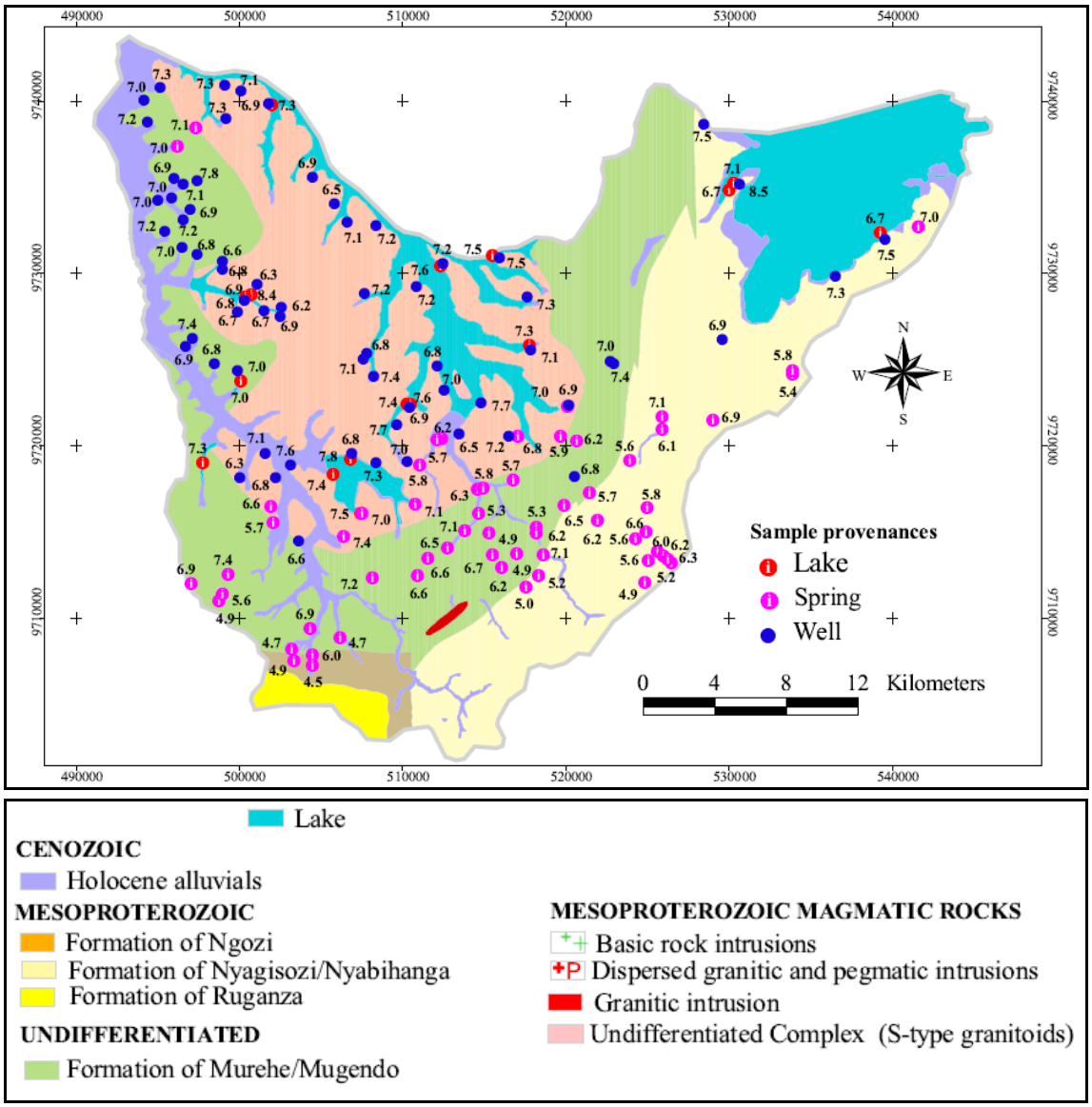

Figure VII.6. Spatial distribution of pH values (values measured in laboratory)

VII.4.2. Hydrochemical parameters

VII.4.2.1. Major ions

Major cations (Ca^{2+}, Mg^{2+}, Na^{+}, K^{+}) and anions (HCO_3^{-}, Cl^{-}, SO_4^{2-}, NO_3^{-}) account for 64.5 to 99.5 % of all the total ionic content. Major cations form 78.4 to 99.9 % of the total cation content, whereas major anions are in the range of 95.3 to 100 % of the total anion content. In this section, a discussion of the abundance and possible sources of major cations and anions is given with a view to inferring the hydrogeochemical processes which are responsible for the chemical composition of water in the study area.

VII.4.2.1.1. Major cations

a. Calcium (Ca^{2+})

Calcium is introduced into the hydrological cycle during the dissolution of readily soluble Ca-rich minerals such as carbonates, fluorites and sulphates, particularly limestone ($CaCO_3$), dolomite ($CaMg(CO_3)_2$), gypsum ($CaSO_4.2H_2O$), anhydrite ($CaSO_4$) and fluorite (CaF_2). The concentration of Ca^{2+} in groundwater in igneous and metamorphic terrains is generally low, due to the low rate of decomposition of aluminosilicate minerals. Groundwater in silicate terrains often contains less than 100 mg/l of Ca^{2+}. However, if carbonate minerals are present in the unsaturated zone and in the aquifer, groundwater may contain more than 100 mg/l of Ca^{2+} (Matthess, 1982). Ca^{2+} concentration in water, and to a lesser extent, magnesium, is responsible for hardness in water. There is no health guideline value for hardness. However, water hardness beyond 200 mg/l can cause scale deposition in the distribution system and kitchen utensils (WHO, 2011).

The Ca^{2+} concentration in the study area is represented in Figure VII.7. It varies between 0.4 mg/l (spring in Narutamwe-Kireka) and 170 mg/l (well in Gasagara I-Rubuga) with an average of 35.9 mg/l. Table VII.8 summarises some descriptive statistics of the Ca^{2+} concentration in the water samples from different sources, i.e. lakes, springs and wells. On average, the highest concentration in Ca^{2+} is observed in water samples from wells, whilst the lowest concentration is associated with water samples from springs.

Table VII.8. Descriptive statistics of Ca^{2+} concentrations in water samples from various sources

	Max mg/l	**Min mg/l**	**Average mg/l**	**Standard deviation mg/l**	**Coefficient of variation %**
All samples	169.9	0.4	35.9	39.8	110.8
Wells	169.9	4.3	65.5	41.0	62.6
Lakes	35.0	9.6	23.2	8.2	35.3
Springs	49.3	0.4	7.1	7.5	104.7

The net contrast in the observed concentration of Ca^{2+} between the immature spring waters and the water samples from the shallow wells confirms that there are hydrochemical processes which progressively increase Ca^{2+} in groundwater as it evolves on its flow path either horizontally or vertically. In spring water samples, relatively high concentrations of Ca^{2+} are found in water samples collected from springs situated within the depression of Bugesera, i.e. Mamfu-Kiyonza (49.3 mg/l, Nr. 44 in Appendix VII.1) and Mukuyo-Kiri (39.6 mg/l Nr. 48 in Appendix VII.1). Except these two springs, all other springs show very low concentrations of Ca^{2+}, which vary between 0.4 mg/l (Narutambwe-Kireka Nr 62 in Appendix VII.1) and 11.7 mg/l (Gihushi-Kiravumba Nr. 27 in Appendix VII.1).

Of the six lakes sampled, Lake Gacamirinda, which is also the most mineralised lake, has the highest concentration in Ca^{2+} whereas Rweru shows the lowest concentration with respect to this parameter. Table VII.9 shows the average concentration of Ca^{2+} in the different lakes sampled. The low Ca^{2+} concentration in Lake Rweru, which is consistent with the overall low mineralisation of this lake, is attributable to the dilution effect induced by the inflow of water from the River Nyabarongo. Moreover, it can be also noticed that, unlike the western side, the wells situated on the eastern side of the lake (Senga-Nyagisozi and Nyange-Kumana) also show low mineralisation and low levels of Ca^{2+}.

Table VII.9. Average concentration of Ca^{2+} (in mg/l) in different lakes sampled

	Cohoha South	**Gacamirinda**	**Nagitamo**	**Narungazi**	**Rweru**	**Rwihinda**
Number of samples	6	2	1	1	3	3
Average Ca^{2+}	22.8	33.9	28	18.5	12.6	23.7

The well in Mago-Gatete which presents the highest mineralisation does not show the highest Ca^{2+} concentration. This implies that Ca-Al-silicates are less abundant in rocks and are therefore not significantly contributing to the hydrochemical evolution of groundwater. Of the 66 wells sampled, only 11 wells have Ca^{2+} concentrations exceeding 100 mg/l. These wells are mainly situated in the western part of the study area. While values of Ca^{2+} concentration lower than 100 mg/l may be consistent with the low solubility of aluminosilicate minerals, these high concentrations of Ca^{2+} are unexpected in such geological environments and the fact that they are localised in the western part of the study area could point to an additional source of Ca^{2+} which might be the dissolution of secondary carbonate minerals. Indeed, Figure VII.7 shows that the highest concentrations of Ca^{2+} are not found in water samples collected within the Undifferentiated Complex where Ca-Al-silicates are likely to occur in the pegmatitic and granitic intrusions comprising this formation.

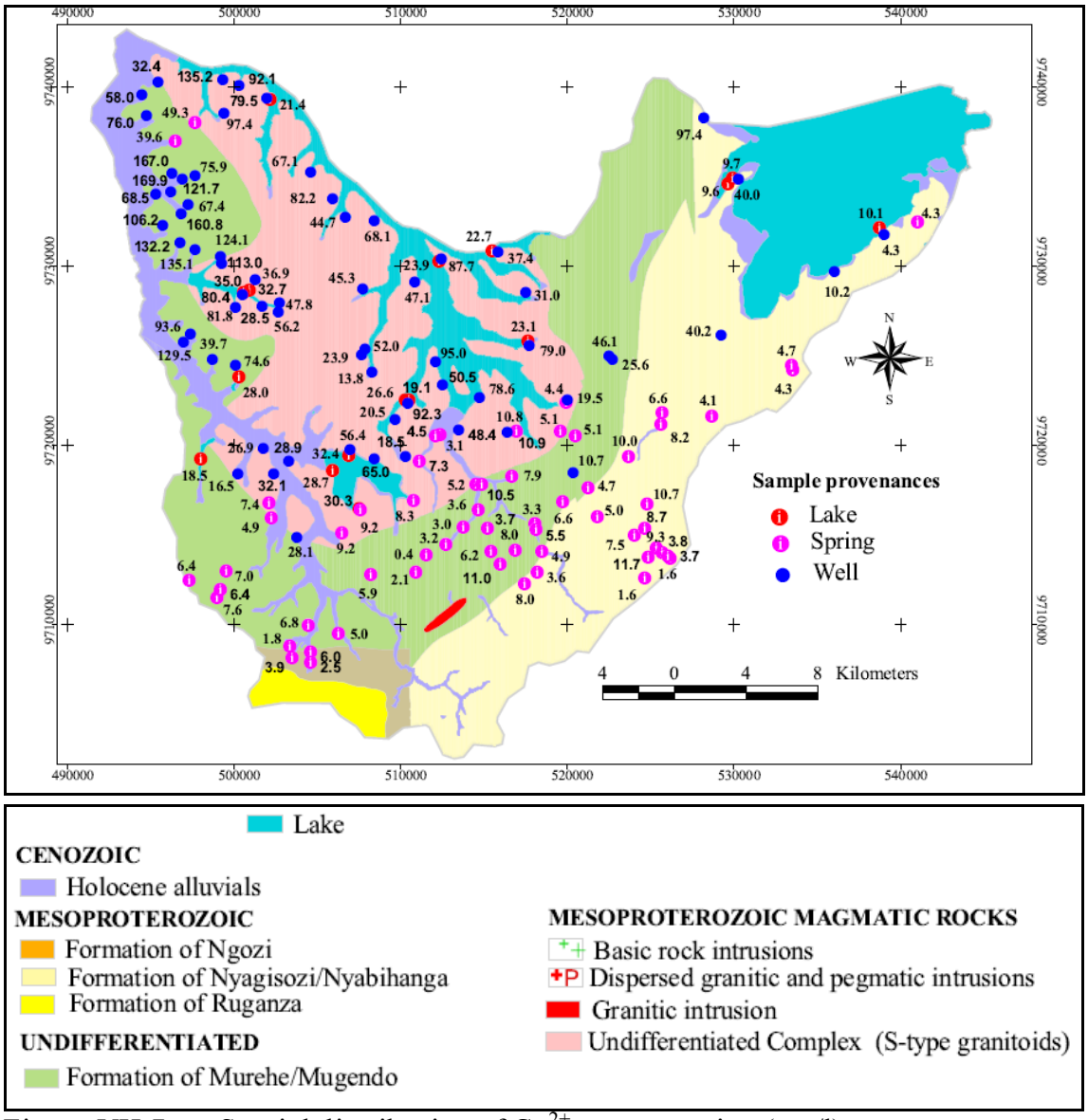

Figure VII.7. Spatial distribution of Ca^{2+} concentration (mg/l)

b. Magnesium (Mg^{2+})

Mg^{2+} is introduced in the hydrological cycle by the weathering of Mg-bearing silicates, such as ferromagnesian minerals, and carbonate minerals, mainly dolomite ($CaMg(CO_3)_2$) and magnesite ($MgCO_3$) (Matthess, 1982). The abundance of Mg^{2+} in all rock types is substantially lower than that of Ca^{2+} and, as a consequence, the concentration of Mg^{2+} in natural waters is generally below that of Ca^{2+} (Selinus *et al.*, 2005). The concentration of Mg^{2+} in groundwater is generally in the range 10 mg/l to 50 mg/l, but higher concentrations may occur in magnesium-rich aquifers such as olivine basalts, serpentine and dolomite (Matthess, 1982).

Figure VII.8 represents the spatial distribution of the concentration of Mg^{2+} across the study area. Table VII.10 shows some descriptive statistics of Mg^{2+} concentration in water samples from different sources. Overall, the concentration of Mg^{2+} in all water

samples varies between 0.9 mg/l (spring in Rugomero-Kiravumba Nr.71 in appendix VII.1) and 74.5 mg/l (well in Bishinzi-Cewe Nr. 78 in Appendix VII.1) with an average of 16.6 mg/l. On average, water samples from wells present the highest concentration of Mg^{2+}, while spring waters are characterised by the lowest concentrations of this element. This observation supports that, like Ca^{2+}, groundwater gets progressively enriched in Mg^{2+} along the flowpath by dissolution of Mg-bearing minerals. Thus, spring waters, which emerge after short residence time and short flowpath, show generally low levels of Mg^{2+}. The springs with relatively high concentrations of Mg^{2+}, i.e. Mamfu-Kiyonza (11.9 mg/l) and Mukuyo-Kiri (9.8 mg/l) are situated within the depression of Bugesera and are also the same with the highest concentration of Ca^{2+}. Except for these two springs, most spring water samples display concentrations of Mg^{2+} lower than 5 mg/l.

Table VII.10. Descriptive statistics of Mg^{2+} concentration in water samples from different sources

	Max mg/l	**Min mg/l**	**Average mg/l**	**Standard deviation mg/l**	**Coefficient of variation %**
All samples	74.5	0.9	16.6	18.6	111.5
Wells	74.5	2	28.7	41	143
Lakes	28.7	6.3	17.5	7.2	41.3
Springs	11.9	0.9	3.4	2	58.1

Table VII.11. Average concentration of Mg^{2+} (in mg/l) in different lakes sampled

	Cohoha South	**Gacamirinda**	**Nagitamo**	**Narungazi**	**Rweru**	**Rwihinda**
Number of samples	6	2	1	1	3	3
Average Mg^{2+}	19.5	23.3	17.3	7.7	6.4	24

While Lake Rweru remains the least mineralized lake also with respect to Mg^{2+} (average concentration of 6.4 mg/l), the highest concentration of this element is not found in Lake Gacamirinda (like for the Ca^{2+}), but in Lake Rwihinda which shows an average concentration in Mg^{2+} of 24 mg/l (Table VII.11). This seems to be consistent with the fact that the water sample with the highest concentration of Mg^{2+} (74.5 mg/l) comes from the well in Bishunzi-Cewe (Nr 78 in Appendix VII.1), which is situated in the watershed of Lake Rwihinda.

Of the 66 water samples collected in wells, 14 samples show Mg^{2+} concentrations exceeding 50 mg/l, which is the maximum typical concentration of this element in groundwater. The lowest concentration of Mg^{2+}, observed in the water sample from the

well at Senga-Nyagisozi, is in line with the general low mineralisation of water from this part of the watershed of Lake Rweru. However, the water sample from the well at Mago-Gatete, which is characterised by the highest TDS and EC values, surprisingly shows a low concentration of Mg^{2+} (3 mg/l). This confirms that Ca-Mg-Al-silicates are less abundant in rocks and do not contribute to the hydrochemical evolution of groundwater. Moreover, the occurrence of high concentration of Mg^{2+} in water samples collected in the western part of the study area seem to confirm the existence of secondary carbonate minerals. Indeed, the same water samples are characterised by elevated concentrations of Ca^{2+}.

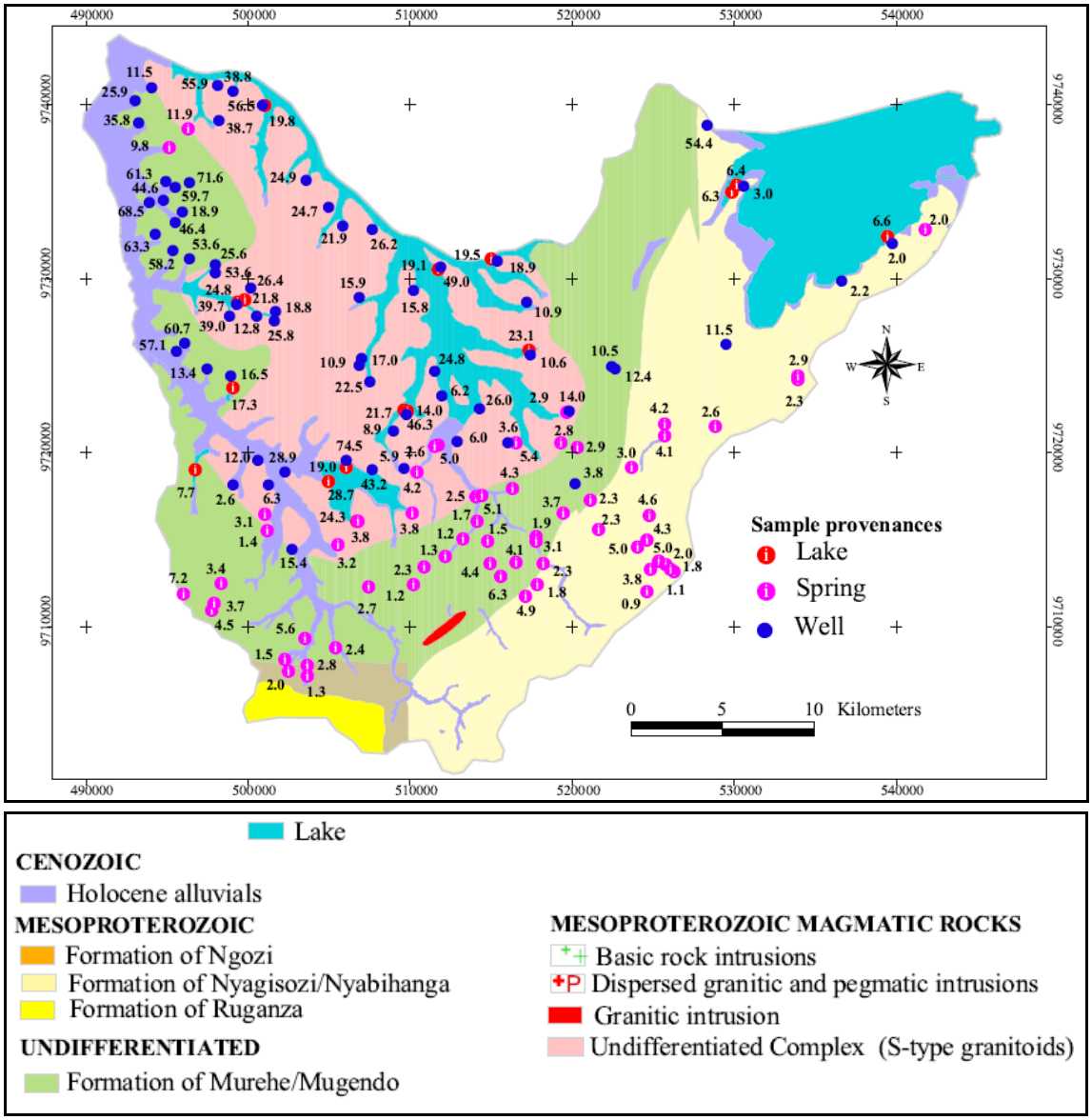

Figure VII.8. Spatial distribution of Mg^{2+} concentration (mg/l)

c. Sodium (Na^+)

Sodium is released in groundwater during the weathering of silicate minerals and especially Na-rich feldspars and feldspathoid minerals (Mathess, 1982). However, the main source of Na^+ to the hydrological cycle is from the ocean in the form of sea spray and its concentrations in rainfall decrease inland. Besides, connate seawater can be a important end member to groundwater, contributing high amounts of Na^+ to groundwater (Walraevens & Van Camp, 2005). Na^+ can also originate from evaporitic concentrations of salts which derive from advanced evaporation of Na-solutions in sediments. The common process which reduces the concentration of Na^+ in groundwater is the adsorption on clay minerals with high cation-exchange capacities. High concentration of Na^+ in groundwater may result from contamination from sewage, industrial effluents, de-icing salts and saltwater intrusion in coastal aquifers (Chapman & Kimstach, 1996).

As of now, there is no health-based guideline for Na^+ concentration in drinking water in the different editions of standards for drinking waters. The proposed guideline of 200 mg/l of Na^+ in groundwater is based on taste considerations. Indeed it is believed that beyond a concentration of 200 mg/l, water may have an unacceptable taste (WHO, 2011).

The Na^+ concentration in the study area is represented in Figure VII.9. Table VII.12 presents descriptive statistics of Na^+ concentration for water samples from different provenances. Na^+ concentration for the bulk of water samples collected for this study varies between a minimum of 1.9 mg/l (spring in Karobogo-Kanyinya, Nr. 36 in Appendix VII.1) and 630 mg/l (well in Mago-Gatete, Nr. 111 in Appendix VII.1) with an average of 78.5 mg/l. Of the 143 water samples collected, Na^+ is the most abundant cation in 114 samples, which represent 80 % of the samples. The highest concentrations of Na^+ are found in water samples collected from wells whereas the lowest concentrations are associated with spring water samples. Of the 143 water samples analysed, 11 samples show concentrations of Na^+ exceeding the taste-based guideline (200 mg/l) and are all from wells.

Table VII.12. Descriptive statistics of Na^+ concentration for water samples of various sources

	Max mg/l	Min mg/l	Average mg/l	Standard deviation mg/l	Coefficient of variation %
All samples	630	1.9	78.5	112.9	143.8
Wells	630	4.1	143	138.2	96.7
Lakes	100.4	11	63.7	29.8	46.8
Springs	123.8	1.9	12.7	15.7	123.4

Except five springs (Bunyari-Rugarama, Gihushi-Kiravumba, Mamfu-Kiyonza, Mukuyo-Kiri and Musave-Rutabo), water samples from other springs have Na^+ concentrations lower than 20 mg/l. The spring in Mukuyo-Kiri, which is located within the depression, has the highest concentration in Na^+ (123.8 mg/l). Hence, as this has already been pointed out for other constituents, this observation confirms that the processes that increase the Na^+ in groundwater may act progressively as the water moves on its flow path. This may explain why samples from wells or springs located in the depression show high levels of dissolved constituents compared to the young spring waters which emerge in the highlands.

Water samples collected from lakes display intermediate concentrations of Na^+. Table VII.13 shows the average concentration of Na^+ in the different lakes sampled. Lake Rwihinda shows the highest concentration of Na^+, whilst Lake Rweru remains with the lowest concentration of this parameter.

Table VII.13. Average concentration of Na^+ (in mg/l) in different lakes sampled

	Cohoha South	**Gacamirinda**	**Nagitamo**	**Narungazi**	**Rweru**	**Rwihinda**
Number of samples	6	2	1	1	3	3
Average Na^+ (mg/l)	68.2	90.2	65.9	40.6	12.1	95.6

Na^+ concentration in water samples from wells shows a wide variation with a minimum of 4.1 mg/l (well in Nyange-Kumana Nr. 127 in Appendix VII.1) and a maximum of 630 mg/l (well in Mago-Gatete Nr. 111 in Appendix VII.1). It is worth to note that the two wells with the extreme concentrations of Na^+ are situated within the watershed of Lake Rweru but on opposite sides of this lake, which shows the lowest mineralisation.
The predominance of Na^+ in most of water samples collected in this study points to the weathering of Na-bearing silicates as the main process controlling the hydrogeochemical evolution of groundwater in the study area. The localised occurences of evaporitic salts such as in Mago-Gatete or in Rubirizi-Bugabira may contribute to some extent, but do not play a major role, as this is evidenced by quite normal levels of chloride in groundwater samples collected close to these salt quarries (e.g. sample Nr. 111 in Appendix VII.1), from the well in Mago-Gatete.

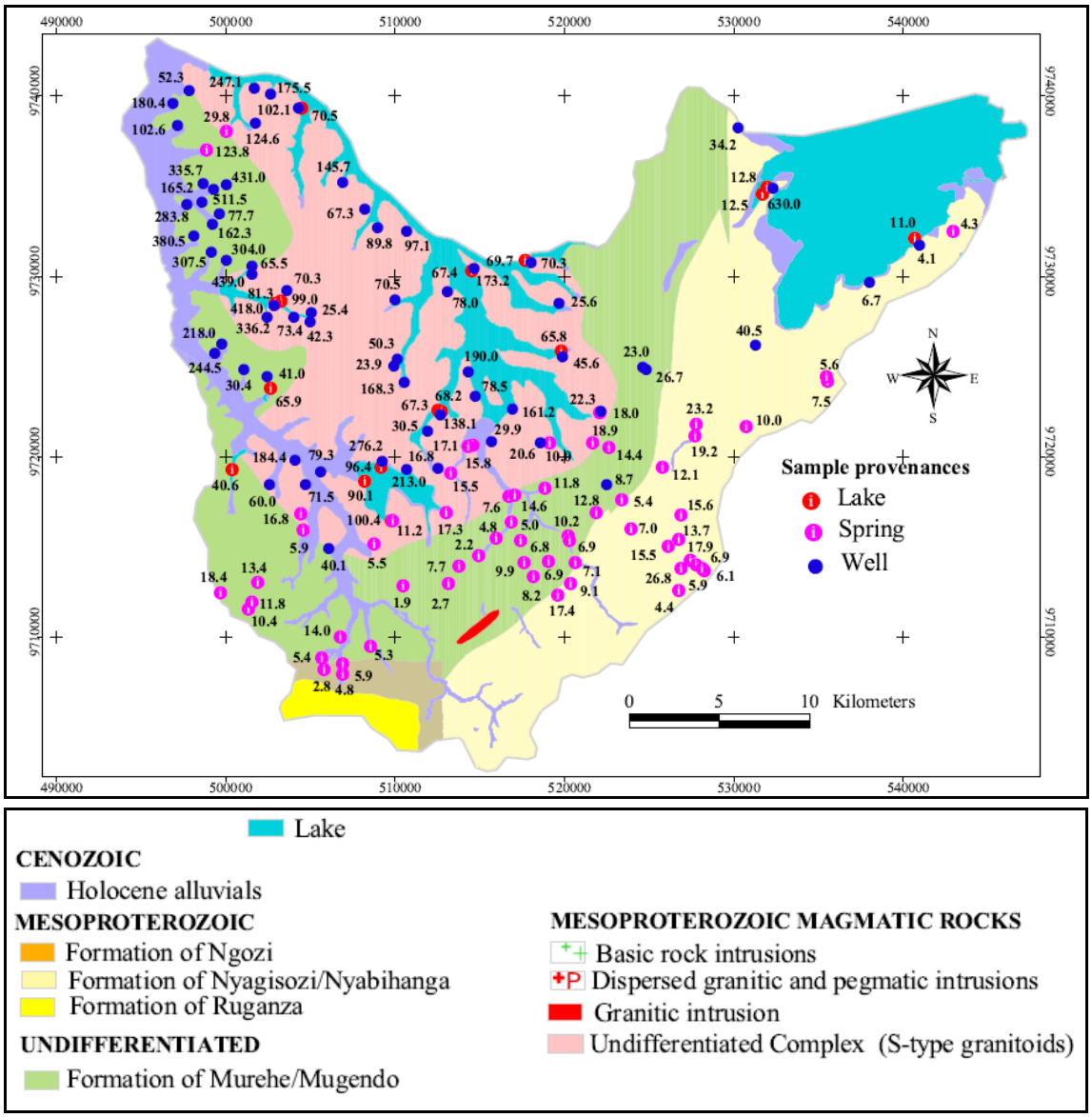

Figure VII.9. Spatial distribution of Na^+ concentration (in mg/l)

d. Potassium (K^+)

Potassium (K^+) is generally released to the groundwater from the weathering of aluminosilicate (K-feldspars, feldspathoids and micas) and clay minerals. It is seldom found in high concentrations in groundwater due to the resistance of K-bearing silicates to weathering combined to its low geochemical mobility in fresh water. High concentrations of potassium may be associated with leaching of evaporatic deposits which contain K-bearing minerals. High levels of K^+ in water may also arise from anthropogenic pollution (agricultural fertilisers, domestic or animal waste) (Matthess, 1982). There is no WHO guideline for the maximum allowable concentration of K^+ in drinking water (WHO, 2009), but European Union proposes a maximum of 12 mg/l (EPA, 2004).

The spatial distribution of the K^+ concentration in the study area is represented in Figure VII.10. Table VII.14 summarises some descriptive statistics of K^+ concentrations for water samples collected from the different sources. Overall, the concentration of K^+ falls within the range of 0.1 mg/l (well in Kigina-Gisenyi I, Nr. 103 in Appendix V.1) to 252 mg/l (well in Mago-Gatete, Nr. 111 in Appendix V.1) with an average of 20.3 mg/l. Of the 143 water samples collected, 60 samples, which represent 42 % of all water samples, have a concentration of K^+ exceeding 12 mg/l, the European Union guideline for K^+ in drinking water. Except one spring water sample, all other water samples with a concentration of K^+ exceeding 12 mg/l are from lakes and wells.

Table VII.14. Some descriptive statistics of the concentration of K^+ for different sources of water samples

	Max mg/l	Min mg/l	Average mg/l	Standard deviation mg/l	Coefficient of variation %
All samples	252.0	0.1	20.3	31.2	153.8
Wells	252.0	0.1	35.8	38.5	107.4
Lakes	49.0	3.4	26.5	16.2	61.2
Springs	20.0	0.1	1.8	2.7	152.0

On average, water samples from wells show the highest average concentration of K^+, whereas samples from springs have the lowest concentration of this parameter. Overall, water samples from wells show relatively elevated concentration of K^+ in the northwestern part of the study area, although the well with the highest concentration of K^+ (252 mg/l) is located in Mago-Gatete (Nr. 111), close to the Lake Rweru (Figure VII.10). The low concentration in wells in Kigina-Gisenyi I (0.1 mg/l) and Kigina-Gisenyi II (0.5 mg/l) is consistent with the fact that these wells are surrounded by outcrops of the quartzite of Burara, whose mineral constituents do not contain potassium. The highest concentration of K^+ (252 mg/l) associated with the well in Mago-Gatete results from the weathering of K-Al-silicates with additional, but not substantial contribution from the leaching of evaporitic deposits situated at a short distance upgradient of the well.

Table VII.15 shows a comparison of the average concentration of K^+ in water samples collected from the 6 lakes. The small Lake Nagitamo has the highest concentration of K^+, while another small lake, i.e. Narungazi has the lowest concentration of this element. The two small lakes are situated in the western part of the study area. However, the two values of K^+ concentration are based on one sample.

Figure VII.10 shows the spatial distribution of K^+ concentration across the study area. It can be observed from the map that the southern highlands where emerge several springs and the eastern part are, overall, characterised by the lowest concentrations of K^+.

Indeed, t he concentration of K^+ in water samples from springs varies between a minimum of 0.14 mg/l (spring at Kinyangurube-Karehe) and a maximum of 20 mg/l, with an average of 1.8 mg/l (Table VII.14)

Table VII.15. Average concentration of K^+ (in mg/l) in different lakes sampled

	Cohoha South	Gacamirinda	Nagitamo	Narungazi	Rweru	Rwihinda
Number of samples	6	2	1	1	3	3
Average K^+ (mg/l)	35.5	25.3	39.0	3.4	6.4	32.7

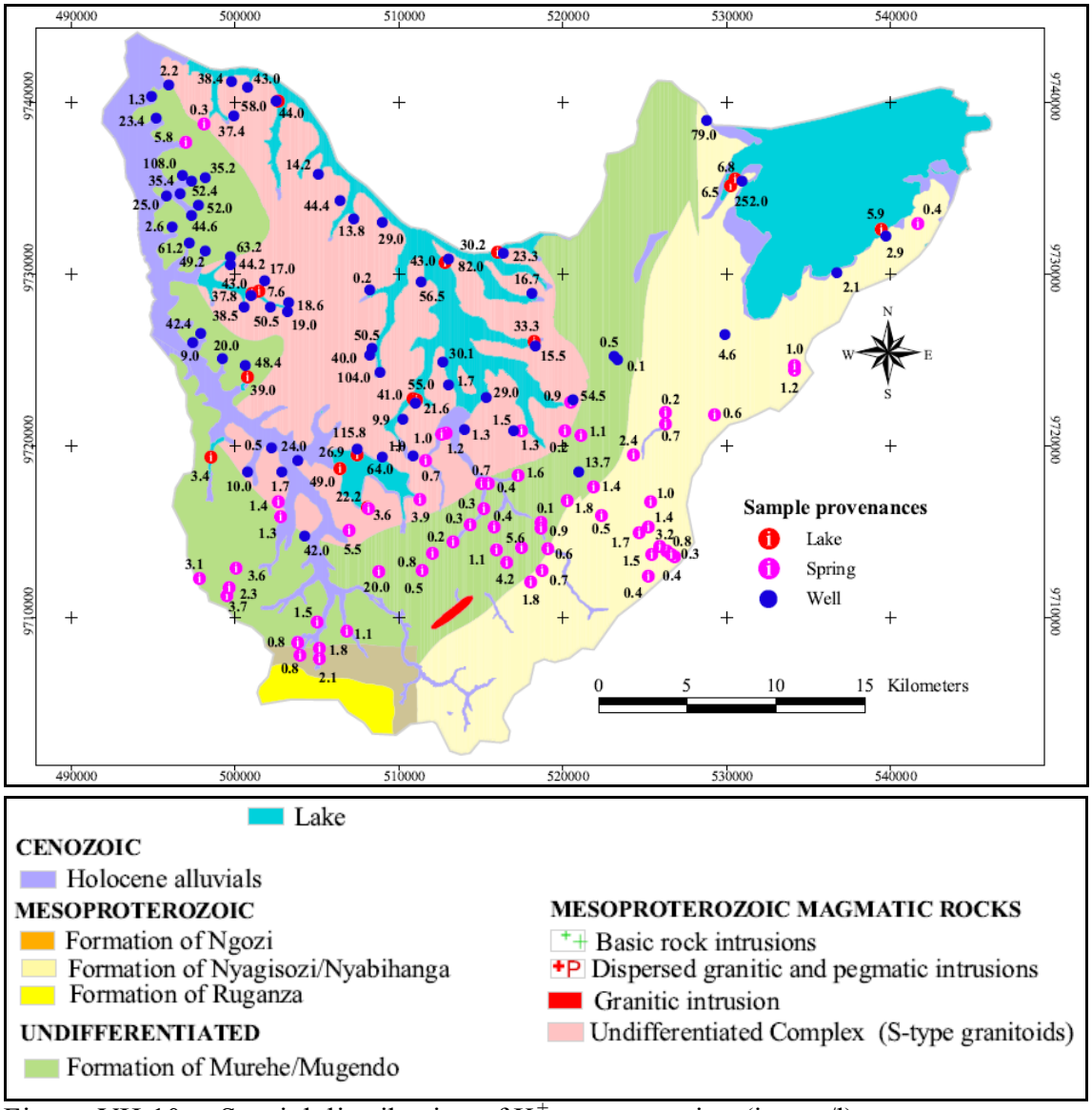

Figure VII.10. Spatial distribution of K^+ concentration (in mg/l)

VII.4.2.1.2. Major anions

a. Bicarbonate (HCO_3^-)

Bicarbonate is formed by the reaction between the percolating water and the dioxide of carbon (CO_2). The latter may originate from the atmosphere or from the soil zone where it is released by the respiration of microorganisms or the aerobic and anaerobic decomposition of organic matter.

The CO_2 reacts with water to form the weak carbonic acid (H_2CO_3) according to the reaction:

$$CO_2+H_2O \leftrightarrow H_2CO_3 \leftrightarrow HCO_3^-+H^+ \leftrightarrow CO_3^{2-}+H^+ \qquad (6.7)$$

The carbonic acid hence formed will further attack and breakdown rock-minerals, resulting in the release of ions responsible for the various hydrochemical facies. The following reactions illustrate the breakdown of carbonate and silicate minerals:

$$CaCO_3 + CO_2 + H_2O \leftrightarrow Ca^{2+} + 2HCO_3^- \qquad (6.8)$$ Calcite

$$2KAlSi_3O_8 + 2H_2CO_3 + 9H_2O \rightleftharpoons Al_2Si_2O_5(OH)_4 + 4H_4SiO_4 + 2K^+ + 2HCO_3^- \qquad (6.9)$$
Orthoclase Kaolinite

The carbonate system is chiefly governed by pH conditions which determine in which form the CO_2 will occur in aqueous solutions. Under usual pH conditions of groundwater (6-8.5), the HCO_3^- species predominates. In the acid (pH<6) and the highly alkaline ranges (pH>10), undissociated $H_2CO_{3(aq)}$ and CO_3^{2-} species are respectively the dominant species.(Appelo & Postma, 2005).

The HCO_3^- concentration in the study area is represented in Figure VII.11. Table VII.16 presents descriptive statistics of bicarbonate concentration in the water samples from the three sources (lakes, springs and wells). Overall, HCO_3^- concentration varies between a minimum of 3.1 mg/l (spring in Twengebuye-Nakabingo) and a maximum of 1984.9 mg/l (well in Mago-Gatete) with an average of 242.7 mg/l. HCO_3^- appears to be the most dominant anion in the majority of the samples. Indeed, out of the 143 water samples collected, HCO_3^- is the dominant anion in 110 samples, which represent 77 % of all water samples.

On average, springs show the lowest concentration of HCO_3^-, whereas water samples from wells display the highest HCO_3^- concentration. The low HCO_3^- concentration in spring waters (average concentration of 27.1 mg/l) can be chiefly explained by the absence of carbonate rocks in the study area, the short flowpath, which implies short residence time, and the attendant low dissolution of silicate minerals. There is a clear

contrast between the HCO_3^- concentration in water samples collected from springs located in the highlands with low concentrations and those located in the depression of Bugesera with the highest concentration of bicarbonate, i.e. Mukuyo-Kiri (328.2 mg/l) and Mamfu- Kiyonza (231.2 mg/l). Apart from these two springs, it is clear that there is a general increase of HCO_3^- concentration in spring waters from the South to the North (Figure VII.11). This observation confirms that the long residence time and flowpath of infiltrating water in the subsurface lead to increased concentration of HCO_3^- and thus to the substantial dissolution of rock-forming minerals, as evidenced by high TDS and EC. Despite the high average concentration of HCO_3^- in water samples from wells, 3 wells, i.e Susa-Gikomero (47 mg/l, Nr. 143 in Appendix VII.1), Rugoma-Kagege (42.7 mg/l, Nr. 128 in Appendix VII.1) and Nyange-Kumana (16.5 mg/l, Nr. 127 in Appendix VII.1) show HCO_3^- concentrations lower than 50 mg/l. The low concentrations of HCO_3^- associated with these wells, which are situated at the the foot of the southern and eastern highlands, reflect short flowpaths and residence time. The water sample from the well situated in Nyange-Kumana is characterised by a general low mineralisation. Although the highest concentration of HCO_3^- is associated with the well at Mago-Gatete, which is situated in the eastern part of the study area, Figure VII.11 shows that the majority of water samples with high HCO_3^- content come from the western part of the study area.

Table VII.16. Some descriptive statistics of the concentration of HCO_3^- for different sources of water samples

	Max mg/l	**Min mg/l**	**Average mg/l**	**Standard deviation mg/l**	**Coefficient of variation %**
All samples	1984.9	3.1	242.7	308.2	127.0
Wells	1984.9	16.5	447.1	343.2	76.8
Lakes	323.9	86.6	221.1	74.8	33.8
Springs	328.2	3.1	27.1	49.2	181.3

Table VII.17. Average concentration of HCO_3^- (in mg/l) in different lakes sampled

	Cohoha South	**Gacamirinda**	**Nagitamo**	**Narungazi**	**Rweru**	**Rwihinda**
Number of samples	6	2	1	1	3	3
Average HCO_3^- (mg/l)	263.6	302.3	229.4	149.5	89.3	234.9

Table VII.17 shows the comparison of average HCO_3^- concentration in water samples from the different lakes. It can be observed that Lake Gacamirinda has the highest concentration of HCO_3^-, while Lake Rweru displays the lowest concentration. The difference in concentration of HCO_3^- among the water samples from the different lakes confirms that, besides the input of bicarbonate from dissolution of atmospheric and soil

zone CO2, there is an important dilution effect which explains the low levels of bicarbonate in Lake Rweru. Indeed, this lake is directly connected to the River Nyabarongo through a narrow and short canal, whereas the other lakes are connected to the River Kanyaru by means of swampy valleys. Hence, Lake Rweru receives more important quantities of water during the high stages of rivers, in April-May, than the other lakes.

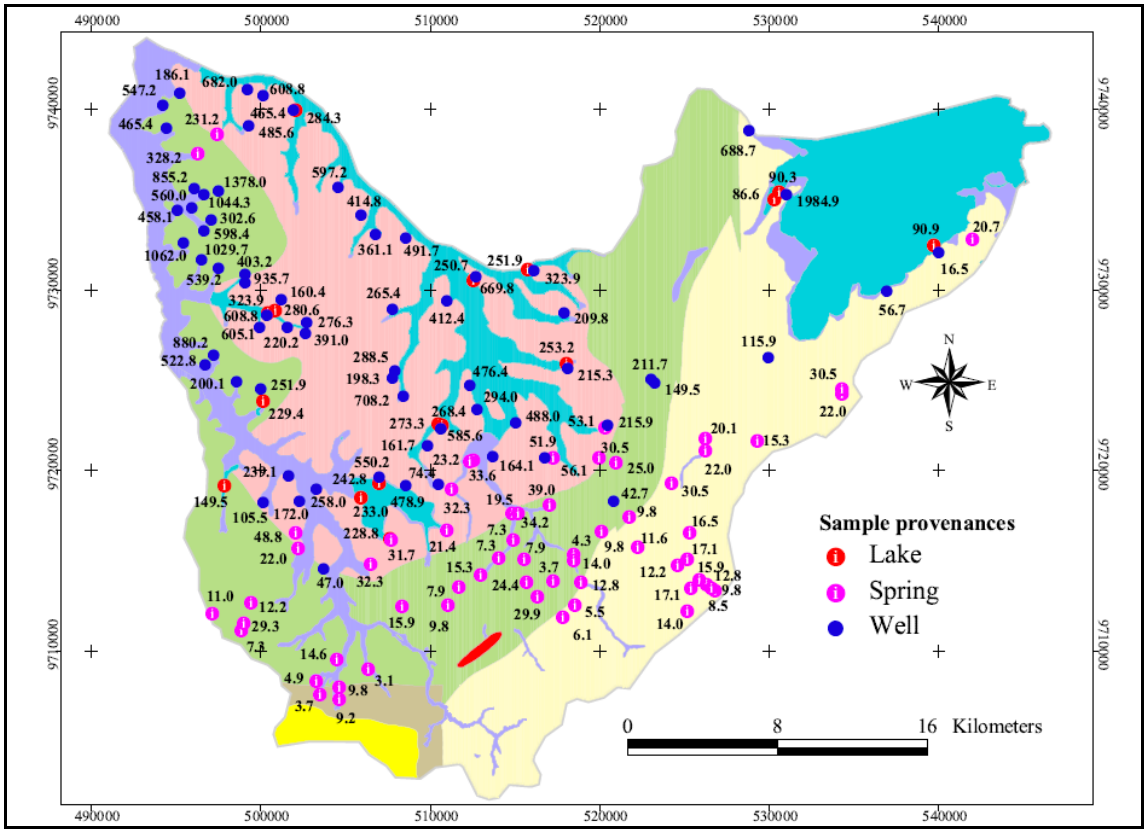

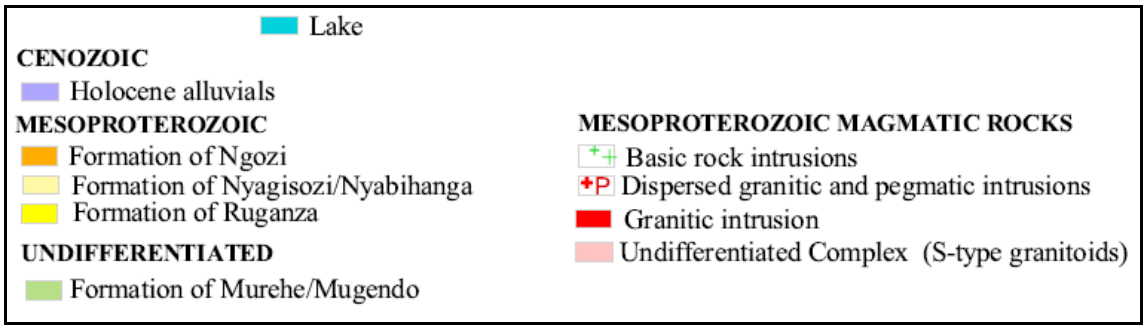

Figure VII.11. Spatial distribution of HCO_3^- concentration (in mg/l)

B Chloride (Cl^-)

Chloride enters the groundwater system with infiltrating rainwater which carries atmospheric deposition of oceanic aerosols and with the weathering of salt deposits. Groundwater in chloride-poor crystalline rocks and sedimentary rocks generally shows low chloride contents (<30 mg/l). Higher concentrations of chloride in groundwater are indicative of anthropogenic pollution or natural processes, such as salt water intrusion,

essentially in coastal aquifers. Chloride is a conservative substance in the sense that it does not participate in any hydrogeochemical processes (Caubel-Forget *et al.*, 2001; Walraevens & Van Camp, 2005) and is not affected by pH and redox conditions. Its concentration therefore varies due to evaporation, dilution, anthropogenic pollution or admixture with (fossil or recent) seawater. So far, there is no health-based standard for chloride concentration in groundwater, however it is considered that a concentration exceeding 250 mg/l is likely to result in a detectable taste, thus rending water unpalatable (WHO, 2008).

The spatial distribution of Cl^- concentration in the study area is represented in Figure VII.12. Table VII.18 shows descriptive statistics of the concentration of Cl^- in water samples collected in this study. Overall, the Cl^- concentration lies in between 0.04 mg/l (spring in Mamfu-Kiyonza, Nr. 44 in Appendix VII.1) and 499.3 mg/l (well in Shenga III-Rugasa, Nr 140 in Appendix VII.1) with an average of 65.7 mg/l. Of all water samples analysed, 7 samples show Cl^- concentrations exceeding the taste-based standard of 250 mg/l and all these samples are from wells. On average, water samples from wells are characterised by the highest concentration of Cl^- whereas samples collected from springs show the lowest concentrations.

Figure VII.12 shows the spatial distribution of the concentration of Cl^- in water samples collected in the study area. The highest concentrations of Cl^- occur in the western part of the study area, where most of the wells with concentrations of Cl^- exceeding the taste-based guideline are located (e.g. Shenga III-Rugasa, Nr.140; Shenga II-Rugasa Nr.141; Gahwijo I-Nyabikenke, Nr. 85). These high concentrations of Cl^- are mainly the result of the evaporative concentration of groundwater along the flowpath with an additional contribution from anthropogenic pollution and dissolution of evaporitic salts. The lowest concentration in Cl^- associated with the well in Senga-Nyagisozi (1.4 mg/l Nr.139 in Appendix VII.1) is in agreement with the overall low concentration of other dissolved consituents in water samples collected on this side of the watershed of Lake Rweru. The well in Mago-Gatete, which is yet characterised by the highest TDS value, does not show a very high concentration of Cl^- (142 mg/l) compared to other dissolved elements, such as Na^+ (630 mg/l) and HCO_3^- (1984.94 mg/l). Despite the presence of halite within the evaporitic salts at Mago-Gatete (Nr. 111 in Appndix VII.2) as revealed by the X-ray analyses, the moderate concentration of Cl^- in this well, which is located in the vicinity of the quarry of these salt deposits, may indicate that the high mineralisation of groundwater in this area is not mainly caused by these salts, but mainly by the weathering of alumino-silicates.

Figure VII.12 also shows that, except some springs like in Gihushi-Kiravumba (56.7 mg/l, Nr. 27 in Appendix VII.1), Bishunzi-Munyinya (33.8 mg/l, Nr. 18 in Appendix

VII.1) or Karira-Gatemere (27.8 mg/l, Nr. 34 in Appendix VII.1) which show relatively high concentrations of Cl^- most probably resulting from anthropogenic pollution, there is a general trend of increasing Cl^- concentration along the flowpath, which could be mainly ascribed to the evaporative concentration. Indeed, it can be observed from the figure that there is a tendency of increasing Cl^- concentration from the South (highlands) towards the North (depression of Bugesera).

Table VII.18. Some descriptive statistics of the concentration of Cl^- for different sources of water samples

	Max mg/l	Min mg/l	Average mg/l	Standard deviation mg/l	Coefficient of variation %
All samples	499.3	0.0	65.7	90.8	138.3
Wells	499.3	1.4	109.9	112.4	102.3
Lakes	166.9	0.3	79.6	51.4	64.5
Springs	115.2	0.0	14.2	17.2	121.2

Table VII.19. Average concentration of Cl^- (in mg/l) in different lakes sampled

	Cohoha South	Gacamirinda	Nagitamo	Narungazi	Rweru	Rwihinda
Number of samples	6	2	1	1	3	3
Average Cl^- (mg/l)	75.7	108.9	102.7	23.6	5.1	153.3

A comparison of the average concentration of Cl^- for the different lake samples shows that Rweru has, by far, the lowest average concentration of Cl^- (5.1 mg/l) while Lake Rwihinda displays the highest concentration (153.3 mg/l) (Table VII.19). Besides the Cl^- amount introduced by rainwater, which should be equally distributed as all the lakes are situated in the same region, this large contrast in concentrations of this element highlights the importance of the dilution, which causes Lake Rweru to have very low concentrations of dissolved solides.

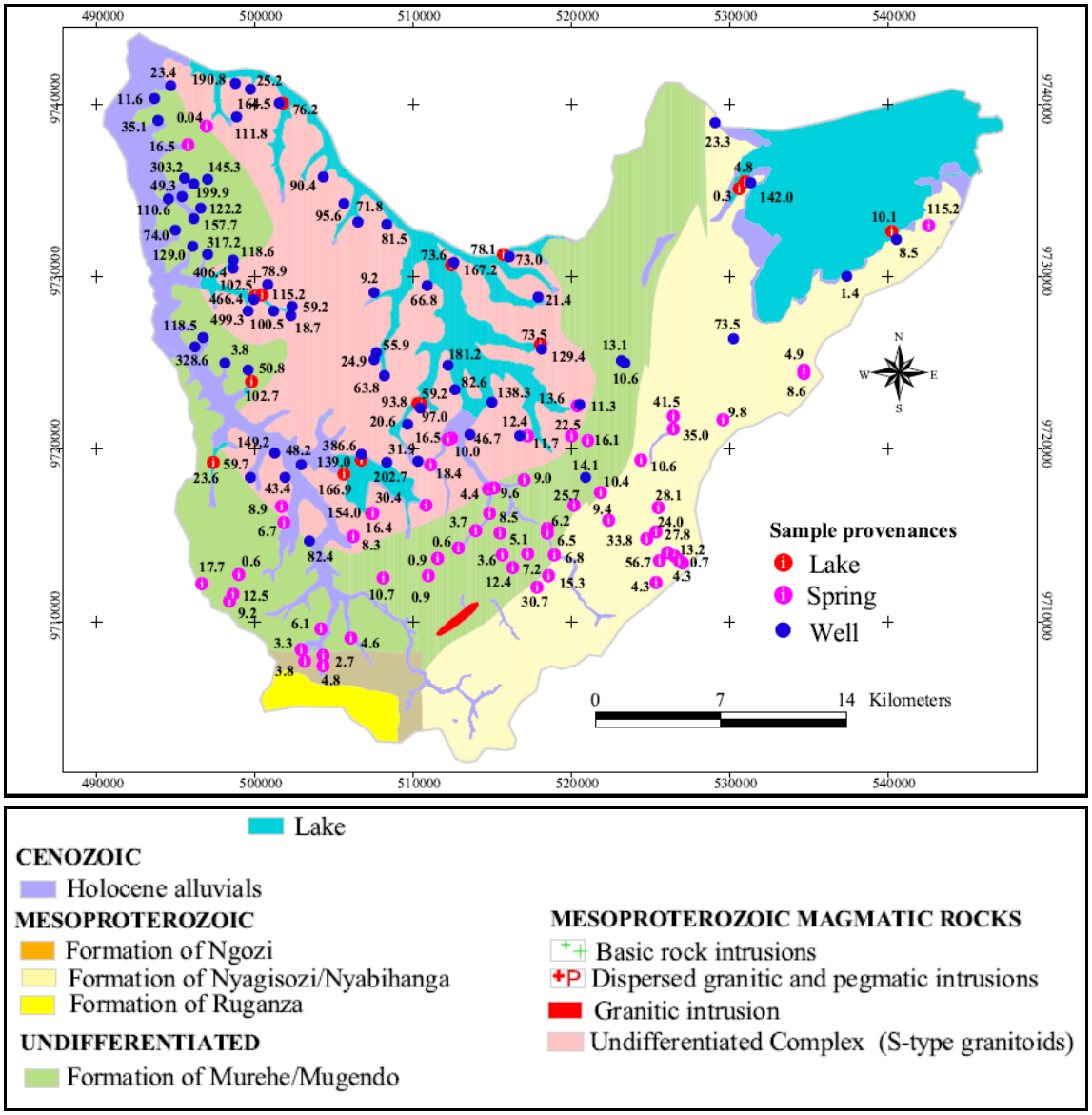

Figure VII.12. Spatial distribution of Cl^- concentration (in mg/l)

C Sulphate (SO_4^{2-})

Sulphur is present in natural waters in the ionic form of SO_4^{2-}. It is the stable oxidized form of sulphur and is readily soluble in water. It is introduced in the hydrological cycle mainly from the atmospheric deposition of oceanic aerosols, saline fossil water in the rocks, the leaching of sulphate minerals such as gypsum ($CaSO_4.2H_2O$), anhydrite ($CaSO_4$) and barite ($BaSO_4$) or the oxidation of sulphide minerals such as pyrite (Fe_2S) or pyrrhotite ($Fe_{1-x}S$). Sulphate content in natural waters falls in the range 2 to 80 mg/l (Chapman & Kimstach, 1996). In crystalline rocks, sulphate content in groundwater generally shows low values (<30 mg/l). However, high concentrations of sulphate exceeding 1000 mg/l may arise from the occurrence of sulphate or sulphide minerals, the pollution from industrial discharges or agricultural fertilisers (Matthess, 1982; Chapman & Kimstach, 1996). Very low or even zero SO_4^{2-} concentration in

groundwater is characteristic of groundwater in which microbiological reduction has taken place (Matthess, 1982).

The SO_4^{2-} concentration across the study area in represented in Figure V.13. Table VII.20 shows descriptive statistics of SO_4^{2-} concentrations in all water samples collected from the study area. Overall, SO_4^{2-} concentrations are in the range between 1 mg/l (spring in Rushubije-Cogo, Nr. 76) and 504.3 mg/l (well in Ntembe I-Kiri, Nr. 124) with an average of 49.8 mg/l. Unlike other dissolved constituents discussed so far, the lowest average SO_4^{2-} concentration is observed in water samples from lakes (2.6 mg/l) whilst the highest average concentration appears in water samples from wells (100 mg/l). Of the 143 water samples collected, 28 samples show concentrations of SO_4^{2-} exceeding 80 mg/l. On the other hand, 81 water samples display concentrations of SO_4^{2-} lower than 10 mg/l, to which belong all 16 water samples from the lakes, 51 water samples from springs and 14 water samples from wells.

Table VII.20. Some descriptive statistics of the concentration of SO_4^{2-} for different sources of water samples

	Max mg/l	**Min mg/l**	**Average mg/l**	**Standard deviation mg/l**	**Coefficient of variation %**
All samples	504.3	1.0	49.8	93.1	187.1
Wells	504.3	1.7	100.1	118.2	118.2
Lakes	3.6	1.4	2.6	0.7	28.1
Springs	96.2	1.0	7.7	14.0	182.6

The highest concentration of SO_4^{2-} observed with the water sample from the spring located in Mukuyo-Kiri (96.2 mg, Nr. 48 in Appendix VII.1) confirms that the enrichment of this anion in groundwater results from long flowpaths and residence time, as this spring emerges in the depression. Indeed, all the springs emerging in the highlands surrounding the depression to the South and East are characterised by low SO_4^{2-} levels, mostly lower than 10 mg/l (51 samples out of 61 water samples from springs). The concentration of SO_4^{2-} in water samples from springs located in the highlands shows low levels which preclude the influence of any additional sources of SO_4^{2-}, except from rainfall recharge.

Figure VII.13 shows particularly elevated concentrations of SO_4^{2-} in water samples from the western part of the study area, in a circumscribed zone situated to the North of Lake Gacamirinda (e.g. wells in Ntembe I-Kiri, Nr.125: 504.3 mg/l; Ntembe II-Kiri, Nr. 124: 337 mg/l; Gasagara II-Rubuga, Nr. 86: 446 mg/l; Kanigo-Cinuma, Nr. 97: 432 mg/l, Kigazi-Nyakarama, Nr. 102: 264 mg/l; Munyinya-Nyakarama, Nr. 117: 256.1 mg/l; Hambiro-Kiyonza, Nr. 90: 253.6 mg/l). Besides agricultural pollution, these localised high concentrations of SO_4^{2-} which are sometimes accompanied by high

concentrations of NO_3^- (e.g. wells in Hambiro-Kiyonza, Nr. 90: 75.5 mg/l; Kanigo-Cinuma, Nr. 97: 57.9 mg/l; Kigazi-Nyakarama, Nr. 102: 80.2 mg/l; Munyinya-Nyakarama, Nr. 117: 79.5 mg/l) or Cl^- (e.g. Gifuruguti-Nyakarama, Nr. 88: 317.2 mg/l; Ntembe II-Kiri, Nr. 124: 303.2 mlg/l; Saruduha I-Rugasa, Nr. 138: 328.6 mg/l) denote pollution from domestic waste. Furthermore, these high concentrations of SO_4^{2-} in groundwater are also likely to be contributed from sulphate minerals (anhydrite or gypsum) associated with salt deposits, whose chemical composition shows high SO_4^{2-} content.

Table V II.21 s hows a comparison of t he a verage c oncentration of S O_4^{2-} in water samples collected from 6 lakes. Lakes Rweru and Narungazi show slightly lower levels of S O42-, w hile Lake Cohoha di splays t he hi ghest c oncentration. H owever, ove rall, there is not a significant difference in concentration of this anion among different lakes. According to Ntakimazi (1985), the low levels of SO42- in these lakes can be ascribed to the fact that this anion is consumed as a nutriet in the primary production process by algae and aquatic vegetation producing organic compounds.

Table VII.21. Average concentration of SO_4^{2-} (in mg/l) in different lakes sampled

	Cohoha South	**Gacamirinda**	**Nagitamo**	**Narungazi**	**Rweru**	**Rwihinda**
Number of samples	6	2	1	1	3	3
Average SO_4^{2-} (mg/l)	3	2.8	2.4	2.3	2.3	2.4

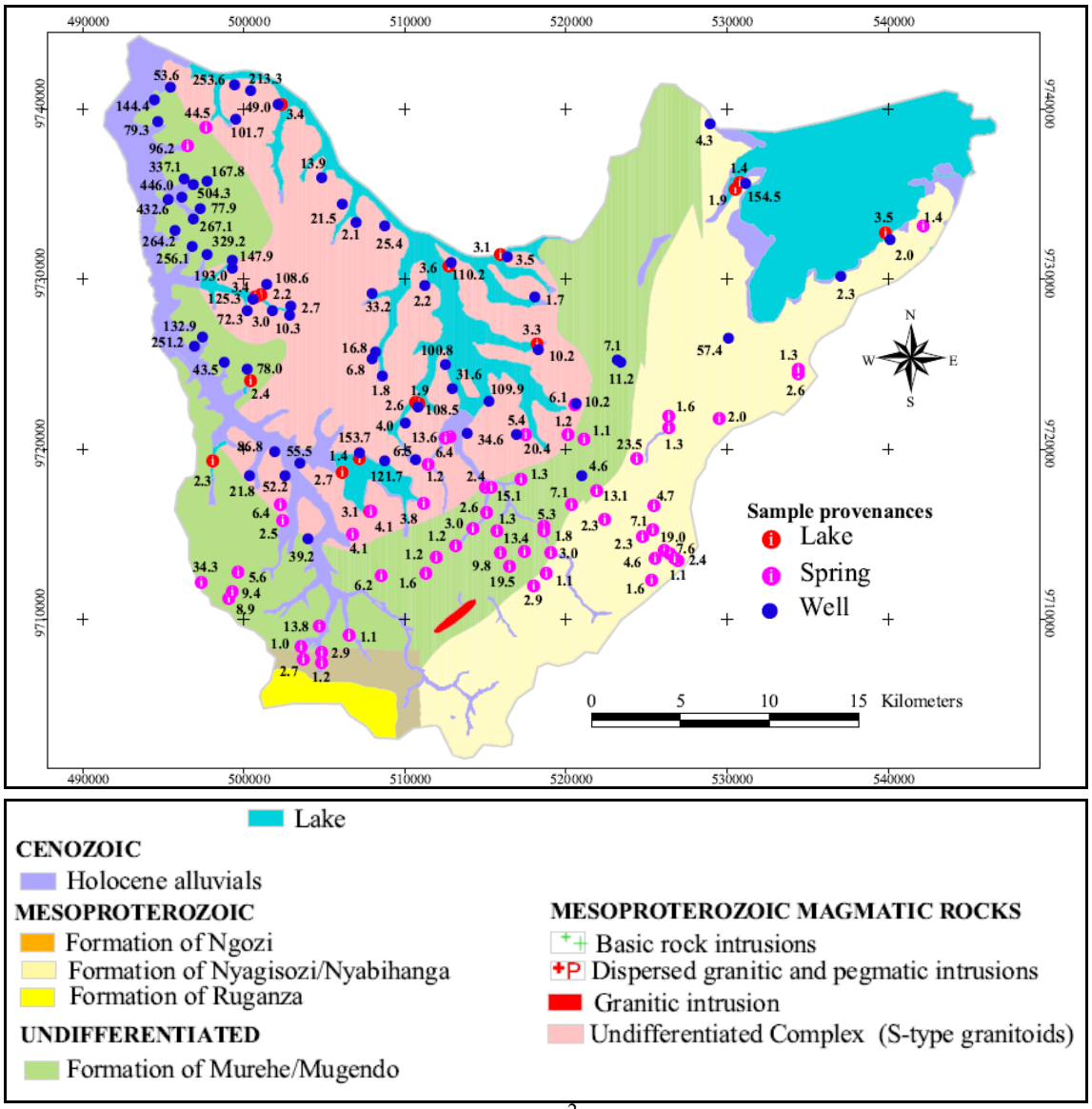

Figure VII.13. Spatial distribution of SO_4^{2-} concentration (mg/l)

d. Nitrates/Nitrites (NO_3^-/NO_2^-)

Nitrates and nitrites are discussed together because they are all forms of nitrogen found in natural waters. Natural concentrations of nitrates in surface water and groundwater, which are generally low, may become significantly enhanced by agricultural, municipal and industrial pollution. Hence, concentrations of NO_3^- exceeding 5 mg/l in surface water are indicative of anthropogenic pollution (Chapman & Kimstach, 1996). Furthermore, nitrate being an essential nutrient for aquatic plants; its concentration may vary seasonally due to growth and decay of plants.

In groundwater, nitrates concentrations are also generally low and concentrations higher than 10 mg/l are usually symptomatic of anthropogenic organic or inorganic inputs (Clabby *et al.*, 2008). Nitrate concentration in groundwater has increased over the last 30 years as a result of intensive use of chemical and manure fertilisers in agriculture.

However, even in unfertilised areas, high nitrate levels in groundwater may also arise from the nitrification of organic matter by bacterial activity (Chapman & Kimstach, 1996)

The WHO health standards for NO_3^- and NO_2^- concentration of respectively 50 mg/l and 3 mg/l (for short–term exposure) in drinking water were established based on epidemiological evidence of methaemoglobinaemia in infants exposed to various levels of nitrates and nitrites. For long-term exposure, a guideline of 0.2 mg/l is proposed by the WHO for nitrite (WHO, 2008).

Figure VII.13 represents the spatial distribution of NO_3^- in the study area. Tables VII.22 and VII.23 present descriptive statistics of the concentration of NO_3^- and NO_2^- in all water samples collected for this study. NO_3^- concentration in the bulk of the samples is in the range of 0.1 mg/l (spring in Kididiri-Buhasa, Nr. 36 in Appendix VII.1) to 83.3 mg/l (well at Kamwayi II-Nyamabuye, Nr. 95 in Appendix VII.1) with an average concentration of 17.6 mg/l. Nitrite concentration varies between a minimum of 0.03 mg/l (e.g. well in Kadobori II-Rubuga, springs in Gatovu-Kanyinya, Kabira-Kanyinya, Karobogo-Kanyinya) and a maximum of 7.2 mg/l (well in Shenga II-Rugasa), with an average concentration of 0.20 mg/l. Of the 143 water samples, 12 samples show levels of NO_3^- exceeding the health-based standard of 50 mg/l, while only 2 samples have concentrations of NO_2^- exceeding the health-based limit of 3 mg/l. A comparison of the average concentration of NO_3^- in water samples of different provenances shows that water samples from wells have the highest nitrate content followed by springs. Like for sulphates, NO_3^- concentration in water samples from lakes shows the lowest concentration, which may be consistent with the use of this anion as a nutrient by aquatic vegetation. On the other hand, the average concentration of NO_2^- shows the highest levels in water samples from wells followed by samples from lakes, whereas the lowest concentrations are associated with water samples from the springs.

All water samples with levels of nitrate and nitrites exceeding the health-based limit are samples from wells. The high concentration of NO_3^- in the well at Kamwayi was expected and is undoubtfully related to contamination of groundwater from human waste. Indeed, the well is located at a distance of less than 10 m from a pit latrine which has been constructed without considering the presence of an operating well in the surroundings. It is also worth to note that the highest values of NO_3^- are located in the northwestern part of the study area (e. g. wells in Kinyamateke, Ntembe II-Kiri, Munyinya-Nyakarama, Kanigo-Cinuma, Kigazi-Nyakarama), where high concentrations of SO_4^{2-} were also observed. These wells are located downslope from small rural agglomerations (e.g. Ntembe II-Kiri, Kinyamateke, Kamwayi, and Munyinya-Nyakarama) or within agricultural fields (e.g. wells in Kanigo-Cinuma, Foko

II-Kiyonza, and Mugombwa-Kiri) (Figure VII.14). Furthermore, it should be mentioned that the study area is a typical rural area with poor or no sanitation system and where extensive breeding contributes to the spreading of animal waste which may be further leached to groundwater.

The low levels of NO_2^- in all water samples are consistent with the fact that in such shallow aquifers and surface water where oxic conditions prevail, denitrification is not a dominant process. Indeed, nitrite is mainly formed by denitrification of NO_3^- under reducing and high pH environments, especially within the human body. On the other hand, the NO_2^- can also be formed through incomplete nitrification as the first step of the oxidation process of ammonia (Hill, 1991). However, the NO_2^- being unstable in the environment, it can rapidly oxidise to NO_3^- and this may explain its low levels observed in water samples.

All the 61 water samples from springs show nitrate concentrations below the maximum allowable level of 50 mg/l for drinking water. The spatial distribution of nitrate in water samples from springs shows that the length of the flow path and the residence time seem not to play an important role in the concentration of nitrate in groundwater (Figure VII.14). Indeed, while for other dissolved elements, the springs located in the depression show the highest concentrations, this seems not to be the case for NO_3^-, for which higher concentrations are mainly observed in water samples collected from springs situated in the highlands (table VII.22), such as Rambo-Gatwe (43.3 mg/l, Nr. 65 in Appendix VII.1), Buhiga-Ntega (41.7 mg/l, Nr. 20 in Appendix VII.1), Mukagezi-Ntogwe (36.2 mg/l, Nr. 47 in Appendix VII.1) and Kagogo-Nyabitare (35.98 mg/l, Nr. 31 in Appendix VII.1). This observation hints to the fact that the concentration of NO_3^- is not controlled by the water-rock interactions but is rather influenced by the existence of a localised source of pollution. None of the water samples from springs shows a concentration of NO_2^- exceeding the health-based standard concentration (short-term exposure) of 3 mg/l..

Table VII.22. Some descriptive statistics of the concentration of NO_3^- for different sources of water samples

	Max mg/l	**Min mg/l**	**Average mg/l**	**Standard deviation mg/l**	**Coefficient of variation %**
All samples	83.3	0.1	17.6	18.5	104.7
Wells	83.3	0.2	23.3	23.9	102.3
Lakes	14.0	1.1	5.6	3.9	69.6
Springs	43.3	0.1	13.5	10.1	75.0

Table VII.23. Some descriptive statistics of the concentration of NO_2^- for different sources of water samples

	Max mg/l	Min mg/l	Average mg/l	Standard deviation mg/l	Coefficient of correlation %
All samples	7.2	0.03	0.2	0.9	360.4
Wells	7.2	0.03	0.4	1.3	323.1
Lakes	1.7	0.04	0.2	0.4	216.2
Springs	0.2	0.03	0.1	0.04	39.1

A comparison of average concentrations of NO_3^- and NO_2^- in the 16 lake samples in given is Tables VII.25 and VII.26. Lake Gacamirinda shows the highest average level of nitrates (11.1 mg/l), while the lowest average concentration of this anion is observed in water samples from Lake Rwihinda. The highest measured concentration of nitrate is however observed in Lake Rweru (14 mg/l in Mago-Gatete) which, yet, shows an overall low concentration for other dissolved constituents. Of the 16 water samples collected from lakes, 5 samples have a concentration of NO_3^- greater than 5 mg/l which, according to Chapman & Kimstach (1996), should be the upper limit of nitrate level in unpolluted surface water. These sporadic relatively high concentrations of nitrate in these small lakes are likely to originate from the decomposition of vegetation and organic matter. Indeed, these lakes are located in swampy valleys and are surrounded by marshy vegetation. On the other hand, a comparison of average concentrations of NO_2^- shows that the small Lake Narungazi has the highest level (1.7 mg/l), but overall, the levels of nitrites in the lakes are very low and do not vary significantly.

Table VII.24. Average concentration of NO_3^- (in mg/l) in different lakes sampled

	Cohoha South	Gacamirinda	Nagitamo	Narungazi	Rweru	Rwihinda
Number of samples	6	2	1	1	3	3
Average NO_3^- (mg/l)	4.3	11.1	4.2	4.4	8.5	2.4

Table VII.25. Average concentration of NO_2^- (in mg/l) in different lakes sampled

	Cohoha South	Gacamirinda	Nagitamo	Narungazi	Rweru	Rwihinda
Number of samples	6	2	1	1	3	3
Average NO_2^- (mg/l)	0.05	0.07	0.06	1.72	0.13	0.15

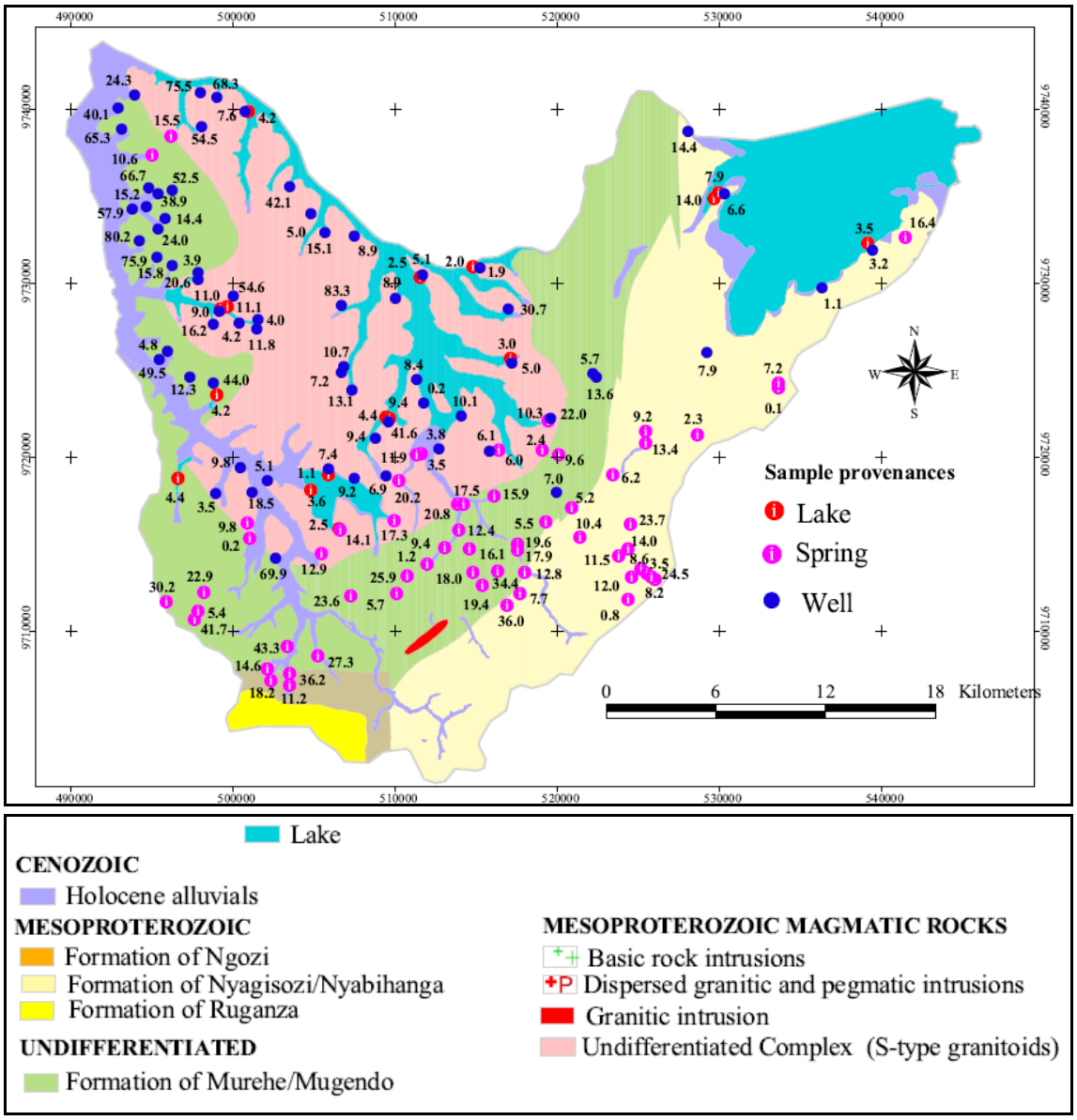

Figure VII.14. Spatial distribution of NO_3^- concentration (in mg/l)

e. Silica

Silica is released in the groundwater as a result of the chemical breakdown of silicate minerals in rocks or in sediments. It occurs in natural water in dissolved, suspended and colloidal forms. Concentration of silica in groundwater is controlled by the intensity of the rock-water interaction which is in turn a function of the aquifer and environmental parameters such as permeability, residence time, lithology, rainfall, temperature and pH (Khan & Umar, 2010; Chapman & Kimstach, 1996).

Silica solubility increases at high temperatures and at pH values below 7 (slight increase) and greater than 7.8 (sharp increase). Dissolved forms of silica are mostly represented by silicic acid (H_4SiO_4) and its dissociation products. Concentration of silica in natural waters varies between 1 mg/l and 30 mg/l but higher concentrations up to 100 mg/l can be encountered in areas where silicate minerals are abundant in local

geology (Khan & Umar, 2010). Silica is a nutrient of some aquatic organisms such as diatoms. Hence, seasonal fluctuations of SiO_2 in aquatic environments may occur due to the uptake of this element during the growing period of these organisms and its release during decomposition and decay (Chapman & Kimstach, 1996). As of now, there is no known health concern for humans but high concentrations of SiO_2 may interfere with treatment techniques designed to remove iron and manganese. Moreover, high concentrations of silica may cause scaling on pipes, thereby impeding flow of water.

The concentration of silica in the study area is represented in Figure VII.15. Concentration of SiO_2 in all water samples varies between 0.1 mg/l (spring in Muyange-Mutetema, Nr. 51) and 30 mg/l (well in Hambiro-Kiyonza, Nr. 90) with an average of 11 mg/l (Table VII.26). On average, the highest concentration of silica (13.8 mg/l) is found within water samples from wells, while the lowest average concentration occurs in water samples from the shallow lakes (6.3 mg/l). Water samples from the springs show intermediate average concentration of silica (9.1 mg/l). While the lowest concentrations of silica should be expected in water samples from springs due to short residence time and flowpaths, it appears that the low levels of silica are rather found in the shallow lakes and reflect the uptake of this dissolved constituent by aquatic vegetation.

Table VII.26. Some descriptive statistics of the concentration of SiO_2 for different sources of water samples

	Max mg/l	Min mg/l	Average mg/l	Standard deviation mg/l	Coefficient of variation %
All samples	30.1	0.1	11	6.8	61.9
Wells	30.1	0.7	13.8	7.2	52.3
Lakes	12.1	0.7	6.3	3.7	58.7
Springs	22.4	0.1	9.1	5.5	60.8

While, overall, most springs with high concentrations of SiO_2, such as the springs at Mukuyo-Kiri (22.4 mg/l, Nr. 48), Mamfu-Kiyonza (17.2 mg/l, Nr. 44), Kabira-Renga (16.7 mg/l, Nr. 30) and Maramvya-Mwenya (18 mg/l, Nr. 45) emerge in the depression, it can be noted that there is a high spatial variability because, locally, some springs located in the depression, like the spring at Gikombe-Ruhita (4.8 mg/l, Nr. 28), Mwenya-Mwenya (1.6 mg/l, Nr. 53), Kigoti-Munzenze (5.7 mg/l, Nr. 38) show low concentrations of SiO_2. On the other hand, relatively high values of silica are observed in some springs emerging in the highlands, like in Buhiga-Ntega (16.3 mg/l), Nakivumbura-Monge (16.6 mg/l), Nakarambo-Rutabo (18.2 mg/l) or Mwenya-Rwimbogo (15 mg/l) (Figure VII.15, Appendix VII.1). Therefore, besides flowpath and residence time, which imply more dissolution of silicate, other factors such as the formation of clay minerals which retains part of the silica released, the types of

lithology and the dissolution of amorphous silica can influence the concentration of silica in groundwater.

The spatial distribution of SiO_2 (Figure VII.15) shows that water samples with high mineralisation such as those collected from the wells in Mago-Gatete (TDS =3229 mg/l, SiO_2 =11.9 mg/l), Shenga II-Rugasa (TDS = 1805 mg/l, SiO_2 = 8.8 mg/l), Shenga III-Rugasa (TDS = 1748.6 mg/l, SiO2 = 5.4 mg/l) or in Bishunzi-Cewe (TDS = 1632.2 mg/l, SiO_2 =5.7 mg/l) do not necessarily have high concentration of SiO_2. This observation confirms that, besides the weathering of silicates, other processes such as the dissolution of evaporitic salts and anthropogenic pollution, which do not increase the silica content, may, accessorily, contribute to the mineralisation of groundwater. Moreover, the variability of silica concentration even within the depression, where high concentrations could be expected, confirms the importance of the incongruent dissolution of aluminosilicates which is accompanied by the formation of authigenic minerals such as kaolinite.

A comparison of the average concentration of silica in different lakes shows that Lake Rwihinda has the highest concentration of silica, whereas Lake Gacamirinda displays the lowest abundance of this dissolved constituent (Table VII.27). The decreasing order of the concentration of SiO_2 in different lakes indicates that the dilution effect due to large volume of water can not alone explain the low concentrations of silica within the lakes. Indeed, while the Lake Nagitamo which is the smallest of the 6 lakes sampled has the second highest concentration of silica, this not the case for the two other small lakes, i.e. Narungazi and Gacamirinda which show the lowest concentration of silica. This seems to confirm that the uptake of dissolved silica by aquatic organisms exerts a significant control over the concentration of silica in the small lakes.

Table VII.27. Average concentration of SiO_2 (in mg/l) in different lakes sampled

	Cohoha South	**Gacamirinda**	**Nagitamo**	**Narungazi**	**Rweru**	**Rwihinda**
Number of samples	6	2	1	1	3	3
Average SiO_2 (mg/l)	6.2	2.7	7.4	4.6	6.7	8.6

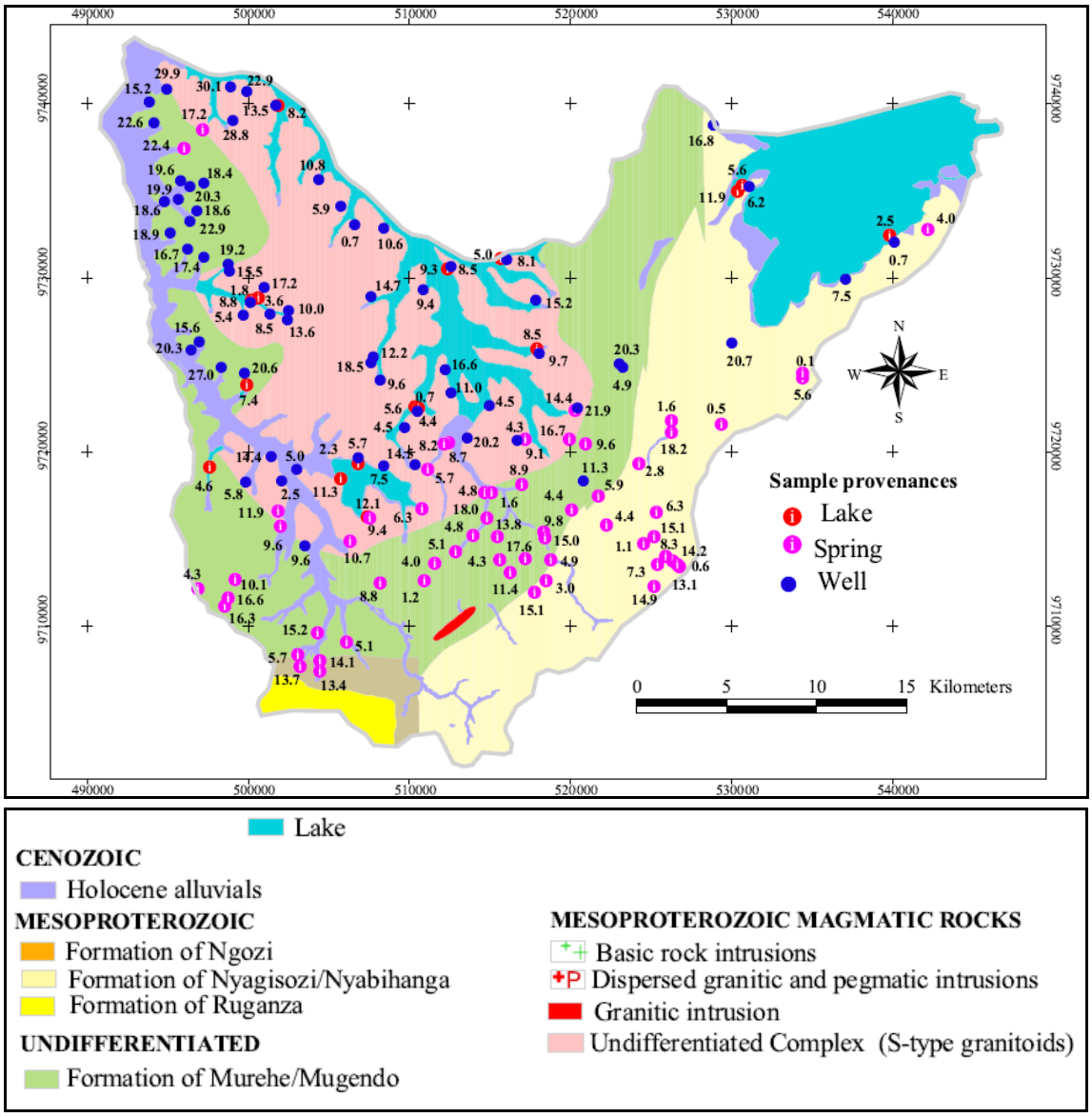

Figure VII.15. Spatial distribution of SiO_2 concentration (in mg/l)

VII.4.2.2. Minor and trace elements

a. Iron (Fe^{2+})

The iron is freed to the hydrological cycle by the weathering of ferromagnesian minerals. Its occurrence in aqueous solution is controlled by environmental conditions, especially redox and pH conditions. In the anaerobic environment, the presence of organic matter can create reducing conditions in which the oxidised forms of iron are reduced resulting in increased concentrations of Fe^{2+}. Iron in most natural waters is found in concentrations ranging from less than 0.001 mg/l to 50 mg/l (Gibbs, 1979; Chapman & Kimstach, 1996). There is no health-based guideline for iron concentration in drinking water. However a guideline of 0.3 mg/l was established by the WHO for aesthetic considerations (WHO, 2008).

The Fe^{2+} concentration in the study area is shown in Figure VII.16. Iron in water samples collected in this study shows concentrations varying between 0.01 mg/l (e.g. spring in Bishunzi-Munyinya, wells in Kiyonza-Foko I, Kinyamateke-Nyabikenke, Nyange-Kumana) and 54 mg/l (well in Shenga III-Rugasa) with an average of 1.99 mg/l (Table VII.28). On average, the highest concentration of iron is observed in water samples from wells, while the lowest levels are found in samples from springs. The lowest concentration of iron characterising water samples from springs reflects oxic or nitric conditions inherent to the shallow flowpaths of spring waters. Of the 143 water samples collected, 51 samples, of which 9 are from lakes, 5 from springs and 37 from wells, show concentrations of Fe^{2+} exceeding the aesthetic standard concentration of 0.3 mg/l.

Figure VII.16 shows the spatial distribution of the concentration of Fe^{2+} across the study area. It can be noted that the highest concentrations of Fe^{2+} are associated with water samples collected from wells located within the Undifferentiated Complex Formation, such as the wells in Shenga III-Rugasa (54 mg/l), Runyangona II-Nyabikenke (25.7 mg/l), Karago-Rukuramigabo (31.9 mg/l) and Mutoza-Yaranda (27.10 mg/l). These high levels of iron can be explained by the weathering of Fe-bearing minerals especially within the granites and pegmatites which comprise the Undifferentiated Complex. Moreover, an important part of this Undifferentiated Complex Formation is overlain by a thick lateritic cover which may be leached by percolating water, resulting in high levels of iron in groundwater.

Elevated iron content in well water in the study area poses a critical quality issue as many wells are squarely abandoned by local villagers who argue that the water from the wells is smelly or tastes salty. This is a widespread problem in the study area which renders the water unpalatable and compels well users to resort to the polluted surface water from the small lakes. Even some of the wells constructed in 2008 by a BTC-funded projected have been abandoned just after completion (e.g. wells at Mutoza-Yaranda, Muhero II-Yaranda, Kuruhura I-Kiyanza, Nunga II-Yaranda), despite a good yield, due to high iron contents. For some wells, the high iron levels could be expected from the beginning because they were constructed in areas covered by thick lateritic cover (e.g. Mutoza-Yaranda, Nunga II-Yaranda, Kiruhura I-Kiyanza).

By comparing the average concentration of Fe^{2+} in water samples from the 6 lakes, it appears that the Lake Gacamirinda has the highest concentration of Fe^{2+}, whereas Lake Cohoha shows the lowest levels of Fe^{2+} (Table VII.29). The low levels of iron in lakes compared to the concentrations observed in water samples collected from wells result from different redox conditions. In lake water there is much more dissolved oxygen and the iron present is precipitated.

Table VII.28. Some descriptive statistics of the concentration of Fe^{2+} for different sources of water samples

	Max mg/l	Min mg/l	Average mg/l	Standard deviation mg/l	Coefficient of variation %
All samples	54.00	0.01	1.99	6.28	316.13
Wells	54.00	0.01	3.98	8.86	222.71
Lakes	3.70	0.17	1.07	0.92	85.64
Springs	2.14	0.01	0.15	0.28	180.17

Table VII.29. Average concentration of Fe^{2+} (in mg/l) in different lakes sampled

	Cohoha South	Gacamirinda	Nagitamo	Narungazi	Rweru	Rwihinda
Number of samples	6	2	1	1	3	3
Average Fe^{2+} (mg/l)	0.28	2.92	0.52	0.57	0.90	0.34

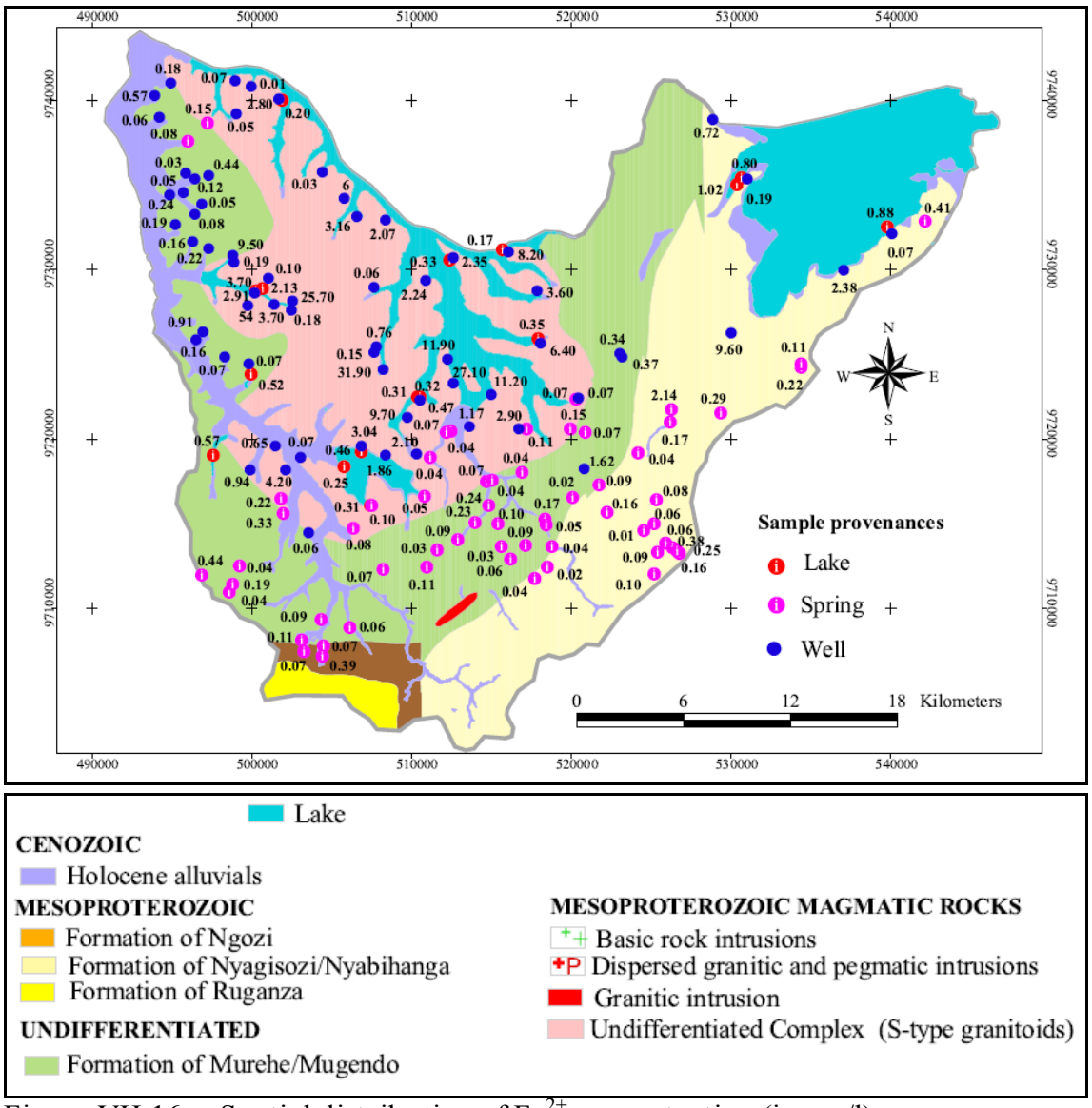

Figure VII.16. Spatial distribution of Fe^{2+} concentration (in mg/l)

b. Manganese (Mn^{2+})

Manganese is naturally occurring in groundwater and surface water resources particularly where reducing conditions prevail. Its occurrence is strongly parallel to that of Fe^{2+}. Mn^{2+} is the most soluble form in groundwater. Concentrations of manganese in groundwater range over several orders of magnitude from less than 0.001 mg/l to values occasionally exceeding 1 mg/l. In shallow aquifers and surface water where oxidizing conditions prevail, manganese is stable in its oxidized form as solid MnO_2 and thus, levels of dissolved Mn in aerobic environment are generally low and even below the analytical detection limit. Under anaerobic conditions, manganese is reduced to its more soluble form Mn^{2+} and therefore high levels of Mn in groundwater may occur (Mathess, 1982, Chapman & Kimstach, 1996). Excessive exposure to manganese through inhalation or drinking water may cause neurological disturbances; a provisional health-based guideline limit of 0.5 mg/l has been established (WHO, 2008).

The spatial distribution of Mn^{2+} concentration in the study area is represented in Figure VII.17. Concentrations of Mn^{2+} in different water samples vary between a minimum of 0.001 mg/l (e.g. well at Kamwayi II) and a maximum of 14.5 mg/l (well at Ceru-Kantuye) with an average of 0.5 mg/l (Table VII.30). In total, 25 water samples of the 143 samples collected have Mn^{2+} concentrations exceeding the provisional health-based guideline for Mn^{2+} concentration in drinking water, i.e. 0.5 mg/l. Of the 25 water samples with Mn^{2+} concentrations exceeding 0.5 mg/l, 2 samples were collected from the lakes, 2 samples are from springs and 21 samples are from wells. On average, spring waters have the lowest concentration of Mn^{2+} (0.09 mg/l), while water samples from the wells display the highest levels of this element (0.94 mg/l). This observation may reflect the fact that, due to shallow flow path and thus oxidizing conditions, the most dominant form of manganese is MnO_2, which is a solid.

Table VII.30. Some descriptive statistics of the concentration of Mn^{2+} for different sources of water samples

	Max mg/l	Min mg/l	Average mg/l	Standard deviation mg/l	Coefficient of variation %
All samples	14.540	0.001	0.505	1.573	311.165
Wells	14.540	0.001	0.936	2.232	238.459
Lakes	1.015	0.092	0.304	0.245	80.489
Springs	1.376	0.002	0.092	0.232	251.152

High levels of Mn^{2+} in some well waters are confirmed by villagers who assert that they do not use water from some wells, such as the well in Kantuye-Ceru (Nr. 98: 14.540 mg/l), because the food cooked with that water turns blackish. Overall, the highest values of Mn^{2+} concentration are associated with wells located within the Undifferentiated Complex Formation, such as the wells at Kantuye-Ceru (Nr. 98: 14.5 mg/l), Gahwijo II-Nyabikenke (Nr. 84: 7.6 mg/l) and Runyonza-Kabonde (Nr. 132: 2.7 mg/l). This observation may reflect the presence of manganese in isomorphic

substitution for some elements like iron or calcium in aluminosilicate and ferromagnesian minerals, which comprise the granite and pegmatite.

A comparison of the average concentration of Mn^{2+} in water samples from the lakes shows that Lake Gacamirinda has the highest Mn^{2+} level (Table VII.31). However, overall, water samples from the lakes are characterised by rather low levels of Mn^{2+}, which are in line with the oxygenated environment of these shallow lakes, which causes most of manganese to precipitate in the form of insoluble MnO_2.

Table VII.31. Average concentration of Mn^{2+} in different lakes sampled

	Cohoha South	Gacamirinda	Nagitamo	Narungazi	Rweru	Rwihinda
Number of samples	6	2	1	1	3	3
Average Mn^{2+} (mg/l)	0.194	0.858	0.466	0.361	0.243	0.143

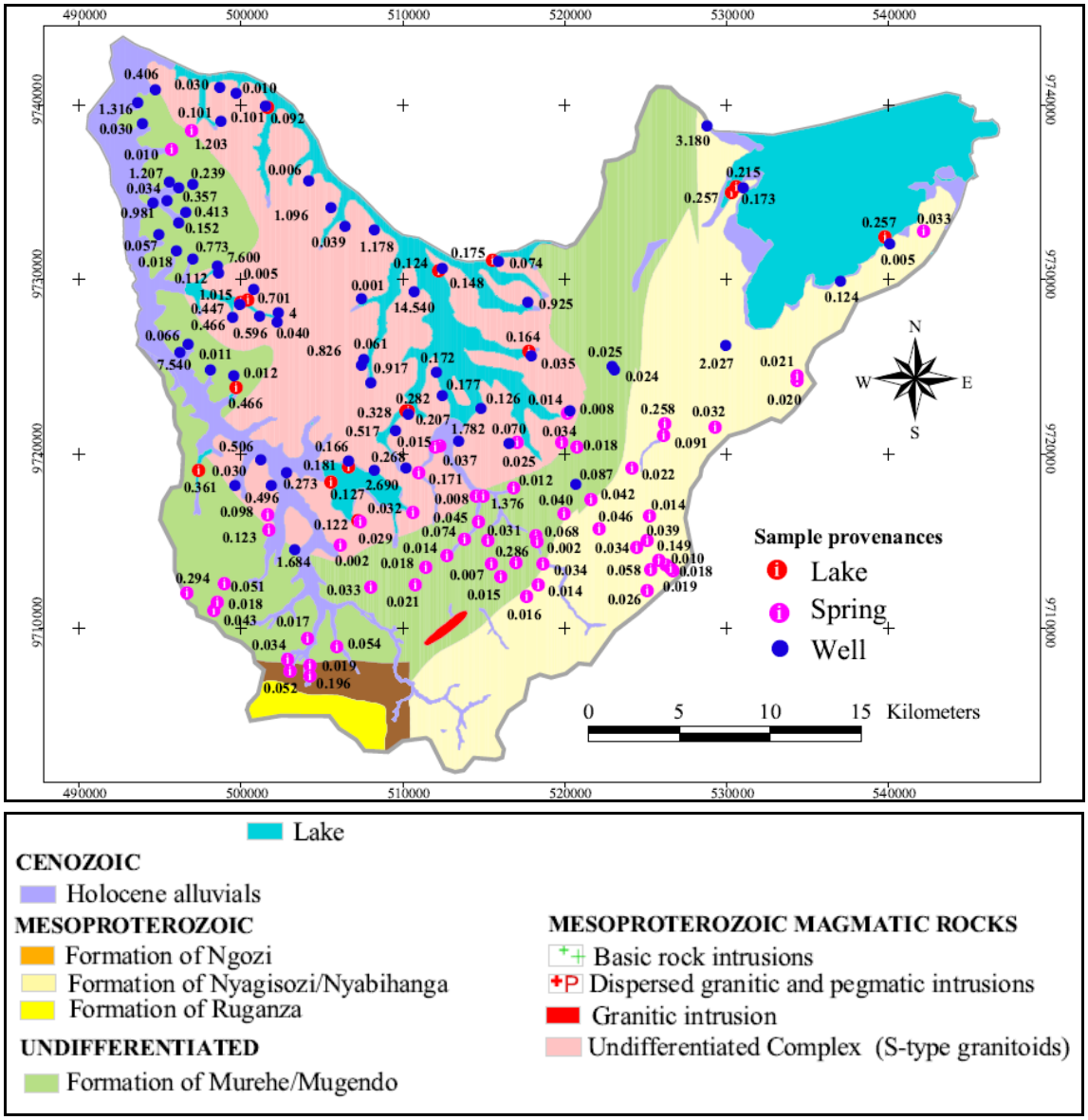

Figure VII.17. Spatial distribution of Mn^{2+} concentrations (in mg/l)

c. Ammonia (NH_4^+)

Ammonia is present in variable concentrations in many surface and groundwater supplies where it may result from the decomposition of nitrogenous organic and inorganic matter in soil and water, excretion by biota, reduction of the nitrogen gas in water by micro-organisms and from gas exchange with the atmosphere. Ammonia can also be brought into water bodies by contamination from industrial effluents and municipal or domestic waste. Ammonia is rapidly oxidised by bacteria, in natural water systems, to nitrite and nitrate in the presence of sufficient dissolved oxygen. Natural levels of ammonium in surface and groundwater are generally below 0.2 mg/l (Chapman & Kimstach, 1996). High levels of ammonia in shallow water are generally symptomatic of possible bacterial, sewage or animal waste pollution (WHO, 2008). There is no direct incidence of ammonia on health and therefore no health-based guideline value has been proposed so far. However, in the guidelines for drinking-water quality, published in 1993, it is recognised that problems of taste and odour may arise from concentrations of ammonia exceeding 35 and 1.5 mg/litre, respectively.

Table VII.32 presents some descriptive statistics of ammonia concentration in water samples from various sources. Overall, the concentration of NH_4^+ ranges between a minimum of 0.0001 mg/l (well in Muhero II-Yaranda, Nr. 116) and a maximum of 5.7 mg/l (well in Murambo-Murambi, Nr. 118), with an average of 0.2 mg/l. Table VII.32 shows that, overall, NH_4^+ concentrations within all water samples are low. Indeed, out of 143 water samples collected, 138 samples, which represent 95.8 % of all the samples, have a concentration of ammonia below the odour-based guideline, i.e. 1.5 mg/l.

All 61 water samples collected from springs have concentrations of ammonia below 1.5 mg/l, the odour-based guideline according to the WHO (2008). These low levels of ammonia in spring water samples are consistent with the fact that there is no important contamination of spring water from domestic or animal waste on one hand, and, on the other hand, the springs emerge from shallow and oxygenated aquifers where most of the ammonia is oxidised to nitrate or nitrite.

The average concentration of ammonia in the different wells sampled, is 0.3 mg/l with a standard deviation of 0.96 mg/l. Of the 66 water samples from wells, 62 samples, which represent 94 % of all water samples from wells, have concentrations of ammonia below the odour-based threshold of 1.5 mg/l. These low levels of ammonia in well waters, especially in these wells where high concentrations of nitrate are observed, like the wells at Gasagara II-Rubuga (0.08 mg/l), Hambiro-Kiyonza (0.12 mg/l), Kamwayi II (0.009 mg/l), Kigazi-Nyakarama (0.14 mg/l) and Susa-Gikomero (0.03 mg/l) may be in agreement with the fact that, in such shallow aquifers where dissolved oxygen may be present in substantial concentrations, an important part of NH_4^+ is oxidised to nitrate.

Table VII.32. Some descriptive statistics of the concentration of NH_4^+ for different sources of water samples

	Max mg/l	Min mg/l	Average mg/l	Standard deviation mg/l	Coefficient of correlation %
All samples	5.67	0.0001	0.21	0.70	327.2
Wells	5.67	0.0001	0.34	0.96	286
Lakes	1.59	0.0002	0.51	0.56	110.3
Springs	0.04	0.0067	0.005	0.005	91.3

A comparison of the average concentration of NH_4^+ in different water samples shows that, unlike other dissolved elements, water samples from the lakes have the highest average concentration of ammonia (0.5 mg/l) compared to the samples of other provenances (Table VII.33).

Of the 16 samples from the lakes, 15 samples are characterised by NH_4^+ concentrations below the odour-based guideline (1.5 mg/l) (Appendix VII.1). These low concentrations of ammonia mainly reflect the oxic conditions of the lakes which cause ammonia to be oxidised to nitrite and nitrate. Moreover, ammonia is consumed by aquatic vegetation as a nutrient. It is also possible that there is no substantial input of ammonia from anthropogenic pollution.

A comparison of the average concentration of NH_4^+ in different lakes sampled, shows that Lake Nagitamo has the highest level of this nutrient, whereas Lake Narungazi has the lowest average concentration (Table VII.32).

Table VII.33. Average concentration of NH_4^+ in different lakes sampled

	Cohoha South	Gacamirinda	Nagitamo	Narungazi	Rweru	Rwihinda
Number of samples	6	2	1	1	3	3
Average NH_4^+ (mg/l)	0.878	0.016	1.486	0.013	0.244	0.207

d. Phosphate (PO_4^{3-})

Phosphate occurs in rocks or minerals, mainly apatite, and is gradually released to natural water systems on weathering and decomposition of organic matter in the form of phosphate ion (PO_4^{3-}) which is soluble in water. Detergents contained in domestic waste-waters, industrial effluents and runoff from agricultural land where PO_4^{3-}-fertilisers are applied, may contribute to increased levels of phosphate in surface and subsurface waters. According to Ross *et al.* (2010), natural background concentrations of phosphate dissolved in water are in the range 0.005-0.05 mg/l. Thus, high concentrations of phosphates are indicative of pollution. Although PO_4^{3-} is not a harmful constituent for human health, its presence in natural water systems, even in

small amounts, may create environmental problems as it boosts the growth of microbes, algae, phytoplankton and aquatic vegetation thereby causing eutrophication of aqueous systems (Miettinen *et al.*, 1997; Rao & Prasad, 1997). Eutrophication and its attendant depletion of dissolved oxygen in surface water may pose a serious threat to aquatic life, especially fishes. Generally, to avoid or minimise algal blooms in water or surfaces in contact with water, Ross *et al.* (2010) proposed to keep phosphate levels in water equal to or less than 0.05 mg/l.

Table VII.34 presents descriptive statistics of the concentration of PO_4^{3-} in water samples from different provenances. Detailed analytical results are presented in Appendix VII.1. Table VII.33 shows that the concentration of phosphate in all water samples is in the range between 0.04 mg/l (e.g. springs in Kabira-Kanyinya, Nr.29; Bunyari-Rugarama, Nr.21; wells in Kanabugiri-Bugera, Nr. 96; Kigina I-Gisenyi, Nr. 103) to 0.86 mg/l (well at Saruduha II, Nr. 138) with an average of 0.11 mg/l. A comparison of the average concentration of PO_4^{3-} in different water samples shows that there is no significant difference between lakes, springs and wells (Table VII.34). Water samples from the lakes show a slightly higher average concentration of phosphate (0.13 mg/l), while springs show the lowest levels of the ion (0.10 mg/l) (Table VII.34). Of the 143 water samples collected, 120 samples show phosphate concentrations exceeding 0.05 mg/l, which is the maximum concentration of phosphate beyond which eutrophication is likely to occur.

Of the 61 water samples collected from springs, 55 samples show phosphate concentrations exceeding the upper level of PO_4^{3-} in natural water beyond which eutrophication may occur, i.e. 0.05 mg/l. This observation may point to the fact that most of the springs which emerge from shallow aquifers are contaminated with PO_4^{3-} from anthropogenic activities particularly agricultural fertilisers, animal and domestic waste. Indeed, it can be noted from Appendix VII.1 that in many springs, high levels of phosphate correspond to relatively high levels of nitrate (e.g. springs at Bihembe-Monge, Nr. 17: 30.2 mg/l; Kagogo-Nyabitare, Nr. 31: 36 mg/l; Mukagezi-Ntogwe, Nr. 47: 36 mg/l; Nakabingo-Gihosha, Nr. 57: 34.4 mg/l; Rambo II-Gatwe, Nr. 66: 43.3 mg/l).

Of the 66 water samples collected from the wells, 49 samples, which represent 74 % of all water samples collected from wells, show concentrations of phosphate greater than the upper limit of 0.05 mg/l. Considering the absence of phosphate minerals in the study area, the enrichment of PO_4^{3-} in some wells is most probably caused by contamination from anthropogenic sources. Indeed, when there is sufficient rainfall, the region of Bugesera and particularly the province of Kirundo constitutes the granary of the whole country for subsistence crops, mainly beans and sorghum. To substantially increase

production, local villagers are increasingly applying a combination of chemical fertilisers and organic manure whose leaching by rainwater may contribute to increased levels of phosphate in groundwater.

Table VII.34. Some descriptive statistics of the concentration of PO_4^{3-} for different sources of water samples

	Max mg/l	**Min mg/l**	**Average mg/l**	**Standard deviation mg/l**	**Coefficient of variation %**
All samples	0.86	0.04	0.11	0.13	124.97
Wells	0.86	0.04	0.11	0.15	136.93
Lakes	0.28	0.06	0.13	0.06	0.49
Springs	0.78	0.04	0.10	0.13	132.49

A comparison of the average concentration of phosphate in different lakes shows that Lake Gacamirinda has the highest level of this nutrient (0.26 mg/l) (Table VII.35). All 16 water samples collected from lakes show concentrations of phosphate greater than 0.05 mg/l, the upper level beyond which excessive growth of aquatic vegetation may occur (Appendix VII.1). These relatively high levels of phosphate in water samples from the lakes may result from anthropogenic inputs. Ntakimazi (1985) observed that the concentrations of phosphate in the Lakes Cohoha and Rweru were low (0.01-0.08 mg/l) and comparable to the levels of phosphates in other equatorial lakes, even those highly productive in terms of primary production.

The relatively high levels of phosphate in water samples collected during this study may bear witness to the fact that the small lakes may progressively evolve towards eutrophication. This phenomenon is materialised by an excessive proliferation of the water hyacinth, an important and pernicious invasive aquatic plant. This plant, which blocks sun light from reaching aquatic flora and deoxygenates water, has negative ecological impacts and particularly hinders the multiplication of aquatic species, mainly fishes. This may explain why local fishermen in the region complain that the fish production of the shallow lakes decreases year after year. According to Ntakimazi (personal communication), this proliferation of water hyacinth in the northern lakes started in late 1990's because, by the time he was carrying out his PhD research in early 1980's, there was no such a plant in the region and the lakes had a good production in terms of fishes.

Table VII.35. Average concentration of PO_4^{3-} in different lakes sampled

	Cohoha South	Gacamirinda	Nagitamo	Narungazi	Rweru	Rwihinda
Number of samples	6	2	1	1	3	3
Average PO_4^{3-} (mg/l)	0.10	0.26	0.21	0.11	0.13	0.09

E Fluoride

Fluoride is mainly released in groundwater from the weathering of F-bearing minerals such as fluorite, micas, apatite and amphiboles which are mostly present as accessory minerals in granites. Fluorite (CaF_2) is the main fluoride mineral whose dissolution constitutes a major source of F^- in groundwater (Jacks *et al.,* 2005). However, atmospheric deposition from soil dust and industrial emissions can also contribute significantly to increased concentrations of fluoride in natural waters. Concentration of fluoride in groundwater is limited by the rather low solubility of the main F-bearing mineral, i.e. fluorite and is strongly controlled by the concentration of Ca^{2+}. High fluoride concentration may occur in Ca^{2+}-poor aquifers and in areas were F-bearing minerals are abundant. Increased concentrations of F^- can also result from the depletion of Ca^{2+} in groundwater which results from the cation exchange of Na^+ for Ca^{2+}. While fluoride has beneficial effects on teeth at low concentrations in drinking waters, exposure to high concentrations of this element (>1.5 mg/l) may cause adverse effects such as dental or skeletal fluorosis (WHO, 2008),

The F^- concentration in the study area is represented in Figure VII.18. Table VII.36 shows that F^- concentrations in the different water samples vary between a minimum of 0.06 mg/l (spring at Kinyangurube-Karehe) and a maximum of 16.53 mg/l (well at Ntwago- Murungurira) with an average of 0.95 mg/l. On average, high concentrations of F^- occur in water samples from wells (1.73 mg/l), while the lowest concentrations are observed in water samples from springs (0.15 mg/l). Of the 143 water samples collected for this study, 21 samples show concentrations of F^- beyond the health-based limit of 1.5 mg/l and are all from wells.

While for other hydrochemical parameters, springs located within the depression show the highest concentrations, this seems not to be the case for F^-. Indeed, the two springs located within the depression, i.e. Mamfu-Kiyonza (Nr 44 in Appendix VII.1) and Mukuyo-Kiri (Nr 48 in Appendix VII.1), show concentrations of F^- of respectively 0.07 mg/l and 0.16 mg/l, whereas springs located at the southern periphery of the depression or within the highlands, such as the springs in Nakabingo-Gatemere (0.37 mg/l), Mukagezi-Ntogwe (0.60 mg/l), Kirunduzi-Mutara (0.54 mg/l) and Buhiga-Ntega (0.39 mg/l) show relatively higher concentrations. This indicates that the length of the flowpath is not the only factor controlling the concentration of F^-.

The average concentration of F^- in well waters (1.73 mg/l) exceeds the health based limit of 1.5 mg/l and shows that this element may pose a health problem. The lowest concentration of F^- (0.12 mg/l) is found within the water sample from the well at Nyange-Kumana (Nr.127 in Appendix VII.1) whose water shows, overall, the lowest mineralisation. The water sample with the highest concentration of F^- (16.53 mg/l) was

collected from the well in Ntwago-Murungurira, which, yet, does not show the highest mineralisation (TDS =741 mg/l). This observation may hint to the fact that the high concentration of F^- may be controlled by some local factors such as the occurrence of F-bearing minerals. Indeed, this water sample has a Ca^{2+} concentration of 26.9 mg/l, which is not the lowest concentration of this element in collected groundwater samples to justify high levels of F^-. Even water samples with lower concentrations of Ca^{2+} such as the wells in Nyange-Kumana (Nr: 127, Ca^{2+} = 4.3 mg/l; F^- = 0.12 mg/l) and Senga-Nyagisozi (Nr: 139: Ca^{2+} = 10.2 mg/l; F^- = 0.43 mg/l) do not show extremely high concentration of F^-. In general, water samples from the wells which are mainly located within the depression, show the highest concentrations of F^-, thereby indicating a possible combination of several hydrochemical processes, including the dissolution of F-bearing minerals and the precipitation of Ca-carbonate minerals resulting from the dissolution of aluminosilicates.

Table VII.36. Some descriptive statistics of the concentration of F^- for different sources of water samples

	Max mg/l	Min mg/l	Average mg/l	Standard deviation mg/l	Coefficient of variation %
All samples	16.53	0.06	0.95	1.80	189.89
Wells	16.53	0.12	1.73	2.40	138.30
Lakes	1.03	0.08	0.74	0.30	40.45
Springs	0.60	0.06	0.15	0.11	72.66

On average, the highest average concentration of F^- in water samples from lakes is found in Lake Cohoha South, while Lake Narungazi shows the lowest concentration (Table VII.37).

Hence, except the small lakes Nagitamo and Narungazi, the other lakes are characterised by levels of F^- which exceed the typical concentration of this element in lakes and rivers (0.5 mg/l) (WHO, 2006).

Table VII.37. Average concentration of F^- in different lakes sampled

	Cohoha South	Gacamirinda	Nagitamo	Narungazi	Rweru	Rwihinda
Number of samples	6	2	1	1	3	3
Average F^- (mg/l)	0.93	0.70	0.50	0.30	0.53	0.77

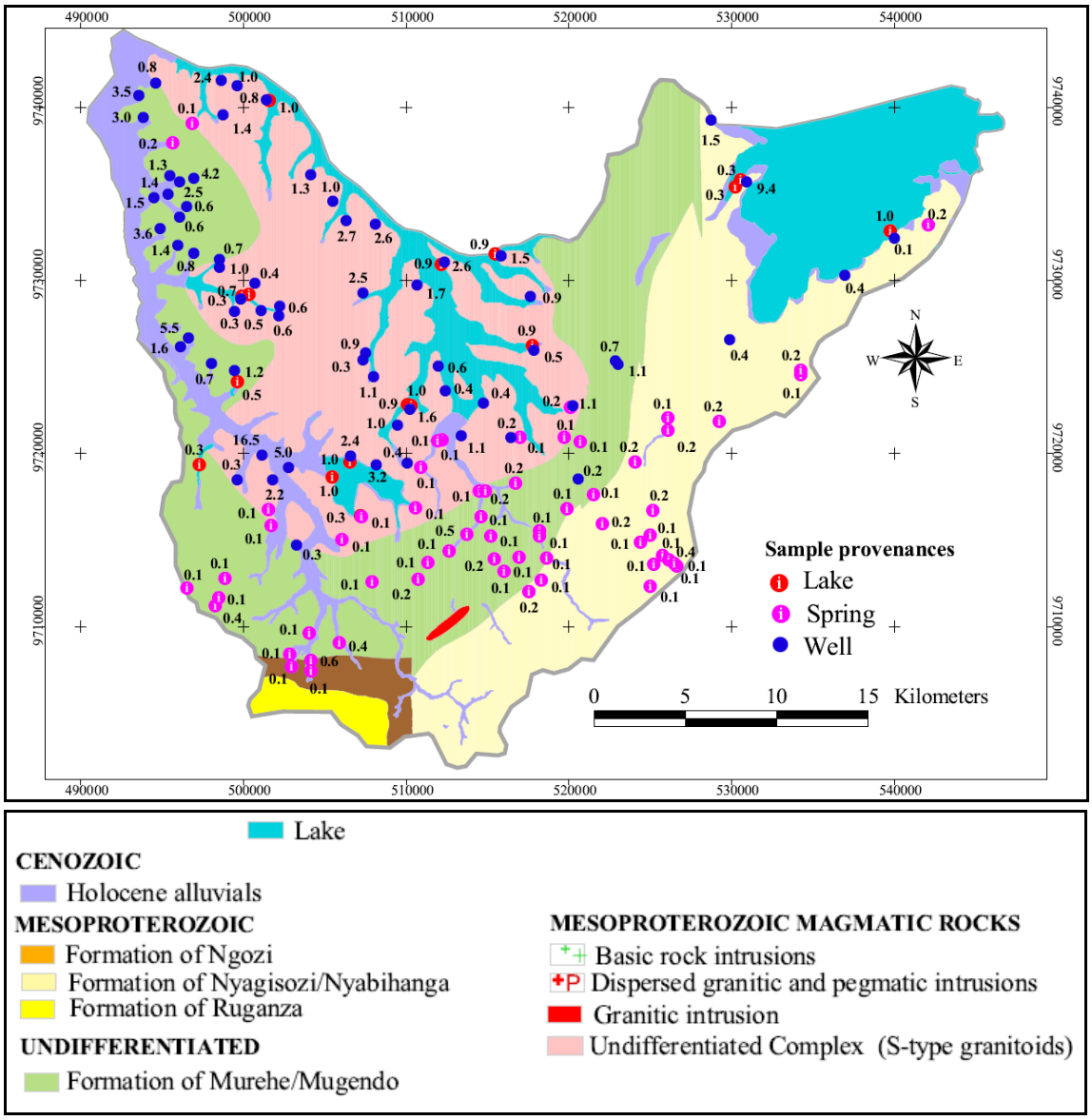

Figure VII.18. Spatial distribution of F^- concentration (mg/l)

VII.4.3. Graphical representation of chemical analyses and hydrochemical classification

VII.4.3.1. Piper diagram and classification based on the dominant ions

Graphical representation of chemical analyses is a commonly used method which facilitates the presentation, the interpretation and the classification of hydrochemical data into different hydrochemical facies (Chadha, 1999; Ahmad *et al.*, 2003; Hossain *et al.*, 2010; Ray & Mukherjee, 2008). The different facies reflect the response of groundwater to hydrochemical processes operating within the lithological framework of an aquifer and the pattern of flow path. Several diagrams are nowadays used for visualisation and classification of hydrochemical data (Güler *et al.*, 2002). In this study, Piper diagram (Piper, 1944) and scatter diagrams will be used.

Piper diagram enables to compare several water samples and to identify the different hydrochemical facies. The latter are determined based on the dominant cation and anion, which are defined as the ones having a concentration greater than 50 % of the sum of cations or anions involved into the classification. A variant of this classification simply considers the dominant ion regardless whether it accounts for more than 50 % of the total sum of concentrations of cations or anions. The last classification, which also considers NO_3^-, is used in this study.

Figure VII.19 shows the projection of the different water samples in the Piper diagram. Details about the classification of all water samples are presented in Appendix VII.2. Table VII.37 summarises the different water types and their respective abundance in terms of frequency. Piper diagram leads to the identification of 10 water types of which $NaHCO_3$, NaCl, $CaHCO_3$ and $NaNO_3$ are the most abundant ones with a respective abundance of 49 %, 19 %, 13 % and 12 %.

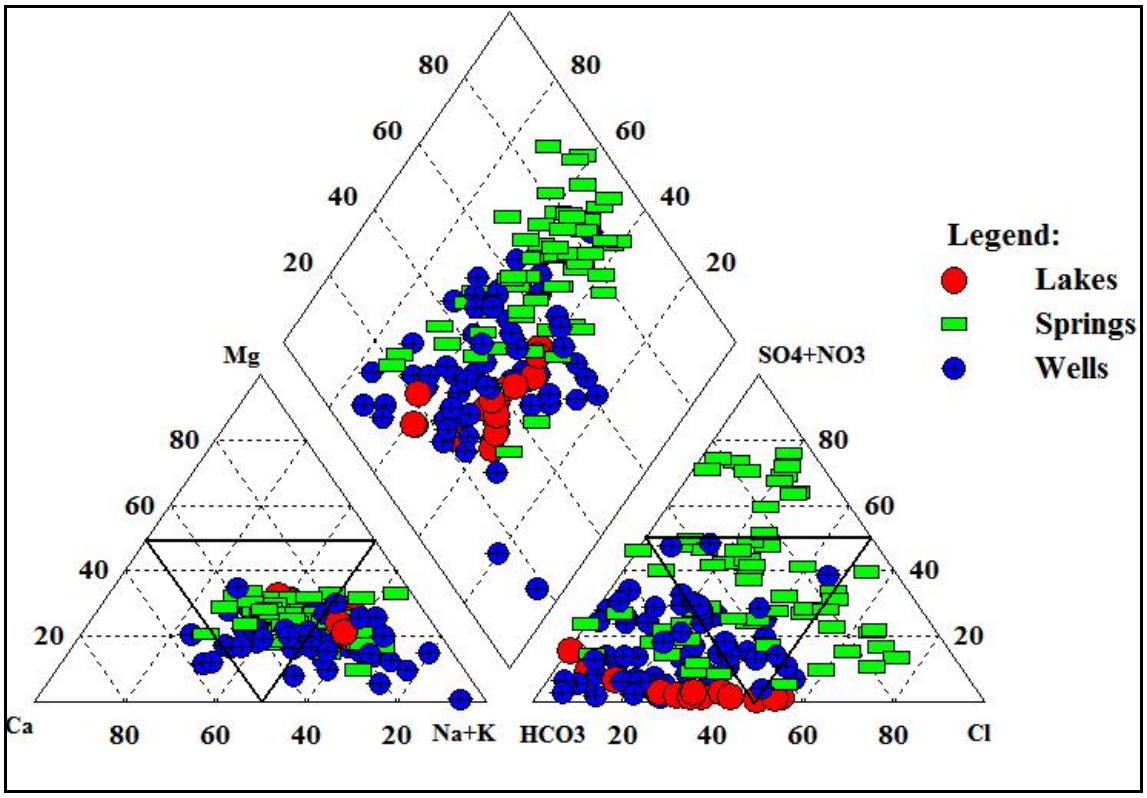

Figure VII.19. Piper diagram showing the projections of the different water samples based on the most abundant ions

A visual inspection of the anion triangle of the Piper diagram (Figure VII.19) shows that most of the samples plot in the lower left corner, thereby indicating that HCO_3^- is the most abundant anion. Indeed, of the 143 water samples collected, 62 % show the dominance of HCO_3^-. The cation triangle shows a scatter of data points in which the pole Na+K dominates for 78 % of the samples while only 16 % of the samples show the dominance of the Ca^{2+}.

Table VII.38. The different water types and their frequency using the classification based on the most abundant cation and anion

S/N	Water types	Frequency	Frequency (%)
1	NaHCO3	70	49
2	NaCl	27	19
3	CaHCO3	18	13
4	NaNO3	17	12
5	NaSO4	4	3
6	CaCl	2	1
7	CaSO4	2	1
8	CaNO3	1	1
9	KHCO3	1	1
10	KNO3	1	1
Total		**143**	**100**

The projection of the cationic and anionic compositions of the 143 water samples on the central diamond of the Piper diagram (Figure VII.20) helps to visualise and compare the different water types as well as to infer the evolutionary trends within the groundwater system. Figure VII.19 shows that the different data points representing the different water samples are characterised by a large spread. However, Figure VII.21 reveals that, by considering the different water types, this graphical representation clearly brings out some interesting hints which help decipher the complexity of the hydrochemical characteristics of the water samples from the different sources. Indeed, Figure VII.21 makes it possible to visualise that the 10 water types form distinct hydrochemical groupings from which an evolutionary sequence can be inferred.

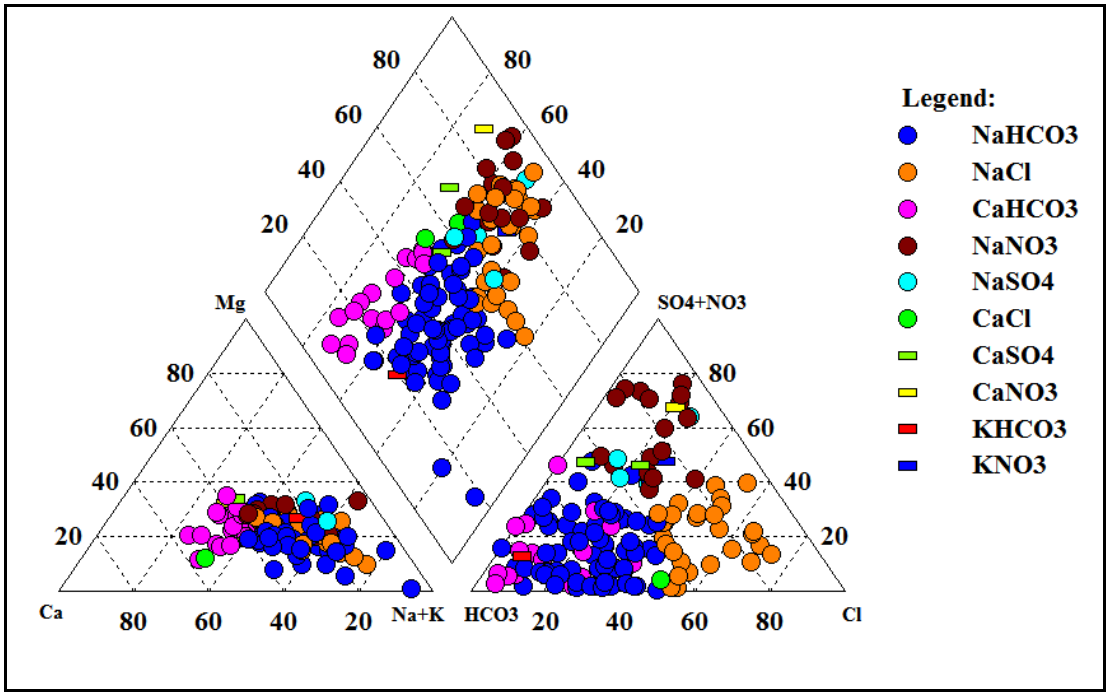

Figure VII.20. Piper diagram showing the different water types based on the dominant cation and anion

Figure VII.21 shows an important cluster of spring water samples, mainly of NaCl and $NaNO_3$ types, and accessorily $CaNO_3$ and $CaSO_4$, at the upper right hand edge of the central diamond, which represents slightly evolved waters of meteoric origin. This group of water types is characterised by low TDS values which are mainly in the range 39.4 mg/l to 142 mg/l with an average of 83 mg/l, as illustrated by the springs at Rushubije-Cogo (Nr. 76: TDS=39.4 mg/l), Rugomero-Gatemere (Nr. 70: TDS = 50.4 mg/l), Burengo-Rushubije (Nr. 22: TDS = 52 mg/l and Gihushi-Kiravumba (Nr. 27: TDS = 142 mg/l). The water sample from the well at Susa-Gikomero which falls within this water type seems to be an outlier, with a TDS value of 366 mg/l. In addition to the low mineralisation, these water samples are also characterised by low levels of silica (0.5-18 mg/l), Na^+ (2-27 mg/l), Ca^{2+} (0.4-12 mg/l), K^+ (0.1-6 mg/l) and HCO_3^- (3.1-34 mg/l), which reflect the low contribution from the weathering of silicate minerals due to short residence time and flow path. However, some springs occur further down towards the lower left edge of the diamond-shaped polygon and are intermixed with water samples from wells and lakes (Figure VII.19). Most of these springs are located inside or close to the depression of Bugesera as this is the case for the springs at Bunyari (Nr. 21: TDS =129 mg/l), Mukuyo-Kiri (Nr. 48: TDS = 654 mg/l), Mamfu-Kiyonza (Nr. 44: TDS = 402 mg/l) and Gihobogo-Murungurira (Nr. 26: TDS = 115 mg/l), Kabira (Nr. 29: TDS = 104 mg/l), Kinyangoro-Kumana (Nr. 39: TDS = 169 mg/l) and Nakabingo (Nr. 58: TDS =116 mg/l).

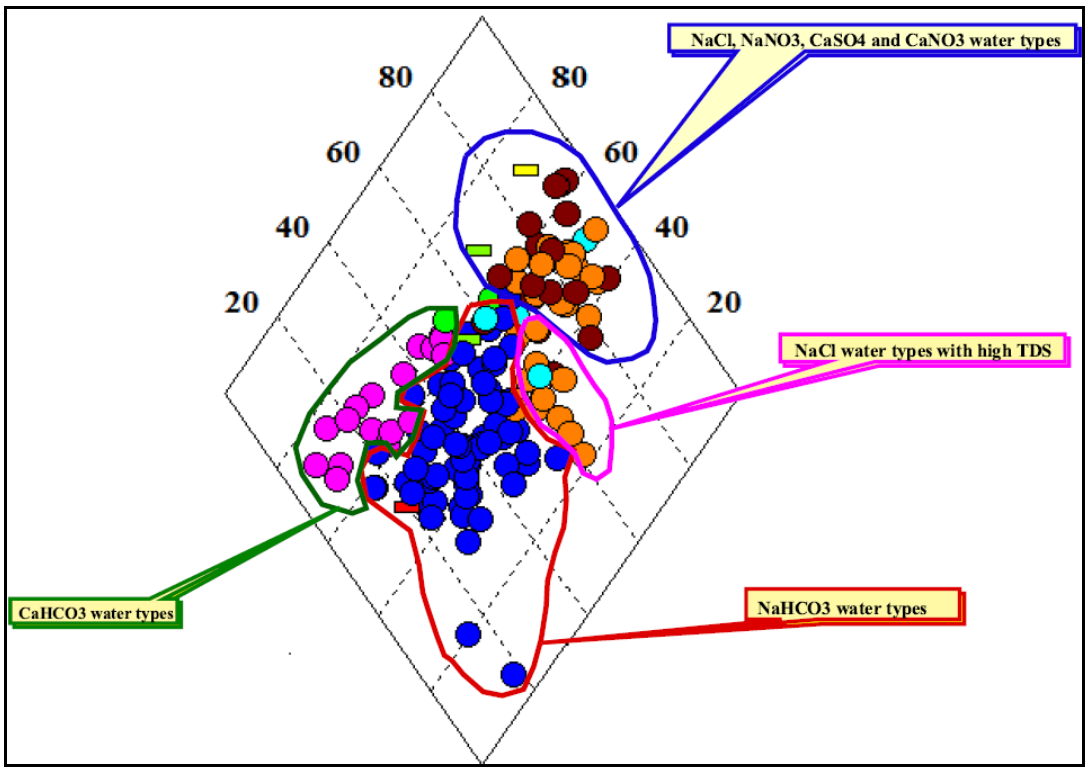

Figure VII.21. Central diamond of the Piper diagram showing the main hydrochemical clusters (legend: same as in Figure VII. 20).

Besides the main cluster of NaCl, $NaNO_3$, $CaSO_4$ and $CaNO_3$ water types, there is another small cluster of mainly NaCl type and accessorily, $NaNO_3$, and $NaSO_4$ which is predominantly formed by water samples from wells. These water samples are characterised by a high mineralisation, as this is illustrated by the wells at Shenga II-Rugasa (Nr. 142: TDS = 1805 mg/l), Kanigo-Cinuma (Nr.97: TDS =1527 mg/l) and Bishunzi-Cewe (Nr. 78: 1632 mg/l). These high TDS values which are associated with high concentrations of HCO_3^- (229-609 mg/l), Na^+ (90-418 mg/l) and Ca^{2+} (27-135 mg/l), confirm an important input from the weathering of feldspar minerals or may result from the concentration of groundwater due to the evapotranspiration process or dissolution of evaporitic salts. Overall, it can be noticed that the concentration of Na^+ is more important than that of Ca^{2+} in the majority of water samples, and this reflects the predominance of Na-feldspars over the Ca-feldspars.

The 17 water samples of $NaNO_3$ water type correspond to spring water with low mineralisation (TDS = 39 -122 mg/l) but which are characterised by relatively important levels of NO_3^- (8-43 mg/l). Most of these spring water samples show NO_3^- concentrations which are even higher than those of HCO_3^- (3-24 mg/l), Na^+ (5-14 mg/l), K^+ (0.1-6 mg/l) and Ca^{2+} (0.4-8 mg/l). This observation indicates that the NO_3^- input is associated with anthropogenic activities such as agricultural fertilisers, human and animal wastes, which contaminate the immature infiltrating waters and which are not degraded by anaerobic bacteria due to short and shallow flow paths in the oxic zone.

The occurrence of $NaHCO_3$ and $CaHCO_3$ water types mainly in the depression (Figure VII.22) with high mineralisation, as illustrated by the wells at Gahwijo II (TDS =2223 mg/l), Gasagara II-Rubuga (TDS =2381 mg/l), Hambiro-Kiyonza (1711 mg/l), Ntambe II-Kiri (TDS = 2257 mg/l), Kadobori II (TDS =1485 mg/l) and Mago-Gatete (3229 mg/l), confirms the importance of the dissolution of feldspars, which is accessorily complemented by the evapotranspiration process along the flow path and the leaching of saline soils.

$NaHCO_3$ water types with low mineralisation and low levels of Na^+, Ca^{2+}, HCO_3^-, Mg^{2+}, K^+ and SiO_2, such as the springs in Narutamwe-Kireka (Nr. 62: TDS = 47 mg/l), Rugomero-Kiravumva (Nr. 71: TDS = 28 mg/l) and Gihobogo-Murungurira (Nr. 26: TDS =103 mg/l), are immature waters, resulting from the infiltration of rain water and which may evolve from NaCl end member to $NaHCO_3$ type due to the dissolution of CO_2 or the oxidation of organic matter and slight weathering of aluminosilicates. The kinetics of dissolution of aluminosilicate minerals being slow, the short residence time does not allow to dissolve substantial amounts of rock-forming minerals.

The geochemical evolutionary track of groundwater in the study area starts by the infiltrating water of NaCl type which evolves towards $NaNO_3$, highly mineralised NaCl, $NaSO_4$, $CaHCO_3$, $CaNO_3$, $CaSO_4$, KNO_3, $KHCO_3$, $NaHCO_3$ water types by the processes of evapotranspiration, anthropogenic pollution, dissolution of evaporitic salts and, more importantly, the weathering of feldspars which brings a substantial contribution of Na^+, Ca^{2+}, HCO_3^-, K^+ and Mg^{2+}. Moreover, the predominance of $NaHCO_3$ and $CaHCO_3$ water types indicates that the dissolution of alumino-silicates, mainly Na-feldspars, is the main process controlling the hydrogeochemical evolution of groundwater in the study area.

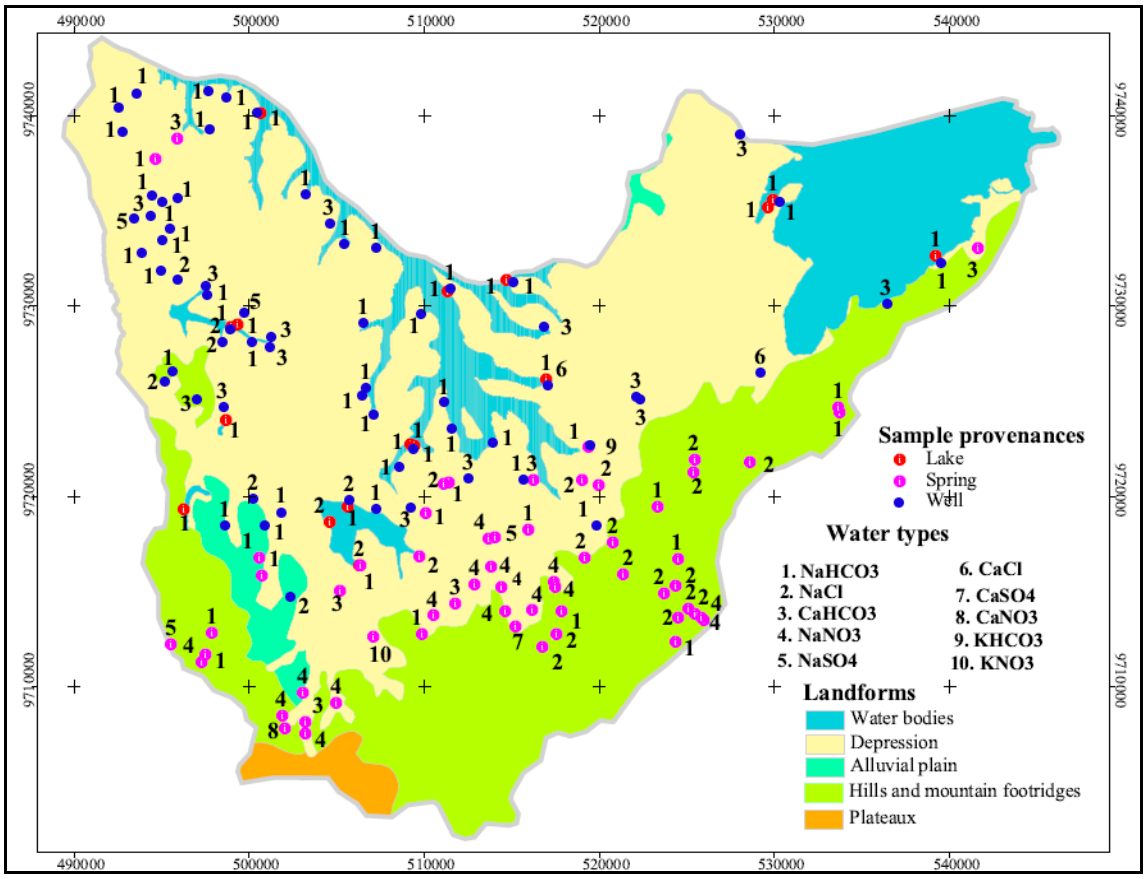

Figure VII.22. Spatial distribution of water types within the different landforms

VII.4.3.2. Classification of De Moor and De Breuck (1969)

De Moor & De Breuck (1969) developed a classification method based on variation of total dissolved solids (TDS) in groundwater as shown in Table VII.38. Simplified empirical relationships between TDS and ρ_w (Ωm, 11°C) and ρ_t (Ωm, 11°C) were further defined by Walraevens & Cnudde (2006) as follows:

- TDS (mg/l) = 10000/ ρ_w (Ωm, 11°C) (6.10)
- ρ_t (Ωm, 11°C) = 4 * ρ_w (Ωm, 11°C) (6.11)

In this classification, groundwater types vary between very fresh (VF) and salt (S) (Table VII.39).

Table VII.39. De Moor and De Breuck (1969) groundwater classification and relation to water resistivity (ρ_w) and formation resistivity (ρ_t).

De Moor & de Breuck (1969)		**Walraevens & Cnudde (2006)**	
Ground water quality	**TDS (mg/l)**	**ρ_w (Ωm, 11°C)**	**ρ_t (Ωm, 11°C)**
Very fresh (VF)	< 200	>50	> 200
Fresh (F)	200-400	50-25	200-100
Moderately fresh (MF)	400-800	25-12.5	100-50
Weakly fresh (WF)	800-1600	12.5-6.25	50-25
Moderately brackish (MB)	1600-3200	6.25-3.13	15-12.5
Brackish (B)	3200-6400	3.13-1.56	12.5-6.25
Very brackish (VB)	6400-12800	1.56-0.78	6.25-3.12
Moderately salt (MS)	12800-25600	0.78-0.39	3.12-1.56
Salt (S)	>25600	< 0.39	< 1.56

The classification of the 143 water samples collected in the study area is presented in Appendix VII.3 and summarised in Table VII.39. The spatial distribution of water types according to this classification is represented in Figure VII.23. Table VII.40 shows the predominance of the very fresh water type (TDS <200 mg/l) which includes all the water samples from the springs located in the highlands which, as it was shown in previous sections, are mostly lowly mineralised. In addition, water samples collected from some wells situated in the southern and eastern parts of the study area, such as the wells at Muhero I-Yaranda (Nr. 115: TDS = 179.4 mg/l), Rugoma-Kagege (Nr. 128: TDS = 129 mg/l), Nyange-Kumana (Nr. 127: TDS = 44.4 mg/l), Senga-Nyagisozi (Nr. 139: TDS= 93.5mg/l) and Kadobogoro-Muramba (Nr. 92: TDS = 134.9 mg/l), fall within the group of very fresh water type. Water samples collected from the two springs located within the depression (Mamfu-Kiyonza, Mukuyo-Kiri) are moderately fresh, i.e. with TDS values comprised between 400 and 800 mg/l.

Table VII.40. Water types according to the classification of De Moor and De Breuck and their frequency

N/S	**Water type**	**Frequency**	**Frequency (%)**
1	Very fresh	67	47
2	Fresh	12	8
3	Moderately fresh	33	23
4	Weakly fresh	19	13
5	Moderately brackish	11	8
6	Brackish	1	1
	Total	**143**	**100**

Water samples collected from the different small lakes are mostly moderately fresh, except 3 samples from the Lake Rweru which are very fresh and the sample from the Lake Narungazi, a tiny lake situated in the western part of the study area, which is fresh.

This classification method shows also that water samples from the wells are predominantly weakly fresh (19 samples) to moderately fresh (17 samples) and to a lesser extent moderately brackish (11 samples), fresh (12 samples), very fresh (5 samples) and brackish (1 sample). The water sample from the well located downstream of the quarry of salty soil at Mago-Gatete (TDS = 3229 mg/l) is the only water sample of brackish water type. The group of wells in the western part of the study area which are characterised by high mineralisation falls within the category of moderately brackish water type (e.g. wells at Gahwijo I, Gifuruguti-Nyakarama, Munyinya-Nyakarama, Ntembe II-Kiri) and weakly fresh type (e.g. wells at Gahwijo II, Kadobori II, Kanigo-Cinuma, GasagaraI-Rubuga).

The distribution of the different water types according to the classification of De Moor and De Breuck (1969) within the different landforms (Figure VII.23) shows a clear demarcation between the depression of Bugesera to the North and the highlands to the South and East. Water samples collected within the depression are classified as fresh (F), moderately fresh (MF), weakly fresh (WF), moderately brackish (MB) and brackish (B), whereas water samples collected from wells and springs situated at the southern and eastern periphery of the depression and in the highlands are systematically very fresh. This classification confirms that the water samples collected from both wells and springs located at the periphery of the depression and in the highlands are newly infiltrated waters of meteoric origin. On the contrary, water samples collected inside the depression are more evolved due to the combination of a number of processes, including the weathering of aluminosilicates, evapotranspiration which contributes to the progressive concentration of groundwater along the flow path and the dissolution of evaporitic salt deposits which are scattered throughout the depression. This is reflected by an elevated mineralisation which reaches even the threshold of brackish water type.

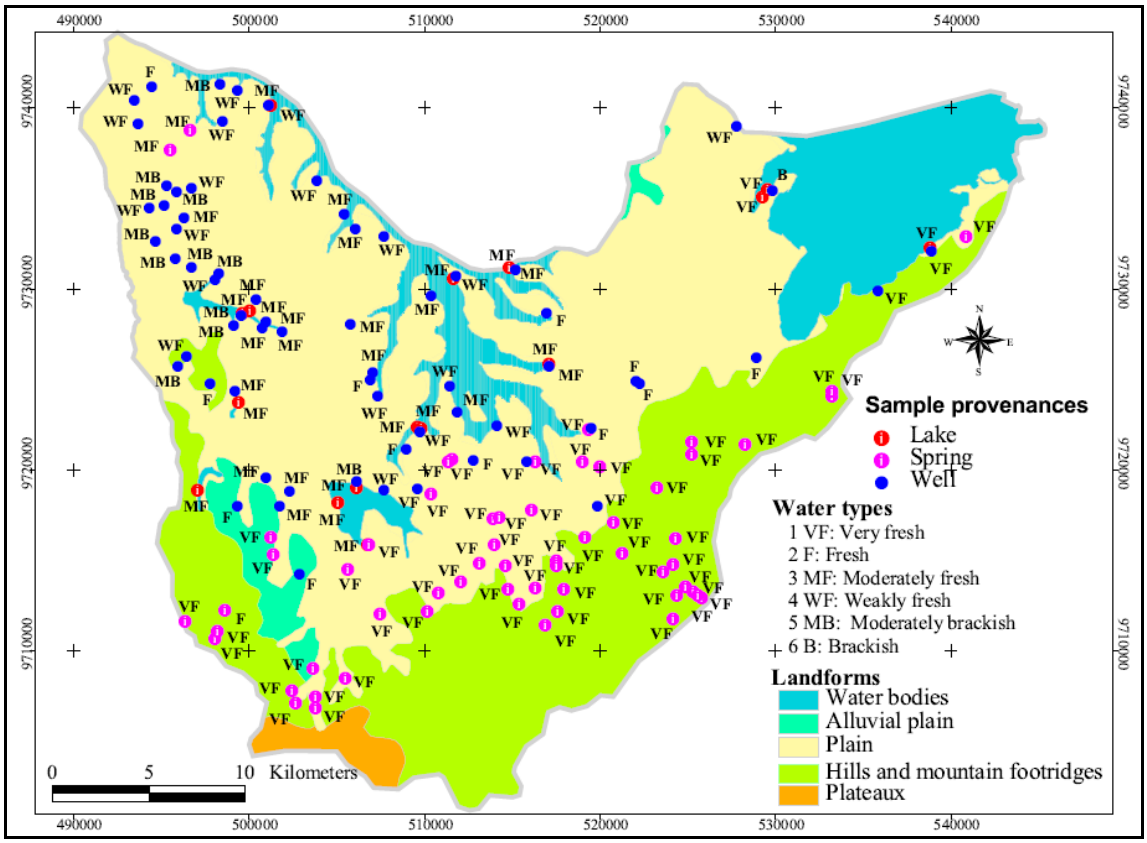

Figure VII.23. Spatial distribution of water types based on the De Moor and De Breuck classification within different landform units.

VII.4.4. Main hydrochemical processes in Bugesera region

In this section a discussion of the main hydrochemical processes which may account for the different hydrochemical characteristics and water types observed in the study area is presented. The discussion presented in the previous sections has shown that the main hydrochemical processes regulating the chemistry of groundwater in Bugesera region include water-rock interactions, predominantly the weathering of silicate minerals and to a lesser extent the dissolution of secondary carbonate minerals, the concentration of different solutes in groundwater resulting from the process of evapotranspiration, and the dissolution of evaporitic salt deposits.

VII.4.4.1. Hydrochemical evolution of groundwater due to evaporative concentration

According to Humphries *et al.* (2011), solutes in groundwater become progressively concentrated under the influence of evapotranspiration, resulting is the saturation, precipitation and accumulation of less soluble compounds. This process may act increasingly along the flow line, thereby progressively augmenting the concentration of solutes from the recharge area towards the discharge area. To evaluate to what extent the evapotranspiration contributes to the increased mineralisation of groundwater along the flow path, the concentration factor was calculated using Cl^- concentration which is

considered as a conservative ion. The evaporative concentration of different dissolved constuents is calculated by considering the lowly mineralised spring water mainly sampled in the highlands as the starting point of the geochemical evolution. Using chloride as a conservative ion, the different water samples were grouped into the following 6 concentration classes: 0-10 mg/l, 10-30 mg/l, 30-60 mg/l, 60-90 mg/l, 90-120 mg/l, 120-150 mg/l and Cl^- concentration greater than 150 mg/l. The first chloride concentration class (0-10 mg/l) was considered as the end member at the start, representing the lowly mineralised water of meteoric origin. It was calculated as the average composition of all water samples belonging to this class.

The geochemical evolution was evaluated through the computation of the concentration factor associated with the subsequent chloride concentration classes. The concentration factor, which is the ratio of the chloride concentration between the considered class to the end member class (Cl^- = 0-10 mg/l), was further used to calculate the concentration of different groundwater solutes which would be expected if evaporation was the only process involved in the hydrochemical evolution of groundwater. Tables VII.41 to VII.46 show the synthesis of the calculations of the concentration factors for different Cl^- concentration classes and the resulting expected concentrations of dissolved constituents. Detailed tables showing these calculations are presented in Appendix VII.5. The Δ concentration represents the difference between the expected concentration due to the evaporation process and the actual concentration as measured in water samples belonging to the considered class.

Despite a certain variability between the different classes, Tables VII.41 to VII.46 show that, overall, as the concentration factor increases, there is progressive deficit in the sum of alkaline and alkaline earth ions ($Na^+ + K^+ + Ca^{2+} + Mg^{2+}$) while HCO_3^- shows a slight increase. The increasing surplus in the concentration of bicarbonate has to be related to the input resulting from the continuing dissolution of CO_2, the oxidation of organic matter or the weathering of aluminosilicates. The increasing deficit in alkaline and alkaline earth ions as the concentration factor increases is somewhat surprising as, due to progressive input from the weathering of aluminosilicates along the flow path, a surplus would be expected. The deficit in alkaline and alkaline earth cations seems to mask the weathering of aluminosilicates and may point to the exaggeration of the concentration factor, due to the fact that the concentration of Cl^- in different classes, used to calculate this factor, might be influenced by other processes than the evaporation such as anthropogenic pollution or dissolution of evaporitic salts.

Next to the cations, it can be noted from Tables VII.41 to VII.46 that calculated concentrations are consistently too high only for NO_3^- and SiO_2, NO_3^- being the highest. For the rest of the solutes, the difference between calculated and actual concentrations

is, on average, negligible. For instance, SO_4^{2-} is fairly well explained by the evaporative concentration model. The deviations of actual concentrations of NO_3^- and SiO_2 with respect to the expected ones are due to the fact that the selected young spring water which was selected for the recharge end member (Cl^- <10mg/l) has already incurred some important aluminosilicate dissolution and some NO_3^- pollution. Indeed, average concentrations of 9.1 mg/l and 16.2 mg/l respectively for SiO_2 and NO_3^- are too high to represent rain water end member. In the actual rainfall water, these concentrations would be lower, such that, after evapoconcentation, the calculated surpluses would not appear.

Figure VII.24 presents a conceptual cross-section of Bugesera aquifer, which summarises the concept of evaporative concentration. Meteoric water infiltrating in the southern highlands will subsequently flow towards the depression which constitues the discharge area. On its flow path to the depression, the concentration of the dissolved constituents in groundwater will progressively increase due to the evapotranspiration which removes part of the solvent, i.e. groundwater. Hence, while water from springs and wells located in and close to the recharge area is characterised by a low mineralisation and low levels of chloride, samples taken from wells further downgradient, i.e. within the depression, show a substantial mineralisation and an increased concentration of chloride, which can be mainly explained by the evaporative concentration.

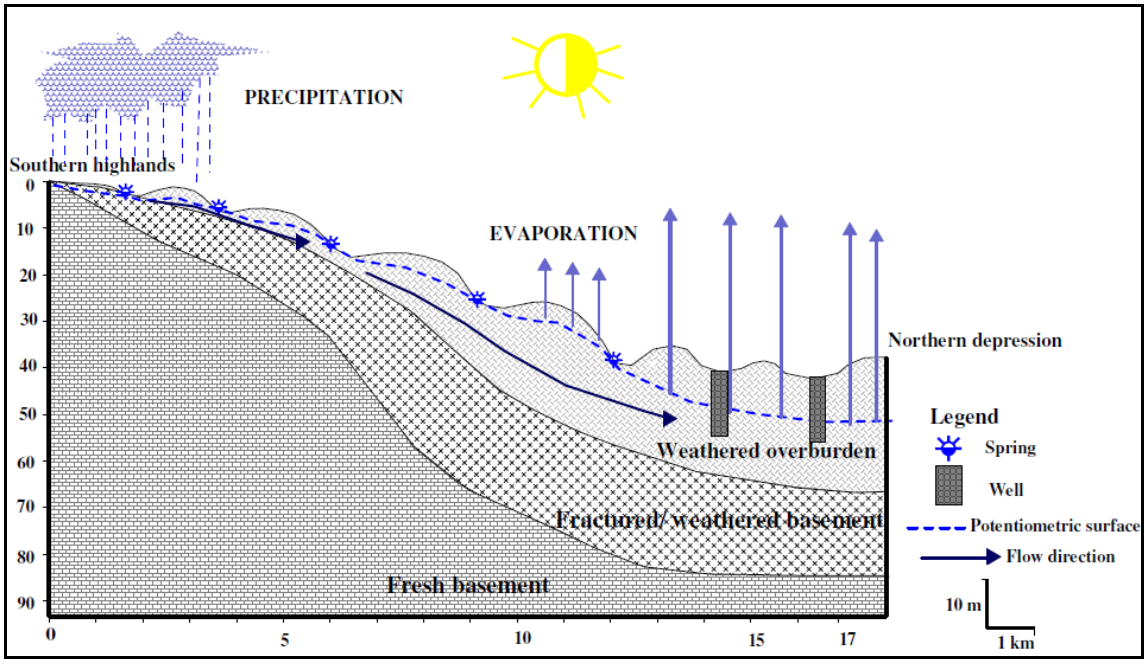

Figure VII.24. A conceptual cross-section illustrating the concept of evaporative concentration in Bugesera aquifer

Table VII.41. Calculation of the concentration factor and water composition expected from evaporative concentration for the class of water samples with Cl^- concentration ranging between 10-30 mg/l

	Cl^- mg/l	HCO_3^- mg/l	SO_4^{2-} mg/l	NO_3^- mg/l	NO_2^- mg/l	NH_4^+ mg/l	PO_4^{3-} mg/l	Ca^{2+} mg/l	Mg^{2+} mg/l	Mn^{2+} mg/l	Fe^{2+} mg/l	K^+ mg/l	Na^+ mg/l	F^- mg/l	SiO_2 mg/l	TDS mg/
Average (Cl <10 mg/l)	5.4	15.5	4.1	16.2	0.1	0.0	0.1	4.8	2.6	0.1	0.1	1.3	7.6	0.2	9.1	67.8
Average (Cl = 10-30 mg/l)	17.1	131.8	22.9	14.8	0.2	0.0	0.1	20.6	9.3	0.2	0.7	10.0	30.7	0.5	11.9	270.9
Concentration factor	3.1															
Expected concentration	17.1	48.7	12.7	50.9	0.3	0.0	0.2	15.2	8.1	0.3	0.4	4.0	23.7	0.5	28.5	212.9
Δ Reaction (mg/l)	0.0	83.1	10.2	-36.2	-0.1	0.0	-0.1	5.4	1.2	-0.1	0.3	5.9	7.0	-0.1	-16.6	58.0
Molar weight		61	96	62	46	18	95	40	24	55		39	23	19	60	
Δ Reaction (mmol/l)		1.4	0.1	-0.6	0.0	0.0	0.0	0.1	0.0	0.0		0.2	0.3	0.0	-0.3	
Sum of alkaline and alkaline earth cations (mmol)								0.6								

Table VII.42. Calculation of the concentration factor and water composition expected from evaporative concentration for the class of water samples with Cl^- concentration ranging between 30-60 mg/l

Site	Cl^- mg/l	HCO_3^- mg/l	SO_4^{2-} mg/l	NO_3^- mg/l	NO_2^- mg/l	NH_4^+ mg/l	PO_4^{3-} mg/l	Ca^{2+} mg/l	Mg^{2+} mg/l	Mn^{2+} mg/l	Fe^{2+} mg/l	K^+ mg/l	Na^+ mg/l	F^- mg/l	SiO_2 mg/l	TDS mg/
Average (Cl<10 mg/l)	5.4	15.5	4.1	16.2	0.1	0.0	0.1	4.8	2.6	0.1	0.1	1.3	7.6	0.2	9.1	67.8
Average (Cl=30-60 mg/l)	44.3	169.7	50.6	17.3	0.1	0.1	0.1	38.4	13.0	0.5	2.4	14.0	47.6	1.1	11.4	410.4
Concentration factor	8.1															
Expected concentration	44.3	126.2	33.0	132.0	0.9	0.0	0.6	39.4	21.1	0.8	1.0	10.5	61.5	1.4	73.8	551.5
Δ Reaction (mg/l)	0.0	43.5	17.6	-114.7	-0.8	0.0	-0.5	-1.0	-8.1	-0.3	1.3	3.5	-13.9	-0.3	-62.4	-141.1
Molar weight		61	96	62	46	18	95	40	24	55		39	23	19	60	
Δ Reaction (mmol/l)		0.7	0.2	-1.9	0.0	0.0	0.0	0.0	-0.3	0.0		0.1	-0.6	0.0	-1.0	
Sum of alkaline and alkaline earth cations (mmol)								-0.8								

Table VII.43. Calculation of the concentration factor and water composition expected from evaporative concentration for the class of water samples with Cl^- concentration ranging between 60-90 mg/l

	Cl^- mg/l	HCO_3^- mg/l	SO_4^{2-} mg/l	NO_3^- mg/l	NO_2^- mg/l	NH_4^+ mg/l	PO_4^{3-} mg/l	Ca^{2+} mg/l	Mg^{2+} mg/l	Mn^{2+} mg/l	Fe^{2+} mg/l	K^+ mg/l	Na^+ mg/l	F^- mg/l	SiO_2 mg/l	TDS mg/
Average (Cl < 10 mg/l)	5.4	15.5	4.1	16.2	0.1	0.0	0.1	4.8	2.6	0.1	0.1	1.3	7.6	0.2	9.1	67.8
Average (Cl =60-90 mg/l)	74.8	397.7	53.6	26.1	0.9	0.6	0.1	47.3	22.8	2.1	8.5	29.4	111.3	1.5	11.6	788.1
Concentration factor	13.8															
Expected concentration	74.8	213.2	55.7	223.0	1.5	0.1	1.0	66.6	35.6	1.3	1.8	17.7	103.9	2.4	124.7	931.9
Δ Reaction (mg/l)	0.0	184.5	-2.1	-197.0	-0.6	0.5	-0.9	-19.3	-12.8	0.7	6.7	11.7	7.4	-0.9	-113.1	-143.8
Molar weight		61	96	62	46	18	95	40	24	55		39	23	19	60	
Δ Reaction (mmol/l)		3.0	0.0	-3.2	0.0	0.0	0.0	-0.5	-0.5	0.0		0.3	0.3	0.0	-1.9	
Sum of alkaline and alkaline earth cations (mmol)								0.4								

Table VII.44. Calculation of the concentration factor and water composition expected from evaporative concentration for the class of water samples with Cl^- concentration ranging between 90-120 mg/l

	Cl^- mg/l	HCO_3^- mg/l	SO_4^{2-} mg/l	NO_3^- mg/l	NO_2^- mg/l	NH_4^+ mg/l	PO_4^{3-} mg/l	Ca^{2+} mg/l	Mg^{2+} mg/l	Mn^{2+} mg/l	Fe^{2+} mg/l	K^+ mg/l	Na^+ mg/l	F^- mg/l	SiO_2 mg/l	TDS mg/
Average (Cl < 10 mg/l)	5.4	15.5	4.1	16.2	0.1	0.0	0.1	4.8	2.6	0.1	0.1	1.3	7.6	0.2	9.1	67.8
Average (Cl =90-120 mg/l)	106.5	451.7	107.0	25.6	0.1	0.7	0.1	73.1	33.8	1.2	2.4	36.9	124.5	1.5	12.9	978.0
Concentration factor	19.6															
Expected concentration	106.5	303.4	79.3	317.4	2.1	0.1	1.4	94.8	50.7	1.9	2.5	25.2	147.8	3.4	177.4	1326.2
Δ Reaction (mg/l)	0.0	148.4	27.7	-291.8	-2.0	0.6	-1.2	-21.7	-16.9	-0.7	-0.2	11.8	-23.3	-1.8	-164.6	-348.2
Molar weight		61	96	62	46	18	95	40	24	55		39	23	19	60	
Δ Reaction (mmol/l)		2.4	0.3	-4.7	0.0	0.0	0.0	-0.5	-0.7	0.0		0.3	-1.0	-0.1	-2.7	
Sum of alkaline and alkaline earth cations (mmol)								-10								

Table VII.45. Calculation of the concentration factor and water composition expected from evaporative concentration for the class of water samples with for the Cl^- concentration ranging between 120-150 mg/l

	Cl^- mg/l	**HCO_3^- mg/l**	**SO_4^{2-} mg/l**	**NO_3^- mg/l**	**NO_2^- mg/l**	**NH_4^+ mg/l**	**PO_4^{3-} mg/l**	**Ca^{2+} mg/l**	**Mg^{2+} mg/l**	**Mn^{2+} mg/l**	**Fe^{2+} mg/l**	**K^+ mg/l**	**Na^+ mg/l**	**F^- mg/l**	**SiO_2 mg/l**	**TDS mg/**
Average (Cl < 10 mg/l)	5.4	15.5	4.1	16.2	0.1	0.0	0.1	4.8	2.6	0.1	0.1	1.3	7.6	0.2	9.1	67.8
Average (Cl =120-150 mg/l)	136.5	445.3	91.5	23.9	3.8	1.8	7.7	57.2	25.7	5.1	2.6	38.4	134.5	3.6	14.3	1062.1
Concentration factor	25.1															
Expected concentration	136.5	388.9	101.7	406.9	2.7	0.1	1.8	121.5	65.0	2.4	3.2	32.3	189.5	4.3	227.4	1700.0
Δ Reaction (mg/l)	0.0	56.4	-10.2	-382.9	1.1	1.7	5.9	-64.3	-39.4	2.7	-0.7	6.1	-55.0	-0.7	-213.2	-637.9
Molar weight		61	96	62	46	18	95	40	24	55		39	23	19	60	
Δ Reaction (mmol/l)		0.9	-0.1	-6.2	0.0	0.1	0.1	-1.6	-1.6	0.0		0.2	-2.4	0.0	-3.6	
Sum of alkaline and alkaline earth cations (mmol)								-5.8								

Table VII.46. Calculation of the concentration factor and water composition expected from evaporative concentration for the class of water samples with Cl^- concentration ranging between >150 mg/l

	Cl^- mg/l	**HCO_3^- mg/l**	**SO_4^{2-} mg/l**	**NO_3^- mg/l**	**NO_2^- mg/l**	**NH_4^+ mg/l**	**PO_4^{3-} mg/l**	**Ca^{2+} mg/l**	**Mg^{2+} mg/l**	**Mn^{2+} mg/l**	**Fe^{2+} mg/l**	**K^+ mg/l**	**Na^+ mg/l**	**F^- mg/l**	**SiO_2 mg/l**	**TDS mg/**
Average (Cl < 10 mg/l)	5.4	15.5	4.1	16.2	0.1	0.0	0.1	4.8	2.6	0.1	0.1	1.3	7.6	0.2	9.1	67.8
Average (Cl > 150 mg/l)	283.7	600.9	154.2	24.3	2.5	1.2	4.3	83.1	38.0	3.1	4.3	51.3	233.8	3.1	14.8	1516.7
Concentration factor	52.1															
Expected concentration	283.7	808.4	211.3	845.7	5.6	0.3	3.7	252.5	135.1	5.0	6.7	67.1	393.9	9.0	472.8	3533.7
Δ Reaction (mg/l)	0.0	-207.5	-57.1	-821.4	-3.1	0.9	0.6	-169.4	-97.1	-1.9	-2.4	-15.8	-160.1	-5.9	-457.9	-2016.9
Molar weight		61	96	62	46	18	95	40	24	55		39	23	19	60	
Δ Reaction (mmol/l)		-3.4	-0.6	-13.2	-0.1	0.1	0.0	-4.2	-4.0	0.0		-0.4	-7.0	-0.3	-7.6	
Sum of alkaline and alkaline earth cations (mmol)								-15.6								

VII.4.4.2. Hydrochemical evolution of groundwater due to mixing with "salt water" resulting from the dissolution of evaporitic salt deposits

VII.4.4.2.1. Origin and occurrences of evaporitic salts

There are several places in the study area where occurrences of salty soils are exploited for cattle feeding. The most well known place is located at Mago-Gatete, in Busoni municipality, where there is a sort of quarry of 3 m-deep where these salts are collected by local cattle breeders (Figures VII.25 to VII.27). According to local villagers, the salty taste of water fetched from some shallow wells in the study area might be due to the presence of these salts which contaminate groundwater.

Since a long time ago, such salty soils were commercialised all over the country and were mainly exploited from the Plain of Imbo, in the region of Bujumbura, where they are locally known as "igitumba". Like the lowlands of Bugesera, the Plain of Imbo is also characterised by relatively elevated air temperatures which may favour the formation of such evaporitic salts in the upper layers of the soil profile. However, while the Plain of Imbo is a sedimentary basin underlain by a mixture of lacustrine and fluviatile sediments, the evaporitic salts of the Bugesera depression occur in the upper layers of the weathered overburden, developed on a Precambrian basement.

Chemical analyses of 63 samples of the evaporitic salts of the Plain of Bujumbura (Nahimana, 1993; unpublished data, Gourdin, 1986 in Nahimana, 1993) at different depths (0 m, 0.5 m and 1 m) have shown the predominance of Na^+ and SO_4^{2-} over the other ions (Table VII.47). Moreover, it was observed that the concentration of the different ions decreases with increasing depth, thereby confirming the fact that the formation of the salts results from the capillary rise which is enhanced by the evapotranspiration process from the shallow water table (2-3 m below the ground surface in Kajaga) (Table VII.47).

Mineralogical analyses of samples from the Plain of Bujumbura by X-ray diffraction have revealed more than eight species of salts including thenardite (Na_2SO_4), halite (NaCl), thermonardite ($Na_2CO_3.H_2O$), nahcolite ($NaHCO_3$), sylvite (KCl), northupite ($Na_6MgCl_2(CO_3)_4$), bischoffite ($MgCl_2.6H_2O$) and calcite ($CaCO_3$).

Chemical analyses of groundwater in the Plain of Bujumbura reflect the chemical composition of the salt deposits. Indeed, it can be observed from Table VII.47 that Na^+ remains the dominant cation in groundwater, whereas HCO_3^- becomes the more abundant anion instead of SO_4^{2-}, which displays the highest concentration in the soil deposits. The relatively elevated concentration of different ions in groundwater results from the contamination of groundwater by infiltrating water which leaches salt deposits in the soil zone. The significant enrichment of groundwater in HCO_3^- compared to the saline soil may be the result of further dissolution of CO_2 and oxidation of organic

matter within the soil zone as infiltrating water progresses towards the saturated zone (Table VII.47).

Table VII.47. Concentration of different cations and anions (in mg/100 mg of soil) in salt soils of the Plain of Bujumbura (Nahimana, 1993)

Sampling depth	Na^+	K^+	Mg^{2+}	Ca^{2+}	CO_3^{2-}	HCO_3^-	Cl^-	SO_4^{2-}	Total
Ground surface	725.8	47.1	28.0	11.0	79.7	603.2	125.6	755.6	2350.8
0.5 m	231.5	15.2	22.0	10.3	24.0	267.5	126.8	376.1	1073.4
1 m	156.3	12.2	16.3	3.4	21.5	207.3	99.0	372.7	888.7
Groundwater (mg/l)	1156	39.0	119.0	132.0	82.0	2756.0	419.0	728.0	5431.0

Figures VII.25 to VII.27 show pictures of the evaporitic salts at the quarry of Mago, in Busoni municipality. Figure VII.28 and VII.29 present schematic cross-sections of the quarries where evaporitic salts are exploited respectively in Mago, in the municipality of Busoni and in Rubirizi, in the municipality of Bugabira. It can be observed from the two cross-sections that the subsurface at the two sites shows a succession of three main lithological layers, including from the ground surface:

- an upper layer made up of coarse materials comprising large lateritic blocks, rock fragments, pebbles and gravels which are slightly cemented by a mixture of clay, silt and sand. The roundness of most of the rock blocks forming this layer denotes a fluviatile origin. The average thickness of this layer is 1 m in Mago and 1.3 m in Rubirizi.
- This upper layer is followed by a relatively thick middle layer where predominate fine materials comprising mainly silt, clay, sand and accessorily a few gravels and blocks scattered throughout the layer. It is in this layer that a concentration of white evaporitic salts is observed on the walls of the quarry of Mago (Busoni) and Rubirizi (Bugabira). These evaporitic salts are exploited by local stockbreeders who scratch the wall of the quarry using shovels or used hoes and trowels. The average thickness of this layer is 4.6 m in Rubirizi (Bugabira) and approximately 3 m in Mago (Busoni).
- The third layer corresponds to the aquifer. It is actually composed of the same materials as the middle layer, but which progressively grade into more coarse materials with an important increase of the proportion of rocks fragments, blocks and gravels, with a little proportion of fine materials. This lithological structure seems to be in agreement with the observations made from the geoelectrical cross-sections, which show that the geoelectrical resistivity can significantly increase below the groundwater table due to the increase of the proportion of coarse materials. The groundwater table was measured at a depth of 3.81 m and 5.91 m respectively from wells at Mago (Busoni) located at approximately 1.7 km downslope of the quarry, and int Rubirizi (Bugabira) which is situated at nearly 300 m upslope of the quarry of salts.

Figure VII.25. A stockbreeder scratching evaporitic salts at the quarry of Mago to feed his cattle

Figure VII.26. Whitish secondary concentrations of the evaporitic salts on the wall of the quarry at Mago (Busoni)

Figure VII.27. Topsoil at the quarry of evaporitic salts of Mago (Busoni) showing coarse materials within the top layer.

The two cross-sections at Mago (Busoni) and Rubirizi (Bugabira) shed sufficient light as regard to the origin of these salts (Figure VII.28 and VII.29). Indeed, in the light of the two cross-sections, it appears clear that, in such a warm environment, these salts result from the upward movement of shallow groundwater through the pores due to the capillary rise, and the seepage across the seepage face of the quarry, and the subsequent evaporation of water, which entails the deposition of the dissolved salts. It stems from what precedes that the evaporitic salts are therefore dispersed in the upper layers of the soil profile above the groundwater table. The white concentrations of evaporitic salts observed on the walls of the quarries at Mago (Busoni) and Rubirizi (Bugabira) may correspond to evaporitic salts of secondary origin associated with the remobilisation of salts within the upper layers of the soil profile by percolating water and subsequent deposition on the wall of the quarries, due to the evaporation of infiltrating water which seeps through the walls of the quarries.

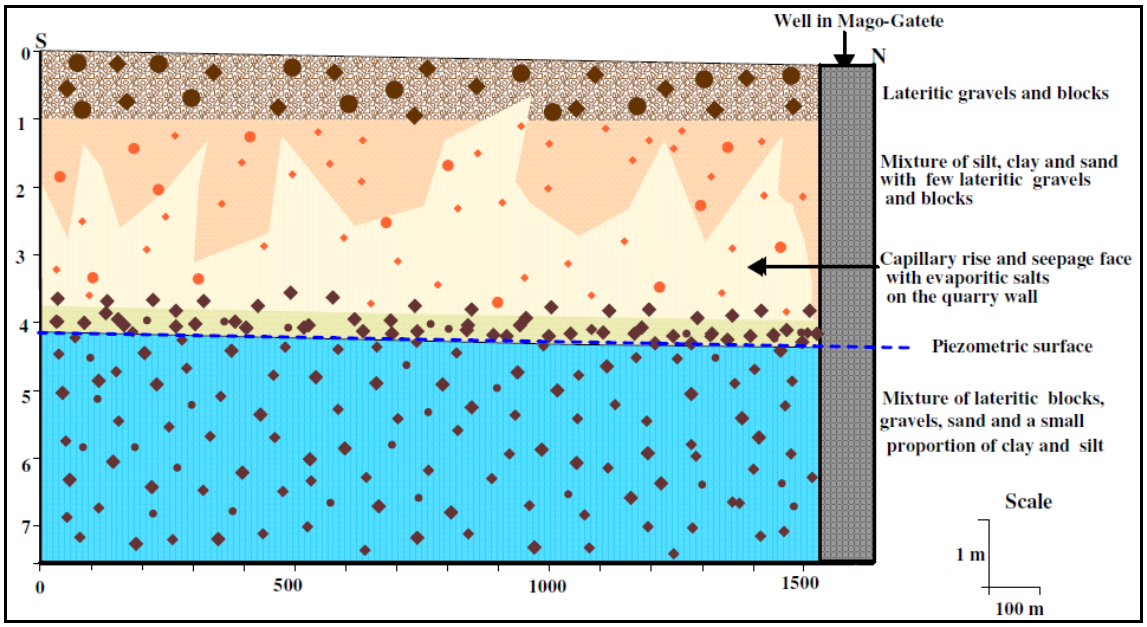

Figure VII.28. Lithological cross-section showing the occurrence of evaporitic salts at Mago in Busoni municipality

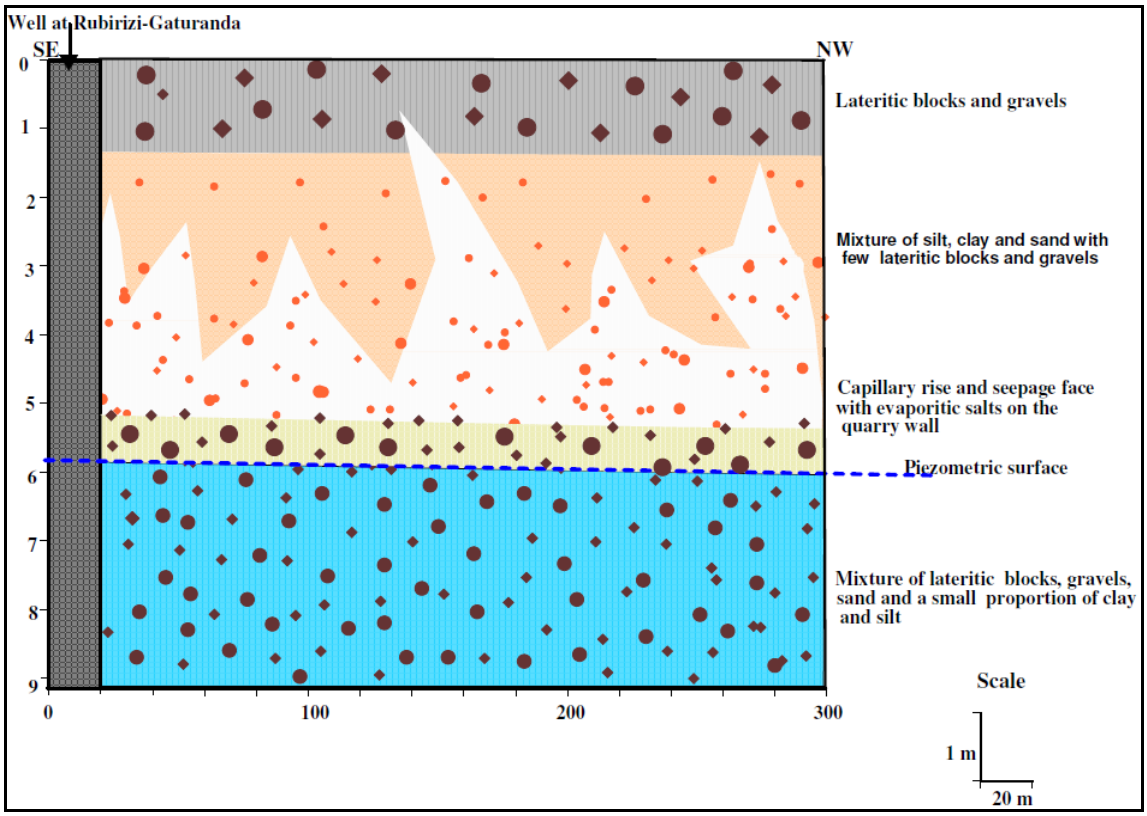

Figure VII.29. Lithological cross-sections showing the occurrence of evaporitic salts at Rubirizi in Bugabira municipality

The precipitation of salts resulting from progressive evaporation of fresh water occurs in a well defined sequence which starts by the less soluble salts such as the alkaline earth carbonates (calcite) and dolomite ($CaMg(CO_3)_2$). Subsequent precipitation of a mineral

sequence of sulphates such as gypsum ($CaSO_4.2H_2O$), silicates like sepiolite ($MgSi_3O_6(OH)_2$) and, in the later stages of the process, highly soluble salts such as halite is controlled by the relative concentration of Na^+, Ca^{2+}, Mg^{2+}, HCO_3^-, SO_4^{2-} and Cl^- (Figure VII.30). As evaporation proceeds and by virtue of the principle of binary salt formation, the species present in larger concentration progressively increase, while those in lower concentration compared to the stoichiometry of the salt will decrease. Figure VII.31 illustrates well this concept based on results of evaporation of typical Sierra Nevada spring water (Appelo & Postma, 1993). Figure VII.30 shows some chemical pathways for natural waters, and salt minerals which are likely to precipitate according to the model developed by Hardie and Eugster (1970, in Appelo and Postma, 1993). Evaporitic salts gradually accumulate in the top soils or on the ground surface through evaporative concentration during the dry season and are flushed into waterways or back to the groundwater during wet periods. This repetitive sequence of evaporation-precipitation-dissolution will enrich groundwater in readily soluble salts.

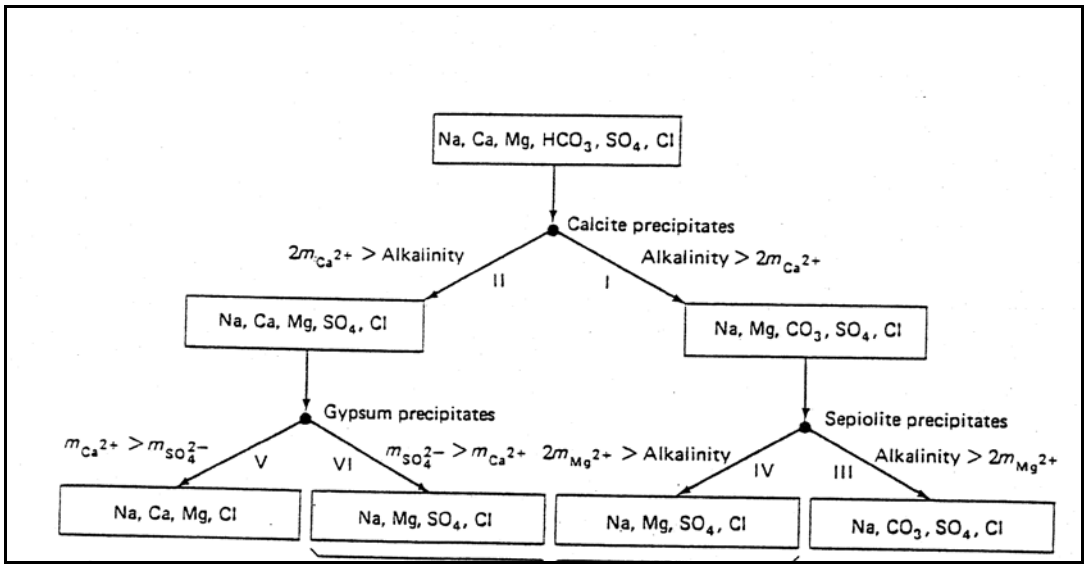

Figure VII.30. Some possible pathways for evaporation of natural waters according to the model of Hardie and Eugster (1970 in Appelo & Postma, 1993)

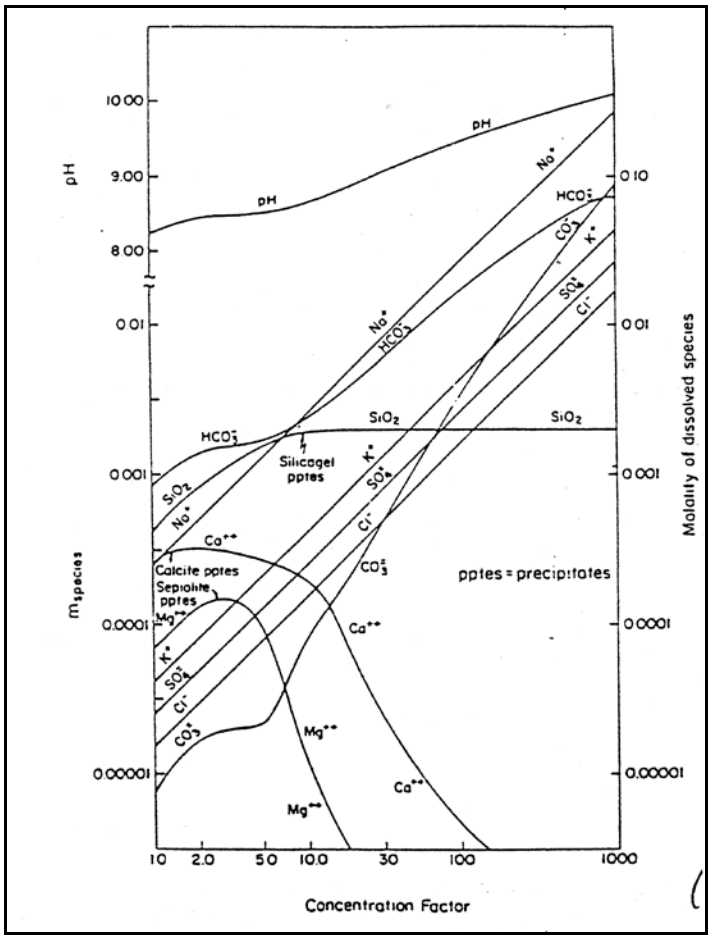

Figure VII.31. Calculated results of evaporation of typical Sierra Nevada spring water at constant temperature in equilibrium with atmospheric CO_2 (Appelo & Postma, 1993)

VII.4.4.2.2. Chemical analyses of the salt soils of Mago (Busoni) and Rubirizi (Bugabira)

a. Sampling

Two samples of salt soils were collected at the quarry of Mago (Busoni) and only one sample was taken at Rubirizi (Bugabira). Two of the three samples, one sample at Mago and another at Rubirizi, were collected by scratching the whitish concentration of salts on the wall of the quarry. As for the third sample taken at Mago, an important block of soil was taken at an area of the soil profile with visible concentrations of salts. All three soil samples consist of reddish-brown to pinkish fine soil mainly constituted of silt, clay and fine sand with a small proportion of coarse materials, including blocks and gravels. The soil samples are all friable. The soil block taken at Mago shows that the white salts form a thin and friable layer covering the wall of the quarry, whereas they are not observed at a certain distance within the wall of the pit. This may therefore confirm that the observed white concentrations of salts are of secondary origin.

b. Analytical method

The chemical composition of the samples of salt soils was analysed following the procedure proposed by Pauwels *et al.* (1992) for chemical analysis of soils. For each soil sample, a solution was prepared by mixing the salt soils and water in the proportion of 1:5 (soil: water). The mixture was then submitted to a prolonged stirring by a glass rod for a duration exceeding 16 hours. Afterwards, the pH was measured using the pH-meter on the stirred solution. After the measurement of pH, the soil-water mixture was filtered and the obtained solution was then used to analyse the different chemical constituents using the standard methods used for the analyses of groundwater chemical constituents.

c. Analytical results and discussion

Table VII.48 shows the results of the chemical analysis of the three samples of salt soils. A quick visual inspection of the analytical results shows that the soil samples analysed are actually salts as evidenced by the high TDS values (1826 -17679 mg/l) and consequently high values of electrical conductivity (2340 -24200 µS/cm-25°). Moreover the salt soils are characterised by high pH values which vary between 8.3 and 8.5. Despite an evident variability of the chemical composition of the salt soils, it can be noted that Na^+ is clearly the most abundant cation with some contribution of Mg^{2+}, Ca^{2+} and K^+, whereas SO_4^{2-} and Cl^-, are the most dominant anions. The other cations and anions show relatively low concentrations. On average, in the three samples of saline soils analysed, Na^+ and SO_4^{2-} contribute respectively 87 % and 68 % of the total sum of cations and anions. The variability of the chemical composition of the three samples may be explained by the way the samples were collected. Indeed, even the two samples which were taken in the same quarry of Mago show significant differences in chemical composition which can be related to the fact that one of the samples was taken by scratching the whitish concentration of secondary salts, whereas the other sample was taken by extracting an entire block of soil from the wall of the quarry. By scratching the secondary concentrations of evaporitic salts, an additional concentration of the secondary salts occurred and this may explain the high concentration of the salinity of this sample. As for the sample taken at Rubirizi in Bugabira municipality, the moderate concentration of the chemical constituents of the salts may be consistent with the fact that, when sampling by scratching the wall of the quarry, an important part of the soil matrix was collected and this may dilute the concentration of the salts.

The predominance of Na^+, Mg^{2+}, Ca^{2+}, K^+, SO_4^{2-} and Cl^- may hint at the plausible precipitation of salts such as carbonates (calcite, dolomite), gypsum ($CaSO_4.2H_2O$), anhydrite ($CaSO_4$), halite (NaCl), sylvite (KCl), thenardite (Na_2SO_4), mirabilite ($Na_2SO_4.10H_2O$),… during the evaporation process which follows the capillary rise. The high salinity of the water sample from the well at Mago-Gatete (TDS = 3229.1 mg/l), which is situated at approximately 1.7 km downslope of the salt quarry, gives evidence of the possible contribution of the evaporitic salts to the salinity of the shallow groundwater.

By coupling the concept of pathways for evaporation of natural waters as developed by Hardie and Eugster (1970, in Appelo & Postma, 1993) to the information provided by the lithological cross-sections of the two sites where saline soils were sampled, the origin of the salts which are reported in many places within Bugesera depression can be clearly understood. Weathering of silicate minerals such as feldspars, biotite and amphiboles to clay and iron hydroxydes progressively releases ions such as Na^+, K^+, Ca^{2+} and Mg^{2+} along with bicarbonate (HCO_3^-) and SiO_2 to surface and groundwater. Alumina and iron are respectively taken up in the authigenic formation of clay minerals and goethite. On the other hand, as groundwater flows from the recharge area towards the discharge area, a progressive concentration occurs due to the evapotranspiration process which removes part of the water from the shallow groundwater system. The evapotranspiration process brings about progressive oversaturation with respect to different salt minerals, which eventually results in precipitation as this is predicted by the model of Hardie and Eugster (1970, in Appelo & Postma, 1993). Capillary action, through the weathered overburden, brings up a fringe of the groundwater, which is further subjected to evapotranspiration, thereby causing different salt minerals to precipitate within the topsoil. Hence, the occurrence of evaporitic minerals in the upper layers of the soil profile in Bugesera can be ascribed to the evaporative concentration along the flow path coupled to the capillary rise. Figure VII.32 shows the evolution of the saturation index as a function of the concentration factor, calculated using the geochemical modelling software Phreeqc. By taking the lowly mineralised spring water as the end member at the start of the geochemical evolution of groundwater, the progressive evaporative concentration, i.e. increasing concentration factor, ultimately leads to the oversaturation and thus the precipitation of different minerals depending of their solubility product. It can be observed from Figure VII.32 that, gypsum being less soluble, oversaturation is rapidly reached (concentration factor 20), whereas halite, which is more soluble, will remain in solution until high values of the concentration factor are reached (concentration factor of 140).

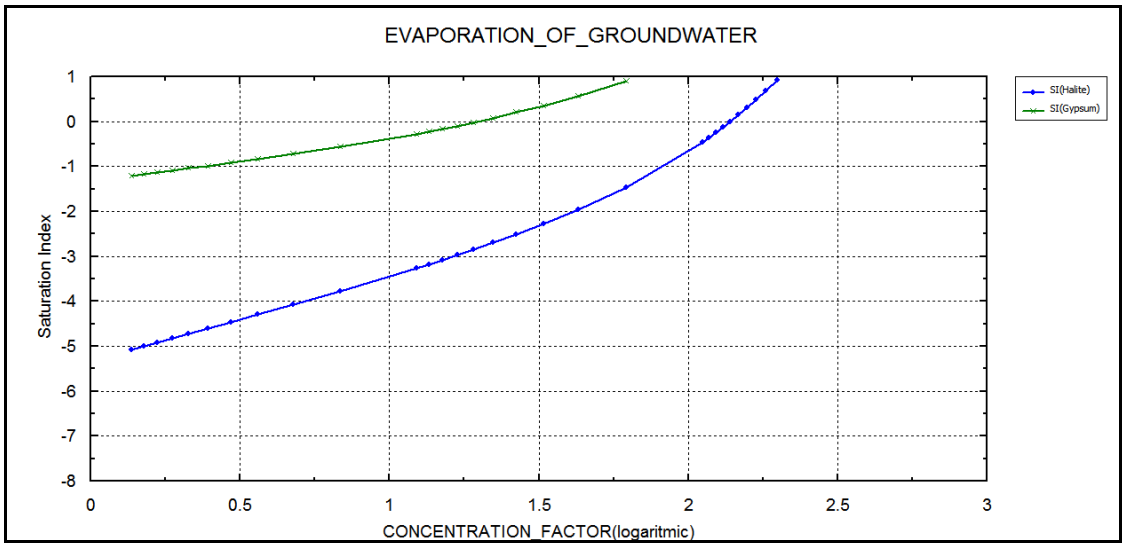

Figure VII.32. Evolution of the saturation index as a function of the evaporative concentration

The whitish concentration of salts on the walls of the quarries, especially along cracks, indicates that part of the salts precipitate as a result of the evaporation of water seeping out of the quarry wall. Therefore, evapoconcentration appears to be the most important process in the formation of the saline encrustations.

Table VII.48. Analytical results of the salt soil samples collected at Mago (Busoni) and Rubirizi (Bugabira)

		Soil block	Scratched sample	Scratched sample	
Site		Mago	Mago	Rubirizi	Average
pH		8.49	8.3	8.49	8.43
EC	µS/cm 25°	7780	24200	2340	11440.00
Na^+	mg/l	1383.00	4892.00	371.00	2215.33
K^+	mg/l	63.00	96.00	14.40	57.80
Ca^{2+}	mg/l	12.80	246.00	114.28	124.36
Mg^{2+}	mg/l	84.00	336.00	61.60	160.53
$Fe^{2+/3+}$	mg/l	0.09	0.23	0.07	0.13
Mn^{2+}	mg/l	0.01	0.04	0.00	0.02
Zn	mg/l	0.07	0.14	0.02	0.08
NH_4^+	mg/l	0.04	0.53	1.14	0.57
Sr^{2+}	mg/l	4.60	45.10	7.35	19.02
Sum		1547.61	5616.04	569.86	2577.84
Cl^-	mg/l	1490.32	3296.05	140.10	1642.16
SO_4^{2-}	mg/l	1304.86	8691.30	1074.20	3690.12
NO_3^-	mg/l	10.57	16.71	0.15	9.14
NO_2^-	mg/l	0.22	0.23	0.15	0.20
HCO_3^-	mg/l	33.55	33.55	29.89	32.33
PO_4^{3-}	mg/l	0.13	0.24	0.06	0.14
SiO_2	mg/l	4.20	13.85	8.70	8.92
F^-	mg/l	10.11	11.45	2.53	8.03
Sum		2853.96	12063.38	1255.78	5391.04
TDS	mg/l	4401.57	17679.42	1825.64	7968.88

VII.4.4.2.3. X-ray analysis of the salt soils of Mago (Busoni) and Rubirizi (Bugabira)

The 3 samples of evaporitic salts were submitted to X-ray analysis with a view to determining the main mineral phases present within the salt occurrences. The analysis was performed at the Laboratory of Soil Science at Ghent University. The determination of the mineral phases is accomplished through the computation of the d-spacing of each

peak by the solution of the Bragg equation for the appropriate value of the wave length λ . Bragg's law is defined as:

$$n\lambda = 2d\sin\theta \qquad (6.12)$$

where n is an integer, λ is the wavelength of incident wave, d is the spacing between the planes in the crystal lattice, and θ is the angle between the incident ray and the scattering planes.

The comparison of the computed d-spacings to the values of d for known minerals provides an identification of the unknown sample, because each mineral has a unique set of d-spacings.

Figures VII.33 to VII.35 show the diffractograms of the 3 samples of evaporitic salts collected at Mago-Gatete and Rubirizi respectively in Busoni and Bugabira municipalities. The interpretation of the 3 X-ray diffractograms (Tables VII.49 to to VII.51, Appendix VII.4) confirms the presence of salt minerals including gypsum ($CaSO_4.2H_2O$), halite (NaCl) and thenardite (Na_2SO_4). Other minerals such as goethite, kaolinite, muscovite and quartz may be part of the soil matrix.

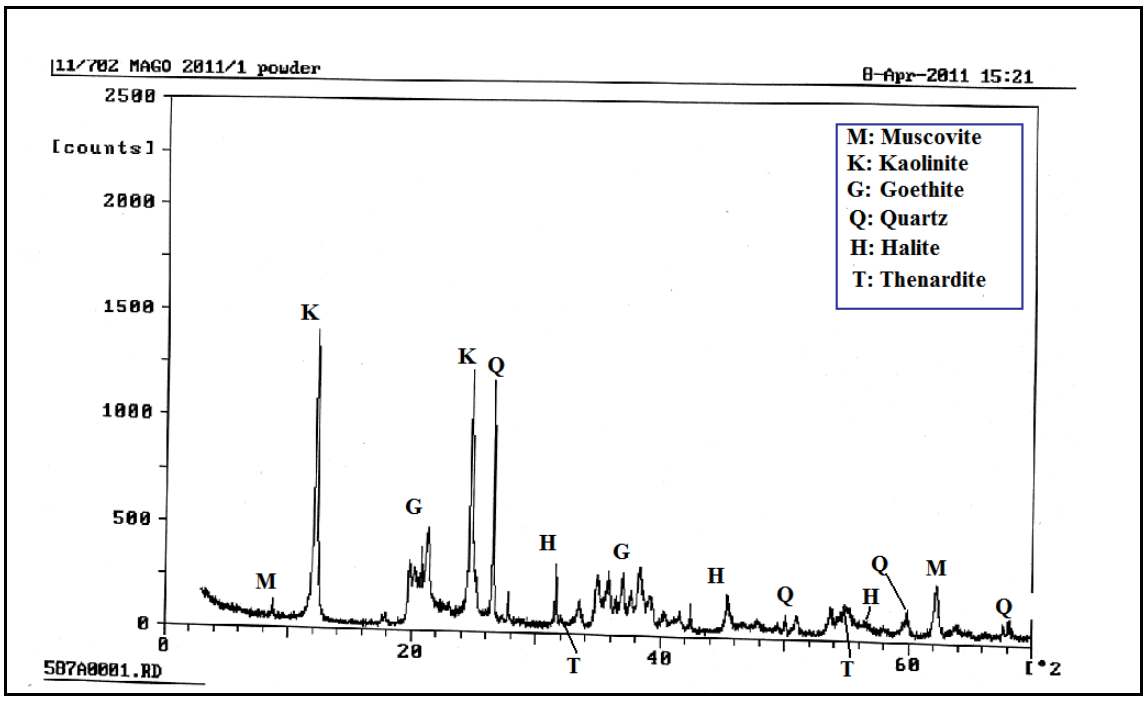

Figure VII.33. X-ray diffractogram of the salt sample Mago 2011/1 (soil block) collected at Mago-Busoni

Table VII.49. Pattern list resulting from the interpretation of the diffractogram of the sample Mago 2011/1

S/N	Reference code	Score	Compound name	Chemical formula	Semi quantitative abundance (%)
1	83-0539	51	Quartz	SiO_2	18
2	80-0885	36	Kaolinite	$Al_2Si_2O_5(OH)_4$	55
3	78-1928	19	Muscovite magnesian	$(K_{0.80}\,Na_{0.02}\,Ca_{0.01})$ $(Al_{1.66}\,Fe_{0.06}$ $Fe_{0.02}Mg_{0.28})(Si_{3.41}Al_{0.59})O_{10}$ $(OH)_2$	26
6			Goethite	FeOOH	
7	75-0306		Halite	NaCl	

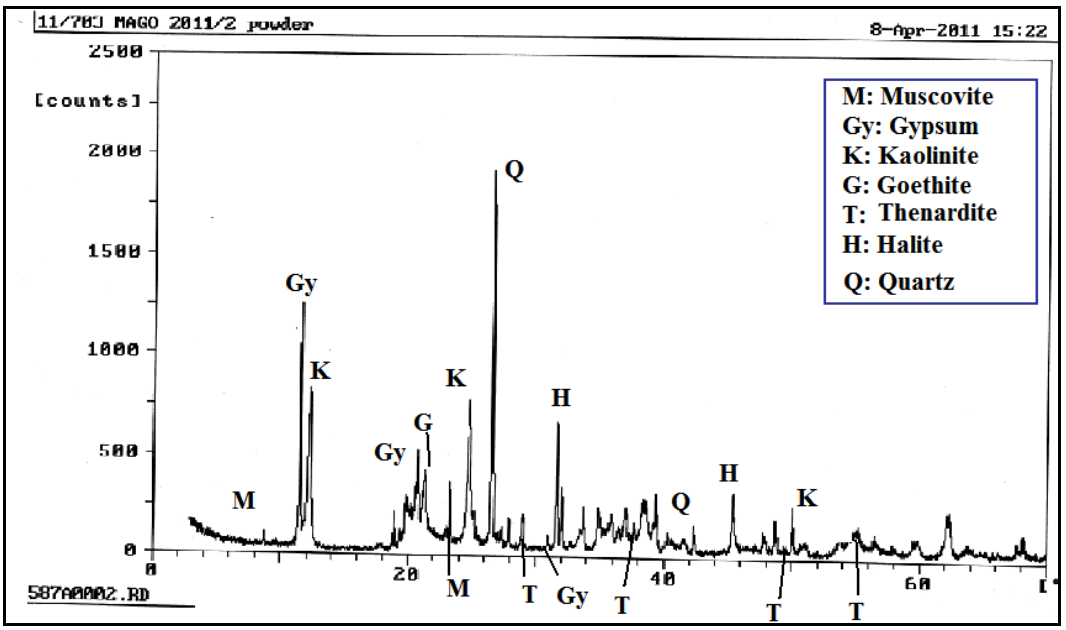

Figure VII.34. X-ray diffractogram of the salt sample Mago 2011/2 (scratched sample) collected at Mago-Busoni

Table VII.50. Pattern list resulting from the interpretation of the diffractogram of the sample Mago 2011/2

S/N	Reference code	Score	Compound name	Chemical formula	Semi quantitative abundance (%)
1	83-0539	53	Quartz	SiO_2	38
2	80-0885	36	Kaolinite	$Al_2Si_2O_5(OH)_4$	37
3	74-2036	33	Thenardite	Na_2SO_4	13
4	74-1904	19	Gypsum	$CaSO_4.H_2O$	8
5	75-0306	31	Halite	NaCl	4
6			Goethite	FeOOH	
7	78-1928	19	Muscovite	$(K_{0.80}\,Na_{0.02}\,Ca_{0.01})$ $(Al_{1.66}\,Fe_{0.06}$ $Fe_{0.02}Mg_{0.28})(Si_{3.41}Al_{0.59})O_{10}$ $(OH)_2$	

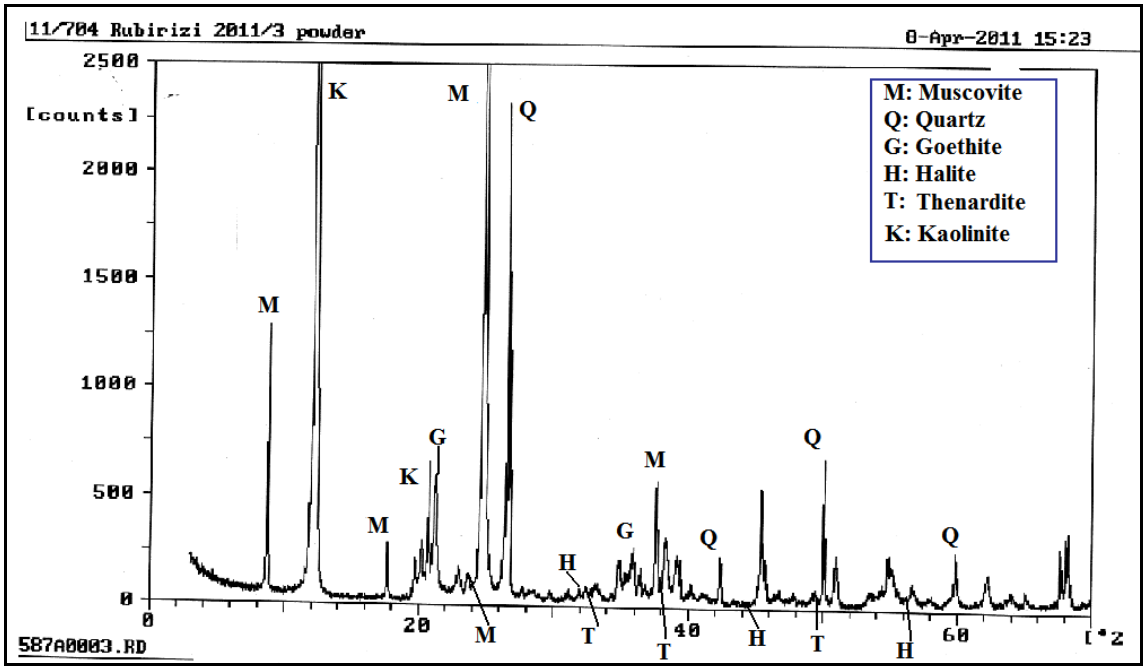

Figure VII.35. X-ray diffractogram of the salt sample Rubirizi 2011/3 (scratched sample) collected at Rubirizi-Bugabira

Table VII.51. Pattern list resulting from the interpretation of the diffractogram of the sample Rubirizi 2011/3

S/N	Reference code	Score	Compound name	Chemical formula	Semi quantitative abundance (%)
1	83-0539	53	Quartz	SiO_2	-
2	80-0885	36	Kaolinite	$Al_2Si_2O_5(OH)_4$	-
3	74-2036	33	Thenardite	Na_2SO_4	-
5	75-0306	31	Halite	NaCl	-
6			Goethite	FeOOH	-
7	78-1928		Muscovite	$(K_{0.80}\,Na_{0.02}\,Ca_{0.01})$ $(Al_{1.66}\,Fe_{0.06}$ $Fe_{0.02}Mg_{0.28})(Si_{3.41}Al_{0.59})O_{10}$ $(OH)_2$	-

VII.4.4.2.4. Hydrochemical evolution of groundwater due to mixing with salt water resulting from the dissolution of evaporitic salt deposits

It has been shown in the section VII.4.4.1 that the evaporative concentration can not be the only process which explains the geochemical evolution of groundwater in the study area. There is indeed a certain discrepancy between the expected composition due to the evaporative concentration and the measured contents of the different dissolved constituents. Hence, the mixing of rainwater and salt water resulting from the

dissolution of saline deposits is evaluated as an alternative hypothesis to the evapoconcentration.

Taking into account the fact that occurrences of evaporitic salts are reported in many places of the study area, the hydrochemical evolution of groundwater was assessed by computing the fractions of meteoric and salt-influenced water which mix to form groundwater. The same 7 classes based on chloride concentration (0-10, 10-30, 30-60, 60-90, 90-120, 120-150 and > 150 mg/l) were used to evaluate the hydrochemical evolution of groundwater on its flow path, i.e. from the main recharge area in the southern highlands to the discharge area which is the depression. The first class of chloride concentration (0-10 mg/l) was used as the fresh end member of the hydrochemical evolution, due to its low levels of Cl^- and mineralisation. The following equation (6.13 & 6.14) was used to determine the proportion of the two end members which mix to form the actual saline groundwater:

$$\left[Cl^-\right]_{spring} * f_{spring} + \left[Cl^-\right]_{salt} * f_{salt} = \left[Cl^-\right]_{GW} \qquad (6.13)$$

$$f_{spring} + f_{salt} = 1 \qquad (6.14)$$

where $[Cl^-]_{spring}$ is the average concentration of Cl^- in the first class of chloride concentration (0-10 mg/l), $[Cl^-]_{salt}$ is the average concentration of Cl^- in the 3 samples of salt soils, $[Cl^-]_{GW}$ is the average concentration of Cl^- in the different classes of Cl^- concentration, f_{spring} and f_{salt} are respectively the fractions of the spring water representing the meteoric water and salt water resulting from the dissolution of the evaporitic salts.

Tables VII.51 to VII.56 show a synthesis of the calculations of the mixing proportions in different classes of chloride concentration. Tables showing detailed calculations of the mixing proportions and the water samples belonging to the different classes are presented in Appendix VII.6. Overall, although this concept of mixing of infiltrating meteoric water with salt-influenced water seems to better predict the concentration of some dissolved constituents, a close look at the Tables VII.52 to VII.57 reveals that the expected concentrations of some dissolved parameters, particularly SO_4^{2-}, are highly overpredicted.

Tables VII.52 to VII.57 show, overall, an increasing surplus of the sum of alkaline and alkaline earth metals ($Na^+ + K^+ + Mg^{2+} + Ca^{2+}$), HCO_3^- and TDS, which indicates that, besides the dissolution of evaporitic salts, there is another input of dissolved constituents of groundwater which can be mostly ascribed to the weathering of aluminosilicates. The substantial increase of HCO_3^- points to the combination of 3 different processes, including weathering of aluminosilicates, dissolution of CO_2 and oxidation of organic matter, which all release this ion to the groundwater. The small surplus of SiO_2, which should normally increase with increasing dissolution of

aluminosilicates, confirms that an important part of this element is retained by the formation of clay minerals, as this is reflected by the stability diagrams.

Other elements such as NO_3^-, NO_2^-, NH_4^+ PO_4^{3-} and F^- do not show a significant change, thereby indicating that there is no further input along the flowpath or that there might not be some processes which remove part of these elements, essentially the nutrients. The deficit of SO_4^{2-} in water samples of all Cl^- concentrations may be related to the fact that the high SO_4^{2-} content in salt deposits results in overestimation of expected concentration of this element in the mixture, regardless of the mixing factors.

The deficit of alkaline and alkaline earth cations in the last class of chloride concentration (> 150 mg/l) may point to an overestimation of the fraction of "salt water", due to high chloride content which might be contributed from other sources such as anthropogenic pollution. This results in the overestimation, in the expected concentration, of the concentration of some ions such as Na^+ which are highly concentrated in the salt soils.

Figure VII.36A & B summarises the concept of hydrochemical evolution of groundwater by mixing between the meteoric water, represented by spring water with the lowest chloride content and the water which has dissolved the evaporitic salts. The infiltrated water is progressively concentrated along its flowpath due to evapotranspiration and the weathering of aluminosilicates. The progressively concentrated groundwater further undergoes capillary rise through the clayey weathered overburden, mostly within the low lying part of the study area, i.e. the depression. When the capillary rise attains the depth of reach of the evaporation, the latter takes over and evaporates the uplifted groundwater, thereby entailing the precipitation of salts within the upper layers of the soil profile (Figure VII.36 A). However, during the rainy season, the salts are again dissolved by the infiltrating water and are washed back to the groundwater, which explains the high TDS values of some wells located in the depression (VII.36 B).

Hence, besides the main hydrogeochemical process which is the weathering of aluminosilicates, it stems from the above discussion that this endless cycle of evaporitic salt formation and dissolution, contributes, to some extent, to the hydrochemical evolution of groundwater within the study area.

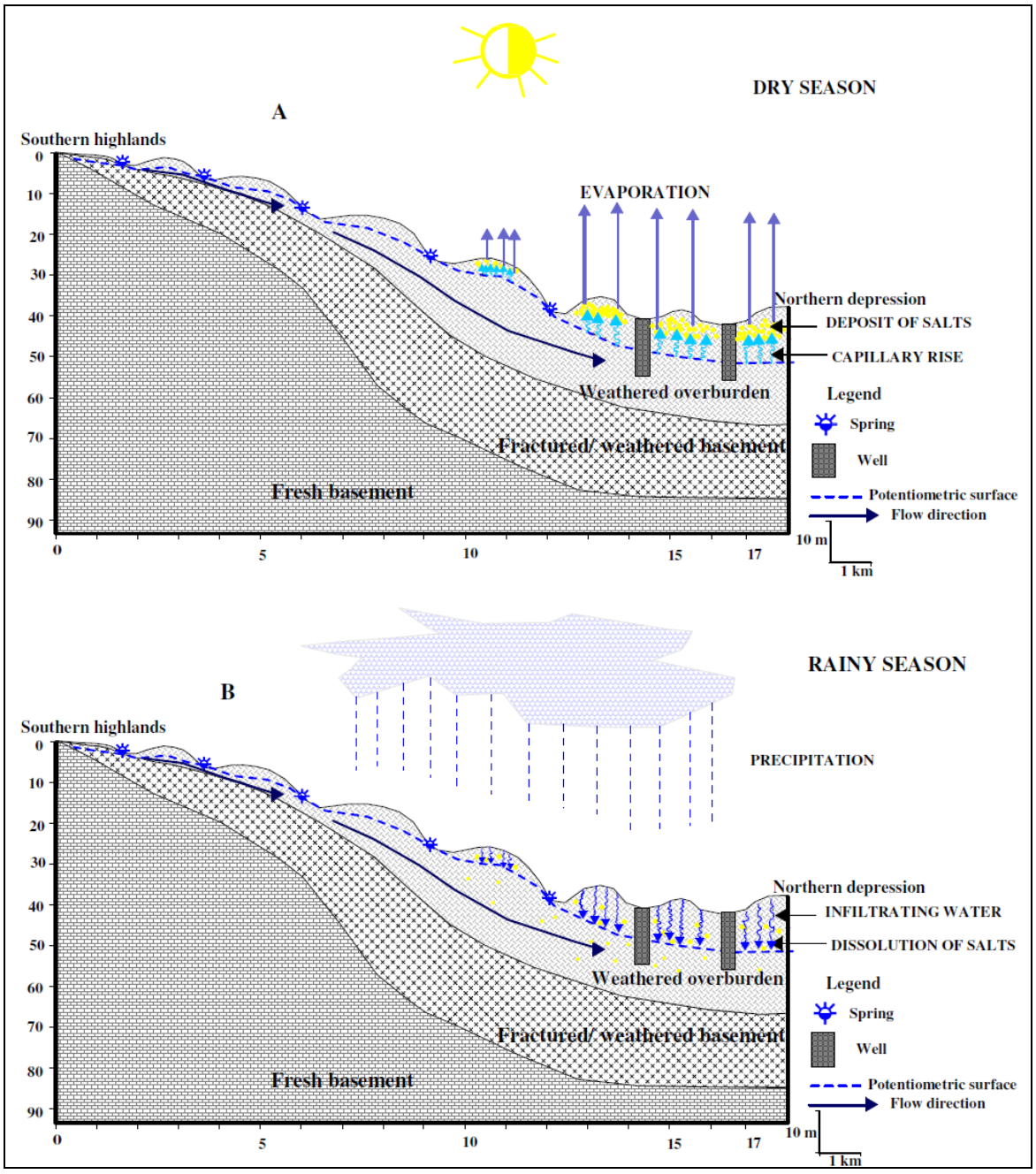

Figure VII.36. Conceptual cross-section showing the formation of evaporitic salts by combined processes of capillary rise and evaporation. A: dry season; B: rainy season

Table VII.52. Calculation of the mixing factor and water composition expected from mixing of two end members for the class of water samples with Cl^- concentration ranging between 10-30 mg/l

		Cl^- mg/l	HCO_3^- mg/l	SO_4^{2-} mg/l	NO_3^- mg/l	NO_2^- mg/l	NH_4^+ mg/l	PO_4^{3-} mg/l	Ca^{2+} mg/l	Mg^{2+} mg/l	Mn^{2+} mg/l	Fe^{2+} mg/l	K^+ mg/l	Na^+ mg/l	F^- mg/l	SiO_2 mg/l	TDS mg/l
Average (Cl < 10 mg/l)		5.4	15.2	4.0	16.2	0.1	0.0	0.1	4.8	2.5	0.1	0.1	1.3	7.5	0.2	8.7	66.5
Average for saline soils		1642.2	32.3	3690.1	9.1	0.2	0.6	0.1	124.4	160.5	0.0	0.1	57.8	2215.3	8.0	8.9	7968.9
Average (Cl = 10-30 mg/l)		17.1	125.2	21.8	15.4	0.2	0.0	0.1	19.9	9.1	0.2	0.6	9.6	30.0	0.4	11.8	262.4
f spring	0.993																
fsalt water	0.007																
Expected concentration		17.1	15.3	30.3	16.2	0.1	0.0	0.1	5.7	3.7	0.1	0.1	1.7	23.3	0.2	8.7	123.0
Δ Reaction (mg/l)		0.0	109.9	-8.5	-0.7	0.0	0.0	0.0	14.2	5.4	0.1	0.5	7.9	6.7	0.2	3.1	139.4
Molar weight (mg)			61	96	62	46	18	95	40	24	55		39	23	19	60	
Δ Reaction (mmol/l)			1.80	-0.09	-0.01	0.00	0.00	0.00	0.36	0.22	0.00		0.20	0.29	0.01	0.05	
Sum of alkaline and alkaline earth cations (mmol)									1.01								

Table VII.53. Calculation of the mixing factor and water composition expected from mixing of two end members for the class of water samples with Cl^- concentration ranging between 30-60 mg/l

		Cl^- mg/l	HCO_3^- mg/l	SO_4^{2-} mg/l	NO_3^- mg/l	NO_2^- mg/l	NH_4^+ mg/l	PO_4^{3-} mg/l	Ca^{2+} mg/l	Mg^{2+} mg/l	Mn^{2+} mg/l	Fe^{2+} mg/l	K^+ mg/l	Na^+ mg/l	F^- mg/l	SiO_2 mg/l	TDS mg/l
Average (Cl < 10 mg/l)		5.4	15.2	4.0	16.2	0.1	0.0	0.1	4.8	2.5	0.1	0.1	1.3	7.5	0.2	8.7	66.5
Average for saline soils		1642.2	32.3	3690.1	9.1	0.2	0.6	0.1	124.4	160.5	0.0	0.1	57.8	2215.3	8.0	8.9	7968.9
Average (Cl = 30-60 mg/l)		44.3	169.7	50.6	17.3	0.1	0.1	0.1	38.4	13.0	0.5	2.4	14.0	47.6	1.1	11.4	410.4
f spring	0.976																
fsalt water	0.024																
Expected concentration		44.3	15.6	91.6	16.1	0.1	0.0	0.1	7.7	6.3	0.1	0.1	2.6	60.0	0.4	8.7	254.3
Δ Reaction (mg/l)		0.0	154.1	-41.0	1.2	0.0	0.1	0.0	30.8	6.7	0.4	2.2	11.4	-12.4	0.7	2.7	156.2
Molar weight (mg)			61	96	62	46	18	95	40	24	55		39	23	19	60	
Δ Reaction (mmol/l)			2.53	-0.43	0.02	0.00	0.00	0.00	0.77	0.28	0.01		0.29	-0.54	0.04	0.05	
Sum of alkaline and alkaline earth cations (mmol)									0.81								

Table VII.54. Calculation of the mixing factor and water composition expected from mixing of two end members for the class of water samples with Cl^- concentration ranging between 60-90 mg/l

		Cl^- mg/l	HCO_3^- mg/l	SO_4^{2-} mg/l	NO_3^- mg/l	NO_2^- mg/l	NH_4^+ mg/l	PO_4^{3-} mg/l	Ca^{2+} mg/l	Mg^{2+} mg/l	Mn^{2+} mg/l	Fe^{2+} mg/l	K^+ mg/l	Na^+ mg/l	F^- mg/l	SiO_2 mg/l	TDS mg/l
Average (Cl < 10 mg/l)		5.4	15.2	4.0	16.2	0.1	0.0	0.1	4.8	2.5	0.1	0.1	1.3	7.5	0.2	8.7	66.5
Average for saline soils		1642.2	32.3	3690.1	9.1	0.2	0.6	0.1	124.4	160.5	0.0	0.1	57.8	2215.3	8.0	8.9	7968.9
Average (Cl = 60-90 mg/l)		74.8	397.7	53.6	26.1	0.9	0.6	0.1	47.3	22.8	2.1	8.5	29.4	111.3	1.5	11.6	788.1
f spring	0.958																
fsalt water	0.042																
Expected concentration		74.8	15.9	160.3	15.9	0.1	0.0	0.1	9.9	9.2	0.1	0.1	3.7	101.1	0.5	8.7	401.5
Δ Reaction (mg/l)		0.0	381.7	-106.7	10.1	0.8	0.6	0.0	37.4	13.5	2.0	8.3	25.8	10.2	1.0	2.9	386.6
Molar weight (mg)			61	96	62	46	18	95	40	24	55		39	23	19	60	
Δ Reaction (mmol/l)			6.26	-1.11	0.16	0.00	0.00	0.00	0.94	0.56	0.04		0.66	0.44	0.05	0.05	
Sum of alkaline and alkaline earth cations (mmol)									2.84								

Table VII.55. Calculation of the mixing factor and water composition expected from mixing of two end members for the class of water samples with Cl^- concentration ranging between 90-120 mg/l

		Cl^- mg/l	HCO_3^- mg/l	SO_4^{2-} mg/l	NO_3^- mg/l	NO_2^- mg/l	NH_4^+ mg/l	PO_4^{3-} mg/l	Ca^{2+} mg/l	Mg^{2+} mg/l	Mn^{2+} mg/l	Fe^{2+} mg/l	K^+ mg/l	Na^+ mg/l	F^- mg/l	SiO_2 mg/l	TDS mg/l
Average (Cl < 10 mg/l)		5.4	15.2	4.0	16.2	0.1	0.0	0.1	4.8	2.5	0.1	0.1	1.3	7.5	0.2	8.7	66.5
Average for saline soils		1642.2	32.3	3690.1	9.1	0.2	0.6	0.1	124.4	160.5	0.0	0.1	57.8	2215.3	8.0	8.9	7968.9
Average (Cl = 90-120 mg/l)		106.5	451.7	107.0	25.6	0.1	0.7	0.1	73.1	33.8	1.2	2.4	36.9	124.5	1.5	12.9	978.0
f spring	0.938																
fsalt water	0.062																
Expected concentration		106.5	16.3	231.6	15.8	0.1	0.0	0.1	12.2	12.3	0.1	0.1	4.8	143.9	0.7	8.7	554.6
Δ Reaction (mg/l)		0.0	435.5	-124.6	9.8	0.0	0.6	0.1	60.9	21.5	1.1	2.2	32.2	-19.4	0.9	4.1	423.4
Molar weight in mg			61	96	62	46	18	95	40	24	55		39	23	19	60	
Δ Reaction (mmol/l)			7.14	-1.30	0.16	0.00	0.00	0.00	1.52	0.89	0.02		0.82	-0.84	0.05	0.07	
Sum of alkaline and alkaline earth cations (mmol)									2.41								

Table VII.56. Calculation of the mixing factor and water composition expected from mixing of two end members for the class of water samples with Cl^- concentration ranging between 120-150 mg/l

		Cl^- mg/l	HCO_3^- mg/l	SO_4^{2-} mg/l	NO_3^- mg/l	NO_2^- mg/l	NH_4^+ mg/l	PO_4^{3-} mg/l	Ca^{2+} mg/l	Mg^{2+} mg/l	Mn^{2+} mg/l	Fe^{2+} mg/l	K^+ mg/l	Na^+ mg/l	F^- mg/l	SiO_2 mg/l	TDS mg/l
Average (Cl < 10 mg/l)		5.4	15.2	4.0	16.2	0.1	0.0	0.1	4.8	2.5	0.1	0.1	1.3	7.5	0.2	8.7	66.5
Average for saline soils		1642.2	32.3	3690.1	9.1	0.2	0.6	0.1	124.4	160.5	0.0	0.1	57.8	2215.3	8.0	8.9	7968.9
Average (Cl = 120-150 mg/l)																	
f spring	0.920																
fsalt water	0.080																
Expected concentration		136.5	16.6	299.2	15.7	0.1	0.1	0.1	14.4	15.2	0.1	0.1	5.8	184.4	0.8	8.7	699.4
Δ Reaction (mg/l)		0.0	788.8	-175.9	9.3	0.0	0.1	0.0	57.0	13.4	0.1	2.6	57.8	78.1	3.9	3.9	837.4
Molar weight in mg			61	96	62	46	18	95	40	24	55		39	23	19	60	
Δ Reaction (mmol/l)			12.93	-1.83	0.15	0.00	0.00	0.00	1.43	0.56	0.00		1.48	3.40	0.21	0.06	
Sum of alkaline and alkaline earth cations (mmol)									6.87								

Table VII.57. Calculation of the mixing factor and water composition expected from mixing of two end members for the class of water samples with Cl^- concentration > 150 mg/l

		Cl^- mg/l	HCO_3^- mg/l	SO_4^{2-} mg/l	NO_3^- mg/l	NO_2^- mg/l	NH_4^+ mg/l	PO_4^{3-} mg/l	Ca^{2+} mg/l	Mg^{2+} mg/l	Mn^{2+} mg/l	Fe^{2+} mg/l	K^+ mg/l	Na^+ mg/l	F^- mg/l	SiO_2 mg/l	TDS mg/l
Average (Cl < 10 mg/l)		5.4	15.2	4.0	16.2	0.1	0.0	0.1	4.8	2.5	0.1	0.1	1.3	7.5	0.2	8.7	66.5
Average for saline soils		1642.2	32.3	3690.1	9.1	0.2	0.6	0.1	124.4	160.5	0.0	0.1	57.8	2215.3	8.0	8.9	7968.9
Average (Cl >150 mg/l)		283.7	645.2	204.9	25.3	0.8	0.6	0.1	107.7	51.0	1.0	5.7	55.1	282.3	1.4	15.1	1679.9
fspring	0.830																
fsalt water	0.170																
Expected concentration		283.7	18.1	630.7	15.0	0.1	0.1	0.1	25.1	29.4	0.1	0.1	10.9	382.9	1.5	8.7	1410.1
Δ Reaction (mg/l)		0.0	627.0	-425.8	10.3	0.6	0.5	0.0	82.6	21.6	0.9	5.6	44.2	-100.6	-0.1	6.4	269.9
Molar weight in mg			61	96	62	46	18	95	40	24	55		39	23	19	60	
Δ Reaction (mmol/l)			10.28	-4.44	0.17	0.00	0.00	0.00	2.06	0.90	0.02		1.13	-4.37	0.00	0.11	
Sum of alkaline and alkaline earth cations (mmol)									-0.26								

VII.4.5. Saturation indices

Saturation indices in groundwater give indication as regards to the state of saturation of groundwater with respect to different mineral species. For this study, this parameter was computed using the software Phreeqc version 2.17.01, an up-to-date version of a geochemical modelling program developed by Parkhurst and Appelo (1999). Phreeqc calculates the saturation index for all mineral species which are likely to be found in groundwater depending on the chemical composition of each water sample. The saturation indices for the different minerals are presented in Appendix VII.7.

Figure VII.37 shows the saturation status with respect to some common mineral phases including calcite, dolomite, fluorite, gypsum, quartz, halite, hematite and goethite. Sample numbers on X-axis refer to the numbers (S/N) of the different water samples as presented in Appendix VII.1. Overall, it can be noted from Figure VII.37 that the saturation indices with respect to the selected 8 mineral phases are systematically lower for spring water samples, while higher values are found in water samples from wells. Water samples from lakes show intermediate values of saturation indices. This observation is in line with the hydrochemical evolution of groundwater in the study area. Indeed, spring waters are generally characterised by a low concentration of dissolved constituents which is explained by the fact that they emerge in or close to the recharge area, after short residence time and flow path. For this reason, spring water samples show undersaturation with respect to most of the common minerals except iron minerals.

The relatively higher values of saturation indices which characterise water samples from wells indicate that the hydrochemical processes taking place along the flow path (aluminosilicate dissolution, evaporative concentration and leaching of salt deposits) progressively increase the saturation status of groundwater with respect to different minerals. Hence, the saturation indices show a clear demarcation between the recharge area, where emerges spring water with the lowest saturation indices, and the discharge area, within the depression, where water samples from wells display increased values of saturation indices towards different minerals.

In comparison to well water, water samples from lakes show low saturation indices with respect to different minerals, which can be ascribed to the dilution effect of precipitation and other tributaries draining into these shallow lakes.

All water samples analysed show an important supersaturation with respect to iron minerals such as hematite (SI $\geq$ 3.4) and goethite (SI $\geq$ 0.7), even in the lowly mineralised spring water samples. This implies that the iron released from the

weathering of ferromagnesian minerals readily precipitates in the form of oxide (hematite) or hydroxide (goethite).

In general, the majority of the samples analysed are undersaturated with respect to calcite and dolomite. Indeed, of the 143 water samples analysed, only 22 samples (15 %), of which 2 are from shallow lakes and 20 are from wells, show a slight oversaturation, whereas only one sample shows saturation with respect to calcite. Similarly, 25 water samples (17 %), of which 3 lake samples and 22 water samples from wells, show a slight oversaturation with respect to dolomite. The overall undersaturation with respect to dolomite and calcite rather reflects the absence of carbonate rocks in the study area. The oversaturation of some water samples with respect to calcite and dolomite may result from the dissolution of secondary carbonate minerals and the dissolution of aluminosilicate minerals, which progressively enrich groundwater in Ca^{2+} and HCO_3^-.

All water samples are undersaturated with respect to gypsum and halite but water samples from wells clearly show higher values of the saturation index with respect to these minerals compared to other samples. Most water samples are characterised by undersaturation with respect to fluorite except three water samples collected from wells (Mago-Gatete, Murungurira-Ntwago, Saruduha II).

In all water samples, saturation indices with respect to quartz plot around the equilibrium line (SI = 0), which suggests that, because some slightly positive saturation indices may occur, this mineral can not precipitate due to the thermodynamic inhibition at low temperature characterising groundwater.

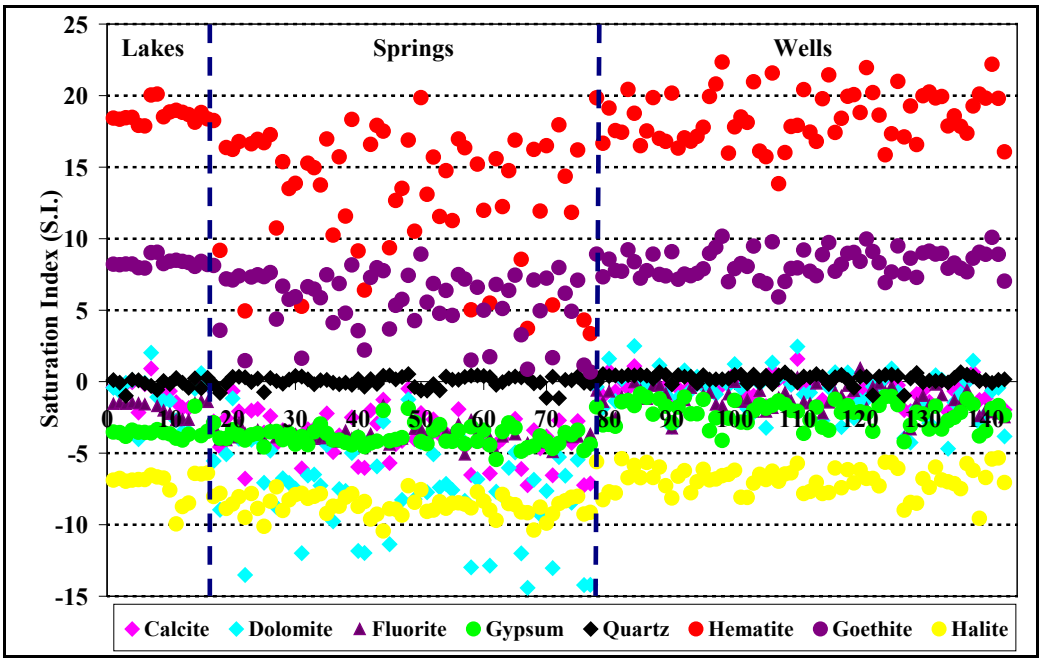

Figure VII.37. Saturation indices for the main mineral phases

VII.4.6. Weathering of silicate and aluminosilicate minerals

The influence of the weathering of aluminosilicate minerals on groundwater chemistry can be evaluated through the computation of the saturation state of groundwater with respect to a given mineral. If we consider the weathering of albite, the congruent dissociation equation can be written as (reaction 6.15):

$$NaAlSi_3O_8 + 4H^+ + 4H_2O \Rightarrow Na^+ + Al^{3+} + 3H_4SiO_4 \qquad (6.15)$$

Albite

$$K = \frac{a_{Na^+} * a_{Al^{3+}} * a^3_{H_2SO_4}}{a^4_{H^-}} \qquad (6.16)$$

The IAP can be determined from each water analysis and then the saturation index can be calculated as:

$$SI = \log\left(\frac{IAP}{K}\right) \qquad (6.17)$$

Equation 6.16 shows that the dissolution of albite is controlled by pH, lower pH values promoting the dissolution. However, it is not reasonable to write the weathering reaction of aluminosilicates as a congruent dissolution, because at the pH values of most natural groundwaters, these mineral phases dissolve incongruently, producing authigenic clay minerals. Helgeson *et al.* (1969, in Appelo & Postma, 2005) report that the dissolution of primary aluminosilicate minerals is a slow and kinetically controlled process, while the precipitation of secondary weathering products is faster and approaches equilibrium.

The saturation index approach of the weathering of aluminosilicate minerals is complicated by a number of drawbacks among which: (1) At typical pH values of groundwater (generally near neutral), the Al^{3+} concentration is very low and difficult to analyse accurately; (2) Clusters of Al-complexes can form in water and may not be completely removed by filtration and are not accounted for in the speciation model; (3) It can be observed that, even for the simple case of albite, the saturation index is controlled by 4 variables which render difficult the graphical representation of the stability of this mineral (equation 6.16).

To overcome these difficulties, aluminosilicate stability diagrams have been devised which assume that all Al^{3+} is preserved in the weathering product. Such diagrams for aluminosilicates contain stability fields for primary aluminosilicates and the possible weathering products such as gibbsite, kaolinite and montmorillonite. In the following sections, stability diagrams for 3 main feldspar minerals, i.e. albite, anorthite and K-feldspar are constructed and discussed.

VII.4.6.1. Stability diagram for anorthite ($CaAl_2Si_2O_8$)

Figure VII.38 depicts the stability diagram of Ca-feldspar and its weathering products which include Ca-montmorillonite, kaolinite and gibbsite. The stability fields for the Ca-feldspar and its possible weathering products are expressed as a function of $\log\left(a_{Ca^{2+}} / a^2_{H^+}\right)$ and $\log a_{H_4SiO_4}$. Table VII.58 gives the reactions governing the transformation of Ca-feldspar into different weathering products. Table VII.59 presents the standard Gibbs free energy for the species involved in the silicate weathering. In Figure VII.38 the boundary between the stability fields for anorthite and gibbsite can be described by the following reaction (6.18):

$$CaAl_2Si_2O_8 + 2H^+ + 6H_2O \Leftrightarrow 2AlOH_3(s) + 2H_4SiO_4 + Ca^{2+} \qquad (6.18)$$

anorthite gibbsite

The aluminium released from anorthite is preserved in gibbsite. The relative stability between the two minerals is therefore controlled by the dissolved silica, Ca^{2+} and pH. The equilibrium constant can be computed from the Gibbs free energy of each individual component as given in Table VII.59. The Gibbs free energy balance for the transformation of anorthite into gibbsite can be calculated as follows:

$$\Delta G_r^0 = ((2(-1159.0) + 2(-1308.0) + (-553.5)) - ((-4017.3) + 2(0) + 6(-237.15)))kJ/mol = 47.3kJ/mol \qquad (6.19)$$

$$\log K = \frac{-\Delta G_r^0}{2.3 * R * T} = 8.3 \qquad (6.20)$$

$$K = \frac{a^2_{H_4SiO_4} * a_{Ca^{2+}}}{a^2_{H^+}} \qquad (6.21)$$

where a is the activity of each dissolved ion

$$\log K = 2\log a_{H_4SiO_4} + \log a_{Ca^{2+}} - 2\log a_{H^+} = 8.3 \qquad (6.22)$$

$$\log\left(a_{Ca^{2+}} / a^2_{H^+}\right) = 8.3 - 2\log a_{H_4SiO_4} \qquad (6.23)$$

Equation 6.23 defines the boundary between anorthite and gibbsite. It is plotted as a straight line with a slope -2 in the stability diagram and the number of variables is reduced to 2.

Similarly, according to the reaction between kaolinite and gibbsite, the aluminium released from gibbsite is preserved in kaolinite. Thus, the relative stability between the two minerals is controlled by the dissolved silica. Considering the equation between kaolinite and gibbsite (Table VII.58), the boundary between the two minerals can be defined by a straight parallel to the Y-axis with -4.49 as the abscissa. Indeed, it can be shown from the equation between gibbsite and kaolinite that:

$$K = \frac{1}{a^2_{H_4SiO_4}} \qquad (6.24)$$

$$\log a_{H_4SiO_4} = -\frac{\log K}{2} = -4.49 \qquad (6.25)$$

According to the reaction between anorthite and kaolinite (Table VII.58), all the silica released from the anorthite is preserved in the kaolinite and the boundary between the two minerals can therefore be defined by the following equations:

$$K = \frac{a_{Ca^{2+}}}{a^2_{H^+}} \qquad (6.26)$$

$$\log K = \log\left(\frac{a_{Ca^{2+}}}{a^2_{H^+}}\right) = 17.27 \qquad (6.27)$$

Hence, the boundary between anorthite and kaolinite is a straight line parallel to the X-axis with 17.27 as the ordinate (Figure VII.38).

From the reaction describing the equilibrium between anorthite and Ca-montmorillonite, the boundary between the two minerals can be defined using the following equations:

$$K = \frac{a^6_{Ca^{2+}}}{a^{12}_{H^+} * a^8_{H_4SiO_4}} \qquad (6.28)$$

$$\log K = 6\log\left(\frac{a_{Ca^{2+}}}{a^2_{H^+}}\right) - 8\log a_{H_4SiO_4} = 133.28 \qquad (6.29)$$

$$\log\left(\frac{a_{Ca^{2+}}}{a^2_{H^+}}\right) = \frac{8\log a_{H_4SiO_4} + 133.28}{6} \qquad (6.30)$$

From the equation 6.30, it can be noted that the boundary between anorthite and Ca-montmorillonite is a straight line with a slope 8/6 in the stability diagram (Figure VII.38).

The reaction between kaolinite and Ca-montmorillonite shows that the boundary between the two minerals can be defined using the following equations:

$$K = \frac{a^2_{H^+}}{a^8_{H_4SiO_4} * a_{Ca^+}} \qquad (6.31)$$

$$\log K = \log\left(\frac{a^2_{H^+}}{a_{Ca^{2+}}}\right) - 8\log a_{H_4SiO_4} = 12.41 \qquad (6.32)$$

$$\log\left(\frac{a_{Ca^{2+}}}{a_{H^+}}\right) = -12.41 - 8\log a_{H_4SiO_4} \qquad (6.33)$$

Therefore, the boundary between the stability fields for anorthite and Ca-montmorillonite is a straight line with a slope -8 in the stability diagram.

The stability diagrams for anorthite, K-feldspar and albite include also the stability lines for quartz and amorphous silica. For both lines, the solubility is discribed by the reaction:

$$SiO_2(s) + 2H_2O \Leftrightarrow H_4SiO_4 \qquad (6.34)$$

H_4SiO_4 remains undissociated at pH values below 9 and the stability of SiO_2 phases is determined by the following equation:

$$K = a_{H_4SiO_4} \qquad (6.35)$$

For quartz, the solubility equation can be written in logarithmic form as:

$$\log K = \log a_{H_4SiO_4} = -4 \qquad (6.36)$$

For amorphous silica, the same equation can be written as:

$$\log K = \log a_{H_4SiO_4} = -2.7 \qquad (6.37)$$

According to Appelo & Postma (2005), quartz has extremely slow reaction kinetics and solutions grossly supersaturated for quartz are common. The slow precipitation of quartz allows the formation of less stable forms of silica such as amorphous silica. The latter is also the most soluble form of silica and thus determines the upper limit of the dissolved silica concentration.

Table VII.58. Chemical reactions used for the construction of the stability diagram for anorthite and corresponding equilibrium constants

Reaction	**ΔG_r^0 (kJ/mol)**	**Log K**
$CaAl_2Si_2O_8 + 2H^+ + 6H_2O \Leftrightarrow 2Al(OH)_3(s) + 2H_4SiO_4 + Ca^{2+}$ Anorthite Gibbsite	-47.3	8.3
$CaAl_2Si_2O_8 + 2H^+ + H_2O \Leftrightarrow Al_2Si_2O_5(OH)_4 + Ca^{2+}$ Anorthite Kaolinite	-98.45	17.3
$7CaAl_2Si_2O_8 + 12H^+ + 8H_4SiO_4 \Leftrightarrow 3[Al_4Si_{7.33}Al_{0.67}O_{20}(OH)_4]Ca_{0.33} + 6Ca^{2+} + 16H_20$ Anorthite Ca-montmorillonite	-759.9	133.3
$2Al(OH)_3(s) + 2H_4SiO_4 \Leftrightarrow AlSi_2O_5(OH)_4 + 5H_2O$ Gibbsite Kaolinite	-51.15	8.97
$7Al_2Si_2O_5(OH)_4 + 8H_4SiO_4 + Ca^{2+} \Leftrightarrow 6[Al_2Si_{3.67}Al_{0.33}O_{10}(OH)_2]Ca_{0.167} + 2H^+ + 23H_20$ Kaolinite Ca-montmorillonite	-70.75	12.41
$SiO_2(quartz) + 2H_2O \Leftrightarrow H_4SiO_4$	22.6	-4
$SiO_2(amorphous) + 2H_2O \Leftrightarrow H_4SiO_4$	15.4	-2.7

Table VII.59. Standard Gibbs free energy for ions and minerals involved in silicate weathering

Phase	Formulae	ΔG_r^0 (kJmol^{-1})	Reference
H+		0	Robie & Waldbaum (1968)
Na^+		-261.9	Robie *et al.* (1979)
K^+		-282.5	Robie *et al.* (1979)
Ca^{2+}		-553.5	Robie *et al.* (1979)
H_2O		-237.15	Robie *et al.* (1979)
H_4SiO_4 (aq)		-1308.0	Robie *et al.* (1979)
Quartz	SiO_2	-856.3	Robie *et al.* (1979)
Amorphous silica	SiO_2	-849.1	Drever (1997)
Albite	$NaAlSi_3O_8$	-3711.7	Robie *et al.* (1979)
Microcline	$KAlSi_3O_8$	3742.3	Robie *et al.* (1979)
Anorthite	$CaAl_2Si_2O_8$	-4017.3	Robie *et al.* (1979)
Muscovite	$KAlSi_3O_{10}(OH)_2$	-5600.7	Robie *et al.* (1979)
Kaolinite	$Al_2Si_2O_5(OH)_4$	-3799.4	Robie *et al.* (1979)
Pyrophyllite	$Al_2Si_4O_{10}(OH)_2$	-5269.3	Garrels (1984)
Gibbsite	$Al(OH)_3$	-1159.0	Garrels (1984)
Illite	$K_{0.8}Al_{1.9}(Al_{0.5}Si_{3.5})O_{10}(OH)_2$	-5471.8	Garrels (1984)
Na-montmorillonite	$Na_{0.33}Al_{2.33}Si_{3.67}O_{10}(OH)_2$	-5368.1	Langmuir (1997)
Ca-monmorillonite	$Ca_{0.167}Al_{2.33}Si_{3.67}O_{10}(OH)_2$	-5371.6	Eby (2004)
K-montmorillonite	$K_{0.3}Al_{1.9}Si_4O_{10}(OH)_2$	-5303.2	Garrels (1984)

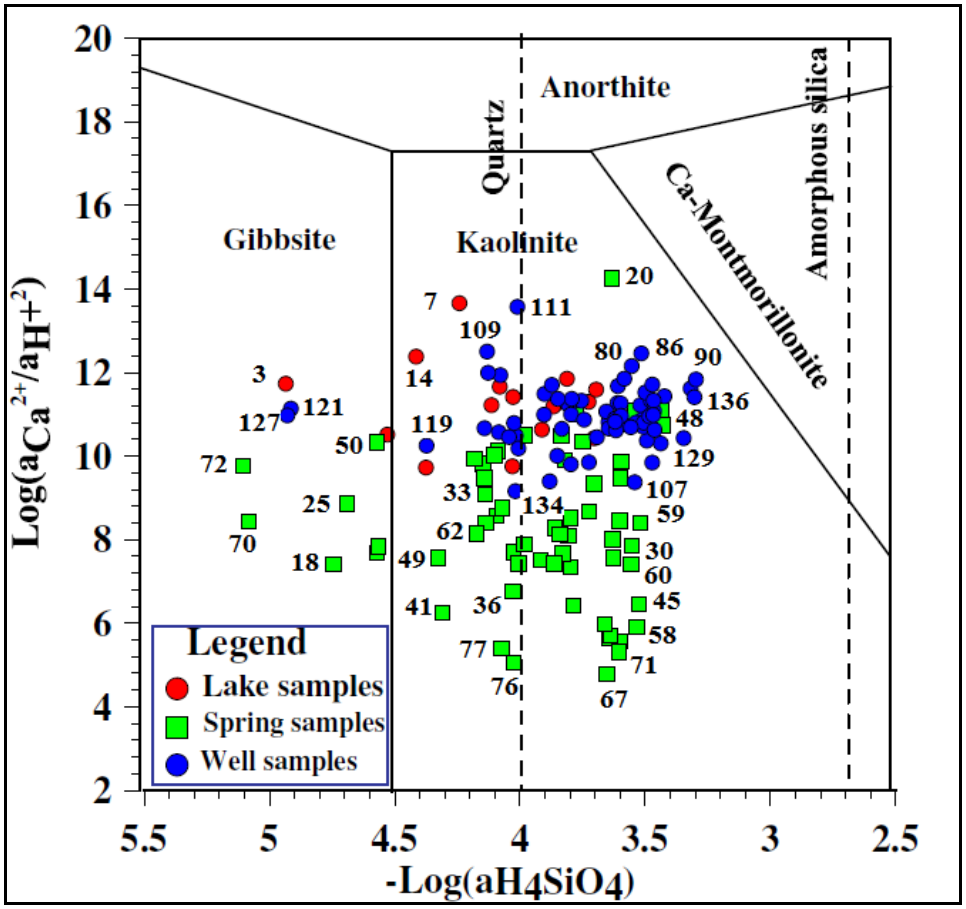

Figure VII.38. Stability of water samples in the system $CaO\text{-}Al_2O_3\text{-}SiO_2\text{-}H_2O$

The approach used for the construction of the stability diagram for anorthite considers this mineral as a pure end-member while it is well established that feldspars, such as plagioclases, are solid solutions of at least two end-members.

VII.4.6.2. Stability diagrams for albite and K-feldspar

Stability diagrams for Na-feldspar and K-feldspar can be constructed in a similar way. Tables VII.60 and VII.61 give the equations and the corresponding ΔG_r° and logK values, which govern equilibrium reactions between the different primary feldspars and their weathering products. However, it should be recalled that considering feldspars as pure end-members is a simplification which implies that the conclusions drawn from such diagrams have to be taken with caution. Indeed, the stability and dissolution/precipitation behaviour of solid solution and of pure end-member minerals will affect the position of the stability boundaries within the diagrams. Moreover, with the slow reaction kinetics of silicate minerals, it is not evident that true equilibrium is ever attained (Appelo & Postma, 2005).

Table VII.60. Reactions used for the construction of the stability diagram for Na-feldspar and the corresponding equilibrium constants

Reaction	ΔG_r^0 **(kJ/mol)**	**Log K**
$NaAlSi_3O_8 + H^+ + 7H_2O \Leftrightarrow AlOH_3(s) + 3H_4SiO_4 + Na^{2+}$ Albite Gibbsite	-51.15	8.97
$2NaAlSi_3O_8 + 2H^+ + 9H_2O \Leftrightarrow Al_2Si_2O_5(OH)_4 + 4H_4SiO_4 + 2Na^+$ Albite Kaolinite	26.85	-4.7
$7NaAlSi_3O_8 + 6H^+ + 20H_2O \Leftrightarrow 3[Al_2Si_{3.67}Al_{0.33}O_{10}(OH)_2]Na_{0.33} + 6Ca^{2+} + 10H_2SiO_4$ Albite Na-montmorillonite	-759.9	133.3
$2Al(OH)_3(s) + 2H_4SiO_4 \Leftrightarrow AlSi_2O_5(OH)_4 + 5H_2O$ Gibbsite Kaolinite	-51.15	8.97
$3.5Al_2Si_2O_5(OH)_4 + 4H_4SiO_4 + Na^{2+} \Leftrightarrow 3[Al_2Si_{3.67}Al_{0.33}O_{10}(OH)_2]Na_{0.33} + H^+ + 11.5H_20$ Kaolinite Na-montmorillonite	-70.75	12.4
$SiO_2(quartz) + 2H_2O \Leftrightarrow H_4SiO_4$	22.6	-4
$SiO_2(amorphous) + 2H_2O \Leftrightarrow H_4SiO_4$	15.4	-2.7

Table VII.61. Reactions used for the construction of the stability diagram for K-feldspar and the corresponding equilibrium constants

Reaction	ΔG_r^0 (kJ/mol)	Log K
$3KAlSi_3O_8 + 2H^+ + 12H_2O \Leftrightarrow KAl_3Si_3O_{10}(OH)_2 + 2K^+ + 6H_4SiO_4$ K-feldspar Muscovite	-59	10.35
$2KAlSi_3O_8 + 2H^+ + 9H_2O \Leftrightarrow Al_2Si_2O_5(OH)_4 + 2K^+ + 4H_4SiO_4$ K-feldspar Kaolinite	22.55	-3.96
$3AlOH_3(s) + 3H_4SiO_4 + K^+ \Leftrightarrow KAl_3Si_3O_{10}(OH)_2 + H^+ + 9H_2O$ Gibbsite Muscovite	-51.35	9.04
$2Al(OH)_3(s) + 2H_4SiO_4 \Leftrightarrow 3Al_2Si_2O_5(OH)_4 + 2K^+$ Gibbsite Kaolinite	-51.15	8.97
$2\ KAl_3Si_3O_{10}(OH)_2 + 2H^+ + 3H_2O \Leftrightarrow 3Al_2Si_2O_5(OH)_4 + 2K^+$ Muscovite Kaolinite	-50.35	8.83
$SiO_2(quartz) + 2H_2O \Leftrightarrow H_4SiO_4$	22.6	-4
$SiO_2(amorphous) + 2H_2O \Leftrightarrow H_4SiO_4$	15.4	-2.7

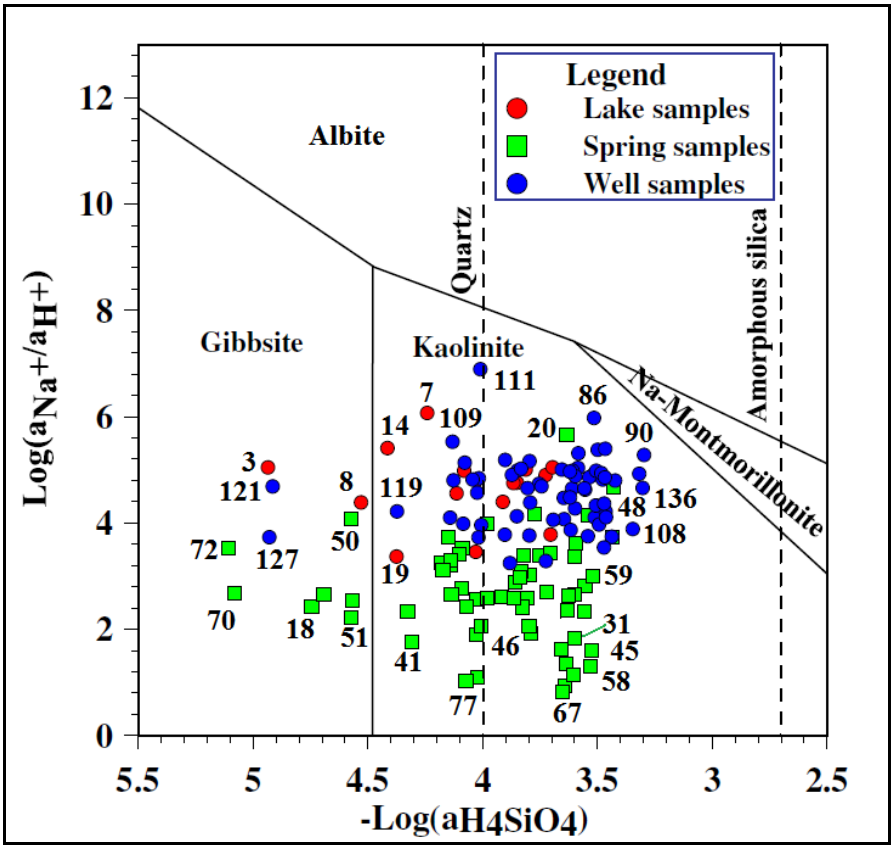

Figure VII.39. Stability of water samples in the system Na_2O-Al_2O_3-SiO_2-H_2O

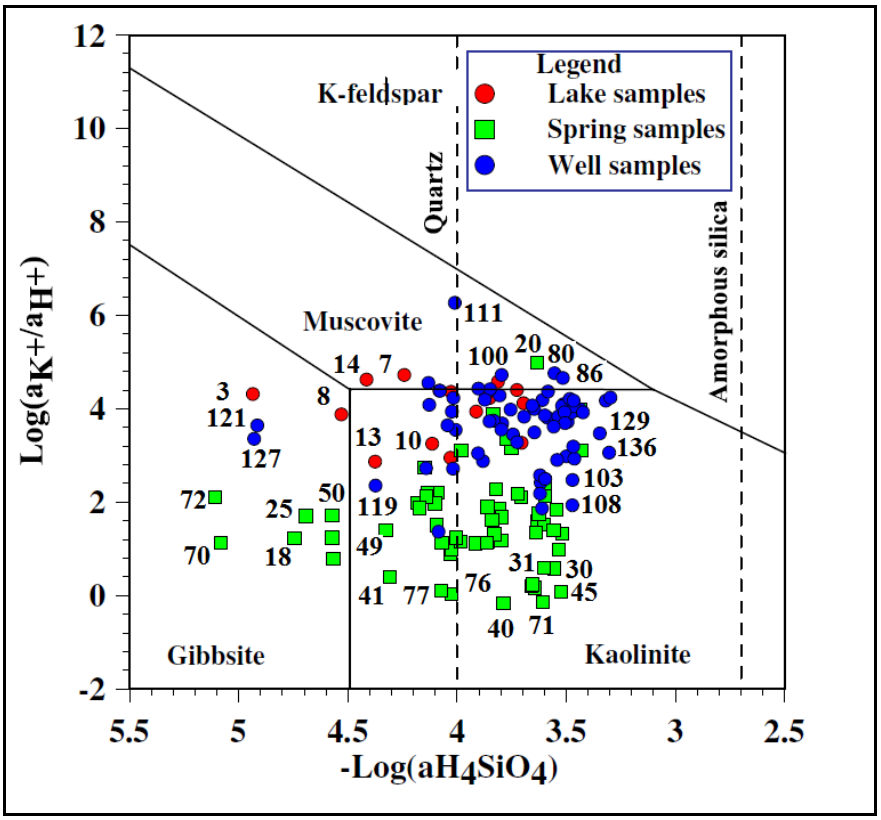

Figure VII.40. Stability of water samples in the system K_2O-Al_2O_3-SiO_2-H_2O

VII.4.6.3. Interpretation of the stability diagrams

Figures VII.38 to VII.40 show the projections of the different water samples analysed in the stability diagrams for Ca-, Na-, and K-feldspars. The numbers in Figures VII.38 to VII.40 correspond to the sample numbers as listed in Appendix VII.1. The activities for Ca^{2+}, Na^+, H^+, K^+ and H_4SiO_4 were calculated using the geochemical modelling software, PHREEQC for windows, version 2.17.01. As a hint to the interpretation of the stability diagrams, it should be understood that a water sample which plots in the kaolinite field suggests that kaolinite is more likely to be the stable mineral phase for this water composition rather than any other weathering product.

Figure VII.38 presents the plots of the 143 water samples in the stability diagram for anorthite. At first glance, most of water samples fall within the stability field of kaolinite. Only 11 water samples among which 2 samples from wells (Ndava II-Nyamabuye, Nr. 122 and Nyange-Kumana, Nr. 127), 2 samples from lakes (Cohoha-Kigozi II, Nr. 3 and Gacamirinda-Shenga II, Nr. 8) and 7 samples from springs lie within the stability field of gibbsite. Compared to the other mineral phases present, kaolinite is therefore the most stable one, which will be in equilibrium with groundwater. The fact that most of the analysed water samples are in equilibrium with kaolinite and to a lesser extent with gibbsite reflects good drainage conditions (Nkotagu, 1996) and is in agreement with the observation by Freeze and Cherry (1979) that in granitic terrain, weathering of feldspar and biotite to kaolinite is a widespread process into the groundwater flow system. Results of X-ray analysis performed on 3 saline soils

collected in the study area confirm the presence of kaolinite in the aquifer matrix (Figures VII.33 to VII.35, Tables VII.49. to VII.51).

The projection of the 143 analysed water samples in the stability diagram for albite (Figure VII.39) equally indicates that most water samples are in thermodynamic equilibrium with kaolinite, while only a few samples (2 wells, 2 lakes and 7 springs) fall within the stability field for gibbsite. It is interesting to note that the 11 water samples falling within the stability field for gibbsite are the same as those on the stability diagram for anorthite. Thus, like within the stability diagram for anorthite, it can be observed from Figure VII.39 that the analysed water samples are mainly in equilibrium with kaolinite and to a lesser extent with gibbsite. This suggests that anorthite and albite, which form the solid solution of plagioclase, are not in equilibrium with groundwater and that they would decompose whenever and wherever in contact with groundwater. The plotting of water samples in the stability field of gibbsite and mostly in the kaolinite stability field suggests hydrological conditions wherein abundant rainfall and the attendant flushing of the soil preclude the formation of montmorillonite.

Figure VII.40 shows the projection of the analysed water samples on the stability diagram for K-feldspar. It can be observed that the majority of the samples plot within the stability field of kaolinite. The same 11 water samples observed in the gibbsite field on the albite and anorthite stability diagrams remain in the same stability field. Moreover, a number of water samples (wells and lakes) form a cluster along the boundary between muscovite and kaolinite, thereby indicating that groundwater is in equilibrium with kaolinite and muscovite. This is consistent with field observations which show that, in some area, for recently constructed wells, aquifer materials excavated at the bottom of the well comprise kaolinite and micas (Figure VII.41). Sample 111 (well at Mago-Gatete) plots far from the boundary between muscovite and kaolinite, in the stability field of muscovite. The forward chemical reaction governing the transformation of micas into kaolinite (Table VII.61) involves a decrease in protons which would result in a pH increase of the groundwater sytem. All the samples plotting along the boundary between the two minerals show neutral to alkaline pH values (6.8-8.5) which are in agreement with a consumption of protons during the weathering of micas.

The stability diagrams for the 3 main feldspars show that the weathering of these aluminosilicate minerals must be an important controlling factor of the hydrochemical evolution of groundwater. On the 3 stability diagrams, it can be noted that lowly mineralised water samples from springs (sample numbers 17-77) plot in the lower part of the stability fields for kaolinite and gibbsite, while water samples from wells (sample numbers 78-143) and lakes (sample numbers 1-16) occupy the upper part. This suggests that the parameter on the Y-axis, i.e. $\log\left(a_{Ca^{2+}}/a_{H^+}^2\right)$, $\log\left(a_{Na^+}/a_{H^+}\right)$ or $\log\left(a_{K^+}/a_{H^+}\right)$, progressively increases on the flow line with increasing residence time and the

consequent dissolution of more aluminosilicate minerals. The increase of the parameter on the Y-axis is accompanied by an increase of the pH and TDS (Figures VII.43 & VII.43), which confirms the progressive dissolution of aluminosilicate minerals. Indeed, the weathering of feldspars consumes protons (H^+) and produces cations (Ca^{2+}, Na^+ and K^+), which implies that groundwater will evolve from low to high values of the parameter on the Y-axis.

Figure VII.41. Photo of aquifer materials excavated in recently constructed wells showing a mixture of kaolinite and muscovite minerals

The stability diagrams for the main feldspar minerals also show two dashed vertical straight lines which represent the saturation state of groundwater with respect to quartz and amorphous silica. Water samples plotting at the right or left of each dashed line are respectively supersaturated or undersaturated with respect to the considered form of silica. On the 3 diagrams, the scatter of the 143 water sample plots shows that all water samples are undersaturated with respect to amorphous silica, which is the most soluble and thus unstable form of silica. This means that no precipitation of amorphous silica can be expected with respect to the chemical composition of the different water samples analysed. On the other hand, it can be observed that most of the water samples analysed (67 %) appear to be supersaturated with respect to quartz, but no precipitation of quartz should be expected because the low temperatures characterising groundwater act as a thermodynamic inhibitor.

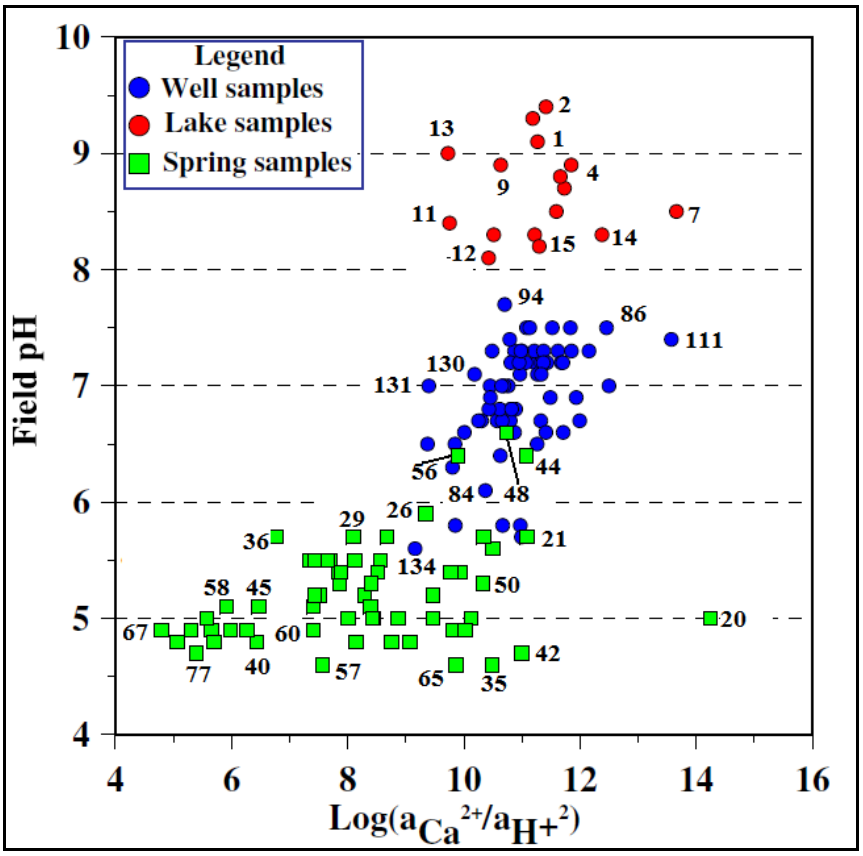

Figure VII.42. pH (field measurements) versus $\log\left(a_{Ca^{2+}}/a_{H^+}^2\right)$ showing that pH values increase with increase of aluminosilicate minerals weathering

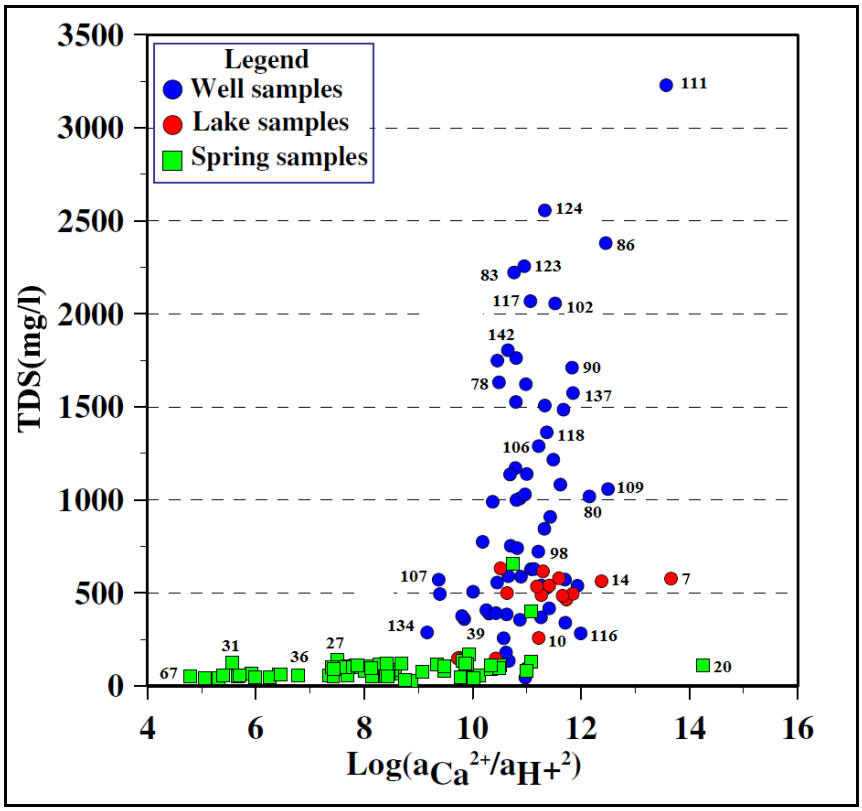

Figure VII.43. TDS versus $\log\left(a_{Ca^{2+}} / a_{H^+}^2\right)$ showing that, overall, TDS values increase with increase of aluminosilicate minerals weathering

VII.4.7. Cross-plots of some hydrochemical parameters

Cross-plots of some hydrochemical parameters (TDS, EC) and the concentration of the major dissolved constituents can help bring out some particular relationships between these parameters. These relationships portray the complex hydrochemical processes which have prevailed during the hydrochemical evolution of groundwater and which have contributed to the present-day chemical characteristics of groundwater. The extent to which the different processes control groundwater chemistry is determined by end members, the residence time, the flow paths and rates as well as the progression of the reaction in an aquifer system.

VII.4.7.1. Electrical conductivity (EC) and major ions

Electrical conductivity (EC) reflects the salinity or the mineralisation of groundwater. High values of TDS indicate mature waters which have been in contact with aquifer materials for a long time and which have, thus, dissolved the possible maximum of rock materials. The EC therefore is the mirror of the influence of the main processes which govern the pace of hydrochemical evolution of groundwater along its flow path. More specifically, the EC in the study area should reflect the combined influence of silicate weathering, the evaporative concentration and the dissolution of evaporitic salts.

Figure VII.44 A to F depicts the relationships between EC and the major ions Na^+, Ca^{2+}, Mg^{2+}, K^+, Cl^- and HCO_3^-, which are mainly contributed by the weathering of aluminosilicates and to a lesser extent by the evaporative concentration and the leaching of evaporitic salts and. It can be observed that there is a significant correlation between EC and Na^+ (R^2 = 0.92), HCO_3^- (R^2 =0.84), Ca^{2+} (R^2 = 0.66) and Mg^{2+} (R^2 = 0.75). Overall, the high linear correlation means that, their concentration increases with increasing EC which also strongly correlates to the TDS. These ions are mainly contributed from rock-water interactions and particularly the weathering of aluminosilicate minerals. This is substantianted by the strong correlation between EC and HCO_3^- (R^2 = 0.84) which reflects the increasing release of HCO_3^- as the weathering of aluminosilicates proceeds. However, it can be observed from all the graphs, that some samples, and especially the sample 111 which was collected close to the quarry of evaporitic salts at Mago-Gatete, fall far from the regression line, which means that, there are several processes which contribute to the salinity of groundwater.

Figure VII. 44 D shows that K^+ has the lowest correlation coefficient (R^2 = 0.48), while there is a large spread of data points above the regression line at lower concentration of K^+. This is due to the fact that the weathering of K-feldspars and micas from which K^+ is released, do not contribute significantly to the salinity of groundwater. Moreover, the low correlation between EC and K^+ seems to be in agreement with the observation by Petrides *et al.* (2006), that the relative amount of K^+ contained in authigenic clay minerals such as kaolinite and gibbsite, resulting from the weathering of aluminosilicates, compared to the concentration in groundwater is much larger than Ca^{2+} and Na^+.

On the other hand, it can be observed from Figure VII.44 F that, despite a relatively high correlation coefficient between the concentration of Cl^- and EC (R^2 = 0.67), there is large spread of dat points above the regression line at lower concentration of Cl^-. This means that the concentration of this anion, which does not necessarily increase with increasing salinity, is not influenced by the weathering of primary aluminosilicates and does not contribute significantly to the salinity of groundwater. This observation confirms that the weathering of aluminosilicates is the main EC-determining process, and not the evaporative concentration nor evaporitic salts dissolution.

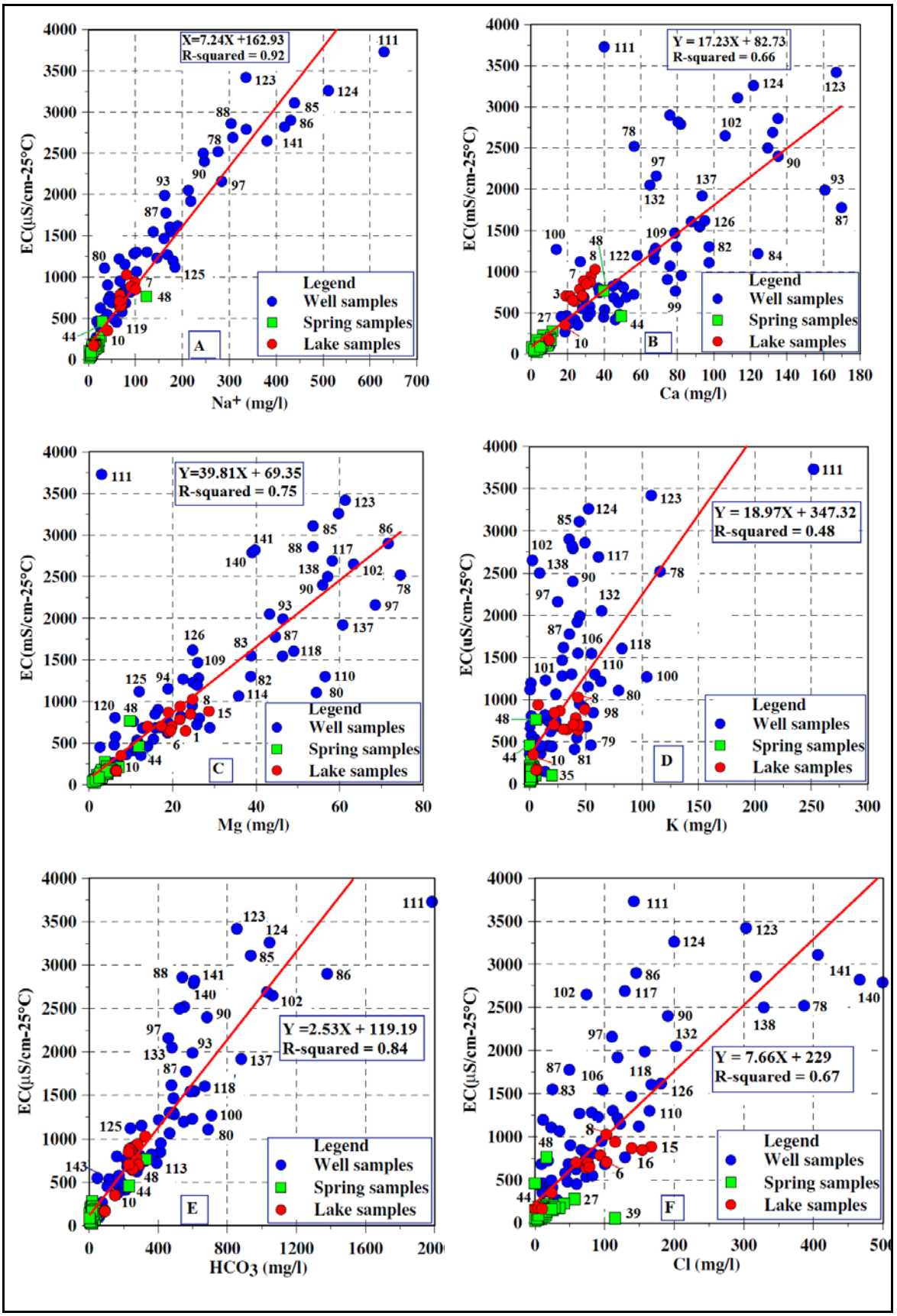

Figure VII.44. Correlation between EC (µS/cm at 25°C) and some major ions

VII.4.7.2. HCO_3^- and major cations (Figures VII.44 A to F)

HCO_3^- and a number of major cations such as Na^+, K^+, Ca^{2+}, Mg^{2+} are released by the acidic weathering of primary aluminosilicate minerals to kaolinite and other clay minerals and oxides. Reactions 6.37 to 6.42 show the main weathering reactions of silicate minerals releasing HCO_3^- and the different cations to groundwater. Ratios are calculated in milliequivalents. While feldspars are the main aluminosilicate minerals found in silicate-bearing rocks such as granites, other silicate mineral like pyroxenes, amphiboles and biotite may be equally present as accessory minerals. Reactions 6.43 to 6.44 show the weathering reactions of carbonate minerals (calcite and dolomite), which also produce HCO_3^-.

$$2NaAlSi_3O_8 + 9H_2O + 2H_2CO_3 \Leftrightarrow Al_2Si_2O_5(OH)_4 + 2Na^+ + 2HCO_3^- + 4H_4SiO_4 \quad (6.37)$$
Albite Kaolinite

$$2KAlSi_3O_8 + 9H_2O + 2H_2CO_3 \Leftrightarrow Al_2Si_2O_5(OH)_4 + 2K^+ + 2HCO_3^- + 4H_4SiO_4 \quad (6.38)$$
K-feldspar Kaolinite

$$2CaAl_2Si_2O_8 + 4CO_2 + 6H_2O \Leftrightarrow 2Al_2Si_2O_5(OH)_4 + 2Ca^{2+} + 4HCO_3^- \quad (6.39)$$
Anorthite Kaolinite

$$2K(Mg_2Fe)(AlSi_3)O_{10}(OH)_2 + 5H_2CO_3 + 7H_2O \Leftrightarrow Al_2Si_2O_5(OH)_4 + 2K^+ + 4Mg^{2+} \quad (6.40)$$
Biotite Kaolinite
$+ 2Fe(OH)_3 + 4H_4SiO_4 + 5HCO_3^-$

$$CaMg(Si_2O_6) + 4CO_2 + 6H_2O \Leftrightarrow Ca^{2+} + Mg^{2+} + 4HCO_3^- + 2H_4SiO_4 \quad (6.41)$$
Pyroxene

$$Ca_2Mg_5Si_8O_{22}(OH)_2 + 14CO_2 + 22H_2O \Leftrightarrow 2Ca^{2+} + 5Mg^{2+} + 14HCO_3^- + 8H_4SiO_4 \quad (6.42)$$
Amphibole

$$CaCO_3 + CO_2 + H_2O \Leftrightarrow Ca^{2+} + 2HCO_3^- \quad (6.43)$$
Calcite

$$CaMg(CO_3)_2 + 2CO_2 + 2H_2O \Leftrightarrow Ca^{2+} + Mg^{2+} + 4HCO_3^- \quad (6.44)$$
Dolomite

The relationship between Ca^{2+} and HCO_3^- is shown in Figure VII.45A. As there are no carbonate rocks in the study area, Ca^{2+} may be mainly released from the weathering of plagioclase (Ca-feldspar, anorthite) and accessorily from pyroxenes, amphiboles and secondary precipitation of carbonate minerals as confirmed by the saturation indices of some water samples with respect to carbonate minerals (aragonite, calcite and dolomite).

Reactions 6.39, 6.41, 6.42, 6.43 and 6.44 show the weathering reactions of the different minerals which are likely to supply Ca^{2+} and HCO_3^- to the groundwater system. Weathering of Ca-feldspar (reaction 6.39) and calcite (reaction 6.43) release HCO_3^- and Ca^{2+} in the equivalent ratio of 1:1, whereas the dissolution of pyroxenes (reaction 6.41) and dolomite (reaction 6.44) produces HCO_3^- and Ca^{2+} in the proportion of 2:1. The dissolution of amphibole (reaction 6.41) liberates HCO_3^- and Ca^{2+} in proportion of 7:2 (Table VII.62).

Table VII.62. Equivalent proportion of different ions released from the weathering of the different aluminosilicate minerals

	Na^+ (meq)	**K^+ (meq)**	**Ca^{2+} (meq)**	**Mg^{2+} (meq)**	**HCO_3^- (meq)**
Albite	2				2
Anorthite			4		4
K-feldspar		2			2
Pyroxenes			2	2	4
Amphiboles			4	10	14
Biotite		2		8	5

The scatter plot of HCO_3^- vs Ca^{2+} (Figure VII.45 A) shows that most of the data points rather plot above the 1:1 line, which indicates an excess of HCO_3^- compared to the amount predicted by the weathering of anorthite and calcite. Only a few water samples like those from the wells in Gasagara I-Rubuga (87), Gahwijo II-Nyabikenke (84), Karago-Kibonde (99) and Susa-Gikomero (143) plot along the 1:1 line. This observation suggests that the weathering of Ca-feldspar is the main source contributing Ca^{2+} to the groundwater but that there are other processes which liberate much more HCO_3^-. The 2:1 line which illustrates the proportions of HCO_3^- and Ca^{2+} deriving from the weathering of pyroxenes and dolomite nearly coincides with a regression line between the two ions. Although the 2:1 and the regression lines lie in the middle of the scatter of data points, the coefficient of determination as shown by the regression line ($R^2 = 0.56$) is very low. Moreover, it can be observed from Figure VII.45 A that nearly all water samples plot below the 7:2 line. This indicates that the weathering of dolomite, pyroxenes and amphiboles is not significantly contributing to hydrogeochemical evolution of groundwater in the study area. Figure VII.45 A also clearly shows that the water sample collected at Mago-Gatete at some distance downstream of the salt quarry (sample 111) and the samples collected at Karago-Rukuramigabo (Nr. 100) and Gasagara II-Rubuga (Nr. 86) plot far above the 1:1, 2:1 and 7:2 lines suggesting higher inputs of HCO_3^- than those predicted by the weathering of plagioclases, calcite, dolomite, amphiboles and pyroxenes.

Figure VII.45 B depicts the relationship between Na^+ and HCO_3^- as predicted by the weathering reaction of albite to kaolinite. From reaction 6.37, it can be noted that the weathering of albite releases Na^+ and HCO_3^- in the equivalent ratio of 1:1 (Table VII.62). Figure VII.45 B shows that, overall, water samples plot along the isoline 1:1,

which indicates that weathering of albite to kaolinite could be the main process which increases Na^+ and HCO_3^- in groundwater in the study area, as confirmed by the predominance of Na^+ and HCO_3^- in most of the water samples. Moreover, the isoline 1:1 nearly coincides with the regression line which reveals a strong linear correlation (R^2= 0.83) between Na^+ and HCO_3^-, thereby suggesting the strong effect of Na-feldspar weathering, which increases along the flowpath, resulting in the progressive build up of Na^+ and HCO_3^- levels in groundwater .

The weathering reactions of K-feldspar (reaction 6.38) and biotite (reaction 6.40) from which K^+ dissolved in groundwater may derive, are depicted in Figure VII.45 C by the lines representing the equivalent ratios of HCO_3^- to K^+ of 1:1 (K-feldspars) and 5:2 (biotite). Also the linear regression between the concentrations of both ions is shown. It can be observed that nearly all data points plot above the lines representing the weathering of biotite (5:2 line) and K-feldspars (1:1 line). This clearly shows that there is a substantial excess of HCO_3^- which results from the weathering of other silicate minerals, also releasing this anion.

Figure VII.45 D shows the relationship between HCO_3^- and Mg^{2+} in comparison to the weathering reaction lines of pyroxenes and dolomite (2:1 line), amphiboles (7:5 line) and biotite (5:8 line), whereby it can be seen that the majority of water samples plot above the 3 lines, suggesting that there is excess of HCO_3^- in comparison with the equivalent proportions predicted by the weathering reactions of pyroxenes, dolomite, amphibole and biotite. Only a few samples plot along the 2:1 and 7:5 lines. This indicates that, although the four minerals may be the source of dissolved Mg^{2+} in groundwater, their weathering reactions do not explain all dissolved HCO_3^-, which is contributed from mixed sources including the different aluminosilicate minerals, and mainly the Na-feldspar (Figure VII.45 B), evaporative concentration and possibly the leaching of the saline soils.

Figure VII.45 E portrays the relationship between HCO_3^- and $Mg^{2+} + Ca^{2+}$ in equivalent ratio of 1:1 as predicted by the weathering reactions of pyroxene, amphibole and dolomite (reactions 6.41, 6.42 and 6.44). This figure shows that a number of samples plots along the 1:1 line with a relatively good correlation between HCO_3^- and $Mg^{2+} + Ca^{2+}$ as evidenced by a coefficient of determination of $R^2 = 0.62$. However, it can be noted that most data points fall above the 1:1 line, thereby suggesting that HCO_3^- is in excess in comparison to the sum of $Ca^{2+} + Mg^{2+}$, as predicted by the weathering reactions of pyroxene, amphibole and dolomite. This indicates that, although the weathering of these 3 minerals may contribute, to some extent, to the amount of dissolved Mg^{2+} and Ca^{2+}, the amount of HCO_3^- is far beyond what is predicted by the weathering reactions of the 3 minerals, which confirms the existence of a substantial contribution of this anion from other sources, and especially the weathering of anorthite and albite.

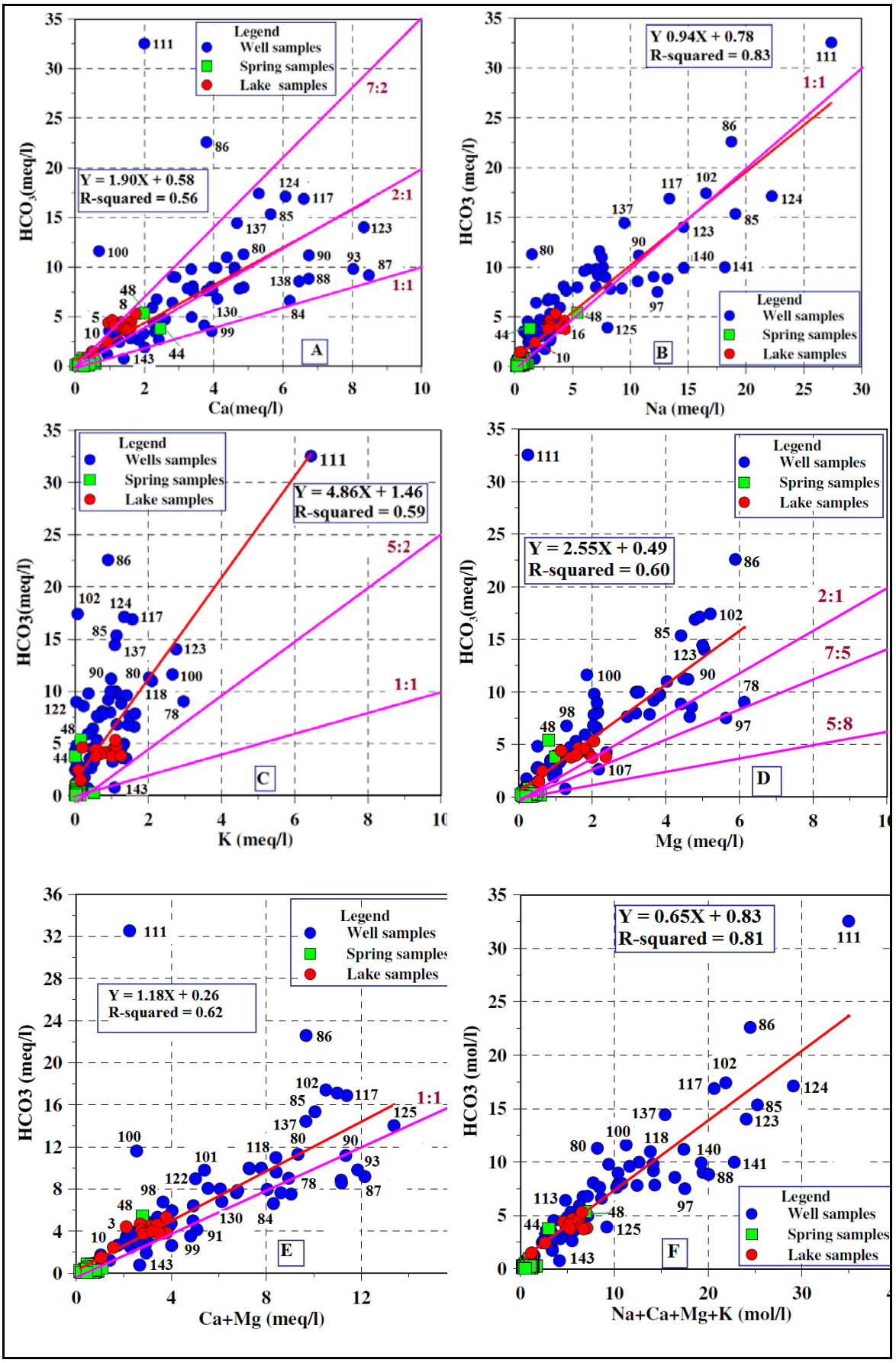

Figure VII.45. Crossplots showing relationships between HCO_3^- and the different cations

Figure VII.45 F illustrates the relationship between HCO_3^- and the sum of alkaline and alkaline earth cations which are added to the groundwater from the weathering of the different aluminosilicate and carbonate minerals (reactions 6.37 to 6.44) (Table VII.62). Overall, Figure VII.45 F shows a strong correlation ($R^2 = 0.81$) between HCO_3^- and the sum of the 4 cations ($Na^+ + K^+ + Ca^{2+} + Mg^{2+}$), which confirms that the weathering of aluminosilicates is the main process which controls the hydrochemistry of groundwater in the study area. The progressive deviation of some water samples from the regression line as the concentrations of HCO_3^- and $Na^+ + K^+ + Ca^{2+} + Mg^{2+}$ increase (e.g. samples 111 and 86) speaks in favour of additional processes which contribute to increased concentration of the different ions.

VII.4.7.3. Calcium and sodium

Figure VII.46 A portrays the relationship between Ca^{2+} and Na^+ in the different water samples whereby it is clear that the scatter of data points is rather large. This is confirmed by the relatively low coefficient of determination between the two cations ($R^2 = 0.49$). Given the absence of carbonate rocks in the study area, Ca^{2+} and Na^+ are mainly supplied to the groundwater by the weathering of aluminosilicates, predominantly plagioclases as illustrated by the reactions 6.37 and 6.39. The weak correlation between Ca^{2+} and Na^+ indicates that the two cations are not released in the same proportions, as this is confirmed by the predominance of Na^+ over Ca^{2+} in the majority of water samples. Moreover, Figure VII.46 A clearly shows that nearly all water samples fall below the 2:1 line, representing the equivalent ratio of Ca^{2+} to Na^+, that would be expected from the weathering of equal amounts of the two aluminosilicates. This evident excess of Na^+ in comparison to Ca^{2+} could be explained by two main reasons. First, it is possible that Na-rich feldspars are predominant in the basement complex underlying the study area in comparison to Ca-feldspars. On the other hand, the predominance of Na^+ in groundwater compared to Ca^{2+} may be explained by the low adsorption affinity of Na^+ onto clay surfaces in comparison to Ca^{2+}. Indeed, when in contact with water, Na^+ which has a smaller valence and and a larger hydrated radius than Ca^{2+}, will tend to be desorbed, while the latter remains tightly bound on the exchange complexes (Rytwo *et al.*, 1996). It is also obvious that the water sample collected at Mago-Gatete, at some distance downgradient the quarry of evaporitic salts, strongly departs from the scatter of other data points, thereby confirming the existence of another source of Na^+, which is manifestly associated with the dissolution of the evaporitic salts. Indeed, the chemical analysis of the saline soils shows the predominance of Na^+, whereas X-ray analyses confirm the presence of halite and thenardite within the saline soil samples.

VII.4.7.4. Calcium and magnesium

Calcium and magnesium can be released to groundwater either as the result of the dissolution of carbonate minerals (calcite or dolomite) or the slow weathering of various silicate minerals. Figure VII.46 B presents the crossplots of Mg^{2+} versus Ca^{2+} wherein the lines representing the weathering reactions of the different minerals which may release both cations to the groundwater are shown. Overall, Figure VII.46 B shows that, despite a relatively large scatter of data points, there is a strong linear correlation between Mg^{2+} and Ca^{2+} as evidenced by the high coefficient of determination (R^2 = 0.72). This suggests that, roughly, the concentration of both cations increases linearly and parallelly as a result of the same hydrochemical process, which is mainly the weathering of aluminosilicate minerals. However, it can be noted that some data points depart from the regression line, thereby indicating that, besides the main process, there are additional hydrochemical processes which may contribute to the differential increase of the two cations in groundwater. These processes may include the dissolution of evaporitic salts, as well as the evaporative concentration along the flowpath. This is evidenced by the fact that the data points progressively deviate from the regression line as the concentration of both cations increases, and particularly in water samples collected from the wells located in the depression (e.g. samples 78, 86, 87, 93, 97) where these additional processes may significantly influence the chemical character of groundwater as a result of long flowpaths and residence time. Indeed, it can be observed that, while other spring samples are located nearly at the origin, the two water samples collected from the 2 springs located in the depression, NW of the study area, i.e. spring at Mamfu-Kiyonza (sample 44) and Mukuyo-Kiri (Sample 48) slightly depart from the regression line.

The 5:2 line represents the weathering reaction of amphiboles (reaction 6.42) whereby Mg^{2+} and Ca^{2+} are released in the equivalent proportion of 5:2 (Table VII.62). The 1:1 line represents the proportions of Mg^{2+} and Ca^{2+} resulting from the weathering of pyroxenes (reaction 6.41) and dolomite (reaction 6.44). Overall, it is obvious that the majority of water samples fall below the 5:2 and 1:1 weathering reaction lines, which suggests an excess of Ca^{2+} in comparison to Mg^{2+}. This observation points to the fact that, considering the sources of Mg^{2+} and Ca^{2+}, the weathering of Ca-feldspar is more important than that of ferromagnesian minerals. Moreover, the dissolution of the evaporitic salts, which contain gypsum, may contribute to increased concentrations of Ca^{2+} in comparison to Mg^{2+}. Furthermore, the fact that the majority of water samples plot below the equiline 1:1 representing the weathering reaction of dolomite and pyroxenes, confirms the predominance of the weathering of feldspars as the main process controlling groundwater chemistry.

VII.4.7.5. Calcium and sulphate

Figure VII. 46 C presents the relationship between SO_4^{2-} and Ca^{2+} which shows a relatively significant coefficient of determination (R^2 = 0.65) between the 2 ions, despite the fact that the scatter of data points is quite large. The addition of Ca^{2+} and SO_4^{2-} to groundwater is mainly contributed from the dissolution of gypsum ($CaSO_4.2H_2O$) and anhydrite ($CaSO_4$) which release the two ions in the molar proportion of 1:1 (reaction 6.45).

$$CaSO_4.2H_2O + H_2O \Leftrightarrow Ca^{2+} + SO_4^{2-} + 3H_2O \qquad (6.45)$$

It can be observed from Figure VII.46 C that a few samples (e.g. samples 48, 83, 86, 88, 102) plot along the 1:1 equiline, which means that they might be influenced by the dissolution of the gypsum which is present into the evaporitic salts as evidenced by X-ray analyses (Figures VII.33 to VII.35). Indeed, all water samples plotting along the 1:1 line were collected from wells or springs located within the depression where these evaporitic salts form. The few samples plotting above the equiline 1:1 highlight an excess of SO_4^{2-} relative to Ca^{2+} which may result from the depletion of Ca^{2+} consecutive to the precipitation of carbonates as this is the case for the water samples 87, 97, 111 and 124 whose saturation indices with respect to calcite and dolomite show a supersaturation. Moreover, Ca^{2+} may be removed from groundwater due to its high bounding affinity to the exchange complexes and particularly of clay minerals.

VII.4.7.6. Sulphate and sodium

Figure VII.46 D shows the relationship between SO_4^{2-} and Na^+. Besides the weathering of gypsum, anhydrite and aluminosilicates, both ions may be contributed from the dissolution of thenardite (Na_2SO_4) according to the reaction (6.46):

$$Na_2SO_4 \Leftrightarrow 2Na^+ + SO_4^{2-} \qquad (6.46)$$

Equation 6.46 indicates that, by weathering of thenardite, SO_4^{2-} and Na^+ are liberated in the equivalent proportions of 1:1. However, Figure VII.46 D shows that nearly all water samples plot below the 1:1 line, which indicates that the weathering of thenardite, which was revealed by X-ray analyses of samples of the saline soils, is not significantly contributing to the chemistry of groundwater in the study area. The fact that the majority of water samples plot below the 1:1 line indicates an excess of Na^+ compared to the equivalent proportions of SO_4^{2-} and Na^+ predicted by the weathering of thenardite, which confirms that the weathering of alumino-silicates and mainly Na-plagioclases is the main process controlling the hydrochemistry of groundwater in the study area. Moreover, the fact that even the water sample 111 which was collected close to the salt quarry of Mago, plots far below the 1:1 line, may indicate that the salt occurrences are localised and are not significantly affecting the overall hydrochemical evolution of groundwater in the study area.

VII.4.7.7. Magnesium and potassium

Mg^{2+} and K^+ are released to groundwater as a result of the weathering of silicate, ferromagnesian and Mg-carbonate minerals. Reaction 6.40 and Table 5.62 show that the dissolution of biotite releases Mg^{2+} and K^+ in equivalent proportions of 4:1. Despite a large scatter of data points as confirmed by the low coefficient of determination (R^2 = 0.28), Figure VII.46 E shows that several water samples fall well along the 4:1 line, thereby indicating that the weathering of biotite is contributing, to some extent, to the chemistry of groundwater.

The deviation of some water samples which plot below the 4:1 line, such as the samples 78, 94, 100, 111, 118, 123, suggests an additional enrichment of K^+ relative to Mg^{2+} in groundwater, particularly in the water sample collected in the vicinity of the quarry of evaporitic salts in Mago-Gatete (sample 111). This indicates that there are additional sources of K^+, such as the weathering of K-feldspar and possibly the leaching of evaporitic salts which mainly occur within the depression.

On the other hand, excess of Mg^{2+} relative to K^+, reflected by a number of water samples like the samples 86, 97, 102 and 138, which plot above the 4:1 line, may derive mainly from the weathering of ferromagnesian minerals and, to a lesser extent, from the dissolution of secondary precipitation of Mg-carbonates within the soil.

VII.4.7.8. Sodium and chloride

Sodium and chloride can be released to the groundwater as a result of the dissolution of several minerals, including halite (reaction 6.47), thenardite (6.46) and silicate minerals (reaction 6.36).

$$NaCl + H_2O \Leftrightarrow Na^+ + Cl^- + H_2O \qquad (6.47)$$

Figure VII.46 F, which depicts the relationship between Na^+ and Cl^-, shows that, while most of the spring waters which are of NaCl water type fall along the 1:1 line representing the dissolution of halite (NaCl) (reaction 6.47) or most probably the Cl:Na ratio of sea water (1.6:1), the majority of water samples, mostly those collected from wells, fall below the equiline 1:1, thereby indicating an excess of Na^+ in comparison to Cl^-. Indeed, spring waters of NaCl type are derived from infiltrating rainwater which has dissolved sea spray. This situation may result from the fact that Na^+ is significantly contributed from different sources including the weathering of aluminosilicates and the dissolution of the evaporitic salts, other than halite (e.g. thenardite) without an equivalent contribution of Cl^-. The increase in concentration of Cl^- is only expected from human pollution, leaching of evaporitic Cl-salts and evaporative concentration which affects all the dissolved constituents. It can be observed that even the water sample from the well at Mago-Gatete (sample 111), which is situated at a short distance downgradient the quarry of evaporitic salts, falls very far from the equiline 1:1, suggesting an excess of Na^+ relative to Cl^-, which indicates that groundwater is not significantly controlled by the dissolution of halite.

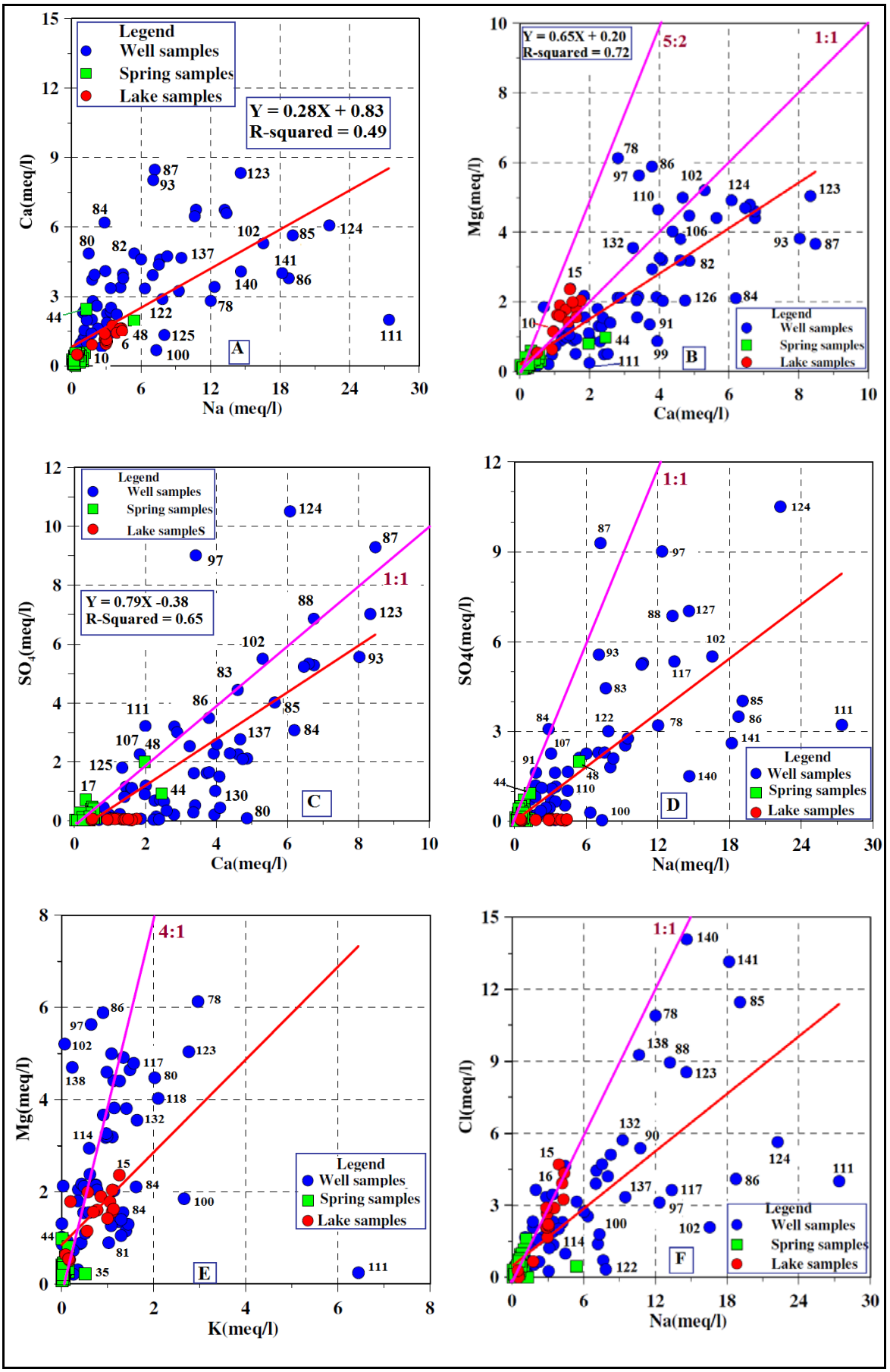

Figure VII.46. Crossplots showing relationship between Ca^{2+} and Na^{+} (A), Mg^{2+} and Ca^{2+} (B), Ca^{2+} and SO_4^{2-} (C), Na^{+} and SO_4^{2-} (D), Mg^{2+} and K^{+} (E), and Cl^{-} and Na^{+} (F).

VII.4.7.9. Calcium and fluoride

Figure VII.47 shows the relationship between Ca^{2+} and F^-, which mainly derives from the dissolution of fluorite (reaction 6.48), an accessory mineral that can occur in igneous, hydrothermal and metamorphic rocks.

$$CaF_{2(s)} + H_2O \Leftrightarrow Ca^{2+} + 2F^- + H_2O \qquad (6.48)$$

F^- can be also present as an impurity in the crystal lattices of some minerals such as apatite, amphiboles and biotite where it isomorphologically substitutes for the hydroxyl group.

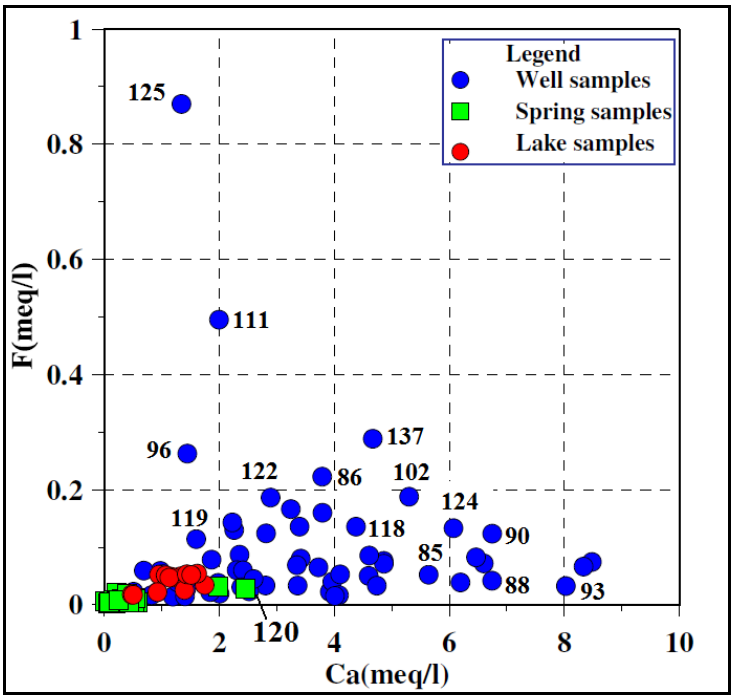

Figure VII.47. Crossplots showing relationship between F^- and Ca^{2+}

It can be noted that most of the water samples are characterised by low concentrations of F^- as illustrated by the scatter of data points which all lie approximately along the X-axis. Indeed, most of the water samples have a concentration of F^- less than or equal to 0.2 meq/l (0.2 mg/l). Despite these low concentrations of F^-, Figure VII.47 roughly depicts an inverse linear relationship between the concentrations of Ca^{2+} and F^-, which are controlled by the solubility of fluorite and calcite. Indeed, several reseachers have already demonstrated that, generally, high Ca^{2+} concentrations in groundwater correspond to low concentrations of F^- and vice versa (e.g. Coetsiers *et al.*, 2008; Rafique *et al.*, 2008; Dhiman & Keshari, 2006). This can be explained by the fact that the weathering of feldspars which consumes protons causes the pH to rise, thus resulting in the dissolution of more CO_2 with the consequent production of more HCO_3^- and CO_3^{2-}. The increase in CO_3^{2-} leads to the precipitation of calcite as groundwater becomes supersaturated with respect to calcite. The precipitation of calcite reduces the Ca^{2+} in groundwater, which becomes undersaturated with respect to fluorite, thereby

resulting in dissolution of fluorite (reaction 6.48) or other F^--bearing minerals. This will increase the concentration of F^- in groundwater.

The saturation indices calculated for the different water samples (Appendix VII.7) show that 22 water samples are supersaturated with respect to calcite, while 3 water samples are oversaturated with respect to fluorite. Water samples whose saturation indices indicate oversaturation with respect to calcite show slight undersaturation (SI = -1.83 to -0.01) to slight oversaturation with respect to fluorite (SI = 0.3-0.96). Water samples 111 and 137 show oversaturation with respect to both calcite and fluorite. This suggests that, with increasing dissolution of fluorite or F^--bearing minerals, the saturation with respect to fluorite is progressively reached, which ultimately results in the precipitation of fluorite. Moreover, the redissolution of the precipitated salts may contribute to high F^- concentration in groundwater. The saturation indices for water sample 96 show equilibrium with respect to calcite (SI = 0) and a slight undersaturation with respect to fluorite (SI = -0.04). The water sample 120 shows an oversaturation with respect to fluorite (SI = 0.95) and undersaturation with respect to calcite (SI = -0.66).

VII.4.7.10. SiO_2 and other parameters

Figure VII.48 A to F shows the relationships between SiO_2 and the hydrochemical parameters Na^+, Ca^{2+}, Mg^{2+}, K^+, HCO_3^- and TDS. Silica in groundwater generally originates from two sources, including the dissolution of quartz or amorphous silica and mainly from the weathering of aluminosilicate minerals. It has been shown that the parameters, which are compared to silica, are also contributed mainly from the weathering of aluminosilicate minerals and that, overall, their concentration increases progressively along the flowpath with increasing mineralisation and residence time. The study area being mainly underlain by silicate-bearing rocks, a positive linear correlation between these parameters and SiO_2 would be logically expected as they are controlled by the same hydrochemical processes along the flowpath. In this respect, Coetsiers & Walraevens (2006) observed that the concentration of SiO_2, in a Neogene aquifer in Belgium, slightly increases along the flow line due to the slow weathering of silicate minerals.

However, it can been noted from Figure VII.48 A to F that there is a poor linear correlation between SiO_2 and the different parameters, where it is clear that the highest concentrations of these parameters do not necessarily correspond to the highest concentration of silica, although there is some tendency. The lack of correlation between silica and the different parameters considered can be ascribed to local lithological variations, some aluminosilicate-bearing rock such as granites being more weatherable than others like quartzites. Indeed, it is well established that the most important factors controlling rates of silica leaching are rock types and the amount of water available for chemical mobilisation of silica (Davis, 1969).

conversion of kaolinite into gibbsite, rather than the dissolution of aluminosilicates.

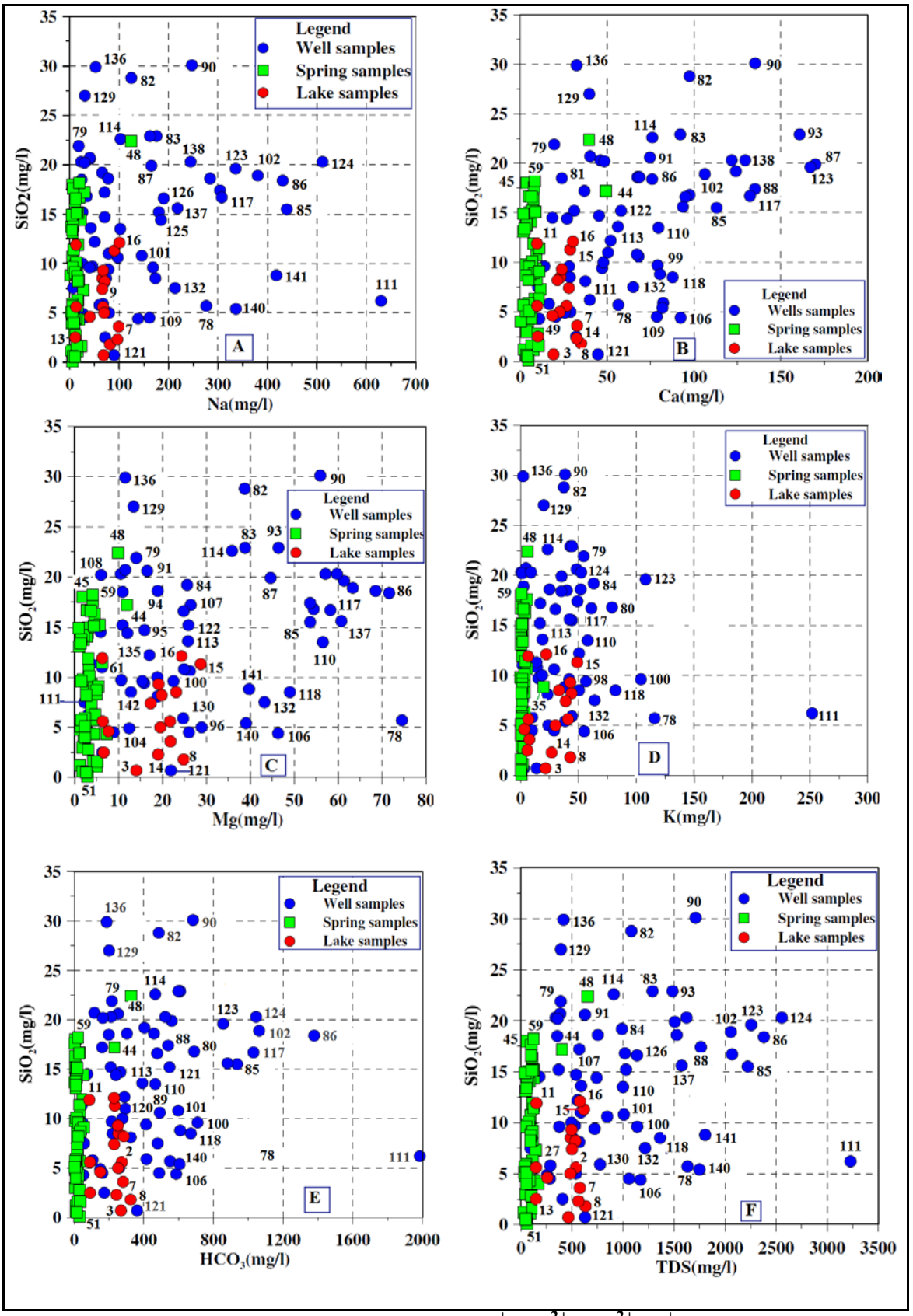

Figure VII.48. Crossplots of SiO_2 versus Na^+, Ca^{2+}, Mg^{2+}, K^+, HCO_3^- and TDS

On the other hand, stability diagrams have shown that most of the water samples plot within the stability field of kaolinite which suggests that part of the silica released from the weathering of aluminosilicates is retained in situ by the neoformation of clay minerals. It can be observed that in Figure VII.48 A, D, E and F, that the water sample from the well at Mago-Gatete (Nr.111) completely departs from the bulk of the data points, which suggests that the elevated concentrations of Na^+, K^+, HCO_3^- and TDS associated with low SiO_2 levels can not be only explained by the weathering of aluminosilicate minerals. On the other hand, all the cross-plots of SiO_2 versus the different hydrochemical parameters (Na^+, K^+, Ca^{2+}, Mg^{2+}, HCO_3^- and TDS) show that water samples collected from springs plot nearly along a vertical line at low values of the different parameters, which suggests that relatively important concentrations of silica (up to 20 mg/l) occur in groundwater at shallow depths and after short residence times.

This observation is consistent with the findings by Davis (1969) who reported that the addition of silica in groundwater is probably more rapid near the ground surface and that the percolating water can have a silica content ranging between 5 and 20 ppm before reaching the groundwater table. The large spread of SiO_2 in spring waters, at remaining low concentration of Na^+, Ca^{2+}, Mg^{2+}, K^+, HCO_3^-, TDS is quite striking and is certainly due to reactions which can be the dissolution of amorphous silica.

VII.5. Conclusions and recommendations

The hydrogeochemistry of the basement aquifer in Bugesera region (Burundi) has been evaluated based on the analytical results of 143 water samples comprising 66 samples from shallow wells, 61 samples from springs, and 16 samples from the shallow lakes. On average, the sequence of the relative abundance of the different dissolved constituents is in the following order: $Na^+ > Ca^{2+} > K^+ > Mg^{2+} > Fe^{2+} > Mn^{2+} > NH_4^+$ and $HCO_3^- > Cl^- > SO_4^{2-} > NO_3^- > NO_2^- > PO_4^{3-}$ for cations and anions respectively.

The maps of the spatial distribution of the different hydrochemical parameters show that there is a clear demarcation between the highlands located to the South and East of the study area, and the depression in which lies the complex of marshlands and shallow lakes. Highlands where emerge several springs are characterised by lowly mineralised waters (TDS = 26-142 mg/l) which represent young infiltrating meteoric waters, as this is confirmed by the low pH values (field pH = 4.6-6.6). On the other hand, water samples collected from the wells, which are in majority located within the depression, show a high mineralisation (TDS = 44-3229 mg/l) and relatively high values of pH (field pH = 5.6-7.7), which reflects long flowpaths and residence time. Water samples from the shallow lakes show intermediate levels of mineralisation (TDS = 147-632 mg/l). Direct precipitation, overland flow and overflow of rivers into the lakes during high stages, induce dilution which explains the relatively low TDS values of water

samples from lakes in comparison to water samples from wells. The high values of pH (field pH = 8.1-9.4) in water samples from lakes are related to the consumption of dissolved CO_2 by aquatic organisms.

The water types were determined by plotting chemical analysis of all water samples on the Piper diagram. The classification based on the dominant cation and anion allows to deduce 10 water types of which $NaHCO_3$, NaCl, $CaHCO_3$ and $NaNO_3$ are the most abundant ones. The appearance of $NaNO_3$, $CaNO_3$, KNO_3 and $NaSO_4$ types reflects contamination by human activities.

The simple classification of De Moor and De Breuck (1969), which is based on the mineralisation of water, confirms the hydrochemical demarcation between the highlands and the depression. Water samples collected within the depression, mostly from the shallow wells, are classified as fresh (F), moderately fresh (MF), weakly fresh (WF), moderately brackish (MB) and brackish (B), whereas water samples collected from wells and springs situated at the southern and eastern periphery of the depression and in the highlands are systematically very fresh (VF).

It is not easy to determine the evolutionary track of groundwater in this shallow basement aquifer due to the complexity of the lithological setting and the flow system. However, the graphical representation of the different water types enabled to visualise distinct groupings of water samples from which the evolutionary sequence can be drawn. Thus, NaCl water types with low mineralisation and low pH represent mainly young infiltrating rain waters and seem to form the starting end member of the hydrochemical evolutionary process. The hydrochemical evolution progressively shifts from young NaCl water types with low TDS, to the different water types including $NaHCO_3$, $CaHCO_3$, $CaSO_4$, $NaSO_4$, $NaNO_3$, $CaNO_3$, CaCl, $KHCO_3$ and KNO_3. This seems to be controlled by a combination of several processes including essentially the weathering of aluminosilicates, evaporative concentration, the dissolution of evaporitic salt deposits and the contamination by human activities.

The projection of the 143 analysed water samples in the stability diagrams for anorthite, albite and K-feldspar indicates that most water samples are in thermodynamic equilibrium with kaolinite, while only a few samples fall within the stability field for gibbsite. The two clay minerals are the main weathering products of aluminosilicates. Moreover, the 3 stability diagrams show that lowly mineralised water samples from springs, plot in the lower part of the stability fields for kaolinite and gibbsite, while water samples from wells and lakes fall in the upper part, thus indicating the progressive increase of the parameter on the Y-axis, i.e. $\log\left(a_{Ca^{2+}}/a_{H^+}^2\right)$, $\log\left(a_{Na^+}/a_{H^+}\right)$ or

$\log\left(a_{K^+}/a_{H^+}\right)$ along the flow line, with increasing residence time and the consequent dissolution of more aluminosilicate minerals. The increase of the parameter on the Y-axis is accompanied by an increase of pH and TDS, which confirms the progressive dissolution of aluminosilicate minerals along the flow line.

The predominance of $NaHCO_3$ and $CaHCO_3$ water types confirms the dissolution of silicate minerals as the main process controlling the hydrochemistry of groundwater in the study area. The weathering of aluminosilicates is also confirmed by the crossplots of the different hydrochemical parameters and particularly the good linear correlation between the EC and Na^+, Ca^{2+}, Mg^{2+} and HCO_3^-, which indicates that the concentration of these elements increases with increasing mineralisation of groundwater. The low correlation between EC and K^+ may suggest that the weathering of K-feldspars and micas does not contribute significantly to the mineralisation of groundwater. The scatter plots of HCO_3^- versus Ca^{2+}, Na^+, Mg^{2+}, K^+; Ca^{2+} versus Na^+; Mg^{2+} versus Ca^{2+}; Mg^{2+} versus K^+; SO_4^{2-} versus Ca^{2+}; Cl^- versus Na^+ also confirm that the weathering of aluminosilicates is the prominent hydrochemical process controlling the chemistry of groundwater in the study area, while the dissolution of gypsum, secondary carbonate minerals and halite may play only a secondary role. This observation is substantiated by the saturation indices which show that only a few samples are oversaturated with respect to carbonate minerals (calcite and dolomite), while all the water samples are undersaturated with respect to gypsum and halite. The lack of correlation between the concentrations of SiO_2 and Na^+, Ca^{2+}, Mg^{2+}, K^+, HCO_3^- and TDS confirms that, by the virtue of the incongruent character of the weathering of aluminosilicates, part of the silica released from the weathering of silicates is taken up into the formation of clay minerals.

The influence of the evaporative concentration on the hydrochemistry was evaluated by the computation of the concentration factor between different classes of increasing Cl^- concentrations and the class considered as the starting end member of the hydrochemical process (Cl^- = 0-10 mg/l class). Overall, despite a certain variability between the different classes of Cl^-, the application of the concept of evapoconcentation alone reveals a progressive deficit in the sum of alkaline and alkaline earth cations ($Na^+ + K^+ + Ca^{2+} + Mg^{2+}$) and SiO_2, while HCO_3^- shows a slight increase, which seems to mask the important contribution of aluminosilicate weathering along the flow path. This deficit of cations may point to the overestimation of the concentration factor because the starting end member is not actually representative of a true recharge water end member as this is evidenced by high levels of SiO_2 and NO_3^- in some water samples belonging to this class (Cl^- <10 mg/l).

The influence of the evaporitic salts on the hydrochemical evolution of groundwater was evaluated through the computation of the fractions of meteoric recharge and salt-influenced waters and the resulting concentration of the end-member mixture. Overall, the concept of mixing of infiltrating water of meteoric origin with salt-influenced water shows an increasing surplus of the sum of alkaline and alkaline earth cations ($Na^+ + K^+ + Mg^{2+} + Ca^{2+}$), HCO_3^- and the TDS, which indicates the important contribution of the weathering of aluminosilicates. However, expected concentrations of SO_4^{2-} are too elevated and seem not to be well predicted by the conceptual model of mixture of rainwater and salt-contaminated end members. Thus, it can be concluded that the hydrochemical evolution of groundwater within the study area is only locally controlled by the evaporitic salt deposits.

CHAPTER VIII. GENERAL CONCLUSIONS AND RECOMMENDATIONS

Burundi, as other Sub-Saharan countries, still has a long walk to go before meeting the Millenium Development Goal with respect to access to safe drinking water, especially in rural areas. To date, the global drinking water coverage in Burundi is estimated at 55 % and 83 % respectively in rural and urban areas. Bugesera region is one of the most potable water-scarce areas in Burundi, despite several attempts to address the issue of potable water since the colonial period. This study was undertaken with a view to achieving a comprehensive understanding of the hydrogeological framework and the hydrogeochemical environment of groundwater resources in Bugesera, a region which, according to the common saying of local inhabitants, is "cursed, damned" due to the scarcity of potable water. This study deals only with one side of a transboundary aquifer extending over the Burundian and Rwandan parts of the Bugesera region because it was impossible to access existing data on the Rwandan side. On the other hand, the two portions of the aquifer being separated by hydrologic boundaries (rivers and lakes) to which discharges the aquifer, each portion can be studied separately and the fact of not incorporating data from the other side does not affect the results. The cross-checking of all results of the investigations conducted within the framework of this study appeals the following conclusions and recommendations.

VIII.1. General conclusions

VIII.1.1. Geology and hydrogeological structure

Geologically, the study area, as the major part of Burundi, belongs to the Karagwe-Ankole belt, a Mesoproterozic belt which comprises two structurally contrasting domains: the Western Domain (WD) and Eastern Domain (ED), separated by an alignment of mafic to ultramafic intrusions known as the Kabanga-Musongati ultramafic and mafic belt. The study area, which entirely belongs to the WD, is predominantly underlain by Precambrian crystalline rocks mainly consisting of metasediments and magmatic intrusions. They belong to five geological formations which are: (1) the Undifferentiated Complex (granitic and pegmatitic intrusions, and relicts of quartzitic metasediments) which covers the centre of the depression, (2) the Formation of Murehe (or Mugendo) (micaschists, quartzites, pegmatitic and granitic intrusions, and quartz veins) which forms an amphitheatre-like feature surrounding the Undifferentiated Complex Formation, (3) the Formation of Ngozi (phyllites, metavolicanites and pegmatitic dykes) occurs in the South-West of the study area, (4) Formation of Ruganza (quartzite, pegmatitic dykes and sporadic mafic rocks) also outcrops in the South-West of the study area, and (5) the Formation of Nyagisozi (or Nyabihanga) (psammites, psammoschists or micaceous sandstones and conglomerates)

forms a NE-SW elongated feature in the East of the study area. Cenozoic formations comprise various types of soils and alluvium in valley bottoms and lower terraces.

The interpretation of two batches of vertical electrical soundings (VES) (AIDR, 1984 and GEOSCI, 2001) and the inferred interpretative cross-sections indicates that the subsurface comprises a complex sequence of 3 to 6 geoelectrical layers with a clear demarcation between the weathered overburden and the basement. These geoelectrical layers are organised in complex sequences which show a general upwards trend of decreasing grain-size in the weathering materials, corroborated by a similar upwards decrease of resistivity. The wide range of resistivity values reflects the variability of the lithological composition which can change from highly clay-rich materials (3-28 Ωm) to mixtures of clay, sand, gravel and rock fragments in variable proportions (28-150 Ωm). The basement is characterised by remarkably high values of resistivity which vary over a wide range: less than 500 Ωm for the weathered/fractured part of the basement and higher values, exceeding 500 Ωm, for the relatively fresh basement. The combination of all geological and geophysical information allows to propose a conceptual hydrogeological model which reveals semi-confined to confined conditions. The main aquifer is composed of a mixture of clay, sand, gravel and rock fragments in variable proportions. The upwards increasing intensity of weathering results in the occurrence of a distinct clay-rich layer at the top of the weathering profile which acts as the (semi-)confining layer. The regolith aquifer is underlain by the fractured/weathered basement which may form the second aquifer. This aquifer is in continuity with the weathered overburden aquifer. The spatial distribution of the average depth to the fresh basement indicates that, with the largest thicknesses of the two components of the aquifer system, the Undifferentiated Complex is endowed with the highest groundwater potential, while in the metasedimentary formations, prospects of groundwater resources appear to be limited.

VIII.1.2. Hydrology and groundwater balance

Groundwater recharge has been computed using the soil moisture balance method in two different ways: Thornthwaite Monthly Water-Balance Model, wherein Hamon's PET equation is embedded, and excel sheets for other 4 PET methods. The comparison of 4 PET (Hargreaves, Thornthwaite, a modification of the Thornthwaite method and Hamon) to the standard Penman-Monteith shows that the Hargreaves method, which overestimates PET by 51 % with a RMSE of 48 mm/month, is definitely not appropriate for the study area. For the other PET methods, while Thornthwaite and Hamon methods underestimate the potential evapotranspiration by 9 % and 12 % respectively, the modification of Thornthwaite method with a coefficient k = 0.69 gives a good estimate of potential evapotranspiration with a overestimation of 1% and RMSE of 5 mm/month.

Groundwater recharge was computed considering 75 mm for plant available water and 37.5 mm for water content at permanent wilting point due to the predominance of clayey soils and shallow rooted plants (subsistence crops) in the study area. This study demonstrates that the use of small time steps in estimating groundwater recharge corresponds to a better approximation of reality and results in an increased recharge. However, given the clayey nature of the top soil, which implies a slow drainage, calculations on a daily basis may overestimate groundwater recharge. In this cas, calculations of groundwater recharge on a 10-day basis could be more appropriate in order to take into account slow drainage of clayey top soils. Moreover, a comparison of monthly estimates of groundwater recharge estimated using different PET methods to the estimate obtained using the standard Penman-Monteith PET on a daily basis (1999/2000-2008/2009) shows that, of all attempted PET methods, the TMWB method (185.40 mm), performs best as it fairly approximates recharge values obtained on a daily basis with Penman-Monteith PET (243.18 mm). This study draws the attention on the importance of errors which can be made by applying an inappropriate PET method while computing groundwater recharge using the soil moisture budget technique. The use of a small effective rooting depth of 0.25 m as suggested by Thornthwaite & Mather (1957) may not take into account the upwards movement of water from the wet subsoil to the dry top soil. Calculations of groundwater recharge using larger effective rooting depths of 0.50 m and 0.75 m result in reduced groundwater recharge**.** The comparison between the annual value of groundwater recharge obtained using the soil moisture balance method (TMWB model) for the calendar year 2008 (221.5 mm) and estimates of groundwater recharge obtained using the groundwater level fluctuation (121.6 mm) and the hybrid water level fluctuation (141.1 mm) methods shows that the two last methods underestimate groundwater recharge. The discrepancy between the two methods and the soil moisture balance method (TMWB model) is mainly due to the use of average values of specific yield and field capacity on one hand, and the fact that evapotranspiration from the groundwater table, which is not evaluated, may lead to a reduced rise of the groundwater level. The groundwater balance demonstrates that the exploitation of groundwater resources is still underdeveloped as it represents only 0.2 % of the recharge. This gives rise to an important baseflow (192.346 Mm^3/annum) which sustains the perennial complex of marshlands and shallow lakes in the Bugesera depression.

VIII.1.3. Hydraulic parameters

Pumping test and recovery data collected during two field campaigns were analysed using the software Aquifer Test Professional 4.2. Different analytical methods including: Theis (1945), Hantush (1960), Jacob-Cooper (1946), Papadopoulos & Cooper (1967), double porosity method and the specific capacity method were examined and compared. The analysis of pumping and recovery test data indicates a widespread conformity of the aquifer response to the Hantush analytical method (27 pumping tests), which confirms the hydrogeological model developed for the study area showing that leaky conditions should prevail. The conformity to the double porosity method is observed mainly in the western part of the study area and seems to be in agreement with the tectonic fracturing associated with the North-South trending fault, along which flows Kanyaru River. The wide variation of the transmissivity (1-377 m^2/d), hydraulic conductivity (0.1-166 m/d) and specific capacity (6.6-1133.6 m^2/d) values, even over short distances, reflects random variation of hydraulic parameters and the importance of heterogeneities which are typical of basement aquifers. The spatial distribution of hydraulic parameters across the three geological formations underlying the study area confirms that the Undifferentiated Complex Formation, which shows the highest hydraulic parameters, has the highest groundwater potential, in comparison to the two metasedimentary formations of Nyagisozi and Murehe. A regression analysis between specific capacity and transmissivity (from the best fit method) shows a strong correlation which is reflected by coefficients of determination of 0.98 and 0.95 respectively for the arithmetic and the log-log plots. This study sheds light to the fact that, despite a random distribution of hydraulic parameters, there are several prospective areas where hydraulic parameters reveal a good groundwater potential.

VIII.1.4. Groundwater flow system

The groundwater flow system in Bugesera region is defined based on the hydraulic head of groundwater in 157 wells and the topographic elevation of 126 springs located mainly in the southern part of the study area. An analysis of the groundwater flow pattern reveals both a local flow towards the perennial and ephemeral streams, and a more regional flow from the southern and eastern highlands towards the complex of marshlands and lakes, within the depression. The groundwater flow system shows a complex pattern which reflects the complexity of the topographic setting. The complex groundwater system can be simplified into 5 groundwater flow basins which are: the basins of Lake Rweru to the East, Lake Cohoha South in the centre, Lake Cohoha North in the North-East, River Navyamo and Lake Rwihinda in the South-West, and River Kanyaru and Lake Gacamirinda in North-West. An analysis of inter-annual variation of groundwater level fluctuation reveals a decreasing trend of groundwater level from 1991 to 2006, while between 2006 and 2008, a peak of groundwater level occurs in

2007. The inter-annual variation of groundwater level is in agreement with the estimates of annual recharge calculated from 1990/1991 to 2007/2008. On a seasonal scale, the analysis of monthly groundwater level fluctuations in 2008 shows the highest amplitudes (average: 0.90 m) in the northeastern part, whereas the lowest amplitudes (average: 0.34 m) occur in the central part of the study area. Intermediate amplitudes (average: 0.54m) are observed in the southwestern part of the study area. The peaks of seasonal groundwater level in the 3 parts of the study area occur in April, May and June respectively for the central, the northeastern and southwestern parts. Beside a possible spatial variability of rainfall, the occurrence of the peak of groundwater level at different times of the year implies different duration for the travel of the recharge, which confirms that the central part of the study area, where the peak of groundwater level occurs early (April), has the highest hydraulic conductivity. The northeastern and southwestern parts of the study area, which are underlain by metasedimentary formations (Nyagisozi and Murehe) where the peaks appear respectively in May and in June, have lower hydraulic conductivities.

VIII.1.5. Groundwater flow model

The steady state groundwater flow model of Bugesera region was successfully conceptualised, constructed, simulated and calibrated using the three dimensional finite difference code Visual Modflow V.3.0. The model domain was discretised into 3 layers, while the grid was defined as consisting of 225 rows and 278 columns with a spatial resolution of 180 m * 180 m for each grid cell. The calibration of the model through a trial and error process, consisting of manually altering the values of hydraulic parameters and the drain conductance, showed that the average hydraulic conductivity of 0.66 m/d calculated from the pumping tests was overestimated. A satisfactory matching between the calculated and measured hydraulic heads was achieved with an average hydraulic conductivity of 0.30 m/d and a drain conductance of 45 m^2/d, as reflected by the low RMSE (5.24 %), the residual mean error (0.42 m) and the standard error of estimate (0.56 m), which confirm the good convergence of the model given the complexity of the topography and the geological heterogeneities. The steady state groundwater flow confirms a regional groundwater flow trend towards the depression and a local flow component towards the myriad of perennial and ephemeral streams. The steady state hydraulic head contours reflect the strong control exerted by the complex topography over the groundwater flow. The discrepancy between the observed and calculated hydraulic heads is due mainly to the use of an average hydraulic conductivity which does not reflect the actual hydraulic conditions mainly in the southern highlands where the weathered overburden thins out or squarely disappears.

VIII.1.6. Hydrochemistry

The hydrogeochemical study is based on the analytical results of 143 water samples collected from hand-dug wells (66), springs (61) and the lakes (16). Overall, the relative abundance of the different dissolved constituents is in the following order: $Na^+ > Ca^{2+} > K^+ > Mg^{2+} > Fe^{2+} > Mn^{2+} > NH_4^+$ and $HCO_3^- > Cl^- > SO_4^{2-} > NO_3^- > NO_2^- > PO_4^{3-}$ for cations and anions respectively. The maps of the spatial distribution of the different hydrochemical parameters show a clear demarcation between the southern and eastern parts, where the low mineralisation (TDS = 26-142 mg/l) and low pH values (field pH = 4.6-6.6) of spring water samples indicate young waters of meteoric origin, and the depression where water samples collected mainly from wells reveal a high mineralisation (TDS = 44-3229 mg/l) and relatively high values of pH (field pH = 5.6-7.7) which correspond to long flowpaths and residence time. The simple classification of De Moor and De Breuck (1969) confirms the hydrogeochemical demarcation between the highlands, where water samples are systematically classified as very fresh (VF), and the depression where several water types: fresh (F), moderately fresh (MF), weakly fresh (WF), moderately brackish (MB) and brackish (B) are observed.

The classification based on the dominant cation and anion allows to deduce 10 water types of which $NaHCO_3$, NaCl, $CaHCO_3$ and $NaNO_3$ are the most abundant ones. The appearance of $NaNO_3$, $CaNO_3$, KNO_3 and $NaSO_4$ types reflect anthropogenic pollution which is reflected by high level of nitrates and sulphates, even in spring waters. The representation of the different water types in a Piper diagram enabled to visualise distinct clusters, which show that the group of lowly mineralised spring waters form the starting end member (NaCl) of the hydrogeochemical evolutionary sequence, which progressively shifts to different water types including $NaHCO_3$, $CaHCO_3$, $CaSO_4$, $NaSO_4$, $NaNO_3$, $CaNO_3$, CaCl, $KHCO_3$ and KNO_3. The hydrogeochemical evolution is controlled by several processes among which the weathering of aluminosilicates appears to be the most important, as this is substantiated by:

- the predominance of $NaHCO_3$ and $CaHCO_3$ water types,
- the projection of the 143 water samples in the stability diagrams for anorthite, albite and K-feldspar, which shows that most water samples are in thermodynamic equilibrium with kaolinite, and to a lesser extent with gibbsite.
- the projection of spring waters in the lower part of the stability diagrams, while water samples from wells and lakes fall in the upper parts, thus indicating the progressive increase of the parameter on the Y-axis, i.e. $\log\left(a_{Ca^{2+}}/a_{H^+}^2\right)$, $\log\left(a_{Na^+}/a_{H^+}\right)$ or $\log\left(a_{K^+}/a_{H^+}\right)$, as a consequence of increasing dissolution of aluminosilicate minerals along the flow path. This increase of the parameter on the Y-axis is accompanied by an increase of pH and TDS.

- the crossplots of the different hydrochemical parameters and particularly the good linear correlation between the EC and Na^+, Ca^{2+}, Mg^{2+} and HCO_3^-, which indicates that the concentration of these elements increases with increasing mineralisation of groundwater.
- the scatter plots of HCO_3^- versus Ca^{2+}, Na^+, Mg^{2+}, K^+; Ca^{2+} versus Na^+; Mg^{2+} versus Ca^{2+}; Mg^{2+} versus K^+; SO_4^{2-} versus Ca^{2+}; Cl^- versus Na^+.

The application of the concept of evapoconcentration reveals a progressive deficit in the sum of alkaline and alkaline earth cations ($Na^+ + K^+ + Ca^{2+} + Mg^{2+}$) and SiO_2, while HCO_3^- shows a slight increase. This deficit of cations reflects the overestimation of the concentration factor because the starting end member is not actually a genuine rain water end member, given the high levels of SiO_2 and NO_3^- in some water samples belonging to this class ($Cl^- < 10$ mg/l). The application of the concept of mixing of infiltrating water of meteoric origin with salt-influenced water shows an increasing surplus of the sum of alkaline and alkaline earth cations ($Na^+ + K^+ + Mg^{2+} + Ca^{2+}$), HCO_3^- and the TDS, which reflects the important contribution of the weathering of aluminosilicates. However, this concept aberrantly overestimates expected concentrations of SO_4^{2-}. It can be therefore concluded that the hydrochemical evolution of groundwater is only locally controlled by the evaporitic salt deposits

VIII.2. General recommendations

This study sheds enough light to the fact Bugesera region is not as "cursed" as local population seems to believe, especially with respect to drinking water resources. Despite the random variation of hydraulic parameters, which is normal for a basement aquifer, this study shows several prospective areas where the hydrogeological structure and hydraulic parameters reveal a good groundwater potential. Therefore, this study recommends the following investigations in order to overcome the challenge of providing enough and clean water to the population:

- Further geophysical investigations coupled with reconnaissance drillings in order to explore the groundwater potential of the fractured/weathered basement.
- To perform VES at prospective sites for well construction, which would focus on exploring the groundwater potential of both the weathered overburden and the fractured/weathered basement. Deepening wells up to the fractured/weathered basement may increase the yield of wells.
- More pumping tests with a representative coverage of the study area, for the sake of reliable and representative hydraulic parameters for the different hydrogeological units.

- A monitoring of groundwater water level fluctuations in Bugesera region using electronic data loggers would definitely give clues as regards to which time scale is appropriate for computing groundwater recharge using the soil moisture balance technique.
- A countrywide programme of regular monitoring of groundwater levels with high-performance equipments, such as electronic divers, especially in regions where potable water is still scarce like Bugesera, the plain of Imbo (Bujumbura) and the eastern depression of Moso. This would help decision-makers to follow closely the availability of this vital resource and to envision adequate measurements in case of severe depletion. This would provide another way of estimating recharge besides the routinely used soil moisture balance technique.
- A regular monitoring of water level fluctuation in the complex of marshlands and lakes, as well as the gauging of discharge in the few streams and rivers, should be undertaken in order to allow a better definition of the boundary conditions for groundwater flow model.
- A seasonal monitoring of groundwater quality to circumscribe the sources of pollution of groundwater is recommended.
- An analysis of heavy metals in groundwater samples in order to assess the impact of the mineralisations of coltan, cassiterite, gold and wolframite, which are being mined in the surroundings of and even inside the study area (e.g. Murehe), on groundwater quality would be very interesting ad important in the perspective of use as drinking water.
- In this study, only data from one weather station are used and assumed to be valid over the whole study area. It is the only weather station present in the area. Also, the long-term average recharge computed using the weather parameters from one station is uniformly applied over the whole study area. However, it was shown in the Chapter V, that the regional pattern indicates that there might be a climatic variability across the study area, with a decreasing trend of precipitation towards the centre of the depression of Bugesera. Hence, this study recommends the installation of a network of weather stations (at least rainfall stations) in order to capture and consider the spatial climatic differences in further investigations.

REFERENCES

Abrams, P., 2001. *The Water Page.* Accessed on 25/08/2011 from http: //www.africanwater.org/nile.htm.

Acworth, R.I., 1987. The development of crystalline basement aquifers in a tropical environment. *Quarterly Journal of Engineering Geology*, 20: 265–272.

Adyalkar, P. G.; Dias, J. P. & Rao, S., 1981. Empirical methods for evaluating hydraulic properties of basaltic water table aquifers with specific capacity values. *Indian Journal of Earth Sciences*, 8(1): 69-75.

Adyalkar, P. G. & Mani, V. V. S., 1972. An attempt at estimating the transmissibilities of trappean aquifers from specific capacity values. *Journal of Hydrology*, 17(3): 237-241.

Ahmad, N.; Sen, Z. & Ahmad, M., 2003. Ground water quality assessment using multi-rectangular diagrams. *Ground Water*, 41(6): 828-832.

Alkaeed, O.; Flores, C.; Jinno, K. & Tsutsumi, A., 2006. Comparison of several reference evapotranspiration methods for Itoshima Peninsula area, Fukuoka, Japan. *Memoirs of the Faculty of Engineering, Kyushu University*, 66(1): 1–14.

Allen, R.G.; Pereira, L.S.; Raes, D. & Smith, M., 1998. Crop evapotranspiration: guidelines for computing crop water requirements. *FAO Irrigation and Drainage Paper*, No. 56, Rome, Italy, 328 p.

Alley, W.M. & Leake, S.A., 2004. The journey from safe yield to sustainability. *Ground Water,* 42(1): 12–16.

Appelo, C.A.J. & Postma, D., 2005. Geochemistry, Groundwater and Pollution. Second edition. A.A., Balkema Publishers, 672 p.

Appelo, C.A.J. & Postma, D., 1993. Geochemistry, groundwater and pollution. A.A., Balkema, Rotterdam, 526 p.

APHA, 1992. Standard Methods for the Examination of Water and Wastewater. 18th edition, American Public Health Association (APHA), American Water Works Association (AWWA) and Water Pollution Control Federation (WPCF), Washington, D.C.

Aquastat, FAO Info, 2005. FAO's Information System on Water and Agriculture. http: //www.fao.org/nr/water/aquastat/countries_regions/burundi/indexfra.stm. Accessed on 16/09/2009.

Asmamaw, A., 2003. A regional scale assessment and modelling of water balance and soil erosion using global climate & internet geodata sets: (Case study of the Upper Rio Grande system, Bolivia). M.Sc. Thesis, International Institute for Geo-information Science and Earth Observation, Enschede, The Netherlands, 107 p.

Bakiewicz, W.; Milnen, D. M. & Pattle, A. D., 1985. Development of public tubewell designs in Pakistan. *Quarterly Journal of Engineering Geology and Hydrogeology,* 18(1): 63-77.

Barcelona, M.J.; Gibb, J. P.; Helfrich, J. A. & Garske, E. E., 1985. Practical guide for groundwater sampling. Illinois State Water Survey, ISWS Contract Report 374, 103 p.

Bannerman, R.R. & Ayibotele, N. B., 1994. Some critical issues with monitoring crystalline rock aquifers for groundwater management in rural areas. In: *Proceedings of the Harare Symposium, July 1984: Challenges in African Hydrology and water resources. IAHS publication*, 144: 47-56.

Barrat, J.M.; Mardhel, V.; Gutirrez, A.; Pinson, S.; Buscarlet, E. & Lallier, S., 2011. Cartes des potentialités en eaux souterraines du Burundi. Étude réalisée dans le cadre du Programme Sectoriel Eau ProSecEau – Burundi contrat n° 81124288007. BRGM/RC- 59751-FR mars 2011, 93 p.

Batelaan, O. & De Smedt, F., 2004. Seepage, a new MODFLOW Drain package. *Ground Water*, 42(4): 576-588.

Batte, A.G.; Muwanga, A.; Sigrist, P.W. & Owor, M., 2008. Vertical electrical sounding as an exploration technique to improve on the certainty of groundwater yield in the fractured crystalline basement aquifers of eastern Uganda. *Hydrogeology Journal*, 16: 1683-1693.

Baudet, D.; Hanon, M.; Lemonne, E. & Theunissen, K., 1989. Lithostratigraphie du domaine sédimentaire de la chaine Kibarienne au Rwanda. *Annales de la Société Géologique Belge*, 112: 225–246.

Bidou, J.E.; Ndayirukiye, S.; Ndayishimiye, J.P. & Sirven, P., 1991. Géographie du Burundi. Hatier, Paris, 288 p.

Bhadra, A.; Panigrah, N.; Singh, R.; Raghuwanshi, N.S; Mal, B.C. & Tripathi, M.P., 2008. Development of a geomorphologic instantaneous unit hydrograph model for scantily geuged watersheds. *Environmental Modeling & software*, 23: 1013-1025.

Bhadra, A.; Panigrahy, N.; Singh, R.; Raghuwanshi, N. S.; Mal, B.C. &. Tripathi, M.P., 2008.

Blaney, H. F. & Criddle, W. D., 1950. Determining water requirements in irrigated area from climatological irrigation data. *US Department of Agriculture, Soil Conservation Service, Technical Paper* No. 96, 48 p.

BLR Ingénierie, 2008. Kagera River basin monograph. Basin development report, final report, 332 p.

Bos, M.G.; Kselik, R.A.L.; Allen, R.G. & Molden, D., 2009. Water requirements for irrigation and the environment. Springer Science + Business Media B.V. 2009, 176 p.

Bourdet, D. & Gringarten, A. C., 1980. Determination of fissured volume and block size in fractured reservoirs by type-curve analysis. In: *Soc. Pet. Eng., Annu. Tech. Conf.* Dallas, TX, Sept. 21–24, 1980, *Pap. SPE 9293* (1980).

Bredehoeft, J.D., 2002. The water budget myth revisited: why hydrogeologists model. *Groundwater*, 40(4): 340-345.

Bredehoeft, J.D., 1997. Safe yield and the water budget myth. *Groundwater*, 35(6): 929.

Bredehoeft, J.D.; Papadopulos, S.S. & Cooper, Jr., 1982. The water-budget myth. In *Scientific basis of water Resources Management*, National Academic Press, pp. 51-57.

Buchwaldt, R.; Toulkeridis, Th.; Todt, W. & Ucakuwun, E.K., 2007. Crustal age domains in the Kibaran belt of SW-Uganda: combined zircon geochronology and Sm-Nd isotopic investigation. *Journal of African Earth Sciences,* 51: 4-20.

Cartes géologiques au 1/100 000 publiées: feuilles Ngozi, S3/29 SE (1983). Muyinga, S3/30 SW (1986) and Busoni, S3/30 NW-NE (1989). Cartes éditées par le Ministère des Travaux Publics, de l'Energie et des Mines du Burundi & le Département de Géologie et de Minéralogie du Musée Royal de l'Afrique Centrale (Belgique).

Castaneda, L. & Rao, P., 2005. Comparison of methods for estimating reference evapotranspiration in southern California. *Journal of Environmental Hydrology*, 13(14): 1-10.

Chenoweth, J., 2008. Minimum water requirement for social and economic development. *Desalination,* 22: 245–256.

Caubel-Forget, V.; Grimaldi, C. & Rouault, F., 2001. Contrasted dynamics of nitrate and chloride in groundwater submitted to the influence of a hedge. *Comptes Rendus de l'Académie des Sciences, Sciences de la Terre et des Planètes/ Earth and Planetary Sciences,* 332: 107–113.

Cazenave-Pierrot, A; Cazenave-Pierrot, F.; Acquier, J.L.; Capecchi, B.; Lopez, A.; Goulin, C.; Sirvin, P. & Nsabimana, S., 1979. Atlas du Burundi. Gradignan, (France): Association pour l'Atlas en Burundi, 138 p.

Chadha, D.K., 1999. A proposed new diagram for geochemical classification of natural waters and interpretation of chemical data. *Hydrogeology Journal*, 7: 431–439.

Chandra, S.; Ahmed, S.; Ram, A. & Dewandel, B., 2008. Estimation of hard rock aquifers hydraulic conductivity from geoelectrical measurements: a theoretical development with field application. *Journal of Hydrology*, 357(3–4): 218–227.

Chapman, D. & Kimstach, V., 1996. Selection of water quality variables. In: Deborah, C. (Ed.), Water quality assessments - A guide to use of biota, sediments and water in environmental monitoring. Second edition. Published on behalf of UNESCO, WHO & UNEP, Tylor and Francis Group, pp 74-133.

Chilton, J. & Seiler, K. P., 2006. Groundwater occurrence and hydrogeological environments. In*:* Schmoll, O., Howard, J., Chilton, J. & Chorus, I. (Eds.), *Protecting groundwater for health: managing the quality of drinking-water sources.* World Health Organization. Published by IWA Publishing, London, UK, 21-46.

Chilton, R. C. & Foster, S.S.D., 1995. Hydrogeological characterization and water supply potential of basement aquifers in tropical Africa. *Hydrogeology Journal*, 3(1): 36-49.

Chilton, R.C. & Smith-Carington, A.K., 1984. Characteristics of the weathered basement aquifer in Malawi in relation to rural water supplies. *IAHS Publication*, 144: 57-72.

Clabby, K.J.; Bradley, C.; Craig, M.; Daly, D.; Lucey, J.; McGarrigle, M.; O'Boyle, S.; Tierney, D. & Bowman, J., 2008. Water quality in Ireland 2004-2006. Environmental Protection Agency, Ireland. 300 p.

Coetsiers, M.; Kilonzo, F. & Walraevens, K., 2008. Hydrochemistry and source of high fluoride in groundwater of the Nairobi area, Kenya. *Hydrological Sciences Journal*, 53(6): 1230-1240.

Coetsiers, M. & Walraevens, K., 2006. Chemical characterization of the Neogene Aquifer, Belgium. *Hydrogeology Journal*, 14: 1556–1568.

Daliakopoulos, I. N.; Coulibaly, P. & Tsanis, I. K., 2005. Groundwater level forecasting using artificial neural networks. *Journal of Hydrology*, 309: 229–240.

Davis, S. N., 1969. Silica in streams and groundwater of Hawaii**.** *Technical report No. 29. Project completion report of identification of irrigation return water in the subsurface, OWRR project No. B-010-HI, Grant agreement No.* 14-01-001-1495, 37 p.

Deblond, A.; Punzalan, L.E.; Boven, A. & Tack, L., 2001. The Malagarazi Supergroup of SE Burundi and its correlative Bukoban Supergroup of NW Tanzania: Neo- and Mesoproterozoic chronostratigraphic constraints from Ar-Ar ages on mafic intrusive rocks. *Journal of African Earth Sciences*, 32: 435-449.

Deblond, A. & Tack, L., 1999. Main characteristics and review of mineral resources of the Kabanga–Musongati alignment in Burundi. *Journal of African Earth Sciences,* 29: 313–328.

Deblond, A., 1990: Late Kibaran layered igneous rocks from eastern Burundi. A Progress Report. *IGCP No. 255 Newsletter Bulletin*, 3: 9-17.

De Moor, G. & De Breuck, W., 1969. De freatische waters in het Oostelijk Kustgebied en in de Vlaamse vallei. *Natuurwet. Tijdschr.,* 51(1-2): 3-68, + 8 annexes.

De Vries, J.J. & Simmers, I., 2002. Groundwater recharge: an overview of processes and challenges. *Hydrogeology Journal*, 10: 5–17.

De Clercq, F.; Muchez, Ph.; Dewaele, S. & Boyce, A., 2008. The tungsten mineralisation at Nyakabingo and Gifurwe (Rwanda): preliminary results. *Geologica Belgica,* 11: 251-258.

Dewaele, S.; De Clercq, F.; Muchez, Ph.; Schneider, J.; Burgess, R.; Boyce, A. & Fernandez-Alonso, M., 2010. Geology of the cassiterite mineralisation in the Rutongo area, Rwanda (Central Africa): current state of knowledge. *Geologica Belgica*, 13(1-2): 91-112.

Dewandel, B.; Lachassagne, P.; Wyns, R.; Marechal, J-C. & Krishnamurthy, N.S., 2006. A generalized 3-D geological and hydrogeological conceptual model of granite aquifers controlled by single or multiphase weathering. *Journal of Hydrology*, 330: 260–284.

Dhiman, S. D. & Keshari, A. K., 2006. Hydrogeochemical evaluation of high-fluoride groundwaters: a case study from Mehsana District, Gujarat, India. *Hydrological Sciences Journal,* 51(6): 1149-1162.

Diop, S. & Tijani, M. N., 2008. Assessing the basement aquifers of eastern Senegal. *Hydrogeology Journal*, 16: 1349-1369.

Dixon, S.A. & Custer, S.G., 2002. Measure of aquifer transmissivity and a test of the hydrogeologic units in Gallatin local water quality district, Gallatin County, Montana. Denver annual meeting, 27-30 October 2002. Abstract available online at: http: //gsa.confex.com/gsa/2002AM/finalprogram/abstract_43392.htm. Cited on 10/09/2010

Domenico, P.A. & Schwartz, F.W., 1990. Physical and chemical hydrogeology. John Wiley & Sons, 824 p.

Domenico, P.A., 1972. Concepts and models in groundwater hydrology. McGraw-Hill, New York, 405 p.

Drever, J. I., 1997. The geochemistry of natural waters: surface and groundwater environments, third edition. Prentice-Hall, New Jersey, USA, 436 p.

Duchesne, J.C.; Liégeois, J.P.; Deblond, A. & Tack, L., 2004. Petrogenesis of the Kabanga-Musongati layered mafic-ultramafic intrusions in Burundi (Kibaran Belt): geochemical, Sr–Nd isotopic constraints and Cr–Ni behaviour. *Journal of African Earth Sciences,* 39: 133–145.

Eby, G.N., 2004. Principles of environmental geochemistry. Thomson Brooks/Cole, Kentucky, USA, 514 p.

El-Fahem, T., 2008. Hydrogeological conceptualisation of a tropical river catchment in a crystalline basement area and transfer into a numerical groundwater flow model - Case study for the Upper Ouémé catchment in Benin -. PhD dissertation, Rheinischen Friedrich–Wilhelms–Universität Bonn, 143 p.

El-Naqa, A., 1994. Estimation of transmissivity from specific capacity data in fractured carbonate rock aquifer, central Jordan. *Environmental Geology*, 23(1): 73-80.

Fabbri, P., 1997. Transmissivity in geothermal Euganean basin: a geostatistical analysis. *Ground Water*, 35: 881-887.

Environmental Protection Agency (EPA), 2004. European Communities. Drinking water regulation, 2000 (S. I. 439 of 2000), a handbook on implementation for sanitary authorities, 155 p.

FAO, 2006. Guidelines for soil description. Fourth edition, 97 p.

FAO, 2005. Aquastat, FAO's Information System on Water and Agriculture. http: //www.fao.org/nr/water/aquastat/countries_regions/burundi/indexfra.stm. Accessed on 16/09/2009.

FAO, 2003. Africover project. Multipurpose Africover databases on environmental resources (MADE) available for 10 countries. Available online at http: //www.africover.org.

Fergusson, B.K. & Debo, T.N., 1990. On-site stormwater management, applications for landscape and engineering, second edition.Van Nostrand Reinhold, New York, 270 p.

Fernandez-Alonso, M.; Dewaele, B.; Tahon, A.; Dewaele, S.; Baudet, D.; Cutten, H. & Tack, L., 2009. The Northeastern Kibaran Belt (NKB): a 1250 Ma-long Proterozoic intracratonic history in Central Africa punctuated by two orogenic events at c.1.0 and 0.55 Ga. Rodinia: Supercontinents, Superplumes and Scotland. *Geological Society London Fermor Meeting, Edinburgh, Scotland, 6–13 September 2009.* Abstracts volume, p. 22.

Fernandez-Alonso, M.; Tack, L.; De Waele, B.; Cutten, H.; Baudet, D. & Tahon, A., 2006. The NE Kibaran Belt (NKB): New uniform stratigraphies and GIS-compiled geological map. *21st Colloquium African Geology (CAG21), 03-05.07.2007, Maputo, Mozambique*. Abstract book: 48- 49 (Poster).

Fernandez-Alonso, M. & Theunissen, K., 1998. Airborne geophysics and geochemistry provide new insights in the intracontinental evolution of the Mesoproterozoic Kibaran belt (Central Africa). *Geological Magazine*, 135: 203–216.

Fetter, C.W., 2001. Applied Hydrogeology, 4th Edition, Prentice Hall, 2001, 598 p.

Finn, M.D.; Gross, M.R.; Eyal, Y. & Draper, G., 2003. Kinematics of throughgoing fractures in jointed rocks. *Tectonophysics*, 376: 151– 166.

Flint, A. L.; Flint, L.E.; Kwicklis, M. E.; Fabryka-Martin, J.T. & Bodvarsson, G.S.; 2002. Estimating recharge at Yucca Mountain, Nevada, USA: comparison of methods. *Hydrogeology Journal*, 10: 180–204.

Foster, S.; Smedley, P. & Candela, L., 1999. Hydrology and water management in the humid tropics. In: Gladwell, J. S.; Fischer, J. & Vargas, R. (Eds.), Hydrology and water management in the humid tropics. Proceedings of the second international colloquium on hydrology and water management in the humid tropics 22 – 26 March 1999, Panama, Republic of Panama. *IHP-V, Technical Documents in Hydrology*, 52: 441-474.

Foster, S.S.D., 1984. African groundwater development - the challenges for hydrogeological science. In: *Challenges in African Hydrology and Water Resources.* Proceedings of the Harare Symposium, July 1984. *IAHS Publication*, 144: 3-12.

Franke, O.L.; Reilly, T.E. & Bennett, G.D., 1987. "Chapter B5", Definition of Boundary and Initial Conditions in the Analysis of Saturated Ground-Water Flow Systems – An Introduction, Book 3, Applications of Hydraulics, U.S. Geological Survey.

Freeze, R. A. & Cherry, J. A., 1979. *Groundwater*. Prentice-Hall, Inc., Englewood Cliffs, New Jersey, 604 p.

Ganyaglo, S.; Y.; Banoeng-Yakubo, B.; Osae, S.; Dampare, S. B.; Fianko, J. R. & Bhuiyan, J.R.F., 2010. Hydrochemical and isotopic characterisation of groundwaters in the Eastern region of Ghana. *Journal of Water Resource and Protection*, 2: 199-208.

Garrels, R. M. 1984. Montmorillonite/illite stability diagrams. *Clays and Clay Minerals*, 32: 161-166.

Gibbs, M.M., 1979. A simple method for the rapid determination of iron in natural waters. *Water Research*, 13(3): 295-297.

Goel, P. K., 2006. Water pollution - causes, effects & control. New Age International Publisher, 413 p.

GEOSCI, 2001. Etude sur la disponibilité en eau potable en province de Kirundo. Volets Géologie, Hydrogéologie et. Géophysique. Rapport définitif, 79 pages + Annexes.

Giddelo, C. S.; Arndt, A. D. & Volckaert, F. A. M., 2002. Impact of rifting and hydrogeography on the genetic structure of Clarias gariepinus in eastern Africa. *Journal of Fish Biology*, 60: 1252–1266.

Giambelluca, T.W. & Oki, D. S., 1987. Temporal disaggregation of monthly rainfall data for water balance modelling. *Proceedings of the Vancouver Symposium, August 1987: The influence of climate change and climatic variability on the hydrology regime and water resources. IAHS Publication,* 168: 255-267.

Gonzalez-Dugo, M.P.; Neale, C.M.U.; Mateos, L.; Kustas, W.P.; Prueger, J.H.; Anderson, M.C. & Li, F., 2009. A comparison of operational remote sensing-based models for estimating crop evapotranspiration. *Agricultural and Forest Meteorology*, 149: 1843–1853.

Govindaraju, R. S., 2000. Artificial neural networks in hydrology I: Preliminary concepts. *Journal of Hydrologic Engineering,* 5: 115-123.

Govindaraju, R. S. & Rao, A.R., 2000: Artificial Neural Networks in Hydrology. *Series: Water Science and Technology Library, Vol. 36.* Kluwer Academic Publisher, 348 p.

Güler, C.;, Thyne, G. D.; McCray, J. E. & Turner, A. K., 2002. Evaluation of graphical and multivariate statistical methods for classification of water chemistry data. *Hydrogeology Journal,* 10: 455–474.

Guitjens, J. C., 1982. Models of Alfalfa Yield and Evapotranspiration. *Journal of the Irrigation and Drainage Division, Proceedings of the American Society of Civil Engineers*, 108(3): 212–222.

Hakiza, G., 2002. Potentialités aquifères de la plaine de la Rusizi. PhD dissertation, Université de Liège, Facultés des Sciences Appliquées, 405 p.

Haitjema, H.M. & Mitchell-Bruker, S., 2005. Are water tables a subdue replica of the topography? *Groundwater,* 43(6): 781-786.

Halford, K. J.; Weight, W. D. & Schreiber, R. P., 2006. Interpretation of transmissivity estimates from single-well pumping aquifer tests. *Ground Water*, 44(3): 467-471.

Halford, K.J. & Hanson, R.T., 2002. User Guide for the Drawdown-Limited, Multi-Node Well (MNW) Package for the U.S. Geological Survey's Modular Three-Dimensional Finite-Difference Ground-Water Flow Model, Versions MODFLOW-96 and MODFLOW-2000. U.S. GEOLOGICAL SURVEY. Open-File Report 02-293, 39 p.

Hamm, S.-Y.; Cheong, J.-Y.; Jang, S.; Jung, C.-Y. & Kim, B.-S., 2005. Relationship between transmissivity and specific capacity in the volcanic aquifers of Jeju Island, Korea. *Journal of Hydrology*, 310: 111-121.

Hamon, W. R., 1963. Computation of direct runoff amounts from storm rainfall. *International Association of Scientific Hydrology Publication,* 63: 52-62.

Harbaugh, J.W.; Banta, E.R.; Hill, M.C. & McDonald, M.G., 2000. MODFLOW-2000. The U.S. Geological Survey's modular ground-water flow model—User guide to modularization concepts and the ground-water flow process: U.S. Geological Survey Open-File Report 00–92, 121 p.

Harbeck, G. E. Jr., 1962. A practical field technique for measuring reservoir evaporation utilizing mass transfer theory. *United States Geological Survey Professional Paper, 272*(E): 101–105.

Hargreaves, G.L. & Samani, Z.A., 1982. Estimating potential evapotranspiration. *Journal of Irrigation and Drainage Engineering*, 108(3): 225–230.

Healy, R.W.; Gray, J.R.; de Vries, M.P. & Mills, P.C., 1989. Water balance at a low level radioactive disposal site. *Water Resource Bulletin*, 25(2): 381-390.

Heath, R.C., 1982. *Basic Groundwater Hydrology*: U.S. Geological Survey, *Water Supply Paper* 2220, 84 p.

Hill, M. J., 1991. Nitrates and nitrites in food and water. Woodhead Publishing Limited, 208 p.

Hirotsugu, A., 2003. Household water consumption and the incidence of diarrhoea. Lessons learned from a case study of the urban poor in Manila. Technical paper presented to WHO/EMRO consultation meeting on minimum household water security requirements and health, Amman, Jordan, 1-3 December 2003, 15 p.

Hossain, G.; Howladar, M. F.; Nessa, L.; Ahmed, S. S. & Quamruzzaman, C., 2010. Hydrochemistry and classification of groundwater resources of Ishwardi Municipal area, Pabna District, Bangladesh. *Geotechnical and Geological Engineering*, 28: 671–679.

Huang, M.; Jacques, G.; Wang, Z. & Monique, G., 2006. A modification to the soil conservation service curve number method for steep slopes in the Loess Plateau of China. *Hydrological processes,* 20(3): 579-589.

Hudak, P.F., 1994. Effective porosity of unconsolidated sand: estimation and impact on capture zone geometry. *Environmental Geology*, 24: 140-143.

Hughes, R.H.; Hughes, J.S. & Bernacsek, G., 1992. Répertoire des zones humides d'Afrique. UICN, Gland, Suisse et Cambridge, Royaume Uni / PNUE, Nairobi, Kenya / CMSC, Royaume Uni xxiv + 808 p. ISBN 2-88032-949-3.

Humphries, M.S.; Kindness, A.; Ellery, W. N. & Hughes, J.C., 2011. Water chemistry and effect of evapotranspiration on chemical sedimentation on the Mkuze River floodplain, South Africa. *Journal of Arid Environments,* 75: 555-565.

Huntley, D.; Nommensen, R. & Steffey, D., 1992. The use of specific capacity to assess transmissivity in fractured-rock aquifers. *Gound Water*, 30(3): 396-402.

Hygecel Ingénieurs conseils, 2005. Etude d'identification pour l'amélioration des services d'eau et d'assainissement dans les provinces de Kirundo et Mwaro, dossier technique 2/13: Commune Busoni. Rapport final, 17 p.

Jabloun, M. & Sahli, A., 2008. Evaluation of FAO-56 methodology for estimating reference evapotranspiration using limited climatic data. Application to Tunisia. *Agricultural Water Management,* 95: 707-715.

Jacks, G.; Bhattacharya, P.; Chaudhary, V. & Singh, K.P., 2005. Controls on the genesis of some high-fluoride groundwaters in India. *Applied Geochemistry,* 20: 221–228.

Jalludin, M. & Razack, M., 2004. Assessment of hydraulic properties of sedimentary and volcanic aquifer systems under arid conditions in the Republic of Djibouti (Horn of Africa). *Hydrogeology Journal*, 12: 159-170.

Jarvis, A.; Reuter, H.I; Nelson, A & E. Guevara, E., 2006. Hole-filled SRTM for the globe, Version 3. CGIAR-CSI SRTM 90 M Database. Available at: http: //srtm.csi.cgiar.org. Accessed on 25 March 2010.

Jatau, B.S. & Bajeh, I., 2008. Hydrogeological appraisal of parts of Jemaa local Government Area, North-Central Kaduna State, Nigeria. *Research Journal of Applied Sciences*, 2(11): 1174-1181.

Jha, M. K.; Jayalekshmi, K.; Machiwal, D.; Kamii, Y. & Chikamori, K., 2004. Determination of hydraulic parameters of an unconfined alluvial aquifer by the floodwave-response technique. *Hydrogeology Journal*, 12: 628–642.

Johnson, A. I.; Moston, R. P. & Versaw, S. F., 1966. Laboratory study of aquifer properties and well design for an artificial recharge site: U.S. Geological Sure by *Water Supply Paper*, no. 1615-H, pp. H23-H25.

Justin, J.D., 1915. Derivation of runoff from rainfall data. Transaction. ASCE 77, 346.

Ministère de l'Aménagement du Territoire et de l'Environnement, République du Burundi, 2000. Convention cadre des Nations Unies sur les changements climatiques, première communication nationale. Unpublished report, 105 p.

Kabundege, G., 1999. Etude hydrologique et hydrogéologique du secteur Ntega (Kirundo), Mémoire de licence inedit, Université du Burundi, Département des Sciences de la Terre, 113 p.

Kalf, F.R.P. & Woolley, D.R., 2005. Applicability and methodology of determining sustainable yield in groundwater systems. *Hydrogeology Journal,* 13: 295–312.

Kendy, E.; Gérard -Marchant, P.; Walter, M.T.; Zhang, Y.; Liu, C. & Steenhuis, T.S., 2003. A soil-water balance approach to quantifying groundwater recharge from irrigated cropland in the North China Plain. *Hydrological Processes* 17: 2011–2031.

Khalil, M.; Sakai, M.; Mizoguchi, M. & Miyazaki, T., 2003. Current and prospective applications of zero flux plane (ZFP) method*. Journal of the Japanese Society of Soil Physics,* 95: 75-90.

Khan, M. M. A & Umar, R., 2010. Significance of silica analysis in groundwater in parts of Central. *Current science,* 98(9): 1237-1240.

Kitching, R.; Edmunds, W.M.; Shearer, T. R.; Walton, N.R.G. & Jacovides, J., 1980. Assessment of recharge to aquifers; *Hydrological Sciences Bulletin,* 25: 217-235.

Kitching, R. & Shearer, T.R., 1982. Construction and operation of a large undisturbed lysimeter to measure recharge to the chalk aquifer, England. *Journal of Hydrology,* 56: 267- 277.

Kitching, R.; Shearer, T.R.; Shedlock, S.L., 1977. Recharge to Bunter sandstone determined from lysimeters. *Journal of Hydrology*, 33: 217–232.

Klerkx, J.; Liégeois, J.P.; Lavreau, J. & Theunissen, K., 1984. Granitoides kibariens précoces et tectonique tangentielle au Burundi: magmatisme bimodal lié a une distention crustale. In: Klerkx, J. & Michot, J. (Eds.), *African Geology*, a Volume in honour of Lucien Cahen. Royal Museum for Central Africa, Tervuren, pp. 29–46.

Klerkx, J.; Liégeois, J.-P.; Lavreau, J. & Claessens, W., 1987. Crustal evolution of the northern Kibaran Belt, eastern and central Africa. In: Kröner, A. (Ed.), *Proterozoic Lithospheric Evolution*. *American Geophysical Union and the Geological Society of America*, 17: 217–233.

Klerkx, J.; Theunissen, K. & Delvaux, D., 1998. Persistent fault controlled basin formation since the Proterozoic along the western branch of the East African Rift. *Journal of African Earth Sciences*, 26: 347–361.

Kokonyangi, J.; Okudaira, T.; Kampunzu, A.B. & Yoshida, M., 2001. Geological evolution of the Kibaride belt, Mitwaba, Democratic Republic of Congo, Central Africa. *Gondwana Research,* 4: 663-664.

Kokonyangi, J.; Armstrong, R.A.; Kampunzu, A.B.; Yoshida, M. & Okudaira, T., 2004. U–Pb zircon geochronology and petrology of granitoids from Mitwaba (Katanga, Congo): implications for the evolution of the Mesoproterozoic Kibaran belt. *Precambrian Research*, 132: 79-106.

Kokonyangi, J. W.; Kampunzu, A.B.; Armstrong, R.; Yoshida, M.; & Okudaira, T.; Arima, M. & Ngulube, D. A., 2006. The Mesoproterozoic Kibaride belt (Katanga, D.R. Congo). *Journal of African Earth Sciences*, 46: 1-35.

Kommadath, A., 2000. Estimation of natural groundwater recharge. In*:* Ramachandra, T.V, Murthy C.R. & Ahlya, N. *(*Eds.*), Groundwater and Hydrogeology*. *Proceedings of Lake 2000. International symposium on restoration of lakes and wetlands, 27th to 29th November 2000, CSIC Auditorium, Indian Institute of Science, Bangalore,* 80-91.

K'Orowe, M.O.; Singh, V.S.; Rao, V.A. & Dhakate, R., 2008. *Current Science*, 95(8): 1067-1071.

Krasny, J., 1993. Classification of transmissivity magnitude and variation. *Ground Water*, 31(2): 231-236.

Krishnamurthy, N.S.; Rao, V.A.; Kumar, D.; Singh, K.K.K & Ahmed, S., 2009. Electrical resistivity imaging technique to delineate coal seam barrier thickness and demarcate water filled voids. *Journal of the Geological Society of India*, 73(5): 639-650.

Kruseman, G. P. & de Ridder, N. A., 1994. Analysis and Evaluation of Pumping Test Data. Second Edition. International Institute for Land Reclamation and Improvement, Wageningen, The Netherlands, 377 p.

Kumar, R.; Chatterjee, C.; Singh, R.D.; Lohani1, A.K; & Kumar, S., 2007. Runoff estimation for ungauged catchments using GIUH. *Hydrological Processes*, 21, 1829–1840.

Languimir, D.1997. Aqueous environmental geochemistry. Prentice Hall, New Jersey, 600 P.

Mahvi, A. H.; Nouri, J.; Babaei, A. A. & Nabizadeh, R., 2005. Agricultural activities impact on groundwater nitrate pollution. *International Journal of Environmental Science and Technology*, 2(1): 41-47.

Lee, C.H., 1915. The determination of safe yield of underground reservoirs of the closed basin type. *Transactions, American Society of Civil Engineers*, 78: 148-251.

Limpert, E.; Stahel, W. A. & Abbt, M., 2001. Log-normal distributions across the sciences: Keys and clues. *Bioscience*, 51(5): 341-352.

Logan, J., 1964. Estimating transmissibility from routine production tests of water wells. *Ground Water,* 2(1): 35–37.

Lopez-Urrea, R.; Martin de Santa, O.F.; Fabeiro, C. & Moratalla, A., 2006. Testing evapotranspiration equations using lysimeter observations in a semiarid climate. *Agricultural Water Management*, 85: 15-26.

Lloyd. J.W., 1999. Water resources of hard rock aquifers in arid and semi-arid zones. *Studies and reports in Hydrology series*, no. 58, UNESCO Publishing, 284 p.

MacDonald, A.M. & Davies, J.A., 2000. Brief review of groundwater for rural water supply in sub- Saharan Africa. *British Geological Survey technical report WC/00/33,* 30 p.

MacDonald, A.; Davies, J.; Calow, R. & Chilton, J., 2005. Developing groundwater: a guide for rural water supply. ITDG Publishing, Rugby, UK, 358 p.

Mace, R. M.; Chowdhury, A. H.; Anaya, R. & Way, S-C., 2000. Groundwater availability of the Trinity aquifer, Hill Country area, Texas: numerical simulations trough 2050. Texas Water Development Board, final report, 174 p.

Mace, R. E.; Smyth, R. C.; Xu, L. & Liang, J., 1999. Transmissivity, Hydraulic Conductivity, and Storativity of the Carrizo-Wilcox Aquifer in Texas. Draft technical report submitted to the Bureau of Economic Geology, The University of Texas at Austin, Texas 78713-8924.

Mace, R. E., 1997. Determination of transmissivity from specific capacity tests in a Karst aquifer. *GroundWater,* 25(5): 738-742.

Mace, R. E.; Nance, H. S. & Dutton, A. R., 1994. Geologic and hydrogeologic framework of regional aquifers in the Twin Mountains, Paluxy, and Woodbine Formations near the SSC site, North-Central Texas: Draft technical report submitted to the TNRLC under contract no. IAC(92-93)-0301 and no. IAC 94-0108, 48 p.

Makkink, G.F., 1957. Testing the Penman formula by means of lysimeters. *Journal of the Institution of Water Engineers,* 11: 277-288.

Maréchal, J. C.; Varma, M.R.R.; Riotte, J.; Vouillamoz, J.M.; Kumar, M.S.M.; Ruiz, L.; Sekhar, M. & Braun, J.J., 2008. Indirect and direct recharges in a tropical forested watershed: Mule Hole, India. *Journal of Hydrology*, 364: 272–284.

Maréchal, J-C., 2010. Editor′s message: the sunk cost fallacy of deep drilling. *Hydrogeology Journal*, 18: 287–289.

Matthess, G., 1982. The properties of groundwater. A Wiley-Interscience Publication, John Wiley & Sons, 399 p.

McCabe, G.J. & Markstrom, S.L., 2007. A monthly water-balance model driven by a graphical user interface. *U.S. Geological Survey Open-File report 2007-1088*, 6 p.

Mjemah, I. C.; Van Camp, M. & Walraevens, K., 2009. Groundwater exploitation and hydraulic parameter estimation for a Quaternary aquifer in Dar-es-Salaam Tanzania. *Journal of African Earth Sciences*, 55: 134-146.

Miettinen, I. T.; Vartiainen, T. & Martikainen, P. J., 1997. Phosphorus and bacterial growth in drinking water. *Applied and Environmental Microbiology,* 63(8): 3242-3245.

Ministère de la Planification du Développement et de la Reconstruction Nationale, 2006. Monographie de la commune Kirundo. Upublished report, 62 p.

Misstear, B.D.R., 2000. Groundwater recharge assessment: a key component of river basin management. In: Irish National Committees of the International Hydrology Programme and the

International Committee for Irrigation and Drainage (Ed.), *Proceedings of National Hydrology Seminar on River Basin Management*, Tullamore, 21 November 2000, 52–59.

Moeyersons, J., 1977. Quelques problèmes relatifs à la morphologie du Rwanda et du Burundi. Musée Royal pour l'Afrique Centrale, Tervuren (Belgique), Département de Géologie et Minéralogie, Rapport annuel 1976, pp.129-142.

Moeyersons, J., 1979 (a). Quelques remarques sur le développement de la dépression du Bugesera au Rwanda. Musée Royal de l'Afrique Centrale, Tervuren (Belgique), Département de Géologie et Minéralogie, Rapport annuel 1978: 127-134.

Moeyersons, J., 1979 (b). Surface d'applanissement, anciens bassins hydrographiques et mouvements tectoniques post-précambriens au Rwanda. *Bulletin de la Société Belge de Géologie*, Tome 88, fascicule 2: 87-96.

Nahimana, L., 1993. Dépots évaporitiques dans les sédiments de la basse Rusizi. Université du Burundi, Département des Sciences de la Terre. Unpublished data.

Nkotagu, H., 1996. The groundwater geochemistry in a semi-arid, fractured crystalline basement area of Dodoma, Tanzania. *Journal of African Earth Sciences*, 23(4): 593-605.

Ntakimazi, G., 1985. Hydrobiologie du Bugesera (Akagera-Haut-Nil), en particulier les lacs Cohoha Sud et Rweru en vue d'une gestion qualitative de la faune piscicole. PhD dissertation, Fondation Universitaire Luxembourgeoise, Volume I, 225 p + appendices.

Nyagwambo, N.L., 2006. Groundwater recharge estimation and water resources assessment in a tropical crystalline basement aquifer. PhD dissertation, Delft University of Technology, Netherlands, 182 p.

Nzeyimana, L., 2003. Rusumo dam-social challenge in Kagera River Basin: participation of the affected people. Unpublished MSc thesis, Linköping University, Department of Water and Environmental Studies, Sweden, 65 p.

Nzigidahera, B.; Fofo, A. & Misigaro A., 2005. Paysage aquatique protégé du Nord du Burundi, étude d'identification. Institut National pour l'Environnement et la Conservation de la Nature, I.N.E.C.N. Unpublished report, 95 p. Available online at: http: //bch-cbd.naturalsciences.be/burundi/contribution/paysageaquatique.pdf.

Olayinka, A.I. & Mbachi, C.N.C., 1992. A technique for the interpretation of electrical sounding from crystalline basement areas of Nigeria. *Journal of Mining and Geology*, 27: 63-69.

Olayinka, A.I. & Sogbetum A.O., 2002. Laboratory measurements of the electrical resistivity of some Nigerian Crystalline basement complex rocks. *African Journal of Science and Technology,* 3: 93–97.

Panabokke, C. R.; Ariyaratne, B. R.; Seneviratne, A. A. A. K. K.; Wijekoon, D. & Molle, F., 2007. Characterization and monitoring of the regolith aquifer within four selected cascades (subwatersheds) of the Malala Oya Basin: *International Water Management Institute (IWMI), Colombo, Sri Lanka, Working Paper 12,* 45 p.

Parkhurst, D.L. & Appelo, C.A.J., 1999. User's guide to phreeqc (version 2) – a computer program for speciation, batch-reaction, one-dimensional transport, and inverse geochemical calculations. USGS Water Resources Investigation Report 99-4259, pp. 310.

Patil, J.P.; Sarangi, A.; Singh, O.P. & Ahmad, T., 2008. Development of a GIS interface for estimation of runoff from Watersheds. *Water Resources Management,* 22: 1221–1239.

Pauwels, J. M.; Van Ranst, E, Verloo, M. G. & Mvondo, Z.A., 1992. Manuel de laboratoire de pedologie. Méthodes d'analyses de sols et de plants, équipement, gestion des stocks de verrerie et de produits chimiques. Publications agricoles 28. Administration générale de la Coopération au Développement, Bruxelles, 265 p.

Peeters, L., 1957. Contribution à l'étude de la genèse du lac Kivu. *Bulletin Société Belge Etudes Géographiques,* 26(1): 155-168.

Pereira, A.R. & Pruitt, W.O., 2004. Adaptation of the Thornthwaite scheme for estimating daily reference evapotranspiration. *Agricultural Water Management*, 66: 251–257.

Petrich, C.R., 2004. Simulation of groundwater flow in the lower Boise river basin. Idaho Water Resources Research Institute. *Research report,* 142 p.

Petrides, B.; Cartwright, I. & Weaver; T.R., 2006. The evolution of groundwater in the Tyrrell catchment, south-central Murray Basin, Victoria, Australia. *Hydrogeology Journal,* 14: 1522-1543.

Phillips, W. S., 1963. Depth of roots in soil. *Ecology,* 44(2): 424.

Piper, A.M., 1944. A graphic procedure in the geochemical interpretation of water analyses. *Transactions of the American Geophysical Union,* 25: 914-928.

Pohl, W. & Günther, M.A., 1991. The origin of Kibaran (late Mid-Proterozoic) tin, tungsten and gold quartz vein deposits in Central Africa: a fluid inclusions study. *Mineralium Deposita*, 26: 51-59.

Pohl, W., 1987. Metallogeny of the northeastern Kibaran belt, Central Africa. *Geological Journal*, 22(S2): 103-119.

Pouclet, A., 1978. Les communications entre les Grands Lacs de l'Afrique Centrale. Implications sur la structure du Rift Occidental, *Rapport Annuel 1977*, Département de Géologie et Minéralogie, Musée Royal de l'Afrique Centrale, Tervuren, Belgique, pp. 145–155.

Prasad, K.L. & Rastogi, A.K., 2001. Estimating net aquifer recharge and zonal hydraulic conductivity values for Mahi Right Bank canal project area, India by genetic algorithm. *Journal of Hydrology,* 243: 149–161.

Priestle, C.H.B. & Taylor, R.J., 1972. On the assessment of surface heat flux and evaporation using large-scale parameters. *Monthly Weather Review,* 100(2): 81–92.

Raes, D.; Steduto, P.; Hsiao, T.C. & Fereres, E., 2010. *Reference manual, chapter 2-AquaCrop, Version 3.1.*Accessed online on 16 September 2011 at http: //www.fao.org/nr/water/docs/aquacrop3_1/AquaCropV31Chapter2.pdf.

Rafique, T.; Naseem, S.; Bhanger, M. I. & Usmani, T. H., 2008. Fluoride ion contamination in the groundwater of Mithi sub-district, the Thar Desert, Pakistan. *Environmental Geology,* 56: 317–326.

Rajurkar, M.P.; Kothyari, U.C. & Chaube, U.C., 2004. Modeling of the daily rainfall-runoff relationship with artificial neural network. *Journal of Hydrology*, 285: 96–113.

Ramakrishnan, D.; Bandyopadhyay, A. & Kusuma, K.N., 2009. SCS-CN and GIS-based approach for identifying potential water harvesting sites in the Kali watershed, Mahi River basin, India. *Journal of Earth System Science*, 118(4): 355-368**.**

Rao, N. S. & Prasad, P. R., 1997. Phosphate pollution in the groundwater of lower Vamsadhara river basin, India. *Environmental Geology,* 31(1/2): 117-122.

Ratto, G. E.; Videla, F.; Maronna, R.; Flores, A & Davila, F. D. P., 2010. Air pollutant transport analysis based on hourly winds in the city of La Plata and surroundings, Argentina. *Water, Air, and Soil Pollution*, 208: 243–257.

Ray, R. K. & Mukherjee, R., 2008. Reproducing the Piper trilinear diagram in rectangular coordinates. *Ground Water*, 46(6): 893-896.

Razack, M. & Huntley, D., 1991. Assessing transmissivity from specific capacity in a large and heterogeneous alluvial aquifer. *Ground Water*, 29(6): 856-861.

Razack, M. & Lasm, T., 2006. Geostatistical estimation of the transmissivity in a highly fractured metamorphic and crystalline aquifer (Man-Danane Region, Western Ivory Coast). *Journal of Hydrology*, 325: 164-178.

République du Burundi, 2011. Cadre stratégique de croissance et de lutte contre la pauvreté - deuxième génération, 148 p.

Reilly, T.E., 2001. System and boundary conceptualization in ground-water flow simulation. Techniques of water resources investigations of the U.S. Geological Survey, Book 3, applications of hydraulics, Chapter B8, 38 p.

Reynolds, J.M., 1997. An introduction to applied and environmental geophysics. John Wiley & Sons Ltd, Chichester & London, 796 p.

Ritter, M.E., 2006. The physical environment: An introduction to Physical Geography. Accessed online, on 31/01/2010 at http: //www.uwsp.edu/geo/faculty/ritter/geog101/textbook/title_page.html.

Robie, R.A.; Hemingway, B.S. & Fisher, J.R., 1979. Thermodynamic properties of minerals and related substances at 298.15°K and 1 bar (10^5 Pa) pressure and at higher temperature. *United States Geological Survey Bulletin*, 1452, 456 p.

Robie, R.A. & Waldbaum, D.R., 1968. Thermodynamic properties of minerals and related substances at 298.15°K (25°C) and one atmosphere (l.013 bars) pressure and at higher temperatures. *United States Geological Survey Bulletin,* 1259: 256 p.

Ross, A.M.; Williams, M.N.; Talham, D.R. & Keaffaber, J.J., 2010. Zirconium phosphate and phosphonate nanoparticles for phosphate removal from water: an aquarium life support system application. Paper presented at the 2010 Aquatic Animal Life Support Operators (AALSO) Symposium, Galveston Texas, 2- 5/5/ 2010.

Rotzoll, K. & El-Kadi, A. I., 2008. Estimating hydraulic conductivity from specific capacity for Hawaii aquifers, USA. *Hydrogeology Journal*, 16: 969-979.

Rushton, K.R.; Eilers, V.H.M. & Carter, R.C., 2006. Improved soil moisture balance methodology for recharge estimation. *Journal of Hydrology*, 318: 379-399.

Rytwo, G.; Banin, A. & Nir, S., 1996. Exchange reactions in the Ca-Mg-Na-Montmorillonite system. *Clays and Clay Minerals,* 44(2): 276-285.

Sammel, E. A., 1974. Aquifer tests in large-diameter wells in India. *Ground Water*, 12(5): 265-272.

Samuel, M. P. & Jha, M. K., 2003. Estimation of aquifer parameters from pumping test data by genetic algorithm optimization technique. *Journal of Irrigation and Drainage Engineering*, 129(5): 348-359.

Sandberg, S.K.; Slater, L.D. & Versteeg, R., 2002. An integrated geophysical investigation of the hydrogeology of an anisotropic unconfined aquifer. *Journal of Hydrology*, 267: 227–243.

Scanlon, B.R.; Healy, R.W. & Cook, P.G., 2002. Choosing appropriate techniques for quantifying groundwater recharge. *Hydrogeology Journal,* 10: 18-39.

Selinus, O.; Alloway, B.; Centeno, J.A.; Finkelman, R.B.; Fuge, R.; Lindh, U. & Smedley, P., (Eds.), 2005. Essentials of Medical Geology, impact of the natural environment on public health. Academic Press, 832 p.

Sentelhas, P.C.; Gillespie, T.J. & Santos, E.A., 2010. Evaluation of FAO Penman-Monteith and alternative methods for estimating reference evapotranspiration with missing data in Southern Ontario, Canada. *Agricultural Water Management,* 97: 635–644.

Sharma, M. L., 1986. Measurement and prediction of natural groundwater recharge - an overview. *New Zealand Journal of Hydrology,* 25(1): 49–56.

SHER Ingénieurs Conseils, 1992. Projet Kirundo, Volet Puits. Etude hydrogéologique, rapport définitif, 38 p. + Annexes.

Singh, S.K., 2008. Aquifer parameters from drawdowns in large-diameter wells: unsteady pumping. *Journal of Hydrologic Engineering*, 13(7): 636-640.

Singhal, B.B.S. & Gupta R.P., 1999. Applied hydrogeology of fractured rocks. Library of cataloguing-in-publication data, 324 p.

Snyder, R.L. & Eching, S., 2003. PMday.xls and PMmon.xls, spreadsheet softwares for estimating daily and monthly reference evapotranspiration using Penman-Monteith equation. *The Regents of the University of California, Davis, California.* Accessed online on 25/08/2011 at online at: http: //biomet.ucdavis.edu/evapotranspiration.html.

Sophocleous, M., 2004. Groundwater recharge. *In* Sylveira, L. & Usunoff, E.J. (Eds.), *Groundwater*, In: *Encyclopedia of Life Support Systems (EOLSS),* Developed under the Auspices of the UNESCO, Eolss Publishers, Oxford, UK, 41 p. (http: //www.eolss.net).

Sophocleous, M., 2000. From safe yield to sustainable development of water resources: The Kansas experience. *Journal of Hydrology,* 235: 27-43.

Sophocleous, M. (Ed.), 1998. Perspectives on sustainable development of water resources in Kansas. *Kansas geological Survey Bulletin,* 239.

Sophocleous, M., 1997. Managing water resources systems: why "safe yield" is not sustainable. *Ground Water*, 35(4): 561.

Sophocleous, M., 1991. Combining the soil-water balance and water-level fluctuation methods to estimate natural groundwater recharge: practical aspects. *Journal of Hydrology,* 124: 229–241.

Sottiaux, G.; Opdecamp, L.; Bigura, C. & Frankart, R., 1988. Carte des sols du Burundi, échelle 1/250000. Note explicative. *AGCD, Publication du Service Agricole* Nr. 9*,* 141 p.

Srivastav, S.K.; Lubczynski, M.W. & Biyani, A.K., 2007. Upscaling of transmissivity, derived from specific capacity: a hydrogeomorphological approach applied to the Doon Valley aquifer in India. *Hydrogeology Journal*, 15: 1251-1264.

Tack, L. & Deblond, A., 1990. Intrusive character of the late Kibaran magmatism in Burundi. *IGCP No. 255 Newsletter,* 3: 81–87.

Tack, L.; Liégeois, J.P.; Deblond, A. & Duchesne, J.C., 1994. Kibaran A-type granitoids and mafic rocks generated by two mantle sources in a late orogenic setting (Burundi). *Precambrian Research,* 68: 323–356.

Tack, L.; Fernandez-Alonso, M.; DeWaele, B.; Tahon, A.; Dewaele, S.; Baudet, D. & Cutten, H., 2006. The Northeastern Kibaran Belt (NKB): a long-lived Proterozoic intraplate history. In: 21st Colloquium African Geology (CAG21), 03-05.07.2006, Maputo, Mozambique, Abstract volume, pp. 149–151.

Tack, L.; Wingate, M.; De Waele, B.; Meert, J.; Griffin, B.; Belousova, E.A.; Tahon, A.; Fernandez-Alonso, M.; Baudet, D.; Cutten, H. & De Waele, S., 2008. The Proterozoic Kibaran Belt in Central Africa: intra-cratonic 1375 Ma emplacement of a LIP. In: 22nd Colloquium African Geology (CAG22), 04-06.11.2008, Hammamet, Tunisia, Abstract volume, p. 89.

Taylor, G. & Eggleton, R.A., 2001. Regolith geology and geomorphology. John Wiley and Sons, 375 p.

Taylor, R.G. & Howard, K.W.F., 2000. A tectonic-geomorphic model of the hydrogeology of deeply weathered crystalline rock: evidence from Uganda. *Hydrogeology Journal*, 8: 279-294.

Taylor, R.G. & Howard, K.W.F., 1999. Lithological evidence for the evolution of weathered mantles in Uganda by tectonically controlled cycles of deep weathering and stripping. *Catena*, 35: 65–94.

TBW Ingénieurs conseils, 1998. Plan directeur national de l'eau. Rapport de base, phase II. Volet 3: Ressources en eau. République du Burundi, Ministère de l'Energie et des Mines,

Direction Générale de l'Eau et de l'Energie Etude hydrométéorologique. Unpublished report 40 p.

TBW Ingénieurs conseils, 1994. Plan directeur national de l'eau. Rapport d'études, phase I. Volet 2: Etude hydrométéorologique. République du Burundi, Ministère des Ressources Naturelles, de l'Environnement et de l'Aménagement du Territoire, Direction Générale de l'Eau et de l'Energie. Unpublished report, 34 p.

Tesfamichael, G.Y.T., 2009. Groundwater flow modeling of the Geba basin, Northern Ethiopia. PhD Dissertation, Vrije Universiteit Brussel, 274 p.

Theis, C.V.; Brown, R. H. & Meyer, R.R., 1963. Estimating the transmissivity of aquifers from specific capacity of wells. In: Bental, R. (Ed.), Methods of determining permeability, transmissivity, and drawdown. *U.S. Geological Survey Water Supply Paper*, 1536(I): 331-340.

Therrien, R.; McLaren, R.G.; Sudicky, E.A. & Panday, S.M., 2010. HydroGeoSphere, a three-dimensional numerical model describing fully-integrated subsurface and surface flow and solute transport. User's Guide, Waterloo, Groundwater Simulations Group, 343 p.

Terzoudi, C.B.; Gemtos, T.A.; Danalatos, N.G. & Argyrokastritis, I., 2007**.** Application of an empirical runoff estimation method in central Greece. *Soil and Tillage Research*, 92: 198-212.

Tessens, E.; Mvuyekure, E.; Muganza, J.P. & Bigura, C., 1991. Guide synoptique pour la carte pédologique semi-détaillée du Burundi. *Publication ISABU* Nr.16, 16 p. + annexes.

Theunissen, K.; Klerkx, K.; Melnikov, A. & Mruma, A., 1996. Mechanisms of inheritance of rift faulting in the western branch of the East African Rift, Tanzania. *Tectonics, 15(4):* 776-790.

Thomasson, H. J.; Olmstead, F. H. & LeRoux, E. R., 1960. Geology, water resources, and usable ground water storage capacity of part of Solano County, CA: U.S. *Geological Survey Water Supply Paper,* 1464, 693 p.

Thornthwaite, C.W. & Mather, J.R., 1957. Instructions and tables for computing potential evapotranspiration and the water balance. *Publications in Climatology*, 10(3): 183 – 311.

Thornthwaite, C.W. & Mather, J.R., 1955. The Water Balance. *Publications in Climatology,* 8(1): 1-104.

Thornthwaite, C.W., 1948. An approach toward a rational classification of climate. *Geographical Review,* 38: 55–94.

Todd, D. K., 1959. Groundwater hydrology. John Wiley and Sons, New York, 336 p.

Trajkovic, S. & Kolakovic, S., 2009. Evaluation of reference evapotranspiration equations under humid conditions. *Water Resources Management,* 23: 3057–3067.

Trefry, M. G. & Muffels, C., 2007. FEFLOW: a finite-element ground water flow and transport modeling tool. *Groundwater*, 45(5): 525-528.

Trescott, P.C., 1975. Documentation of a finite difference model for simulation of three dimensional groundwater flow. *U.S. Geological Survey, Open-File Report* 75-438, p. 48**.**

UNEP, 1992. World atlas of desertification. Edward Arnold, London, 69 p. ISBN No: 340555122.

UNESCO, 1979. Map of the world distribution of arid regions. *Man and Biosphere Technical Notes* No. 7. Paris, France: 1 map-sheet + 54 p. explanatory note. Scale =1/25000000.

UNICEF/WHO JMP, 2012. Progress on drinking water and sanitation: 2012 update. WHO/UNICEF Joint Monitoring Programme for water supply and sanitation, 66 p.

USDA-SCS (U.S. Department of Agriculture-Soil Conservation Service), 1972. National Engineering Handbook, Section 4, Hydrology, Chapter 10: Estimation of direct runoff from storm rainfall. U.S. Government Printing Office. Washington, D.C, pp. 10.1-10.24.

USDA-NRCS (United States Department of Agriculture-Natural Resources Conservation Services), 1986. Urban hydrology for small watersheds. *Technical release,* 55, 26 p.

Van Camp, M.; Coetsiers, M.; Martens, K. & Walraevens, K., 2010. Effects of multi-annual climate variability on the hydrodynamic evolution (1833 to present) in a shallow aquifer system in nothern Belgium. *Hydrological Sciences Journal*, 55(5): 763-779.

Verbovsek, T., 2008. Estimation of transmissivity and hydraulic conductivity from specific capacity and specific capacity index in dolomite aquifers. *Journal of Hydrologic Engineering*, 9: 817-823.

Vissers**, M.** J.M. & Van der Perk, M., 2008. The stability of groundwater flow systems in unconfined sandy aquifers in the Netherlands. *Journal of Hydrology*, 348: 292-304.

Wallroth, T. & Rosenbaum, M. S., 1996. Estimating the spatial variability of specific capacity from a swedish regional database. *Marine and Petroleum Geology*, 13(4): 457-461.

Wright, E.P., 1992. The hydrogeology of crystalline basement aquifers in Africa. *Geological Society Special Publication,* 66: 1-27.

Walraevens, K.; Vandecasteele, I.; Martens, K.; Nyssen, J.; Moeyersons, J.; Gebreyohannes, T.; De Smedt, F. & Poesen, J., 2009. Groundwater recharge and flow in a small catchment in the Tigray region in North Ethiopia. *Hydrological Sciences Journal*, 54(4): 739 – 753.

Walraevens, K. & Cnudde, J.P., 2006. Applied Geophysics. Lecture notes, Ghent University, Belgium.

Walraevens, K. & Van Camp, M., 2008. Groundwater recharge and flow in a small catchment in the Tigray region in North Ethiopia. *Groundwater & Climate in Africa an international conference-Kampala, Uganda, 24th-28th June 2008*. Abstract book, p. 39.

Walraevens, K. & Van Camp, M., 2005. Advances in understanding natural groundwater quality controls in coastal aquifers. In: Custodio, A. & Manzano, M.A. (Eds.), *Groundwater and saline intrusion, selected papers from the 18th Salt Water Intrusion Meeting, Cartagena 2004,* 449-463.

Walvoord, M.A.; Plumer, M.A.; Phillips, F.M. & Wolfsberg, A.V., 2002. Deep arid system hydrodynamics 1. Equilibrium states and response times in thick desert vadose zones. *Water Resources Research*, 38(12): 1308, doi: 10.1029/2001WR000824, 15 p.

Waterloo Hydrogeologic Inc., 2002. User's Manual. Software-consulting-training, Waterloo Hydrogeologic Inc., Waterloo, Ontario, Canada, 386 p.

Weight, W.D., 2008. Hydrogeology field manual. Second edition, The McGraw-Hill Compagnies Inc. 751 p.

WHO, 2011. Guidelines for drinking-water quality. Fourth edition. WHO Library Cataloguing-in-Publication Data, 518 p.

WHO, 2009. Background document for development of WHO guidelines for drinking-water quality. WHO Document Production Services, 12 p.

WHO, 2008. Guidelines for drinking-water quality (electronic resource): incorporating 1st and 2nd addenda, volume1, recommendations. 3rd edition. WHO Library Cataloguing-in-Publication Data, 668 p.

WHO, 1984. Guidelines for drinking water quality. Volume 1. Recommendations Geneva. Switzerland.

WHO & UNICEF, 2000. Global water supply and sanitation assessment 2000 Report. WHO/UNICEF, Geneva/New York, 77 p.

Winter, T. C., 1999. Relation of streams, lakes, and wetlands to groundwater flow systems. *Hydrogeology Journal,* 7: 28-45.

Winter, T. C.; Harvey, J.W.; Franke, O.L. & Alley, W.M., 1998, Groundwater and surface water, a single resource. *U.S. Geological Survey Circular,* 1139, 87 p.

Wright, E.P., 1992. The hydrogeology of crystalline basement aquifers in Africa. *Geological Society, London, Special Publications,* 66: 1-27.

Wyns, R.; Baltassat, J.M.; Lachassagne, P.; Legchenko, A.; Vairon, J. & Mathieu, F., 2004. Application of SNMR soundings for groundwater reserves mapping in weathered basement rocks (Brittany, France). *Bulletin de la Société Géologique de France*, 175(1): 21–34.

Xiao, H.; Meissner, R.; Seeger, J.; Rupp, H. & Borg, H., 2009. Testing the precision of a weighable gravitation lysimeter. *Journal of Plant Nutrition and Soil Science,* 172(2): 194-200.

Xu, C.-Y. & Singh, V.P., 2002. Cross comparison of empirical equations for calculating potential evapotranspiration with data from Switzerland. *Water Resources Management,* 16: 197–219.

Xu, Y. & Beekman, H.E., 2003. Groundwater Recharge Estimation in Southern Africa. *UNESCO IHP Series* No. 64, 206 p.

Xu, C.Y. & Chen, D., 2005. Comparison of seven models for estimation of evapotranspiration and groundwater recharge using lysimeter measurement data in Germany. *Hydrological Processes*, 19(18): 3717-3734.

Yazdani, M.R.; Saghafian, B.; Mahdian, M.H. & Soltani, S., 2009. Monthly runoff estimation using artificial neural networks. *Journal of Agricultural Science and Technology*, 11: 355-362.

Zekai S., 1991. Drawdown Distribution During Recovery around a Large Diameter Well, *Nordic Hydrology,* 22: 253-264.

Zhou, Y., 2009. A critical review of groundwater budget myth, safe yield and sustainability. *Journal of Hydrology*, 370: 20.

Zhou, Y. & Wenpeng, L., 2011. A review of regional groundwater flow modelling. *Geoscience Frontiers,* 2(2): 205-214.

Hydrogeological and Hydrogeochemical Investigation of a Precambrian Basement Aquifer in Bugesera Region (Burundi)

APPENDICES

Charles BAKUNDUKIZE

Dissertation submitted in fulfilment of the requirements for the award of the degree of Doctor in Sciences: Geology

Academic year: 2011-2012

Promotor: Prof. Dr. Kristine Walraevens

Appendix II. 1. Inversion results of the 136 VES

Sounding station AIDR 1-VES 411			**Sounding station AIDR 1-VES 412**		
L (m)	l (m)	ρ_a (Ωm)	L (m)	l (m)	ρ_a (Ωm)
2	1	336.9	2	1	132.0
4	1	118.7	4	1	96.4
6	1	67.3	6	1	79.5
10	1	63.9	10	1	69.2
14	2	66.8	14	2	64.4
20	2	68.4	20	2	57.9
30	2	67.8	30	2	48.2
40	2	65.7	40	2	41.7
60	10	61.2	60	10	36.2
80	10	58.6	80	10	35.8
100	10	57.8	100	10	37.7
150	10	61.1	150	10	46.5
200	40	69.1	200	40	57.0
300	40	91.0	300	40	77.4
Model	**RMS error (%) = 4.1**		**Model**	**RMS error (%) = 3.7**	
Layer	Resistivity (Ωm)	Thickness(m)	Layer	Resistivity (Ωm)	Thickness(m)
1	525.5	0.6	1	153.6	0.7
2	21.3	0.5	2	67.6	6.2
3	73.7	10.4	3	29.4	40.3
4	49.9	66.9	4	264.9	
5	707				

Sounding station AIDR 1-VES 413			**Sounding station AIDR 1-VES 414**		
L (m)	L (m)	ρ_a (Ωm)	L (m)	l (m)	ρ_a (Ωm)
2	1	36.2	2	1	28.3
4	1	40.7	4	1	21.1
6	1	47.7	6	1	26.5
10	1	58.7	10	1	34.9
14	2	64.1	14	2	40.7
20	2	64.8	20	2	46.1
30	2	58.5	30	2	50.6
40	2	51.5	40	2	52.9
60	10	43.2	60	10	56.6
80	10	40.4	80	10	61.0
100	10	40.0	100	10	66.0
150	10	43.4	150	10	78.6
200	40	49.1	200	40	89.2
300	40	61.7	300	40	103.9
Model	**RMS error (%) = 3.5**		**Model**	**RMS error (%) =**	
Layer	Resistivity (Ωm)	Thickness(m)	Layer	Resistivity (Ωm)	Thickness(m)
1	35.3	1.6	1	89	0.3
2	112.6	3.6	2	14	1.2
3	34.9	60	3	66.2	4.4
4	148.4		4	50.9	21.7
			5	139.1	

Sounding station AIDR 2-VES 421		
L (m)	l (m)	ρ_a (Ωm)
2	1	13.1
4	1	14.6
6	1	17.2
10	1	22.2
14	2	26.1
20	2	30.2
30	2	34.5
40	2	37.5
60	10	42.4
80	10	47.7
100	10	53.6
150	10	70.3
200	40	86.9
300	40	116.3
Model	**RMS error (%) = 3.4**	
Layer	Resistivity (Ωm)	Thickness(m)
1	12.8	1.7
2	41.2	31.6
3	320.8	

Sounding station AIDR 2-VES 422		
L (m)	l (m)	ρ_a (Ωm)
2	1	11.9
4	1	11.0
6	1	14.5
10	1	19.7
14	2	23.4
20	2	27.2
30	2	31.1
40	2	33.6
60	10	37.5
80	10	41.4
100	10	45.9
150	10	59.9
200	40	75.6
300	40	106.8
Model	**RMS error (%) = 2.4**	
Layer	Resistivity (Ωm)	Thickness(m)
1	22	0.4
2	4.7	0.6
3	37.5	39.6
4	627.9	

Sounding station AIDR 2-VES 423		
L (m)	L (m)	ρ_a (Ωm)
2	1	19.9
4	1	23.3
6	1	26.9
10	1	33.0
14	2	37.1
20	2	41.2
30	2	45.1
40	2	47.8
60	10	52.9
80	10	59.0
100	10	66.3
150	10	87.3
200	40	108.6
300	40	146.4
Model	**RMS error (%) = 2.3**	
Layer	Resistivity (Ωm)	Thickness(m)
1	18.4	0.6
2	23.5	1
3	49.3	32.4
4	433.8	

Sounding station AIDR 2-VES 424		
L (m)	l (m)	ρ_a (Ωm)
2	1	26.2
4	1	25.1
6	1	30.1
10	1	35.3
14	2	37.9
20	2	40.1
30	2	41.9
40	2	43.2
60	10	46.3
80	10	50.7
100	10	56.3
150	10	73.7
200	40	92.4
300	40	127.2
Model	**RMS error (%) = 2.4**	
Layer	Resistivity (Ωm)	Thickness(m)
1	56.6	0.3
2	10.3	0.4
3	42.9	37.4
4	481.2	

Sounding station AIDR 3-VES 431		
L (m)	l (m)	ρ_a (Ωm)
2	1	13.1
4	1	14.6
6	1	17.2
10	1	22.2
14	2	26.1
20	2	30.2
30	2	34.5
40	2	37.5
60	10	42.4
80	10	47.7
100	10	53.6
150	10	70.3
200	40	86.9
300	40	116.3
Model	**RMS error (%) = 3.6**	
Layer	Resistivity (Ωm)	Thickness(m)
1	559.3	0.4
2	60.3	25.5
3	229	40.1
4	2271.5	

Sounding station AIDR 3-VES 432		
L (m)	l (m)	ρ_a (Ωm)
2	1	83.4
4	1	64.1
6	1	56.5
10	1	52.7
14	2	52.1
20	2	52.8
30	2	56.0
40	2	61.3
60	10	75.3
80	10	91.2
100	10	107.5
150	10	148.0
200	40	187.6
300	40	261.6
Model	**RMS error (%) = 4.8**	
Layer	Resistivity (Ωm)	Thickness(m)
1	97.7	1.2
2	50.5	31.4
3	183.4	56.6
4	1216.5	

Sounding station AIDR 3-VES 433		
L (m)	L (m)	ρ_a (Ωm)
2	1	94.1
4	1	43.4
6	1	37.7
10	1	39.5
14	2	42.1
20	2	44.2
30	2	44.9
40	2	45.3
60	10	48.6
80	10	55.6
100	10	64.9
150	10	91.9
200	40	119.8
300	40	174.1
Model	**RMS error (%) = 6.1**	
Layer	Resistivity (Ωm)	Thickness(m)
1	184.1	0.4
2	32.2	2.3
3	56.4	4.2
4	36.7	21.9
5	489.6	23.5
6	1827.8	

Sounding station AIDR 3-VES 434		
L (m)	l (m)	ρ_a (Ωm)
2	1	95.9
4	1	41.7
6	1	35.5
10	1	40.5
14	2	46.8
20	2	53.0
30	2	57.0
40	2	57.9
60	10	60.3
80	10	67.2
100	10	77.6
150	10	110.2
300	20	213.3
100	40	77.6
150	40	110.2
200	40	144.9
Model	**RMS error (%) = 3.5**	
Layer	Resistivity (Ωm)	Thickness(m)
1	178.1	0.5
2	27.8	2.5
3	96.4	4.7
4	38.5	19.2
5	523.4	14.9
6	3659.3	

Sounding station AIDR 4-VES 441		
L (m)	l (m)	ρ_a (Ωm)
2	1	122.3
4	1	42.3
6	1	29.4
10	1	28.5
14	2	31.4
20	2	37.3
30	2	47.5
40	2	56.2
60	10	70.3
80	10	82.1
100	10	92.9
150	10	119.6
200	40	146.2
300	40	196.3
Model	**RMS error (%) = 4.2**	
Layer	Resistivity (Ωm)	Thickness(m)
1	233.5	0.5
2	24.9	5.2
3	104.1	38.2
4	637.7	

Sounding station AIDR 4-VES 442		
L (m)	l (m)	ρ_a (Ωm)
2	1	114.8
4	1	37.2
6	1	24.5
10	1	24.6
14	2	28.4
20	2	35.5
30	2	47.0
40	2	57.3
60	10	75.6
80	10	92.9
100	10	110.0
150	10	152.5
200	40	193.2
300	40	266.9
Model	**RMS error (%) = 3.7**	
Layer	Resistivity (Ωm)	Thickness(m)
1	217.3	0.5
2	20	4.4
3	113.9	24.5
4	1006.9	

Sounding station AIDR 4-VES 443		
L (m)	L (m)	ρ_a (Ωm)
2	1	93.4
4	1	47.8
6	1	28.3
10	1	21.6
14	2	22.0
20	2	24.8
30	2	32.0
40	2	40.3
60	10	56.8
80	10	72.2
100	10	86.5
150	10	117.8
200	40	144.1
300	40	185.6
Model	**RMS error (%) = 2.2**	
Layer	Resistivity (Ωm)	Thickness(m)
1	120.8	0.7
2	18.9	7.9
3	147.5	6.9
4	370.1	

Sounding station AIDR 4-VES 444		
L (m)	l (m)	ρ_a (Ωm)
2	1	85.8
4	1	58.4
6	1	37.9
10	1	25.4
14	2	23.8
20	2	25.3
30	2	30.6
40	2	37.0
60	10	50.3
80	10	63.5
100	10	76.7
150	10	110.1
200	40	143.0
300	40	205.1
Model	**RMS error (%) = 3.2**	
Layer	Resistivity (Ωm)	Thickness(m)
1	96.2	1
2	20.6	8.3
3	95.3	21.5
4	1453.2	

Sounding station AIDR 5-VES 451		
L (m)	l (m)	ρ_a (Ωm)
2	1	225.3
4	1	257.9
6	1	243.6
10	1	181.7
14	2	128.7
20	2	88.3
30	2	73.5
40	2	77.9
60	10	98.6
80	10	121.7
100	10	143.7
150	10	190.8
200	40	228.6
300	40	

Model	**RMS error (%) = 4.7**	
Layer	Resistivity (Ωm)	Thickness(m)
1	151	0.3
2	319	2
3	56	14
4	481.7	

Sounding station AIDR 5-VES 452		
L (m)	l (m)	ρ_a (Ωm)
2	1	203.3
4	1	221.3
6	1	202.5
10	1	148.7
14	2	109.3
20	2	81.7
30	2	70.9
40	2	71.8
60	10	82.6
80	10	98.1
100	10	115.2
150	10	156.5
200	40	192.7

Model	**RMS error (%) = 3.5**	
Layer	Resistivity (Ωm)	Thickness(m)
1	87.4	0.1
2	259.2	2
3	61.4	22
4	551.4	

Sounding station AIDR 5-VES 453		
L (m)	L (m)	ρ_a (Ωm)
2	1	179.0
4	1	175.1
6	1	165.7
10	1	137.7
14	2	109.3
30	2	66.9
40	2	69.0
60	10	82.9
80	10	96.6
100	10	107.9
150	10	128.1
200	40	141.0

Model	**RMS error (%) = 5.3**	
Layer	Resistivity (Ωm)	Thickness(m)
1	179.6	3.3
2	45.4	10.1
3	179.8	

Sounding station AIDR 5-VES 454		
L (m)	l (m)	ρ_a (Ωm)
2	1	175.8
4	1	171.6
6	1	161.7
10	1	133.4
14	2	106.2
20	2	79.7
30	2	62.8
40	2	59.0
60	10	60.9
80	10	66.8
100	10	74.2
150	10	93.3
200	40	109.9

Model	**RMS error (%) = 4.9**	
Layer	Resistivity (Ωm)	Thickness(m)
1	176.5	3.1
2	51.9	27.4
3	216	

Sounding station AIDR 5-VES 455		
L (m)	l (m)	ρ_a (Ωm)
2	1	42.6
4	1	39.5
6	1	35.6
10	1	30.9
14	2	29.4
20	2	29.8
30	2	33.8
40	2	40.2
60	10	55.6
80	10	71.3
100	10	85.9
150	10	116.5
200	40	139.1
Model	**RMS error (%) = 5.2**	
Layer	Resistivity (Ωm)	Thickness(m)
1	43.4	1.4
2	26.3	12.7
3	3136.6	9.2
4	67.2	

Sounding station AIDR 6-VES 461		
L (m)	L (m)	ρ_a (Ωm)
2	1	24.1
4	1	18.6
6	1	14.1
10	1	12.7
14	2	15.3
20	2	20.4
30	2	29.3
40	2	38.3
60	10	56.3
80	10	74.0
100	10	91.5
150	10	133.4
200	40	173.2
Model	**RMS error (%) = 4**	
Layer	Resistivity (Ωm)	Thickness(m)
1	26	1.1
2	7.1	2.6
3	65.2	7.3
4	1482.1	

Sounding station AIDR 6-VES 462		
L (m)	l (m)	ρ_a (Ωm)
2	1	26.6
4	1	9.2
6	1	9.1
10	1	12.6
14	2	16.2
20	2	20.9
30	2	27.7
40	2	33.8
60	10	45.6
80	10	57.7
100	10	70.2
150	10	101.5
200	40	131.7
Model	**RMS error (%) = 2.7**	
Layer	Resistivity (Ωm)	Thickness(m)
1	70	0.4
2	6.2	2
3	51.1	18.4
4	1193.1	

Sounding station AIDR 6-VES 463			**Sounding station AIDR 6-VES 464**		
L (m)	l (m)	ρ_a (Ωm)	L (m)	l (m)	ρ_a (Ωm)
2	1	18.9	2	1	35.1
4	1	9.7	4	1	9.9
6	1	9.6	6	1	7.8
10	1	12.2	10	1	8.1
14	2	15.6	8	2	7.8
20	2	20.5	14	2	9.3
30	2	27.5	20	2	11.7
40	2	33.5	30	2	16.2
60	10	43.4	40	2	21.0
80	10	52.1	60	10	30.6
100	10	60.4	80	10	40.3
150	10	81.6	100	10	50.1
200	40	103.6	150	10	74.0
			200	40	97.2
Model	**RMS error (%) = 3**		**Model**	**RMS error (%) = 4**	
Layer	Resistivity (Ωm)	Thickness(m)	Layer	Resistivity (Ωm)	Thickness(m)
1	39.9	0.4	1	96	0.4
2	7.6	2.8	2	7	5.3
3	71.8	38.1	3	49.5	10.3
4	1165		4	1613.7	

Sounding station AIDR 7-VES 471			**Sounding station AIDR 7-VES 472**		
L (m)	L (m)	ρ_a (Ωm)	L (m)	l (m)	ρ_a (Ωm)
2	1	65.6	2	1	80.4
4	1	20.1	4	1	71.1
6	1	13.9	6	1	56.1
10	1	17.4	10	1	33.5
14	2	21.7	14	2	23.6
20	2	27.1	20	2	19.6
30	2	34.1	30	2	20.4
40	2	40.0	40	2	23.1
60	10	51.0	60	10	29.4
80	10	62.9	80	10	35.9
100	10	75.9	100	10	42.7
150	10	111.0	150	10	60.9
200	40	147.5	200	40	80.1
300	40	220.5	300	40	119.1
Model	**RMS error (%) = 3.8**		**Model**	**RMS error (%) = 2.7**	
Layer	Resistivity (Ωm)	Thickness(m)	Layer	Resistivity (Ωm)	Thickness(m)
1	122.2	0.5	1	82.5	1.8
2	8.4	1.8	2	15.7	9.8
3	51.6	23.7	3	47.1	28
4	24326.1		4	6751.8	

Sounding station AIDR 7-VES 473			**Sounding station**		
L (m)	l (m)	ρ_a (Ωm)	L (m)	l (m)	ρ_a (Ωm)
2	1	64.8			
4	1	48.8			
6	1	36.4			
10	1	32.2			
14	2	35.9			
20	2	41.5			
30	2	48.0			
40	2	52.9			
60	10	62.0			
80	10	72.3			
100	10	84.5			
150	10	120.3			
200	40	159.1			
300	40	238.0			
Model	**RMS error (%) = 4.2**		**Model**	**RMS error (%) =**	
Layer	Resistivity (Ωm)	Thickness(m)	Layer	Resistivity (Ωm)	Thickness(m)
1	70.3	1.1			
2	15.3	1.4			
3	58.5	30.5			
4	39918.9				

Sounding station AIDR 8-VES 481			**Sounding station AIDR 8-VES 482**		
L (m)	L (m)	ρ_a (Ωm)	L (m)	l (m)	ρ_a (Ωm)
2	1	80.3	2	1	95.1
4	1	57.5	4	1	77.8
6	1	46.5	6	1	61.7
10	1	39.5	10	1	46.6
14	2	36.1	14	2	40.5
20	2	31.7	20	2	36.1
30	2	27.3	30	2	33.4
40	2	26.8	40	2	33.3
60	10	32.4	60	10	36.3
80	10	41.4	80	10	41.0
100	10	51.3	100	10	46.7
150	10	76.3	150	10	63.3
200	40	101.3	200	40	82.0
300	40	150.6	300	40	121.1
Model	**RMS error (%) = 6.2**		**Model**	**RMS error (%) = 4.3**	
Layer	Resistivity (Ωm)	Thickness(m)	Layer	Resistivity (Ωm)	Thickness(m)
1	93.9	0.8	1	100.7	1.1
2	39.1	5.4	2	42.3	3.1
3	14.9	10	3	28.8	14.3
4	63.4	9.6	4	48.3	30.6
5	5221.8		5	5197.5	

Sounding station AIDR 8-VES 483			**Sounding station AIDR 8-VES 484**		
L (m)	L (m)	ρ_a (Ωm)	L (m)	l (m)	ρ_a (Ωm)
2	1	118.7	2	1	249.6
4	1	163.3	4	1	181.7
6	1	183.1	6	1	172.7
10	1	193.3	10	1	170.0
14	2	183.2	14	2	155.9
20	2	153.3	20	2	123.4
30	2	104.0	30	2	76.2
40	2	74.3	40	2	51.1
60	10	57.3	60	10	38.8
80	10	59.9	80	10	41.2
100	10	67.9	100	10	46.9
150	10	93.2	150	10	63.4
200	40	121.8	200	40	81.9
300	40	180.0	300	40	120.7
Model	**RMS error (%) = 4.3**		**Model**	**RMS error (%) = 2.3**	
Layer	Resistivity (Ωm)	Thickness(m)	Layer	Resistivity (Ωm)	Thickness(m)
1	63.4	0.3	1	331.4	0.5
2	232.5	5.4	2	134.5	1
3	24.4	5.2	3	216	4
4	53.6	30.2	4	22.1	11.5
5	4851.4		5	51.7	34.5
			6	5092.5	

Sounding station AIDR 9-VES 491			**Sounding station AIDR 9-VES 492**		
L (m)	L (m)	ρ_a (Ωm)	L (m)	l (m)	ρ_a (Ωm)
2	1	83.0	2	1	56.0
4	1	75.0	4	1	43.0
6	1	60.8	6	1	30.0
10	1	36.8	10	1	18.8
14	2	26.5	14	2	16.4
20	2	25.2	20	2	16.9
30	2	31.6	30	2	20.2
30	2	31.6	40	2	24.5
40	10	38.1	60	10	33.0
60	10	48.5	80	10	40.7
80	10	56.9	100	10	47.5
100	10	64.2	150	10	62.0
150	10	81.1	200	40	74.4
200	40	97.8	300	40	95.5
300	40	131.4			
Model	**RMS error (%) = 5.1**		**Model**	**RMS error (%) = 3.9**	
Layer	Resistivity (Ωm)	Thickness(m)	Layer	Resistivity (Ωm)	Thickness(m)
1	84.6	2	1	59.9	1.2
2	9	2.8	2	13.7	9.1
3	83	50.8	3	106.2	54.9
4	569.4		4	246.8	

Sounding station AIDR 9-VES 493			**Sounding station**		
L (m)	L (m)	ρ_a (Ωm)	L (m)	l (m)	ρ_a (Ωm)
2	1	51.2			
4	1	27.2			
6	1	16.4			
10	1	12.6			
14	2	13.0			
20	2	15.1			
30	2	19.8			
40	2	24.5			
60	10	33.1			
80	10	40.3			
100	10	46.7			
150	10	60.1			
200	40	71.9			
300	40	94.4			
Model	**RMS error (%) = 3.4**		**Model**	**RMS error (%) =**	
Layer	Resistivity (Ωm)	Thickness(m)	Layer	Resistivity (Ωm)	Thickness(m)
1	64.9	0.8			
2	10.8	6.8			
3	92	80.8			
4	680.7				

Sounding station AIDR 10-VES 501			**Sounding station AIDR10-VES 502**		
L (m)	L (m)	ρ_a (Ωm)	L (m)	l (m)	ρ_a (Ωm)
2	1	163.0	2	1	164.6
4	1	123.9	4	1	117.7
6	1	102.6	6	1	99.6
10	1	76.0	10	1	77.1
14	2	61.8	14	2	65.3
20	2	55.0	20	2	58.8
30	2	57.2	30	2	58.3
40	2	61.8	40	2	61.0
60	10	69.2	60	10	66.9
80	10	74.3	80	10	71.5
100	10	78.7	100	10	75.4
150	10	90.1	150	10	84.4
200	40	104.1	200	40	94.8
300	40	139.9	300	40	121.9
Model	**RMS error (%) = 3.4**		**Model**	**RMS error (%) = 2.2**	
Layer	Resistivity (Ωm)	Thickness(m)	Layer	Resistivity (Ωm)	Thickness(m)
1	195.9	0.5	1	234	0.4
2	110.1	1.9	2	109.5	1.8
3	38.9	4.9	3	49.8	8.4
4	81.3	74.2	4	80.7	84.1
5	3104.7		5	1973.5	

Sounding station AIDR 10-VES 503		
L (m)	L (m)	ρ_a (Ωm)
2	1	148.9
4	1	115.3
6	1	87.5
10	1	66.6
14	2	61.4
20	2	59.6
30	2	60.1
40	2	62.0
60	10	67.0
80	10	71.2
100	10	73.9
150	10	76.1
200	40	77.8
300	40	89.3

Model	**RMS error (%) = 2.9**	
Layer	Resistivity (Ωm)	Thickness(m)
1	160.8	1
2	57.1	17.5
3	139	15.3
4	42.3	57.9
5	2057.5	

Sounding station AIDR 10-VES 504		
L (m)	l (m)	ρ_a (Ωm)
2	1	136.9
4	1	123.7
6	1	102.8
10	1	71.4
14	2	57.6
20	2	53.2
30	2	57.9
40	2	64.7
60	10	74.7
80	10	79.1
100	10	80.2
150	10	79.8
200	40	83.0
300	40	102.8

Model	**RMS error (%) = 3.8**	
Layer	Resistivity (Ωm)	Thickness(m)
1	139.8	1.8
2	42.1	8
3	152	14.2
4	41.8	49
5	2565	

Sounding station AIDR 11-VES 511		
L (m)	L (m)	ρ_a (Ωm)
2	1	150.3
4	1	127.0
6	1	101.9
10	1	77.8
14	2	71.2
20	2	70.6
30	2	74.0
40	2	76.9
60	10	79.0
80	10	77.8
100	10	75.7
150	10	73.8
200	40	79.2
300	40	102.7

Model	**RMS error (%) = 2.6**	
Layer	Resistivity (Ωm)	Thickness(m)
1	157.1	1.2
2	62.1	5.8
3	92.6	23.5
4	28.9	27.2
5	696.1	

Sounding station AIDR 11-VES 512		
L (m)	l (m)	ρ_a (Ωm)
2	1	135.6
4	1	121.9
6	1	102.4
10	1	76.3
14	2	65.5
20	2	61.3
30	2	62.5
40	2	65.5
60	10	69.0
80	10	68.4
100	10	65.6
150	10	58.0
200	40	56.0
300	40	65.8

Model	**RMS error (%) = 2.1**	
Layer	Resistivity (Ωm)	Thickness(m)
1	138.8	1.6
2	54.3	9.3
3	106	16
4	28.3	56.2
5	1708.7	

Sounding station AIDR 11-VES 513			**Sounding station**		
L (m)	L (m)	ρ_a (Ωm)	L (m)	l (m)	ρ_a (Ωm)
2	1	59.2			
4	1	53.2			
6	1	45.6			
10	1	38.0			
14	2	38.0			
20	2	42.9			
30	2	51.1			
40	2	56.6			
60	10	61.3			
80	10	61.2			
100	10	59.4			
150	10	55.3			
200	40	56.3			
300	40	70.2			
Model	**RMS error (%) = 2.6**		**Model**	**RMS error (%) =**	
Layer	Resistivity (Ωm)	Thickness(m)	Layer	Resistivity (Ωm)	Thickness(m)
1	60.7	1.5			
2	25.2	3.2			
3	86.7	19			
4	29.9	52.8			
5	1930.7				

Sounding station AIDR 12-VES 521			**Sounding station AIDR 12-VES 522**		
L (m)	L (m)	ρ_a (Ωm)	L (m)	l (m)	ρ_a (Ωm)
2	1	69.6	2	1	74.0
4	1	26.4	4	1	24.5
6	1	16.3	6	1	14.0
10	1	15.0	10	1	14.2
14	2	16.6	14	2	17.4
20	2	20.5	20	2	22.8
30	2	27.8	30	2	31.1
40	2	34.6	40	2	38.3
60	10	46.5	60	10	50.4
80	10	56.6	80	10	60.6
100	10	65.4	100	10	69.8
150	10	84.9	150	10	91.9
200	40	103.1	200	40	114.9
300	40	139.7	300	40	164.1
Model	**RMS error (%) = 4.2**		**Model**	**RMS error (%) = 2.8**	
Layer	Resistivity (Ωm)	Thickness(m)	Layer	Resistivity (Ωm)	Thickness(m)
1	112.7	0.6	1	125.1	0.6
2	12.8	5.6	2	10.1	3.6
3	118.6	68.5	3	100.2	53.1
4	1357.8		4	4192.8	

Sounding station AIDR 12-VES 523			**Sounding station AIDR12-VES 524**		
L (m)	L (m)	ρ_a (Ωm)	L (m)	l (m)	ρ_a (Ωm)
2	1	70.4	2	1	107.2
4	1	34.4	4	1	47.1
6	1	18.4	6	1	24.0
10	1	15.8	10	1	18.6
14	2	19.6	14	2	21.0
20	2	25.7	20	2	26.3
30	2	34.4	30	2	34.9
40	2	41.8	40	2	42.4
60	10	54.0	60	10	55.0
80	10	64.7	80	10	66.0
100	10	74.8	100	10	76.5
150	10	101.1	150	10	103.7
200	40	129.6	200	40	133.2
300	40	190.0	300	40	195.6
Model	**RMS error (%) = 3.5**		**Model**	**RMS error (%) = 2.7**	
Layer	Resistivity (Ωm)	Thickness(m)	Layer	Resistivity (Ωm)	Thickness(m)
1	90.1	0.8	1	145.7	0.723
2	9	2.6	2	14.4	4.4
3	89.1	42.3	3	93.2	42
4	7824.1		4	10337.2	

Sounding station AIDR 13-VES 531			**Sounding station AIDR 13-VES 532**		
L (m)	L (m)	ρ_a (Ωm)	L (m)	l (m)	ρ_a (Ωm)
2	1	54.7	2	1	27.6
4	1	12.7	4	1	11.1
6	1	9.1	6	1	12.0
10	1	11.4	10	1	15.4
14	2	14.4	14	2	19.5
20	2	18.4	20	2	25.3
30	2	23.7	30	2	33.3
40	2	28.0	40	2	39.9
60	10	35.3	60	10	50.2
80	10	42.2	80	10	58.7
100	10	49.5	100	10	66.5
150	10	69.5	150	10	86.1
200	40	91.0	200	40	106.7
300	40	134.9	300	40	148.8
Model	**RMS error (%) = 12.6**		**Model**	**RMS error (%) = 5.5**	
Layer	Resistivity (Ωm)	Thickness(m)	Layer	Resistivity (Ωm)	Thickness(m)
1	132.7	0.5	1	143.5	0.3
2	6.5	2.3	2	9.8	2.8
3	44	31.7	3	76.4	44.7
4	4543.4		4	920.8	

Sounding station AIDR 13-VES 533		
L (m)	L (m)	ρ_a (Ωm)
2	1	44.7
4	1	9.1
6	1	10.5
10	1	14.5
14	2	18.4
20	2	23.3
30	2	29.4
40	2	33.9
60	10	40.2
80	10	44.6
100	10	48.4
150	10	57.4
200	40	67.9
300	40	92.8
Model	**RMS error (%) = 4.3**	
Layer	Resistivity (Ωm)	Thickness(m)
1	322.1	0.3
2	7.2	2
3	52.3	67.5
4	1547	

Sounding station AIDR 8-VES 534		
L (m)	l (m)	ρ_a (Ωm)
2	1	51.3
4	1	20.3
6	1	25.6
10	1	34.1
14	2	40.5
20	2	47.4
30	2	58.7
40	2	64.2
60	10	54.4
80	10	68.6
100	10	73.4
150	10	88.8
200	40	108.6
300	40	154.1
Model	**RMS error (%) = 5**	
Layer	Resistivity (Ωm)	Thickness(m)
1	318.8	0.3
2	15.2	1.3
3	67.5	56.1
4	2275.4	

Sounding station AIDR 14-VES 541		
L (m)	L (m)	ρ_a (Ωm)
2	1	170.8
4	1	90.0
6	1	58.3
10	1	38.5
14	2	31.4
20	2	27.7
30	2	26.7
40	2	27.5
60	10	31.3
80	10	36.7
100	10	42.8
150	10	57.8
200	40	71.0
300	40	92.5
Model	**RMS error (%) = 4.4**	
Layer	Resistivity (Ωm)	Thickness(m)
1	232.6	1.3
2	55.5	3.3
3	24.5	47
4	200.6	

Sounding station AIDR 14-VES 542		
L (m)	l (m)	ρ_a (Ωm)
2	1	133.8
4	1	96.7
6	1	60.0
10	1	31.0
14	2	25.1
20	2	23.7
30	2	23.6
40	2	23.9
60	10	25.3
80	10	27.8
100	10	31.1
150	10	41.8
200	40	53.8
300	40	77.7
Model	**RMS error (%) = 2**	
Layer	Resistivity (Ωm)	Thickness(m)
1	145	1.2
2	12.9	0.5
3	23	39.1
4	721.2	

Sounding station AIDR 14-VES 543		
L (m)	L (m)	ρ_a (Ωm)
2	1	423.0
4	1	223.8
6	1	107.6
10	1	44.5
14	2	33.8
20	2	30.9
30	2	30.4
40	2	31.0
60	10	33.7
80	10	37.8
100	10	42.6
150	10	55.2
200	40	66.4
300	40	84.0
Model	**RMS error (%) = 4.1**	
Layer	Resistivity (Ωm)	Thickness(m)
1	521.8	0.8
2	99.2	0.9
3	29	28.5
4	155.8	

Sounding station AIDR 14-VES 544		
L (m)	l (m)	ρ_a (Ωm)
2	1	92.9
4	1	69.4
6	1	53.9
10	1	40.9
14	2	34.4
20	2	28.7
30	2	25.0
40	2	24.5
60	10	26.7
80	10	30.7
100	10	35.3
150	10	46.5
200	40	56.2
300	40	71.2
Model	**RMS error (%) = 2.3**	
Layer	Resistivity (Ωm)	Thickness(m)
1	103.4	0.8
2	43	2.9
3	21	22.8
4	131.8	

Sounding station AIDR 15-VES 551		
L (m)	L (m)	ρ_a (Ωm)
2	1	136.3
4	1	93.3
6	1	73.2
10	1	61.8
14	2	56.9
20	2	50.3
30	2	40.8
40	2	35.2
60	10	32.8
80	10	36.0
100	10	40.9
150	10	53.4
200	40	64.0
300	40	80.2
Model	**RMS error (%) = 2.7**	
Layer	Resistivity (Ωm)	Thickness(m)
1	162.3	0.7
2	60.3	6.4
3	21.7	18.6
4	139	

Sounding station AIDR 10-VES 552		
L (m)	l (m)	ρ_a (Ωm)
2	1	85.2
4	1	92.9
6	1	92.0
10	1	83.3
14	2	72.2
20	2	58.8
30	2	47.8
40	2	44.4
60	10	45.1
80	10	49.3
100	10	55.1
150	10	71.8
200	40	88.1
300	40	115.5
Model	**RMS error (%) =**	
Layer	Resistivity (Ωm)	Thickness(m)
1	53.4	0.2
2	99.2	3.3
3	38.5	30.7
4	267.2	

Sounding station AIDR 15-VES 553			**Sounding station AIDR 15-VES 554**		
L (m)	L (m)	ρ_a (Ωm)	L (m)	l (m)	ρ_a (Ωm)
2	1		2	1	210.8
4	1		4	1	264.4
6	1		6	1	259.6
10	1		10	1	196.9
14	2		14	2	131.0
20	2		20	2	72.7
30	2		30	2	43.0
40	2		40	2	39.1
60	10		60	10	44.1
80	10		80	10	53.5
100	10		100	10	64.8
150	10		150	10	95.5
200	40		200	40	126.6
300	40		300	40	188.3
Model	**RMS error (%) = 9.4**		**Model**	**RMS error (%) = 2.9**	
Layer	Resistivity (Ωm)	Thickness(m)	Layer	Resistivity (Ωm)	Thickness(m)
1	122	1.3	1	59.5	0.3
2	389.1	2.9	2	361.8	4.4
3	16.6	15.4	3	31.9	49
4	509.3		4	6994	

Sounding station AIDR 16-VES 561			**Sounding station AIDR 16-VES 562**		
L (m)	L (m)	ρ_a (Ωm)	L (m)	l (m)	ρ_a (Ωm)
2	1	94.4	2	1	126.4
4	1	43.0	4	1	76.2
6	1	43.0	6	1	65.3
10	1	46.2	10	1	50.3
14	2	45.2	14	2	38.6
20	2	41.3	20	2	30.7
30	2	37.0	30	2	30.9
40	2	36.8	40	2	36.3
60	10	42.8	60	10	48.8
80	10	51.0	80	10	60.3
100	10	59.1	100	10	70.3
150	10	76.4	150	10	90.6
200	40	89.7	200	40	105.8
Model	**RMS error (%) = 2.6**		**Model**	**RMS error (%) = 1.1**	
Layer	Resistivity (Ωm)	Thickness(m)	Layer	Resistivity (Ωm)	Thickness(m)
1	233.3	0.4	1	197.3	0.5
2	31.4	1.4	2	53	0.8
3	94.9	1.5	3	96.6	1.2
4	26.6	14.3	4	19.5	8.8
5	161.9		5	181.7	

Sounding station AIDR 16-VES 563			**Sounding station AIDR 16-VES 564**		
L (m)	L (m)	ρ_a (Ωm)	L (m)	l (m)	ρ_a (Ωm)
2	1	164.2	2	1	130.0
4	1	95.5	4	1	117.7
6	1	76.6	6	1	109.7
10	1	57.6	10	1	90.6
14	2	45.9	14	2	73.1
20	2	37.6	20	2	57.0
30	2	35.8	30	2	48.9
40	2	39.2	40	2	50.3
60	10	50.5	60	10	60.5
80	10	63.1	80	10	72.1
100	10	75.3	100	10	82.8
150	10	102.4	150	10	104.2
200	40	125.1	200	40	119.8
Model	**RMS error (%) = 2.3**		**Model**	**RMS error (%) = 5.2**	
Layer	Resistivity (Ωm)	Thickness(m)	Layer	Resistivity (Ωm)	Thickness(m)
1	259.1	0.5	1	170.7	0.3
2	78.7	2.4	2	118	2.9
3	28.1	14.1	3	37.4	13.8
4	317.9		4	188.6	

Sounding station GEOSCI 5-60			**Sounding station GEOSCI 5-61**		
L (m)	L (m)	ρ_a (Ωm)	L (m)	l (m)	ρ_a (Ωm)
2	0.5	56.9	2	0.5	70.4
3	0.5	54.4	3	0.5	79.3
4	0.5	53.3	4	0.5	83.1
6	0.5	52.2	6	0.5	82.5
8	0.5	50.9	8	0.5	77.6
10	0.5	49.4	10	0.5	71.0
12	2	47.6	12	2	64.8
16	2	43.5	16	2	55.5
20	2	39.6	20	2	50.8
24	2	36.3	24	2	49.7
30	2	33.6	30	2	52.1
40	6	33.9	40	6	61.9
50	6	37.8	50	6	74.8
60	6	43.7	60	6	88.9
80	6	57.2	80	6	118.1
100	6	71.4	100	6	147.5
120	6	85.6	120	6	177.0
160	20	114.0	160	20	236.0
200	20	142.4	200	20	294.9
240	20	170.7	240	20	353.9
300	20	213.0	300	20	442.2
400	20	283.3	400	20	589.3
Model	**RMS error (%) = 5.8**		**Model**	**RMS error (%) = 4.1**	
Layer	Resistivity (Ωm)	Thickness(m)	Layer	Resistivity (Ωm)	Thickness(m)
1	68.2	0.3	1	36.6	0.2
2	52.5	5.5	2	99.6	2.3
3	14.4	8.1	3	33.7	9.5
4	212.4	6	4	129.6	3.6
5	25664.4		5	298730.2	

Sounding station GEOSCI 5-62			**Sounding station GEOSCI 5-63**		
L (m)	L (m)	ρ_a (Ωm)	L (m)	l (m)	ρ_a (Ωm)
2	0.5	53.6	2	0.5	78.1
3	0.5	49.1	3	0.5	84.4
4	0.5	47.1	4	0.5	87.3
6	0.5	44.4	6	0.5	88.2
8	0.5	41.8	8	0.5	86.8
10	0.5	39.7	10	0.5	84.1
12	2	38.4	12	2	81.0
16	2	38.9	16	2	75.6
20	2	42.1	20	2	72.9
24	2	47.0	24	2	73.0
30	2	55.6	30	2	76.8
40	6	70.7	40	6	88.1
50	6	85.9	50	6	101.3
60	6	101.1	60	6	114.9
80	6	132.0	80	6	143.0
100	6	163.7	100	6	172.4
120	6	195.7	120	6	203.3
160	20	260.4	160	20	267.4
200	20	325.3	200	20	333.0
240	20	390.1	240	20	398.9
300	20	487.2	300	20	497.8
400	20	648.7	400	20	661.9

Model	**RMS error (%) = 5.2**		**Model**	**RMS error (%) = 3**	
Layer	Resistivity (Ωm)	Thickness(m)	Layer	Resistivity (Ωm)	Thickness(m)
1	88.5	0.2	1	47.6	0.2
2	46.9	2.8	2	94.1	3.9
3	13.3	2.1	3	26	2.6
4	193.4	16.7	4	159.4	24.2
5	111675.5		5	58770.7	

Sounding station GEOSCI 5-64			**Sounding station GEOSCI 5-65**		
L (m)	L (m)	ρ_a (Ωm)	L (m)	l (m)	ρ_a (Ωm)
2	0.5	47.5	2	0.5	62.0
3	0.5	54.9	3	0.5	70.5
4	0.5	59.4	4	0.5	80.5
6	0.5	62.8	6	0.5	98.2
8	0.5	62.4	8	0.5	107.8
10	0.5	59.9	10	0.5	111.4
12	2	56.5	12	2	110.7
16	2	50.2	16	2	103.0
20	2	46.0	20	2	94.1
24	2	44.3	24	2	87.2
30	2	44.9	30	2	82.5
40	6	50.1	40	6	85.7
50	6	56.6	50	6	94.9
60	6	62.9	60	6	106.2
80	6	74.3	80	6	128.5
100	6	84.2	100	6	150.0
120	6	93.5	120	6	171.0
160	20	111.4	160	20	213.5
200	20	129.9	200	20	257.0
240	20	149.4	240	20	301.1
300	20	180.0	300	20	367.1
400	20	233.0	400	20	474.0
Model	**RMS error (%) = 4.8**		**Model**		**RMS error (%) = 7.5**
Layer	Resistivity (Ωm)	Thickness(m)	Layer	Resistivity (Ωm)	Thickness(m)
1	34.9	0.4	1	56.3	1.1
2	77.1	2.8	2	299.4	1.7
3	23.6	5.7	3	18.7	3
4	121	63.6	4	219.7	42
5	3752.5		5	3716	

Sounding station GEOSCI 5-66			**Sounding station GEOSCI 5-67**		
L (m)	L (m)	ρ_a (Ωm)	L (m)	l (m)	ρ_a (Ωm)
2	0.5	56.1	2	0.5	55.5
3	0.5	57.2	3	0.5	57.0
4	0.5	58.8	4	0.5	58.9
6	0.5	62.3	6	0.5	62.2
8	0.5	64.3	8	0.5	63.5
10	0.5	64.8	10	0.5	63.1
12	2	63.9	12	2	61.6
16	2	60.0	16	2	57.6
20	2	56.0	20	2	54.5
24	2	53.1	24	2	53.2
30	2	51.2	30	2	53.8
40	6	52.7	40	6	59.1
50	6	56.8	50	6	65.9
60	6	61.7	60	6	72.7
80	6	72.2	80	6	85.5
100	6	83.3	100	6	97.5
120	6	95.3	120	6	109.4
160	20	121.0	160	20	133.8
200	20	147.9	200	20	158.7
240	20	175.1	240	20	183.8
300	20	215.4	300	20	220.6
400	20	280.4	400	20	278.2

Model	**RMS error (%) = 2.5**		**Model**	**RMS error (%) = 2.6**	
Layer	Resistivity (Ωm)	Thickness(m)	Layer	Resistivity (Ωm)	Thickness(m)
1	55.4	1.6	1	54.5	1.3
2	91.2	2.7	2	82.4	2.7
3	21.5	3.7	3	23.6	4
4	77.6	32.4	4	116.5	40.8
5	2755.4		5	1186.6	

Sounding station GEOSCI 7-40			**Sounding station GEOSCI 7-41**		
L (m)	L (m)	ρ_a (Ωm)	L (m)	l (m)	ρ_a (Ωm)
2	0.5	197.8	2	0.5	151.0
3	0.5	202.8	3	0.5	96.4
4	0.5	185.5	4	0.5	85.2
6	0.5	133.8	6	0.5	83.6
8	0.5	97.2	8	0.5	82.0
10	0.5	75.6	10	0.5	82.4
12	2	64.7	12	2	82.8
16	2	58.4	16	2	84.5
20	2	60.7	20	2	87.5
24	2	66.2	24	2	91.6
30	2	77.3	30	2	99.8
40	6	98.7	40	6	117.8
50	6	121.3	50	6	139.3
60	6	143.8	60	6	162.7
80	6	187.7	80	6	211.8
100	6	229.9	100	6	261.7
120	6	270.5	120	6	311.2
160	20	347.4	160	20	408.9
200	20	419.1	200	20	504.1
240	20	486.1	240	20	597.1
300	20	578.9	300	20	732.2
400	20	715.7	400	20	947.0
Model	**RMS error (%) = 3.3**		**Model**	**RMS error (%) = 4.4**	
Layer	Resistivity (Ωm)	Thickness(m)	Layer	Resistivity (Ωm)	Thickness(m)
1	119.3	0.3	1	596.5	0.3
2	329.7	0.8	2	80.6	13.5
3	44.6	8.5	3	740.8	12.7
4	2075.7		4	7024.2	

Sounding station GEOSCI 7-42			**Sounding station GEOSCI 7-43**		
L (m)	L (m)	ρ_a (Ωm)	L (m)	l (m)	ρ_a (Ωm)
2	0.5	154.1	2	0.5	88.3
3	0.5	147.7	3	0.5	84.7
4	0.5	137.3	4	0.5	79.3
6	0.5	111.3	6	0.5	66.9
8	0.5	89.1	8	0.5	57.3
10	0.5	73.2	10	0.5	51.1
12	2	63.0	12	2	47.6
16	2	54.1	16	2	45.6
20	2	52.8	20	2	47.2
24	2	55.0	24	2	50.5
30	2	61.4	30	2	57.1
40	6	76.2	40	6	69.5
50	6	93.2	50	6	82.0
60	6	111.1	60	6	93.8
80	6	147.3	80	6	115.4
100	6	183.4	100	6	135.0
120	6	219.3	120	6	153.4
160	20	290.3	160	20	188.5
200	20	360.4	200	20	223.4
240	20	429.6	240	20	259.1
300	20	531.5	300	20	314.2
400	20	697.2	400	20	409.4
Model	**RMS error (%) = 6**		**Model**	**RMS error (%) = 4.8**	
Layer	Resistivity (Ωm)	Thickness(m)	Layer	Resistivity (Ωm)	Thickness(m)
1	157.8	1.7	1	90.4	1.6
2	40.7	9.5	2	36.2	7.9
3	114.4	2.7	3	270.5	66
4	9757.6		4	13779.2	

Sounding station GEOSCI 7-44			**Sounding station GEOSCI 7-45**		
L (m)	L (m)	ρ_a (Ωm)	L (m)	l (m)	ρ_a (Ωm)
2	0.5	146.3	2	0.5	104.2
3	0.5	145.0	3	0.5	122.6
4	0.5	142.4	4	0.5	127.1
6	0.5	133.7	6	0.5	116.0
8	0.5	122.8	8	0.5	101.4
10	0.5	111.3	10	0.5	88.7
12	2	101.1	12	2	79.8
16	2	86.5	16	2	70.4
20	2	79.2	20	2	67.1
24	2	77.2	24	2	66.7
30	2	79.9	30	2	69.0
40	6	92.1	40	6	76.7
50	6	108.4	50	6	87.7
60	6	126.4	60	6	100.9
80	6	165.0	80	6	130.6
100	6	205.0	100	6	162.1
120	6	245.5	120	6	194.1
160	20	327.0	160	20	258.2
200	20	408.3	200	20	322.0
240	20	489.6	240	20	385.5
300	20	611.2	300	20	480.4
400	20	813.2	400	20	637.1
Model	**RMS error (%) = 4.9**		**Model**	**RMS error (%) = 5.6**	
Layer	Resistivity (Ωm)	Thickness(m)	Layer	Resistivity (Ωm)	Thickness(m)
1	147	2.8	1	19.4	0.1
2	53.8	8.1	2	754.4	0.3
3	154.3	11.5	3	58.8	17.6
4	93296.2		4	28425.6	

Sounding station GEOSCI 7-46			**Sounding station**		
L (m)	L (m)	ρ_a (Ωm)	L (m)	l (m)	ρ_a (Ωm)
2	0.5	103.4			
3	0.5	112.6			
4	0.5	107.4			
6	0.5	80.7			
8	0.5	57.7			
10	0.5	42.6			
12	2	34.4			
16	2	30.0			
20	2	32.3			
24	2	36.9			
30	2	45.4			
40	6	60.2			
50	6	75.0			
60	6	89.8			
80	6	119.2			
100	6	148.3			
120	6	177.1			
160	20	234.0			
200	20	290.0			
240	20	344.9			
300	20	425.7			
400	20	555.9			
Model	**RMS error (%) = 5**		**Model**	**RMS error (%) =**	
Layer	Resistivity (Ωm)	Thickness(m)	Layer	Resistivity (Ωm)	Thickness(m)
1	68.1	0.4			
2	329.1	0.5			
3	16.9	5.4			
4	6071.5				

Sounding station GEOSCI 9-68			**Sounding station GEOSCI 9-69**		
L (m)	L (m)	ρ_a (Ωm)	L (m)	l (m)	ρ_a (Ωm)
2	0.5	92.8	2	0.5	50.7
3	0.5	72.7	3	0.5	46.9
4	0.5	60.7	4	0.5	43.7
6	0.5	48.5	6	0.5	39.9
8	0.5	41.5	8	0.5	38.3
10	0.5	36.2	10	0.5	37.5
12	2	32.4	12	2	37.2
16	2	27.6	16	2	37.0
20	2	25.5	20	2	37.2
24	2	24.7	24	2	37.7
30	2	24.8	30	2	38.8
40	6	26.9	40	6	41.5
50	6	30.3	50	6	45.3
60	6	34.4	60	6	49.7
80	6	43.8	80	6	59.6
100	6	53.7	100	6	70.1
120	6	63.6	120	6	80.9
160	20	82.8	160	20	103.0
200	20	101.3	200	20	125.7
240	20	119.0	240	20	149.0
300	20	144.2	300	20	184.4
400	20	183.2	400	20	243.8
Model	**RMS error (%) = 2.8**		**Model**	**RMS error (%) = 3.5**	
Layer	Resistivity (Ωm)	Thickness(m)	Layer	Resistivity (Ωm)	Thickness(m)
1	126.1	0.5	1	54.5	0.7
2	50.2	2	2	36	18.4
3	20.8	17.4	3	147.2	40.8
4	837.4		4	9611.7	

Sounding station GEOSCI 9-70			**Sounding station GEOSCI 9-71**		
L (m)	L (m)	ρ_a (Ωm)	L (m)	l (m)	ρ_a (Ωm)
2	0.5	38.9	2	0.5	104.7
3	0.5	42.8	3	0.5	90.4
4	0.5	43.0	4	0.5	77.4
6	0.5	39.6	6	0.5	64.0
8	0.5	36.7	8	0.5	62.1
10	0.5	34.7	10	0.5	62.8
12	2	33.9	12	2	63.8
16	2	34.0	16	2	64.2
20	2	35.3	20	2	63.4
24	2	37.1	24	2	62.4
30	2	40.0	30	2	61.3
40	6	44.4	40	6	61.0
50	6	48.0	50	6	62.4
60	6	51.1	60	6	64.6
80	6	56.4	80	6	70.5
100	6	61.5	100	6	77.0
120	6	66.8	120	6	83.7
160	20	78.9	160	20	97.6
200	20	92.8	200	20	112.3
240	20	107.9	240	20	127.9
300	20	131.5	300	20	152.0
400	20	171.1	400	20	191.9
Model	**RMS error (%) = 1.9**		**Model**	**RMS error (%) = 1.4**	
Layer	Resistivity (Ωm)	Thickness(m)	Layer	Resistivity (Ωm)	Thickness(m)
1	17	0.2	1	116.8	1
2	65.9	0.7	2	23.9	0.7
3	28.3	5.4	3	117.9	1.5
4	61.1	53.1	4	53.2	15.4
5	2050.5		5	97	53
			6	1040.5	

Sounding station GEOSCI 12-124			**Sounding station GEOSCI 12- 125**		
L (m)	L (m)	ρ_a (Ωm)	L (m)	l (m)	ρ_a (Ωm)
2	0.5	66.3	2	0.5	407.5
3	0.5	76.8	3	0.5	535.9
4	0.5	81.3	4	0.5	614.6
6	0.5	80.8	6	0.5	656.6
8	0.5	77.3	8	0.5	622.9
10	0.5	73.7	10	0.5	551.9
12	2	70.9	12	2	476.4
16	2	67.6	16	2	354.4
20	2	66.1	20	2	288.1
24	2	65.5	24	2	263.3
30	2	65.4	30	2	261.5
40	6	65.7	40	6	292.3
50	6	65.9	50	6	323.0
60	6	65.6	60	6	344.4
80	6	64.0	80	6	369.0
100	6	62.1	100	6	381.6
120	6	60.8	120	6	390.6
160	20	60.3	160	20	413.0
200	20	62.4	200	20	443.9
240	20	66.3	240	20	480.3
300	20	73.8	300	20	536.2
400	20	88.1	400	20	618.5
Model	**RMS error (%) = 4.7**		**Model**	**RMS error (%) = 9.3**	
Layer	Resistivity (Ωm)	Thickness(m)	Layer	Resistivity (Ωm)	Thickness(m)
1	47.4	0.5	1	134.8	0.3
2	181.1	0.5	2	5305.4	0.4
3	62	11.9	3	29	1.3
4	118.6	4.7	4	3077	3.3
5	47.7	71	5	55.5	6.6
6	273		6	1052	

Sounding station GEOSCI 12-126			**Sounding station GEOSCI 12- 127**		
L (m)	L (m)	ρ_a (Ωm)	L (m)	l (m)	ρ_a (Ωm)
2	0.5	41.1	2	0.5	140.1
3	0.5	47.2	3	0.5	154.7
4	0.5	53.2	4	0.5	152.3
6	0.5	62.0	6	0.5	130.5
8	0.5	67.4	8	0.5	114.8
10	0.5	72.0	10	0.5	107.2
12	2	76.6	12	2	106.4
16	2	87.1	16	2	113.4
20	2	98.5	20	2	123.8
24	2	109.9	24	2	133.7
30	2	125.9	30	2	146.8
40	6	148.7	40	6	165.0
50	6	167.1	50	6	180.8
60	6	182.3	60	6	195.1
80	6	205.9	80	6	220.2
100	6	223.4	100	6	241.2
120	6	237.3	120	6	258.6
160	20	259.1	160	20	285.2
200	20	277.6	200	20	304.0
240	20	295.0	240	20	317.7
300	20	320.9	300	20	332.0
400	20	364.1	400	20	346.5
Model	**RMS error (%) = 9.4**		**Model**	**RMS error (%) = 4.8**	
Layer	Resistivity (Ωm)	Thickness(m)	Layer	Resistivity (Ωm)	Thickness(m)
1	36.1	0.9	1	71.2	0.3
2	323.3	0.3	2	345.9	0.6
3	50.3	2.6	3	55.1	2
4	284.6	92.6	4	188.3	13.7
5	792.9		5	374.8	

Sounding station GEOSCI 12-128			**Sounding station GEOSCI 12- 129**		
L (m)	L (m)	ρ_a (Ωm)	L (m)	l (m)	ρ_a (Ωm)
2	0.5	101.0	2	0.5	134.3
3	0.5	124.8	3	0.5	168.0
4	0.5	143.1	4	0.5	186.2
6	0.5	160.7	6	0.5	191.1
8	0.5	162.2	8	0.5	179.6
10	0.5	155.7	10	0.5	162.4
12	2	146.8	12	2	146.5
16	2	131.1	16	2	124.1
20	2	122.4	20	2	112.1
24	2	119.9	24	2	106.5
30	2	122.5	30	2	103.5
40	6	134.3	40	6	103.6
50	6	148.3	50	6	105.8
60	6	162.2	60	6	109.0
80	6	187.8	80	6	117.4
100	6	209.6	100	6	127.0
120	6	227.9	120	6	137.0
160	20	256.2	160	20	155.4
200	20	276.7	200	20	170.8
240	20	291.9	240	20	183.4
300	20	308.3	300	20	198.1
400	20	325.5	400	20	215.1
Model	**RMS error (%) = 5**		**Model**	**RMS error (%) = 4.1**	
Layer	Resistivity (Ωm)	Thickness(m)	Layer	Resistivity (Ωm)	Thickness(m)
1	75.4	0.6	1	55.4	0.3
2	373.3	1.2	2	414.9	1
3	51.4	2.2	3	73.1	2
4	133.1	10.6	4	99.8	25.9
5	361.9		5	261.6	

Sounding station GEOSCI 13-118			**Sounding station GEOSCI 13- 119**		
L (m)	L (m)	ρ_a (Ωm)	L (m)	l (m)	ρ_a (Ωm)
2	0.5	109.7	2	0.5	23.4
3	0.5	81.1	3	0.5	23.6
4	0.5	63.5	4	0.5	24.1
6	0.5	51.5	6	0.5	25.8
8	0.5	52.6	8	0.5	28.2
10	0.5	57.8	10	0.5	30.9
12	2	64.6	12	2	33.8
16	2	79.0	16	2	39.1
20	2	92.1	20	2	43.7
24	2	103.3	24	2	47.6
30	2	116.4	30	2	52.2
40	6	130.2	40	6	57.5
50	6	136.8	50	6	61.1
60	6	139.2	60	6	63.4
80	6	138.5	80	6	65.7
100	6	137.2	100	6	66.2
120	6	138.0	120	6	66.1
160	20	146.7	160	20	65.6
200	20	160.5	200	20	66.8
240	20	175.3	240	20	70.0
300	20	195.9	300	20	77.3
400	20	223.4	400	20	93.1
Model	**RMS error (%) = 3.4**		**Model**	**RMS error (%) = 4.2**	
Layer	Resistivity (Ωm)	Thickness(m)	Layer	Resistivity (Ωm)	Thickness(m)
1	147.5	0.6	1	23.2	2.9
2	38.1	3.1	2	76.1	38.8
3	820.8	3.6	3	18.5	20.5
4	23	7.3	4	386.9	
5	340.4				

Sounding station GEOSCI 13-120			**Sounding station GEOSCI 13- 121**		
L (m)	L (m)	ρ_a (Ωm)	L (m)	l (m)	ρ_a (Ωm)
2	0.5	18.2	2	0.5	64.3
3	0.5	22.4	3	0.5	58.2
4	0.5	25.0	4	0.5	51.6
6	0.5	27.6	6	0.5	41.4
8	0.5	29.6	8	0.5	37.0
10	0.5	31.7	10	0.5	35.7
12	2	34.1	12	2	36.2
16	2	39.0	16	2	39.5
20	2	43.7	20	2	44.1
24	2	47.8	24	2	48.8
30	2	52.8	30	2	55.5
40	6	59.0	40	6	65.0
50	6	63.5	50	6	72.9
60	6	66.8	60	6	79.5
80	6	71.6	80	6	90.6
100	6	75.0	100	6	100.0
120	6	77.9	120	6	108.4
160	20	83.6	160	20	124.1
200	20	89.9	200	20	138.4
240	20	97.1	240	20	151.4
300	20	109.4	300	20	168.5
400	20	132.2	400	20	191.2
Model	**RMS error (%) = 3.4**		**Model**	**RMS error (%) = 4.9**	
Layer	Resistivity (Ωm)	Thickness(m)	Layer	Resistivity (Ωm)	Thickness(m)
1	11.5	0.5	1	68.8	1
2	71.1	0.5	2	27.9	4.4
3	12.7	1.1	3	114.7	38.7
4	80	92.5	4	289.4	
5	600.1				

Sounding station GEOSCI 13-122			**Sounding station GEOSCI 13- 123**		
L (m)	L (m)	ρ_a (Ωm)	L (m)	l (m)	ρ_a (Ωm)
2	0.5	20.1	2	0.5	13.5
3	0.5	12.1	3	0.5	13.4
4	0.5	10.6	4	0.5	14.0
6	0.5	12.1	6	0.5	16.2
8	0.5	13.8	8	0.5	18.9
10	0.5	15.9	10	0.5	21.6
12	2	18.0	12	2	24.1
16	2	22.2	16	2	28.4
20	2	26.4	20	2	31.9
24	2	30.4	24	2	34.8
30	2	35.8	30	2	38.3
40	6	43.9	40	6	42.6
50	6	50.9	50	6	46.0
60	6	57.0	60	6	48.8
80	6	67.5	80	6	53.9
100	6	76.4	100	6	59.3
120	6	84.2	120	6	65.3
160	20	98.2	160	20	79.2
200	20	110.9	200	20	94.8
240	20	122.8	240	20	111.2
300	20	139.2	300	20	136.1
400	20	162.8	400	20	176.9
Model	**RMS error (%) = 5.6**		**Model**	**RMS error (%) = 5.8**	
Layer	Resistivity (Ωm)	Thickness(m)	Layer	Resistivity (Ωm)	Thickness(m)
1	48.4	0.4	1	16.8	0.3
2	3	0.3	2	12.2	1.8
3	13.5	2.9	3	53.9	46.6
4	112.1	49.8	4	1710.3	
5	312.9				

Sounding station GEOSCI 14-103			**Sounding station GEOSCI 14- 104**		
L (m)	L (m)	ρ_a (Ωm)	L (m)	l (m)	ρ_a (Ωm)
2	0.5	31.9	2	0.5	32.0
3	0.5	17.6	3	0.5	17.8
4	0.5	12.2	4	0.5	11.7
6	0.5	10.6	6	0.5	9.0
8	0.5	11.6	8	0.5	9.3
10	0.5	13.0	10	0.5	10.2
12	2	14.5	12	2	11.2
16	2	17.3	16	2	13.4
20	2	20.1	20	2	15.6
24	2	22.8	24	2	17.6
30	2	27.1	30	2	20.5
40	6	34.6	40	6	25.2
50	6	42.6	50	6	29.9
60	6	50.8	60	6	34.8
80	6	67.5	80	6	45.1
100	6	84.4	100	6	55.9
120	6	101.3	120	6	66.8
160	20	135.0	160	20	88.9
200	20	168.7	200	20	111.0
240	20	202.4	240	20	133.0
300	20	253.0	300	20	166.0
400	20	337.2	400	20	220.8
Model	**RMS error (%) = 7.6**		**Model**	**RMS error (%) = 9.4**	
Layer	Resistivity (Ωm)	Thickness(m)	Layer	Resistivity (Ωm)	Thickness(m)
1	65	0.5	1	61.7	0.5
2	7.8	2.1	2	7.2	3
3	27.9	8.9	3	33.5	15.6
4	223499.2		4	20233.8	

Sounding station GEOSCI 14-105			**Sounding station GEOSCI 14- 106**		
L (m)	L (m)	ρ_a (Ωm)	L (m)	l (m)	ρ_a (Ωm)
2	0.5	32.5	2	0.5	46.8
3	0.5	21.6	3	0.5	29.0
4	0.5	14.7	4	0.5	18.7
6	0.5	10.4	6	0.5	12.4
8	0.5	10.8	8	0.5	12.6
10	0.5	12.4	10	0.5	14.2
12	2	14.0	12	2	16.1
16	2	17.0	16	2	19.9
20	2	19.7	20	2	23.4
24	2	22.2	24	2	26.7
30	2	25.6	30	2	31.6
40	6	30.8	40	6	39.6
50	6	36.1	50	6	47.8
60	6	41.5	60	6	56.3
80	6	53.1	80	6	73.9
100	6	65.4	100	6	92.1
120	6	78.0	120	6	110.3
160	20	103.8	160	20	147.0
200	20	129.7	200	20	183.7
240	20	155.6	240	20	220.4
300	20	194.5	300	20	275.4
400	20	259.2	400	20	366.9
Model	**RMS error (%) = 13**		**Model**	**RMS error (%) = 6**	
Layer	Resistivity (Ωm)	Thickness(m)	Layer	Resistivity (Ωm)	Thickness(m)
1	46.3	0.7	1	72.1	0.6
2	5.5	1.6	2	7.8	2.2
3	39.6	18.2	3	52.2	13.2
4	215445.2		4	111846.9	

Sounding station GEOSCI 14-107			**Sounding station GEOSCI 14- 108**		
L (m)	L (m)	ρ_a (Ωm)	L (m)	l (m)	ρ_a (Ωm)
2	0.5	30.9	2	0.5	34.1
3	0.5	19.1	3	0.5	21.9
4	0.5	12.4	4	0.5	15.1
6	0.5	8.5	6	0.5	10.9
8	0.5	8.9	8	0.5	11.1
10	0.5	10.3	10	0.5	12.2
12	2	11.9	12	2	13.6
16	2	15.2	16	2	16.4
20	2	18.4	20	2	19.0
24	2	21.6	24	2	21.4
30	2	26.1	30	2	24.8
40	6	33.3	40	6	30.2
50	6	40.3	50	6	35.7
60	6	47.3	60	6	41.3
80	6	61.5	80	6	53.3
100	6	76.0	100	6	65.9
120	6	90.7	120	6	78.8
160	20	120.6	160	20	104.9
200	20	150.6	200	20	131.1
240	20	180.6	240	20	157.3
300	20	225.7	300	20	196.6
400	20	300.8	400	20	261.9
Model	**RMS error (%) = 6.8**		**Model**	**RMS error (%) = 7.6**	
Layer	Resistivity (Ωm)	Thickness(m)	Layer	Resistivity (Ωm)	Thickness(m)
1	47.8	0.6	1	52.2	0.6
2	5.3	2.4	2	7.7	2.5
3	92.3	18.9	3	39.1	16.6
4	112185		4	112381.9	

Sounding station GEOSCI 15-109			**Sounding station GEOSCI 15- 110**		
L (m)	L (m)	ρ_a (Ωm)	L (m)	l (m)	ρ_a (Ωm)
2	0.5	16.2	2	0.5	10.4
3	0.5	14.1	3	0.5	9.6
4	0.5	14.5	4	0.5	10.5
6	0.5	17.4	6	0.5	13.2
8	0.5	20.8	8	0.5	16.1
10	0.5	24.8	10	0.5	19.5
12	2	28.9	12	2	23.1
16	2	36.8	16	2	30.5
20	2	44.2	20	2	38.0
24	2	51.1	24	2	45.6
30	2	60.7	30	2	56.9
40	6	74.7	40	6	75.6
50	6	86.9	50	6	94.3
60	6	97.6	60	6	112.8
80	6	115.7	80	6	149.6
100	6	130.8	100	6	185.9
120	6	144.1	120	6	221.9
160	20	167.8	160	20	292.8
200	20	190.5	200	20	362.2
240	20	213.8	240	20	430.3
300	20	250.8	300	20	529.9
400	20	318.4	400	20	689.7
Model	**RMS error (%) = 8.3**		**Model**	**RMS error (%) = 18**	
Layer	Resistivity (Ωm)	Thickness(m)	Layer	Resistivity (Ωm)	Thickness(m)
1	150.6	0.2	1	93.1	0.2
2	12.6	2.3	2	3.7	0.2
3	202.6	89.5	3	11.3	2.3
4	11307		4	6460. 8	

Sounding station GEOSCI 15-111			**Sounding station GEOSCI 15- 112**		
L (m)	L (m)	ρ_a (Ωm)	L (m)	l (m)	ρ_a (Ωm)
2	0.5	20.5	2	0.5	35.7
3	0.5	11.3	3	0.5	15.4
4	0.5	10.7	4	0.5	12.1
6	0.5	13.0	6	0.5	13.4
8	0.5	15.4	8	0.5	15.2
10	0.5	18.4	10	0.5	17.6
12	2	21.3	12	2	19.7
16	2	26.6	16	2	23.5
20	2	31.6	20	2	26.8
24	2	36.0	24	2	29.6
30	2	42.1	30	2	33.1
40	6	50.7	40	6	37.7
50	6	57.9	50	6	41.5
60	6	64.3	60	6	45.0
80	6	75.3	80	6	51.8
100	6	85.1	100	6	59.0
120	6	94.5	120	6	66.9
160	20	113.2	160	20	84.3
200	20	132.0	200	20	103.1
240	20	150.9	240	20	122.2
300	20	178.5	300	20	150.9
400	20	220.9	400	20	197.6
Model	**RMS error (%) = 4.6**		**Model**	**RMS error (%) = 4.9**	
Layer	Resistivity (Ωm)	Thickness(m)	Layer	Resistivity (Ωm)	Thickness(m)
1	165.2	0.3	1	173.7	0.3
2	9.3	2.2	2	10.1	2.2
3	103.6	45.9	3	50.8	37
4	721.7		4	2624.6	

Sounding station GEOSCI 15-113			**Sounding station GEOSCI 15- 114**		
L (m)	L (m)	ρ_a (Ωm)	L (m)	l (m)	ρ_a (Ωm)
2	0.5	8.4	2	0.5	7.0
3	0.5	6.3	3	0.5	7.1
4	0.5	6.3	4	0.5	7.4
6	0.5	7.6	6	0.5	8.3
8	0.5	8.9	8	0.5	9.6
10	0.5	10.6	10	0.5	11.0
12	2	12.2	12	2	12.3
16	2	15.3	16	2	15.0
20	2	18.1	20	2	17.3
24	2	20.7	24	2	19.3
30	2	24.3	30	2	21.8
40	6	29.6	40	6	25.2
50	6	34.4	50	6	28.0
60	6	39.0	60	6	30.6
80	6	47.8	80	6	35.6
100	6	56.9	100	6	41.1
120	6	66.4	120	6	47.1
160	20	86.3	160	20	60.2
200	20	106.8	200	20	73.8
240	20	127.6	240	20	87.4
300	20	158.8	300	20	107.4
400	20	210.3	400	20	139.4
Model	**RMS error (%) = 4.1**		**Model**	**RMS error (%) = 3.6**	
Layer	Resistivity (Ωm)	Thickness(m)	Layer	Resistivity (Ωm)	Thickness(m)
1	69.3	0.2	1	6.9	2.6
2	5.6	2.3	2	39.9	14.6
3	57.9	29.8	3	12.2	6.7
4	7777.9		4	1194.3	

Sounding station GEOSCI 15-115			**Sounding station GEOSCI 15- 116**		
L (m)	L (m)	ρ_a (Ωm)	L (m)	l (m)	ρ_a (Ωm)
2	0.5	17.1	2	0.5	9.2
3	0.5	15.1	3	0.5	9.6
4	0.5	13.5	4	0.5	10.1
6	0.5	12.8	6	0.5	11.7
8	0.5	14.3	8	0.5	13.2
10	0.5	16.5	10	0.5	14.6
12	2	18.9	12	2	15.9
16	2	23.3	16	2	18.0
20	2	27.3	20	2	19.9
24	2	30.8	24	2	21.7
30	2	35.6	30	2	24.3
40	6	42.8	40	6	28.6
50	6	49.4	50	6	32.9
60	6	56.0	60	6	37.1
80	6	69.4	80	6	45.6
100	6	83.5	100	6	54.3
120	6	98.1	120	6	63.3
160	20	127.8	160	20	82.1
200	20	157.4	200	20	101.4
240	20	186.4	240	20	120.8
300	20	228.8	300	20	149.8
400	20	296.3	400	20	197.3
Model	**RMS error (%) = 6.7**		**Model**	**RMS error (%) = 9.2**	
Layer	Resistivity (Ωm)	Thickness(m)	Layer	Resistivity (Ωm)	Thickness(m)
1	18.7	1	1	9	1.7
2	3.4	0.7	2	22.6	7.7
3	65.5	23.1	3	62.4	27.5
4	2297.9		4	3944.8	

Sounding station GEOSCI 15-117			**Sounding station**		
L (m)	L (m)	ρ_a (Ωm)	L (m)	l (m)	ρ_a (Ωm)
2	0.5	9.0	2	0.5	
3	0.5	9.8	3	0.5	
4	0.5	10.9	4	0.5	
6	0.5	13.6	6	0.5	
8	0.5	15.9	8	0.5	
10	0.5	18.1	10	0.5	
12	2	19.9	12	2	
16	2	23.3	16	2	
20	2	26.4	20	2	
24	2	29.3	24	2	
30	2	33.4	30	2	
40	6	39.7	40	6	
50	6	45.7	50	6	
60	6	51.5	60	6	
80	6	63.4	80	6	
100	6	75.9	100	6	
120	6	89.0	120	6	
160	20	116.5	160	20	
200	20	144.8	200	20	
240	20	173.3	240	20	
300	20	216.0	300	20	
400	20	286.6	400	20	
Model	**RMS error (%) = 1.8**		**Model**	**RMS error (%) =**	
Layer	Resistivity (Ωm)	Thickness(m)	Layer	Resistivity (Ωm)	Thickness(m)
1	8.4	1.3			
2	28.3	4.7			
3	68.2	25.2			
4	14547.3				

Sounding station GEOSCI 16-96			**Sounding station GEOSCI 16-97**		
L (m)	L (m)	ρ_a (Ωm)	L (m)	l (m)	ρ_a (Ωm)
2	0.5	72.0	2	0.5	42.9
3	0.5	52.0	3	0.5	32.8
4	0.5	45.6	4	0.5	25.7
6	0.5	39.6	6	0.5	19.0
8	0.5	34.5	8	0.5	17.1
10	0.5	31.2	10	0.5	16.4
12	2	28.9	12	2	16.3
16	2	27.1	16	2	16.5
20	2	27.4	20	2	17.1
24	2	28.8	24	2	18.1
30	2	32.2	30	2	20.0
40	6	39.6	40	6	24.2
50	6	48.0	50	6	28.9
60	6	56.6	60	6	34.0
80	6	73.4	80	6	44.1
100	6	89.7	100	6	54.0
120	6	105.2	120	6	63.6
160	20	134.3	160	20	81.6
200	20	161.2	200	20	98.5
240	20	186.1	240	20	114.2
300	20	220.2	300	20	136.0
400	20	269.7	400	20	168.2
Model	**RMS error (%) = 4.7**		**Model**	**RMS error (%) = 6.6**	
Layer	Resistivity (Ωm)	Thickness(m)	Layer	Resistivity (Ωm)	Thickness(m)
1	219.8	0.3	1	54.8	0.7
2	46.5	1.7	2	15.2	12.5
3	21.7	9.9	3	489.7	
4	696.3				

Sounding station GEOSCI 16-98			**Sounding station GEOSCI 16-99**		
L (m)	L (m)	ρ_a (Ωm)	L (m)	l (m)	ρ_a (Ωm)
2	0.5	19.5	2	0.5	53.8
3	0.5	12.7	3	0.5	27.8
4	0.5	10.1	4	0.5	17.5
6	0.5	9.1	6	0.5	12.7
8	0.5	9.3	8	0.5	12.4
10	0.5	9.9	10	0.5	12.9
12	2	10.9	12	2	13.9
16	2	13.2	16	2	16.4
20	2	16.0	20	2	19.6
24	2	18.9	24	2	23.1
30	2	23.4	30	2	28.6
40	6	31.0	40	6	38.0
50	6	38.4	50	6	47.5
60	6	45.7	60	6	57.0
80	6	60.0	80	6	76.0
100	6	73.8	100	6	95.0
120	6	87.3	120	6	113.9
160	20	113.1	160	20	151.8
200	20	137.6	200	20	189.5
240	20	160.7	240	20	227.2
300	20	193.4	300	20	283.7
400	20	242.9	400	20	377.4
Model	**RMS error (%) = 6.3**		**Model**	**RMS error (%) = 5.9**	
Layer	Resistivity (Ωm)	Thickness(m)	Layer	Resistivity (Ωm)	Thickness(m)
1	37	0.4	1	112.9	0.5
2	8	4.9	2	10.9	5.7
3	886.9		3	40628.8	

Sounding station GEOSCI 16-100			**Sounding station GEOSCI 16-101**		
L (m)	L (m)	ρ_a (Ωm)	L (m)	l (m)	ρ_a (Ωm)
2	0.5	16.0	2	0.5	17.1
3	0.5	7.2	3	0.5	11.3
4	0.5	6.6	4	0.5	9.3
6	0.5	7.7	6	0.5	8.5
8	0.5	8.4	8	0.5	8.8
10	0.5	9.7	10	0.5	9.5
12	2	11.2	12	2	10.4
16	2	14.5	16	2	12.8
20	2	18.0	20	2	15.6
24	2	21.6	24	2	18.6
30	2	27.0	30	2	23.1
40	6	36.0	40	6	30.8
50	6	45.0	50	6	38.6
60	6	53.9	60	6	46.3
80	6	71.9	80	6	61.7
100	6	89.9	100	6	77.1
120	6	107.9	120	6	92.5
160	20	143.8	160	20	123.3
200	20	179.7	200	20	154.2
240	20	215.7	240	20	185.0
300	20	269.5	300	20	231.2
400	20	359.3	400	20	308.2
Model	**RMS error (%) = 9.9**		**Model**	**RMS error (%) = 7.6**	
Layer	Resistivity (Ωm)	Thickness(m)	Layer	Resistivity (Ωm)	Thickness(m)
1	330.3	0.2	1	32.9	0.4
2	6.6	3.6	2	7.5	4.8
3	297179.6		3	303753.9	

Sounding station GEOSCI 16-102			**Sounding station**		
L (m)	L (m)	ρ_a (Ωm)	L (m)	l (m)	ρ_a (Ωm)
2	0.5	29.6			
3	0.5	19.7			
4	0.5	14.3			
6	0.5	10.6			
8	0.5	9.9			
10	0.5	10.0			
12	2	10.4			
16	2	11.7			
20	2	13.4			
24	2	15.5			
30	2	18.9			
40	6	25.0			
50	6	31.2			
60	6	37.5			
80	6	50.0			
100	6	62.4			
120	6	74.9			
160	20	99.9			
200	20	124.8			
240	20	149.8			
300	20	187.2			
400	20	249.6			
Model	**RMS error (%) = 6.7**		**Model**	**RMS error (%) =**	
Layer	Resistivity (Ωm)	Thickness(m)	Layer	Resistivity (Ωm)	Thickness(m)
1	45.4	0.6			
2	8.8	7			
3	248347.8				

Sounding station GEOSCI 20-145			**Sounding station 20-146**		
L (m)	L (m)	ρ_a (Ωm)	L (m)	l (m)	ρ_a (Ωm)
2	0.5	81.8	2	0.5	74.6
3	0.5	92.4	3	0.5	82.3
4	0.5	98.7	4	0.5	92.6
6	0.5	104.5	6	0.5	114.4
8	0.5	106.4	8	0.5	130.1
10	0.5	106.4	10	0.5	140.8
12	2	105.7	12	2	147.1
16	2	104.7	16	2	152.1
20	2	106.2	20	2	153.2
24	2	110.6	24	2	153.9
30	2	120.4	30	2	156.8
40	6	140.5	40	6	167.4
50	6	160.0	50	6	180.3
60	6	177.1	60	6	192.5
80	6	204.4	80	6	209.5
100	6	224.0	100	6	217.7
120	6	238.0	120	6	220.3
160	20	255.3	160	20	218.7
200	20	265.8	200	20	217.5
240	20	274.8	240	20	220.8
300	20	292.6	300	20	235.1
400	20	338.2	400	20	278.4
Model	**RMS error (%) = 5.5**		**Model**	**RMS error (%) =4.8**	
Layer	Resistivity (Ωm)	Thickness(m)	Layer	Resistivity (Ωm)	Thickness(m)
1	60	0.4	1	69.8	1.3
2	116.3	4	2	339.8	1.8
3	35	2.1	3	86.6	5.6
4	363.4	47	4	404.1	17.5
5	55.4	22.7	5	134.9	80
6	31971.4		6	6154.4	

Sounding station GEOSCI 20-147			**Sounding station 20-148**		
L (m)	L (m)	ρ_a (Ωm)	L (m)	l (m)	ρ_a (Ωm)
2	0.5	76.7	2	0.5	109.4
3	0.5	90.1	3	0.5	113.8
4	0.5	104.4	4	0.5	120.5
6	0.5	128.8	6	0.5	137.4
8	0.5	144.6	8	0.5	151.3
10	0.5	154.6	10	0.5	161.0
12	2	160.1	12	2	166.2
16	2	163.1	16	2	168.4
20	2	160.9	20	2	166.2
24	2	157.3	24	2	163.8
30	2	152.9	30	2	162.6
40	6	150.9	40	6	167.5
50	6	154.0	50	6	175.9
60	6	159.1	60	6	184.8
80	6	169.6	80	6	199.8
100	6	177.5	100	6	211.2
120	6	183.1	120	6	220.3
160	20	191.6	160	20	235.8
200	20	200.3	200	20	251.0
240	20	211.2	240	20	267.8
300	20	232.6	300	20	297.1
400	20	279.3	400	20	356.5
Model	**RMS error (%) = 5.8**		**Model**	**RMS error (%) = 3.8**	
Layer	Resistivity (Ωm)	Thickness(m)	Layer	Resistivity (Ωm)	Thickness(m)
1	66.3	0.9	1	107	1.7
2	244.8	3.1	2	371.5	1.9
3	107.8	8.9	3	64.1	2.9
4	256.8	13.8	4	241.1	120.6
5	171.9	96.9	5	6088.4	
6	6060.9				

Sounding station GEOSCI 20-149			**Sounding station 20-150**		
L (m)	L (m)	ρ_a (Ωm)	L (m)	l (m)	ρ_a (Ωm)
2	0.5	89.1	2	0.5	122.6
3	0.5	105.2	3	0.5	125.3
4	0.5	120.7	4	0.5	130.0
6	0.5	144.5	6	0.5	143.0
8	0.5	158.6	8	0.5	155.7
10	0.5	166.2	10	0.5	165.9
12	2	169.1	12	2	172.7
16	2	166.5	16	2	178.6
20	2	159.1	20	2	179.2
24	2	150.8	24	2	178.4
30	2	140.9	30	2	179.1
40	6	132.8	40	6	187.2
50	6	131.9	50	6	200.3
60	6	133.9	60	6	215.0
80	6	138.2	80	6	241.6
100	6	140.4	100	6	263.4
120	6	141.5	120	6	281.4
160	20	146.2	160	20	311.5
200	20	156.4	200	20	338.8
240	20	171.7	240	20	366.4
300	20	199.2	300	20	411.3
400	20	248.1	400	20	496.6
Model	**RMS error (%) = 3.7**		**Model**	**RMS error (%) = 5.1**	
Layer	Resistivity (Ωm)	Thickness(m)	Layer	Resistivity (Ωm)	Thickness(m)
1	75.1	0.8	1	121.1	2
2	233.7	3.7	2	318.1	2.7
3	85.8	9	3	65.7	3.3
4	288.8	11.7	4	347.9	112.5
5	57.4	27.6	5	6204.5	
6	1087				

Sounding station GEOSCI 21-130			**Sounding station GEOSCI 21-131**		
L (m)	L (m)	ρ_a (Ωm)	L (m)	l (m)	ρ_a (Ωm)
2	0.5	64.5	2	0.5	73.7
3	0.5	72.2	3	0.5	80.4
4	0.5	81.6	4	0.5	89.6
6	0.5	98.7	6	0.5	108.4
8	0.5	108.1	8	0.5	120.6
10	0.5	111.9	10	0.5	126.7
12	2	112.0	12	2	127.8
16	2	107.5	16	2	121.7
20	2	103.5	20	2	112.3
24	2	102.4	24	2	103.8
30	2	106.1	30	2	96.6
40	6	121.4	40	6	96.6
50	6	139.8	50	6	104.1
60	6	157.4	60	6	113.6
80	6	185.8	80	6	129.7
100	6	205.6	100	6	140.0
120	6	219.0	120	6	146.0
160	20	234.0	160	20	151.3
200	20	242.4	200	20	154.7
240	20	250.2	240	20	159.9
300	20	267.1	300	20	173.3
400	20	311.6	400	20	208.5
Model	**RMS error (%) = 3.6**		**Model**	**RMS error (%) = 6.1**	
Layer	Resistivity (Ωm)	Thickness(m)	Layer	Resistivity (Ωm)	Thickness(m)
1	59.4	1.2	1	69.5	1.3
2	341.6	1.4	2	393.6	1.6
3	20.6	2.4	3	17.2	2.9
4	770.3	17.2	4	822.7	8.2
5	40.1	20.3	5	49.7	38.3
6	10340.4		6	7442.2	

Sounding station GEOSCI 21-132			**Sounding station GEOSCI 21-133**		
L (m)	L (m)	ρ_a (Ωm)	L (m)	l (m)	ρ_a (Ωm)
2	0.5	70.1	2	0.5	121.1
3	0.5	88.6	3	0.5	125.3
4	0.5	98.8	4	0.5	126.9
6	0.5	103.6	6	0.5	127.5
8	0.5	101.7	8	0.5	126.9
10	0.5	98.6	10	0.5	125.2
12	2	96.8	12	2	123.0
16	2	98.0	16	2	117.6
20	2	102.6	20	2	111.9
24	2	108.0	24	2	107.1
30	2	115.5	30	2	102.6
40	6	124.5	40	6	101.8
50	6	130.1	50	6	105.8
60	6	133.4	60	6	111.3
80	6	135.6	80	6	119.7
100	6	134.6	100	6	123.1
120	6	132.2	120	6	122.3
160	20	127.1	160	20	115.4
200	20	125.3	200	20	108.4
240	20	128.2	240	20	104.9
300	20	139.5	300	20	106.6
400	20	171.0	400	20	123.6
Model	**RMS error (%) = 3.9**		**Model**	**RMS error (%) = 3.9**	
Layer	Resistivity (Ωm)	Thickness(m)	Layer	Resistivity (Ωm)	Thickness(m)
1	34.6	0.4	1	97.6	0.2
2	388.1	0.6	2	130	6
3	23.9	0.9	3	54.9	6.8
4	153.4	37.8	4	301.3	17
5	58.2	51	5	31.7	45.7
6	7610.3		6	6836.4	

Sounding station GEOSCI 21-134			**Sounding station GEOSCI 21-135**		
L (m)	L (m)	ρ_a (Ωm)	L (m)	l (m)	ρ_a (Ωm)
2	0.5	75.8	2	0.5	76.9
3	0.5	82.1	3	0.5	82.7
4	0.5	87.4	4	0.5	89.1
6	0.5	92.5	6	0.5	98.9
8	0.5	92.7	8	0.5	102.6
10	0.5	91.7	10	0.5	103.0
12	2	91.1	12	2	101.7
16	2	94.2	16	2	98.7
20	2	101.6	20	2	97.4
24	2	111.1	24	2	98.3
30	2	126.3	30	2	102.3
40	6	147.8	40	6	112.4
50	6	163.3	50	6	122.2
60	6	173.2	60	6	129.7
80	6	180.5	80	6	137.2
100	6	177.5	100	6	137.8
120	6	170.1	120	6	135.1
160	20	154.0	160	20	129.5
200	20	145.1	200	20	129.2
240	20	144.6	240	20	135.8
300	20	153.8	300	20	153.9
400	20	182.1	400	20	196.1
Model	**RMS error (%) = 4.1**		**Model**	**RMS error (%) = 5.1**	
Layer	Resistivity (Ωm)	Thickness(m)	Layer	Resistivity (Ωm)	Thickness(m)
1	70.1	0.8	1	72.8	1.1
2	128.4	1.5	2	182	1.1
3	46.3	2.8	3	75.8	8.5
4	399.1	17	4	387.8	12
5	19.6	14.4	5	27	23
6	677		6	30089.8	

Sounding station GEOSCI 21-136			**Sounding station GEOSCI 21-137**		
L (m)	L (m)	ρ_a (Ωm)	L (m)	l (m)	ρ_a (Ωm)
2	0.5	76.3	2	0.5	67.1
3	0.5	82.8	3	0.5	74.5
4	0.5	89.5	4	0.5	76.9
6	0.5	98.5	6	0.5	74.0
8	0.5	101.2	8	0.5	68.5
10	0.5	100.8	10	0.5	63.3
12	2	99.3	12	2	60.0
16	2	96.6	16	2	59.0
20	2	96.0	20	2	62.4
24	2	97.4	24	2	67.7
30	2	101.6	30	2	76.1
40	6	110.6	40	6	88.0
50	6	118.7	50	6	97.1
60	6	125.2	60	6	104.0
80	6	133.3	80	6	113.0
100	6	136.6	100	6	117.7
120	6	137.4	120	6	119.7
160	20	136.4	160	20	120.2
200	20	137.1	200	20	120.1
240	20	141.8	240	20	122.0
300	20	155.5	300	20	129.6
400	20	191.0	400	20	153.2
Model	**RMS error (%) = 4.9**		**Model**	**RMS error (%) = 4.9**	
Layer	Resistivity (Ωm)	Thickness(m)	Layer	Resistivity (Ωm)	Thickness(m)
1	71.5	1	1	31.3	0.2
2	187.6	0.9	2	92.3	2
3	75.6	6.5	3	20	1.8
4	178.3	32.3	4	153	38
5	52.4	39.3	5	55	52.9
6	5317.7		6	4615.6	

Sounding station GEOSCI 21-138			**Sounding station**		
L (m)	L (m)	ρ_a (Ωm)	L (m)	l (m)	ρ_a (Ωm)
2	0.5	51.7			
3	0.5	53.6			
4	0.5	55.3			
6	0.5	55.8			
8	0.5	53.0			
10	0.5	49.1			
12	2	45.6			
16	2	42.3			
20	2	43.1			
24	2	46.4			
30	2	53.1			
40	6	63.8			
50	6	72.4			
60	6	78.7			
80	6	86.3			
100	6	89.6			
120	6	90.8			
160	20	92.3			
200	20	96.1			
240	20	103.5			
300	20	119.2			
400	20	152.6			
Model	**RMS error (%) = 3.9**		**Model**	**RMS error (%) =**	
Layer	Resistivity (Ωm)	Thickness(m)	Layer	Resistivity (Ωm)	Thickness(m)
1	50.2	1.1			
2	91.9	1.3			
3	11.8	2.3			
4	539.7	5.9			
5	28	29.7			
6	17393.7				

Sounding station GEOSCI 22-139			**Sounding station GEOSCI 22-140**		
L (m)	L (m)	ρ_a (Ωm)	L (m)	l (m)	ρ_a (Ωm)
2	0.5	48.0	2	0.5	292.5
3	0.5	38.0	3	0.5	246.0
4	0.5	33.5	4	0.5	198.9
6	0.5	29.3	6	0.5	132.1
8	0.5	27.3	8	0.5	101.1
10	0.5	27.3	10	0.5	86.2
12	2	28.7	12	2	79.5
16	2	34.0	16	2	75.7
20	2	40.9	20	2	76.9
24	2	47.9	24	2	80.3
30	2	58.3	30	2	87.7
40	6	74.7	40	6	103.1
50	6	90.0	50	6	119.4
60	6	104.3	60	6	135.4
80	6	130.3	80	6	164.9
100	6	153.6	100	6	191.2
120	6	174.8	120	6	215.1
160	20	212.3	160	20	258.7
200	20	245.5	200	20	300.0
240	20	275.8	240	20	341.0
300	20	318.0	300	20	404.4
400	20	382.6	400	20	516.3

Model	**RMS error (%) = 5.9**		**Model**	**RMS error (%) = 3.3**	
Layer	Resistivity (Ωm)	Thickness(m)	Layer	Resistivity (Ωm)	Thickness(m)
1	78.9	0.4	1	331.6	0.9
2	32.2	1.7	2	109.5	0.8
3	10.9	1.8	3	65.7	10.1
4	414.7	87.9	4	388.8	87.6
5	1281.4		5	24554.7	

Sounding station GEOSCI 22-141			**Sounding station GEOSCI 22-142**		
L (m)	L (m)	ρ_a (Ωm)	L (m)	l (m)	ρ_a (Ωm)
2	0.5	88.6	2	0.5	103.0
3	0.5	81.4	3	0.5	102.2
4	0.5	71.7	4	0.5	100.7
6	0.5	53.7	6	0.5	96.1
8	0.5	44.8	8	0.5	90.8
10	0.5	42.1	10	0.5	85.9
12	2	43.3	12	2	81.8
16	2	49.2	16	2	76.5
20	2	55.9	20	2	74.2
24	2	61.8	24	2	73.9
30	2	69.5	30	2	75.7
40	6	80.1	40	6	82.0
50	6	89.1	50	6	90.1
60	6	97.4	60	6	99.0
80	6	113.9	80	6	117.2
100	6	131.5	100	6	135.9
120	6	150.4	120	6	155.2
160	20	190.8	160	20	196.2
200	20	232.5	200	20	239.7
240	20	274.0	240	20	284.7
300	20	334.6	300	20	353.3
400	20	430.5	400	20	467.5
Model	**RMS error (%) = 4.2**		**Model**	**RMS error (%) = 4.8**	
Layer	Resistivity (Ωm)	Thickness(m)	Layer	Resistivity (Ωm)	Thickness(m)
1	93.3	1.4	1	103.5	2.3
2	15	1.4	2	63.8	11.1
3	110.5	32.3	3	164.9	36.3
4	2749.3		4	17002.2	

Sounding station GEOSCI 22-143			**Sounding station GEOSCI 22-144**		
L (m)	L (m)	ρ_a (Ωm)	L (m)	l (m)	ρ_a (Ωm)
2	0.5	114.4	2	0.5	131.5
3	0.5	110.3	3	0.5	128.2
4	0.5	103.7	4	0.5	122.0
6	0.5	87.4	6	0.5	103.6
8	0.5	73.8	8	0.5	84.5
10	0.5	64.1	10	0.5	68.3
12	2	58.0	12	2	56.8
16	2	52.9	16	2	45.9
20	2	52.7	20	2	43.4
24	2	54.8	24	2	44.3
30	2	59.9	30	2	47.7
40	6	70.3	40	6	53.1
50	6	81.0	50	6	58.0
60	6	91.5	60	6	62.9
80	6	111.5	80	6	73.4
100	6	131.1	100	6	85.4
120	6	151.1	120	6	98.7
160	20	192.6	160	20	127.8
200	20	236.1	200	20	158.4
240	20	280.7	240	20	189.5
300	20	348.4	300	20	236.2
400	20	461.1	400	20	313.5
Model	**RMS error (%) = 5.3**		**Model**	**RMS error (%) = 5.3**	
Layer	Resistivity (Ωm)	Thickness(m)	Layer	Resistivity (Ωm)	Thickness(m)
1	116.8	1.8	1	133.4	2.3
2	41.9	8.2	2	9.7	1.1
3	173.8	36.7	3	63.5	29.2
4	16930.6		4	225	7.4
			5	17631.1	

Appendix III.1. Spring discharge

S/N	Site	Elevation	Discharge (l/sec)	Discharge (m^3/d)	Discharge (m^3/y)
1	Bicankingi	1535	0.07	6.05	2209.21
2	Bihembe-Monge	1473	0.3	25.92	9468.06
3	Bishunzi-Munyinya	1493	1	86.40	31560.19
4	Bugorora-Gakana	1407	0.2	17.28	6312.04
5	Buhasa I	1485	2	172.80	63120.38
6	Buhasa II	1483	2	172.80	63120.38
7	Buhiga-Ntega	1424	0.4	34.56	12624.08
8	Bunyari-Rugarama	1348	0.27	23.33	8521.25
9	Burengo-Rushubije	1416	0.1	8.64	3156.02
10	Burima	1500	0.22	19.01	6943.24
11	Cinka	1475	0.1	8.64	3156.02
12	Cogo	1505	0.2	17.28	6312.04
13	Gacabwoya I	1612	1.2	103.68	37872.23
14	Gacabwoya II	1638	2	172.80	63120.38
15	Gaharata-Murama	1360	0.3	25.92	9468.06
16	Gaherere	1533	0.4	34.56	12624.08
17	Gahombo	1604	1	86.40	31560.19
18	Gakenke	1690	1.2	103.68	37872.23
19	Gasuga	1585	0.08	6.91	2524.82
20	Gasura I	1569	0.5	43.20	15780.10
21	Gatovu-Kanyinya	1377	0.51	44.06	16095.70
22	Gatunguru-Rugero	1418	0.2	17.28	6312.04
23	Gihobogo-Murungurira	1381	0.5	43.20	15780.10
24	Gihushi-Kiravumba	1485	1	86.40	31560.19
25	Gikombe-Ruhita	1362	4	345.60	126240.77
26	Kabingo	1608	0.2	17.28	6312.04
27	Kabira	1362	0.2	17.28	6312.04
28	Kabira-Renga	1355	0.3	25.92	9468.06
29	Kabungera	1506	0.2	17.28	6312.04
30	Kagobe	1513	0.5	43.20	15780.10
31	Kagogo-Nyabitare	1466	0.4	34.56	12624.08
32	Kanyamanza	1370	0.2	17.28	6312.04
33	Kanyamateke	1539	2	172.80	63120.38
34	Kararire-Kagege	1509	0.2	17.28	6312.04
35	Karira	1513	0.3	25.92	9468.06
36	Karira-Gatemere	1448	0.2	17.28	6312.04
37	Karobogo	1385	0.7	60.48	22092.13
38	Kibande	1506	0.2	17.28	6312.04
39	Kididiri-Buhasa	1465	3	259.20	94680.58
40	Kigarama	1489	0.09	7.78	2840.42
41	Kigomero-Munyinya	1529	0.3	25.92	9468.06
42	Kigoti-Munzenze	1362	0.5	43.20	15780.10
43	Kikombe	1502	0.7	60.48	22092.13
44	Kinyangoro-Kumana	1315	0.18	15.55	5680.83
45	Kinyangurube-Karehe	1394	0.3	25.92	9468.06
46	Kinywamagana-Kigarama	1436	0.7	60.48	22092.13

S/N	Site	Elevation	Discharge (l/sec)	Discharge (m^3/d)	Discharge (m^3/y)
47	Kiramata-Monge	1432	0.1	8.64	3156.02
48	Kirunduzi-Mutara	1379	1.1	95.04	34716.21
49	Kivyuka	1580	0.08	6.91	2524.82
50	Mamfu-Kiyonza	1346	0.3	25.92	9468.06
51	Maramya-Mwenya	1383	2.4	207.36	75744.46
52	Marimano	1386		0.00	0.00
53	Mugatoboramana	1719	0.1	8.64	3156.02
54	Mubira	1520	0.12	10.37	3787.22
55	Mucogo	1498	1	86.40	31560.19
56	Mudahinyuka-Kigina II	1361	0.2	17.28	6312.04
57	Mugakore	1597	0.07	6.05	2209.21
58	Mugaseno	1564	0.6	51.84	18936.12
59	Mugasuga	1535	0.09	7.78	2840.42
60	Mugatovu	1643	0.6	51.84	18936.12
61	Mugisongati	1581	0.7	60.48	22092.13
62	Muguruka I	1499	0.08	6.91	2524.82
63	Muguruka II	1503	0.08	6.91	2524.82
64	Mukabakene	1696	0.7	60.48	22092.13
65	Mukabingo	1572	0.12	10.37	3787.22
66	Mukabirizi	1458	4	345.60	126240.77
67	Mukadahoka I	1582	0.4	34.56	12624.08
68	Mukadahoka II	1504	0.08	6.91	2524.82
69	Mukagezi-Ntogwe	1387	0.4	34.56	12624.08
70	Mukanyoni	1643	0.24	20.74	7574.45
71	Mukuyo-Kiri	1358	0.2	17.28	6312.04
72	Mumarenga	1495	0.5	43.20	15780.10
73	Mumugoti	1529	0.12	10.37	3787.22
74	Munkombe	1597	0.07	6.05	2209.21
75	Mununga	1455	0.4	34.56	12624.08
76	Murugomero I	1531	0.5	43.20	15780.10
77	Murugomero II	1709	3	259.20	94680.58
78	Murugomero III	1634	0.7	60.48	22092.13
79	Murunyinya	1535	0.09	7.78	2840.42
80	Murusave I	1561	0.07	6.05	2209.21
81	Murusave II	1527	0.07	6.05	2209.21
82	Murutare	1525	0.17	14.69	5365.23
83	Muruzegezege	1636	0.7	60.48	22092.13
84	Muryaruhuma	1757	1.04	89.86	32822.60
85	Musave-Mugobe	1398	0.5	43.20	15780.10
86	Musave-Rutabo	1364	0.2	17.28	6312.04
87	Mushundahe	1537	1	86.40	31560.19
88	Mutetema-Muyange	1432	0.2	17.28	6312.04
89	Mvyayingabo-Mutara	1394	1.5	129.60	47340.29
90	Mwenya-Mwenya	1368	2.5	216.00	78900.48
91	Mwenya-Rwimbogo	1397	0.2	17.28	6312.04

S/N	Site	Elevation	Discharge (l/sec)	Discharge (m^3/d)	Discharge (m^3/y)
92	Mwibamba	1500	0.17	14.69	5365.23
93	Nagikono-Kinyangurube	1386	7	604.80	220921.34
94	Nakabingo	1343	0.38	32.83	11992.87
95	Nakabingo-Gatemere	1494	1	86.40	31560.19
96	NakabingoII-Gihosha	1425	0.1	8.64	3156.02
97	Nakarambo-Rutabo	1376	0.2	17.28	6312.04
98	Nakavumu	1399	0.2	17.28	6312.04
99	Nakivumbura-Monge	1416	0.4	34.56	12624.08
100	Naruhangangara	1503	0.08	6.91	2524.82
101	Narukere-Gihosha	1389	0.4	34.56	12624.08
102	Narutambwe-Kireka	1403	0.2	17.28	6312.04
103	Nganji-Murama	1474	0.4	34.56	12624.08
104	Nyabitare	1475	0.18	15.55	5680.83
105	Nyabitare-Munyinya	1427	0.3	25.92	9468.06
106	Nyamugari	1495	0.5	43.20	15780.10
107	Nyamvura	1474	7	604.80	220921.34
108	Nyaruziba-Mutara	1434	0.6	51.84	18936.12
109	RamboII-Gatwe	1369	0.5	43.20	15780.10
110	Rubira-Gatemere	1534	1	86.40	31560.19
111	Rugangazi-Ntogwe	1422	0.3	25.92	9468.06
112	Rugero-Nakarinzi	1383	0.2	17.28	6312.04
113	Rugoma-Kagege	1513	0.3	25.92	9468.06
114	Rugomero-Gatemere	1524	1.2	103.68	37872.23
115	Rugomero-Kiravumba	1539	2	172.80	63120.38
116	Rugomero-Nyabugeni	1513	0.8	69.12	25248.15
117	Rugunga II-Kavomo	1365	3.4	293.76	107304.65
118	Rugunga I-Kavomo	1364	0.9	77.76	28404.17
119	Ruhara	1503	0.7	60.48	22092.13
120	Ruhongore-Munyinya	1459	1	86.40	31560.19
121	Rushubije-Cogo	1390	0.2	17.28	6312.04
122	Rusumba	1516	0.24	20.74	7574.45
123	Ruvogo	1518	3	259.20	94680.58
124	Rwinago	1480	0.4	34.56	12624.08
125	Ryasebukanu	1530	2.2	190.08	69432.42
126	Twengebuye-Nakabingo	1378	0.1	8.64	3156.02
127	Mutumba-Regideso				27288
128	Pumping station-Kirundo				232661
129	Overflow-pumping station		6.5	562	205141
Total					**3493606**

Appendix IV.1. Lithological cross-sections of some recently constructed wells in the study area (BTC-Funded project, 2008)

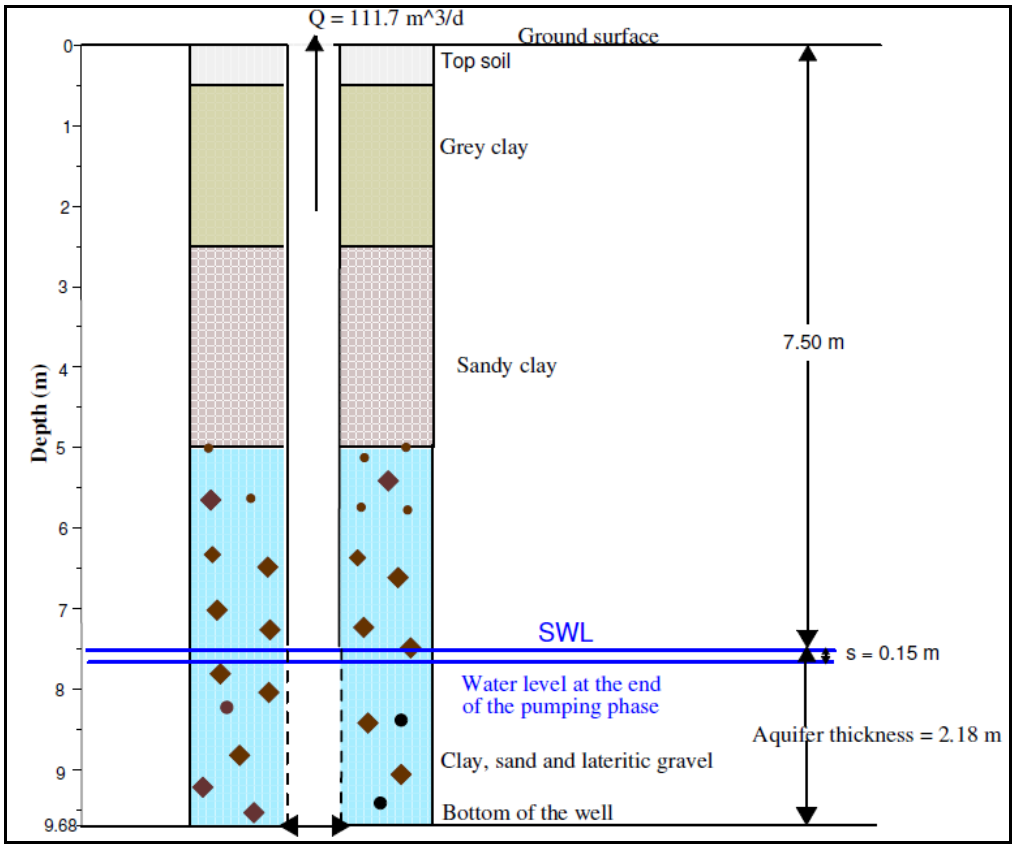

Figure IV.1.1. Lithological log of the well in Kabonde-Runyonza

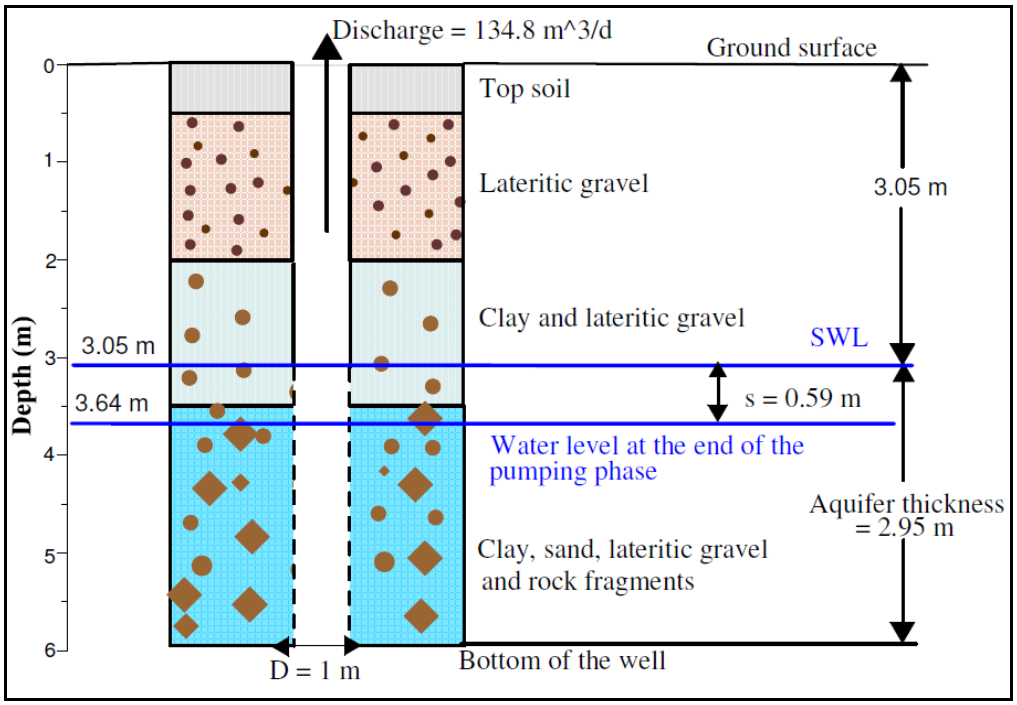

Figure IV.1.2. Lithological log of the well in Kiruhurura I-Kiyanza

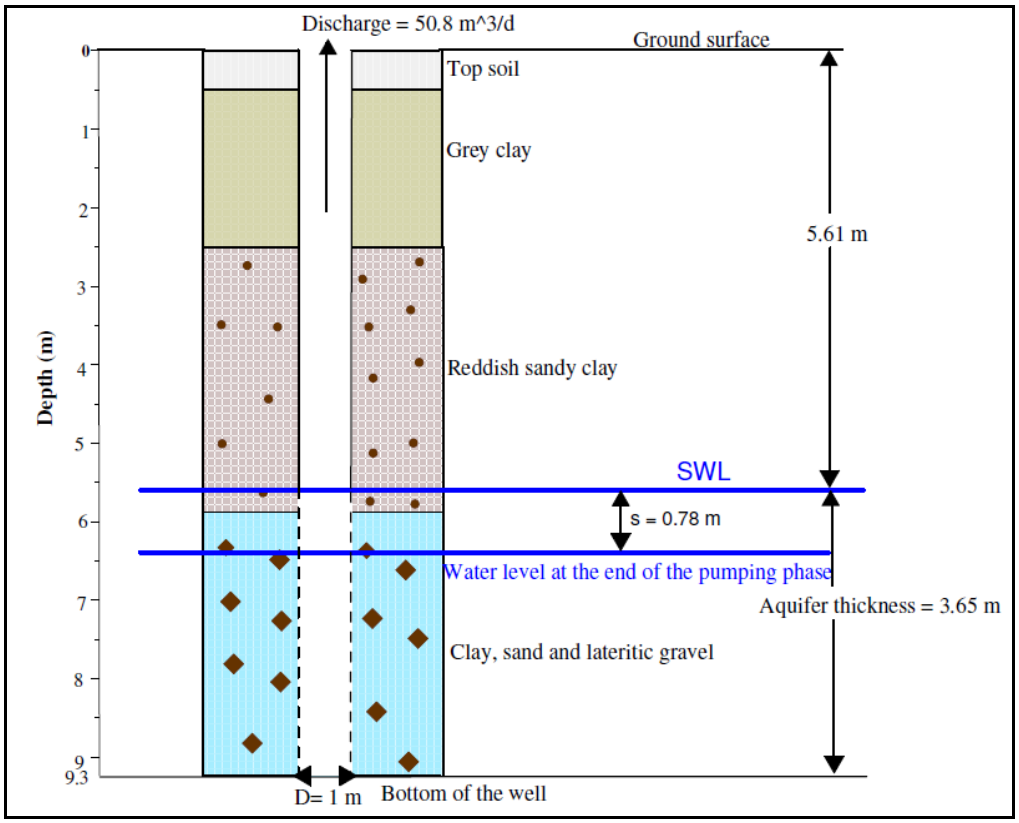

Figure IV.1.3. Lithological log of the well in Kiruhura II-Muramba

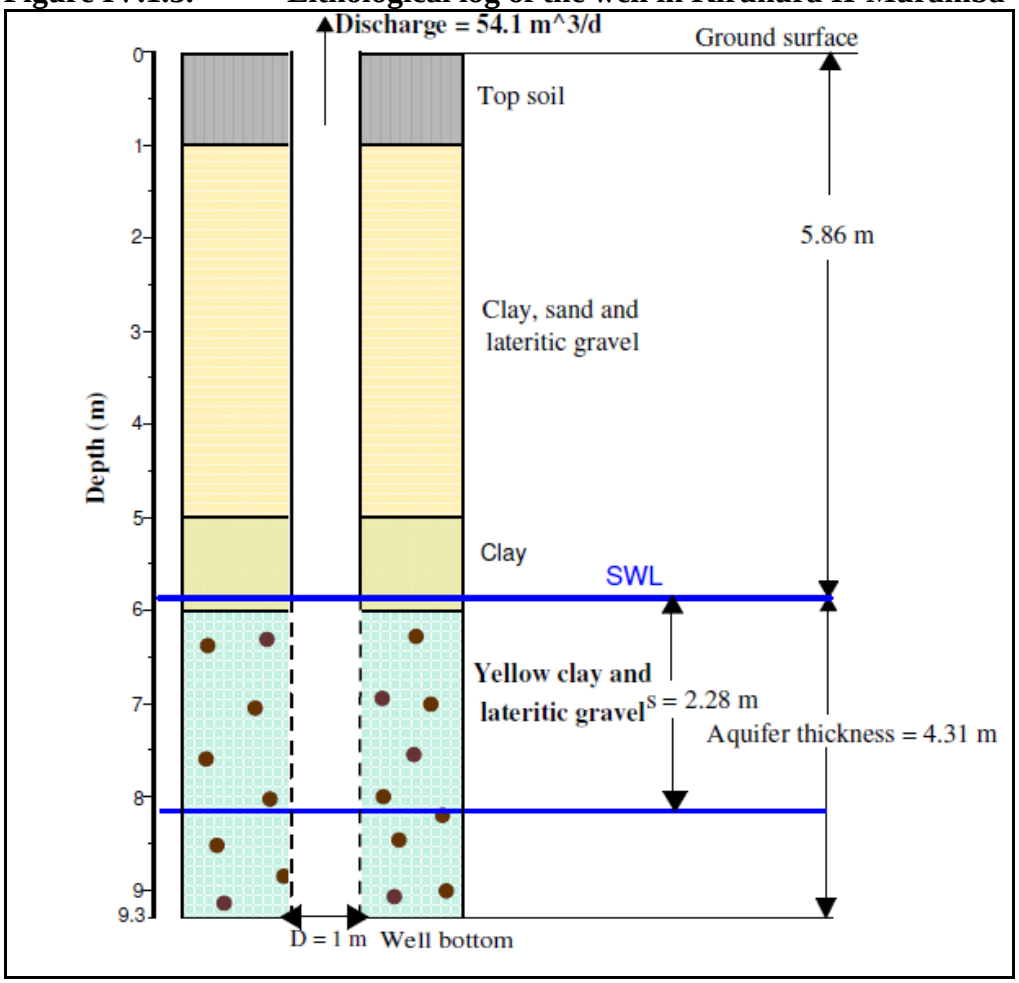

Figure IV.1.4. Lithological log of the well in Kigoma-Gatare

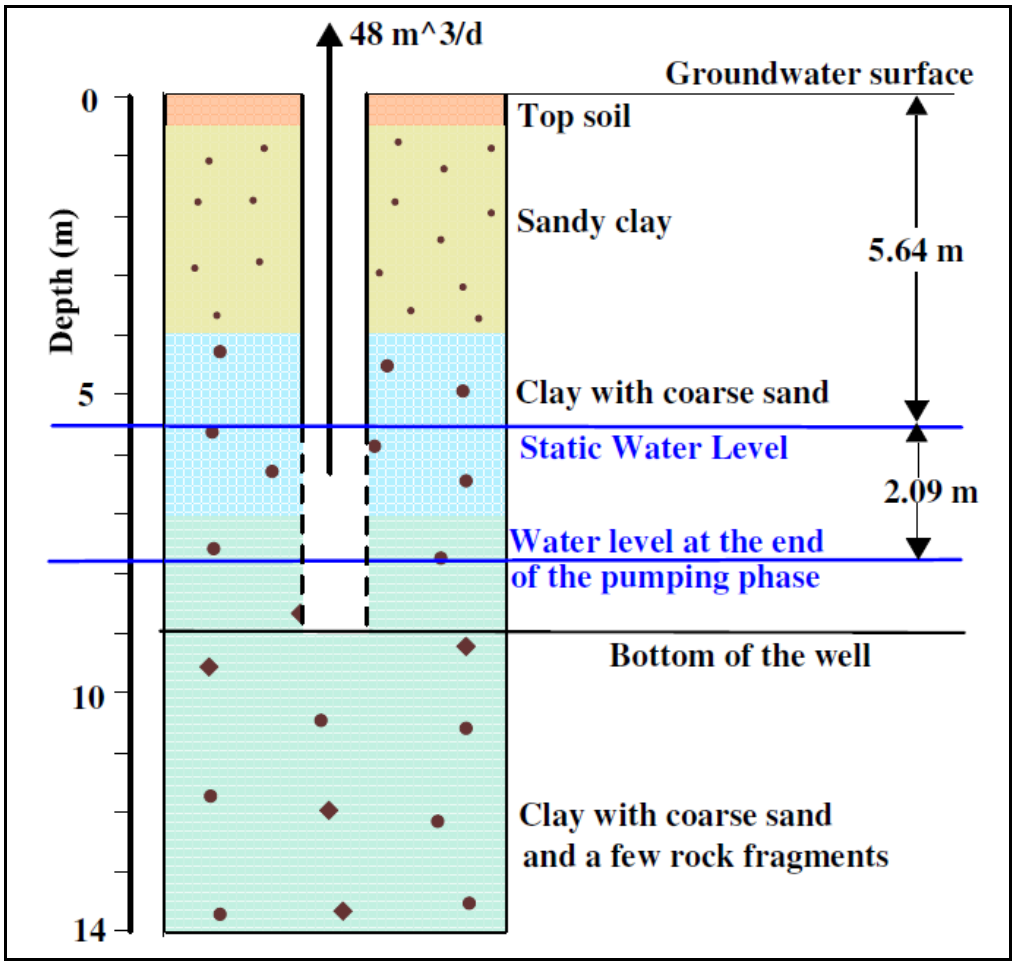

Figure IV.1.5. Lithological log of the well in Kinyamateke-Nyabikenke

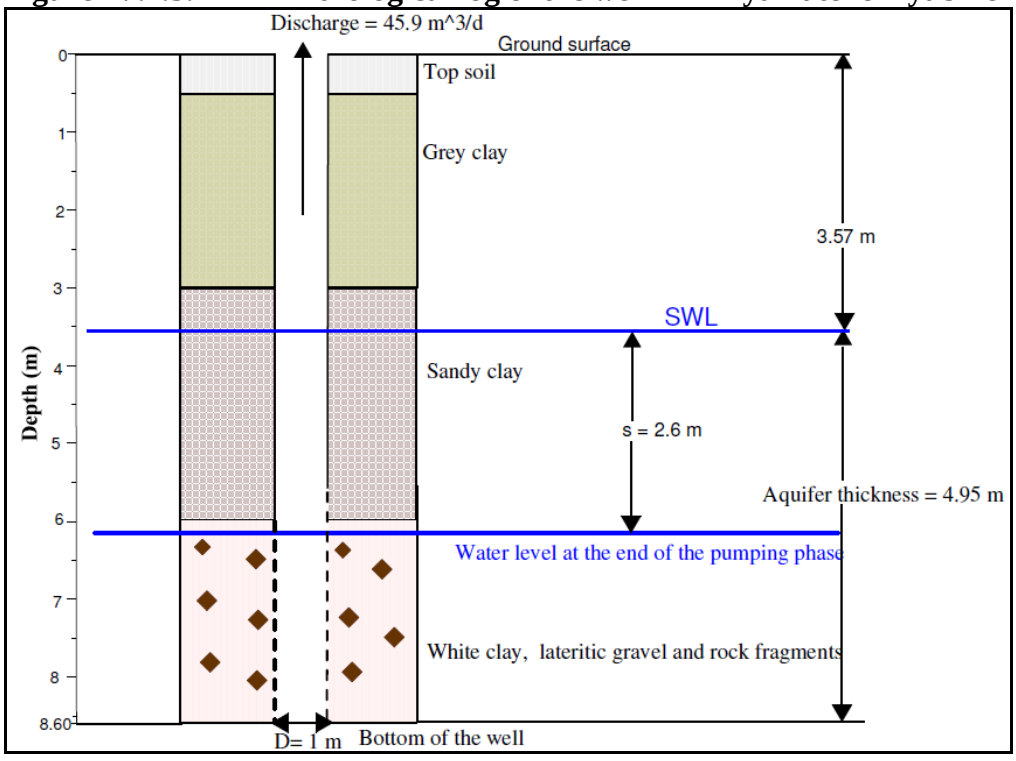

Figure IV.1. 6. Lithological log of the well in Marembo-Marembo

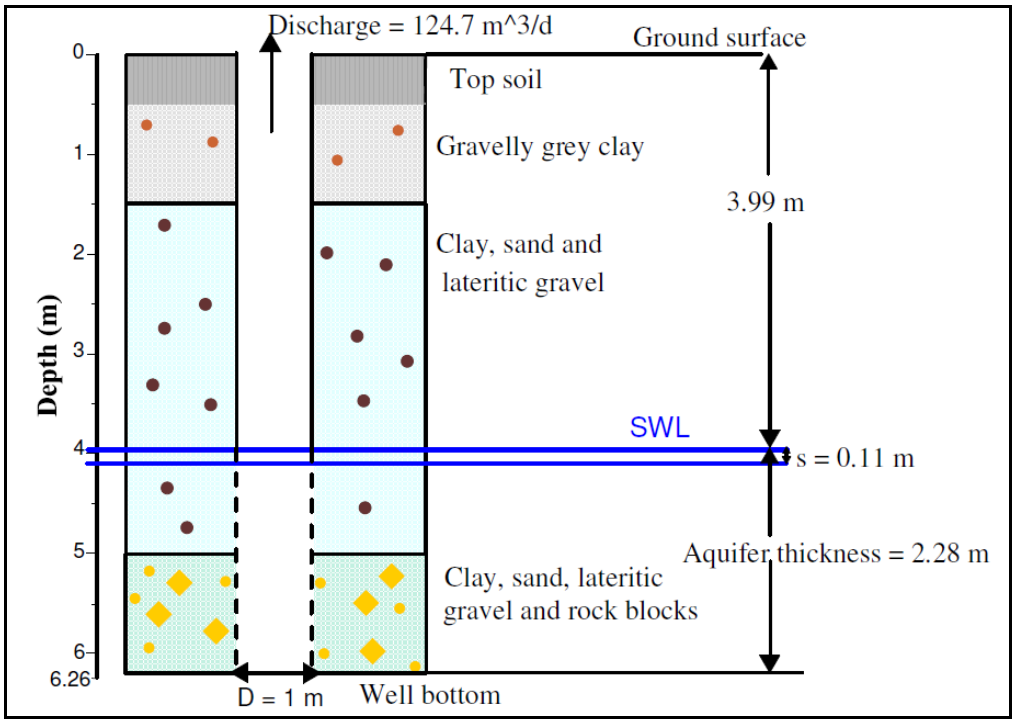

Figure IV.2.7. Lithological log of the well in Muhero II-Yaranda

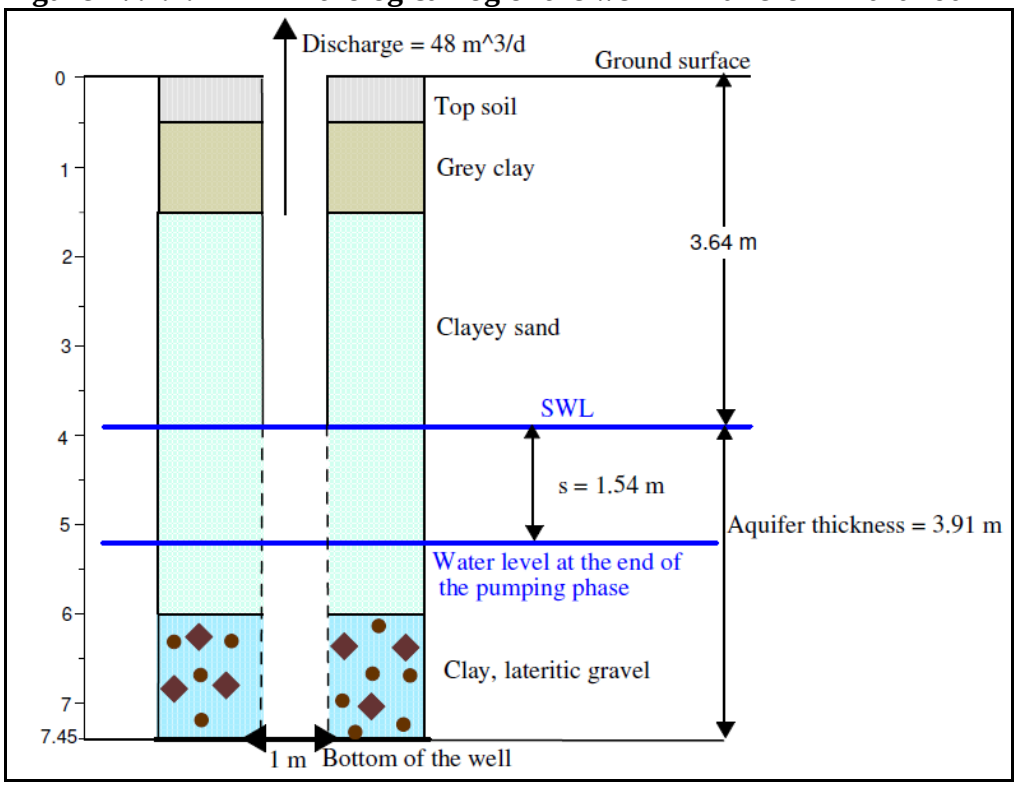

Figure IV.2.8. Lithological log of the well in Mutoza-Yaranda

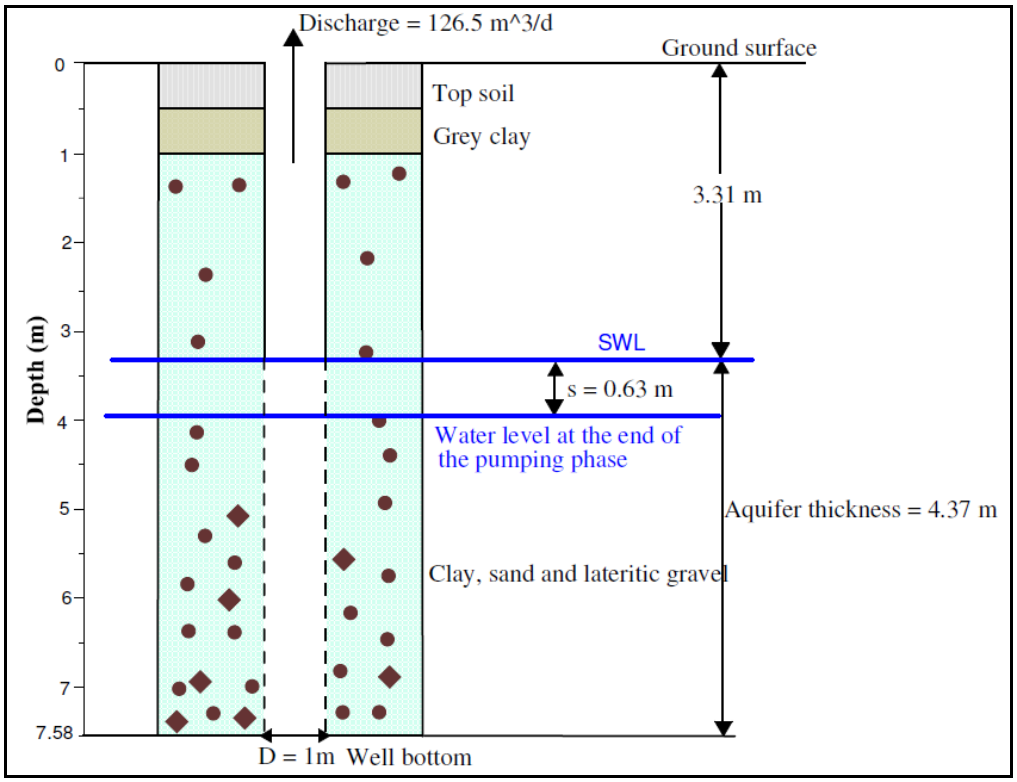

Figure IV.2.9. Lithological log of the well in Nunga II-Yaranda

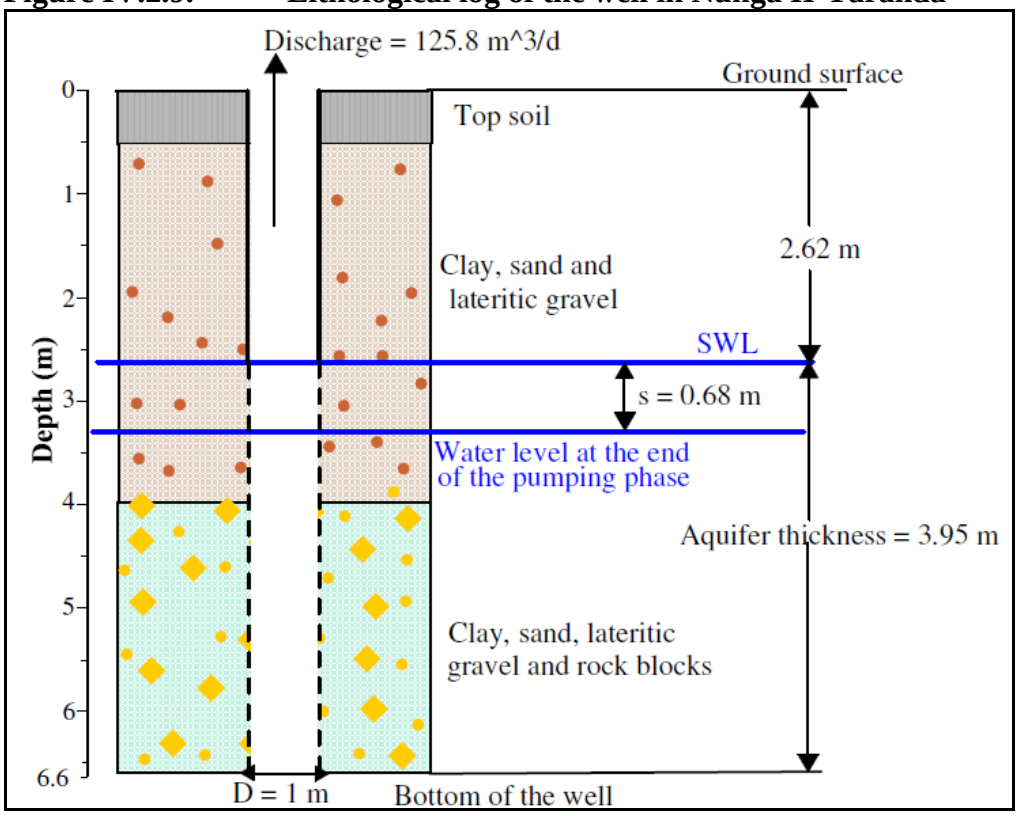

Figure IV.2.10. Lithological log of the well in Senga-Nyagisozi

Appendix IV.2. Pumping test analytical curves

Location: Bugesera (Burundi)	Pumping Test: Large diameter well Bishunzi	Pumping Well: PW
Test Conducted by: Charles		Test Date: 17/07/2008
Analysis Performed by: Charles	Huntush	Analysis Date: 03/02/2009
Aquifer Thickness: 4.65 m	Discharge Rate: 2.005117317 [m³/h]	

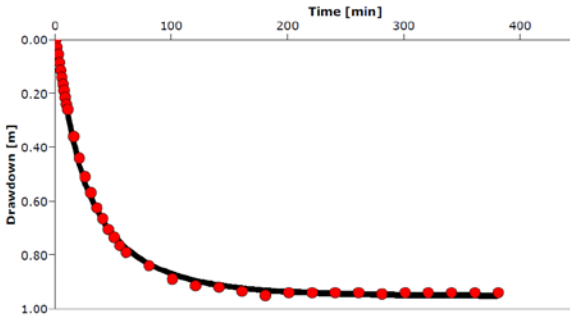

Calculation after Hantush

Observation Well	Transmissivity [m²/d]	Hydraulic Conductivity [m/d]	Storage coefficient	Ratio K(v)/K(h)	Hydr. resistance [min]
PW	7.24×10^{0}	1.56×10^{0}	4.50×10^{-1}	1.00×10^{-3}	1.88×10^{2}

Figure IV.2.1: Analysis of pumping test for the well in Bishunzi-Cewe using Hantush method (test Nr.1)

Location: Bugesera (Burundi)	Pumping Test: Large diameter well Bishunzi	Pumping Well: PW
Test Conducted by: Charles		Test Date: 17/0
Analysis Performed by: Charles	Cooper & Jacob	Analysis Date:
Aquifer Thickness: 4.65 m	Discharge Rate: 2.005117317 [m³/h]	

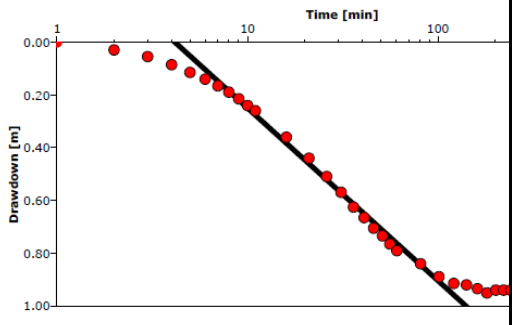

Calculation after Cooper & Jacob

Observation Well	Transmissivity [m²/d]	Hydraulic Conductivity [m/d]	Storage coefficient	Radial Dista PW [m]
PW	1.35×10^{1}	2.89×10^{0}	3.50×10^{-1}	0.5

Figure IV.2.2: Analysis of pumping test data for the well in Bishunzi- Cewe using the Cooper & Jacob method (test Nr.1)

Location: Bugesera (Burundi)	Pumping Test: Large diameter well Cewe_Bishunzi	Pumping Well: PW
Test Conducted by: Charles		Test Date: 17/07/2008
Analysis Performed by: Charles	Huntush	Analysis Date: 03/02/2009
Aquifer Thickness: 4.65 m	Discharge Rate: 2.005 [m³/h]	

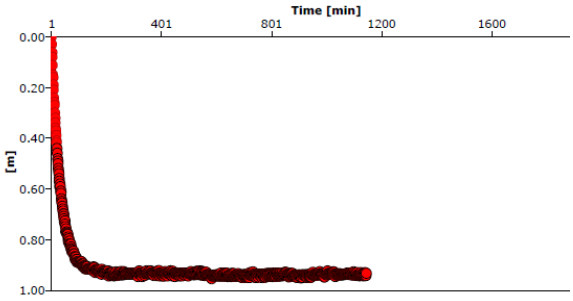

Calculation after Hantush

Observation Well	Transmissivity [m²/d]	Hydraulic Conductivity [m/d]	Storage coefficient	Hydr. resistance [min]	Radial [PW [m]
PW	5.56×10^{0}	1.20×10^{0}	4.57×10^{-1}	1.39×10^{2}	0.5

Figure IV.2.3: Analysis of recovery test data for the well in Bishunzi-Cewe using the Hantush analytical method (test Nr.1)

Location: Bugesera (Burundi)	Pumping Test: Large diameter well Cewe_Bishunzi	Pumping Well: PW
Test Conducted by: Charles		Test Date: 17/07/20
Analysis Performed by: Charles	Cooper & Jacob	Analysis Date: 04/0
Aquifer Thickness: 4.65 m	Discharge Rate: 2.005 [m³/h]	

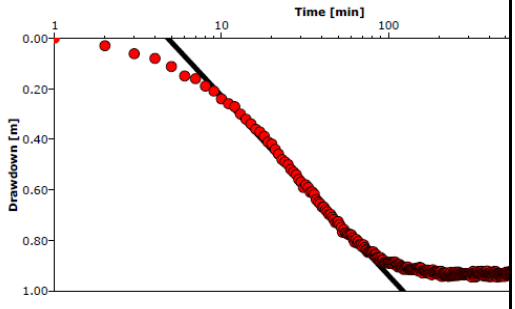

Calculation after Cooper & Jacob

Observation Well	Transmissivity [m²/d]	Hydraulic Conductivity [m/d]	Storage coefficient	Radial Distance PW [m]
PW	1.24×10^{1}	2.67×10^{0}	3.69×10^{-1}	0.5

Figure IV.2.4: Analysis of recovery test data for the well in Cewe-Bishunzi using the Cooper & Jacob analytical method (test Nr.1)

Location: Bugesera (Burundi)	Pumping Test: Large diameter well Cimbogo_Gatete	Pumping Well: PW
Test Conducted by: Charles		Test Date: 06/08/2008
Analysis Performed by: Charles	Huntush	Analysis Date: 12/02/2009
Aquifer Thickness: 1.79 m	Discharge Rate: 2.731224612 [m³/h]	

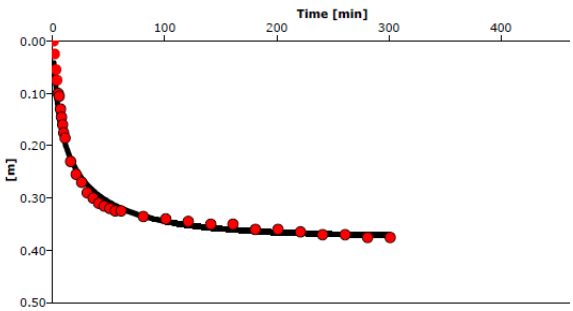

Calculation after Hantush

Observation Well	Transmissivity [m²/d]	Hydraulic Conductivity [m/d]	Storage coefficient	Hydr. resistance [min]	Radi PW [m]
PW	5.43×10^{1}	3.03×10^{1}	5.00×10^{-1}	2.47×10^{2}	0.5

Figure IV.2.5: Analysis of pumping test data for the well in Cimbogo-Gatete using the Hantush analytical method (test Nr.2)

Location: Bugesera (Burundi)	Pumping Test: Large diameter well Cimbogo_Gatete	Pumping Well: PW
Test Conducted by: Charles		Test Date: 06/08/2
Analysis Performed by: Charles	Cooper & Jacob	Analysis Date: 12/
Aquifer Thickness: 1.79 m	Discharge Rate: 2.731224612 [m³/h]	

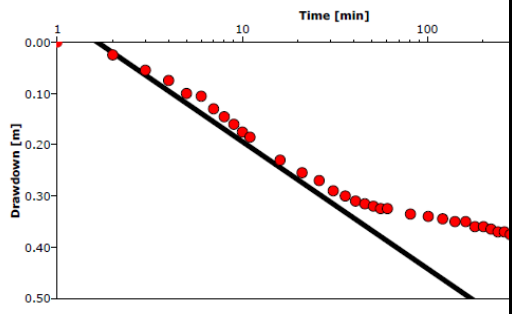

Calculation after Cooper & Jacob

Observation Well	Transmissivity [m²/d]	Hydraulic Conductivity [m/d]	Storage coefficient	Radial Distance PW [m]
PW	4.84×10^{1}	2.71×10^{1}	5.00×10^{-1}	0.5

Figure IV.2.6: Analysis of pumping test data for the well in Cimbogo-Gatete using the Cooper & Jacob method (test Nr. 2)

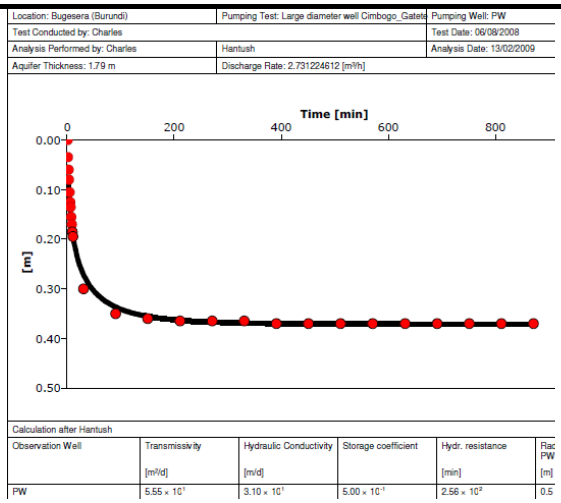

Figure IV.2.7: Analysis of recovery test data for the well in Cimbogo- Gatete using the Hantush analytical method (test Nr. 2)

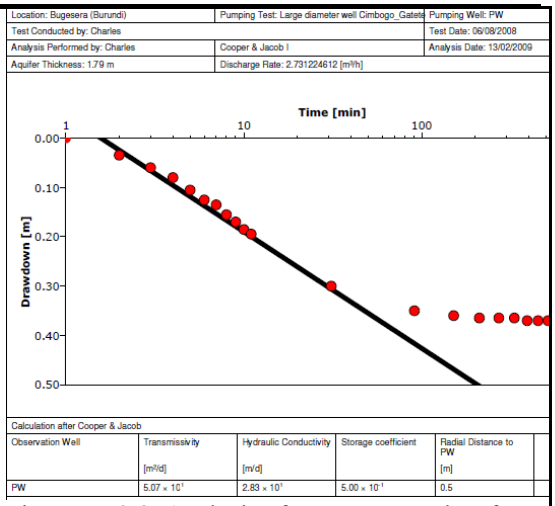

Figure IV.2.8: Analysis of recovery test data for the well in Cimbogo-Gatete using the Cooper & Jacob analytical method (test Nr. 2)

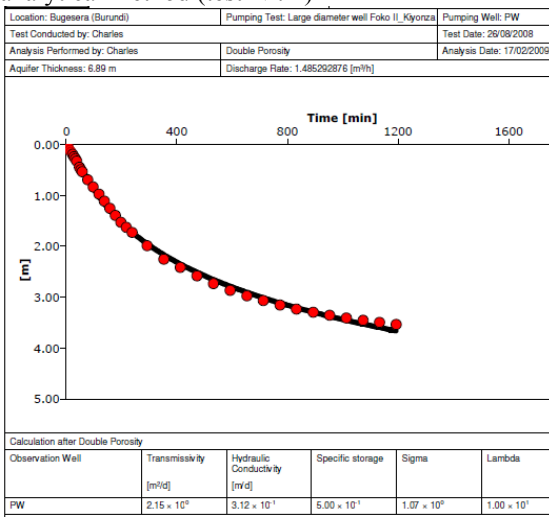

Figure IV.2.9: Analysis of recovery test data for the well in Foko II-Kiyonza using the double porosity analytical solution (test Nr. 3)

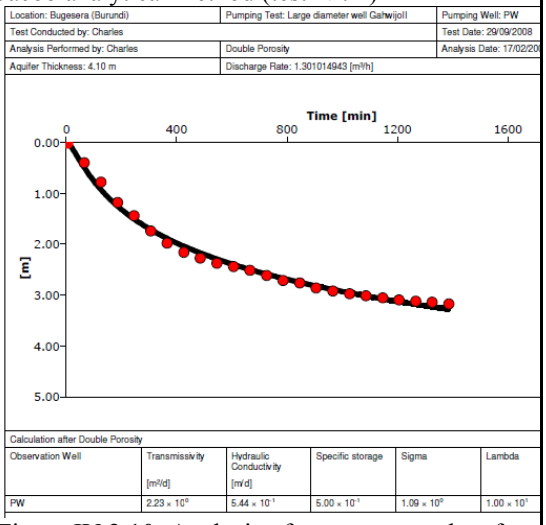

Figure IV.2.10: Analysis of recovery test data for the well in Gahwijo II using the double porosity analytical solution (test Nr. 4)

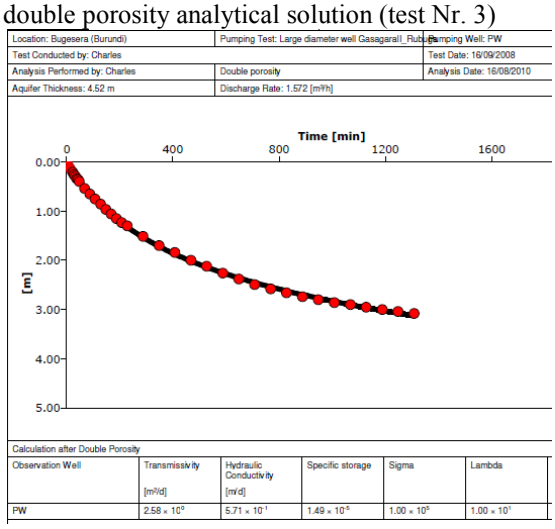

Figure IV.2.11: Analysis of recovery test data for the well in Gasagara II using the double porosity analytical solution (test Nr. 5)

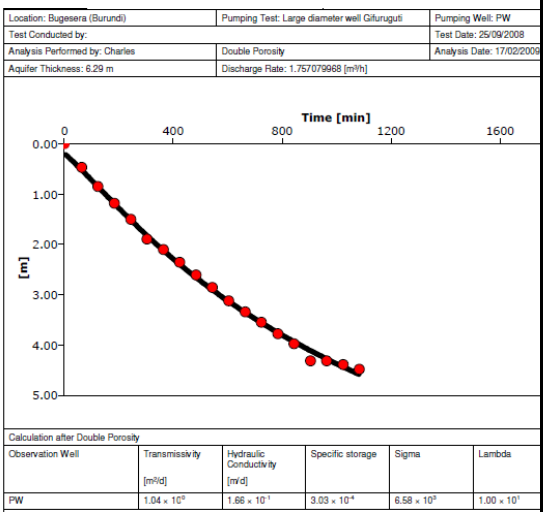

Figure IV.2.12: Analysis of recovery test data for the well in Gifuruguti-Nyakarama using the double porosity model (test Nr. 6)

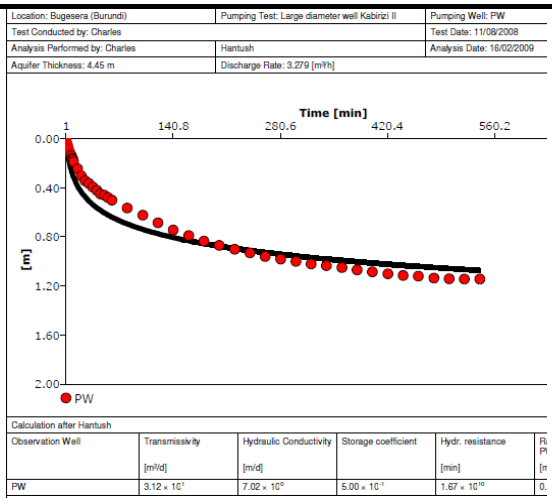

Figure IV.2.13: Analysis of pumping test data for the well in Kabirizi II-Kigoma using the Hantush analytical model (test Nr. 7)

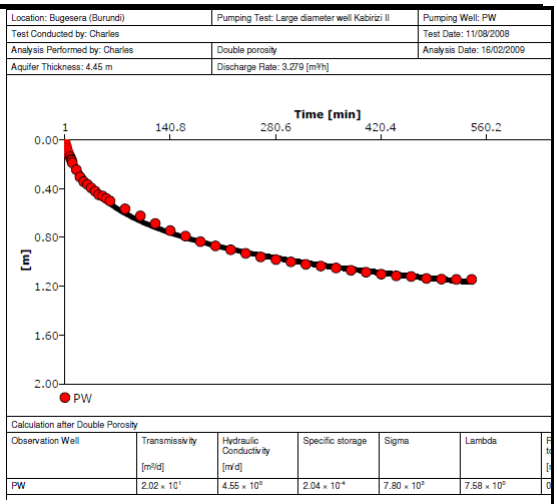

Figure IV.2.14: Analysis of pumping test data for the well in Kabirizi II-Kigoma using the double porosity analytical method (test Nr.7)

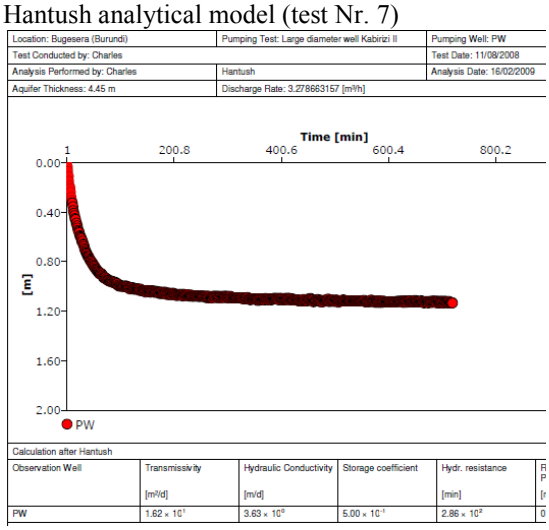

Figure IV.2.15: Analysis of recovery test data for the well in Kabirizi II-Kigoma using the Hantush analytical method (test Nr. 7)

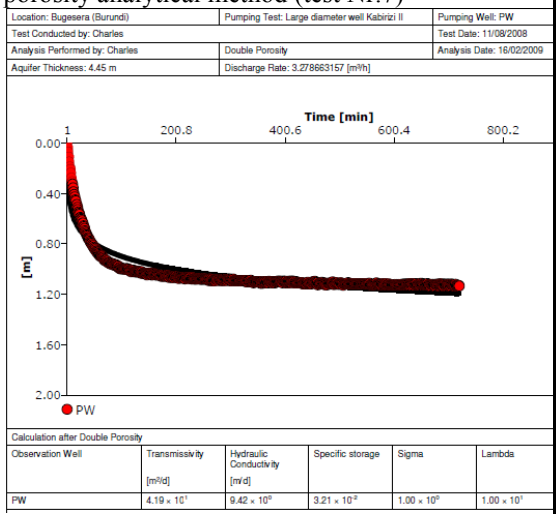

Figure IV.2.16: Analysis of recovery test data for the well in Kabirizi II-Kigoma using the double porosity analytical method (test Nr. 7)

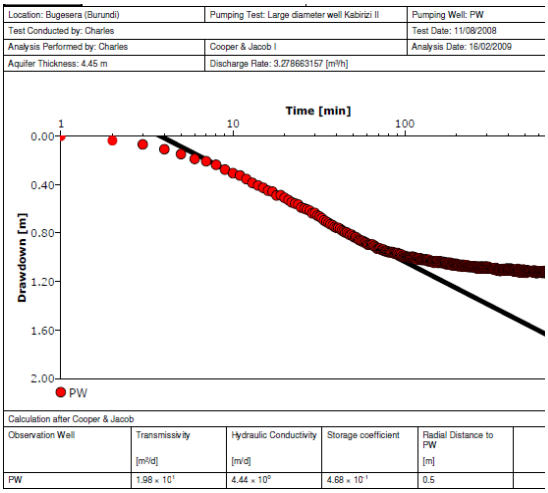

Figure IV.2.17: Analysis of recovery test data for the well in Kabirizi II-Kigoma using the Cooper & Jacob analytical method (test Nr. 7)

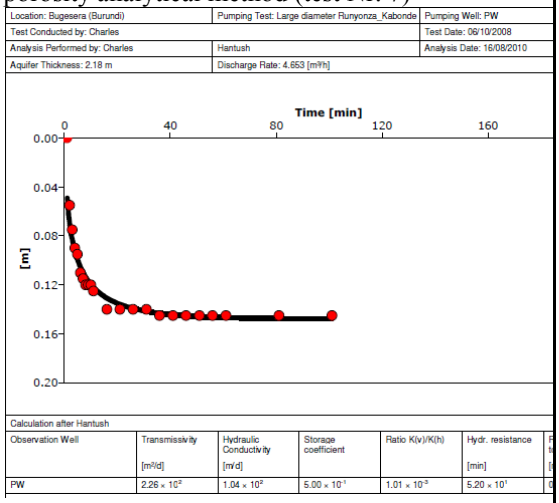

Figure IV.2.18: Analysis of pumping test data for the well in Kabonde-Runyonza using the Hantush analytical method (test Nr. 8)

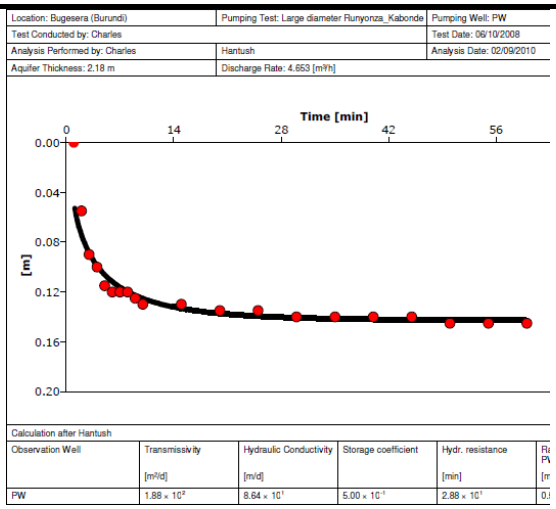

Figure IV.2.19: Analysis of recovery test data for the well in Kabonde-Runyonza using the Hantush analytical method (test Nr. 8)

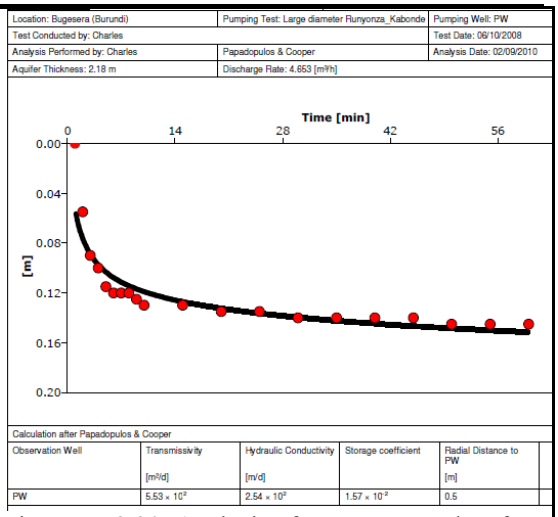

Figure IV.2.20: Analysis of recovery test data for the well in Kabonde-Runyonza using the Papadopulos & Cooper method (test Nr. 8)

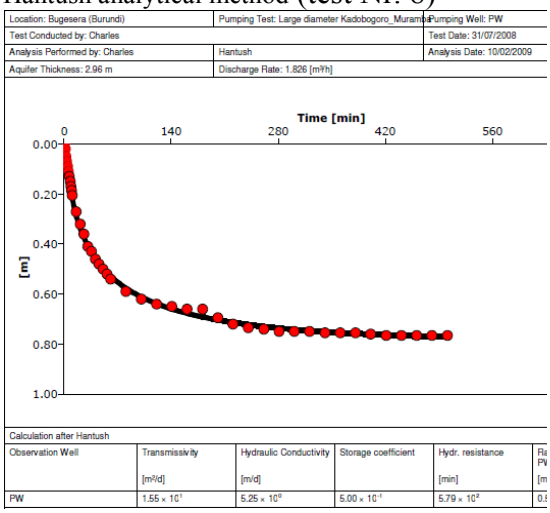

Figure IV.2.21: Analysis of pumping test data for the well in Kadobogoro-Muramba using the Hantush analytical method (test Nr. 9)

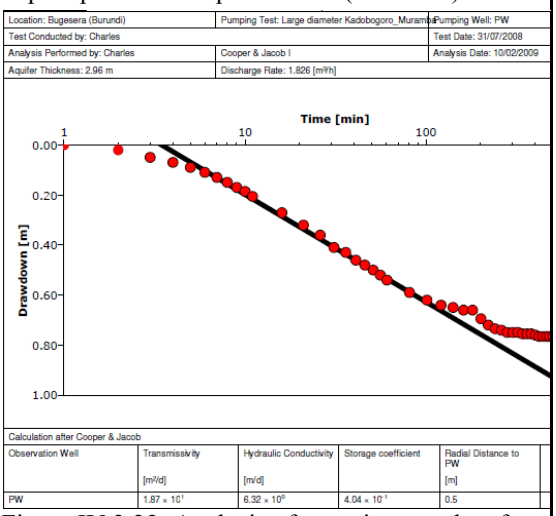

Figure IV.2.22: Analysis of pumping test data for the well in Kadobogoro-Muramba using the Cooper & Jacob method (test Nr. 9)

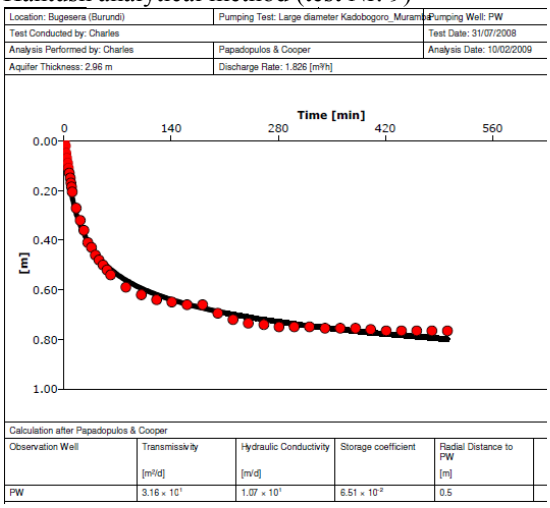

Figure IV.2.23: Analysis of pumping test data for the well in Kadobogoro-Muramba using the Papadopulos & Cooper method (test Nr. 9)

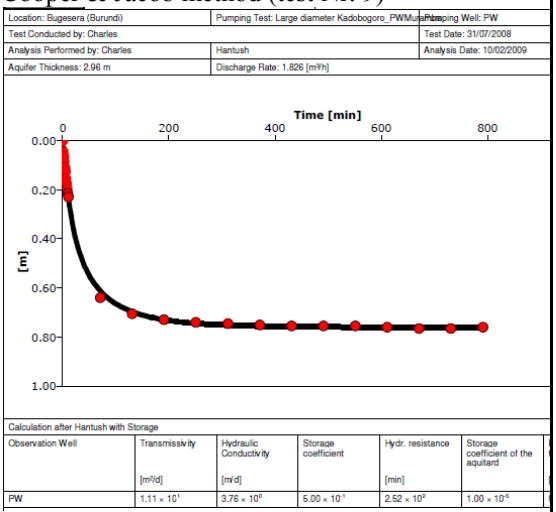

Figure IV.2.24: Analysis of recovery test data for the well in Kadobogoro-Muramba using the Hantush analytical method (test Nr. 9)

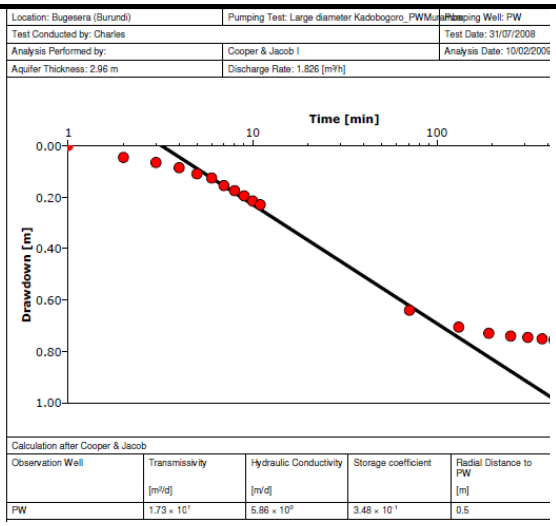

Figure IV.2.25: Analysis of recovery test data for the well in Kadobogoro-Muramba using the Cooper & Jacob analytical method (test Nr. 9)

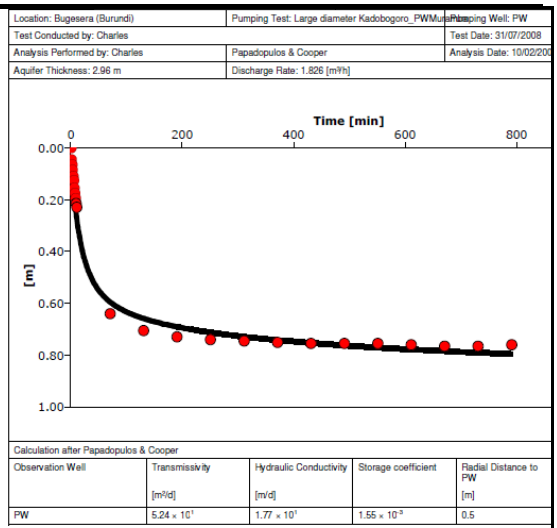

Figure IV.2.26: Analysis of recovery test data for the well in Kadobogoro-Muramba using the Papadopulos & Cooper method (test Nr. 9)

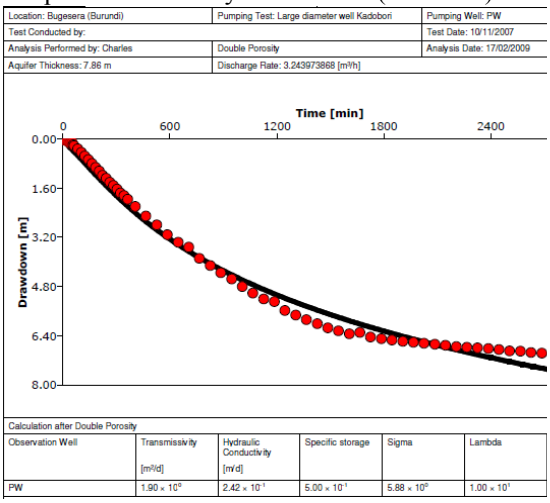

Figure IV.2.27: Analysis of recovery test data for the well in Kadobori II-Rubuga using the double porosity method
(test Nr. 10)

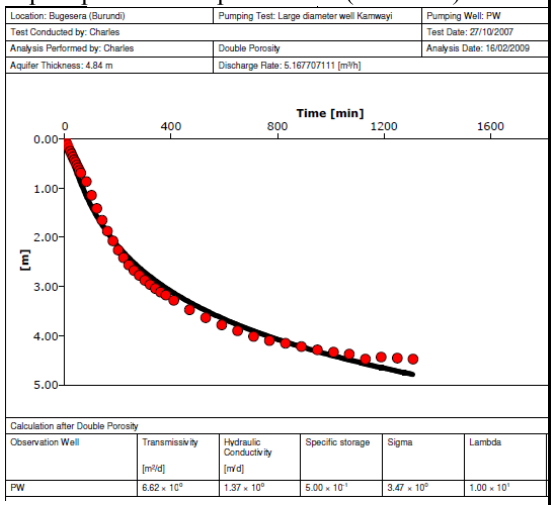

Figure IV.2.28: Analysis of recovery test data for the well in Kamwayi II-Nyamabuye using the double porosity method (test Nr. 11)

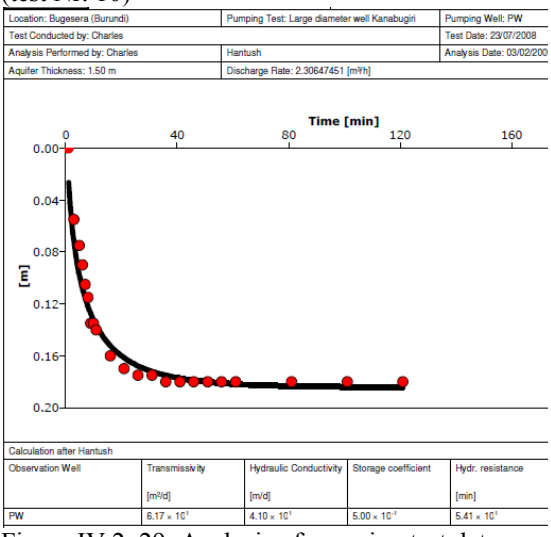

Figure IV.2. 29: Analysis of pumping test data for the well in Kanabugiri-Bugera using the Hantush analytical method (test Nr. 12)

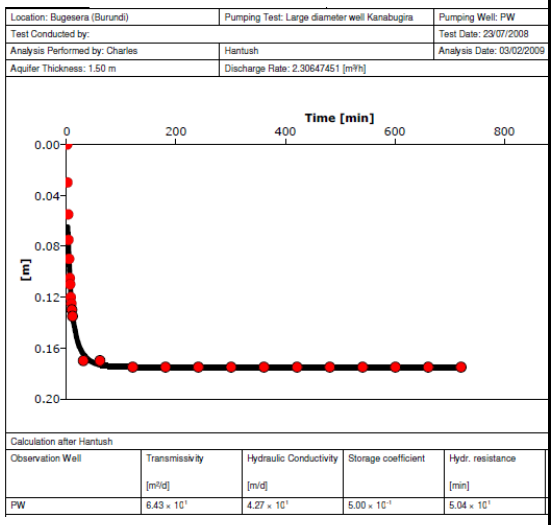

Figure IV.2. 30: Analysis of recovery test data for the well in Kanabugiri-Bugera using the Hantush analytical method (test Nr. 12)

Location: Bugesera (Burundi)	Pumping Test: Large diameter well Kanabugira	Pumping Well: PW
Test Conducted by:		Test Date: 23/07/2008
Analysis Performed by: Charles	Cooper & Jacob I	Analysis Date: 03/02/2009
Aquifer Thickness: 1.50 m	Discharge Rate: 2.30647451 [m³/h]	

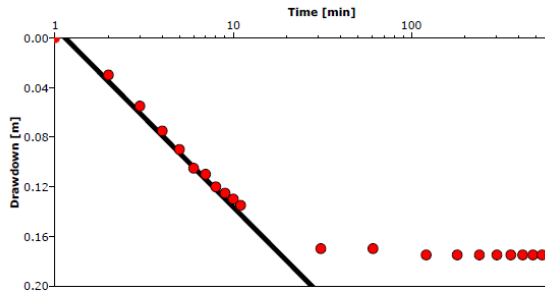

Calculation after Cooper & Jacob

Observation Well	Transmissivity [m²/d]	Hydraulic Conductivity [m/d]	Storage coefficient	Radial Distance to PW [m]
PW	7.01×10^{1}	4.66×10^{1}	5.00×10^{-1}	0.5

Figure IV.2.31: Analysis of recovery test data for the well in Kanabugiri-Bugera using the Cooper & Jacob analytical method (test Nr. 12)

Location: Bugesera (Burundi)	Pumping Test: Large diameter well Kanigo_Cinuma	Pumping Well: PW
Test Conducted by: Charles		Test Date: 23/09/2008
Analysis Performed by: Charles	Double Porosity	Analysis Date: 17/02/2009
Aquifer Thickness: 5.64 m	Discharge Rate: 1.822382913 [m³/h]	

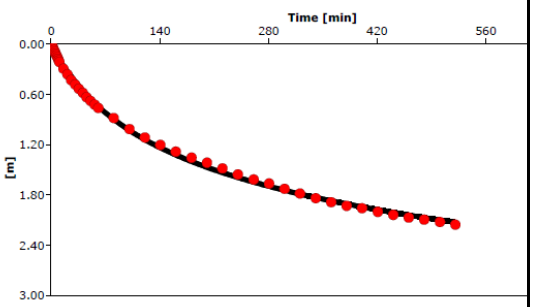

Calculation after Double Porosity

Observation Well	Transmissivity [m²/d]	Hydraulic Conductivity [m/d]	Specific storage	Sigma	Lambda
PW	4.78×10^{0}	8.46×10^{-1}	1.87×10^{-3}	4.61×10^{0}	8.85×10^{0}

Figure IV.2.32: Analysis of pumping test data for the well in Kanigo-Cinuma using the double porosity analytical method (test Nr. 13)

Location: Bugesera (Burundi)	Pumping Test: Large diameter well Kanigo_Cinuma	Pumping Well: PW
Test Conducted by: Charles		Test Date: 23/09/2008
Analysis Performed by: Charles	Hantush	Analysis Date: 17/02/2009
Aquifer Thickness: 5.64 m	Discharge Rate: 1.822382913 [m³/h]	

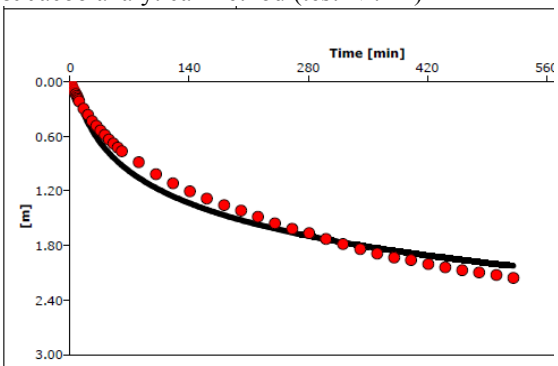

Calculation after Hantush

Observation Well	Transmissivity [m²/d]	Hydraulic Conductivity [m/d]	Storage coefficient	Hydr. resistanc [min]
PW	6.45×10^{0}	1.14×10^{0}	5.00×10^{-1}	1.67×10^{10}

Figure IV.2. 33: Analysis of pumping test data for the well in Kanigo-Cinuma using the Hantush analytical method (test Nr.13)

Location: Bugesera (Burundi)	Pumping Test: Large diameter well Kanigo_Cinuma	Pumping Well: PW
Test Conducted by: Charles		Test Date: 23/09/2008
Analysis Performed by: Charles	Hantush	Analysis Date: 17/02/2009
Aquifer Thickness: 5.64 m	Discharge Rate: 1.822382913 [m³/h]	

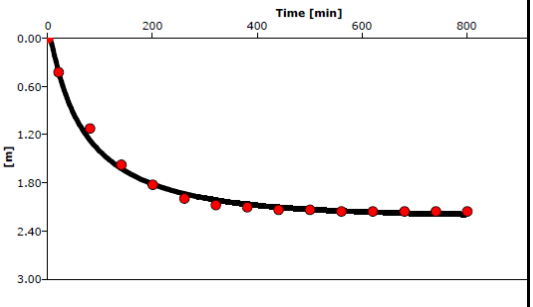

Calculation after Hantush

Observation Well	Transmissivity [m²/d]	Hydraulic Conductivity [m/d]	Storage coefficient	Hydr. resistance [min]	Rad PW [m]
PW	3.37×10^{0}	5.96×10^{-1}	5.00×10^{-1}	6.03×10^{2}	0.5

Figure IV.2.34: Analysis of recovery test data for the well in Kanigo-Cinuma using the Hantush analytical method (test Nr.13)

Location: Bugesera (Burundi)	Pumping Test: Large diameter well Kanigo_Cinuma	Pumping Well: PW
Test Conducted by: Charles		Test Date: 23/09/2008
Analysis Performed by: Charles	Double porosity	Analysis Date: 17/02/2009
Aquifer Thickness: 5.64 m	Discharge Rate: 1.822382913 [m³/h]	

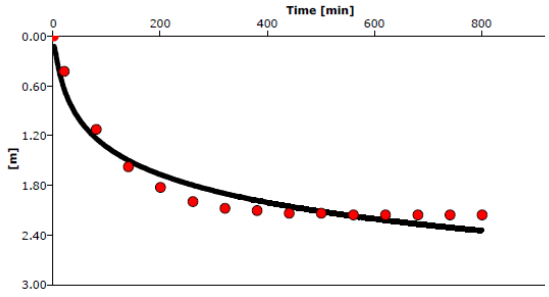

Calculation after Double Porosity

Observation Well	Transmissivity [m²/d]	Hydraulic Conductivity [m/d]	Specific storage	Sigma	Lambda
PW	7.04×10^{0}	1.25×10^{0}	3.07×10^{-6}	1.00×10^{5}	1.00×10^{1}

Figure IV.2.35: Analysis of recovery test data for the well in Kanigo-Cinuma using the double porosity analytical method (test nr.13)

Location: Bugesera (Burundi)	Pumping Test: Large diameter well Kanigo_Cinuma	Pumping Well: PW
Test Conducted by: Charles		Test Date: 23/09/2008
Analysis Performed by: Charles	Cooper & Jacob I	Analysis Date: 17/02/2009
Aquifer Thickness: 5.64 m	Discharge Rate: 1.822382913 [m³/h]	

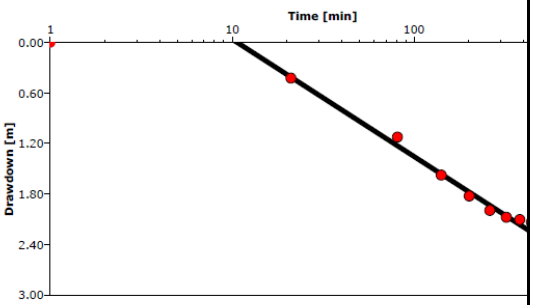

Calculation after Cooper & Jacob

Observation Well	Transmissivity [m²/d]	Hydraulic Conductivity [m/d]	Storage coefficient	Radial Distance to PW [m]
PW	5.74×10^{0}	1.02×10^{0}	3.82×10^{-1}	0.5

Figure IV.2.36: Analysis of recovery test data for the well in Kanigo-Cinuma using the Cooper & Jacob method (test Nr. 13)

Location: Bugesera (Burundi)	Pumping Test: Large diameter well Ceru_Kantuye	Pumping Well: PW
Test Conducted by:		Test Date: 15/11/2007
Analysis Performed by: Charles	Double porosity	Analysis Date: 16/02/2009
Aquifer Thickness: 1.84 m	Discharge Rate: 2.145124585 [m³/h]	

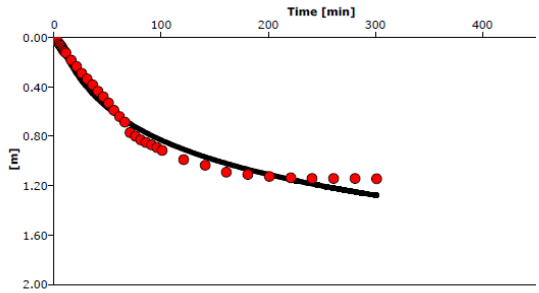

Calculation after Double Porosity

Observation Well	Transmissivity [m²/d]	Hydraulic Conductivity [m/d]	Specific storage	Sigma	Lambda
PW	9.55×10^{0}	5.17×10^{0}	4.69×10^{-1}	1.00×10^{0}	1.00×10^{-1}

Figure IV.2.37: Analysis of recovery test data for the well in Ceru-Kantuye using the double porosity method (test Nr. 14)

Location: Bugesera (Burundi)	Pumping Test: Large diameter well Ruseno_Kanyagu	Pumping Well: PW
Test Conducted by: Charles		Test Date: 14/10/2008
Analysis Performed by: Charles	Double Porosity	Analysis Date: 17/02/2009
Aquifer Thickness: 3.60 m	Discharge Rate: 1.238713751 [m³/h]	

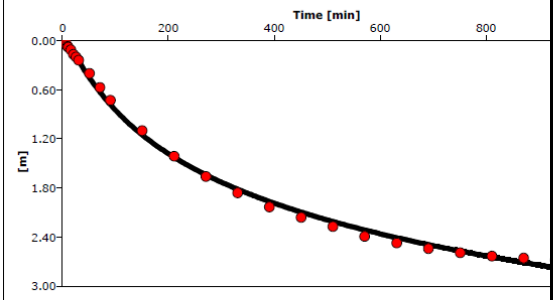

Calculation after Double Porosity

Observation Well	Transmissivity [m²/d]	Hydraulic Conductivity [m/d]	Specific storage	Sigma	Lambda
PW	2.40×10^{0}	6.66×10^{-1}	4.03×10^{-1}	1.15×10^{0}	8.20×10^{0}

Figure IV.2.38: Analysis of recovery test data for the well in Kanyagu-Ruseno using the double porosity method (test Nr. 15)

Location: Bugesera (Burundi)	Pumping Test: Large diameter well Ruseno_Kanyagu	Pumping Well: PW
Test Conducted by: Charles		Test Date: 14/10/2008
Analysis Performed by: Charles	Theis	Analysis Date: 17/02/2009
Aquifer Thickness: 3.60 m	Discharge Rate: 1.238713751 [m³/h]	

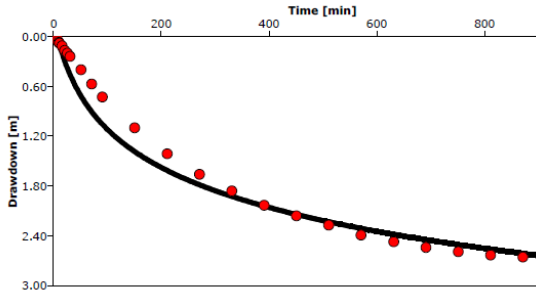

Calculation after Theis

Observation Well	Transmissivity [m²/d]	Hydraulic Conductivity [m/d]	Storage coefficient	Radial Distance to PW [m]
PW	3.24×10^{0}	8.98×10^{-1}	5.00×10^{-1}	0.5

Figure IV.2.39: Analysis of recovery test data for the well in Kanyagu-Ruseno using the Theis method (test Nr. 15)

Location: Bugesera (Burundi)	Pumping Test: Large diameter well Ruseno_Kanyagu	Pumping Well: PW
Test Conducted by: Charles		Test Date: 14/10/2008
Analysis Performed by: Charles	Papadopulos & Cooper	Analysis Date: 17/02/2009
Aquifer Thickness: 3.60 m	Discharge Rate: 1.238713751 [m³/h]	

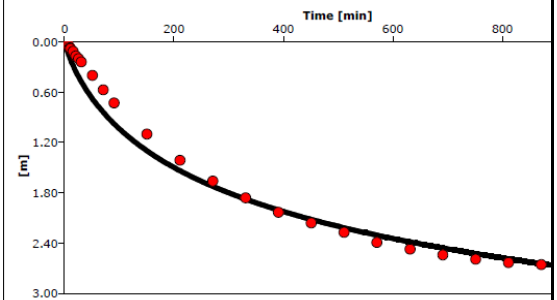

Calculation after Papadopulos & Cooper

Observation Well	Transmissivity [m²/d]	Hydraulic Conductivity [m/d]	Storage coefficient	Radial Distance to PW [m]
PW	3.06×10^{0}	8.50×10^{-1}	5.00×10^{-1}	0.5

Figure IV.2.40: Analysis of recovery test data for the well in Kanyagu-Ruseno using the Papadopulos & Cooper method (test Nr. 15)

Location: Bugesera	Pumping Test: Large diameter Kigina_Gisenyil	Pumping Well: PW
Test Conducted by: Charles		Test Date: 08/08/2008
Analysis Performed by: Charles	Hantush	Analysis Date: 11/02/2009
Aquifer Thickness: 2.32 m	Discharge Rate: 3.361338146 [m³/h]	

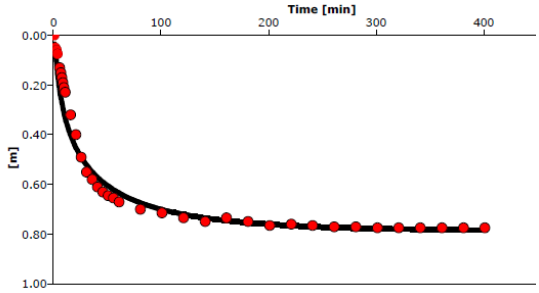

Calculation after Hantush

Observation Well	Transmissivity [m²/d]	Hydraulic Conductivity [m/d]	Storage coefficient	Hydr. resistance [min]	R P [n
PW	2.77×10^{1}	1.20×10^{1}	5.00×10^{-1}	2.93×10^{2}	0.

Figure IV.2. 41: Analysis of pumping test data for the well in Kigina I-Gisenyi using the Hantush analytical method (test Nr. 17)

Location: Bugesera	Pumping Test: Large diameter Kigina_Gisenyil	Pumping Well: PW
Test Conducted by: Charles		Test Date: 08/08/2008
Analysis Performed by: Charles	Hantush	Analysis Date: 11/02/2009
Aquifer Thickness: 2.32 m	Discharge Rate: 3.361338146 [m³/h]	

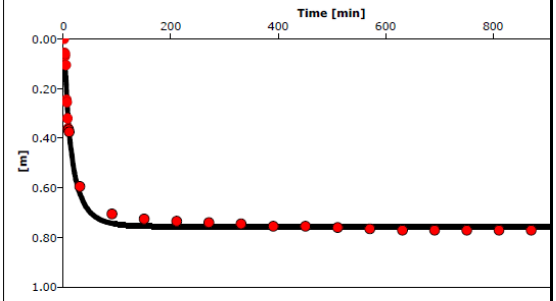

Calculation after Hantush

Observation Well	Transmissivity [m²/d]	Hydraulic Conductivity [m/d]	Storage coefficient	Hydr. resistance [min]	Ra PW [m]
PW	1.26×10^{1}	5.41×10^{0}	5.00×10^{-1}	7.21×10^{1}	0.5

Figure IV.2.42: Analysis of recovery test data for the well in Kigina I-Gisenyi using the Hantush analytical method (test Nr.17)

Location: Bugesera	Pumping Test: Large diameter Kigina_Gisenyil	Pumping Well: PW
Test Conducted by: Charles		Test Date: 08/08/2008
Analysis Performed by: Charles	Cooper & Jacob I	Analysis Date: 11/02/2009
Aquifer Thickness: 2.32 m	Discharge Rate: 3.361338146 [m³/h]	

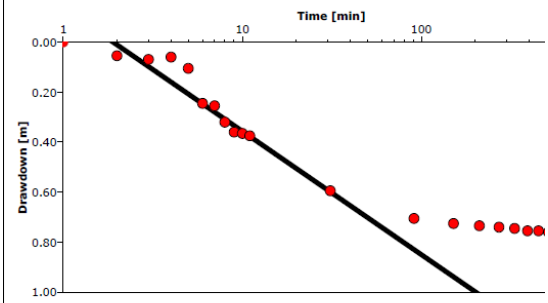

Calculation after Cooper & Jacob

Observation Well	Transmissivity [m²/d]	Hydraulic Conductivity [m/d]	Storage coefficient	Radial Distance to PW [m]
PW	2.99×10^{1}	1.29×10^{1}	3.54×10^{-1}	0.5

Figure IV.2.43: Analysis of recovery test data for the well in Kigina I-Gisenyi using the Cooper & Jacob analytical method (test Nr. 17)

Location: Bugesera (Kirundo)	Pumping Test: Large diameter Well Kigina Gisenyil 2	Pumping Well: PW
Test Conducted by: Charles		Test Date: 18/10/2007
Analysis Performed by: Charles	Hantush	Analysis Date: 11/02/2009
Aquifer Thickness: 2.00 m	Discharge Rate: 3.392971579 [m³/h]	

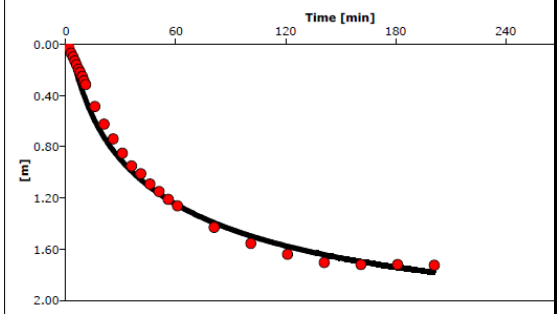

Calculation after Hantush

Observation Well	Transmissivity [m²/d]	Hydraulic Conductivity [m/d]	Storage coefficient	Hydr. resistance [min]
PW	1.04×10^{1}	5.23×10^{0}	5.00×10^{-1}	7.64×10^{2}

Figure IV.2. 44: Analysis of pumping test data for the well in Kigina II-Gisenyi using the Hantush analytical method (test Nr.18)

Location: Bugesera (Kirundo)	Pumping Test: Large diameter Well Kigina Gisenyil 2	Pumping Well: PW
Test Conducted by: Charles		Test Date: 18/10/2007
Analysis Performed by: Charles	Cooper & Jacob I	Analysis Date: 11/02/2009
Aquifer Thickness: 2.00 m	Discharge Rate: 3.392971579 [m³/h]	

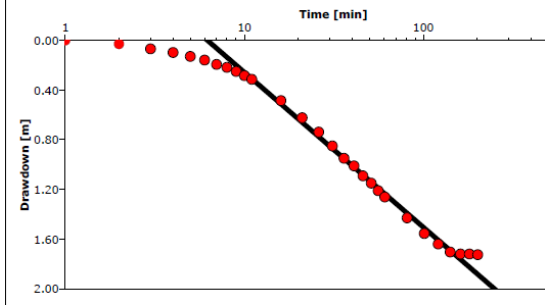

Calculation after Cooper & Jacob

Observation Well	Transmissivity [m²/d]	Hydraulic Conductivity [m/d]	Storage coefficient	Radial Distance to PW [m]
PW	1.19×10^{1}	5.99×10^{0}	4.64×10^{-1}	0.5

Figure IV.2.45: Analysis of pumping test data for the well in Kigina II-Gisenyi using the Cooper & Jacob analytical method (test Nr. 18)

Location: Bugesera	Pumping Test: Large diameter Kigina_Gisenyil	Pumping Well: PW
Test Conducted by: Charles		Test Date: 08/08/2008
Analysis Performed by: Charles	Hantush	Analysis Date: 11/02/2009
Aquifer Thickness: 2.00 m	Discharge Rate: 3.392971579 [m³/h]	

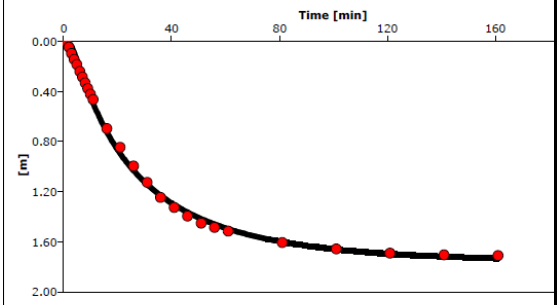

Calculation after Hantush

Observation Well	Transmissivity [m²/d]	Hydraulic Conductivity [m/d]	Storage coefficient	Hydr. resistance [min]	Rad PW [m]
PW	5.17×10^{0}	2.59×10^{0}	3.90×10^{-1}	1.59×10^{2}	0.5

Figure IV.2.46: Analysis of recovery test data for the well in Kigina II-Gisenyi using the Hantush analytical method (test Nr.18)

Location: Bugesera	Pumping Test: Large diameter Kigina_Gisenyil	Pumping Well: PW
Test Conducted by: Charles		Test Date: 08/08/2008
Analysis Performed by: Charles	Cooper & Jacob I	Analysis Date: 11/02/2009
Aquifer Thickness: 2.00 m	Discharge Rate: 3.392971579 [m³/h]	

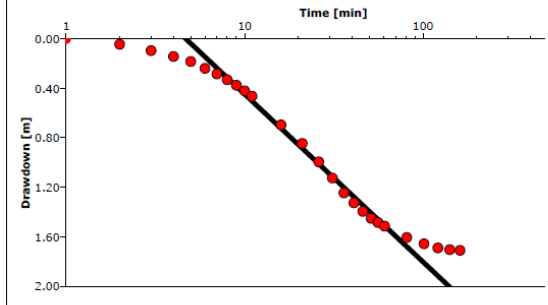

Calculation after Cooper & Jacob

Observation Well	Transmissivity [m²/d]	Hydraulic Conductivity [m/d]	Storage coefficient	Radial Distance to PW [m]
PW	1.10×10^{1}	5.51×10^{0}	3.22×10^{-1}	0.5

Figure IV.2.47: Analysis of recovery test data for the well in Kigina II-Gisenyi using the Cooper & Jacob method (test Nr. 18)

Location: Bugesera (Burundi)	Pumping Test: Large diameter Kigoma Gatare	Pumping Well: PW
Test Conducted by: Charles		Test Date: 09/10/2008
Analysis Performed by: Charles	Hantush	Analysis Date: 15/02/2009
Aquifer Thickness: 3.65 m	Discharge Rate: 2.25220943 [m³/h]	

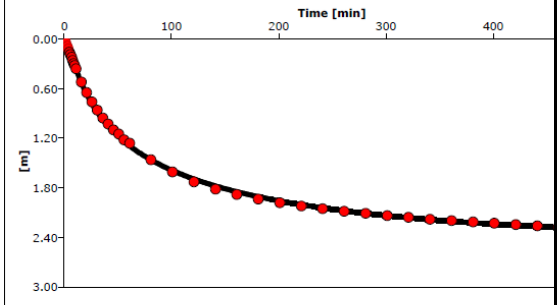

Calculation after Hantush

Observation Well	Transmissivity [m²/d]	Hydraulic Conductivity [m/d]	Storage coefficient	Hydr. resistance [min]	Rad PW [m]
PW	5.67×10^{0}	1.55×10^{0}	3.98×10^{-1}	1.19×10^{3}	0.5

Figure IV.2.48: Analysis of pumping test data for the well in Kigoma-Gatare using the Hantush analytical method (test Nr. 19)

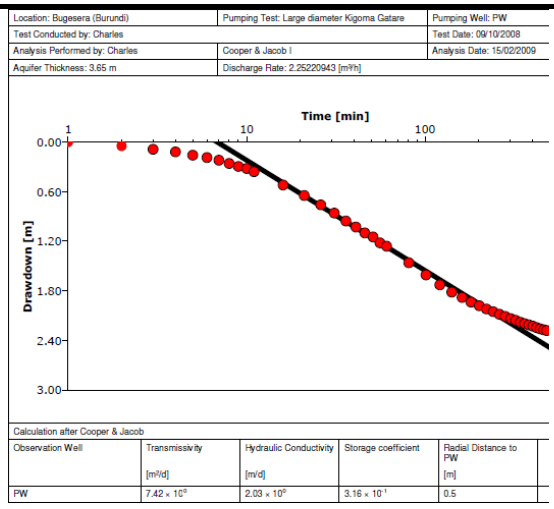

Figure IV.2.49: Analysis of pumping test data for the well in Kigoma-Gatare using the Cooper & Jacob analytical method (test Nr. 19)

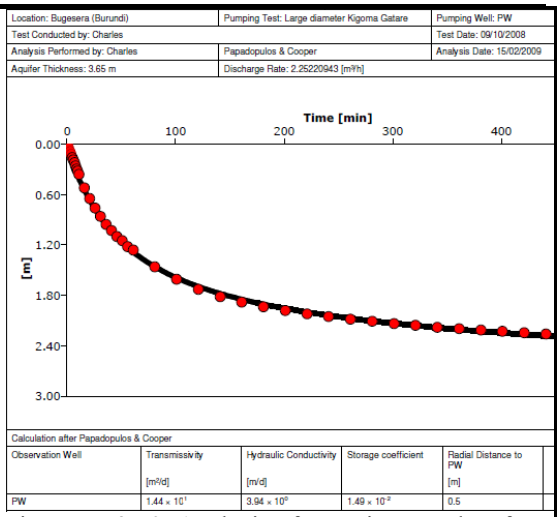

Figure IV.2.50: Analysis of pumping test data for the well in Kigoma-Gatare using the Papadopulos & Cooper method (test Nr. 19)

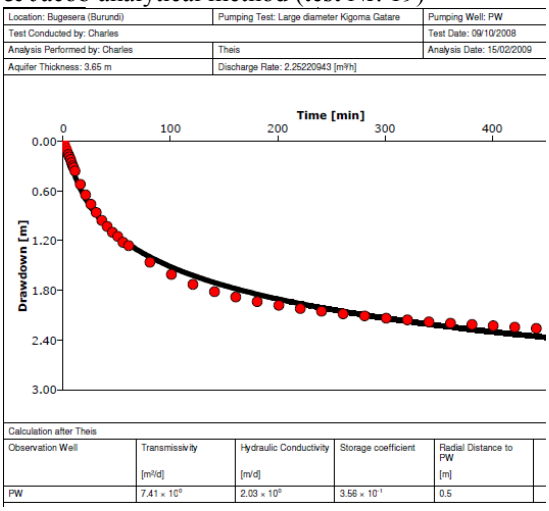

Figure IV.2.51: Analysis of pumping test data for the well in Kigoma-Gatare using the Theis method (test Nr 18)

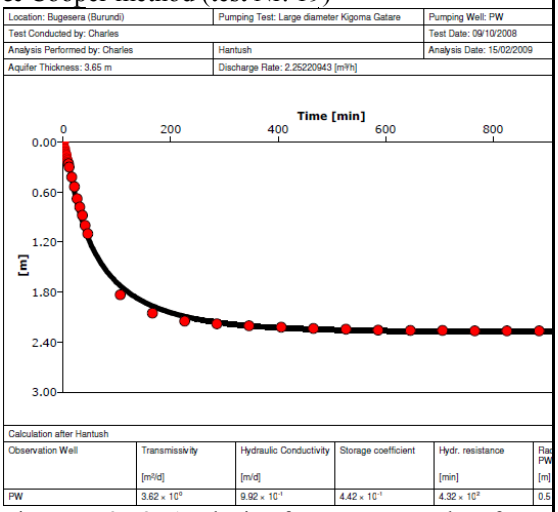

FigureIV.2.52: Analysis of recovery test data for the well in Kigoma-Gatare using the Hantush method (test Nr. 19)

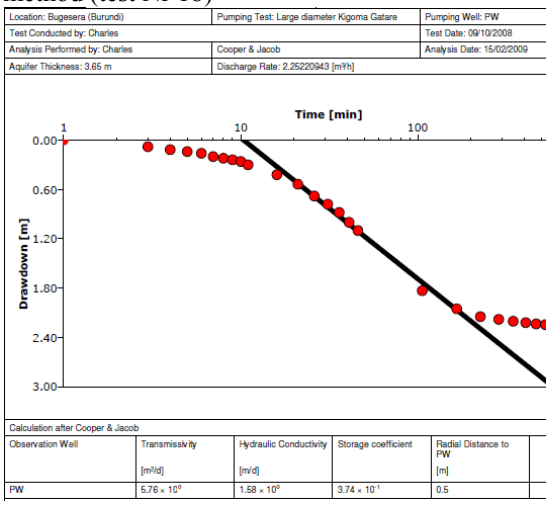

Figure IV.2.53: Analysis of recovery test data for the well in Kigoma-Gatare using the Cooper & Jacob method (test Nr. 19)

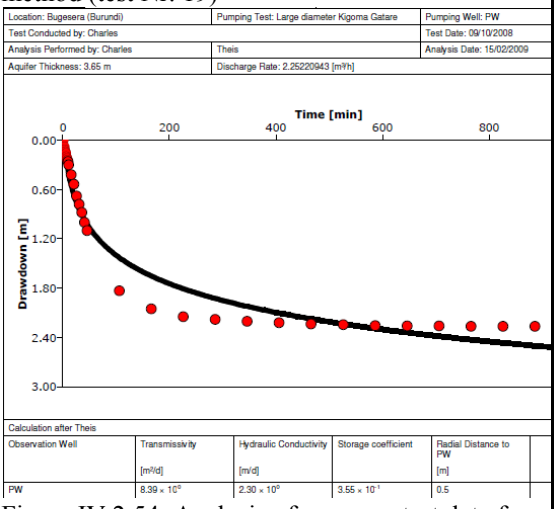

Figure IV.2.54: Analysis of recovery test data for the well in Kigoma -Gatare using the Theis method (test Nr. 19)

Location: Bugesera (Burundi)	Pumping Test: Large diameter Kigoma Gatare	Pumping Well: PW
Test Conducted by: Charles		Test Date: 09/10/2008
Analysis Performed by: Charles	Papadopulos & Cooper	Analysis Date: 15/02/2009
Aquifer Thickness: 3.65 m	Discharge Rate: 2.25220943 [m³/h]	

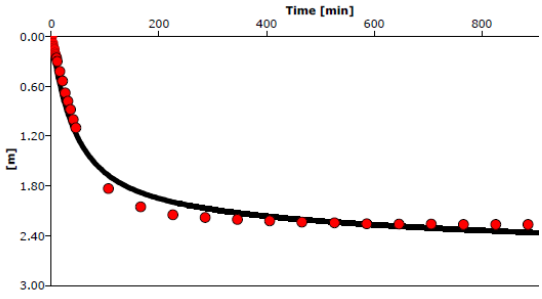

Calculation after Papadopulos & Cooper

Observation Well	Transmissivity [m²/d]	Hydraulic Conductivity [m/d]	Storage coefficient	Radial Distance to PW [m]
PW	2.08×10^{1}	5.70×10^{0}	1.12×10^{-3}	0.5

Figure IV.2.54: Analysis of recovery test data for the well in Kigoma-Gatare using the Papadopulos & Cooper method (test Nr. 19)

Location: Bugesera (Burundi)	Pumping Test: Large diameter well Kigozi_Yaranda	Pumping Well: PW
Test Conducted by:		Test Date: 16/11/2007
Analysis Performed by: Charles	Double Porosity	Analysis Date: 16/02/2009
Aquifer Thickness: 2.48 m	Discharge Rate: 2.555926198 [m³/h]	

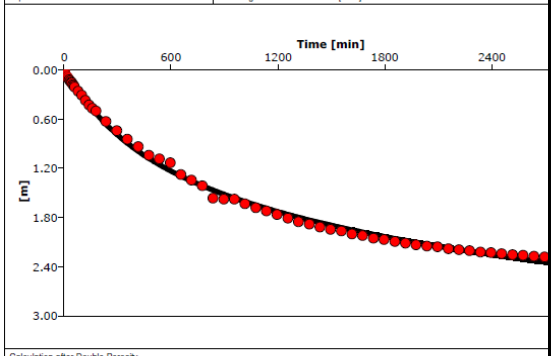

Calculation after Double Porosity

Observation Well	Transmissivity [m²/d]	Hydraulic Conductivity [m/d]	Specific storage	Sigma	Lambda
PW	6.14×10^{0}	2.48×10^{0}	4.44×10^{-1}	1.16×10^{1}	1.00×10^{1}

Figure IV.2.56: Analysis of recovery test data for the well in Kigozi-Yaranda using the double porosity method (test Nr. 20)

Location: Bugesera (Burundi)	Pumping Test: Large diameter well Kinyamateke	Pumping Well: PW
Test Conducted by:		Test Date: 14/08/2008
Analysis Performed by: Charles	Hantush	Analysis Date: 16/02/2009
Aquifer Thickness: 2.61 m	Discharge Rate: 1.443288174 [m³/h]	

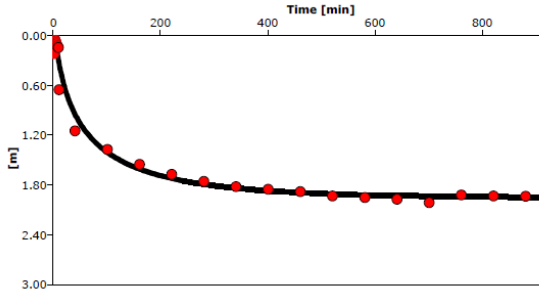

Calculation after Hantush

Observation Well	Transmissivity [m²/d]	Hydraulic Conductivity [m/d]	Storage coefficient	Hydr. resistance [min]	Ra PW [m]
PW	3.94×10^{0}	1.51×10^{0}	2.76×10^{-1}	1.08×10^{3}	0.5

Figure IV.2.57: Analysis of recovery test data for the well in Kinyamateke well using the Hantush analytical method (test Nr.21)

Location: Bugesera (Burundi)	Pumping Test: Large diameter well Kinyamateke	Pumping Well: PW
Test Conducted by:		Test Date: 14/08/2008
Analysis Performed by: Charles	Papadopulos & Cooper	Analysis Date: 16/02/2009
Aquifer Thickness: 2.61 m	Discharge Rate: 1.443288174 [m³/h]	

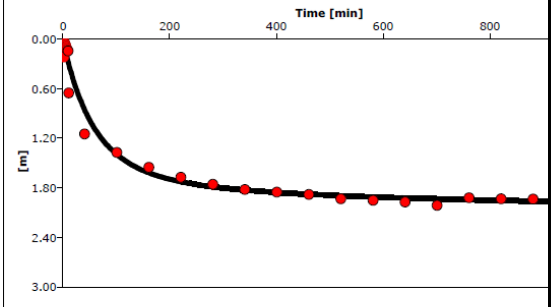

Calculation after Papadopulos & Cooper

Observation Well	Transmissivity [m²/d]	Hydraulic Conductivity [m/d]	Storage coefficient	Radial Distance to PW [m]
PW	2.70×10^{1}	1.03×10^{1}	5.76×10^{-7}	0.5

Figure IV.2.58: Analysis of recovery test data for the well in Kinyamateke using the Papadopulos & Cooper method (test Nr. 21)

Location: Bugesera (Burundi)	Pumping Test: Large diameter Well Muramba_Kiruhura	Pumping Well: PW
Test Conducted by:		Test Date: 04/10/2008
Analysis Performed by: Charles	Hantush	Analysis Date: 06/02/2009
Aquifer Thickness: 3.68 m	Discharge Rate: 2.114959659 [m³/h]	

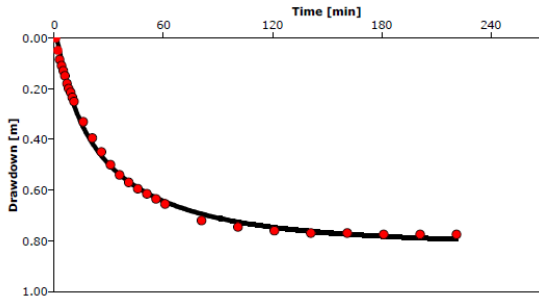

Calculation after Hantush

Observation Well	Transmissivity [m²/d]	Hydraulic Conductivity [m/d]	Storage coefficient	Hydr. resistance [min]
PW	1.20×10^{1}	3.27×10^{0}	4.84×10^{-1}	2.31×10^{2}

Figure IV.2.59: Analysis of pumping test data for the well in Kiruhura II-Muramba using the Hantush method (test Nr. 22)

Location: Bugesera (Burundi)	Pumping Test: Large diameter Well Muramba_Kiruhura	Pumping Well: PW
Test Conducted by:		Test Date: 04/10/2008
Analysis Performed by: Charles	Cooper & Jacobl	Analysis Date: 06/02/2009
Aquifer Thickness: 3.68 m	Discharge Rate: 2.114959659 [m³/h]	

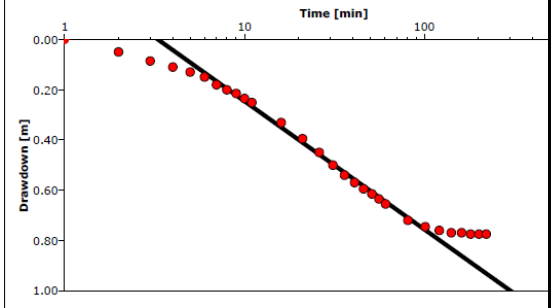

Calculation after Cooper & Jacob

Observation Well	Transmissivity [m²/d]	Hydraulic Conductivity [m/d]	Storage coefficient	Radial Distance to PW [m]
PW	1.82×10^{1}	4.94×10^{0}	3.76×10^{-1}	0.5

Figure IV.2.60: Analysis of pumping test data for the well in Kiruhura II-Muramba l using the Cooper & Jacob method (test Nr. 22)

Location: Bugesera (Burundi)	Pumping Test: Large diameter Well Muramba_Kiruhura	Pumping Well: PW
Test Conducted by:		Test Date: 04/10/2008
Analysis Performed by: Charles	Papadopulos & Cooper	Analysis Date: 06/02/2009
Aquifer Thickness: 3.68 m	Discharge Rate: 2.114959659 [m³/h]	

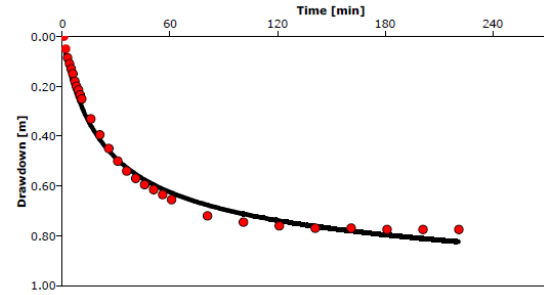

Calculation after Papadopulos & Cooper

Observation Well	Transmissivity [m²/d]	Hydraulic Conductivity [m/d]	Storage coefficient	Radial Distance to PW [m]
PW	3.57×10^{1}	9.70×10^{0}	2.84×10^{-2}	0.5

Figure IV.2.61: Analysis of pumping test data for the well in Kiruhura II-Muramba using the Papadopulos & Cooper method (test Nr. 22)

Location: Bugesera (Burundi)	Pumping Test: Large diameter well Muramba-Kiruhura	Pumping Well: PW
Test Conducted by:		Test Date: 04/10/2008
Analysis Performed by: Charles	Theis	Analysis Date: 06/02/2009
Aquifer Thickness: 3.68 m	Discharge Rate: 2.115 [m³/h]	

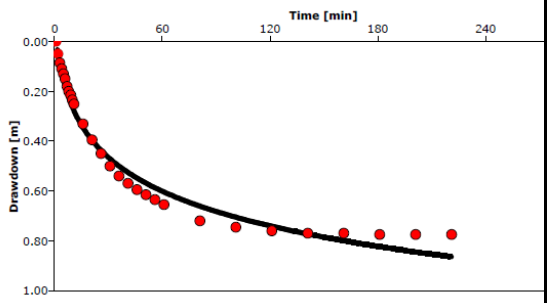

Calculation after Theis

Observation Well	Transmissivity [m²/d]	Hydraulic Conductivity [m/d]	Storage coefficient	Radial Distance to PW [m]
PW	1.97×10^{1}	5.35×10^{0}	4.07×10^{-1}	0.5

Figure IV.2.62: Analysis of pumping test data for the well in Kiruhura II-Muramba using the Theis method (test Nr. 22)

Location: Bugesera (Burundi)	Pumping Test: Large diameter well Muramba-Kiruhura	Pumping Well: PW
Test Conducted by: Charles		Test Date: 05/10/2008
Analysis Performed by: Charles	Hantush	Analysis Date: 10/02/2009
Aquifer Thickness: 3.68 m	Discharge Rate: 2.114959659 [m³/h]	

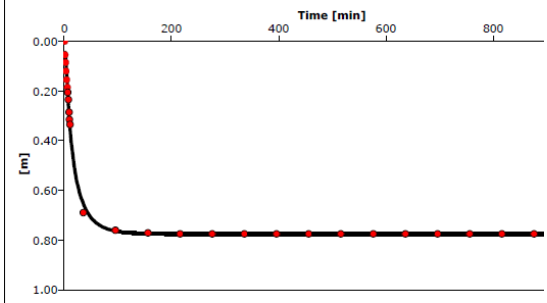

Calculation after Hantush

Observation Well	Transmissivity [m²/d]	Hydraulic Conductivity [m/d]	Storage coefficient	Hydr. resistance [min]	R P [r
PW	6.97×10^{0}	1.89×10^{0}	3.39×10^{-1}	1.08×10^{2}	0

Figure IV.2.63: Analysis of recovery test data for the well in Kiruhura II-Muramba using the Hantush method (test Nr. 22)

Location: Bugesera (Burundi)	Pumping Test: Large diameter well Muramba-Kiruhura	Pumping Well: PW
Test Conducted by: Charles		Test Date: 05/10/2008
Analysis Performed by: Charles	Cooper & Jacob I	Analysis Date: 10/02/2009
Aquifer Thickness: 3.68 m	Discharge Rate: 2.114959659 [m³/h]	

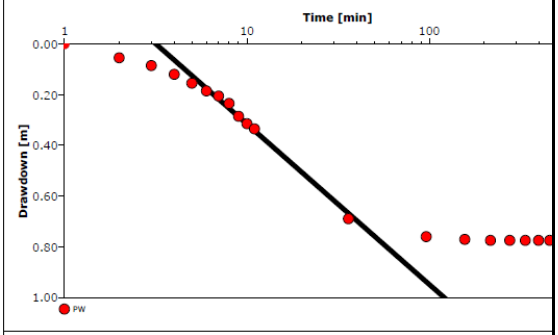

Calculation after Cooper & Jacob

Observation Well	Transmissivity [m²/d]	Hydraulic Conductivity [m/d]	Storage coefficient	Radial Distance to PW [m]
PW	1.47×10^{1}	3.99×10^{0}	2.91×10^{-1}	0.5

Figure IV.2.64: Analysis of recovery test data for the well in Kiruhura II-Muramba using the Cooper and Jacob method (test Nr. 22)

Location: Bugesera (Burundi)	Pumping Test: Large diameter well Kiyanza_Kiruhura	Pumping Well: PW
Test Conducted by: Charles		Test Date: 03/10/2008
Analysis Performed by: Charles	Hantush	Analysis Date: 10/02/2009
Aquifer Thickness: 2.95 m	Discharge Rate: 3.471111111 [m³/h]	

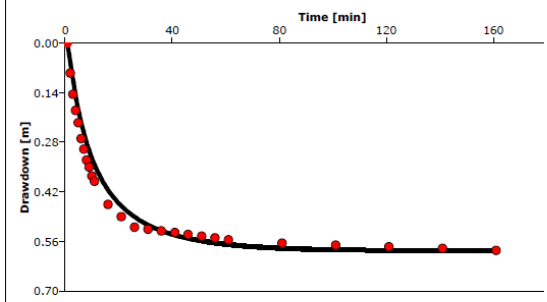

Calculation after Hantush

Observation Well	Transmissivity [m²/d]	Hydraulic Conductivity [m/d]	Storage coefficient	Ratio K(v)/K(h)	Hydr. resistance [min]
PW	1.92×10^{1}	6.51×10^{0}	5.00×10^{-1}	1.20×10^{-1}	6.25×10^{1}

Figure IV.2.65: Analysis of pumping test data for the well in Kiruhura I-Kiyanza using the Hantush analytical method (test Nr. 23)

Location: Bugesera (Burundi)	Pumping Test: Large diameter well Kiyanza_Kiruhura	Pumping Well: PW
Test Conducted by: Charles		Test Date: 03/10/2008
Analysis Performed by: Charles	Cooper & Jacob I	Analysis Date: 10/02/2009
Aquifer Thickness: 2.95 m	Discharge Rate: 3.471111111 [m³/h]	

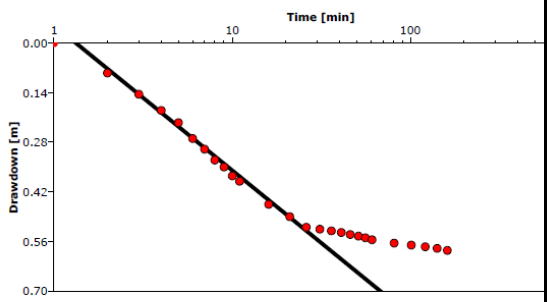

Calculation after Cooper & Jacob

Observation Well	Transmissivity [m²/d]	Hydraulic Conductivity [m/d]	Storage coefficient	Radial Distance to PW [m]
PW	3.72×10^{1}	1.26×10^{1}	3.08×10^{-1}	0.5

Figure IV.2.66: Analysis of pumping test data for the well in Kiruhura I-Kiyanza using the Cooper & Jacob analytical method (test Nr. 23)

Location: Bugesera (Burundi)	Pumping Test: Large diameter well Kiyanza_Kiruhura	Pumping Well: PW
Test Conducted by: Charles		Test Date: 03/10/2008
Analysis Performed by: Charles	Papadopulos & Cooper	Analysis Date: 10/02/2009
Aquifer Thickness: 2.95 m	Discharge Rate: 3.471111111 [m³/h]	

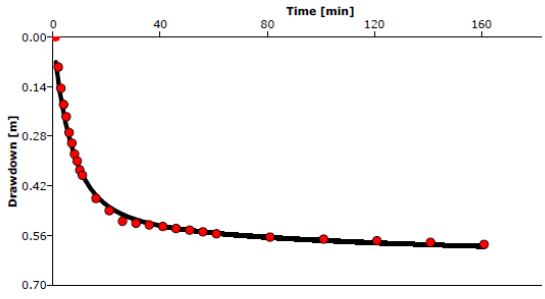

Calculation after Papadopulos & Cooper

Observation Well	Transmissivity [m²/d]	Hydraulic Conductivity [m/d]	Storage coefficient	Radial Distance to PW [m]
PW	2.09×10^{2}	7.07×10^{1}	1.57×10^{-5}	0.5

Figure IV.2.67: Analysis of pumping test data for the well in Kiruhura I-Kiyanza using the Papadopulos & Cooper method (test Nr. 23)

Location: Bugesera (Burundi)	Pumping Test: Large diameter well Kiyanza_Kiruhura	Pumping Well: PW
Test Conducted by: Charles		Test Date: 03/10/2008
Analysis Performed by: Charles	Hantush	Analysis Date: 10/02/2009
Aquifer Thickness: 2.95 m	Discharge Rate: 3.471111111 [m³/h]	

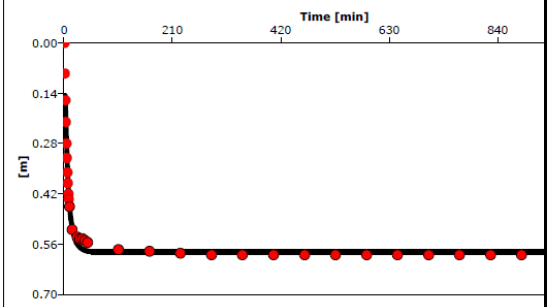

Calculation after Hantush

Observation Well	Transmissivity [m²/d]	Hydraulic Conductivity [m/d]	Storage coefficient	Hydr. resistance [min]
PW	1.20×10^{1}	4.07×10^{0}	3.00×10^{-1}	4.19×10^{1}

Figure IV.2 68: Analysis of recovery test data for the well in Kiruhura I-Kiyanza using the Hantush method (test Nr. 23)

Location: Bugesera (Burundi)	Pumping Test: Pumping large Diameter Mago_Gatete	Pumping Well: PW
Test Conducted by: Charles		Test Date: 25/11/2008
Analysis Performed by: Charles	Hantush	Analysis Date: 13/02/2009
Aquifer Thickness: 4.13 m	Discharge Rate: 2.1610489 [m³/h]	

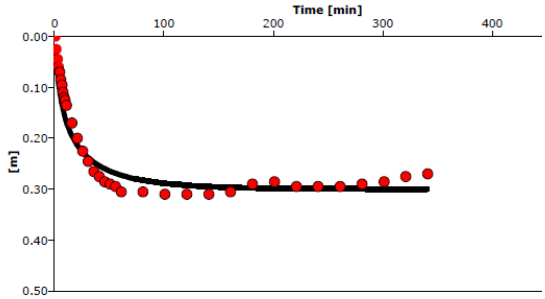

Calculation after Hantush

Observation Well	Transmissivity [m²/d]	Hydraulic Conductivity [m/d]	Storage coefficient	Hydr. resistance [min]
PW	4.39×10^{1}	1.06×10^{1}	5.00×10^{-1}	1.47×10^{2}

Figure IV.2.69: Analysis of pumping test data for the well in Mago-Gatete using the Hantush method (test Nr. 24)

Location: Bugesera (Burundi)	Pumping Test: Pumping large Diameter Mago_Gatete	Pumping Well: PW
Test Conducted by: Charles		Test Date: 25/11/2008
Analysis Performed by: Charles	Hantush	Analysis Date: 13/02/2009
Aquifer Thickness: 4.13 m	Discharge Rate: 2.1610489 [m³/h]	

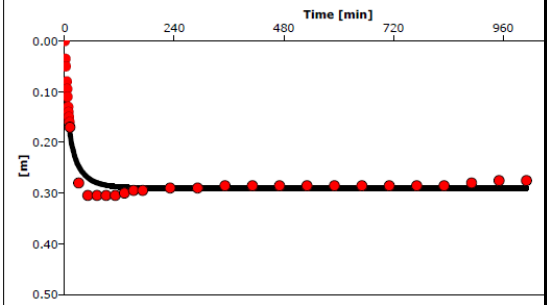

Calculation after Hantush

Observation Well	Transmissivity [m²/d]	Hydraulic Conductivity [m/d]	Storage coefficient	Hydr. resistance [min]
PW	3.73×10^{1}	9.02×10^{0}	5.00×10^{-1}	9.41×10^{1}

Figure IV.2.70: Analysis of recovery test data for the well in Mago-Gatete using the Hantush method (test Nr.24)

Location: Bugesera	Pumping Test: Large diameter Marembo_Marembo	Pumping Well: PW
Test Conducted by: Charles		Test Date: 01/10/2008
Analysis Performed by: Charles	Hantush	Analysis Date: 12/02/2009
Aquifer Thickness: 4.95 m	Discharge Rate: 1.911353853 [m³/h]	

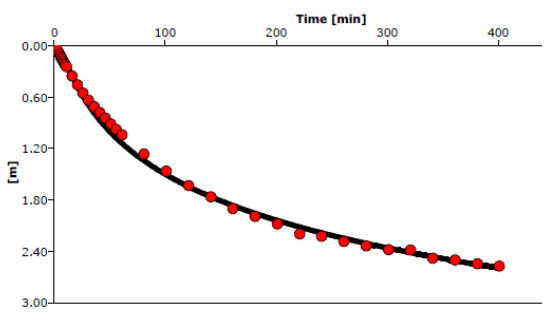

Calculation after Hantush

Observation Well	Transmissivity [m²/d]	Hydraulic Conductivity [m/d]	Storage coefficient	Hydr. resistance [min]
PW	4.38×10^{0}	8.84×10^{-1}	5.00×10^{-1}	1.67×10^{10}

Figure IV.2.71: Analysis of pumping test data for the well in Marembo-Marembo using the Hantush method (test Nr. 25)

Location: Bugesera	Pumping Test: Large diameter Marembo_Marembo	Pumping Well: PW
Test Conducted by: Charles		Test Date: 01/10/2008
Analysis Performed by: Charles	Jacob & Cooper	Analysis Date: 12/02/2009
Aquifer Thickness: 4.95 m	Discharge Rate: 1.911353853 [m³/h]	

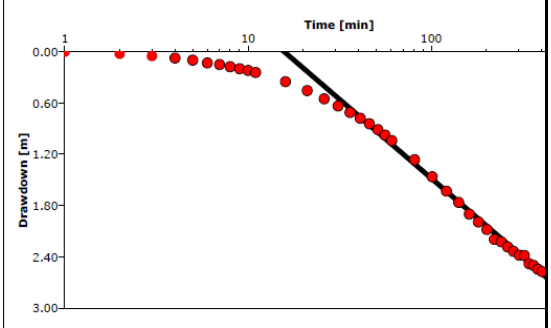

Calculation after Cooper & Jacob

Observation Well	Transmissivity [m²/d]	Hydraulic Conductivity [m/d]	Storage coefficient	Radial Distance to PW [m]
PW	4.55×10^{0}	9.19×10^{-1}	4.47×10^{-1}	0.5

Figure IV.2.72: Analysis of pumping test data for the well in Marembo-Marembo using the Cooper & Jacob method (test Nr. 25)

Location: Bugesera	Pumping Test: Large diameter Marembo_Marembo	Pumping Well: PW
Test Conducted by: Charles		Test Date: 01/10/2008
Analysis Performed by: Charles	Theis	Analysis Date: 12/02/2009
Aquifer Thickness: 4.95 m	Discharge Rate: 1.911353853 [m³/h]	

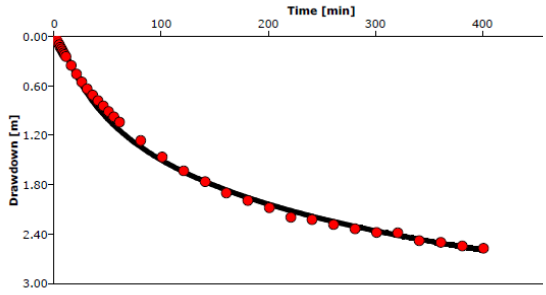

Calculation after Theis

Observation Well	Transmissivity [m²/d]	Hydraulic Conductivity [m/d]	Storage coefficient	Radial Distance to PW [m]
PW	4.38×10^{0}	8.84×10^{-1}	5.00×10^{-1}	0.5

Figure IV.2.73: Analysis of pumping test data for the well in Marembo-Marembo using the Theis method (test Nr. 25)

Location: Bugesera	Pumping Test: Large diameter Marembo_Marembo	Pumping Well: PW
Test Conducted by: Charles		Test Date: 01/10/2008
Analysis Performed by: Charles	Hantush	Analysis Date: 12/02/2009
Aquifer Thickness: 4.95 m	Discharge Rate: 1.911353853 [m³/h]	

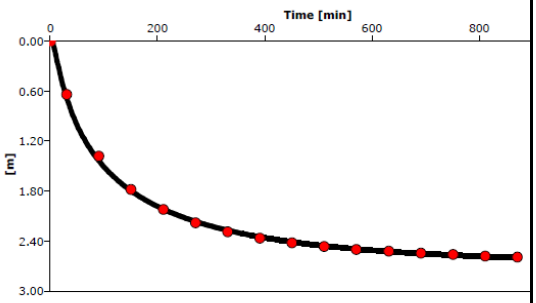

Calculation after Hantush

Observation Well	Transmissivity [m²/d]	Hydraulic Conductivity [m/d]	Storage coefficient	Hydr. resistance [min]	R PW [m]
PW	3.67×10^{0}	7.40×10^{-1}	5.00×10^{-1}	1.02×10^{3}	0

Figure IV.2.74: Analysis of recovery test data for the well in Marembo-Marembo using the Hantush method (test Nr. 25)

Location: Bugesera	Pumping Test: Large diameter Marembo_Marembo	Pumping Well: PW
Test Conducted by: Charles		Test Date: 01/10/2008
Analysis Performed by: Charles	Cooper & Jacob I	Analysis Date: 12/02/2009
Aquifer Thickness: 4.95 m	Discharge Rate: 1.911353853 [m³/h]	

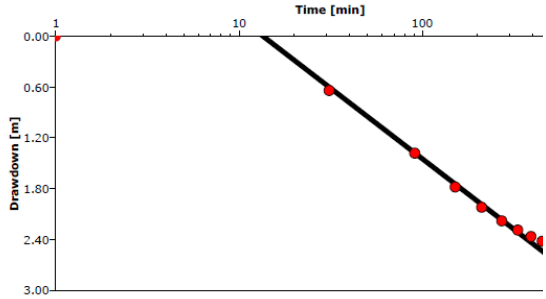

Calculation after Cooper & Jacob

Observation Well	Transmissivity [m²/d]	Hydraulic Conductivity [m/d]	Storage coefficient	Radial Distance to PW [m]
PW	5.04×10^{0}	1.02×10^{0}	4.25×10^{-1}	0.5

Figure IV.2.75: Analysis of recovery test data for the well in Marembo-Marembo using the Cooper & Jacob method (test Nr. 25)

Location: Bugesera	Pumping Test: Large diameter Marembo_Marembo	Pumping Well: PW
Test Conducted by: Charles		Test Date: 01/10/2008
Analysis Performed by: Charles	Theis	Analysis Date: 12/02/2009
Aquifer Thickness: 4.95 m	Discharge Rate: 1.911353853 [m³/h]	

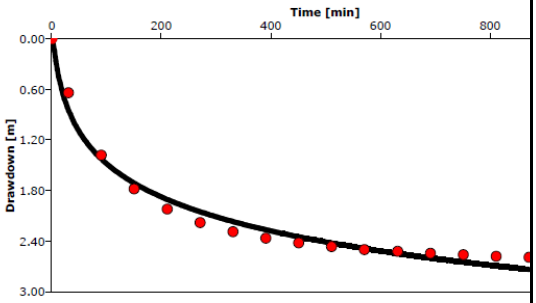

Calculation after Theis

Observation Well	Transmissivity [m²/d]	Hydraulic Conductivity [m/d]	Storage coefficient	Radial Distance to PW [m]
PW	6.16×10^{0}	1.25×10^{0}	3.32×10^{-1}	0.5

Figure IV.2.76: Analysis of recovery test data for the well in Marembo-Marembo using the Theis method (test Nr. 25)

Location: Bugesera (Burundi)	Pumping Test: Large diameter well Mugombwa_ Kiri	Pumping Well: PW
Test Conducted by: Charles		Test Date: 05/11/2007
Analysis Performed by: Charles	Hantush	Analysis Date: 17/02/2009
Aquifer Thickness: 3.05 m	Discharge Rate: 2.733830026 [m³/h]	

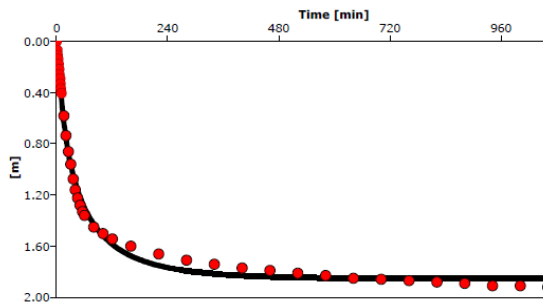

Calculation after Hantush

Observation Well	Transmissivity [m²/d]	Hydraulic Conductivity [m/d]	Storage coefficient	Hydr. resistance [min]
PW	7.20×10^{0}	2.36×10^{0}	3.85×10^{-1}	4.52×10^{2}

Figure IV.2.77: Analysis of recovery test data for the well in Mugombwa-Kiri using the Hantush method (test Nr. 26)

Location: Bugesera (Burundi)	Pumping Test: Large diameter well Mugombwa_ Kiri	Pumping Well: PW
Test Conducted by: Charles		Test Date: 05/11/2007
Analysis Performed by: Charles	Papadopulos & Cooper	Analysis Date: 17/02/2009
Aquifer Thickness: 3.05 m	Discharge Rate: 2.733830026 [m³/h]	

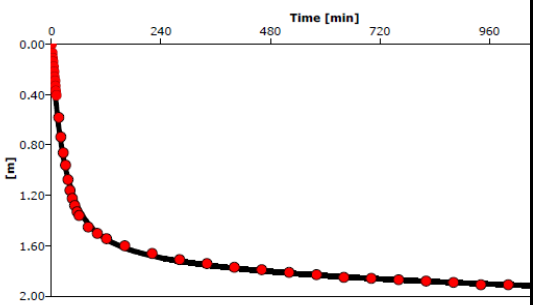

Calculation after Papadopulos & Cooper

Observation Well	Transmissivity [m²/d]	Hydraulic Conductivity [m/d]	Storage coefficient	Radial Distance to PW [m]
PW	4.04×10^{1}	1.32×10^{1}	9.04×10^{-5}	0.5

Figure 78: Analysis of recovery test data for the well in Mugombwa-Kiri using the Papadopulos & Cooper method (test Nr. 26)

Location: Bugesera (Burundi)	Pumping Test: Large diameter Muheroll Yaranda	Pumping Well: PW
Test Conducted by: Charles		Test Date: 29/10/2008
Analysis Performed by: Charles	Hantush	Analysis Date: 04/02/2
Aquifer Thickness: 2.27 m	Discharge Rate: 5.195449356 [m³/h]	

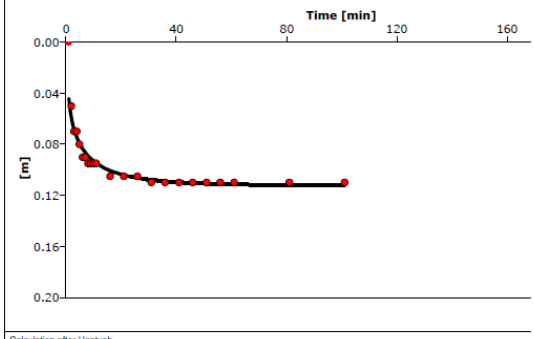

Calculation after Hantush

Observation Well	Transmissivity [m²/d]	Hydraulic Conductivity [m/d]	Storage coefficient	Hydr. resistance [min]
PW	3.77×10^{2}	1.66×10^{2}	5.00×10^{-1}	5.24×10^{1}

Figure IV.2.79: Analysis of pumping test data for the well in Muhero-Yaranda II using the Hantush method (test Nr. 27)

Location: Bugesera (Burundi)	Pumping Test: Large diameter Muheroll Yaranda	Pumping Well: PW
Test Conducted by: Charles		Test Date: 29/10/2008
Analysis Performed by: Charles	Hantush	Analysis Date: 04/02/2009
Aquifer Thickness: 2.27 m	Discharge Rate: 5.195449356 [m³/h]	

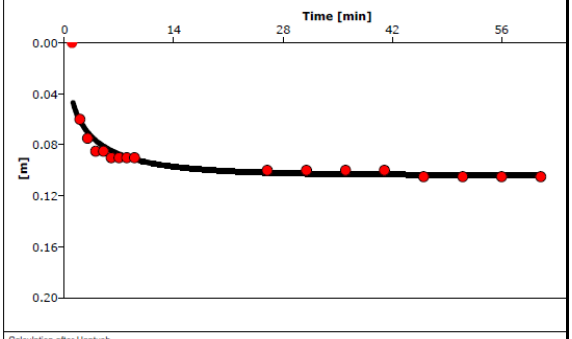

Calculation after Hantush

Observation Well	Transmissivity [m²/d]	Hydraulic Conductivity [m/d]	Storage coefficient	Hydr. resistance [min]	Radi PW [m]
PW	3.43×10^{2}	1.51×10^{2}	5.00×10^{-1}	2.85×10^{1}	0.5

Figure IV.2.80: Analysis of recovery test data for the well in Muhero-Yaranda I using the Hantush method (test Nr. 27)

Location: Bugesera (Burundi)	Pumping Test: Large diameter Muhero Yarandal	Pumping Well: PW
Test Conducted by: Charles		Test Date: 21/11/2008
Analysis Performed by: Charles	Hantush	Analysis Date: 04/02/2009
Aquifer Thickness: 3.57 m	Discharge Rate: 1.840732368333 [m³/h]	

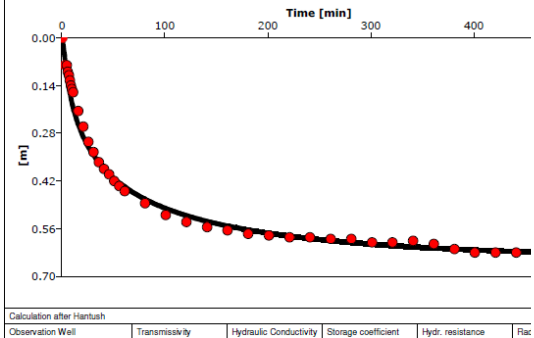

Calculation after Hantush

Observation Well	Transmissivity [m²/d]	Hydraulic Conductivity [m/d]	Storage coefficient	Hydr. resistance [min]	Rad PW [m]
PW	2.16×10^{1}	6.06×10^{0}	5.00×10^{-1}	6.98×10^{2}	0.5

Figure IV.2.81: Analysis of pumping test data for the well in Muhero-Yaranda I using the Hantush method (test Nr. 28)

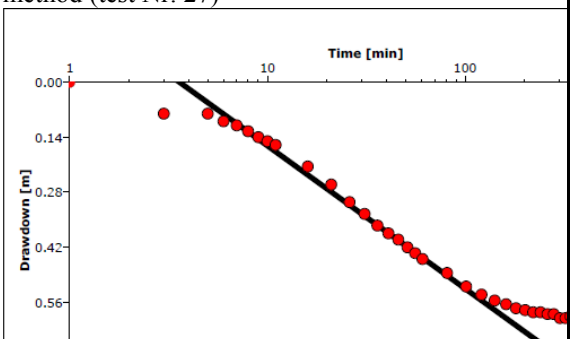

Calculation after Cooper & Jacob

Observation Well	Transmissivity [m²/d]	Hydraulic Conductivity [m/d]	Storage coefficient	Radial Distance to PW [m]
PW	2.22×10^{1}	6.23×10^{0}	5.00×10^{-1}	0.5

Figure IV.2.82: Analysis of pumping test data for the well in Muhero-Yaranda I using the Cooper & Jacob method (test Nr. 28)

Location: Bugesera (Burundi)	Pumping Test: Large diameter Muhero Yarandal	Pumping Well: PW
Test Conducted by: Charles		Test Date: 21/11/2008
Analysis Performed by: Charles	Papadopulos & Cooper	Analysis Date: 04/02/200
Aquifer Thickness: 3.57 m	Discharge Rate: 1.840732368333 [m³/h]	

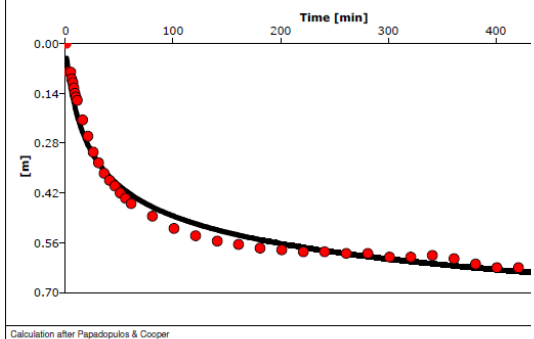

Calculation after Papadopulos & Cooper

Observation Well	Transmissivity [m²/d]	Hydraulic Conductivity [m/d]	Storage coefficient	Radial Distance to PW [m]
PW	3.63×10^{1}	1.02×10^{1}	1.20×10^{-1}	0.5

Figure IV.2.83: Analysis of pumping test data for the well in Muhero-Yaranda I well using the Papadopulos & Cooper method (test Nr. 28)

Location: Bugesera (Burundi)	Pumping Test: Large diameter Muhero Yarandal	Pumping Well: PW
Test Conducted by: Charles		Test Date: 21/11/2008
Analysis Performed by: Charles	Hantush	Analysis Date: 04/02/2009
Aquifer Thickness: 3.57 m	Discharge Rate: 1.840732368333 [m³/h]	

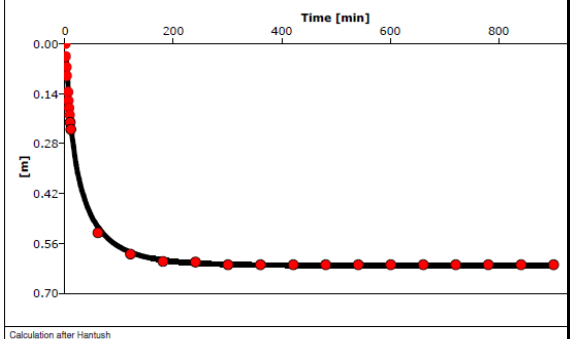

Calculation after Hantush

Observation Well	Transmissivity [m²/d]	Hydraulic Conductivity [m/d]	Storage coefficient	Hydr. resistance [min]	Radi PW [m]
PW	1.31×10^{1}	3.67×10^{0}	5.00×10^{-1}	1.89×10^{2}	0.5

Figure IV.2.84: Analysis of recovery test data for the well in Muhero-Yaranda I using the Hantush method (test Nr. 28)

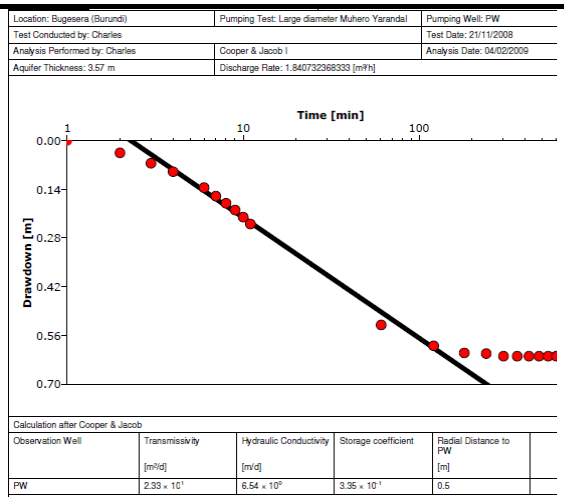

Figure IV.2.85: Analysis of pumping test data for the well in Muhero-Yaranda II using the Hantush method (test Nr. 28)

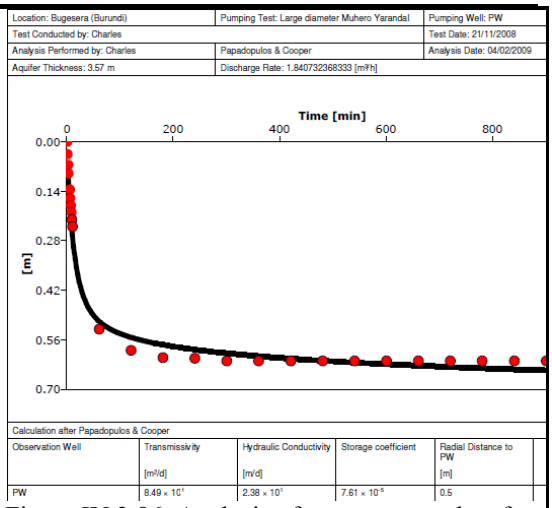

Figure IV.2.86: Analysis of recovery test data for the well in Muhero-Yaranda I using the Papadopulos & Cooper method (test Nr. 28)

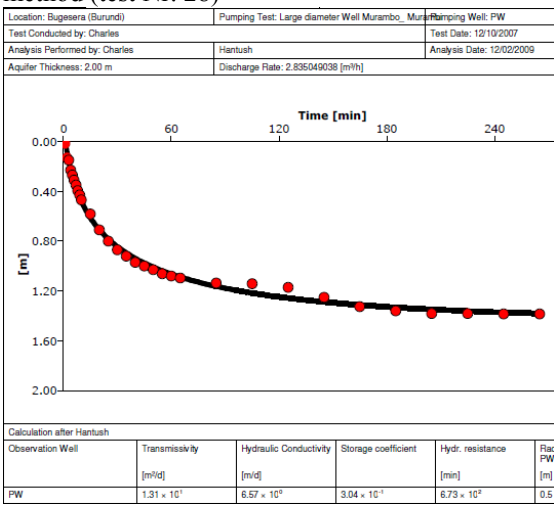

Figure IV.2.87: Analysis of pumping test data for the well in Murambo-Murambi using the Hantush method (test Nr. 30)

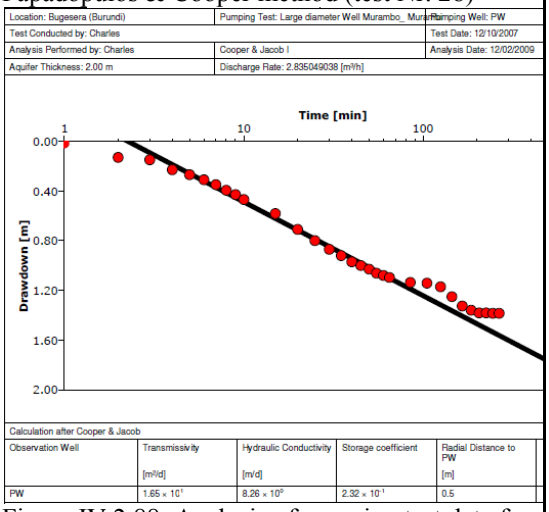

Figure IV.2.88: Analysis of pumping test data for the well in Murambo-Murambi using the Cooper & Jacob method (test Nr. 30)

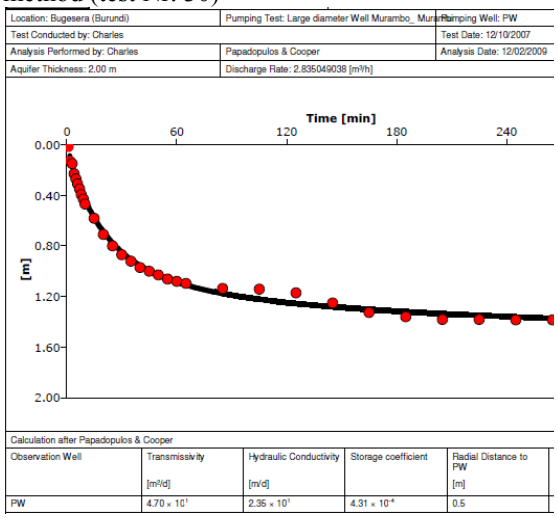

Figure IV.2.89: Analysis of recovery test data for the well in Murambo-Murambi using the Papadopulos & Cooper method (test Nr. 30)

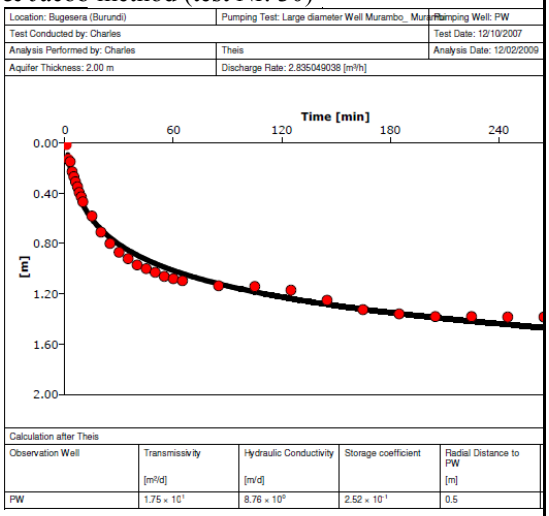

Figure IV.2.90: Analysis of pumping test data for the well in Murambo-Murambi using the Theis method (test Nr. 30)

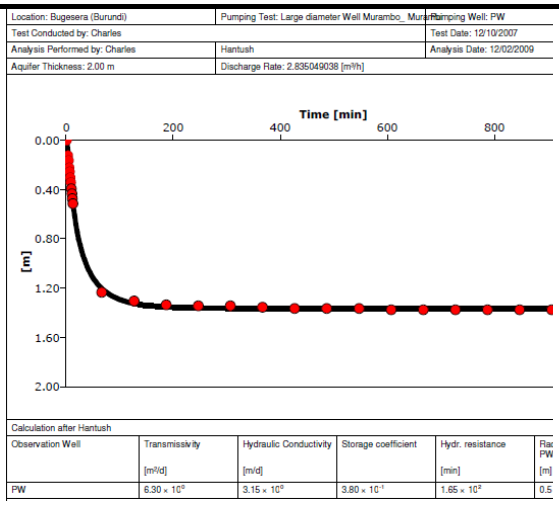

Figure IV.2.91: Analysis of recovery test data for the well in Murambo-Murambi using the Papadopulos & Cooper method (test Nr. 30)

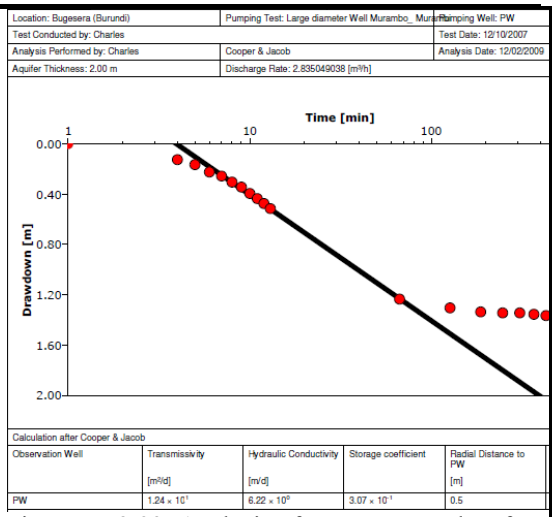

Figure IV.2.92: Analysis of recovery test data for the well in Murambo-Murambi using the Cooper & Jacob method (test Nr. 30)

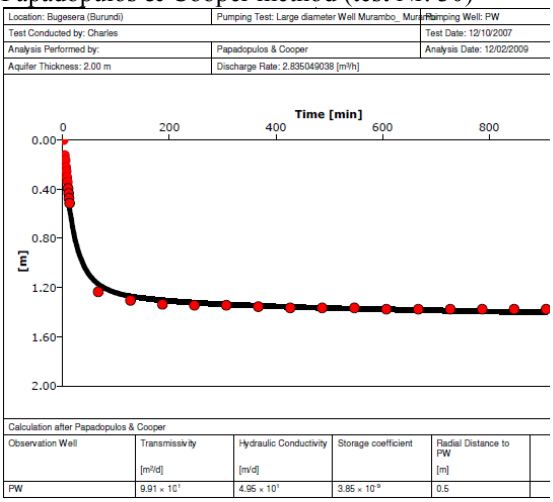

Figure IV.2.93: Analysis of recovery test data for the well in Murambo-Murambi using the Papadopulos & Cooper method (test Nr. 30)

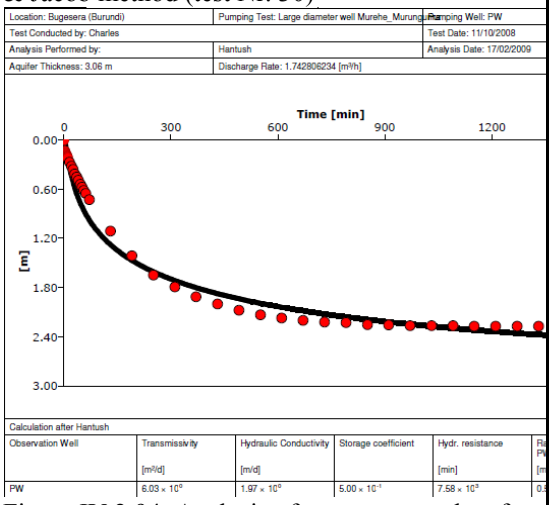

Figure IV.2.94: Analysis of recovery test data for the well in Murehe-Murungurira using the Hantush method (test Nr. 31)

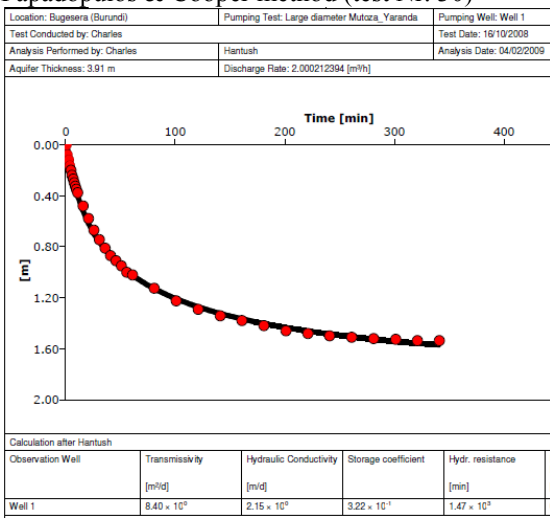

Figure IV.2.95: Analysis of pumping test data for the well Mutoza-Yaranda using the Hantush method (test Nr. 32)

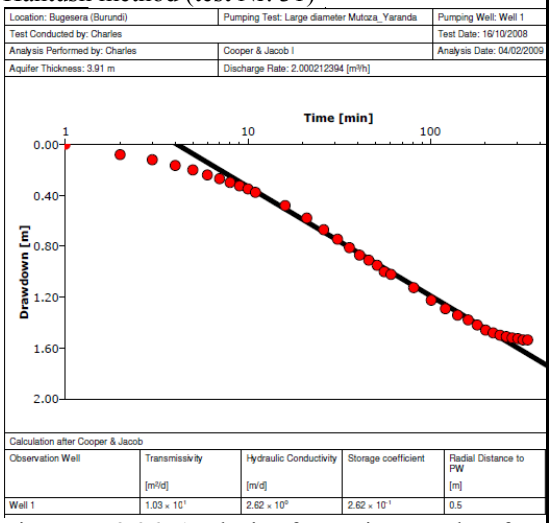

Figure IV.2.96: Analysis of pumping test data for the well in Mutoza-Yaranda using the Cooper & Jacob method (test Nr.32)

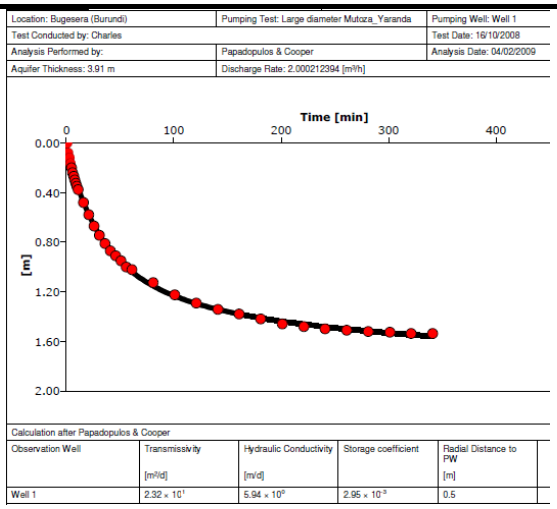

Figure IV.2.97: Analysis of pumping test data for the well in Mutoza-Yaranda using the Papadopulos & Cooper method (test Nr. 32)

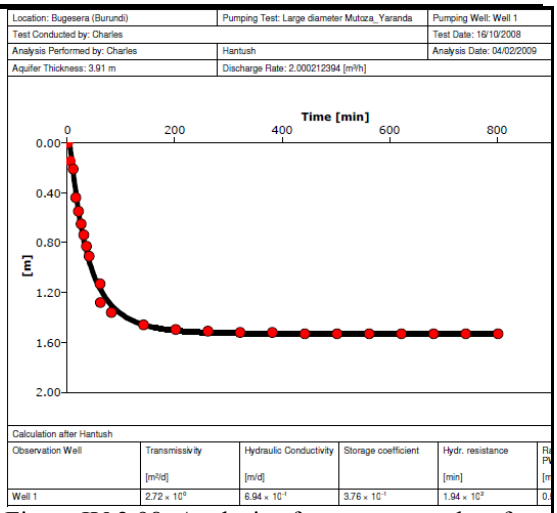

Figure IV.2.98: Analysis of recovery test data for the well in Mutoza-Yaranda using the Hantush method (test Nr. 32)

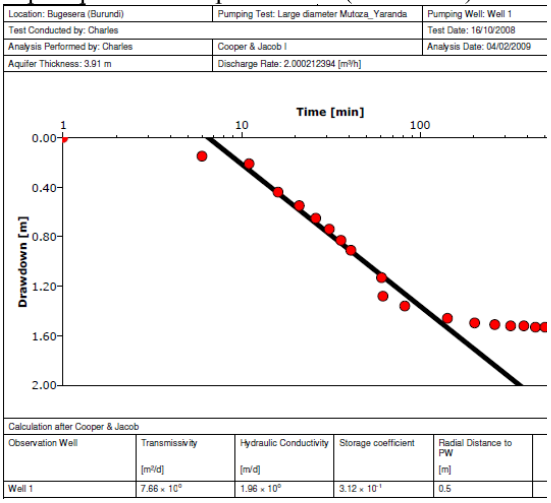

Figure IV.2.99: Analysis of recovery test data for the well in Mutoza-Yaranda using the Cooper & Jacob method (test Nr. 32)

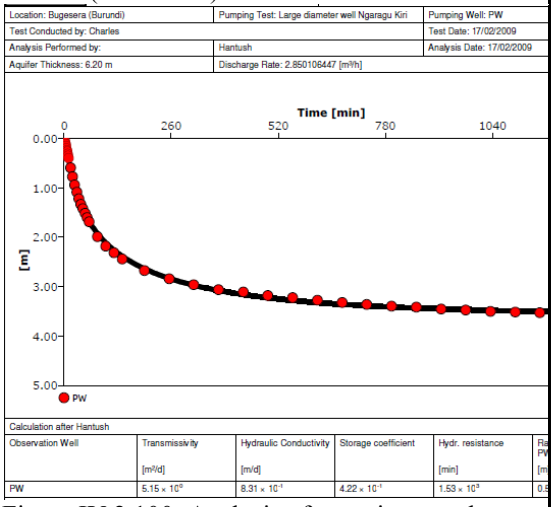

Figure IV.2.100: Analysis of pumping test data for the well in Ngaragu-Kiri using the Hantush method (test Nr. 33)

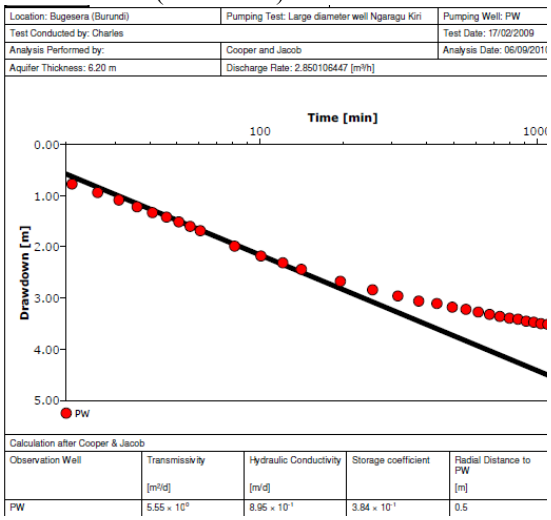

Figure 101: Analysis of pumping test data for the well in Ngaragu-Kiri using the Cooper & Jacob method (test Nr. 33)

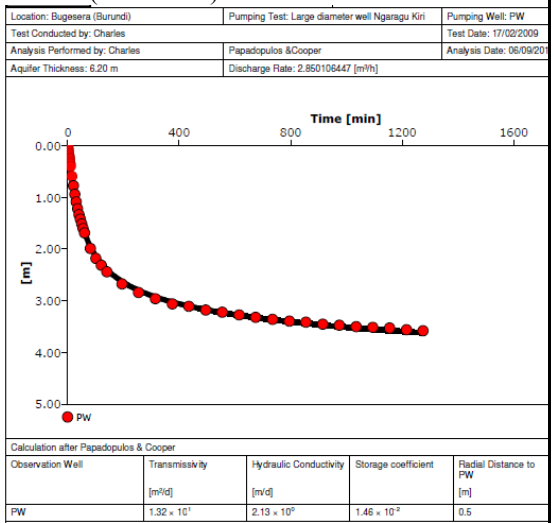

Figure IV.2.102: Analysis of pumping test data for the well in Ngaragu-Kiri using the Papadopulos & Cooper method (test Nr. 33)

Location: Bugesera (Burundi)	Pumping Test: Large diameter well Ngaragu Kiri	Pumping Well: PW
Test Conducted by: Charles		Test Date: 17/02/2009
Analysis Performed by:	Theis	Analysis Date: 06/09/2010
Aquifer Thickness: 6.20 m	Discharge Rate: 2.850106447 [m³/h]	

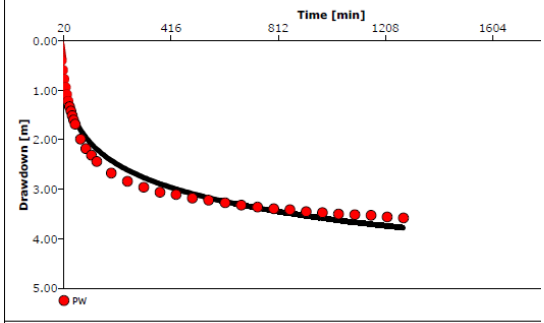

Calculation after Theis

Observation Well	Transmissivity [m²/d]	Hydraulic Conductivity [m/d]	Storage coefficient	Radial Distance to PW [m]
PW	7.46×10^{0}	1.20×10^{0}	3.36×10^{-1}	0.5

Figure IV.2.103: Analysis of pumping test data for the well in Ngaragu-Kiri using the Theis method (test Nr. 33)

Location: Bugesera (Burundi)	Pumping Test: Large diameter well Ngaragu Kiri	Pumping Well: PW
Test Conducted by: Charles		Test Date: 17/02/2009
Analysis Performed by: Charles	Hantush	Analysis Date: 17/02/2009
Aquifer Thickness: 6.20 m	Discharge Rate: 2.850106447 [m³/h]	

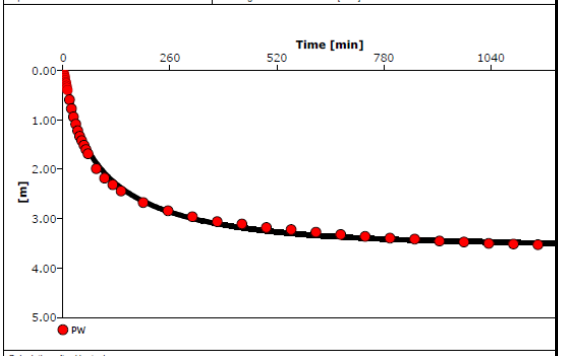

Calculation after Hantush

Observation Well	Transmissivity [m²/d]	Hydraulic Conductivity [m/d]	Storage coefficient	Hydr. resistance [min]	Radi PW [m]
PW	4.41×10^{0}	7.11×10^{-1}	5.00×10^{-3}	1.03×10^{3}	0.5

Figure IV.2.104: Analysis of recovery test data for the well in Ngaragu-Kiri using the Hantush method (test Nr. 33)

Location: Bugesera (Burundi)	Pumping Test: Large diameter well Ngaragu Kiri	Pumping Well: PW
Test Conducted by: Charles		Test Date: 17/02/2009
Analysis Performed by: Charles	Cooper & Jacob I	Analysis Date: 17/02/2009
Aquifer Thickness: 6.20 m	Discharge Rate: 2.850106447 [m³/h]	

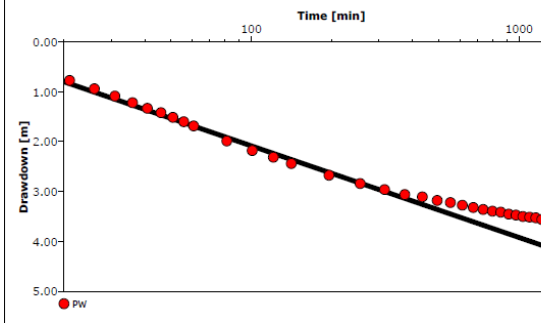

Calculation after Cooper & Jacob

Observation Well	Transmissivity [m²/d]	Hydraulic Conductivity [m/d]	Storage coefficient	Radial Distance to PW [m]
PW	6.82×10^{0}	1.10×10^{0}	3.11×10^{-1}	0.5

Figure IV.2.105: Analysis of recovery test data for Ngaragu-Kiri well using the Cooper & Jacob method (test Nr. 33)

Location: Bugesera (Burundi)	Pumping Test: Large diameter well Ngaragu Kiri	Pumping Well: PW
Test Conducted by: Charles		Test Date: 17/02/2009
Analysis Performed by: Charles	Papadopulos & Cooper	Analysis Date: 17/02/2009
Aquifer Thickness: 6.20 m	Discharge Rate: 2.850106447 [m³/h]	

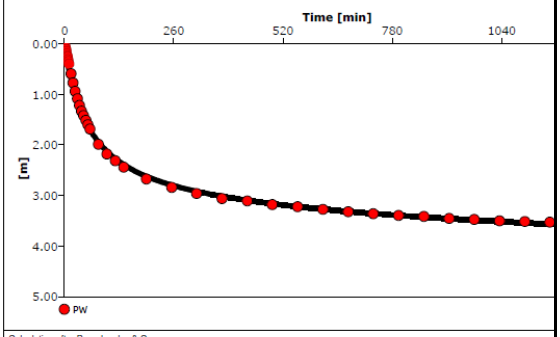

Calculation after Papadopulos & Cooper

Observation Well	Transmissivity [m²/d]	Hydraulic Conductivity [m/d]	Storage coefficient	Radial Distance to PW [m]
PW	1.32×10^{1}	2.14×10^{0}	1.46×10^{-2}	0.5

Figure IV.2.106: Analysis of recovery test data for Ngaragu-Kiri well using the Papadopulos & Cooper method (test Nr. 33)

Location: Bugesera (Burundi)	Pumping Test: Large diameter well Ngaragu Kiri	Pumping Well: PW
Test Conducted by: Charles		Test Date: 17/02/2009
Analysis Performed by: charles	Theis	Analysis Date: 17/02/2009
Aquifer Thickness: 6.20 m	Discharge Rate: 2.850106447 [m³/h]	

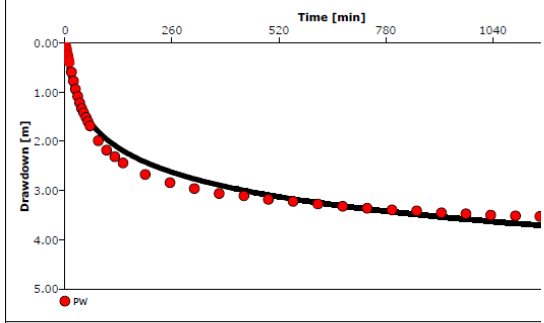

Calculation after Theis

Observation Well	Transmissivity [m²/d]	Hydraulic Conductivity [m/d]	Storage coefficient	Radial Distance to PW [m]
PW	7.46×10^{0}	1.20×10^{0}	3.36×10^{-1}	0.5

Figure IV.2.107: Analysis of recovery test data for the well in Ngaragu-Kiri using the Theis method (test Nr. 33)

Location: Bugesera (Burundi)	Pumping Test: Large diameter well Ntembe II Kiri	Pumping Well: PW
Test Conducted by: Charles		Test Date: 02/11/2007
Analysis Performed by: Charles	Hantush	Analysis Date: 17/02/2009
Aquifer Thickness: 4.45 m	Discharge Rate: 2.437059233 [m³/h]	

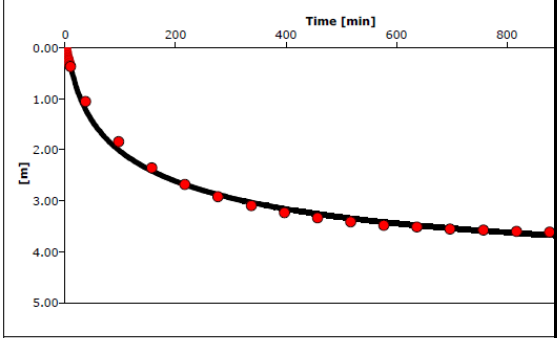

Calculation after Hantush

Observation Well	Transmissivity [m²/d]	Hydraulic Conductivity [m/d]	Storage coefficient	Hydr. resistance [min]
PW	4.76×10^{0}	1.07×10^{0}	3.80×10^{-1}	4.01×10^{3}

Figure IV.2.108: Analysis of recovery test data for the well in Ntembe-Kiri using the Hantush method (test Nr. 34)

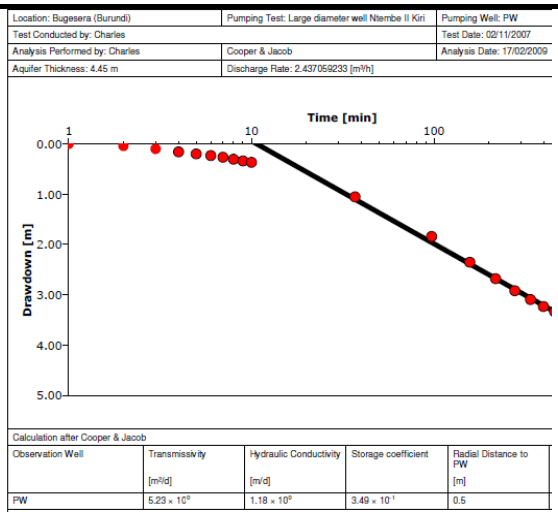

Figure IV.2.109: Analysis of recovery test data for the well in Ntembe-Kiri using the Cooper & Jacob method (test Nr. 34)

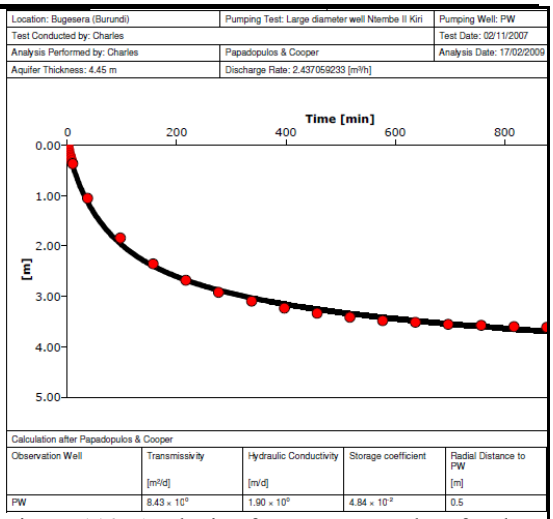

Figure 110: Analysis of recovery test data for the well in Ntembe-Kiri using the Papadopulos & Cooper method (test Nr. 34)

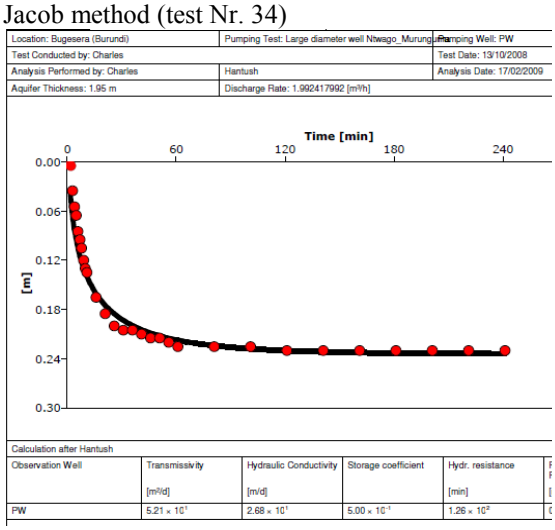

Figure IV.2.111: Analysis of pumping test data for the well in Ntwago-Murungurira using the Hantush method (test Nr. 35)

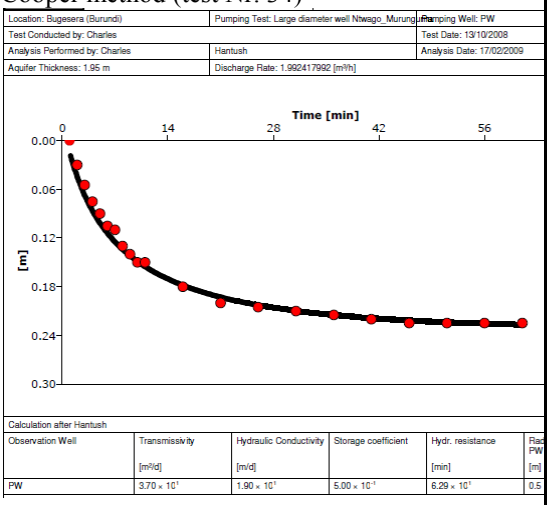

Figure IV.2.112: Analysis of recovery test data for Ntwago-Murungurira well using the Hantush method (test Nr. 35)

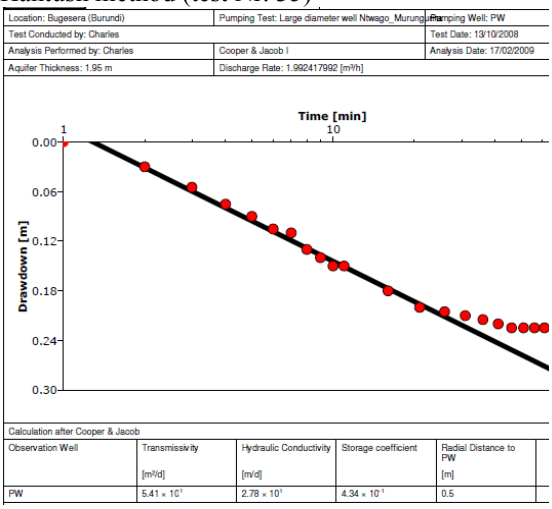

Figure IV.2.113: Analysis of recovery test data for Ntwago-Murungurira well using the Cooper & Jacob method (test Nr. 35)

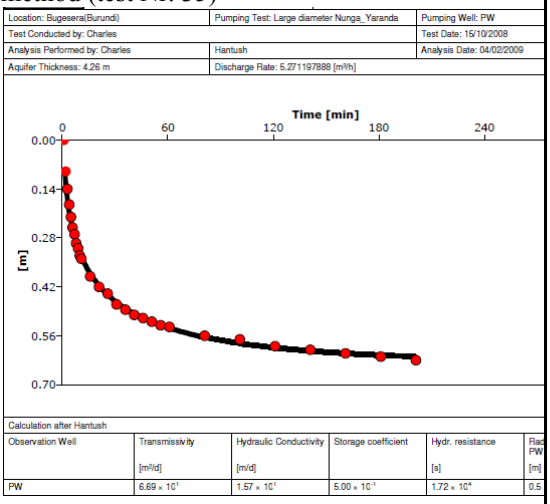

Figure IV.2.114: Analysis of pumping test data for the well in Nunga II-Yaranda using the Hantush method (test Nr. 36)

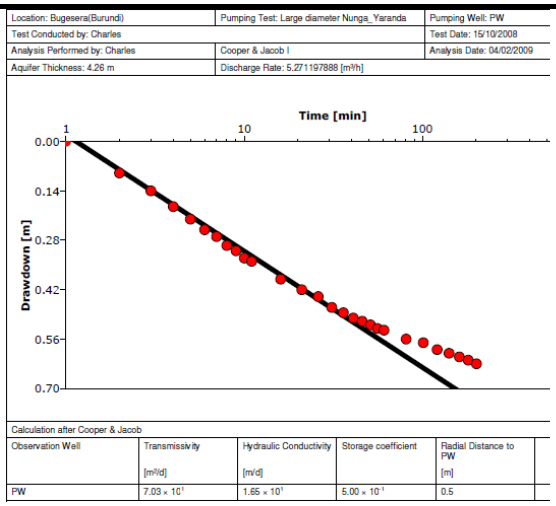

Figure IV.2.115: Analysis of pumping test data for the well in Nunga II-Yaranda using the Cooper & Jacob method (test Nr.36)

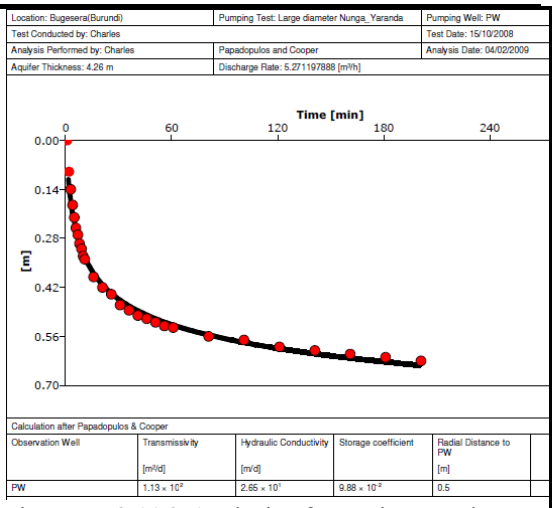

Figure IV.2.116: Analysis of pumping test data for the well in Nunga II-Yaranda using the Papadopulos & Cooper method (test Nr. 36)

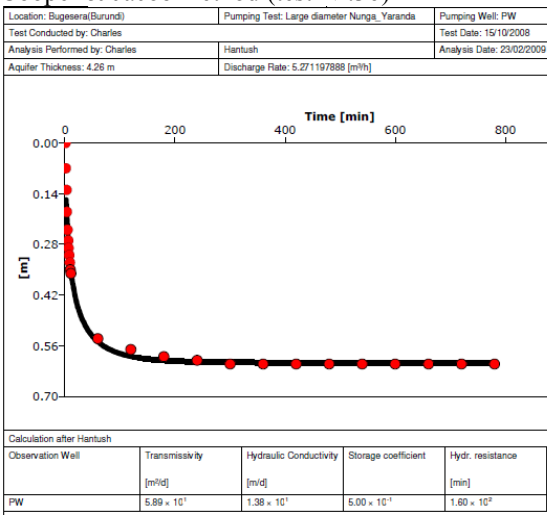

Figure IV.2.117: Analysis of recovery test data for the well in Nunga II-Yaranda using the Hantush method (test Nr. 36)

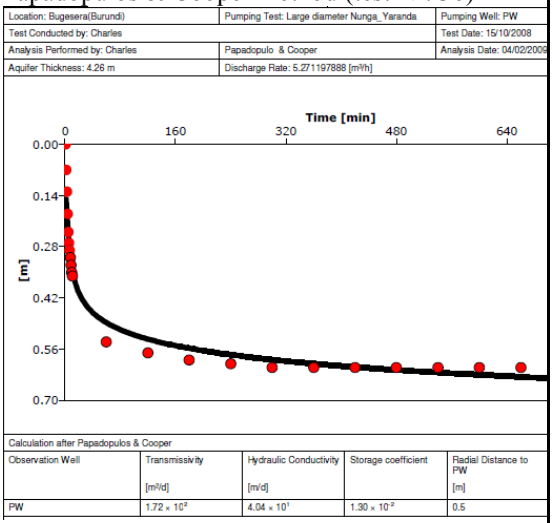

Figure IV.2.118: Analysis of pumping test data for the well in Nunga II-Yaranda using the Papadopulos & Cooper method (test Nr.36)

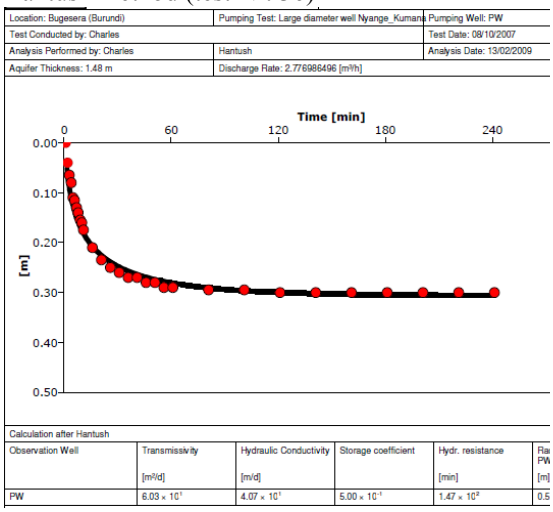

Figure 119: Analysis of pumping test data for the well in Nyange-Kumana using the Hantush method (test Nr. 37)

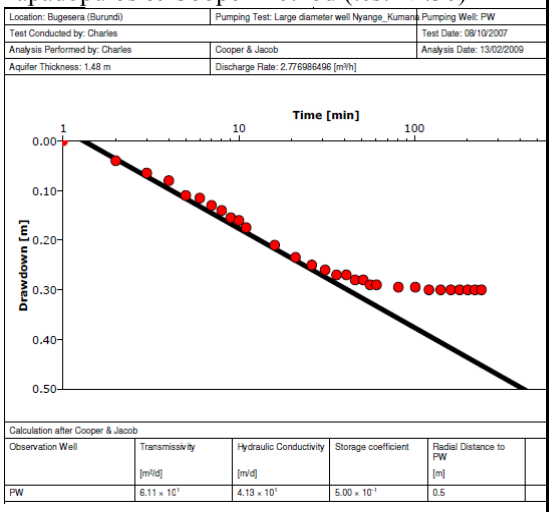

Figure IV.2.120: Analysis of pumping test data for the well in Nyange-Kumana using the Cooper and Jacob method (test Nr. 37)

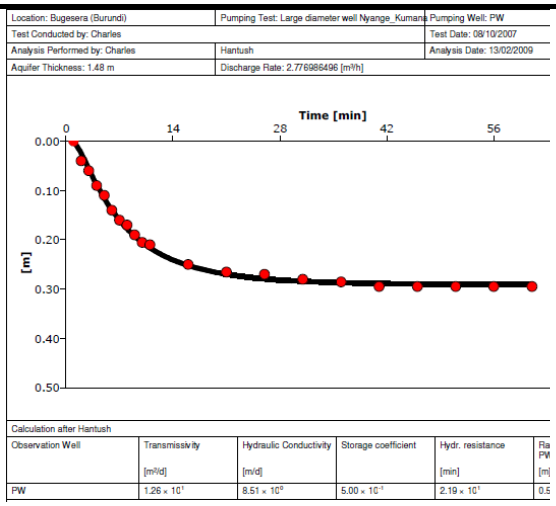

Figure IV.2.121: Analysis of recovery test data for the well in Nyange-Kumana using the Hantush method (Well Nr 37)

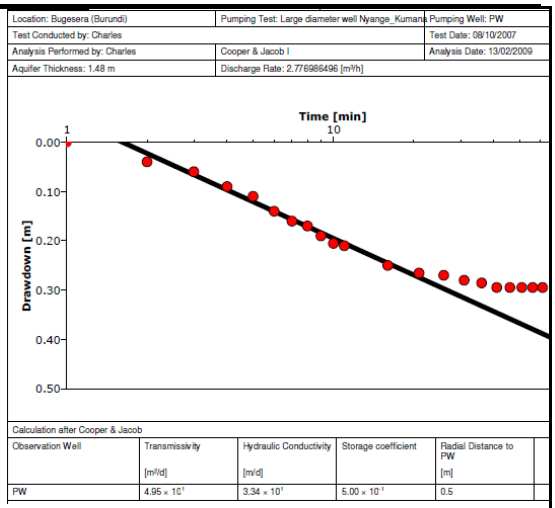

Figure IV.2.122: Analysis of recovery test data for the will in Nyange-Kumana using the Cooper & Jacob method (test Nr. 37)

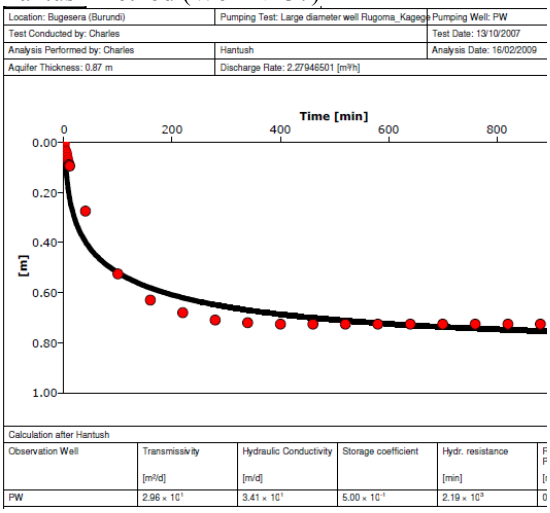

Figure IV.2.123: Analysis of recovery test data for the well in Rugoma-Kagege using the Hantush method (test Nr. 38)

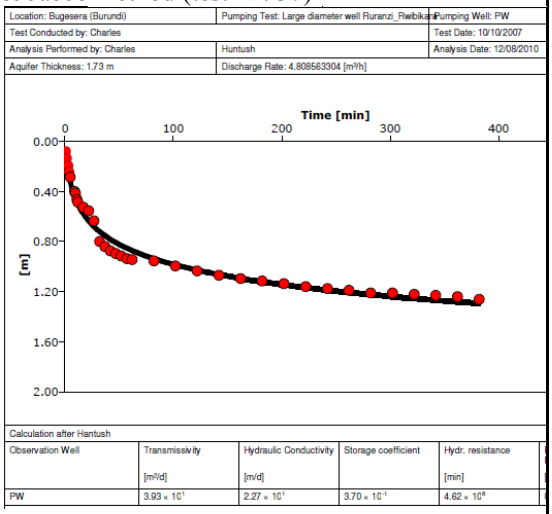

Figure IV.2.124: Analysis of pumping test data for the well in Ruranzi-Rwibikara using the Hantush method (test Nr. 39)

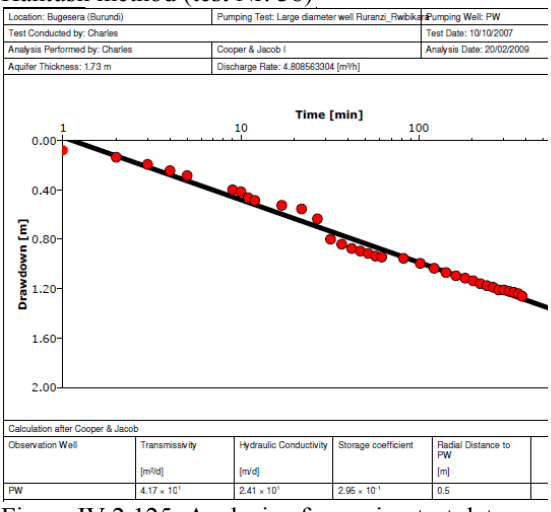

Figure IV.2.125: Analysis of pumping test data for the well in Ruranzi-Rwibikara well using the Cooper & Jacob method (test Nr. 39)

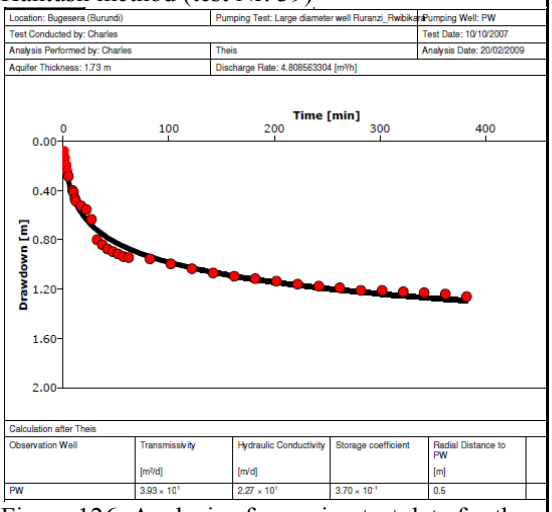

Figure 126: Analysis of pumping test data for the well in Ruranzi-Rwibikara using the Theis method (test Nr. 39)

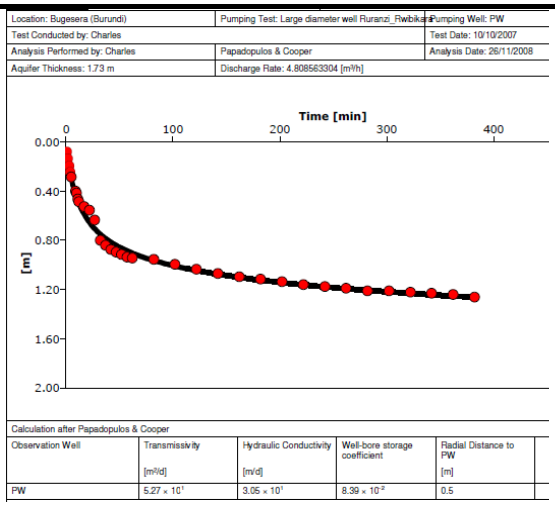

Figure IV.2.127: Analysis of pumping test data for the well in Ruranzi-Rwibikara using the Papadopulos & Cooper method (test Nr. 39)

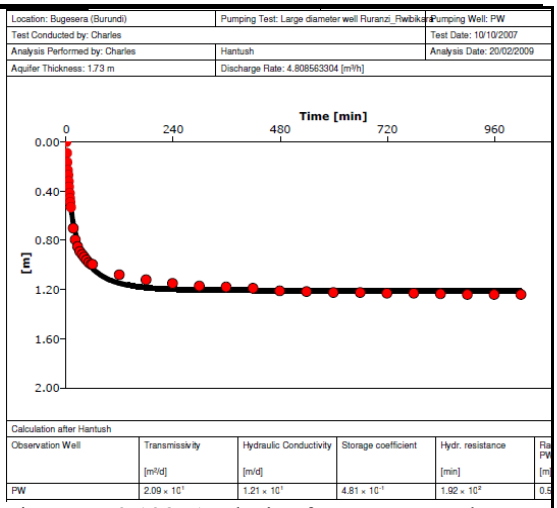

Figure IV.2.128: Analysis of recovery test data for the well in Ruranzi-Rwibikara using the Hantush method (test Nr. 39)

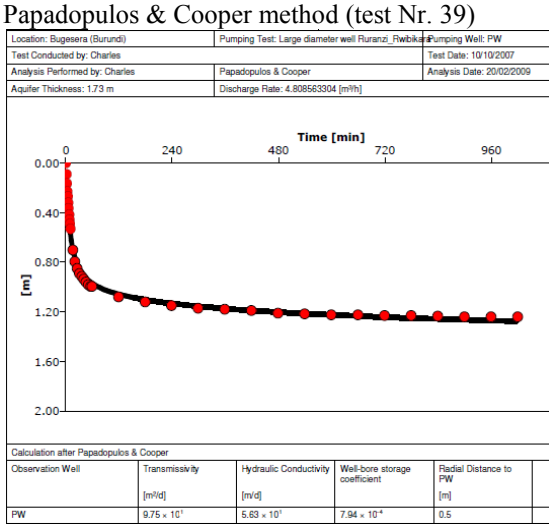

Figure IV.2.129: Analysis of recovery test data for the well in Ruranzi-Rwibikara using the Papadopulos & Cooper method (test Nr. 39)

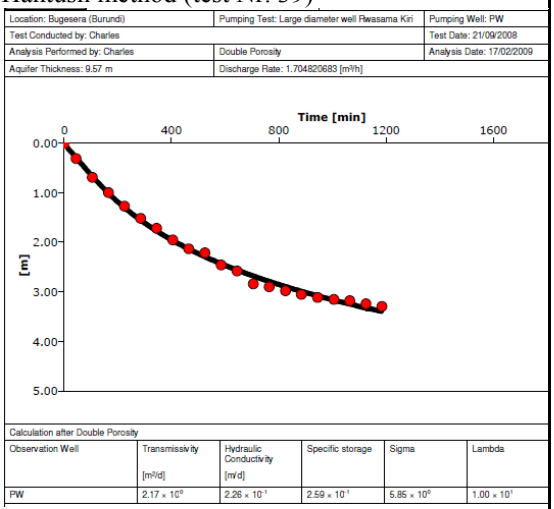

Figure IV.2.130: Analysis of recovery test data for the well in Rwasama-Kiri using the double porosity method (test Nr. 40)

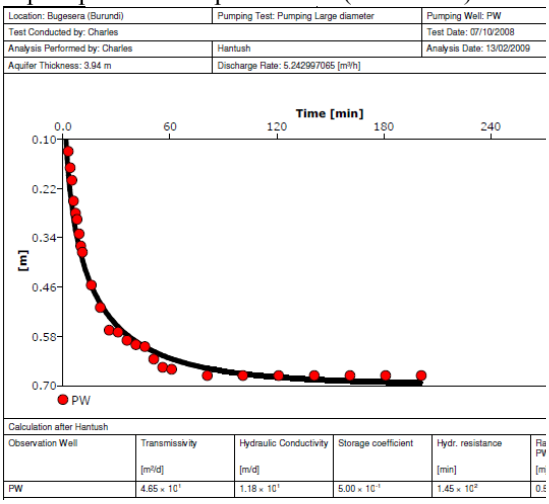

Figure IV.2.131: Analysis of pumping test data for the well in Senga-Nyagisozi using the Hantush method (test Nr. 41)

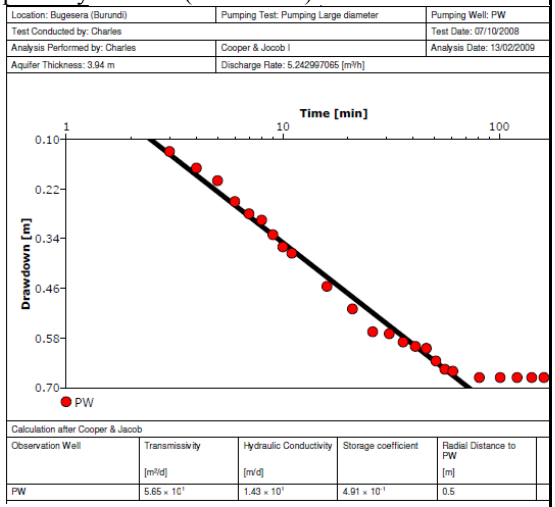

Figure IV.2.132: Analysis of pumping test data for the well in Senga-Nyagisozi using the Cooper & Jacob method (test Nr. 41)

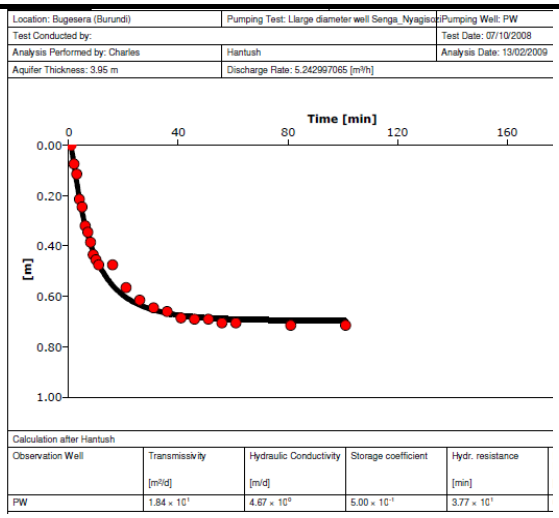

Calculation after Hantush

Observation Well	Transmissivity [m²/d]	Hydraulic Conductivity [m/d]	Storage coefficient	Hydr. resistance [min]
PW	1.84×10^{1}	4.67×10^{0}	5.00×10^{-1}	3.77×10^{1}

Figure IV.2.133 Analysis of recoverytest data for the well in Senga-Nyagisozi using the Hantush method (test Nr. 41)

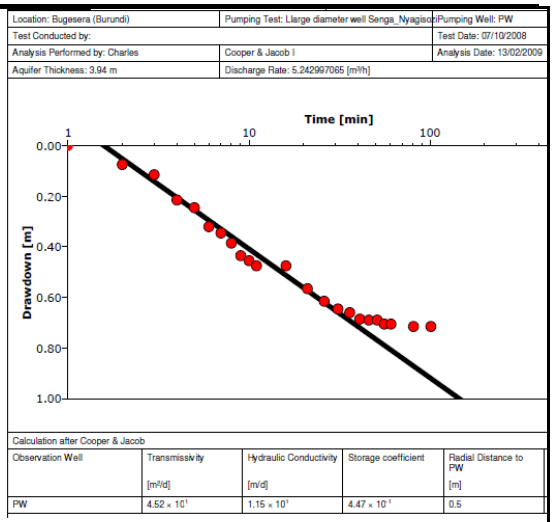

Calculation after Cooper & Jacob

Observation Well	Transmissivity [m²/d]	Hydraulic Conductivity [m/d]	Storage coefficient	Radial Distance to PW [m]
PW	4.52×10^{1}	1.15×10^{1}	4.47×10^{-1}	0.5

Figure IV.2.134 Analysis of recovery data for the well in Senga-Nyagisozi using the Hantush method (test Nr. 41)

Appendix IV.3. Storage coefficient and specific storage calculated using different analytical methods from pumping and recovery test data collected during the field work in 2007 and 2008.

Well name	Pumping test					Recovery test					Best fit method
	Hantush	Theis	Papadopulos & Cooper	Cooper & Jacob	Double porosity	Hantush	Theis	Papadopulos & Cooper	Cooper & Jacob	Double porosity	
Cewe-Bishunzi	0.45	-	-	0.35	-	0.46	-	-	0.37		Hantush
Ceru-Kantuye	-	-	-	-	-	-	-	-	-	0.47	Double porosity
Cimbogo-Gatete	0.50	-	-	0.50	-	0.50	-	-	0.50	-	Hantush
FokoII-Kiyonza	-	-	-	-	-	-	-	-	-	0.50	Double porosity
GahwijoII-Nyabikenke	-	-	-	-	-	-	-	-	-	0.50	Double porosity
GasagaraII-Rubuga	-	-	-	-	-	-	-	-	-	$1.49x10^{-5}$	Double porosity
Gifuruguti-Nyakarama	-	-	-	-	-	-	-	-	-	$3.03x10^{-4}$	Double porosity
Kabirizi II-Kigoma	0.50	-	-	-	$2.04x10^{-4}$	0.50	-	-	0.47	$3.21x10^{-2}$	Double porosity (Pumping)-Hantush (Recovery)
Kabonde-Runyonza	0.50	-	-	-	-	0.50	-	$1.57x10^{-2}$	-	-	Hantush
Kadobogoro-Muramba	0.50	-	0.065	0.40	-	0.50	-	$1.55x10^{-3}$	0.35	-	Hantush
Kadobori II-Rubuga	-	-	-	--	-	-	-	-	-	0.50	Double porosity
Kamwayi II-Nyamabuye	-	-	-	-	-	-	-	-	-	0.50	Double porosity
Kanabugiri-Bugera	0.50	-	-	-	-	0.50	-	-	0.50	-	Hantush
Kanigo-Cinuma	0.50	-	-	-	$1.87x10^{-3}$	0.50	-	-	-	$3.07x10^{-6}$	Double porosity (Pumping)-Hantush (Recovery)
Kanyagu-Ruseno	-	-	-	-	-	-	0.50	0.50	-	$4.03x10^{-1}$	Double porosity
Kigina I-Gisenyi	0.50	-	-	-	-	0.50	-	-	0.35	-	Hantush
Kigina II-Gisenyi	0.50	-	-	0.46	-	0.39	-	-	0.32	-	Hantush
Kigoma-Gatare	0.40	0.36	0.015	0.32	-	0.44	0.36	$1.12x10^{-3}$	0.37	-	Hantush
Kigozi-Yaranda	-	-	-	-	-	-	-	-	-	0.44	Double porosity
Kinyamateke	-	-	-	-	-	0.28		$5.76x10^{-7}$			Hantush
Kiruhura I-Kiyanza	0.50	-	$1.57x10^{-6}$	0.31	-	0.30	-	-	-	-	Hantush
Kiruhura II-Muramba	0.48	0.41	$2.28x10^{-2}$	0.38	-	0.34	-	-	0.29	-	Hantush
Mago-Gatete	0.50	-	-	-	-	0.50	-	-	-	-	Hantush
Marembo-Marembo	0.50	0.50	-	0. 45	-	0.50	0.33	-	0.43	-	Hantush
Mugombwa-Kiri	-	-	-	-	-	0.39	-	$9.04x10^{-5}$	-	-	Hantush
Muhero I-Yaranda	0.50	-	0.12	0.50	-	0.50	-	$7.61x10^{-5}$	0.34	-	Hantush
Muhero II-Yaranda	0.50	-	-	-	-	0.50	-	-	-	-	Hantush
Mukuyo-Kiri	-	-	-	-	-	-	-	-	-	0.50	Double porosity
Murambo-Murambi	0.30	-	$4.33x10^{-4}$	0.23	-	0.38	0.25	$3.85x10^{-9}$	0.31	-	Hantush
Murehe-Murungurira	-	-	-	-	-	0.50	-	-	-	-	Hantush

NB: Values calculated with double porosity method are specific storage

Well name	**Pumping test**					**Recovery test**					**Best fit method**
	Hantush	Theis	Papadopulos & Cooper	Cooper & Jacob	Double porosity	Hantush	Theis	Papadopulos & Cooper	Cooper & Jacob	Double porosity	
Mutoza-Yaranda	0 .32	-	$2.95x10^{-3}$	0.26	-	0.38	-	-	0.31	-	Hantush
Ngaragu-Kiri	0.42	-	$1.46x10^{-2}$	0.38	-	0.50	-	$1.42x10^{-2}$	0.31	-	Hantush
Ntembe II-Kiri	-	-	-	-	-	0.38	-	$4.84x10^{-2}$	0.35	-	Hantush
Ntwago-Murungurira	0.50	-	-	0.43	-	0.50	-	-	-	-	Hantush
Nunga II-Yaranda	0.50	-	$9.88x10^{-2}$	0.50	-	0.50	-	$1.30x10^{-2}$	-	-	Hantush
Nyange-Kumana	0.50	-	-	0.50	-	0.50	-	-	0.50	-	Hantush
Rugoma-Kagege	-	-	-	-	-	0.50	-	-	-	-	Hantush
Ruranzi-Rwibikara	0.37	0.37	$8.39x10^{-2}$	0.30	-	0.48	-	$7.94x10^{-4}$	-	-	Hantush
Rwasama-Kiri	-	-	-	-	-	-	-	-	-	0.26	Double porosity
Senga-Nyagisozi	0.50			0.49	-	0.5	-	-	0.45	-	Hnatush

Appendix V.1. Piezometric measurements showing the depth to the groundwater table, the elevation of the site and the deducted hydraulic head (in m above the local datum, Arc 1950 for Burundi)

S/N	X	Y	Site	Source	Date of mesurement	Depth to water (m)	Elevation (m)	Hydraulic head (m)
1	516921	9706756	Bicankingi	Spring	n.d.	0.00	1535	1535.00
2	499004	9712471	Bihembe-Monge	Spring	14/10/2008	0.00	1473	1473.00
3	523811	9715010	Bishunzi-Munyinya	Spring	13/09/2008	0.00	1493	1493.00
4	518655	9714117	Bugorora-Gakana	Spring	30/09/2008	0.00	1407	1407.00
5	531259	9723417	Buhasa I	Spring	n.d.	0.00	1485	1485.00
6	530311	9723858	Buhasa II	Spring	n.d.	0.00	1483	1483.00
7	500547	9711523	Buhiga-Ntega	Spring	17/10/2008	0.00	1424	1424.00
8	519983	9722409	Bunyari-Rugarama	Spring	03/09/2008	0.00	1348	1348.00
9	504727	9708162	Burengo-Rushubije	Spring	17/10/2008	0.00	1416	1416.00
10	512928	9704605	Burima	Spring	n.d.	0.00	1500	1500.00
11	513452	9707372	Cinka	Spring	n.d.	0.00	1475	1475.00
12	515524	9706609	Cogo	Spring	n.d.	0.00	1505	1505.00
13	514249	9709222	Gacabwoya I	Spring	n.d.	0.00	1612	1612.00
14	514635	9709190	Gacabwoya II	Spring	n.d.	0.00	1638	1638.00
15	511492	9716917	Gaharata-Murama	Spring	16/10/2007	0.00	1360	1360.00
16	519436	9708969	Gaherere	Spring	n.d.	0.00	1533	1533.00
17	519085	9708973	Gahombo	Spring	n.d.	0.00	1604	1604.00
18	503297	9706435	Gakenke	Spring	n.d.	0.00	1690	1690.00
19	519018	9709229	Gasuga	Spring	n.d.	0.00	1585	1585.00
20	511393	9704391	Gasura I	Spring	n.d.	0.00	1569	1569.00
21	507484	9715137	Gatovu-Kanyinya	Spring	16/10/2007	0.00	1377	1377.00
22	511613	9712941	Gatunguru-Rugero	Spring	30/09/2008	0.00	1418	1418.00
23	503453	9716809	Gihobogo-Murungurira	Spring	11/10/2008	0.00	1381	1381.00
24	524547	9713801	Gihushi-Kiravumba	Spring	13/09/2008	0.00	1485	1485.00
25	514974	9717806	Gikombe-Ruhita	Spring	30/09/2008	0.00	1362	1362.00
26	519165	9708506	Kabingo	Spring	n.d.	0.00	1608	1608.00
27	508550	9716418	Kabira-Kanyinya	Spring	16/10/2007	0.00	1362	1362.00
28	519650	9720768	Kabira-Renga	Spring	13/09/2008	0.00	1355	1355.00
29	514448	9706784	Kabungera	Spring	n.d.	0.00	1506	1506.00
30	514162	9703519	Kagobe	Spring	n.d.	0.00	1513	1513.00
31	517699	9712287	Kagogo-Nyabitare	Spring	30/09/2008	0.00	1466	1466.00
32	520524	9720519	Kanyamanza-Kagege	Spring	13/09/2008	0.00	1370	1370.00
33	503351	9707252	Kanyamateke	Spring	n.d.	0.00	1539	1539.00
34	519792	9716858	Kararire-Kagege	Spring	13/09/2008	0.00	1509	1509.00
35	515367	9707320	Karira	Spring	n.d.	0.00	1513	1513.00
36	525018	9714274	Karira-Gatemere	Spring	15/09/2008	0.00	1448	1448.00
37	509141	9712820	Karobogo-Kanyinya	Spring	16/10/2007	0.00	1385	1385.00
38	514977	9706240	Kibande	Spring	n.d.	0.00	1506	1506.00
39	532612	9724206	Kididiri-Buhasa	Spring	13/09/2008	0.00	1465	1465.00
40	511089	9705202	Kigarama	Spring	n.d.	0.00	1489	1489.00
41	521719	9716017	Kigomero-Munyinya	Spring	13/09/2008	0.00	1529	1529.00
42	511789	9719116	Kigoti-Munzenze	Spring	30/09/2008	0.00	1362	1362.00
43	510956	9704808	Kikombe	Spring	n.d.	0.00	1502	1502.00
44	539579	9732462	Kinyangoro-Kumana	Spring	08/10/2008	0.00	1315	1315.00
45	518266	9715625	Kinyangurube-Karehe	Spring	30/09/2008	0.00	1394	1394.00
46	518375	9712936	Kinywamagana-Kigarama	Spring	30/09/2008	0.00	1436	1436.00
47	501068	9713013	Kiramata-Monge	Spring	11/10/2008	0.00	1432	1432.00
48	514292	9715455	Kirunduzi-Mutara	Spring	30/09/2008	0.00	1379	1379.00
49	518935	9708358	Kivyuka	Spring	n.d.	0.00	1580	1580.00
50	499295	9738023	Mamfu-Kiyonza	Spring	16/09/2008	0.00	1346	1346.00

S/N	X	Y	Site	Source	Date of mesurement	Depth to water (m)	Elevation (m)	Hydraulic head (m)
51	515076	9716410	Maramya-Mwenya	spring	30/09/2008	0.00	1383	1383.00
52	510530	9714820	Marimano	Spring	n.d.	0.00	1386	1386.00
53	515473	9704426	Mubira	Spring	n.d.	0.00	1520	1520.00
54	520761	9710756	Mucogo	Spring	n.d.	0.00	1498	1498.00
55	503572	9715942	Mudahinyuka-Kigina II	Spring	11/10/2008	0.00	1361	1361.00
56	517120	9708742	Mugakore	Spring	n.d.	0.00	1597	1597.00
57	509412	9704811	Mugaseno	Spring	n.d.	0.00	1564	1564.00
58	519834	9708616	Mugasuga	Spring	n.d.	0.00	1535	1535.00
59	517861	9710185	Mugatoboramana	Spring	n.d.	0.00	1719	1719.00
60	508685	9704916	Mugatovu	Spring	n.d.	0.00	1643	1643.00
61	509306	9704971	Mugisonga	Spring	n.d.	0.00	1581	1581.00
62	520050	9709323	Muguruka I	Spring	n.d.	0.00	1499	1499.00
63	519837	9709010	Muguruka II	Spring	n.d.	0.00	1503	1503.00
64	508040	9705157	Mukabakene	Spring	n.d.	0.00	1696	1696.00
65	516067	9704114	Mukabingo	Spring	n.d.	0.00	1572	1572.00
66	520356	9711533	Mukabirizi	Spring	n.d.	0.00	1458	1458.00
67	515781	9705274	Mukadahoka I	Spring	n.d.	0.00	1582	1582.00
68	515181	9704839	Mukadahoka II	Spring	n.d.	0.00	1504	1504.00
69	505777	9708511	Mukagezi-Ntogwe	Spring	17/10/2008	0.00	1387	1387.00
70	518145	9708133	Mukanyoni	Spring	n.d.	0.00	1643	1643.00
71	498228	9736991	Mukuyo-Kiri	Spring	16/09/2008	0.00	1358	1358.00
72	513171	9705058	Mumarenga	Spring	n.d.	0.00	1495	1495.00
73	513723	9703922	Mumugoti	Spring	n.d.	0.00	1529	1529.00
74	518131	9708635	Munkombe	Spring	n.d.	0.00	1597	1597.00
75	510910	9705757	Mununga	Spring	n.d.	0.00	1455	1455.00
76	520693	9709509	Murugomero I	Spring	n.d.	0.00	1531	1531.00
77	507566	9705243	Murugomero II	Spring	n.d.	0.00	1709	1709.00
78	520752	9709019	Murugomero III	Spring	n.d.	0.00	1634	1634.00
79	521042	9709615	Murunyinya	Spring	n.d.	0.00	1535	1535.00
80	517386	9709500	Murusave I	Spring	n.d.	0.00	1561	1561.00
81	517522	9709147	Murusave II	Spring	n.d.	0.00	1527	1527.00
82	519572	9708994	Murutare	Spring	n.d.	0.00	1525	1525.00
83	508221	9705435	Muruzegezege	Spring	n.d.	0.00	1636	1636.00
84	503914	9706028	Muryaruhuma	Spring	n.d.	0.00	1757	1757.00
85	523501	9719404	Musave-Mugobe	Spring	13/09/2008	0.00	1398	1398.00
86	525327	9721819	Musave-Rutabo	Spring	13/09/2008	0.00	1364	1364.00
87	511183	9704586	Mushundahe	Spring	n.d.	0.00	1537	1537.00
88	532591	9724442	Mutetema-Muyange	Spring	13/09/2008	0.00	1432	1432.00
89	515800	9714103	Mvyayingabo-Mutara	Spring	30/09/2008	0.00	1394	1394.00
90	515311	9717830	Mwenya-Mwenya	Spring	30/09/2008	0.00	1368	1368.00
91	518306	9715320	Mwenya-Rwimbogo	Spring	30/09/2008	0.00	1397	1397.00
92	513928	9704841	Mwibamba	Spring	n.d.	0.00	1500	1500.00
93	516988	9718270	Nagikono-Kinyangurube	Spring	30/09/2008	0.00	1386	1386.00
94	517213	9720763	Nakabingo	Spring	n.d.	0.00	1343	1343.00
95	525380	9714027	Nakabingo-Gatemere	Spring	13/09/2008	0.00	1494	1494.00
96	517176	9714170	NakabingoII-Gihosha	Spring	30/09/2008	0.00	1425	1425.00
97	525296	9721153	Nakarambo-Rutabo	Spring	13/09/2008	0.00	1376	1376.00
98	512790	9714168	Nakavumu	Spring	n.d.	0.00	1399	1399.00
99	500721	9711947	Nakivumbura-Monge	Spring	11/10/2008	0.00	1416	1416.00
100	513757	9704960	Naruhanga	Spring	n.d.	0.00	1503	1503.00

S/N	X	Y	Site	Source	Date of mesurement	Depth to water (m)	Elevation (m)	Hydraulic head (m)
101	515628	9715365	Narukere-Gihosha	Spring	30/09/2008	0.00	1389	1389.00
102	512189	9713898	Narutambwe-Kireka	Spring	30/09/2008	0.00	1403	1403.00
103	512611	9715724	Nnganji-Murama	Spring	n.d.	0.00	1474	1474.00
104	510977	9705400	Nyabitare	Spring	n.d.	0.00	1475	1475.00
105	524491	9716753	Nyabitare-Munyinya	Spring	13/09/2008	0.00	1427	1427.00
106	512309	9705386	Nyamugari	Spring	n.d.	0.00	1495	1495.00
107	505919	9706731	Nyamvura	Spring	n.d.	0.00	1474	1474.00
108	516339	9713377	Nyaruziba-Mutara	Spring	30/09/2008	0.00	1434	1434.00
109	505651	9709994	RamboII-Gatwe	Spring	15/10/2008	0.00	1369	1369.00
110	525802	9713684	Rubira-Gatemere	Spring	13/09/2008	0.00	1534	1534.00
111	505769	9707913	Rugangazi-Ntogwe	Spring	17/10/2008	0.00	1422	1422.00
112	513320	9714508	Rugero-Nakarinzi	Spring	30/09/2008	0.00	1383	1383.00
113	521253	9717613	Rugoma-Kagege	Spring	13/09/2008	0.00	1513	1513.00
114	525645	9713821	Rugomero-Gatemere	Spring	13/09/2008	0.00	1524	1524.00
115	524358	9712586	Rugomero-Kiravumba	Spring	13/09/2008	0.00	1539	1539.00
116	528111	9721649	Rugomero-Nyabugeni	Spring	13/09/2008	0.00	1513	1513.00
117	512966	9720619	Rugunga II-Kavomo	Spring	30/09/2008	0.00	1365	1365.00
118	512723	9720563	Rugunga I-Kavomo	Spring	30/09/2008	0.00	1364	1364.00
119	513047	9704431	Ruhara	Spring	n.d.	0.00	1503	1503.00
120	524366	9715387	Ruhongore-Munyinya	Spring	13/09/2008	0.00	1459	1459.00
121	504583	9708830	Rushubije-Cogo	Spring	17/10/2008	0.00	1390	1390.00
122	516438	9706801	Rusumba	Spring	n.d.	0.00	1516	1516.00
123	504419	9707304	Ruvogo	Spring	n.d.	0.00	1518	1518.00
124	515340	9706761	Rwinago	Spring	n.d.	0.00	1480	1480.00
125	506278	9706731	Ryasebukanu	Spring	n.d.	0.00	1530	1530.00
126	507312	9709497	Twengebuye-Nakabingo	Spring	17/10/2008	0.00	1378	1378.00
127	502990	9735790	Bambo-Rubuga	Well	08/10/2008	2.20	1348	1345.80
128	529431	9736842	Bidogo-Gatete	Well	28/10/2008	4.91	1336	1331.09
129	518351	9728973	Bifu II-Marembo	Well	27/10/2008	4.17	1348	1343.83
130	518042	9728495	Bifu I-Marembo	Well	27/10/2008	5.03	1365	1359.97
131	504401	9723359	Bikombe-Kigoma	Well	10/10/2008	2.90	1404	1401.10
132	507941	9719750	Bishunzi-Cewe	Well	30/10/2008	3.22	1372	1368.78
133	509423	9721566	Bitozi-Rukuramigabo	Well	30/10/2008	12.35	1363	1350.65
134	506857	9718443	Bugera-Bugera	Well	30/10/2008	4.28	1369	1364.72
135	520113	9722504	Bunyari-Rugarama	Well	27/10/2008	3.39	1366	1362.61
136	507025	9719948	Cewe-Nunga	Well	07/10/2008	6.22	1379	1372.78
137	506944	9721604	Cewe-Nyagahama	Well	30/10/2008	3.08	1389	1385.92
138	506131	9719892	Cewe-Nyakariba	Well	30/10/2008	6.17	1370	1363.83
139	527657	9738234	Cimbogo-Gatete I	Well	28/10/2008	2.21	1328	1325.79
140	527623	9738559	Cimbogo-Gatete II	Well	28/10/2008	4.85	1324	1319.15
141	504623	9735023	Cimvuzo-Gaturanda	Well	09/10/2008	4.73	1357	1352.27
142	508633	9725032	Cinyambo-Gitwe	Well	10/10/2008	6.95	1355	1348.05
143	500944	9738506	Foko II-Kiyonza	Well	08/10/2008	6.82	1370	1363.18
144	501761	9740091	Foko I-Kiyonza	Well	08/10/2008	2.66	1361	1358.34
145	511517	9716849	Gaharata-Murama	Well	30/10/2008	3.13	1364	1360.87
146	499599	9720802	Gahenda-Mugendo	Well	03/10/2008	3.89	1367	1363.11
147	500747	9730542	Gahwijo III-Nyabikenke	Well	07/10/2008	4.40	1355	1350.60
148	501049	9730892	Gahwijo I-Nyabikenke	Well	07/10/2008	0.37	1365	1364.63
149	500781	9730118	Gahwijo II-Nyabikenke	Well	07/10/2008	3.55	1387	1383.45
150	502641	9722135	Gakindo-Kigoma	Well	10/10/2008	3.65	1384	1380.35

S/N	X	Y	Site	Source	Date of mesurement	Depth to water (m)	Elevation (m)	Hydraulic head (m)
151	499352	9735036	Gasagara II-Rubuga	Well	08/10/2008	1.85	1395	1393.15
152	497952	9734114	Gasagara I-Rubuga	Well	08/10/2008	11.93	1361	1349.08
153	518247	9719887	Gashoka-Muramba	Well	30/10/2008	2.14	1372	1369.86
154	503708	9736919	Gatorondero-Gaturanda	Well	09/10/2008	6.09	1382	1375.91
155	507520	9715116	Gatovu-Kanyinya	Well	30/20/2008	1.78	1377	1375.23
156	506199	9722341	Gatovu-Kigoma	Well	30/10/2008	3.89	1375	1371.12
157	503293	9734011	Gaturanda-Gaturanda	Well	09/10/2008	6.30	1358	1351.70
158	499356	9730896	Gifuruguti-Nyakarama	Well	09/10/2008	5.69	1361	1355.31
159	536620	9730751	Gikombe-Nyagisozi	Well	28/10/2008	4.92	1329	1324.08
160	504990	9714863	Gikomero-Susa	Well	01/10/2008	4.78	1370	1365.22
161	500425	9738234	Gikono-Kiyonza	Well	08/10/2008	8.00	1353	1351.98
162	514651	9727322	Gitamo II-Murambi	Well	27/10/2008	5.33	1363	1357.67
163	513777	9728084	Gitamo I-Murambi	Well	27/10/2008	8.00	1365	1357.01
164	515323	9728079	Gitamo III-Murambi	Well	27/10/2008	7.31	1367	1359.69
165	509324	9732510	Haga II-Nyamabuye	Well	10/10/2008	5.61	1394	1388.39
166	510115	9730715	Haga I-Nyamabuye	Well	10/10/2008	8.33	1362	1353.67
167	505208	9716851	Haga-Susa	Well	01/10/2008	6.40	1357	1350.60
168	500866	9740404	Hambiro-Kiyonza	Well	08/10/2008	11.90	1384	1372.10
169	508606	9716366	Kabira-Kanyinya	Well	30/10/2008	2.72	1372	1369.29
170	501618	9724437	Kabirizi II-Kigoma	Well	11/10/2008	2.51	1361	1358.49
171	516750	9720755	Kadobogoro-Muramba	Well	30/10/2008	3.51	1359	1355.49
172	498573	9732876	Kadobori II-Rubuga	Well	09/10/2008	3.19	1379	1375.81
173	498969	9733459	Kadobori I-Rubuga	Well	09/10/2008	9.63	1377	1367.37
174	509556	9729414	Kamwayi III-Nyamabuye	Well	10/10/2008	3.57	1401	1397.43
175	507602	9727945	Kamwayi II-Nyamabuye	Well	10/10/2008	6.97	1366	1359.03
176	508652	9728716	Kamwayi I-Nyamabuye	Well	10/10/2008	5.94	1368	1362.06
177	504550	9719120	Kanabugiri I-Bugera	Well	30/10/2008	3.39	1373	1369.61
178	505823	9717420	Kanabugiri II-Bugera	Well	30/10/2008	4.33	1372	1367.67
179	497161	9733971	Kanigo-Cinuma	Well	09/10/2008	7.19	1362	1354.81
180	511564	9729125	Kantuye-Ceru	Well	30/10/2008	9.63	1370	1360.37
181	517976	9725554	Karago-Kibonde	Well	27/10/2008	2.00	1369	1367.00
182	509190	9724077	Karago-Runyonza	Well	30/10/2008	2.71	1374	1371.29
183	501741	9720652	Kariba-Kanyagu	Well	05/10/2008	4.94	1359	1354.06
184	505765	9735220	Karisha-Kigina	Well	10/10/2008	8.10	1375	1366.90
185	509182	9712886	Karobogo-Kanyinya	Well	30/10/2008	6.90	1398	1391.10
186	515394	9725642	Kibonde-Nunga	Well	27/10/2008	3.31	1374	1370.69
187	497510	9732243	Kigazi-Nyakarama	Well	09/10/2008	12.21	1376	1363.79
188	519465	9731664	Kigeri II-Rwibikara	Well	27/10/2008	3.51	1348	1344.49
189	519997	9731492	Kigeri I-Rwibikara	Well	27/10/2008	10.35	1355	1344.65
190	522431	9724962	Kigina I-Gisenyi	Well	28/10/2008	3.00	1414	1411.00
191	522598	9724794	Kigina II-Gisenyi	Well	28/10/2008	3.15	1416	1412.85
192	506819	9734930	Kigina-Kigina	Well	10/10/2008	7.57	1393	1385.43
193	506433	9732978	Kigina-Ntaho	Well	10/10/2008	4.02	1398	1393.98
194	528684	9726152	Kigoma-Gatare	Well	09/10/2008	5.86	1343	1337.14
195	504235	9722206	Kigoma-Kigoma	Well	07/10/2008	4.32	1383	1378.68
196	511210	9722323	Kigozi-Yaranda	Well	30/10/2008	5.48	1376	1370.53
197	502703	9729227	Kinyamateke-Nyabikenke	Well	07/10/2008	5.81	1365	1359.20
198	499482	9738822	Kiri-Kiri	Well	08/10/2008	2.64	1369	1366.36
199	515207	9722641	Kiruhura I-Kiyanza	Well	02/10/2008	3.05	1375	1371.95
200	505219	9736653	Kiryama-Gaturanda	Well	09/10/2008	8.54	1355	1346.46

S/N	X	Y	Site	Source	Date of mesurement	Depth to water (m)	Elevation (m)	Hydraulic head (m)
201	515723	9723725	Kiyanza-Muramba	Well	30/10/2008	2.18	1364	1361.82
202	503340	9739347	Kiyonza-Nunga	Well	08/10/2008	2.18	1348	1345.82
203	529635	9734846	Mago I-Gatete	Well	28/10/2008	4.07	1332	1327.93
204	529116	9734328	Mago II-Gatete	Well	28/10/2008	2.01	1329	1326.99
205	517787	9728512	Marembo-Marembo	Well	01/10/2008	3.87	1362	1358.13
206	503999	9727440	Mataka-Rugasa	Well	10/10/2008	15.32	1360	1344.68
207	517800	9723918	Migirye-Kibonde	Well	27/10/2008	9.07	1365	1355.93
208	518875	9729151	Mitanga-Ruranzi	Well	27/10/2008	4.48	1357	1352.52
209	496589	9738358	Mugombwa-Kiri	Well	08/10/2008	7.32	1381	1373.68
210	510497	9721413	Muhero II-yaranda	Well	29/10/2008	3.98	1368	1364.02
211	511070	9719349	Muhero I-Yaranda	Well	30/10/2008	3.62	1357	1353.38
212	503253	9721036	Mukaro-Kigoma	Well	10/10/2008	4.77	1376	1371.23
213	498307	9736972	Mukuyo-Kiri	Well	08/10/2008	1.89	1367	1365.11
214	498483	9731330	Munyinya-Nyakarama	Well	09/10/2008	7.95	1376	1368.05
215	517614	9727884	Murama I-Higiro	Well	27/10/2008	6.59	1369	1362.41
216	516618	9727933	Murama II-Higiro	Well	27/10/2008	3.87	1378	1374.13
217	513994	9720843	Muramba-Kiruhura II	Well	04/10/2008	5.23	1378	1372.77
218	513078	9730415	Murambo-Murambi	Well	27/10/2008	9.46	1369	1359.54
219	503693	9718435	Murehe-Murungurira	Well	06/10/2008	5.50	1387	1381.50
220	499392	9719262	Murungazi-Mugendo	Well	03/10/2008	1.68	1381	1379.32
221	513115	9723341	Mutoza-Yaranda	Well	16/10/2008	3.48	1366	1362.52
222	507722	9732708	Ndava II-Nyamabuye	Well	10/08/2008	8.39	1388	1379.61
223	508484	9733915	Ndava I-Nyamabuye	Well	10/08/2008	4.45	1364	1359.55
224	496361	9739565	Ngaragu-Kiri	Well	08/10/2008	5.14	1377	1371.87
225	509343	9728506	Ngugo I-Gitwe	Well	10/10/2008	7.04	1363	1355.96
226	509440	9726783	Ngugo III-Nyamabuye	Well	10/10/2008	4.60	1356	1351.40
227	500032	9719913	Ngugo II-Kanyagu	Well	03/10/2008	3.77	1373	1369.23
228	501106	9720121	Ngugo I-Kanyagu	Well	03/10/2008	3.91	1370	1366.09
229	515359	9722922	Ntarabwa-Kiyanza	Well	30/10/2008	6.10	1367	1360.90
230	498070	9735152	Ntembe II-Kiri	Well	08/10/2008	8.18	1372	1363.82
231	498592	9734829	Ntembe I-Kiri	Well	08/10/2008	3.89	1389	1385.11
232	504061	9722339	Ntwago III-Kigoma	Well	10/10/2008	1.89	1363	1361.11
233	505840	9722092	Ntwago II-Kigoma	Well	10/10/2008	4.89	1362	1357.11
234	503106	9719806	Ntwago-Murungurira	Well	05/10/2008	4.82	1376	1371.18
235	512765	9724667	Nunga II-Yaranda	Well	15/10/2008	3.31	1348	1344.69
236	512824	9725255	Nunga I-Yaranda	Well	30/10/2008	4.68	1358	1353.32
237	501290	9729175	Nyabikenke-Nyabikenke	Well	07/10/2008	12.50	1385	1372.50
238	529510	9729530	Nyakiganga-Gatare	Well	28/10/2008	12.22	1340	1327.78
239	497149	9731252	Nyamabuye-Nyakarama	Well	09/10/2008	7.61	1371	1363.39
240	537741	9731738	Nyange-Kumana	Well	28/10/2008	8.60	1332	1323.40
241	499094	9722516	Rabiro-Rutagara	Well	02/10/2008	4.00	1389	1385.00
242	506396	9712376	Rambo-Kanyinya	Well	30/10/2008	5.62	1384	1378.38
243	505171	9714125	Renga II-Gitwenzi	Well	01/10/2008	4.46	1358	1353.54
244	504131	9738524	Rubirizi-Gaturanda	Well	09/10/2008	5.25	1369	1363.75
245	500877	9732978	Rubuga-Ninda	Well	09/10/2008	3.67	1442	1438.33
246	503444	9734123	Rubuga-Rubuga I	Well	09/10/2008	3.23	1350	1346.77
247	504781	9738088	Rubuga-Rubuga II	Well	09/10/2008	2.80	1375	1372.20
248	503444	9735863	Rubuga-Rubuga III	Well	09/10/2008	3.20	1374	1370.80
249	499760	9727632	Rugasa-Nyamata	Well	10/10/2008	2.86	1365	1362.14
250	498376	9729059	Rugasa-Rugasa	Well	10/10/2008	4.21	1351	1346.79

S/N	X	Y	Site	Source	Date of mesurement	Depth to water (m)	Elevation (m)	Hydraulic head (m)
251	520425	9718462	Rugoma-Kagege	Well	30/10/2008	5.20	1430	1424.80
252	503777	9734980	Ruhando-Gaturanda	Well	09/10/2008	3.45	1380	1376.55
253	512314	9722327	Ruhuzu-Yaranda	Well	30/10/2008	10.90	1366	1355.10
254	528586	9735993	Rukera-Gatete	Well	28/10/2008	5.10	1339	1333.90
255	500313	9724817	Rukindo-Rugasa	Well	10/10/2008	5.21	1372	1366.79
256	506971	9733736	Rukore II-Kigina	Well	07/10/2008	7.61	1380	1372.40
257	506493	9732376	Rukore I-Kigina	Well	07/10/2008	3.10	1348	1344.90
258	504062	9727972	Runyangona II-Nyabikenke	Well	07/10/2008	5.68	1363	1357.32
259	503233	9728064	Runyangona I-Nyabikenke	Well	07/10/2008	10.65	1365	1354.35
260	509334	9719271	Runyonza-Kabonde	Well	06/10/2008	7.50	1366	1358.50
261	510811	9719267	Runyonza-Muhero	Well	30/10/2008	4.02	1357	1352.98
262	510359	9722324	Runyonza-Rukuramigabo	Well	30/10/2008	2.45	1349	1346.55
263	510884	9723498	Runyonza-Ruzirakabogi	Well	30/10/2008	4.05	1362	1357.96
264	516201	9730751	Ruranzi-Rwibikara	Well	27/10/2008	6.61	1375	1368.39
265	501718	9718420	Ruseno-Kanyagu	Well	05/10/2008	4.14	1358	1353.86
266	500386	9730451	Rutamo-Nyakarama	Well	09/10/2008	9.99	1367	1357.01
267	515490	9726623	Rutanga II-Murambi	Well	01/10/2008	2.99	1359	1356.01
268	517469	9726086	Rutanga I-Murambi	Well	01/10/2008	4.12	1359	1354.88
269	510702	9725363	Rutare I-Ceru	Well	30/10/2008	12.35	1373	1360.65
270	508969	9726154	Ruyivyi I-Gitwe	Well	10/10/2008	7.32	1356	1348.68
271	508786	9725389	Ruyivyi II-Gitwe	Well	10/10/2008	13.47	1356	1342.53
272	497282	9740266	Rwasama-Kiri	Well	08/10/2008	1.66	1380	1378.34
273	519039	9728717	Rwibikara	Well	02/10/2008	4.35	1381	1376.65
274	516747	9722406	Rwiri-Mwaro	Well	30/10/2008	7.85	1368	1360.15
275	499077	9726224	Saruduha II-Rugasa	Well	10/10/2008	9.60	1384	1374.40
276	498657	9725745	Saruduha I-Rugasa	Well	10/10/2008	2.89	1377	1374.11
277	535002	9729669	Senga-Nyagisozi	Well	08/10/2008	2.62	1354	1351.38
278	501572	9727706	Shenga III-Rugasa	Well	11/10/2008	2.02	1360	1357.98
279	501948	9728377	Shenga II-Rugasa	Well	11/10/2008	10.44	1382	1371.56
280	503043	9727738	Shenga I-Rugasa	Well	11/10/2008	9.33	1378	1368.67
281	539727	9734484	Sigu-Kumana	Well	28/10/2008	3.31	1323	1319.70
282	527472	9732698	Vyanzo I-Gatete	Well	28/10/2008	6.45	1330	1323.54
283	528347	9734431	Vyanzo II-Gatete	Well	28/10/2008	4.79	1327	1322.21

N.B.:

- The date of measurement for springs is the date of sampling
- n.d. for the date of measurement means that the spring was not sampled

Appendix V.2. Groundwater level fluctuations for the year 2008 (in m above the local datum, Arc 1950 for Burundi)

S/N	Site	Depth	Jan	Feb	Mar	Ap	May	June	July	Aug	Sept	Oct	Nov	Dec	Max	Min	Amplitude	Observation
128	Bidogo-Gatete	5.56	1331.82	1331.90	1332.12	1332.43	1332.62	1332.52	1332.25	1331.90	1331.69	1331.73	1331.78	1331.85	1332.62	1331.69	0.93	NP
139	Cimbogo-Gatete I	3.60	1325.97	1326.04	1326.28	1326.64	1326.83	1326.70	1326.43	1326.15	1325.87	1325.79	1325.94	1326.00	1326.83	1325.79	1.04	NP
159	Gikombe Nyagisozi	8.22	1324.22	1324.31	1324.53	1324.78	1325.01	1324.90	1324.65	1324.38	1324.12	1324.08	1324.21	1324.27	1325.01	1324.08	0.93	NP
203	Mago-Gatete	8.40	1328.10	1328.21	1328.41	1328.69	1328.90	1328.82	1328.57	1328.20	1328.03	1327.93	1328.06	1328.12	1328.90	1327.93	0.97	NP
238	Nyakiganga-Gatare	12.57	1327.85	1327.91	1328.03	1328.25	1328.45	1328.46	1328.31	1328.05	1327.91	1327.78	1327.80	1327.82	1328.46	1327.78	0.68	NP
281	Sigu-Kumana	5.76	1319.84	1319.94	1320.17	1320.49	1320.69	1320.57	1320.31	1319.90	1319.72	1319.70	1319.84	1319.90	1320.69	1319.70	0.99	NP
282	Vyanzo I-Gatete	7.70	1323.53	1323.57	1323.68	1324.01	1324.26	1324.25	1324.06	1323.88	1323.69	1323.55	1323.53	1323.50	1324.26	1323.50	0.76	NP
283	Vyanzo II-Gatete	6.22	1322.31	1322.37	1322.57	1322.87	1323.08	1323.01	1322.81	1322.57	1322.33	1322.21	1322.28	1322.30	1323.08	1322.21	0.87	NP
132	Bishunzi-Cewe	8.10	1368.90	1368.99	1369.17	1369.22	1369.20	1369.12	1369.02	1368.93	1368.84	1368.78	1368.74	1368.72	1369.22	1368.72	0.51	FTP
138	Cewe-Nyakariba	9.78	1363.94	1364.02	1364.25	1364.33	1364.26	1364.20	1364.08	1363.98	1363.89	1363.83	1363.80	1363.77	1364.33	1363.77	0.56	NP
145	Gaharata-Murama	6.60	1360.89	1360.92	1361.14	1361.19	1361.04	1361.02	1360.97	1360.92	1360.88	1360.87	1360.86	1360.86	1361.19	1360.86	0.33	NP
146	Gitamo I-Murambi	9.52	1359.09	1359.06	1359.11	1359.18	1359.19	1359.21	1359.19	1359.09	1359.06	1359.01	1359.00	1358.97	1359.21	1358.97	0.25	NP
163	Gitamo II-Murambi	8.76	1359.78	1359.74	1359.79	1359.83	1359.83	1359.85	1359.82	1359.77	1359.71	1359.67	1359.67	1359.64	1359.85	1359.64	0.21	NP
180	Kantuye-Ceru	11.46	1360.47	1360.45	1360.50	1360.53	1360.51	1360.52	1360.48	1360.44	1360.40	1360.37	1360.36	1360.33	1360.53	1360.33	0.20	NP
215	Murama I-Higiro	7.41	1362.51	1362.50	1362.57	1362.64	1362.63	1362.64	1362.56	1362.43	1362.41	1362.41	1362.41	1362.33	1362.64	1362.33	0.31	NP
264	Ruranzi-Rwibikara	8.65	1368.53	1368.52	1368.57	1368.66	1368.64	1368.63	1368.55	1368.48	1368.42	1368.40	1368.38	1368.34	1368.66	1368.34	0.32	NP
160	Gikomero-Susa	7.15	1365.29	1365.38	1365.41	1365.58	1365.69	1365.74	1365.51	1365.34	1365.15	1365.22	1365.32	1365.36	1365.74	1365.15	0.59	NP
167	Haga-Susa	6.27	1350.74	1350.73	1350.75	1350.98	1351.09	1351.24	1350.76	1350.61	1350.56	1350.61	1350.63	1350.68	1351.24	1350.56	0.67	NP
183	Kariba-Kanyagu	6.86	1354.29	1354.33	1354.35	1354.41	1354.49	1354.51	1354.27	1354.13	1354.03	1354.06	1354.20	1354.24	1354.51	1354.03	0.48	NP
219	Murehe-Murungurira	8.82	1381.67	1381.64	1381.75	1381.98	1381.96	1382.04	1381.76	1381.62	1381.43	1381.50	1381.49	1381.54	1382.04	1381.43	0.62	NP
220	Murungazi - Mugendo	4.49	1379.48	1379.57	1379.58	1379.65	1379.56	1379.85	1379.59	1379.42	1379.30	1379.32	1379.39	1379.37	1379.85	1379.30	0.55	NP
234	Ntwago-Murungurira	7.28	1371.23	1371.20	1371.28	1371.40	1371.54	1371.55	1371.29	1371.15	1371.15	1371.19	1371.05	1371.23	1371.55	1371.05	0.50	NP
243	Renga II-Gitwenzi	6.10	1353.66	1353.66	1353.74	1353.89	1353.90	1353.88	1353.76	1353.60	1353.49	1353.54	1353.57	1353.58	1353.90	1353.49	0.42	NP
227	Ngugo II-Kanyagu	6.01	1369.47	1369.10	1369.54	1369.55	1369.58	1369.64	1369.43	1369.26	1369.17	1369.23	1369.26	1369.28	1369.64	1369.10	0.54	NP
135	Bunyari-Rugarama	11.42	1362.30	1362.14	1362.39	1362.97	1361.87	1361.90	1356.66	1355.30	1362.70	1362.61	1362.85	1362.90	1362.97	1355.30	7.67	FTP
171	Kadobogoro-Muramba	6.41	1355.45	1355.48	1355.65	1355.66	1355.59	1355.57	1355.56	1355.52	1355.49	1355.49	1355.49	1355.48	1355.66	1355.45	0.20	FTP
190	Kigina I-Gisenyi	5.10	1411.05	1410.99	1411.10	1411.69	1411.16	1411.23	1411.03	1411.01	1411.00	1411.00	1410.82	1410.93	1411.69	1410.82	0.87	FTP
191	Kigina II-Gisenyi	5.17	1412.84	1412.77	1412.85	1413.33	1413.03	1413.10	1412.90	1412.87	1412.83	1412.85	1412.55	1412.70	1413.33	1412.55	0.78	FTP
196	Kigozi-Yaranda	7.00	1371.09	1371.05	1371.30	1371.37	1371.36	1370.35	1370.42	1370.41	1370.40	1370.53	1370.50	1370.37	1371.37	1370.35	1.02	FTP
211	Muhero I-Yaranda	7.33	1353.30	1353.35	1353.46	1353.45	1353.43	1353.43	1353.40	1353.40	1353.40	1353.39	1353.40	1353.39	1353.46	1353.30	0.16	FTP
218	Murambo-Murambi	11.78	1359.66	1359.68	1359.71	1359.81	1359.80	1359.81	1359.75	1359.68	1359.60	1359.54	1359.53	1359.48	1359.81	1359.48	0.33	FTP
265	Ruseno-Kanyagu	7.61	1353.75	1354.07	1353.98	1354.01	1354.11	1354.13	1353.96	1353.78	1353.71	1353.86	1354.21	1354.22	1354.22	1353.71	0.51	FTP

S/N	Site	Depth	Jan	Feb	Mar	Ap	May	June	July	Aug	Sept	Oct	Nov	Dec	Max	Min	Amplitude	Observation
156	Gatovu-Kanyinya	3.87	1375.15	1375.16	1375.34	1375.33	1375.30	1375.28	1375.26	1375.25	1375.23	1375.23	1375.24	1375.23	1375.34	1375.15	0.19	NP
146	Gahenda-Mugendo	5.66	1363.44	1363.51	1363.66	1363.45	1363.55	1363.57	1363.32	1363.16	1363.07	1363.11	1363.18	1363.19	1363.66	1363.07	0.59	NP
169	Kabira-Kanyinya	4.75	1369.27	1369.29	1369.45	1369.47	1369.46	1369.45	1369.40	1369.35	1369.30	1369.28	1369.28	1369.27	1369.47	1369.27	0.20	NP
177	Kanabugiri-Bugera	8.10	1369.79	1369.96	1370.24	1370.16	1370.06	1369.96	1369.86	1369.75	1369.65	1369.61	1369.62	1369.63	1370.24	1369.61	0.63	NP
181	Karago-Kibonde	10.32	1367.18	1367.19	1367.27	1367.33	1367.24	1367.16	1367.09	1367.04	1367.00	1367.01	1367.02	1366.96	1367.33	1366.96	0.37	NP
182	Karago-Runyonza	12.10	1370.92	1371.35	1371.53	1371.60	1371.55	1371.53	1371.45	1371.40	1371.35	1371.30	1371.27	1371.23	1371.60	1370.92	0.68	NP
185	Karobogo-Kanyinya	9.20	1391.27	1391.30	1391.91	1391.71	1391.48	1391.38	1391.20	1391.17	1391.15	1391.13	1391.10	1391.09	1391.91	1391.09	0.82	NP
189	Kigeri I-Rwibikara	12.63	1345.04	1344.96	1344.95	1345.06	1344.98	1344.94	1344.85	1344.73	1344.71	1344.65	1344.62	1344.56	1345.06	1344.56	0.50	NP
208	Mitanga-Ruranzi	13.66	1352.50	1352.47	1352.57	1352.68	1352.62	1352.74	1352.53	1352.35	1352.52	1352.53	1352.64	1352.47	1352.74	1352.35	0.39	NP
216	Murama II-Higiro	0.00	1374.39	1374.35	1374.41	1374.47	1374.48	1374.48	1374.40	1374.10	1374.24	1374.13	1374.02	1374.01	1374.48	1374.01	0.47	NP
228	Ngugo I-Kanyagu	6.41	1365.67	1366.07	1365.64	1365.63	1365.70	1365.81	1365.61	1365.45	1365.36	1365.40	1365.45	1365.49	1366.07	1365.36	0.71	NP
229	Ntarabwa-Kiyanza	7.18	1360.98	1360.94	1360.95	1360.96	1360.99	1360.98	1360.94	1360.89	1360.84	1360.80	1360.79	1360.77	1360.99	1360.77	0.22	NP
236	Nunga I-Yaranda	5.73	1353.53	1353.48	1353.56	1353.59	1353.60	1353.60	1353.53	1353.45	1353.37	1353.32	1353.32	1353.28	1353.60	1353.28	0.32	NP
240	Nyange-Kumana	10.20	1323.70	1323.82	1324.04	1324.33	1324.54	1324.52	1324.15	1323.70	1323.57	1323.57	1323.73	1323.78	1324.54	1323.57	0.97	NP
242	Rambo-Kanyinya	6.94	1378.39	1378.41	1378.57	1378.56	1378.54	1378.50	1378.47	1378.43	1378.39	1378.38	1378.37	1378.34	1378.57	1378.34	0.23	NP
253	Ruhuzu-Yaranda	12.13	1355.11	1355.18	1355.24	1355.95	1355.24	1355.23	1355.20	1355.17	1355.14	1355.11	1355.09	1355.06	1355.95	1355.06	0.89	NP
254	Rukera-Gatete	6.43	1334.03	1334.12	1334.30	1334.59	1334.79	1334.73	1334.52	1334.35	1334.00	1333.90	1334.51	1334.02	1334.79	1333.90	0.88	NP
261	Runyonza-Muhero	6.78	1352.93	1352.97	1353.10	1353.08	1353.05	1353.05	1353.02	1353.00	1352.99	1352.98	1352.97	1352.96	1353.10	1352.93	0.17	NP
263	Runyonza-Ruzirakabogi	8.14	1357.66	1357.63	1357.66	1357.69	1357.70	1357.69	1357.95	1357.93	1357.91	1357.90	1357.87	1357.84	1357.95	1357.63	0.32	NP

N.B.:

- NP: Non producing wells
- FTP: Full time producing wells

Appendix V.3. Comparison of groundwater levels in 1991, 2006, 2007 and 2008 (in m above the local datum, Arc 1950 for Burundi)

S/N	Site	Depth	August 1991	September 2006	October 2007	October 2008	Observations
128	Bidogo-Gatete	5.56	1331.71	1331.46	1331.60	1331.09	Non producing well
139	Cimbogo-Gatete	3.60	n.d.	1325	1325.73	1325.79	Non producing well
159	Gikombe-Nyagisozi	8.22	n.d.	1323.96	1324.11	1324.08	Non producing well
203	Mago I-Gatete	8.40	1328.68	1327.83	1328.00	1327.93	Non producing well
254	Rukera-Gatete	5.79	1334.17	1333.54	1333.81	1333.79	Non producing well
281	Sigu-Kumana	5.76	n.d.	1319.43	1319.75	1319.70	Non producing well
282	Vyanzo I-Gatete	7.70	1325.76	1325.06	1325.3	1325.21	Non producing well
283	Vyanzo II-Gatete	6.22	n.d.	1320.17	1320.64	1320.55	Non producing well
134	Bugera-Bugera	5.12	1364.67	1364.53	1364.81	1364.72	Non producing well
135	Bunyari-Rugarama	11.42	1357.43	1355.58	1362.67	1362.61	Intermittently producing well
145	Gaharata-Murama	6.60	n.d.	1360.68	1360.9	1360.87	Non producing well
164	Gitamo I-Murambi	9.52	n.d.	1358.87	1359.17	1359.01	Non producing well
163	Gitamo II-Murambi	8.06	1359.40	1359.32	1359.86	1359.67	Non producing well
182	Karago-Runyonza	12.10	1371.92	1371.16	1371.48	1371.16	Non producing well
236	Nunga I-Yaranda	5.73	1354.74	1352.90	1353.64	1353.32	Non producing well
264	Ruranzi-Rwibikara	8.65	1370.31	1368.20	1368.62	1368.40	Non producing well l
146	Gahenda-Mugendo	5.66	n.d.	1362.81	1363.53	1363.11	Non producing well
160	Gikomero-Susa	7.15	n.d.	1365.03	1365.43	1365.22	Producing untill 2006l
183	Kariba-Kanyagu	6.86	n.d.	1354.02	1354.36	1354.06	Non producing well
219	Murehe-Murungurira	8.82	1381.81	1381.14	1381.66	1381.50	Non producing well
228	Ngugo I-Kanyagu	6.41	1365.89	1366.03	1366.38	1366.09	Non producing well
234	Ntwago-Murungurira	7.28	1371.62	1370.88	1371.24	1371.19	Non producing well
243	Renga II-Gitwenzi	6.10	n.d.	1353.28	1353.62	1353.54	Non producing well
265	Ruseno-Kanyagu	7.61	1354.22	1353.42	1353.77	1353.86	Operating well untill Spetember 2008
170	Kabirizi II-Kigoma	7.35	1357.51	1357.43	1358.61	1358.49	Producing untill 2006
179	Kanigo-Cinuma	13.15	1356.3	1354.7	1354.91	1354.81	Full time producing well
197	Kinyamateke-Nyabikenke	9.00	1360.9	1359.63	1360.17	1359.19	Full time producing well
213	Mukuyo-Kiri	8.25	1359.93	1364.82	1365.23	1365.11	Non producing well
224	Ngaragu-Kiri	11.52	1373.18	1370.60	1371.13	1371.87	Full time producing well
244	Rubirizi-Gaturanda	9.93	1365.23	1363.27	1363.74	1363.75	Non producing well
255	Rukindo-Rugasa	9.71	1367.27	1365.92	1366.9	1366.79	Full time producing well
276	Saruduha I-Rugasa	6.10	1374.06	1373.4	1373.86	1374.11	Full time producing well

S/N	Site	Depth	August 1991	September 2006	October 2007	October 2008	Observations
130	Bifu I-Marembo	6.18	1360.96	1360.16	1360.07	1359.98	Non operating well
142	Cinyambo-Gitwe	9.60	1347.28	1347.08	1348.03	1348.05	Operating well
154	Gatorondero-Gaturanda	8.35	1377.60	1375.1	1375.87	1374.91	Non operating well
158	Gifuruguti-Nyakarama	11.60	1352.49	1352.71	1352.67	1355.31	Operating well
168	Hambiro-Kiyonza	13.40	1371.85	1374.77	1371.32	1372.1	Operating well
177	Kanabugiri I-Bugera	5.00	1369.7	1369.21	1369.75	1369.61	Operating well
181	Karago-Kibonde	10.32	n.d.	1366.74	1367.24	1367.01	Non operating well
185	Karobogo-Kanyinya	9.20	1391.99	1391.28	1391.27	1391.13	Non operating well
183	Kigeri I-Rwibikara	12.63	1347.34	1344.20	1344.49	1344.65	Non operating well
190	Kigina I-Gisenyi	5.10	n.d.	1410.58	1411.07	1411.00	Operating well
191	Kigina II-Gisenyi	5.17	n.d.	1412.70	1412.82	1412.85	Operating well
196	Kigozi-Yaranda	7.00	1372.68	1371.06	1371.64	1370.53	Operating well
206	Mataka-Rugasa	17.88	1350.93	1345.70	1344.35	1344.68	Operating well
208	Mitanga-Ruranzi	13.66	1350.01	1351.91	1352.50	1352.53	Waste thrown inside the well which raises the water level
209	Mugombwa-Kiri	12.12	1375.92	1374.29	1374.44	1373.68	Operating in 2006
215	Murama I-Higiro	12.00	1363.54	1362.53	1362.56	1362.56	Non operating well
218	Murambo-Murambi	11.78	1362.24	1359.68	1359.78	1359.54	Operating well deepened in 2000
220	Murungazi-Mugendo	4.49	n.d.	1379.20	1379.58	1379.32	Non operating well
227	Ngugo II-Kanyagu	6.01	n.d.	1368.98	1369.55	1369.23	Non operating well
236	Nunga-Kiyonza	5.07	1344.67	1345.44	1344.96	1344.84	Operating well
240	Nyange-Kumana	10.20	n.d.	1323.27	1323.53	1323.40	Operating well
242	Rambo-Kanyinya	6.94	1379.11	1378.3	1378.43	1378.38	Non operating well
251	Rugoma-Kagege	6.46	n.d.	1425.15	1425.31	1424.81	Operating well
261	Runyonza-Muhero	6.78	1352.58	1352.58	1352.95	1352.98	Non operating well
272	Rwasama-Kiri	12.82	1376.41	1374.82	1378.03	1378.34	Non operating well

Appendix VII.1. Groundwater chemical analysis results

S/N	Site	Source	EC µS/cm-25°C	T °C	pH	HCO3 mg/l	Cl mg/l	SO4 mg/l	NO3 mg/l	NO2 mg/l	NH4 mg/l	PO4 mg/l	Ca mg/l	Mg mg/l	Mn mg/l	Fe mg/l	K mg/l	Na mg/l	F mg/l	SiO2 mg/l	Al mg/l	TDS mg/l	Error %
1	Cohoha-Kibonde	Lake	647.0		7.3	253.2	73.5	3.3	3.0	0.0	0.9	0.1	23.1	23.1	0.2	0.4	33.3	65.8	0.9	8.5	**0.0**	489.0	3.71
2	Cohoha-Kigozi I	Lake	784.0	23.0	7.4	273.3	93.8	2.6	4.4	0.1	1.6	0.1	26.6	21.7	0.3	0.3	41.0	67.3	0.9	5.6	0.0	539.6	0.41
3	Cohoha-Kigozi II	Lake	702.0	26.0	7.6	268.4	59.2	1.9	9.4	0.1	0.0	0.2	19.1	14.0	0.3	0.3	21.6	68.2	1.0	0.7	0.0	464.4	5.24
4	Cohoha-Murambi	Lake	640.0	27.9	7.6	250.7	73.6	3.6	2.5	0.0	0.7	0.1	23.9	19.1	0.1	0.3	43.0	67.4	0.9	9.3	0.0	495.3	4.16
5	Cohoha-Nunga	Lake	700.0	28.7	7.3	284.3	76.2	3.4	4.2	0.1	1.1	0.1	21.4	19.8	0.1	0.2	44.0	70.5	1.0	8.2	0.0	534.3	0.01
6	Cohoha-Ruranzi	Lake	651.0	24.4	7.5	251.9	78.1	3.1	2.0	0.0	1.0	0.1	22.7	19.5	0.2	0.2	30.2	69.7	0.9	5.0	0.0	484.6	1.32
7	Gacamirinda-Kinyamateke	Lake	941.0	25.9	8.4	280.6	115.2	2.2	11.1	0.1	0.0	0.3	32.7	21.8	0.7	2.1	7.6	99.0	-	3.6	0.0	576.8	0.40
8	Gacamirinda-Shenga II	Lake	1027.0	23.4	6.9	323.9	102.5	3.4	11.0	0.0	0.0	0.2	35.0	24.8	1.0	3.7	43.0	81.3	0.7	1.8	0.0	632.4	0.79
9	Nagitamo-Kabirizi I	Lake	706.0	25.2	7.0	229.4	102.7	2.4	4.2	0.1	1.5	0.2	28.0	17.3	0.5	0.5	39.0	65.9	0.5	7.4	0.0	499.4	0.13
10	Narungazi-Murungazi	Lake	351.0	28.5	7.3	149.5	23.6	2.3	4.4	1.7	0.0	0.1	18.5	7.7	0.4	0.6	3.4	40.6	0.3	4.6	0.0	257.7	2.61
11	Rweru-Mago I	Lake	166.1	24.5	6.7	86.6	0.3	1.9	14.0	0.1	0.0	0.1	9.6	6.3	0.2	0.8	6.5	12.5	0.3	11.9	0.0	151.1	0.42
12	Rweru-Mago II	Lake	174.7	29.1	7.1	90.3	4.8	1.4	7.9	0.1	0.0	0.1	9.7	6.4	0.3	1.0	6.8	12.8	0.3	5.6	0.0	147.6	1.26
13	Rweru-Nyange	Lake	166.0	24.9	6.7	90.9	10.1	3.5	3.5	0.2	0.7	0.1	10.1	6.6	0.3	0.9	5.9	11.0	1.0	2.5	0.0	147.3	4.16
14	Rwihinda-Bishunzi	Lake	868.0	26.3	7.8	242.8	139.0	1.4	1.1	0.1	0.0	0.1	32.4	19.0	0.2	0.5	26.9	96.4	1.0	2.3	0.0	563.2	0.80
15	Rwihinda-Bugera	Lake	885.0	27.3	7.4	233.0	166.9	2.7	3.6	0.3	0.4	0.1	28.7	28.7	0.1	0.3	49.0	90.1	1.0	11.3	0.0	616.2	2.00
16	Rwihinda-Kabira	Lake	848.0	26.6	7.5	228.8	154.0	3.1	2.5	0.0	0.3	0.1	30.3	24.3	0.1	0.3	22.2	100.4	0.3	12.1	0.0	578.6	1.62
17	Bihembe-Monge	Spring	215.0	23.5	6.9	11.0	17.7	34.3	30.2	0.1	0.0	0.1	6.4	7.2	0.3	0.4	3.1	18.4	0.1	4.3	0.1	133.5	1.86
18	Bishunzi-Munyinya	Spring	168.8	22.4	5.6	12.2	33.8	2.3	11.5	0.1	0.0	0.1	7.5	5.0	0.0	0.0	1.7	15.5	0.1	1.1	0.1	90.9	3.91
19	Bugorora-Gakana	Spring	90.2	22.7	7.1	12.8	6.5	3.0	12.8	0.1	0.0	0.1	4.9	2.3	0.0	0.0	0.6	7.1	0.1	4.9	0.1	55.3	6.23
20	Buhiga-Ntega	Spring	144.6	23.4	4.9	7.3	9.2	8.9	41.7	0.1	0.0	0.1	7.6	4.5	0.0	0.0	3.7	10.4	0.4	16.3	0.0	110.2	2.30
21	Bunyari-Rugarama	Spring	155.7	24.4	7.0	53.1	13.6	6.1	10.3	0.1	0.0	0.0	4.4	2.9	0.0	0.1	0.9	22.3	0.2	14.4	0.0	128.6	3.22
22	Burengo-Rushubije	Spring	54.0	22.9	4.9	3.7	3.8	2.7	18.2	0.1	0.0	0.1	3.9	2.0	0.1	0.1	0.8	2.8	0.1	13.7	0.1	52.1	1.89
23	Gaharata-Murama	Spring	197.0	24.2	7.1	21.4	30.4	3.8	17.3	0.0	0.0	0.0	8.3	3.8	0.0	0.1	3.9	17.3	0.1	6.3	0.0	112.6	0.34
24	Gatovu-Kanyinya	Spring	102.5	25.2	7.4	32.3	8.3	4.1	12.9	0.0	0.0	0.0	9.2	3.2	0.0	0.1	5.5	5.5	0.1	10.7	0.0	91.9	1.98
25	Gatunguru-Rugero	Spring	34.1	23.1	6.6	9.8	0.9	1.6	5.7	0.1	0.0	0.1	2.1	1.2	0.0	0.1	0.5	2.7	0.2	1.2	0.1	26.3	3.57
26	Gihobogo-Murungurira	Spring	150.4	24.2	6.6	48.8	8.9	6.4	9.8	0.1	0.0	0.1	7.4	3.1	0.1	0.2	1.4	16.8	0.1	11.9	0.0	115.0	2.07
27	Gihushi-Kiravumba	Spring	279.0	22.4	5.6	17.1	56.7	4.6	12.0	0.1	0.0	0.1	11.7	3.8	0.1	0.1	1.5	26.8	0.1	7.3	0.1	141.8	1.68
28	Gikombe-Ruhita	Spring	79.6	24.2	6.3	19.5	4.4	2.4	20.8	0.1	0.0	0.1	5.2	2.5	0.0	0.1	0.7	7.6	0.1	4.8	0.1	68.3	0.93
29	Kabira-Kanyinya	Spring	156.0	24.7	7.0	31.7	16.4	4.1	14.1	0.0	0.0	0.0	9.2	3.8	0.0	0.1	3.6	11.2	0.1	9.4	0.0	103.9	2.19
30	Kabira-Renga	Spring	148.1	24.5	5.9	30.5	22.5	1.2	2.4	0.1	0.0	0.1	5.1	2.8	0.0	0.2	0.2	18.9	0.1	16.7	0.1	101.0	4.82

S/N	Site	Source	EC µS/cm-25°C	T °C	pH	HCO3 mg/l	Cl mg/l	SO4 mg/l	NO3 mg/l	NO2 mg/l	NH4 mg/l	PO4 mg/l	Ca mg/l	Mg mg/l	Mn mg/l	Fe mg/l	K mg/l	Na mg/l	F mg/l	SiO2 mg/l	Al mg/l	TDS mg/l	Error %
31	Kagogo-Nyabitare	Spring	191.0	22.7	5.0	6.1	30.7	2.9	36.0	0.1	0.0	0.1	8.0	4.9	0.0	0.0	1.8	17.4	0.2	15.1	0.1	123.3	0.19
32	Kanyamanza-Kagege	Spring	127.4	24.7	6.2	25.0	16.1	1.1	9.6	0.1	0.0	0.1	5.1	2.9	0.0	0.1	1.1	14.4	0.1	9.6	0.1	85.3	4.78
33	Kararire-Kagege	Spring	149.2	23.3	6.5	9.8	25.7	7.1	5.5	0.1	0.0	0.1	6.6	3.7	0.0	0.0	1.8	12.8	0.1	4.4	0.1	77.7	4.69
34	Karira-Gatemere	Spring	201.0	22.5	6.0	15.9	27.8	19.0	8.6	0.1	0.0	0.1	9.3	5.0	0.1	0.1	3.2	17.9	0.1	8.3	0.1	115.5	4.74
35	Karobogo-Kanyinya	Spring	105.2	23.0	7.2	15.9	10.7	6.2	23.6	0.0	0.0	0.0	5.9	2.7	0.0	0.1	20.0	1.9	0.1	8.8	0.1	96.0	1.70
36	Kididiri-Buhasa	Spring	72.7	21.8	5.4	22.0	8.6	2.6	0.1	0.1	0.0	0.1	4.3	2.3	0.0	0.2	1.2	7.5	0.1	5.6	0.3	55.1	7.43
37	Kigomero-Munyinya	Spring	85.7	22.3	6.2	11.6	9.4	2.3	10.4	0.1	0.0	0.1	5.0	2.3	0.0	0.2	0.5	7.0	0.2	4.4	0.1	53.4	5.74
38	Kigoti-Munzenze	Spring	162.4	24.1	5.8	32.3	18.4	1.2	20.2	0.1	0.0	0.1	7.3	4.2	0.2	0.0	0.7	15.5	0.1	5.7	0.0	106.0	0.26
39	Kinyangoro-Kumana	Spring	55.8	24.1	7.0	20.7	115.2	1.4	16.4	0.1	0.0	0.1	4.3	2.0	0.0	0.4	0.4	4.3	0.2	4.0	0.1	169.5	4.31
40	Kinyangurube-Karehe	Spring	118.9	23.7	5.3	4.3	6.2	5.3	19.6	0.1	0.0	0.1	3.3	1.9	0.1	0.2	0.1	10.2	0.1	9.8	0.0	61.1	6.84
41	Kinywamagana-Kigarama	Spring	87.7	23.6	5.2	5.5	15.3	1.1	7.7	0.1	0.0	0.1	3.6	1.8	0.0	0.0	0.7	9.1	0.1	3.0	0.0	48.1	5.16
42	Kiramata-Monge	Spring	155.2	23.6	7.4	12.2	0.6	5.6	22.9	0.1	0.0	0.1	7.0	3.4	0.1	0.0	3.6	13.4	0.1	10.1	0.1	79.3	4.99
43	Kirunduzi-Mutara	Spring	44.6	23.7	7.1	7.3	3.7	3.0	9.4	0.2	0.0	0.1	3.0	1.2	0.1	0.2	0.3	4.8	0.5	4.8	1.1	39.6	3.10
44	Mamfu-Kiyonza	Spring	459.0	24.5	7.1	231.2	0.0	44.5	15.5	0.1	0.0	0.8	49.3	11.9	1.2	0.2	0.3	29.8	0.1	17.2	0.0	402.0	2.07
45	Maramvya-Mwenya	Spring	48.4	23.0	5.3	7.3	8.5	2.6	12.4	0.1	0.0	0.1	3.6	1.7	0.0	0.2	0.3	5.0	0.1	18.0	0.9	60.8	5.61
46	Mudahinyuka-Kigina II	Spring	69.2	24.7	5.7	22.0	6.7	2.5	0.2	0.1	0.0	0.1	4.9	1.4	0.1	0.3	1.3	5.9	0.1	9.6	0.1	55.2	4.61
47	Mukagezi-Ntogwe	Spring	89.0	22.7	6.0	9.8	2.7	2.9	36.2	0.1	0.0	0.1	6.0	2.8	0.0	0.1	1.8	5.9	0.6	14.1	0.1	83.1	2.88
48	Mukuyo-Kiri	Spring	766.0	24.3	7.0	328.2	16.5	96.2	10.6	0.1	0.0	0.5	39.6	9.8	0.0	0.1	5.8	123.8	0.2	22.4	1.7	655.3	1.70
49	Musave-Mugobe	Spring	179.8	22.5	5.6	30.5	10.6	23.5	6.2	0.1	0.0	0.1	10.0	3.0	0.0	0.0	2.4	12.1	0.2	2.8	0.1	101.7	2.19
50	Musave-Rutabo	Spring	225.0	25.5	7.1	20.1	41.5	1.6	9.2	0.1	0.0	0.1	6.6	4.2	0.3	2.1	0.2	23.2	0.1	1.6	0.1	110.9	2.57
51	Mutetema-Muyange	Spring	74.4	22.7	5.8	30.5	4.9	1.3	7.2	0.1	0.0	0.1	4.7	2.9	0.0	0.1	1.0	5.6	0.2	0.1	0.1	58.7	2.73
52	Mvyayingabo-Mutara	Spring	129.3	24.2	6.7	24.4	3.6	9.8	18.0	0.1	0.0	0.1	6.2	4.4	0.0	0.0	1.1	9.9	0.2	4.3	0.1	82.2	6.13
53	Mwenya-Mwenya	Spring	196.9	23.2	5.8	34.2	9.6	15.1	17.5	0.1	0.0	0.1	10.5	5.1	1.4	0.0	0.4	14.6	0.2	1.6	0.1	110.3	6.64
54	Mwenya-Rwimbogo	Spring	87.2	23.8	6.2	14.0	6.8	1.8	17.9	0.1	0.0	0.1	5.5	3.1	0.0	0.1	0.9	6.9	0.1	15.0	0.1	72.3	6.50
55	Nagikono-Kinyangurube	Spring	134.7	24.1	5.7	39.0	9.0	1.3	15.9	0.1	0.0	0.1	7.9	4.3	0.0	0.0	1.6	11.8	0.2	8.9	0.0	100.1	4.79
56	Nakabingo	Spring	169.1	25.6	6.8	56.1	11.7	5.4	6.0	0.0	0.0	0.0	10.8	5.4	0.0	0.1	1.3	10.0	0.1	9.1	0.0	116.2	0.13
57	Nakabingo II-Gihosha	Spring	134.6	22.9	4.9	3.7	7.2	13.4	34.4	0.1	0.0	0.1	8.0	4.1	0.3	0.1	5.6	6.9	0.1	17.6	0.1	101.7	4.11
58	Nakabingo-Gatemere	Spring	59.1	22.0	6.2	12.8	13.2	7.6	3.5	0.2	0.0	0.1	3.8	2.0	0.0	0.4	0.8	6.9	0.4	14.2	0.9	66.8	7.51
59	Nakarambo-Rutabo	Spring	174.3	23.7	6.1	22.0	35.0	1.3	13.4	0.1	0.0	0.1	8.2	4.1	0.1	0.2	0.7	19.2	0.2	18.2	0.1	122.7	0.61
60	Nakivumbura-Monge	Spring	134.4	23.6	5.6	29.3	12.5	9.4	5.4	0.1	0.0	0.1	6.4	3.7	0.0	0.2	2.3	11.8	0.1	16.6	0.6	98.5	3.45

S/N	Site	Type	EC µS/cm-25°C	T °C	pH	HCO3 mg/l	Cl mg/l	SO4 mg/l	NO3 mg/l	NO2 mg/l	NH4 mg/l	PO4 mg/l	Ca mg/l	Mg mg/l	Mn mg/l	Fe mg/l	K mg/l	Na mg/l	F mg/l	SiO2 mg/l	Al mg/l	TDS mg/l	Error %
61	Narukere-Gihosha	Spring	57.3	23.1	4.9	7.9	5.1	1.3	16.1	0.2	0.0	0.1	3.7	1.5	0.0	0.1	0.4	6.8	0.1	13.8	0.0	57.1	4.29
62	Narutambwe-Kireka	Spring	80.7	23.3	6.6	7.9	0.9	1.2	25.9	0.1	0.0	0.1	0.4	2.3	0.0	0.0	0.8	7.7	0.1	4.0	0.1	51.5	3.74
63	Nyabitare-Munyinya	Spring	179.5	22.5	5.8	16.5	28.1	4.7	23.7	0.1	0.0	0.1	10.7	4.6	0.0	0.1	1.0	15.6	0.2	6.3	0.1	111.6	2.42
64	Nyaruziba-Mutara	Spring	167.4	22.9	6.2	29.9	12.4	19.5	19.4	0.1	0.0	0.1	11.0	6.3	0.0	0.1	4.2	8.2	0.1	11.4	0.0	122.4	1.11
65	Rambo II-Gatwe	Spring	178.6	23.6	6.9	14.6	6.1	13.8	43.3	0.2	0.0	0.1	6.8	5.6	0.0	0.1	1.5	14.0	0.1	15.2	0.1	121.6	1.64
66	Rubira-Gatemere	Spring	55.4	23.1	5.2	8.5	4.3	1.1	8.2	0.1	0.0	0.1	1.6	1.1	0.0	0.2	0.4	5.9	0.1	13.1	0.0	44.6	2.69
67	Rugangazi-Ntogwe	Spring	62.2	22.9	4.5	9.2	4.8	1.2	11.2	0.1	0.0	0.1	2.5	1.3	0.2	0.4	2.1	4.8	0.1	13.4	0.1	51.3	2.00
68	Rugero-Nakarinzi	Spring	22.6	23.6	6.5	15.3	0.6	1.2	1.2	0.1	0.0	0.7	3.2	1.3	0.0	0.1	0.2	2.2	0.1	5.1	0.1	31.5	4.22
69	Rugoma-Kagege	Spring	75.4	21.6	5.7	9.8	10.4	4.6	5.2	0.1	0.0	0.1	4.7	2.3	0.0	0.1	1.4	5.4	0.1	5.9	0.1	50.1	4.20
70	Rugomero-Gatemere	Spring	60.6	22.1	6.3	9.8	0.7	2.4	24.5	0.1	0.0	0.1	3.7	1.8	0.0	0.3	0.3	6.1	0.1	0.6	0.7	51.1	1.42
71	Rugomero-Kiravumba	Spring	38.6	23.3	4.9	14.0	4.3	1.6	0.8	0.1	0.0	0.1	1.6	0.9	0.0	0.1	0.4	4.4	0.1	14.9	0.1	43.4	6.35
72	Rugomero-Nyabugeni	Spring	104.4	22.2	6.9	15.3	9.8	2.0	2.3	0.1	0.0	0.1	4.1	2.6	0.0	0.3	0.6	10.0	0.2	0.5	0.1	47.9	4.54
73	Rugunga II- Kavomo	Spring	166.9	23.8	6.2	33.6	10.0	13.6	3.5	0.1	0.0	0.1	3.1	5.0	0.0	0.0	1.2	15.8	0.1	8.7	0.1	94.8	4.30
74	Rugunga I-Kavomo	Spring	135.7	24.2	5.7	23.2	16.5	6.4	11.9	0.1	0.0	0.1	4.5	2.6	0.0	0.1	1.0	17.1	0.1	8.2	0.1	91.9	1.47
75	Ruhongore-Munyinya	Spring	162.5	22.3	6.6	17.1	24.0	7.1	14.0	0.1	0.0	0.1	8.7	4.3	0.0	0.1	1.4	13.7	0.1	15.1	0.1	105.9	3.03
76	Rushubije-Cogo	Spring	53.1	23.8	4.7	4.9	3.3	1.0	14.6	0.1	0.0	0.1	1.8	1.5	0.0	0.1	0.8	5.4	0.1	5.7	0.0	39.4	3.92
77	Twengebuye-Nakabingo	Spring	86.5	23.6	4.7	3.1	4.6	1.1	27.3	0.1	0.0	0.1	5.0	2.4	0.1	0.1	1.1	5.3	0.4	5.1	0.0	55.7	4.36
78	Bishunzi-Cewe	Well	2520.0	22.9	6.8	550.2	386.6	153.7	7.4	0.0	0.0	0.0	56.4	74.5	0.2	3.0	115.8	276.2	2.4	5.7	0.0	1632.2	1.66
79	Bunyari-Rugarama	Well	462.0	24.3	6.9	215.9	11.3	10.2	22.0	0.0	0.0	0.1	19.5	14.0	0.0	0.1	54.5	18.0	1.1	21.9	0.0	388.8	1.45
80	Cimbogo-Gatete	Well	1108.0	23.3	7.5	688.7	23.3	4.3	14.4	0.1	0.0	0.6	97.4	54.4	3.2	0.7	79.0	34.2	1.5	16.8	0.0	1018.4	2.75
81	Cinyambo-Gitwe	Well	414.0	26.6	7.1	198.3	24.9	6.8	7.2	0.0	0.0	0.1	23.9	10.9	0.8	0.2	40.0	23.9	0.3	18.5	0.0	355.8	0.32
82	Foko II-Kiyonza	Well	1302.0	24.1	7.3	485.6	111.8	101.7	54.5	0.0	0.1	0.1	97.4	38.7	0.1	0.1	37.4	124.6	1.4	28.8	0.0	1082.0	1.10
83	Foko I-Kiyonza	Well	1550.0	23.4	7.1	608.8	25.2	213.3	68.3	0.1	0.1	0.1	92.1	38.8	0.0	0.0	43.0	175.5	1.0	22.9	0.0	1289.1	0.87
84	Gahwijo II-Nyabikenke	Well	3110.0	24.2	6.8	935.7	406.4	193.0	20.6	0.0	0.1	0.1	113.0	53.6	0.1	0.2	44.2	439.0	1.0	15.5	0.0	2222.6	1.42
85	Gahwijo I-Nyabikenke	Well	1219.0	24.3	6.6	403.2	118.6	147.9	3.9	0.0	0.7	0.1	124.1	25.6	7.6	9.5	63.2	65.5	0.7	19.2	0.0	989.8	1.21
86	Gasagara II-Rubuga	Well	1777.0	25.9	7.0	560.0	49.3	446.0	15.2	0.0	0.1	0.1	169.9	44.6	0.0	0.1	35.4	165.2	1.4	19.9	0.0	1507.2	0.33
87	Gasagara I-Rubuga	Well	2900.0	26.3	7.8	1378.0	145.3	167.8	52.5	0.0	0.1	0.1	75.9	71.6	0.2	0.4	35.2	431.0	4.2	18.4	0.0	2380.7	2.80
88	Gifuruguti-Nyakarama	Well	2860.0	23.8	6.8	539.2	317.2	329.2	15.8	0.0	0.1	0.1	135.1	53.6	0.8	0.2	49.2	304.0	0.8	17.4	0.0	1762.6	1.51
89	Haga II-Nyamabuye	Well	1282.0	27.3	7.2	491.7	81.5	25.4	8.9	0.1	0.5	0.1	68.1	26.2	1.2	2.1	29.0	97.1	2.6	10.6	0.0	844.8	1.76
90	Hambiro-Kiyonza	Well	2400.0	23.6	7.3	682.0	190.8	253.6	75.5	0.0	0.1	0.1	135.2	55.9	0.0	0.1	38.4	247.1	2.4	30.1	0.0	1711.2	0.03

S/N	Site	Type	EC µS/cm-25°C	T °C	pH	HCO3 mg/l	Cl mg/l	SO4 mg/l	NO3 mg/l	NO2 mg/l	NH4 mg/l	PO4 mg/l	Ca mg/l	Mg mg/l	Mn mg/l	Fe mg/l	K mg/l	Na mg/l	F mg/l	SiO2 mg/l	Al mg/l	TDS mg/l	Error %
91	Kabirizi II-Kigoma	Well	903.0	24.3	7.0	251.9	50.8	78.0	44.0	0.1	0.1	0.1	74.6	16.5	0.0	0.1	48.4	41.0	1.2	20.6	0.0	627.4	1.26
92	Kadobogoro-Muramba	Well	210.0	22.9	7.2	51.9	12.4	20.4	6.1	0.1	0.0	0.1	10.9	3.6	0.1	2.9	1.5	20.6	0.2	4.3	0.0	134.9	4.16
93	Kadobori II-Rubuga	Well	1990.0	25.0	7.2	598.4	157.7	267.1	24.0	0.0	0.1	0.1	160.8	46.4	0.2	0.1	44.6	162.3	0.6	22.9	0.0	1485.4	0.39
94	Kadobori I-Rubuga	Well	1153.0	26.5	6.9	302.6	122.2	77.9	14.4	0.0	0.0	0.1	67.4	18.9	0.4	0.1	52.0	77.7	0.6	18.6	0.0	752.9	3.13
95	Kamwayi II-Nyamabuye	Well	682.0	24.7	7.2	265.4	9.2	33.2	83.3	0.1	0.0	0.1	45.3	15.9	0.0	0.1	0.2	70.5	2.5	14.7	0.0	540.3	0.04
96	Kanabugiri-Bugera	Well	685.0	24.4	7.6	258.0	48.2	55.5	5.1	0.0	0.0	0.0	28.9	28.9	0.3	0.1	24.0	79.3	5.0	5.0	0.0	538.5	7.28
97	Kanigo-Cinuma	Well	2160.0	24.5	7.0	458.1	110.6	432.6	57.9	0.2	0.1	0.1	68.5	68.5	1.0	0.2	25.0	283.8	1.5	18.6	0.0	1526.7	3.49
98	Kantuye-Ceru	Well	848.0	25.3	7.2	412.4	66.8	2.2	8.9	6.7	0.0	0.1	47.1	15.8	14.5	2.2	56.5	78.0	1.7	9.4	0.0	722.2	0.64
99	Karago-Kibonde	Well	762.0	25.3	7.1	215.3	129.4	10.2	5.0	0.0	0.0	0.0	79.0	10.6	0.0	6.4	15.5	45.6	0.5	9.7	0.7	528.0	0.33
100	Karago-Rukuramigabo	Well	1270.0	24.1	7.4	708.2	63.8	1.8	13.1	0.1	0.0	0.1	13.8	22.5	0.9	31.9	104.0	168.3	1.1	9.6	0.0	1139.2	0.11
101	Karisha-Kigina	Well	1230.0	24.1	6.9	597.2	90.4	13.9	42.1	0.1	0.1	0.1	67.1	24.9	0.0	0.0	14.2	145.7	1.3	10.8	0.0	1007.8	4.76
102	Kigazi-Nyakarama	Well	2650.0	27.8	7.2	1062.0	74.0	264.2	80.2	0.0	0.2	0.1	106.2	63.3	0.1	0.2	2.6	380.5	3.6	18.9	0.0	2056.0	1.57
103	Kigina I-Gisenyi	Well	415.0	23.7	7.0	211.7	13.1	7.1	5.7	0.1	0.0	0.0	46.1	10.5	0.0	0.4	0.5	23.0	0.7	20.3	0.0	339.3	3.92
104	Kigina II-Gisenyi	Well	352.0	23.8	7.4	149.5	10.6	11.2	13.6	0.3	0.0	0.0	25.6	12.4	0.0	0.3	0.1	26.7	1.1	4.9	0.1	256.5	1.27
105	Kigoma-Gatare	Well	536.0	23.7	6.9	115.9	73.5	57.4	7.9	0.1	0.0	0.1	40.2	11.5	2.0	9.6	4.6	40.5	0.4	20.7	0.0	384.2	0.50
106	Kigozi-Yaranda	Well	1547.0	25.7	6.9	585.6	97.0	108.5	41.6	0.0	0.1	0.1	92.3	46.3	0.2	0.5	55.0	138.1	1.6	4.4	0.0	1171.2	1.88
107	Kinyamateke	Well	799.0	25.1	6.3	160.4	78.9	108.6	54.6	0.1	0.1	0.3	36.9	26.4	0.0	0.1	17.0	70.3	0.4	17.2	0.0	571.2	3.18
108	Kiruhura II-Muramba	Well	478.0	23.8	6.5	164.1	46.7	34.6	3.8	0.1	0.0	0.1	48.4	6.0	1.8	1.2	1.3	29.9	1.1	20.2	0.0	359.3	4.90
109	Kiruhura I-Kiyanza	Well	1468.0	24.8	7.7	488.0	138.3	109.9	10.1	0.2	0.4	0.1	78.6	26.0	0.1	11.2	29.0	161.2	0.4	4.5	0.0	1058.0	0.42
110	Kiyonza-Nunga	Well	1301.0	25.6	6.9	465.4	164.5	49.0	7.6	0.0	0.0	0.0	79.5	56.5	0.1	2.8	58.0	102.1	0.8	13.5	0.0	999.8	4.38
111	Mago I-Gatete	Well	3730.0	26.4	8.5	1984.9	142.0	154.5	6.6	0.1	0.0	0.1	40.0	3.0	0.2	0.2	252.0	630.0	9.4	6.2	0.0	3229.1	4.98
112	Marembo-Marembo	Well	454.0	24.3	7.3	209.8	21.4	1.7	30.7	0.1	0.0	0.1	31.0	10.9	0.9	3.6	16.7	25.6	0.9	15.2	0.0	368.6	4.97
113	Mataka-Rugasa	Well	722.0	24.1	6.9	391.0	18.7	10.3	11.8	0.0	0.0	0.1	56.2	25.8	0.0	0.2	19.0	42.3	0.6	13.6	0.0	589.6	0.56
114	Mugombwa-Kiri	Well	1066.0	24.2	7.2	465.4	35.1	79.3	65.3	0.1	0.1	0.1	76.0	35.8	0.0	0.1	23.4	102.6	3.0	22.6	0.0	909.1	2.04
115	Muhero I - Yaranda	Well	267.0	25.0	7.0	74.4	31.9	6.5	6.9	0.1	0.0	0.1	18.5	5.9	0.3	2.1	1.0	16.8	0.4	14.5	0.0	179.4	2.58
116	Muhero II - Yaranda	Well	362.0	24.7	7.7	161.7	20.6	4.0	9.4	0.9	0.0	0.1	20.5	8.9	0.5	9.7	9.9	30.5	1.0	4.5	0.0	282.1	2.88
117	Munyinya-Nyakarama	Well	2690.0	24.4	7.0	1029.7	129.0	256.1	75.9	0.2	0.1	0.1	132.2	58.2	0.0	0.2	61.2	307.5	1.4	16.7	0.0	2068.4	1.39
118	Murambo-Murambi	Well	1606.0	25.5	7.2	669.8	167.2	110.2	5.1	0.2	5.7	0.0	87.7	49.0	0.1	2.4	82.0	173.2	2.6	8.5	0.0	1363.5	0.98
119	Murehe-Murungurira	Well	577.0	24.4	6.8	172.0	43.4	52.2	18.5	0.1	0.0	0.1	32.1	6.3	0.5	4.2	1.7	71.5	2.2	2.5	0.0	407.2	0.01
120	Murungurira-Ntwago	Well	1120.0	24.3	7.1	239.1	149.2	86.8	9.8	0.1	0.0	0.1	26.9	12.0	0.5	0.7	0.5	184.4	16.5	14.4	0.0	741.0	1.49

S/N	Site	Type	EC µS/cm-25°C	T °C	pH	HCO3 mg/l	Cl mg/l	SO4 mg/l	NO3 mg/l	NO2 mg/l	NH4 mg/l	PO4 mg/l	Ca mg/l	Mg mg/l	Mn mg/l	Fe mg/l	K mg/l	Na mg/l	F mg/l	SiO2 mg/l	Al mg/l	TDS mg/l	Error %
121	Mutoza-Yaranda	Well	807.0	24.5	7.0	294.0	82.6	31.6	0.2	1.6	1.9	0.1	50.5	6.2	0.2	27.1	1.7	78.5	0.4	11.0	0.0	587.5	1.82
122	Ndava II-Nyamabuye	Well	821.0	24.1	7.1	361.1	71.8	2.1	15.1	0.1	1.4	0.0	44.7	21.9	0.0	3.2	13.8	89.8	2.7	0.7	0.0	628.5	1.47
123	Ngaragu-Kiri	Well	1196.0	24.8	7.0	547.2	11.6	144.4	40.1	0.0	0.1	0.1	58.0	25.9	1.3	0.6	1.3	180.4	3.5	15.2	0.0	1029.5	0.05
124	Ntembe II-Kiri	Well	3420.0	23.8	6.9	855.2	303.2	337.1	66.7	0.1	0.1	0.3	167.0	61.3	1.2	0.0	108.0	335.7	1.3	19.6	0.0	2256.5	0.16
125	Ntembe I-Kiri	Well	3260.0	22.7	7.1	1044.3	199.9	504.3	38.9	0.1	0.1	0.0	121.7	59.7	0.4	0.1	52.4	511.5	2.5	20.3	0.0	2556.3	1.01
126	Nunga II-Yaranda	Well	1618.0	24.6	6.8	476.4	181.2	100.8	8.4	0.2	1.0	0.1	95.0	24.8	0.2	11.9	30.1	190.0	0.6	16.6	0.0	1137.1	3.62
127	Nyange-Kumana	Well	37.5	25.2	7.5	16.5	8.5	2.0	3.2	0.0	0.0	0.0	4.3	2.0	0.0	0.1	2.9	4.1	0.1	0.7	0.0	44.4	2.50
128	Rugoma-Kagege	Well	149.2	23.6	6.8	42.7	14.1	13.1	7.0	1.8	0.2	0.0	10.7	3.8	0.1	1.6	13.7	8.7	0.2	11.3	0.0	129.0	3.67
129	Rukindo-Rugasa	Well	447.0	22.6	6.8	200.1	3.8	43.5	12.3	0.3	0.0	0.1	39.7	13.4	0.0	0.1	20.0	30.4	0.7	27.0	0.0	391.4	4.43
130	Rukore-II-Kigina	Well	951.0	25.4	6.5	414.8	95.6	21.5	5.0	0.0	4.9	0.0	82.2	24.7	1.1	6.0	44.4	67.3	1.0	5.9	0.0	774.4	3.33
131	Runyangona II-Nyabikenke	Well	625.0	22.0	6.2	276.3	59.2	2.7	4.0	0.0	0.7	0.0	47.8	18.8	4.0	25.7	18.6	25.4	0.6	10.0	0.0	493.8	2.27
132	Runyonza-Kabonde	Well	2050.0	24.7	7.3	478.9	202.7	121.7	9.2	2.8	0.6	0.1	65.0	43.2	2.7	1.9	64.0	213.0	3.2	7.5	0.0	1216.3	4.62
133	Ruranzi-Rwibikara	Well	746.0	25.1	7.5	323.9	73.0	3.5	1.9	0.0	1.8	0.0	37.4	18.9	0.1	8.2	23.3	70.3	1.5	8.1	0.1	571.9	0.07
134	Ruseno-Kanyagu	Well	452.0	24.3	6.3	105.5	59.7	21.8	3.5	0.1	0.0	0.7	16.5	2.6	0.0	0.9	10.0	60.0	0.3	5.8	0.0	287.3	0.21
135	Ruyivyi II-Gitwe	Well	687.0	25.8	6.8	288.5	55.9	16.8	10.7	0.1	0.0	0.1	52.0	17.0	0.1	0.8	50.5	50.3	0.9	12.2	0.0	555.8	4.67
136	Rwasama-Kiri	Well	496.0	24.2	7.3	186.1	23.4	53.6	24.3	0.1	0.0	0.2	32.4	11.5	0.4	0.2	2.2	52.3	0.8	29.9	0.0	417.3	3.11
137	Saruduha II-Rugasa	Well	1920.0	23.4	7.4	880.2	118.5	132.9	4.8	0.0	0.1	0.9	93.6	60.7	0.1	0.9	42.4	218.0	5.5	15.6	0.0	1574.2	0.93
138	Saruduha I-Rugasa	Well	2500.0	22.1	6.9	522.8	328.6	251.2	49.5	0.0	0.1	0.2	129.5	57.1	7.5	0.2	9.0	244.5	1.6	20.3	0.1	1622.2	3.38
139	Senga-Nyagisozi	Well	96.2	25.9	7.3	56.7	1.4	2.3	1.1	0.2	0.0	0.1	10.2	2.2	0.1	2.4	2.1	6.7	0.4	7.5	0.0	93.5	3.80
140	Shenga I- Rugasa	Well	680.0	23.8	6.7	220.2	100.5	3.0	4.2	0.1	0.0	0.0	28.5	12.8	0.6	3.7	50.5	73.4	0.5	8.5	0.0	506.4	3.87
141	Shenga III-Rugasa	Well	2790.0	24.2	6.7	605.1	499.3	72.3	16.2	0.0	0.0	0.0	81.8	39.0	0.5	54.0	38.5	336.2	0.3	5.4	0.0	1748.6	1.83
142	Shenga II-Rugasa	Well	2820.0	23.3	6.8	608.8	466.4	125.3	9.0	7.2	0.0	0.0	80.4	39.7	0.4	2.9	37.8	418.0	0.3	8.8	0.0	1805.0	0.94
143	Susa-Gikomero	Well	548.0	24.3	6.6	47.0	82.4	39.2	69.9	0.1	0.0	0.1	28.1	15.4	1.7	0.1	42.0	40.1	0.3	9.6	0.0	375.7	4.81

Appendix VII.2. Comparison of Physico-chemical parameters measured in field and laboratory

S/N	Name	Source	T (°C)	Field pH	Laboratory pH	Field EC (µS/cm-25°C)	Laboratory EC (µS/cm-25°C)
1	Cohoha-Kibonde	Lake	n.d	9.1	7.3	n.d.	647.0
2	Cohoha-Kigozi I	Lake	23.0	9.4	7.4	n.d.	784.0
3	Cohoha-Kigozi II	Lake	26.0	8.9	7.6	809.0	702.0
4	Cohoha-Murambi	Lake	27.9	8.9	7.6	n.d.	640.0
5	Cohoha-Nunga	Lake	28.7	9.3	7.3	n.d.	700.0
6	Cohoha-Ruranzi	Lake	24.4	8.8	7.5	n.d.	651.0
7	Gacamirinda-Kinyamateke	Lake	25.9	8.5	8.4	1090.0	941.0
8	Gacamirinda-Shenga II	Lake	23.4	8.3	6.9	n.d.	1027.0
9	Nagitamo-Kabirizi I	Lake	25.2	8.9	7	n.d.	706.0
10	Narungazi-Murungazi	Lake	28.5	8.3	7.3	n.d.	351.0
11	Rweru-Mago I	Lake	24.5	8.4	7.1	445.0	166.1
12	Rweru-Mago II	Lake	29.1	8.1	6.7	210.0	174.7
13	Rweru-Nyange	Lake	25.4	9	6.7	n.d.	166.0
14	Rwihinda-Bishunzi	Lake	29.1	8.3	7.8	1030.0	868.0
15	Rwihinda-Bugera	Lake	27.3	8.2	7.4	n.d.	885.0
16	Rwihinda-Kabira	Lake	26.6	8.5	7.5	n.d.	848.0
17	Bihembe-Monge	Spring	23.5	4.9	6.9	235.0	215.0
18	Bishunzi-Munyinya	Spring	22.4	5.1	5.6	227.0	168.8
19	Bugorora-Gakana	Spring	22.7	5	7.1	108.0	90.2
20	Buhiga-Ntega	Spring	23.4	5	4.9	172.0	144.6
21	Bunyari-Rugarama	Spring	24	5.7	7	190	155.7
22	Burengo-Rushubije	Spring	22.9	4.9	4.9	79.0	54.0
23	Gaharata-Murama	Spring	24.2	5.6	7.1	n.d.	197.0
24	Gatovu-Kanyinya	Spring	25.2	5.7	7.4	n.d.	102.5
25	Gatunguru-Rugero	Spring	23.1	5	6.6	41.0	34.1
26	Gihobogo-Murungurira	Spring	24.2	5.9	6.6	169.0	150.4
27	Gihushi-Kiravumba	Spring	22.4	5.2	5.6	336.0	279.0
28	Gikombe-Ruhita	Spring	24.2	5.5	6.3	103.0	79.6
29	Kabira-Kanyinya	Spring	24.7	5.7	7	n.d.	156.0
30	Kabira-Renga	Spring	24.5	5.3	5.9	164	148.1
31	Kagogo-Nyabitare	Spring	22.7	5	5	212.0	191.0
32	Kanyamanza-Kagege	Spring	24.7	5.4	6.2	161.0	127.4
33	Kararire-Kagege	Spring	23.3	4.8	6.5	189.0	149.2
34	Karira-Gatemere	Spring	22.5	5.2	6	243.0	201.0
35	Karobogo	Spring	23	4.6	7.2	n.d.	105.2
36	Kididiri-Buhasa	Spring	21.8	5.7	5.4	97.7	72.7
37	Kigomero-Munyinya	Spring	22.3	5.1	6.2	99.0	85.7
38	Kigoti-Munzenze	Spring	24.1	5.5	5.8	178.0	162.4
39	Kinyangoro-Kumana	Spring	24.1	5.4	7	58.0	55.8
40	Kinyagurube-Karehe	Spring	23.7	4.8	5.3	109.0	118.9
41	Kinywamagana-Kigarama	Spring	23.6	4.9	5.2	101.0	87.7
42	Kiramata-Monge	Spring	23.6	4.7	7.4	146.0	155.2
43	Kirunduzi-Mutara	Spring	23.7	4.9	7.1	52.0	44.6
44	Mamfu-Kiyonza	Spring	24.5	6.4	7.1	541.0	459.0
45	Maramvya-Mwenya	Spring	23.0	5.1	5.3	57.0	48.4
46	Mudahinyuka-Kigina II	Spring	24.7	5.5	5.7	84.0	69.2
47	Mukagezi-Ntogwe	Spring	22.7	5	6	118.0	89.0
48	Mukuyo-Kiri	Spring	24.7	6.6	7	906.0	766.0
49	Musave-Mugobe	Spring	22.5	5.5	5.6	224.0	179.8
50	Musave-Rutabo	Spring	23.5	5.3	7.1	270.0	225.0

S/N	Name	Source	T (°C)	Field pH	Laboratory pH	Field EC(µS/cm-25°C)	Laboratory EC(µS/cm-25°C)
51	Mutetema-Muyange	Spring	22.7	5.5	5.8	98.9	74.4
52	Mvyayingabo-Mutara	Spring	24.2	5.2	6.7	150.0	129.3
53	Mwenya-Mwenya	Spring	23.2	5.4	5.8	204.0	196.9
54	Mwenya-Rwimbogo	Spring	23.8	5	6.2	97.2	87.2
55	Nagikono-Kinyangurube	Spring	24.1	5.5	5.7	157.0	134.7
56	Nakabingo	Spring	25.6	6.4	6.8	n.d.	169.1
58	Nakabingo II-Gihosha	Spring	22.9	4.6	4.9	162.0	134.6
57	Nakabingo-Gatemere	Spring	22.0	5.1	6.2	82.0	59.1
59	Nakarambo-Rutabo	Spring	23.7	5.3	6.1	229.0	174.3
60	Nakivumbura-Monge	Spring	23.6	4.9	5.6	153.0	134.4
61	Narukere-Gihosha	Spring	23.1	4.8	4.9	72.0	57.3
62	Narutambwe-Kireka I	Spring	23.3	4.8	6.6	91.0	80.7
63	Nyabitare-Munyinya	Spring	22.5	5.4	5.8	225.0	179.5
64	Nyaruziba_Mutara	Spring	22.9	5.7	6.2	190.0	167.4
65	RamboII-Gatwe	Spring	23.6	4.6	6.9	191.0	178.6
66	Rubira-Gatemere	Spring	23.1	4.9	5.2	74.0	55.4
67	Rugangazi-Ntongwe	Spring	22.9	4.9	4.5	79.0	62.2
68	Rugero-Nakarinzi	Spring	23.6	4.8	6.5	34.0	22.6
69	Rugoma-Kagege	Spring	21.6	5.2	5.7	97.0	75.4
70	Rugomero-Gatemere	Spring	22.1	5	6.3	76.0	60.6
71	Rugomero-Kiravumba	Spring	23.3	4.9	4.9	55.0	38.6
72	Rugomero-Nyabugeni	Spring	22.2	5.4	6.9	127.0	104.4
73	Rugunga II-Kavomo	Spring	23.8	5.5	6.2	191.0	166.9
74	Rugunga I Kavomo	Spring	24.2	5.5	5.7	156.0	135.7
75	Ruhongore-Munyinya	Spring	22.3	5	6.6	192.0	162.5
76	Rushubije-Cogo	Spring	23.8	4.8	4.7	68.1	53.1
77	Twengebuye-Nakibingo	Spring	23.6	4.7	4.7	109.0	86.5
78	Bishunzi-Cewe	Well	23.0	7.3	6.8	2700.0	2520.0
79	Bunyari-Rugarama	Well	24.3	6.7	6.9	n.d.	462.0
80	Cimbogo-Gatete	Well	23.3	7.3	7.5	1770.0	1108.0
81	Cinyambo-Gitwe	Well	26.6	6.6	7.1	n.d.	414.0
82	Foko II-Kiyonza	Well	26.2	7.3	7.3	1770	1302.0
83	Foko I-Kiyonza	Well	23.4	7.2	7.1	n.d.	1550.0
84	Gahwijo II-Nyabikenke	Well	25.3	6.1	6.6	3290	3110.0
85	Gahwijo I-Nyabikenke	Well	24.2	7	6.8	n.d.	1219.0
86	Gasagara II-Rubuga	Well	25.3	7.5	7.8	2180	1777.0
87	GasagaraI-Rubuga	Well	26.3	7.2	7	n.d.	2900.0
88	Gifuruguti-Nyakarama	Well	23.7	6.8	6.8	3020	2860.0
89	Haga II-Nyamabuye	Well	27.3	6.7	7.2	n.d.	1282.0
90	Hambiro-Kiyonza	Well	23.6	7.5	7.3	n.d.	2400.0
91	Kabirizi II-Kigoma	Well	23.5	7.5	7	1000	903.0
92	Kadobogoro-Muramba	Well	25.5	5.8	7.2	270.0	210.0
93	Kadobori II-Rubuga	Well	26	7.2	7.2	n.d.	1990.0
94	Kadobori I-Rubuga	Well	26.5	7.7	6.9	n.d.	1153.0
95	Kamwayi II-Nyamabuye	Well	24.7	7.1	7.2	n.d.	682.0
96	Kanabugiri-Bugera	Well	23.8	6.9	7.6	950	685.0
97	Kanigo-Cinuma	Well	24	6.7	7	2630	2160.0
98	Kantuye-Ceru	Well	25.4	7.3	7.2	n.d.	848.0
99	Karago-Kibonde	Well	25.3	7.3	7.1	n.d.	762.0
100	Karago-Rukuramigabo	Well	24.1	7.3	7.4	1590.0	1270.0

S/N	Name	Source	T (°C)	Field pH	Laboratory pH	Field EC (µS/cm-25°C)	Laboratory EC(µS/cm-25°C)
101	Karisha-Kigina	Well	24.1	7.3	6.9	n.d.	1230.0
102	Kigazi-Nyakarama	Well	27.8	7.5	7.2	n.d.	2650.0
103	Kigina I-Gisenyi	Well	24	6.6	7	420	415.0
104	Kigina II-Gisenyi	Well	23.8	6.7	7.4	n.d.	352.0
105	Kigoma-Gatare	Well	23.7	6.4	6.9	599.0	536.0
106	Kigozi-Yaranda	Well	25.5	7.4	6.9	1920	1547.0
107	Kinyamateke-Nyabikenke	Well	23.7	6.5	6.3	1050	799.0
108	Kiruhura II-Muramba	Well	23.8	6.5	6.5	504.0	478.0
109	Kiruhura I-Kiyanza	Well	24.8	7	7.7	1630.0	1468.0
110	Kiyonza-Nunga	Well	25.6	7.2	6.9	n.d.	1301.0
111	Mago I-Gatete	Well	26.4	7.4	8.5	4800.0	3730.0
112	Marembo-Marembo	Well	24.3	6.5	7.3	476.0	454.0
113	Mataka-Rugasa	Well	14.1	6.7	6.9	n.d.	722.0
114	Mugombwa-Kiri	Well	24.2	7.2	7.2	n.d.	1066.0
115	Muhero I-Yaranda	Well	24.6	6.8	7	336	267.0
116	Muhero II-Yaranda	Well	24.7	6.7	7.7	401.0	362.0
117	Munyinya-Nyakarama	Well	24.4	7.2	7	n.d.	2690.0
118	Murambo-Murambi	Well	26	7.2	7.2	n.d.	1606.0
119	Murehe-Murungurira	Well	24.4	6.7	6.8	630.0	577.0
120	Mutoza-Yaranda	Well	24.5	6.8	7	938.0	807.0
121	Ndava II-Nyamabuye	Well	24.1	7.5	7.1	n.d.	821.0
122	Ngaragu-Kiri	Well	24.8	7.1	7	n.d.	1196.0
123	Ntembe II-Kiri	Well	24.3	7.2	6.9	n.d.	3420.0
124	Ntembe I-Kiri	Well	22.7	7.1	7.1	n.d.	3260.0
125	Ntwago-Murungurira	Well	24.3	6.8	7.1	1220.0	1120.0
126	Nunga II-Yaranda	Well	24.6	7	6.8	1810.0	1618.0
127	Nyange-Kumana	Well	25	5.8	7.5	n.d.	37.5
128	Rugoma-Kagege	Well	24.4	5.8	6.8	n.d.	149.2
129	Rukindo-Rugasa	Well	22.6	6.8	6.8	n.d.	447.0
130	Rukore II-Kigina	Well	25.4	7.1	6.5	n.d.	951.0
131	Runyangona II-Nyabikenke	Well	22	7	6.2	n.d.	625.0
132	Runyonza-Kabonde	Well	24.7	6.9	7.3	2180.0	2050.0
133	Ruranzi-Rwibikara	Well	25.1	7.2	7.5	n.d.	746.0
134	Ruseno-Kanyagu	Well	25.0	5.6	6.3	467.0	452.0
135	Ruyivyi II-Gitwe	Well	25.8	7	6.8	n.d.	687.0
136	Rwasama-Kiri	Well	24.2	6.6	7.3	558.0	496.0
137	Saruduha II-Rugasa	Well	23.4	7.3	7.4	n.d.	1920.0
138	Saruduha I-Rugasa	Well	22.1	7.3	6.9	n.d.	2500.0
139	Senga-Nyagisozi	Well	25.9	5.7	7.3	84.9	96.2
140	Shenga III-Rugasa	Well	24.2	6.9	6.8	n.d.	2790.0
141	Shenga II-Rugasa	Well	23.3	7	6.7	n.d.	2820.0
142	Shenga I-Rugasa	Well	23.8	6.6	6.7	n.d.	680.0
143	Susa-Gikomero	Well	24.3	6.3	6.6	n.d.	548.0

Appendix VII.3. Classification based of the dominant ions and De Moor & De Breuck (1969)

S/N	Site	Source	EC µS/cm-25°C	pH	Na %	K %	N+K %	Ca %	Mg %	HCO_3 %	Cl %	SO_4 %	NO_3 %	NO_3+SO_4 %	TDS mg/l	Dominant ion	De Moor & De Breuck (1969)
1	Cohoha-Kibonde	Lake	647.0	7.3	42.3	12.6	54.9	17.0	28.1	65.5	32.7	1.1	0.8	1.8	489.0	NaHCO3	Moderately fresh (MF)
2	Cohoha-Kigozi I	Lake	784.0	7.4	41.3	14.8	56.1	18.7	25.2	61.8	36.5	0.7	1.0	1.7	539.6	NaHCO3	Moderately fresh (MF)
3	Cohoha-Kigozi II	Lake	702.0	7.6	52.7	9.8	62.6	17.0	20.5	70.3	26.7	0.6	2.4	3.1	464.4	NaHCO3	Moderately fresh (MF)
4	Cohoha-Murambi	Lake	640.0	7.6	43.1	16.2	59.3	17.6	23.2	65.2	32.9	1.2	0.6	1.8	495.3	NaHCO3	Moderately fresh (MF)
5	Cohoha-Nunga	Lake	700.0	7.3	44.5	16.4	60.9	15.5	23.6	67.1	30.9	1.0	1.0	2.0	534.3	NaHCO3	Moderately fresh (MF)
6	Cohoha-Ruranzi	Lake	651.0	7.5	46.3	11.8	58.1	17.3	24.5	64.2	34.3	1.0	0.5	1.5	484.6	NaHCO3	Moderately fresh (MF)
7	Gacamirinda-Kinyamateke	Lake	941.0	5.9	54.4	2.4	56.8	20.6	22.6	57.0	40.2	0.6	2.2	2.8	576.8	NaHCO3	Moderately fresh (MF)
8	Gacamirinda-Shenga II	Lake	1027.0	6.9	42.0	13.1	55.0	20.7	24.2	62.8	34.2	0.9	2.1	3.0	632.4	NaHCO3	Moderately fresh (MF)
9	Nagitamo-Kabirizi I	Lake	706.0	7.0	42.9	14.9	57.8	20.9	21.3	55.5	42.8	0.7	1.0	1.7	499.4	NaHCO3	Moderately fresh (MF)
10	Narungazi-Murungazi	Lake	351.0	7.3	51.7	2.5	54.2	27.1	18.6	75.8	20.6	1.5	2.2	3.7	257.7	NaHCO3	Moderately fresh (MF)
11	Rweru-Mago I	Lake	166.1	6.7	32.0	10.0	41.9	27.8	30.3	83.5	7.7	1.6	7.2	8.8	151.1	NaHCO3	Very fresh (VF)
12	Rweru-Mago II	Lake	174.7	7.1	31.7	9.7	41.5	28.1	30.5	83.8	0.5	2.3	13.3	15.6	147.6	NaHCO3	Very fresh (VF)
13	Rweru-Nyange	Lake	166.0	6.7	28.5	9.0	37.5	30.0	32.5	78.3	14.9	3.8	2.9	6.7	147.3	NaHCO3	Very fresh (VF)
14	Rwihinda-Bishunzi	Lake	868.0	7.8	52.0	8.5	60.5	20.1	19.4	50.1	49.3	0.4	0.2	0.6	563.2	NaHCO3	Moderately fresh (MF)
15	Rwihinda-Bugera	Lake	885.0	7.4	43.7	14.0	57.7	16.0	26.4	44.2	54.5	0.7	0.7	1.3	616.2	NaCl	Moderately fresh (MF)
16	Rwihinda-Kabira	Lake	848.0	7.5	51.7	6.7	58.4	17.9	23.6	45.7	53.0	0.8	0.5	1.3	578.6	NaCl	Moderately fresh (MF)
17	Bihembe-Monge	Spring	215.0	6.9	44.7	4.4	49.2	17.7	33.1	9.6	26.5	38.0	25.9	63.9	133.5	NaSO4	Very fresh (VF)
18	Bishunzi-Munyinya	Spring	168.8	5.6	44.9	2.8	47.8	24.9	27.3	14.4	68.8	3.4	13.4	16.8	90.9	NaCl	Very fresh (VF)
19	Bugorora-Gakana	Spring	90.2	7.1	40.6	2.0	42.6	32.1	25.3	31.7	27.7	9.5	31.1	40.6	55.3	NaHCO3	Very fresh (VF)
20	Buhiga-Ntega	Spring	144.6	4.9	34.8	7.3	42.1	29.2	28.7	9.7	21.1	14.9	54.3	69.2	110.2	NaNO3	Very fresh (VF)
21	Bunyari-Rugarama	Spring	155.7	7.0	66.6	1.6	68.3	15.1	16.6	56.2	24.8	8.2	10.8	19.0	128.6	NaHCO3	Very fresh (VF)
22	Burengo-Rushubije	Spring	54.0	4.9	24.3	4.2	28.6	39.3	32.2	11.6	20.8	11.0	56.6	67.6	52.1	CaNO3	Very fresh (VF)
23	Gaharata-Murama	Spring	197.0	7.1	47.7	6.3	54.0	26.4	19.6	22.4	54.8	5.0	17.8	22.8	112.6	NaCl	Very fresh (VF)
24	Gatovu-Kanyinya	Spring	102.5	7.4	21.8	12.8	34.6	41.7	23.7	50.2	22.1	8.0	19.7	27.7	91.9	CaHCO3	Very fresh (VF)
25	Gatunguru-Rugero	Spring	34.1	6.6	35.4	4.0	39.4	32.0	28.6	51.5	8.3	10.6	29.7	40.2	26.3	NaHCO3	Very fresh (VF)
26	Gihobogo-Murungurira	Spring	150.4	6.6	52.5	2.5	55.1	26.4	18.6	59.6	18.6	10.0	11.8	21.7	115.0	NaHCO3	Very fresh (VF)
27	Gihushi-Kiravumba	Spring	279.0	5.6	55.5	1.8	57.3	27.8	14.9	12.9	73.7	4.4	8.9	13.3	141.8	NaCl	Very fresh (VF)
28	Gikombe-Ruhita	Spring	79.6	6.3	40.5	2.2	42.7	31.7	25.6	38.7	14.9	5.9	40.5	46.4	68.3	NaNO3	Very fresh (VF)

S/N	Site	Source	EC µS/cm-25°C	pH	Na %	K %	N+K %	Ca %	Mg %	HCO_3 %	Cl %	SO_4 %	NO_3 %	NO_3+SO_4 %	TDS mg/l	Dominant ions	De Moor & De Breuck (1969)
29	Kabira-Kanyinya	Spring	156.0	7.0	36.0	6.8	42.8	33.9	23.2	40.1	35.8	6.6	17.5	24.1	103.9	NaHCO3	Very fresh (VF)
30	Kabira-Renga	Spring	148.1	5.9	62.5	0.4	62.9	19.5	17.7	41.7	52.9	2.1	3.3	5.3	101.0	NaCl	Very fresh (VF)
31	Kagogo-Nyabitare	Spring	191.0	5.0	47.1	2.8	49.9	25.0	25.1	6.2	53.9	3.7	36.1	39.8	123.3	NaCl	Very fresh (VF)
32	Kanyamanza-Kagege	Spring	127.4	6.2	54.5	2.5	57.0	22.1	20.9	39.4	43.6	2.2	14.9	17.1	85.3	NaCl	Very fresh (VF)
33	Kararire-Kagege	Spring	149.2	6.5	44.9	3.7	48.6	26.6	24.8	14.2	64.6	13.2	7.9	21.2	77.7	NaCl	Very fresh (VF)
34	Karira-Gatemere	Spring	201.0	6.0	44.8	4.7	49.5	26.8	23.7	16.5	49.6	25.1	8.8	33.9	115.5	NaCl	Very fresh (VF)
35	Karobogo-Kanyinya	Spring	105.2	7.2	7.5	46.2	53.6	26.4	20.0	24.2	28.2	12.1	35.5	47.6	96.0	KNO3	Very fresh (VF)
36	Kididiri-Buhasa	Spring	72.7	5.4	43.1	4.2	47.2	28.0	24.7	54.7	36.8	8.2	0.3	8.5	55.1	NaHCO3	Very fresh (VF)
37	Kigomero-Munyinya	Spring	85.7	6.2	40.3	1.8	42.0	33.0	25.0	28.3	39.6	7.2	24.9	32.1	53.4	NaCl	Very fresh (VF)
38	Kigoti-Munzenze	Spring	162.4	5.8	48.1	1.3	49.4	25.9	24.7	37.9	37.1	1.7	23.3	25.0	106.0	NaHCO3	Very fresh (VF)
39	Kinyangoro-Kumana	Spring	55.8	7.0	32.9	1.7	34.6	37.2	28.2	53.5	0.2	4.7	41.6	46.3	169.5	CaHCO3	Very fresh (VF)
40	Kinyangurube-Karehe	Spring	118.9	5.3	58.2	0.5	58.7	21.4	19.9	10.4	25.9	16.5	47.1	63.6	61.1	NaNO3	Very fresh (VF)
41	Kinywamagana-Kigarama	Spring	87.7	5.2	53.2	2.3	55.5	24.3	20.2	13.4	64.6	3.3	18.6	21.9	48.1	NaCl	Very fresh (VF)
42	Kiramata-Monge	Spring	155.2	7.4	41.9	6.6	48.4	29.1	22.5	43.7	8.6	11.2	36.5	47.7	79.3	NaHCO3	Fresh (F)
43	Kirunduzi-Mutara	Spring	44.6	7.1	45.1	1.7	46.8	32.0	21.2	27.4	23.8	14.4	34.4	48.9	39.6	NaNO3	Very fresh (VF)
44	Mamfu-Kiyonza	Spring	459.0	7.1	27.3	0.1	27.5	51.8	20.7	76.3	0.0	18.7	5.0	23.7	402.0	CaHCO3	Fresh (F)
45	Maramya-Mwenya	Spring	48.4	5.3	39.8	1.2	41.0	33.5	25.6	19.5	39.2	8.9	32.4	41.3	60.8	NaNO3	Very fresh (VF)
46	Mudahinyuka-Kigina II	Spring	69.2	5.7	39.6	5.1	44.7	37.6	17.7	59.7	31.2	8.6	0.5	9.1	55.2	NaHCO3	Very fresh (VF)
47	Mukagezi-Ntogwe	Spring	89.0	6.0	31.0	5.4	36.4	35.7	28.0	18.2	8.5	6.9	66.4	73.3	83.1	NaNO3	Very fresh (VF)
48	Mukuyo-Kiri	Spring	766.0	7.0	64.7	1.8	66.5	23.8	9.7	67.1	5.8	25.0	2.1	27.1	655.3	NaHCO3	Moderately fresh (MF)
49	Musave-Mugobe	Spring	179.8	5.6	39.5	4.5	44.0	37.4	18.5	36.0	21.5	35.3	7.2	42.5	101.7	NaHCO3	Very fresh (VF)
50	Musave-Rutabo	Spring	225.0	7.1	59.8	0.3	60.0	19.5	20.4	19.6	69.6	1.9	8.9	10.8	110.9	NaCl	Very fresh (VF)
51	Mutetema-Muyange	Spring	74.4	5.8	33.2	3.5	36.7	31.4	31.9	64.0	17.7	3.5	14.9	18.3	58.7	NaHCO3	Very fresh (VF)
52	Mvyayingabo-Mutara	Spring	129.3	6.7	38.2	2.5	40.8	27.5	31.8	40.2	10.1	20.6	29.2	49.7	82.2	NaNO3	Very fresh (VF)
53	Mwenya-Mwenya	Spring	196.9	5.8	40.1	0.7	40.8	32.9	26.2	39.3	19.0	22.0	19.7	41.8	110.3	NaSO4	Very fresh (VF)
54	Mwenya-Rwimbogo	Spring	87.2	6.2	35.3	2.6	37.9	32.2	29.9	30.8	25.6	5.0	38.6	43.6	72.3	NaNO3	Very fresh (VF)
55	Nagikono-Kinyangurube	Spring	134.7	5.7	39.6	3.1	42.7	30.3	27.0	54.4	21.5	2.3	21.8	24.1	100.1	NaHCO3	Very fresh (VF)
56	Nakabingo	Spring	169.1	6.8	29.9	2.3	32.2	37.1	30.7	63.0	22.7	7.7	6.6	14.4	116.2	CaHCO3	Very fresh (VF)

S/N	Site	Source	EC µS/cm-25°C	pH	Na %	K %	N+K %	Ca %	Mg %	HCO_3 %	Cl %	SO_4 %	NO_3 %	NO_3+SO_4 %	TDS mg/l	Dominant ion	De Moor & De Breuck (1969)
57	Nakabingo II-Gihosha	Spring	134.6	4.9	25.5	12.1	37.6	33.9	28.5	5.5	18.6	25.5	50.5	76.0	101.7	NaNO3	Very fresh (VF)
58	Nakabingo-Gatemere	Spring	59.1	6.2	44.2	3.0	47.3	28.3	24.4	26.3	46.7	19.9	7.0	27.0	66.8	NaCl	Very fresh (VF)
59	Nakarambo-Rutabo	Spring	174.3	6.1	52.2	1.1	53.3	25.6	21.0	22.7	62.1	1.6	13.6	15.2	122.7	NaCl	Very fresh (VF)
60	Nakivumbura-Monge	Spring	134.4	5.6	42.8	4.9	47.8	26.8	25.4	43.0	31.6	17.5	7.9	25.4	98.5	NaHCO3	Very fresh (VF)
61	Narukere-Gihosha	Spring	57.3	4.9	48.1	1.7	49.8	30.3	19.9	23.2	25.6	4.9	46.3	51.2	57.1	NaNO3	Very fresh (VF)
62	Narutambwe-Kireka	Spring	80.7	6.6	59.8	3.5	63.3	3.5	33.2	21.8	4.1	4.2	70.0	74.2	51.5	NaNO3	Very fresh (VF)
63	Nyabitare-Munyinya	Spring	179.5	5.8	41.9	1.5	43.5	33.0	23.6	17.5	51.3	6.4	24.8	31.1	111.6	NaCl	Very fresh (VF)
64	Nyaruziba-Mutara	Spring	167.4	6.2	23.3	7.1	30.3	35.9	33.8	31.5	22.4	26.0	20.1	46.1	122.4	CaSO4	Very fresh (VF)
65	RamboII-Gatwe	Spring	178.6	6.9	42.0	2.6	44.5	23.6	31.9	17.2	12.4	20.6	49.9	70.5	121.6	NaNO3	Very fresh (VF)
66	Rubira-Gatemere	Spring	55.4	5.2	58.9	2.3	61.2	17.8	21.0	33.7	29.1	5.4	31.7	37.2	44.6	NaNO3	Very fresh (VF)
67	Rugangazi-Ntogwe	Spring	62.2	4.5	41.8	10.8	52.6	25.6	21.8	30.5	27.7	5.1	36.6	41.8	51.3	NaNO3	Very fresh (VF)
68	Rugero-Nakarinzi	Spring	22.6	6.5	26.0	1.3	27.4	43.7	28.9	79.6	5.7	8.3	6.4	14.7	31.5	CaHCO3	Very fresh (VF)
69	Rugoma-Kagege	Spring	75.4	5.7	33.9	5.1	39.0	33.9	27.1	25.2	46.4	15.1	13.3	28.4	50.1	NaCl	Very fresh (VF)
70	Rugomero-Gatemere	Spring	60.6	6.3	44.3	1.3	45.6	30.3	24.1	25.6	3.2	8.0	63.2	71.2	51.1	NaNO3	Very fresh (VF)
71	Rugomero-Kiravumba	Spring	38.6	4.9	54.1	2.9	56.9	23.1	20.0	57.7	30.6	8.4	3.3	11.7	43.4	NaHCO3	Very fresh (VF)
72	Rugomero-Nyabugeni	Spring	104.4	6.9	50.0	1.9	51.9	23.7	24.4	31.2	58.9	5.3	4.5	9.9	47.9	NaCl	Very fresh (VF)
73	Rugunga II- Kavomo	Spring	166.9	6.2	53.8	2.4	56.1	12.0	31.8	47.0	24.1	24.2	4.8	29.0	94.8	NaHCO3	Very fresh (VF)
74	Rugunga I-Kavomo	Spring	135.7	5.7	61.6	2.2	63.8	18.5	17.7	32.4	39.7	11.4	16.4	27.8	91.9	NaCl	Very fresh (VF)
75	Ruhongore-Munyinya	Spring	162.5	6.6	41.9	2.5	44.4	30.5	25.1	21.0	50.8	11.2	17.0	28.1	105.9	NaCl	Very fresh (VF)
76	Rushubije-Cogo	Spring	53.1	4.7	50.2	4.3	54.5	19.3	26.2	18.6	21.8	5.0	54.5	59.6	39.4	NaNO3	Very fresh (VF)
77	Twengebuye-Nakabingo	Spring	86.5	4.7	32.5	4.0	36.5	35.3	28.3	7.8	20.3	3.7	68.3	72.0	55.7	NaNO3	Very fresh (VF)
78	Bishunzi-Cewe	Well	2520.0	6.8	50.2	12.4	62.6	11.8	25.6	38.8	46.9	13.8	0.5	14.3	1632.2	NaCl	Moderately brackish (MB)
79	Bunyari-Rugarama	Well	462.0	6.9	18.1	32.4	50.6	22.7	26.8	79.9	7.2	4.8	8.0	12.8	388.8	KHCO3	Fresh (F)
80	Cimbogo I-Gatete	Well	1108.0	7.5	11.6	15.7	27.3	37.8	34.8	92.0	5.4	0.7	1.9	2.6	1018.4	CaHCO3	Weakly fresh (WF)
81	Cinyambo-Gitwe	Well	414.0	7.1	25.0	24.6	49.7	28.7	21.6	77.2	16.7	3.4	2.8	6.1	355.8	NaHCO3	Fresh (F)
82	Foko II-Kiyonza	Well	1302.0	7.3	37.6	6.6	44.2	33.7	22.0	56.4	22.3	15.0	6.2	21.2	1082.0	NaHCO3	Weakly fresh (WF)
83	Foko I-Kiyonza	Well	1550.0	7.1	46.2	6.7	52.8	27.8	19.3	61.5	4.4	27.4	6.8	34.1	1289.1	NaHCO3	Weakly fresh (WF)
84	Gahwijo II-Nyabikenke	Well	1219.0	6.6	22.3	12.7	35.0	48.5	16.5	50.5	25.5	23.5	0.5	24.0	989.8	CaHCO3	Weakly fresh (WF)

S/N	Site	Source	EC µS/cm-25°C	pH	Na %	K %	N+K %	Ca %	Mg %	HCO_3 %	Cl %	SO_4 %	NO_3 %	NO_3+SO_4 %	TDS mg/l	Dominant ion	De Moor & De Breuck (1969)
85	Gahwijo I-Nyabikenke	Well	3110.0	6.8	63.1	3.7	66.8	18.6	14.6	49.2	36.8	12.9	1.1	14.0	2222.6	NaHCO3	Moderately brackish (MB)
86	Gasagara II-Rubuga	Well	2900.0	7.8	63.9	3.1	67.0	12.9	20.1	72.8	13.2	11.3	2.7	14.0	2380.7	NaHCO3	Moderately brackish (MB)
87	Gasagara I-Rubuga	Well	1777.0	7.0	35.5	4.5	40.0	41.9	18.1	45.7	6.9	46.2	1.2	47.4	1507.2	CaSO4	Weakly fresh (WF)
88	Gifuruguti-Nyakarama	Well	2860.0	6.8	51.6	4.9	56.5	26.3	17.2	35.5	35.9	27.5	1.0	28.6	1762.6	NaCl	Moderately brackish (MB)
89	Haga II-Nyamabuye	Well	1282.0	7.2	40.2	7.1	47.2	32.3	20.5	73.1	20.8	4.8	1.3	6.1	844.8	NaHCO3	Weakly fresh (WF)
90	Hambiro-Kiyonza	Well	2400.0	7.3	46.6	4.3	50.8	29.2	19.9	48.5	23.3	22.9	5.3	28.2	1711.2	NaHCO3	Moderately brackish (MB)
91	Kabirizi II-Kigoma	Well	903.0	7.0	22.0	15.3	37.3	46.0	16.7	52.3	18.2	20.6	9.0	29.6	627.4	CaHCO3	Moderately fresh (MF)
92	Kadobogoro-Muramba	Well	210.0	7.2	50.6	2.2	52.8	30.6	16.6	49.3	20.4	24.6	5.7	30.3	134.9	NaHCO3	Very fresh (VF)
93	Kadobori II-Rubuga	Well	1990.0	7.2	35.2	5.7	40.9	40.1	19.1	48.5	22.0	27.5	1.9	29.5	1485.4	NaHCO3	Weakly fresh (WF)
94	Kadobori I-Rubuga	Well	1153.0	6.9	35.1	13.8	48.9	34.9	16.1	48.3	33.6	15.8	2.3	18.1	752.9	NaHCO3	Moderately fresh (MF)
95	Kamwayi II-Nyababuye	Well	682.0	7.2	46.2	0.1	46.2	34.0	19.7	65.5	3.9	10.4	20.2	30.6	540.3	NaHCO3	Moderately fresh (MF)
96	Kanabugiri I-Bugera	Well	685.0	7.6	43.7	7.8	51.5	18.3	30.2	62.0	19.9	16.9	1.2	18.1	538.5	NaHCO3	Moderately fresh (MF)
97	Kanigo-Cinuma	Well	2160.0	7.0	56.0	2.9	58.9	15.5	25.6	36.5	15.2	43.8	4.5	48.3	1526.7	NaSO4	Weakly fresh (WF)
98	Kantuye-Ceru	Well	848.0	7.2	39.9	17.0	57.0	27.7	15.3	76.5	21.3	0.5	1.6	2.1	722.2	NaHCO3	Moderately fresh (MF)
99	Karago-Kibonde	Well	762.0	7.1	27.6	5.5	33.1	54.8	12.1	47.2	48.8	2.9	1.1	3.9	528.0	CaCl	Moderately fresh (MF)
100	Karago-Rukuramigabo	Well	1270.0	7.4	58.5	21.3	79.7	5.5	14.8	85.0	13.2	0.3	1.6	1.8	1139.2	NaHCO3	Weakly fresh (WF)
101	Karisha-Kigina	Well	1230.0	6.9	52.4	3.0	55.4	27.7	16.9	73.6	19.2	2.2	5.1	7.3	1007.8	NaHCO3	Weakly fresh (WF)
102	Kigazi-Nyakarama	Well	2650.0	7.2	61.0	0.2	61.3	19.6	19.2	66.2	7.9	20.9	4.9	25.9	2056.0	NaHCO3	Moderately brackish (MB)
103	Kigina I-Gisenyi	Well	415.0	7.4	23.9	0.3	24.2	55.2	20.6	85.0	9.0	3.6	2.3	5.9	339.3	CaHCO3	Fresh (F)
104	Kigina II-Gisenyi	Well	352.0	7.0	33.5	0.1	33.6	36.9	29.5	76.5	9.3	7.3	6.9	14.1	256.5	CaHCO3	Fresh (F)
105	Kigoma-Gatare	Well	536.0	6.9	36.5	2.4	38.9	41.6	19.5	35.9	39.1	22.6	2.4	25.0	384.2	CaCl	Fresh (F)
106	Kigozi-Yaranda	Well	1547.0	6.9	37.9	8.9	46.8	29.1	24.1	62.9	17.9	14.8	4.4	19.2	1171.2	NaHCO3	Weakly fresh (WF)
107	Kinyamateke-Nyabikenke	Well	799.0	6.3	40.7	5.8	46.5	24.5	28.9	32.9	27.8	28.3	11.0	39.3	571.2	NaSO4	Moderately fresh (MF)
108	Kiruhura II-Muramba	Well	478.0	6.5	30.7	0.8	31.4	56.9	11.6	56.1	27.5	15.1	1.3	16.4	359.3	CaHCO3	Fresh (F)
109	Kiruhura I-Kiyanza	Well	1468.0	7.7	50.7	5.4	56.1	28.4	15.5	55.7	27.2	15.9	1.1	17.1	1058.0	NaHCO3	Weakly fresh (WF)
110	Kiyonza-Nunga	Well	1301.0	6.9	30.5	10.2	40.7	27.3	32.0	56.9	34.6	7.6	0.9	8.5	999.8	NaHCO3	Weakly fresh (WF)
111	Mago I-Gatete	Well	3730.0	8.5	75.9	17.9	93.8	5.5	0.7	81.6	10.0	8.1	0.3	8.3	3229.1	NaHCO3	Brackish (B)
112	Marembo-Marembo	Well	454.0	7.3	28.0	10.7	38.7	38.8	22.5	75.2	13.2	0.8	10.8	11.6	368.6	CaHCO3	Fresh (F)

S/N	Site	Source	EC (µS/cm-25°C)	pH	Na %	K %	N+K %	Ca %	Mg %	HCO_3 %	Cl %	SO_4 %	NO_3 %	NO_3+SO_4 %	TDS mg/l	Dominant ion	De Moor & De Breuck (1969)
113	Mataka-Rugasa	Well	722.0	6.9	25.4	6.7	32.1	38.7	29.3	87.3	7.2	2.9	2.6	5.5	589.6	CaHCO3	Moderately fresh (MF)
114	Mugombwa-Kiri	Well	1066.0	7.2	37.8	5.1	42.9	32.2	25.0	67.4	8.7	14.6	9.3	23.9	909.1	NaHCO3	Weakly fresh (WF)
115	Muhero I -Yaranda	Well	267.0	7.0	33.7	1.2	34.9	42.6	22.4	51.5	38.1	5.7	4.7	10.4	179.4	CaHCO3	Very fresh (VF)
116	Muhero II - Yaranda	Well	362.0	7.7	39.8	7.6	47.4	30.7	21.9	76.4	16.8	2.4	4.4	6.8	282.1	NaHCO3	Fresh (F)
117	Munyinya-Nyakarama	Well	2690.0	7.0	50.8	5.9	56.7	25.1	18.2	62.3	13.4	19.7	4.5	24.2	2068.4	NaHCO3	Moderately brackish (MB)
118	Murambo-Murambi	Well	1606.0	7.2	41.8	11.6	53.4	24.3	22.3	60.8	26.1	12.7	0.5	13.2	1363.5	NaHCO3	Weakly fresh (WF)
119	Murehe-Murungurira	Well	577.0	6.8	59.0	0.8	59.9	30.4	9.8	51.9	22.5	20.0	5.5	25.5	407.2	NaHCO3	Moderately fresh (MF)
120	Mutoza-Yaranda	Well	807.0	7.0	52.6	0.7	53.3	38.9	7.9	61.7	29.8	8.4	0.0	8.5	587.5	NaHCO3	Moderately fresh (MF)
121	Ndava II-Nyamabuye	Well	821.0	7.1	47.1	4.3	51.4	26.9	21.7	71.9	24.6	0.5	3.0	3.5	628.5	NaHCO3	Moderately fresh (MF)
122	Ngaragu-Kiri	Well	1196.0	7.0	60.8	0.3	61.1	22.4	16.5	69.3	2.5	23.2	5.0	28.2	1029.5	NaHCO3	Weakly fresh (WF)
123	Ntembe II-Kiri	Well	3420.0	6.9	47.5	9.0	56.5	27.1	16.4	45.7	27.9	22.9	3.5	26.4	2256.5	NaHCO3	Moderately brackish (MB)
124	Ntembe I-Kiri	Well	3260.0	7.1	64.3	3.9	68.2	17.6	14.2	50.5	16.6	31.0	1.9	32.8	2556.3	NaHCO3	Moderately brackish (MB)
125	Ntwago-Murungurira	Well	1120.0	7.1	77.4	0.1	77.5	13.0	9.5	38.8	41.7	17.9	1.6	19.5	741.0	NaCl	Moderately fresh (MF)
126	Nunga II-Yaranda	Well	1618.0	6.8	52.2	4.9	57.1	30.0	12.9	51.5	33.7	13.9	0.9	14.7	1137.1	NaHCO3	Weakly fresh (WF)
127	Nyange-Kumana	Well	37.5	7.5	27.8	11.7	39.6	33.9	26.5	44.8	39.8	6.9	8.6	15.4	44.4	NaHCO3	Very fresh (VF)
128	Rugoma-Kagege	Well	149.2	6.8	24.0	22.3	46.3	34.0	19.7	47.1	26.8	18.4	7.7	26.1	129.0	NaHCO3	Very fresh (VF)
129	Rukindo-Rugasa	Well	447.0	6.8	26.9	10.4	37.3	40.3	22.4	73.0	2.4	20.2	4.4	24.6	391.4	CaHCO3	Fresh (F)
130	Rukore-II-Kigina	Well	951.0	6.5	28.7	11.1	39.9	40.2	19.9	67.8	26.9	4.5	0.8	5.3	774.4	CaHCO3	Moderately fresh (MF)
131	Runyangona II-Nyabikenke	Well	625.0	6.2	20.0	8.6	28.7	43.3	28.1	71.7	26.4	0.9	1.0	1.9	493.8	CaHCO3	Moderately fresh (MF)
132	Runyonza-Kabonde	Well	2050.0	7.3	52.3	9.3	61.6	18.3	20.1	48.3	35.2	15.6	0.9	16.5	1216.3	NaHCO3	Weakly fresh (WF)
133	Ruranzi-Rwibikara	Well	746.0	7.5	43.2	8.4	51.7	26.4	21.9	71.1	27.6	1.0	0.4	1.4	571.9	NaHCO3	Moderately fresh (MF)
134	Ruseno-Kanyagu	Well	452.0	6.3	67.0	6.6	73.5	21.1	5.4	44.1	42.9	11.6	1.4	13.0	287.3	NaHCO3	Fresh (F)
135	Ruyivyi II-Gitwe	Well	687.0	6.8	29.3	17.3	46.6	34.7	18.7	69.2	23.1	5.1	2.5	7.7	555.8	NaHCO3	Moderately fresh (MF)
136	Rwasama-Kiri	Well	496.0	7.3	46.5	1.2	47.6	33.1	19.3	58.5	12.6	21.4	7.5	28.9	417.3	NaHCO3	Fresh (F)
137	Saruduha II-Rugasa	Well	1920.0	7.4	46.9	5.4	52.2	23.1	24.7	70.0	16.2	13.4	0.4	13.8	1574.2	NaHCO3	Weakly fresh (WF)
138	Saruduha I-Rugasa	Well	2500.0	6.9	48.3	1.0	49.3	29.4	21.3	35.9	38.8	21.9	3.3	25.3	1622.2	NaCl	Moderately brackish (MB)
139	Senga-Nyagisozi	Well	96.2	7.3	28.3	5.2	33.5	49.3	17.2	89.8	3.8	4.6	1.8	6.4	93.5	CaHCO3	Very fresh (VF)
140	Shenga III-Rugasa	Well	2790.0	6.7	63.9	4.3	68.2	17.8	14.0	38.5	54.6	5.8	1.0	6.9	1748.6	NaCl	Moderately brackish (MB)
141	Shenga II-Rugasa	Well	2820.0	6.8	68.8	3.7	72.5	15.2	12.4	38.6	50.8	10.1	0.6	10.6	1805.0	NaCl	Moderately brackish (MB)
142	Shenga I- Rugasa	Well	680.0	6.7	45.9	18.6	64.4	20.4	15.1	54.9	43.1	1.0	1.0	2.0	506.4	NaHCO3	Moderately fresh (MF)
143	Susa-Gikomero	Well	548.0	6.6	31.8	19.6	51.3	25.6	23.1	15.3	46.1	16.2	22.4	38.6	375.7	NaCl	Fresh (F)

Appendix VII.4. Details of the X-ray analysis of the salt soils

VI.4.1. Details of the X-ray analysis of the salt sample Mago 2011/1 (Busoni)

File: 587A0001.DI 8-Apr-2011 15:25

PC-APD, Diffraction software PC-APD, Diffraction software

Sample identification:	11/702 powder
Data measured at:	8-Apr-2011 11:32:00
Diffractometer type:	PW3710 BASED
Tube anode:	Cu
Generator tension [kV]:	40
Generator current [mA]:	30
Wavelength Alpha1 [Å]:	1.54060
Wavelength Alpha2 [Å]:	1.54439
Intensity ratio (alpha2/alpha1):	0.500
Divergence slit:	AUTOMATIC
Irradiated length [mm]:	12
Receiving slit:	0.1
Monochromator used:	YES
Start angle [°2θ]:	3.010
End angle [°2θ]:	69.990
Step size [°2θ]:	0.020
Maximum intensity:	3203.560
Time per step [s]:	1.000
Type of scan:	CONTINUOUS
Intensities converted to:	FIXED
Peak positions defined by:	Minimum of 2nd derivative of peak
Minimum peak tip width:	0.20
Maximum peak tip width:	1.00
Peak base width:	2.00
Minimum significance:	0.75
Number of peaks:	36

Angle [°2θ]	d-value α1 [Å]	d-value α2 [Å]	Peak width [°2θ]	Peak int [counts]	Back. int [counts]	Rel. int [%]	Signif.
8.775	10.0691	10.0939	0.240	161	166	5.0	1.05
12.280	7.2019	7.2196	0.200	3204	106	100.0	15.88
17.935	4.9418	4.9540	0.480	52	45	1.6	3.89
19.785	4.4837	4.4947	0.200	400	46	12.5	3.87
21.340	4.1604	4.1706	0.200	605	48	18.9	4.54
23.025	3.8596	3.8691	0.240	98	46	3.1	1.14
24.800	3.5872	3.5960	0.200	1369	48	42.7	12.68
26.565	3.3527	3.3610	0.240	756	49	23.6	7.77
27.320	3.2618	3.2698	0.200	24	49	0.7	0.81
31.630	2.8265	2.8334	0.240	213	36	6.7	4.23
32.090	2.7870	2.7938	0.200	23	35	0.7	1.22
33.535	2.6701	2.6767	0.240	94	32	2.9	1.55
34.880	2.5702	2.5765	0.320	185	30	5.8	9.07
35.855	2.5025	2.5086	0.200	180	29	5.6	2.59
36.990	2.4283	2.4342	0.200	174	28	5.4	3.31
37.655	2.3869	2.3928	0.200	119	27	3.7	2.10
38.330	2.3464	2.3522	0.280	204	26	6.4	5.59
39.225	2.2949	2.3005	0.400	98	25	3.1	4.27
40.320	2.2351	2.2406	0.240	52	24	1.6	1.23
41.595	2.1695	2.1748	0.320	44	22	1.4	1.99
42.425	2.1289	2.1341	0.240	42	21	1.3	1.44

Halite ?

goethite α, FeOOH

File: 587A0001.DI 8-Apr-2011 15:25

PC-APD, Diffraction software PC-APD, Diffraction software

Angle [°2θ]	d-value α1 [Å]	d-value α2 [Å]	Peak width [°2θ]	Peak int [counts]	Back. int [counts]	Rel. int [%]	Signif.
45.380	1.9969	2.0018	0.200	110	19	3.4	3.32
46.615	1.9468	1.9516	0.400	23	18	0.7	0.89
47.890	1.8979	1.9026	0.240	34	18	1.1	3.26
49.525	1.8390	1.8436	0.320	18	16	0.6	0.94
50.055	1.8208	1.8253	0.200	37	16	1.2	2.23
51.005	1.7891	1.7935	0.320	40	16	1.2	3.20
53.765	1.7036	1.7078	0.200	59	15	1.9	1.96
54.815	1.6734	1.6775	0.240	74	15	2.3	1.77
56.570	1.6256	1.6296	0.480	26	15	0.8	0.77
58.045	1.5877	1.5917	0.320	16	16	0.5	0.99
59.935	1.5421	1.5459	0.320	37	16	1.2	2.48
62.180	1.4917	1.4954	0.200	108	16	3.4	3.03
63.740	1.4589	1.4625	0.240	18	17	0.6	1.37
66.270	1.4092	1.4127	0.480	6	17	0.2	1.41
68.190	1.3741	1.3775	0.320	18	18	0.6	2.41

Peak List

No.	Pos. [°2Th.]	Height [cts]	FWHM [°2T	d-spacing [Å]	Rel. Int. [%]	Tip width [°	Matched by
1	8,7679	33,09	0,2880	10,07719	3,21	0,2400	78-1928
2	12,2891	906,50	0,1680	7,19655	87,88	0,1400	80-0885
3	17,8177	18,89	0,5760	4,97407	1,83	0,4800	78-1928
4	19,7721	174,90	0,2400	4,48659	16,96	0,2000	80-0885; 78-1928
5	20,7950	196,44	0,1440	4,26814	19,04	0,1200	83-0539
6	21,3255	275,37	0,2400	4,16315	26,70	0,2000	80-0885 → goethite
7	24,7871	853,00	0,1200	3,58904	82,69	0,1000	80-0885
8	26,5619	1031,50	0,0720	3,35312	100,00	0,0600	83-0539; 80-0885; 78-1928
9	27,7831	117,04	0,0720	3,20845	11,35	0,0600	
10	31,6283	250,16	0,0960	2,82660	24,25	0,0800	80-0885
11	33,4977	76,29	0,1440	2,67301	7,40	0,1200	78-1928
12	34,8646	156,93	0,2880	2,57127	15,21	0,2400	80-0885; 78-1928
13	35,8250	148,14	0,3840	2,50452	14,36	0,3200	80-0885; 78-1928
14	36,9582	164,64	0,1920	2,43028	15,96	0,1600	78-1928
15	37,5902	107,41	0,2880	2,39086	10,41	0,2400	80-0885; 78-1928
16	38,3250	186,62	0,3360	2,34670	18,09	0,2800	80-0885; 78-1928
17	39,1020	99,01	0,3840	2,30183	9,60	0,3200	80-0885
18	40,2961	45,87	0,2880	2,23634	4,45	0,2400	83-0539; 80-0885; 78-1928
19	41,4577	38,65	0,5760	2,17632	3,75	0,4800	80-0885; 78-1928
20	42,3897	115,20	0,0720	2,13060	11,17	0,0600	83-0539; 80-0885
21	45,3700	129,18	0,1920	1,99733	12,52	0,1600	80-0885; 78-1928
22	50,0513	48,40	0,1440	1,82093	4,69	0,1200	83-0539; 80-0885; 78-1928
23	50,9687	51,26	0,2880	1,79029	4,97	0,2400	80-0885
24	53,7596	65,33	0,2880	1,70375	6,33	0,2400	80-0885; 78-1928
25	54,9770	55,90	0,9600	1,66887	5,42	0,8000	83-0539; 80-0885; 78-1928
26	59,8818	81,34	0,1440	1,54336	7,89	0,1200	83-0539; 80-0885; 78-1928
27	62,1875	183,51	0,2400	1,49156	17,79	0,2000	80-0885; 78-1928
28	63,7974	30,13	0,5760	1,45774	2,92	0,4800	83-0539; 80-0885; 78-1928
29	67,6603	50,54	0,1920	1,38361	4,90	0,1600	83-0539; 78-1928
30	68,1032	74,87	0,1440	1,37568	7,26	0,1200	83-0539; 80-0885; 78-1928

VI.2.2. Details of the X-ray analysis of the salt sample Mago 2011/2 (Busoni)

File: 587A0002.DI 8-Apr-2011 15:2

PC-APD, Diffraction software PC-APD, Diffraction softwar

Sample identification:	11/703 powder
Data measured at:	8-Apr-2011 12:28:00
Diffractometer type:	PW3710 BASED
Tube anode:	Cu
Generator tension [kV]:	40
Generator current [mA]:	30
Wavelength Alpha1 [Å]:	1.54060
Wavelength Alpha2 [Å]:	1.54439
Intensity ratio (alpha2/alpha1):	0.500
Divergence slit:	AUTOMATIC
Irradiated length [mm]:	12
Receiving slit:	0.1
Monochromator used:	YES
Start angle [°2θ]:	3.010
End angle [°2θ]:	69.990
Step size [°2θ]:	0.020
Maximum intensity:	2209.000
Time per step [s]:	1.000
Type of scan:	CONTINUOUS
Intensities converted to:	FIXED
Peak positions defined by:	Minimum of 2nd derivative of peak
Minimum peak tip width:	0.20
Maximum peak tip width:	1.00
Peak base width:	2.00
Minimum significance:	0.75
Number of peaks:	42

Angle [°2θ]	d-value α1 [Å]	d-value α2 [Å]	Peak width [°2θ]	Peak int [counts]	Back. int [counts]	Rel. int [%]	Signif.
8.790	10.0519	10.0767	0.240	100	146	4.5	0.75
9.620	9.1864	9.2090	0.240	30	128	1.4	1.00
11.535	7.6653	7.6841	0.240	2209	90	100.0	8.71
12.285	7.1990	7.2167	0.280	1832	79	82.9	18.49
17.850	4.9651	4.9774	0.320	35	44	1.6	1.51
18.945	4.6806	4.6921	0.240	210	41	9.5	2.96
19.850	4.4692	4.4802	0.240	384	40	17.4	2.64
20.735	4.2804	4.2909	0.240	543	37	24.6	3.45
21.360	4.1565	4.1667	0.200	529	37	23.9	5.04
23.320	3.8114	3.8208	0.240	339	34	15.3	2.72
24.805	3.5865	3.5953	0.200	870	31	39.4	9.26
26.580	3.3509	3.3591	0.240	1475	29	66.8	11.69
29.005	3.0760	3.0836	0.200	154	27	7.0	4.82
31.790	2.8126	2.8195	0.480	125	25	5.7	5.83
32.735	2.7335	2.7403	0.240	36	24	1.6	1.18
33.785	2.6509	2.6575	0.240	137	23	6.2	1.88
34.925	2.5670	2.5733	0.240	166	23	7.5	4.89
35.915	2.4984	2.5046	0.200	144	22	6.5	2.59
36.485	2.4607	2.4668	0.200	86	22	3.9	1.70
37.025	2.4261	2.4320	0.200	159	21	7.2	3.13
38.355	2.3449	2.3507	0.200	188	21	8.5	1.95

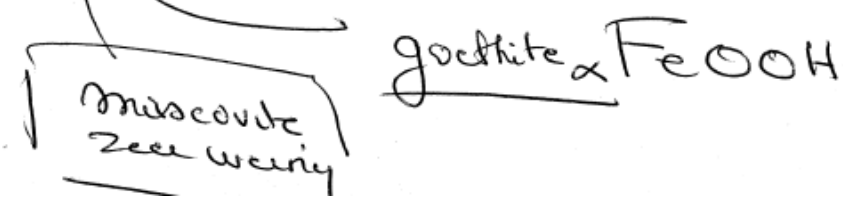

File: 587A0002.DI 8-Apr-2011 15:24

PC-APD, Diffraction software PC-APD, Diffraction software

Angle [°2θ]	d-value α1 [Å]	d-value α2 [Å]	Peak width [°2θ]	Peak int [counts]	Back. int [counts]	Rel. int [%]	Signif.
39.345	2.2882	2.2938	0.240	149	20	6.7	2.19
40.210	2.2409	2.2464	0.200	56	19	2.5	1.17
41.595	2.1695	2.1748	0.240	48	20	2.2	1.02
42.430	2.1287	2.1339	0.320	46	19	2.1	14.92
45.420	1.9952	2.0002	0.240	169	18	7.7	3.84
47.835	1.9000	1.9047	0.240	53	18	2.4	1.89
48.740	1.8668	1.8714	0.200	96	17	4.3	3.69
49.465	1.8411	1.8457	0.240	18	17	0.8	0.76
50.125	1.8184	1.8229	0.240	74	17	3.3	2.78
51.125	1.7852	1.7896	0.320	30	16	1.4	1.67
53.755	1.7039	1.7081	0.240	50	16	2.3	2.69
55.170	1.6635	1.6676	0.480	64	16	2.9	3.52
56.480	1.6280	1.6320	0.320	37	16	1.7	1.30
58.030	1.5881	1.5920	0.240	17	16	0.8	2.02
59.485	1.5527	1.5565	0.240	31	16	1.4	0.76
59.930	1.5422	1.5460	0.240	36	16	1.6	0.76
62.220	1.4909	1.4945	0.360	96	16	4.3	11.45
63.770	1.4583	1.4619	0.400	18	15	0.8	1.22
64.990	1.4338	1.4374	0.320	8	16	0.4	1.44
66.315	1.4084	1.4118	0.480	5	15	0.2	1.43
68.170	1.3745	1.3779	0.240	25	16	1.1	1.51

Peak List

No.	Pos. [°2Th.]	Height [cts]	FWHM [°2Td-spacing [Å]	Rel. Int. [%]	Tip width [°	Matched by
1	11,5812	888,06	0,1440	7,63480	53,69	0,1200	74-1904
2	12,3061	502,76	0,1680	7,18666	30,39	0,1400	80-0885
3	17,8479	15,64	0,5760	4,96571	0,95	0,4800	
4	18,9692	152,43	0,0960	4,67464	9,21	0,0800	74-2036
5	19,3990	71,86	0,1440	4,57203	4,34	0,1200	
6	19,8022	175,17	0,1440	4,47985	10,59	0,1200	80-0885
7	20,7850	389,71	0,0720	4,27019	23,56	0,0600	83-0539; 74-1904
8	21,3459	268,13	0,2400	4,15922	16,21	0,2000	80-0885
9	23,3220	290,90	0,0960	3,81109	17,59	0,0800	80-0885; 74-2036; 74-1904
10	24,7738	556,24	0,1440	3,59094	33,63	0,1200	80-0885; 74-1904
11	26,5697	1654,16	0,0960	3,35215	100,00	0,0800	83-0539; 80-0885
12	27,3480	80,77	0,1440	3,25849	4,88	0,1200	75-0306
13	27,9609	142,43	0,0960	3,18844	8,61	0,0800	74-2036; 74-1904
14	29,0644	115,82	0,0720	3,06985	7,00	0,0600	74-2036; 74-1904
15	31,0177	57,02	0,1440	2,88083	3,45	0,1200	74-1904
16	31,6117	601,30	0,1200	2,82805	36,35	0,1000	80-0885; 75-0306
17	32,0685	224,05	0,1200	2,78879	13,54	0,1000	74-2036; 74-1904
18	33,4334	61,38	0,7680	2,67800	3,71	0,6400	74-1904
19	33,7751	154,82	0,0720	2,65168	9,36	0,0600	74-2036
20	34,9022	150,96	0,1920	2,56859	9,13	0,1600	80-0885
21	35,2922	69,48	0,7680	2,54109	4,20	0,6400	80-0885; 74-1904
22	35,8617	137,60	0,1920	2,50204	8,32	0,1600	80-0885; 74-2036; 74-1904
23	37,0171	143,55	0,2400	2,42655	8,68	0,2000	
24	38,4244	136,22	0,4800	2,34085	8,23	0,4000	80-0885; 74-2036
25	39,3421	259,26	0,0720	2,28834	15,67	0,0600	83-0539; 80-0885; 74-1904
26	40,2670	50,70	0,2880	2,23788	3,06	0,2400	83-0539; 80-0885
27	41,5290	44,42	0,3840	2,17275	2,69	0,3200	80-0885
28	42,3281	110,71	0,0960	2,13356	6,69	0,0800	83-0539; 80-0885; 74-1904
29	45,4110	235,87	0,1200	1,99562	14,26	0,1000	80-0885; 74-1904; 75-0306
30	47,7543	84,13	0,1440	1,90302	5,09	0,1200	80-0885; 74-2036; 74-1904
31	48,7380	169,59	0,0720	1,86688	10,25	0,0600	80-0885; 74-2036; 74-1904
32	50,0809	227,25	0,0720	1,81993	13,74	0,0600	83-0539; 80-0885
33	50,6351	20,11	1,1520	1,80130	1,22	0,9600	83-0539; 80-0885; 74-2036; 74-1904
34	53,7353	68,99	0,2880	1,70446	4,17	0,2400	80-0885; 74-1904; 75-0306
35	55,0093	70,04	0,9600	1,66796	4,23	0,8000	83-0539; 80-0885; 74-2036; 74-1904
36	56,4276	65,75	0,1440	1,62936	3,97	0,1200	80-0885; 75-0306
37	59,6661	35,18	0,7680	1,54842	2,13	0,6400	83-0539; 80-0885; 74-2036; 74-1904
38	62,2083	156,10	0,2880	1,49111	9,44	0,2400	80-0885; 74-2036; 74-1904
39	63,8083	25,90	0,5760	1,45752	1,57	0,4800	83-0539; 80-0885; 74-1904
40	67,6720	45,25	0,1680	1,38340	2,74	0,1400	83-0539; 74-2036; 74-1904
41	68,1012	103,91	0,0960	1,37572	6,28	0,0800	83-0539; 80-0885; 74-2036

VI.4.3. Details of the X-ray analysis of the salt sample Rubirizi 2011/3 (Bugabira)

File: 587A0003.DI 8-Apr-2011 15:2

PC-APD, Diffraction software PC-APD, Diffraction softwar

Sample identification:	11/704 powder
Data measured at:	8-Apr-2011 13:25:00
Diffractometer type:	PW3710 BASED
Tube anode:	Cu
Generator tension [kV]:	40
Generator current [mA]:	30
Wavelength Alpha1 [Å]:	1.54060
Wavelength Alpha2 [Å]:	1.54439
Intensity ratio (alpha2/alpha1):	0.500
Divergence slit:	AUTOMATIC
Irradiated length [mm]:	12
Receiving slit:	0.1
Monochromator used:	YES
Start angle [°2θ]:	3.010
End angle [°2θ]:	69.990
Step size [°2θ]:	0.020
Maximum intensity:	18686.89
Time per step [s]:	1.000
Type of scan:	CONTINUOUS
Intensities converted to:	FIXED
Peak positions defined by:	Minimum of 2nd derivative of peak
Minimum peak tip width:	0.20
Maximum peak tip width:	1.00
Peak base width:	2.00
Minimum significance:	0.75
Number of peaks:	38

Angle [°2θ]	d-value α1 [Å]	d-value α2 [Å]	Peak width [°2θ]	Peak int [counts]	Back. int [counts]	Rel. int [%]	Signif.
8.740	10.1093	10.1342	0.320	1584	196	8.5	2.09
12.250	7.2194	7.2372	0.240	18687	106	100.0	29.88
17.705	5.0055	5.0178	0.240	299	44	1.6	3.53
20.245	4.3828	4.3936	0.240	357	37	1.9	2.55
21.220	4.1836	4.1939	0.200	756	36	4.0	6.93
23.010	3.8621	3.8716	0.200	182	32	1.0	2.66
23.670	3.7558	3.7651	0.200	142	31	0.8	2.29
24.790	3.5886	3.5975	0.240	6368	30	34.1	24.14
26.620	3.3459	3.3542	0.320	1246	28	6.7	21.13
28.480	3.1315	3.1392	0.480	40	27	0.2	0.93
29.760	2.9997	3.0070	0.240	36	25	0.2	0.91
31.100	2.8734	2.8805	0.240	34	24	0.2	0.96
31.910	2.8023	2.8092	0.240	35	24	0.2	2.26
32.430	2.7585	2.7653	0.240	49	23	0.3	2.11
33.340	2.6853	2.6919	0.560	62	23	0.3	6.01
34.845	2.5727	2.5790	0.200	156	22	0.8	4.00
35.920	2.4981	2.5043	0.200	207	21	1.1	4.31
37.620	2.3890	2.3949	0.200	428	19	2.3	11.30
38.280	2.3494	2.3551	0.320	210	19	1.1	10.78
39.250	2.2935	2.2991	0.400	121	18	0.6	7.52
41.175	2.1906	2.1960	0.480	27	18	0.1	1.34

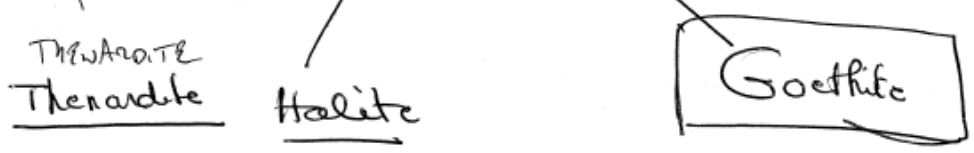

File: 587A0003.DI 8-Apr-2011 15:24

PC-APD, Diffraction software PC-APD, Diffraction software

Angle [°2θ]	d-value α1 [Å]	d-value α2 [Å]	Peak width [°2θ]	Peak int [counts]	Back. int [counts]	Rel. int [%]	Signif.
42.365	2.1318	2.1370	0.240	104	18	0.6	3.20
43.540	2.0769	2.0821	0.480	7	17	0.0	0.81
45.410	1.9957	2.0006	0.320	250	16	1.3	9.22
46.750	1.9415	1.9463	0.560	28	16	0.2	2.53
47.735	1.9037	1.9084	0.280	22	15	0.1	1.77
49.395	1.8436	1.8481	0.400	32	15	0.2	2.86
50.100	1.8193	1.8238	0.240	196	15	1.0	5.90
50.945	1.7911	1.7955	0.280	119	14	0.6	10.65
53.460	1.7126	1.7168	0.320	29	14	0.2	1.44
54.785	1.6743	1.6784	0.240	108	14	0.6	3.47
56.670	1.6230	1.6270	0.240	44	15	0.2	1.14
58.035	1.5880	1.5919	0.320	18	16	0.1	1.34
59.905	1.5428	1.5466	0.320	81	16	0.4	5.52
62.210	1.4911	1.4947	0.280	62	17	0.3	4.93
64.045	1.4527	1.4563	0.400	17	17	0.1	1.85
65.100	1.4317	1.4352	0.240	25	18	0.1	1.38
68.180	1.3743	1.3777	0.320	85	18	0.5	5.93

Peak List

No.	Pos. [°2Th.]	Height [cts]	FWHM [°2T	d-spacing [Å]	Rel. Int. [%]	Tip width [°	Matched by
1	8,7860	872,69	0,0960	10,05646	13,98	0,0800	46-1409
2	12,2781	6241,61	0,1440	7,20297	100,00	0,1200	83-0971
3	17,6949	176,17	0,0720	5,00832	2,82	0,0600	46-1409
4	19,7325	127,82	0,1920	4,49551	2,05	0,1600	83-0971; 46-1409
5	20,2290	186,03	0,1440	4,38628	2,98	0,1200	83-0971
6	20,7650	498,46	0,0960	4,27424	7,99	0,0800	83-0539
7	21,2074	373,07	0,2400	4,18607	5,98	0,2000	83-0971
8	22,9825	84,76	0,2880	3,86661	1,36	0,2400	83-0971
9	24,7864	4552,71	0,1200	3,58914	72,94	0,1000	83-0971
10	26,5450	2034,40	0,0720	3,35521	32,59	0,0600	83-0539; 83-0971
11	26,7404	927,28	0,0720	3,33114	14,86	0,0600	83-0539; 46-1409
12	33,3260	37,65	0,5760	2,68638	0,60	0,4800	
13	34,8370	127,71	0,2400	2,57325	2,05	0,2000	83-0971; 46-1409
14	35,9108	177,53	0,2400	2,49872	2,84	0,2000	83-0971; 46-1409
15	36,4191	81,18	0,1920	2,46501	1,30	0,1600	83-0539; 83-0971
16	37,5958	446,62	0,1440	2,39052	7,16	0,1200	
17	38,2159	190,91	0,3840	2,35314	3,06	0,3200	83-0971
18	39,1152	152,02	0,1440	2,30109	2,44	0,1200	83-0971
19	39,3733	150,44	0,0720	2,28659	2,41	0,0600	83-0539; 83-0971
20	40,1903	70,01	0,1440	2,24198	1,12	0,1200	83-0539; 83-0971
21	42,3470	193,92	0,1200	2,13265	3,11	0,1000	83-0539; 83-0971; 46-1409
22	45,4044	471,73	0,0720	1,99589	7,56	0,0600	83-0971; 46-1409
23	45,7129	172,54	0,0960	1,98314	2,76	0,0800	83-0539; 83-0971; 46-1409
24	50,0604	671,96	0,0720	1,82063	10,77	0,0600	83-0539
25	50,9540	173,83	0,1680	1,79077	2,79	0,1400	
26	54,7938	151,69	0,1920	1,67401	2,43	0,1600	83-0539; 83-0971; 46-1409
27	55,1725	97,26	0,1920	1,66341	1,56	0,1600	83-0539; 83-0971
28	56,6170	54,72	0,2880	1,62435	0,88	0,2400	83-0971
29	57,9425	15,42	0,5760	1,59031	0,25	0,4800	83-0971
30	59,8658	219,13	0,0960	1,54373	3,51	0,0800	83-0539; 83-0971
31	62,2097	97,74	0,2880	1,49108	1,57	0,2400	83-0971
32	63,9425	28,54	0,5760	1,45478	0,46	0,4800	83-0539; 83-0971
33	65,0519	58,43	0,1920	1,43263	0,94	0,1600	83-0971
34	67,6458	261,81	0,0960	1,38387	4,19	0,0800	83-0539
35	68,0713	292,69	0,0960	1,37625	4,69	0,0800	83-0539; 83-0971
36	68,2707	184,16	0,0720	1,37272	2,95	0,0600	83-0539; 83-0971

Pattern List

No	Ref. Code	Score	Compound Name	Chemical Formula	Scale Fact	Displacem	RIR	SemiQuan
1	83-0539	48	Quartz	Si O2	0,105	0,000	3,070	-
2	83-0971	31	Kaolinite 1\ITA\RG	Al2 (Si2 O5) (O H)4	0,125	0,000	1,040	-
3	46-1409	23	Muscovite-2\ITM\RG#	(K , Ba , Na)0.75 (Al , Mg , Cr	0,036	0,000	0,000	-

Appendix VII.5. Estimation of the evaporative concentration using the concentration factor

S/N	Site	Source	EC µS/cm-25°C	pH	Cl mg/l	HCO_3 mg/l	SO_4 mg/l	NO_3 mg/l	NO_2 mg/l	NH_4 mg/l	PO_4 mg/l	Ca mg/l	Mg mg/l	Mn mg/l	Fe mg/l	K mg/l	Na mg/l	F mg/l	SiO_2 mg/l	TDS mg/l
19	Bugorora-Gakana	Spring	90.2	7.1	6.5	12.8	3.0	12.8	0.1	0.0	0.1	4.9	2.3	0.0	0.0	0.6	7.1	0.092	4.9	55.3
20	Buhiga-Ntega	Spring	144.6	4.9	9.2	7.3	8.9	41.7	0.1	0.0	0.1	7.6	4.5	0.0	0.0	3.7	10.4	0.391	16.3	110.2
22	Burengo-Rushubije	Spring	54.00	4.86	3.8	3.66	2.74	18.19	0.09	0.00	0.06	3.92	1.95	0.05	0.07	0.82	2.79	0.11	13.68	52.06
24	Gatovu-Kanyinya	Spring	102.5	7.4	8.3	32.3	4.1	12.9	0.0	0.0	0.0	9.2	3.2	0.0	0.1	5.5	5.5	0.127	10.7	91.9
25	Gatunguru-Rugero	Spring	34.10	6.59	0.9	9.76	1.58	5.71	0.11	0.01	0.08	2.14	1.16	0.02	0.11	0.52	2.72	0.18	1.22	26.32
26	Gihobogo-Murungurira	Spring	150.4	6.6	8.9	48.8	6.4	9.8	0.1	0.0	0.1	7.4	3.1	0.1	0.2	1.4	16.8	0.076	11.9	115.0
28	Gikombe-Ruhita	Spring	79.6	6.3	4.4	19.5	2.4	20.8	0.1	0.0	0.1	5.2	2.5	0.0	0.1	0.7	7.6	0.139	4.8	68.3
36	Kididiri-Buhasa	Spring	72.7	5.4	8.6	22.0	2.6	0.1	0.1	0.0	0.1	4.3	2.3	0.0	0.2	1.2	7.5	0.077	5.6	55.1
37	Kigomero-Munyinya	Spring	85.7	6.2	9.4	11.6	2.3	10.4	0.1	0.0	0.1	5.0	2.3	0.0	0.2	0.5	7.0	0.158	4.4	53.4
40	Kinyangurube-Karehe	Spring	118.9	5.3	6.2	4.3	5.3	19.6	0.1	0.0	0.1	3.3	1.9	0.1	0.2	0.1	10.2	0.063	9.8	61.1
42	Kiramata-Monge	Spring	155.2	7.4	0.6	12.2	5.6	22.9	0.1	0.0	0.1	7.0	3.4	0.1	0.0	3.6	13.4	0.108	10.1	79.3
43	Kirunduzi-Mutara	Spring	44.60	7.10	3.7	7.32	3.03	9.36	0.15	0.01	0.09	2.96	1.19	0.07	0.23	0.30	4.79	0.54	4.76	39.61
45	Maramvya-Mwenya	Spring	48.4	5.3	8.5	7.3	2.6	12.4	0.1	0.0	0.1	3.6	1.7	0.0	0.2	0.3	5.0	0.085	18.0	60.8
46	Mudahinyuka-Kigina II	Spring	69.2	5.7	6.7	22.0	2.5	0.2	0.1	0.0	0.1	4.9	1.4	0.1	0.3	1.3	5.9	0.090	9.6	55.2
47	Mukagezi-Ntogwe	Spring	89.00	5.95	2.7	9.76	2.90	36.24	0.14	0.00	0.06	5.95	2.83	0.02	0.07	1.75	5.93	0.60	14.06	83.08
51	Mutetema-Muyange	Spring	74.4	5.8	4.9	30.5	1.3	7.2	0.1	0.0	0.1	4.7	2.9	0.0	0.1	1.0	5.6	0.178	0.1	58.7
52	Mvyayingabo-Mutara	Spring	129.30	6.68	3.6	24.40	9.81	17.99	0.09	0.01	0.07	6.20	4.36	0.01	0.03	1.12	9.91	0.20	4.34	82.17
53	Mwenya-Mwenya	Spring	196.9	5.8	9.6	34.2	15.1	17.5	0.1	0.0	0.1	10.5	5.1	1.4	0.0	0.4	14.6	0.156	1.6	110.3
54	Mwenya-Rwimbogo	Spring	87.2	6.2	6.8	14.0	1.8	17.9	0.1	0.0	0.1	5.5	3.1	0.0	0.1	0.9	6.9	0.131	15.0	72.3
55	Nagikono-Kinyangurube	Spring	134.7	5.7	9.0	39.0	1.3	15.9	0.1	0.0	0.1	7.9	4.3	0.0	0.0	1.6	11.8	0.223	8.9	100.1
58	Nakabingo II-Gihosha	Spring	134.6	4.9	7.2	3.7	13.4	34.4	0.1	0.0	0.1	8.0	4.1	0.3	0.1	5.6	6.9	0.122	17.6	101.7
61	Narukere-Gihosha	Spring	57.3	4.9	5.1	7.9	1.3	16.1	0.2	0.0	0.1	3.7	1.5	0.0	0.1	0.4	6.8	0.106	13.8	57.1
62	Narutambwe-Kireka	Spring	80.70	6.60	0.9	7.93	1.20	25.93	0.13	0.00	0.07	0.39	2.25	0.02	0.03	0.76	7.67	0.09	4.03	51.45
65	Rambo II-Gatwe	Spring	178.6	6.9	6.1	14.6	13.8	43.3	0.2	0.0	0.1	6.8	5.6	0.0	0.1	1.5	14.0	0.067	15.2	121.6
66	Rubira-Gatemere	Spring	55.40	5.22	4.3	8.54	1.08	8.16	0.08	0.00	0.06	1.55	1.11	0.02	0.16	0.39	5.90	0.10	13.14	44.59
67	Rugangazi-Ntogwe	Spring	62.2	4.5	4.8	9.2	1.2	11.2	0.1	0.0	0.1	2.5	1.3	0.2	0.4	2.1	4.8	0.069	13.4	51.3
68	Rugero-Nakarinzi	Spring	22.60	6.45	0.6	15.25	1.24	1.25	0.09	0.00	0.71	3.19	1.28	0.01	0.09	0.19	2.18	0.12	5.12	31.47
70	Rugomero-Gatemere	Spring	60.60	6.26	0.7	9.76	2.41	24.51	0.13	0.01	0.08	3.66	1.77	0.02	0.25	0.30	6.14	0.06	0.63	51.14
71	Rugomero-Kiravumba	Spring	38.60	4.87	4.3	14.03	1.62	0.81	0.09	0.00	0.06	1.62	0.85	0.03	0.10	0.39	4.35	0.09	14.89	43.35
72	Rugomero-Nyabugeni	Spring	104.4	6.9	9.8	15.3	2.0	2.3	0.1	0.0	0.1	4.1	2.6	0.0	0.3	0.6	10.0	0.169	0.5	47.9
76	Rushubije-Cogo	Spring	53.10	4.73	3.3	4.88	1.04	14.58	0.08	0.00	0.07	1.80	1.48	0.03	0.11	0.79	5.37	0.15	5.67	39.40
77	Twengebuye-Nakabingo	Spring	86.5	4.7	4.6	3.1	1.1	27.3	0.1	0.0	0.1	5.0	2.4	0.1	0.1	1.1	5.3	0.421	5.1	55.7
		Average			**5.4**	**16.0**	**3.9**	**15.4**	**0.1**	**0.0**	**0.1**	**4.8**	**2.5**	**0.1**	**0.1**	**1.3**	**7.6**	**0.2**	**8.4**	**65.8**

S/N	Site	Source	EC µS/cm-25°C	pH	Cl mg/l	HCO_3 mg/l	SO4 mg/l	NO_3 mg/l	NO_2 mg/l	NH_4 mg/l	PO_4 mg/l	Ca mg/l	Mg mg/l	Mn mg/l	Fe mg/l	K mg/l	Na mg/l	F mg/l	SiO_2 mg/l	TDS mg/l
17	Bihembe-Monge	Spring	215.0	6.9	17.7	11.0	34.3	30.2	0.1	0.0	0.1	6.4	7.2	0.3	0.4	3.1	18.4	0.078	4.3	133.5
21	Bunyari-Rugarama	Spring	155.7	7.0	13.6	53.1	6.1	10.3	0.1	0.0	0.0	4.4	2.9	0.0	0.1	0.9	22.3	0.168	14.4	128.6
29	Kabira-Kanyinya	Spring	156.0	7.0	16.4	31.7	4.1	14.1	0.0	0.0	0.0	9.2	3.8	0.0	0.1	3.6	11.2	0.135	9.4	103.9
30	Kabira-Renga	Spring	148.1	5.9	22.5	30.5	1.2	2.4	0.1	0.0	0.1	5.1	2.8	0.0	0.2	0.2	18.9	0.084	16.7	101.0
32	Kanyamanza-Kagege	Spring	127.4	6.2	16.1	25.0	1.1	9.6	0.1	0.0	0.1	5.1	2.9	0.0	0.1	1.1	14.4	0.086	9.6	85.3
33	Kararire-Kagege	Spring	149.2	6.5	25.7	9.8	7.1	5.5	0.1	0.0	0.1	6.6	3.7	0.0	0.0	1.8	12.8	0.079	4.4	77.7
34	Karira-Gatemere	Spring	201.0	6.0	27.8	15.9	19.0	8.6	0.1	0.0	0.1	9.3	5.0	0.1	0.1	3.2	17.9	0.104	8.3	115.5
35	Karobogo	Spring	105.2	7.2	10.7	15.9	6.2	23.6	0.0	0.0	0.0	5.9	2.7	0.0	0.1	20.0	1.9	0.097	8.8	96.0
38	Kigoti-Munzenze	Spring	162.4	5.8	18.4	32.3	1.2	20.2	0.1	0.0	0.1	7.3	4.2	0.2	0.0	0.7	15.5	0.113	5.7	106.0
41	Kinywamagana-Kigarama	Spring	87.7	5.2	15.3	5.5	1.1	7.7	0.1	0.0	0.1	3.6	1.8	0.0	0.0	0.7	9.1	0.122	3.0	48.1
48	Mukuyo-Kiri	Spring	766.0	7.0	16.5	328.2	96.2	10.6	0.1	0.0	0.5	39.6	9.8	0.0	0.1	5.8	123.8	0.161	22.4	655.3
49	Musave-Mugobe	Spring	179.8	5.6	10.6	30.5	23.5	6.2	0.1	0.0	0.1	10.0	3.0	0.0	0.0	2.4	12.1	0.196	2.8	101.7
56	Nakabingo	Spring	169.1	6.8	11.7	56.1	5.4	6.0	0.0	0.0	0.0	10.8	5.4	0.0	0.1	1.3	10.0	0.068	9.1	116.2
57	Nakabingo-Gatemere	Spring	59.1	6.2	13.2	12.8	7.6	3.5	0.2	0.0	0.1	3.8	2.0	0.0	0.4	0.8	6.9	0.365	14.2	66.8
60	Nakivumbura-Monge	Spring	134.4	5.6	12.5	29.3	9.4	5.4	0.1	0.0	0.1	6.4	3.7	0.0	0.2	2.3	11.8	0.114	16.6	98.5
63	Nyabitare-Munyinya	Spring	179.5	5.8	28.1	16.5	4.7	23.7	0.1	0.0	0.1	10.7	4.6	0.0	0.1	1.0	15.6	0.205	6.3	111.6
64	Nyaruziba-Mutara	Spring	167.4	6.2	12.4	29.9	19.5	19.4	0.1	0.0	0.1	11.0	6.3	0.0	0.1	4.2	8.2	0.125	11.4	122.4
69	Rugoma-Kagege	Spring	75.4	5.7	10.4	9.8	4.6	5.2	0.1	0.0	0.1	4.7	2.3	0.0	0.1	1.4	5.4	0.083	5.9	50.1
73	Rugunga II- Kavomo	Spring	166.9	6.2	10.0	33.6	13.6	3.5	0.1	0.0	0.1	3.1	5.0	0.0	0.0	1.2	15.8	0.119	8.7	94.8
74	Rugunga I-Kavomo	Spring	135.7	5.7	16.5	23.2	6.4	11.9	0.1	0.0	0.1	4.5	2.6	0.0	0.1	1.0	17.1	0.091	8.2	91.9
75	Ruhongore-Munyinya	Spring	162.5	6.6	24.0	17.1	7.1	14.0	0.1	0.0	0.1	8.7	4.3	0.0	0.1	1.4	13.7	0.079	15.1	105.9
79	Bunyari-Rugarama	Well	462.0	6.9	11.3	215.9	10.2	22.0	0.0	0.0	0.1	19.5	14.0	0.0	0.1	54.5	18.0	1.121	21.9	388.8
80	Cimbogo-Gatete	Well	1108.0	7.5	23.3	688.7	4.3	14.4	0.1	0.0	0.6	97.4	54.4	3.2	0.7	79.0	34.2	1.450	16.8	1018.4
81	Cinyambo-Gitwe	Well	414.0	7.1	24.9	198.3	6.8	7.2	0.0	0.0	0.1	23.9	10.9	0.8	0.2	40.0	23.9	0.272	18.5	355.8
83	Foko I-Kiyonza	Well	1550.0	7.1	25.2	608.8	213.3	68.3	0.1	0.1	0.1	92.1	38.8	0.0	0.0	43.0	175.5	0.956	22.9	1289.1
92	Kadobogoro-Muramba	Well	210.0	7.2	12.4	51.9	20.4	6.1	0.1	0.0	0.1	10.9	3.6	0.1	2.9	1.5	20.6	0.163	4.3	134.9
103	Kigina I-Gisenyi	Well	415.0	7.4	13.1	211.7	7.1	5.7	0.1	0.0	0.0	46.1	10.5	0.0	0.4	0.5	23.0	0.743	20.3	339.3
104	Kigina II-Gisenyi	Well	352.0	7.0	10.6	149.5	11.2	13.6	0.3	0.0	0.0	25.6	12.4	0.0	0.3	0.1	26.7	1.146	4.9	256.5
112	Marembo-Marembo	Well	454.0	7.3	21.4	209.8	1.7	30.7	0.1	0.0	0.1	31.0	10.9	0.9	3.6	16.7	25.6	0.875	15.2	368.6
113	Mataka-Rugasa	Well	722.0	6.9	18.7	391.0	10.3	11.8	0.0	0.0	0.1	56.2	25.8	0.0	0.2	19.0	42.3	0.640	13.6	589.6
116	Muhero II - Yaranda	Well	362.0	7.7	20.6	161.7	4.0	9.4	0.9	0.0	0.1	20.5	8.9	0.5	9.7	9.9	30.5	1.017	4.5	282.1
122	Ngaragu-kiri	Well	1196.0	7.0	11.6	547.2	144.4	40.1	0.0	0.1	0.1	58.0	25.9	1.3	0.6	1.3	180.4	3.540	15.2	1029.5
128	Rugoma-Kagege	Well	149.2	6.8	14.1	42.7	13.1	7.0	1.8	0.2	0.0	10.7	3.8	0.1	1.6	13.7	8.7	0.150	11.3	129.0
136	Rwasama-Kiri	Well	496.0	7.3	23.4	186.1	53.6	24.3	0.1	0.0	0.2	32.4	11.5	0.4	0.2	2.2	52.3	0.822	29.9	417.3
	Average				**17.1**	**131.8**	**22.9**	**14.8**	**0.2**	**0.0**	**0.1**	**20.6**	**9.3**	**0.2**	**0.7**	**10.0**	**30.7**	**0.5**	**11.9**	**270.9**

			EC µS/cm-25°C	pH	Cl mg/l	HCO_3 mg/l	SO_4 mg/l	NO_3 mg/l	NO_2 mg/l	NH_4 mg/l	PO_4 mg/l	Ca mg/l	Mg mg/l	Mn mg/l	Fe mg/l	K mg/l	Na mg/l	F mg/l	SiO_2 mg/l	TDS mg/l
	Average (Cl = 10-30 mg/l)				**17.1**	**131.8**	**22.9**	**14.8**	**0.2**	**0.0**	**0.1**	**20.6**	**9.3**	**0.2**	**0.7**	**10.0**	**30.7**	**0.5**	**11.9**	**270.9**
	Concentration factor				**3.1**															
	Expected concentration				**17.1**	**50.1**	**12.1**	**48.3**	**0.3**	**0.0**	**0.3**	**14.9**	**7.9**	**0.3**	**0.4**	**3.9**	**23.9**	**0.5**	**26.4**	**206.8**
	Δ Reaction (mg/l)				**0.0**	**81.6**	**10.8**	**-33.6**	**-0.2**	**0.0**	**-0.2**	**5.7**	**1.4**	**0.0**	**0.2**	**6.1**	**6.8**	**0.0**	**-14.5**	**64.0**
	Molar weight					**61**	**96**	**62**	**46**	**18**	**95**	**40**	**24**	**55**		**39**	**23**	**19**	**60**	
	Δ Reaction (mmol/l)					**1.3**	**0.1**	**-0.5**	**0.0**	**0.0**	**0.0**	**0.1**	**0.1**	**0.0**		**0.2**	**0.3**	**0.0**	**-0.2**	

	Site	Source	EC µS/cm-25°C	pH	Cl mg/l	HCO_3 mg/l	SO_4 mg/l	NO_3 mg/l	NO_2 mg/l	NH_4 mg/l	PO_4 mg/l	Ca mg/l	Mg mg/l	Mn mg/l	Fe mg/l	K mg/l	Na mg/l	F mg/l	SiO_2 mg/l	TDS mg/l
23	Gaharata	Spring	197.0	7.1	30.4	21.4	3.8	17.3	0.0	0.0	0.0	8.3	3.8	0.0	0.1	3.9	17.3	0.147	6.3	112.6
18	Bishunzi-Munyinya	Spring	168.8	5.6	33.8	12.2	2.3	11.5	0.1	0.0	0.1	7.5	5.0	0.0	0.0	1.7	15.5	0.087	1.1	90.9
27	Gihushi-Kiravumba	Spring	279.0	5.6	56.7	17.1	4.6	12.0	0.1	0.0	0.1	11.7	3.8	0.1	0.1	1.5	26.8	0.097	7.3	141.8
31	Kagogo-Nyabitare	Spring	191.0	5.0	30.7	6.1	2.9	36.0	0.1	0.0	0.1	8.0	4.9	0.0	0.0	1.8	17.4	0.154	15.1	123.3
50	Musave-Rutabo	Spring	225.0	7.1	41.5	20.1	1.6	9.2	0.1	0.0	0.1	6.6	4.2	0.3	2.1	0.2	23.2	0.136	1.6	110.9
59	Nakarambo-Rutabo	Spring	174.3	6.1	35.0	22.0	1.3	13.4	0.1	0.0	0.1	8.2	4.1	0.1	0.2	0.7	19.2	0.171	18.2	122.7
87	Gasagara I-Rubuga	Well	1777.0	7.0	49.3	560.0	446.0	15.2	0.0	0.1	0.1	169.9	44.6	0.0	0.1	35.4	165.2	1.417	19.9	1507.2
91	Kabirizi II-Kigoma	Well	903.0	7.0	50.8	251.9	78.0	44.0	0.1	0.1	0.1	74.6	16.5	0.0	0.1	48.4	41.0	1.237	20.6	627.4
96	Kanabugiri-Bugera	Well	685.0	7.6	48.2	258.0	55.5	5.1	0.0	0.0	0.0	28.9	28.9	0.3	0.1	24.0	79.3	4.990	5.0	538.5
108	Kiruhura II-Muramba	Well	478.0	6.5	46.7	164.1	34.6	3.8	0.1	0.0	0.1	48.4	6.0	1.8	1.2	1.3	29.9	1.141	20.2	359.3
114	Mugombwa-Kiri	Well	1066.0	7.2	35.1	465.4	79.3	65.3	0.1	0.1	0.1	76.0	35.8	0.0	0.1	23.4	102.6	3.040	22.6	909.1
115	Muhero I - Yaranda	Well	267.0	7.0	31.9	74.4	6.5	6.9	0.1	0.0	0.1	18.5	5.9	0.3	2.1	1.0	16.8	0.420	14.5	179.4
119	Murehe-Murungurira	Well	577.0	6.8	43.4	172.0	52.2	18.5	0.1	0.0	0.1	32.1	6.3	0.5	4.2	1.7	71.5	2.170	2.5	407.2
131	Runyangona II-Nyabikenke	Well	625.0	6.2	59.2	276.3	2.7	4.0	0.0	0.7	0.0	47.8	18.8	4.0	25.7	18.6	25.4	0.582	10.0	493.8
134	Ruseno-Kanyagu	Well	452.0	6.3	59.7	105.5	21.8	3.5	0.1	0.0	0.7	16.5	2.6	0.0	0.9	10.0	60.0	0.320	5.8	287.3
135	Ruyivyi II-Gitwe	Well	687.0	6.8	55.9	288.5	16.8	10.7	0.1	0.0	0.1	52.0	17.0	0.1	0.8	50.5	50.3	0.851	12.2	555.8
	Average (Cl = 30-60 mg/l)				**44.3**	**169.7**	**50.6**	**17.3**	**0.1**	**0.1**	**0.1**	**38.4**	**13.0**	**0.5**	**2.4**	**14.0**	**47.6**	**1.1**	**11.4**	**410.4**
	Concentration factor				**8.1**															
	Expected concentration				**44.3**	**129.9**	**31.5**	**125.3**	**0.9**	**0.0**	**0.8**	**38.7**	**20.4**	**0.8**	**1.1**	**10.2**	**61.9**	**1.3**	**68.5**	**535.9**
	Δ Reaction (mg/l)				**0.0**	**39.8**	**19.1**	**-108.0**	**-0.8**	**0.0**	**-0.7**	**-0.3**	**-7.4**	**-0.3**	**1.2**	**3.8**	**-14.3**	**-0.3**	**-57.0**	**-125.4**
	Molar weight					**61**	**96**	**62**	**46**	**18**	**95**	**40**	**24**	**55**		**39**	**23**	**19**	**60**	
	Δ Reaction (mmol/l)					**0.7**	**0.2**	**-1.7**	**0.0**	**0.0**	**0.0**	**0.0**	**-0.3**	**0.0**		**0.1**	**-0.6**	**0.0**	**-1.0**	

	Site	Source	EC µS/cm-25°C	pH	Cl mg/l	HCO_3 mg/l	SO_4 mg/l	NO_3 mg/l	NO_2 mg/l	NH_4 mg/l	PO_4 mg/l	Ca mg/l	Mg mg/l	Mn mg/l	Fe mg/l	K mg/l	Na mg/l	F mg/l	SiO_2 mg/l	TDS mg/l
89	Haga II-Nyamabuye	Well	1282.0	7.2	81.5	491.7	25.4	8.9	0.1	0.5	0.1	68.1	26.2	1.2	2.1	29.0	97.1	2.580	10.6	844.8
98	Kantuye-Ceru	Well	848.0	7.2	66.8	412.4	2.2	8.9	6.7	0.0	0.1	47.1	15.8	14.5	2.2	56.5	78.0	1.655	9.4	722.2
100	Karago-Rukuramigabo	Well	1270.0	7.4	63.8	708.2	1.8	13.1	0.1	0.0	0.1	13.8	22.5	0.9	31.9	104.0	168.3	1.131	9.6	1139.2
102	Kigazi-Nyakarama	Well	2650.0	7.2	74.0	1062.0	264.2	80.2	0.0	0.2	0.1	106.2	63.3	0.1	0.2	2.6	380.5	3.570	18.9	2056.0
103	Kigoma-Gatare	Well	536.0	6.9	73.5	115.9	57.4	7.9	0.1	0.0	0.1	40.2	11.5	2.0	9.6	4.6	40.5	0.370	20.7	384.2
105	Kinyamateke	Well	799.0	6.3	78.9	160.4	108.6	54.6	0.1	0.1	0.3	36.9	26.4	0.0	0.1	17.0	70.3	0.420	17.2	571.2
120	Mutoza-Yaranda	Well	807.0	7.0	82.6	294.0	31.6	0.2	1.6	1.9	0.1	50.5	6.2	0.2	27.1	1.7	78.5	0.448	11.0	587.5
121	Ndava II-Nyamabuye	Well	821.0	7.1	71.8	361.1	2.1	15.1	0.1	1.4	0.0	44.7	21.9	0.0	3.2	13.8	89.8	2.720	0.7	628.5
133	Ruranzi-Rwibikara	Well	746.0	7.5	73.0	323.9	3.5	1.9	0.0	1.8	0.0	37.4	18.9	0.1	8.2	23.3	70.3	1.490	8.1	571.9
143	Susa-Gikomero	Well	548.0	6.6	82.4	47.0	39.2	69.9	0.1	0.0	0.1	28.1	15.4	1.7	0.1	42.0	40.1	0.283	9.6	375.7
	Average (Cl =60-90 mg/l)				**74.8**	**397.7**	**53.6**	**26.1**	**0.9**	**0.6**	**0.1**	**47.3**	**22.8**	**2.1**	**8.5**	**29.4**	**111.3**	**1.5**	**11.6**	**788.1**
	Concentration factor				**13.8**															
	Expected concentration				**74.8**	**219.5**	**53.2**	**211.6**	**1.5**	**0.1**	**1.3**	**65.4**	**34.5**	**1.3**	**1.9**	**17.2**	**104.6**	**2.2**	**115.7**	**905.5**
	Δ Reaction (mg/l)				**0.0**	**178.1**	**0.4**	**-185.6**	**-0.6**	**0.5**	**-1.2**	**-18.1**	**-11.7**	**0.8**	**6.6**	**12.2**	**6.7**	**-0.7**	**-104.1**	**-117.3**
	Molar weight					**61**	**96**	**62**	**46**	**18**	**95**	**40**	**24**	**55**		**39**	**23**	**19**	**60**	
	Δ Reaction (mmol/l)					**2.9**	**0.0**	**-3.0**	**0.0**	**0.0**	**0.0**	**-0.5**	**-0.5**	**0.0**		**0.3**	**0.3**	**0.0**	**-1.7**	

	Site	Source	EC µS/cm-25 °C	pH	Cl mg/l	HCO_3 mg/l	SO_4 mg/l	NO_3 mg/l	NO_2 mg/l	NH_4 mg/l	PO_4 mg/l	Ca mg/l	Mg mg/l	Mn mg/l	Fe mg/l	K mg/l	Na mg/l	F mg/l	SiO_2 mg/l	TDS mg/l
39	Kinyangoro-Kumana	Spring	55.8	7.0	115.2	20.7	1.4	16.4	0.1	0.0	0.1	4.3	2.0	0.0	0.4	0.4	4.3	0.158	4.0	169.5
84	Gahwijo II-Nyabikenke	Well	1219.0	6.6	118.6	403.2	147.9	3.9	0.0	0.7	0.1	124.1	25.6	7.6	9.5	63.2	65.5	0.740	19.2	989.8
97	Kanigo-Cinuma	Well	2160.0	7.0	110.6	458.1	432.6	57.9	0.2	0.1	0.1	68.5	68.5	1.0	0.2	25.0	283.8	1.527	18.6	1526.7
101	Karisha	Well	1230.0	6.9	90.4	597.2	13.9	42.1	0.1	0.1	0.1	67.1	24.9	0.0	0.0	14.2	145.7	1.311	10.8	1007.8
106	Kigozi-Yaranda	Well	1547.0	6.9	97.0	585.6	108.5	41.6	0.0	0.1	0.1	92.3	46.3	0.2	0.5	55.0	138.1	1.628	4.4	1171.2
108	Foko II-Kiyonza	Well	1302.0	7.3	111.8	485.6	101.7	54.5	0.0	0.1	0.1	97.4	38.7	0.1	0.1	37.4	124.6	1.357	28.8	1082.0
130	Rukore-II-Kigina	Well	951.0	6.5	95.6	414.8	21.5	5.0	0.0	4.9	0.0	82.2	24.7	1.1	6.0	44.4	67.3	1.006	5.9	774.4
137	Saruduha II-Rugasa	Well	1920.0	7.4	118.5	880.2	132.9	4.8	0.0	0.1	0.9	93.6	60.7	0.1	0.9	42.4	218.0	5.480	15.6	1574.2
142	Shenga I- Rugasa	Well	680.0	6.7	100.5	220.2	3.0	4.2	0.1	0.0	0.0	28.5	12.8	0.6	3.7	50.5	73.4	0.499	8.5	506.4
	Average (90-120 mg/l)				**106.5**	**451.7**	**107.0**	**25.6**	**0.1**	**0.7**	**0.1**	**73.1**	**33.8**	**1.2**	**2.4**	**36.9**	**124.5**	**1.5**	**12.9**	**978.0**
	Concentration factor				**19.6**															
	Expected concentration				**106.5**	**312.4**	**75.7**	**301.2**	**2.1**	**0.1**	**1.9**	**93.1**	**49.1**	**1.8**	**2.7**	**24.5**	**148.9**	**3.2**	**164.6**	**1288.6**
	Δ Reaction (mg/l)				**0.0**	**139.3**	**31.4**	**-275.6**	**-2.0**	**0.6**	**-1.7**	**-20.0**	**-15.3**	**-0.7**	**-0.3**	**12.4**	**-24.4**	**-1.6**	**-151.7**	**-310.6**
	Molar weight					**61**	**96**	**62**	**46**	**18**	**95**	**40**	**24**	**55**		**39**	**23**	**19**	**60**	
	Δ Reaction (mmol/l)					**2.3**	**0.3**	**-4.4**	**0.0**	**0.0**	**0.0**	**-0.5**	**-0.6**	**0.0**		**0.3**	**-1.1**	**-0.1**	**-2.5**	

	Site	Source	EC µS/cm-25°C	pH	Cl mg/l	HCO_3 mg/l	SO_4 mg/l	NO_3 mg/l	NO_2 mg/l	NH_4 mg/l	PO_4 mg/l	Ca mg/l	Mg mg/l	Mn mg/l	Fe mg/l	K mg/l	Na mg/l	F mg/l	SiO_2 mg/l	TDS mg/l
86	Gasagara II-Rubuga	Well	2900.0	7.8	145.3	1378.0	167.8	52.5	0.0	0.1	0.1	75.9	71.6	0.2	0.4	35.2	431.0	4.230	18.4	2380.7
94	Kadobori I-Rubuga	Well	1153.0	6.9	122.2	302.6	77.9	14.4	0.0	0.0	0.1	67.4	18.9	0.4	0.1	52.0	77.7	0.638	18.6	752.9
99	Karago-Kibonde	Well	762.0	7.1	129.4	215.3	10.2	5.0	0.0	0.0	0.0	79.0	10.6	0.0	6.4	15.5	45.6	0.478	9.7	528.0
109	Kiruhura I-Kiyanza	Well	1468.0	7.7	138.3	488.0	109.9	10.1	0.2	0.4	0.1	78.6	26.0	0.1	11.2	29.0	161.2	0.430	4.5	1058.0
111	Mago - Gatete	Well	3730.0	8.5	142.0	1984.9	154.5	6.6	0.1	0.0	0.1	40.0	3.0	0.2	0.2	252.0	630.0	9.410	6.2	3229.1
117	Munyinya-Nyakarama	Well	2690.0	7.0	129.0	1029.7	256.1	75.9	0.2	0.1	0.1	132.2	58.2	0.0	0.2	61.2	307.5	1.369	16.7	2068.4
125	Ntwago-Murungurira	Well	1120.0	7.1	149.2	239.1	86.8	9.8	0.1	0.0	0.1	26.9	12.0	0.5	0.7	0.5	184.4	16.530	14.4	741.0
	Average (Cl = 120-150 mg/l)				**136.5**	**445.3**	**91.5**	**23.9**	**3.8**	**1.8**	**7.7**	**57.2**	**25.7**	**5.1**	**2.6**	**38.4**	**134.5**	**3.6**	**14.3**	**1062.1**
	Concentration factor				**25.1**															
	Expected concentration				**136.5**	**400.5**	**97.0**	**386.1**	**2.7**	**0.1**	**2.4**	**119.3**	**63.0**	**2.4**	**3.4**	**31.4**	**190.8**	**4.0**	**211.0**	**1651.8**
	Δ Reaction (mg/l)				**0.0**	**44.8**	**-5.5**	**-362.1**	**1.1**	**1.6**	**5.3**	**-62.1**	**-37.3**	**2.7**	**-0.9**	**7.0**	**-56.3**	**-0.5**	**-196.7**	**-589.7**
	Molar weight					**61**	**96**	**62**	**46**	**18**	**95**	**40**	**24**	**55**		**39**	**23**	**19**	**60**	
	Δ Reaction (mmol/l)					**0.7**	**-0.1**	**-5.8**	**0.0**	**0.1**	**0.1**	**-1.6**	**-1.6**	**0.0**		**0.2**	**-2.4**	**0.0**	**-3.3**	

	Site	Type	EC µS/cm-25°C	pH	Cl mg/l	HCO_3 mg/l	SO_4 mg/l	NO_3 mg/l	NO_2 mg/l	NH_4 mg/l	PO_4 mg/l	Ca mg/l	Mg mg/l	Mn mg/l	Fe mg/l	K mg/l	Na mg/l	F mg/l	SiO_2 mg/l	TDS mg/l
78	Bishunzi -Cewe	Well	2520.0	6.8	386.6	550.2	153.7	7.4	0.0	0.0	0.0	56.4	74.5	0.2	3.0	115.8	276.2	2.360	5.7	1632.2
85	Gahwijo I-Nyabikenke	Well	3110.0	6.8	406.4	935.7	193.0	20.6	0.0	0.1	0.1	113.0	53.6	0.1	0.2	44.2	439.0	0.995	15.5	2222.6
88	Gifuruguti-Nyakarama	Well	2860.0	6.8	317.2	539.2	329.2	15.8	0.0	0.1	0.1	135.1	53.6	0.8	0.2	49.2	304.0	0.798	17.4	1762.6
90	Hambiro-Kiyonza	Well	2400.0	7.3	190.8	682.0	253.6	75.5	0.0	0.1	0.1	135.2	55.9	0.0	0.1	38.4	247.1	2.350	30.1	1711.2
93	Kadobori II-Rubuga	Well	1990.0	7.2	157.7	598.4	267.1	24.0	0.0	0.1	0.1	160.8	46.4	0.2	0.1	44.6	162.3	0.622	22.9	1485.4
110	Kiyonza-Nunga	Well	1301.0	6.9	164.5	465.4	49.0	7.6	0.0	0.0	0.0	79.5	56.5	0.1	2.8	58.0	102.1	0.765	13.5	999.8
118	Murambo-Murambi	Well	1606.0	7.2	167.2	669.8	110.2	5.1	0.2	5.7	0.0	87.7	49.0	0.1	2.4	82.0	173.2	2.580	8.5	1363.5
123	Ntembe II-Kiri	Well	3420.0	6.9	303.2	855.2	337.1	66.7	0.1	0.1	0.3	167.0	61.3	1.2	0.0	108.0	335.7	1.264	19.6	2256.5
124	Ntembe I-Kiri	Well	3260.0	7.1	199.9	1044.3	504.3	38.9	0.1	0.1	0.0	121.7	59.7	0.4	0.1	52.4	511.5	2.530	20.3	2556.3
126	Nunga II-Yaranda	Well	1618.0	6.8	181.2	476.4	100.8	8.4	0.2	1.0	0.1	95.0	24.8	0.2	11.9	30.1	190.0	0.632	16.6	1137.1
132	Runyonza-Kabonde	Well	2050.0	7.3	202.7	478.9	121.7	9.2	2.8	0.6	0.1	65.0	43.2	2.7	1.9	64.0	213.0	3.160	7.5	1216.3
138	Saruduha I	Well	2500.0	6.9	328.6	522.8	251.2	49.5	0.0	0.1	0.2	129.5	57.1	7.5	0.2	9.0	244.5	1.568	20.3	1622.2
140	Shenga III-Rugasa	Well	2790.0	6.7	499.3	605.1	72.3	16.2	0.0	0.0	0.0	81.8	39.0	0.5	54.0	38.5	336.2	0.320	5.4	1748.6
141	Shenga II-Rugasa	Well	2820.0	6.8	466.4	608.8	125.3	9.0	7.2	0.0	0.0	80.4	39.7	0.4	2.9	37.8	418.0	0.295	8.8	1805.0
	Average (Cl >150 mg/l)				**283.7**	**600.9**	**154.2**	**24.3**	**2.5**	**1.2**	**4.3**	**83.1**	**38.0**	**3.1**	**4.3**	**51.3**	**233.8**	**3.1**	**14.8**	**1516.7**
	Concentration factor				**52.1**															
	Expected concentration				**283.7**	**832.5**	**201.6**	**802.5**	**5.6**	**0.3**	**4.9**	**248.0**	**130.9**	**4.9**	**7.1**	**65.3**	**396.7**	**8.4**	**438.6**	**3433.5**
	Δ Reaction (mg/l)				**0.0**	**-231.6**	**-47.4**	**-778.2**	**-3.2**	**0.9**	**-0.6**	**-164.9**	**-92.9**	**-1.8**	**-2.8**	**-14.0**	**-162.9**	**-5.3**	**-423.8**	**-1916.7**
	Molar weight					**61**	**96**	**62**	**46**	**18**	**95**	**40**	**24**	**55**		**39**	**23**	**19**	**60**	
	Δ Reaction (mmol/l)					**-3.8**	**-0.5**	**-12.6**	**-0.1**	**0.0**	**0.0**	**-4.1**	**-3.9**	**0.0**		**-0.4**	**-7.1**	**-0.3**	**-7.1**	

Appendix VII.6. Calculations of the mixing fractions of rain and salt-influenced waters

S/N	Site	Type	EC µS/cm-25°C	pH	Cl mg/l	HCO_3 mg/l	SO_4 mg/l	NO_3 mg/l	NO_2 mg/l	NH4 mg/l	PO_4 mg/l	Ca mg/l	Mg mg/l	Mn mg/l	Fe mg/l	K mg/l	Na mg/l	F mg/l	SiO_2 mg/l	TDS mg/l
19	Bugorora-Gakana	Spring	90.2	7.1	6.5	12.8	3.0	12.8	0.1	0.0	0.1	4.9	2.3	0.0	0.0	0.6	7.1	0.092	4.9	55.3
20	Buhiga-Ntega	Spring	144.6	4.9	9.2	7.3	8.9	41.7	0.1	0.0	0.1	7.6	4.5	0.0	0.0	3.7	10.4	0.391	16.3	110.2
22	Burengo-Rushubije	Spring	54.0	4.9	3.8	3.7	2.7	18.2	0.1	0.0	0.1	3.9	2.0	0.1	0.1	0.8	2.8	0.112	13.7	52.1
24	Gatovu-Kanyinya	Spring	102.5	7.4	8.3	32.3	4.1	12.9	0.0	0.0	0.0	9.2	3.2	0.0	0.1	5.5	5.5	0.127	10.7	91.9
25	Gatunguru-Rugero	Spring	34.1	6.6	0.9	9.8	1.6	5.7	0.1	0.0	0.1	2.1	1.2	0.0	0.1	0.5	2.7	0.176	1.2	26.3
26	Gihobogo-Murungurira	Spring	150.4	6.6	8.9	48.8	6.4	9.8	0.1	0.0	0.1	7.4	3.1	0.1	0.2	1.4	16.8	0.076	11.9	115.0
28	Gikombe-Ruhita	Spring	79.6	6.3	4.4	19.5	2.4	20.8	0.1	0.0	0.1	5.2	2.5	0.0	0.1	0.7	7.6	0.139	4.8	68.3
36	Kididiri-Buhasa	Spring	72.7	5.4	8.6	22.0	2.6	0.1	0.1	0.0	0.1	4.3	2.3	0.0	0.2	1.2	7.5	0.077	5.6	55.1
37	Kigomero-Munyinya	Spring	85.7	6.2	9.4	11.6	2.3	10.4	0.1	0.0	0.1	5.0	2.3	0.0	0.2	0.5	7.0	0.158	4.4	53.4
40	Kinyangurube-Karehe	Spring	118.9	5.3	6.2	4.3	5.3	19.6	0.1	0.0	0.1	3.3	1.9	0.1	0.2	0.1	10.2	0.063	9.8	61.1
42	Kiramata-Monge	Spring	155.2	7.4	0.6	12.2	5.6	22.9	0.1	0.0	0.1	7.0	3.4	0.1	0.0	3.6	13.4	0.108	10.1	79.3
43	Kirunduzi-Mutara	Spring	44.6	7.1	3.7	7.3	3.0	9.4	0.2	0.0	0.1	3.0	1.2	0.1	0.2	0.3	4.8	0.540	4.8	39.6
45	Maramvya-Mwenya	Spring	48.4	5.3	8.5	7.3	2.6	12.4	0.1	0.0	0.1	3.6	1.7	0.0	0.2	0.3	5.0	0.085	18.0	60.8
46	Mudahinyuka-Kigina II	Spring	69.2	5.7	6.7	22.0	2.5	0.2	0.1	0.0	0.1	4.9	1.4	0.1	0.3	1.3	5.9	0.090	9.6	55.2
47	Mukagezi-Ntogwe	Spring	89.0	6.0	2.7	9.8	2.9	36.2	0.1	0.0	0.1	6.0	2.8	0.0	0.1	1.8	5.9	0.604	14.1	83.1
51	Mutetema-Muyange	Spring	74.4	5.8	4.9	30.5	1.3	7.2	0.1	0.0	0.1	4.7	2.9	0.0	0.1	1.0	5.6	0.178	0.1	58.7
52	Mvyayingabo-Mutara	Spring	129.3	6.7	3.6	24.4	9.8	18.0	0.1	0.0	0.1	6.2	4.4	0.0	0.0	1.1	9.9	0.199	4.3	82.2
53	Mwenya-Mwenya	Spring	196.9	5.8	9.6	34.2	15.1	17.5	0.1	0.0	0.1	10.5	5.1	1.4	0.0	0.4	14.6	0.156	1.6	110.3
54	Mwenya-Rwimbogo	Spring	87.2	6.2	6.8	14.0	1.8	17.9	0.1	0.0	0.1	5.5	3.1	0.0	0.1	0.9	6.9	0.131	15.0	72.3
55	Nagikono-Kinyangurube	Spring	134.7	5.7	9.0	39.0	1.3	15.9	0.1	0.0	0.1	7.9	4.3	0.0	0.0	1.6	11.8	0.223	8.9	100.1
58	Nakabingo II-Gihosha	Spring	134.6	4.9	7.2	3.7	13.4	34.4	0.1	0.0	0.1	8.0	4.1	0.3	0.1	5.6	6.9	0.122	17.6	101.7
61	Narukere-Gihosha	Spring	57.3	4.9	5.1	7.9	1.3	16.1	0.2	0.0	0.1	3.7	1.5	0.0	0.1	0.4	6.8	0.106	13.8	57.1
62	Narutambwe-Kireka	Spring	80.7	6.6	0.9	7.9	1.2	25.9	0.1	0.0	0.1	0.4	2.3	0.0	0.0	0.8	7.7	0.085	4.0	51.5
65	RamboII-Gatwe	Spring	178.6	6.9	6.1	14.6	13.8	43.3	0.2	0.0	0.1	6.8	5.6	0.0	0.1	1.5	14.0	0.067	15.2	121.6
66	Rubira-Gatemere	Spring	55.4	5.2	4.3	8.5	1.1	8.2	0.1	0.0	0.1	1.6	1.1	0.0	0.2	0.4	5.9	0.097	13.1	44.6
67	Rugangazi-Ntogwe	Spring	62.2	4.5	4.8	9.2	1.2	11.2	0.1	0.0	0.1	2.5	1.3	0.2	0.4	2.1	4.8	0.069	13.4	51.3
68	Rugero-Nakarinzi	Spring	22.6	6.5	0.6	15.3	1.2	1.2	0.1	0.0	0.7	3.2	1.3	0.0	0.1	0.2	2.2	0.117	5.1	31.5
70	Rugomero-Gatemere	Spring	60.6	6.3	0.7	9.8	2.4	24.5	0.1	0.0	0.1	3.7	1.8	0.0	0.3	0.3	6.1	0.057	0.6	51.1
71	Rugomero-Kiravumba	Spring	38.6	4.9	4.3	14.0	1.6	0.8	0.1	0.0	0.1	1.6	0.9	0.0	0.1	0.4	4.4	0.089	14.9	43.4
72	Rugomero-Nyabugeni	Spring	104.4	6.9	9.8	15.3	2.0	2.3	0.1	0.0	0.1	4.1	2.6	0.0	0.3	0.6	10.0	0.169	0.5	47.9
76	Rushubije-Cogo	Spring	53.1	4.7	3.3	4.9	1.0	14.6	0.1	0.0	0.1	1.8	1.5	0.0	0.1	0.8	5.4	0.145	5.7	39.4
77	Twengebuye-Nakabingo	Spring	86.5	4.7	4.6	3.1	1.1	27.3	0.1	0.0	0.1	5.0	2.4	0.1	0.1	1.1	5.3	0.421	5.1	55.7
	Average (Cl = 0-10 mg/l)				**5.4**	**15.2**	**4.0**	**16.2**	**0.1**	**0.0**	**0.1**	**4.8**	**2.5**	**0.1**	**0.1**	**1.3**	**7.5**	**0.2**	**8.7**	**66.5**

S/N	Site	Type	EC µS/cm-25°C	pH	Cl mg/l	HCO_3 mg/l	SO_4 mg/l	NO_3 mg/l	NO_2 mg/l	NH_4 mg/l	PO_4 mg/l	Ca mg/l	Mg mg/l	Mn mg/l	Fe mg/l	K mg/l	Na mg/l	F mg/l	SiO_2 mg/l	TDS mg/l
17	Bihembe-Monge	Spring	215.0	6.9	17.7	11.0	34.3	30.2	0.1	0.0	0.1	6.4	7.2	0.3	0.4	3.1	18.4	0.078	4.3	133.5
21	Bunyari	Spring	155.7	7.0	13.6	53.1	6.1	10.3	0.1	0.0	0.0	4.4	2.9	0.0	0.1	0.9	22.3	0.168	14.4	128.6
29	Kabira-Kanyinya	Spring	156.0	7.0	16.4	31.7	4.1	14.1	0.0	0.0	0.0	9.2	3.8	0.0	0.1	3.6	11.2	0.135	9.4	103.9
30	Kabira-Renga	Spring	148.1	5.9	22.5	30.5	1.2	2.4	0.1	0.0	0.1	5.1	2.8	0.0	0.2	0.2	18.9	0.084	16.7	101.0
32	Kanyamanza-Kagege	Spring	127.4	6.2	16.1	25.0	1.1	9.6	0.1	0.0	0.1	5.1	2.9	0.0	0.1	1.1	14.4	0.086	9.6	85.3
33	Kararire-Kagege	Spring	149.2	6.5	25.7	9.8	7.1	5.5	0.1	0.0	0.1	6.6	3.7	0.0	0.0	1.8	12.8	0.079	4.4	77.7
34	Karira-Gatemere	Spring	201.0	6.0	27.8	15.9	19.0	8.6	0.1	0.0	0.1	9.3	5.0	0.1	0.1	3.2	17.9	0.104	8.3	115.5
35	Karobogo	Spring	105.2	7.2	10.7	15.9	6.2	23.6	0.0	0.0	0.0	5.9	2.7	0.0	0.1	20.0	1.9	0.097	8.8	96.0
38	Kigoti-Munzenze	Spring	162.4	5.8	18.4	32.3	1.2	20.2	0.1	0.0	0.1	7.3	4.2	0.2	0.0	0.7	15.5	0.113	5.7	106.0
41	Kinywamagana-Kigarama	Spring	87.7	5.2	15.3	5.5	1.1	7.7	0.1	0.0	0.1	3.6	1.8	0.0	0.0	0.7	9.1	0.122	3.0	48.1
48	Mukuyo-Kiri	Spring	766.0	7.0	16.5	328.2	96.2	10.6	0.1	0.0	0.5	39.6	9.8	0.0	0.1	5.8	123.8	0.161	22.4	655.3
49	Musave-Mugobe	Spring	179.8	5.6	10.6	30.5	23.5	6.2	0.1	0.0	0.1	10.0	3.0	0.0	0.0	2.4	12.1	0.196	2.8	101.7
56	Nakabingo	Spring	169.1	6.8	11.7	56.1	5.4	6.0	0.0	0.0	0.0	10.8	5.4	0.0	0.1	1.3	10.0	0.068	9.1	116.2
57	Nakabingo-Gatemere	Spring	59.1	6.2	13.2	12.8	7.6	3.5	0.2	0.0	0.1	3.8	2.0	0.0	0.4	0.8	6.9	0.365	14.2	66.8
60	Nakivumbura-Monge	Spring	134.4	5.6	12.5	29.3	9.4	5.4	0.1	0.0	0.1	6.4	3.7	0.0	0.2	2.3	11.8	0.114	16.6	98.5
63	Nyabitare-Munyinya	Spring	179.5	5.8	28.1	16.5	4.7	23.7	0.1	0.0	0.1	10.7	4.6	0.0	0.1	1.0	15.6	0.205	6.3	111.6
64	Nyaruziba-Mutara	Spring	167.4	6.2	12.4	29.9	19.5	19.4	0.1	0.0	0.1	11.0	6.3	0.0	0.1	4.2	8.2	0.125	11.4	122.4
69	Rugoma-Kagege	Spring	75.4	5.7	10.4	9.8	4.6	5.2	0.1	0.0	0.1	4.7	2.3	0.0	0.1	1.4	5.4	0.083	5.9	50.1
73	Rugunga II- Kavomo	Spring	166.9	6.2	10.0	33.6	13.6	3.5	0.1	0.0	0.1	3.1	5.0	0.0	0.0	1.2	15.8	0.119	8.7	94.8
74	Rugunga I-Kavomo	Spring	135.7	5.7	16.5	23.2	6.4	11.9	0.1	0.0	0.1	4.5	2.6	0.0	0.1	1.0	17.1	0.091	8.2	91.9
75	Ruhongore-Munyinya	Spring	162.5	6.6	24.0	17.1	7.1	14.0	0.1	0.0	0.1	8.7	4.3	0.0	0.1	1.4	13.7	0.079	15.1	105.9
79	Bunyari-Rugarama	Well	462.0	6.9	11.3	215.9	10.2	22.0	0.0	0.0	0.1	19.5	14.0	0.0	0.1	54.5	18.0	1.121	21.9	388.8
80	Cimbogo-Gatete	Well	1108.0	7.5	23.3	688.7	4.3	14.4	0.1	0.0	0.6	97.4	54.4	3.2	0.7	79.0	34.2	1.450	16.8	1018.4
81	Cinyambo	Well	414.0	7.1	24.9	198.3	6.8	7.2	0.0	0.0	0.1	23.9	10.9	0.8	0.2	40.0	23.9	0.272	18.5	355.8
92	Kadobogoro-Muramba	Well	210.0	7.2	12.4	51.9	20.4	6.1	0.1	0.0	0.1	10.9	3.6	0.1	2.9	1.5	20.6	0.163	4.3	134.9
103	Kigina I-Gisenyi	Well	415.0	7.4	13.1	211.7	7.1	5.7	0.1	0.0	0.0	46.1	10.5	0.0	0.4	0.5	23.0	0.743	20.3	339.3
104	Kigina II-Gisenyi	Well	352.0	7.0	10.6	149.5	11.2	13.6	0.3	0.0	0.0	25.6	12.4	0.0	0.3	0.1	26.7	1.146	4.9	256.5
83	Foko I-Kiyonza	Well	1550.0	7.1	25.2	608.8	213.3	68.3	0.1	0.1	0.1	92.1	38.8	0.0	0.0	43.0	175.5	0.956	22.9	1289.1
112	Marembo-Marembo	Well	454.0	7.3	21.4	209.8	1.7	30.7	0.1	0.0	0.1	31.0	10.9	0.9	3.6	16.7	25.6	0.875	15.2	368.6
113	Mataka-Rugasa	Well	722.0	6.9	18.7	391.0	10.3	11.8	0.0	0.0	0.1	56.2	25.8	0.0	0.2	19.0	42.3	0.640	13.6	589.6
116	Muhero II - Yaranda	Well	362.0	7.7	20.6	161.7	4.0	9.4	0.9	0.0	0.1	20.5	8.9	0.5	9.7	9.9	30.5	1.017	4.5	282.1
122	Ngaragu-kiri	Well	1196.0	7.0	11.6	547.2	144.4	40.1	0.0	0.1	0.1	58.0	25.9	1.3	0.6	1.3	180.4	3.540	15.2	1029.5
128	Rugoma-Kagege	Well	149.2	6.8	14.1	42.7	13.1	7.0	1.8	0.2	0.0	10.7	3.8	0.1	1.6	13.7	8.7	0.150	11.3	129.0
136	Rwasama-Kiri	Well	496.0	7.3	23.4	186.1	53.6	24.3	0.1	0.0	0.2	32.4	11.5	0.4	0.2	2.2	52.3	0.822	29.9	417.3
	Average (Cl =10-30 mg/l)				**17.1**	**131.8**	**22.9**	**14.8**	**0.2**	**0.0**	**0.1**	**20.6**	**9.3**	**0.2**	**0.7**	**10.0**	**30.7**	**0.5**	**11.9**	**270.9**

			EC µS/cm-25°C	pH	Cl mg/l	HCO_3 mg/l	SO_4 mg/l	NO_3 mg/l	NO_2 mg/l	NH_4 mg/l	PO_4 mg/l	Ca mg/l	Mg mg/l	Mn mg/l	Fe mg/l	K mg/l	Na mg/l	F mg/l	SiO_2 mg/l	TDS mg/l
	Average (Cl = 10-30 mg/l)				**17.1**	**131.8**	**22.9**	**14.8**	**0.2**	**0.0**	**0.1**	**20.6**	**9.3**	**0.2**	**0.7**	**10.0**	**30.7**	**0.5**	**11.9**	**270.9**
	Saline soils (average)		**11440.0**	**8.4**	**1642.2**	**32.3**	**3690.1**	**9.1**	**0.2**	**0.6**	**0.1**	**124.4**	**160.5**	**0.0**	**0.1**	**57.8**	**2215.3**	**8.0**	**8.9**	**7968.9**
	f spring		**0.993**																	
	fsalt water		**0.007**																	
	Expected concentration				**17.1**	**15.3**	**30.3**	**16.2**	**0.1**	**0.0**	**0.1**	**5.7**	**3.7**	**0.1**	**0.1**	**1.7**	**23.3**	**0.2**	**8.7**	**123.0**
	Δ Reaction (mg/l)				**-0.1**	**116.4**	**-7.4**	**-1.4**	**0.0**	**0.0**	**0.0**	**14.9**	**5.7**	**0.2**	**0.5**	**8.3**	**7.4**	**0.2**	**3.2**	**147.9**
	Molar weight (mg)					**61**	**96**	**62**	**46**	**18**	**95**	**40**	**24**	**55**		**39**	**23**	**19**	**60**	
	Δ Reaction (mmol/l)					**1.91**	**-0.08**	**-0.02**	**0.00**	**0.00**	**0.00**	**0.37**	**0.24**	**0.00**		**0.21**	**0.32**	**0.01**	**0.05**	

S/N	Site	Type	EC µS/cm-25°C	pH	Cl mg/l	HCO_3 mg/l	SO_4 mg/l	NO_3 mg/l	NO_2 mg/l	NH4 mg/l	PO4 mg/l	Ca mg/l	Mg mg/l	Mn mg/l	Fe mg/l	K mg/l	Na mg/l	F mg/l	SiO_2 mg/l	TDS mg/l
23	Gaharata	Spring	197.0	7.1	30.4	21.4	3.8	17.3	0.0	0.0	0.0	8.3	3.8	0.0	0.1	3.9	17.3	0.147	6.3	112.6
31	Kagogo-Nyabitare	Spring	191.0	5.0	30.7	6.1	2.9	36.0	0.1	0.0	0.1	8.0	4.9	0.0	0.0	1.8	17.4	0.154	15.1	123.3
114	Muhero I - Yaranda	Well	267.0	7.0	31.9	74.4	6.5	6.9	0.1	0.0	0.1	18.5	5.9	0.3	2.1	1.0	16.8	0.420	14.5	179.4
18	Bishunzi-Munyinya	Spring	168.8	5.6	33.8	12.2	2.3	11.5	0.1	0.0	0.1	7.5	5.0	0.0	0.0	1.7	15.5	0.087	1.1	90.9
59	Nakarambo-Rutabo	Spring	174.3	6.1	35.0	22.0	1.3	13.4	0.1	0.0	0.1	8.2	4.1	0.1	0.2	0.7	19.2	0.171	18.2	122.7
113	Mugombwa-Kiri	Well	1066.0	7.2	35.1	465.4	79.3	65.3	0.1	0.1	0.1	76.0	35.8	0.0	0.1	23.4	102.6	3.040	22.6	909.1
50	Musave-Rutabo	Spring	225.0	7.1	41.5	20.1	1.6	9.2	0.1	0.0	0.1	6.6	4.2	0.3	2.1	0.2	23.2	0.136	1.6	110.9
119	Murehe-Murungurira	Well	577.0	6.8	43.4	172.0	52.2	18.5	0.1	0.0	0.1	32.1	6.3	0.5	4.2	1.7	71.5	2.170	2.5	407.2
117	Muramba-Kiruhura II	Well	478.0	6.5	46.7	164.1	34.6	3.8	0.1	0.0	0.1	48.4	6.0	1.8	1.2	1.3	29.9	1.141	20.2	359.3
94	Kanabugiri-Bugera	Well	685.0	7.6	48.2	258.0	55.5	5.1	0.0	0.0	0.0	28.9	28.9	0.3	0.1	24.0	79.3	4.990	5.0	538.5
85	Gasagara I-Rubuga	Well	1777.0	7.0	49.3	560.0	446.0	15.2	0.0	0.1	0.1	169.9	44.6	0.0	0.1	35.4	165.2	1.417	19.9	1507.2
89	Kabirizi II-Kigoma	Well	903.0	7.0	50.8	251.9	78.0	44.0	0.1	0.1	0.1	74.6	16.5	0.0	0.1	48.4	41.0	1.237	20.6	627.4
135	Ruyivyi II	Well	687.0	6.8	55.9	288.5	16.8	10.7	0.1	0.0	0.1	52.0	17.0	0.1	0.8	50.5	50.3	0.851	12.2	555.8
27	Gihushi-Kiravumba	Spring	279.0	5.6	56.7	17.1	4.6	12.0	0.1	0.0	0.1	11.7	3.8	0.1	0.1	1.5	26.8	0.097	7.3	141.8
131	Runyangona II-Nyabikenke	Well	625.0	6.2	59.2	276.3	2.7	4.0	0.0	0.7	0.0	47.8	18.8	4.0	25.7	18.6	25.4	0.582	10.0	493.8
134	Ruseno-Kanyagu	Well	452.0	6.3	59.7	105.5	21.8	3.5	0.1	0.0	0.7	16.5	2.6	0.0	0.9	10.0	60.0	0.320	5.8	287.3
	Average (Cl = 30-60 mg/l)				44.3	169.7	50.6	17.3	0.1	0.1	0.1	38.4	13.0	0.5	2.4	14.0	47.6	1.1	11.4	410.4
	Saline soils (average)		11440.0	8.4	1642.2	32.3	3690.1	9.1	0.2	0.6	0.1	124.4	160.5	0.0	0.1	57.8	2215.3	8.0	8.9	7968.9
	f spring		0.976																	
	fsalt water		0.024																	
	Expected concentration				44.3	15.6	91.6	16.1	0.1	0.0	0.1	7.7	6.3	0.1	0.1	2.6	60.0	0.4	8.7	254.3
	Δ Reaction (mg/l)				-0.1	154.1	-41.0	1.2	0.0	0.1	0.0	30.8	6.7	0.4	2.2	11.4	-12.4	0.7	2.7	156.2
	Molar weight in mg					61	96	62	46	18	95	40	24	55		39	23	19	60	
	Δ Reaction (mmol/l)					2.53	-0.43	0.02	0.00	0.00	0.00	0.77	0.28	0.01		0.29	-0.54	0.04	0.05	

S/N	Site	Type	EC µS/cm-25°C	pH	Cl mg/l	HCO_3 mg/l	SO_4 mg/l	NO_3 mg/l	NO_2 mg/l	NH_4 mg/l	PO_4 mg/l	Ca mg/l	Mg mg/l	Mn mg/l	Fe mg/l	K mg/l	Na mg/l	F mg/l	SiO_2 mg/l	TDS mg/l
98	Karago-Rukuramigabo	Well	1270.0	7.4	63.8	708.2	1.8	13.1	0.1	0.0	0.1	13.8	22.5	0.9	31.9	104.0	168.3	1.131	9.6	1139.2
96	Kantuye-Ceru	Well	848.0	7.2	66.8	412.4	2.2	8.9	6.7	0.0	0.1	47.1	15.8	14.5	2.2	56.5	78.0	1.655	9.4	722.2
122	Ndava II	Well	821.0	7.1	71.8	361.1	2.1	15.1	0.1	1.4	0.0	44.7	21.9	0.0	3.2	13.8	89.8	2.720	0.7	628.5
133	Ruranzi-Rwibikara	Well	746.0	7.5	73.0	323.9	3.5	1.9	0.0	1.8	0.0	37.4	18.9	0.1	8.2	23.3	70.3	1.490	8.1	571.9
103	Kigoma-Gatare	Well	536.0	6.9	73.5	115.9	57.4	7.9	0.1	0.0	0.1	40.2	11.5	2.0	9.6	4.6	40.5	0.370	20.7	384.2
100	Kigazi-Nyakarama	Well	2650.0	7.2	74.0	1062.0	264.2	80.2	0.0	0.2	0.1	106.2	63.3	0.1	0.2	2.6	380.5	3.570	18.9	2056.0
105	Kinyamateke	Well	799.0	6.3	78.9	160.4	108.6	54.6	0.1	0.1	0.3	36.9	26.4	0.0	0.1	17.0	70.3	0.420	17.2	571.2
87	Haga II	Well	1282.0	7.2	81.5	491.7	25.4	8.9	0.1	0.5	0.1	68.1	26.2	1.2	2.1	29.0	97.1	2.580	10.6	844.8
143	Susa-Gikomero	Well	548.0	6.6	82.4	47.0	39.2	69.9	0.1	0.0	0.1	28.1	15.4	1.7	0.1	42.0	40.1	0.283	9.6	375.7
121	Mutoza-Yaranda	Well	807.0	7.0	82.6	294.0	31.6	0.2	1.6	1.9	0.1	50.5	6.2	0.2	27.1	1.7	78.5	0.448	11.0	587.5
	Average (Cl = 60-90 mg/l)				74.8	397.7	53.6	26.1	0.9	0.6	0.1	47.3	22.8	2.1	8.5	29.4	111.3	1.5	11.6	788.1
	Saline soils (average)		11440.0	8.4	1642.2	32.3	3690.1	9.1	0.2	0.6	0.1	124.4	160.5	0.0	0.1	57.8	2215.3	8.0	8.9	7968.9
	f spring		0.958																	
	fsalt water		0.042																	
	Expected concentration				74.8	15.9	160.3	15.9	0.1	0.0	0.1	9.9	9.2	0.1	0.1	3.7	101.1	0.5	8.7	401.5
	Δ Reaction (mg/l)				0.0	381.7	-106.7	10.1	0.8	0.6	0.0	37.4	13.5	2.0	8.3	25.8	10.2	1.0	2.9	386.6
	Molar weight in mg					61	96	62	46	18	95	40	24	55		39	23	19	60	
	Δ Reaction (mmol/l)					6.26	-1.11	0.16	0.00	0.00	0.00	0.94	0.56	0.04		0.66	0.44	0.05	0.05	

S/N	Site	Type	EC µS/cm-25°C	pH	Cl mg/l	HCO_3 mg/l	SO_4 mg/l	NO_3 mg/l	NO_2 mg/l	NH_4 mg/l	PO_4 mg/l	Ca mg/l	Mg mg/l	Mn mg/l	Fe mg/l	K mg/l	Na mg/l	F mg/l	SiO_2 mg/l	TDS mg/l
99	Karisha	Well	1230.0	6.9	90.4	597.2	13.9	42.1	0.1	0.1	0.1	67.1	24.9	0.0	0.0	14.2	145.7	1.311	10.8	1007.8
130	Rukore-II-Kigina	Well	951.0	6.5	95.6	414.8	21.5	5.0	0.0	4.9	0.0	82.2	24.7	1.1	6.0	44.4	67.3	1.006	5.9	774.4
104	Kigozi-Yaranda	Well	1547.0	6.9	97.0	585.6	108.5	41.6	0.0	0.1	0.1	92.3	46.3	0.2	0.5	55.0	138.1	1.628	4.4	1171.2
140	Shenga I- Rugasa	Well	680.0	6.7	100.5	220.2	3.0	4.2	0.1	0.0	0.0	28.5	12.8	0.6	3.7	50.5	73.4	0.499	8.5	506.4
95	Kanigo-Cinuma	Well	2160.0	7.0	110.6	458.1	432.6	57.9	0.2	0.1	0.1	68.5	68.5	1.0	0.2	25.0	283.8	1.527	18.6	1526.7
108	Kiyonza-Foko II	Well	1302.0	7.3	111.8	485.6	101.7	54.5	0.0	0.1	0.1	97.4	38.7	0.1	0.1	37.4	124.6	1.357	28.8	1082.0
39	Kinyangoro-Kumana	Spring	55.8	7.0	115.2	20.7	1.4	16.4	0.1	0.0	0.1	4.3	2.0	0.0	0.4	0.4	4.3	0.158	4.0	169.5
138	Saruduha II	Well	1920.0	7.4	118.5	880.2	132.9	4.8	0.0	0.1	0.9	93.6	60.7	0.1	0.9	42.4	218.0	5.480	15.6	1574.2
83	Gahwijo II	Well	1219.0	6.6	118.6	403.2	147.9	3.9	0.0	0.7	0.1	124.1	25.6	7.6	9.5	63.2	65.5	0.740	19.2	989.8
	Average (Cl = 90-120 mg/l)				106.5	451.7	107.0	25.6	0.1	0.7	0.1	73.1	33.8	1.2	2.4	36.9	124.5	1.5	12.9	978.0
	Saline soils (average)		11440.0	8.4	1642.2	32.3	3690.1	9.1	0.2	0.6	0.1	124.4	160.5	0.0	0.1	57.8	2215.3	8.0	8.9	7968.9
	f spring		0.938																	
	fsalt water		0.062																	
	Expected concentration				106.5	16.3	231.6	15.8	0.1	0.0	0.1	12.2	12.3	0.1	0.1	4.8	143.9	0.7	8.7	554.6
	Δ Reaction (mg/l)				0.0	435.5	-124.6	9.8	0.0	0.6	0.1	60.9	21.5	1.1	2.2	32.2	-19.4	0.9	4.1	423.4
	Molar weight in mg					61	96	62	46	18	95	40	24	55		39	23	19	60	
	Δ Reaction (mmol/l)					7.14	-1.30	0.16	0.00	0.00	0.00	1.52	0.89	0.02		0.82	-0.84	0.05	0.07	

S/N	Site	Type	EC µS/cm-25°C	pH	Cl mg/l	HCO_3 mg/l	SO_4 mg/l	NO_3 mg/l	NO_2 mg/l	NH4 mg/l	PO_4 mg/l	Ca mg/l	Mg mg/l	Mn mg/l	Fe mg/l	K mg/l	Na mg/l	F mg/l	SiO_2 mg/l	TDS mg/l
91	Kadobori I	Well	1153.0	6.9	122.2	302.6	77.9	14.4	0.0	0.0	0.1	67.4	18.9	0.4	0.1	52.0	77.7	0.638	18.6	752.9
116	Munyinya-Nyakarama	Well	2690.0	7.0	129.0	1029.7	256.1	75.9	0.2	0.1	0.1	132.2	58.2	0.0	0.2	61.2	307.5	1.369	16.7	2068.4
97	Karago-Kibonde	Well	762.0	7.1	129.4	215.3	10.2	5.0	0.0	0.0	0.0	79.0	10.6	0.0	6.4	15.5	45.6	0.478	9.7	528.0
106	Kiruhura I-Kiyanza	Well	1468.0	7.7	138.3	488.0	109.9	10.1	0.2	0.4	0.1	78.6	26.0	0.1	11.2	29.0	161.2	0.430	4.5	1058.0
110	Mago - Gatete	Well	3730.0	8.5	142.0	1984.9	154.5	6.6	0.1	0.0	0.1	40.0	3.0	0.2	0.2	252.0	630.0	9.410	6.2	3229.1
84	Gasagara II-Rubuga	Well	2900.0	7.8	145.3	1378.0	167.8	52.5	0.0	0.1	0.1	75.9	71.6	0.2	0.4	35.2	431.0	4.230	18.4	2380.7
120	Murungurira-Ntwago	Well	1120.0	7.1	149.2	239.1	86.8	9.8	0.1	0.0	0.1	26.9	12.0	0.5	0.7	0.5	184.4	16.530	14.4	741.0
	Average				136.5	805.4	123.3	24.9	0.1	0.1	0.1	71.4	28.6	0.2	2.7	63.6	262.5	4.7	12.6	1536.9
	Saline soils (average)		11440.0	8.4	1642.2	32.3	3690.1	9.1	0.2	0.6	0.1	124.4	160.5	0.0	0.1	57.8	2215.3	8.0	8.9	7968.9
	f spring		0.920																	
	fsalt water		0.080																	
	Expected concentration				136.5	16.6	299.2	15.7	0.1	0.1	0.1	14.4	15.2	0.1	0.1	5.8	184.4	0.8	8.7	699.4
	Δ Reaction (mg/l)				0.0	788.8	-175.9	9.3	0.0	0.1	0.0	57.0	13.4	0.1	2.6	57.8	78.1	3.9	3.9	837.4
	Molar weight in mg					61	96	62	46	18	95	40	24	55		39	23	19	60	
	Δ Reaction (mmol/l)					12.93	-1.83	0.15	0.00	0.00	0.00	1.43	0.56	0.00		1.48	3.40	0.21	0.06	

S/N	Site	Type	EC µS/cm-25°C	pH	Cl mg/l	HCO_3 mg/l	SO_4 mg/l	NO_3 mg/l	NO_2 mg/l	NH_4 mg/l	PO_4 mg/l	Ca mg/l	Mg mg/l	Mn mg/l	Fe mg/l	K mg/l	Na mg/l	F mg/l	SiO_2 mg/l	TDS mg/l
92	Kadobori II	Well	1990.0	7.2	157.7	598.4	267.1	24.0	0.0	0.1	0.1	160.8	46.4	0.2	0.1	44.6	162.3	0.622	22.9	1485.4
109	Kiyonza-Nunga	Well	1301.0	6.9	164.5	465.4	49.0	7.6	0.0	0.0	0.0	79.5	56.5	0.1	2.8	58.0	102.1	0.765	13.5	999.8
118	Murambo-Murambi	Well	1606.0	7.2	167.2	669.8	110.2	5.1	0.2	5.7	0.0	87.7	49.0	0.1	2.4	82.0	173.2	2.580	8.5	1363.5
126	Nunga II-Yaranda	Well	1618.0	6.8	181.2	476.4	100.8	8.4	0.2	1.0	0.1	95.0	24.8	0.2	11.9	30.1	190.0	0.632	16.6	1137.1
88	Hambiro-Kiyonza	Well	2400.0	7.3	190.8	682.0	253.6	75.5	0.0	0.1	0.1	135.2	55.9	0.0	0.1	38.4	247.1	2.350	30.1	1711.2
125	Ntembe I-Kiri	Well	3260.0	7.1	199.9	1044.3	504.3	38.9	0.1	0.1	0.0	121.7	59.7	0.4	0.1	52.4	511.5	2.530	20.3	2556.3
132	Runyonza-Kabonde	Well	2050.0	7.3	202.7	478.9	121.7	9.2	2.8	0.6	0.1	65.0	43.2	2.7	1.9	64.0	213.0	3.160	7.5	1216.3
124	Ntembe II-Kiri	Well	3420.0	6.9	303.2	855.2	337.1	66.7	0.1	0.1	0.3	167.0	61.3	1.2	0.0	108.0	335.7	1.264	19.6	2256.5
86	Gifuruguti-Nyakarama	Well	2860.0	6.8	317.2	539.2	329.2	15.8	0.0	0.1	0.1	135.1	53.6	0.8	0.2	49.2	304.0	0.798	17.4	1762.6
137	Saruduha I	Well	2500.0	6.9	328.6	522.8	251.2	49.5	0.0	0.1	0.2	129.5	57.1	7.5	0.2	9.0	244.5	1.568	20.3	1622.2
78	Bishunzi -Cewe	Well	2520.0	6.8	386.6	550.2	153.7	7.4	0.0	0.0	0.0	56.4	74.5	0.2	3.0	115.8	276.2	2.360	5.7	1632.2
82	Gahwijo I	Well	3110.0	6.8	406.4	935.7	193.0	20.6	0.0	0.1	0.1	113.0	53.6	0.1	0.2	44.2	439.0	0.995	15.5	2222.6
142	Shenga II-Rugasa	Well	2820.0	6.8	466.4	608.8	125.3	9.0	7.2	0.0	0.0	80.4	39.7	0.4	2.9	37.8	418.0	0.295	8.8	1805.0
141	Shenga III-Rugasa	Well	2790.0	6.7	499.3	605.1	72.3	16.2	0.0	0.0	0.0	81.8	39.0	0.5	54.0	38.5	336.2	0.320	5.4	1748.6
	Average (Cl > 150 mg/l)				283.7	645.2	204.9	25.3	0.8	0.6	0.1	107.7	51.0	1.0	5.7	55.1	282.3	1.4	15.1	1679.9
	Saline soils (average)		11440.0	8.4	1642.2	32.3	3690.1	9.1	0.2	0.6	0.1	124.4	160.5	0.0	0.1	57.8	2215.3	8.0	8.9	7968.9
	f spring		0.830																	
	fsalt water		0.170																	
	Expected concentration				283.7	18.1	630.7	15.0	0.1	0.1	0.1	25.1	29.4	0.1	0.1	10.9	382.9	1.5	8.7	1410.1
	Δ Reaction (mg/l)				0.0	627.0	-425.8	10.3	0.6	0.5	0.0	82.6	21.6	0.9	5.6	44.2	-100.6	-0.1	6.4	269.9
	Molar weight in mg					61	96	62	46	18	95	40	24	55		39	23	19	60	
	Δ Reaction (mmol/l)					10.28	-4.44	0.17	0.00	0.00	0.00	2.06	0.90	0.02		1.13	-4.37	0.00	0.11	

Appendix VII.7. Saturation indices for different water samples

Phase	1	2	3	4	5	6	7	8	9	10	11	12	13	14	15	16	17	18	Formulae
Amm (g)	-8.03	-7.74		-7.88	-7.98	-7.79	-9.16	-9.96	-8.16	-9.97	-10.64	-10.83	-8.73	-8.43	-9.94	-8.46	-10.73	-12.08	NH_3
Anhydrite	-3.75	-3.78	-4.03	-3.61	-3.76	-3.77	-3.81	-3.58	-3.79	-3.88	-4.31	-4.18	-3.9	-1.94	-3.99	-3.69	-3.1	-4.18	$CaSO_4$
Aragonite	-0.53	-0.62	-0.29	-0.18	-2.31	-0.33	0.78	-0.79	-0.89	-0.8	-1.97	-1.58	-1.98	-0.57	0.09	-0.36	-2.92	-4.71	$CaCO_3$
Calcite	-0.39	-0.48	-0.15	-0.04	-2.16	-0.18	0.92	-0.64	-0.75	-0.66	-1.82	-1.44	-1.84	-0.42	0.23	-0.22	-2.78	-4.57	$CaCO_3$
Chalcedony	-0.3	-0.48	-1.38	-0.26	-0.32	-0.53	-0.69	-0.98	-0.36	-0.56	-0.48	-0.15	-0.82	-0.17	-0.86	-0.14	-0.6	-1.19	SiO_2
Chrysotile	-5.44	-5.62	-6.62	-4.18	-5.83	-4.92	0.46	-9.51	-8.09	-7.26	-10.89	-8.22	-11.67	-5.13	-3.92	-4.45	-11.43	-19.34	$Mg_3Si_2O_5(OH)_4$
CO_2(g)	-1.99	-2.22	-2.21	-2.22	-3.68	-2.17	-3.07	-1.49	-1.71	-2.2	-1.91	-2.19	-1.89	-2.05	-2.47	-2.14	-2.92	-2.31	CO_2
Dolomite	-0.43	-0.69	-0.08	0.09	-4.02	-0.08	2.03	-1.08	-1.35	-1.34	-3.48	-2.71	-3.5	-0.5	0.59	-0.18	-5.55	-8.96	$CaMg(CO_3)_2$
$Fe(OH)_3$ (a)	2.32	2.27	2.33	2.34	2.06	2.05	3.13	3.16	2.36	2.53	2.52	2.59	2.44	2.17	2.51	2.29	2.23	-2.31	$Fe(OH)_3$ (a)
Fluorite	-1.55	-1.47	-1.55	-1.47	-1.5	-1.58		-1.7	-2.01	-2.25	-2.64	-2.69	-2.67	-1.5	-1.35	-1.41	-3.08	-4.04	CaF_2
Goethite	8.21	8.17	8.22	8.23	7.96	7.94	9.02	9.05	8.25	8.42	8.41	8.48	8.33	8.06	8.4	8.18	8.12	3.59	FeOOH
Gypsum	-3.53	-3.56	-3.82	-3.39	-3.54	-3.55	-3.59	-3.36	-3.57	-3.66	-4.09	-3.96	-3.68	-1.72	-3.77	-3.47	-2.88	-3.96	$CaSO_4.2H_2O$
H_2 (g)	-29.36	-29.52	-30.44	-30.32	-29.2	-30.16	-33.92	-27.52	-27.92	-29.36	-26.92	-28.28	-26.84	-29.44	-31.32	-29.8	-27.44	-22.44	H_2 (g)
H_2O (g)	-1.51	-1.51	-1.51	-1.51	-1.51	-1.51	-1.51	-1.51	-1.51	-1.51	-1.51	-1.51	-1.51	-1.51	-1.51	-1.51	-1.51	-1.51	H_2O (g)
Halite	-6.89	-6.77	-6.96	-6.88	-6.84	-6.84	-6.53	-6.66	-6.74	-7.57	-8.74	-9.95	-8.49	-6.42	-6.45	-6.39	-8.03	-7.81	NaCl
Hausmannite	-5.17	-3.58	-1.91	-3.29	-5.82	-3.13	6.69	-7.3	-7.21	-3.85	-10.09	-6.97	-10.29	-5.45	-0.46	-4.5	-8.58	-23.8	Mn_3O_4
Hematite	18.42	18.34	18.45	18.47	17.92	17.88	20.04	20.1	18.51	18.85	18.83	18.97	18.67	18.14	18.81	18.37	18.25	9.18	Fe_2O_3
Jarosite-K	-3.69	-4.04	-5.06	-4.15	-4.22	-5.18	-5.68	0.31	-2.67	-4.19	-2.46	-3	-1.9	-0.4	-5.42	-4.42	-1.23	-13.72	$KFe_3(SO_4)_2(OH)_6$
Manganite	-1.83	-1.27	-0.56	-1.04	-2.07	-1.01	2.89	-2.84	-2.75	-1.39	-3.88	-2.61	-3.95	-1.91	0.07	-1.53	-3.28	-9.19	MnOOH
Melanterite	-11.62	-11.92	-12.89	-12.52	-11.72	-12.71	-15.54	-8.94	-10.27	-11.49	-9.24	-10.39	-8.84	-10.03	-13.76	-12.14	-8.64	-9.36	$FeSO_4.7H_2O$
O_2 (g)	-24.47	-24.15	-22.31	-22.55	-24.79	-22.87	-15.35	-28.15	-27.35	-24.47	-29.35	-26.63	-29.51	-24.31	-20.55	-23.59	-28.31	-38.31	O_2 (g)
Pyrochroite	-6.37	-5.89	-5.64	-6.06	-6.53	-5.95	-3.93	-6.46	-6.57	-5.93	-7.2	-6.61	-7.23	-6.49	-5.45	-6.29	-6.86	-10.27	$Mn(OH)_2$
Pyrolusite	-3.19	-2.55	-1.38	-1.92	-3.51	-1.97	3.81	-5.12	-4.83	-2.75	-6.46	-4.51	-6.57	-3.23	-0.31	-2.67	-5.6	-14.01	$MnO_2.H_2O$
Quartz	0.11	-0.07	-0.98	0.14	0.09	-0.12	-0.29	-0.57	0.04	-0.16	-0.07	0.25	-0.42	0.23	-0.46	0.26	-0.19	-0.79	SiO_2
Rhodochrosite	-0.17	0.07	0.33	-0.09	-2.03	0.05	1.18	0.23	-0.1	0.05	-0.92	-0.62	-0.94	-0.35	0.26	-0.25	-1.6	-4.4	$MnCO_3$
Sepiolite	-4.34	-4.75	-6.93	-3.43	-4.62	-4.38	-1.06	-8.18	-6.21	-5.99	-8.27	-5.95	-9.36	-3.92	-4.27	-3.42	-8.83	-15.09	$Mg_2Si_3O_7.5OH.3H_2O$
Sepiolite (d)	-7.24	-7.65	-9.83	-6.33	-7.52	-7.28	-3.96	-11.08	-9.11	-8.89	-11.17	-8.85	-12.26	-6.82	-7.17	-6.32	-11.73	-17.99	$Mg_2Si_3O_7.5OH.3H_2O$
Siderite	-3.7	-4.05	-4.45	-4.38	-5.56	-4.56	-6.25	-1.44	-2.66	-3.7	-2.2	-3.09	-2.22	-3.94	-4.97	-4.1	-3.76	-5.18	$FeCO_3$
SiO_2(a)	-1.14	-1.32	-2.22	-1.1	-1.15	-1.37	-1.53	-1.82	-1.2	-1.4	-1.32	-0.99	-1.66	-1.01	-1.7	-0.98	-1.44	-2.03	$SiO_{2\,(a)}$
Talc	-2.34	-2.87	-5.69	-1	-2.76	-2.28	2.77	-7.77	-5.11	-4.68	-8.15	-4.83	-9.62	-1.78	-1.95	-1.04	-8.93	-18.03	$Mg_3Si_4O_{10}(OH)_2$

Phase	19	20	21	22	23	24	25	26	27	28	29	30	31	32	33	34	35	36	Formulae
Amm (g)	-11.46	-9.49	-9.71	-12.96		-10.26	-10.87	-11.13		-11.42		-11.5	-12.39	-11.32	-11.04	-11.75		-12.09	NH_3
Anhydrite	-4.19	-3.59	-3.98	-4.31	-3.94	-3.83	-4.79	-3.73	-3.71	-4.28	-3.83	-4.59	-4.06	-4.63	-3.73	-3.19	-3.83	-4.31	$CaSO_4$
Aragonite	-2.69	-0.79	-2.23	-6.92	-2.17	-2.05	-3.72	-2.54	-4.46	-3.54	-3.67	-3.93	-6.21	-3.47	-3.44	-3.81	-2.36	-5.06	$CaCO_3$
Calcite	-2.55	-0.65	-2.08	-6.78	-2.03	-1.91	-3.57	-2.4	-4.32	-3.39	-3.52	-3.78	-6.06	-3.33	-3.3	-3.67	-2.22	-4.92	$CaCO_3$
Chalcedony	-0.54	-0.08	-0.07	-0.09	-0.43	-0.2	-1.14	-0.15	-0.37	-0.54	-0.26	0	-0.05	-0.25	-0.59	-0.31	-0.28	-0.48	SiO_2
Chrysotile	-10.33	3.01	-9.58	-22.77	-9.05	-9.4	-15.14	-12.05	-18.32	-14.97	-16	-15.87	-20.93	-14.33	-13.35	-15.22	-8.77	-20.11	$Mg_3Si_2O_5(OH)_4$
CO_2(g)	-3	-5.14	-2.33	-2.77	-2.86	-2.59	-2.77	-2.07	-2.15	-2.29	-1.96	-1.97	-2.55	-2.18	-2.7	-2.29	-3.04	-2.02	CO_2
Dolomite	-5.07	-1.17	-4	-13.52	-4.06	-3.94	-7.07	-4.82	-8.77	-6.75	-7.08	-7.48	-11.99	-6.56	-6.49	-7.26	-4.43	-9.77	$CaMg(CO_3)_2$
$Fe(OH)_3$ (a)	1.29	1.22	1.5	-4.43	1.41	1.58	1.45	1.74	-1.53	0.79	-0.14	0.04	-4.26	0.74	0.58	-0.02	1.58	-1.77	$Fe(OH)_3$ (a)
Fluorite	-4.09	-3.89	-2.87	-3.62	-3.69	-3.38	-4.09	-3.33	-3.89	-3.39	-3.44	-3.7	-3.96	-3.59	-4	-3.95	-3.88	-4.05	CaF_2
Goethite	7.18	7.11	7.39	1.47	7.31	7.47	7.34	7.63	4.37	6.68	5.75	5.93	1.63	6.63	6.47	5.87	7.47	4.12	FeOOH
Gypsum	-3.97	-3.37	-3.76	-4.09	-3.72	-3.61	-4.57	-3.51	-3.49	-4.06	-3.61	-4.37	-3.84	-4.41	-3.51	-2.97	-3.61	-4.09	$CaSO_4.2H_2O$
H_2 (g)	-28.2	-17.98	-27.92	-19.44	-28.56	-28.12	-26.36	-26.32	-22.28	-25.04	-23.64	-23.64	-19.88	-24.96	-25.88	-24.04	-28.8	-21.6	H_2 (g)
H_2O (g)	-1.51	-1.51	-1.51	-1.51	-1.51	-1.51	-1.51	-1.51	-1.51	-1.51	-1.51	-1.51	-1.51	-1.51	-1.51	-1.51	-1.51	-1.51	H_2O (g)
Halite	-8.86	-8.55	-8.05	-9.49	-7.82	-8.87	-10.12	-8.36	-7.36	-9.01	-8.27	-7.9	-7.81	-8.16	-8.02	-7.84	-9.22	-8.71	NaCl
Hausmannite	-9.36	-8.08	-11.79	-30.66	-8.74		-14.52	-12.77	-23.51	-19.14	-20.97	-20.78	-31.2	-16.54	-14.99	-17.93	-8.08	-26.52	Mn_3O_4
Hematite	16.36	16.23	16.78	4.94	16.62	16.94	16.7	17.26	10.74	15.37	13.5	13.87	5.27	15.27	14.96	13.75	16.96	10.24	Fe_2O_3
Jarosite-K	-7.4	-11.74	-5.2	-17.89	-6.37	-5.28	-6.08	-3.66	-10.74	-6.66	-7.28	-9.04	-17.45	-7.22	-6.58	-5.96	-4.83	-11.43	$KFe_3(SO_4)_2(OH)_6$
Manganite	-3.42	-4.7	-4.27	-11.98	-3.15		-5.44	-4.87	-9.12	-7.2	-8.05	-7.98	-12.08	-6.35	-5.68	-6.97	-2.89	-10.24	MnOOH
Melanterite	-11.37	-9.76	-10.6	-8.36	-11.55	-10.89	-9.62	-8.74	-8.13	-8.82	-8.13	-8.47	-8.66	-9.12	-9.4	-7.76	-11.37	-7.89	$FeSO_4.7H_2O$
O_2 (g)	-26.79	-47.24	-27.35	-44.31	-26.07	-26.95	-30.47	-30.55	-38.63	-33.11	-35.91	-35.91	-43.43	-33.27	-31.43	-35.11	-25.59	-39.99	O_2 (g)
Pyrochroite	-7.38	-3.54	-8.09	-11.56	-7.29		-8.48	-7.89	-10.12	-9.58	-9.73	-9.66	-11.88	-8.69	-8.48	-8.85	-7.15	-10.9	$Mn(OH)_2$
Pyrolusite	-5.36	-11.75	-6.35	-18.3	-4.91		-8.3	-7.75	-14.02	-10.72	-12.27	-12.2	-18.18	-9.91	-8.78	-10.99	-4.53	-15.48	$MnO_2.H_2O$
Quartz	-0.13	0.33	0.34	0.31	-0.02	0.21	-0.74	0.25	0.04	-0.14	0.15	0.4	0.36	0.16	-0.18	0.1	0.12	-0.07	SiO_2
Rhodochrosite	-2.2	-0.5	-2.24	-6.14	-1.97		-3.07	-1.78	-4.09	-3.69	-3.5	-3.46	-6.25	-2.68	-3	-2.95	-2.01	-4.74	$MnCO_3$
Sepiolite	-7.99	1.67	-6.71	-15.55	-6.96	-6.81	-12.2	-8.5	-13.04	-11.09	-11.31	-10.8	-14.25	-10.17	-10.09	-10.88	-6.53	-14.41	$Mg_2Si_3O_7.5OH.3H_2O$
Sepiolite (d)	-10.89	-1.23	-9.61	-18.45	-9.86	-9.71	-15.1	-11.4	-15.94	-13.99	-14.21	-13.7	-17.15	-13.07	-12.99	-13.78	-9.43	-17.31	$Mg_2Si_3O_7.5OH.3H_2O$
Siderite	-5.16	-2.26	-4.14	-6.26	-5.08	-4.42	-3.84	-2.84	-4.17	-3.37	-3.27	-3.1	-6.1	-3.26	-4.41	-3.68	-5.2	-3.95	$FeCO_3$
SiO_2(a)	-1.38	-0.92	-0.91	-0.93	-1.27	-1.04	-1.98	-0.99	-1.21	-1.38	-1.1	-0.84	-0.89	-1.09	-1.43	-1.15	-1.12	-1.32	$SiO_{2\,(a)}$
Talc	-7.7	6.56	-6.02	-19.26	-6.21	-6.1	-13.72	-8.65	-15.35	-12.35	-12.81	-12.18	-17.33	-11.12	-10.82	-12.14	-5.63	-17.36	$Mg_3Si_4O_{10}(OH)_2$

Phase	**37**	**38**	**39**	**40**	**41**	**42**	**43**	**44**	**45**	**46**	**47**	**48**	**49**	**50**	**51**	**52**	**53**	**54**	**Formulae**
Amm (g)	-11.15	-12.17	-10.75	-12	-12.35	-10.38	-10.39	-10.48	-12.34	-11.68	-12.43	-10.46	-11.95	-10.26	-12.12	-10.62	-11.95	-11.54	NH_3
Anhydrite	-4.3	-4.47	-4.64	-4.12	-4.76	-4.51	-4.38	-2.24	-4.36	-4.26	-4.14	-2.09	-3.05	-4.41	-4.57	-3.61	-3.23	-4.38	$CaSO_4$
Aragonite	-3.9	-4.02	-2.64	-6.11	-6.16	-2.16	-3.08	-1.4	-5.84	-4.52	-4.28	-0.64	-4.16	-2.34	-4.08	-2.78	-3.86	-3.76	$CaCO_3$
Calcite	-3.76	-3.88	-2.49	-5.96	-6.02	-2.02	-2.93	-1.26	-5.69	-4.37	-4.14	-0.49	-4.02	-2.19	-3.93	-2.64	-3.71	-3.62	$CaCO_3$
Chalcedony	-0.58	-0.47	-0.63	-0.24	-0.76	-0.22	-0.55	0.01	0.03	-0.25	-0.08	0.12	-0.78	-1.02	-1.02	-0.59	-1.01	-0.05	SiO_2
Chrysotile	-15.66	-17.2	-11.13	-20.58	-22.28	-7.07	-10.89	-7.25	-20.2	-18.72	-15.76	-8.02	-19.09	-10.3	-18.26	-11.88	-18.1	-14.14	$Mg_3Si_2O_5(OH)_4$
CO_2(g)	-2.48	-1.91	-2.76	-2.72	-2.61	-3.34	-3.28	-2.67	-2.49	-2.06	-2.48	-1.56	-1.91	-2.85	-1.95	-2.44	-1.89	-2.4	CO_2
Dolomite	-7.51	-7.64	-4.98	-11.83	-11.98	-4.01	-5.92	-2.79	-11.37	-8.95	-8.26	-1.25	-8.21	-4.24	-7.73	-5.08	-7.39	-7.14	$CaMg(CO_3)_2$
$Fe(OH)_3$ (a)	0.96	-1.11	2.27	-2.33	-3.69	1.4	2.07	1.86	-2.21	-0.56	-0.14	1.54	-1.64	3.03	-0.35	0.95	-1.13	0.48	$Fe(OH)_3$ (a)
Fluorite	-4.19	-3.43	-3.97	-3.75	-4.5	-3.66	-4.1	-1.65	-4.4	-4.1	-3.98	-1.73	-3.29	-3.3	-3.72	-3.39	-3.09	-3.54	CaF_2
Goethite	6.85	4.78	8.16	3.56	2.2	7.29	7.96	7.75	3.68	5.33	5.75	7.43	4.26	8.92	5.55	6.85	4.77	6.37	FeOOH
Gypsum	-4.08	-4.25	-4.42	-3.9	-4.54	-4.29	-4.16	-2.02	-4.14	-4.04	-3.92	-1.87	-2.83	-4.19	-4.35	-3.39	-3.01	-4.16	$CaSO_4.2H_2O$
H_2 (g)	-24.72	-23.04	-28	-21.16	-20.72	-29.64	-28.4	-28.28	-21.12	-22.64	-23.8	-27.92	-22.52	-28.4	-23.36	-26.72	-23.04	-24.76	H_2 (g)
H_2O (g)	-1.51	-1.51	-1.51	-1.51	-1.51	-1.51	-1.51	-1.51	-1.51	-1.51	-1.51	-1.51	-1.51	-1.51	-1.51	-1.51	-1.51	-1.51	H_2O (g)
Halite	-8.71	-8.08	-7.84	-8.72	-8.38	-9.61	-9.27	-10.44	-8.89	-8.92	-9.33	-7.27	-8.43	-7.55	-9.08	-8.98	-8.39	-8.85	NaCl
Hausmannite	-17.65	-20.19	-10.02	-29	-29.18	-5.27	-7.81	-4.79	-26.65	-21.55	-21.11	-12.42	-24.2	-6.32	-22.06	-15.18	-17.52	-21.64	Mn_3O_4
Hematite	15.71	11.57	18.33	9.13	6.4	16.58	17.92	17.51	9.36	12.66	13.51	16.88	10.52	19.85	13.1	15.7	11.54	14.75	Fe_2O_3
Jarosite-K	-6.05	-11.53	-5.19	-13.09	-17.57	-8.3	-5.46	-4.06	-13.06	-8.58	-7.95	-2.76	-9.58	-3.5	-9.16	-6.03	-9.58	-7.55	$KFe_3(SO_4)_2(OH)_6$
Manganite	-6.76	-7.89	-3.67	-11.14	-11.27	-1.81	-2.87	-1.88	-10.36	-8.41	-8.07	-4.48	-9.31	-2.37	-8.46	-5.6	-7	-8.08	MnOOH
Melanterite	-8.33	-9.05	-10.54	-7.7	-9.32	-13.17	-10.77	-9.84	-7.84	-7.74	-8.42	-9.48	-7.75	-10.15	-8.53	-9.73	-7.96	-8.98	$FeSO_4.7H_2O$
O_2 (g)	-33.75	-37.11	-27.19	-40.87	-41.75	-23.91	-26.39	-26.63	-40.95	-37.91	-35.59	-27.35	-38.15	-26.39	-36.47	-29.75	-37.11	-33.67	O_2 (g)
Pyrochroite	-8.98	-9.27	-7.53	-11.58	-11.49	-6.49	-6.93	-5.88	-10.78	-9.59	-9.83	-8.3	-10.43	-6.43	-10	-8.82	-8.38	-10.32	$Mn(OH)_2$
Pyrolusite	-10.44	-12.41	-5.71	-16.6	-16.95	-3.03	-4.71	-3.78	-15.84	-13.13	-12.21	-6.56	-14.09	-4.21	-12.82	-8.28	-11.52	-11.74	$MnO_2.H_2O$
Quartz	-0.18	-0.07	-0.22	0.17	-0.35	0.18	-0.15	0.41	0.43	0.16	0.33	0.53	-0.37	-0.62	-0.62	-0.18	-0.61	0.36	SiO_2
Rhodochrosite	-3.28	-3	-2.11	-6.12	-5.92	-1.66	-2.03	-0.37	-5.09	-3.46	-4.12	-1.68	-4.16	-1.1	-3.77	-3.08	-2.08	-4.55	$MnCO_3$
Sepiolite	-11.62	-12.47	-8.68	-14.33	-16.33	-5.3	-8.39	-5.03	-13.63	-13.1	-10.85	-5.35	-14.23	-8.78	-14.09	-9.12	-13.97	-9.72	$Mg_2Si_3O_7.5OH.3H_2O$
Sepiolite (d)	-14.52	-15.37	-11.58	-17.23	-19.23	-8.2	-11.29	-7.93	-16.53	-16	-13.75	-8.25	-17.13	-11.68	-16.99	-12.02	-16.87	-12.62	$Mg_2Si_3O_7.5OH.3H_2O$
Siderite	-3.23	-3.89	-3.83	-4.98	-6.01	-6.11	-4.76	-4.3	-4.61	-3.29	-3.86	-3.33	-4.16	-3.37	-3.33	-4.19	-3.88	-3.65	$FeCO_3$
SiO_2(a)	-1.42	-1.31	-1.47	-1.08	-1.6	1.06	-1.39	-0.83	-0.81	-1.09	-0.92	-0.72	-1.61	-1.86	-1.86	-1.43	-1.85	-0.89	$SiO_{2\,(a)}$
Talc	-13.13	-14.45	-8.69	-17.35	-20.1	-3.82	-8.29	-3.53	-16.45	-15.51	-12.22	-4.08	-16.94	-8.64	-16.6	-9.36	-16.43	-10.54	$Mg_3Si_4O_{10}(OH)_2$

Phase	55	56	57	58	59	60	61	62	63	64	65	66	67	68	69	70	71	72	Formulae
Amm (g)	-11.65	-10.51	-12.96	-11.69	-11.88	-11.88	-12.69	-11.36	-12.44	-11.56	-10.73	-12.39	-12.81	-11.21	-12.8	-11.04	-12.95	-10.41	NH_3
Anhydrite	-4.39	-3.66	-3.38	-4.56	-4.4	-3.61	-4.65	-5.66	-3.72	-3.11	-3.45	-5.09	-4.84	-4.72	-4.02	-4.4	-4.89	-4.54	$CaSO_4$
Aragonite	-3.97	-2.06	-6.66	-4.68	-3.58	-4.34	-6.55	-4.54	-4.14	-3.2	-2.75	-6.25	-7.38	-3.55	-4.81	-3.98	-6.69	-2.85	$CaCO_3$
Calcite	-3.83	-1.92	-6.52	-4.54	-3.43	-4.19	-6.41	-4.4	-4	-3.06	-2.6	-6.1	-7.24	-3.4	-4.66	-3.84	-6.55	-2.71	$CaCO_3$
Chalcedony	-0.28	-0.27	0.02	-0.07	0.03	-0.01	-0.09	-0.62	-0.43	-0.17	-0.05	-0.11	-0.1	-0.52	-0.45	-1.53	-0.05	-1.56	SiO_2
Chrysotile	-17.02	-10.38	-21.74	-14.92	-14.27	-17.16	-22.94	-13.2	-16.96	-13.69	-9.42	-21.35	-25.34	-14.6	-18.22	-17.39	-23.68	-13.06	$Mg_3Si_2O_5(OH)_4$
CO_2(g)	-1.82	-2.15	-2.77	-2.43	-2.27	-1.93	-2.43	-2.87	-2.21	-2.07	-2.79	-2.42	-2.36	-2.49	-2.42	-2.59	-2.18	-2.81	CO_2
Dolomite	-7.58	-3.79	-12.98	-8.33	-6.82	-8.28	-12.87	-7.69	-8.01	-6.02	-4.95	-12	-14.42	-6.86	-9.29	-7.64	-13.03	-5.27	$CaMg(CO_3)_2$
$Fe(OH)_3$ (a)	-1.26	1.58	-4.39	1.28	0.71	-0.9	-4.15	0.9	-0.78	0.48	1.54	-2.62	-5.03	1.22	-0.94	1.35	-4.22	2.08	$Fe(OH)_3$ (a)
Fluorite	-3.55	-2.97	-2.68	-5.09	-3.61	-3.41	-3.98	-5	-3.82	-3.05	-3.68	-4.79	-4.29	-4.45	-3.85	-4.25	-4.92	-4.14	CaF_2
Goethite	4.63	7.48	1.5	7.17	6.6	4.99	1.74	6.79	5.11	6.37	7.44	3.27	0.86	7.11	4.96	7.24	1.67	7.97	FeOOH
Gypsum	-4.17	-3.44	-3.16	-4.34	-4.18	-3.39	-4.43	-5.44	-3.5	-2.89	-3.23	-4.87	-4.62	-4.5	-3.8	-4.18	-4.67	-4.32	$CaSO_4.2H_2O$
H_2 (g)	-22.88	-27.12	-19.4	-24.64	-24.36	-22.56	-19.56	-26.4	-23.08	-24.68	-27.44	-20.88	-18.08	-25.8	-22.84	-25.04	-19.48	-27.64	H_2 (g)
H_2O (g)	-1.51	-1.51	-1.51	-1.51	-1.51	-1.51	-1.51	-1.51	-1.51	-1.51	-1.51	-1.51	-1.51	-1.51	-1.51	-1.51	-1.51	-1.51	H_2O (g)
Halite	-8.5	-8.47	-8.83	-8.56	-7.71	-8.36	-8.98	-9.7	-7.89	-8.53	-8.6	-9.11	-9.16	-10.37	-8.77	-9.89	-9.24	-8.53	NaCl
Hausmannite	-24.04	-12.35	-28.63	-19.84	-17.74	-24.32	-31.03	-14.65	-23.38	-19.33	-12.25	-28.34	-35.36	-16.45	-22.46	-18.06	-31.42	-10.84	Mn_3O_4
Hematite	11.26	16.96	5.02	16.35	15.2	11.98	5.49	15.58	12.23	14.75	16.88	8.55	3.72	16.24	11.92	16.49	5.36	17.95	Fe_2O_3
Jarosite-K	-11.42	-4.93	-15.6	-3.49	-7.02	-8.2	-18.09	-7.88	-9.23	-4.8	-4.42	-14.64	-18.98	-7	-9.31	-5.32	-18.03	-5.1	$KFe_3(SO_4)_2(OH)_6$
Manganite	-9.2	-4.59	-11.31	-7.5	-6.85	-9.34	-12.08	-5.48	-8.94	-7.33	-4.51	-10.96	-13.77	-6.18	-8.68	-6.84	-12.22	-4	MnOOH
Melanterite	-8.99	-9.78	-7.62	-7.4	-8.52	-7.45	-8.51	-10.34	-8.16	-7.89	-9.73	-8.37	-7.95	-9.4	-8.05	-8.24	-8.4	-10.29	$FeSO_4.7H_2O$
O_2 (g)	-37.43	-28.95	-44.39	-33.91	-34.47	-38.07	-44.07	-30.39	-37.03	-33.83	-28.31	-41.43	-47.03	-31.59	-37.51	-33.11	-44.23	-27.91	O_2 (g)
Pyrochroite	-10.5	-8.01	-10.87	-9.68	-8.89	-10.48	-11.72	-8.54	-10.34	-9.53	-8.09	-11.26	-12.67	-8.94	-9.96	-9.22	-11.82	-7.68	$Mn(OH)_2$
Pyrolusite	-13.8	-7.07	-17.65	-11.22	-10.71	14.1	-18.34	-8.32	-13.44	-11.03	-6.83	-16.56	-20.77	-9.32	-13.3	-10.36	-18.52	-6.22	$MnO_2.H_2O$
Quartz	0.13	0.13	0.42	0.33	0.44	0.4	0.32	-0.22	-0.03	0.23	0.36	0.3	0.3	-0.11	-0.05	-1.13	0.35	-1.15	SiO_2
Rhodochrosite	-4.14	-1.98	-5.45	-3.93	-2.88	-4.23	-5.97	-3.23	-4.37	-3.42	-2.7	-5.5	-6.85	-3.25	-4.2	-3.63	-5.83	-2.31	$MnCO_3$
Sepiolite	-12.02	-7.58	-14.68	-10.29	-9.67	-11.66	-15.65	-10.05	-12.24	-9.62	-6.57	-14.63	-17.27	-10.81	-13.12	-14.35	-16.09	-11.51	$Mg_2Si_3O_7.5OH.3H_2O$
Sepiolite (d)	-14.92	-10.48	-17.58	-13.19	-12.57	-14.56	-18.55	-12.95	-15.14	-12.52	-9.47	-17.53	-20.17	-13.71	-16.02	-17.25	-18.99	-14.41	$Mg_2Si_3O_7.5OH.3H_2O$
Siderite	-3.87	-3.47	-6.2	-2.82	-2.99	-3.46	-5.71	-4.52	-3.87	-3.28	-4.32	-4.82	-5.79	-3.52	-4.12	-3.11	-5.49	-3.9	$FeCO_3$
SiO_2(a)	-1.12	-1.11	-0.82	-0.91	-0.81	-0.85	-0.93	-1.46	-1.27	-1.01	-0.88	-0.95	-0.94	-1.36	-1.29	-2.37	-0.89	-2.4	$SiO_{2\,(a)}$
Talc	-13.88	-7.22	-18.01	-11.37	-10.5	-13.48	-19.42	-10.75	-14.13	-10.33	-5.81	-17.87	-21.84	-11.94	-15.43	-16.75	-20.09	-12.48	$Mg_3Si_4O_{10}(OH)_2$

Phase	73	74	75	76	77	78	79	80	81	82	83	84	85	86	87	88	89	90	Formulae
Amm (g)	-11.95	-11.74	-11.68	-12.89	-12.78	-10.22	-9.95	-11.22	-9.89	-9.39	-9.36	-8.9	-9.49	-8.68	-9.18	-9.64	-8.51	-8.96	NH_3
Anhydrite	-3.78	-3.93	-3.62	-5.05	-4.6	-1.99	-3.25	-3.21	-3.34	-1.83	-1.57	-1.55	-1.64	-1.9	-1.08	-1.32	-2.5	-1.42	$CaSO_4$
Aragonite	-3.71	-4.43	-2.89	-7.39	-7.26	-0.57	-1.16	0.61	-0.83	0.16	0.01	-0.62	-0.06	0.94	0.12	-0.25	-0.04	0.45	$CaCO_3$
Calcite	-3.56	-4.28	-2.75	-7.24	-7.12	-0.42	-1.02	0.75	-0.69	0.31	0.16	-0.48	0.08	1.08	0.27	-0.1	0.11	0.59	$CaCO_3$
Chalcedony	-0.29	-0.31	-0.05	-0.47	-0.52	-0.47	0.11	0	0.04	0.23	0.03	0.06	-0.03	0.04	0.07	0.02	-0.2	0.25	SiO_2
Chrysotile	-14.25	-17.68	-11.25	-24.66	-24.45	-7.72	-7.95	-2.93	-6.98	-4.53	-6.06	-9.49	-7.39	-1.26	-6.28	-7.43	-6.33	-3.82	$Mg_3Si_2O_5(OH)_4$
CO_2(g)	-2.02	-2.05	-2.55	-2.64	-2.84	-1.24	-1.65	-1.73	-1.89	-1.64	-1.39	-1.18	-1.01	-1.71	-1.4	-1.24	-1.55	-1.57	CO_2
Dolomite	-6.57	-8.46	-5.45	-14.22	-14.2	-0.36	-1.83	1.61	-1.36	0.56	0.28	-1.3	0.19	2.49	0.29	-0.26	0.15	1.14	$CaMg(CO_3)_2$
$Fe(OH)_3$ (a)	0.29	-0.98	1.2	-4.74	-5.22	3.03	1.44	2.67	1.88	1.11	0.03	3.32	1.82	2.48	1.35	1.87	3.03	1.61	$Fe(OH)_3$ (a)
Fluorite	-3.75	-3.88	-3.84	-4.61	-3.66	-0.62	-1.41	-0.69	-2.55	-0.75	-1.12	-1.15	-1.08	-0.04	-0.58	-1.19	-0.28	-0.24	CaF_2
Goethite	6.18	4.91	7.09	1.15	0.67	8.92	7.33	8.56	7.77	7	5.92	9.21	7.71	8.38	7.24	7.76	8.92	7.5	FeOOH
Gypsum	-3.56	-3.71	-3.4	-4.83	-4.38	-1.77	-3.03	-2.99	-3.12	-1.61	-1.35	-1.33	-1.42	-1.68	-0.86	-1.1	-2.28	-1.2	$CaSO_4.2H_2O$
H_2 (g)	-24.64	-22.92	-26.44	-18.92	-18.72	-27.32	-27.52	-30.04	-28.48	-22.5	-22.16	-26.28	-27.32	-31.12	28.12	-27.24	-28.64	-29.28	H_2 (g)
H_2O (g)	-1.51	-1.51	-1.51	-1.51	-1.51	-1.51	-1.51	-1.51	-1.51	-1.51	-1.51	-1.51	-1.51	-1.51	-1.51	-1.51	-1.51	-1.51	H_2O (g)
Halite	-8.33	-8.08	-8.02	-9.26	-9.14	-5.6	-8.25	-7.7	-7.78	-6.45	-6.97	-6.71	-5.39	-5.85	-6.72	-5.65	-6.7	-5.97	NaCl
Hausmannite	-18.21	-23.65	-13.65	-32.49	-32.43	-10.56	-13.12	-0.32	-5	-13.58	-18.01	-7.92	-11.41	-2	-10.97	-8.85	-4.64	-8.28	Mn_3O_4
Hematite	14.36	11.83	16.19	4.3	3.35	19.84	16.67	19.12	17.55	16.01	13.84	20.43	17.43	18.76	16.5	17.53	19.85	17	Fe_2O_3
Jarosite-K	-6.16	-9.37	-5.29	-19.28	-20.38	3.52	-3.64	-2.8	-3.52	-4.24	-6.28	4.99	-0.38	-1.44	-1.69	0.37	0.58	-2.3	$KFe_3(SO_4)_2(OH)_6$
Manganite	-6.96	-9.06	-5.14	-12.67	-12.69	-3.96	-4.78	-0.1	-1.92	-5.77	-7.31	-3.26	-4.25	-0.48	-3.97	-3.41	-1.77	-2.88	MnOOH
Melanterite	-8.18	-8.04	-9.36	-8.56	-8.82	-7.35	-10.12	-11.96	-10.81	-7.83	-8.08	-5.99	-8.48	-11.67	-9.36	-8.11	-9.36	-10.53	$FeSO_4.7H_2O$
O_2 (g)	-33.91	-37.35	-30.31	-45.35	-45.75	-28.55	-28.15	-23.11	-26.23	-38.19	-38.87	-30.63	-28.55	-20.95	-26.95	-28.71	-25.91	-24.63	O_2 (g)
Pyrochroite	-9.14	-10.38	-8.22	-11.99	-11.91	-7.48	-8.4	-4.98	-6.02	-6.88	-8.25	-6.26	-7.77	-5.9	-7.89	-6.89	-5.95	-7.38	$Mn(OH)_2$
Pyrolusite	-10.68	-13.64	-7.96	-19.25	-19.37	-6.34	-7.06	-1.12	-3.72	-10.56	-12.27	-6.16	-6.63	-0.96	-5.95	-5.83	-3.49	-4.28	$MnO_2.H_2O$
Quartz	0.12	0.09	0.36	-0.07	-0.12	-0.06	0.52	0.4	0.44	0.64	0.44	0.46	0.37	0.44	0.48	0.42	0.2	0.66	SiO_2
Rhodochrosite	-2.97	-4.25	-2.59	-6.45	-6.57	-0.54	-1.87	1.47	0.28	-0.34	-1.46	0.75	-0.6	0.58	-1.1	0.06	0.68	-0.77	$MnCO_3$
Sepiolite	-10.19	-12.52	-7.79	-17.44	-17.38	-6.13	-5.32	-2.17	-4.8	-2.84	-4.2	-6.44	-5.19	-0.99	-4.27	-5.14	-4.77	-2.34	$Mg_2Si_3O_7.5OH.3H_2O$
Sepiolite (d)	-13.09	-15.42	-10.69	-20.34	-20.28	-9.03	-8.22	-5.07	-7.7	-5.74	-7.1	-9.34	-8.09	-3.89	-7.17	-8.04	-7.67	-5.24	$Mg_2Si_3O_7.5OH.3H_2O$
Siderite	-3.4	-3.84	-3.92	-6.19	-6.77	-1.22	-3.32	-3.44	3.6	-1.13	-1.8	-0.35	-2.2	-4.13	-3.45	-2.33	-2.19	-3.95	$FeCO_3$
SiO_2(a)	-1.13	-1.15	-0.89	-1.31	-1.36	-1.3	-0.73	-0.84	-0.8	-0.61	-0.81	-0.78	-0.87	-0.8	-0.77	-0.82	-1.04	-0.59	$SiO_{2\,(a)}$
Talc	-11.12	-14.61	-7.64	-21.91	-21.79	-4.95	-4.02	0.76	-3.2	-0.36	-2.3	-5.67	-3.76	2.52	-2.43	-3.7	-3.03	0.39	$Mg_3Si_4O_{10}(OH)_2$

Phase	91	92	93	94	95	96	97	98	99	100	101	102	103	104	105	106	107	108	Formulae
Amm (g)	-9.47	-10.3	-9.31	-9.78	-10.12	-9.21	-9.62	-9.67	-9.71	-10.7	-9.54	-8.87	-9.61	-10.05	-10.92	-9.71	-9.97	-11.11	NH_3
Anhydrite	-1.94	-3.1	-1.3	-2	-2.47	-2.47	-1.47	-3.66	-2.76	-4.33	-2.78	-1.53	-3.06	-3.08	-2.25	-1.84	-2.08	-2.36	$CaSO_4$
Aragonite	-0.44	-1.65	0.35	-0.61	-0.39	-0.14	-0.44	-0.23	-0.32	-0.37	-0.22	0.41	-0.22	-1.11	-1.13	-0.24	-1.86	-1.45	$CaCO_3$
Calcite	-0.3	-1.51	0.49	-0.46	-0.24	0	-0.29	-0.09	-0.18	-0.23	-0.07	0.56	-0.07	-0.96	-0.99	-0.1	-1.71	-1.31	$CaCO_3$
Chalcedony	0.09	-0.59	-0.06	0.04	-0.06	-0.53	0.05	-0.25	-0.24	-0.24	-0.19	0.05	0.08	-0.53	0.09	-0.47	0.01	0.08	SiO_2
Chrysotile	-7.22	-9.28	-5.36	-8.12	-6.34	-3.91	-6.19	-6.94	-7.63	-5.49	-7.74	-4.66	-5.29	-8.95	-8.23	-8.12	-10.96	-11.68	$Mg_3Si_2O_5(OH)_4$
CO_2(g)	-1.7	-2.5	-1.52	-1.5	-1.84	-2.26	-1.42	-1.63	-1.88	-1.56	-1.28	-1.3	-2.11	-1.87	-1.94	-1.22	-1.42	-1.48	CO_2
Dolomite	-0.9	-3.15	0.79	-1.13	-0.59	0.35	-0.25	-0.3	-0.88	0.11	-0.24	1.23	-0.44	-1.9	-2.17	-0.15	-3.22	-3.17	$CaMg(CO_3)_2$
$Fe(OH)_3$ (a)	1.5	3.19	1.63	1.27	1.51	1.67	2	3.07	3.51	4.28	1.09	2.01	2.36	2.16	3.58	1.16	0.97	2.31	$Fe(OH)_3$ (a)
Fluorite	-0.84	-3.26	-1.29	-1.48	-0.42	-0.04	-0.93	-0.77	-1.6	-1.69	-0.88	-0.01	-1.4	-1.26	-2.09	-0.63	-2.09	-1	CaF_2
Goethite	7.39	9.08	7.52	7.16	7.4	7.57	7.89	8.96	9.4	10.17	6.98	7.9	8.25	8.05	9.48	7.05	6.86	8.2	FeOOH
Gypsum	-1.72	-2.88	-1.08	-1.78	-2.25	-2.25	-1.25	-3.44	-2.54	-4.11	-2.56	-1.31	-2.84	-2.86	-2.03	-1.62	-1.86	-2.14	$CaSO_4.2H_2O$
H_2 (g)	-28.04	-28.68	-28.8	-27.4	-28.8	-30.56	27.84	-28.68	-28.52	-29.4	-27.76	-28.92	-29.6	-27.8	-27.6	-27.4	-25.24	-25.84	H_2 (g)
H_2O (g)	-1.51	-1.51	-1.51	-1.51	-1.51	-1.51	-1.51	-1.51	-1.51	-1.51	-1.51	-1.51	-1.51	-1.51	-1.51	-1.51	-1.51	-1.51	H_2O (g)
Halite	-7.27	-8.13	-6.22	-6.61	-7.77	-7	-6.13	-6.87	-6.81	-6.57	-6.48	-6.19	-8.09	-8.1	-7.1	-6.48	-6.84	-7.42	NaCl
Hausmannite	-12.05	-7.42	-7.22	-8.84		-1.73	-7.04	-1.15	-8.98	-3.42	-13.05	-8.49	-7.2	-10.9	-5.97	-8.97	-18.85	-10.48	Mn_3O_4
Hematite	16.79	20.17	17.04	16.32	16.81	17.14	17.79	19.93	20.81	22.34	15.98	17.81	18.5	18.12	20.96	16.12	15.73	18.41	Fe_2O_3
Jarosite-K	-2.32	-0.08	-1.73	-2.52	-5.91	-4.24	0.3	-1.09	1.11	2.05	-5.42	-1.93	-4.84	-4.29	3.1	-2.67	-1.94	-0.38	$KFe_3(SO_4)_2(OH)_6$
Manganite	-4.34	-2.69	-2.6	-3.38		-0.48	-2.7	-0.6	-3.24	-1.24	-4.72	-3.01	-2.46	-4	-2.39	-3.42	-7.07	-4.18	MnOOH
Melanterite	-9.78	-9.16	-10	-9.38	-10.87	-12.25	-8.43	-10.39	-9.12	-10	-10.68	-9.74	-11.46	-9.63	-7.33	-9.41	-7.35	-7.05	$FeSO_4.7H_2O$
O_2 (g)	-27.11	-25.83	-25.59	-28.39	-25.59	-22.07	-27.51	-25.83	-26.15	-24.39	-27.67	-25.35	-23.99	-27.59	-27.99	-28.39	-32.71	-31.51	O_2 (g)
Pyrochroite	-8.22	-6.89	-6.86	-6.94		-5.62	-6.48	-4.8	-7.36	-5.8	-8.46	-7.33	-7.12	-7.76	-6.05	-6.98	-9.55	-6.96	$Mn(OH)_2$
Pyrolusite	-6.36	-4.39	-4.24	-5.72		-1.24	-4.82	-2.3	-5.02	-2.58	-6.88	-4.59	-3.7	-6.14	-4.63	-5.76	-10.49	-7.3	$MnO_2.H_2O$
Quartz	0.49	-0.19	0.35	0.45	0.35	-0.12	0.45	0.15	0.16	0.16	0.21	0.46	0.49	-0.13	0.49	-0.07	0.41	0.48	SiO_2
Rhodochrosite	-1.74	-1.21	-0.2	-0.25		0.3	0.28	1.75	-1.05	0.83	-1.56	-0.44	-1.06	-1.44	0.19	-0.02	-2.79	-0.26	$MnCO_3$
Sepiolite	-4.88	-7.38	-3.88	-5.55	-4.54	-3.7	-4.26	-5.26	-5.7	-4.28	-5.69	-3.23	-3.61	-7.07	-5.55	-6.41	-7.5	-7.87	$Mg_2Si_3O_7.5OH.3H_2O$
Sepiolite (d)	-7.78	-10.28	-6.78	-8.45	-7.44	-6.6	-7.16	-8.16	-8.6	-7.18	-8.59	-6.13	-6.51	-9.97	-8.45	-9.31	-10.4	-10.77	$Mg_2Si_3O_7.5OH.3H_2O$
Siderite	-3.57	-3	-3.64	-3.28	-4.08	-5.22	-2.69	-2.25	-1.97	-1.33	-3.41	-3.09	-3.91	-2.95	-1.51	-3.1	-2.41	-1.44	$FeCO_3$
SiO_2(a)	-0.75	-1.43	-0.9	-0.8	-0.9	-1.37	-0.79	-1.09	-1.08	-1.08	-1.03	-0.79	-0.76	-1.37	-0.75	-1.31	-0.83	-0.76	$SiO_{2\,(a)}$
Talc	-3.35	-6.76	-1.78	-4.33	-2.76	-1.27	-2.4	-3.75	-4.42	-2.28	-4.42	-0.85	-1.43	-6.32	-4.36	-5.37	-7.24	-7.82	$Mg_3Si_4O_{10}(OH)_2$

Phase	109	110	111	112	113	114	115	116	117	118	119	120	121	122	123	124	125	126	Formulae
Amm (g)	-8.73	-9.85	-8.95	-10.36	-10.17	-9.23	-9.97	-11.6	-9.26	-7.43	-10.58	-8.06	-8.02	-9.6	-9.67	-9.24	-10.35	-8.55	NH_3
Anhydrite	-1.87	-2.23	-2.3	-3.83	-2.91	-2	-3.4	-3.61	-1.45	-1.89	-2.37	-2.43	-3.69	-1.88	-1.27	-1.26	-2.32	-1.83	$CaSO_4$
Aragonite	0.59	-0.35	1.45	-0.54	-0.53	0.01	-1.43	-0.34	0.19	0.13	-1.22	-0.54	-0.34	-0.25	0.07	0.3	-0.81	-0.38	$CaCO_3$
Calcite	0.73	-0.2	1.59	-0.4	-0.39	0.15	-1.28	-0.2	0.33	0.27	-1.08	-0.39	-0.19	-0.11	0.21	0.44	-0.66	-0.24	$CaCO_3$
Chalcedony	-0.58	-0.1	-0.46	-0.05	-0.09	0.13	-0.07	-0.58	-0.1	-0.3	-0.82	-0.07	-1.36	-0.05	0.07	0.09	-0.07	-0.01	SiO_2
Chrysotile	-3.75	-6.85	-2.1	-6.31	-7.87	-5.08	-8.42	-4.91	-6.73	-5.9	-11.68	-8.84	-8.9	-6.77	-6.97	-5.43	-7.43	-8.34	$Mg_3Si_2O_5(OH)_4$
CO_2(g)	-2.1	-1.34	-2.31	-1.99	-1.38	-1.61	-2.23	-2.52	-1.07	-1.43	-1.66	-1.62	-1.66	-1.4	-1.07	-1.22	-1.81	-1.26	CO_2
Dolomite	1.33	-0.21	2.45	-0.9	-0.77	0.33	-2.72	-0.41	0.65	0.64	-2.53	-1.25	-0.34	-0.17	0.33	0.92	-1.34	-0.72	$CaMg(CO_3)_2$
$Fe(OH)_3$ (a)	3.89	2.02	2.06	3.31	1.83	1.51	2.99	3.83	1.82	3.08	3.14	4.08	3.21	2.42	1.03	1.77	2.51	3.6	$Fe(OH)_3$ (a)
Fluorite	-1.83	-1.34	0.3	-1.42	-1.52	-0.12	-2.22	-1.45	-0.74	-0.28	-0.64	-1.84	-0.36	-0.13	-0.73	-0.31	0.96	-1.41	CaF_2
Goethite	9.78	7.91	7.95	9.2	7.72	7.4	8.88	9.72	7.71	8.97	9.03	9.97	9.1	8.31	6.92	7.66	8.4	9.49	FeOOH
Gypsum	-1.65	-2.01	-2.08	-3.61	-2.69	-1.78	-3.18	-3.39	-1.23	-1.67	-2.15	-2.21	-3.47	-1.66	-1.05	-1.04	-2.1	-1.61	$CaSO_4.2H_2O$
H_2 (g)	-30.96	-21.76	-34.16	-29.04	-27.4	-28.8	-28.12	-30.84	-27.8	-28.64	-27.04	-27.96	-28.56	-28.16	-27.4	-28.52	-28.44	-27.16	H_2 (g)
H_2O (g)	-1.51	-1.51	-1.51	-1.51	-1.51	-1.51	-1.51	-1.51	-1.51	-1.51	-1.51	-1.51	-1.51	-1.51	-1.51	-1.51	-1.51	-1.51	H_2O (g)
Halite	-6.26	-6.38	-5.71	-7.82	-7.68	-7.04	-7.82	-7.76	-6.04	-6.15	-7.08	-6.77	-6.77	-7.29	-5.64	-5.65	-6.15	-6.07	NaCl
Hausmannite	-2.27	-16.33	3.13	-3.53	-11.86	-9.06	-7.09	0.09	-12.53	-7.6	-9.24	-8.49	-9.06	-5.78	-8.08	-7.16	-6	-10.78	Mn_3O_4
Hematite	21.57	17.83	17.91	20.41	17.44	16.8	19.78	21.44	17.42	19.95	20.07	21.95	20.21	18.63	15.85	17.33	18.81	20.99	Fe_2O_3
Jarosite-K	2.64	-0.86	-4.14	-1.24	-3.01	-3.26	-1.47	-0.49	-0.35	2.31	1.71	3.32	-1.22	-0.77	-1.98	-0.53	-1.42	4.53	$KFe_3(SO_4)_2(OH)_6$
Manganite	-0.6	-6.81	1.74	-1.33	-4.38	-3.22	-2.67	0.17	-4.54	-2.76	-3.57	-3.17	-3.26	-2.23	-3.12	-2.63	-2.26	-4.06	MnOOH
Melanterite	-10.2	-6.14	-15.14	-10.54	-9.68	-10.57	-9.32	-11.44	-8.84	-8.74	-7.24	-7.47	-10.14	-8.74	-9.13	-9.32	-9.1	-6.74	$FeSO_4.7H_2O$
O_2 (g)	-21.27	-39.67	-14.87	-25.11	-28.39	-25.59	-29.95	-21.51	-27.59	-25.91	-29.11	-27.27	-26.07	-26.87	-28.39	-26.15	-26.31	-28.87	O_2 (g)
Pyrochroite	-5.94	-7.55	-5.2	-5.71	-7.94	-7.48	-6.59	-5.11	-8.3	-6.94	-6.95	-7.01	-7.4	-6.17	-6.68	-6.75	-6.34	-7.5	$Mn(OH)_2$
Pyrolusite	-1.16	-11.97	2.78	-2.85	-6.72	-4.86	-4.65	-0.45	-6.68	-4.48	-6.09	-5.23	-5.02	-4.19	-5.47	-4.41	-4.08	-6.52	$MnO_2.H_2O$
Quartz	-0.17	0.31	-0.05	0.36	0.31	0.53	0.34	-0.17	0.3	0.11	-0.42	0.34	-0.96	0.36	0.47	0.49	0.34	0.4	SiO_2
Rhodochrosite	0.15	-0.72	0.67	0.48	-1.14	-0.9	-0.64	0.56	-1.18	-0.18	-0.43	-0.44	-0.87	0.61	0.43	0.21	0.03	-0.58	$MnCO_3$
Sepiolite	-3.68	-4.94	-2.38	-4.5	-5.61	-3.39	-5.94	-4.44	-4.87	-4.64	-9.37	-6.22	-8.42	-4.8	-4.74	-3.69	-5.28	-5.78	$Mg_2Si_3O_7.5OH.3H_2O$
Sepiolite (d)	-6.58	-7.84	-5.28	-7.4	-8.51	-6.29	-8.84	-7.34	-7.77	-7.54	-12.27	-9.12	-11.32	-7.7	-7.64	-6.59	-8.18	-8.68	$Mg_2Si_3O_7.5OH.3H_2O$
Siderite	-3.04	0.45	-6.68	-2.55	-2.6	-3.85	-2.64	-3.46	-2.5	-2.01	-1.39	-0.86	-2.08	-2.41	-3.09	-3.06	-2.87	-0.59	$FeCO_3$
SiO_2(a)	-1.42	-0.94	-1.3	-0.89	-0.93	-0.71	-0.91	-1.42	-0.94	-1.14	-1.66	-0.91	-2.2	-0.88	-0.77	-0.75	-0.91	-0.85	$SiO_{2\,(a)}$
Talc	-1.21	-3.34	0.68	-2.71	-4.36	-1.13	-4.86	-2.36	-3.24	-2.79	-9.63	-5.28	-7.93	-3.16	-3.13	-1.56	-3.86	-4.65	$Mg_3Si_4O_{10}(OH)_2$

Phase	127	128	129	130	131	132	133	134	135	136	137	138	139	140	141	142	143	Formulae
Amm (g)	-9.79	-9.23	-10.03	-8.09	-9.22	-8.3	-7.61	-11.42	-9.78	-10.07	-9.17	-9.31	-9.69	-10.02	-9.92	-10.65	-10.27	NH_3
Anhydrite	-4.42	-3.28	-2.36	-2.48	-3.53	-1.94	-3.54	-2.95	-2.71	-2.36	-1.82	-1.43	-4.02	-2.11	-1.9	-3.67	-2.56	$CaSO_4$
Aragonite	-2.13	-2.22	-1.01	-0.77	-1.57	0	-0.11	-2.26	-0.8	-0.52	0.51	-0.15	-1.43	-0.47	-0.36	-1.29	-2.1	$CaCO_3$
Calcite	-1.99	-2.07	-0.87	-0.63	-1.42	0.14	0.04	-2.11	-0.66	-0.37	0.65	-0.01	-1.28	-0.33	-0.21	-1.15	-1.96	$CaCO_3$
Chalcedony	-1.38	-0.17	0.21	-0.46	-0.33	-0.35	-0.32	-0.47	-0.14	0.25	-0.03	0.08	-0.35	-0.49	-0.28	-0.3	-0.25	SiO_2
Chrysotile	-9.46	-10.81	-8.37	-10.57	-12.33	-5.42	-5.07	-14.53	-9.03	-5.28	-3.72	-6.61	-8.41	-9.22	-8.28	-10.27	-10.52	$Mg_3Si_2O_5(OH)_4$
CO_2(g)	-3.29	-2.26	-1.63	-1.14	-1.15	-1.68	-2	-1.61	-1.44	-2.12	-1.53	-1.32	-2.6	-1.11	-1.19	-1.49	-2.09	CO_2
Dolomite	-3.96	-4.25	-1.86	-1.43	-2.9	0.45	0.13	-4.69	-1.46	-0.85	1.47	-0.02	-2.89	-0.62	-0.42	-2.29	-3.83	$CaMg(CO_3)_2$
$Fe(OH)_3$ (a)	1.66	2.74	1.39	3.09	3.23	3.02	3.07	2.04	2.4	2.03	2.74	1.79	3.15	4.2	3.01	3.01	1.14	$Fe(OH)_3$ (a)
Fluorite	-3.88	-3.33	-1.51	-0.99	-1.63	-0.21	-0.95	-2.54	-1.28	-1.49	0.36	-0.6	-2.4	-2.13	-2.22	-1.98	-2.48	CaF_2
Goethite	7.55	8.63	7.28	8.99	9.12	8.91	8.96	7.93	8.29	7.92	8.63	7.68	9.04	10.09	8.9	8.9	7.03	FeOOH
Gypsum	-4.2	-3.06	-2.14	-2.26	-3.31	-1.72	-3.32	-2.73	-2.49	-2.14	-1.6	-1.21	-3.8	-1.89	-1.68	-3.45	-2.34	$CaSO_4.2H_2O$
H_2 (g)	-30	-27.04	-27.2	-26.16	-24.96	-29.12	-29.84	-25.36	-27.04	-29.36	-29.6	-27.6	-29.32	-26.88	-27.32	-26.64	-26.24	H_2 (g)
H_2O (g)	-1.51	-1.51	-1.51	-1.51	-1.51	-1.51	-1.51	-1.51	-1.51	-1.51	-1.51	-1.51	-1.51	-1.51	-1.51	-1.51	-1.51	H_2O (g)
Halite	-8.98	-8.45	-8.5	-6.78	-7.39	-5.98	-6.87	-7	-7.13	-7.48	-6.21	-5.73	-9.55	-5.41	-5.34	-6.7	7.05	NaCl
Hausmannite	-9.48	-11.12	-13.93	-10.62	-11.67	-2.53	0.97	-16.88	-12.85	-3.86	-6.54	-4.95	-5.03	-10.31	-9.34	-10	-9.5	Mn_3O_4
Hematite	17.11	19.27	16.57	19.98	20.25	19.83	19.93	17.87	18.58	17.85	19.27	17.37	20.1	22.19	19.8	19.81	16.06	Fe_2O_3
Jarosite-K	-7.29	0.39	-2.78	2.66	1.89	1.79	-1.92	-0.23	-0.14	-3.24	0.42	-1.11	-2.36	6.27	2.82	0.58	-2.59	$KFe_3(SO_4)_2(OH)_6$
Manganite	-3.16	-4.2	-5.11	-4.18	-4.73	-0.99	0.3	-6.4	-4.77	-1.39	-2.24	-2.05	-1.79	-3.95	-3.56	-3.89	-3.79	MnOOH
Melanterite	-12.97	-8.16	-9.24	-6.89	-6.41	-9.21	-11.33	-6.99	-8.53	-10.67	-9.97	-8.67	-10.76	-6.05	-7.45	-8.22	-8.58	$FeSO_4.7H_2O$
O_2 (g)	-23.19	-29.11	-28.79	-30.87	-33.27	-24.95	-23.51	-32.47	-29.11	-24.47	-23.99	-27.99	-24.55	-29.43	-28.55	-29.91	-30.71	O_2 (g)
Pyrochroite	-8.02	-7.58	-8.57	-7.12	-7.07	-5.41	-4.48	-8.94	-8.15	-5.93	-6.9	-5.71	-6.31	-7.25	-7.08	-7.07	-6.77	$Mn(OH)_2$
Pyrolusite	-4.2	-6.72	-7.55	-7.14	-8.29	-2.47	-0.82	-9.76	-7.29	-2.75	-3.49	-4.29	-3.17	-6.55	-5.94	-6.61	-6.71	$MnO_2.H_2O$
Quartz	-0.97	0.23	0.61	-0.05	0.07	0.05	0.08	-0.06	0.26	0.65	0.37	0.49	0.05	-0.09	0.12	0.11	0.16	SiO_2
Rhodochrosite	-3.13	-1.65	-2.01	-0.08	-0.03	1.1	1.7	-2.36	-1.42	0.13	-0.25	1.15	-0.73	-0.18	-0.09	-0.37	-0.68	$MnCO_3$
Sepiolite	-8.82	-7.71	-5.45	-8.02	-8.98	-4.41	-4.13	-10.68	-6.47	-3.32	-2.74	-4.48	-6.41	-7.18	-6.2	-7.56	-7.64	$Mg_2Si_3O_7.5OH.3H_2O$
Sepiolite (d)	-11.72	-10.61	-8.35	-10.92	-11.88	-7.31	-7.03	-13.58	-9.37	-6.22	-5.64	-7.38	-9.31	-10.08	-9.1	-10.46	-10.54	$Mg_2Si_3O_7.5OH.3H_2O$
Siderite	-5.98	-2.38	-3.18	-0.47	0.25	-2.56	-3.2	-1.59	-1.91	-4.12	-2.93	-2.68	-3.46	0.3	-1.2	-1.14	-3.42	$FeCO_3$
SiO_2(a)	-2.22	-1.01	-0.63	-1.29	-1.17	-1.19	-1.16	-1.31	-0.98	-0.59	-0.87	-0.76	-1.19	-1.33	-1.12	-1.14	-1.09	$SiO_{2\,(a)}$
Talc	-8.52	-7.46	-4.26	-7.78	-9.3	-2.43	-2.01	-11.77	-5.61	-1.09	-0.08	-2.74	-5.42	-6.51	-5.14	-7.17	-7.32	$Mg_3Si_4O_{10}(OH)_2$